

*Carnegie
Institution*

OF WASHINGTON


Year Book 67

1967-1968



A. D. SINGER

DIRECTOR'S OFFICE



Digitized by the Internet Archive
in 2012 with funding from
LYRASIS Members and Sloan Foundation

*Carnegie
Institution*

OF WASHINGTON

Year Book 67

1967-1968

Library of Congress Catalog Card Number 3-16716
Port City Press, Baltimore, Maryland

Contents

	<i>page</i>
Officers and Staff	v
Report of the President	1
Reports of Departments and Special Studies	1
Mount Wilson and Palomar Observatories	3
Geophysical Laboratory	71
Department of Terrestrial Magnetism	281
Committee on Image Tubes for Telescopes	387
Department of Embryology	393
Department of Plant Biology	471
Genetics Research Unit	553
Bibliography	569
Report of the Executive Committee	571
Report of Auditors	573
Abstract of Minutes of the Seventieth Meeting of the Board of Trustees	589
Articles of Incorporation	591
By-Laws of the Institution	595
Index	601

President and Trustees

PRESIDENT

Caryl P. Haskins

BOARD OF TRUSTEES

James N. White
Chairman

Henry S. Morgan
Vice-Chairman

Garrison Norton
Secretary

Sir Eric Ashby
Amory H. Bradford
Omar N. Bradley ¹
Vannevar Bush
Michael Ference, Jr.
Carl J. Gilbert
Crawford H. Greenewalt
Caryl P. Haskins
Alfred L. Loomis
Robert A. Lovett
William McC. Martin, Jr.
Keith S. McHugh
Henry S. Morgan
Seeley G. Mudd ²
William I. Myers
Garrison Norton
Robert M. Pennoyer
Richard S. Perkins
William M. Roth
William W. Rubey
Frank Stanton
Charles P. Taft
Charles H. Townes
Juan T. Trippe
James N. White

¹ Retired May 3, 1968.

² Died March 10, 1968.

Trustees (continued)

AUDITING COMMITTEE

Keith S. McHugh, *Chairman*
Alfred L. Loomis
Juan T. Trippe

EXECUTIVE COMMITTEE

Henry S. Morgan, *Chairman*
Carl J. Gilbert
Crawford H. Greenewalt
Caryl P. Haskins
Keith S. McHugh
William I. Myers
Garrison Norton
Richard S. Perkins
Frank Stanton
James N. White

RETIREMENT COMMITTEE

Frank Stanton, *Chairman*
Amory H. Bradford
Garrison Norton
Richard S. Perkins

COMMITTEE ON ASTRONOMY

Crawford H. Greenewalt, *Chairman*
Amory H. Bradford
William McC. Martin, Jr.

FINANCE COMMITTEE

Richard S. Perkins, *Chairman*
Crawford H. Greenewalt
Alfred L. Loomis
Keith S. McHugh
Henry S. Morgan

COMMITTEE ON BIOLOGICAL SCIENCES

Alfred L. Loomis, *Chairman*
William I. Myers
Charles P. Taft

NOMINATING COMMITTEE

Carl J. Gilbert, *Chairman*
Crawford H. Greenewalt
Keith S. McHugh
James N. White

COMMITTEE ON TERRESTRIAL SCIENCES

Juan T. Trippe, *Chairman*
Richard S. Perkins

Staff

MOUNT WILSON AND PALOMAR OBSERVATORIES

813 Santa Barbara Street
Pasadena, California 91106

Horace W. Babcock, *Director*
Halton C. Arp
Ira S. Bowen, *Distinguished*
Service Member

Edwin W. Dennison
Armin J. Deutsch
Jesse L. Greenstein
Robert F. Howard
Robert P. Kraft ¹
Robert B. Leighton
Guido Münch
J. Beverley Oke
Bruce H. Rule
Allan R. Sandage
Wallace L. W. Sargent
Maarten Schmidt
Arthur H. Vaughan, Jr.
Olin C. Wilson
Harold Zirin
Fritz Zwicky ²

GEOPHYSICAL LABORATORY

2801 Upton Street, N.W.
Washington, D.C. 20008

Philip H. Abelson, *Director*
Peter M. Bell
Francis R. Boyd, Jr.
Felix Chayes
Gordon L. Davis
Gabrielle Donnay
Joseph L. England
P. Edgar Hare
Thomas C. Hoering
Thomas E. Krogh
Gunnar Kullerud
Donald H. Lindsley
J. Frank Schairer
Hatten S. Yoder, Jr.

DEPARTMENT OF TERRESTRIAL MAGNETISM

5241 Broad Branch Road, N.W.
Washington, D.C. 20015

Ellis T. Bolton, *Director*
L. Thomas Aldrich, *Associate*
Director
Merle A. Tuve, *Distinguished*
Service Member

Roy J. Britten
Louis Brown
Dean B. Cowie
Scott E. Forbush
W. Kent Ford, Jr.³
Stanley R. Hart
David E. Kohne
Richard B. Roberts
Vera C. Rubin
I. Selwyn Sacks
T. Jefferson Smith ⁴
John S. Steinhart
Kenneth C. Turner

¹ Resigned July 31, 1968.

² Retired June 30, 1968.

³ On leave of absence to August 31, 1967.

⁴ On leave of absence October 1, 1967, to March 31, 1968. Resigned June 30, 1968.

Staff (continued)

DEPARTMENT OF PLANT BIOLOGY

Stanford, California 94305

C. Stacy French, *Director*
Olle Björkman
Jeanette S. Brown
Jens C. Clausen, *Emeritus*
David C. Fork
William M. Hiesey
Malcolm A. Nobs
James H. C. Smith, *Emeritus*

DEPARTMENT OF EMBRYOLOGY

*115 West University Parkway
Baltimore, Maryland 21210*

James D. Ebert, *Director*
David W. Bishop¹
Bent G. Böving
Donald D. Brown
Igor B. Dawid
Robert L. DeHaan
Elizabeth M. Ramsey

GENETICS RESEARCH UNIT

*Cold Spring Harbor
New York 11724*

Alfred D. Hershey, *Director*
Barbara McClintock, *Distinguished
Service Member*
Elizabeth Burgi

*Cytogenetics Laboratory
Ann Arbor, Michigan*

Helen Gay

¹ Retired June 30, 1967.

Staff (continued)

OFFICE OF ADMINISTRATION

1530 P Street, N.W., Washington, D.C. 20005

Caryl P. Haskins	<i>President</i>
Edward A. Ackerman	<i>Executive Officer</i>
James W. Boise	<i>Bursar; Secretary-Treasurer, Retirement Trust; Executive Secretary to the Finance Committee</i>
Marjorie H. Walburn	<i>Assistant to the President</i>
Donald J. Patton	<i>Director of Publications</i>
Sheila A. McGough	<i>Editor</i>
Kenneth R. Henard	<i>Assistant Bursar; Assistant Treasurer, Retirement Trust</i>
Pamela W. Thomas	<i>Assistant Editor</i>
Joseph M. S. Haraburda	<i>Assistant to the Bursar</i>
A. Gerald Thompson	<i>Assistant to the Director of Publications</i>
Marshall Hornblower	<i>Counsel</i>

STAFF MEMBERS IN SPECIAL SUBJECT AREAS

Tatiana Proskouriakoff

Anna O. Shepard ¹

¹ Retired June 30, 1968.

Staff (continued)

RESEARCH ASSOCIATES OF THE CARNEGIE INSTITUTION

Mateo Casaverde

Lima, Peru

Richard A. Chase

Johns Hopkins University

Louis B. Flexner

University of Pennsylvania

Irwin Konigsberg

University of Virginia

J. D. McGee

Imperial College of Science and Technology, University of London

Jan H. Oort

University of Leiden

Harry E. D. Pollock

Carnegie Institution

Reynaldo Salgueiro

La Paz, Bolivia

Shigeji Suyehiro

Japan Meteorological Agency

Former Presidents and Trustees

PRESIDENTS

Daniel Coit Gilman, 1902-1904 John Campbell Merriam, 1921-1938;
Robert Simpson Woodward, 1904-1920 *President Emeritus 1939-1945*
Vannevar Bush, 1939-1955

TRUSTEES

Alexander Agassiz	1904-05	Seth Low	1902-16
George J. Baldwin	1925-27	Wayne MacVeagh	1902-07
Thomas Barbour	1934-46	Andrew W. Mellon	1924-37
James F. Bell	1935-61	Margaret Carnegie Miller	1955-67
John S. Billings	1902-13	Roswell Miller	1933-55
Robert Woods Bliss	1936-62	Darius O. Mills	1902-09
Lindsay Bradford	1940-58	S. Weir Mitchell	1902-14
Robert S. Brookings	1910-29	Andrew J. Montague	1907-35
John L. Cadwalader	1903-14	William W. Morrow	1902-29
William W. Campbell	1929-38	William Church Osborn	1927-34
John J. Carty	1916-32	James Parmelee	1917-31
Whitefoord R. Cole	1925-34	Wm. Barclay Parsons	1907-32
Frederic A. Delano	1927-49	Stewart Paton	1916-42
Cleveland H. Dodge	1903-23	George W. Pepper	1914-19
William E. Dodge	1902-03	John J. Pershing	1930-43
Charles P. Fenner	1914-24	Henning W. Prentis, Jr.	1942-59
Homer L. Ferguson	1927-52	Henry S. Pritchett	1906-36
Simon Flexner	1910-14	Gordon S. Rentschler	1946-48
W. Cameron Forbes	1920-55	David Rockefeller	1952-56
James Forrestal	1948-49	Elihu Root	1902-37
William N. Frew	1902-15	Elihu Root, Jr.	1937-67
Lyman J. Gage	1902-12	Julius Rosenwald	1929-31
Walter S. Gifford	1931-66	Martin A. Ryerson	1908-28
Cass Gilbert	1924-34	Henry R. Shepley	1937-62
Frederick H. Gillett	1924-35	Theobald Smith	1914-34
Daniel C. Gilman	1902-08	John C. Spooner	1902-07
John Hay	1902-05	William Benson Storey	1924-39
Barklie McKee Henry	1949-66	Richard P. Strong	1934-48
Myron T. Herrick	1915-29	William H. Taft	1906-15
Abram S. Hewitt	1902-03	William S. Thayer	1929-32
Henry L. Higginson	1902-19	James W. Wadsworth	1932-52
Ethan A. Hitchcock	1902-09	Charles D. Walcott	1902-27
Henry Hitchcock	1902	Frederic C. Walcott	1931-48
Herbert Hoover	1920-49	Henry P. Walcott	1910-24
William Wirt Howe	1903-09	Lewis H. Weed	1935-52
Charles L. Hutchinson	1902-04	William H. Welch	1906-34
Walter A. Jessup	1938-44	Andrew D. White	1902-03
Frank B. Jewett	1933-49	Edward D. White	1902-03
Samuel P. Langley	1904-06	Henry White	1913-27
Ernest O. Lawrence	1944-58	George W. Wickersham	1909-36
Charles A. Lindbergh	1934-39	Robert E. Wilson	1953-64
William Lindsay	1902-09	Robert S. Woodward	1905-24
Henry Cabot Lodge	1914-24	Carroll D. Wright	1902-08

Under the original charter, from the date of organization until April 28, 1904, the following were ex officio members of the Board of Trustees: the President of the United States, the President of the Senate, the Speaker of the House of Representatives, the Secretary of the Smithsonian Institution, and the President of the National Academy of Sciences.



Report OF
THE President

Mankind is now in one of its rare moods of shifting its outlook. The mere compulsion of tradition has lost its force. It is the business of philosophers, students, and practical men to re-create and re-enact a vision of the world, conservative and radical, including those elements of reverence and order without which society lapses into riot, a vision penetrated through and through with unflinching rationality. Such a vision is the knowledge which Plato identified with virtue.

ALFRED NORTH WHITEHEAD—Introduction to *Business Adrift*,

by W. B. DONHAM, 1931

There are inherent in the scientific method ethical values which, if they were to command common assent, would have an immense stabilizing value on public affairs. I cannot do more than catalogue them here. There is the scientist's undogmatic attitude to truth and error; his acknowledgement that truth is always changing, approaching an asymptote of perfection, but never reaching it. And error? Error is not evil: it is only discarded approximations to truth. . . .

And lastly there is the internationalism of science: it is the one remaining force of cohesion between peoples who may be at war on every other issue. Whether the man who upsets my scientific theories is my countryman or my enemy is immaterial: the theories are upset all the same. Perhaps, then, it is through reflection on the ethical and moral implications of science and technology, that is to say the influences of these studies on humanism, that a country may make its greatest contribution to civilization.

SIR ERIC ASHBY—"Machines, Understanding, and Learning, Reflections on Technology in Education," *The Graduate Journal*, University of Texas, 1967

We live in a world of unreality and dreams. To give up our imaginary position as the center, to renounce it, not only intellectually but in the imaginative part of our soul, that means to waken to what is real and eternal, to see the true light and hear the true silence. . . . It is a transformation analogous to that which takes place in the dusk of evening on a road, where we suddenly discern as a tree what we had at first seen as a stooping man; or where we suddenly recognize as a rustling of leaves what we thought at first were whispering voices. We see the same colors; we hear the same sounds, but not in the same way.

SIMONE WEIL—*Waiting for God*, 1959

THIS IS A YEAR OF WATERSHED. In our swift-moving and protean world every new year must carry a particular significance, must bring fresh opportunities, and at the same time must carry forward and renew a panorama of already existing concerns. This is as true in the realm of science as in any other segment of national, or indeed of world, affairs. It is a normal situation, and one which we have long since learned to expect.

Yet by any standard, and from any aspect, the year just past and the year ahead may be viewed in retrospect as marking a dividing range in many of the greatest concerns of our society and our time—in the very evolution, indeed, of our nation. Surely, in terms of major political and social tides in both national and international affairs, the critical nature of the past year, and its aspect of watershed, are so compellingly evident as to make further emphasis superfluous. But as a rising ocean tide affects the character and course of every creek and river and winding estuary that enters it, and is in turn affected by their flow, so the events of the past

year—and the shape of deeper social trends that these events reflect—have deeply scored their marks in other areas as well, areas such as science, that preoccupy us both as individuals and as a nation, and that are importantly and indissolubly of the nexus of those events. It is somewhat striking to reflect that in this year, the two hundredth anniversary of the birth of that great French mathematical physicist Jean Baptiste Joseph Fourier at Auxerre in Yonne, we find the affairs of science as sensitively responsive to elements of their larger social background, as intimately reflecting them and bounded by them, as Fourier found in a very different context of place and time and circumstance—and, so finding, managed personally to span the gulf between them during the years of his scientific greatness and of the French Revolution. For American science, as for other national concerns, the shape of the year's events has indeed had some aspects of a watershed whose outlines and influence could significantly affect the contours of our scientific landscape for some time to come, or even, indeed, permanently. How we respond over the next few years to very real crises in the scientific affairs of the nation could leave an important and perhaps enduring imprint on our fortunes.

A century and a half ago, Thomas Jefferson wrote, in a letter to John Adams, "I like the dreams of the future better than the history of the past." As in so many other aspects of his life and work, it seems very clear today that Jefferson, in that single sentence, epitomized with extraordinary clarity a creed of the young nation that quite literally had the quality of a faith. It was a faith that is hard to define precisely. But perhaps it can best be expressed as a consuming passion for the wonder of the world—both the natural world and the world of man—and a total dedication to growth and movement and aspiration, which taken together sum to the quality of hope which today is surely our most precious, and perhaps our most threatened, common possession, the very root of our vitality as a people, the quality to which men over all the world will respond, particularly in our time, as they will to nothing else. And there was a third facet to that faith. It comprehended a real reverence, with all the power and the inspiration that the fact of reverence conveys.

Through the centuries since Jefferson's death the society that he knew, shaped and motivated in good measure by that faith, has grown to proportions of which he could hardly have dreamed. It has also, quite obviously, changed in structure and character in ways that would have quite defied his imagination. New problems have replaced the old at the forefront of our concerns. New views of nature and of man have swept like swift, re-

current tides over the nation, as they have over a world society transformed by experience and development beyond anything that a Jeffersonian society could have comprehended in its most soaring flights of imagination. Superficially it sometimes appears that we are so different a people today, buffeted by such new orders of challenge and demand, beset by such new kinds of imperatives for our very survival let alone our further growth, that bonds with that past have dissolved and vanished.

Yet a strong case can be made for the contrary view. The basic precepts around which a society crystallizes, upon which the foundations of a nation are laid, the precepts which have supported and guided such a people to maturity and unexampled power, and also to genuine greatness, can be discarded only at the most serious peril to the cohesiveness and effectiveness and indeed to the basic health of that society. In social as in biological evolution, the fundamental elements of structure and of function must be retained at all costs, however rapid the pace of evolution in more peripheral elements. To deviate from this principle is to jeopardize survival itself—a fact illustrated everywhere in the living world, and recognized at a deep and pervading level by most societies and nations, including our own. The evidence is very strong indeed—and deeply salutary for our future—that our devotion to growth and vitality and aspiration, and our reverence for these sustaining elements of hope, and the incentives to individual excellence that they imply, continue importantly to mold our ethos as a people, despite threats and impediments and even denials that abound on every hand. And it is especially noteworthy that there has been no national concern, from the time of Jefferson to this, where these elements of faith and hope and devotion to movement and growth have been more vividly exemplified than in the philosophy underlying and motivating the scientific way.

But it would be idle, and worse, to ignore the threats to that ethos of growth and vitality and aspiration and reverence posed by the nature of our time, or to minimize their dangers. Some seem intrinsic to that passion, which has possessed us from the beginning, to dominate our physical environment and to use it to the utmost, indeed to consume it with an unexampled deadly effectiveness and often enough, indeed, with an unexampled greed. A prescient observer has pointed out that in any closed system, as our environment essentially is, there cannot be overweening mastery and organization in one part without correlative disordering and destruction elsewhere, unless special thought and effort are tirelessly given to the problem. We are only now beginning to implement that basic principle, so crucial to our continuing welfare, in any telling way. As we have all become suddenly aware, the ethos of movement and growth upon which we founded our society, and which has brought us to our present stature,

also has its obverse potential. The most sobering task for our time, perhaps, is to learn how so to live and plan that the following generation, too, can have its chance. For, as Coleridge so truly said: "in today already walks tomorrow."

Nowhere in our national life are the hazards of the times more explicitly illustrated than in the field of science itself. In this year of change, it is worthwhile to give special attention to some examples of such scientific hazards.

Since the time of Newton, an unusually rapid rate of growth has been one of the hallmarks of science. As Derek Price presciently pointed out some years ago, the volume of scientific work in the world, whether measured by the number of scientific papers issued, or by the number of scientific journals, or by the number of scientists themselves, has been increasing at an exponential rate such as to approximately double every ten to fifteen years, multiplying itself roughly tenfold two or three times each century. This is not a new relation. It has clearly held true over the centuries since Newton. Neither is it in any way unique in kind. For it seems probable that the rate at which all knowledge has expanded—and perhaps the acceleration of many other human activities as well, over the last century at least—has also been exponential. But, as Price has suggestively demonstrated, there seems to be a special structuring to the research front of science that has resulted in a growth rate far in excess of those of other human activities. An illustration of this that comes close to home involves the growth of the population of those men and women holding scientific and technical degrees in the United States over the century from 1800 to 1900. It has been estimated that in 1800 there were approximately one thousand individuals in the country who held such degrees. In 1850 the number was about ten thousand. By 1900 it had swelled to the neighborhood of one hundred thousand. Currently it is believed that the number of those trained in science and technology—the scientific pool—has increased by twenty percent since 1964, and its present size is estimated as high as eight hundred thousand or more men and women. By such criteria, rapid growth seems of the essence of the scientific way.

John R. Platt has provided particularly vivid illustrations of this growth rate in quite a different context—that of the products of scientific thought embodied in some fields of contemporary technology. Toward the end of the third decade of this century, for instance, atomic particles could be accelerated to speeds equivalent to approximately five hundred thousand volts. During the century's fourth decade, that ceiling climbed to about

twenty million electron volts. In the fifth decade, it reached approximately a half billion. By the middle 1960s it stood at about thirty billion, and current aspirations, of course, reach much further, to two hundred, and then possibly to one thousand billion electron volts or more. Over a considerable period, the energies of such machines have increased by a factor of ten approximately every seven years.

Another and more immediately relevant indicator of the dynamic growth that is so characteristic a quality of both science and technology is the proportion of our national income that has been expended in its support over the last decades. In 1940, for example, the total national budget for research and development was reckoned at \$74 million. A decade later, after World War II, it had burgeoned to approximately \$1.2 billion. In 1953, at the close of the Korean war, it had reached \$3 billion, and in 1956 it amounted to approximately \$3.5 billion. It is interesting to notice the steady and considerable, but not explosive, expansion over the years of the Korean conflict. Then came Sputnik, and by 1959 the part of the national budget labeled for research and development had reached \$5.8 billion. Four years later, in 1963, it amounted to \$11.9 billion, a sum greater than the total funds spent in this category over all the years from the American Revolution to and through World War II, and amounting to nearly fifteen percent of the entire expendable Federal budget. By the following year, the figure had grown to \$14.6 billion. Over the eventful decade preceding 1964, the estimated Federal budget for research and development had expanded by more than four hundred percent, and a projection of continued growth at essentially this extraordinary rate, so kindling to our tradition of coupling faith and hope with dynamic movement and dynamic growth, had become widely assumed in the communities concerned with both research and development. For those communities, as for the nation at large, it was a heady period.

Then, in 1965, there came a sharp turn. The Federal budget allocation for science for that year showed an increase over the preceding one of only \$0.2 billion. The causes of this sudden leveling seem initially to have been largely internal. In part, there was concern in the Congress that a rise so steep as that of the preceding decade could not be projected much further without producing a serious imbalance in the total pattern of national commitments. Partly it was caused, clearly, by the need strongly felt in the Executive branch to impose some structure on the extraordinary tangle which this precipitate expansion had created—to try to find some ordering of priorities. That task, of course, has proved of overwhelming difficulty. Indeed, in the field of basic research, with its fundamental and proper unpredictability, this particular problem, by its very nature, may never be solved.

By 1966, external factors of immense magnitude had been added to these internal pressures for reduction of the growth rate. The Federal budget for research and development rose to \$16.1 billion in that year, but increased only to an estimated \$16.7 billion for 1967, to about \$16.9 billion in 1968, and to approximately \$17.2 billion for 1969. At no time, to be sure, had there been a formal reduction in budgeted funds. But after 1964 the rate of growth, once of the order of twenty percent per year, shrank to an average of about two and a half percent. It is to be remembered, too, that the purchasing power of the research dollar itself had been falling constantly for more than a decade and a half, because of the combined effects of inflationary forces on salaries in science and on the purchase price of equipment, and, most important, because as any science advances, the sophistication and power and complexity and hence the cost of the instrumentation required tends constantly to augment. Thus Dael Wolfe has calculated that one dollar spent for research in 1965 had roughly the purchasing power of eighty-two cents in 1960, of fifty-seven cents in 1955, and of forty-one cents in 1950. So it is a genuine question whether there has been any real increase in Federal funding of research and development, considered together, since 1965.

This year, to the powerful budgetary constraint of the Vietnamese war have been added two further constraining forces. Each threatens to impose very severe limitations on the Federal support of both science and technology. Yet each is undeniable in its extraordinary importance for the nation. The first is the \$6 billion cut in national expenditures, which may finally amount to something in the neighborhood of \$7 billion, and is likely to fall especially heavily on Federal support for research and development in the next year or two. The second constraint results from the vast demands which must be made on our revenues, for as many years ahead as we can see, by the plight of the cities and the vital need to restore our environment. It is difficult to see where funds for substantial expansion of the Federal budget for research and development, taken together, can come from for several years ahead. Indeed, it is hard to see how an actual decline can be avoided.

Now there can be no doubt that, during the period of explosive expansion in Federal support for research and development, a great deal of money was spent, and a great deal of energy and time were consumed, in projects that were less than well conceived. It is possible to argue with some weight that a period of consolidation, a period in which we must address ourselves to the difficult questions of priorities that have never really been answered, a period in which we must make the hard choices that we dislike to make—and have always disliked to make in the context of rapid and chaotic growth that has shaped our society from the beginning—can redound to our real benefit.

Furthermore, as Platt has sensitively pointed out, growth curves of the kind that we have witnessed in the power of accelerators, or, for another example, in speeds of transportation, have many of the characteristics of a chain reaction, well illustrated by a flame. And chain reactions, by their very nature, do not go on forever—or if they do, they consume all before them. Accelerators cannot continue to increase in power indefinitely, else the revenues required to build them would exceed the capacities of any one nation, or even a combination of nations. Speeds of travel cannot increase indefinitely, for at velocities of less than twenty thousand miles per hour we have left the earth and are in orbit—where, indeed, we are already. Perhaps we are now face-to-face, at least temporarily, with some problems of this kind in the Federal funding of research and development.

In this context, a challenging further dimension for thought and analysis has recently been opened by some new and suggestive findings of Derek Price. In a series of penetrating studies, he has been able to show that the contribution of the various nations of the globe to the world's store of scientific information *per se*, as measured by the share of the world's scientific papers in various fields annually issuing from them, is remarkably coordinate, not with their total populations, not with their own estimates of the funds which their governments expend in research and development—which may vary from less than 1 percent of their annual budgets to the high of approximately 3.5 percent of the gross national product reckoned for our own country—but, remarkably enough, with their overall national wealth. That proportion turns out to be extraordinarily uniform among all nations which are making significant contributions to the global accumulation of scientific knowledge. Whether their wealth be large or small, their expenditures for research, defined as the effort to create and publish new knowledge, appear to approximate 0.7 per cent of the gross national product for each of them. In our own case, the disparity between that figure and our own present estimate of 3.5 percent of our gross national product spent for research and development is accounted for largely by expenditures for development, expenditures directed primarily to the utterly essential, but different, objectives of technological growth and particularly national defense.

But, although this figure of 0.7 percent, as the minimum expenditure required of any nation that is significantly contributing to the world store of scientific knowledge, seems generally consistent among the contributing countries at the moment, it has not been—and the indications are that it will not in future be—constant with time. Price finds, for instance, that in 1956 it amounted to approximately 0.3 percent, roughly half the present figure. In the absence of important damping influences, the present 0.7 percent is projected to double approximately every decade.

But of course such a projection suggests an ultimate picture that is quite impossible. To express our current stated commitment of Federal funds to research and development, this figure of 0.7 percent of the G.N.P. must be multiplied by about five. If the same ratio were to hold in the future, then this projection would require us, by the year 2000, to spend roughly one half to two thirds of our gross national product on research and development, a situation which, literally interpreted in terms of our present concepts of such categories, would clearly be absurd. So it is evident that we may well experience some real and serious deceleration of proportional, though not perhaps of absolute, growth rate in the Federal support of research and development between now and the end of the century whatever external circumstances prevail; and that, whether we do or not, we may have to evolve some really new conceptions of the whole issue.

The first warnings of this challenge may be with us today. For it may be true that some real immediate and practical benefits can be derived from a relatively short period of forced consolidation in Federal support of the national scientific effort, with its compulsion to face hard assessments, which we do not like to make and almost certainly would not make without such pressures. But it is evident that prolonged stagnation would pose hazards of major proportions, and that these dangers, moreover, would mount swiftly with time. It is well worth our pondering the nature of some of those hazards, and considering carefully ways in which they might be overcome, or circumvented, or at the very least alleviated.

Greatest of all the dangers of course, and underlying all of them, is the risk to spirit and vitality and hope that deceleration must always bring to a people who from the beginning have identified all three so much with growth and expansion and change. But there are others of a more practical kind.

In the unremitting competition of our planet, it is crystal clear that any nation which permits its scientific resources to wither, or even to diminish, over any considerable period of time is *ipso facto* gravely compromising its position in the world. And the greatest of these resources, of course, is the human one, that "pool" of the scientifically trained within the population, and, most important, the new generation of the gifted young just now entering upon their lives' work, who over the next decade will be manning our research frontiers. One of the gravest dangers of the deceleration that confronts us is that, unless we manage most carefully, it is likely to be particularly damaging to just this group. For it is, after all, a ubiquitous human tendency to cling especially tenaciously to the known and the tested when the going is difficult and uncertain. That temptation is no less strong

in the fields of science than elsewhere. Some time ago, for instance, the House of Representatives approved a reduction in the funding of the National Science Foundation by one fifth—from the \$500 million requested for the 1969 budget to \$400 million, while the Senate approved a budget only \$10 million higher. Under pressures of this kind, as it becomes impossible for the granting agencies supporting scientific research to fund more than a fraction of the excellent proposals placed before them, the temptation to choose in favor of mature established investigators, with high reputations and fine records of successful research already publicly supported, over unknown but potentially innovating newcomers is understandably great. There is a persuasive immediate logic to this course. Yet these are exactly the choices that can be particularly dangerous to our scientific future. Fortunately, those presently conducting the affairs of the Federal granting agencies seem aware of this danger, and clearly they are making considerable efforts to moderate it.

But the threat to that most precious scientific resource that we have, our population of nearly mature scientific trainees who have shown brilliant promise, the predoctoral candidates and the candidates for postdoctoral fellowships, stems from other quarters too. The training grants of the National Aeronautics and Space Administration, for example, which were originally established to replenish qualified young talent from the universities as the space effort drained them away, and which since 1961 have supported work for the Ph.D. by more than a thousand young men and women, have dropped to a twentieth since 1966. A survey of one hundred nineteen physics departments in universities, recently conducted by the American Institute of Physics, revealed that sixteen percent of their senior personnel had lost all government research support this year, and the figure was expected to rise to twenty-one percent next year. Until 1964, appropriations for the National Institutes of Health rose between fifteen and thirty percent a year, a figure that was sometimes almost embarrassingly large. But since that year support has almost leveled off, and the gulf between resources and opportunities is certainly as great this year as it is in other sectors of Federally supported research. Such indicators, it is evident, are but the iceberg's tips, visible hints of possibly greater problems ahead.

If, then, the flame must be damped for some time to come, how can we manage the containment to the least disadvantage? How can we live with diminished growth without stifling developing buds beneath the hardening bark, and so gravely compromising our future? That is indeed a major question for our time. There are, of course, no clear answers at present. But it is surely imperative to think hard about some specific features of the situation, and more broadly about the nature of research itself, now and in the future.

First of all, it is worth reflecting that one of the most traumatic features of the deceleration that we are witnessing may not lie so much in its actual magnitude as in *the suddenness and unexpectedness of the event*. Since science is, above all, a cumulative discipline, where new knowledge typically grows within the structure of knowledge already won, the basic requirement for its health is not to be measured so much in *amount* of support as in its *stability and continuity*. Unlike many other activities, the level of productivity of the scientific way is neither strictly proportional to the amounts spent on it, nor can science, like an activity of entrepreneurial character, be rapidly expanded or contracted in response to sudden and swift changes in the base of support. The adjustments that must be made to effect either expansion or contraction on any major scale are much too basic and massive and time-consuming for this. Moreover, there is a "critical volume" for every successful scientific endeavor, however modest it may be—a "critical volume" of facilities and equipment, but above all of the number of fine minds engaged—below which it simply becomes ineffective. So unexpected fluctuations in the base, major swings from under- to over-commitment, uncertainty and unpredictability, are inherently ruinous—far more harmful than a somewhat parsimonious, yet assured and consistent, undergirding. This salient element of a policy for support of science has been well known for many years in many places. Awareness of it, both in this country and abroad, has motivated many suggestions and some policy, such as the trend to extend the terms of Federal research grants from one year to three years or five years; or such as the weighing of institutional versus project grants that has occurred in many Federal agencies over several years, and has recently been a particular concern of, among others, the Wescoe Committee reporting to the National Institutes of Health. But it is one thing to manage matters so that these hazards of instability can be minimized on a relatively small, or local, scale. It is quite something else to do it effectively over the whole front of research support.

Perhaps, during the next years, we should concentrate less on trying to determine realistic *ceilings* for our research expenditures, and give more thought to how we might provide *assured floors* to our support of research. Just as universities and private research institutes have in recent years attempted to order their affairs so that during times of austerity their tenured faculties or staffs continue to be supported with their own research assured at levels at least sufficient to provide continuity, so, perhaps, in the domain of Federal funding we ought to consider very carefully what minimal orders of support could, with a fair degree of probability, be assured over several years to come. Psychological adjustments to that kind of floor—bringing some sense of security and of the possibility of longer-range

planning as much as anything else—might catalyze hope and verve to a degree that should not be underestimated.

The analyses of Price and his colleagues may provide both a central idea and a specific basis around which such an approach could be built. For if, as he has demonstrated, the figure of 0.7 percent of G.N.P. for support of research is at present an operational one among the nations currently making significant contributions to the world's store of scientific knowledge, perhaps this suggests such a natural "floor" for the Federal support of science itself. It is notable, of course, that this proposed "floor" in fact represents only one fifth of the estimated 3.5 percent of our gross national product that we have actually committed at present to research and development considered together. But the total 3.5 percent merges the support of what, as Price has cogently emphasized, are in many respects two quite different activities—research, "basic" and "applied" on the one hand, and technology on the other. Their distinctiveness in this context, and equally their close relationships in other frames of reference, are worth scrutiny and emphasis.

Often, of course, there is a close-knit functional connection, and a vital one, between research and technological development. One need only cite the drama of the transistor to illustrate this point, or the evolution of penicillin, from its initial discovery, to the development of extraordinarily high-yielding strains of the parent mold selected from among X-ray-induced mutants of *Penicillium notatum*, to the wholly artificial syntheses of the drug recently announced. And the vital quality of this relationship is just as clearly illustrated by the limitations imposed on one partner by the absence of the other. It may well be, for instance, that computer technology is approaching a serious intellectual barrier at present that can only be surmounted by further research in three or four related branches of fundamental science.

The development of the maser and the laser offers one of the best examples of how intimate and powerful this sort of linkage can be. As Charles Townes has recently and cogently pointed out, the relationship here is particularly striking not only because of the extraordinary advances in technology which have resulted—advances of a different order of magnitude than could possibly have been achieved, or even imagined, through "straight-line" technological approaches to the same goals. A reverse effect is equally arresting. For here not only did major scientific conquests bring revolution to whole areas of technology. Reciprocally, these conquests were themselves stimulated and supported by contemporary technological advance. Under the pressures of World War II, the technique of microwave oscillators was developed to the point where a new branch of physics, microwave spectroscopy, the study of the interaction between

gaseous molecules and microwaves, was generated and productively developed, at first primarily in industrial laboratories. Yet the commitment to that course of research soon waned there. The basic invention of the maser in 1951 issued instead from Columbia University, to be followed very shortly by similar developments at the University of Maryland and the Lebedev Institute in Russia. Clearly, it was the fusion of the essentially "pure" research field of microwave spectroscopy—itself an outgrowth of intensive applied work originally having predominantly military ends in view—with applied electronics that provided the setting from which the maser and the laser could emerge.

At the far end of the scale of development, the practical consequences, present and potential, of the maser principle are of course so utterly extraordinary in their scope and power and variety as already to be legendary: from its applications to transoceanic communications; through satellites of hitherto unattained orders of range and precision; to the taking of scientific measurements of hitherto unrealized sensitivity; to instrumenting the world's most precise clock, so accurate that if it were to run three hundred thousand years its estimated error would be about one second; to the production, by the laser, of light beams of intensities millions of times greater than ever before achieved, for the first time making it possible to reflect a beam of light from the moon's surface and receive it again on earth; to the precise drilling of holes in materials as refractory as diamond; to the provision of a linear measure of enormous precision applicable to the most conventional operations in civil engineering on the one hand and to the laying out of the course of the first great linear accelerator on the other; to ultrahigh-speed photography and holography; to new modes of high-speed processing, storage, and retrieval of information; to the performance of delicate eye surgery, notably operations for detached retinae—the range and scope and novelty of the uses of the principle seem virtually limitless. And the end, clearly, lies far in the future.

Rather similar circumstances, of course, surrounded the development of the principle of the transistor, which has had such enormous application. Again a technological environment, coupled with the atmosphere and the freedom characteristic of basic research, made possible advances in fundamental understanding that transformed the technical practices of the day, as undoubtedly they will those of the future.

Thus the evidence is crystal clear that research and development can be, and in some strikingly successful enterprises have been, wedded in extraordinarily intimate working partnerships, with spectacular consequences for both. But it is equally clear that functionally the two activities are by no means identical. There are real and deep-lying differences between them, differences in both character and mode and in the environments best suited

for their prosecution. In the broad area of national support of research and development, it is rare in practice that these two kinds of activity are not distinct, and indeed they are rarely responsive to the same kinds of relationship to Federal support.

Volumes have been written about the differences between "basic" and "applied" research. In Great Britain, at the national level, the two categories are actually administered by separate government departments. Yet such a distinction, if it is at all real, is not strongly reflected in the training or the capability or, basically, in the philosophy of the investigator, nor in the kinds of environment demanded for his best work. At most, it can only touch his stated objectives. But it does seem evident that there is a sharp contrast between science and technology. Between an activity having the primary goal of the winning, publication, and storage of new knowledge, and an activity oriented to developing, perfecting, and distributing specific technical items, there do seem to be basic differences that are sharply reflected in both the orientation and the preferred methodology of the professional in the two fields. It is well to keep these differences in mind when viewing the 0.7 percent of G.N.P. that appears as the "standard" support among nations making significant contributions to the world's stock of published information, and, contrastingly, the higher percentage of the U.S. G.N.P. allocated for the support of science, which combines expenditures for research with the much more massive sums for technological development, whose fruits are primarily of practical application in national concerns, public and private. Thus the United States spends considerably more in the Federal support of research and development than does any European country. It is this combined total that we reckon as our 3.5 percent of G.N.P. which compares with about 2.5 percent for Great Britain, and 2 percent for The Netherlands, the current leaders on the European scene. But of two dollars so spent in our own country, one goes for research in space and defense. The total reflects very imperfectly our actual Federal commitment of dollars devoted to the winning of new knowledge.

All this suggests that there may be real merit in a formal budgetary separation of the estimated Federal support of research from that of development. Such a move might make possible the formal establishment of a realistic and more stable "floor" for research support. It might well be set in the general region of this 0.7 percent proportion of the G.N.P. The concept of such a separation, of course, is not new. It was, in fact, put into effect several years ago. In retrospect, there seems little doubt that this was an excellent move. It sharpened concepts. Equally important, it made possible a continuing real, if modest, increase in the support of research *per se*,

well into the lean years. This policy may well have been related, though indirectly, to an evolution illustrated by the following figures. While it has been calculated that in 1953 somewhat less than seven percent of the total Federal commitment to research and development went to research, by 1965 that figure had increased to an estimated eleven percent. In 1966-1967 it was possible, even in the face of stringently tightened circumstances, to increase the separated research budget by more than ten percent—maintaining roughly the same rate of growth for research that had characterized the combined research and development budget in some earlier years. It may never be possible to estimate the real effectiveness of such budgetary separation in cushioning the worst effects of the shocks attendant upon deceleration. But it is clear that its benefits had special impact upon young research talent just emerging on the scene.

In the new Federal budget for 1969, this separation of research and development has been abandoned. Is not this move, far from being progressive, actually a retrogressive one? Should it not be reversed?

In this context of the future growth of the scientific effort and of the significance of that growth for the nation, another interesting characteristic of the scientific way may prove important. Price has pointed out that over a span of years almost great enough to set a tradition, only about one fifth of the young postgraduates in science, newly equipped with doctoral degrees in their fields, have returned to academic environments. This "surplus" in the production of scientists suggests that, if we are careful to protect our resources of teaching in the future, we can legitimately anticipate that a goodly number of scientifically well-trained men and women will become available each year who will be free—and often, no doubt, eager—to enter fields of direct practical and social concern related to their specialties—sometimes, indeed, much broader than their specialties. It is from the ranks of such young people particularly that we may expect to draw a substantial proportion of those who must plan for the courses of science in the nation in the future—a planning process which we can no longer escape, a prospect which, much as we inherently dislike it, we can no longer in good conscience deny. But at least equally important, this "surplus" of trained scientists constitutes a highly significant reservoir of talent and effort available for some of the immense and urgent practical tasks that surely lie ahead for this generation and the next: the problems of the cities, the problems of the preservation and the building of our total environment that so preoccupy our thinking but cannot, to the degree that is so supremely necessary, commandeer our action today. So we may expect that a considerable proportion of the talent which will be developed today and to-

morrow with the aid of Federal funds formally designated for "scientific" purposes will, in the years of their maturity, repay the nation manyfold in areas that today we may think of as quite apart from those of science in the stricter sense.

Indeed, it is probably difficult to overestimate the weight of the effective talent that people so trained could bring to national problems of this order, provided that the limitations as well as the capacities inherent in such training are kept soberly in mind. It must always be remembered, of course, that this definition of "surplus" can only be valid if the deployment of trained men and women is to the same general fields as those in which they were prepared. What must be guarded against is the all-too-common and all-too-human tendency to regard a training in science—or indeed in scientific technology—as providing the tools for attacking these questions in a *general* sense. To imagine, for instance, that the vast and interlocked congeries of problems involved in attempts to rescue deteriorating environments from further degradation can be solved by scientific skills *alone*, or even in principal part by them, is to gravely underestimate the nature of those problems, and at the same time to misapprehend both the strengths and the limitations of the scientific way. It is a temptation that planners and implementers alike must firmly and consistently resist.

Such considerations, of course, lay very special emphasis on the significance of the teacher of science for the whole future of our nation, and further emphasize how very important it is, from the standpoint of Federal expenditures, that the deceleration in the rate of support to the universities for science teaching—teaching being, of course, the inseparable partner of academic research—be minimized as far as it possibly can be over the coming years. These same considerations further suggest that the significance of scientific skills in national affairs in the future may come to be even broader than we conceive it to be at present. This may offer the strongest of all imperatives to guard against reducing the Federal support of science, now and in the future, so far as we possibly can.

There is a further characteristic of scientific research that should make it easier to accommodate continuing growth in its support over the lean years ahead, or at least substantially to cushion the shock of deceleration, provided the budgets for research and development can once again be separately considered. It is now generally recognized that the costs of research, by and large, are far smaller, both relatively and absolutely, than those of corresponding programs of development. For in ways as fundamental to our spiritual welfare and growth as to our material substance, science and the humanities make common cause. In an era when the work of vast teams

has replaced that of the individual in so many areas, for many of the sciences it is still as true as it is for the humanities that original and powerful individuals remain the most significant finders of fresh paths. Abetted by the training and experience that is theirs, and in the case of science by the modern instrumentation which plays so key a role in scientific advance; immensely helped, again particularly in the case of science, by students or assistants or colleagues who form with them the close-knit cohesive working groups that continue to constitute the most stimulating and effective environments for creative research, nevertheless it is still basically these exceptional individual investigators who, in their thousands, pioneer, and will continue to pioneer, the new ways. In each new age, it is such youthful individuals recently entered upon research who typically create for their generation fresh visions of the world, visions rooted in and owing much to those of their teachers, but nonetheless distinctive and responsive to the new circumstances of the time. The evidence for this, both historical and contemporary, is compelling. In coming years our society will need to rely even more heavily on these recruits to guide us across the difficult watershed that is the terrain of our time. We must do everything within our power to assure to the coming generations the tools, the aids, the working environments, and above all the individual scope for individual thought that they will require.

Surely one of the most important things that we can do is to preserve and enhance and increase, to the greatest extent that we are able, those centers of excellence in both formal and practical research training that are so critical to preparation for scientific greatness. Hans Krebs has recently emphasized how vital such centers are, and what unequalled opportunity they can offer to the gifted young individual at a critical period in his career, molding him to the stature of those exceptional older men with whom he associates. A specific and remarkable example of this is provided by the life of Krebs himself. Destined to become a Nobel laureate in chemistry, he had the opportunity, during that critical period of development spanning his twenty-fifth to his twenty-ninth years, of working closely with Otto Warburg, and indeed of collaborating in a subsidiary capacity in the very investigation that brought the Nobel award to Warburg in 1931. And it is striking that the career of Warburg himself followed almost exactly the same course. As a young man, he was associated closely with Emil Fischer, who in 1902 had been awarded the Nobel prize for his work on the chemistry of sugars. Fischer, in turn, had worked with Adolf von Baeyer, who, for his discoveries in the chemistry of dyestuffs, particularly for his synthesis of indigo, also received the Nobel award, in 1905. And so the genealogy continues, back to the period when the formal acclaim of Nobel awards, with all their shortcomings as well as their virtues, was yet

unknown. For von Baeyer was a pupil of Kekulé, most famous today, perhaps, for his vision of the structure of the benzene molecule. And Kekulé, in turn, studied with Liebig, who may fairly be said to have laid the foundations of organic chemistry. Liebig, again, had worked in Paris in the laboratory of Gay-Lussac, who discovered some of the fundamental laws of the behavior of gases. Later Liebig referred to this experience as a critically determining one for the whole course of his life. Gay-Lussac, in his turn, learned especially from Berthollet, the pioneer in theories of combustion, who, among other pioneering achievements, abandoned the notions of phlogiston that in his time were still so entrenched. And Berthollet, finally, was a pupil of the great Lavoisier.

Arne Tiselius has spoken movingly of this same relationship, again from the depths of personal experience. "To most research workers," he has written, "the decisive factor in preparing their minds is obviously their impressions and experiences during their university years, particularly if they have the good fortune of having a great scientist as their teacher. This was so in my case and it should be obvious to all those familiar with the work in physical and biochemistry in Sweden how much I owe to The Svedberg—a great personality and a great friend. . . . In my experience, I have come to the conclusion (also expressed by many others in similar activities): in the support of fundamental research, the individual research worker is more essential than the research project, when judging priorities."

In every instance, as both Krebs and Tiselius emphasize, this association of pupil with teacher occurred at a period of research training roughly corresponding to the years that today would be comprehended in the doctoral and postdoctoral periods. And this was no casual or part-time connection. It was intense and prolonged. Upon the intimacy of this relationship, as upon the qualities of both master and pupil, its unique effectiveness depended. It also depended, very clearly, upon the environment in which the experience took place. A glance at the history of the centers of training of great scientists through two centuries is enough to show that it is in the free and flexible and rather small research group, centered about a few figures of real stature both in research and teaching, which, in this context, are of course essentially identical, that the great figures of the following generation have developed, and continue to develop. From Liebig's laboratory no less than sixty leaders of science were "propagated" in succeeding generations from his day to ours, and more than thirty of these have been Nobel laureates.

This situation is as contemporary as it is historical. Krebs has pointed to some interesting statistics concerning the sources of highly distinguished science—and scientists—in Great Britain over approximately the past twenty years. While in the earlier part of this period the universities clearly

were a main source of scientific excellence, more recently the lead has passed in considerable measure to the research institutes, where teaching and administrative duties are traditionally light and time is available to concentrate upon substance. Thus, of thirty-two new Fellows elected to the Royal Society in March, 1967, only thirteen had conducted the work decisive to their selection within universities, and some of these had held research professorships there. The British Medical Research Council, in whose laboratories Kendrew, Perutz, Wilkins, Crick, and Watson worked, among others, and where the crucial discoveries about the structure of DNA were consummated, operates with something like five percent of the research funds available to the universities and with perhaps one tenth the number of scientists. Yet, of a total of eighteen Nobel awards in all scientific areas made in Britain since 1950, no less than seven came to members of the staff of the Medical Research Council—an astonishingly large share. It would be hard to find more striking evidence of the essential place of the research institution and the flexible center of excellence, whose members are adequately protected from the grueling demands for the diversion of time and energy that are so omnipresent with us today. As Krebs has stressed, in our age, and particularly in these years of watershed, the cultivation of excellence in science is no academic exercise, but a fundamental source of national strength, both economic and political.

There can be no more vivid nor contemporary tribute to the continuing relevance and great importance of the individual, of the close-knit research group, and of the research center of distinction in which the individual works, and no greater satisfaction of that "need to know" that lies so close to the center of our beings and constitutes such a vital element of our spiritual heritage, than that afforded by any set of vignettes, however briefly and lightly sketched, of a randomly selected few of the advances in the understanding of nature that have marked the year just past.

In astronomy, for instance, the strange quasars, the quasi-stellar sources that were first detected through the recording of their radio emissions at the British radio observatory at Jodrell Bank, and then, after being identified as optically observable objects, were discovered at the Mount Wilson and Palomar Observatories to have extraordinary redshifts, continue to pose profound questions at the deepest level of cosmology. For the astonishing values of their redshifts, if interpreted in the usual fashion, indicate that they lie at such vast distances that, so far, no explanation satisfactory to all astronomers has been offered as to how they can be visible at all. And this year there has come the discovery of yet a new quasar, apparently more distant from us even than the farthest hitherto found, with a redshift

of 2.358, once again the greatest ever observed. It has been several times suggested, as a possible resolution of this dilemma of the quasars, that perhaps they are not in fact so distant, that a part or all of their enormous redshifts may be correlated with conditions other than distance, and that perhaps, after all, they are rather local objects. This would indeed explain their visibility. But studies of the numbers and the distribution of the radio-quiet quasars in the sky—made during the year just past, again at the Mount Wilson and Palomar Observatories—seem to eliminate that hypothesis. So the mystery continues.

At the same time, once again from the Mount Wilson and Palomar Observatories, there has come this year a new determination of the rate of expansion of the universe, and new explorations, too, have been undertaken which now make a convincing argument, not only that the expanding universe was initiated by a gigantic “big-bang” explosion, but that the history of the universe may go back much further than this. In fact, the universe may have been alternating between expansion and contraction to a dense mass, then expansion again, with a total time cycle of approximately 8×10^{10} years, an interval that defies the imagination.

Now to the mystery of the quasars is added another: that of the pulsating radio stars, or pulsars. The first of these was discovered at Cambridge in December of 1967. It emitted bursts of energy at radio frequencies with a period of approximately one and one third seconds, a period which is remarkably constant, to the order of one part in ten million. In rather rapid succession, three more similar objects were recorded: two with virtually the same highly constant period as the first, the third with a shorter period, also highly constant, of about a quarter of a second. A fourth, the first to be recorded from an American source, was detected at the Harvard Observatory. It, too, pulsed with a frequency maintained with extraordinary precision, at intervals of about seven tenths of a second, each pulse lasting for about one fiftieth of a second. Ten pulsars are now known—two discovered by the Australians, one at Arecibo, one at Harvard, and the remainder in England.

What are these strange objects, and what can account for both the regularity and the comparatively high frequency of the energy bursts which they emit? Because of the delaying effect of electrons along a radio path, an effect to which lower frequency radio waves are especially sensitive, the portions of the energy pulse that lie in lower frequencies may reach the earth seconds later than those at higher frequencies, and this delay can be used as a measure of the distance of the objects. Calculations of this kind have led to general agreement that, in marked contrast to the quasars, pulsars are, in astronomical terms, relatively nearby objects, ranging perhaps from fifty to three hundred light-years away. Thus they lie within

our own galaxy—and indeed may be neighbors of our solar system within the Milky Way.

Four nights of intensive examination with the two-hundred-inch telescope on Palomar Mountain failed to confirm the existence of any visible object corresponding to Pulsar CP 1919, one of the Cambridge discoveries which had earlier been suspected of emitting light in the visible range. What then can be the nature of these dark objects, and what the secret of their extraordinarily regular periodicity, or, even more remarkable, of the extremely short intervals between pulses? Highly rhythmic phenomena, such as the movements of a pair of binary stars around one another or such as, for that matter, the spin of the earth, are of course common and characteristic phenomena in celestial nature. But if the rhythm of the radio bursts from a pulsar is to be explained as being due to its rotation—as though, indeed, it were a rotating searchlight whose beam swept the earth once in every quarter second, or even once in every one and one third seconds—a far higher rate of revolution would be required than is commonly met with in the cosmos. Such an extraordinary rate of revolution in turn demands that the quasars be extremely small and extremely dense bodies. These qualifications might be fulfilled by a “white dwarf”—a star which, in a cataclysmic burst of energy as a nova, has burned its nuclear fuel and collapsed to a small, dense, and ultimately cold body. It has been urged that the spinning neutron stars, of extremely small diameter and intense magnetic fields, might be even more likely candidates. It has been proposed that the plasma stream from the surface of such a star may spiral out along magnetic field lines, its tangential velocity increasing as its radius increases until, when this velocity equals that of light, a burst of synchrotron radiation is emitted in a narrow cone, sweeping the earth on each rotation of the star. But at this frontier of knowledge there is still great doubt, and no theory has yet won general acceptance.

Just one hundred years ago this year Louis Pasteur, having moved to the École Normale as director of scientific studies, at last was able to proclaim definitively that the fermentation of wine results from the action of minute, invisible living organisms within it, and that when a fermentation fails to proceed normally, it is because the necessary organism either is absent or has not grown properly. It was in 1868 that Pasteur announced that he had isolated the causative organism of the disease of silkworms that was ruining the French silk industry, and that he had found a method of detecting infected stock, and of preventing contagion.

It is interesting to reflect a century later how Pasteur, were he living at this hour, would have regarded the discovery of viruses, or the whole

complex of problems revolving about the coding and translation of information in heredity, to which the bacilli that he detected have themselves contributed so much information. How would he have reacted to the achievement of the laboratory copying of the genome of an infectious RNA virus, using naturally occurring biological templates and enzymes, by Sol Spiegelman at the University of Illinois? How, again, would he have reacted to the extension of that dramatic accomplishment this year: the copying of the genome of a virus with a DNA core, likewise using information and enzymes derived from living cells—a virus which then replicated itself within a living cell—by Goulian, Kornberg, and Sinsheimer? And most important, one wonders what Pasteur, whose gifts of prophecy were so dramatically exemplified in that work of a century ago, would have to say about the implications and the possible consequences of these contemporary achievements for the greatest goal, which lies yet in the future—the goal of the genuinely artificial creation of genetically competent DNA.

What would Pasteur as a chemist have had to say about the remarkable accomplishment reported this year from the Max Planck Institute for Cell Chemistry in Munich, in which the fatty acid synthetase, obtained from yeast, with a molecular weight of 2.3 million, was successfully crystallized? This huge molecule, which acts almost like a chemical factory in catalyzing the immensely complex synthesis of fatty acid building blocks within the yeast cell, is by far the largest structure of its type ever to be crystallized intact. The achievement for the first time provides an opportunity to make an X-ray structural analysis of an extensive and highly organized “community” of enzymes, and suggests the possibility, at some future time, of really knowing the constitution of this functioning molecular “organism,” and of understanding the way that its parts are operationally related.

Again, what would Pasteur have thought of the complete synthesis of the substance glucagon at the Max Planck Institute for Albumen Research, also in Munich, announced during the year just past? Glucagon is an essential hormone of the pancreas, appearing to play a role in the gastrin-secretion-histamine mechanism, and perhaps also in liver function. It is sufficiently rare, and sufficiently difficult to extract from its natural source, that it has always been in short supply. Quite apart from the technical brilliance of the synthesis itself, supplies of the synthetic substance which it may make available could have a marked impact upon the treatment of hyperglycemic shock, among other things.

What would Pasteur the chemist have thought of the accomplishment involved in a complete synthesis of penicillin from so common and apparently unlikely a substance as isobutyraldehyde, yielding, finally, an isomer of penicillin V, announced this year from the laboratories of the Stevens

Institute of Technology? What would he have thought of the synthesis of artificial polypeptides by the solid phase method reported last year from the Rockefeller University? Until about 1932, it was difficult to synthesize polypeptides at all. Now, with the new method, it becomes feasible to add new amino acids to a growing chain, one by one. Thus it seems possible that a chain of almost any length and composition can be synthesized. When one considers the impressive biological and medical significance of many known polypeptides, such as, for example, vasopressin, which raises the blood pressure by contracting capillaries and arteries; or eledoisin, isolated from a Mediterranean species of octopus, a substance ten thousand times more potent in affecting rate of heart beat than quinidine, at present the drug most used for this purpose and itself recently synthesized; or physalaemin, derived from the frog *Xenopus*, a powerful inducer of abnormally high blood pressure, the potentialities of the new method become even more impressive.

It will be just eleven decades ago in July of 1969 that a communication entitled "On the Tendency of Species to Form Varieties; and on the Perpetuation of Varieties and Species by Means of Selection" was jointly presented to the Linnean Society by Charles Darwin and Alfred Russel Wallace. A little more than a year later there issued a publication called *On the Origin of Species by Means of Natural Selection, or the Preservation of Favoured Races in the Struggle for Life*—and the theory of evolution had been placed before the world. How excited, and perhaps amazed, Darwin would be, were he among us today, to review the most recent evidence that his basic principle can be adumbrated as vividly at the levels of cells, and of genes, and indeed of biological molecules, as at those of the entire organism and the populations of organisms with which he dealt. Perhaps he would be even more moved to see that, more than a century later, new discoveries continue to be made, new facets of his insights uncovered, at the very levels of life that most concerned him—the levels of organisms and their integrated populations.

How deeply he would have been interested in the exciting demonstrations, first made at the Carnegie Institution and now widely extended, that replication of certain genetic loci, sometimes hundreds, or thousands, and, in at least one instance, a million times, seems to occur frequently in the chromosomes of higher many-celled organisms throughout the animal and the plant kingdoms. What would have been his conjectures about the adaptive quality of this extraordinary, and until recently unsuspected, phenomenon, so widespread in the animal and vegetable kingdoms? Had he been familiar with the knowledge, discovered only in very recent years,

that in higher vertebrates there may exist several chemical forms of the blood protein-pigment hemoglobin, each specified by a single gene locus; with the fact, for instance, that a change, brought about through mutation of the genetic message instructing it, in a single one of the 514 amino acids of which hemoglobin is composed (a change from glutamic acid to valine in the 6-position of β -hemoglobin) could produce the pathological hereditary condition of sickle cell anemia, how deeply interested he surely would have been! Had he known, further, as we now know, that individuals carrying the gene determining this same sickle cell anemia, when they are heterozygous for it, are actually more resistant to certain forms of malaria, and so better adapted for survival than normal persons in localities where such malaras are rampant, though less well adapted in regions free of them, would he have seen this as one of the most poignant examples of survival equilibrium in polymorphic populations? How the universality of his theory at all levels of life would have been driven home to him!

In that primitive fishlike animal the lamprey, there is only one form of hemoglobin. Would Darwin have speculated, as a discerning scientist did this year, that, in the course of the evolution of early vertebrates, replication of the single locus for hemoglobin might have had the effect of providing some new organism with "spare" genetic copies: evolutionary insurance, as it were, allowing normal functions to be preserved through the continuing control of the original, unchanged genetic locus while new hemoglobin-modifying mutations, derived from one or more genetic copies, could be "experimented with," leading ultimately, perhaps, to the establishment of a multiple series of hemoglobin pigments in the blood, such as we find today in higher vertebrates, with the physiological versatility that this provides? Would he have looked on this case, now so well documented because of our new-found knowledge of the details of hemoglobin structure and its relation to genetic constitution, as a possible paradigm for similar kinds of evolution elsewhere? How would Darwin, who was keenly aware of the great evolutionary questions involved in the evident differences in rates of evolution of different organisms—problems that continue to baffle us so today—have related the phenomenon of genetic replication to this mystery?

How Darwin would have delighted in Spiegelman's brilliant demonstration and use of the principle of natural selection in an entirely new domain—at the level of the information stored in the cores of infective RNA viruses. By providing natural strands of RNA in the test tube with supplies of nucleotides to serve as raw materials for the synthesis of new strands, together with stores of the replicating enzyme replicase, new RNA strands were readily produced. By maintaining an abundant supply of both raw materials and enzyme, and then transferring newly synthesized

strands of the RNA to fresh tubes as soon as they appeared, it was possible to carry out what in fact was an experiment in intensified Darwinian selection, of the type often undertaken at the level of multicellular organisms, such as fruit flies. This process, repeated through seventy-five "generations" of new RNA, resulted in a population of strands which could replicate far faster than the originals. The striking point then demonstrated was that these RNA strands, selected through seventy-five passages of intense competition for rapidity in replication, had changed markedly in composition. More than eighty percent of the information originally carried by the virus strand had been lost. Supplied with abundant available substrate for RNA synthesis and in the presence of adequate supplies of the replicating enzyme, freed from the necessity of coding for the structures necessary to the natural virus, such as the protein coat the particle must have to maintain an independent existence during its passage from one host cell to another, and the protein "apparatus" requisite for attachment of the virus to a new host cell, the selected RNA strands appeared to have "shed" a large part of the information code providing for these features. The "new" viruses in fact proved less infective than the originals. What had been conserved, however, and increased, was the capacity for rapid replication. So these strands of RNA had indeed demonstrated as truly an adaptive response to intensive selection as Darwin ever described among man's domestic animals. In further experiments of a basically similar kind, the triphosphate in the medium was lowered to a level barely usable by the normal virus. Triphosphate is vitally essential. Under pressure of this deprivation, a variant form of RNA, capable of utilizing triphosphate at lower concentrations than the normal form, appeared and rapidly dominated the culture, again in a pattern of Darwinian selection. A possible practical application of work of this kind, using some of the artificially modified types of RNA as tools to combat natural RNA viruses in infection by competing with them for substrates, is for the future to reveal. How that possibility, too, would have excited the men of Darwin's generation, had they been able to apprehend it!

It was just a century in 1968 since Gregor Johann Mendel was elected Abbot of the monastery of Bränn, and his most active scientific work thereby brought to a close, three years after he had presented that momentous two-part paper before the Natural Science Society, the paper that laid the very foundations of genetics. In the library of the monastery there have been unearthed editions of Darwin's writings with their margins liberally annotated by Mendel, presumably during the period of his most intense work in the monastery gardens. So it is clear that the man who first grasped the very concept of those genetic elements whose mutational changes provide the basic raw material for organic evolution must also have thought

deeply about the nature and the pattern of that organic evolution. One cannot help wondering, in this connection, how Mendel may have speculated about the processes of evolution in those genetic mechanisms themselves. Over the years since Mendel's death many answers to such questions have been set forth, and much evidence uncovered to demonstrate that there has indeed been a highly complex evolution at the level of chromosomes, and even of genes—an evolution as complex and reticulate and beautiful as that at the level of the gross forms of organisms. But how, one may finally ask, did the mechanisms for information storage and retrieval themselves develop and become elaborated, in the very earliest evolution of life?

Here the rejoinders must still all be speculative. For, while the essence of genetic replication, in which identical copies of preexisting genetic material are made, inheres in reactions involving base-pairing—the fundamental nature of which we can reasonably hope eventually to comprehend even though we are still vastly ignorant of all its details—real understanding of the processes of translation, by which the genetic information is ultimately given tangible expression in the structure of proteins, is more difficult. How were the particular “rules” developed that now govern the relationships between the sixty-four possible trinucleotides and the arrangement of the amino acids in proteins—rules apparently universally followed throughout the panoply of living things? We are far indeed from answers to these questions today. And until such answers are found, we will be able to say little that is definite about the way in which the processes of translation evolved. What a new dimension Darwin would have found in this field of evolutionary thought!

Again, how Darwin's keen eye for form and his sense of its significance throughout the living world would have been challenged by those investigations of development and its mechanisms that constitute one of the most exciting frontiers of modern biology. One can imagine, for example, how the phenomenon of “programmed cell death” in development would have arrested his attention: the fact that the orderly, predetermined death of certain cells, occurring at the very time that neighboring cells are rapidly proliferating, and playing a vital role in molding the organism's ultimate form and structure and function, is truly the final “acting out” of instructions coded originally within the DNA of the whole organism, and represents a genuine example of specialization. How much Darwin might have been tempted to speculate about such examples of extreme specialization in terms of natural selection. Perhaps he would have pondered especially the following circumstance. Whereas an individual of unusually adaptive endowment living as an independent element in a polymorphic, panmictic breeding population commonly increases in numbers more rapidly than its fellows, so that its type may come to form a larger proportion of the whole

as the generations pass, specialized high adaptive efficiency in the cell or organism that is tightly bound within a dynamically interacting, close-knit biological or social complex, in which the constituent living units are deeply and immediately interdependent, may have precisely the opposite consequence in evolution, drastically limiting the numbers of such a cell or organism and rigidly fixing the numerical proportions of the whole.

And surely Darwin would have taken special interest in findings of this year in areas of inquiry that were already very familiar to him in the context of natural selection and that one might have imagined would long ago have been exhaustively explored. In the *Origin of Species* Darwin had much to say of the description, then but newly given, of mimetic butterflies associated with their models along the Amazon, and of reports of similar cases of mimicry brought by Wallace from Malaya. Both Bates and Wallace had interpreted their findings as we would interpret them today, and Darwin, in a chapter of the *Origin* called "Analogical Resemblances," discusses at some length and with evident satisfaction the ways in which these remarkable instances of mimicry both confirm and extend the theory of natural selection. But how delighted Darwin might be, were he here today, to reflect that, after more than a century's exploration of this subject by a multitude of investigators, the year just past has revealed yet more examples of a new, and intricately wonderful, order of this phenomenon. In a genus of solitary wasps long known for the striking mimicry of a more powerful solitary hunting form exhibited by some of its members, it has recently been discovered that several species go much further. They show a dual, sex-limited kind of mimicry that simultaneously involves two very different models. The males mimic species of social wasps common within their range. The females mimic a solitary hunting wasp likewise abundant in their territory. Thus these versatile organisms wring "double dividends," as it were, from the protective resemblances so well known to Darwin, and offer fascinating examples of yet another variation of the pattern of natural selection at the level of living things where the theory of natural selection itself was first adduced.

One of the arresting features common to this sampling of contemporary advances in our understanding of nature, and in our power to exploit newly discovered features of the natural world, is that all of them, despite their wide diversity in subject and approach, were achieved either by individual scientific leaders or, more often, by rather limited numbers of outstandingly trained and gifted investigators, working in those small, intense teams that so characteristically form the optimum environments for the highest scientific productivity. Moreover, although some of the investigations demanded very costly instruments, such as powerful telescopes, the

material needs of the majority were relatively modest. The order of monetary support required for each of these achievements was, by usual standards of development, truly minuscule. It is clear that the best research is often extraordinarily economical, in both money and the actual number of men and women involved—though not of the training and quality of these investigators.

This characteristic economy becomes important to reckon with in the context of the present. Even under relatively severe economic constrictions, it should be possible, given sufficient care and imagination and insight, so to manage matters over the next few years that we do not unduly disrupt that flow in the creation of new knowledge that is so vital for our future, both spiritually and materially. The wisdom that we shall require here must evidently comprehend, among other things, a clear vision of the separate roles of research and development in our nation. It must also include as precise an estimate as we can achieve of their relative costs. It bears reiteration, in this connection, that the attempt made in past years to distinguish the costs of research and of development in Federal accounting takes on a special significance today. If this attempt were continued in future, it might well be found that, even if a fairly considerable reduction in Federal funds available for research and development, taken together, proved necessary for the coming year or two, support for research *per se* over the next critical years might not have to be reduced so severely, if indeed at all.

But there are other dangers, of a more deep-lying and subtle kind, that may threaten us in the climate of deceleration of the next few years. They will demand vigilant and understanding attention. One of them stems from apprehensions about science that undoubtedly lie dormant in our society.

Misunderstanding of the real nature of the scientific way is an ever-lurking danger with us, as it is all over the world. But the intensity of the problem varies greatly with circumstances. In a time like the present the threat is apt to be particularly severe. In such periods our concepts of the relationship of science to society are all too likely to polarize about either of two extremes. At one pole, science may come to be commonly regarded as an activity quite apart from the mainstream of society—even, in part at least, as a culturally enriching luxury, desirable, to be sure, but essentially remote from the principal currents of national concern. If this characterization gains wide acceptance in a society, it can be menacing. For, as Graham Hough has recently remarked in a different context: "In good times it is possible to pursue a multitude of remote and unpractical activities without feeling the painful sense of their disconnection with the actual and the

present. . . . One of the functions of civilization is to provide room for innumerable pursuits that have no *direct* connection with the daily business of living. For in good times there are all manner of unseen threads that link the old with the new, and make even scholarship and criticism a part of the national life. The past can live in the present without a violent distortion of its real nature. . . . Today this seems hardly possible."

In the absence of a keen appreciation of the relevance of even the most abstract science to the broader concerns of the society that supports it; in the absence of a clear understanding that it is in just those situations where viewpoints from the past and of the present are dangerously sundered that the scientific way can provide one of the most powerful of cohesive forces, one of the most durable of bridges across the gap, Hough's analysis, originally applied to other areas of culture, can only too easily become, for science, self-fulfilling prophecy. With this danger there is another that may be yet more serious. This view of science is all too apt to set off its own reaction: the demand for secularization; the demand that science be plunged *too fully* into the mainstream; the demand that science, if it is to be supported by society, should immediately and demonstrably be usable by society, and should be deliberately cultivated for its pragmatically *anticipated* results. One of the dangerous aspects of this line of thought, of course, is that once the consequences of research are generally regarded as being predictable in this way research then logically becomes subject to the same sort of regulation and control, the same kinds of efficiency ratings, that are properly applied to activities with predictable results everywhere in the society. Precisely because science is intrinsically unpredictable, its whole essence, both as a spiritual and a material resource, can easily be destroyed if this sort of misapprehension generally obtains.

This conceptual battle was fought and, on the whole, won, many years ago. Yet it is never really ended. It is in times like the present that we must pay special attention to the dangers of losing ground once gained.

But critical times like these may, at the opposite extreme, exacerbate a precisely opposite misconception of the social impact of science, which can carry an equal danger. This is the presumption that science has become all *too* socially relevant; that, with technology, it has in our day quite literally captured the world, and is proceeding on a course of its own, Frankenstein-like, largely independent of social direction and largely escaped from social control. Titles of such recent books as *The Temporary Society*, *The Technological Society*, and *The Accidental Century* reflect this apprehension well.

There are undoubtedly powerful and readily understandable reasons for this feeling. Conditioned as we often are to associate the technologies of World War II and of the Sputnik era primarily with science, we are at a point where the *possibilities* that now seem accessible to us, whether or not they can or will ever be realized, seem far more radical than ever before. As we peer into the future, we can, without any undue stretch of credibility, see ourselves taking the first steps toward navigation of our solar system before many years have passed. When Johannes Kepler, in *The Dream*, written in 1609 and first published in Latin in 1634, discussed trips from the planet earth to its moon in future, this must have seemed wildly visionary to his contemporaries, as indeed the title of the work suggests that he himself regarded it. Yet how soberly prophetic, in many ways, this work seems today, particularly when the author warns that solar radiation will constitute a major hazard for space travelers. Only a bit further in the future seem to lie the many possible consequences of biological and behavioral control, with their vast potential social impacts, which, though we may sometimes be inclined to overdraw them because we simply cannot, at this stage, assess them accurately, have nevertheless received some emphasis in suggestive experimental work during this very year. Here, of course, we are dealing with what is basically technology, or technology closely interwoven with science.

When we speak of the possibilities of future science, we are on yet more uncertain ground, where imagination and hope and fear have less to tram-mel them, because of the unpredictability that is so deeply characteristic of the scientific way. It is indeed a basic unpredictability. For, as Sir Peter Medawar has cogently pointed out, to predict a really new idea is to have that new idea, and if the idea has already occurred, of course, it can no longer be the subject of prediction. A quotation from the great English physiologist J. S. Haldane, the father of J. B. S. Haldane, is suggestive in this connection. In 1931 he wrote concerning the modes by which people were just beginning to suspect that the chromosomes operated, and by which heredity mediated development. Two investigators of the day, Ewald Hering and Richard Semon, "assume," says Haldane, "... that germ-cells are furnished with a system of engrams, functioning as guideposts to all the normal stages of development. . . . But," Haldane continues, "this theory has quite evidently all the defects of other attempts at mechanistic explanations of development. How such an amazingly complicated system of signposts could function by any physico-chemical process or reproduce itself indefinitely often is inconceivable." That was published only thirteen years before the pioneering experiments of Oswald Avery and his colleagues, in which mutant strains of bacteria were genetically transformed to the normal type by the action of purified DNA from the normal

form, were to lay the observational foundations from which have grown our contemporary concepts of the nature of these very engrams.

There is a further psychological factor which can be important in this general context. It may well be that the imperatives to adjust to technological change in our time are actually no greater than those that faced our predecessors. Nonetheless, they differ importantly. In our time not only is there reasonable promise of developments far more radical and more unfamiliar than any we face now and with those developments a threat of probing far more deeply and meaningfully into our most closely guarded personal domains. In addition, many of those anticipated innovations, and the futures that they imply, have been in our minds now for quite a long time. It seems quite possible that we are living with a cumulative effect of a long-continued awareness and expectation which, under the right circumstances, can be subtly and profoundly disconcerting to us.

Our reactions range, often with abrupt swings, from anxious doubts to what may be worse—over-credulity: an exaggerated faith in the powers of science, and more especially of technology, to work miracles in our society far beyond the limits of their capacity or relevance. Both these extremes of feeling arise from misconceptions which we must particularly guard against in such times as the present. Overdrawn credulity, especially, can lead to errors that may be costly not only in money but in terms of the careers of men and women. Furthermore, the cost of such mistakes is not to be measured merely in immediate and concrete losses, heavy though these may be. With our immense powers of recuperation, our superb capacities to rectify our errors, such consequences can in general be mitigated with time. What is more truly serious is that memories of such mistakes, once made, are apt to linger, and to exacerbate the oscillations from over- to under-valuation of the scientific mode. In extreme cases, this effect can be most harmful.

There is a final source of unease, primarily concerning technology, that affects us all in greater or less measure, and which unless, once again, we are vigilant, could have subtle and dangerous social consequences. Our own society is perhaps more vulnerable to this particular danger than any other on the globe—in part because we have so eagerly embraced technology and live by its products to so great a degree. We are continually assailed, of course, by the problems of comprehending and coping with the sometimes too-localized over-plenty that massive and highly advanced technologies, applied in the sphere of daily living, can bring, with the social stresses and dislocations that frequently accompany them. But beyond this, it is probably no exaggeration to say that the technologies which so pervade

our everyday lives have, cumulatively over the years, come to pose real threats to our concepts of reality. Urban or suburban life absorbs a larger and larger fraction of our nation. More and more people are shut off from nearly all daily contact with the natural environment, living in homes and working in buildings well isolated from the outside world, moving between them, often enough, in sealed and air-conditioned vehicles, enjoying relaxation through representations and using products that alike are predominantly humanly conceived and executed. We may well come to conclude with Ian Jarvie that our all-embracing modern technology is indeed assaulting the most fundamental classifications of our experience. We may well ask with him "What remains of the basic distinction between the natural and the artificial when we are confronted with modern technology?"

Does this blurring of distinctions matter? There is much to suggest that it may matter very seriously indeed. For when such a confusion is combined with the pressure of all the imagined things that science and technology may bring us in the near future, a situation could be created in which the fundamental dividing line between imagination and reality becomes very badly blurred. There is evidence that this is happening on a significant scale in our society today, and its effects could be grave. For there is nothing more painfully frustrating than to have embraced the imagined on the assumption that it is real, to have wholeheartedly pinned one's vision of the future on something that is at best half plausible and never finally materializes. One then feels cheated; one feels that what is in fact impossible has been willfully withheld. This is a peculiarly acute and dangerous kind of suffering. The threat of experiencing it can only be turned aside by a realignment of the very processes of apprehension and judgment, by the inward reestablishment of a firm boundary between what actually exists, or has a reasonable probability of existing, and what is, in essence, fictitious. This is a kind of stringent therapy which we, in common with a large share of the rest of the world, surely need. Should the situation grow worse over the coming years, it could threaten seriously the integrity, and indeed the safety, of our society.

Both technology and science have significant parts to play in resolving this crisis. The role of technology, which is essentially to act as a bridge, is perhaps especially vital. The part of science in this combination is clearly that of stabilizer. For the natural sciences early defined "reality" by an extension in precision and percipience and control of the traditional mode by which laymen also defined reality—as that which could be experimentally verified. Verification, of course, originally meant confirmation by the senses. It also meant verification, not by the senses of one man only, but by those of many. Likewise it implied consistency through time, in the sense that the same processes undertaken at another time brought consequences which

could be apprehended in the same way. This is still an acceptable basic sketch of the *process* by which verification is secured in the natural sciences, though the tests of interpretation are now, of course, far more sophisticated. It is implicit in our thinking that such tests are practical rather than philosophical. Indeed, as Martin Johnson long ago remarked, at a philosophical level we probably should regard verification, and so "reality," primarily as a measure of *communication* among scientists. But the practical tests, over a great part of the vast front of science, remain in this general mold—a mold, of course, which continues to be the one in which the criteria of "reality" for most of our everyday affairs are set; where, too, these criteria provide the most powerful and reliable medium of individual communication available to us.

When we enter truly social realms, however, we encounter a very different situation. Here, as Donald MacKay has observed so truly, the comparatively invariant criteria of the senses no longer suffice. The questions asked of social science, and for which the social sciences are seeking the answers, cannot be regarded as either "true" or "valid" in the conventional sense. For the content of these questions is sensitively responsive to the interpretation of the receiver of the information as well as to that of the sender. Here the attitude of the audience, the impressions, beliefs, extrapolations that may enter, all have a highly operative function in the defining of "reality," and their influence may greatly bias our conceptions of it.

Now this approach to "reality" is necessarily quite different from that of the natural sciences. Indeed, it can sometimes lie—and properly—quite outside their tradition, and if the integrity and effectiveness of the natural sciences are to be preserved, it probably must remain so. And yet we live in a world where, with increasing frequency, these two definitions of "reality" are placed in apposition, or are actually conjoined around the same substantive concerns. And those concerns commonly involve technology. This, perhaps, is one of the significant causes of the erosion of the once-clear line between imagination and reality, or, perhaps more accurately, the growing confusion of different kinds of "reality" that so haunts us today. There is no clear and present way out of the dilemma. But there can be no doubt that trying to fathom its unknowns and contradictions will pose a challenge of very high priority over the years ahead, and our answers to this challenge will have extraordinary practical as well as theoretical importance for our society.

One final concern must be deeply significant for our time. Just before Christmas in 1954, the first real success in transplanting a vital organ from one individual to another—a human dream ever since stories of sixteenth-

century Europe had erroneously credited Gasparo Tagliacozzi, the great Italian surgeon, with this accomplishment—was achieved when a kidney was removed from a Boston twin and transplanted to his brother. Since that time, more than twelve hundred kidney transplants have been attempted, with a rising percentage of success. In December of last year the first transplantation of a human heart was made. Although the patient quickly succumbed, the operation was shortly followed by a second which was more successful. Some nine months later, in August of the year just past, the twenty-seventh such operation had been completed, and the condition of the patient reported as satisfactory. A lung has recently been transplanted in an Edinburgh hospital. Transplantations have been made of liver and pancreas. Thanks to intensive research on such antiimmunogenic substances as antilymphocyte globulin, designed to suppress the normal rejection mechanisms of the body to foreign objects; thanks to improved methods and enhanced efficiencies in tissue typing and in the matching of appropriate donors and recipients, it seems quite possible that the transplantation of unpaired as well as paired vital organs between unrelated individuals may ultimately achieve a recognized position in surgical therapy comparable to the use of artificial hearts and kidneys to which we are accustomed today.

With all the brilliant work that has been done, and the brilliant, if limited, successes so far achieved, that day is not yet. But the potentialities have been so clearly indicated that, with our penchant for running beyond the event in imagination, we are already in the process of psychologically adjusting to a very new situation. And that adjustment, of course, brings with it all kinds of difficult questions that are new for us. When do we have the moral right to remove the vital organs from a body: at what point can we morally consider a person to be dead? What is to be considered a "success" in terms of the patient-recipient? How long must he survive the operation? What condition of body and mind, and what order of social value, must he show promise of achieving to make us feel that the operation, however brilliantly successful in a technical sense, has been humanly justified? These, and a host of associated problems equally difficult and challenging, will surely be with us as far into the future as we can see, and they will be answered differently by various people at various times and places.

But there is a deeper and more general issue underlying these matters that we must surely keep most critically in mind. In times of crisis, in a period when the experience of many kinds of violence to human life and the memory of that experience are all too vivid with us; in a period when the recollection of the catastrophic destruction of some of the most cherished monuments of human will and effort and of human reverence remains all too close, there is some real risk that the tremendous recent advances in the

sciences of life, with the new possibilities that they hold for the betterment of the human condition—of which the history of organ transplant forms an especially dramatic chapter—might yet be accompanied, bit by bit and almost imperceptibly, by a trend to hold human life itself less sacred than it has been in the best periods of our past. There is the associated possibility that the *capacity for reverence* itself, perhaps our most precious moral and social quality, might slowly be eroded.

Clearly there exist powerful bulwarks in our society against these dangers. They inhere primarily in those vital qualities of hope and devotion to movement and expansion that have always been so much at the forefront of our thought and feeling. In that context, science itself, with its own dedication to those qualities, with its total dependence upon them for its own welfare and integrity, must form one of the most stable and steadfast of such bulwarks. This, perhaps, is the greatest reason why we should give the most critical thought, in this year of watershed, to protecting and cultivating, in every way that we can conceive, the vitality, and above all the verve, of the scientific way.

One may long, as I do, for a gentler flame, a respite, a pause for musing. But perhaps there is no other peace for the artist than what he finds in the heat of combat. "Every wall is a door," Emerson correctly said. Let us not look for the door, and the way out, anywhere but in the wall against which we are living. Instead, let us seek the respite where it is—in the very thick of the battle. . . . Some will say that this hope lies in a nation; others, in a man. I believe rather that it is awakened, revived, nourished by millions of solitary individuals whose deeds and works every day negate frontiers and the crudest implications of history. As a result, there shines forth fleetingly the ever threatened truth that each and every man, on the foundation of his own sufferings and joys, builds for all.

ALBERT CAMUS—*Resistance, Rebellion, and Death*, 1957

The Year in Review

And by that destiny to perform an act
Whereof what's past is prologue, what to come
Is yours and my discharge.

—SHAKESPEARE, *The Tempest*,
Act II, Scene 1, lines 260–262

Dr. James D. Ebert, Director of the Department of Embryology, states in the Introduction to his report this year: “. . . it has been uncommonly difficult to summarize work already completed while conveying an idea of new directions. The problems encountered in reaching a proper balance of ‘old’ and ‘new’ are illustrated in . . . our activities.” Dr. Ebert’s words apply equally well to the programs of all the Departments of the Institution, and perhaps to those of any vital research organization.

Like a “normal” biological population, a research organization’s interests at a given time are composed of old and new, the budding and the closing, the ascendant and the waning. In a sense the great questions, like the analysis of the structure and content of the cosmos, or the analysis of the particulate composition and structure of energy and matter, are timeless and at once both old and new. When we examine the progress of any field of inquiry and its content at any one time, Dr. Ebert’s observations do indeed apply.

The distinction is operationally important, for in these days of rapid communication the time span between the new and the old may be relatively short, as a “lode” is soon mined by hundreds of scientists. Or rapid senescence may supervene, or premature abandonment of once-flourishing fields of inquiry occur. And fields may even be “rejuvenated,” as the tide of interest turns again and energizes them.

Dr. Ebert’s remarks call special attention to the nature of all our *Year Books*. They are, above all, progress reports and not statements of conclusions. *Year Book 67* is no exception. In summarizing the content of its individual reports this year it seems appropriate to stress explicitly what

has always been implicit in these Reviews: that progress in the work of the Institution, as elsewhere, represents a combination of the old and the new, of the emergent problem and the matured field.

In a delightfully worded and penetrating Introduction to his report this year Alfred D. Hershey, Director of the Genetics Research Unit, aptly characterizes the essence of most progress in science. He remarks that "discovery and description of natural phenomena are ends in themselves" to practicing scientists. "One notices a phenomenon that looks interesting. After suitable thought and labor, one performs an experiment that ought to be instructive. What it actually does is to turn up a second phenomenon not related in a simple way to the first. This sequence of events makes for lively research. It does not provide explanations . . . we have to consider the possibility that (this) sequence . . . may prove endless, giving an indefinitely complicated description of nature. . . . This seems to be the state of affairs in research on the structure of matter at both ends of the scale of magnitude. For somewhat similar reasons, what goes on in atomic nuclei, outer space, and living cells might prove equally refractory to explanation." That is, the new in science does not often produce broad generalizing explanations. It only gives a slightly different view of the infinite than was there before. A number of such views are provided by the Institution's work in astronomy and astrophysics, nuclear physics, geophysics and geochemistry, and biophysics, biochemistry, and biology during a very rewarding year.

Astronomy and Astrophysics

Astronomy surely ranks among the most ancient of all scientific subjects. At the same time it is a scientific subject for which there is as yet not even a theoretical end to the imagined.

The year's work at the Mount Wilson and Palomar Observatories can once again be summarized in categories that have become familiar to readers of these Reviews.

Work in one of these categories, that of solar astronomy, reaches back close to the origin of the Mount Wilson Observatory. Indeed the founder of that Observatory, the late George Ellery Hale, selected Mount Wilson as its site at least in part because of the peculiar advantages it offered for solar observation. Solar study has continued without interruption at the Mount Wilson Observatory ever since 1904. The sun's magnetic properties have been a subject of investigation since 1908, when Dr. Hale discovered the magnetic field of sunspots. Solar physics has been a major research interest of Horace W. Babcock, present Director of the Observatories, who was the co-inventor of the now widely used solar magnetograph. Robert Howard,

Harold Zirin, and their colleagues thus continue a program which now has more than half a century behind it.

Study of the magnetic properties of the sun continues to be an important part of the solar program today. Solar magnetograms, which have been a feature of the Observatories' operations since 1953, now are reduced by computer analysis. They provide the basis for calculations of the integrated magnetic-field strength and fluxes for each day's observation. The magnetograph may also be used in the "velocity mode" for producing "Dopplergrams," or maps of differential velocity patterns on the sun. Studies of the differential solar rotation with the aid of isotachial¹ plots have been initiated. The first results show no large-scale meridional currents.

In collaboration with V. Bumba of the Ondrejov Observatory of Czechoslovakia, Howard found that low-latitude patterns of magnetic fields on the sun persist for periods as long as one or two years with rotation rates of about 27 days. The 27-day period of these long-lived magnetic "streams" on the sun undoubtedly is connected with recurrent magnetic disturbances in the vicinity of the earth.

Howard and J. M. Wilcox, of the University of California, Berkeley, have studied the relation of the interplanetary magnetic field with that of the sun's photosphere. The solar field is found to have a pattern different from that which may be expected from the usual solar differential rotation. For example, the rotationally most advanced part of the field is at 15° north latitude, not at the equator, as would be projected in differential rotation in the photosphere.

Study of the solar events of another year produced one of the more interesting insights on the solar process. H. Zirin and Mrs. D. R. Lackner, a NASA postdoctoral fellow, studied in detail the records of the great flare of August 28, 1966, one of the largest proton flares observed in the present solar cycle. This flare appeared qualitatively different from a normal solar flare in the very large size of the area over which energy was released, as though a chain reaction of energy release had occurred. From the observed area of the flare and assumptions as to its height, it was possible to make models of the emitting material. The X-ray emission and microwave bursts traceable to the flare can only be explained by assuming that they occurred at temperatures greater than a billion degrees.

Laboratory study also provided the first convincing identifications from an astrophysical source of the "forbidden" lines of neutral sulfur in the Fraunhofer spectrum, whose presence was first suggested in 1948 by I. S. Bowen. D. L. Lambert, in collaboration with J. P. Swings and N. Grevesse of the University of Liège, Belgium, has provided an accurate wavelength

¹ An isotach is a contour line denoting equal velocity.

for two neutral sulfur forbidden lines. The observed intensities in the solar spectrum are in good agreement with predictions based upon theory.

Pulsars. The most remarkable astronomical discovery announced during the year was that of the rapidly pulsating radio source in the constellation Vulpecula, announced by A. Hewish and his collaborators at Cambridge University in February 1968.² This discovery brought to astronomers' attention a whole new class of objects with very unusual properties. The most remarkable of these is the radiation of brief pulses of radio energy with a period of extremely high constancy. Thus the name "pulsar." The pulse recurrence interval for this first pulsar was measured at 1.3372795 seconds by F. D. Drake and collaborators at the Arecibo Observatory in Puerto Rico.³

Soon after announcement of the first pulsars, H. Arp, A. Sandage, J. Kristian, and others of the Mount Wilson and Palomar Observatories attempted to identify them optically. A major part of the search has centered on the field of CP 1919, the first pulsar with an accurately determined radio position. The fields of sources CP 0950 and CP 1133 also were examined, but with negative results. An object of magnitude 17.5, apparently a star, in the field of the pulsar CP 1919 was searched for periodic fluctuations in brightness with the aid of a signal-averaging computer. No periodicity in the light was detected. However, measurements and detailed analysis of pulsar data are continuing at the Observatories because of the obvious interest in the physics of pulsars. Further, it is thought that more precise measurement of astronomical distances than ever before achieved may be possible, as well as the establishment of the plasma distribution in the galaxy with greater accuracy and in more detail.⁴

Quasi-stellar Sources. An equally if not more remarkable class of objects is that of the quasi-stellar source, first identified optically at the Mount Wilson and Palomar Observatories in 1962. They continue to present some of the more difficult problems encountered in the recent history of astronomy and have aroused at least one lively controversy as to their characteristics and position. This controversy centers on the distance of the quasars. Are some or all of them "local," that is, within or relatively near to our Galaxy? Or are they at cosmological distances, as the large redshifts of many quasars indicate? Members of the staff of the Observatories believe they have adduced convincing evidence during the year that the quasars are not "local."

² A. Hewish, S. J. Bell, J. D. H. Pilkington, P. F. Scott, and R. A. Collins, "Observation of a Rapidly Pulsating Radio Source," *Nature*, 217, 1968, p. 709.

³ F. D. Drake, E. J. Gunbermann, D. L. Jauncey, J. M. Comella, G. A. Zeissig, H. D. Craft, Jr., "The Rapidly Pulsating Radio Source in Vulpecula," *Science*, 3 May 1968, p. 503.

⁴ Drake, *et al.*, *op. cit.*, p. 507.

Quasi-stellar sources may be divided among radio-emitting sources and radio-quiet objects. All are optically blue. A. Sandage completed during the year photoelectric photometry of 300 blue objects and concluded that a major change in the nature of blue objects occurs at the visual magnitude designated 15. Radio-quiet quasars begin to occur at about this magnitude and increase in frequency with increasingly fainter apparent magnitudes.

Study of the quasar component of the blue objects investigated became sufficiently precise during the year to afford a first tentative estimate of the number of radio-quiet quasars in the sky. On the basis of Sandage's photoelectric photometry and spectrometry by A. Braccesi and R. Lynds, an estimate of 0.4 QSOs per square degree was made to blue magnitude 17.1, 5 per square degree to magnitude 18.5, and 100 per square degree to 21.5. A quantitative growth relation can be calculated from the observed distribution by magnitude. Although the determination of the growth function for the radio-quiet quasars is tentative, Sandage and W. J. Luyten, of the University of Minnesota, are convinced that the number of such objects is very large. The suggested function for the growth relationship results in an estimate of 10 million quasars over the entire sky to a faintness of magnitude 22. Sandage believes that such a large number of objects having either a constant space density or a positive density gradient outward, virtually eliminates the "local" hypothesis for quasar distances.

An important distinguishing feature of quasi-stellar sources is their optical variation with time. Rapid fluctuations of nonthermal radiation (continuous emission not attributable to stars) in quasars over periods of days is cited by some astronomers in support of a contention that quasars are "local." It is also suggested that there may be another explanation for the observed redshift.

To examine the validity of this position a search was started for nonthermal radiation in objects whose cosmological distances are not disputed. A kind of galaxy known as the N-type displays nonthermal radiation, and has been shown by Sandage to lie at cosmological distances.

Sandage and J. B. Oke found that the N-type galaxy 3C 371 varied optically by nearly a factor of 2 in intensity between June 1966 and September 1967. Oke found variations of 10 to 15 percent within only a few days. Later observations by Sandage on other N-type galaxies also revealed significant variations in brightness. It was concluded that large variations of radiation within a matter of days cannot in themselves contradict the cosmological distance scale of quasars.

M. Schmidt, observing objects identified by E. T. Olsen of the University of Michigan, continued spectroscopic observation of quasi-stellar radio sources. A most interesting discovery was the quasi-stellar source 4C 25.5, identified by Olsen as a blue stellar object of visual magnitude about 17.5.

It has an emission-line redshift of 2.358, the largest yet recorded. If the redshift is an indicator of relative distance from the earth, once again we may record the observation of an object still farther from the earth than the farthest known the year before.

Compact Galaxies and Groups of Galaxies. Further evidence of the enormous variety and great richness of the sky in classes of astronomical objects is given in investigations of compact galaxies and chain galaxies. F. Zwicky, Arp, Oke, W. L. W. Sargent, and G. Neugebauer have made spectroscopic investigations of several hundred compact galaxies. They have found that among the compact galaxies are objects that match the spectra, colors, and absolute magnitudes of other extragalactic objects originally considered unique, like the quasars. Observations by Zwicky, Arp, Sargent, and T. Fairall demonstrate that there exist compact galaxies that form a continuous link between ordinary galaxies and quasars. One of these, the "iron galaxy" (I Zw 0051 = 12), with an absolute magnitude of -23.1 , is considered to be as luminous as some quasi-stellar sources.

Compact galaxies in some cases have been found in clusters which contain dozens to hundreds of objects. Three of the more remarkable of these clusters, known by their numbers in the Zwicky list, (Zw Cl) 1710, 1849, and 0658, contain respectively 345, 324, and 189 galaxies each. A feature of these clusters appears to be a large velocity dispersion. Zw Cl 1710, for example, has two galaxies with individual velocities of recession of 23,820 kilometers per second and 21,440 kilometers per second.

Other clusters of galaxies contain fewer members. Sargent began a study of motions of galaxies in small groups. One of the clusters, VV 172,⁵ contains five galaxies in an almost linear chain, isolated from others of similar brightness (Plate 1). The mass of the whole system is equivalent to at least 400 billion solar masses. Image-tube spectra obtained of each galaxy in the chain show redshifts of approximately 16,000 kilometers per second for four of the galaxies, but one of almost 37,000 kilometers per second for the fifth. The four galaxies have a systematic trend of redshift indicating their rotation as a system. The anomalous fifth must be either a background galaxy, or one that was expelled from the chain with tremendous energy about 100 million years ago. VV 172, incidentally, is not unique. Two other galactic clusters, Stephan's Quintet and the triple system IC 3481, also have an anomalous galaxy, but in these the redshift is much smaller than in the remainder of the group. VV 172 is the first to be found with an anomalous galaxy apparently receding at such a rapid rate from its system.

An Unusual Near Neighbor in Space. Arp and J. Greenstein have made some observations of the star Wolf 359, one of the nearest neighbors to the

⁵ From the discoverer, B. A. Vorontsov-Velyaminov, whose study of the National Geographic-Palomar Observatory Sky Survey identified a number of unusual astronomical objects.



Plate 1. The chain of five galaxies known as VV 172. The second galaxy from the top of the chain has a redshift more than twice that of any one of the other four galaxies. (From H. Arp, *Atlas of Peculiar Galaxies*, Pasadena, 1966: No. 329.)

earth, with the image-tube spectrograph. On the very first observation they found this very faint star to have a flare. Wolf 359 is a member of what is called the "old disk population" of stars in the Galaxy. Such strong chromospheric activity is unexpected among these stars, and particularly in one of such low luminosity. An additional unusual feature was discovered in observations by Neugebauer and E. Becklin which showed unusual brightness in the infrared. The star has an apparent visual magnitude of 13.3, but a magnitude of 5.8 at the 3.4-micron wavelength. The infrared brightness may be explained by low temperature, but the temperature would have to lie far below that expected for any of the "main-sequence" stars, where Wolf 359 was thought to fit. These observations suggest that a part of the luminosity-temperature function generally accepted by astronomers may be subject to reinterpretation.

Radio Observations in the Southern Hemisphere. A significant tentative conclusion about the Magellanic Clouds, our Galaxy's nearest neighbors, was derived from southern hemisphere radio observations. Aided by the installation of a new low-noise parametric amplifier and a complete digital data acquisition system, the recently established Carnegie-Argentina Radio Astronomy Station at La Plata continued investigation of the dynamic history of the system comprising our Galaxy and the two Magellanic Clouds. Using equations of motion, observed radio velocities, and assumed velocities perpendicular to the line of sight, computer studies of the possible history of the Galaxy and the Magellanic Clouds were undertaken. Two conclusions may be drawn. One is that the radial velocities of the material between the two clouds are consistent with an explosive origin for the two clouds. The second is that the Magellanic Clouds are probably not an oblique twin system, but are most likely independent celestial bodies passing close to one another. K. C. Turner, of the Department of Terrestrial Magnetism, concludes "there seem to be no considerations other than aesthetic ones which require the clouds to be permanent pair."

Refining the Tools for Analyzing the Cosmos. One of the most fascinating questions in all astronomy, if not in all science, is that involving the history and processes of the cosmos. As W. H. McCrea has observed, modern cosmology is in a supremely interesting state.⁶ The original static model of the universe proposed by Einstein in 1917 has long since been superseded, and the more recent steady-state model of Bondi, Gold, and Hoyle has been called into serious question. There remains the "big-bang" hypothesis, whose main predictions "appear to have been almost suddenly found to be fulfilled."⁷ However, in spite of the satisfactory fit to the big-bang model that large-scale computing seems to be giving recent observations, McCrea notes

⁶ W. H. McCrea, "Cosmology after Half a Century," *Science*, 21 June 1968, p. 1295.

⁷ *Ibid.*

that there still remain both empirical and conceptual difficulties about the acceptance of such a model.⁸

One other possible interpretation is that of an oscillating universe, in a sense a variant of the big-bang model. The question of choice among alternative models still remains. The concept of a "fireball" (or "big-bang") origin for the observed universe seems to be generally accepted, although the date of this epochal event is still uncertain.

The key to a decision among known models and to elaboration of the features of whatever cosmological model is chosen lies in refinement of the parameters H_0 , q_0 , and σ_0 used in its construction. These are, respectively, Hubble's constant (ratio of speed of recession to distance), the deceleration parameter, and the density parameter.

Sandage developed during the year a new method of determining the Hubble constant. By calculating the apparent magnitude-redshift relation for the brightest elliptical galaxies in clusters at distances lying beyond the effects of "local" inhomogeneities in our part of the universe, he has arrived at a determination of the constant that narrows considerably the range between possible upper and lower limits. These he states to be 75 and 50 kilometers per second megaparsec.⁹ The reciprocal of the constant may be stated in years. Taken together with the deceleration parameter (q_0) of +1, the new determination gives an estimate of the time since the "fireball" of the big-bang as about 11 billion years. Sandage notes that such an estimate lies within the range of the estimated age of globular clusters of stars (about 10 billion years) and the presently determined age of the heavy chemical elements (greater than 6.6 billion years) that make up the earth's crust.

The value of the Hubble constant is of such obvious importance to cosmology that Sandage, in collaboration with J. Kristian, has already begun a check on the new method by making a second and different type of determination, in which the angular sizes of ionized hydrogen patches in nearby spiral (Sc) galaxies are measured on high-quality photographs made with the 200-inch telescope.

In collaboration with J. B. Oke, Sandage has also attacked the problem of defining more accurately the deceleration parameter (q_0). The problem is to determine the correction necessary for measured intensities of redshifted galaxies to compensate for the redshifting of the continuum energy distribution through the measuring bands. As part of this determination Oke and Sandage examined the energy distribution in eight giant E (elliptical) galaxies. They found it to be identical for all eight of the galaxies, thus supporting the view that elliptical systems are similar in their stellar content.

⁸ *Ibid.*, pp. 1297-1299.

⁹ One megaparsec equals 3.26 million light years.

These data were compared with new photoelectric measurements for galaxies in 32 clusters. The function predicted from the study of the giant galaxies agreed with the photoelectric measurements over the entire range of redshifts with a probable error of less than ± 0.02 magnitude. Such agreement, they say, shows that no significant change in energy distribution has occurred through evolution of the stellar content of the E galaxies during a period of 2.5 billion years. The results are consistent with a new estimate by Sandage that the change in magnitude over time in such systems is less than 0.05 magnitude per billion years, as determined from study of the evolutionary pattern of relevant stars.

The ultimate purpose of the energy distribution corrections is a decision between a "big-bang" (ever-expanding) model of the universe, and an oscillating model. The new data had been given a preliminary analysis by Sandage and J. D. Peach. They report that the data favor the oscillating model, and suggest a total cycle of time between fireballs of about 80 billion years.

Improved Instrumentation in Astronomy. In keeping with a long tradition the scientists of the Institution have continued to be alert to possible improvements in the instrumentation of astronomical observation. In these days, when the pressure for observing time generated by the increasing number of astronomers has intensified greatly, the potential contributions of improved instrumentation are enormously greater than ever before. At least two of the activities of the Mount Wilson and Palomar Observatories, extension of photoelectric data systems using digital recording, and the Carnegie Southern Observatory, bear special mention. So also does the continued work on image tubes for telescopes, a particular interest of the Department of Terrestrial Magnetism to which the Observatories also have contributed.

One of the longest continued single projects in the Institution's history has been that of the Committee on Image Tubes for Telescopes. The Committee was started at the Department of Terrestrial Magnetism in February 1954 to investigate the possible use of electronic techniques to supplant or supplement the prevailing photographic techniques of recording observations from optical telescopes. First supported by a grant from the Carnegie Corporation of New York and then by grants from the National Science Foundation, the Committee, with the cooperation of the Radio Corporation of America and other industrial laboratories, has had outstanding success in developing a satisfactory image tube intensifier for optical telescopes. The first successful two-stage cascaded tubes, developed in the RCA laboratories, became available at the end of 1963. Since that time 35 tubes have been distributed by the Committee and the National Science Foundation to astronomers on a priority basis, 14 of them within the last year.

Meanwhile, further technical development of the tubes and associated optics or other instrumentation has continued. The RCA laboratory now has under development an improved version of the image tube that promises to increase the image resolution obtained on tubes of the present design.

One notable event during the year was the first use of the image tube on the 200-inch Palomar telescope as part of a new Cassegrain image tube spectrograph designed by I. S. Bowen. For equivalent resolution, the new spectrograph gave a speed gain of about 15, measured in the blue part of the spectrum, as compared to the prior "unaided" instrument. The use of this spectrograph thus can substantially improve the effectiveness of the 200-inch by permitting the scheduling of more observations.

A most important advance in the mode of operating the three major telescopes of the Observatories has been designed and gradually installed over the last few years. Photoelectric data systems using digital recording now take care of a majority of the observing nights on the 60-inch telescope (57 percent) and on the 100-inch (68 percent), and now are used for nearly a third of the nights on the 200-inch. The tedious and time-consuming task of installing digital data cables and many coaxial cables on the 200-inch telescope was essentially completed during the year. About 120 digital conductors now link that telescope with the data room. An additional 56 cables were installed to operate a multichannel spectrum scanner at the Cassegrain focus.

The data systems already have contributed notably to efficiency and flexibility in the use of the telescopes. For the future, use of integrated circuit modules, high-capacity, compact, low-cost computers, and direct lines to large computers at distant laboratories offer proven possibilities for further steps towards more effective use of these valuable instruments.

A third important step towards effective instrumentation in optical astronomy was taken by the Institution's Board of Trustees during the year in approving the establishment of an optical observatory to be located in central Chile and administered by the Mount Wilson and Palomar Observatories. Thus the first fruits of the careful site survey investigations that have been conducted for several years past are now in sight. Engineering activities are now proceeding.

Nuclear Physics

Nuclear physics has held the attention of some Institution scientists since the early 1920s. Ellis T. Bolton, Director of the Department of Terrestrial Magnetism, relates in the Introduction of his report the story of one exciting event in the history of that interest, when Richard Roberts, Lawrence Hafstad, and Robert Meyer gave one of the early demonstrations of nuclear

fission by bombarding uranium 238 with neutrons from lithium and deuterium in the Department's Van de Graaff accelerator. The successful demonstration was conducted in the presence of Niels Bohr, Enrico Fermi, Gregory Breit, L. Rosenfeld, and Edward Teller. Although it was unknown at the time, prior demonstrations of fission had been conducted 12 days before by Frisch in Copenhagen, and three days previously by Dunning and his colleagues at Columbia University. Bohr witnessed the Roberts-Hafstad-Meyer experiment without knowing that Frisch had already successfully completed his experiment.

Within the last few years interest in nuclear physics has revived at the Department of Terrestrial Magnetism. Descriptions will be found in the *Year Book* of experiments conducted during the past year by L. Brown, C. Petitjean, and W. Trächslin on the lithium-helium transmutations [${}^7\text{Li}(p,\alpha){}^4\text{He}$ and ${}^6\text{Li}(p,{}^3\text{He}){}^4\text{He}$] with the use of a polarized proton beam. The reactions studied proved to be strongly sensitive to polarization. Brown, Petitjean, and Trächslin note that the energy range shown in the lithium-helium transmutation experiments "covers a region where the structure of the intermediate nuclei ${}^8\text{Be}$ and ${}^7\text{Be}$ is still uncertain after 30 years of research with unpolarized protons." Thus it appears possible that atomic nuclei as complicated as that of the beryllium atom could be described in terms not much more complicated than for the helium atom.

Another finding of interest to these investigators concerned an earlier helium-to-helium experiment (*Year Book* 66). R. G. Satchler, of Oak Ridge National Laboratory, has found that the DTM measurements of ${}^4\text{He}(p,p){}^4\text{He}$ fit a concept of nuclear structure known as the *optical model*, which hitherto has applied only to nuclear scattering at high energies on medium and heavy nuclei. The application of the optical model to a light element is significant, explain Brown, Petitjean, and Trächslin, because "The fit of theory to data . . . had to be made with a reduced number of parameters, since the usual complex potentials¹⁰ must be replaced with real ones because no inelastic processes¹¹ are possible." The possibility definitely is opened that concepts of nuclear structure can be somewhat simplified, permitting a choice among the known theoretical alternatives, and possibly a single system of statistical probabilities.

Geophysics and Geochemistry

Research in geophysics has as long and as distinguished a record in the Institution as research in astronomy. Plans for a geophysical laboratory and an "International Magnetic Bureau" were presented in the second *Year*

¹⁰ Of overlapping levels in the nucleus.

¹¹ An inelastic process is one in which the bombarded nucleus is left in an "excited" state.

Book (1903), and the "Department of International Research in Terrestrial Magnetism" commenced operation on April 1, 1904. The geophysical program of the Institution has continued uninterrupted ever since, through its two departments, the Geophysical Laboratory, and the Department of Terrestrial Magnetism. The principal objective of our geophysical research is knowledge of the history and composition of the earth—the enormously complex universe of rock and molten material lying under us.

The investigative programs themselves are indicative of the complexity of the subject with which they are concerned. The search for understanding of the earth's properties and processes in the 1967–1968 programs included identification of the mineral components of the earth; identification, description, and laboratory reproduction of the processes of rock formation, energy flow, and structural formation; and the relations of the planet to its immediate environment in space.

Identification of New Minerals and Other Components of the Earth's Crust. Nothing illustrates better the earth's complexity than the number of known minerals found in its crust. More than 2500 minerals already are known. To the layman it may come as a mild surprise that today, after thousands of years of mineral identification, new minerals are being discovered. Indeed, three of them were discovered or identified at the Geophysical Laboratory during the year.

A. El Goresy discovered a new allotropic form of carbon, which he and Gabrielle Donnay studied by means of X rays. There are three other known forms, diamond, graphite, and lonsdaleite. The newly discovered mineral has a hexagonal form, a metallic gray-to-white reflection color, and is slightly harder than graphite. It was found in polished sections of "shocked" graphite gneisses from the Ries meteorite crater in Germany. It is to be called chaoite in honor of Dr. Edward Chao of the United States Geological Survey.

The second new mineral was discovered by Gabrielle Donnay. It has been named ewaldite, and is a complex sodium-calcium-barium carbonate found in three-dimensional intergrowth with a previously known mineral, mckelveyite, from the Green River formation of the United States.

The third new mineral, now called sonoraite, was discovered by Richard R. V. Gaines, of the Universidad Nacional Autónoma de Mexico, in the Moctezuma tellurium-gold mine in the state of Sonora, Mexico. It is an iron tellurite occurring as highly lustrous, yellowish-green rosettes. The crystal structure was determined by Gabrielle Donnay in cooperation with J. Zemann of the University of Vienna, and J. M. Stewart of the University of Maryland, and a chemical analysis was made by M. H. Hey of the British Museum.

One of the more intriguing problems in the identification of rock components concerns evidences of life in the ancient rocks. For several years

P. H. Abelson and his colleagues at the Geophysical Laboratory have been seeking these evidences. They have been particularly interested in the fatty acid and amino acid traces to be found in sedimentary rocks and their relations to modern fatty acids and amino acids. Problems lie not only in the identification and measurement of life-derived materials, but also in detecting contamination of ancient rocks by more recent additions.

The contamination problem was illustrated in an analysis made this year of the amino acid content of the 1.9 billion-year-old Gunflint iron formation of Ontario, where microfossils embedded in chert were discovered about 15 years ago. Other investigators have reported finding amino acids in the chert that they believed to have been residual in it for 1.9 billion years. However, because of the conditions under which the chert specimens were found, and the presence of specific amino acids not considered stable over time, Abelson and Hare replicated the experiments. They concluded from a number of analytical results, such as the observed ratio of alloisoleucine to isoleucine, that the amino acids found in the chert are of recent origin.

The organic geochemistry group of the Geophysical Laboratory made significant progress during the year in identifying the products with life origins that are stable under geologic conditions. The group also developed further the laboratory-simulated production of these compounds. The combination of gas-liquid chromatography with a mass spectrometer, used by T. C. Hoering for analysis of molecular structure, aided much in gaining new understanding. As Dr. Abelson explains in his Introduction to the Geophysical Laboratory report, this combination gives unique information on molecular structure even when only tiny samples are available.

Using these methods, Hoering analyzed samples of marine sediment from the continental shelf off Southern California for fatty acid content and found a surprisingly large content of the branched-chain acids, particularly of the isoprenoid type. Such acids, although known in lipides, are usually considered to be relatively rare.

In separate experiments Hoering, P. E. Hare, and R. M. Mitterer succeeded in reproducing in the laboratory the pattern of amino acids and other life compounds to be found in ancient sediments. Hoering's experiments were a continuation of a set started last year on the application of elevated temperatures to a recent marine sediment. Analyzing the porphyrins that resulted from this treatment, he found the distribution of molecular weights very similar to that in materials separated from ancient sediments. His data suggest that alkylation and transalkylation may be important organic reactions occurring in sedimentary rocks in addition to hydrogenation, dehydrogenation, cyclization, and hydrolysis.

Hare and Mitterer experimented with the incubation of fragments of modern moluscan shells at temperatures from 185° to 90°C for periods from

one day to three months in varying environments. Their experimental procedure produced changes in the amino acid content almost identical with those seen in fossils (Fig. 1). The detailed data on changes under different conditions over time suggested potential uses for amino acid ratios in fossil study. If the temperature is known, an approximate age can be calculated. On the other hand, incubation temperature may be inferred for material whose date of origin is known. Such knowledge could be used in stratigraphic correlation, as in connection with deep-sea sediment cores.

Identification and Reproduction of Rock-Forming Processes. Much of the research interest of the Geophysical Laboratory now centers on studies of phase relations and other mineralogical attributes that may give clues about the composition and structure of the crust, mantle, and core of the earth. They are directed towards not only information concerning the composition of the earth in all its complexities, but also an understanding of how it became what it is. Laboratory experiment has now become a prime source of such information, but the older tradition of field study for understanding the earth by no means has been abandoned.

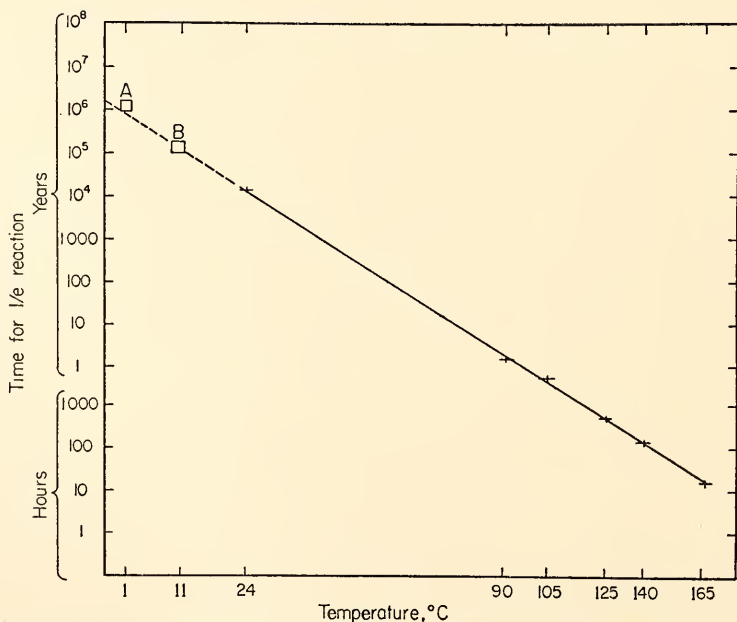


Fig. 1. Comparison of reaction times for laboratory-observed conversion of isoleucine to alloisoleucine (lower right) with radio carbon-dated fossil shell materials (upper end of solid line), materials from an Antarctic deep-sea core (A), and Upper Pleistocene materials from Wailes Bluff, Maryland, locality. The plot shown is for an Arrhenius equation that relates the rate constant of a reaction to the absolute temperature. The data obtained by Hare and Mitterer in their laboratory experiments show that extrapolation of laboratory-observed values to fossil specimens may be possible.

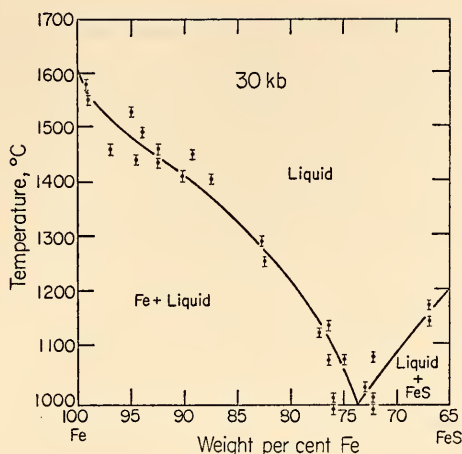


Fig. 2. Temperature-composition section for the Fe-FeS system at 30 kb pressure. Increasing sulfur content of a mixture of iron and sulfur shown with distance to the right on the diagram. The eutectic temperature (minimum melting temperature) for the liquid is near 1000°C. The same melting temperature has been observed at 1 atmosphere of pressure, but 3.5 percent more sulfur is required to reach the eutectic temperature. This observation suggests that even a small amount of sulfur at the earth's core may have a significant influence on its melting temperature.

From a series of experiments conducted by P. R. Brett of the U. S. Geological Survey and P. M. Bell of the Geophysical Laboratory, an interesting inference can be made about the temperature of the earth's core. It has been known for some time that a mixture of iron and sulfur had a lower melting temperature than iron alone under atmospheric conditions. Brett and Bell experimented with the Fe-FeS system under 30 kb of pressure. The minimum melting (eutectic) temperature was found to be almost exactly the same at 30 kb as at one atmosphere (about 990°C). However, the amount of sulfur needed to reach the eutectic temperature in the mixture was 3.5 percent less at 30 kb than under one atmosphere (Fig. 2). These results suggest that even a small amount of sulfur, if present in the earth's core, would lower the melting temperature of the iron there significantly. The difference between the melting temperature of 100 percent iron and the eutectic iron-sulfur combination is more than 600°C.

A unique and imaginative method of studying deep-lying rocks is described in the report of H. O. A. Meyer and F. R. Boyd on mineral inclusions in diamonds. The high temperatures and pressure required for the formation of diamonds under natural conditions are such that it seems most likely

that diamonds have come from depths below 100 kilometers, that is, from far below the base of the earth's crust. The chemical compositions of other minerals sometimes included within natural diamonds were determined quantitatively for the first time by Meyer and Boyd with an electron probe. The inclusions are far too small to have been studied by the classic methods of analytical chemistry. The olivine, garnet, chromite, and diopside inclusions within the diamonds studied were found to be grossly similar to those from ultramafic nodules in the kimberlite where the diamonds occur. All of the inclusions were discovered to be monomineralic (i.e., one mineral per inclusion), suggesting that the diamonds were formed by a solid-state process rather than by crystallization from a magma. Another interesting observation is that the garnet and chromite inclusions were unusually rich in chromium, whereas a single diopside inclusion was found to contain unusually little chromium. Furthermore, other characteristics of the diopsides imply a relatively low temperature for the formation of the diamonds, probably 950°C. Boyd observes that this temperature is low in comparison to the range in which diamonds have been synthesized in the laboratory.

The distribution of water in the earth's crust and mantle and its function in rock-forming processes have long been subjects of geophysical and geochemical study. Theories of the genesis of magmas must make allowances for the manner in which water is distributed within the earth's mantle. The occurrence of water within the deep mantle is a problem of special interest. The minerals known as amphiboles, hydrous compounds stable at temperatures up to 1000°C at low pressure, have been proposed as mineral phases that could hold water deep within the mantle. M. C. Gilbert, a Fellow at the Geophysical Laboratory, experimented with the pressure effect on amphibole stability, and showed that calcic amphiboles are not likely to be stable at depths greater than 70 to 100 km. Gilbert concludes that amphiboles may be significant in the petrology of the lower crust and upper mantle, but cannot be the water bearers at greater depths. One more constraint upon the composition of the mantle thus has been discovered.

The effects of water comprised an important part of another Geophysical Laboratory study on the genesis of basalt magmas—very important sources of rocks in the earth's crust. H. S. Yoder, Jr., and I. Kushiro studied the melting relations of enstatite (MgSiO_3) and forsterite (Mg_2SiO_4) in the presence of water. Their results suggest that silica-saturated magmas can be formed in the presence of water at considerable depths in the upper mantle by partial melting of enstatite or fractional crystallization. These results are considered significant indicators of the origins of silica-rich magmas, such as the andesitic magmas in mountain-building zones, thought to be formed by fractional crystallization of basalt magmas at high water pressures.

An interesting tool of theoretical significance has been developed by W. B. Bryan of the Geophysical Laboratory. The study of an intrusive igneous rock suite evolved from a magma, or possibly the mixing of two or more magmas, involves complex relations in crystal-melt equilibria, assimilation, etc. Bryan has written a computer program that will generate an estimate of the composition of the magma at any arbitrarily chosen stage of evolution. A large number of alternative hypotheses may thus be tested rapidly, as well as the capacity of an inferred mechanism to account for observed trends in the evolution.

Studies of Meteorites and Meteorite Effects. Several interesting studies of meteorites and their impact were undertaken during the year at the Geophysical Laboratory. P. M. Bell and E. Chao have experimented for the first time with the formation and annealing of synthetic dense glasses composed of feldspars. Such glasses are observed at the surface of the earth in the impact zones surrounding meteor craters. They are formed by the high-pressure shock-wave that accompanies the meteoric impact, and they are extraordinarily dense. A comparison of such impact products with the products of other explosive events, such as volcanic eruptions, is expected to be useful in the analysis of samples from the moon or other planets when they become available.

G. Kullerud and A. El Goresy have explained one of the anomalies of meteorite mineralogy as compared to terrestrial assemblages: the lack of equilibrium between minerals in the same assemblage. The lack of equilibrium need not indicate a lack of differentiation in meteoritic bodies, as previously believed, but can be more readily explained as the effect of shock in at least some instances.

Geophysical Field Studies. Although laboratory experiment has become the dominant interest of geophysical research workers in the Institution, the long tradition of field observation that began with the Department of International Research in Terrestrial Magnetism in 1904 continues as a highly useful approach to new knowledge about the interior of the earth. The program of seismological observations of the Department of Terrestrial Magnetism depends upon field operation. An unusual geophysical field investigation of heat flow from the earth's interior was started in 1966 and completed this year.

J. S. Steinhart, S. R. Hart, and T. J. Smith of the Department of Terrestrial Magnetism report this year on their regional survey of heat flow from the earth's crust as measured from the bottom of Lake Superior. Working from the U. S. Coast Guard Cutter *Woodrush*, measurements were recorded in 1967 of sediment temperature gradients and thermal conductivities of these sediments at 95 heat-flow sites. The data made available from these measurements made possible the compilation of a regional heat-flow map of

Lake Superior (Fig. 3). Steinhart and his colleagues describe it as a "significant advance in our understanding of regional heat-flow patterns."

The range of heat-flow values found by Steinhart, Hart, and Smith is surprisingly large, varying by a factor of almost three, in some places within very short distances. In general the variations of heat flow in the Lake correlate rather well with the known geologic, gravity, and magnetic features of the Lake bottom and surrounding shores. Volcanic rock areas, for example, are highly magnetic, relatively dense, and have a low heat flow (being low in radioactivity). Using gravity, magnetic, and heat-flow data, Steinhart, Hart, and Smith have constructed a "near-surface" model of the geologic structure of the Lake Superior basin. The model shows relatively thick (10-kilometer) sections of nonmagnetic, moderately dense, and quite radioactive sediments with high heat flow in the central and eastern sections of the lake. The western lake bottom is described as one of non-radioactive, very light, nonmagnetic sediments of lesser thickness (5-kilometer). Such rocks are known on the surface of the Apostle Islands in the western part of the Lake.

The geologic structure model is considered to explain the main features of regional gravity, magnetic and heat-flow variations "in terms consistent with the known or inferred geology." The investigators have found that there is a close relationship between gravity and heat flow in areas dominated by crystalline rocks. Although they recognize that heat-flow variations also are influenced by geological complexities at deeper levels, such as variations in crustal thickness, they consider it reasonable to ascribe most of the heat-flow variations observed on the Lake Superior bottom to variations in the radioactivity of the upper crustal rocks (within 10 kilometers). This study, confirming the hypothesis that relatively dramatic variations in energy flow from the interior of the earth to its surface can occur within a few kilometers, shows that horizontal variations in the crustal structure of the earth, no less than depth variations, are important arbiters of the earth's geophysical features.

Biochemical, Biophysical, and Biological Investigations

In the essay to which I alluded at the beginning of this Review, Alfred Hershey speaks of "the DNA revolution." He remarks that it is "one of a small class of successful scientific revolutions, and should renew significantly our confidence that the structure of the universe is eventually decipherable." Hershey further observes that revelation of the structure of DNA has "set off a numerous and continuing train of successes in the analysis of the living machine."

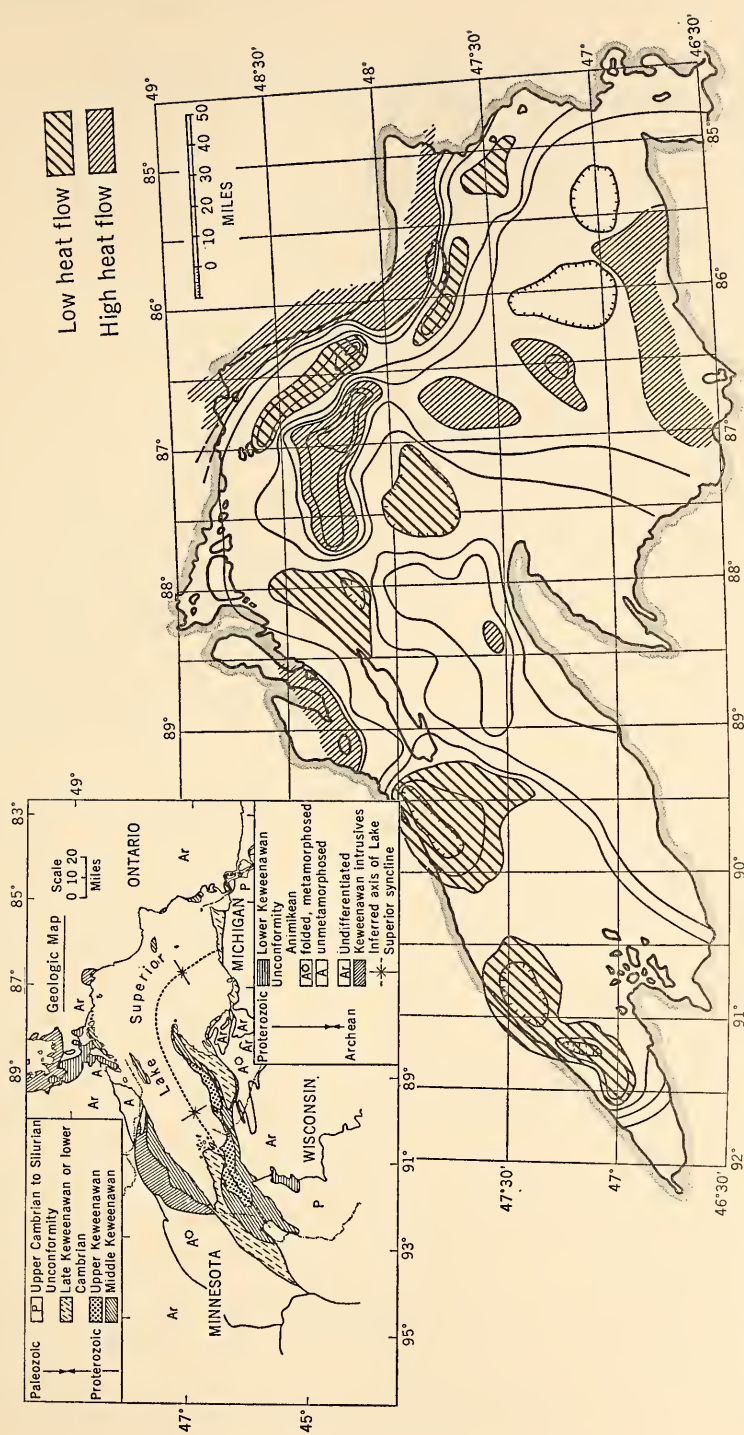


Fig. 3. Completed contour map of the Lake Superior region. Contours are in terms of heat-flow units ($1 \text{ hfu} = 10^{-6} \text{ cal/cm}^2/\text{sec}$). This map represents completion of observations whose progress was reported in the 1967 Report of the President (Figure 5, page 47). Inset: Known geology of the Lake Superior region.

The DNA revolution itself, in the terms of this report, is no longer "new." However, each succeeding year brings forth fresh evidence that the frontal wave of analyses which it started is continuing extremely actively. The impact of this wave, first fully evident on a broad scale in the Institution during our last report year, continued strongly in three of the departments undertaking research on biological problems: Dr. Hershey's own Genetics Research Unit, the Biophysics Section of the Department of Terrestrial Magnetism, and the Department of Embryology.

By far the longest-continued program in the Institution directly focused on the story of DNA is that of the Genetics Research Unit. In the concluding section of his report, entitled "The T4- λ Universe," Hershey gives some elegant insights that bridge a decade of thought and experiment in analyzing the DNA message. T4 and λ , of course, refer to two viruses that are favorite materials for DNA analyses. In his account Hershey begins with the classical Crick-Watson DNA model and from it derives a model structure for T4 DNA, known to be characterized by terminal repetition and circular permutation, attributes not contemplated in the classical model. The complexity of even this simplest of all life forms is disclosed in Hershey's observation that "T4 DNA molecules exist as isomeric systems representing, perhaps, 200,000 permuted structures." On the other hand, λ phage is known in only *one* molecular form. DNA molecules from λ phage particles are all alike.

Centering attention on terminal repetition and permutation, Hershey concludes, "DNA language is not human language and information theory of the message variety is not serviceable for both . . . DNA language is a chemical language obeying special topological rules, rules that are enforced by the special kind of twofold redundancy usually found in its messages." Hershey takes some pains to elaborate this critical difference because the term "redundancy" derives from the theory of open messages, and he considers it inappropriate to DNA language theory. Instead of the term "terminal redundancy" Hershey prefers "joining sequences" (Fig. 4).

After describing the experimental evidence from both T4 and λ phages, Hershey says "The nature of the T4- λ DNA message suggests that DNA replication depends on at least four categories of genetic elements: one or more starting sequences; one or more enzymes . . . directly responsible for DNA synthesis, including something that recognizes starting sequences; joining sequences; and a mechanism for the regeneration of joining sequences from joined sequences." The latter element can be supplied either by a cutting enzyme or by a hypothetical device for measuring lengths of DNA.

Hershey continues with a description of experimental evidence for the starting sequences and joining sequences in λ phage, noting that "in λ clustering of genes of related function is not a principle but a fact." How-

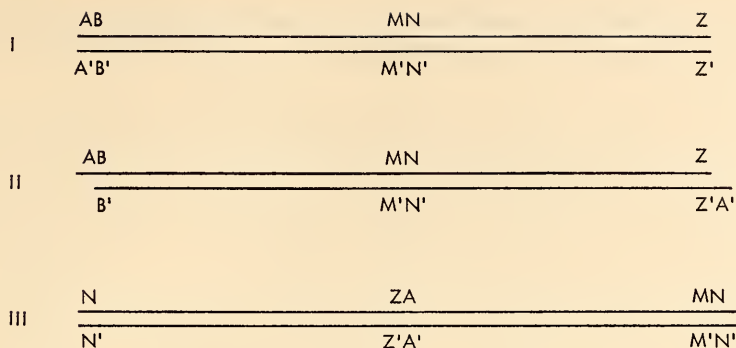


Fig. 4. Alfred Hershey's illustration of DNA "language." Three bihelical DNA molecules are represented as information diagrams. Each letter signifies a nucleotide sequence of arbitrary length. The prime of each letter indicates the corresponding complementary sequence on the second strand of a helix. Structure I conforms to the classic Crick-Watson model, but is not known to exist. It is an open sequence with a twofold redundancy of language in a code of paired complementarity. Structure II contains slightly more information per nucleotide than Structure I, and has the sequence Z' A' which is missing from Structure I. Joining the complementary ends of Structure II results in a closed sequence with exactly twofold redundancy. The extra information in Structure II thus is the potentiality of closure. Structure II does exist, as the DNA of λ phage. Structure III has the same information content as Structure II, but differs in mass to the extent of the additional N and N'. It can also form a closed sequence of exactly twofold redundancy. It differs further from the preceding two structures in sentence order. This illustrates the possibility of permutations, 26 of which would be permitted by the alphabet used in the illustration. Structure III and its cyclic permutations represent T4 DNA, which is characterized by terminal repetition and circular permutation.

Using these illustrations Hershey comments upon the difference between human language and DNA language. "Consider a message A through Z in which sentence Z is a paraphrase of A. Then, for purposes of human communication, we have $A-Z = A-YA = AY$, and Z serves only to minimize errors of transmission. In the language of DNA chemistry, A-Y and A-YA are not equivalent, and open sequences of the type A-Y may well be meaningless. Furthermore, we can write $A-YA = N-YA-N$ for DNA language, a rule implying a degree of independence in the meaning of individual sentences not common in human messages. . . . In short, DNA language is a chemical language obeying special topological rules, rules that are enforced by the special kind of twofold redundancy usually found in its messages."

ever, also "in λ , the joining sequences at the molecular ends form the most obligatory sort of functional unit but are scarcely clustered in the genetic map." He adds his opinion that the clustering of genes is a radical principle in relation to genetic combination, a useful device, but one perhaps seldom exploited in chromosomes at large. Hershey concludes that the radical clustering principle first suggested by R. A. F. Fisher nearly 40 years ago has a conservative counterpart, an "unclustering principle." Referring to evolution, he says that "history is inscrutable to us precisely because, as Pareto noticed some years back, it mixes incompatible principles." Nor should one underestimate the significance of the adventitious in evolution, as when "*E. coli*, in persuading λ to center its joining sequence¹² in the

¹² The adjacent genes on either side of the joining sequence are symmetrical; development may proceed from either side.

prophage map, just made the best of a second-rate opportunity." Hershey's "unclustering principle" may indeed be at least partly dependent on the random event.

Isolation of a Gene Cluster. Another striking illustration of the continuing nature of the DNA revolution is presented this year in the work of David Kohne of the Biophysics Section of the Department of Terrestrial Magnetism. Kohne has actually succeeded in chemically isolating certain genes. He has isolated and purified the nucleotide sequences in DNA that specify the ribosomal RNAs in the bacteria *E. coli* and *Proteus mirabilis*. By coincidence, Kohne treats one example of the genetic phenomenon of clustering to which Hershey referred. In his experiments this year he isolated ribosomal RNA cistrons (clusters composed of several functionally related genes) from the two bacterial species. The RNA cistrons may be regarded as the fraction of the total bacterial cell DNA that codes, that is, carries the message for, the formation of ribosomal RNA. This is believed to be the first instance of the essentially complete purification of deoxyribonucleotide sequences characteristic for any specific gene function.

This isolation of the ribosomal RNA cistron depended on knowledge gained earlier at the Biophysics Section of the reassociation kinetics of bacterial DNA¹³ and on the capability achieved there to separate reassociated DNA from unreassociated DNA. It provides a particularly good example of the extraordinary effectiveness of a combination of intimate knowledge of a difficult technology, painstaking experimental work, and comprehensive imagination.

Kohne's basic procedure may be summarized in two stages. First came the reaction of nonradioactive ribosomal RNA with radioactive DNA under controlled conditions such that very little DNA-DNA reassociation occurred, although all but a small fraction of the DNA complementary to the ribosomal RNA formed rRNA-DNA hybrids. Second came the separation of the reassociated and unreassociated DNA by passing the incubation mixture through an hydroxyapatite column. Under predetermined conditions the rRNA-DNA adsorbs onto the hydroxyapatite while the unreassociated DNA passes on through the column.

By these methods Kohne found that *E. coli* contains about five separate ribosomal RNA cistrons per cell, and *Proteus mirabilis* has about six such cistrons. Thermal stability studies of the reassociated cistrons suggested that the isolated cistrons have a higher guanine-cytosine content than does "bulk" DNA of the whole genome of *E. coli* (about 55 percent as compared to 52 percent). (Fig. 5.) The same appears to be true for *Proteus mirabilis*.

¹³ The recombination in vitro of separate DNA strands into their normal double-stranded configuration.

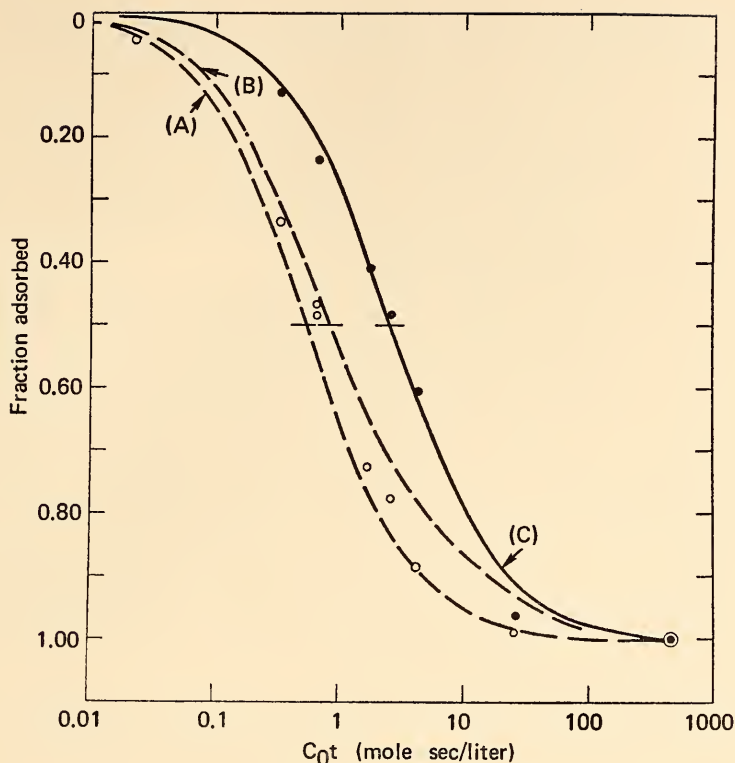


Fig. 5. The reassociation kinetics of a mixture of radioactive *E. coli* rRNA cistrons and *E. coli* unlabeled bulk DNA. C_0t represents the product of the concentration of DNA and the time of incubation (moles of nucleotide \times seconds per liter). Curve C (solid line) is a reaction curve for bulk DNA. Curves A and B are theoretical reaction curves calculated for situations where: A. All the rRNA cistrons are identical; and B. Four of the rRNA cistrons are identical and one is different.

The open circles represent the observed reassociation of rRNA cistrons in David Kohne's experiments to determine the heterogeneity of rRNA cistrons.

The existence of multiple rRNA cistrons in each bacterial cell has raised a question as to the possible heterogeneity of the ribosomal RNA. Isolation of the rRNA cistrons has made it feasible to examine this question of heterogeneity. Further reassociation experiments by Kohne indicate that probably three quarters of the cistrons in *E. coli* and *Proteus mirabilis* are very similar to one another. A high degree of homogeneity therefore appears to exist in the ribosomal RNA gene clusters in these species.

Comparison of the ribosomal RNA cistrons in different species was the next logical problem. Again using similar hybridization techniques, small quantities of radioactive labelled *E. coli* ribosomal RNA cistrons were reassociated with unlabelled DNA from other bacterial species. The species

examined exhibited more than 90 percent relatedness between their ribosomal RNA cistrons as compared to a 4 to 40 percent relatedness between the whole DNAs of the same species. Kohne observes in his *Year Book* report that the ribosomal RNA-cistron relatedness indicates that these cistrons apparently have been "strongly conserved during bacterial evolution and . . . the great majority of nucleotide sequences have diverged at a much faster rate than the rR-cistrons." This confirms independently previous findings of other investigators.

Kohne's experiments clearly demonstrate that the small amounts of repeated nucleotide sequences which are involved in a known physiological function, that of protein synthesis, occur in the bacterial genome. However, it is not yet determined whether all of the member sequences are used in the synthesis. The experiments further show that theoretically any gene may be chemically identified, and that directed "repair" or "engineering" of specific gene structure is not impossibly visionary. Further, the technique developed in these experiments provides a powerful tool for fractionating DNA so as to detect the expression of that DNA during the life cycle of a cell or organism. It may have great usefulness in the study of differential gene expression occurring in developing organisms. I turn next to the Institution's recent work in precisely this field.

Development of the Individual Organism. Inquiry into the modes of development and differentiation of the individual many-celled organism has been a long-term interest within the Institution, having been a continuous part of the program of the Department of Embryology for more than 60 years. Today, in spite of the long history of attention to the subject, "the orderly morphogenesis of the fertilized egg into complex and highly differentiated multicellular organisms" still presents some of the most formidable problems on the frontier of molecular biology.¹⁴ Now that ethologists, or behaviorists, see the need for embarking on "a full program of experimental embryology of behavior,"¹⁵ the prime importance of embryology and developmental biology among the life sciences can no longer be questioned.

The complexity of the highly coordinated processes that ultimately produce a mature organism has been eloquently described in Arthur Koestler's *The Ghost in the Machine*. Koestler reminds us that "it takes fifty-six generations of cells to produce a human being out of a single fertilized egg cell." He enumerates the steps involved: the multiplication of cells, the subsequent growth of daughter-cells, cell specialization, and the shaping of the organism. Developmental mechanisms, Koestler argued, require multilevel analyses.

¹⁴ Gunther S. Stent, "That Was the Molecular Biology That Was," *Science*, 26 April 1968, p. 394.

¹⁵ N. Tinbergen, "On War and Peace in Animals and Man," *Science*, 28 June 1968, p. 1416.

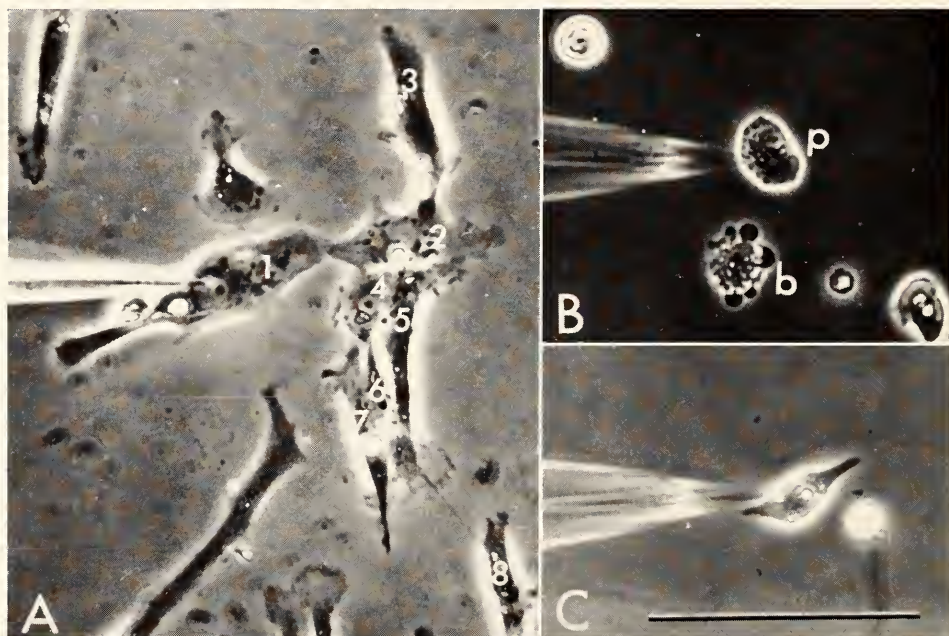


Plate 2. Illustrations of Robert DeHaan's microelectrode recording activity of seven-day chick embryo heart cells that have been 48 hours in culture. Scale equals 100 microns. A. Electrode penetrating a myocardial cell in a group of seven cells in contact. B. Unsuccessful impalements. C. Successfully impaled myocardial cell.

Perhaps the easier and certainly the more popular level for research in our day is the molecular and the cellular. The problems confronting the research worker whose attention focuses on the supracellular levels remain formidable, even though "some reasonable molecular mechanisms for cellular differentiation can at least be *imagined*."¹⁶

One Staff Member of the Department of Embryology, Robert DeHaan, has consistently kept this focus in his research. In a lecture presented at the annual symposium of the Society for Developmental Biology he emphasized that it is necessary to explore the processes of development not only at the molecular level and the levels of supramolecular aggregates, but also at the level of cells and their parts and of tissues if we are ultimately to achieve a real understanding of organogenesis and the emergence of a new individual. In this context, DeHaan has made steady progress on several fronts in his continuing study of the developing heart.

DeHaan and his co-workers have contributed particularly to our understanding of the origins of the heart-forming mesoderm—that is, the location and boundaries of prospective cardiac tissue and to the organization of that tissue within those boundaries. His study has further included investigation of the movements of tissue through which a flat sheet of mesoderm is converted into a primitive tubular heart. It has involved the microanatomy and behavioral properties of embryonic heart cells as seen both in the intact heart and in tissue culture, and the adhesive relations of those cells. Most recently he has been interested in the functional properties and population dynamics of the pacemaking cells, those heart cells which beat spontaneously.

During 1967–1968, DeHaan continued this multilevel approach. Probably the most important event during the year was a technical advance, by which more accurate observation of attributes of the pacemaking cells can be made. DeHaan and Sheldon Gottlieb, an undergraduate student at Johns Hopkins University, succeeded in impaling and electrophysiologically analyzing isolated embryonic heart cells (Plate 2). Their achievement almost certainly will make possible more rapid advance in further study of the origin and characteristics of pacemaker cells.

Often in scientific progress technical advances provide powerful keys to ultimate understanding. Several further accomplishments of this kind at the Department of Embryology during the year illustrate this situation.

Peter Tuft of the University of Edinburgh, who spent the year as a Carnegie Fellow at the Department, achieved a technical innovation that should facilitate significant further advances of knowledge at the levels of cell and tissue. Tuft and B. G. Böving studied the uptake of water by the

¹⁶ Stent, *op. cit.*

rabbit blastocyst, a thin-walled sphere of cells resulting from cleavage that outwardly appear to be undifferentiated. Study of the liquid content of the blastocyst is considered important because the accumulation of fluid in the blastocyst cavity is the stimulus for the equidistant spacing of the blastocytes (undifferentiated cells) and, more generally, because it exemplifies an important feature of embryogenesis. The blastocyst forms the first of a series of relatively large, transient, liquid-filled intercellular cavities arising in embryonic development. The formation of this first cavity is astonishingly rapid. Four days after mating the rabbit blastocyst begins to expand, and within another four days its volume has increased ten-thousandfold. Nearly all of the increase in volume is due to the uptake of water.

Tuft's and Böving's technical advance comprises a modification of existing techniques for determining freezing points, adapting them to the microscale required for studying individual blastocytes. Their technique enabled them to make reliable determinations of the properties of water in the blastocyst and its maternal environment. Their findings demonstrate convincingly that the accumulation of liquid in the blastocyst does not result from a passive flow of water, but requires energy-coupled reactions for its formation.

A majority of the studies at the Department of Embryology were at the molecular level, where technical advances also played an important role during the year. One such advance was the development by Donald Brown, Igor Dawid, and others, of a method of isolating large amounts of ribosomal DNA from bulk DNA.

Brown, Dawid, and their colleagues have shown that the oocytes (early-stage eggs) of five amphibian species as well as those of an echiuroid worm, *Urechis caupo*, contain many extra copies of the genes for the ribosomal RNAs known as 28S and 18S. For example, an oocyte nucleus of the frog *Xenopus laevis* contains about 1000 times as many genes for 28S and 18S ribosomal RNA as does the nucleus of a somatic (body) cell. The oocytes of these animals all synthesize large quantities of ribosomes for storage and the extra gene copies apparently act as templates in this synthesis. The genes are active only in oocytes and no longer function after the first division of the cell (meiosis) and ovulation.

This event is of considerable biological interest because it is so highly specific. Only about 0.1 to 0.2 percent of the germ cell's DNA has been selected for repeated copying. Knowledge of the mechanism of replication therefore is being sought. Alternative hypotheses as to the mechanism postulate changes in the nucleotide sequence of the genes for the ribosomal RNA, subtle cues in the structure of the nucleolar organizer site of the chromosomes, and the involvement of polymerase enzymes.

An important clue may lie in the finding reported this year by Brown, Dawid, and Ronald H. Reeder, a Fellow of the Helen Hay Whitney Founda-

tion, that the extrachromosomal copies of ribosomal DNA (rDNA) are subtly different from the rDNA associated with the chromosomes in somatic cells. The extra copies of rDNA in the germinal vesicle (oocyte nucleus) have a higher buoyant density than somatic-cell DNA. Explaining this difference in buoyant densities is considered of major importance by the Director of the Department, and is the present focus of research interest of the Brown-Dawid group.

Brown, Dawid, and Reeder recently coupled the now-standard cesium chloride technique for obtaining density gradients with an initial precipitation of DNA by means of polylysine. Polylysine precipitates adenine-thymine-rich DNA before DNA rich in guanine-cytosine. More than 90 percent of the bulk DNA from *Xenopus laevis* can be precipitated by polylysine under conditions where at least 50 percent of the rDNA remains in solution. This method has permitted the purification of large amounts of pure rDNA from somatic-cell DNA. Evidence can now be sought (and is being sought) as to why the buoyant densities of the two rDNAs differ.

Two earlier technical advances, that of cloned-cell culture and that of somatic-cell hybridization, were extended and applied effectively in several experiments at the molecular level during the year at the Department of Embryology. Mary Weiss, a Fellow of the U. S. Public Health Service, cooperating with Boris Ephrussi (University of Paris) and L. J. Scaletta (Case Western Reserve University) has studied the nature of the relation between a viral genome and the host cell transformed by that virus. One inquiry has concerned her and her colleagues. Is the tumor virus actually integrated into the genome or does it persist in a cell as an episome-like free particle? An extraordinary—and highly useful—property of hybrid cells is that all the chromosomes of one “parent” may ultimately be eliminated from the descendant hybrid cells. Earlier experiments by Dr. Weiss and H. Green showed that man-mouse hybrid cells in subsequent divisions undergo rapid and extensive segregation of human chromosomes with no accompanying loss of the mouse chromosome of the genome. Taking advantage of this phenomenon, Dr. Weiss transformed human cells by a tumor virus, SV₄₀, and then hybridized these cells with normal mouse cells. After a suitable number of generations, tests for the viral antigen (T) show it to be absent in hybrid cells that have lost most or all of their human chromosomes. This is taken as strong evidence that the viral genome was actually integrated with the human chromosomes of transformed cells.

Two additional technical advances opened new vistas in the techniques of cell culture. In collaboration with Carnegie Fellow H. G. Coon, Dr. Weiss obtained substantial increases in the spontaneous mating rate of hybridizing cell lines by assisting their fusion with inactivated virus. Employing an inactivated Sendai virus and two mouse “L” cell lines known as A9 and

Cl 1 D, Drs. Coon and Weiss found that artificial induction of fusion did indeed assist the formation of these propagating hybrid strains. The same increase in virus-assisted mating rates was observed in combinations of the cell line Cl 1 D and normal rat liver cells, a hybrid that should be of considerable future laboratory interest.

The rat liver cells used for the virus-assisted hybridization themselves represented an important technical advance. They were obtained during the year by Dr. Coon, who cloned liver cells from infant rats to produce in culture typical epithelial pavement cells. Cells which have been serially subcultured show the same characteristics of phase-dense cytoplasm and tightly packed nuclei. Individual cells form colonies upon transfer, and they produce some of the normal serum antigens, but it is not yet known whether or not these subcultured cells are capable of other complex functions of normal liver cells.

Plant Biology

Most of the remaining biological investigations of the Institution concern plants. The Department of Plant Biology is primarily concerned with two aspects of the life of plants. Its interest in the first, experimental taxonomy—the relation of plant speciation and physiology to environment—can be traced to the earliest years of the Institution, having begun in the Desert Laboratory of the Institution at Tucson, Arizona, in 1903. The second is more strongly focused on a single biological process, the fragile, complex, immensely important system of photosynthesis. The biochemical investigations of photosynthesis were commenced at the Institution's Department of Botanical Research at Tucson in 1910. After 58 years of work, the major questions still remain unsolved, and the objective of these investigations remains substantially the same, although, of course, significant progress has been made in the intervening half century.

C. Stacy French, Director of the Department of Plant Biology, discusses some of the reasons for the measured progress that biochemists have experienced in this field and why full understanding of the processes of photosynthesis is yet to come. Dr. French says, "As the basic questions about (photosynthesis) became more clearly formulated the more easily definable problems were taken up by chemists and physicists, usually with the expectation of a quick breakthrough from the application of their more sharply defined methods of experimentation and interpretation. . . . We seem to have passed through the period of naïveté in the application of the more rigorous disciplines to biological problems. Rather than being considered a limitation on precise experimentation the diversity of species and of physiological states of living plants is now being exploited. . . . Excellence of

chemical and physical procedures combined with weak biology, or the converse situation, is no longer a characteristic of our subject." Dr. French may take a certain amount of satisfaction in the trend that he has reported for his field, because few research groups concerned with photosynthesis elsewhere in the world have so consistently supported biophysical-biochemical research and physiological-environmental studies side by side as has his own.

Research during the year at the Department of Plant Biology also illustrated vividly, once again, the influence of technical advances upon research results. The model of the photosynthetic mechanism that is gradually evolving still has many uncertainties because the components of the systems concerned have not been isolated in vitro in their natural, functional form. One of the more pressing problems involving the isolating of components is that of separating the parts of chloroplasts that drive the distinct yet highly interrelated photochemical reactions. Detergents like Triton X-100 and digitonin have been widely used to obtain chloroplast fractions for experiment. Although the detergents greatly facilitate the separation of the fractions, they have the disadvantage of becoming incorporated in the fraction isolated and may damage the activity of the isolated pigment and bias the experimental measurement of the activity.

This year Jean-Marie Michel and Marie-Rose Michel-Wolwertz, Fellows at the Department, devised a procedure for separating chloroplast fractions that avoids the use of detergents. Their method uses a needle-valve homogenizer developed at the Department in 1950 with a buffered salt solution, followed by centrifugation in a sucrose concentration gradient. The Michels' method was tested on both spinach chloroplasts and those of *Chlorella pyrenoidosa*. Tests made of the absorption spectra and activities of the three fractions obtained in this way showed that the first (low-density) fraction displayed photosynthetic activity and spectral characteristics of the component known as system 1, as previously identified from action spectra of live plants. The two "heavier" fractions showed absorption spectra and photochemical characteristics of the component known as system 2. Thus, the method has been shown to separate the two principal postulated systems of the photosynthetic process.

By coincidence, a natural plastome mutant fractionation of the two photochemical systems was discovered by Ulrich Heber, a Carnegie Corporation Fellow, in mutant leaves of the evening primrose, *Oenothera*. Some of the leaves Professor Heber found to have only system 1 functioning, whereas others had only system 2 activity. Chloroplast particles from mutant system 1 leaves were found to have similar absorption spectra to those of the system 1 fractions isolated from spinach or *Chlorella*. The chloroplasts of the mutant system 2 leaves resemble the system 2 fraction

from normal plants in photochemical and spectral properties. The detection and analysis of these mutants emphasizes Dr. French's comment about the combination of biochemistry and biology that now characterizes research on photosynthesis.

Action and absorbance spectra are important means of measuring and identifying activity in the photosynthetic system. Their correct interpretation is an enduring problem in photosynthesis research. The curves which record the spectra are always composites, and the correlation of elements in the shapes of the curves with postulated components of the system has been an important source of the understanding thus far achieved about the mechanism of photosynthesis.

This year the Department experimented with a new means of analyzing spectral curves. For the first time a digital computer was employed in this task. This was made possible by the installation of a cable connection between the Department and the Computation center of Stanford University. French, J. S. Brown, L. Prager, and M. Lawrence describe in the Department's report their first efforts at analyzing by computer the spectra of natural chlorophyll complexes. Curve analysis may show that evidence previously assumed to be indicative of an individual chlorophyll component may in fact represent only variations in bandwidth of chlorophyll components having the same peak wavelengths. This appears to be true, for instance, for spectral differences between the low-density and high-density *Chlorella* fractions obtained by the Michels' new method.

On the other hand, curve analysis may also suggest the existence of hitherto unrecognized components. Such may be the case for the absorbance spectrum of the mutant system 1 *Oenothera* leaves described above. The original absorbance curves and the computer analysis of the curve are shown in Figure 6. The wide "tail" of the original absorbance curve may be due to a component having a 708-nm (7080 angstroms) peak. French and his colleagues state, however, that the accuracy of the records is not yet sufficient to do more than suggest the presence of such a long wavelength component. Nonetheless, it is obvious that the new method of spectral curve analysis is promising enough to contribute to the objective described by Dr. French in the Introduction to his report: "To find out how many . . . forms of chlorophyll exist, (and) which of them are part of the two photochemical systems of photosynthesis."

The intricacies of identifying portions of even one set of the components of the photosynthetic system are well illustrated by questions involving the yellow pigments known as carotenoids. All photosynthesizing plants contain carotenoids, and a variety of answers have been proposed as to their functions. Some, but not all, of the carotenoids may be light absorbers, passing on their absorbed energy to chlorophyll. They are thought also to act as

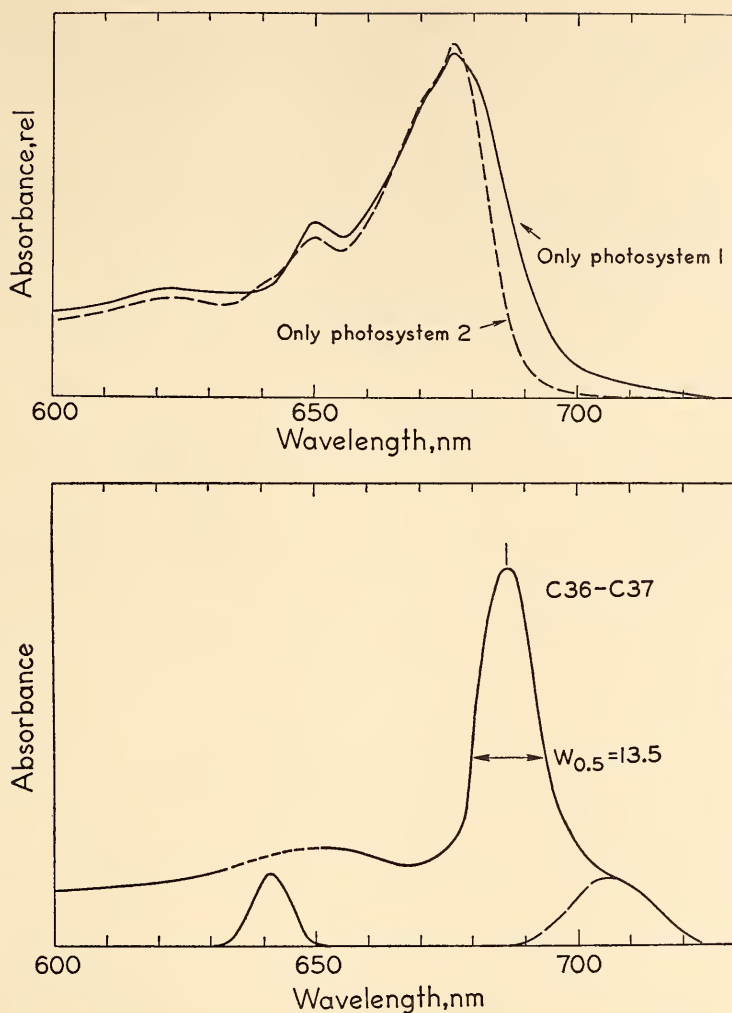


Fig. 6. The upper diagram gives the absorption spectra measured at 77° K for chloroplast particles isolated for *Oenothera* (primrose) mutants having only photosystem 1 or photosystem 2 activity. The lower diagram indicates the possible additional components in photosystem 1 missing from photosystem 2.

internal light filters, protecting chlorophyll from bleaching, and to participate in the oxygen-evolving step of photosynthesis. Extending a study begun earlier, David Fork continued the study of carotenoid responses in the yellow-green alga, *Botrydiopsis*, which lacks chlorophyll *b*, a pigment that interferes with the measurement of carotenoid changes. Dr. Fork found in experiments that activation of either system 1 or system 2 of this alga gave identical changes in the carotenoids. He found that the changes were in the

same direction regardless of which of the two photosystems was activated. He concludes that the same carotenoid pigment is modified by both of the photosystems, and that it is not a link between the two main photochemical reactions.

Experimental Taxonomy. For many years the experimental taxonomy group in the Department of Plant Biology has studied the effects of climatic and atmospheric differences dependent on altitude and latitude, concentrating particularly on an examination of covariance with altitude of species and race characteristics in the monkey flower, *Mimulus*. The investigation has involved the comparative examination of a number of physical and physiological characteristics in hybrid progenies from a number of contrasting forms of *Mimulus*, growing in very different altitudinal environments.

Extensive study of 16 genetic markers that distinguish the parent races used in the *Mimulus* hybrids has been carried out on thousands of plants over a 20-year period. They have shown that ability to survive in specific environments is correlated to a significant degree with certain combinations of morphological characteristics. These characteristics can be recognized as early as the third generation of progeny among the hybrids. The third generation hybrids, indeed, begin to approach the status of recognizable ecological races.

An illustration of the versatility of *Mimulus* as a botanical research material is provided in the report by W. M. Hiesey, M. A. Nobs and O. Björkman on photosynthesis in an amphiploid *Mimulus*. They note that amphiploidy (the inheritance of *all* chromosomes from two parent species) has played an important evolutionary role in the synthesis of new species from ancestral forms of restricted ecological or geographical distribution. Such species frequently are successful in invading new environments not occupied by the parent species. Measurements of the photosynthetic rates of *M. lewisii* from 10,500 feet elevation in the Sierra Nevada of California and of *M. nelsonii* from Mexico with that of their amphiploid descendants showed that the amphiploid had an equal or higher rate of photosynthesis than its parents at lower temperatures (22°C or below). On the other hand, the rate at higher temperatures (38°C) was a third or less that of either of its parents. Hiesey, Nobs, and Björkman consider the measurements significant in that a combination genome of two species occurring through amphiploidy appears to have the capacity of notably altering some basic physiological functions.

Björkman, E. Gauth, Hiesey, and Nobs also report on the beginning of a study designed to compare photosynthetic responses of plants from widely contrasting latitudes. As their material they chose the liverwort *Marchantia polymorpha*, one of the simplest of green plants. It ranges from

the arctic polar regions to the equator, and its relatively simple structure favors studies of its photosynthesis in vivo. Dr. Björkman developed during the year a rapid method of measuring photosynthetic rates in liverwort tissue by means of an oxygen electrode. Björkman's method makes possible study in vivo of variations in photosynthetic activity, including those resulting from rapid changes of temperature, light intensity, and other causes.

During the summer of 1968 Björkman and Gauhl collected *Marchantia* specimens from the Point Barrow area of Alaska as well as from California. Laboratory study of the effects of temperature and oxygen concentration levels on photosynthesis in California specimens of *Marchantia* was commenced during the year.

Dr. Björkman plans to compare the properties of some selected enzymes known to be of key importance in the metabolism of green plants among the three general types of *Marchantia*. One of these enzymes is carboxydismutase (ribulose-1, 5-diphosphate carboxylase), whose activity Björkman studied during the year in goldenrod (*Solidago*), plantain (*Plantago*), and other species. His studies were directed toward a comparison of species normally growing in shade with those normally growing in full sunlight. They demonstrated quite strikingly the much higher carboxydismutase activity in the plants adapted to full sunlight. Björkman is now developing methods for preparing extracts of this and other enzymes, like phosphoribulokinase, and citrate synthase, the condensing enzyme, from *Marchantia* tissues.

These studies would seem to have the potentiality of carrying investigations of ecology and of speciation to a new level of biochemical refinement, demonstrating further Dr. French's comment that biochemistry and biology are now achieving an increasingly effective working relationship.

Observations on Nervous System and Brain Function

It is appropriate to end this discussion of the year's activities with the mention of a field comparatively new for the Institution. Gunther Stent recently observed, "There now seems to remain only one major frontier of biological inquiry for which reasonable molecular mechanisms still cannot be even imagined: the higher nervous system. Its fantastic attributes continue to pose a problem as hopelessly difficult and intractably complex as the hereditary mechanism did a generation ago."¹⁷

For several years, with the aid of the Carnegie Corporation, the Institution has sponsored a modest number of fellowships for study of this most fascinating, most difficult, and perhaps most important of all biological fields. Such fellowships have been held by both senior and postdoctoral

¹⁷ Stent, *op. cit.*, p. 395.

research workers at McGill University, Johns Hopkins University, the National Physical Laboratory (Teddington, England), and the University of Sussex. For a longer period Dr. Richard B. Roberts, working in the Biophysics Section of the Department of Terrestrial Magnetism, has been collaborating with Drs. L. B. and J. B. Flexner at the University of Pennsylvania in an experimental program in this general field.

Already the fellowships have produced some significant accretions to our knowledge of the functioning of nervous systems. Such was Dr. Thomas B. Mulholland's discovery of the relation of the alpha rhythm in the brain to the oculomotor function during his tenure as a Carnegie Fellow at the National Physical Laboratory in 1964-1965. This discovery called into question the use of the alpha rhythm as a measure of alertness. The significance of the discovery was attested at the International Conference on Attention in Neurophysiology conducted at Teddington on October 3-5, 1967, with the partial support of the Institution. It was described by one of the principal participants, Dr. H. H. Jasper of Montreal, as a landmark in the field.

Dr. Roberts and his colleague, A. V. Rake, report in this *Year Book* on their long-term studies of the mechanisms of memory in the brain. Roberts and Rake report that there appear to be three forms of memory: a long-term memory persisting over the lifetime of an individual, having a basis similar to inherited behavior patterns and requiring protein synthesis for formation and maintenance; a very short-term memory of some seconds duration, probably based on electrical reverberation, and erasable with electroconvulsive shock; and an intermediate-term memory of several hours duration, postulated to have a nonprotein chemical basis, but capable of surviving electroconvulsive shock. Drs. Roberts and Rake suggest that the latter two forms of memory, the very short-term and the intermediate-term, together make up a system having different properties from those exhibited by either type operating alone. The combination of the two types they designate as short-term memory.

They postulate a model of short-term memory in which an initial burst of reverberation causes chemical changes that facilitate further reverberation and greater chemical change. The reverberation is then quenched by inhibition of the cells concerned. Chemical tracers would decay during the periods of quenching. A succeeding burst of reverberation would restore or increase the chemical trace. Duration of short-term memory therefore would depend on both the initial strength of the chemical trace and on the frequency of bursts of reverberation.

Experiments on laboratory mice during the year by Roberts and Rake were directed toward: (1) observation of biochemical changes correlated with learning; and (2) attempts to affect learning and memory by drug

injection. All experiments directed toward observing biochemical correlates of learning in live animals had negative results. Attention therefore was shifted to cell culture of neurons, which is now in progress. Experiments on the behavioral effects of drugs were more promising. Injection with cycloheximide (a protein synthesis inhibitor) and pentobarbitol (a depressant or reverberation inhibitor) produced severe memory impairment, although neither drug alone showed such an effect. Although Roberts and Rake do not regard their results as conclusive they hope that this kind of experimental approach ultimately may give some indication of the duration of short-term memory and the time required for the establishment of a protein-based long-term memory.

This year the Institution was favored at its Annual Trustees' Lecture on May 3, 1968, by a report from one of the most imaginative of the students of nervous system function, Professor Donald MacKay of the University of Keele in England. MacKay chose to discuss the eventual impact upon the personal aspect of human nature of "mechanical" answers from investigations like those reported by Roberts and Rake. As Dr. MacKay put it, "What status would be left to our conscious experience in a mechanistic scheme of brain function?"

Stent, in the *Science* article published the week prior to Dr. MacKay's lecture, raised essentially the same question: "... the higher nervous system does ... present the most ancient and best-known paradoxes in the history of human thought: the relation of mind to matter, or of free will to determinism."¹⁸ Stent believes that the old question has renewed scientific importance because "increasing numbers of veteran molecular biologists of the informational ... school are now turning toward the nervous system ... But it is also possible that study of the nervous system is bringing us to the limits of human understanding, in that the brain may not be capable ... of providing an explanation for itself ... there exist processes which, though they clearly obey the laws of physics, can *never* be explained."¹⁹

Professor MacKay remarked: "... even though our brains were as mechanical as clockwork we, as we know one another as individuals, are in a certain essential sense, indeterminate and free. ... trying to link experience onto brain mechanism as if it were a kind of additional invisible extra cause, is rather like trying to find room for the equation being solved by a computer in the electronic theory of its workings. ... The mystery of our being doesn't consist in the mechanical inexplicability of our brains. ..."

Here indeed is a new frontier for scientific investigation, with significant problems, as Lord Adrian said at the Conference on Attention in Neurophysiology, sufficient for centuries.

¹⁸ *Ibid.*

¹⁹ *Ibid.*

Losses . . .

It is with a sense of deep personal loss, and an even greater sense of the loss to the Institution, that I record here the death of Seeley Greenleaf Mudd, a Trustee and great friend of the Institution. In his passing, in Pasadena on March 10, 1968, at the age of 73, the Institution lost a wise leader and counselor.

There are men who lift the age they inhabit so that all men walk on higher ground. Dr. Mudd was surely one of these. Generous, resourceful, humane, a man of limitless energy and dedication, he inspired all who knew him.

Dr. Mudd became a Trustee of the Institution in 1940 and remained on its Board until his death. As a member of the Astronomy Committee, he was very active in the affairs of the Mount Wilson and Palomar Observatories. As a Trustee also of the California Institute of Technology, he forged notable links between the two institutions that jointly operate the Observatories.

Dr. Mudd also was a Trustee of Pomona College, of Stanford University, the University of Southern California, and the National Fund for Medical Education. He served as physician, scholar, educator, advisor to governments and institutions. As a student, he first enrolled at Stanford University, later transferring to Columbia, where he received a B.S. degree in 1917. He received the M.D. from Harvard in 1924 and after completing house officership at Massachusetts General Hospital, entered practice in cardiology in Los Angeles. He was an associate in cancer research at the California Institute of Technology from 1931 to 1935, and from 1935 to 1945 he was professor of radiation therapy at the same institution. From 1941 to 1943 he served as dean of the medical school at the University of Southern California.

Dr. Mudd was a Diplomate of the American Board of Internists, a member of the Aesculapian Club, the Los Angeles Academy of Medicine, the National Research Council Advisory Committee on Aviation Medicine (1942-1945), the Pacific Interurban Clinical Club, the Radiological Society of North America, and the American Heart Association. He was also Director of the Finney-Howell Research Foundation in Baltimore from 1936 to 1946, and later Director of the Good Hope Hospital Association of Los Angeles. To these many organizations, as to the Carnegie Institution, he gave his services unstintingly. All of us who knew him and worked with him will miss him deeply.

The year has been further saddened by the passing of several scientists who had made indispensable contributions to the professional life of the Institution.

On April 8, 1968, the Institution lost Dr. Harold D. Babcock. He had served as a Staff Member of the Mount Wilson and Palomar Observatories for almost 40 years (1909-1948). A solar physicist of the highest distinction, he was a pioneer, with George Ellery Hale, in solar research. Among his many published contributions, his authorship, with others, of *Revision of Rowland's Preliminary Table of Solar Spectrum Wave-Lengths, with an Extension to the Present Limit of the Infra-Red*, and, with Charlotte E. Moore of *The Solar Spectrum λ 6600 to λ 13495* may be especially noted. His life and work provided an outstanding chapter in the research history of the Institution. His son, Dr. Horace W. Babcock, is currently Director of the Observatories.

Dr. Robert B. Sosman, who worked as a physicist and served as Assistant Director at the Geophysical Laboratory from 1908 to 1928, died on October 30, 1967. He was a pioneer in American ceramics and in 1953 won the Albert Victor Bleining Award, the highest honor a ceramicist can receive. In 1937 Dr. Sosman served as President of the American Ceramic Society. Co-ordinator of the Day and Sosman high-temperature scale, he was the author of the definitive study *The Properties of Silica*.

Dr. Carl G. Hartman, a Staff Member at the Department of Embryology from 1925 to 1941, died on March 5, 1968, at the age of 88. A biologist whose discoveries in embryology helped develop the principles of birth control, Dr. Hartman will long be remembered for his work and his personal contribution to the Institution.

Another long-time associate in the Department of Embryology, Dr. George W. Bartelmez, author of many of the articles in the well-known series *Contributions to Embryology*, also died this year. Dr. Bartelmez' remarkable career encompassed two major areas in embryology: the development of the reproductive tract, and the development of the embryonic nervous system. In the latter area he laid the groundwork for what is clearly emerging as a major field of study.

Miss Henrietta Swope, a Research Fellow at the Mount Wilson and Palomar Observatories since 1952, formally completed a most distinguished career with the Institution this year. At its April meeting the American Astronomical Society announced the presentation of the Annie Jump Cannon Award to Miss Swope. The award commemorates the Harvard astronomer Annie Jump Cannon, herself a renowned investigator of variable stars.

A devoted friend of the Observatories, Miss Swope studied numerous cepheid variable stars in several dwarf galaxies and in M 31, the great

Andromeda Galaxy. Her precise and detailed investigation of the periods, amplitudes and colors of these variable stars led to calibration of the distance moduli of the galaxies in which they occur. One of her most significant contributions was the calibration—the most accurate to date—of the distance of the Andromeda Galaxy. This measurement has become the “celestial yardstick” by which other distances in the universe are calculated.

Dr. Anna O. Shepard, a most distinguished Staff Member in the former Department of Archaeology, retires this year. Since the formal closing of the Department in 1958, she has served as a special research associate. She holds a unique position in archaeology as a ceramics technologist, and is the author of many authoritative works on this subject, which she has pioneered. Her book *Ceramics for the Archaeologist* is a classic.

Dr. David W. Bishop, a Staff Member of the Department of Embryology since 1952, also retires this year. A specialist in human reproductive systems and spermatology, Dr. Bishop did much pioneering work at the Department.

. . . and Gains

In the year just past, the Institution has been particularly fortunate in gaining three new Trustees of great experience and reputation, all elected to the Board on May 3, 1968. Michael Ference, Jr., Robert Morgan Pennoyer, and William Matson Roth are our newly elected Board Members.

Michael Ference, Jr., was born in Whiting, Indiana, in 1911. He received his B.S. degree in 1933 from the University of Chicago. After obtaining his Ph.D. from the same institution in 1936, Dr. Ference became a teacher of physics at the University. During the war he served as civilian consultant to the Air Force. After spending some years with the Signal Corps England Laboratories, first as Chief Scientist, then as Technical Director, in 1953 Dr. Ference entered his present association with the Ford Motor Company, as Chief Scientist. He served successively as Associate Director, Director, and Executive Director, and since 1958 has been Vice-President of Research for the Ford Motor Company.

Dr. Ference is a member of the President's Science Advisory Committee, and the National Academy of Sciences. He is a Trustee of the RAND Corporation, the Argonne Universities Association and Case Western Reserve University, a member of the Board of Governors of Wayne State University, and a member of the Governor's Scientific Advisory Board of

Michigan. He is also an advisor to the Group Weather Modification Committee of the National Science Foundation, and a member of the Research and Development Advisory Council.

Robert Morgan Pennoyer was born in New York City in 1925. After receiving his undergraduate education at Harvard College and serving two years in the U. S. Naval Reserve, he studied law at Columbia University. In 1951 he was admitted to the New York State Bar. He was associated with the law firm of Davis Polk, Wardell, Sunderland & Kiendl in New York City until 1953, when he became Assistant U. S. Attorney for the Southern District of New York. Two years later he joined the staff of the Office of the Secretary of Defense. Since 1958 Mr. Pennoyer has been Associate, then Partner, in the firm of Patterson, Belknap & Webb in New York City.

His trusteeships include the Union Theological Seminary, the Metropolitan Museum of Art, and the American Place Theatre. He serves on the Board of Visitors of Columbia Law School, and is a member of the Council on Foreign Relations, Inc., and a director of the Association of Harvard Alumni.

William Matson Roth was born in San Francisco in 1916. He was graduated from Yale University in 1939. In 1947 he became associated with the Barber Oil Company, and the following year joined the Honolulu Oil Corporation, of which he is now a member of the Board of Directors. Mr. Roth has been Vice-President of Finance, and Director of the Matson Navigation Company and Subsidiaries in San Francisco, and Chairman of the Board of the Pacific National Life Assurance Company. In 1963 he became Deputy Special Representative for Trade Negotiations for the U. S. Government. At present he is serving the Federal Government as Ambassador Without Portfolio, in the capacity of Special Representative for Trade Negotiations.

Mr. Roth has been a Trustee of the Committee for Economic Development, and a Regent of the University of California.

It gives me the greatest pleasure to record the following honors which have come to Staff Members of the Institution during the past year.

Dr. Barbara McClintock, Distinguished Service Member of the Genetics Research Unit, was awarded the honorary degree of Doctor of Science by the University of Missouri for "distinguished service and leadership in research and education."

Dr. Philip H. Abelson, Director of the Geophysical Laboratory, received the honorary degree of Doctor of Humane Letters from the University of Puget Sound.

Dr. Horace W. Babcock, Director of the Mount Wilson and Palomar Observatories, was elected a corresponding member of the Société Royale des Sciences de Liège.

Dr. James D. Ebert of the Department of Embryology was elected to membership on the Board of Directors of Oak Ridge Associated Universities. He was invited to deliver a National Institutes of Health Lecture, and, in addition, offered a series of E. B. Wilson Lectures at the University of Texas and gave the Yamagiwa Memorial Lecture at the Cancer Institute of Tokyo.

Dr. Allan R. Sandage of the Mount Wilson and Palomar Observatories was elected to the Organizing Committee of the Commission Scientifique de Physique des Instituts Internationaux, Solvay. He gave the Halley Lecture at Oxford University and spoke on radio galaxies and quasars to the International Astronomical Union in August 1967. At a meeting of the Rittenhouse Society honoring his studies on cosmology and his work on such recently discovered cosmic objects as quasars, Dr. Sandage was given the Rittenhouse Medal.

Dr. William M. Hiesey of the Department of Plant Biology was awarded the Certificate of Merit of the Botanical Society of America "in recognition of distinguished achievement in and contributions to the advancement of botanical science. Ecological physiologist, . . . a pioneer in elucidating the genecological nature of species; he has done much to encourage and help students in all areas of plant science."

Dr. Felix Chayes of the Geophysical Laboratory served as President of the Mineralogical Society of America during the year 1967-1968.

Dr. Robert Howard of the Mount Wilson and Palomar Observatories with Dr. V. Bumba of the Ondrejov Observatory received the Astronomy Prize from the Czechoslovak Academy of Sciences in November 1967 for their work on large-scale magnetic fields.

Dr. Olle Björkman of the Department of Plant Biology was awarded the degree of Doctor of Philosophy "with great distinction" at the University of Uppsala in December 1967. This degree is awarded only to outstanding scholars, and confers the title of Member of the Faculty at the University of Uppsala.

Reports of Departments and Special Studies

Mount Wilson and Palomar Observatories

Geophysical Laboratory

Department of Terrestrial Magnetism

Committee on Image Tubes for Telescopes

Department of Embryology

Department of Plant Biology

Genetics Research Unit

Mount Wilson and Palomar Observatories

Operated by Carnegie Institution of Washington
and California Institute of Technology

Pasadena, California

Horace W. Babcock
Director

OBSERVATORY COMMITTEE

Horace W. Babcock
Chairman

Carl D. Anderson

Jesse L. Greenstein

Robert B. Leighton

Allan R. Sandage

Olin C. Wilson

Contents

Introduction	7	Classification system for galactic globular clusters	30
Observing Conditions	9	Interstellar Gas and Gaseous Nebulae .	30
Physics of the Sun	9	Interstellar absorption lines	30
Large-scale solar magnetic fields .	9	Orion nebula	31
Magnetograms	10	Planetary nebulae	32
Active regions	10	Crab nebula	32
H α filaments and magnetic fields .	11	Infrared Sky Survey	33
Studies of velocity fields on the solar surface	11	Observational Cosmology	33
The solar cycle	12	New determination of the Hubble constant	33
Solar activity	12	New values for the redshift <i>K</i> -cor- rection	34
K-line cinematography	13	Galaxies	34
Extreme ultraviolet	13	Distance to the Virgo cluster . .	34
Composition of the solar photosphere.	14	Galaxies in groups	35
Coronal physics	14	Association of galaxies and radio sources	36
Forbidden lines in the Fraunhofer spectrum	15	Markarian blue galaxies	36
Planets and the Moon	16	Seyfert galaxies	36
Mars	16	Infrared observations	36
Jupiter	16	Dwarf systems	36
Satellites of Jupiter	16	Polarization	36
Planetary photography	17	Radio galaxies	37
Stellar Spectroscopy and Photometry .	17	Radio observations of peculiar galaxies	37
White dwarfs	17	Catalog of galaxies and of clusters of galaxies	38
Dwarf Me stars	18	Compact galaxies	38
Model atmospheres of M-dwarf stars	18	Clusters of compact galaxies . . .	39
Spectroscopy and photometry of cool stars	19	Sizes of rich clusters of galaxies .	40
Temperature, gravity, and mass of τ Herculis, Vega, and Sirius . .	19	Area of the sky covered by clusters of galaxies	40
Early-type main-sequence stars .	19	The Galaxy	40
Faint blue stars	20	Supernovae	41
Spectroscopic binaries	20	Absolute magnitudes	41
Peculiar A stars	21	Frequency	41
Variable stars	21	Photometry and light curves . .	41
Measurements of H and K flux . .	22	Spectra	42
Infrared scanning	23	Pulsating Radio Sources	42
Classification	23	X-Ray Sources	43
Blue stragglers	24	Scorpius X-1	43
Stellar composition	24	Cygnus X-2	44
He ³ in magnetic stars	26	Quasi-Stellar Sources	45
Absolute Spectrophotometry	26	Spectroscopic observations . . .	45
Star Clusters	27	Radio-quiet quasars and white dwarfs.	45
Gaps in the giant branch of M 15 .	27	Optical variations of quasars and N-type galaxies	46
M 92	27	Spectral energy distribution . . .	47
M 69	27	Polarization	47
NGC 6553	28	Parkes source 0237-23	48
NGC 6171	28	Source 3C 287	48
NGC 6981	28		
NGC 7099	29		
Blue stars	29		
R associations	29		
Praesepe cluster	29		

Theoretical Studies	49	Polarimeter	59
Stability of rotating systems	49	60-inch photometric telescope . .	59
Dissociation equilibrium of H^- . .	50	Modification of Mount Wilson	
Nonthermal radiation	50	60-inch telescope	60
Variations of extragalactic sources .	50	Solar instrumentation	60
Guest Investigators	51	Robinson solar telescope	60
Astroelectronics Laboratory	56	Photoheliograph for Apollo . . .	61
200-inch data system	56	Photographic Laboratory	61
Other data systems	57	Site Investigation	62
General laboratory projects	58	Chile	62
Instrumentation	58	Big Bear solar observatory . . .	62
Optical design	58	Bibliography	63
Image-tube spectrograph	58	Staff and Organization	68
Multichannel spectrometer	58		

INTRODUCTION

This year marks the centenary of the birth of George Ellery Hale, founder of the Kenwood, Yerkes, Mount Wilson and Palomar Observatories. It is also the 60th anniversary of his discovery of the magnetic field of sunspots. A unique figure in science, Hale, with his extraordinary imagination, insight, and organizational ability is responsible, more than any other individual, for the great advances in astronomy that we are privileged to see in the 20th century. Innovator and builder of great telescopes—the Yerkes 40-inch refractor (1897), the Mount Wilson 60-inch (1908) and 100-inch reflectors (1918), and the 200-inch on Palomar Mountain (1948), each the largest of its time—Hale also set goals that inspired and guided his co-workers and his followers. It is fortunate that the story of Hale's life is now readily available through the recent biography, *Explorer of the Universe*, by Helen Wright (1966).

Hale wrote in 1905, "The prime object of the [Mount Wilson] Solar Observatory is to apply new instruments and methods of research in a study of the physical elements of the problem of stellar evolution."

As Harold Zirin has said, "Only a profound mind could produce such a goal for a solar observatory; only such goals and programs, coupled with Hale's talents, could make it successful."

How gratified Hale would have been as a result of the action of the Trustees of the Carnegie Institution this year in approving the establishment of a major new observatory to be located in central Chile, and how enthusiastic about the expanded goals of the Mount Wilson and Palomar Observatories, whose instruments, with new methods of research, are now applied in a study of the physical elements and evolution of the universe itself.

The quasi-stellar sources (quasars) retain a position in the front rank of interest and attention notwithstanding the challenges raised by X-ray stars and the newly discovered pulsating radio sources. Among the recently identified quasars observed spectroscopically by Maarten Schmidt in the year just past is 4C 25.5. This is a blue object, starlike in appearance, of visual magnitude about 17.5. Two broad emission lines in its spectrum at $\lambda 4082$ and $\lambda 5200$ are identified by Schmidt as Lyman α of hydrogen ($\lambda_0 = 1215$) and λ_0 1549 of triply ionized carbon. The redshift $(\lambda - \lambda_0)/\lambda_0$ is 2.358, the largest so far observed. An unusual feature is the appearance of absorption lines on the longward side of the corresponding emission lines; the absorption lines have a redshift of 2.3683, indicating that the absorbing material is moving toward the emitting parts of the source at about 900 km/sec.

The quasar with the richest known spectrum and the sharpest lines is Parkes 0237-23. Greenstein and Sargent, analyzing an excellent spectrogram made with the 200-inch telescope, have compiled a very selected list of 49 absorption lines for most of which they have measured equivalent widths, half-widths, and central depths. Using a systematic identification procedure devised by Professor John Bahcall, the three investigators found that it was necessary to segregate the absorption lines into five separate sets characterized by different redshifts: 2.2015, 1.6706, 1.6560, 1.5132, and 1.2642. The authors conclude that it is at present impossible to decide whether the lines arise in intergalactic space, in galaxies in the line of sight, or in clouds that have been expelled from the object and are moving at speeds up to 0.3 c relative to the source of the emission lines.

Additional confirmation of the optical

variation of quasars on a time scale of days has been made. Such rapid fluctuations of the nonthermal radiation (continuous emission not attributable to stars) constitute one of the phenomena that have been cited by some who hold that quasars are at the "local" and not the "cosmological" distances indicated by their redshifts. This argument against the cosmological distance scale for quasars has fallen, for it has been found independently by both Sandage and Oke that certain N-type galaxies (specifically 3C 371) changed by a factor of nearly 2 in optical intensity in a little over a year. It is generally conceded that N-type galaxies, like others, are at distances represented by their redshifts in the conventional Hubble diagram.

Another strong argument for cosmological distances of quasars has emerged from the recent estimates of the great number of the radio-quiet quasars and the rate at which the number increases to fainter limits. Sandage has been able to arrive at a first tentative estimate of the number of radio-quiet quasars per square degree to three increasingly faint levels of apparent magnitude. Based on photometry with the 200-inch telescope of a field centered on Selected Area 57 and on earlier work, it is estimated that there are 0.4 radio-quiet quasars per square degree to a limit $B=18.1$ (apparent magnitude in blue light), 5 per square degree to $B=18.5$, and 100 per square degree to $B=21.5$. These figures suggest that the number of quasars over the whole sky to $B=22$ is very large, probably approaching 10^7 . Sandage believes that such a large number of objects having either a constant space density or a positive density gradient outward eliminates the local hypothesis for quasar distances.

It was early in 1968 that a group of Cambridge radio astronomers headed by Dr. A. R. Hewish announced the discovery of four rapidly pulsating radio sources of remarkably stable frequency of the order of 1 second. The radio posi-

tion of one of these "pulsars," CP 1919, is close to a relatively conspicuous optical object that was suggested by Ryle and Bailey as a possible candidate for identification.

Astronomers at Mount Wilson and Palomar, as at many other observatories, immediately started efforts at optical identification, but no peculiar objects are found near the radio positions of three of the pulsars, and for CP 1919 careful observations with the 200-inch telescope by Kristian, Sandage, Schmidt, Snellen, and Westphal, using the digital data recording and harmonic analysis, yielded no evidence of optical pulsation of the suggested blue source. The probability is that the known pulsars are so faint as to be beyond the reach of even the 200-inch telescope for effective observation, if not for detection. On this problem, as for the quasars and others, one can anticipate increasing demands for instruments of the greatest practicable light-gathering power.

The Observatories have been fortunate in having as a guest investigator Dr. Willem J. Luyten of the University of Minnesota, an astronomer who has specialized in the determination of the proper motions of stars. Some years ago, Luyten pointed out that the 48-inch schmidt telescope is a nearly ideal instrument for proper-motion work. The *National Geographic Society-Palomar Observatory Sky Survey*, completed under the supervision of R. Minkowski with the 48-inch in 1957, constitutes an excellent set of first-epoch plates for such measurements. In recent years, Luyten has obtained many second-epoch plates of the sky with the same instrument, and on this program a total of 752 repeat plates have now been taken; only 184 remain.

During the year, Luyten and his associates at Minnesota examined 20 pairs of schmidt plates, finding more than 11,000 proper-motion stars, among which are several degenerate objects of unusually high velocity. Soon an automated pro-

gram of blinking all the plates for detection and measurement of proper-motion stars will be commenced by Luyten, using a machine especially constructed for the purpose by the Control Data Corporation under a grant from the National Aeronautics and Space Ad-

ministration. It is to be expected that a very large amount of basic data on stellar motions will result. This is one of the extended large-scale programs of a "sustaining" nature that are important for the orderly advance of astronomy.

OBSERVING CONDITIONS

Mount Wilson received 26.98 inches of precipitation during the year. The 64-year average is 35.76 inches. Total snowfall was 27 inches. The highest temperature reached 90°F and the lowest, on December 14, was 9°F.

At Palomar Mountain the total rainfall was 24.63 inches, with a snowfall of 40.8 inches. A minimum temperature of 10°F was recorded. A major earthquake centered at Ocotillo Wells, some 33 miles from the Palomar Observatory, occurred on April 8, 1968. The telescopes and buildings shook intensely but no equipment damage was noted. A few

rock slides were in evidence on the mountain slopes.

As limited by weather conditions, the hours worked with the major telescopes, of a possible 3800 nighttime hours, were as shown in Table 1.

TABLE 1. Observations

Telescope	Complete Nights	Partial Nights	Total Hours Worked
60-inch	213	68	2486
100-inch	237	51	2586
200-inch	238	62	2554

PHYSICS OF THE SUN

Routine solar observations were made by Thomas Cragg, Robert Howard, and Merwyn Utter on 323 days. The records of various kinds made between June 1, 1967, and May 31, 1968, were as follows:

Direct photographs	333
H α spectroheliograms, 30-foot focus	592
K2 spectroheliograms, 30-foot focus	601
Full-disk magnetograms	272
Fine-scan magnetograms	1207
Sunspot drawings	270

Magnetic classifications of sunspot groups were made visually on 225 days during the year.

Synoptic charts of solar magnetic fields observed at Mount Wilson between August 1959 and July 1966 were published in the form of an atlas by the Carnegie Institution of Washington (Publication 626). The authors are Robert Howard, Dr. V. Bumba of the

Astronomical Institute of the Czechoslovak Academy of Sciences, Ondrejov, and Sara F. Smith of the Lockheed Solar Observatory. Funds for the reduction of the data and the publication of the atlas were provided in part by the Office of Naval Research.

Large-Scale Solar Magnetic Fields

Howard, on a six-month leave of absence at the Ondrejov Observatory, Czechoslovakia, collaborated with Dr. V. Bumba in a study of the large-scale magnetic fields of the sun as observed in recent years at Mount Wilson. They found that low-latitude patterns of magnetic fields persist for intervals as long as one or two years, with rotation rates of very nearly 27.0 days (synodic). Many regions contribute magnetic flux to make up these patterns, and the long

lifetimes of the patterns indicate that regions tend to occur at a preferred phase in the 27-day period for long intervals of time. The 27.0-day period is undoubtedly connected with recurrent geomagnetic disturbances. The patterns that seem correlated with these recurrent disturbances are preferentially of positive polarity (over the seven-year period studied) and precede the large Unipolar Magnetic Regions, which during this time were predominantly negative. Further study of the development of activity in the long-lived magnetic "streams" is planned.

Dr. John M. Wilcox of the Space Sciences Laboratory, University of California, Berkeley, and Howard have compared an interpolated pattern of the interplanetary magnetic field with the photospheric magnetic field. This comparison reveals that there is a pattern in the solar field which extends over a wide range of latitude on both sides of the solar equator. This pattern shows characteristics that differ from the usual solar differential rotation in three respects: (1) If this particular interplanetary sector pattern persisted for two years, as seems likely, then the sector boundaries would be stretched in longitude by differential rotation at a much larger amount than is observed. (2) Differential rotation would lead to the rotationally most advanced part of the feature being located at the equator, while the most advanced part of the feature is actually at about 15° north latitude. (3) The evolution with time of the photospheric sector pattern (during 1964) is distinctly different from that to be expected simply from differential rotation.

Magnetograms

The computer programs that reduce the magnetic and other data from the daily full-disk magnetograms were largely rewritten during the year in order to make them faster and more eco-

nomical. The daily magnetograms, which require about 45 minutes to obtain at the telescope, and which are made with a square aperture 17 arc-sec on a side, continue to be reduced by velocity as well as magnetic data. For each day's observation, the differential rotation of the sun is calculated in the form of the coefficients of a $\sin^2 + \sin^4$ expansion in the solar latitude. This project continues as a long-term study of possible changes in the differential rotation with the solar activity cycle. In addition, integrated magnetic-field strengths and fluxes are calculated for polar and other latitude regions for each day's observation. This large amount of material has not yet been analyzed in detail. This program is supported in part by the Office of Naval Research.

From the residuals in the least-squares equation for the differential rotation, it is possible to construct a "Dopplergram" or isotach contour map of the solar surface. The observations for these programs were completed during the year and the first few test Dopplergrams were obtained. Preliminary results give no evidence for the existence of meridional or Rossby-type large-scale currents down to the present limiting line-of-sight velocity of 100 meters/sec.

Active Regions

Mrs. Sara F. Smith of the Lockheed Solar Observatory, Burbank, and Howard continued a study of the magnetic classifications of solar active regions. The Mount Wilson magnetograms were used to investigate the configurations of the associated magnetic fields. Such data are preferable to the sunspot magnetic-field configurations because the sunspots are relatively short-lived and do not always reflect an inherent magnetic complexity in a region. Truly complex regions show a great deal of flare activity. A further study of the orientations of magnetic axes in active regions has been undertaken in collaboration

with Mrs. Dora Lackner. In particular, regions of reversed polarity will be investigated because in a preliminary study it appeared that such configurations were associated with the production of many flares.

Rust continued his magnetographic observations of active regions in hopes of detecting magnetic-field fluctuations in the photosphere at the time of solar flares. The magnetograph at the 150-foot tower, operated on the $\lambda 5250$ line of Fe I, was programmed to scan entire active centers in 5 to 10 minutes with 10 arc-sec resolution. During the summer observation season, over 2000 magnetograms were thus obtained and reduced on the IBM 7094 computer at Caltech. Funds for this extensive reduction process were provided by the Office of Naval Research. First results indicate that the magnetic energy in an active region increases in the half hour preceding a flare. During flares, the magnetic energy decreases and the energy losses are comparable to estimated flare energies of about 10^{30} ergs. Contour maps of the longitudinal components of the photospheric fields indicate that flares start near small ($\ll 10''$) magnetic features that are of polarity opposite to that of the surrounding magnetic fields. Rust calls these features "satellite sunspots" because they usually appear clustered around the outer edge of the penumbra of a large visible sunspot. Satellite sunspots themselves are not always visible in integrated light, but they are quite apparent on maps of the magnetic fields and they are the seats of Ellerman bombs and of many surges observed in $H\alpha$ photographs. The fields of satellite sunspots weaken simultaneously with flares and explosive surges. Rust is continuing to analyze these data at the Sacramento Peak Observatory.

H α Filaments and Magnetic Fields

Rust took advantage of the excellent solar seeing conditions present at the

150-foot tower in the early summer mornings to make several maps at 3" and 5" resolution of the magnetic fields near large, quiescent filaments. He has compared the magnetic flux measured in the photosphere near filaments with that measured in filaments when they appear as bright prominences at the solar limb. The limb measurements were obtained by the observers at the High Altitude Observatory's Climax, Colorado, station. The observations show that the flux available for filament support on the Kippenhahn and Schlüter prominence model is about equal to that actually measured in the prominence. The magnetic-field distribution in the photosphere under quiescent filaments seems to determine filament shape, position, and stability on the solar disk.

Studies of Velocity Fields on the Solar Surface

Howard, in collaboration with Dr. J. M. Wilcox and Mr. Andrew Tanenbaum of the Space Sciences Laboratory, University of California, Berkeley, has investigated velocity fields on the solar surface by means of a newly developed technique. Using the magnetograph and guiding system at the 150-foot tower telescope at Mount Wilson, they scanned one straight line on the sun's disk back and forth for several hours. The digitized magnetic, velocity, brightness, and position data are plotted in such a way that one can follow the velocity or other quantities for each point on the scan line. Thus an accurate one-dimensional picture of the field may be constructed. A large amount of data was accumulated during the summer and only a preliminary reduction has been carried out. The reduction of amplitudes of the oscillatory motions in the photosphere in a plage region is quite evident in these observations, as is the absence of oscillations in sunspots. In quiet regions there appears to be a structuring of the oscillatory field. There are some places where the

amplitudes are consistently high, and others where the amplitudes are consistently low. This study is still in progress, and it is hoped that it may be possible to determine which quiet-sun features are associated with high amplitudes and which with low amplitudes.

The Solar Cycle

Leighton continued his investigation, begun in 1965, of a magnetokinematic model of the solar cycle. It seems capable of reproducing many of the properties of the solar cycle with a precision equaling that with which the properties are now known. This comprehensive model, soon to be published, represents a significant advance in our understanding of the sun.

Solar Activity

A number of interesting and novel events were observed with the photoheliograph on Robinson Laboratory. In particular, on January 29, 1968, an eruptive arch prominence was observed in $H\alpha$ light directly on the disk through its entire trajectory. The eruptive prominence began with a spiraling motion and rose slowly (10–50 km/sec) to a height of approximately 200,000 km above the disk. It then descended toward a nearby sunspot group with velocities up to 200 km/sec. The falling material produced chromospheric brightening. Most interesting is that the eruptive arch appeared bright against the disk near the top of its trajectory. Because this requires high density, as well as high temperature, it is suggested that shocks are developed through the top of the orbit. These problems are currently under study by Zirin.

In another case, a quiescence prominence was observed to brighten without any nearby flare but with obvious density and temperature increase; it erupted upward in a surge, and then reappeared in its former state an hour later.

A number of interesting solar flares have been observed, each giving new insight into the flare process. Some flares have been observed with rise times as short as 10 seconds. There appears to be considerable interaction between neighboring spot groups in setting off flares, and a number of records suggesting exchange of material between neighboring spot groups have been obtained. The Robinson photoheliograph has been operated every clear day by Messrs. Bohlin, Lorenz, Lambert, and Zirin, assisted by several Caltech undergraduates.

Mrs. Dora Russo Lackner, NASA postdoctoral fellow, and Zirin made a detailed investigation of the large flare of August 28, 1966, which was observed in $H\alpha$ at Mount Wilson. This was one of the largest proton flares in the present solar cycle. This large flare appeared qualitatively different from the normal small solar flare in that energy was released over a very large area of the sunspot. It was as though a small preliminary eruption set off the chain energy release through the entire group. The rise of the flare was characterized by a rapid elongation of two bright strands, which then separated rapidly with a velocity of 150 km/sec. The time of increase in X-ray emission agreed well with the period of elongation and separation of the $H\alpha$ strands. From the observed area of the flare and assumptions on the height, it is possible to make models of the emitting material. It is found that the X rays and the microwave bursts must be explained by temperatures, or at least particle energies, greater than 10^9 degrees (or greater than 80 keV). If these energetic electrons are spread over the entire volume, they make up about 10^{-3} of the material (i.e., their density is $10^8/\text{cm}^3$); if the hard X rays and microwave bursts are produced in a small kernel, then the density in the kernel must be much higher, and a true temperature of 10^9 degrees might be achieved there. The radio emission may be explained by synchrotron action,

with a cutoff due to absorption by the corona, or possibly by the Razin effect as has been advocated by Ramaty and Lingenfelter (1967).

K-Line Cinematography

The Lockheed Solar Observatory kindly lent a birefringent filter for the K-line which, with the new guider, has been used for observations of chromospheric structure and active regions at the Hale Solar Laboratory. These investigations have been pursued by Julian, Lackner, Zirin, and Eric Persson, a Caltech graduate student. Although cinematography of active regions has not been particularly interesting, beautiful details may be observed in the chromosphere. Films of chromospheric oscillations have been obtained and it is confirmed that the K-line shows the horizontal oscillations similar to those seen in $H\alpha$. The oscillations, however, are much more complex, with both bright and dark regions showing motion. The bright faculae at the edges of the K-network remain fixed during this oscillation.

Observations of the $H\alpha$ oscillation in the chromosphere have been obtained also. Zirin and Lambert, using the 150-foot solar tower at Mount Wilson, obtained a series of movies of the $H\alpha$ line at the limb of the sun. These films confirm that there is substantial measurable velocity in the horizontal oscillation of the chromosphere. The periods of these oscillations are around 180 seconds. It appears the amplitudes may be as high as 10 km/sec. It is hoped to combine the $H\alpha$ and K-line observations soon for a more comprehensive understanding of the chromospheric oscillation.

Extreme Ultraviolet

Much information about the upper atmosphere of the sun is contained in spectrograms in the extreme ultraviolet, and in recent years these have increased in quality and reliability. Zirin has been studying their interpretation. He finds

that the determination of abundances of elements from the ultraviolet spectra is difficult and contradictory, particularly for lines in the transition zone. Some of Zirin's results differ from the abundance determinations of Pottasch (*Astrophys. J.*, 137, 945, 1963) and Athay (*Astrophys. J.*, 145, 784, 1966). It appears that considerably more study is required before the transition zone can be understood. On the other hand, abundance determinations for coronal ions from the extreme ultraviolet appear reliable.

Recent spectroheliograms in the extreme ultraviolet line obtained at the Naval Research Laboratory are a rich source of information on the structure of the chromosphere. In particular, most of the transition-zone lines show a flat brightness distribution across the disk. Only a very narrow and sharp limb-brightening near the limb is seen. Therefore, the normal concept of a secant distribution is invalid. Zirin has developed a model in which roughness and inhomogeneity of the chromosphere explain this flat distribution of emission.

Another interesting aspect of the extreme ultraviolet spectroheliograms is that He II radiation at $\lambda 304$ is observed in the corona. Calculation of the ionization equilibrium of helium shows that there is always a moderate amount of singly ionized helium present in the corona. Therefore, one may predict interesting effects in the $\lambda 304$ resonance line, such as reflection by coronal clouds or ultraviolet emission from plages. Similar effects are observed in Lyman α , and Zirin has proposed that the self-reversal of Lyman α is, in fact, due to absorption in the corona.

Kozlovsky and Zirin have calculated the ionization equilibrium of oxygen in the corona. This was aimed at solving the contradiction that the O VI lines are extremely strong, yet they belong to an intermediate ionization level not observed to be strong in the transition zone. They found that because of

the lithiumlike configuration there is a considerable amount of O VI at temperatures up to 2×10^6 °K. Therefore, a large part of the O VI in fact comes from the corona rather than the transition zone. This has been confirmed by the observation of the secant distribution in this line by the Orbiting Solar Observatory experiment of Harvard College Observatory.

In conjunction with the effort to understand the chromosphere from studies of limb-brightening in the ultraviolet, Simon and Zirin have attempted to gain information from the radio emission of the sun. A number of scans of the sun at 3 cm and 13 cm were obtained by Dr. Alan Moffet with the Goldstone antenna of the Jet Propulsion Laboratory. In addition, data on brightness distribution have been collected from other sources. When the effect of solar active regions is eliminated, the brightness distribution is flat at almost all frequencies. This means that the sun is essentially rough at all these frequencies. Investigation of these matters is continuing.

A new step in our understanding of the outer solar corona and zodiacal light was obtained in photographs made by Surveyors V and VI. Zirin participates as a member of the working committee of astronomy, and Bohlin is actively working with the results. After the sun sets behind the lunar horizon, it has been possible to take long exposures of the solar corona with various Polaroids. Photographs have been obtained showing the K-corona up to 60 radii from the center of the sun.

Composition of the Solar Photosphere

Lambert has continued work on a comprehensive reinvestigation of the composition of the solar photosphere. New results for the alkaline earths—magnesium, calcium, strontium, and barium—have been obtained in cooperation with Dr. B. Warner of the University of Texas. The abundances are

$$\begin{array}{ll} \log N(\text{Mg}) = 7.48 & \log N(\text{Ca}) = 6.33 \\ \log N(\text{Sr}) = 2.82 & \log N(\text{Ba}) = 1.90 \end{array}$$

on the standard scale where $\log N(\text{H}) = 12.00$. Nine trace elements were studied in collaboration with Drs. B. Warner and E. A. Mallia of the Department of Astrophysics in Oxford, England. The results are

$$\begin{array}{ll} \log N(\text{Zn}) = 4.42 & \log N(\text{Ga}) = 2.84 \\ \log N(\text{Ca}) = 2.07 & \log N(\text{In}) = 1.71 \\ \log N(\text{Hg}) < 3.0 & \log N(\text{Ti}) \leq 0.2 \end{array}$$

$$\begin{array}{l} \log N(\text{Ge}) = 3.32 \\ \log N(\text{Sn}) = 1.71 \\ \log N(\text{Pb}) = 1.90 \end{array}$$

The isotopic abundance ratio $\text{C}^{12}/\text{C}^{13}$ was derived by Lambert from a measurement of the isotopic line $\text{R}_{1,2} \text{ } ^2\Delta\text{-X } ^2\pi$ band. This line was discussed recently by Richter and Tonner (*Z. Astrophys.*, 67, 155, 1967). A new measurement of the equivalent width was obtained from scans made with the Oxford spectrometer. The derived photospheric abundance ratio is $\text{C}^{12}/\text{C}^{13} = 150 \pm 30$, which exceeds the terrestrial ratio ($\text{C}^{12}/\text{C}^{13} = 89$) by almost a factor of 2. This result is in agreement with a prediction made by Fowler, Greenstein, and Hoyle (*Geophys. J. Roy. Astron. Soc.*, 6, 148, 1961). This investigation and work in progress on isotopic lines in the C_2 Swan band was carried out in collaboration with Dr. Mallia.

Coronal Physics

Recent studies of the coronal-line spectrum have emphasized that differences in composition appear to exist between the photosphere and the corona. In an attempt to resolve this outstanding problem, Lambert has begun a thorough evaluation of the methods employed in the determination of the coronal composition and the possible processes that might be responsible for the composition difference. A. G. W. Cameron (*Astrophys. Letters*, 1, 35, 1967) suggested that the overabundance of heavy elements in the solar corona was due to an enhanced

rate of ejection of ions from the underlying chromosphere and that radiation pressure through line absorption was the responsible factor. A quantitative study of this proposal has shown that the effective force produced by radiation pressure is insufficient to explain the observed enhancement.

As a continuation and final summary of work begun at the High Altitude Observatory, Bohlin is investigating the evolution, structure, and associated phenomena of white-light solar coronal streamers. The data for this study are direct photographs of the corona from both the 1965 eclipse and three unmanned, stratospheric balloon flights of an externally occulted coronagraph during 1964–1965 (the Coronascope II project under the direction of Dr. Gordon Newkirk, High Altitude Observatory, and assisted by Bohlin). Complementing these direct photographs are nearly daily photoelectric scans of the inner K-corona ($r \leq 1\frac{3}{4} R_{\odot}$) made with the High Altitude Observatory K-coronameter in Hawaii. Cross-identification of features seen in the photographs and by the K-coronameter led to a sample of eight coronal streamers whose positions on the solar disk could be found with considerable certainty.

This study shows that streamers co-rotate with the sun and exhibit considerable stability in basic configurations over periods of several rotations. While rather slow evolution was the general rule for coronal structure during this period of solar minimum, occasionally growth and decay of major streamers within periods of 14 days were detected. The lifetime of one high-latitude “helmet” streamer was 4 to 5 solar rotations; another streamer overlying a complex region of activity lasted for over 7 rotations. One equatorial streamer that overlay an intense, flaring active region lived for only one rotation and was clearly related to an intense geomagnetic storm as well as to magnetic and

solar-wind velocity structure in interplanetary space.

The average coronal streamer could be adequately described by a three-dimensional density model having a radially dependent core density which decreases as a Gaussian perpendicular from the core line. The $1/e$ -density cross-section contour at $r \simeq 1\frac{1}{4} R_{\odot}$ was $\sim 25^\circ$ in latitude by $\sim 40^\circ$ in longitude. Calculations showed that such a feature will remain visible for about four days on either side of limb passage. The most promising method of predicting coronal streamer structure lay in calculating the magnetic potential lines of force above the solar surface, using as a source the surface fields as observed by the Mount Wilson magnetograph.

This program is being extended by Bohlin to study the quasi-stationary patterns of coronal structure in 1965, both as related to solar activity and also to the “sector structure” of the interplanetary medium observed by satellites. These quasi-stationary coronal patterns are being averaged to provide a basis for the derivation of a nonsymmetric density model of the entire inner corona during mid-1965.

Bohlin has also begun analysis of the Jet Propulsion Laboratory photographs of the extended solar corona observed at sunset from the lunar surface by Surveyor moon-probe satellites. These photographs should eventually provide intensity and polarization observations of the extended ($10 \lesssim r < 50 R_{\odot}$) corona and zodiacal light, which has hitherto been poorly observed.

Forbidden Lines in the Fraunhofer Spectrum

The possible presence of [S I] and [Ca II] lines in the Fraunhofer spectrum was first suggested in 1948 by Bowen (*Rev. Mod. Phys.*, 20, 109). Recent laboratory measurements of forbidden lines and the ultraviolet spectrum have provided accurate wavelengths for the

S I forbidden lines which arise from transitions within the $3s^2 3p^4$ ground configuration. Lambert, in collaboration with Drs. J. P. Swings and N. Grevesse of the Institut d'Astrophysique in Liège, Belgium, has carried out a search for [S I] lines in the solar spectrum. Two lines were successfully identified and are the first convincing identifications of [S I] lines in an astrophysical source. Their observed intensities are in good agreement with predictions based upon theoretical transition probabilities and the sulphur abundance derived by Lambert and Warner (*Monthly Notices Roy. Astron. Soc.*, 138, 181, 1968).

The [Ca II] transition $4s^2S_{1/2} - 3d^2D_{3/2}$ was searched for by Lambert in collaboration with Drs. Mallia and Warner. The line was identified in the Fraunhofer spectrum for the first time. The observed intensity is in approximate agreement with a prediction based upon a theoretical estimate of the transition probability and the revised Ca abundance derived by Lambert and Warner. Accurate observations were not possible because the line is blended with a stronger telluric line. This study confirms the independent identification of the [Ca II] line by Grevesse and Swings (*C.R. Acad. Sci. Paris*, 266, 110, 1968).

PLANETS AND THE MOON

Mars

The reduction and analysis of the measurements of the absorption lines in the weak $5\nu_3$ band of CO_2 at $\lambda 8690$ in the spectrum of Mars, carried out interferometrically by Münch at the 1967 opposition (*Year Book 66*, p. 260), have been completed. Individual or average tracings of the R8, R10, or R12 rotational lines were fitted by least squares to the observed instrumental profile, which approximates the shape of an Airy function with half-intensity width of 0.038 \AA . The average equivalent width for these lines, reduced to the center of the disk, is $3.67 \pm 0.032 \text{ m\AA}$. It is believed that this result, involving some 60,000 pulse counts per spectral element, is the most accurate measurement of a weak absorption line ever carried out in any astronomical source except the sun, and demonstrates the great power and possibilities of Fabry-Perot spectroscopy.

Jupiter

The intensity of absorption lines in the NH_3 band at $\lambda 6450$ in the spectrum of Jupiter is being measured by Münch at the 100-inch coude by means of Fabry-Perot interferometers, as a function of

position over the planetary disk. It is hoped to derive from these measurements information about the mechanism of line formation and scattering properties of the atmosphere.

Difference spectra in spectral regions containing strong CH_4 bands, between the various zones and bands in the Jupiter disk, are also being obtained by Münch with the 100-inch coude scanner under medium resolution ($\Delta\lambda = 3.5 \text{ \AA}$). From these measures it is possible to derive in principle the concentration of the scattering solid particles relative to the gas at various heights over the different areas. Further observational work on this problem is needed to find out whether it will lead to profitable results.

Satellites of Jupiter

Low-resolution spectra of the Galilean satellites of Jupiter in the regions $\lambda 1.4 - 1.7$ and $2.0 - 2.4 \mu$ have been obtained by Münch and Neugebauer at the east-arm focus of the 200-inch telescope for the purpose of verifying previous reports regarding the existence of considerable variations in the reflectivity of the various satellites. Preliminary analysis of the data, now in the process of reduction, confirms such variations.

Planetary Photography

Murray continued experiments aimed at improving photography of the planets. Photographs of Mercury were made shortly after sunrise at the coudé focus

of the 100-inch telescope using both full and reduced (45-inch) aperture. Multiple printing of one set of negatives by Dr. Bradford Smith of New Mexico State University yielded recognizable detail on the disk of the planet.

STELLAR SPECTROSCOPY AND PHOTOMETRY

White Dwarfs

In observations of the Lowell proper-motion stars, with special concentration on those of moderately small proper motion, Greenstein discovered approximately 40 more white dwarfs. In enormous preponderance are those of spectral type DA, although several new helium-rich stars have been found. An interesting discovery is a group of three relatively bright sdO subdwarfs, GD 298, 299, and 300.

At the opposite end of the white-dwarf sequence lie the cool degenerate stars, for which there have been extensive searches by Eggen and Greenstein. It is now clear that the difficulty of discovery of these objects is based on a genuine physical effect—the rapid cooling as the interior solidifies into a lattice, so that no more free energy is available from the nucleons. This rapid cooling would be reflected in a drop in the frequency as a function of absolute visual magnitude, since the stars would rapidly reach large bolometric corrections. Spectra obtained by Greenstein of suspected candidates for red degenerate stars have shown in almost every case that the stars are weak-lined K or even M stars with no outstanding peculiarities. The ultraviolet excess found by Eggen may be explained in large part by the line blanketing being much less in sdK stars than in the main-sequence stars. Of 23 stars suspected by Eggen to have very large space motions if they are main-sequence stars of luminosity given by their $B-V$ color, 2 were yellowish degenerate stars of spectral type DC, and 1 was DA. All others were classified as sdG, sdK, or dMp.

However, the change in derived absolute magnitude using the ultraviolet excess was insufficient to reduce the mean space motions of these stars to an acceptable value. Of 19 stars for which tangential velocities could be derived, 5 had space motions greater than 500 km/sec. The most reasonable interpretation of these extraordinary large motions, which are not borne out by the observed low-dispersion radial velocities, is that the stars are, in fact, subluminescent and lie between the main sequence and the red degenerate stars. The motions become reasonable if the stars lie at least 1.5 mag below the main sequence; they may, in fact, lie as much as 3 mag below the main sequence.

Tsuji computed the effective line blanketing in a star of 4000° effective temperature and very low metal abundance. This star approaches the blackbody line if its metal abundance is less than about 10^{-2} that of the sun, and is essentially on the blackbody line at 10^{-4} solar metal abundance. The change in $B-V$ is small, however, so that Eggen's selection of the high-velocity proper-motion stars has, in fact, disclosed a group that is intermediate in luminosity between main-sequence and fully degenerate stars. Almost all these stars are faint, and none of this type has yet been found among those analyzed spectroscopically. The lines are quite sharp, although there is a chance that strong lines may, in fact, be broadened by high pressure, which would be consistent with very low metal abundance. In such stars, Rayleigh scattering becomes a dominant opacity source because of the weakness

of the negative hydrogen-ion contribution.

Dwarf Me Stars

An observation made with the image-tube spectrograph concerns the star Wolf 359, one of our nearest neighbors in space, with a parallax of 0.4 arc-second. This very faint star, with $M_V = +16.6$, was found by Arp and Greenstein to show a spectroscopic flare on the first observation. Three subsequent spectra showed a normal dMe spectrum with strong hydrogen-line and K-line emission. During the flare, the hydrogen lines broadened very greatly and the neutral helium lines appeared. The velocities may have become slightly more negative. The star is a member of the old disk population with space motions U, V, W , of $+27$, -45 , and -20 km/sec. Wolf 359 was noted to have had a visual flare by Prof. H. U. Sandig, but no other observations are available. It is unexpected to find a strong chromospheric activity persisting in a very old disk star, and especially one of such low luminosity. However, observations by Neugebauer and Becklin have further compounded the mystery of this unusual object. They observed the infrared brightness at 1.6, 2.2, and 3.4 microns on several dates. They did not find any significant variation. On the other hand, they found that this star of apparent visual magnitude 13.3 had magnitude 5.8 at 3.4 μ . This extremely large infrared color index can possibly be explained by low temperature, approximately 2200°K, far below that expected for any main-sequence star even of spectral type dM8. The TiO bands are not outstandingly strong in the blue-green portion of the spectrum. Combining the information from the infrared with *UBV* photometry by Eggen, one finds that the object radiates 10^4 times more strongly at 3.4 μ than in the ultraviolet at 0.4 μ . Thus the shape of the lower end of the main sequence is very much at issue.

Krzeminski contained photoelectric *UBV* observations of a sample of dMe stars to establish the character of their light variability. New observations of BD+34° 106 gave a period of 2.170 days for sinusoidal light variation. Change in amplitude and phase shift between 1966 and 1967 observations was found in HDE 234677, although the period of light variations of 3.336 days remains constant.

Model Atmospheres of M-Dwarf Stars

In order to construct model atmospheres of M-dwarf stars, Tsuji has evaluated molecular-line opacities such as are due to vibration-rotation bands of H_2O and CO , pure rotation bands of H_2O , and electronic bands of TiO , MgH , CaH , and SiH . The effect of line structure on molecular opacity is approximately taken into account by the probability distribution function corresponding to the Elsasser-band model. This is characterized by two parameters, the mean absorption coefficient and the mean line separation at each wavelength interval. The absorption coefficient of the collision-induced vibration-rotation bands of H_2 is calculated, and it turns out to be of comparable importance with the absorption of H_2^+ (*ff*) around 2 μ in M-dwarf stars. The Rosseland mean opacity at relatively high pressures is also calculated. Atomic-line absorptions, however, are not considered.

Based on these opacity sources, a model atmosphere of M-dwarf stars with $T_e = 3000^\circ K$, $\log g = 4.8$, $v_t = 2$ km/sec, and solar metal content has been calculated by Tsuji. The resulting model in radiative equilibrium shows very low surface temperature near 1100°K. The emergent flux calculated from this model shows appreciable flux excess around 1 μ and 1.6 μ , while it shows general flux deficiency in the infrared. This is because 1 μ and 1.6 μ are the windows of molecular absorptions, and because their spectral regions correspond to the maximum

of Planck radiation of 3000°K. As a whole, the opacity of cool atmospheres is high in the infrared because of the strong absorptions by H₂O and CO, while it is relatively low below 1 μ even if TiO and other molecular absorptions are taken into account. For this reason the red-dwarf stars are blue as compared with the blackbody radiation. If this fact is taken into account in the analysis of Johnson's infrared multicolor photometry, the temperature scale of M-dwarf stars appears to be lower by 200°K or more than that estimated without considering the model effect. Then the effective temperature at type M4V is about 3000°K rather than 3200°K. This study is being extended to several other effective temperatures, and the effect of convective energy transport is considered. Some opacity data are also improved.

Spectroscopy and Photometry of Cool Stars

Coudé spectrograms of the M2V star HD 95735 have been obtained by Tsuji in the near infrared as well as in the blue and yellow. These plates are to be analyzed by the use of model atmospheres now under calculation. The Mira variable, α Ceti, was observed at several phases between August 1967 and February 1968 in the near infrared.

Tsuji observed several K-giant stars, including one Ba II star, ζ Capricorni, in the near infrared mainly for a study of the red system of CN and possibly for investigation of the abundance of C¹³.

To supplement the analysis of high-dispersion spectrograms of two R-type stars, HD 156074 and HD 182040, taken by Greenstein with the 200-inch telescope, photoelectric scanning of the spectra of these stars is being carried out with the 60-inch Cassegrain scanner. Molecular opacities such as are due to C₂, CN, and CH, which are important in these stars, are investigated by the same method adopted to calculate the molecular opacity for M stars. Photoelectric

scans of several cool carbon stars are also being attempted.

Temperature, Gravity, and Mass of τ Herculis, Vega, and Sirius

Heintze derived from high-dispersion spectrograms profiles of the Balmer lines of the B5 IV star τ Her (HD 147392; $\alpha(1900)=16^h16^m7$, $\delta(1900)=+46^\circ33'$) and compared them with theoretical predicted line profiles. Monochromatic continuum magnitudes of the star were also observed and compared with monochromatic continuum fluxes derived from models. The effective temperature of τ Her is found to be $14500 \pm 500^\circ\text{K}$ and $\log g = 3.5 \pm 0.2$. It is pointed out that τ Her is not reddened, that the rotational velocity is very low, and that departures from LTE very likely occur in the hydrogen spectrum.

For α Lyrae, Heintze found the effective temperature to be 10,000°K and $\log g = 3.6$; furthermore, he concluded that the mass is 1.3 ± 0.4 solar masses. Finally, he provides some evidence that Sirius A itself is a binary system. An additional conclusion is that the true Balmer jump (BJ) of α Lyr is 1^m43 , and that for B-type stars the following relation is valid: $\text{BJ} = 1.20 (U - B) + 1^m45$. The Balmer jump derived from Balmer-line-blanketed models of Mihalas (1966) seems to agree with the observations. Those derived in 1965 require a correction of -0^m06 . The $U - B$ colors compiled by Mihalas (1966) require a correction of $+0^m07_s$, while those derived by him in 1965 need a correction of $+0^m02_s$.

Early-Type Main-Sequence Stars

With the scanner on the 60-inch telescope at Mount Wilson, Kodaira is studying the continuous radiative flux ($\lambda\lambda 3300-6000$) of B3 V stars brighter than about the fifth magnitude and north of -15° declination. He is also using the X-spectrograph to obtain plates for studying the variation of radial velocity of these stars.

Computer programs for the quantitative interpretation of early-type spectra by means of model-atmosphere techniques are being constructed by Scholz, and some are already in use.

High-dispersion spectra of several stars (O,B,F) were taken. An investigation of τ Scorpii (B0 V) and λ Leporis (B0.5 IV) will be completed soon by Scholz in collaboration with J. Hardorp of Hamburg. The evaluation of plates of HD 58343 (B3 Ve), which is supposed to be a rapid pole-on rotator, has been started with Kodaira. Models of the α Lyr atmosphere proposed recently are being checked by comparison with published and unpublished observations.

Faint Blue Stars

Sargent and Dr. Leonard Searle of the Mount Stromlo Observatory completed work on the spectra of 30 of the brighter stars in Feige's list of blue stars at high galactic latitudes. The spectra were obtained earlier at the Lick Observatory, and had a dispersion of 48 Å/mm. The spectrograms were classified on a system that used measured equivalent widths, line profiles, and colors in addition to visual inspection (*Astrophys. J.*, 152, 443, 1968).

The main result of this work was the discovery that Feige 86, a B star with weak helium lines of a type commonly found in the galactic halo, has additional peculiarities in its spectrum, including an abnormally strong line of P II. The star has a large proper motion and, on kinematic grounds, must be a horizontal-branch star of Population II. Sargent and Searle concluded that the existence of Feige 86 means that the weak helium lines in the spectra of halo blue stars can no longer be taken as an indication of a low helium abundance in the material from which the star formed. Following this work, Greenstein and Sargent began a survey of the spectra of halo B stars down to $M_V \sim 11$ in order to see if other peculiar stars could be found. They

used the Palomar coude spectrograph at 18 Å/mm. It was found that BD+5°2468, a ninth magnitude object having the *UBV* colors appropriate to a B5 star, has an abnormal spectrum similar to that of a λ 4500-Si-type Ap star. This star has a fairly large proper motion that leads to a transverse velocity of over 300 km/sec if it is on the main sequence. BD+5°2468 provides additional evidence that peculiar A and B stars of the kind found in Population I also exist in Population II.

In their work on the brighter Feige stars, Sargent and Searle studied the properties of several B stars with abnormally broad H lines. They found that these sdB stars always show an abnormally small ratio of the strengths of the singlets to the triplets among the He I lines. The sdB stars sometimes, but not always, have weak He I lines for their colors; the singlet-triplet anomaly exists irrespective of the absolute strengths of the He I lines. In order to obtain more understanding of this effect, Sargent is cooperating with Drs. Searle and Baschek of the Mount Stromlo Observatory in a detailed spectrophotometric study of AC+9°6-12. This is a ninth magnitude sdB star for which Sargent has obtained 18-Å/mm Palomar coude spectrograms.

Sargent and Greenstein have continued their search for interesting objects of the halo population of spectral type B. These are selected from lists by Feige and Luyten, who found many proper-motion stars and other sources. A few objects of special interest may be noted. These are stars with weak helium lines, notwithstanding a photoelectric color that sets them close to the main sequence at spectral types B5 or earlier. One is -12°6299; another, +5°2468. The latter may be a spectrum variable of the silicon type belonging to the halo population.

Spectroscopic Binaries

Deutsch has now found approximate periods for two other A stars that are

interesting spectroscopic binaries. One is 51 Tauri, an A8 star on the Hyades main sequence. This is a double-line spectroscopic binary with a period of about 12.3 years. The secondary has a spectral type near G0. Visual observers should take the opportunity to search for it during the five years beginning in 1971, when its separation will be of the order of 0".15. The other spectroscopic binary is 53 Camelopardalis, an A2p star in which H. W. Babcock has found a strong magnetic field that reverses with a period of 8.03 days. The star also exhibits large-amplitude spectrum variation and small-amplitude radial-velocity variation, both with the same period. Velocities from Babcock's plates and Deutsch's show also that 53 Cam is a single-line spectroscopic binary with an orbit of large eccentricity and a period of about 6.7 years. Babcock has drawn attention to certain relatively small irregularities in the magnetic cycle, in which the phase of the magnetic curve appears at some epochs to lead the phase in a strictly periodic ephemeris and at some epochs to lag. These irregularities prove to be too large for attribution to the effects of light-transit time across the binary orbit; they appear to be caused by actual deformations of the field in the stellar reversing layer.

Peculiar A Stars

Sargent, working in cooperation with Drs. S. Strom and K. Strom of the Harvard College Observatory, completed an abundance analysis of HD 204411, an unusual Ap star. Its main peculiarity is a deficiency of carbon by a factor of about 20, together with slight widening of the iron peak.

Mrs. A. I. Sargent, Greenstein, and Sargent completed a study of the spectra of about 15 Ap stars in the red region of the spectrum. This was aimed particularly at a study of the neon abundance. Lines of this element are not found in normal stars cooler than about

B7. Only a few Ap stars are hotter than this. However, for six stars that were sufficiently hot for Ne I lines to be expected if the element is in normal abundance, the following results were found: Ne was absent in 3 stars of the $\lambda 4200$ -Si group; Ne lines slightly stronger than normal were found in 3 B stars with weak He I lines.

Miss Judith Cohen has studied microphotometer tracings and wavelength measures of numerous coude plates in the visual spectrum of α^2 Canum Venaticorum. Greenstein and Deutsch obtained these spectrograms at various phases during several cycles of this well-known spectrum variable and magnetic reverser, which has a period of 5.5 days. Concurrent observations of other kinds were obtained by Conti, Danziger, Oke, and Sargent. Miss Cohen's discussion is the first to yield satisfactory identifications of most lines in the visual region of this rich spectrum. Like earlier investigators, she assigned each line to one of three different systems that vary distinctively in intensity and radial velocity. Her work establishes that lines of Gd III and Cl II occur, and that their intensity and velocity variations are indistinguishable from those of Gd II, Eu II, and other singly ionized rare earths. Dr. P. Swings of the Institut d'Astrophysique, Belgium, has reported a similar result for Gd III and several other doubly ionized species that produce lines in the region $\lambda\lambda 3070$ –3300. Miss Cohen questions earlier attributions of lines to Hg II and Pb II, and she finds no evidence for P II.

Variable Stars

Z Camelopardalis, the prototype of a subclass of dwarf novae, has been studied spectroscopically and photometrically by Kraft, Krzeminski, and Dr. G. S. Mumford of the Tufts University. The star is found to be a double-line spectroscopic binary [sdBe+G(?)] with an orbital period of 0.289845 days and mass ratio near unity; masses of the components are

around 1 M_{\odot} . Although eclipses have not been detected, the light curves show a number of features that recur with the same period as the spectroscopic one. Of these, the most pronounced is a "shoulder" reminiscent of that in U Geminorum and VV Puppis. The moment of spectroscopic conjunction, when the blue star is behind, comes on the descending branch of the shoulder and is accompanied by a $(U-B)$ excess amounting to 0.1 mag. The mean colors at maximum light are $B-V=0.00$, $U-B=-0.80$, and at minimum are $B-V=+0.50$, $U-B=-0.75$. The model advanced previously by Kraft (*Adv. Astron. Astrophys.*, 2, 43, 1965) for old and dwarf novae appears entirely applicable to Z Cam.

Garrison has completed his two-year classification dispersion survey of long-period variable stars brighter than 9th magnitude and north of -30° . Approximately 900 spectrograms of 150 Mira variables were obtained. Spectra were taken of some stars at all phases, but for most stars preference was given to maximum and premaximum phases. This program was carried out in collaboration with Deutsch and P. C. Keenan, who are continuing to obtain spectrograms at 20 Å/mm in the blue and violet for the study of systematic anomalies in various absorption lines and bands. One of the results of this two-year combined program is the discovery of A10 emission in R Piscium, R Corvi, R Cassiopeiae, and RT Librae. In the past this rare phenomenon had been seen on only two occasions—Mira in 1924 and R Serpentis in 1960. A discussion of the anomalous behavior of the A10 bands in Mira variables is in preparation.

The distance of the 149 classical Cepheid SU Cassiopeiae was determined by Racine using nearby field stars that, like the variable, are seen to illuminate reflection nebulae and are presumably connected with the same dust cloud. Its absolute magnitude was found to be $\langle M_V \rangle = -2.45 \pm 0.2$ mag, in good agree-

ment with predictions based on modern calibrations of the period-luminosity relation.

In June 1967, Deutsch found that the bright combination variable CH Cygni had sustained another outburst like that first seen in 1963. The hot continuum was invisible on plates of March 1961 and September 1966, as were the permitted emission lines of hydrogen and helium. The M star appears to change its radial velocity slowly, as though in an orbit with period of the order of 10 years.

Measurements of H and K Flux

Wilson has continued his photoelectric measurements of the flux at the center of stellar H and K lines. More suitable blue-sensitive photomultipliers were acquired and have been in operation since August 1967. About this time also, changes were made in the observational program. Numerous Strömgren-Perry stars were dropped; those retained were the stars with known H-K emission, some others with measured flux only slightly less than these, and a selection of stars with minimum flux to serve as standards, i.e., as a check on the observations. Added to the program were a number of later-type main-sequence stars, mostly known to have H-K emission components and extending from G5 to M2.

For the earlier-type stars, F5 to G2, there have been so far no unambiguous variations in H-K flux. Hence it may be concluded that any cyclical changes for these objects must be of long period compared to the interval of slightly over two years during which they have been observed, or else that the technique used is insufficiently sensitive.

Some of the later-type main-sequence stars show variations in H-K flux which are probably real. The time covered by the observations of these objects has, however, not been long enough to reveal any certain evidence of variations of a cyclical nature. Enough has now been

done to indicate that this project is necessarily long range. Unfortunately, there is no real evidence to indicate ultimate success in uncovering stellar analogues of the solar-activity cycle.

Infrared Scanning

Hyland is using the infrared scanner in collaboration with E. Groth and H. Butcher, Caltech physics students, at the Cassegrain foci of the 24-inch, 60-inch, and 100-inch telescopes to scan K and M giants in the 1.5–1.8 μ and 2.1–2.5 μ ranges to obtain integrated band intensities for the vibration rotation bands of CO. Initial results for α Tauri, β Geminorum, α Ursae Majoris, and δ Virginis, with a resolution of 32 Å for the 1.5–1.8 μ region and 67 Å for the 2.1–2.4 μ region are promising. They show that accurate band strengths can be obtained. The theoretical interpretation of these band strengths still presents a major problem, the solution of which, however, should yield, in combination with high-dispersion spectra, dependable values of the C/O ratio for late-type stars.

Classification

The spectrum of the very peculiar star HD 147010, which is a member of the upper Scorpius complex of stars, gas, and dust, has been studied by Garrison using a high-dispersion plate taken by Münch. The Fe II, Cr II, Si II, and Ti II lines are similar in strength to those of an early A-type supergiant, while the H and He I lines are similar to those of a late B-type giant.

The spectrum of NGC 2024 No. 1, an extremely heavily reddened star in the Orion association, has been classified by Garrison. He has found it to be identical to that of θ^2 Orionis B (B0.5 Vp with very broad hydrogen lines). A comparison of the photometry for the two stars indicates that the ratio of total to selective absorption is less than 4, contradicting previously suggested higher values

for Orion. The resulting absolute magnitudes for the two stars are consistent with the appearance of their spectra.

The cluster Tr 37 is very close to the position of the very-high-luminosity red supergiant μ Cephei. In order to investigate the relationship between μ Cep, the cluster, and the association I Cephei, Garrison has taken classification dispersion spectrograms of stars in and around Tr 37. The stars in this cluster also have an important bearing on the question of the ratio of total to selective absorption since H. L. Johnson has suggested that it is higher in this region than normal.

Garrison and Schild have finished classification of the spectra of all southern OB stars earlier than B8 in the bright star catalog. Some B8–A2 supergiants were also included. The plates were taken by Dr. W. A. Hiltner using a 1-prism classification spectrograph and the 16-inch telescope at Cerro Tololo.

Stellar spectra are usually classified on the basis of suitable line ratios, since estimates of these can be very sensitive to temperature changes but relatively insensitive to abundance anomalies, luminosity effects, or the densitometric properties of the spectrograms. In classifying M giants, however, it is usually necessary to assign spectral types on the basis of the absolute intensities of TiO bands rather than on the basis of band ratios. At 10 Å/mm, however, temperature-sensitive line ratios can still be isolated in the spectra of K and M giants. Deutsch, Wilson, and Keenan have found that these confirm the spectral types based on TiO. Although some M giants have moderately high velocities—of the order of 120 km/sec—and reveal some evidence of mild metal-deficiency line weakening, their spectral types from TiO bands nevertheless are reliable temperature indicators. One by-product of this collaboration is the development of a simple null method, based on lines judged to be of equal strength, for determining

g and M stars of known excitation temperature and chemical composition. Another by-product is the discovery that in some, perhaps all, of the high-velocity M giants the Balmer lines have variable intensity. On many plates they are conspicuously stronger than in standard giants of the same spectral type.

Blue Stragglers

Continuing his study of blue stragglers in old open clusters, Deutsch has found that Fagerholm 190 in M 67 is a single-line spectroscopic binary with a period of 4.198 days and a velocity amplitude of about 18 km/sec. He also has inconclusive evidence for duplicity in other blue stragglers in the same cluster. These results lend support to the McCrea hypothesis for the formation of such stars by evolution of close binary stars with mass exchange. The results also militate against the view that the blue stragglers are single stars that have returned to the main sequence after passing through the red-giant phase of stellar evolution. If the McCrea hypothesis is indeed correct, the rotational velocities of 50–100 km/sec, reported by Deutsch in previous *Year Books*, can no longer be adduced as evidence in support of a Dicke-type model for the rotation of solar-type stars. However, Sargent's mass determinations for three other blue stragglers still tend to favor the idea that these stars have no close companions and have already been red giants.

Stellar Composition

The study of peculiar elemental abundances in unevolved stars has led to an unexpected result concerning the K dwarfs discovered by Spinrad some years ago to have exceptionally strong metallic lines. In HD 75732 and HD 145675, which proved to be essentially normal K1 main-sequence stars, Greenstein and Oinas have found that not only are the metallic lines enhanced, but a large num-

ber of molecular features are detectable both in the spectrum and in the spectrophotometric scans. The CN molecule is strong, as is the Swan system of C_2 . The latter bands are well resolved, but would not, unfortunately, be strong enough to permit detection of C^{13} atoms if they were present. The great strength of carbon features in unevolved stars cannot be caused by internal nucleosynthesis. The possibilities are (1) that the oxygen abundance in these stars is abnormally low, so that the C/O ratio exceeds unity, or (2) both carbon and oxygen are enhanced in abundance, with carbon more enhanced than oxygen. In any case, it is apparent that the strong metallic lines and the change of the C/O ratio from its solar value in old disk-population stars must be connected with a spotty chemical element concentration in the interstellar gas out of which these stars were formed. The possibility exists that the high abundance of oxygen already noted in Arcturus and the high abundance of carbon here detected are connected with explosions in super-massive stars formed early in the history of the disk. Oinas will continue to measure and observe further stars of this type for carbon, oxygen, and metallic-line peculiarities.

A complete and accurate analysis has been made of three horizontal-branch A stars by Kodaira, Greenstein, and Oke. Kodaira had already published a model-atmosphere analysis of HD 161817. The two additional stars, HD 86986 and HD 109995, had been observed spectroscopically by Greenstein at Palomar and spectrophotometrically by Oke. Since the fine analysis of HD 161817 was available, and since the temperatures of the three stars were nearly the same, it was possible to make an accurate differential analysis of HD 96986 and HD 109995 with respect to HD 161817. The effective temperatures are near 7800°K, and the surface gravity is low ($\log g=3.0$). Rotation is small. The mean metal deficiencies with respect to the sun

were, in the logarithm, -1.54 for HD 86986, -1.76 for HD 109995, and -1.16 for HD 161817. Thus the horizontal-branch A stars of very high velocity show a range of metal deficiency from a factor of 15 below the sun to 60. The systematic trends among the abundance deficiencies are similar to those already noted for the very metal-poor giant HD 122563. The α -particle nuclei (Mg, Al, Si) are least deficient; those of the s-process (Sr, Y, Cr, Ba) are the most deficient. The differences in abundance anomalies are greatest in the most metal-poor star. A tentative analysis of the carbon and oxygen content, using lines very near the limit of detectability, seems to indicate that both carbon and oxygen are in high abundance relative to metals, i.e., not very much lower than in the sun. This is in agreement with earlier observations of the slightly metal-deficient red giants in which oxygen showed a surprisingly high abundance. The masses deduced for the stars are below 1 solar mass and the space motions over 300 km/sec.

From data obtained by Conti, Danziger, and herself, Ann Merchant Boesgaard has found that the beryllium content of F-G dwarf stars increases with increasing $B-V$. For the same stars, the lithium content decreases with $B-V$. The decreases in lithium can be understood in terms of convective depletion. The apparent increase in beryllium, however, requires either (1) the postulation of a new depletion or production mechanism, or (2) a variation in the spallation production parameters, e.g., duration and energy spectrum of bombarding particles.

Mrs. Boesgaard has completed an analysis of the isotopic abundances of magnesium in 10 late-type stars from the 0, 0 band of MgH. The stars studied give evidence for Mg²⁵ and Mg²⁶ in amounts similar to the terrestrial abundance ratios relative to Mg²⁴.

A spectrogram exposed in the ultra-

violet to $\lambda 3100$ of ζ Capricorni, a hot Ba II star, has been obtained by Mrs. Boesgaard for the purpose of searching for the strong Tc II lines in that spectral region. There can be no positive identification of Tc II, however, since this region of the spectrum is very crowded with atomic lines. An upper limit to the line strengths will be estimated.

Palomar high-dispersion spectrograms of BD+39°4926 (cf. Oke, Greenstein, and Gunn, in *Stellar Evolution*, p. 399, R. F. Stein and A. G. W. Cameron, eds., Plenum Press, New York, 1966) are being analyzed by Kodaira. They show numerous O I, C I, and weak ionized metallic lines. Tentative results suggest that this star has the physical parameters $\log g=1$ and $\theta_e=0.7$, normal oxygen and carbon abundances, and a moderate deficiency in metallic elements.

A curve-of-growth analysis has been undertaken by Hyland for several hot Si $\lambda 4200$ stars from material obtained at Mount Stromlo Observatory. From spectra of the blue-wavelength region only it has been found that in each case (1) the excitation temperature is only slightly lower than the effective temperature obtained from photoelectric scans, (2) the derived value of the microturbulence is very low, and (3) the chromium-iron ratio is greatly enhanced compared with normal stars. These results are in direct opposition to those obtained by Searle *et al.* (*Astrophys. J.*, 145, 141, 1966) from a consideration of the ultraviolet spectra of similar peculiar stars, and may be due to an extreme depth dependence of the relevant quantities through the atmospheres.

The silicon star HD 221006 has been found by Hyland to be a spectrum variable showing extreme variations of its Si II lines. No definitive period has yet been obtained for the variations. All measured lines of Si II vary in phase with one another, and Si III $\lambda 4552$ also varies in the same phase. The lines of Mg II and Fe II appear to vary slightly

and in phase with Si II, whereas C II $\lambda 4267$ varies slightly in antiphase with the other elements. He $\lambda 4471$ does not show any systematic variation and is always very weak for the high ($\sim 16,000^\circ\text{K}$) effective temperature of the star. It has been estimated that $N_{\text{He}}/N_{\text{H}} < 0.01$. The value is in good agreement with the helium abundances Hyland obtained for silicon stars in galactic clusters, where it was shown that the anomalously low helium abundance was purely atmospheric.

From a study of the absolute energy distributions and $\text{H}\gamma$ profiles of 40 B stars, Hyland has determined an effective-temperature scale as a function of $Q = (U - B) - 0.72 (B - V)$. This scale agrees well with the fundamental temperatures of Hanbury-Brown *et al.* (*Monthly Notices, Roy. Astron. Soc.*, 137, 393, 1967) and with the scale proposed by Morton and Adams (*Astrophys. J.*, 151, 61, 1968), but predicts considerably higher temperatures than those found by Heintze (*Bull. Astron. Inst. Neth.*, 20, 1-25, 1968). This scale has been used to derive helium abundances for 9 cluster B stars and leads to a mean

result of $N_{\text{He}}/N_{\text{H}} = 0.11$, in good agreement with most recent direct and indirect determinations.

He³ in Magnetic Stars

Zirin has studied the $\lambda 10830$ line in a number of magnetic stars in order to confirm the result of Sargent and Jugaku on the presence of He³ in 3 Centauri A. The infrared image tube of the 72-inch camera of the 200-inch was used with a new transfer lens composed of two Canon f/0.9 camera lenses face to face that has made possible considerable gain in speed. The presence of the He³ line in 3 Cen A is confirmed. He³ is also found in ϵ Ursae Majoris. Both He³ and He⁴ are found in γ^1 Virginis. The helium line could not be detected in α^2 Canis Venaticorum, α Andromedae, β Coronae Borealis, and several other magnetic variable stars. The $\lambda 10830$ line is favorable for such observations because it is the strongest of helium lines. Also, the He³-He⁴ shift is about 1 Å.

The $\lambda 10830$ line has been studied in various other stars also, one of the most interesting results being the observations of $\lambda 10830$ emission in R Scuti.

ABSOLUTE SPECTROPHOTOMETRY

A program of absolute calibration of the flux of α Lyrae is being continued by Oke and Schild. All equipment for the calibration, including the 4-inch Newtonian telescope, the 200-inch prime-focus scanner, the data system, and the platinum blackbody furnace, is now in operation at Palomar. A number of observations of the furnace and α Lyrae are now in hand, but reductions are not yet complete. One problem being encountered is that the extinction along the horizontal path between the source and the 4-inch telescope seems to be greater than was expected. This extinction is being measured by means of a quartz-iodine lamp that is operated alternately on the roof of the powerhouse

and atop a tower located midway between the powerhouse and the 4-inch telescope. From the difference between these two measurements, with allowance made for the reciprocal square decrease of brightness and distance, the horizontal extinction can be deduced. Careful measurements of this extinction are being made each night in which absolute calibration work is done.

Schild is measuring absolute fluxes of bright B and A stars to visual magnitude 3.5 with special emphasis on the stars near the galactic poles, which are presumably not appreciably reddened. These data will be used for a careful comparison with detailed models when the absolute calibration is available. Several

bright stars visible from the northern hemisphere for which direct radius determinations are available from the interferometer work by Dr. R. Hanbury-Brown at the Narrabri Observatory are also being observed.

The 4-inch telescope and scanner are also being used by Oke and Schild to measure absolute fluxes of bright elliptical galaxies, especially NGC 4472. From these data, the K -corrections needed in the luminosity-redshift relation will be derived. It is important to observe the elliptical galaxies in their entirety since population differences between the nuclei and outer regions are thought to exist.

The 4-inch telescope is an ideal instrument with which to make such measurements, since it has a large field and a chopper with which the contribution of the night sky radiation can be continuously monitored.

Visvanathan and Oke completed the observation of 25 stars in the Pleiades cluster. Absolute fluxes in selected 50-Å bands in the region of $\lambda\lambda 3400$ –8000 and $H\gamma$ line strengths have been obtained with an S20 cell at the 60-inch telescope. For the bright early-B stars, the line strength of the He I $\lambda 4472$ was observed with the coudé scanner of the 100-inch telescope.

STAR CLUSTERS

Gaps in the Giant Branch of M 15

The newly modified Sartorius iris photometer has been used to measure a color-magnitude diagram for the globular cluster M 15 that is sufficiently precise so that fine structure has begun to appear. Katem measured 664 uncrowded stars brighter than $V=17$ on ten plates taken by Sandage in each of two colors.

The major new result of the investigation is the appearance of a distinct gap, about 0.5 mag wide in V , centered at $\Delta V=0.9$ mag above the horizontal branch. Other deeper but narrower gaps are probable at $V=15.5$ and $V=16.1$. With respect to a smooth distribution, the deficiency of stars in the major gap is 4.2 times the standard deviation. In addition, a similar structure at the same distance above the horizontal branch also seems to occur in previous color-magnitude diagrams of other globular clusters, including M 5, M 2, M 3, NGC 7006, NGC 362, NGC 5897, and perhaps M 53.

Kristian found it possible to estimate that the intrinsic width of the giant branch in M 15 is less than ± 0.01 mag in $B-V$ at constant luminosity by comparing the known measuring errors with observed dispersion in the color-magni-

tude diagram. This corresponds to a surface temperature difference of $\Delta T/T < \pm 0.01$ and to a difference in radius of $\Delta R/R < \pm 0.02$.

The presence of gaps along the giant sequence suggests that stars do not evolve at a uniform rate along this sequence. If real, the gaps provide constraints on models of nuclear burning in interior shells as evolution proceeds. In order further to confirm the results found for M 15, a similar study of the globular cluster M 3 has been started.

M 92

Using photographic plates and a photoelectric sequence obtained by Sandage with the 200-inch reflector, Hartwick has made star counts to a limiting magnitude $V \simeq 21.5$ in the globular cluster M 92. These counts are being used to obtain semi-empirical evolutionary tracks with the object of obtaining the helium content of M 92.

M 69

Hartwick and Sandage have obtained a color-magnitude (C-M) diagram for the strong-line globular cluster M 69. A photometric sequence was set up in the

cluster by means of a photographic transfer from NGC 6356, in which a photoelectric sequence exists. The C-M diagram shows a stubby red horizontal branch and a relatively gently sloped giant branch resembling 47 Tucanae in both of these respects. With an adopted reddening of 0.2 mag and an assumed magnitude of $M_V = +0.5$ for the horizontal branch, the true distance modulus for M 69 is $(m-M)_0 = 15.2 \pm 0.5$. The membership of four long-period variables near the top of the giant branch seems certain.

NGC 6553

Using photographic plates obtained by Sandage, Hartwick has obtained a color-magnitude diagram for the globular cluster NGC 6553. This cluster is of interest because it has been classified by W. W. Morgan as being among the strongest-lined of all the galactic globular clusters. The cluster is projected on an extremely rich star field, making photometry difficult. A sequence was set up by photographic transfer from NGC 6356, and the scale and zero point of the sequence were established by Racine by photoelectric observations of three of the stars with the 100-inch telescope. While the topology of the C-M diagram of NGC 6553 is similar to that of M 69, the giant branch is less steeply sloped. By adopting a reddening of 0.71 mag and an absolute magnitude for the horizontal branch of $M_V = +0.5$, a true distance modulus of $(m-M)_0 = 14.42 \pm 0.5$ was found. The membership of two long-period variables near the top of the giant branch, as well as one RR Lyrae star, seems certain.

Using photographic plates calibrated with photoelectric standards, Dickens has been studying the following globular clusters in three colors (*U*, *B*, and *V*). The observations were made with the 100-inch and 60-inch telescopes.

NGC 6171

Work on the RR Lyrae variables in this cluster is nearing completion. With the help of Philip Rust, a Caltech student, more than 10,000 star measurements were made on 80 plates using the digitized Sartorius iris-diaphragm photometer. The program included many horizontal-branch stars as well as RR Lyrae variables. Computer programs were written and used to produce light curves for the variables, and also color-magnitude and two-color diagrams for the variables at mean light and for the horizontal-branch stars. Analysis of the residuals of comparison stars also measured indicates that magnitudes and colors averaged over more than 20 plates have a mean error ~ 0.01 mag.

There is quite a sharp separation in color between variable and nonvariable stars along the horizontal branch. There is also a complete separation in color between a- and c-type variables, with a gap of about 0.05 mag between the reddest c-type and the bluest a-type. This is in marked contrast with metal-poor clusters, such as ω Centauri, that show an overlap in color between the two types of variable star. The mean period-amplitude relationship for NGC 6171 occurs at considerably shorter periods than that for variables in metal-poor clusters. Since NGC 6171 appears to be metal rich, its variables can presumably be identified with those in the field with small values of the line strength parameter Δs . These delineate a mean period-amplitude relation at shorter periods than those of large Δs (metal poor). Since NGC 6171 contains large amplitude variables with periods ~ 0.4 day, these variables probably represent the cluster counterparts of the short-period, large-amplitude a-type variable stars previously known to occur only in the field.

NGC 6981

The color-magnitude and two-color diagrams have been obtained by Dickens

for stars in and above the horizontal branch, which occurs at $V=16.9$. Although the integrated spectrum of the cluster is G3, the color-magnitude diagram does not appear to be typical of very metal-rich clusters in that it has nearly equal numbers of stars on each side of the variable gap. Provisional values of the reddening and ultraviolet excess are $E(B-V)=0.07$ and $\delta(U-B)=0.20$.

NGC 7099

Dickens has obtained the color-magnitude and two-color diagrams for stars brighter than $V=17$. The horizontal branch occurs at $V=15.5$, which, using the provisional value of $E(B-V)=0.10$ from *UBV* measurements of field stars, indicates a distance of 9 kpc, assuming $M_V=+0.4$ for the RR Lyrae variables. The cluster appears to be extremely metal poor (integrated spectrum A7) with a heavy concentration of stars on the blue side of the variable gap and an ultraviolet excess of $\delta(U-B)=0.28$. The horizontal-branch stars lie to the left of the standard relationship in the $U-B/B-V$ diagram.

Blue Stars

Sargent continued earlier work on the spectra of blue stars in globular clusters (*Year Book 66*, p. 275). Greenstein (*Astrophys. J.*, 152, 431, 1968) suggested that the sharp K lines of Ca II found by Sargent and others in the spectra of globular-cluster blue stars and attributed to the interstellar medium might be due to the unresolved background of late-type stars in the clusters. Sargent found preliminary evidence against this hypothesis in that a blue star in M 15, twice as far from the center of the cluster as those previously observed, still has a strong, sharp K line.

R Associations

Racine has initiated a photometric and spectroscopic study of *R* associations in

an attempt to investigate the evolutionary characteristics of their illuminating stars as well as the law of interstellar reddening and absorption. The observations are essentially completed for two groups of reflection nebulae in Monoceros and Canis Majoris. Monoceros R2 ($\alpha=6^h05^m$; $\delta=-6^\circ20'$, 1900) contains some 30 members with a range of nearly 1 mag in $E(B-V)$. Canis Majoris ($\alpha=7^h00^m$; $\delta=-11^\circ20'$, 1900) is possibly associated with Canis Majoris OB1, and is set within a long arc of H II emission terminated by a vast reflection nebula illuminated by HD 53623. Among the probable members of CMa R1 one finds the N star W Canis Majoris and the R Coronae-type variable Z Canis Majoris (MWC 165). This star, at the tip of the very small nebula NGC 2327, shows strong P Cygni emission over a peculiar F-type spectrum. Becklin and Neugebauer observed the star in the infrared and found an excess reminiscent of R Monoceros. Other stars possibly related to this group are the R star EM Monoceros and the P Cygni star HD 51480.

The final analysis of the data for these two *R* associations is in progress and observations of similar groups are being made in the summer Milky Way.

Praesepe Cluster

The effect of axial rotation on the colors and magnitudes of stars in Praesepe was further examined by Dickens, Kraft, and Krzeminski. As mentioned in *Year Book 66*, (p. 276), deviations $\delta(U-B)$ for a fixed $(B-V)$ are found to be less well correlated with $Y=(V \sin i)/\langle V \sin i \rangle$ than is the case in the Hyades, and correlation found by Strittmatter between excessive brightness and $(V \sin i)^2$ is poorly confirmed. A study of Strömgren-type photometric parameters made available by Crawford suggests that the unexpectedly poor correlation found for the Praesepe stars may be a result of a very slight differential reddening.

Classification System for Galactic Globular Clusters

In view of recent suggestions by S. van den Bergh (*Astron. J.*, 72, 70, 1967; *Publ. Astron. Soc. Pacific*, 79, 460, 1967) and Sandage and Wildey on the possibility that the helium abundance affects the distribution of stars along the horizontal branch in globular clusters, Hartwick has proposed a two-dimensional classification in which the two indices are the quantity $(B - V)_{0, g}$ defined by Sandage and Smith (*Astrophys. J.*, 144, 886, 1966) and a parameter S defined as the slope of the line joining the intersection of the horizontal and giant branches and a point on the giant branch 2.5 mag

brighter. According to theoretical computations of Demarque, Giesler, and Iben, both of the above indices depend on the helium as well as on the metal abundance of the cluster. The dependences were separated by plotting each quantity against the Morgan class, which is essentially an indicator of metal abundance only. When the two indices for each of the 27 globular clusters with available C-M diagrams are plotted, a two-dimensional progression of horizontal-branch shape is found as one proceeds along a path of constant Y , varying Z , and a path of varying Y , constant Z , thus confirming the suggestion of van den Bergh, Sandage, and Wildey.

INTERSTELLAR GAS AND GASEOUS NEBULAE

Interstellar Absorption Lines

Münch and Vaughan have continued their analysis of high-resolution interferometric observations of interstellar absorption lines in the spectra of nearby early-type stars. A curve-of-growth analysis of the sodium D lines had indicated a typical internal rms velocity dispersion, for apparently single components, of as low as 0.5–1.0 km/sec. Thus hyperfine splitting must be taken into account in interpreting both the curve of growth and the observed profiles. One result of considerable interest is the possible existence of several unusually massive interstellar sodium clouds, which may tend to show lower turbulence than the more common, less massive (or more highly ionized) clouds. In connection with this work, a new larger-aperture Fabry-Perot etalon designed to give improved resolution in the violet has been acquired recently. Further observations of interstellar Ca II (H and K), CN, and CH⁺ in this region are planned.

Vaughan and Danziger used the 100-inch coude interferometric scanner in an attempt to obtain an improved upper

limit on the abundance of interstellar lithium in the directions of ζ Ophiuchi and α Cygni. The observations, which are currently being reduced, were concentrated in five selected bands of 2 km/sec width on and near the expected radial velocities of interstellar absorption. On the basis of a recent study of the H I clouds near ζ Oph by Herbig (*Z. Astrophys.*, 68, 243, 1968), it is considered that, if the hoped-for detection limit of $W_\lambda \leq 0.5$ mÅ at $\lambda 6707$ can be reached, a negative result would imply an interstellar lithium-silicon abundance ratio not greater than the chondritic value.

The spectrum of ζ Oph has been scanned photoelectrically by Münch through a Fabry-Perot interferometer around the expected wavelength $\lambda 8757.69$ Å of the R0 line in the (2, 0) band of the Phillips system of the C₂ molecule. So far no line stronger than 5 mÅ has been detected at an 80% confidence level, but it is planned to continue the observations in order to set a sharper upper limit.

The interstellar Ca II lines have been noted for some time to be present in stars of high-galactic latitude. Since a vertical path through the normal layer of gas at

the galactic pole is supposed to traverse only 100 parsecs, the presence of the K line on low-dispersion spectra of halo blue stars was rather remarkable. The line has now been measured by Greenstein in 33 halo stars of various spectral types and distances from the galactic plane. In stars of moderate galactic latitude, intensities reach 0.55 \AA ; if the absorbing layer is assumed to be plane-parallel, the equivalent width of the interstellar K line reduced to the galactic poles is found to range from 0.35 \AA to 0.10 \AA . There is some indication that the line still increases in strength 500 pc above the galactic plane. There are nine stars whose spectra have been obtained at sufficient dispersion so that velocities are meaningful. After correction for solar motion and the normal galactic rotation terms, the residual velocities of the interstellar clouds at high latitudes are found to run from $+7$ to -34 km/sec . Of the nine, only one has a positive residual cloud velocity. The preponderance of negative velocities is similar to that found in the 21-cm line observations of high-latitude neutral hydrogen. However, the velocities are very much lower, presumably reflecting the higher density of the clouds. The line is also observed to be surprisingly strong in very blue globular-cluster stars; spectra at 90 \AA/mm are available for a few. There is an apparent paradox in that the K line sometimes gives a high velocity similar to that of the globular cluster itself. It is possible that there is some contamination from the background light of red subgiants on the slit of the spectrograph. In M 13, the star Barnard 29 observed at 18 \AA/mm showed a star velocity of -244 and a K-line velocity of -33 km/sec , suggesting that the K line was interstellar in origin. In other cluster stars it is clear that the K line is partly stellar and partly interstellar in M 13. Where the cluster velocity is about -245 km/sec , the K-line velocity observed runs from -141 to -33 .

Orion Nebula

The Orion Nebula has been mapped extensively by Greenstein with emphasis on the spectral region near the Balmer series limit. Coudé spectrograms at 18 \AA/mm were used. Because of velocity broadening, the lines begin to merge near principal quantum number $n=35$. However, the shape of the blended intensity curve in this region, and also near $n=75$ where the lines are completely blended, and just beyond the series limit have all been measured. Plates have also been taken to show the doublet ratio of the [O II] lines of $\lambda\lambda 3726$ and 3729 . In cooperation with Prof. Goldberg at Harvard, and a student, Don Halder, an attempt has been made to fit the run of intensity of the higher members of the Balmer series to obtain the values of b_n (the occupation numbers) for high values of n . This is quite sensitive to electron density, at densities below $n_e=10^4$, and is also somewhat sensitive to temperature if the electron temperature is very low. General agreement with the expected curves computed by Halder has been found; new collisional cross sections have been derived for this purpose. A quite low electron temperature has been derived for NGC 7027, suggestive of a very efficient cooling mechanism. Goldberg, on the basis of elaborate computations of collisional excitation cross sections, has suggested that the cooling mechanism is the forbidden emission of the singly and doubly ionized metals of the iron group. There is a complicating link between the derived electron temperature and electron density, but in the Orion Nebula the electron density can be checked by the variation of the $\lambda 3726/\lambda 3729$ ratio on the assumption that the hydrogen and the forbidden oxygen lines are produced in the same region. In the very inhomogeneous planetary nebula this method may not be so successful. Neugebauer, Becklin, and Hilgeman have continued infrared studies of the Orion Nebula and other regions of pos-

sible star formation. In Orion, 2.2- and 1.65- μ scans were made on the 60-inch telescope of the region surrounding the infrared point source, the nonthermal OH source (observed by Raimond and Elliasen, 1967), and the 20- μ nebula (Kleinman and Low, 1967). The scans showed a large concentration of 2.2- μ radiation in the region and an additional point source of infrared radiation. The source has the same color but is fainter than the first Orion-nebula infrared source found. No image of the source is seen on photographic plates. Low-resolution infrared spectral scans of the Orion nebula were also made with the 24-inch telescope on Mount Wilson. Detection of the Brackett- γ line of hydrogen was made. The strength of this line will be useful in providing information about the radiation from the nebula, as well as the physical characteristics of the nebula itself.

Observations at 2.2 and 1.65 μ were also made on the 200-inch and 60-inch telescopes at the positions of three non-thermal OH sources, W3, W51, and W75. Infrared radiation was detected near all three sources. The sources at W75 and W51 appear extended, whereas the source near W3 is pointlike. None of the infrared sources associated with OH emission can be identified with a visible object on the *Palomar Sky Survey* schmidt prints.

In their survey of the internal kinematics of the Orion Nebula, Wilson and Münch discovered that in certain areas the emission lines become very broad or even double (*Year Book 56*, p. 55). In order to establish the origin of the large mass motions revealed in this fashion, Münch has started a detailed study of line profiles in representative areas of the nebula, using Fabry-Perot interferometers of various resolving powers. The much greater efficiency of the photoelectric detector and larger throughput of the interferometer allow the study of lines fully two orders of magnitude

fainter than was possible photographically. The observed complex profiles of the line [O III] $\lambda 4363$ and their comparison with those of the N1 and N2 lines have shown that the electron temperature is essentially the same in the two gas masses that give rise to the double lines. If the line-doubling is a manifestation of a strong shock wave, then this shock is nearly isothermal. Further observations in the [O II] and [O I] lines are planned in order to obtain information about densities and ionization conditions in the various line components.

Planetary Nebulae

The internal motions in the planetary nebula NGC 6543, which on visual inspection has a markedly helical form, have been studied by Münch on multi-slit plates taken at the 200-inch coude with 4.5 Å/mm dispersion. The radial velocities of various points in the nebula that cover a range between -100 and -25 km/sec suggest that the nebular material is contained on two helical surfaces nearly symmetrical with respect to the central star and moving away from it. The observed arms are not isolated features but are condensations on these helical sheets, which contain sufficient matter to shield the outer regions from the ultraviolet radiation of the central star, as required by a pronounced ionization stratification.

Crab Nebula

Further study of the motions of the line-emitting filaments in the Crab Nebula were carried out by Virginia Trimble (*Year Book 66*, p. 277). The measurement of proper motions for filaments with known radial velocity has allowed the construction of three-dimensional models for the nebula. The motions of the filaments together with other nondynamical data indicate a most probable distance to the object of 2.02 kpc. The proper motion and radial velocity

derived for the nebula as a whole lead to the conclusion that the nebula is moving 112 km/sec faster than the galactic rotation at its position. The proper motion of the so-called central star translates into an equally unlikely space motion, but this result, as well as the motion of the whole nebula, is quite uncertain. The likelihood of a physical connection between the star and the nebula has thus been diminished, but not completely ruled out, as a consequence of these measurements.

The line-emitting filaments have been found to be distributed throughout the nebula rather than on a thin outer envelope, as previously supposed. The motions of the filaments are nevertheless largely radial, each having a velocity nearly proportional to its distance from the expansion center. The mean deviation from this proportionality is 0.01 arc-sec/yr, or 70 km/sec, an amount compatible with the scatter of the filaments around the expansion center in the year 1140 A.D.

INFRARED SKY SURVEY

The infrared survey of the sky funded by the National Aeronautics and Space Administration was completed by Neugebauer and Becklin with the assistance of Edward Groth. A catalog of about 5500 objects, essentially complete to $K=3$, is being prepared for publication

this summer. Descriptions of the instrumentation and preliminary results have been given in previous *Year Books*. It is currently planned to transport the telescope from Mount Wilson to Cerro Tololo in Chile, and thus to survey the entire sky.

OBSERVATIONAL COSMOLOGY

New Determination of the Hubble Constant

A new method to determine the value of the expansion rate of the universe has been used by Sandage. Difficulties with previous methods have centered around a possible local non-Hubble flow in the expansion field for redshifts in the range $0 < c\Delta\lambda/\lambda_0 \leq 4000$ km/sec due to perturbations of the local nonhomogeneous distribution of matter. The new method circumvents this difficulty by (1) reading the apparent-magnitude-redshift relation (the Hubble diagram) for first-ranked E galaxies in clusters at redshifts beyond the local anisotropy ($c\Delta\lambda/\lambda_0 \simeq 10,000$ km/sec), (2) using the fact that such cluster galaxies are remarkably constant in absolute luminosity [$\sigma(M_V) \simeq \pm 0.26$ mag], and (3) calibrating M_V of the first-ranked E cluster galaxy with NGC 4472, which is

the brightest E galaxy in the Virgo cluster.

The distance to the Virgo cluster was found from Racine's photometry of 200-inch plates of globular clusters in NGC 4486 (M 87) taken by Sandage. Racine showed that the luminosity function for these clusters is steep and begins near $B=21.3$ in M 87. If the brightest of these star clusters has the same M_V as the brightest globular cluster in M 31 at $M_V = -9.83$, then the apparent modulus of the Virgo cluster in blue light ($\bar{\lambda} \simeq 4400$ Å) is $m-M=31.1$. The absolute magnitude of NGC 4472 is determined to be $M_B = -21.68$, which, when combined with a new Hubble diagram obtained by Sandage for 42 first-ranked E galaxies in clusters, gives for the Hubble constant $H = 75.3^{+19}_{-15}$ km/sec Mpc, or $H^{-1} = 13^{+3.7}_{-2.7} \times 10^9$ years.

This determination gives an *upper limit* because the brightest globular

cluster of the 2000 clusters in M 87 is likely to be *brighter* than the most luminous cluster in M 31 with only 250 globular-cluster members. Taking this statistical effect into account, it seems possible that H could be as low as 50 km/sec Mpc, or H^{-1} could be as large as 19×10^9 years. The importance of this result is that it removes the difficulty with the time scale given by older estimates of H that were as high as 120 km/sec Mpc ($H^{-1} = 8.1 \times 10^9$ years). If $H^{-1} = 19 \times 10^9$ years, and if the deceleration parameter is $q_0 \simeq +1$, then the time since the fireball is $0.571 H_0^{-1} = 11 \times 10^9$ years, which is consistent with the age of the globular clusters ($T \simeq 10 \times 10^9$ years) and the age of the heavy chemical elements ($T \geq 6.6 \times 10^9$ years) that make up the earth's crust.

Work by Kristian and Sandage has continued on a second method of finding H by use of the angular sizes of ionized hydrogen patches in nearby Sc galaxies. The data are not yet sufficient for a solution. The value of H is of such obvious importance to all theories of cosmology that all efforts to check the new method are desirable.

New Values for the Redshift K-Correction

The corrections to measured intensities of redshifted galaxies to compensate for the shifting of the continuum energy distribution through the measuring bands must be accurately known before the deceleration parameter, q_0 , can be measured via the Hubble diagram.

Oke and Sandage completed a new determination of K_B , K_V , and K_R for the broadband B , V , and R magnitude systems as a function of redshift in the range $0 \leq \Delta\lambda/\lambda_0 \leq 0.30$. New measurements of the energy distribution of 8

giant E galaxies were completed in the wavelength range $3200 \text{ \AA} < \lambda_0 < 11,000 \text{ \AA}$ with a spectral resolution of 50 Å. It was found that $I(\lambda)$ was identical for all eight E galaxies, supporting the view that elliptical systems with $M_V \gtrsim -18$ mag are similar in their stellar content.

The individual results were combined to form a mean $I(\lambda)$ function that was numerically redshifted through the photometric sensitivity functions, $S(\lambda)$, of the three broadband filter functions.

New photoelectric measurements of the $B-V$ color of the first several brightest galaxies in 32 clusters, whose redshifts range from $0 \leq \Delta\lambda/\lambda_0 \leq 0.20$, were compared with the calculations. The predicted $K_B - K_V = f(\Delta\lambda/\lambda_0)$ agree with the observations over the entire redshift range to better than ± 0.02 mag, showing the absence of the Stebbins-Whitford effect, at least to this level of accuracy. Such agreement shows that no change in the shape of $I(\lambda)$ has occurred due to evolution of the stellar content of these E galaxies during the look-back time of $\sim 0.154_0^{-1} \simeq 2.5 \times 10^9$ years. These data provide constraints on the change of integrated luminosity of E galaxies due to evolution of the stellar content. The results are consistent with a new estimate by Sandage that $dV/dt \ll 0.05$ mag/ 10^9 yrs from considerations of the evolutionary pattern of the relevant stars.

The new K -corrections have been used to refine the Hubble diagram reported in previous *Year Books*. The ultimate purpose is to determine the deceleration parameter for a decision between an ever-expanding model or an oscillating universe. The new data, which have been analyzed in a preliminary fashion by Peach and by Sandage, favor the oscillating case with a total cycle time of about 80×10^9 years.

GALAXIES

Distance to the Virgo Cluster

Racine has used plates of M 87 taken with the Hale telescope to obtain colors

and magnitudes for the globular-star clusters associated with this giant elliptical galaxy, which is a member of the

Virgo cluster of galaxies. These globular clusters in M 87 are found to have a mean intrinsic color $\langle(B-V)\rangle = +0.74$, which is not significantly different from the mean colors of globular clusters in the Galaxy or in M 31. The apparent-luminosity function of the M 87 clusters rises steeply at $B=21.2$ mag, and appears to reach a maximum at $B=23.2$ mag. By comparing with the luminosities of the globular clusters in the Galaxy and in M 31, the distance of the Virgo cluster of galaxies is found to be 12 Mpc, and a value of 79 ± 12 km/sec/Mpc is obtained for the Hubble constant.

Galaxies in Groups

Sargent has begun a study of the motions of galaxies in small groups by obtaining spectra of galaxies in four systems discovered by Vorontsov-Velyaminov—VV 144, 150, 165, and 172. (These objects are all illustrated in Arp's *Atlas of Peculiar Galaxies*.) VV 144, which is also I Zw 1122+54, consists of a nucleus that E. M. and G. R. Burbidge found earlier to have a broad $H\alpha$ emission line in its spectrum. A jet projecting from the nucleus has a prominent knot halfway along it. Image-tube spectra of the nucleus of VV 144 confirmed that it resembles a Seyfert galaxy. There are broad emission lines of hydrogen and much sharper emission lines of [O II] and [O III] in the blue region of the spectrum. Spectrograms were obtained with the slit along the jet of VV 144. Although the jet is easily visible to the eye at the telescope, no trace of its spectrum was found, so that it clearly does not radiate a predominantly emission-line spectrum. On the other hand, the knot has an absorption-line spectrum similar to that of an A5 star. The redshift of the knot is 6467 km/sec, as compared to 6169 km/sec for the nucleus. This leads to a minimum mass for the system of about $2 \times 10^{11} M_{\odot}$.

VV 150 and VV 165 both consist of irregular chains, each containing four galaxies. The spectra of these objects

have not yet been measured, but it is evident from visual inspection that in each system the random velocities of the component galaxies do not exceed a few hundred kilometers per second. However, this is not the case for VV 172. This system consists of an almost linear chain of five galaxies about 1 arc-min in projected length and fairly isolated from other galaxies of similar brightness. At least two image-tube spectra have been obtained of each galaxy in the chain. If we denote the galaxies by A, B, C, D, and E, proceeding north to south along the chain, the redshifts are found to be $V_A=16,070$, $V_B=36,880$, $V_C=15,820$, $V_D=15,690$, and $V_E=15,480$ km/sec. Thus galaxy B has a redshift that is 20,000 km/sec greater than those of the other four galaxies. This galaxy is the only one that shows an emission line, $\lambda 3727$ of [O II], in addition to H and K absorption lines. Neglecting galaxy B, the other four galaxies in VV 172 have a systematic trend of redshift along the chain, indicative of rotation. This leads to a lower limit for the mass of the whole system of $\sim 4 \times 10^{11} M_{\odot}$. It is clear that galaxy B is not gravitationally bound to the system if its redshift is a true Doppler shift. Preliminary calculations indicate that the sharpness of the emission and absorption lines in galaxy B rule out the possibility that its excess redshift is gravitational. We are left with the possibilities either that galaxy B is a background galaxy or that it has been expelled from the chain with a kinetic energy of about 10^{60} ergs about 10^7 years ago. Sargent intends to investigate other small groups of interacting galaxies in the future. However, it is already clear that VV 172 is not unique. It merely displays in an extreme form a kind of phenomenon already discovered in Stephan's Quintet and in the interacting triple system IC 3481, Anon, IC 3483. In both these last two cases, the anomalous galaxy has a much *smaller* redshift than the rest of the group.

Association of Galaxies and Radio Sources

Arp continued his investigation of the apparent association of objects with attention to the surroundings of the 13 brightest E galaxies. He concluded that 10 of these galaxies appear to be members of chains of galaxies, and that where radio-source extensions from the central galaxy are well marked, the lines of these extensions coincide with the line of direction of the chain.

Markarian Blue Galaxies

Following a visit by Dr. E. Khachikian of the Burakan Astrophysical Observatory, Armenia, U.S.S.R., Sargent began a program to obtain spectra of blue galaxies discovered by Markarian which had not previously been observed. Satisfactory spectra were obtained of Markarian Nos. 18, 20, 21, 29, 38, 43, 47, and 48, of which Nos. 20, 38, 39, and 43 revealed sharp emission lines.

Seyfert Galaxies

Oke and Sargent have done further work on NGC 4151. The forbidden lines and cores of the hydrogen lines are formed in clouds with $N_e = 5000 \text{ cm}^{-3}$ and $T_e = 20,000^\circ\text{K}$; these clouds fill only a small fraction of the total volume of the nucleus. The intensities of the observed coronal lines can be explained by postulating a hot gas with $T_e = 10^6^\circ\text{K}$, which fills the entire nucleus of the galaxy and for which $N_e = 100 \text{ cm}^{-3}$. The cool clouds and hot medium are nearly in pressure equilibrium. The origin of the very broad wings of the hydrogen lines and the ionized helium line $\lambda 4686$ is still uncertain. They could be produced by a very dense gas in violent motion or possibly by electron scattering.

Infrared Observations

Neugebauer and Becklin also have begun a program of measuring Seyfert

galaxies, compact galaxies, radio galaxies, and related objects at 1.65 and 2.2 μ . About 12 of these galaxies have been measured so far. Several show an infrared excess suggestive of a non-thermal source of radiation.

Dwarf Systems

In combining the period-luminosity curves of variables in the Leo II system with those of other dwarf systems, Miss Swope noticed that the variables brighter than the usual RR Lyrae cluster variables found in these systems may form a period-luminosity curve of their own that falls somewhere between that of the classical Cepheids of Population I and the W Virginis-type Cepheids found in globular clusters. However, the material is still too limited to permit deriving the slope of the curve. But both the Ursa Minor system of van Agt and the Leo II system seem to indicate that this curve extends to variables with period in the usual RR Lyrae range but brighter than the other RR Lyrae variables in the system. Otherwise the work on the Leo II system still awaits a photoelectric sequence in order to determine the photovisual scale and whether there is any reddening in the system.

Polarization

Sandage and Visvanathan have observed photoelectrically at the prime focus of the 200-inch telescope the large-scale filaments of M 82 for polarization and colors in the U, B, V system. The apertures used were 17" and 28" in diameter. A preliminary analysis shows the following: (1) The percentage of polarization varies from 13% to 32%. (2) The position angle of the electric vector is found to be perpendicular to the filamentary structure. (3) Colors show large ultraviolet excess and they fit with the energy spectrum of synchrotron radiation.

A program by Visvanathan is in progress to observe polarization in Seyfert

galaxies, N-type galaxies, and compact galaxies. A number of optically variable quasi-stellar sources, N-type galaxies, and compact galaxies are being observed for polarization and colors.

Visvanathan and Oke have separated the continuum of the Seyfert galaxy into thermal and nonthermal components from the polarization observations and scanner data. The polarization data were obtained with different apertures and the use of *U*, *B*, *V*, and *R* filters at the 100-inch and 60-inch telescopes. Polarization is high in the ultraviolet and gradually decreases toward longer wavelengths. Scanner observations from ultraviolet to infrared have been obtained at the prime focus of the 200-inch telescope. By assuming that the nonthermal component has no wavelength dependence of polarization and that the observed change in percentage polarization with λ is due to the addition of unpolarized galaxy radiation, the continuum of NGC 1068 is separated into thermal and nonthermal components. The derived nonthermal component is smooth and similar to the energy distribution of the quasi-stellar source 3C 273 from 0.33 to 1.0 μ .

Radio Galaxies

Oke discovered that the nucleus of the N-type radio galaxy 3C 371 changed by more than 1 mag during the past two years and could change by 0.10–0.15 mag over intervals of a few days. The absolute luminosity is approximately 10% of that of 3C 48 if 3C 48 is assumed to be at a cosmological distance. It can be concluded that rapid variability cannot now be used in an argument against the cosmological nature of quasars. Using the spectral-energy distribution and the observed strengths of the H and K lines and Mg II line, it is possible to separate the radiation of the background galaxy from that of the nonthermal variable nucleus.

Oke, Sargent, Neugebauer, and Becklin have made scanner observations and

infrared measures of two Zwicky compact galaxies, I Zw 1727+50 and 3C 120. The first of these is variable in light and color, and there must be a substantial nonthermal component. The fact that the energy distribution flattens in the infrared suggests, however, that the stellar contribution is by no means small. The spectral-energy distribution in 3C 120 continues to increase rapidly in the infrared, indicating a strong nonthermal contribution to the observed radiation.

Oke is continuing to obtain spectral-energy distributions of radio galaxies such as NGC 1068, NGC 1275, and Cygnus A. The last is an extremely red object, even when corrections are made for reddening, and its large optical size suggests that there must be a large stellar contribution to the radiation. The accuracy of the observations is not yet sufficient to indicate whether the H and K lines are present in absorption.

Radio Observations of Peculiar Galaxies

Most of the Zwicky compact galaxies do not appear in the catalogs of radio sources, despite the fact that many of these galaxies have spectra that resemble those quasi-stellar objects (e.g., I Zw 0051+12) or radio galaxies. It is possible that many of these galaxies are radio sources which, however, are optically thick at frequencies below 1000 Mc/s where the conventional surveys, such as the 4C, have been carried out. Accordingly, Sargent collaborated with Dr. A. T. Moffet of the California Institute of Technology in a search for radio emission from peculiar galaxies. Observations were made with the Owens Valley interferometer at a base line of 500 feet EW at wavelengths of 21 cm and 3 cm. The objects observed included 50 galaxies in Zwicky's lists and 25 Markarian blue galaxies. At 3 cm none of the peculiar galaxies were detected, indicating an upper limit to the radio flux of about 0.2 flux units. At 21 cm a few objects were detected, including Markarian

3 which is in the 4C catalogue. However, none of the galaxies with broad emission lines in their optical spectra and with colors similar to quasi-stellar objects were detected at either wavelength.

Catalogue of Galaxies and of Clusters of Galaxies

The work on all six volumes covering the unobscured areas from Dec -3° to $+90^\circ$ has now been completed. The manuscripts of the last two volumes, Nos. IV and VI, will be sent to the printer within the next few months. An important contribution to these volumes was made by Herzog with his invention of a simple graph from which values of the precession in all parts of the sky can immediately be measured off. It is expected that the finished volumes will become available at the end of the year. The compilation has been produced under the direction of Zwicky by Herzog, Kowal, Gates, Barbon, Fairall, and others, with funding by the National Science Foundation.

Compact Galaxies

While surveying the 48-inch schmidt plates for clusters of galaxies to be included in the *Catalogue*, Zwicky has continued to select the more obvious compact galaxies. In addition to the five lists previously issued by Zwicky, two more lists (VI and VII) have been assembled which contain 222 and 938 objects, respectively. Altogether the seven lists contain 2309 objects. Of these, several hundred have been investigated directly and spectroscopically by Zwicky, Arp, Oke, Sargent, and Neugebauer at Palomar, and, working with Zwicky, by R. Barbon and T. Fairall using the large reflectors at the Kitt Peak and McDonald Observatories. Some of the main results found are that among the compact galaxies are objects which match the spectra, colors, and absolute magnitudes of other extragalactic objects

that were originally thought to be unique, such as the Seyfert galaxies, N galaxies, and quasars.

Most important for cosmological theory is the fact that some of the extremely compact galaxies that appear starlike when photographed with the 200-inch have larger, and occasionally very much larger, redshifts than the supposedly brightest cluster galaxies of the same magnitude. Examples are:

VII Zw 1354.3+6457. An almost starlike emission-line object even with the 200-inch telescope. Estimated $m_{pg}=16.4$, $U-B=-0.8$, $B-V=+0.6$, and symbolic velocity of recession $V_s=2100$ km/sec, that is, indicative absolute magnitude $M_{pg}=-20.2$.

II Zw 0430.5+0515. A new intrinsically bright Seyfert emission-line galaxy of variable brightness $m=13.1$ to 14.6.

I Zw 1727.1+5015. A variable radio-quiet galaxy with featureless spectrum.

I Zw 0051.0+1225. A luminous compact galaxy with strong Fe II emission lines and $V=13.90$, $U-B=-0.80$, and $B-V=0.36$. With $V_s=18150$ km/sec, an indicative absolute magnitude $M_V=-22.6$ is obtained.

II Zw 2130.0+0956. A new very bright Seyfert galaxy. With $m_p=14.80$ and $V_s=18750$ km/sec, the indicative absolute magnitude becomes $M_p=-21.6$.

The above data are based on observations by Zwicky, Arp, Sargent, and Fairall. These findings demonstrate that there exist compact galaxies which form a continuous link between the ordinary galaxies and the quasars.

Sargent has made spectroscopic observations of 127 objects in Zwicky's first five lists of "Compact Galaxies and Compact Parts of Galaxies." About 100 of these spectra were obtained with the image-tube spectrograph at the Cassegrain focus of the Hale telescope. The rest were obtained with the prime-focus spectrograph. Forty-six of the galaxies have spectra containing emission lines. Usually the emission lines are sharp,

but five galaxies have broad emission lines similar to those in the spectra of Seyfert galaxies. If galaxies in Zwicky's lists are selected for observation on the basis that they appear blue on the *Palomar Sky Atlas* prints, the proportion of emission-line objects is greater than 50%. Some details of the more interesting objects are given below.

1. The "iron galaxy" I Zw 0051+12. The spectrum of this object has been described by Sargent in *Astrophys. J. (Letters)*, 152, L31, 1968. The galaxy has a starlike nucleus of $m_v=14.0$, which gives a spectrum composed of broad emission lines of H and Fe II in a blue continuum. With a redshift of 18,150 km/sec, this object has $M_v=-23.1$ and is as luminous as some quasi-stellar sources if the latter are at cosmological distances.

2. II Zw 2130+09. This is an N-type galaxy having a starlike nucleus of magnitude $V=14.6$. This object has a spectrum similar to that of a Seyfert galaxy with very broad emission lines of H and He II and sharper emission lines of [O II] and [O III]. However, it is unusual in that weak permitted emission lines of Fe II are also visible. This object has a redshift of 18,350 km/sec and $M_v=-22.7$. There is a preliminary indication that Fe II emission lines are indicative of high intrinsic luminosity, since Wampler and Oke have identified these lines in the spectrum of 3C 273.

3. Several compact galaxies, notably II Zw 0553+03, II Zw 0508-02, II Zw 0448+03, I Zw 1535+55, I Zw 1634+52, and II Zw 1448+35, have very strong emission lines principally of H, [O II], and [O III] on a blue continuous background. All these objects have small redshifts and appear to be intrinsically faint. For example, II Zw 0553+03 has a redshift of 617 km/sec and $M_v\sim-15$. No stellar absorption lines have been seen in the spectra of these objects; the mode of excitation of the hot gas remains obscure.

Sargent made *UBV* observations of about 30 compact galaxies in an attempt to relate the colors to the spectra of these objects. The following preliminary results were obtained:

1. The galaxies having very broad emission lines have colors that fall in the region occupied by QSOs in the ($B-V$, $U-B$) diagram.

2. The objects having sharp emission lines occupy a band below the QSOs. Although they are blue, they do not have such pronounced ultraviolet excesses as the QSOs.

3. The objects having weak, sharp emission lines and A-type absorption spectra fall in the region of the ($B-V$, $U-B$) diagram occupied by the Magellanic Irregulars.

4. The compact galaxies with G-type absorption spectra have colors similar to ordinary elliptical galaxies. This is borne out by observations of the continuous energy distribution of a few such objects.

Objects in Zwicky's list of compact galaxies continue to be observed by Arp as well as by Sargent. Arp reports a nearly stellar blue compact, VII Zw 1354+64, with a Seyfert spectrum with the relatively high redshift of $z=0.075$. A blue compact at $17^h9^m+64^\circ17'$ has an early-type absorption spectrum and the relatively high redshift of $z=0.90$. Arp has taken direct, good-seeing photographs and numerous spectra of 3C 371, the galaxy first noted by Oke to be variable in optical light. Aside from a very small, faint haze directly around the nucleus, the galaxy is shown to be optically stellar. Low-contrast emission lines have been recorded in the spectrum, and analysis of the material is proceeding in collaboration with Visvanathan.

Clusters of Compact Galaxies

Among the 2309 objects in Zwicky's seven lists there are many close double, triple, and multiple compact galaxies. Most interesting, however, are larger groups and clusters of compact galaxies

which contain dozens to hundreds of objects. Some of the groups found by Zwicky are the following:

Zw Cl 0152.0+3337. A cluster composed of very compact galaxies, the brightest of which have $m_p=17.3$.

Zw Gr 0338.3+1510. A beautiful group of about 50 compact galaxies, including some close pairs. The brightest members have $m_p=16.3$.

Zw Cl 0658.3+6320. A rich medium-distant cluster with 189 galaxies listed in the *Catalogue*. The redshift of galaxy No. 1, that is of Zw Cl 0658.3+6320-1, is $V_s=28,600$ km/sec. The brightest members have $m_p \cong 16.9$.

Zw Cl 1710.4+6401. A rich cluster of 345 medium-compact and compact galaxies. The symbolic velocity of recession is $V_s=23,820$ km/sec for member No. 3, and 21,440 km/sec for No. 5. The brightest member has about $m_p=15.9$.

Zw Cl 1849.1+7724. An open cluster containing about 325 compact galaxies. For the brightest members, $m_p=15.7$.

Sargent obtained image-tube spectra of the brightest galaxy in each of five Abell clusters—Nos. 655, 963, 2029, 2204, and 2224—in order to determine redshifts as part of a long-term program in cooperation with Sandage and Kristian. Spectra were obtained also of galaxies in two clusters of compact galaxies discovered by Zwicky. Two galaxies in Zw Cl 1710+64 gave redshifts of 21,440 and 23,820 km/sec. This is a preliminary indication that this cluster has an unusually large velocity disper-

sion. A redshift of 28,600 km/sec was obtained for a galaxy in Zw Cl 0659+63.

Sizes of Rich Clusters of Galaxies

From a preliminary survey (*Publ. Astron. Soc. Pacific*, 50, 218, 1938) with the 18-inch schmidt telescope, Zwicky in 1938 determined the size of the average cell occupied by each of the hundred nearest rich clusters of galaxies as $D=7.8$ million parsecs, assuming a Hubble constant $H=550$ km/sec million pc, or $D_0=43$ million pc indicative (for $H=100$ km/sec million pc). Analyzing the distribution of 9800 clusters of galaxies listed in the six volumes of the *Catalogue*, Zwicky has now redetermined D_0 and obtained $D_0=40$ million pc, in good agreement with the value derived in 1938 and the long-standing prediction that no clusters of clusters exist among the objects listed in the *Catalogue*.

Area of the Sky Covered by Clusters of Galaxies

The projected central areas of the rich clusters of galaxies to distances corresponding to symbolic velocities of recession $V_s=c z=75000$ km/sec, as listed in the *Catalogue*, in the least obscured areas cover 60% of the sky. To distances corresponding to $z=2$ instead of $z=1/4$, these central parts of the clusters would cover the sky five times, or actually many more times if the increase in density with distance, in agreement with the cosmological interpretation of the large redshifts of quasars, were taken into account.

THE GALAXY

Studies of the center of the Galaxy at infrared wavelengths have been continued by Neugebauer and Becklin. With the 60-inch telescope, spatial scans at 1.65 and 2.2 μ were made of a region $2^\circ \times 1^\circ$ around the galactic center. In addition to producing much more precise

color measurements of sources at the center, the scans show that most of the extended infrared sources lie within $1/2^\circ$ of that point. In the spring of 1968, similar observations were made, also at 5.0 and 10 μ . The data are still being reduced. Low-resolution (~ 400 Å) spec-

tral scans of the central "point" source at the galactic center were obtained with the 200-inch telescope. These scans, which cover the wavelength regions between 2 and 2.5 μ , will be compared in

detail with similar scans of the extended background obtained at the Newtonian focus. No strong emission or absorption features were observed.

SUPERNOVAE

The search for supernovae with the Palomar schmidt telescopes, supported in large part by the National Science Foundation, has been continued. Ten supernovae (1 each by Herzog and Kowal, 8 by Zwicky) have been discovered in the period from June 1, 1967, to May 31, 1968. In the same period, supernovae were found by the members of the Committee for Research on Supernovae within Commission 28 of the International Astronomical Union. Most remarkable among these is the fourth supernova found in NGC 6946 since 1917. The statistical investigation by Zwicky of multiple appearances of supernovae in certain galaxies indicates that there are stellar systems which in a given long period produce up to 10 times as many supernovae as other systems that structurally and in other known respects have the same characteristics.

Absolute Magnitudes

Indicative absolute photographic magnitudes of 23 supernovae were determined by Kowal and it was found that they are grouped about an absolute value $M_p = 18.6$, with a dispersion of about $\Delta M_p = 0.75$. Kowal also plotted a new symbolic velocity (V_s)—apparent-magnitude (m_p) relation and found (using 7 supernovae of type I in the Virgo and Coma Clusters) $5 \log V_s = m_p + 3.59$, in good agreement with the relation first derived by Zwicky in 1961 (*Publ. Astron. Soc. Pacific*, 73, 185). From 15 supernovae in cluster galaxies and field galaxies, Kowal derives $5 \log V_s = m_p + 3.27$.

Frequency

The frequency of supernovae was originally determined by Zwicky (*Astrophys. J.*, 96, 28, 1942) from his survey, with J. J. Johnson, of 836 galaxies listed in the Shapley-Ames Catalogue, using the 18-inch schmidt telescope. The net result was a frequency of one supernova per 359 years per galaxy, on the average. No preference was found for any of the various structural types of galaxies, except that no supernovae of the type II occurred in any spherical or elliptical galaxies. Barbon, in collaboration with Zwicky, has now redetermined the average frequency of appearance, ν . A total of 2144 galaxies brighter than $m_p = 15.7$ listed in the Catalogue and 45 supernovae appearing in them September 1957 and June 1967 were considered. The net result was $\nu_1 = 1$ supernova per 316 years per galaxy, in close agreement with Zwicky's original result.

Separating the 45 supernovae into 37 that appeared in cluster galaxies and 8 in field galaxies, Barbon obtained

$\nu_{cl} = 1$ supernova per 335 years per cluster galaxy

$\nu_{field} = 1$ supernova per 229 years per field galaxy.

Photometry and Light Curves

Zwicky, Rudnicki, Kowal, Herzog, and Fairall have constructed the light curves of about two dozen supernovae, which will be published in the near future. Photometric data for all known supernovae have been compiled by Kowal, who also derived indicative absolute magnitudes for about 40 objects for

which the maxima have been observed. For type I the maximum photographic magnitude is -18.6 , and for type II the maximum is -6.5 , on the average. It is anticipated that supernovae can be used soon to derive the Hubble constant and the second-order term in the magnitude-redshift relation.

Spectra

Sargent obtained spectra of five supernovae with the image-tube spectrograph at the 200-inch telescope. The supernova in Anon 0813+20 was observed on

April 25, 1968, and found to be of type I. The redshift of the parent galaxy is 12,800 km/sec. The supernova in Anon 1256+27 was observed April 25 and is also of type I. The redshift of the parent galaxy is 12,050 km/sec. The supernova in NGC 6946 was observed on April 25 and found to be of type II. On May 16, 1968, Sargent observed the supernova in NGC 4891; it appears to be of type I. The supernova in the semicompact galaxy Anon 1404+53 was observed the same night. Its spectrum was not readily identifiable.

PULSATING RADIO SOURCES

Following the announcement of the remarkable discovery of pulsating radio sources by Hewish and his collaborators in February 1968, a program was started toward their optical identification.

Photographs of the field of CP 1919 by Arp include sky-limited $H\alpha$ interference-filter plates with the 48-inch schmidt, and limiting exposures in the blue, visual, and red regions with the 200-inch telescope. The best 200-inch photograph, made in good seeing, goes to about $m_{pg}=23$ and is being used by various investigators in the attempted optical identification of the source.

Efforts have so far centered on CP 1919, in part because it was the first source with an accurately determined radio position, and in part because there is a relatively conspicuous optical object at that position that has been suggested by Ryle and Bailey as a possible candidate. The object shows H and K in absorption at a radial velocity of -40 km/sec, according to Sargent and Schmidt. Photoelectric photometry by Sandage and Kristian give $V=17.5$, $B-V=+1.4$, and $U-B=+0.8$.

A search for optical variations in this and other objects has been started by Kristian, Sandage, Schmidt, Grant Snellen of the Caltech Computing Cen-

ter, and Westphal. Pulses from the 200-inch prime-focus photometer are recorded directly on magnetic tape, along with a 12 KHz timing signal, so that the arrival time of each photon can be determined. These data are being searched for periodic fluctuations in brightness, with preliminary results that are negative. One 2-hour run on CP 1919, for example, was played back through a 1024 channel signal-averaging computer that was cycled at twelve times the radio period P , so that periodicities of P , $2P$, $3P$, $4P$, $6P$, or $12P$ with sufficient amplitude should have been detected. The data from the averager were then folded into the submultiples of $12P$ and digitally smoothed with filters of varying widths in order to improve the precision. No periodicity was detected, with results ranging from pulse widths of 50 msec at $12P$ with counting statistics of 1% to quasi-sinusoidal oscillations at $2P$ with counting statistics of 0.2%. Measurements and more detailed analysis of the data are continuing.

For the other two sources with fairly accurate radio positions, photographs of the fields have been obtained by Kristian with the 48-inch schmidt telescope and IIIa-J plates. For CP 0950, there are only two or three objects close to the

plate limit near the radio position. Several objects near the position of CP 1133 as determined by Moffet and Ekers have been investigated spectroscopically by Schmidt. None of the stellar objects

seemed peculiar. The object closest to the radio position turned out to be a compact 16–17 mag galaxy of early-type spectrum. The Balmer lines are seen in absorption at a redshift of 11%.

X-RAY SOURCES

Scorpius X-1

Spectroscopic and photometric data obtained in 1966–1967 have been analyzed in detail and discussed by Kristian, Sandage, and Westphal. Eleven spectrograms were remeasured with the extensive use of digital techniques. The plates, some of which were single-trailed, were scanned in successive strips with a microphotometer whose photoelectric output was amplified and sent by underground cable to the Caltech computing center. There the signal was converted to digital form and stored on magnetic tape by a high-speed analogue-to-digital converter. All subsequent analysis of the plate material was done by computer, using the digitized data. The digital techniques proved quite powerful, both for radial velocity measurements and faint line detection.

Radial velocity changes of the order of 100 km/sec over several hours were found, with the emission lines He II $\lambda 4686$ and the Balmer series moving in opposite directions. In addition to these velocity changes within a single night, there also appear to be systematic night-to-night changes of the same magnitude over a period of a week. The available data are not yet sufficient to determine whether the velocity changes are due to orbital motions or to other effects, such as gas streaming. A minimum statement is that some systematic motion is present, and in this respect Sco X-1 is similar to the binary source Cygnus X-2 (see below).

In addition to the prominent lines previously mentioned here and elsewhere, many faint emission features

were noted, including numerous lines of He I, He II at $\lambda\lambda 3858$ and 4541, several weak lines tentatively identified as due to Fe II, a number of weak, broad features between $\lambda\lambda 4350$ and 4600, and several unidentified lines. No convincing identifications of forbidden lines were made, but the identification problem awaits further study.

A firm lower limit for the distance to Sco X-1, based on Wallerstein's investigation of the line strengths of interstellar Ca II K, is 300 pc. An upper limit, assuming that Sco X-1 is like the brightest old novae, is 1000 pc. Distance estimates based on the number of hydrogen atoms in the line of sight and on the X-ray optical depth, while more uncertain, are consistent with these limits.

The optical flux of Sco X-1 has been monitored on five separate nights for intervals of 2 to 4 hours, and the object was found to be highly and erratically variable. Rapid optical flickering with amplitudes of a few hundredths of a magnitude on a time scale of a few minutes is always present, superposed on slower continuous variations with amplitudes of the order of 0.15 mag and occasional bursts of 0.2 mag lasting for intervals of the order of 10 min and having very rapid rise and decay times.

Two indirect, order-of-magnitude estimates suggest that the flickering may be in some way related to the X-ray output. Assuming that the X rays are produced in a homogeneous bremsstrahlung source, the cooling time is of the order of minutes, which is the characteristic time of the flicker. If the flicker were produced by a low- Q , low-order harmonic pulsation of the star, then,

for plausible parameters, the acoustic energy delivered to the stellar atmosphere would be of the same order as the observed X-ray output, if a mechanism were available to convert one to the other. A test of this idea would be to look for a correlation between the amplitude of the flicker and the X-ray output.

To improve our understanding of the physics of X-ray sources, it is now desirable to observe such a source simultaneously for several hours in the X-ray and optical regions of the spectrum and to test for possible correlations of its variations in the two regions. An early attempt at such an experiment is planned.

Neugebauer, Oke, Becklin, and Garmire have completed a study of Sco X-1 by scanning into the infrared. Photoelectric spectrum scans from $\lambda\lambda 3300$ to $10,800$ and infrared photometric measures at 1.65 and 2.2μ have been obtained on many nights. The observed spectral energy distribution f_ν is nearly flat from 0.33 to 1.0μ and then turns down in the infrared, approaching an $f_\nu \propto \nu^2$ law. The observations rule out free-free radiation from a transparent gas; they also rule out synchrotron radiation unless some self-absorption mechanism operates in the visible. The X rays can be explained by free-free radiation from a gas with a temperature of 5×10^7 K. This same mass of gas can also explain the observed fluxes in the visible and infrared if a reasonable amount of interstellar absorption is assumed, since it can be shown that the optical depth in the visible and infrared is large.

Cygnus X-2

The object tentatively identified as Cyg X-2 has been observed photometrically and spectroscopically by Kristian, Sandage, and Westphal and the identification confirmed.

The photometric data show variations similar to those of the first identified source, Sco X-1. Broad-band *UBV* data

on seven nights showed variations up to 0.3 mag between successive nights. A 5-hour run of continuous monitoring, using a special two-channel ratio photometer developed by Thomas McCord of the Division of Geological Sciences at Caltech, showed short-peaked oscillations of about 0.04 mag and time scales of a few minutes, superposed on a longer fluctuation period of about 1 hour and amplitude 0.10 mag; underlying these was a gradual decline of 0.5 mag over the 5-hour interval.

A 200-inch prime-focus spectrogram was analyzed by means of the digital techniques described above for the Sco X-1 spectra. Among the remarkable features of this spectrogram are (1) very broad hydrogen lines in absorption, with a notable absence of damping wings such as are found in white-dwarf spectra; (2) narrow lines of He II $\lambda 4686$ in emission and circumstellar Ca II in absorption; (3) a strong asymmetry just shortward of $H\gamma$ and of $H\delta$; (4) an absorption feature at $\lambda 4460$ that may be He II $\lambda 4471$; and (5) a faint emission line due to He I $\lambda 4713$. According to Greenstein, the presence of both $\lambda 4713$ and He II $\lambda 4686$ in the same spectrum is very rare. The features (1), (3), and (4) may indicate the presence in the object of gas streams with velocities in excess of 700 km/sec.

The spectrogram is consistent with a suggestion made earlier by C. R. Lynds and E. M. Burbidge that Cyg X-2 is a spectroscopic binary whose components are associated with the He II line and the absorption lines, respectively. The available data are minimal, but the assumption of circular orbits gives a lower limit of 300 km/sec for the relative orbital velocity, approximately equal masses, a period less than 0.4 M days, a separation less than 0.01 M $_\odot$ a.u., and a systematic velocity of -250 km/sec. This velocity would reflect almost entirely the sun's motion in the Galaxy, which would suggest that Cyg X-2 is a Population II object.

For three independent reasons, it appears that the optical flux from the object cannot primarily be nonthermal radiation connected with the production of the X rays: (1) there are quasi-periodic fluctuations as short as a few minutes; (2) the central depth is at least

$A_c=0.4$ for the Ca II K shell line, and the hydrogen lines have appreciable depths; and (3) there is disagreement between the observed brightness and color of the object and an extrapolated bremsstrahlung spectrum fitted to the X-ray data.

QUASI-STELLAR SOURCES

Spectroscopic Observations

Spectroscopic observations of quasi-stellar radio sources are being continued by Schmidt. Most of the sources observed have been identified by Edward T. Olsen of the University of Michigan from accurate positions obtained for 4C radio sources. More than half of the identifications are confirmed by the spectroscopic nature of the objects. Relatively few redshifts have been determined so far.

The most interesting quasi-stellar source is 4C 25.5, which was identified by Olsen with a blue stellar object of visual magnitude around 17.5. Its spectrum shows broad emission lines at wavelengths of 4082 and 5200 Å. These lines are identified as Lyman- α and C IV $\lambda 1549$ emission at a redshift of 2.358, the largest redshift recorded to date. Absorption lines due to Ly- α and C IV are seen on the red side of the emission lines. The absorption-line redshift is 2.3683. Apparently the absorbing material is flowing toward the emitting parts of the quasi-stellar source with a speed of around 900 km/sec. Several other absorption lines have not yet been identified.

Schmidt is undertaking a systematic spectroscopic study of blue stellar objects identified by Sandage and Luyten in fields at 8^h28^m , $+18^\circ$ and 15^h10^m , $+24^\circ$. The objective is to obtain a sample of quasi-stellar sources complete to a limiting magnitude near 18. This will allow a derivation of the space distribution similar to that reported in *Year Book 66* (p. 292) for quasi-stellar radio sources in the revised 3C catalog.

Radio-Quiet Quasars and White Dwarfs

Sandage has completed photoelectric photometry of 300 blue objects listed in the catalogs of the general survey discussed in *Year Book 66* (p. 292). Most of the objects lie in the magnitude range $15 < V < 19.2$. Analysis of the nature of these objects was begun from a study of the $U-B$, $B-V$ diagram. Two major regions of the distribution are along the blackbody line and within the F and G subdwarf domain. There are virtually no stars along the luminosity class III-VI line of the $U-B$, $B-V$ diagram, contrary to the situation for blue stars brighter than $V \simeq 15$. This result confirms the earlier conclusion that a major change in the nature of the blue objects occurs near $V=15$. Although the change is not abrupt, it is clearly present.

Spectra by Schmidt show that all objects above the blackbody line with $0.6 > B-V > 0.0$ are radio-quiet quasars. A number of objects below the blackbody line are also quasars, but the contamination of the sample by nearby white dwarfs is also appreciable.

Sandage and Luyten conclude that brighter than $V \simeq 15$ the blue population consists of stars that follow the luminosity class III-VI line of the $U-B$, $B-V$ diagram. These are hot OB subdwarfs, runaway main-sequence B stars, and hot horizontal-branch stars. Fainter than $V \simeq 15$, the number of these objects decreases drastically due to the steep density gradient perpendicular to the galactic plane. However, at about this magnitude the volume of space sampled for white dwarfs with $V \simeq +10$ and

fainter ($D \leq 100$ pc) becomes large enough so that appreciable numbers of white dwarfs begin to appear. Radio-quiet quasars also begin to occur.

Work on the quasar component became sufficiently precise during the report year to permit a first tentative estimate of the number of radio-quiet quasars per square degree at various apparent-magnitude levels. Spectra by Braccesi and Lynds of the interloper field of Sandage and Véron, together with photoelectric photometry by Sandage in a 200-inch field of 0.04 square degree centered on SA 57, combined with work reported last year, suggest that there are 0.4 QSO per square degree to $B=18.1$, 5 per square degree to $B=18.5$, and 100 per square degree to $B=21.5$. These are consistent with a growth relation

$$\log N(B) = 0.75 B - 14.0$$

for the number of radio-quiet quasars per square degree brighter than magnitude B . The data are not yet of sufficient accuracy to determine whether the difference of the coefficient in B from the constant-density value of 0.6 is significant, but Sandage and Luyten note that their result is consistent with Schmidt's earlier result, based on a smaller but more homogeneous sample of radio quasars, that $d \log N(B)/dB > 0.6$.

Although this determination of the growth function of radio-quiet quasars is tentative, Sandage and Luyten are convinced that the number of such objects per square degree at $B \simeq 22$ is very large. The suggested function gives 10^7 quasars over the entire sky to $B=22$. Sandage believes that such a large number of objects that have either a constant space density [$d \log N(B)/dB = 0.6$] or a positive density gradient outward virtually eliminates the local hypothesis for quasar distances.

Optical Variations of Quasars and N-Type Galaxies

One of the principal distinguishing features of quasi-stellar sources is their

optical variation. Rapid fluctuations of the nonthermal radiation (continuous emission not attributable to stars) in quasars on a time scale of days is one of the phenomena cited by some astronomers in their contention that quasars are at local distances, contrary to the evidence presented by the large redshifts.

This particular argument against cosmological distances for quasars would fall if similar optical variations of nonthermal radiation could be discovered in objects whose cosmological distances were not in dispute.

In 1963 Burbidge, Burbidge, and Sandage pointed out the similarity of the nuclei of Seyfert galaxies and quasars. More recently, the nonthermal radiation in highly nucleated N-type galaxies, isolated by Morgan at the Yerkes Observatory, has been recognized to be of the same type. Because Seyfert galaxies and N-type systems are at distances given by their redshifts, the discovery of optical variations in the nuclei of either of these galaxy types would be crucial.

From repeated photometric observations, Sandage, and independently Oke, found that the optical flux ($3300 \text{ \AA} < \lambda < 10,000 \text{ \AA}$) of the N-type galaxy 3C 371 changed by $\Delta V \simeq 0.7$ mag (nearly a factor of 2 in intensity) between June 1966 and September 1967. Oke found that the time scale for variations of 10–15% was only a few days.

Sandage showed that the N-type galaxies are at their Hubble distances by noting that all members of the class (11 objects) studied to October 1967 follow the redshift-apparent magnitude relation (the Hubble diagram) defined by radio galaxies not classed as N; and that the visual magnitudes, which form the abscissa of the Hubble diagram, are not contaminated with the nonthermal component by more than 0.3 mag for N galaxies with redshifts less than $\Delta\lambda/\lambda_0 = 0.3$. The contamination is less than the spread of radio E galaxies about the

mean line in the Hubble diagram. Because (1) the radio N galaxies contain a radio E system underlying the non-thermal radiation, (2) the radio E galaxies are constant in absolute luminosity to within $\sigma \simeq \pm 0.5$ mag, and therefore define a meaningful Hubble diagram, and (3) there is no dispute over the distances of E galaxies, these data show that N galaxies are at their Hubble distances to within the statistics of the E galaxies with which they are compared.

Later observations by Sandage in August to September 1967 showed that the N galaxies 3C 109 and 3C 390.3 also vary in brightness by at least 0.3 mag. The compact galaxy I Zw 1727+50 was found to be an optical variable by Sandage, and independently by Oke, Sargent, Neugebauer, and Becklin. These discoveries appear to give clear evidence that large variations of radiation on a time scale of days cannot, in themselves, contradict the cosmological distance scale of quasars because the N-type galaxies where such variations have now been observed are at their Hubble distances.

Spectral Energy Distribution

E. J. Wampler at the Lick Observatory and Oke have continued to scan 3C 446 to study the changes in the spectral energy distribution with time and to measure absolute line intensities of C IV $\lambda 1550$ and C III $\lambda 1909$. No line-intensity changes have been observed since the original outburst in 1966. This suggests that the size of the region giving rise to the emission lines is at least one light year. During the summer of 1967, 3C 446 dropped back to near minimum light. The flux in the red, however, remained abnormally high; this may indicate that two distinct energy distributions, one of which is variable, are present.

Oke, Neugebauer, and Becklin have been carrying out a program to determine overall spectral energy distribu-

tions of many quasi-stellar sources. Oke has obtained detailed scan data from $\lambda\lambda 3300$ to 6000 , and a few selected wavelengths between $\lambda\lambda 6000$ and $10,000$. Neugebauer and Becklin, with the 200-inch telescope, have made measurements at 1.65 and 2.2μ . Data now are available for more than 20 objects. In the great majority of cases, the fluxes f_ν change smoothly with wavelength, usually increasing toward the infrared. In a few, as in 3C 273, the spectra are flat and abruptly brighten in the infrared. Occasional objects show very abnormal energy distributions.

Neugebauer and Becklin have attempted measurements of 42 quasars; of these, 29 have been observed to have a K magnitude larger than 15. In the region of the sky between R.A. = $13^h - 0^h - 5^h$ with Dec -30° , 23 of the 26 known quasars brighter than $V=17.0$ have been measured. For this sample the average $V-K$ color index equals 3.1 with a scatter of 0.7. If it is assumed the source of radiation is nonthermal, then this color index corresponds to a spectral index α of 0.6 ± 0.3 . (The flux is proportional to $2^{-\alpha}$.) In general, the $2.2\text{-}\mu$ flux density lies on or near the line connecting the radio and visual flux densities.

Of the 39 sources measured, 19 were measured twice or more at 2.2μ , with the result that only two sources showed variations larger than those expected from normal statistics. These two sources, 3C 279 and 3C 345, are known visual variables. The brightness of 3C 345 decreased by a factor of 3 between summer of 1967 and the spring of 1968. The results of the infrared measurements of quasars are being prepared for publication in collaboration with Oke.

Polarization

Visvanathan has started a program at the 100-inch to measure the polarization in sources that show nonthermal continuum. Fourteen QSS were observed for polarization. Seven of the 14 show mea-

surable intrinsic polarization in the range from 0.014 to 0.087 mag. The source 3C 454.3, which is optically variable, shows polarization of 0.087 mag, and the polarization elements seem to have remained the same on the nights observed. Other QSS that have been observed on different nights do not show variation in P and θ .

Parkes Source 0237-23

An elaborate investigation of the absorption-line spectrum of this object has been completed spectroscopically by Greenstein and Sargent, working at 90 and 190 Å/mm. The best spectrum required observations on two nights. A large number of lines are suspected to be present, and a very selected list of 49 absorption lines in the wavelength range $\lambda\lambda 3300\text{--}4800$ has been obtained. Equivalent width, half widths, and central depths are given for 38 of these at λ greater than 3650 Å. The first observed fact is that the lines are barely resolved, if they are resolved, even at this dispersion. In other words, the lines are very much sharper than in most other quasi-stellar sources. In addition, a large number of lines could not be identified with the first redshift proposed by Arp, Bolton, and Kinman. Work by Greenstein and Schmidt a year ago had already suggested that two separate redshifts were present at $z=2.202$ and 1.956. However, an attempt to identify the full absorption-line list led to great difficulties, so that the only satisfactory procedure, eventually, was the use of a systematic method invented by Bahcall, involving an elaborate computing machine program. Bahcall's program permits the isolation of candidate redshifts on the basis of a comparison of a list of lines expected to be present with the observed list of lines. Bahcall decided to use only lines of singly to quadruply ionized common elements, arising from their ground state. (The latter assumption is required if one expects the lines to be

formed at relatively low electron density.) Bahcall's procedure turned out a large number of redshifts; next it was necessary to isolate those that seemed to be physically reasonable. Therefore, criteria such as the presence of Lyman- α and other strong lines, the identification of the strongest lines for each element, the identification of those expected to be strongest with normal composition, etc., had to be made. The redshifts thus revealed were $z=2.2015$, 1.6706, 1.6560, 1.5132, and 1.3642. In the paper by Bahcall, Greenstein, and Sargent, there is no strong evidence for an absorption redshift at 1.955 that had been found by earlier workers. However, reexamination of this possibility subsequent to submission for publication suggests that, in fact, a shift of 1.9550 may be possible. There is some slight evidence for the presence of a line from a low excited state in one of the shells, but in all the others no excited states are present. It is impossible to conclude whether the lines arise in intergalactic space, in galaxies in the line of sight, or in clouds which have been expelled from the object and which are moving at speeds up to 0.3 the velocity of light relative to the source of the emission lines.

Source 3C 287

A report by T. A. Matthews at the University of Maryland of time-varying nebulosity associated with the quasar 3C 287 has been investigated and not confirmed. Matthews has compared a 100-inch plate taken in 1965 with a 48-inch plate taken in 1966. He reported seeing a "bridge" on the 100-inch plate between the quasar and a fainter, redder star some 3 arc-sec away. On the 48-inch plate he reported that the bridge had expanded into a nebulosity about 4 sec wide, and, assuming expansion at less than the velocity of light, deduced an upper limit of $\frac{1}{4}$ -million light years for the distance of the quasar.

Following early reports of this work,

Kristian and Peach examined twelve 48-inch and four 200-inch plates of 3C 287, taken in 1950, 1964, 1967, and 1968, for evidence of the nebulosity and failed to detect it. In particular, all the 200-inch plates, with better resolution and fainter limiting magnitude than those on which the nebulosity was reported, show the images of the quasar and the nearby star to be distinctly stellar, with no associated nebulosity between or around them. The first of these was taken by Sandage in 1964, a year before the reported changes, and the second by Arp in 1967.

The other two 200-inch plates, taken in 1968 by Kristian and Peach, were compared with two 48-inch plates taken three weeks earlier. The 200-inch plates show no nebulosity. One of the 48-inch plates was taken in exceptionally good seeing. Because of the smaller scale size and the sphero-chromatic aberration of the schmidt telescope, the images are blended, with a perceptible "waist" between them. The second schmidt plate was taken on the following night in poorer seeing and shows the images even more smeared, the waist having disap-

peared. The image on this plate looks similar to that on prints of Matthews' plate. From this comparison and an examination of the appearance of 3C 287 on earlier 48-inch plates, some of them taken on the same nights and others only a month apart, it was concluded that atmospheric, optical, and photographic effects could be sufficient to account for the appearance of the 1966 plate without having to attribute any part of the image to nebulosity.

Several attempts to obtain a 100-inch plate of the object were unsuccessful because of poor weather. An examination of randomly selected plates in the files, however, showed that spurious "bridges" (as photographic artifacts) between pairs similar to 3C 287 and its companion are very common on 100-inch plates.

It appears also that the faint star may have a proper motion. This is based on a comparison of the *Sky Survey* red plate with the later 48-inch plates. The quality of the image on the *Sky Survey* plate, however, is not good, and this result can only be verified in time by a later epoch plate.

THEORETICAL STUDIES

Stability of Rotating Systems

The gravitational stability of thin, rotating disks of stars with respect to small-scale, axisymmetric disturbances has been reexamined by Julian, taking into account possible overstabilities. These overstabilities have been shown to be absent whenever the density of stars in phase space is a decreasing function of the size of the Lindblad epicycle. The existence in such cases of a maximum wavelength of disturbance and a maximum r.m.s. random velocity beyond which all simple instabilities are avoided has been established. On the other hand, overstability has been shown to occur for no rotation if the distribu-

tion of stellar velocities in any given direction has a sufficiently high relative maximum at a nonzero velocity. Moreover, overstabilities have also been shown to arise even in the presence of rotation for that velocity distribution wherein all the Lindblad epicycles are equal in size. This work suggests that stable velocity distributions for the stars in disk galaxies must be similar to the Schwarzschild one.

Electron cyclotron masers are currently being studied by Peter Goldreich of the Geological Sciences Division and Julian with possible applications to radio sources. The effects on the maser phenomenon of various electron distribution functions are being pursued by numerical

analysis of the dispersion equation for electromagnetic waves in a plasma.

The structure of the magnetic field surrounding a rapidly rotating neutron star with a relativistic, co-rotating magnetosphere is being studied by Goldreich and Julian with possible application to pulsating radio sources.

Dissociation Equilibrium of H^-

The assumption that the source function for continuous thermal radiation due to the negative hydrogen (H^-) ion in solar-type stellar atmospheres is equivalent to the Planck function has previously been justified on the grounds that the dissociation equilibrium of the H^- ion is governed by the associative detachment reaction $H^- + H \rightarrow H_2 + e$. Lambert and Dr. B. E. J. Pagel of the Royal Greenwich Observatory, Herstmonceux, England, have rediscussed this assumption on the basis of recent experimental and theoretical estimates for the rates of the important processes controlling the H^- equilibrium. They conclude that the assumption is justified for the photospheres of main-sequence stars and of normal giants, at least for those giants in the range of spectral types G5 III to K5 III. This conclusion is confirmed by an analysis of the observed infrared color indices.

Nonthermal Radiation

Dr. Leonard Searle of the Mount Stromlo Observatory and Sargent found that the equivalent width of the $H\beta$ emission line is about 50 Å in all extragalactic objects having broad emission lines for which this quantity is known. They summarized the existing data for 15 objects, including 6 Seyfert galaxies, 1 N-type galaxy, 3 Zwicky compacts, 2 blue stellar objects, and 2 quasi-stellar radio sources. The expected equivalent width of $H\beta$ due to recombinations in a gas at 20,000°K, the temperature characteristically found for these objects, is

500 Å. It has commonly been supposed that objects of the kind listed have non-thermal optical continua. In order to explain why the optical nonthermal radiation should always weaken the $H\beta$ emission line by about the same amount, Searle and Sargent suggest that the gas in these objects is ionized by the non-thermal radiation. Calculations show that this suggestion is reasonable if the nonthermal radiation has the same spectral index in all the objects and if this value of the spectral index persists below the Lyman limit.

Variations of Extragalactic Sources

A study of the radio flux variations of extragalactic radio sources was carried out by Rees and Simon. It was shown that although the observations suggest that the variable flux arises in an expanding component emitting synchrotron radiation, such a model is untenable for both 3C 120 (a compact galaxy) and 3C 273 (a QSS) unless the expansion velocities are relativistic. A relativistically expanding model would be compatible with the present data in both cases, and very long baseline interferometers should soon provide a further test. It was noted also that the occurrence of relativistic expansion would reduce the estimated severity of inverse Compton losses in the optically variable QSSs.

The character of the optical variations of 3C 273 was studied by Simon and T. Manwell of Cornell University. By analysis of the spectral density of the observed luminosity functions, it was shown that there is considerable difficulty with the hypothesis that the variations are periodic, and it was argued that they may be the result of a random process. Specific attention was directed to the problems of misleading resolution in spectral-density estimates of records of finite length, and the appropriateness of the various statistical tests that had been used in past studies of the fluctuations.

GUEST INVESTIGATORS

Dr. R. d'E. Atkinson of the University of Indiana spent some weeks at the Observatories scanning and remeasuring a number of Humason's early spectrograms of galaxies. He concluded that, when small and large redshifts are compared, there is no significant evidence for a change with time in the atomic fine-structure constant.

Dr. Lawrence A. Aller of the University of California at Los Angeles and Dr. Stanley S. Czyzak of Ohio State University, with the 100-inch and 60-inch telescopes at Mount Wilson, continued their observations of planetary nebulae. Spectrograms of NGC 6572, 7009, 112165, 114997, and 115217 were obtained, and also plates of suitable comparison stars, i.e., θ Crateris and ξ_2 Ceti.

During the first six months of 1968, they were able to secure necessary photoelectric data on the following nebulae in the blue and visible regions, at the 60-inch telescope: blue: NGC 2003, 6886, 111717, and 115217; visible: NGC 2440, 3242, 4361, 6210, 6309, and 113568. The comparison star for these objects was α Leonis.

Investigations on the following nebulae, based on Mount Wilson observations, have been accepted for publication during the past year: NGC 604, 2440, 6543, 112149, and 112165. Also, a paper on the "Chemical Composition of Planetary Nebulae" will appear in the *Intern. Astron. Union Symp. No. 34, Planetary Nebulae*, p. 209. Here Aller and Czyzak have employed certain of their observational data with their latest theoretical results on forbidden transitions and collision strengths in the study of the nebular chemical composition. The observational data in IC 1747, 3568, 5217, and NGC 2003, 4361, 6309, 7026 have been reduced and work has been completed for publication.

With the recent improvements and developments in the calculation of collision strengths of forbidden transitions, and in

particular that of the fine-structure collision strengths, the study of the physical processes in gaseous nebulae demands a more careful analysis of the photoelectric and photographic photometry. A greater stress has to be placed on the observational data, i.e., a more detailed study of the objects has to be made.

Dr. Roberto Barbon of the Osservatorio Astrophisico, Asiago, used the 48-inch schmidt telescope for part of a program on the luminosity function of supernovae. Light curves of the following four supernovae appearing in the Coma cluster of galaxies were obtained: SN 1962a, 1962i, 1963c, and 1963m.

From the material of the 48-inch schmidt supernova search assembled during the last ten years, Barbon investigated the frequency of occurrence of supernovae in clusters of galaxies. The value derived—one supernova per galaxy per 316 years—is in satisfactory agreement with the previous estimates made by Zwicky in 1942 from the material obtained with the 18-inch schmidt telescope.

From May 1966 through November 1967, the 18-inch schmidt has been used by Barbon in surveying spectroscopically the regions surrounding the galactic poles in a search for bright compact galaxies and quasi-stellar objects. The limiting magnitude of the survey is about $13.5 m_{pg}$, and the dispersion is 370 \AA/mm at H_γ . The survey covers approximately 2100 square degrees around the north galactic pole between Dec $+18^\circ$ and $+48^\circ$ and RA 22^h to 16^h , and about 2500 square degrees in the southern galactic cap between Dec -12° and $+12^\circ$ and RA 22^h to 4^h . The reduction of the material is still in progress. While many known red stars, Me variables, and emission-line galaxies have been identified, this spectroscopic survey disclosed no bright compact galaxy or quasi-stellar object.

With the 48-inch telescope, Barbon

searched 13 fields in the southern galactic cap, not covered by the Haro-Luyten survey, for faint blue stars by the three-color method. Thus far 937 new blue stars have been found in the six fields already inspected. A catalog giving positions, magnitudes, and colors is being compiled.

In collaboration with Drs. A. Braccesi and R. Fanti of the University of Bologna, who provided the radio data, Barbon found that seven radio sources from the *Fourth Cambridge Catalogue* could be optically identified with blue stars.

Coudé spectrograms of γ Geminorum were measured by Dr. Wallace R. Beardsley of the Allegheny Observatory in order to obtain accurate radial velocities during the cycle 1942-1955. These velocities are being analyzed to determine whether an apparent shift in the velocity of the system, observed for other cycles, exists for this cycle also. The accurate velocities will also permit a definitive orbit to be calculated. At the suggestion of Greenstein, several measures of coudé spectra of Groombridge 1830 also were made for the period 1948 to date. These measures are being continued in an effort to define a possible radial velocity orbit to the visual companion discovered recently by Worley.

Dr. Alessandro Braccesi of the Institute of Physics, Bologna, obtained multi-color plates with the 48-inch schmidt telescope for identification of radio-quiet quasars by means of the infrared excess technique. Initial tests were promising, as shown by spectrographic confirmation in a number of cases. An iris photometer for measurement of the plates has been built and put into operation in Bologna.

Dr. Robert G. Chambers of the Brackett Observatory, Pomona College, obtained spectrograms in the near infrared ($\lambda \approx 8500$ Å) of 5 Be stars and 13 MK standard stars, using the X spectrograph on the 60-inch reflector. The purpose is to exploit the higher shell transparency expected at longer wavelengths for classification of later Be stars.

During the first week of August 1967, H. Dickel and H. Wendker of the University of Illinois Observatory completed the first half of an $H\alpha$ survey of the emission nebulosities in the Cygnus X complex (near the star γ Cygni). The observational material for the $H\alpha$ survey consists of 28 direct-photographic plates taken with an 80-Å wide $H\alpha$ interference filter on the 48-inch schmidt telescope. Most of the 103aE plates were "preflashed" for 2 sec before being exposed for 75 min at the telescope. Each plate has a set of calibration spots made with the spot sensitometer. Measurements of the surface brightness in $H\alpha$ for the four brightest H II regions (IC 1318a,b,c and HS 191) were made at the Lowell Observatory and will be used to calibrate the plates. Each plate has a usable field of $1.5^\circ \times 1.5^\circ$. The overlapping network of 28 plates is centered on $\alpha(1950.0) \sim 20^h 18^m$, $\delta(1950.0) \sim +41.5^\circ$, or $\ell^{II} \sim 79^\circ$, $b^{II} \sim +30^\circ$. The plates cover the region from approximately $\ell^{II} = 74^\circ - 84^\circ$ and $b^{II} = 0^\circ - 5.5^\circ$.

The Cygnus X region has also been observed at centimeter wavelengths by Wendker. This complex contains many radio sources, of which at least 29 have well-determined thermal spectra. All but four of these coincide with optically visible nebulae on prints of the *Palomar Sky Atlas*. The distribution of $H\alpha$ emission across the nebulae will be obtained from the microphotometry of the plates. These distributions will be compared with the hydrogen continuum emission at the radio wavelengths in order to determine the amount and distribution of interstellar absorption in the region. A comparison of the values of the $H\alpha$ absorption with star-reddening data will give an independent determination of the distances and dimensions of the nebulae. Since these H II regions presumably lie in the local spiral arm which one views tangentially, their distribution in depth along the arm may be derived.

As a guest investigator with the 200-

inch telescope and coude spectrograph, John Danziger of the Harvard College Observatory has completed lithium observations in 17 main-sequence stars between spectral types F5 and K0 in the Coma cluster. There is a marked decrease of lithium with decrease in effective temperature, and at the later spectral types the lithium abundance falls between those observed in the Pleiades and Hyades clusters. This is consistent with an inverse main-sequence age versus lithium abundance correlation and reinforces the previous observational results that lithium is being depleted in the main-sequence phase of stars slightly less massive than the sun. Lithium observations were made also in a number of main-sequence field stars with spectral types as late as M0. At least two stars later than K0 have measurable amounts of lithium, and this extends the region of spectral type in which lithium has been found. An interpretation awaits further observations.

With the Cassegrain scanner on the 100-inch telescope, Danziger has accumulated continuum scans for a number of short-period variables, either dwarf Cepheids or δ Scuti stars. An interpretation of their gravities and temperatures, and hence their evolutionary status, depends on the reliable absolute calibration of the primary standard. This should be forthcoming in the near future.

Dr. O. J. Eggen of the Mount Stromlo and Siding Spring Observatories observed with the 100-inch and 200-inch telescopes in February. His program was concerned with photometry of faint proper-motion stars from Giclas' lists and with some faint stars in Selected Area 57. Poor weather severely limited the results.

During three nights in February and six nights in March, Dr. Erik Holmberg of Uppsala University used the 48-inch schmidt telescope for photometric observations of the Virgo cluster of galaxies, the aim being to determine total magnitudes in the *UBV* system for as

many cluster members as possible. The cluster was covered with two series of plates in each of the three wavelength regions; to calibrate the plates, extrafocal exposures were made of two fields of standard stars. It is hoped that a detailed study of the final magnitudes and colors will, among other things, help to solve the problem presented by the color excesses known to exist for a number of the cluster members.

Coude spectrograms of the blue region of Mira variables, taken with the 100-inch and 200-inch telescopes by Dr. Philip C. Keenan of the Perkins Observatory during the summer of 1967 and preceding summers, provided estimates of the strength of the absorption bands of aluminum oxide. On the average, the AlO absorption is stronger in Mira variables of type Me than in ordinary giant stars at the same temperature. These bands fluctuate greatly from cycle to cycle, and their occasional reversal to emission suggests that when they appear abnormally weak the absorption is reduced by incipient emission. This work was done in collaboration with Deutsch and Garrison, and was reported by Garrison in a joint paper at the April 1968 meeting of the American Astronomical Society.

With the cooperation of Wilson and Deutsch, their coude spectrograms of giants in the range of types K2 to M6 were classified by Keenan, using ratios of atomic lines. These temperature types were found to be consistent with the usual types estimated from the strengths of TiO bands, and the small group of M giants with space velocities ≥ 80 km/sec showed no discrepancies in type. The temperature scale of M giants is thus nearly independent of space motion.

Dr. E. Khachikian of the Burakan Astrophysical Observatory, Armenia, U.S.S.R., visited the Mount Wilson and Palomar Observatories for several weeks in 1968. At Palomar he obtained spectrograms of a number of the Markarian "blue galaxies."

Dr. F. J. Low of the University of Arizona, with the assistance of Mr. A. W. Davidson, carried out infrared observations at the Palomar Observatory in July 1967. Using a newly developed helium-cooled germanium photodetector operating at an effective wavelength of 1.5 microns, observations of about 35 quasars and related objects were made with the 200-inch telescope. All objects investigated were readily detected. The results were consistent with similar observations carried out by Neugebauer and Becklin at 2.2 microns. A single measurement of the polarization of 3C 273 at 1.5 microns yielded the surprisingly large value of $38 \pm 10\%$. Unfortunately, this single observation could not be repeated. Observations at 5 and 10 microns were made on a number of different objects, including a detailed study of the structure of the infrared core in the planetary nebulae NGC 7027. It was found that the bright infrared core is much smaller in diameter than the optical nebula.

During two dark runs in March and May 1968, Dr. Willem J. Luyten of the University of Minnesota took 102 plates in the program of repeating the *Palomar Observatory-National Geographic Society Survey* plates for proper motions. Sixty-seven more plates were taken by Charles Kowal, thus bringing the total of new repeat plates to 752. Only 184 remain to be taken. Some twenty pairs of plates were examined and more than 11,000 proper-motion stars found, among which are several degenerate objects of exceedingly high velocity. In the systematic search for blue stars and quasars, three more plates taken by Sandage with Haro's three-image method have been examined and 1100 more faint blue stars found and published.

Dr. Beverly T. Lynds of the University of Arizona made two visits to the Observatories to undertake a study of the distribution of dark nebulae in galaxies. Photographs of galaxies in the files were examined and notes were made

of the more promising objects for future study. Then measurements were made of the size and position of the dark nebulae relative to the bright features defining the structure of the individual galaxy. To date, Mrs. Lynds has measured M 74, 83, 100, 101, and NGC 5248. These Sc spirals were selected for the initial study because the dark clouds are relatively easily identified and because H α interference photographs were available for delineation of H II spiral features. It is hoped to continue this work and to extend the analysis to both the earlier normal and the barred spirals.

The Snow telescope was used by Dr. Walter E. Mitchell, Jr., of Perkins Observatory through the month of September 1967 in conducting trials and making observations with a solar image slicer and a signal averager. Opposing limbs of the sun were fed in rapid alternation to the spectrograph slit and the observation repeated in the continuum and in the center of a strong Fraunhofer line. The photomultiplier signal was amplified and recorded in a computer of average transients (Technical Measurements, Inc.) so that the scans of opposing limbs were juxtaposed on the instrument's oscilloscope screen. The integrated line and continuum scans were subsequently rendered on chart paper for ease of measurement. The method was demonstrated to have promise for the determination of chromospheric heights relatively free from the effects of poor seeing. Mr. Philip E. Barnhart assisted in this program.

Dr. C. R. O'Dell of the Yerkes Observatory employed the prime-focus scanner of the 200-inch and the Cassegrain-focus scanner on the 100-inch telescope for two investigations. Helium and Balmer line-ratio changes as a function of position in several double-shell planetary nebulae were sought in order to quantitatively evaluate the role of He I triplet self-absorption. Because of bad weather, too few observations were obtained, so that no statement on the results can be made. A search for the

$\lambda 3080$ band of OH, expected to be bright under several models of OH radio sources, was also planned, but again the weather intervened.

Dr. U. W. Steinlin of the University of Basel took plates with the 48-inch schmidt from January through April 1968 for the continuation of work on galactic structure. Attention was concentrated on two fields toward the anti-center for an investigation of the distribution of stars of different age across a spiral arm and for the determination of the exact location of star formation within a spiral arm. Plates were taken in the *RGU* system. Also, plates were taken in both *RGU* and *UBV* systems of a field surrounding the globular cluster M 5, first for deriving the exact relation between the two systems for Population II stars, and secondly for investigating density and luminosity functions across the inner part of the galactic halo.

Dr. S. Strom of the Smithsonian Astrophysical Observatory and Mr. A. Wood, a Harvard graduate student, obtained spectrum scans of the A stars in the Coma cluster using Oke's scanner on the 60-inch telescope. These scans will be used in conjunction with model atmospheres to provide an accurate choice of T_{eff} and gravity for these stars. Abundance analyses of several of these stars are currently under way and will permit a discussion of the variation of metal-to-hydrogen ratio between this cluster and the Hyades.

Observations with the 48-inch schmidt telescope were made in July 1967 by Dr. S. van den Bergh of the David Dunlap Observatory, University of Toronto. The primary purpose was to continue his ten-year program on bright variable stars in members of the Local Group. Multicolor observations were obtained of the galaxies M 31, M 33, and NGC 6822. A second program involved observations of absorbing interstellar clouds. These observations were used to establish a simple classification system for interstellar clouds. On July 10

a plate was obtained of Nova Delphini 1967. Comparison of this plate with the *Sky Survey* led to the identification of a blue star with $12 < V < 13$ as the prenova (van den Bergh and Racine, *Intern. Astron. Union Information Bull. on Variable Stars No. 212*). A plate of the field of the first identified pulsating radio source (Ryle and Bailey, *Nature*, 217, 907, 1968) was obtained on July 5, 1967. Comparison with a *Sky Survey* plate obtained June 15, 1950, shows that the star that Ryle and Bailey identify with the radio source has a proper motion $\mu \leq 0.030$ arc-sec per year. The brightness of this star on the two red plates differs by less than 0.5 mag.

Dr. G. Wallerstein of the University of Washington has obtained 15 Å/mm spectrograms of the 45-day Cepheid SV Vulpeculae from shortly after minimum light to a little beyond maximum. Radial velocity curves for lines of different excitation and ionization levels will be derived. A displaced component at H α appears near mid-rising light and remains until after maximum. The same phenomenon was found by Kraft in the 16-day Cepheid X Cygni.

Wallerstein has obtained spectrograms of several double-line binaries in the Hyades as part of the cooperative program with Dr. A. Batten at the Dominion Astrophysical Observatory. The primary purpose of the program is to obtain minimum masses that may be compared with the rather low masses derived by Eggen from the visual binaries and moving parallaxes. A byproduct will be the derivation of lithium abundances in binaries of various periods and the comparison with lithium abundances of single stars in the Hyades.

An 18 Å/mm spectrogram of RS Ophiuchi taken four months before the outburst of October 26, 1967, showed an A-type shell spectrum similar to that observed by Sanford in 1947 and by Wallerstein from 1960 to 1966. Two spectra of RS Oph in the red taken in February 1968, four months after maxi-

mum, show the [Fe X], [Fe XIV], [Ca XV], and other coronal lines. Theoretical calculations have been initiated to describe the temperature and density structure behind an expanding shock wave as it penetrates a circumstellar envelope. Preliminary print-outs show that strong X-ray emission down to 0.1 Å may be expected during the early phases of the outburst. Coronal line strengths will be predicted and compared with relative intensities obtained with a wide slit.

An unsuccessful search for C^{13} was made in two stars with strong CN bands, ϵ Pegasi (K2 Ib) and α Serpentis (K2 IIIp), using the (2, 0) CN bands in the near infrared. In cooperation with Mr. Thomas Greene, Wallerstein found in α Ser that the ratio of C^{12}/C^{13} is greater than 10. This is unfortunately below the ratio of 30 expected from the nitrogen excess predicted by stellar-evolution models and observed in α Ser.

Robert L. Younkin of the Douglas Aircraft Company has used the pulse-

counting equipment now available with the scanner and 60-inch reflector to extend previous infrared measurements of planets and satellites. Radiance measurements of Io, Ganymede, Uranus, and Neptune were carried out to 1.08 μ . Special attention was given to accurate determination of the radiance of Uranus and Neptune in strong methane bands, where the planets are approximately of the 10th and 12th magnitudes. This will permit calculation of the optical depths of the scattering layer above the methane. This was particularly important in the case of Uranus, where comparison with similar measurements in about 1986, when the planet will be viewed end-on, will yield information on the altitude variation of methane and other gaseous constituents.

An attempt was made to verify previous indications of anomalous limb darkening in strong methane bands on Uranus. The results were inconclusive because of unsatisfactory seeing.

ASTROELECTRONICS LABORATORY

As a measure of the acceptance of photoelectric data systems using digital recording, the following table is provided to indicate utilization of such systems during the 12-month interval ending on May 1, 1968.

Telescope	Elec- tronic Setup	Number of Nights	Total Percentage of Nights Using Data System
200-inch	40*	127	29%
100-inch	63	248	68%
60-inch	52	208	57%

* In addition, 14 electronic setups were made for image tubes.

200-Inch Data System

Under the direction of Dennison, the principal effort of the laboratory was

centered on equipment for the 200-inch Hale Telescope. The newly installed data system was designed to include two reversing counters, an acquisition-interval timer, and a timer that could be adjusted to work with the various optical chopper disks used in front of both the prime-focus scanner and the new multichannel Cassegrain scanner. In addition, this system will accept information from the two telescope encoders, a large variety of digital alpha-numeric switches, which can be used for miscellaneous information, and information taken directly from microswitches on the observing equipment. As an example of the latter type of input, microswitches have been placed on the photometer base so that the observer automatically records whether he is observing a star or the sky background. The data from all the various channels, which can be put in

any order the observer wishes, are recorded on printed paper tape as well as on punched cards for computer use at a later time. If the observer so desires, he may set the data system to restart automatically after each recording cycle so that it is possible to collect a series of accurately timed photometric measurements over a period of several hours. This information can be rapidly put into the computer and the time spectrum of optical variations in the source can be derived easily.

As reported last year, the system also contains the digital control logic for the 200-inch coude spectrograph scanning photometer. The first operation of this entire system, including the use of closed-circuit television for the purpose of remotely displaying digital panels, was successfully used in November 1967. A strip-chart recorder was also employed to read the digital output from the pulse counters, so that the observer could monitor his data while the observations were in progress.

The time-consuming and tedious task of installing digital data cables, as well as many coaxial cables, on the 200-inch telescope was virtually completed during the year. The total number of digital conductors linking the telescope with the data room is approximately 120. Fifty-six cables were also installed in the 200-inch to permit the multichannel spectrum scanner to operate at the Cassegrain focus. A high-voltage power supply and temporary high-voltage cables have been installed on the telescope to permit the operation of the Cassegrain image-tube spectrograph.

Other Data Systems

A semiportable data system for Oke was constructed during the year, and initial tests at Palomar indicate that this system is successful. This system includes a sidereal or civil-time digital clock which is accurate to a fraction of a second per day, and which can be

easily set. A high-speed dual counter permits the recording of both channels, and an internal digital subtraction circuit displays the difference between the two data channels. The system also contains an interval timer and a chopper disk timer, and the necessary electronics to prepare the output of a digital encoder for automatic recording. The recording is done on printed paper tape, but if future requirements arise for summary punched-card recording for computer analysis, this can be added at a later date with relatively minor changes in circuitry. The data system includes controls for starting, stopping, resetting, recording, and holding or suspending the data-gathering operations. Stepping motor controls also permit the observer to set the wavelength of the prime-focus scanner from a considerable distance. In fact, during the operation of this data system with the 4-inch telescope attached to the prime-focus scanner mounted on the 18-inch telescope at Palomar, it has been possible to point the telescope at a star and then to control remotely the entire operation from the operating area, which is one floor below the observing floor.

A similar system is nearing completion for investigation in the Division of Geological Sciences, which will be used for astronomical measurements and also infrared measurements at Mount Wilson. The outstanding difference between the two data systems lies in the fact that the "Geology System" will accept either ratios between the two numbers in the dual-channel counter or differences, as in the case of the absolute-calibration program.

Deutsch has developed some design considerations for a stellar spectrograph that would operate in the mode of a two-dimensional pulse-counter. Such an instrument would provide important advantages over conventional spectrographs, notably in latitude, speed, and photometric precision, while retaining high spectral resolution and finesse. In

order to find whether existing low-noise video cameras could serve in such a spectrograph, he has proposed to make laboratory tests of their signal-to-noise characteristics at very low light levels.

General Laboratory Projects

In the planning of digital data systems for astronomical telescopes, it is necessary to look far ahead to accommodate the probable needs of observers as well as to plan for the most efficient and flexible use of the possibilities offered by a rapidly developing technology. During the past year, Howard Sachs, senior engineer, extended the formulation of general concepts to guide such development. These concepts are designed to adapt to the current technological change from logic elements constructed of indi-

vidual components to integrated circuit modules. The new integrated circuit modules are, in general, not only smaller and more reliable, but are notably less expensive than the assemblies they are designed to replace. The logical functions served by these modules are unchanged, however, so that fundamental circuit designs remain substantially the same. Another important technological factor is the introduction of new high-capacity, compact, high-performance, low-cost computers. Data systems employing such computers at the telescope offer, for the future, many attractive possibilities for efficiency and flexibility. They may also permit the data system at the telescope to communicate directly with larger computers at distant laboratories.

INSTRUMENTATION

Optical Design

The design of the Gascoigne-type corrector lens for the Cassegrain focus of the Palomar 60-inch photoelectric telescope has been completed by Bowen and Vaughan. The lens, both elements of which are of fused silica, gives images of $\frac{1}{2}$ second or smaller over a field $1\frac{1}{4}^\circ$ in diameter.

Bowen has continued his investigations of optics for use with image-intensifier tubes. These include a spectrograph camera of the solid block, concentric-mirror Cassegrain-schmidt type, operating at a focal ratio of $f/1.4$, and various mirror systems for reimaging the phosphor on the photographic plate.

Image-Tube Spectrograph

The design and construction of a nebular spectrograph utilizing a Carnegie-RCA image tube has been reported in preceding year books. The instrument was first used on the 200-inch telescope in August 1967. The speed gain of the

instrument over unaided photographic spectroscopy is about 15 in the blue part of the spectrum. This gain is derived from the ratio of exposure times required to obtain a well-exposed spectrogram with the prime-focus spectrograph at 400 Å/mm and the Cassegrain image-tube spectrograph at 200 Å/mm. The different dispersions used in the comparison reflect the ratio of resolving power for the two instruments.

The instrument has been in general use since December 1967, when the large instrument adapter with offset guider was installed at the Cassegrain focus of the 200-inch telescope. This adapter accommodates both the Cassegrain spectrograph and the new 33-channel spectrometer; it will be available also for other auxiliary instruments.

Multichannel Spectrometer

The new spectrometer, built with a grant provided by the Advanced Research Projects Agency, has been completed and installed at Palomar on the

200-inch Hale telescope. Since only one of the two cold boxes is operational, observations during the next few months will be made with 16 channels covering the spectral range from $\lambda\lambda 5500$ to $11,200$. Within the next two months, the blue cold box, with 13 of the 17 possible photomultiplier tubes, will be mounted on the instrument. The data system has at present enough counters to accommodate 20 channels. Advantage will be taken of the fact that a small computer is to be added to the 200-inch data system during the next six months. With the computer it will be possible to activate all 33 channels without the addition of more bulky pulse-counters. Laboratory tests have shown that there will be little difficulty in operating a large number of photomultiplier tubes, amplifiers, and counters. High reliability is achieved by using pulse-counting techniques and solid-state electronics.

Polarimeter

The construction of the single-channel sky-compensated polarimeter has been completed. It was put into operation at both the 100-inch and 60-inch telescopes by Visvanathan. Observations of twelve standard polarized stars from Hiltner's list give a mean difference in P (Visvanathan-Hiltner) of ± 0.003 mag, or 0.15% , and $\pm 1.8^\circ$ in θ .

60-Inch Photometric Telescope

This project for the Palomar Observatory is proceeding under the grant made by the National Science Foundation to the Carnegie Institution. The 60-inch fused silica disk has been fine-lapped on the 72-inch grinding machine close to the final radius of curvature prior to figuring to the final Ritchey-Chrétien design.

All major mechanical components of the telescope and most subassembly items have now been fabricated and tested; shop assembly is proceeding un-

der the direction of Rule. The main declination and right ascension gears have been made and tested; the drive gearing units are complete and ready for assembly in proper order with the overall schedule. The oil pad and pumping system are complete and temporarily in use for shop assembly and tests. Bearing tests and gear burnishing are proceeding. The upper tube and secondary mirror cage are ready for mounting.

The 60-inch primary cells and mirror-support units were completed in 1967 and all units have now been thoroughly inspected, tested, and calibrated in all attitudes and for all mirror load conditions. The 18 axial lever-support units under all load conditions show total friction of less than 0.1% , as do the 18 radial compound lever units. The flip-cage and secondary focus unit are complete with mirror cells and are ready for drive tests. Limit switches, covers, and accessories are being made and fitted as the assembly proceeds.

Since the approval of the telescope site at Palomar in 1967, much has been done to prepare the site for construction of the Oscar G. Mayer Memorial Dome. Surveys were completed for location, roads, power lines, and utilities. Foundation investigations and site borings were made, resulting in recommendations for location of telescope pier and coudé support on sound bedrock. The site was stripped of topsoil to the rock outcropping level, ready for building foundations. An access road 18 feet wide with maximum grade of about 8% was completed and trenches dug for underground water, telephone, and temporary power service. All site development was ready by May 1, 1968. Building contractors are expected to start construction by the end of June.

Two new Palomar cottages were completed—one for the night assistant at the 60-inch telescope, the other as a staff cottage and lodge annex.

Modification of Mount Wilson 60-inch Telescope

With completion of major modifications to the dome, considerable progress has been made in design and shop fabrication of components required for improvement and renovation of the telescope itself. The remounting of secondary Cassegrain and coudé mirrors into a back-to-back turnover mounting has been completed. The new declination drive gear and mechanism, with remote coordinating readout, is nearing completion. The right-ascension drive-gear unit is under construction, while polar-axis-drive modifications are being planned. Revision of the tube for the 3-mirror coudé system and design work on the coudé room base will be completed shortly.

Solar Instrumentation

A Littrow spectrograph for the new solar equatorial telescope was engineered by Boller and Chivens Division of Perkin-Elmer Corporation under the supervision of Zirin; completion is scheduled for December 1968. The spectrograph has a focal length of 945 inches. A special fluorite-BK2 lens designed by Dr. Richard Dunn of Sacramento Peak Observatory provides essentially achromatic images from $\lambda\lambda 3000$ to 10,000. The spectrograph will be mounted vertically at the coudé focus of the equatorial telescope. It includes a rapid film transport, stepping slit, grating control, and various other provisions to permit rapid-sequence solar spectroscopy. Two interchangeable gratings will be used.

Instrumental improvements at the Hale Solar Laboratory include a photoelectric guider built by Julian, a variable-speed grating drive, and a tilted slit mechanism that permits photography of the slit jaws during the making of spectrograms.

Two small photoheliographs designed by Mr. George Carroll of Lockheed Solar Observatory have been installed, one in

Tel Aviv, Israel, and one on top of the Robinson Laboratory. These 5-inch refractors are equipped with Halle birefringent filters for H α and pulse cameras, as well as photoelectric tracking units. The two locations, Israel and California, present the possibility of obtaining nearly continuous records of the sun. Selected portions of the 50-mm solar image are recorded on 35-mm film. The telescope on Robinson Laboratory has been successful, and results are described elsewhere. The Tel Aviv telescope has suffered from filter problems but is currently in operation.

Robinson Solar Telescope

Rehabilitation of the Robinson Laboratory Solar Telescope is rapidly nearing completion. This work is funded by a NASA contract to Zirin and has been directed by J. David Bohlin. The telescope is an integral part of Robinson Laboratory and was originally designed and 90% completed over thirty years ago (Hale, G. E., *Astrophys. J.*, 82, 111-139, 1935). The coelostat consists of 36-inch and 30-inch diameter flats housed under a 23-foot dome on the Robinson roof. A free-standing, octagonal shaft extends 65 feet deep. The lower 75 feet was planned for vertical spectrographs (never constructed), while the upper 50-foot section contains the image-forming mirror system. The coelostat mirrors illuminate a 26-inch off-axis parabola located 5 feet above the first basement level (the observing level). The primary f/16 beam is folded by a Cassegrain secondary mirror that may be either a flat or any one of three convex mirrors, giving final solar-image diameters of about 4, 8, 14, or 22 inches.

The first phase of rehabilitation will put the telescope into operation as originally designed (using just the 8-inch diameter image), followed by a second phase of additional instrumentation when operational characteristics have been evaluated. General overhaul of various

mechanical and electrical systems was begun in 1967. A two-level observing floor was installed in the shaft at the first basement level in January 1968. New cells for the 30-inch and 26-inch mirrors were fabricated by Boller and Chivens. The mirrors originally constructed for the solar telescope have been realuminized and overcoated with silicon-oxide; they were installed in May. The 36-inch coelostat flat is a glass-on-metal type produced by the Philips Lamp Works of Holland prior to 1935. It consists of about one inch of glass fused onto a ribbed-case iron base having the same coefficient of expansion as the glass. The 30-inch flat is the first of the ribbed Pyrex blanks cast by Corning Glass Works as part of the 200-inch project. The 26-inch is solid Pyrex while the Cassegrain secondaries are early-type fused silica. Final optical and mechanical adjustments are in progress leading to an operational evaluation.

Photoheliograph for Apollo

Howard and Zirin have been conducting in coordination with the Jet Propulsion Laboratory a design study of a proposed high-resolution solar telescope for the Apollo applications program of the National Aeronautics and Space Administration. The aim is to secure both white-light and filter photographs of high quality. During this year, funding for the project was received, and considerable progress was made by a group working at the Jet Propulsion Laboratory. An optical design of a Gregorian system was completed and approved, and a primary mirror of internally cooled ultra-low-expansion fused silica was designed. A quarter-scale model has been built and work is now under way on a full-scale flight-verification unit. It is felt that despite uncertainties of the national space program and the various problems involved with space telescopes, this project will eventually be necessary in the quest for high resolution.

PHOTOGRAPHIC LABORATORY

The Photographic Laboratory under the supervision of William C. Miller continued the program of routine tests of all photographic materials received from the manufacturers. An improved system of reporting results of such tests to the Staff is under development; it will provide observers with a curve for each emulsion, giving speeds at all wavelengths rather than at only one, as is the case with the existing system.

Difey has devoted most of his time to the production of publication and work prints for the Staff and to assisting with plate tests. Of particular interest are the results that he and Miller obtained in formulating an improved developer for astronomical use with the Kodak spectroscopic plates. The new developer has been tested extensively both in the laboratory and in the dome. After

submitting samples to several of our Staff, samples were sent to interested members of other observatories for evaluation. All reports to date have been favorable. For a density of 0.3 above fog, IIa plates developed in the new solution require only 60% of the exposure needed for plates developed in D-76. At a density of 1.0 above fog, the figure is 80%. With the 103a plates the new developer required only 55% as much exposure to produce a density of 1.0 above fog, as with D-19. All other physical characteristics of the developed images produced by the new solution were at least as good as those with the older developers. Of particular interest is a marked decrease in image-edge effects produced by the new formula. The only possible criticism so far is that contrast cannot be controlled by varying develop-

ment time with the new developer. The old formulae will gradually be replaced in all darkrooms by the new solution.

Tests of possible reduction of reciprocity failure at long exposure times by refrigerating the photographic plates were conducted in cooperation with Westphal, who designed the cold box and temperature-control units. Optimum results with spectroscopic plates were achieved at -20°C , but gains were so small that they did not justify the mechanical and optical difficulties involved in providing refrigerated plate boxes at the telescopes. Gains through other means, such as baking, pre-exposure, and the new developer formula, exceeded those resulting from refrigeration.

The demand for astronomical photographs as educational and teaching aids became so great that steps were taken to increase their availability to schools and colleges, and simultaneously de-

crease the time spent by Miller in administering the Observatories' system of distribution and sale, by negotiating a contract with the Hubbard Scientific Company of Northbrook, Illinois, a leader in the distribution at wholesale of educational material and teaching aids to schools and colleges.

Cooperation has continued with the Eastman Kodak Company in mutual efforts to improve materials and methods for astronomical photography. Information for their data books has been given, and Miller is cooperating with their technical writers in the preparation of a new booklet devoted to technical and practical information of use to astronomical photographers.

Miller has actively participated in meetings of both the International Astronomical Union and American Astronomical Society Working Groups on Photographic Materials.

SITE INVESTIGATION

Chile

Work in Chile, under the immediate supervision of Buck, has been directed mainly toward planning for the development of Cerro Morado. Operation of the two astronomical seeing monitors was continued there until the end of the report year. Recording of microthermal fluctuations of the air by means of thermistors at four levels on each of four 100-foot towers, as installed by Westphal, was continued. The resulting data are definitely useful in the selection of specific telescope sites on the summit area. The recording of meteorological data continues, however, not only on Morado but on some other summits in the same general area of Chile. The interest and cooperation offered by the Associated Universities of Research in Astronomy, the University of Chile, and the government of Chile have supported

and justified the further formulation and study of comprehensive plans to develop Cerro Morado as a site for a major astronomical observatory. From Morado field data, and with consideration of requirements based on experience at Mount Wilson and Palomar, Rule has prepared a site development plan for telescope locations, road access, power, water, and other services, providing for optimum utilization of the summit area.

In May 1968, J. W. Boise, Bursar of the Carnegie Institution, joined with Babcock, Rule, and Buck in a visit to Chile for site studies and for a meeting with representatives of AURA to discuss specific plans for boundary locations and for land use by the Institution.

Big Bear Solar Observatory

A search for a new observing station that would permit observation of the

sun with good seeing for extended intervals throughout the day was begun some years ago by Leighton, Howard, and Zirin. It has now been decided to locate at Big Bear Lake in the San Bernardino Mountains. The site offers a 6700-foot altitude and a stable daytime air mass produced by the cool water of the lake; sky transparency is good. The California Institute of Technology has leased from the Bear Valley Mutual Water Company approximately seven acres of land, including 500 feet of lake frontage and a

1000-foot long strip into the lake. Grants from the Max Fleischmann Foundation of Nevada, the National Science Foundation and the National Aeronautics and Space Administration will permit the construction of a solar observatory with a 50-foot concrete tower on a small island about 1000 feet from the north shore of the lake. The new solar equatorial telescope, now completed, will be erected on top of the tower. A laboratory and residence building will be constructed on shore.

BIBLIOGRAPHY

- Anderson, Jean H., *see* Luyten, Willem J.
- Arp, Halton, Radio sources and their galaxies of origin. *Astrofizika* (Burakan), 4, 59-91, 1968.
- Arp, Halton, Analysis of stellar content and Cepheid evolution in NGC 1866. *Astrophys. J.*, 149, 91-108, 1967.
- Arp, Halton, Investigations of the association between radio sources and peculiar galaxies. *Astrophys. J.*, 152, 633-637, 1968.
- Arp, Halton, A compact galaxy (III Zw 2) and a compact radio galaxy (3C 120) with Seyfert-type spectra. *Astrophys. J.*, 152, 1101-1107, 1968.
- Arp, Halton, A counter-jet in M 87. *Astrophys. Letters* (England), 1, 1-5, 1967.
- Arp, Halton, Lines of galaxies from radio sources. *Publ. Astron. Soc. Pacific*, 80, 129-154, 1968.
- Arp, Halton, Nature of the ring around M 81. *Sky and Telescope*, 35, 11, 1968.
- Arp, Halton, and Jeffrey D. Scargle, A high-latitude planetary nebula. *Astrophys. J.*, 150, 707-710, 1967.
- Arp, Halton, and A. D. Thackeray, The star cluster NGC 1866 and its Cepheids. *Astrophys. J.*, 149, 73-89, 1967.
- Arp, Halton, E. Khachikian, C. R. Lynds, and D. W. Weedman, Two new Seyfert galaxies. *Astrophys. J. (Letters)*, 152, L103-L104, 1968.
- Babcock, Horace W., Frederick Hanley Seares (1873-1964), in *Am. Phil. Soc. Year Book*, 1967, pp. 145-148.
- Babcock, Horace W., Optical astronomy in perspective. *Astron. Soc. Pacific Leaflet No. 462*, 8 pp., December 1967.
- Babcock, Horace W., Concentration of elements over the surface of a magnetic star, in *Magnetic and Related Stars*, pp. 97-100, 1000-foot long strip into the lake. Grants from the Max Fleischmann Foundation of Nevada, the National Science Foundation and the National Aeronautics and Space Administration will permit the construction of a solar observatory with a 50-foot concrete tower on a small island about 1000 feet from the north shore of the lake. The new solar equatorial telescope, now completed, will be erected on top of the tower. A laboratory and residence building will be constructed on shore.
- Robert C. Cameron, ed., Mono Book Corporation, Baltimore, Md., 1967.
- Bahcall, John, and Maarten Schmidt, Does the fine-structure constant vary with cosmic time? *Phys. Rev. Letters*, 19, 1294-1295, 1967.
- Bahcall, John N., Wallace L. W. Sargent, and Maarten Schmidt, An analysis of the absorption spectrum of 3C 191. *Astrophys. J. (Letters)*, 149, L11-L15, 1967.
- Barbon, R., A. Braccisi, and R. Fanti, Identification of seven 4C sources with blue objects. *Il Nuovo Cimento, LII-B*, No. 1, 262-266, 1967.
- Barbon, R., *see also* Zwicky, Fritz.
- Baum, William A., *see* McGee, J. D.
- Becklin, E. E., *see* Oke, J. B.
- Bertola, F., *see* Gates, Howard S.
- Boesgaard, Ann Merchant, Observations of beryllium in stars, in *Highlights of Astronomy as Presented at the XIIIth General Assembly, Intern. Astron. Union, Prague, 1967*, pp. 237-242, L. Perek, ed., D. Reidel Publishing Co., Dordrecht-Holland, 1968.
- Bowen, Ira S., Astronomical optics, in *Ann. Rev. Astron. Astrophys.*, Vol. 5, pp. 45-66, Annual Reviews, Inc., Palo Alto, Calif., 1967.
- Braccisi, A., Lynds, R., and Sandage, A., Spectroscopic and photometric data for a sample of quasi-stellar objects identified by their infrared excess. *Astrophys. J. (Letters)*, 152, L105-L110, 1968.
- Braccisi, A., *see also* Barbon, R.
- Bumba, V., Robert Howard, and Sara F. Smith, The sun as a magnetic star, in *Magnetic and Related Stars*, pp. 131-138, Robert C. Cameron, ed., Mono Book Corp., Baltimore, Md., 1967.
- Bumba, V., R. Howard, M. J. Martres, and I. Soru-Iscovici, Patterns of active-region,

- magnetic-field development, in *Intern. Astron. Union Symp. No. 35*, pp. 13-24, K. O. Kiepenheuer, ed., D. Reidel Publishing Co., Dordrecht-Holland, 1968.
- Bumba, V., *see also* Howard, Robert; Krüger, A.
- Ciatti, F., *see* Gates, Howard S.
- Cohen, J. G., and G. L. Grasdalen, Limits on the C^{12}/C^{13} ratio in metal-deficient stars. *Astrophys. J. (Letters)*, 151, L41-L44, 1968.
- Conti, Peter S., Metallic-line stars in the Pleiades, in *Magnetic and Related Stars*, pp. 321-327, Robert C. Cameron, ed., Mono Book Corp., Baltimore, Md., 1967.
- Danziger, I. J., and R. J. Dickens, Spectrophotometry of new short-period variable stars. *Astrophys. J.*, 149, 55-72, 1967.
- Danziger, I. J., *see also* Kuhl, L. V.
- Davis, Dorothy N., Is there technetium in HR 1105? *Astrophys. J. (Letters)*, 152, L13-L15, 1968.
- Davis, Dorothy N., *see also* Schadee, Aert.
- Deutsch, Armin J., Magnetic fields (stellar), in *Encyclopedia of Atmospheric Sciences and Astrogeology*, pp. 534-535, Rhodes W. Fairbridge, ed., Reinhold Publishing Corp., New York, 1967.
- Deutsch, Armin J., Inferences from the statistics of stellar rotation, in *Magnetic and Related Stars*, pp. 181-207, Robert C. Cameron, ed., Mono Book Corp., Baltimore, Md., 1967.
- Dickens, R. J., Robert P. Kraft, and W. Krzeminski, The effect of rotation on the colors and magnitudes of stars in Praesepe. *Astron. J.*, 73, 6-13, 1968.
- Dickens, R. J., *see also* Danziger, I. J.
- Eggen, Olin J., Narrow- and broad-band photometry of red stars, I, Northern giants. *Astrophys. J., Suppl. Ser.*, 14, No. 131, 307-358, 1967.
- Eggen, Olin J., and Jesse L. Greenstein, Observations of proper-motion stars, III. *Astrophys. J.*, 150, 927-942, 1967.
- Fanti, R., *see* Barbon, R.
- Garrison, R. F., Stellar associations. *Astron. Soc. Pacific Leaflet No. 465*, 8 pp., March 1968.
- Garrison, R. F., The spectrum of star No. 1 in NGC 2024. *Publ. Astron. Soc. Pacific*, 80, 20-24, 1968.
- Gates, Howard S., F. Zwicky, F. Bertola, F. Ciatti, and K. Rudnicki, The supernova SN 1966b (Z SN-177) in NGC 4688. *Astron. J.*, 72, 912-914, 1967.
- Grasdalen, G. L., *see* Cohen, J. G.
- Greenstein, Jesse L., Astronomy, in *Americana Annual*, pp. 85-88, The Americana Corporation, New York, 1968.
- Greenstein, Jesse L., Horizontal-branch stars and interstellar lines at high latitude. *Astrophys. J.*, 152, 431-437, 1968.
- Greenstein, Jesse L., and Virginia L. Trimble, Einstein redshift in white dwarfs. *Astrophys. J.*, 149, 283-289, 1967.
- Greenstein, Jesse L., *see also* Eggen, Olin J.
- Gunn, James E., *see* Norton, Robert H.
- Herzog, Emil R., On the identification of five galaxies in the Virgo cluster. *Publ. Astron. Soc. Pacific*, 79, 627-629, 1967.
- Howard, Robert, Magnetic field of the sun (observational), in *Ann. Rev. Astron. Astrophys.*, Vol. 5, pp. 1-24, Annual Reviews, Inc., Palo Alto, Calif., 1967.
- Howard, Robert, Solar magnetism, in *Encyclopedia of Atmospheric Sciences and Astrogeology*, pp. 880-881, Rhodes W. Fairbridge, ed., Reinhold Publishing Corp., New York, 1967.
- Howard, Robert, Budapest Symposium on solar active regions. *Sky and Telescope*, 34, 296, 1967.
- Howard, Robert, Velocity fields in the solar atmosphere. *Solar Physics*, 2, 3-33, 1967.
- Howard, Robert, and William C. Livingston, Some observations bearing on the problem of short-period oscillations. *Solar Physics*, 3, 434-438, 1968.
- Howard, Robert, V. Bumba, and Sara F. Smith, *Atlas of Solar Magnetic Fields, August 1959-June 1966*, Carnegie Inst. of Washington Publ. No. 626, Washington, D.C., 1967.
- Howard, Robert, Andrew W. Tanenbaum, and John M. Wilcox, A new method of magnetograph observations of the photospheric brightness, velocity, and magnetic fields. *Solar Physics*, 4, 286-299, 1968.
- Howard, Robert, *see also* Bumba, V.; Krüger, A.; Smith, Sara F.; Wilcox, John M.
- Irwin, John B., The need for two large Schmidts, in *Vistas Astron.*, Vol. 10, pp. 143-147, Arthur Beer, ed., Pergamon Press, Oxford and New York, 1968.
- Joy, Alfred H., Eclipsing stars, *Astron. Soc. Pacific Leaflet No. 464*, 8 pp., February 1968.
- Joy, Alfred H., Frederick Hanley Seares (1873-1964), in *Biographical Memoirs*, 39, 417-44, published for National Academy of Sciences of the United States by Columbia University Press, New York, 1967.
- Joy, Alfred H., Mount Wilson solar physicist dies (Harold D. Babcock). *Sky and Telescope*, 35, 350, 1968.
- Jugaku, Jun, and Wallace L. W. Sargent, Studies of the peculiar A stars, V, Continuous

- energy distributions. *Astrophys. J.*, 151, 259-263, 1968.
- Khachikian, E., *see* Arp, Halton.
- Karpowicz, M., On the non-existence of clusters of clusters of galaxies, III. *Z. Astrophys.*, 67, 139-142, 1967.
- Karpowicz, M., *see also* Zwicky, Fritz.
- Khogali, A., *see* McGee, J. D.
- Kleczek, J., *see* Krüger, A.
- Koelbloed, David, Abundances in two extremely high-velocity stars. *Astrophys. J.*, 149, 299-315, 1967.
- Kraft, Robert P., The possible presence of Ap stars in young stellar groups, in *Magnetic and Related Stars*, pp. 303-309, Robert C. Cameron, ed., Mono Book Corp., Baltimore, Md., 1967.
- Kraft, Robert P., On the structure and evolution of W Ursae Majoris stars. *Publ. Astron. Soc. Pacific*, 79, 395-413, 1967.
- Kraft, Robert P., *see also* Dickens, R. J.; McGee, J. D.
- Kristian, Jerome, Allan Sandage, and J. A. Westphal, Rapid photometric and spectroscopic variations of the X-ray source Cyg X-2. *Astrophys. J. (Letters)*, 150, L99-L106, 1967.
- Kristian, Jerome, and John V. Peach, The optical image of 3C 237. *Astrophys. J. (Letters)*, 152, L161-L164, 1968.
- Krüger, A., V. Bumba, R. Howard, and J. Kleczek, The interplanetary sector structure and solar radio emission. *Bull. Astron. Inst. Czechoslovakia*, 19, 180-181, 1968.
- Krzeminski, W., *see* Dickens, R. J.
- Kuhi, L. V., and I. J. Danziger, A spectrophotometric study of Delta Scuti and Delta Delphini. *Astrophys. J.*, 149, 47-53, 1967.
- Lambert, D. L., and E. A. Mallia, The C^{12}/C^{13} ratio in the solar photosphere. *Astrophys. Letters (England)*, 1, 85-87, 1968.
- Lambert, D. L., and B. Warner, The abundances of the elements in the solar photosphere, V, The alkaline earths Mg, Ca, Sr, Ba. *Monthly Notices Roy. Astron. Soc.*, 140, 197-221, 1968.
- Lasker, Barry M., The energization of the interstellar medium by ionization-limited H II regions. *Astrophys. J.*, 149, 23-28, 1967; and in *Intern. Astron. Union Symp. No. 31, Radio Astronomy and the Galactic System*, pp. 125-126, H. van Woerden, ed., Academic Press, London, 1967.
- Livingston, William C., *see* Howard, Robert; Norton, Robert H.
- Luyten, Willem J., Jean H. Anderson, and Allan Sandage, Faint blue stars in a field centered at 9:32+24°. *Search for Faint Blue Stars*, A, Pt. XLVIII, 1 p., published by The Observatory, University of Minnesota, Minneapolis, Minn., 1968.
- Luyten, Willem J., Jean H. Anderson, and Allan Sandage, Faint blue stars in a field centered at 12:34+30°. *op. cit.*, Pt. XLIX, 1 p., 1968.
- Lynds, C. R., *see* Arp, Halton; Braccisi, A.
- McCammon, D., *see* Münch, Guido.
- McGee, J. D., A. Khogali, W. A. Baum, and R. P. Kraft, Stellar rotations observed with a spectracon. *Monthly Notices, Roy. Astron. Soc.*, 137, 303-310, 1967.
- Makita, Mitsugu, A study of the green TiO band in the sunspot spectrum. *Solar Physics*, 3, 557-562, 1968.
- Mallia, E. A., *see* Lambert, D. L.
- Manwell, Tom, and Michal Simon, Are the optical luminosity functions of 3C 273 random? *Nature*, 217, 931, 1968.
- Marsden, B. G., *see* Rudnicki, K.
- Martres, M. J., *see* Bumba, V.
- Moffet, A. T., M. Schmidt, C. H. Slater, and A. R. Thompson, The radio source 3C 17. *Astrophys. J.*, 148, 283-286, 1967.
- Münch, Guido, The emission in the central regions of M 31, in *Intern. Astron. Union Symp. No. 29, Instability Phenomena in Galaxies*, pp. 71-74, M. Arakelpan, ed., Meždunarodnaja Kniga, Moscow, 1968.
- Münch, Guido, Internal motions in the planetary nebula NGC 6543, in *Intern. Astron. Union Symp. No. 34, Planetary Nebulae*, pp. 259-266, D. E. Osterbrock and C. R. O'Dell, eds., D. Reidel Publishing Co., Dordrecht-Holland, 1968.
- Münch, Guido, Interstellar absorption lines, in *Stars and Stellar Systems*, Vol. VII, *Nebulae and Interstellar Matter*, chap. 7, pp. 365-402, Barbara M. Middlehurst and Lawrence H. Aller eds., University of Chicago Press, 1968.
- Münch, Guido, G. Neugebauer, and D. McCammon, Infrared coronal lines, II, Observation of [Si X] $\lambda 1.43 \mu$ and [Mg VIII] $\lambda 3.03 \mu$. *Astrophys. J.*, 149, 681-686, 1967.
- Neugebauer, G., *see* Münch, Guido; Oke, J. B.
- Newkirk, G. A., *see* Norton, Robert H.
- Norton, Robert H., James E. Gunn, W. C. Livingston, G. A. Newkirk, and H. Zirin, Surveyor I observations of the solar corona. *J. Geological Res.*, 72, 815-817, 1967.
- Oke, J. B., Effective temperatures and gravities of λ Bootis stars. *Astrophys. J.*, 150, 513-520, 1967.
- Oke, J. B., Optical variations in the radio galaxy 3C 371. *Astrophys. J. (Letters)*, 150, L5-L8, 1967.

- Oke, J. B., A study of the Seyfert galaxy NGC 4151. *Proc. Astron. Soc. Australia*, 1, 7, 1966.
- Oke, J. B., Photoelectric spectrophotometry of quasi-stellar sources, in *Intern. Astron. Union Symp. No. 29, Instability Phenomena in Galaxies*, pp. 328-341, M. Arakeljan, ed., Meždunarodnaja Kniga, Moscow, 1967.
- Oke, J. B., A study of the nucleus of the Seyfert galaxy NGC 4151 *op. cit.*, pp. 91-96.
- Oke, J. B., Report on absolute spectrophotometry, in *Trans. Intern. Astron. Union*, Vol. 13A, *Reports on Astronomy*, pp. 637-638, L. Perek, ed., D. Reidel Publishing Co., Dordrecht-Holland, 1967.
- Oke, J. B., and Wallace L. W. Sargent, Nucleus of the Seyfert galaxy, NGC 4151. *Astrophys. J.*, 151, 807-824, 1968.
- Oke, J. B., and Rudolph E. Schild, A practical multiple-reflection technique for improving the quantum efficiency of photomultiplier tubes. *Applied Optics*, 7, 617-622, 1968.
- Oke, J. B., W. L. W. Sargent, G. Neugebauer, and E. E. Becklin, A variable radio-quiet compact galaxy, I Zw 1727+50. *Astrophys. J. (Letters)*, 150, L173-L176, 1967.
- Oke, J. B., *see also* Visvanathan, N.
- Peach, John V., *see* Kristian, Jerome.
- Racine, René, Preliminary colors of faint objects around M 87. *Publ. Astron. Soc. Pacific*, 80, 326-329, 1968.
- Rees, M. J., and Michal Simon, Evidence for relativistic expansion in variable radio sources. *Astrophys. J. (Letters)*, 152, L145-L148, 1968.
- Rudnicki, K., Observations of 5 old supernovae. *Astron. Nachr.*, 290, 85-87, 1967.
- Rudnicki, K., Observations of 6 supernovae. *Astron. Nachr.*, 290, 135-139, 1967.
- Rudnicki, K., General features of clusters of galaxies. *Soviet Astron.-A.J.*, 11, 59-62, 1967.
- Rudnicki, K., and B. G. Marsden, Periodic comet Grigg-Skjellerup (1966f). *Intern. Astron. Union Circular No. 2029*, August 9, 1967.
- Rudnicki, K., *see also* Gates, Howard S.; Zwicky, Fritz.
- Rust, David M., Chromospheric explosions and satellite sunspots, in *Intern. Astron. Union Symp. No. 35, Structure and Development of Solar Active Regions*, pp. 77-84, K. O. Kiepenheuer, ed., D. Reidel Publishing Co., Dordrecht-Holland, 1968.
- Sandage, Allan, Additional data on the optical variation of 3C 371 and other properties of N-type galaxies. *Astrophys. J. (Letters)*, 150, L9-L12, 1967.
- Sandage, Allan, Redshifts of nine radio galaxies. *Astrophys. J. (Letters)*, 150, L145-L146, 1967.
- Sandage, Allan, Optical variation of the nuclei of three compact galaxies together with new photometric data for Seyfert galaxies. *Astrophys. J. (Letters)*, 150, L177-L182, 1967.
- Sandage, Allan, A new determination of the Hubble constant from globular clusters in M 87. *Astrophys. J. (Letters)*, 152, L149-L154, 1968.
- Sandage, Allan, The time scale for creation, in *Galaxies and the Universe*, pp. 75-112, Lodewijk Woltjer, ed., Columbia University Press, New York, 1968.
- Sandage, Allan, Radio galaxies and quasars, II, in *Highlights of Astronomy as Presented at the XIIIth General Assembly of the Intern. Astron. Union, Prague 1967*, pp. 45-70, L. Perek, ed., D. Reidel Publishing Co., Dordrecht-Holland, 1968.
- Sandage, Allan, Three photoelectric measurements of LP 93-21. *Intern. Astron. Union Circular No. 2069*, April 26, 1968.
- Sandage, Allan, Observational cosmology. *Observatory*, 88, 91-106, 1968.
- Sandage, Allan, Optical data on quasi-stellar sources, in *Trans. Intern. Astron. Union*, Vol. 13A, *Reports on Astronomy*, pp. 579-587, L. Perek, ed., D. Reidel Publishing Co., Dordrecht-Holland, 1967.
- Sandage, Allan, and G. A. Tammann, A composite period-luminosity relation for Cepheids at mean and maximum light. *Astrophys. J.*, 151, 531-546, 1968.
- Sandage, Allan, and Robert Wildey, The anomalous color-magnitude diagram of the remote globular cluster NGC 7006. *Astrophys. J.*, 150, 469-482, 1967.
- Sandage, Allan, *see also* Braccisi, A.; Kristian; Jerome; Luyten, Willem J.; Tammann, A. G.
- Sargent, Wallace L. W., Spectra and masses of the blue "horizontal-branch" stars in M 67. *Astrophys. J.*, 152, 885-889, 1968.
- Sargent, Wallace L. W., A luminous compact galaxy with strong Fe II emission lines. *Astrophys. J. (Letters)*, L31-L34, 1968.
- Sargent, Wallace L. W., A new intrinsically bright Seyfert galaxy. *Publ. Astron. Soc. Pacific*, 79, 369-371, 1967.
- Sargent, Wallace L. W., and Leonard Searle, The interpretation of the helium weakness in halo stars. *Astrophys. J. (Letters)*, 150, L33-L38, 1967.
- Sargent, Wallace L. W., and Leonard Searle, A quantitative description of the spectra of the brighter Feige stars. *Astrophys. J.*, 152, 443-452, 1968.

- Sargent, Wallace L. W., *see also* Bahcall, John N.; Jugaku, Jun; Oke, J. B.
- Scargle, Jeffrey D., The Crab Nebula—913 years after its outburst. *Astron. Soc. Pacific Leaflet No. 457*, 8 pp., July 1967.
- Scargle, Jeffrey D., A note on relativistic magnetohydrodynamics. *Astrophys. J.*, *151*, 791–796, 1968.
- Scargle, Jeffrey D., *see* Arp, Halton.
- Schadee, Aert, Molecular band intensities in G and K stars. *Astrophys. J.*, *151*, 239–258, 1968.
- Schadee, Aert, and Dorothy N. Davis, Zirconium isotope ratios in HR 1105. *Astrophys. J.*, *152*, 169–179, 1968.
- Schild, Rudolph E., *see* Oke, J. B.
- Schmidt, Maarten, Radio galaxies and the origin of cosmic rays. *Astrophys. J. (Letters)*, *149*, L39, 1967.
- Schmidt, Maarten, Space distribution and luminosity functions of quasi-stellar radio sources. *Astrophys. J.*, *151*, 393–410, 1968.
- Schmidt, Maarten, *see also* Bahcall, John N.; Moffet, A. T.
- Searle, Leonard, *see* Sargent, Wallace L. W.
- Simon, Michal, *see* Manwell, Tom; Rees, M. J.
- Slater, C. H., *see* Moffet, A. T.
- Smith, Sara F., and Robert Howard, Magnetic classification of active regions. *Intern. Astron. Union Symp. No. 35, The Structure and Development of Solar Active Regions*, pp. 33–42, K. O. Kiepenheuer, ed., D. Reidel Publishing Co., Dordrecht-Holland, 1968.
- Smith, Sara F., *see* Bumba, V.; Howard, Robert.
- Soru-Iscovici, I., *see* Bumba V.
- Spiegel, E. A., *see* Stein, Robert F.
- Stein, Robert F., and E. A. Spiegel, Radiative damping of sound waves. *J. Acoust. Soc. Am.*, *42*, 866–869, 1967.
- Swope, Henrietta H., Progress report on the Leo II system. *Publ. Astron. Soc. Pacific*, *79*, 430–440, 1967.
- Tammann, G. A., and Allan Sandage, The stellar content and distance of the galaxy NGC 4203 in the M 81 group. *Astrophys. J.*, *151*, 825–860, 1968.
- Tammann, G. A., *see* Sandage, Allan.
- Tanenbaum, Andrew W., *see* Howard, Robert.
- Thackeray, A. D., *see* Arp, Halton.
- Thompson, A. R., *see* Moffet, A. T.
- Trimble, Virginia L., *see* Greenstein, Jesse L.
- Utter, Merwyn G., The heavens in 1968. *Astron. Soc. Pacific, Ann. Ser.*, 8 pp., January 1968.
- Vaughan, Arthur H., Jr., Astronomical interference spectroscopy. *Ann. Rev. Astron. Astrophys.*, Vol. 5, pp. 139–166, Annual Reviews, Inc., Palo Alto, Calif., 1967.
- Vaughan, Arthur H., Jr., Interferometer measurement of star diameters (a one-hundredth anniversary). *Astron. Soc. Pacific Leaflet No. 458*, 8 pp., August 1967.
- Vaughan, Arthur H., Jr., and Harold Zirin, The helium line $\lambda 10830 \text{ \AA}$ in late-type stars. *Astrophys. J.*, *152*, 123–139, 1968.
- Visvanathan, N., Interstellar polarization. *Astron. Soc. Pacific Leaflet No. 463*, 8 pp., January 1968.
- Visvanathan, N., Polarization observations in the radio galaxy 3C 371 and X-ray source Cyg X-2. *Astrophys. J. (Letters)*, *150*, L149–L152, 1967.
- Visvanathan, N., and J. B. Oke, Non-thermal compound in the continuum of NGC 1068. *Astrophys. J.*, *152*, L165–L168, 1968.
- Warner, B., *see* Lambert, David L.
- Weedman, D. W., *see* Arp, Halton.
- Weistrop, Donna, Equivalent widths of H α in late-type stars. *Publ. Astron. Soc. Pacific*, *79*, 546–550, 1967.
- Westphal, J. A., *see* Kristian, Jerome.
- Wilcox, John M., and Robert Howard, Persistent solar magnetic pattern extending over equatorial latitudes. *Phys. Rev. Letters*, *20*, 1252–1254, 1968.
- Wilcox, John M., *see also* Howard, Robert.
- Willey, Robert, *see* Sandage, Allan.
- Wilson, Olin C., Radial velocities of dK and dM stars. *Astron. J.*, *72*, 905–912, 1967.
- Wilson, Olin C., Stellar chromospheres. *Encyclopedia of Atmospheric Sciences and Astrogeology*, pp. 947–949, Rhodes W. Fairbridge, ed., Reinhold Publishing Corp., New York, 1967.
- Woerden, Hugo van, Structure and motions in the interstellar medium, in *Intern. Astron. Union Symp. No. 31, Radio Astronomy and the Galactic System*, pp. 3–30, H. van Woerden, ed., Academic Press, London, 1967.
- Zirin, Harold, The excitation of coronal emission lines as a measure of electron density. *Astrophys. J.*, *151*, 383–388, 1968.
- Zirin, Harold, He⁺ in several magnetic stars. *Astrophys. J. (Letters)*, *152*, L177–L178, 1968.
- Zirin, Harold, The solar atmosphere, in *The Earth in Space*, pp. 25–32, Hugh Odishaw, ed., Basic Books, New York, 1967; condensed version, *Astron. Soc. Pacific Leaflet No. 466*, 8 pp., April 1968.
- Zirin, Harold, The solar atmosphere, in *Proc. Intern. School of Physics, Enrico Fermi, Course 39, Plasma Astrophysics*, pp. 124–141, P. A. Sturrock, ed., Academic Press, New York and London, 1967.

- Zirin, Harold, *see also* Norton, Robert H.; Vaughan, Arthur H., Jr.
- Zwicky, Fritz, Compact and dispersed cosmic matter, Part 1, in *Advances in Astronomy and Astrophysics*, Vol. 5, pp. 267-343, Z. Kopal, ed., Academic Press, New York, 1967.
- Zwicky, Fritz, Neutron-star-studded compact galaxies. *Astrophysics, Acad. Sci. Armenian SSR*, 3, 519-524, 1967.
- Zwicky, Fritz, Blue compact galaxies in the Leo A and B clusters. *op. cit.*, 525-528.
- Zwicky, Fritz, Découverte des deux premiers amas formés par des galaxies compactes. *C. R. Acad. Sci. Paris*, 266, 103-105, 1968.
- Zwicky, Fritz, Systematische Entdeckung von Kosmischen Objekten. *Die Sterne*, 43, 105-112, 1967.
- Zwicky, Fritz, Discovery of two supernovae. *Intern. Astron. Union Circular No. 2070*, April 29, 1968.
- Zwicky, Fritz, Morphology of the instability of galaxies, in *Intern. Astron. Union Symp. No. 29, Instability of Phenomena in Galaxies*, pp. 46-70, M. Arakeljan, ed., Meždunarodnaja Kniga, Moscow, 1967.
- Zwicky, Fritz, List of compact galaxies and compact parts of galaxies, eruptive galaxies and post-eruptive galaxies, Sixth and Seventh, June 1968, California Institute of Technology, Pasadena, Calif.
- Zwicky, Fritz, The 1966 Palomar supernova search. *Publ. Astron. Soc. Pacific*, 79, 456-459, 1967.
- Zwicky, Fritz, and R. Barbon, Supernova 1962a of type I in the Coma cluster of galaxies. *Astron. J.*, 72, 1366-1367, 1967.
- Zwicky, Fritz, Maria Karpowicz, and K. Rudnicki, Photographic observation of 3C 273. *Z. Astrophys.*, 67, 243-245, 1967.
- Zwicky, Fritz, *see also* Gates, Howard S.

STAFF AND ORGANIZATION

Professor Jan H. Oort, Director of the University Observatory, Leiden, The Netherlands, held an appointment as Research Associate during the year, and visited the Observatories during the months of December, January, and February.

Dr. Leonard T. Searle became a Staff Member of the Observatories on June 21, 1968. Recently on the staff of the Mount Stromlo Observatory, Australian National Observatory, Dr. Searle is well known here, having held an appointment as research fellow at the Mount Wilson and Palomar Observatories from 1960 to 1963.

Miss Henrietta Swope, research fellow at the Observatories, retired after sixteen years during which she made important contributions to the study of variable stars in dwarf galaxies of the local group as well as in the Andromeda Galaxy, M 31. Her work, initiated in collaboration with the late Walter Baade, resulted in the most precise calibration of the distance to external galaxies.

Dr. Fritz Zwicky, a Staff Member of the Observatories since 1948, retired on June 30, 1968. His prolific researches, characterized by an independent ap-

proach and conducted with great energy, covered a wide range in the fields of cosmology and astrophysics. He organized large-scale collaborative programs for the discovery of supernovae and for the cataloging of galaxies.

Research Division

Distinguished Service Member, Carnegie Institution of Washington

Ira S. Bowen

Research Associate

Jan H. Oort

Staff Members

Halton C. Arp

Horace W. Babcock, Director

Edwin W. Dennison

Armin J. Deutsch

Jesse L. Greenstein¹

Robert F. Howard

Robert P. Kraft²

Robert B. Leighton³

Guido Münch⁴

J. Beverley Oke⁴

Bruce H. Rule, Chief Engineer

Allan R. Sandage

Wallace L. W. Sargent⁵

Leonard T. Searle

Maarten Schmidt⁴

Arthur H. Vaughan, Jr.
 Olin C. Wilson
 Harold Zirin ⁶
 Fritz Zwicky ⁷

Staff Member Engaged in Post-Retirement Studies

Alfred H. Joy

Staff Associates

Bruce C. Murray ⁸
 Gerry Neugebauer ⁹
 James A. Westphal ¹⁰

Senior Research Fellow

Jun Jugaku ¹¹

Carnegie Fellows

Robert Dickens ¹²
 Jerome Kristian
 Wojciech Krzeminski ¹³
 John V. Peach ¹⁴
 René Racine
 David M. Rust ¹⁵
 Natarajan Visvanathan

Research Council of Canada Fellowship

F. David A. Hartwick ¹⁶

NATO Fellow

Alessandro Braccesi ¹⁷

Research Fellows

Ann Merchant Boesgaard ¹⁸
 J. David Bohlin
 J. W. R. Heintze ²
 Ardon R. Hyland
 William H. Julian
 Keiichi Kodaira
 Dora Russo Lackner ¹⁹
 David L. Lambert
 Mitsugu Makita ²⁰
 Martin J. Rees ²¹
 M. T. Scholz
 Rudolf E. Schild
 Michal Simon
 Robert Stein ²²
 Henrietta H. Swope ⁷
 Takashi Tsuji

Senior Research Assistant

Dorothy D. Locanthi

Research Assistants

Frank J. Brueckel
 Sylvia Burd

Thomas A. Cragg
 Robert F. Garrison ¹⁶
 Howard Gates ¹⁶
 Emil Herzog ¹⁶
 Basil Katem
 Margaret Katz
 Charles T. Kowal
 A. Louise Lowen
 Kathleen Reynolds ²³
 Malcolm S. Riley
 Annilla Sargent
 Merwyn G. Utter
 Grace D. Vess

Student Observers

Saul J. Adelman
 Christopher M. Anderson
 Kurt S. Anderson
 Dennis Baker
 Eric Becklin
 Judith Cohen
 Edward J. Groth
 Theodore Hilgeman
 Thomas B. McCord
 Dennis Matson
 Robert O'Connell
 Patrick S. Osmer
 Arsine V. Peterson
 Bruce A. Peterson
 Virginia L. Trimble
 Donna E. Weistrop

Photographic Laboratory

William C. Miller, Photographer
 John A. Difley, Photographic Technician
 Clare Neal, Solar Photographic Assistant

Librarian

Marline Gerrity ²⁴
 Charlotte Fournier

Instrument Design and Construction

Lawrence E. Blakeé, Senior Electronic Technician
 Maynard K. Clark, Senior Electronic Engineering Assistant
 Floyd E. Day, Head Optician
 Raymond Dreiling, Machinist
 Loyal Elam, Jr., Draftsman ²⁵
 Robert D. Georgen, Machinist
 Fred Idzinga, Electronics Specialist
 Melvin W. Johnson, Optician
 Wilfred H. Leckie, Draftsman
 Ernest O. Lorenz, Engineering Assistant
 Richard Lucinio, Engineering Assistant
 Frederick O'Neill, Machinist

Michael Morrill, Technical Aide ²⁶
 Gerald Preston, Technical Aide
 John D. Raphael, Electronics Specialist
 Rudolf E. Ribbens, Designer and Superintendent of Instrument Shop
 Howard G. Sachs, Engineer
 Benny W. Smith, Electronics Specialist
 Robert G. Stiles, Optician
 David Thompson, Technical Assistant
 Virgal Z. Vaughan, Electronics Specialist
 Ralph W. Wilson, Machinist
 Madeleine Williams, Draftsman
 Felice Woodworth, Draftsman-Illustrator

Maintenance and Operation

Mount Wilson Observatory and Offices

Wilma J. Berkebile, Secretary
 Fern V. Borgen, Stenographer and Receptionist
 Clyde B. Bornhurst, Mechanic
 Hugh T. Couch, Superintendent of Construction
 Helen S. Czaplicki, Typist-Editor
 Hazel Fulton, Stewardess
 Eugene L. Hancock, Night Assistant
 Mark D. Henderson, Custodian ⁷
 Anne Hopper, Accountant
 Rienaldo Jacques, Night Assistant
 Ethel Marzalek, Stewardess
 Frances Maynor, Stewardess
 Alfred H. Olmstead, Laborer
 Glen Sanger, Driver
 William D. St. John, Custodian
 Henry F. Schaefer, Night Assistant
 Elizabeth M. Shuey, Secretary
 Benjamin B. Traxler, Mountain Superintendent
 Fredrick P. Woodson, Assistant to the Director

¹ Professor of Astrophysics and Executive Officer for Astronomy, California Institute of Technology.

² Resigned July 31, 1968.

³ Professor of Physics, California Institute of Technology.

⁴ Professor of Astronomy, California Institute of Technology.

⁵ Associate Professor of Astronomy, California Institute of Technology.

⁶ Professor of Astrophysics, California Institute of Technology.

⁷ Retired June 30, 1968.

⁸ Professor of Planetary Science, California Institute of Technology.

⁹ Associate Professor of Physics, California Institute of Technology.

¹⁰ Senior Research Fellow in Planetary Science, California Institute of Technology.

Palomar Observatory and Robinson Laboratory

Fred Anderson, Machinist ²⁷
 Ray L. Ballard, Administrative Assistant
 Jan A. Bruinsma, Custodian
 Maria J. Bruinsma, Stewardess
 Eleanor G. Ellison, Secretary and Librarian
 Beulah Greenlee, Stewardess
 Frank K. Greenlee, Custodian
 Daniel J. Hargraves, Mechanic and Relief Night Assistant
 Liselotte M. Hauck, Secretary
 Victor A. Hett, Night Assistant
 Helen D. Holloway, Secretary
 Charles E. Kearns, Assistant Superintendent
 J. Luz Lara, Mechanic
 Carl D. Palm, Night Assistant
 Catherine T. Paul, Secretary
 Marilynne Rice, Secretary
 Carol Russell, Secretary ²⁸
 Robert T. Snow, Mechanic and Relief Night Assistant
 Barrett A. Staples, Mechanic ²⁹
 Gary M. Tuton, Night Assistant
 William C. Van Hook, Mountain Superintendent
 Betty A. Wallace, Secretary
 Ardith Walthers, Secretary
 Warren L. Weaver, Mechanic

Site-Testing Operations, Chile

Donald L. Buck, Project Supervisor
 Manuel Blanco, Laborer
 Manuel Casanova, Observer and Utility Employee ¹⁶
 Roberto Ramos, Laborer
 Tomas Veliz, Trainee Observer ¹⁶
 Manfred Wagner, Camp Chief

¹¹ Resigned October 31, 1967.

¹² Resigned September 20, 1967.

¹³ Resigned November 30, 1967.

¹⁴ Resigned April 22, 1968.

¹⁵ Resigned February 27, 1968.

¹⁶ Resigned June 30, 1968.

¹⁷ Resigned March 15, 1968.

¹⁸ Resigned August 31, 1967.

¹⁹ Resigned June 13, 1968.

²⁰ Resigned December 15, 1967.

²¹ Resigned May 17, 1968.

²² Resigned September 1, 1967.

²³ Resigned October 2, 1967.

²⁴ Resigned May 15, 1968.

²⁵ Resigned March 1, 1968.

²⁶ Resigned October 7, 1967.

²⁷ Resigned February 9, 1968.

²⁸ Resigned February 2, 1968.

²⁹ Resigned January 4, 1968.

Geophysical Laboratory

Washington, District of Columbia

Philip H. Abelson
Director

Contents

Introduction	75	Silicate systems including a vapor phase	153
Silicate Mineralogy and Phase-Equilibria Studies	80	Melting of forsterite and enstatite at high pressures under hydrous conditions (Kushiro and Yoder).	153
Pyroxenes	80	Liquidus relations in the system forsterite-diopside-silica-H ₂ O at 20 kb (Kushiro)	158
Synthesis and stability of iron-free pigeonite in the system MgSiO ₃ -CaMgSi ₂ O ₆ at high pressures (Kushiro)	80	Melting of a hydrous phase: phlogopite (Yoder and Kushiro)	161
Electron-probe study of pyroxene exsolution (Boyd and Brown)	83	Reconnaissance study of the stability of amphiboles at high pressure (Gilbert)	167
Ortho-clino inversion in ferrosilite (Lindsley and Munoz)	86	Control of fugacities in fluorine-bearing hydrothermal systems (Munoz)	170
Subsolidus relations on the join hedenbergite-ferrosilite at 20 kb (Munoz and Lindsley)	88	Sulfide Mineralogy and Phase-Equilibria Studies	175
Unit-cell parameters of clinopyroxenes along the join hedenbergite-ferrosilite (Lindsley, Munoz, and Finger)	91	Ore minerals	175
Optical properties of synthetic clinopyroxenes on the join hedenbergite-ferrosilite (Myer and Lindsley)	92	The Fe-Se system (Kullerud)	175
Oxidation of Ca-rich clinopyroxenes (Huckenholz)	94	The Cu-Zn-S system (Craig and Kullerud)	177
Stability of omphacite	96	Cubic \rightleftharpoons hexagonal inversions in some M ₂ S ₄ -type sulfides (Kullerud)	179
Stability of omphacite in the absence of excess silica (Bell and Kalb)	97	Meteorite minerals	182
Stability of omphacite in the presence of excess silica (Kushiro)	98	The Cr-S and Fe-Cr-S systems (El Goresy and Kullerud)	182
The temperature-compression melting relation (Gilbert)	100	Sulfide assemblages in the Odessa meteorite (Kullerud and El Goresy)	187
Feldspars and highly feldspathic rocks. The melilite-plagioclase incompatibility dilemma in igneous rocks (Yoder and Schairer)	101	Sulfur-isotope fractionation in minerals (Puchelt)	192
The join albite-anorthite-akermanite (Schairer and Yoder)	101	Synthesis of β Cr ₂ FeS ₄ at 35 kb (El Goresy, Bell, and England)	197
Anorthite-akermanite and albite-soda melilite reaction relations (Yoder)	104	Melting relations in the Fe-rich portion of the system Fe-FeS at 30 kb pressure (Brett and Bell)	198
Experiments bearing on the origin of anorthositic intrusions (Emslie and Lindsley)	105	Biogeochemistry	199
Syenites (Morse)	108	Reactions of the organic matter in a Recent marine sediment (Hoering)	199
Feldspars (Morse)	112	Branched-chain fatty acids in Recent sediments (Hoering)	201
Annealing characteristics of dense feldspar glass (Chao and Bell)	120	Fatty alcohols in sedimentary rocks (Hoering)	202
Diamond inclusions, aluminum silicates, β -quartz, andradite	126	Fichtelite hydrocarbons in fossil wood (Hoering)	203
Mineral inclusions in diamonds (Meyer and Boyd)	130	Laboratory simulation of amino-acid diagenesis in fossils (Hare and Mitterer)	205
The andalusite-sillimanite transition and the aluminum silicate triple point (Gilbert, Bell, and Richardson)	130	Recent amino acids in the Gunflint chert (Abelson and Hare)	208
X-ray properties and stability relations of β -quartz solid solutions along the join LiAlSi ₂ O ₆ -SiO ₂ (Munoz)	135	Computer Reduction of Electron-Probe Data (Boyd, Finger, and Chayes)	210
Synthesis and stability of Ti-andradite (Huckenholz)	137	Crystallography	215
		A new hexagonal form of carbon from the Ries Crater (El Goresy and Donnay)	215
		Determination of cation distributions by least-squares refinement of single-crystal X-ray data (Finger)	216

Magnetic susceptibility and exchange coupling in ardennite (Senftle, Thorpe, and Donnay)	218	Curve-fitting in the ternary diagram (Chayes)	236
"McKelveyite," a syntactic intergrowth of two phases (Donnay and Donnay)	218	A last look at G1-W1 (Chayes)	239
Crystalline heterogeneity	219	Materials balance in igneous rock suites (Bryan)	241
Evidence from electron-probe study of Brazilian tourmaline (Donnay)	219	A least-squares approximation for estimating the composition of a mixture (Bryan, Finger, and Chayes)	243
Evidence from source-image distortion (Young, Wagner, Pollard, and Donnay)	220	Chemical and optical petrography (Bryan)	244
Structure refinement of elbaite (Donnay and Barton)	221	Volcanic rocks from the Bunya Mountains, Queensland, Australia	244
Improvements of crystallographic equipment (Donnay)	222	An olivine gabbro-microsyenite intrusion from the Carnarvon Range, Queensland, Australia	247
Sonorait (Gaines, Donnay, Hey, and Zemann)	223	Structural Geology	251
The crystal structure of sonoraite, $\text{Fe}_2\text{-Te}_2\text{O}_5(\text{OH})_4 \cdot \text{H}_2\text{O}$ (Donnay, Stewart, and Zemann)	223	Experiments in flow deformation (Scott)	251
Geochronology and Geochemistry (Davis, Krogh, Hart, Aldrich, Morse, and Ishizaka)	224	Movement directions and the axial-plane fabrics of flexural folds (Scott and Hansen)	254
Geochronology of the Grenville Province (Krogh and Davis)	224	On the "drag folds" of Van Hise and Leith (1911) (Hansen and Scott)	258
Fractionation of potassium and rubidium in a layered intrusion (Morse and Davis)	231	Slip folds in planes of unsystematic orientation (Hansen)	263
Petrology	233	Staff Activities	265
Statistical petrography	233	Aluminum Silicate Conference	265
Identity of expected interdependence between pairs of Niggli numbers and pairs of analogous remaining-space variables (Chayes)	235	<i>Journal of Petrology</i>	266
Transformations designed to eliminate negative elements from sample estimates of the vector of open variances (Chayes)	236	Lectures	266
		Petrologists' Club	267
		Bibliography	268
		References Cited	269
		Personnel	276

INTRODUCTION

A creative enterprise depends for its success first on gifted people. Over the years the Geophysical Laboratory has had its share of them. If a laboratory is to be more than just a collection of individuals, however, a symbiotic relationship must exist among the staff. Together they must create an atmosphere that is both stimulating and sustaining of intellectual endeavor. This atmosphere is likely to occur if certain factors are present and others are suppressed. Positive factors include a common allegiance to scholarship as one of the highest forms of human endeavor. They include mutual respect among the staff. They include freedom for the individual to choose his own program within reasonable but broad limits, with the choice based solely on intellectual criteria. Negative factors that must be suppressed are excessive bureaucracy and red tape and the dominance of criteria for choice of program other than purely intellectual.

For nearly two decades scientific research in this country was carried out under circumstances that permitted great creativity. Generous support was widely available, with few strings attached. Of late, the climate has changed drastically. Budget cuts, though substantial, are of small consequence in comparison to other factors. Government regulations are placing on universities and their staffs an irritating burden of paper work. More serious is a deterioration in the intellectual atmosphere of the university. The cries of students and of some faculty for "relevance" are basically a manifestation of anti-intellectualism.

A further, related negative influence on the creative enterprise is the adverse effect resulting from a changed attitude on the part of government toward the value of basic research. Maynard Hutchins outlined the scope of the problem when discussing the huge modern university.

"The multiversity, which will do for the society anything the society will pay for, exists to flatter the spirit of the age. One trouble with flattering the spirit of the age is that all of a sudden it may turn and bite you. Something of the sort appears to be happening in California. The popular desire, which was formerly, for reasons never made clear, to have a famous multiversity, is now the desire, for reasons equally obscure, to have a cheap one, with clean-shaven students, and relatively few of them. What are you to say to people whose immediate needs you are striving to meet, and even to anticipate, when they tell you they've changed their minds and do not need you any more?"

Today there is widespread continuing deterioration in the environment for basic research in this country. These trends make it essential that at least a few places be maintained where creative scholarship is a way of life.

At the Geophysical Laboratory we are fortunate in functioning under circumstances that lend themselves to scholarly effort. We enjoy freedom from red tape and flexibility of programs, and we seek to maximize the proportion of independently creative minds among us. In such circumstances men are creative. Highlights of some of the accomplishments of the past year follow.

Meyer and Boyd have used the electron probe to make the first chemical study of olivine, garnet, chromite, and diopside inclusions from natural diamonds. Because of the high pressures and temperatures required for stable crystallization of diamond in the earth it is very probable that natural diamonds recovered from kimberlite have come from depths greater than 100 km. The minerals found as inclusions are similar in a gross way to those from the ultramafic nodules in kimberlite but there are a number of remarkable differences. It has been found

that garnet and chromite inclusions are unusually rich in chromium, whereas a diopside inclusion contains unusually little chromium. An important feature not yet explained is the monomineralic nature of the inclusions, no polyminerally inclusion having yet been found.

Exsolution features are especially well developed in pyroxenes from large layered intrusives, and their study provides insight into the solid-state response of these minerals to conditions of slow cooling. Boyd and Brown have analyzed both host and exsolved lamella in a grain of inverted pigeonite and in a coexisting grain of augite from the Bushveld gabbro. Their analyses show that the minor elements Al, Cr, Mn, Ti, and Na have fractionated in the exsolution process. The composition of an augite lamella in inverted pigeonite is almost identical with that of the separate augite host, and the composition of a clinohypersthene lamella in augite is very similar to that of the inverted pigeonite host. These relations indicate that equilibrium has been maintained for a considerable period during cooling below the solidus.

The phase relations of Ca-Fe pyroxenes have continued to be of major interest to Lindsley. With Munoz he has investigated the subsolidus relations of pyroxenes on the join hedenbergite-ferrosilite at 20 kb. Finger joined them in determining the unit-cell parameters of these pyroxenes, and Myer determined their optical properties. The results of this study provide information concerning the subsolidus phase relations in the pyroxene quadrilateral and offer valuable insights concerning the crystallization history of layered intrusive igneous rocks. Munoz also made a determination of the unit-cell parameters and stability relations of β -quartz solid solutions on the join $\text{LiAlSi}_2\text{O}_6$ - SiO_2 at high pressures.

Huckenholz carried out a detailed study of the join andradite-Ti-garnet and its relationships in the join wolastonite-perovskite-hematite. He concluded that the appearance of Ti-bearing

garnets and ferri-diopsides is a natural consequence of crystallization at or near atmospheric conditions and is not necessarily the result of special deep-seated processes. Further experiments on natural clinopyroxenes show that the association of andraditic garnets and ferri-diopsides is favored in magmas crystallizing under oxidizing conditions.

The pyroxene omphacite ($\text{NaAlSi}_2\text{O}_6$ - $\text{CaMgSi}_2\text{O}_6$) is probably formed under high pressures, occurring at great depths in the earth. Bell, Kalb, and Kushiro have been studying the stability of omphacite, with particular attention to the effect of exchanging diopside for jadeite in the solid solution.

Kushiro and Yoder studied the melting relations for MgSiO_3 and Mg_2SiO_4 compositions under hydrous conditions to determine the effect of water on the genesis of basaltic magmas. They found that enstatite melts incongruently to forsterite and liquid in the presence of water at pressures up to at least 30 kb, compared with about 5 kb under anhydrous conditions. Kushiro studied the melting relations in the system forsterite-diopside-silica-water at high pressures and found that the field of silica relative to those of diopside and enstatite solid solutions is greatly reduced at 20 kb water pressure. The results suggest that silica-rich magmas such as andesitic and dacitic magmas can be formed by fractional crystallization of basaltic magmas at high water pressures. The process may be related to the origin of calcalkali rocks in the orogenic zones.

Kushiro reinvestigated the system diopside-enstatite at 20 kb under anhydrous conditions and found a narrow field of pigeonitic clinopyroxene in the subsolidus region of this system, results significant for an understanding of the crystallization of pigeonite-bearing rocks. The synthesis of "iron-free pigeonite" was made in this and adjoining fields.

Plagioclase and melilite do not coexist in igneous rocks, yet they crystallize together in the laboratory. This dilemma

has been the focus of an intensive effort by Yoder and Schairer. The association of plagioclase and melilite persists up to relatively moderate pressures (Yoder), in the presence of water (Yoder and Schairer), and over a wide range of compositions (Schairer and Yoder). The presence of ferric iron and titanium may greatly restrict the association but other factors, not yet discovered, are being sought to account for the incompatibility of these two minerals in natural lavas.

Efforts by Yoder and Kushiro to investigate the system involving the principal minerals of kimberlite, forsterite-calcite-phlogopite, resulted in many difficulties in the interpretation of the experimental products. Two of the principal minerals, forsterite and phlogopite, were successfully studied individually in the presence of water. Liquids with which forsterite and phlogopite are stable to depths of about 60 km are rich in alkalis and lie outside the range of compositions of the principal minerals of kimberlite. At greater depths, where phlogopite may melt congruently, the existence of a kimberlite magma may be possible.

Field deductions suggest that natural magmas are water-undersaturated under the conditions of generation. Yoder and Kushiro have demonstrated with the hydrous mineral phlogopite that the undersaturation exists in the partial melting of mantle materials consisting of an assemblage of hydrous and anhydrous phases in the absence of a free gas phase. The new data help to resolve the apparent discrepancy between the large amounts of water soluble in silicate liquids in the laboratory and the small amounts of water believed to be contained in natural magmas.

Schairer and Yoder have been studying phase-equilibrium relations in simplified systems related to the origin of basaltic and alkaline rocks. In the join albite-anorthite-akermanite, they have found the presence of four crystalline phases with a liquid over a considerable

range of temperature, indicating the complex nature of the solid solution. It is evident that, not a quaternary, but at least a quinary equilibrium is involved.

The manner in which H_2O is contained in the mantle plays a role in theories of the genesis of magmas. Amphiboles, because they are hydrous compounds stable at temperatures up to $1000^\circ C$ at low pressure, have been proposed as phases that could hold water at depth. In a reconnaissance study of the pressure effect on amphibole stability, Gilbert has shown that calcic amphiboles are not likely to be stable at depths greater than 70 to 100 km, thus placing one more constraint on the phase assemblages present in the upper mantle.

Petrogenetic grids for metamorphic rocks rely heavily on the polymorphs of Al_2SiO_5 —kyanite, andalusite, and sillimanite—for their pressure-temperature coordinates. Gilbert, Bell, and Richardson have extended the work reported last year to a study of the andalusite-sillimanite transition. During the andalusite-sillimanite grade of metamorphism, temperatures were in the range 625° to $850^\circ C$. Determination of this transition has also made possible a better definition of the aluminum silicate triple point. It is now clear that pressures during kyanite-sillimanite metamorphism must have been above 5 kb.

When meteorites strike the earth at high velocity, a high-pressure shock wave results. One of the effects observed in impact zones on the surface of the earth is the conversion of minerals from the crystalline state to an extraordinarily dense glass. Bell and Chao have experimentally investigated for the first time the formation and annealing of synthetic dense glasses of feldspar composition. An understanding of impact products as compared with other products of natural explosive events, such as volcanic eruptions, will be useful in the analysis of samples from the moon and from other planets as they become available.

Morse has shown that the alkali feldspars are related by a "eutectic," rather than a "minimum," at $P_{H_2O}=5$ kb, and that new positions of the solvus limbs were required. These positions were located by a bracketing technique. Morse expanded the studies into the nepheline syenite portion of petrogeny's residua system, demonstrating the persistence of the feldspar join as a thermal barrier between nepheline syenites and granites, alone and with diopside, up to $P_{H_2O}=10$ kb.

Emslie and Lindsley continued their investigations into the origin of anorthosite, studying the high-pressure melting relations of compositions in the join forsterite-albite-anorthite and of the chilled margin of the Michikamau anorthosite complex.

Hoering has constructed and put into operation a mass spectrometer for the analysis of the molecular structure of organic compounds found in sedimentary rocks. A combination of gas-liquid chromatography by mass spectrometry gives unique information on molecular structure with microgram quantities of pure samples. Using this tool Hoering has identified a large number of fatty acids occurring in a Recent marine sediment. Surprisingly, he found a relatively large amount of highly branched acids. Mass spectrometry has been used to identify the homologous series of porphyrins generated by mild thermal treatment of a Recent marine sediment. The distribution of molecular weights obtained this way is very similar to that found in material separated from ancient sediments.

In the laboratory Hare and Mitterer have simulated processes requiring millions of years in fossils. The incubation of shells at temperatures from 185° to 90°C for 1 day to 3 months produces changes in the amino content almost identical with those seen in fossils. A partial conversion of isoleucine to allo-isoleucine is of particular potential usefulness—in dating when the temperature

is known or as a thermometer when the age of the specimens is known accurately.

Abelson and Hare have examined amino acids present in the 1900-million-year-old Gunflint chert. A number of lines of evidence converge toward the conclusion that these amino acids are of recent origin.

Using the methods of dating rocks based on the accumulation of radiogenic daughter isotopes and the accompanying changes in the ratio of radiogenic to non-radiogenic isotopes, Krogh and Davis have been able to prove the widespread occurrence of rocks and sediments as old as 1800 m.y. in the 1000-m.y.-old Grenville province of the Canadian shield. It has been possible to set limits in time for periods of regional metamorphism and deformation in areas that later were remetamorphosed. The interface between the old Superior rocks and the younger rocks to the south, the Grenville Front, has been an active zone for the past 1800 m.y.

Kullerud has shown that spinel-type sulfide minerals containing metal to sulfur in the 3:4 atomic ratio all have high-pressure polymorphs.

Applications of pertinent phase diagrams, produced by experimental studies on synthetic systems, have shown that lack of equilibrium between minerals in meteorites is not a rare occurrence and that equilibrium between assemblages, often only a few millimeters apart, is usually not achieved. Kullerud and El Goresy have shown that some of the nonequilibrium assemblages found in meteorites may be explained as effects of shock.

The mineral daubréelite is very common in iron meteorites, enstatite chondrites, and achondrites. For this reason the systems Cr-S and Cr-Fe-S have been studied over a large temperature range by El Goresy and Kullerud, who have shown that daubréelite occurs in two polymorphic forms and that some sulfides in the Cr-S system occur as minerals.

Brett and Bell have examined the

system Fe-FeS to determine what effect the addition of sulfur to iron would have on the melting point of iron at high pressure. The effect at 30 kb is several hundred degrees, suggesting that even a small amount of sulfur present in the earth's core would lower the melting temperature.

Puchelt has studied isotope effects in inorganic reactions of sulfides. He has shown that atoms in sulfur vapor readily exchange with sulfur in a number of ore-forming sulfides and has applied this result to sulfide minerals from the Bodenmais, Germany, ore deposit to show how the original heterogeneous distribution of sulfur-isotope ratios has been altered during the metamorphism of the original sedimentary ore deposit.

El Goresy has discovered a new allotropic form of carbon, which he and Donnay have studied by X rays. Three other forms are known—graphite, diamond, and lonsdaleite. The new hexagonal phase of carbon is present in polished sections of shocked graphite gneisses from the Ries Crater in Germany. So far, the mineral (to be called chaoite) has been found only in powdered form. The unit cell is large ($a=8.948$, $c=14.978$ Å); a single crystal is needed for the structure determination. Chaoite is slightly harder than graphite.

In another study El Goresy, Bell, and England have synthesized $\beta\text{Cr}_2\text{FeS}_4$ at high pressures. This new phase may be stable in meteorites at the time of their formation and later invert to the alpha form, which is commonly observed.

Two other new minerals were studied by Donnay. Sonoraite was found in the field by R. V. Gaines. Its chemical formula, fully established only with the help of the crystal-structure determination, is $\text{Fe}_2^{3+}\text{Te}_2^{4+}\text{O}_5(\text{OH})_4 \cdot \text{H}_2\text{O}$. The structure was solved by Donnay in cooperation with Stewart and Zemmann. It consists of pairs of edge-sharing oxygen-hydroxyl octahedra about Fe^{3+} , $\text{Fe}_2\text{OH}_4\text{O}_5$ groups that share an OH corner. The Fe-Fe distance within a pair is only about 3.1 Å.

Additional cross-linking of these pairs is performed by oxygen triangles bonded to tellurium.

Ewaldite, a complex carbonate occurring in three-dimensional intergrowth with mckelveyite from the Green River formation, was discovered by Donnay by single-crystal X-ray diffraction study.

Finger worked on theoretical and computational aspects of the refinement of crystal structures of minerals where the average occupancy of a site is to be determined by means of least-squares analyses of X-ray data.

From a detailed examination of published analyses of two silicate reference materials, G1 and W1, Chayes concludes that interlaboratory biases must account for a very considerable proportion of the observed dispersion. Sampling variance and random error are confounded in the experimental design, and no separate estimate of either can be obtained from the data. In 50 paired analyses, i.e., analyses of both materials by the same analyst, however, correlations between results for the same constituents are consistently far too strong to be dismissed as random.

In his continuing study of petrographic correlation, Chayes has found a simple linearizing transformation for use with ternary closed data and has been able to show that expected correlations between what he terms "remaining-space" variables (see *Year Book 66*) are in fact identical with those calculated for analogous pairs of the widely used Niggli numbers. Extending preliminary work described last year, Chayes has found a reasonable linear transformation that yields open variance vectors free of negative elements for all arrays so far examined; he points out that in such instances it is both impossible and unnecessary to recast the (transformed) data either as remaining-space variables or as Niggli numbers.

Many basalts from eastern Australia project in the normative composition field Ol'-Di'-Hy', resembling in this re-

spect basalts of the deep ocean ridges, as previously discussed by Chayes (*Year Book 64*). Bryan's study of the petrographic and chemical details of these basalts and of associated andesitic rocks has provided further insight into genetic relations and problems of classification. In a related study of chemically equivalent intrusive gabbro intimately associated with a microsyenite ring-dike, he has shown that crystal fractionation of a parent liquid lying close to the normative Ol'-Di' join may lead ultimately to an oversaturated residual liquid enriched in potash relative to soda.

Genetic hypotheses involving crystal-melt equilibria, assimilation, or mixing of two or more magmas, have been frequently proposed. Bryan has now written a computer program which generates an estimate of the inferred parent liquid or of the inferred residual liquid at any arbitrarily chosen stage of magmatic evolution. This program makes it possible to test rapidly many alternative hypotheses, using any reasonable number of components simultaneously, or to test the ability of an inferred mechanism to simulate observed variation trends. A direct numerical analogue of current graphical procedures, his method shares with them the restriction that the observer is required to select from among a number of possible solutions, each based on only part of the data. In a late and not yet extensively tested development, Bryan, Finger, and Chayes have formu-

lated the problem as one in least-squares approximation, a procedure which of course yields only one solution for a given set of data, and should also lead to more satisfactory hypothesis testing.

During the report year, Hansen has spent much of his time writing a book called *Strain Facies*, which presents new approaches and concepts in the description and analysis of folds in rocks. He has continued testing and calibrating the 10 kb-1000°C gas apparatus for rock deformation, in part with the collaboration of J. L. England. During the final months of the current year, Scott completed construction of a flow-deformation apparatus for the study of folding induced in low-viscosity fluids. Initial experiments on finely layered stitching wax in Vaseline, within a flow environment that involved constriction of the layers, as well as simple shear parallel with the layers (compound and velocity gradient flow), yielded sets of asymmetric flexural-slip folds with planar distributions of fold axes. The relationships between the imposed flow environment and the induced fabric of the folds confirmed part of the theory of the "separation angle," which is used to deduce the movement directions in which natural folds develop within the earth. Both Scott and Hansen have continued the structural analysis of natural folds and report relationships between axial-plane fabrics, height-width ratios, and the movement histories of folded rocks.

SILICATE MINERALOGY AND PHASE-EQUILIBRIA STUDIES

PYROXENES

SYNTHESIS AND STABILITY OF IRON-FREE PIGEONITE IN THE SYSTEM MgSiO_3 - $\text{CaMgSi}_2\text{O}_6$ AT HIGH PRESSURES

I. Kushiro

Pigeonite occurs in tholeiitic basalts, dolerites, and andesites. Many tholeiitic

gabbros also contain hypersthene with augite lamellae, now often interpreted as an inversion product of pigeonite due to slow cooling and referred to below as "inverted pigeonite." The stability fields of pigeonite and ferro-pigeonite have been considered to be at higher temperatures than that of orthopyroxene of the same Mg/Fe²⁺ ratio.

This conclusion is based on their natural occurrence and the clinopyroxene-orthopyroxene relations in the system MgSiO_3 - FeSiO_3 at 1 atm, given by Bowen and Schairer (1935), with the assumption that the presence of a small amount of Ca does not essentially change the clinopyroxene-orthopyroxene stability relations. Foster (1951) and Atlas (1952) have shown that clinoenstatite is not stable but protoenstatite is stable at high temperatures ($>985^\circ \pm 10^\circ\text{C}$) for MgSiO_3 composition. Boyd and Schairer (1964) suggested that clinoenstatite is formed from protoenstatite during quenching, that protoenstatite has a stability field only in the Mg-rich region, and that pigeonite may have its own stability field above the orthopyroxene stability field in the relatively iron-rich region of the join MgSiO_3 - FeSiO_3 . Kuno (1966) has suggested similar stability relations. Yoder, Tilley, and Schairer (*Year Book* 62, pp. 84-95), on the basis of experiments on natural pigeonites, suggested two possibilities: pigeonite may be an inversion product of protohypersthene or a quenched stable product. Thus, notwithstanding many investigations, the stability field of pigeonite is still controversial, and even synthesis of pigeonite has not been achieved.

During the course of studies on the join diopside-enstatite at 20 kb, clinopyroxene showing the 231 reflection in its X-ray powder pattern was observed in the subsolidus region (Kushiro, *Year Book* 63, pp. 104-105). The 231 reflection, a strong reflection with $h+k$ odd, is not derived from the diopside structure ($C2/c$) but from the clinoenstatite (or pigeonite) structure ($P2_1/c$). This evidence suggests that there may be a field of pigeonitic clinopyroxene in the subsolidus region of the join diopside-enstatite. In the present investigation, the subsolidus region of this join has been restudied more carefully at 20 kb in the compositional range from $\text{Di}_{10}\text{En}_{90}$ to $\text{Di}_{56}\text{En}_{44}$ (wt %). The runs were made

with a piston-cylinder, solid-media pressure apparatus similar to that designed by Boyd and England (1960). Starting materials were glass prepared by Boyd and Schairer (1964) and glass crystallized to diopside and clinoenstatite solid solutions at 1 atm. Mechanical mixtures of pure diopside and pure orthoenstatite were also used as starting material. The runs lasted $\frac{1}{2}$ to 1 hour for temperatures above 1600°C and $\frac{2}{3}$ to 3 hours for temperatures between 1400° and 1600°C . The results are shown in Fig. 1. Most of the runs above and some below the solidus have been reported previously (Kushiro, *Year Book* 63, pp. 103-105).

For compositions between diopside and $\text{Di}_{53}\text{En}_{47}$, diopside solid solution is stable at 1600°C . Between the compositions $\text{Di}_{50}\text{En}_{50}$ and $\text{Di}_{20}\text{En}_{80}$, however, two different clinopyroxenes appear to coexist. Their X-ray powder diffraction patterns show a split in the 311 reflection (Fig. 2) and also the 220 reflection, although the split of the latter reflection is not so clear as that of the former. Other peaks change so little with composition that they will not show a split for the composition range shown here. A mechanical mixture of pure diopside (40 wt %) and pure orthoenstatite (60 wt %) held at 1600°C for 1 hour also recrystallized into clinopyroxene(s) showing a split 311 peak without orthoenstatite. The clinopyroxene formed from a glass of composition $\text{Di}_{40}\text{En}_{60}$ at 1600°C showed no split in the 311 and 220 reflections; when this clinopyroxene was held at 1620°C for 30 minutes, however, both reflections were clearly separated. The possible reflections derived from diopside solid solution are not in accord with one of the split peaks. The relative intensities, but not the position, of the two separate peaks for the 311 reflection appear to change with the bulk composition of the starting material (Fig. 2). The intensity of the 231 reflection increases with increase of MgSiO_3 in the bulk composition.

The clinopyroxene(s) crystallized from

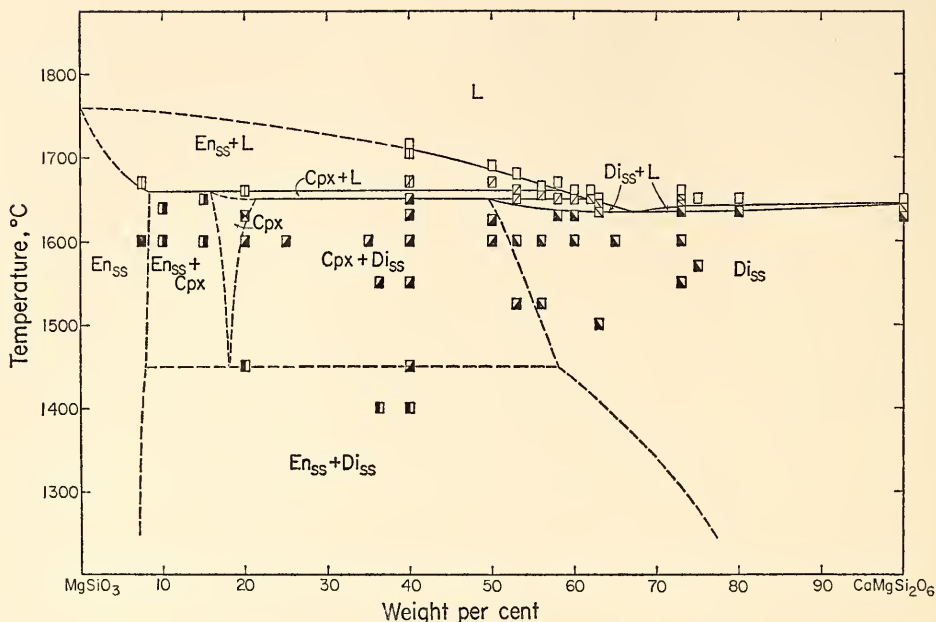


Fig. 1. Phase-equilibrium diagram of the system diopside ($\text{CaMgSi}_2\text{O}_6$)-enstatite (MgSiO_3) at 20 kb under anhydrous conditions. Cpx, pigeonitic clinopyroxene; Di_{ss}, diopside solid solution; En_{ss}, orthoenstatite solid solution; L, liquid.

the composition $\text{Di}_{20}\text{En}_{80}$ at 1600°C shows a split 311 peak, one part of which is strong and the other weak; whereas at 1630°C, a single clinopyroxene, showing a single 311 peak with a sharp 231 peak, was obtained from the same composition. The X-ray powder diffraction pattern is very similar to those of natural

pigeonites (Fig. 3). This pigeonitic clinopyroxene may be called "iron-free pigeonite" on the basis of appropriate Ca content as well as structure. Lindsley and Munoz (this report) synthesized "iron pigeonite" on the join hedenbergite-ferrosilite.

In the compositions between $\text{Di}_{15}\text{En}_{85}$ and $\text{Di}_{10}\text{En}_{90}$, orthoenstatite and pigeonitic clinopyroxene coexist at temperatures between 1600°C and 1650°C, and for the composition $\text{Di}_{7.5}\text{En}_{92.5}$ only orthoenstatite was obtained at 1600°C. The field of pigeonitic clinopyroxene is limited, therefore, to a region near the composition $\text{Di}_{20}\text{En}_{80}$, as shown in Fig. 1. At 1400°C, diopside and orthoenstatite solid solutions were obtained from a glass ($\text{Di}_{40}\text{En}_{60}$) and a mechanical mixture of pure diopside and orthoenstatite ($\text{Di}_{36.3}\text{En}_{63.7}$). At 1450°C, diopside solid solution and pigeonitic clinopyroxene crystallized from a glass of composition $\text{Di}_{40}\text{En}_{60}$, and diopside and orthoenstatite solid solution crystallized from composi-

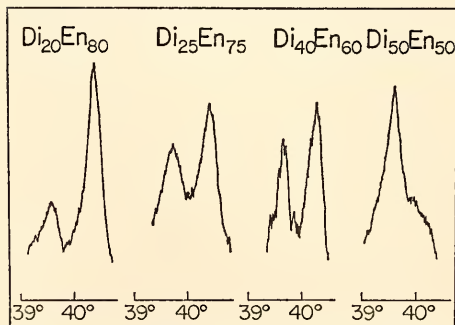


Fig. 2. X-ray powder diffraction patterns of 311 reflections ($\text{CuK}\alpha$) of clinopyroxenes crystallized from mixtures of compositions $\text{Di}_{20}\text{En}_{80}$, $\text{Di}_{25}\text{En}_{75}$, $\text{Di}_{40}\text{En}_{60}$, and $\text{Di}_{50}\text{En}_{50}$ (wt %) at 1600°, 1600°, 1650°, and 1600°C, respectively.

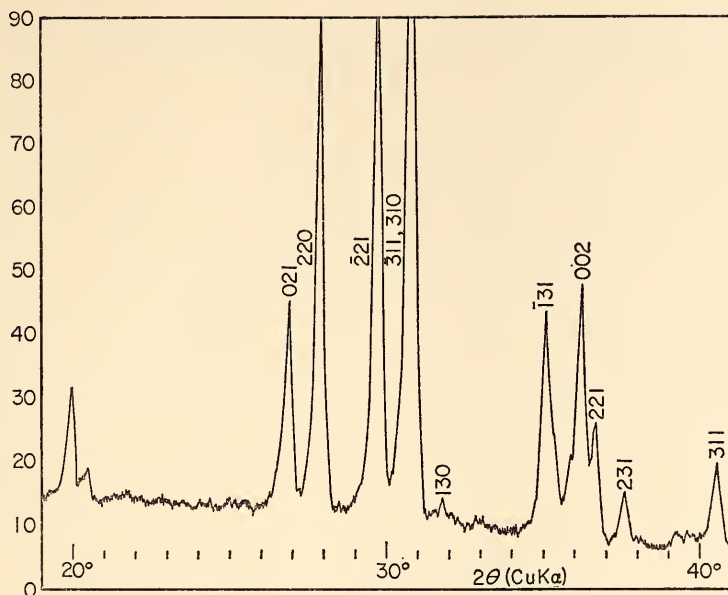


Fig. 3. X-ray powder diffraction pattern (CuK α) of a single pigeonitic clinopyroxene synthesized from a mixture of composition $\text{Di}_{20}\text{En}_{80}$ at 1630°C and 20 kb.

tion $\text{Di}_{20}\text{En}_{80}$. The field of pigeonitic clinopyroxene is limited, therefore, to temperatures at least above 1450°C, as shown in Fig. 1.

The $\text{Ca}/(\text{Ca}+\text{Mg})$ ratio of the pigeonitic clinopyroxene field, 0.08 to 0.10, is very similar to the $\text{Ca}/(\text{Ca}+\text{Mg}+\text{Fe}^{2+})$ ratio of natural pigeonites. The limited $\text{Ca}/(\text{Ca}+\text{Mg}+\text{Fe}^{2+})$ ratio of natural pigeonites may be explained by the narrow field suggested by the present experiments. On the basis of the present experimental results, it is suggested that pigeonite has more Ca than clinoenstatite, protoenstatite, or orthoenstatite (orthopyroxene) and that pigeonite is stable only near the solidus temperatures and inverts to orthopyroxene with exsolution of diopside solid solution (augite) at lower temperatures. These suggestions are also consistent with the natural evidence.

The pigeonitic clinopyroxene field shown in Fig. 1 would change with pressure and iron content. It may be expected from natural evidence that the temperature of the pigeonitic clinopyroxene field

is lowered with decreasing pressure or increasing iron content, or both, and for the $\text{Fe}^{2+}/(\text{Mg}+\text{Fe}^{2+})$ ratios and the conditions of crystallization of natural basaltic magmas, pigeonites with $\text{Fe}^{2+}/(\text{Mg}+\text{Fe}^{2+})$ ratio greater than 0.3 would crystallize. It is also likely that at 1 atm there is a narrow field of pigeonite near the $\text{Ca}/(\text{Ca}+\text{Mg}+\text{Fe}^{2+})$ ratio of 0.10 in the system $\text{MgSiO}_3\text{-FeSiO}_3\text{-CaSiO}_3$.

ELECTRON-PROBE STUDY OF PYROXENE EXSOLUTION

*F. R. Boyd and G. M. Brown**

A wealth of exsolution features in pyroxenes and other minerals has been opened up for chemical study by the advent of the electron probe. These features are of interest because they contain information on the solid-state response of various igneous and metamorphic rocks and ores to conditions of slow cooling. Exsolution features in pyroxenes are particularly well developed

* Department of Geology, University of Durham, Durham, England.

in rocks from large, basic intrusions such as the Bushveld, Skaergaard, and Stillwater. A qualitative survey (*Year Book 66*) of exsolved pyroxenes in a variety of gabbroic rocks from these intrusions showed remarkably regular but intricate patterns of exsolution. Coarse exsolution lamellae sometimes exsolve fine lamellae on further cooling, and the patterns are particularly complex in the inverted pigeonites where multiple sets of lamellae are common.

Quantitative analyses of lamella-host pairs have been undertaken to determine whether or not all cations in these pyroxenes participate in the exsolution process and to determine whether equilibrium is maintained between exsolving pyroxene phases as cooling proceeds.

A gabbro from the Bushveld intrusion (SA 1019) was chosen for the quantitative study. This specimen contains augite with fine, even lamellae of clinohypersthene ranging in width from 1 μm up to about 15 μm . Associated with the augite are inverted pigeonite grains with blebs of exsolved augite ranging up to several hundred micrometers in width. The grain of augite and the grain of pigeonite that were selected for analysis lie several centimeters apart in the same thin section.

Quantitative analyses were made of a

single clinohypersthene lamella in augite, as well as of adjacent areas of the augite host. The lamella is doubly terminated within the augite crystal and is about 12 to 15 μm thick. The original shape of the lamella was evidently that of a flat lens, and the thin section has cut a segment from the edge of this lens. Consistently low Ca counts were found only in the middle portion of the lamella, indicating that the beam was penetrating into underlying augite toward the ends. A scan across the augite grain monitoring $\text{CaK}\alpha$ X rays is shown in Fig. 4. This augite crystal contains many fine lamellae 1 to 3 μm thick as well as a more coarse set. As can be seen in Fig. 4, there are areas of augite host immediately adjacent to the analyzed clinohypersthene lamella that are free of the fine lamellae, and the augite host analyses were made here. These areas are restricted, and it was necessary to repolish the section when the analyses were about half completed to remove contamination spots left by the electron beam.

The augite lamella in pigeonite and the adjacent areas of pigeonite host which were selected for analysis are relatively free of secondary exsolution features. Nevertheless other pigeonite grains in this gabbro are exotic examples of the development of multiple sets of lamellae.

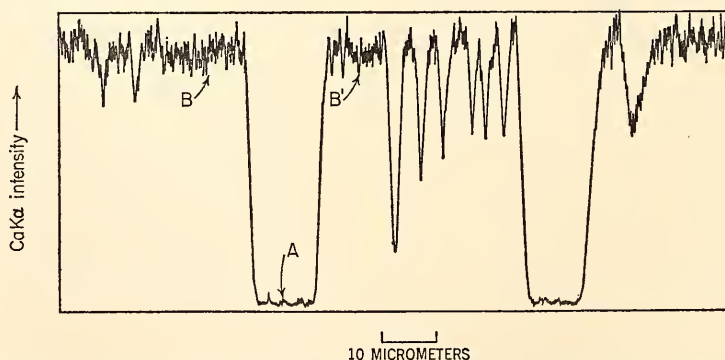


Fig. 4. Scan across an augite crystal containing exsolution lamellae of clinohypersthene; Bushveld gabbro, specimen no. SA 1019. The clinohypersthene analyses were made in the vicinity of point A, and the analyses for the augite host were made in the vicinities of points B and B'.

The analyzed augite lamella is an elongate bleb, ranging up to about 50 μm in width, and the area available for analysis was much greater than needed.

Analyses were made at 20 kV for Fe, Cr, and Mn, and at 15 kV for other elements. The specimen current was 0.03 to 0.04 μa with an X-ray spot size of 2 to 3 μm . The principal standard used was a glass prepared by H. G. Huckenholz containing Ca, Mg, Fe, and Si. Pure Cr and Mn were used along with other standards described in *Year Book 66*. The data were reduced with the use of the computer programs and correction procedures described elsewhere in this report.

Results of the analyses given in Table 1 show that all the cations,

except probably silicon, have participated in the unmixing process. This is true of the minor elements as well as Ca, Mg, and Fe. Even Cr, which is present at a concentration level on the order of 100 ppm, is fractionated between lamellae and host crystals. Ti, Na, Cr, and Al are concentrated in the Ca-rich pyroxene phases, and Mn is concentrated in the Ca-poor phases. The composition of the clinohypersthene lamella in augite is similar to the composition of the inverted pigeonite host, and the composition of the augite lamella in pigeonite is almost identical with the augite host.

These analyses are plotted in the pyroxene quadrilateral in Fig. 5 along with trend lines for pyroxenes from the

TABLE 1. Electron-Probe Analyses of Coexisting Pyroxenes from the Bushveld Intrusion

Inverted Pigeonite					Augite			
Host (hypersthene)			Lamella (augite)		Host (augite)		Lamella (clinohypersthene)	
SiO ₂	53.0	2	52.4	2	51.8	3	52.5	6
TiO ₂	0.3	...	0.5	...	0.5	...	0.2	...
Al ₂ O ₃	0.73	1	1.34	6	1.52	3	0.85	2
Cr ₂ O ₃	<0.01	...	0.02	...	0.02	...	<0.01	...
FeO*	23.6	2	11.2	19	10.8	6	25.6	3
MnO	0.5	...	0.3	...	0.3	...	0.6	...
CaO	1.36	15	21.0	21	21.2	6	0.77	3
MgO	20.7	2	13.6	3	13.3	1	19.6	3
Na ₂ O	0.05	...	0.2	...	0.2	...	0.05	...
K ₂ O	<0.005	...	<0.01	...	<0.005	...	<0.01	...
Totals	100.3		100.5		99.5		99.9	
Atomic Proportions for 6 Oxygen Atoms								
Si	1.98	} 2.000	1.96	} 2.000	1.95	} 2.000	1.98	} 2.000
Ti	0.008		0.01		0.01		0.006	
Al	0.012		0.03		0.04		0.014	
Al	0.020	} 1.998	0.029	} 2.009	0.028	} 2.000	0.024	} 2.001
Fe	0.740		0.349		0.340		0.812	
Mn	0.02		0.009		0.01		0.02	
Ca	0.055		0.842		0.857		0.031	
Mg	1.16		0.760		0.748		1.11	
Na	0.003		0.02		0.017		0.004	
Atomic %								
Ca	2.8		43.2		44.1		1.6	
Mg	59.2		38.9		38.4		56.8	
Fe	38.0		17.9		17.5		41.6	

* Total Fe as FeO.

Note: Numbers in italics are for the ratio σ/\sqrt{N} where σ is the standard deviation and N is the mean count.

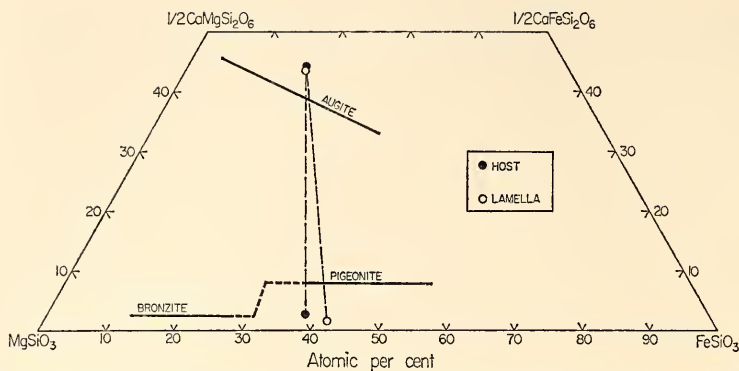


Fig. 5. A plot of the analytical data from Table 1 in the pyroxene quadrilateral. Trend lines established by bulk analyses of pyroxene pairs from the Bushveld intrusion (Wager and Brown, 1968) are also shown.

Bushveld intrusion established by wet-chemical analyses of bulk pyroxene separates (Wager and Brown, 1968). The pyroxenes from SA 1019 have not been separated and analyzed by wet chemical methods, but to a close approximation the bulk compositions of the augite and the inverted pigeonite can be taken as the points of intersection of the host-lamellae tie lines with their respective trend lines. A tie line established by joining these points of intersection has a slope compatible with those established by bulk analyses of other augite-inverted pigeonite pairs. The exsolution process shifts the compositions of the host and lamellae phases to more Ca-rich compositions on the augite side and to more Ca-poor compositions on the pigeonite side, as would be expected by slow cooling through an expanding two-pyroxene field.

The similarity in composition of the two Ca-rich phases and to a lesser extent the two Ca-poor phases implies that equilibrium was maintained for a period of time as the cooling proceeded. Values for the ratio σ/\sqrt{N} suggest that there are inhomogeneities in these phases but that they are not grossly inhomogeneous.

ORTHO-CLINO INVERSION IN FERROSILITE

D. H. Lindsley and J. L. Munoz

In the few years since ferrosilite was first synthesized at high pressures the apparent relations between orthoferrosilite (OFs; FeSiO_3 with space group *Pbca*) and clinoferrosilite (ClFs, FeSiO_3 with space group *P2₁/c*) have been a source of confusion. Lindsley, Davis, and MacGregor (1964) reported that they synthesized OFs at higher temperatures than ClFs, but they did not claim that this was an equilibrium relation. At the same time, Akimoto, Fujisawa, and Katsura (1964) reported the high-pressure synthesis of two polymorphs of ferrosilite; they identified one as OFs and the other as protoferrosilite (which was later shown to be ClFs). Lindsley, MacGregor, and Davis (*Year Book 63*, p. 175) next presented a phase diagram in which fields of ClFs and and ferrosilite III (Fs III; a pyroxenoid form of FeSiO_3) occur just below the solidus and a field of OFs appears at lower temperatures. The diagram was confirmed by reversed reaction between each pair of the three polymorphs, and it appeared that the true equilibrium relations had been determined. But some

anomalies remained. Although both OFs and ClFs readily invert to Fs III when held for a few hours in the pressure and temperature conditions of the reported Fs III field, experiments lasting 24 hours sometimes yielded ClFs at the same pressures and temperatures. Furthermore, synthesis experiments on oxide mixes within the Fs III field occasionally quenched to an orthorhombic form, which then rapidly inverted to ClFs at ambient pressure and temperature. The inversion, which could be observed under the petrographic microscope immediately after quenching, was too rapid to permit X-ray identification of the orthorhombic material; but this behavior was strongly reminiscent of protoenstatite. It appeared, then, that the field of Fs III given by Lindsley, MacGregor, and Davis might actually represent the stability field of yet another nonquenchable polymorph.

Spurred by the report of a low-temperature field for clinoenstatite (Selar, Carrison, and Schwartz, 1964), Lindsley (*Year Book 64*, pp. 148–149) discovered a field of ClFs lying below about 800°C over a wide pressure range. A field boundary between OFs (above 800°C) and ClFs (below 800°C) was confirmed by reversed reaction. (Akimoto *et al.*, 1965, presented a somewhat different boundary between these fields, but they too reported ClFs as the low-temperature polymorph.) It now appeared that there were two distinct fields of ClFs, one at high temperatures and one at low temperatures, separated by the field of OFs, and with each field boundary confirmed by reversed reaction. Although such a relation is theoretically possible, Lindsley suggested that high-temperature ClFs as well as Fs III might form upon cooling of a nonquenchable polymorph, perhaps protoferrosilite. Experiments at 20 kb on the composition $\text{Fe}_{0.4}\text{Mg}_{0.6}\text{SiO}_3$ indicated that the monoclinic polymorph was the stable low-temperature polymorph of intermediate Fe-Mg pyroxenes as well as of the end members (*Year Book 64*,

pp. 149–150). These results seemed inconsistent with data from natural pyroxenes, for pigeonites evidently form at higher temperatures than hypersthene. Furthermore, hypersthene rather than clinohypersthene is the common Ca-poor pyroxene in charnockites and pyroxene granulites. Kuno (1966) proposed a diagram for the Fe-Mg pyroxenes, which had a field of high-temperature clinopyroxene—to account for pigeonite—as well as a field of low-temperature clinopyroxene, extrapolated from the high-pressure studies, but it was still not clear why so few, if any, natural hypersthene inverted to the low-temperature monoclinic form on cooling.

In a study of the join hedenbergite-ferrosilite (*Year Book 65*, pp. 230–234), Lindsley reported fields of clinopyroxene (space group presumed to be $C2/c$) and of a pyroxenoid at 5, 7.5, 10, and 15 kb. Preliminary data obtained above 15 kb were not published, but the relations between Cpx and pyroxenoid for the compositions $\text{Fs}_{95}\text{Wo}_5$ and $\text{Fs}_{90}\text{Wo}_{10}$ were grossly consistent with the fields of ClFs and Fs III reported for pure FeSiO_3 (*Year Book 63*, p. 175), both fields lying immediately below the solidus, with ClFs occurring at higher pressures. No further evidence was found regarding the possible existence of a protoferrosilite field immediately below the solidus.

Riecker and Rooney (1967) reported the conversion of clinoenstatite from rhombic enstatite under shearing conditions at temperatures up to 1000°C—well within the rhombic enstatite field as reported by Selar, Carrison, and Schwartz (1964), and Boyd and England (*Year Book 64*, pp. 117–120). Munoz (*Year Book 66*, pp. 269–370) confirmed the findings of Riecker and Rooney. Evidently shearing stress increases the stability field of clinoenstatite. Inasmuch as there is inevitably a component of shear in dry experiments performed in solid-media pressure apparatus, it appeared that the entire low-clinopyroxene field might owe its existence to shearing

stress. Munoz sought to test this hypothesis by experiments on enstatite polymorphs, employing a hydrostatic cell at 20 kb. No reaction was observed in these experiments; clearly, shearing stress influences the kinetics of the ortho-clino inversion in enstatite, regardless of whether it also displaces the equilibrium. Water added to the starting material might increase the reaction rates, but it would also have resulted in the formation of hydrous phases when added to MgSiO_3 . Hydrous ferrous silicates form much less readily than do their magnesian counterparts, however, and it appeared that high-pressure hydrothermal experiments on ferrosilite might resolve the ortho-clino inversion problem.

We have successfully performed high-pressure hydrothermal experiments on FeSiO_3 using silver capsules in piston-and-cylinder pressure apparatus; water was retained in the capsules, no redox reaction took place (indicating that the experiments were effectively closed to H_2O and H_2), and no obvious hydrous phases were formed. The presence of a vapor phase at pressure and temperature is demonstrated by the leaching of small amounts of silica from the charge and the subsequent deposition of this silica as small globules with low refractive index. We converted ClFs to OFs at 20 kb and at temperatures as low as 650°C —in the ClFs field and 160° below the OFs-ClFs inversion curve (*Year Book 64*, p. 149). In duplicate dry (and therefore shearing) experiments, OFs inverted to ClFs.

There are only two logical explanations for these results: either shearing stress stabilizes clinoferrosilite at low temperatures; or small, thus far undetected, amounts of water enter the orthoferrosilite structure and stabilize it. We have seen no difference in the optical properties or X-ray diffraction patterns of orthoferrosilite synthesized under wet and dry conditions, and we suspect that the former explanation—stabilization of ClFs by shearing stress—is correct.

However, particularly in view of the hydrous magnesium orthosilicates (with apparent pyroxene structures) synthesized at 35 to 65 kb by Selar, Carrison, and Stewart (1968b), we cannot categorically reject the second possibility.

If further work should demonstrate that clinopyroxene is stable at low pressure only under shearing stress, the presence of hypersthene (rather than clinohypersthene) in many rocks is no longer enigmatic. It is still curious that clinohypersthene is rare in alpine-type peridotites, many of which may have been intruded essentially in the solid state and presumably under conditions of shearing stress; evidently much of the shearing is confined to restricted zones, with the bulk of the rock acting as inert blocks.

Even if the field of low-temperature clinopyroxene disappears under conditions of low shearing stress, the actual stability of high-temperature clinopyroxenes is still under question; it is not yet clear whether pigeonites are stable at high temperatures or whether they form upon cooling of some non-quenchable polymorph. The solution to this problem seems to require X-ray diffraction data obtained at high temperatures (and, for pure FeSiO_3 , at high pressure as well).

SUBSOLIDUS RELATIONS ON THE JOIN HEDENBERGITE-FERROSILITE AT 20 KB

J. L. Munoz and D. H. Lindsley

Previous investigation of the join hedenbergite ($\text{Ca}_{0.5}\text{Fe}_{0.5}\text{SiO}_3$, Hd)-ferrosilite (FeSiO_3 , Fs) at high pressures indicated the existence of a broad field of clinopyroxene (Cpx) at temperatures just below the solidus (*Year Book 65*, pp. 230-234). Reaction rates are slow in dry experiments along this join at temperatures below 1000°C , however, and it was impossible to determine whether a two-pyroxene field existed below that temperature. During the past year we have extended our investigation

of the Hd-Fs join to the range 700° to 1010°C using hydrothermal experiments at 20 kb. We have found a two-pyroxene field: Cpx plus OFs_{88} , orthoferrosilite with approximately 5 mole % CaSiO_3 (Fig. 6A).

Three types of starting materials were employed: single-phase clinopyroxenes of intermediate compositions, mechanical mixtures of Hd and OFs, and mechanical mixtures of two clinopyroxenes ($\text{Fs}_{90}\text{Wo}_{10}$ and $\text{Fs}_{60}\text{Wo}_{40}$). From 10 to 15 mg of appropriate starting material, plus 0.5 to 2 mg water, and approximately 0.5 mg silica glass (to saturate the vapor phase with SiO_2) was packed into a silver capsule, which was then capped with a tightly fitting silver lid. The loaded capsules were reacted at the desired pressure and temperature in piston-and-cylinder apparatus for durations ranging from 16 hours to 27 days. The presence of water at the conclusion of each experiment in all but one or two charges and the absence of magnetite (which would have indicated oxidation of the charge by preferential escape of hydrogen) show that the mechanically sealed capsules were effectively closed to water and hydrogen, and thus no external redox buffer was required. Compositions of OFs_{88} were determined by electron-microprobe analysis; compositions of Cpx were determined by X-ray methods and confirmed by microprobe analysis.

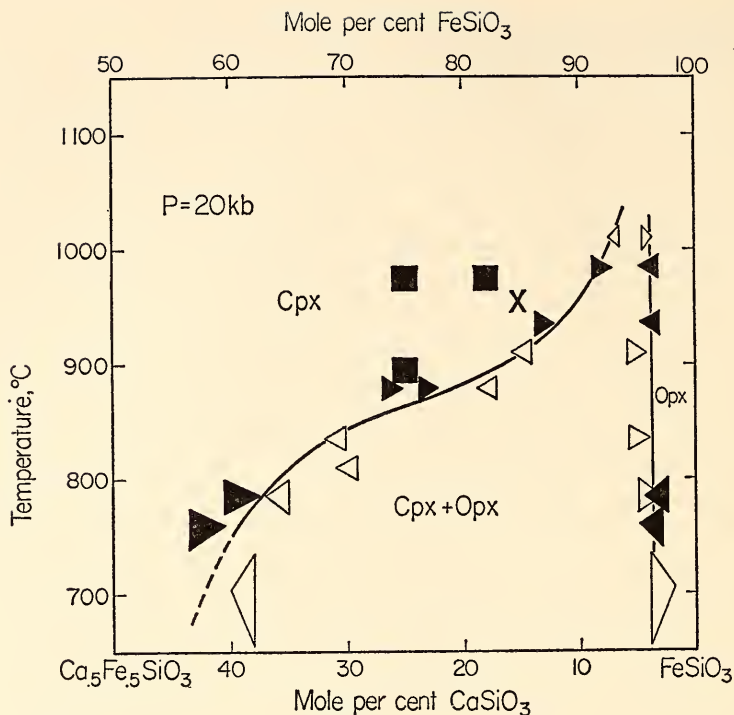
Clinopyroxene starting materials that broke down to two pyroxenes invariably produced discrete grains of the two phases and never lamellae of OFs_{88} in a Cpx host.

The shape of the curve for the composition of Cpx in equilibrium with OFs_{88} (Fig. 6A) is similar to that given by Davis and Boyd (1966) for Cpx on the join diopside-enstatite at 30 kb. In view of Kushiro's discovery of a two-Cpx field for the same join at 20 kb (discussed elsewhere in this report), we have searched carefully for a two-Cpx field on the join Hd-Fs, such as is shown

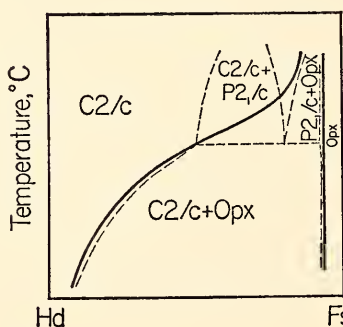
hypothetically in Fig. 6(B), but have not found one.

A clinopyroxene synthesized by us has been shown, on the basis of single-crystal X-ray photographs, to have the pigeonite ($P2_1/c$) structure (C. W. Burnham, personal communication, 1968; the single crystal was shown to have the nominal composition $\text{Fs}_{85}\text{Wo}_{15}$ by its unit-cell parameters). Thus, any two-Cpx field must lie at compositions more Ca rich than $\text{Fs}_{85}\text{Wo}_{15}$. We have homogenized mixtures of two clinopyroxenes ($\text{Fs}_{90}\text{Wo}_{10}$ and $\text{Fs}_{60}\text{Wo}_{40}$) with bulk compositions $\text{Fs}_{75}\text{Wo}_{25}$ and $\text{Fs}_{82}\text{Wo}_{18}$ (see Fig. 6A). The homogenization is indicated by powder X-ray studies of the run products and confirmed by electron-microprobe examination. We conclude that at 1000°C and 20 kb there is continuous solid solution between Hd and the composition $\text{Fs}_{92}\text{Wo}_8$. We cannot categorically eliminate a narrow (less than 10 mole % wide) two-clinopyroxene field that might indicate a first-order transition between clinopyroxenes of the pigeonite structure (space group $P2_1/c$) and the diopside structure (space group $C2/c$). We have tacitly assumed this conclusion in our interpretation of Fig. 6(A) as resulting from a two-Cpx field that has penetrated the lower but not the upper boundary of a Cpx-Opx transition loop (Fig. 6C). Under this interpretation the narrow two-pyroxene field above about 950°C in Fig. 6(A) corresponds to a pigeonite-hypersthene transition loop in Mg-bearing pyroxenes. We have been unable to extend this field to its presumed intersection at pure FeSiO_3 because a liquid appears in hydrothermal experiments above 1010°C and a pyroxenoid replaces both pyroxenes above $1085^\circ \pm 15^\circ\text{C}$ in dry experiments.

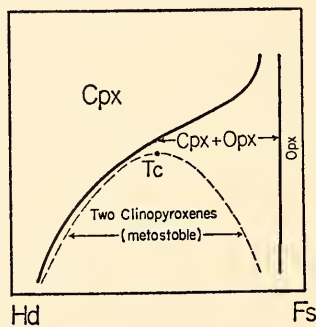
Assuming (1) that the Cpx series is a regular solution, (2) that the presumed miscibility gap in that series is symmetrical, and (3) that the interpretation shown in Fig. 6(C) is correct, we can extrapolate the critical temperature (T_c , about 870°C, in Fig. 6C) to low pres-



A



B



C

Fig. 6. Phase relations for the join hedenbergite-ferrosilite at 20 kb. (A) Data points and probable phase boundaries; (B, C) schematic interpretations of data. (A) Open triangles, compositions of pyroxenes formed by breakdown of single-phase Cpx. Solid triangles, compositions of pyroxenes formed by reaction of Hd + OFs pairs. Solid squares, compositions of Cpx homogenized from mixtures of $\text{Fe}_{80}\text{Wo}_{20}$ and $\text{Fe}_{80}\text{Wo}_{10}$, both Cpx. Horizontal extent of each symbol indicates uncertainty in composition; vertical extent indicates uncertainty in temperature. X indicates the synthesis conditions of a Cpx shown (by C. W. Burnham) to have the pigeonite ($P2_1/c$) structure. (B) Interpretation of relations in A as resulting from the intersection of three two-pyroxene regions along an isothermal three-phase line. We have not observed a two-clinopyroxene field ($C2/c + P2_1/c$), but it might escape detection by X-ray diffraction if less than about 10 mole % in width. (C) Interpretation of relations in A as resulting from the intersection of a two-Cpx field with the lower but not the upper boundary of a Cpx-Opx transition loop. T_c is the critical temperature of the assumed miscibility gap. This is our preferred interpretation.

tures. Using the excess volume of mixing for the series— $1.4 \pm 0.5 \text{ Å}^3$ at the composition $\text{Fs}_{75}\text{Wo}_{25}$ (Lindsley, Munoz, and Finger, this report)—and the method of Bell and Davis (*Year Book 64*, p. 122), we calculate that the critical temperature lies at approximately 820°C at 1 atm. This result provides a metastable (the stable assemblage is $\text{Cpx} + \text{fayalite} + \text{silica}$) terminus for the crest of the two-pyroxene field in the pyroxene quadrilateral diopside-hedenbergite-enstatite-ferrosilite. It appears that the two-pyroxene field might not intersect the solidus in the Mg-poor portion of that quadrilateral.

UNIT-CELL PARAMETERS OF CLINOPYROXENES ALONG THE JOIN HEDENBERGITE-FERROSILITE

D. H. Lindsley, J. L. Munoz, and L. W. Finger

Unit-cell parameters for clinopyroxenes synthesized along the join hedenbergite ($\text{Ca}_{0.5}\text{Fe}_{0.5}\text{SiO}_3$)-ferrosilite (FeSiO_3) have been determined through least-squares refinement of powder X-ray diffraction data (Fig. 7). The data were collected at a scanning rate of $1/4^\circ/\text{minute}$ in the range 19° to $65^\circ 2\theta$, with $\text{CuK}\alpha$ and $\text{CuK}\alpha_1$ radiation. CaF_2 was used as an internal standard in all but one powder mount, for which ($\text{Fs}_{65}\text{Wo}_{35}$) a correction term for 2θ was calculated

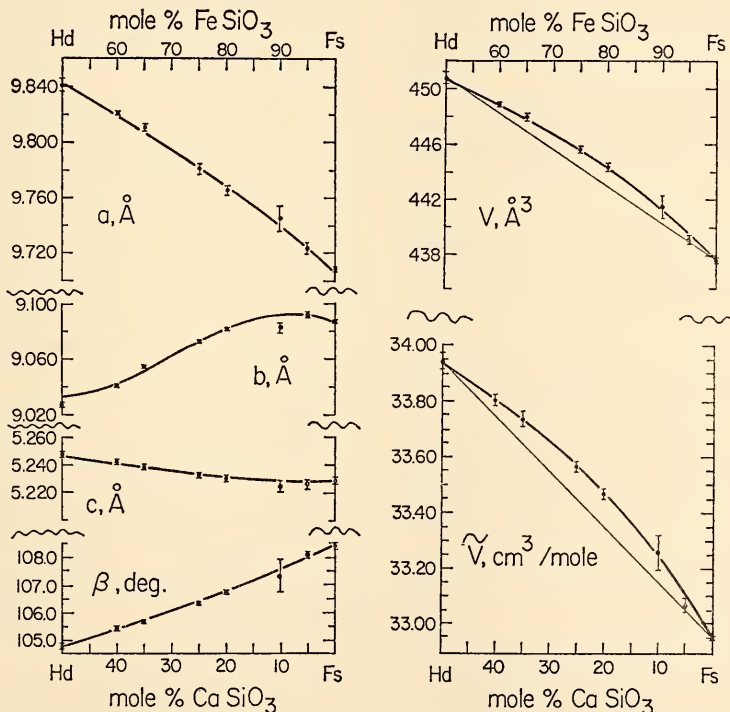


Fig. 7. Unit-cell parameters for clinopyroxenes synthesized on the join hedenbergite-ferrosilite. Values for hedenbergite are from powder data (J. Nolan, personal communication), and for ferrosilite from single-crystal data (Burnham, *Year Book 64*). All cell dimensions for intermediate pyroxenes were determined by least-squares refinement of powder diffractometer data. Conditions of synthesis: $\text{Fs}_{80}\text{Wo}_{20}$, 25 kb, 1210°C , dry; $\text{Fs}_{65}\text{Wo}_{35}$, 20 kb, 1210°C , dry; $\text{Fs}_{75}\text{Wo}_{25}$, 20 kb, 940°C , hydrothermal; $\text{Fs}_{80}\text{Wo}_{20}$, 25 kb, 1230°C , dry; $\text{Fs}_{65}\text{Wo}_{35}$, 37 kb, 1325°C , dry. Molar volumes (\tilde{V}) calculated on the basis of $Z = 8(\text{Ca,Fe})\text{SiO}_3$ per unit cell.

as a variable in the least-squares refinement, with the use of a program adapted from Burnham (*Year Book 64*, pp. 200–202). This term was insignificant, resulting in a change of $0.006^\circ 2\theta$ for each observation.

The variation of the unit-cell parameters with composition is presented in Fig. 7. The data were fitted by using weighted regression analysis, and the solution having the smallest standard error of estimate was plotted. The data for a and β require quadratic solutions; the data for the other parameters are best described by cubic equations, although only for b is there a large difference between the quadratic and cubic solutions.

The data in Fig. 7 should be useful in constructing grids of unit-cell parameters for the pyroxene quadrilateral. In addition, the small positive volume of mixing indicates that the size of the two-pyroxene field at 20 kb (Munoz and Lindsley, this report) should decrease at lower pressures.

OPTICAL PROPERTIES OF SYNTHETIC CLINOPYROXENES ON THE JOIN HEDENBERGITE-FERROSILITE

G. H. Myer and D. H. Lindsley*

Accurate data on the optical properties of synthetic clinopyroxenes along the join hedenbergite ($\text{Ca}_{0.5}\text{Fe}_{0.5}\text{SiO}_3$; Hd)-ferrosilite (FeSiO_3 ; Fs) have long been needed to provide one set of limiting conditions to the optical properties of clinopyroxenes lying in the quadrilateral diopside-hedenbergite-enstatite-ferrosilite. Unsuitable morphology and fine grain size prevented Bowen, Schairer, and Posnjak (1933, pp. 260–261) from determining n_β and $2V$, and limited the precision of their measurements of n_α and n_γ to ± 0.003 . We have measured the optical properties of clinopyroxenes synthesized at pressures of 20 kb or

above, where ferrosilite and FeSiO_3 -rich solid solutions are stable.

The clinopyroxenes were first synthesized in iron capsules in a large-volume ($\frac{3}{4}$ -inch bore) solid-media, piston-and-cylinder pressure device. Products that appeared homogeneous (with the exception of 1 to 2% fayalite + quartz in a few samples) upon X-ray and cursory optical examination, were then recrystallized in iron capsules for several hours at temperatures just below the solidus. Examination of these recrystallized samples in thin section reveals a porphyroblastic texture, the larger grains being about $100\ \mu$ in length. The demonstration of a two-clinopyroxene field intersecting the solidus at 20 kb for the join diopside-enstatite (Kushiro, this report) suggests that this bimodal distribution of grain size might reflect two clinopyroxenes of different composition. However, the smooth variation of both optical properties and unit-cell parameters with bulk composition of the samples is inconsistent with the existence of a miscibility gap, 10 mole % or more in width, on the join Hd-Fs. Inasmuch as the porphyroblastic texture is found over a wide range of compositions, it cannot have resulted from a narrow miscibility gap; instead, it probably reflects a variable growth rate among crystals of the same composition.

Clinopyroxenes of the compositions $\text{Fs}_{65}\text{Wo}_{35}$, $\text{Fs}_{75}\text{Wo}_{25}$, and $\text{Fs}_{85}\text{Wo}_{15}$ were too fine-grained when treated as above to permit good optical measurements. Additional samples of these compositions were therefore recrystallized hydrothermally at 20 kb by techniques described by Munoz and Lindsley (this report).

The clinopyroxenes were studied as grains in immersion oils—free on glass slides, mounted on epoxy resin substrates or mounted on glass spindles—and in thin sections. Refractive-index measurements were made in sodium vapor light; oils matching an index were transferred by micropipet to a Leitz-

* Department of Geological Sciences, University of Maine, Orono, Maine.

Jelley microrefractometer for immediate calibration. Precision of the refractive-index determinations is considered to be ± 0.001 . The optic angle, $2V_z$, was measured in sodium light by the interference-figure method of Tobi (1956) and by orthoscopic universal-stage techniques; both optic axes were observed as recommended by Munro (1963).

The refractive indices are plotted in Fig. 8 along with the data of Bowen, Schairer, and Posnjak (1933) for n_a and n_γ . The curves for n_a and n_β must intersect between $\text{Fs}_{95}\text{Wo}_5$ and $\text{Fs}_{100}\text{Wo}_0$. Composition $\text{Fs}_{98}\text{Wo}_2$ is predicted to have $n_a = n_\beta$ and thus to be pseudo-uniaxial.

The β refractive index of clinoferrosilite given by Lindsley, MacGregor, and

Davis (Year Book 63, p. 176) is 1.767 ± 0.002 . The new measurements give 1.765 ± 0.001 , which is at their low extreme. The data of Bowen, Schairer, and Posnjak (1933) for n_a and n_γ of hedenbergite and intermediate compositions lie consistently above the new curves. The small amount of fayalite+quartz in some of our samples would bias our results in the right direction but to an insufficient extent to account for this difference; we cannot explain it.

Between $\text{Fs}_{50}\text{Wo}_{50}$ and $\text{Fs}_{95}\text{Wo}_5$ the optic plane is parallel to (010), hence $Y=b$. The monoclinic inclined dispersion with $v > r$ is weak for $\text{Fs}_{50}\text{Wo}_{50}$ and increases to strong for $\text{Fs}_{95}\text{Wo}_5$. Interference figures, as observed in white light, exhibit one black isogyre and the other

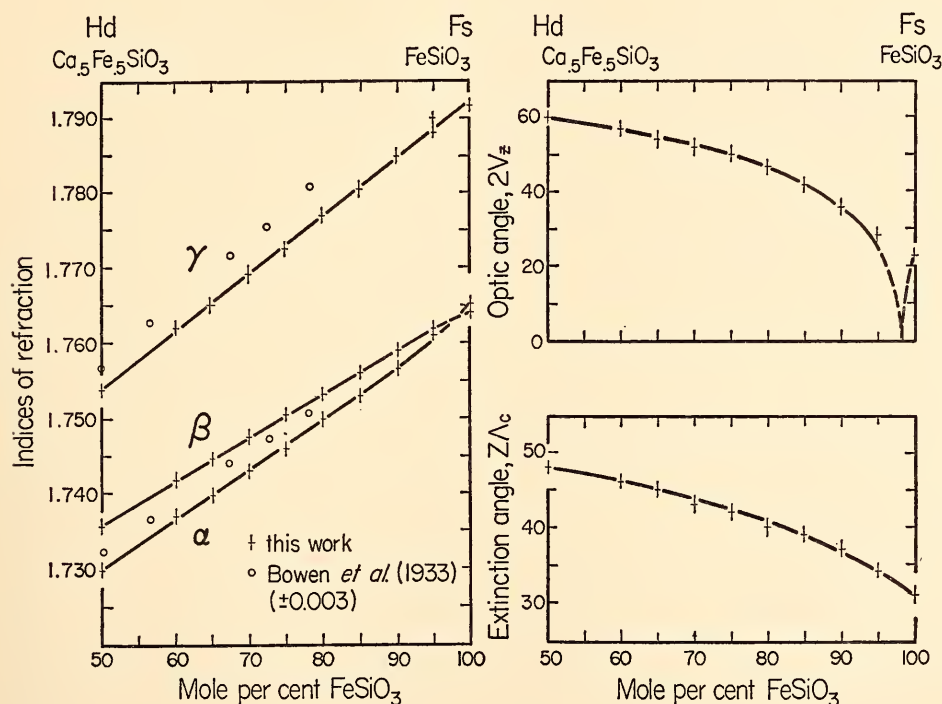


Fig. 8. Variation of optical properties with composition for synthetic clinopyroxenes along the join hedenbergite-ferrosilite. Crosses are data points: horizontal bar gives preferred value of parameter; extent of vertical bar gives estimated uncertainty. Curves are visual estimates. Open circles give values of n_a and n_γ reported by Bowen, Schairer, and Posnjak (1933, pp. 260-261). The optic angle $2V_z$ must go to zero between $\text{Fs}_{95}\text{Wo}_5$ and Fs_{100} because the orientation of the optic plane changes from parallel to (010) to perpendicular to (010) in that interval.

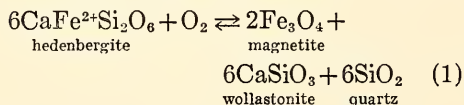
strongly colored. Clinoferrosilite, on the other hand, has the optic plane perpendicular to (010) and $X=b$. The monoclinic horizontal dispersion is strong: both isogyres are colored with $v > r$. $2V_z$ must decrease to zero between $\text{Fs}_{95}\text{Wo}_5$ and $\text{Fs}_{100}\text{Wo}_0$, rather than at $\text{Fs}_{94}\text{Wo}_6$ as predicted by Hess (1949) and by Muir (1951).

Extinction angle $Z \wedge c$ (Fig. 8) could not be measured to better than $\pm 2^\circ$ because of imperfect morphology. Twinning is developed often on (100) and occasionally on (001). Extinction angles for twinned and untwinned grains agreed to within 3° .

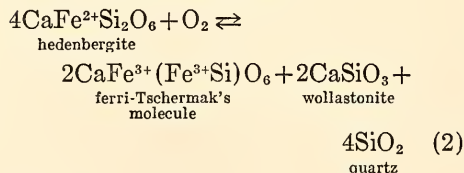
OXIDATION OF Ca-RICH CLINOPYROXENES

H. G. Huckenholz

The activities of SiO_2 in magmas are believed to be strongly controlled by oxidation, according to Osborn (1959). The change from ferrous to ferric iron causes silica enrichment, and magmas originally Ne normative may change to Hy- or even Qz-normative bulk composition. Yoder and Tilley (1962) discussed and illustrated the effect of oxidation on olivines and suggested a similar reaction for Ca-rich clinopyroxenes:

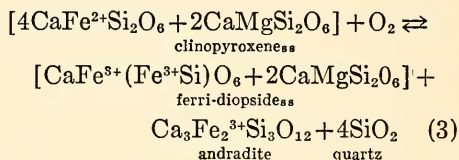


In the event that ferric iron is retained in the clinopyroxene structure, the following reaction should take place:



The nature of the incorporation of ferric iron in Ca-rich clinopyroxene, particularly in diopside, is now known (Huckenholz, Schairer, and Yoder, *Year Book 66*). Diopside may take up in solid solution 33% by weight of the ferri-

Tschermak's molecule (FTs), and as much as 19% Fe_2O_3 may be retained in the diopside structure in the absence of soda at 1157°C and 1 atm pressure. Additional substitution of the ferri-Tschermak's molecule in a clinopyroxene solid solution is not stable as a single phase, and phase assemblages of clinopyroxene_{ss} + hematite, clinopyroxene_{ss} + hematite + andradite, and hematite + andradite are formed. Above 1157°C polyphase assemblages occur in which andradite is replaced by wollastonite, pseudowollastonite, and additional hematite. Therefore, reaction 2, outlined by Yoder and Tilley (1962), should be modified with regard to andradite as follows:



In order to test reaction 3, a series of natural Ca-rich clinopyroxenes (Table 1) were treated at 1125°C and 1 atm over a period of 3 weeks. The envelopes containing the samples were perforated to achieve better circulation of air. It is believed that treatment like this converts most of the Fe^{2+} into Fe^{3+} , and the analyses of the clinopyroxenes have been recalculated on an Fe^{3+} basis. As plotted on the wollastonite-diopside-hematite join of Fig. 9 (neglecting the excess of free silica), oxidation of augites and hedenbergites yields a phase assemblage of clinopyroxene_{ss} + hematite (+cristobalite) in sample 1, whereas in samples 2, 3, and 4 an assemblage of clinopyroxene_{ss} + hematite + andradite_{ss} (+cristobalite) is obtained. One would expect from equation 3 that no hematite should be formed. Its appearance is caused by the ferrosilite content of the natural clinopyroxenes, however, as can be seen in the norm of the clinopyroxenes.

In all four samples the reaction produces fine-grained intergrowths of the phases, sometimes with oriented hematite

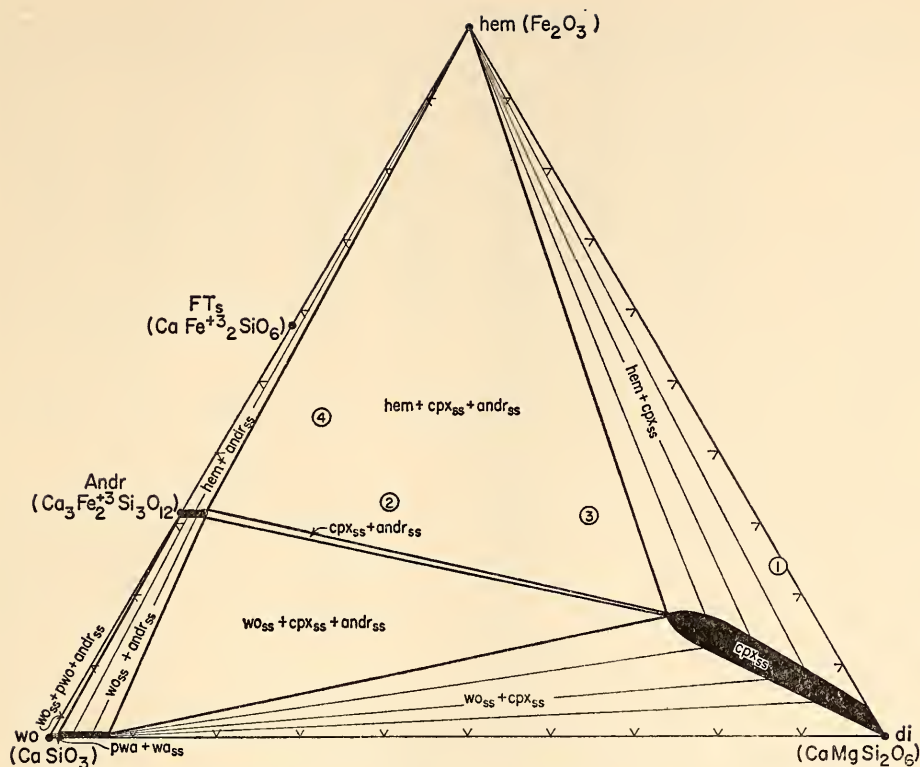


Fig. 9. Wollastonite-diopside-hematite join below 1137°C and the composition of natural clinopyroxenes after "oxidation," neglecting cristobalite. Phases encountered: FTs, ferri-Tschermak's molecule; andr, andradite; wo, wollastonite; pwo, pseudowollastonite; di, diopside; cpx, clinopyroxene; hem, hematite. Numbers refer to samples, as indicated in Table 2.

and cristobalite parallel to (001) of the new clinopyroxene. The composition of the light yellow to yellow-brown ferri-diopside may be traced by using the angular separation of $2\theta(240)-2\theta(041)$ (Huckenholz, Schairer, and Yoder): about $\text{di}_{95}\text{hem}_5$ in sample 1, and about $\text{di}_{67}\text{hem}_{17}\text{wo}_{16}$ in samples 2, 3, and 4. The garnet formed in sample 2 is almost a pure andradite with minor amounts of a grossularite component, whereas the garnet of samples 3 and 4 contains both a grossularite and a Ti-garnet component, as revealed by the size of their cell edges, and by the Al and Ti contents of the samples (Table 2, samples 2, 3, and 4).

From the data at hand it is evident

that the formation of ferri-diopside and andradite is favored in addition to Fe^{3+} -bearing oxides if a magma crystallizes under oxidizing conditions. However, ferri-diopside is very often associated with those igneous rocks that have undergone oxidation and that contain small amounts of alkalis, especially sodium. Large amounts of sodium lead to the formation of the acmite molecule, whereas potassium enters the diopside structure only in very small amounts. If the sodium content of a magma is high and insufficient Al_2O_3 is available, a preferred formation of acmite molecules or even of acmite itself may take place under oxidizing conditions.

TABLE 2. Analyses of Natural Clinopyroxenes Oxidized in this Study

	1	1a	2	2a	3	3a	4	4a
Analyses								
SiO ₂	50.58	49.8	48.34	47.4	49.44	48.3	47.09	45.9
Al ₂ O ₃	2.20	2.1	0.30	0.3	1.31	1.3	0.80	0.8
Fe ₂ O ₃	1.57	18.5	1.50	26.5	0.88	24.3	1.61	32.3
FeO	15.53	...	22.94	...	21.64	...	28.41	...
MnO	0.28	0.3	3.70	3.6	0.42	0.4	0.64	0.6
MgO	12.60	12.4	1.06	1.1	6.92	6.8	1.19	1.1
CaO	16.40	16.1	21.30	20.9	18.23	17.8	18.99	18.5
Na ₂ O	0.24	0.2	0.14	0.1	0.29	0.3
K ₂ O	0.03	...	0.03	...	0.03	...	0.05	...
TiO ₂	0.61	0.6	0.08	0.1	0.83	0.8	0.83	0.8
Cr ₂ O ₃	<0.01	<0.02	...
H ₂ O	0.46	0.14	...
Totals	100.04	100.0	99.85	100.0	99.99	100.0	99.97	100.0
Norms								
Q	...		1.29		...		1.27	
Or	0.18		0.18		0.18		0.30	
Ab	2.03		1.18		2.45		...	
An	4.84		0.10		2.18		2.04	
Di	62.98		93.33		75.00		81.46	
Hy	25.20		1.02		16.79		10.66	
Ol	1.38		...		0.54		...	
Mt	2.28		2.17		1.28		2.33	
Il	1.16		0.15		1.58		1.58	
Molecular Fs/En ratio in Hy	0.39		0.93		0.63		0.93	
Composition in di, wo, hem, and cr after Oxidation, wt %								
di		66.3		19.2		40.3		7.9
wo		...		34.3		16.5		34.2
hem		20.7		26.2		25.6		33.9
cr		13.0		20.3		17.6		24.0
Results of Oxidation								
Ferri-diopside	*			*		*		*
Andradite _{ss}	†			*		*		*
			(12.037 ± 0.003 Å)		(12.09 ± 0.01 Å)		(12.055 ± 0.005 Å)	
Hematite	*			*		*		*
Cristobalite	*			*		*		*

* Present.

† Absent.

1. Augite (4330), recalculated as "oxidized" augite (1a), from ferrogabbro MZ, Skaergaard intrusion, east Greenland (Brown, 1957). Donated by G. M. Brown.

2. Hedenbergite, recalculated as "oxidized" hedenbergite (2a), from a skarn rock close to a diorite intrusion, Herault, Shasta County, California. (Wyckoff, Merwin, and Washington, 1925). Collection of H. S. Yoder, Jr.

3. Ferroaugite (EG 4316), recalculated as "oxidized" ferroaugite (3a), from ferrodiorite UZb, Skaergaard intrusion, east Greenland (Brown and Vincent, 1963). Donated by G. M. Brown.

4. Ferrohedenbergite (K 3381), recalculated as "oxidized" ferrohedenbergite (4a), from ferro-syenite, Kiglapait intrusion, Labrador, Canada. (C. O. Ingamells, analyst; contains 0.02 Cr₂O₃, 0.20 NiO, 0.005 SrO, and 0.02 P₂O₅.) Donated by S. A. Morse.

STABILITY OF OMPHACITE

Omphacite, a clinopyroxene solid solution consisting mainly of diopside (CaMgSi₂O₆) and jadeite (NaAlSi₂O₆) components, is one of the major constitu-

ent minerals of eclogites. It also occurs in some glaucophane schists and associated metamorphic rocks. In the absence of free silica, omphacite breaks down to nepheline, albite, and a more diopside-

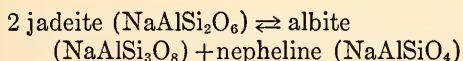
rich omphacite with less jadeite component at lower pressures or at higher temperatures. In the presence of free silica, omphacite reacts with silica to form albite and a more diopside-rich omphacite with less jadeite component at lower pressures or at higher temperatures.

In the present experiments the stability field of omphacite has been determined in the joins diopside-jadeite (free silica absent) and diopside-albite (free silica present).

Stability of Omphacite in the Absence of Excess Silica

P. M. Bell and J. Kalb

The pure jadeite end member has been studied experimentally in the subsolidus by Robertson, Birch, and MacDonald (1957) and by Bell (*Year Book 63*, pp. 171-174). Pure jadeite breaks down by means of the univariant reaction:



In the present study the primary aim has been to evaluate the effect on the univariant reaction of the addition of diopside ($\text{CaMgSi}_2\text{O}_6$). The breakdown of jadeite is highly pressure sensitive and has provided a useful geobarometer for

eclogitic rocks even though most natural jadeites are omphacitic since they contain an average of at least 10 to 15% diopside (see Coleman *et al.*, 1965). It is essential to know how the presence of the diopside component affects the jadeite geobarometer.

Jadeite is in equilibrium with albite and nepheline along a curve that is very steep to the pressure axis: at 1150°C the curve lies at 22 kb, and at 1225°C the curve lies at 24 kb. These two temperatures, 1150° and 1225°C, were chosen for experimental isotherms. The reaction omphacite₁ \rightleftharpoons plagioclase + nepheline + diopside pyroxene (omphacite₂) was investigated isothermally for the compositions $\text{Jd}_{50}\text{Di}_{50}$ and $\text{Jd}_{70}\text{Di}_{30}$ wt % with the piston-cylinder, solid-media apparatus. The reaction is sensitive to the compositions of the phases. Thus in selecting starting materials for the right-hand side of the reaction (low-pressure assemblage), the compositions of the phases must be those that are at equilibrium on the phase boundary. Theoretically, therefore, the boundary must be known before it can be studied. In order to avoid this paradox, glasses and crystalline mixes were used to reconstitute the phase boundaries. Boundaries produced by using these starting materials were

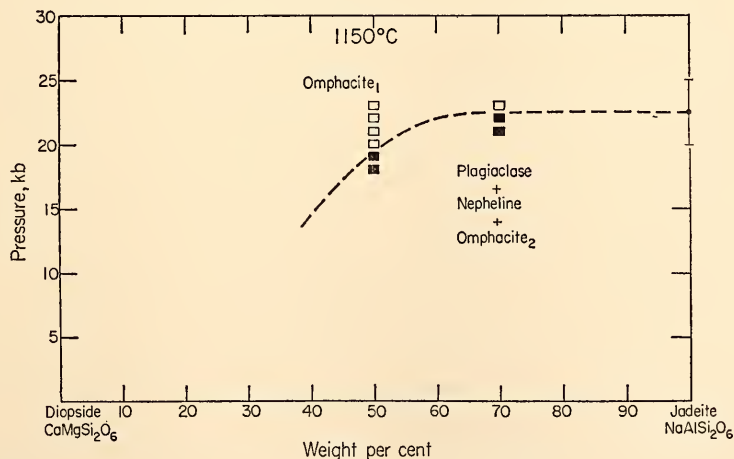


Fig. 10. Pressure-composition section for omphacite at 1150°C.

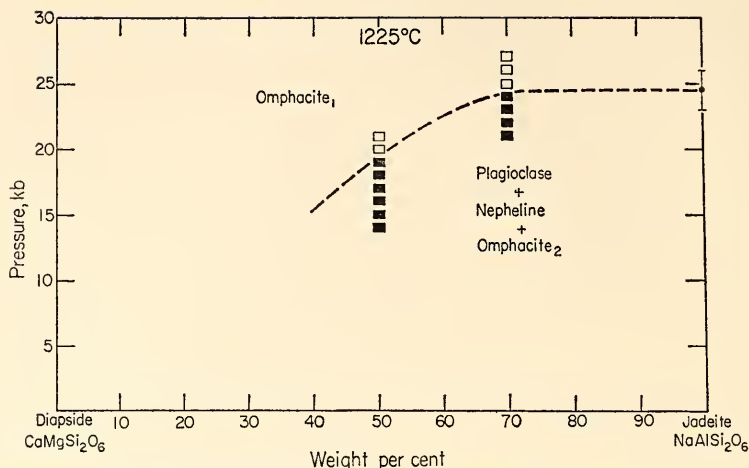


Fig. 11. Pressure-composition section for omphacite at 1225°C.

metastable but were useful in giving a general location for the equilibria. By trial and error, the correct assemblages were synthesized close to the boundary and used as starting materials. The assemblage plagioclase + nepheline + omphacite₂ was added in equal proportions to the omphacite₁, and an increase or decrease in the amount of reactant or products was used as an indication of the direction of reaction. The disappearance of plagioclase was used to fix the phase boundary.

Experimental points determined for the isotherms 1150° and 1225°C are shown in Figs. 10 and 11. The results suggest that the breakdown of jadeite is not sensitive to the presence of diopside in solid solution with it unless the concentration of diopside is greater than 30 wt %. These results confirm the theoretical result of Bell and Davis (*Year Book* 64, pp. 120–123) and the preliminary experiments with natural samples of Newton and Smith (1967). The view of Robertson, Birch, and MacDonald (1957) that the presence of omphacite in rocks suggests that they formed at high pressure appears to be valid.

Stability of Omphacite in the Presence of Excess Silica

I. Kushiro

The subsolidus region of the join diopside-albite was studied previously in the pressure range 10 to 32 kb and the temperature range 1050° to 1350°C, with piston-cylinder, solid-media apparatus (*Year Book* 64, pp. 113–115). It was shown that the stability field of an omphacite + quartz assemblage relative to that of an omphacite + albite-rich plagioclase + quartz assemblage expands toward albite with an increase of pressure at constant temperature. Starting materials used in those experiments were glass of compositions on the join diopside (Di)-albite (Ab) made by Schairer and Yoder (1960). It is possible, however, that metastable assemblages may be formed from glass even at high temperatures. The present experiments have been made by the piston-out technique with crystalline starting materials. Experiments were performed for the three compositions $\text{Di}_{55}\text{Ab}_{45}$, $\text{Di}_{40}\text{Ab}_{60}$, and $\text{Di}_{25}\text{Ab}_{75}$ (wt %) at 1250°C in the pressure range 25 to 34.5 kb.

For the composition $\text{Di}_{55}\text{Ab}_{45}$, the omphacite + plagioclase + quartz assemblage

was converted to omphacite+quartz at 27.5 kb and the omphacite+quartz assemblage was converted to omphacite+plagioclase+quartz at 25.5 kb in 5 to 6 hours. The boundary between these two assemblages for $\text{Di}_{55}\text{Ab}_{45}$ composition is located, therefore, at 26.5 ± 1 kb at 1250°C , about 0.5 kb higher than that determined with the use of glass as starting material (Fig. 12). For the composition $\text{Di}_{40}\text{Ab}_{60}$, the reversal reactions took place at 32.5 and 29 kb, respectively. The boundary for this composition then, is 30.8 ± 1.8 kb at 1250°C , about 1.2 kb higher than that given in the previous experiments. It appears that the reaction rate is slower for more albite-rich compositions. For the composition $\text{Di}_{25}\text{Ab}_{75}$, complete disappearance of plagioclase was not observed in the runs at pressures up to 34.5 kb for 5 to 6 hours at 1250°C , and the boundary could not be determined successfully. The amount of plagioclase relative to omphacite and quartz, estimated from the relative in-

tensities of X-ray reflections, decreases with increasing pressure. This decrease could occur in both the omphacite+plagioclase+quartz field and the omphacite+quartz field, however, and cannot be used to locate the boundary curve.

Extrapolation of the boundary to albite composition suggests that the breakdown of albite into jadeite+quartz would take place at 33.5 ± 2 kb at 1250°C . The value is consistent with that obtained by extrapolating the breakdown curves of albite given by Birch and LeComte (1960) and Newton and Smith (1967).

Comparison of the previous results with those obtained in the present experiments suggests that the boundary between the field of the omphacite+quartz assemblage and that of the omphacite+plagioclase+quartz assemblage given in the previous experiments is nearly correct for compositions more diopside rich than $\text{Di}_{50}\text{Ab}_{50}$ at temperatures at least near 1250°C . For compositions more albite

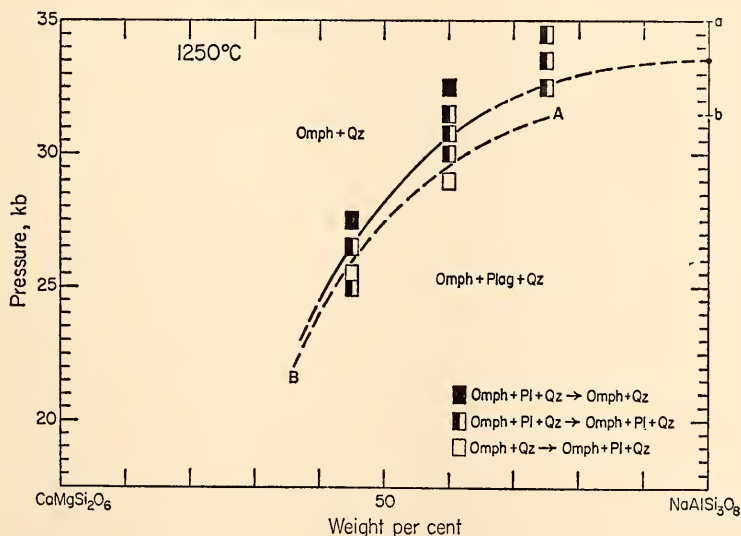


Fig. 12. Subsolidus phase relations in the join diopside-albite at 1250°C . The dashed curve A-B is a boundary between the field of the omphacite+quartz assemblage and that of the omphacite+plagioclase+quartz assemblage given in the previous experiments (*Year Book 64*, p. 113). The range a-b is the uncertainty of pressure for the reaction albite=jadeite+quartz at 1250°C in the extrapolation of the data of Birch and LeComte (1960) and Newton and Smith (1967).

rich than $\text{Di}_{50}\text{Ab}_{50}$, however, the corrected boundary lies at 1 to 2 kb higher pressure than that of the previous experiments.

THE TEMPERATURE-COMPRESSION MELTING RELATION

M. C. Gilbert

A "new melting law" of the form $T_M = T_M^\circ (1 + C \Delta V/V_0)$, for application at high pressures, has recently been proposed by Kraut and Kennedy (1966a). It was based on the observation that plots of melting temperature at pressure against isothermal (room-temperature) compression of the solid phase appeared to give a linear relation. These authors originally suggested that "this result seems to apply to all substances examined which melt with an increase in volume . . ." Shortly thereafter Kraut and Kennedy (1966b) indicated that some solidified gases did not obey this relationship. More recent work by Luedemann and Kennedy (1968) has shown that the linear relation also breaks down for the alkali metals as melting maxima are approached, and compression of the solid reaches 35 to 40%. The latter authors speculated that the results may indicate that, at equivalent compressions for silicates (in the deep mantle and core), fusion maxima would be encountered. In the light of these arguments it seemed of interest to examine such a plot for aegirite, which melts incongruently (Fig. 13). The melting relations were reported previously in *Year Book 65* (pp. 241-244). Compressibility values are derived from ultrasonic measurements on a specimen of aegirite (Birch, 1966, Tables 7-10 and 7-12; Alexandrov and Ryzhova, 1961).

It is clear that no linear relation between $\Delta V/V_0$ and melting temperature exists for aegirite. In fact, the resulting curve is similar in form to the fusion curve itself. It was thought possible that deviation from linearity might be due to

incongruent melting. For comparison, plots of melting temperature versus compressibility for other silicates are shown in the inset of Fig. 13. Fayalite (Fe_2SiO_4), which melts incongruently up to 40 kb (Hsu, 1967), and sanidine (KAlSi_3O_8), which melts incongruently up to 20 kb (Lindsley, 1966) show linear relationships over that region; thus, incongruent behavior cannot be used to explain curvature. In contrast, diopside, which melts congruently (Boyd and England, 1963), and sanidine, which melts congruently above 20 kb (Lindsley, 1966), do not show linear relations. On the whole, the relationships for silicates shown in Fig. 13 reflect the form of the fusion curves: linear fusion curves result in linear T_M versus $\Delta V/V_0$ curves; fusions with marked curvature result in curved T_M versus $\Delta V/V_0$ relations, with the exception of albite.

A pressure effect on the emf of thermocouples cannot be used to account for the nonlinear T_M - $\Delta V/V_0$ curves presented here, because all curves shown are plotted without this correction so that differences between curves are real. Nothing in the experimental techniques used to determine the melting curves can be appealed to since all these curves were determined by the same type of apparatus and technique. It is possible that the compressibility measurements at lower pressures for silicates may have larger uncertainties than expected and that extrapolation to higher pressure of low-pressure measurements is unwarranted. In any case, difficulties in the simple temperature-compression relation are not limited to silicates. Some of the elements and simple compounds considered by Kennedy and co-workers also do not show linear behavior. There would seem to be no *a priori* reason why a melting law that does not take into account properties of both solid and liquid phases should work. Whatever the reasons, the "new law of melting" does not seem to be substantiated by silicates over the pressure range thus far investigated.

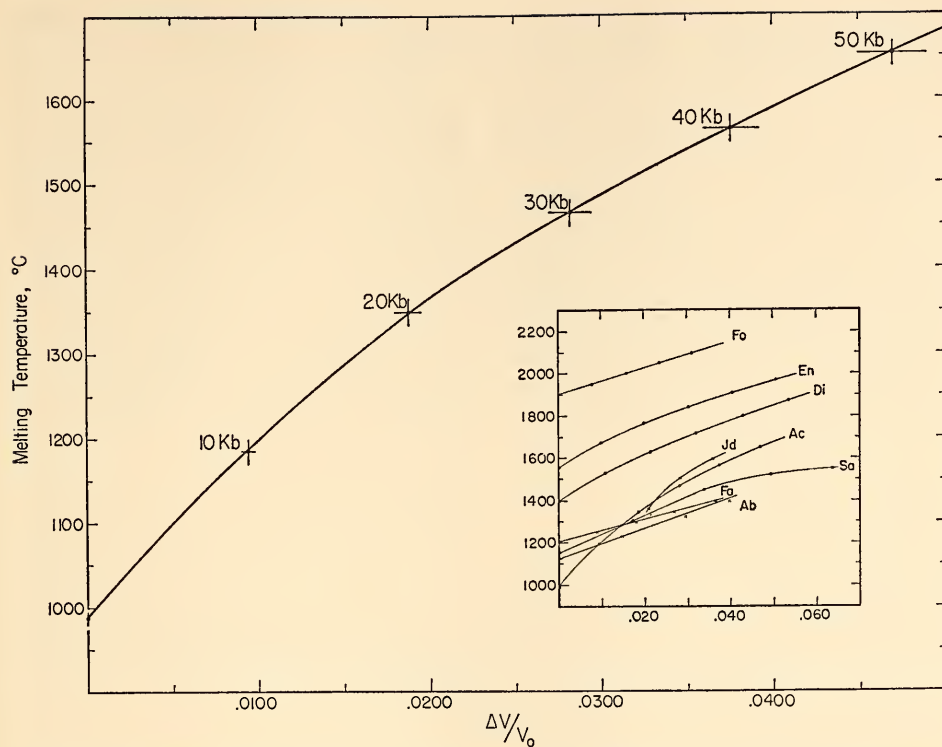


Fig. 13. Melting temperature of acmite versus its compression at room temperature. Inset shows similar plots for other silicates. Compression data summarized in Birch (1966, Table 7-10). Melting curves for Fo, forsterite, Mg_2SiO_4 (Davis and England, 1964); En, enstatite, MgSiO_3 (Boyd, England, and Davis, 1964); Di, diopside, $\text{CaMgSi}_2\text{O}_6$, and Ab, albite, $\text{NaAlSi}_3\text{O}_8$ (Boyd and England, 1963); Jd, jadeite, $\text{NaAlSi}_2\text{O}_6$ (Bell, *Year Book 63*); Ac, acmite; Sa, sanidine, KAlSi_3O_8 (Lindsley, 1966); Fa, fayalite, Fe_2SiO_4 (Hsu, 1967). The points shown on the curves in the inset represent 10-kb steps in pressure. The first point on the jadeite curve represents 30 kb.

FELDSPARS AND HIGHLY FELDSPATHIC ROCKS

THE MELILITE-PLAGIOCLASE INCOMPATIBILITY DILEMMA IN IGNEOUS ROCKS

H. S. Yoder, Jr., and J. F. Schairer

Field occurrences clearly indicate the incompatibility of plagioclase and melilite in lavas of the alkali suites. Volcanic centers of the same province eject either plagioclase-bearing pyroclastics and lavas or melilite-bearing lavas, and occasionally extrude both lava types separated by long intervals of time. The field association is close and definitive; the genetic relationship, however, is not as

yet evident from field deductions. Because plagioclase and melilite are the key minerals to the major trends of alkali igneous rock, the system albite (Ab)-anorthite (An)-akermanite (Ak) at 1 atm was studied by Schairer and Yoder (this report). The results, surprisingly enough, demonstrated that a plagioclase and a melilite were compatible with liquid over much of the range of plagioclase, with the exception of compositions on the join Ab-Ak. Although the plagioclase compositions were not determined, it was obvious that plagioclase and melilite were compatible over a significant range of plagioclase

composition, in direct contradiction to the field observations. The simplified nature of the laboratory experiments was believed to be the cause in part of the dilemma, and other factors, such as the presence or absence of water, were considered relevant to the problem on the basis of field observations. Nixon and Clark (1967, p. 470) believed that magma richer in volatiles and calcium produced melilite-bearing lavas rather than plagioclase-bearing lavas. Melilite was present in the more calcium-rich compositions in the simple Ab-An-Ak system, however, with plagioclase. The

effect of volatiles, specifically H_2O , was therefore investigated as well.

Compositions on or close to the $Ab_{50}Ak_{50}$ - $An_{50}Ak_{50}$ were studied at temperatures from 700° to $1175^\circ C$ at $P_{H_2O} = 2$ kb. These conditions were chosen because of the restrictions of the stability of akermanite itself (Yoder, *Year Book 66*, p. 473) and the limitations imposed by $An_{50}Ak_{50}$ (Yoder, this report). The anhydrous phase relations are shown in Fig. 14 by a series of lines, indicating the appearance or disappearance of phases. The anhydrous composition close to $Ab_{37}An_{13}Ak_{50}$ marks the change at the

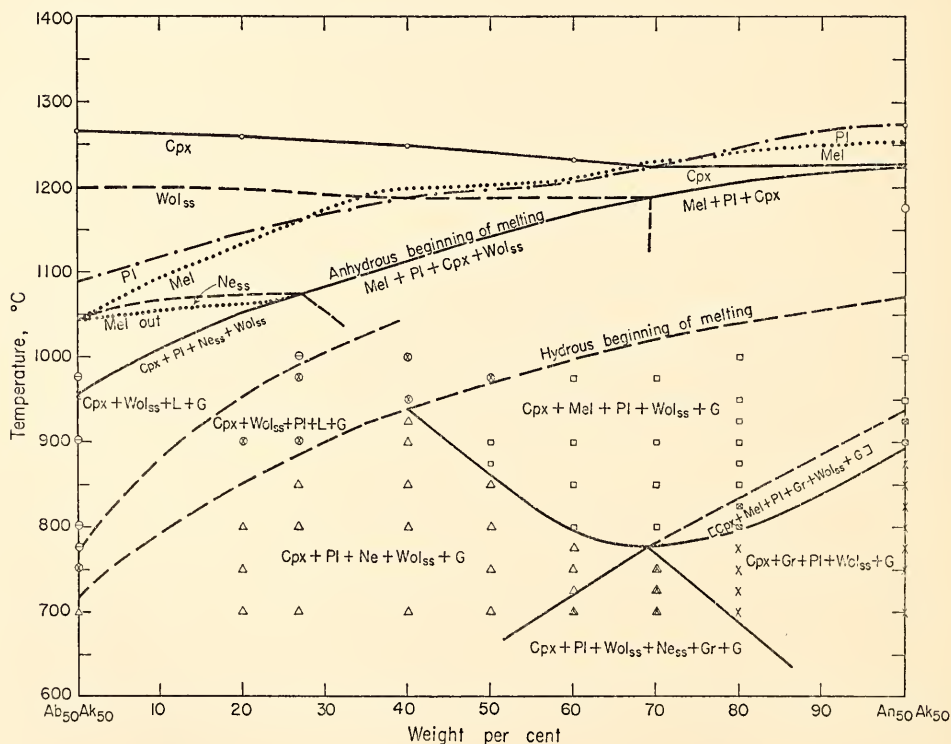


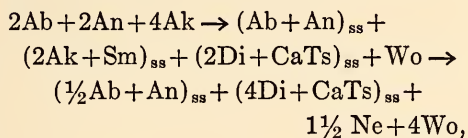
Fig. 14. At the higher temperatures are presented the 1-atm thermal relations of compositions on or near the join albite₅₀akermanite₅₀-anorthite₅₀akermanite₅₀ (see Fig. 15, Schairer and Yoder, this report). The appearance of each phase and the disappearance of melilite (Mel) is indicated by a patterned curve. At the lower temperatures are presented the hydrothermal relations in an excess of water at $P_{H_2O} = 2$ kb for the same compositions. The curves mark the boundaries between assemblages. The assemblage $Cpx + Mel + Pl + Gr + Wol_{ss} + G$ is believed to be due to metastable growth and persistence of garnet (Gr). Cpx, clinopyroxene; Pl, plagioclase; Wol_{ss} , wollastonite solid solution; G, gas; L, liquid. Water content, if any, of the garnet was not determinable optically because of the small grain size.

solidus from the assemblage melilite + plagioclase + clinopyroxene + wollastonite to nepheline + plagioclase + clinopyroxene + wollastonite. On the same figure are shown the assemblages found under $P_{H_2O}=2$ kb. The beginning of melting is drastically lowered and the change of assemblage at the anhydrous solidus extends to more calcium-rich compositions. Additional assemblages involving a garnet (mainly grossularite) were encountered at the most calcium-rich composition at lower temperatures, as predicted from the study of $An_{50}Ak_{50}$ (Yoder, this report). It is evident that melilite and plagioclase coexist in the presence of water at reasonable magma temperatures. Preliminary results at higher water pressures, e.g., 5 kb, indicate a drastic temperature rise in the stability of the garnet-bearing assemblages, and the melilite assemblages do not appear. Appeal to such water pressures does not seem appropriate for the lavas but may account for the absence of melilite in the pyroclastics. The dilemma remains for the lavas on the basis of these experiments.

A natural melilite (approximately $\frac{2}{3}$ akermanite and $\frac{1}{3}$ soda melilite) and a natural plagioclase (close to An_{50}) were mixed in equal proportions and heated at 1 atm at a series of temperatures. No reaction was observed below 800°C. At and above 850°C, to the beginning of melting and through much of the melting region, the assemblage was mostly melilite and plagioclase, with some diopside and wollastonite solid solutions. Under hydrous conditions ($P_{H_2O}=2$ kb) the natural minerals reacted completely to clinopyroxene + plagioclase + wollastonite + nepheline at 700°, 800°, and 900°C. Melting of the synthetic composition $Ab_{25}An_{25}Ak_{50}$ begins at about 970°C under $P_{H_2O}=2$ kb, and the melilite-bearing assemblage, whose plagioclase and melilite compositions are believed to be in accord with the natural

minerals chosen (see equations below), is stable down to about 860°C (Fig. 14). Apparently the additional constituents in the natural materials are the cause of the difference in results in the hydrous experiments, whereas rate problems prohibited attainment of equilibrium in the anhydrous experiments.

The two principal assemblages exhibited in Fig. 14, $Cpx + Pl + Ne_{ss} + Wo_{ss}$ and $Cpx + Mel + Pl + Wo_{ss}$, may be related, with an initial composition of 1Ab:1An:2Ak for example, as follows:



where Sm represents soda melilite; Di, diopside; CaTs, calcium Tschermak's molecule; Ne, nepheline; and Wo, wollastonite. All possible solid solutions are not adequately represented; however, the apparent incompatibility of nepheline and melilite, which are found coexisting in other compositions in Ab-An-Ak (Fig. 15 of Schairer and Yoder, this report), is outlined. (Attempts to test these relationships by means of microprobe analyses of the phases failed because of the exceedingly small grain size.) The reactions postulated depend in part on solid solution of soda melilite in akermanite and of "plagioclase" in nepheline (see Fig. 17 of Yoder, this report). Both types of solid solution series are reasonable on the basis of analysis of natural minerals and phase relations in less complex synthetic systems. From another viewpoint, desilication of albite to nepheline and anorthite to calcium Tschermak's molecule brings about silication of the akermanite to diopside and wollastonite. The complexities of the solid solutions do not yield an unambiguous solution to the relationship of the two principal assemblages with the data at hand.

THE JOIN ALBITE-ANORTHITE- AKERMANITE

J. F. Schairer and H. S. Yoder, Jr.

The phase-equilibrium diagram for the join albite-anorthite-akermanite is given here as Fig. 15. Data for the limiting system albite-anorthite were given by Bowen (1913), and additional data were obtained by Schairer (1957, p. 232, Fig. 35) in his studies of the system nepheline-anorthite-silica, which confirmed exactly the liquidus curve of Bowen but slightly modified the solidus curve. Data for the limiting system anorthite-akermanite were given by deWys and Foster (1956). Data obtained in the present investigation show that anorthite and akermanite do not show simple eutectic relations, that

crystals of a slightly aluminous diopside solid solution appear in some of these compositions, in addition to anorthite and a melilite (probably nearly but not exactly of akermanite composition), and that beginning of melting occurs through a range of temperatures below that of the "eutectic" composition anorthite-akermanite. Data for the limiting system albite-akermanite were obtained by Schairer and Yoder (*Year Book 63*, p. 69, Fig. 5; p. 70, Fig. 6) in their study of the joins albite-akermanite-diopside and nepheline-akermanite-albite.

Twenty-eight compositions in the join albite-anorthite-akermanite (shown as black dots in Fig. 15) were prepared and studied by the method of quenching. Fields of melilite, diopside solid solution, and plagioclase appear on the liquidus

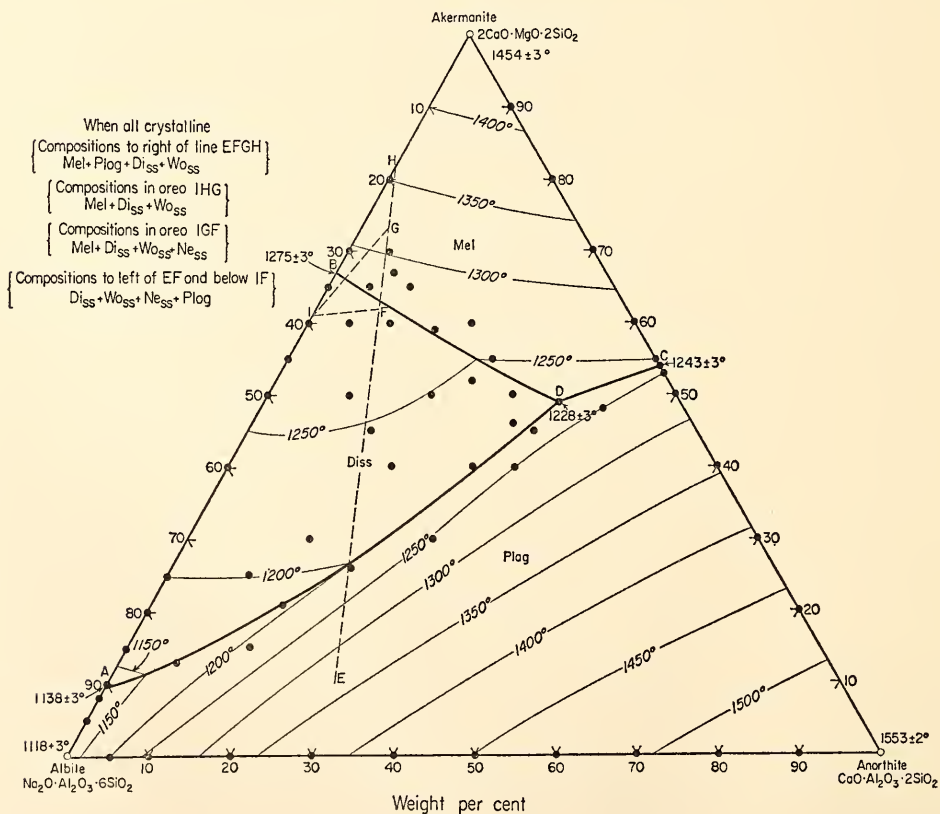


Fig. 15. Phase equilibrium diagram for the join albite-anorthite-akermanite at 1 atm.

surface. Wollastonite solid solution appears as one of the solid phases in all compositions studied at some temperature below the liquidus, and crystals of a nepheline solid solution appear at some temperature below the liquidus in all compositions to the left of the dashed line *EFG* and below the dashed line *IG* (Fig. 15). There is only one piercing point in the join, which lies at *D*, at $1228^{\circ} \pm 3^{\circ}\text{C}$, at the composition albite 15, anorthite 36, akermanite 49 wt %, where the univariant curve melilite + diopside solid solution + plagioclase + liquid pierces the join.

One significant piece of information emerges from the quenching data on the pseudoternary join: Four solid phases are in equilibrium with a liquid over a considerable range of temperature. In a quaternary system at 1 atm pressure, four solid phases with a liquid can coexist only at one temperature. The join albite-anorthite-akermanite is exhibiting quinary equilibrium. Many of the compositions studied show the presence of the four crystalline phases melilite + diopside solid solution + wollastonite solid solution + plagioclase with a liquid phase over a range of temperature as much as 75°C . Other compositions studied show the presence of the four crystalline phases diopside solid solution + wollastonite solid solution + plagioclase + nepheline solid solution with a liquid over a range of temperature as much as 25°C .

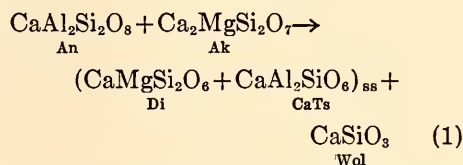
All the crystalline phases encountered in the join albite-anorthite-akermanite are complex solid solutions. The melilites are ternary solid solutions of akermanite, soda melilite, and a little gehlenite. The clinopyroxenes are aluminous diopsides. The wollastonites are solid solutions of CaSiO_3 and diopside with a possible small Al_2O_3 content. The feldspars are plagioclases. The nepheline solid solutions probably have appreciable contents of albite or anorthite, or both. The compositions of none of the solid solutions are known precisely. We were

not able to determine the compositions of the feldspars in equilibrium with melilites or with nephelines that coexist with diopsides, wollastonites, and liquids by means of the quenching method. The crystals obtained thus far are not of sufficient size to determine by means of the electron microprobe.

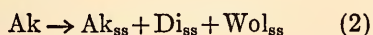
ANORTHITE-AKERMANITE AND ALBITE-SODA MELILITE REACTION RELATIONS

H. S. Yoder, Jr.

Plagioclase and melilite are stable together in some metamorphic rocks but do not coexist in alkali igneous rocks. A study of a composition containing equal proportions by weight of anorthite (An) and akermanite (Ak) yielded results that bear on the limits of compatibility of these phases. In Fig. 16 it is seen that where anorthite (An) and melilite (Mel) coexist, a clinopyroxene (Cpx) and a wollastonite solid solution (Wol_{ss}) (not identified at 1 atm) are also produced from the bulk composition $\text{An}_{50}\text{Ak}_{50}$. The reaction may be in principle:



where Di represents diopside, and CaTs, calcium Tschermak's molecule. The system anorthite-akermanite is no longer considered to be binary (*cf.* deWys and Foster, 1956; Schairer and Yoder, this report). The wollastonite no doubt contains some clinopyroxene in solid solution because the inversion of wollastonite to pseudowollastonite is not observed, wollastonite being stable some 65° to 100°C above the inversion of pure CaSiO_3 (Kushiro, *Year Book 63*, p. 84). On the other hand, the reaction may also be, at least in part:



as described by Schairer, Yoder, and

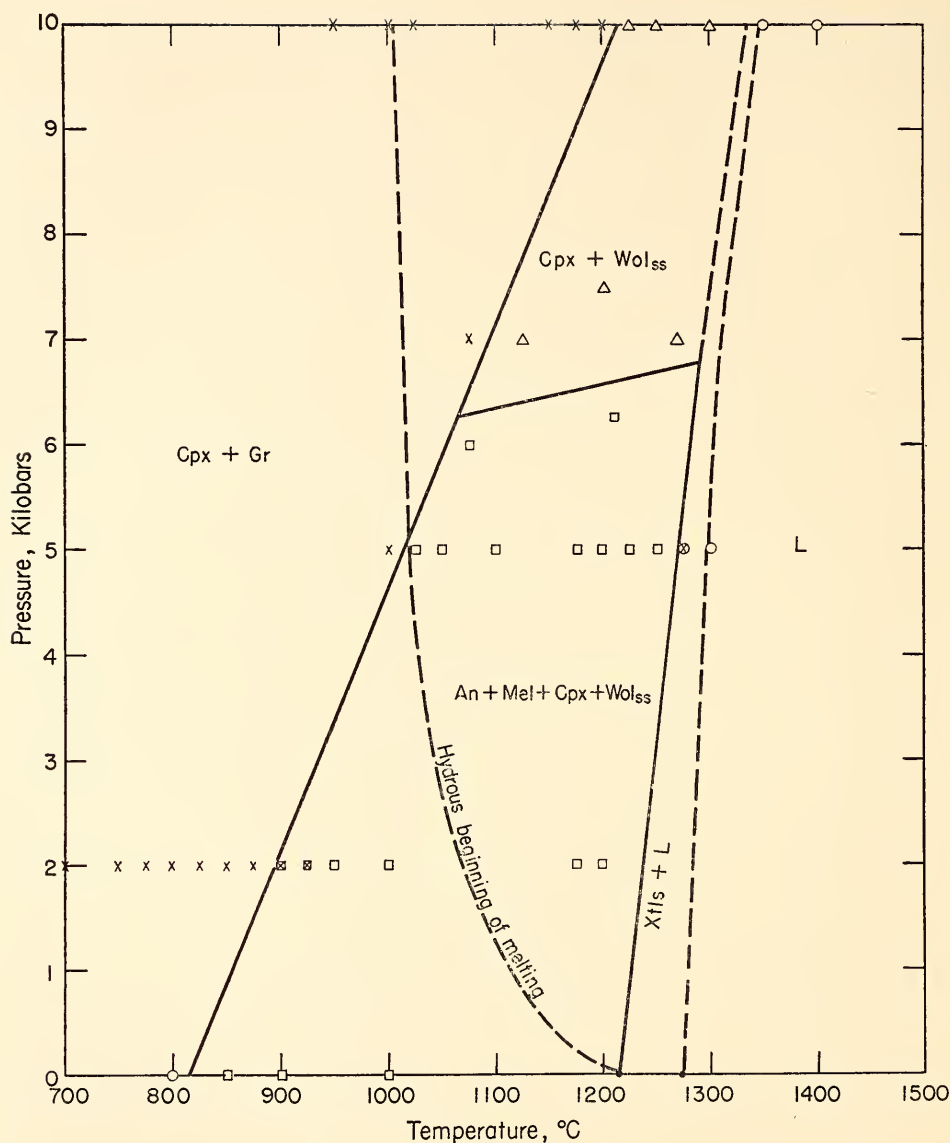


Fig. 16. Pressure-temperature diagram for the bulk composition anorthite 50 akermanite 50 by weight. Cpx, clinopyroxene; Wol_{ss}, wollastonite solid solution; An, anorthite; Mel, melilite; Gr, garnet; L, liquid; Xtls, various assemblages of some of the above-named crystalline phases. One-atm data from Schairer and Yoder (this report).

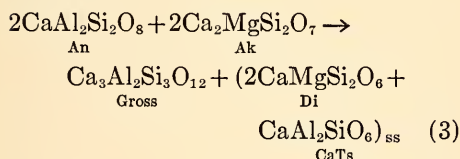
Tilley (*Year Book 65*, pp. 217-219) wherein a complex solid solution, as yet undefined, of akermanite was formed.

With increasing total pressure the relative proportions of anorthite and melilite (ss?) decrease and clinopyrox-

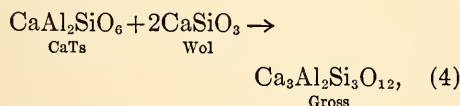
ene + wollastonite_{ss} increase, mainly by solid solution as indicated in equation 1. At about 6½ kb and higher, only clinopyroxene and wollastonite_{ss} were formed in the region outlined in Fig. 16. The clinopyroxene solid solu-

tion (1Di:1CaTs) suggested is reasonable, since calcium Tschermak's molecule itself is stable above about 12 kb (Hays, 1966) and some solid solution occurs at 1 atm, although the amount is not yet known with certainty (Hytönen and Schairer, *Year Book 60*, pp. 125–141; Clark, Schairer, and de Neufville, *Year Book 61*, pp. 59–68). Due note was made of the warning of Hytönen and Schairer (*Year Book 60*, p. 139) in regard to metastable solid solutions: reversal of reactions was obtained.

With lowering temperatures a sluggish reaction takes place, whereby the bulk composition $An_{50}Ak_{50}$ is converted to a clinopyroxene and a grossularite garnet (Gross). The reaction may be written in principle as:



Solid solution of pyrope in the garnet no doubt occurs. At least 5 wt % pyrope was found in solid solution in grossularite at 10 kb by Yoder and Chinner (*Year Book 59*, p. 79) in the grossularite-pyrope- H_2O join. The products of equation 1 are related to the products of equation 3 by reaction of a type represented by



thereby reducing the aluminous character of the clinopyroxene. Similar decrease in alumina content of pyroxene has been observed in other reactions involving the appearance of garnet (see Boyd and England, *Year Book 63*, pp. 157–161).

The upper stability limit of the garnet-bearing assemblage is close to that for pure grossularite itself (Hays, *Year Book 65*, p. 239). The high-pressure

termination of the coexistence of akermanite and anorthite is about 1 kb lower than that for forsterite and anorthite (Kushiro and Yoder, 1966; Yoder, *Year Book 65*, p. 276).

A preliminary beginning-of-melting curve under hydrous conditions is also shown in Fig. 16. Further limitation of the field of coexistence of anorthite and akermanite is evident.

These results indicate severe constraints on assemblages containing anorthite and akermanite; a broad region of coexistence still persists, however, within the pressure-temperature conditions where lavas and shallow intrusives are to be expected. Factors other than elevated pressures or presence of water appear to be necessary to account for the discrepancy between field studies of igneous rocks and laboratory observations. The present results are, however, in accord with the observation of melilite and plagioclase in metamorphic aureoles.

Oxidizing conditions may tend to increase the clinopyroxene + garnet field at the expense of plagioclase and melilite. Recently, Huckenholz, Schairer, and Yoder (*Year Book 66*, pp. 335–346) showed that an andradite garnet and a diopside saturated with a ferri-Tschermak's molecule were stable up to 1157°C, almost up to the beginning of melting. Presence of titanium would also increase the stability field of a clinopyroxene (titanaugite) and garnet (melanite) association (see Huckenholz, this report). Both ferric iron and titanium are enriched in alkali igneous rocks relative to other major magma series. Addition of albite to the system initially enlarges the field of coexistence of plagioclase and melilite, then diminishes the field as illustrated in Fig. 14 (Yoder and Schairer, this report).

Preliminary experiments on the reaction relations of albite-soda melilite, soda analogues of anorthite-akermanite, indicate that at pressures below about 6.5 kb the assemblage nepheline + wol-

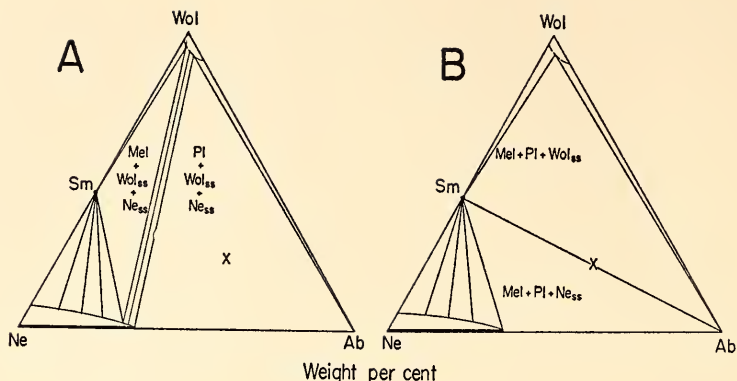


Fig. 17. Schematic representation of the assemblages immediately below (A) and above (B) about 6.5 kb for the system nepheline (Ne)-wollastonite (Wol)-albite (Ab). The 1-atm assemblage is nepheline solid solution + wollastonite + plagioclase according to Foster (1942) at the piercing point of the system.

lastonite + plagioclase is stable. Above that pressure melilite + plagioclase are the stable phases. The relationships are illustrated schematically in Fig. 17; the solid solutions are complex and cannot be adequately defined. These experiments lead to the conclusion that the nepheline-wollastonite-diopside plane in the expanded basalt tetrahedron of Schairer and Yoder (*Year Book* 63, p. 65), which prohibits the coexistence of albite and akermanite, may be penetrated by a family of joins connecting albite with soda-rich melilites. The prohibition of the coexistence of an akermanite-rich melilite and albite remains.

The data now at hand do not yield a satisfactory solution to the melilite-plagioclase dilemma of the alkali igneous rocks.

EXPERIMENTS BEARING ON THE ORIGIN OF ANORTHOSITIC INTRUSIONS

R. F. Emslie and D. H. Lindsley*

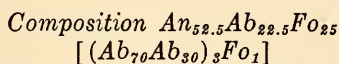
We report here the results of some experiments on natural and synthetic systems that have a bearing on the origin of anorthosites. Although the high content of intermediate plagioclase in batholithic anorthosites is explainable

in part by plagioclase accumulation, the conclusion that the parent liquid was enriched in the components of intermediate plagioclase seems inescapable. Consequently, our experiments were directed toward investigating suitable mechanisms by which such enrichment might be accomplished. We reported last year (*Year Book* 66, pp. 497-480) work that led us to believe that the system albite-anorthite-diopside could not provide an adequate model for the generation of anorthositic magmas at crustal pressures. This year we have focused attention on compositions in the system albite-anorthite-forsterite at pressures up to 20 kb. We have also examined the P - T relations of a sample of the "chilled margin" of the Michikamau intrusion, a large unmetamorphosed body in Labrador with characteristics intermediate between typical anorthosite complexes and stratiform mafic intrusions (Emslie, 1965, 1968). The rock assemblage of the Michikamau intrusion strongly suggests that basaltic magma played a dominant role in its development. Recent strontium and oxygen isotopic evidence (Epstein and Taylor, 1967; Heath, 1966) from widespread anorthositic intrusions also supports arguments relating them to basaltic

* Geological Survey of Canada.

magma. The approach adopted, therefore, is to examine conditions under which basaltic liquids, or their derivatives, might be induced to crystallize large volumes of intermediate plagioclase. In effect, this reduces to finding processes by which the alumina content and the Na/Ca ratio of basaltic liquids may be increased simultaneously.

Experiments at pressures between 5 and 20 kb were done in a solid-media, piston-and-cylinder apparatus under dry conditions.



The composition $\text{An}_{52.5}\text{Ab}_{22.5}\text{Fo}_{25}$ (mole ratio) lies in the plagioclase field at

1 atm (Fig. 18, inset). It was chosen to illustrate boundary-curve shifts and reactions between forsterite and plagioclase with increasing pressure. Starting materials included forsterite plus plagioclase crystals, glass, and a high-pressure assemblage synthesized at 20 kb that contained clinopyroxene, plagioclase, spinel, and some forsterite (presumably residual). All runs were made in platinum capsules.

With increasing pressure, plagioclase is replaced by spinel as the liquidus phase, demonstrating that the spinel field is enlarged by application of pressure (Fig. 18). Up to about 19 kb, plagioclase joins spinel with decreasing temperature, but at higher pressure

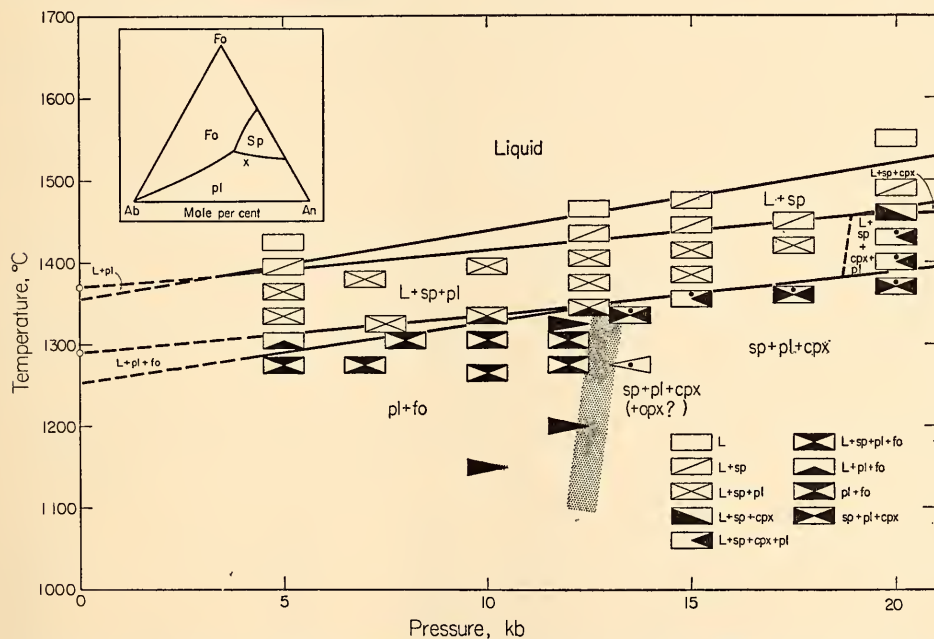


Fig. 18. *P-T* diagram for the composition $\text{An}_{52.5}\text{Ab}_{22.5}\text{Fo}_{25}$ (mole %). Inset at upper left is the liquidus diagram at 1 atm for the system forsterite-albite-anorthite (converted to mole percentage from *Yearbook Book 65*, p. 206) with the composition $\text{An}_{52.5}\text{Ab}_{22.5}\text{Fo}_{25}$ indicated by an X. One-atmosphere temperatures plotted in the figure are from the same source. Triangular symbols indicate that the starting material was a high-pressure assemblage containing cpx, pl, sp, and fo. Solid triangles indicate that fo grew and cpx and sp decreased. Open triangle indicates that cpx and sp grew and fo decreased. Symbols containing a solid circle are runs in which fo was present as residual phase; with repeated grinding and rerunning the fo decreased in amount and cpx and sp increased. L, liquid; sp, spinel; pl, plagioclase; cpx, clinopyroxene; opx, orthopyroxene; fo, forsterite; ab, albite; an, anorthite.

spinel is followed first by clinopyroxene and then plagioclase. Liquid + forsterite + plagioclase is stable up to a maximum pressure of about 13 kb. At subsolidus temperatures the reaction forsterite + plagioclase \rightleftharpoons spinel + plagioclase + clinopyroxene (+orthopyroxene?) is indicated as a stippled zone of some finite but unknown width. Because plagioclase and the pyroxene are solid solutions, the reaction must proceed over a P - T range. The presence of orthopyroxene on the high-pressure side of the stippled zone is suspected but not verified. At higher pressures orthopyroxene is believed to disappear by entry into solid solution in the clinopyroxene.

Fractional crystallization of spinel at high pressures is capable of driving the liquid to more plagioclase-rich compositions and presumably to compositions richer in albite relative to anorthite because spinel removes alumina and enriches the liquid in silica. Addition of silica to the starting composition to produce normative pyroxene would drastically decrease the size of the liquid + spinel field, however, and it is unlikely that natural basic magmas can precipitate sufficient amounts of spinel to make this an effective mechanism in the production of anorthositic liquids.

Some experiments were performed on the composition $An_{37.5}Ab_{37.5}Fo_{25}$ [$(An_{50}Ab_{50})_3Fo_1$]. Plagioclase is the first phase to occur at the liquidus up to about 11 kb, but at higher pressures spinel again takes its place. It is clear, however, that if spinel crystallization were suppressed by a slightly more silica-rich starting composition, clinopyroxene would be present at the liquidus at pressures at least as low as 15 kb. We are presently determining the Al_2O_3 contents of the high-pressure clinopyroxene. At present we assume that the Al_2O_3 contents are less than those in the co-existing liquids. Fractional crystallization of such clinopyroxene should be capable of increasing both the alumina

content of the liquid and its Na/Ca ratio.

The stippled subsolidus reaction boundary in Fig. 18 may be compared to curve *A* of Kushiro and Yoder (*Year Book 64*, Fig. 14) for the composition forsterite 1: anorthite 1 (mole). The comparison illustrates that addition of albite stabilizes the assemblage forsterite + plagioclase to higher pressure. Presumably troctolites, especially those with magnesian olivine, are stable throughout most or all of the continental crust. This conclusion is of importance in assessing the maximum depth of crystallization of some of the largest anorthositic plutons with olivine-plagioclase assemblages in Quebec and Labrador.

Michikamau Chilled Margin

A recently obtained sample of very fine-grained rock taken a few inches from the contact of the Michikamau intrusion is interpreted as approximating a liquid composition that was chilled against the wall at the time of emplacement. An analysis and norm of the rock (EC66-21A5) are given in Table 3. Field evidence suggests that the bulk magma (liquid + crystals) was probably considerably richer in plagioclase than this sample (Emslie, 1965, 1968). The

TABLE 3. Chemical Analysis and Norm of Michikamau Chilled Margin EC66-21A5

Analysis		Norm	
SiO ₂	47.56	Qz	...
Al ₂ O ₃	18.33	Or	0.56
Fe ₂ O ₃	0.30	Ab	10.49
FeO	11.66	An	44.24
MgO	6.40	Di	10.44
CaO	12.07	Hy	29.11
MnO	0.21	Ol	0.86
K ₂ O	0.08	Il	2.28
Na ₂ O	1.25	Mt	0.46
P ₂ O ₅	0.28	Ap	0.66
TiO ₂	1.24	Ct	0.40
H ₂ O	0.09	Remainder	0.18
H ₂ O	0.09		
CO ₂	0.16	Total	99.68
Total	99.72		

Note: Analyst, J. L. Bouvier.

sample is clearly aluminous and could be described as a basalt with a high alumina content, as might be expected from its association with a plagioclase-rich rock assemblage. Assuming that the liquid was derived from the mantle, it is of interest to examine its phase relations under conditions similar to those at which it formed or to which it was subjected during its rise into the crust.

Finely ground rock powder from the chilled margin and a glass prepared from it were used as starting materials. Most of the high-pressure experiments were run in platinum capsules. It is well known that iron-bearing silicates and liquids tend to lose iron to platinum containers.

We evaluated the approximate extent of the iron loss by microprobe analysis of duplicate samples and their platinum capsules: for a sample of the Michikamau chilled margin run for $\frac{1}{2}$ hour

at 1340°C and 10 kb (well within the liquid field) the Fe loss is 3–5% of the amount present, or about 0.4–0.6 wt % FeO. The loss of iron to the capsule results in the release of oxygen, and thus the FeO/Fe₂O₃ ratio, as well as the total iron content is lowered. Our results must be interpreted with these facts in mind; we believe, however, that though the iron loss affects the details of our diagrams, it does not modify the general conclusions drawn from them.

The experimental results are shown in Fig. 19. Plagioclase is the first crystalline phase to appear on cooling at pressures up to 12 kb. From 12 kb to about 16.5 kb clinopyroxene is the primary phase, and at higher pressures garnet crystallizes first. With decreasing temperatures these phases are joined by pyroxene(s) or plagioclase, or both.

Early plagioclase crystallization rapidly depletes the alumina content of the liquid, and it is clear that at pressures

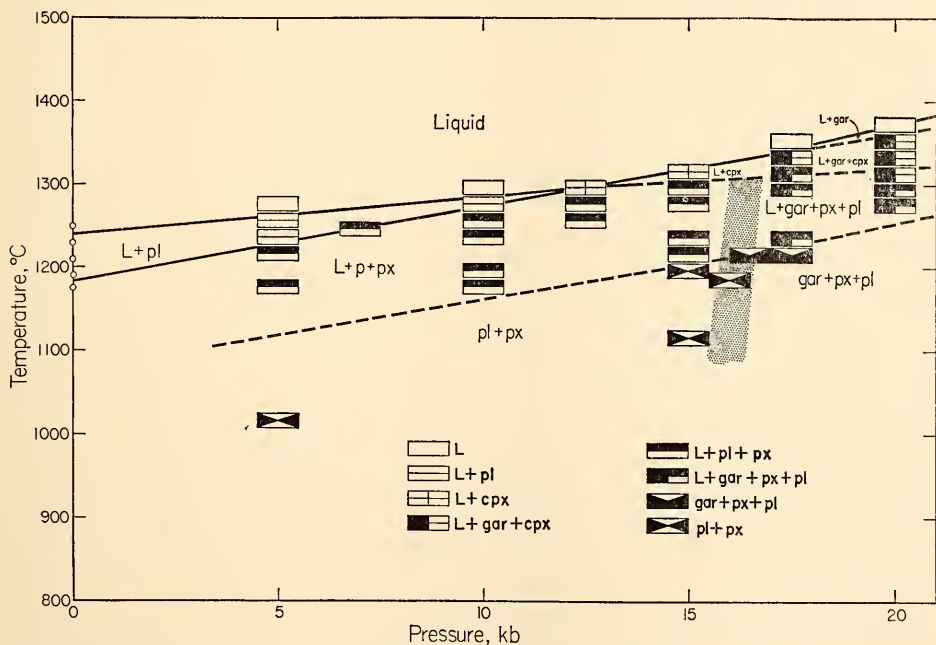


Fig. 19. *P-T* diagram for the Michikamau chilled margin EC66-21A5. One-atmosphere runs were made in evacuated silica tubes through the courtesy of J. F. Schairer. L, liquid; pl, plagioclase; cpx, clinopyroxene; gar, garnet; px, clinopyroxene + orthopyroxene.

below 12 kb fractional crystallization cannot enrich the liquid in alumina. At higher pressures, fractional crystallization of clinopyroxene should be capable of enriching the liquid in alumina and soda. Selective removal of garnet at still higher pressures, on the other hand, may be expected to cause alumina depletion of the liquid. At pressures at least up to 20 kb, however, garnet is closely followed by clinopyroxene with decreasing temperature, and it is probable that fractional crystallization of garnet+clinopyroxene could lead to enrichment of the liquid in components of intermediate plagioclase so long as the ratio of garnet to clinopyroxene is not high. The extent of this enrichment depends, of course, on the extent of the garnet+clinopyroxene phase volume and on the composition of the clinopyroxene.

Of the crystalline phases that occur at and near liquidus temperatures in basaltic magmas at moderate to high pressures, clinopyroxene appears most likely to play an important role in crystal fractionation processes capable of producing anorthositic liquids. There is probably a pressure range—say 10–15 kb—at which clinopyroxene is enriched in Ca-Tschermak's molecule relative to jadeite; its removal would enrich the liquid in albite relative to anorthite, as well as enriching it in alumina, because the pyroxene is lower in Al_2O_3 than the liquid. Such clinopyroxene coexists with liquid or with garnet and liquid only at pressures expected near and below the base of the continental crust. Maximum pressures under which suitable fractionation could occur are limited by (1) the increasing amount of garnet that crystallizes early and (2) breakdown of the albite component of plagioclase, which also goes into solid solution (as jadeite) in clinopyroxene. An estimate of the upper pressure limit under which fractional crystallization of clinopyroxene or garnet plus clinopyroxene from basaltic liquids can lead to anorthositic compositions is approximately 20 kb, de-

pending on compositions (see also Green, 1966, p. 220).

SYENITES

S. A. Morse

Syenites and their extrusive equivalents trachytes appear to occupy a paradoxical position among igneous rocks. On the one hand, their small volume in the crust and frequent well-defined association with logically parental magma series render their derivation by fractionation from basalt quite credible, and in some cases the parent-daughter relationship is clearly demonstrable. On the other hand, syenites and trachytes are critically undersaturated rocks in the sense of Yoder and Tilley (*Year Book* 59, p. 68) and lie in projection on a critical undersaturation line (the alkali feldspar join) in petrogeny's residua system (Schairer, 1950). From all apparent evidence, these residual liquids lie on a thermal maximum relative to their neighbors, granite (or rhyolite) and nepheline syenite (or phonolite). What mechanism can cause a magma to remain critically saturated throughout its fractionation history and terminate on a thermal maximum instead of fractionating off toward either oversaturated or undersaturated compositions? The question is fundamental, not only because of the economic importance of syenites, which often contain unusual abundances of valuable metals and rare-earth elements, but also because one or more basic concepts of magmatic fractionation have apparently escaped our notice.

Initial investigations during the past year have helped to define the problem and narrow the working hypotheses to a manageable number. Aside from a characterization of the natural occurrences, a reinvestigation has been made of the alkali feldspar-water system at 5 kb, discussed elsewhere in this report, and the syenite-nepheline syenite portion of petrogeny's residua system has been

investigated at 5 kb water pressure. Studies in the system diopside-albite-orthoclase have been begun at 1 atmosphere and at 5 kb water pressure.

Characterization of Syenites

Syenites are rocks dominated by lime-poor feldspar and contain little or no quartz or feldspathoid; by addition of these minerals they grade into quartz syenite or nepheline syenite, respectively. In its simplest form, the mafic mineralogy is essentially that of basalts: augite, olivine, and Fe-Ti oxide, although of course the first two are richer in ferrous iron than those in basalts. Numerous natural examples support this characterization of syenite, among them the layered intrusions of Labrador (Kiglapait, Michikamau) and southwest Greenland (e.g., Kûngnât). Trachytes occur in which members of the augite-ferroaugite series, olivine, and Fe-Ti oxide are the dominant mafics, although partially resorbed biotite phenocrysts are usually present as well.

The Labrador and Greenland syenites, and many trachytic suites, show a single hypersolvus feldspar of the plagioclase-anorthoclase series dominating the fractionation path. A second, K-rich feldspar may appear in the very late stages, but attainment of the two-feldspar boundary would not appear to be critical to syenitic fractionation.

In the plutonic examples just mentioned, the assemblage fayalite+magnetite+alkali feldspar is common, and the oxygen fugacity defined by this assemblage is presumably very close to that defined by fayalite+magnetite+quartz (FMQ). The oxygen fugacity of the magmas during fractionation is probably well modeled by the FMQ buffer curve (Morse and Stoiber, 1966).

In summary, it appears that a reasonable model for the fractionation trend from basaltic to syenitic liquids can be generated by consideration of the four solid solution series, feldspar, augite,

olivine, and magnetite, crystallizing under conditions of oxidation corresponding to the FMQ buffer. Hydrous, peralkaline, and peraluminous syenites may be treated as special cases requiring further explanation.

Syenitic Trends

Within the syenitic kindred there exist fractionation trends toward both oversaturation and undersaturation with silica; examples of these can be found with any of the following mafic mineralogies: olivine+sodic pyroxene, olivine+ferroaugite, ferroaugite alone, and sodic pyroxene alone, all with Fe-Ti oxides. The existence of such trends and their apparent indifference to mafic mineralogy suggest their origin by fractionation of feldspar, a process that is evidently ineffectual early in the fractionation history.

Most hydrous syenites (those containing amphibole or biotite) in the Greenland-Labrador province have silica-oversaturated trends, which may be accounted for by oxidation of normative olivine during fractionation due to elevated P_{H_2O} . Fractionation of amphibole or biotite itself could also have the effect of silica enrichment.

Projection of the normative salic components of chemical analyses into petrogeny's residual system (nepheline-kalsilite-silica) has often served to illustrate the correspondence between rock compositions and experimentally determined melting minima, as for example with granites (Tuttle and Bowen, 1958; Luth, Jahns, and Tuttle, 1964) and nepheline syenites (Hamilton and MacKenzie, 1965). As the plots of the latter authors show, however, the example fails with syenites, a fact that should prove to be very instructive. The relationships of 81 modern analyses of syenitic rocks from the Gardar province of Greenland (Watt, 1966) are summarized in Fig. 20, which shows a strong maximum on the feldspar join at Or_{40} , with subsidiary

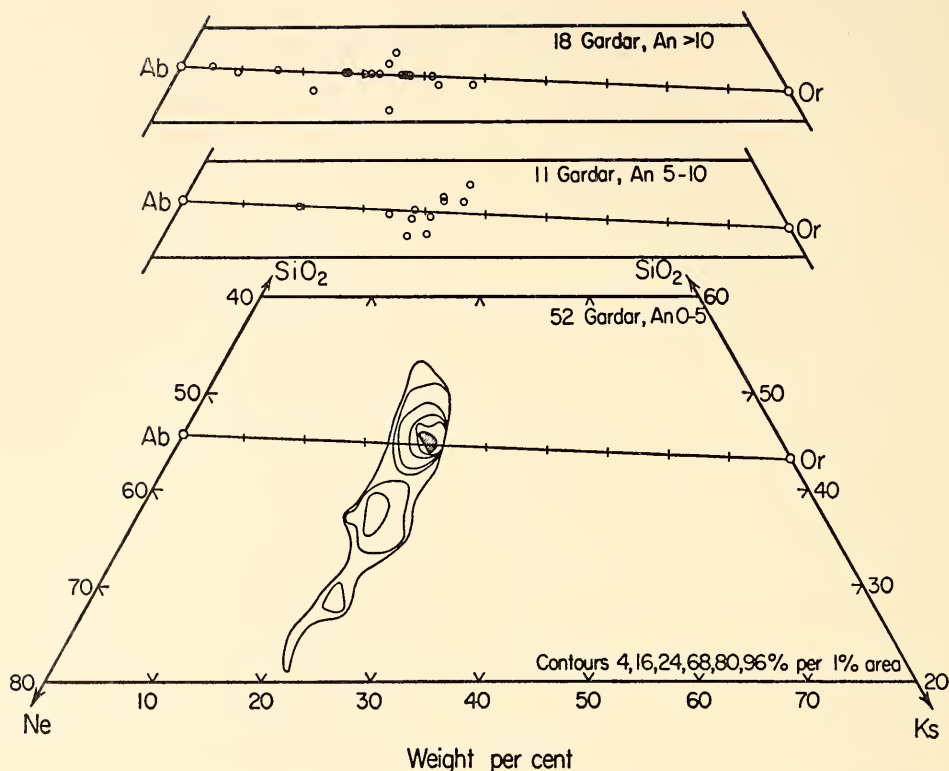


Fig. 20. The salic components of 81 natural syenites from the Gardar province, Greenland (Watt, 1966), projected from An onto the system Ne-Ks-Sil. The diagrams, classified from top to bottom by decreasing anorthite content, illustrate the trend of syenites in the ternary feldspar plane toward the maximum near Or_{40} and then away from the feldspar join in the low-Ca residua system (bottom).

trends toward granite and nepheline syenite. By contrast, the minimum or eutectic in the pure feldspar join, as determined experimentally, varies from near Or_{35} at 1 bar to less than Or_{30} at 5 kb P_{H_2O} . These natural syenites, therefore, are not well modeled by alkali feldspar alone, as should also be apparent from their far from modest mafic and anorthite content.

Anorthite in the feldspar should cause a shift toward Or in projection, judging from the trend of the two-feldspar boundary in the ternary feldspar system (e.g., Yoder, Stewart, and Smith, *Year Book 56*, pp. 206-214). Addition of anorthite alone should not generate a strong maximum when projected onto

the alkali feldspar join but rather a continuum of syenite compositions along the join. Moreover, for reasons stated above, the two-feldspar boundary seems of little importance except in the last stages of syenitic differentiation. The persistent syenitic maximum near Or_{40} suggests a crystal \rightleftharpoons liquid control, and this is probably generated by the confluence of the boundary surfaces of plagioclase, ferroaugite, fayalitic olivine, Fe-Ti oxide, and liquid. Although the calcic pyroxene might be expected to be dominant in this respect because of its stabilization of Ca-bearing plagioclase in place of pure albite (Schairer and Yoder, 1960), preliminary experiments in the system diopside-albite-orthoclase

(see below) suggest movement of the trace of the feldspar minimum in the right direction but somewhat short of the required magnitude.

There are thus at least two parts to the syenite problem: first, the maintenance of critical undersaturation during fractionation, and second, the generation of liquids that project toward Or from the alkali feldspar minimum. The two may not be unrelated.

Experimental Evidence

The most obvious question that might be asked about syenitic liquids is whether or not they do indeed occupy a thermal maximum relative to granite and nepheline syenite. A qualified answer to this question is given by current experimental work in petrogeny's residua system at 5 kb P_{H_2O} .

Nepheline-kalsilite-silica at 5 kb P_{H_2O} . The silica-oversaturated portion of this system has been reported in detail by Luth, Jahns, and Tuttle (1964). The alkali feldspar-water join at 5 kb was studied by Yoder, Stewart, and Smith (*Year Book 56*, pp. 206-214) and re-studied by Morse during the past year (discussed elsewhere in this report). The silica-undersaturated portion has been studied at 1 kb P_{H_2O} by Hamilton and MacKenzie (1965), and portions of the bounding system Ab-Ne- H_2O involving analcite were studied by Peters, Luth, and Tuttle (1966). Part of the interest in the 5-kb isobaric section reported here lies in the determination of the alkali feldspar solvus for undersaturated compositions, and part of it lies in the appearance of analcite and the assemblage analcite-K feldspar at subsolidus temperatures.

The liquidus diagram for the residua system at 5 kb P_{H_2O} as presently known is shown in Fig. 21. The region involving leucite was not investigated in this study. The beginning of melting of nepheline-syenitic compositions occurs at $635^\circ \pm 3^\circ\text{C}$ at an isobaric eutectic projecting

very near the 1-kb minimum and the 1-atm reaction point, as sketched in Fig. 22. This implies that fractionation at almost any geologically reasonable water pressure and, less certainly, most reasonable total pressures under water-undersaturated conditions should lead to nepheline syenites of limited compositional variation, as appears to be true in nature (Hamilton and MacKenzie, 1965, Fig. 4).

A series of isobaric, isothermal sections, shown in Figs. 23-27, illustrates the equilibria encountered by a nepheline-syenitic liquid in its crystallization and subsolidus history. The tie lines in the 665°C section are not schematic but are determined by X-ray methods for feldspar and by electron-probe analysis of nepheline. The probe analyses show the amount of silica dissolved in nepheline at this pressure to be measurable, although appreciably less than found at lower pressures (Hamilton and MacKenzie, 1960, p. 61), as expected. The analyzed series lies within experimental error on a straight line from $\text{SiO}_2=2.6\%$ on the Ne- SiO_2 join to $\text{Ks}=40\%$ on the Ne-Ks join. There is no evidence for a two-feldspathoid region.

It is to be noted that the liquid field extends to the Ne-Ab sideline at 665°C ; the assemblage $\text{Ne}_{ss}\text{-Ab}_{ss}$ does not appear. On further cooling from 665°C , the liquid field shrinks away from the Ne-Ab sideline, but as it does so, the assemblage analcite-liquid becomes stable, again preventing the assemblage $\text{Ns}_{ss}+\text{Ab}_{ss}$, as shown in the 640°C isothermal section. At some temperature lower than 640°C but greater than 635°C , the assemblage $\text{Ab}+L$ must become unstable through the reaction $\text{Ab}+L=\text{Anl}+\text{Kf}$ (K feldspar) + G , since the beginning of melting occurs at a eutectic within the $\text{Anl}+\text{Kf}+\text{Ne}$ field, which dominates much of the diagram at subsolidus temperatures (see the 600°C isothermal, isobaric section, Fig. 25). This necessitates a narrow field of anal-

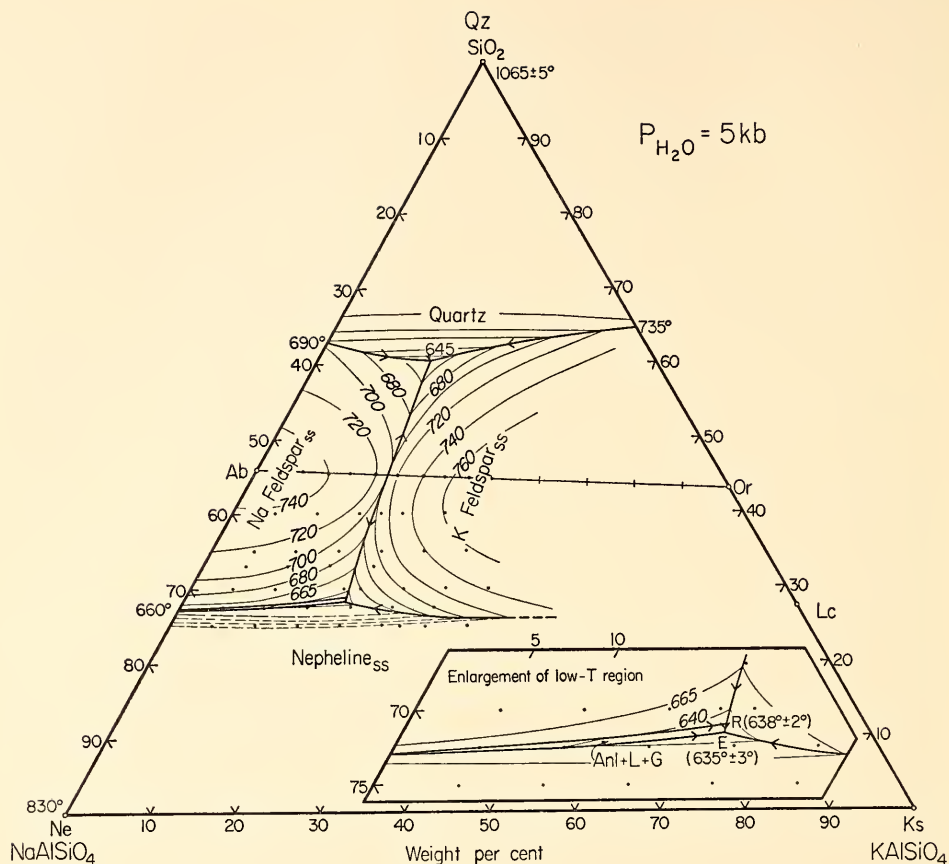


Fig. 21. Liquidus diagram of petrogeny's residua system at 5 kb P_{H_2O} , omitting relationships involving leucite. The granite portion is replotted from Luth, Jahns, and Tuttle (1964), and data on Ne-Ab- H_2O are incorporated from Peters, Luth, and Tuttle (1966). Points show compositions studied in this work.

cite on the liquidus diagram and a reaction point R where the two-feldspar+liquid boundary curve meets the $Anl+Ab+L$ boundary curve (see inset in Fig. 21). On cooling below R , liquids produce analcite and K feldspar, until the eutectic is reached, at which point nepheline joins the assemblage and crystallization is completed isothermally.

It is noteworthy that the commonly observed assemblage $Ne_{ss}+Ab_{ss}$ has no field of stability at 5 kb P_{H_2O} ; therefore rocks that show this assemblage must have formed under some lower water pressure. The termination of the $Ne_{ss}+$

Ab_{ss} stability field in the hydrous system occurs at a quaternary invariant point involving $Ab+Kf+Ne+Anl+L+G$ at some pressure not far below 5 kb and a temperature not far above 535°C. Data are as yet insufficient to permit accurate delineation of the univariant curves around this invariant point, but experiments between 2 and 10 kb are underway for this purpose.

From the data incorporated in Fig. 21, a profile can be drawn along the two-feldspar+liquid boundary curve from the granite eutectic through the feldspar join and to the nepheline syenite eutectic.

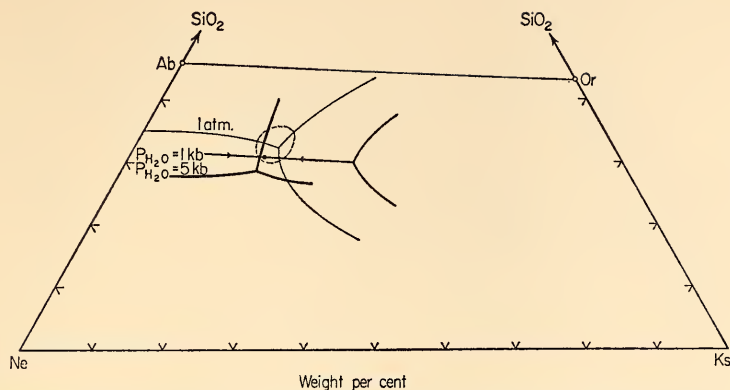


Fig. 22. Positions of nepheline syenite minima in petrogeny's residua system at 1 atm and 1 and 5 kb P_{H_2O} . The 1-atm boundaries are from Schairer (1950); the 1-kb boundaries are from Hamilton and MacKenzie (1965); and the 5-kb boundaries are from the present study. The 1-atm minimum lies very near the leucite reaction point. The dashed circle is the contour around the statistical maximum of nepheline syenite analyses from Hamilton and MacKenzie (1965).

This profile, projected parallel to lines of equal silica content onto the line $Ne/Ks=1$, is shown in Fig. 26, along with comparable projections at lower and higher pressures. The profiles at 1 atm and 1 kb P_{H_2O} are those of the minimum liquidus temperatures on the

feldspar+liquid boundary surface. The profile at 10 kb in the nepheline syenite portion is supported by a few reconnaissance experiments made during the current study. It is clear from these profiles that haplosyenites represented by petrogeny's residua system do indeed lie

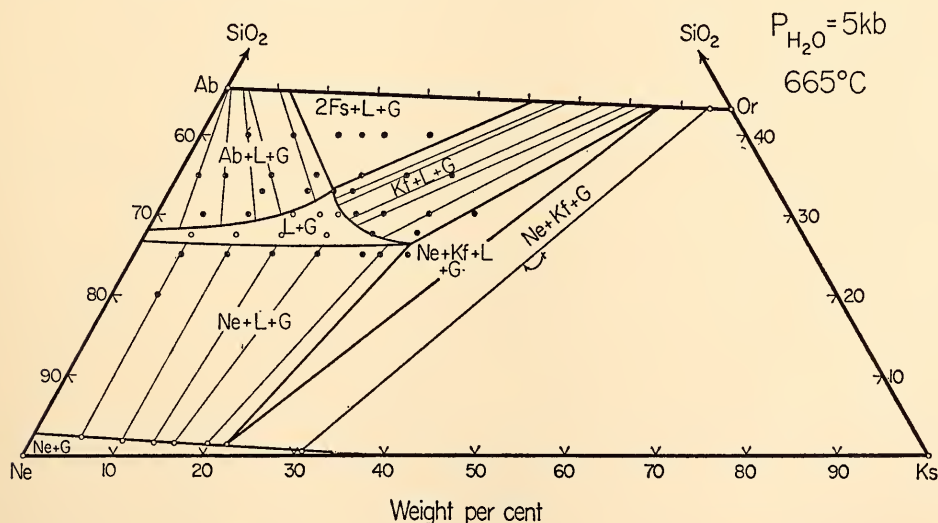


Fig. 23. Isothermal, isobaric section, at 665°C and 5 kb, of the nepheline syenite region of $Ne-Ks-SiO_2-H_2O$. The tie lines are not schematic but determined directly by X-ray composition of feldspars (except Or_{65}) and electron-probe analyses of nephelines and the most potassic feldspar. Fs, feldspar; Kf, K feldspar.

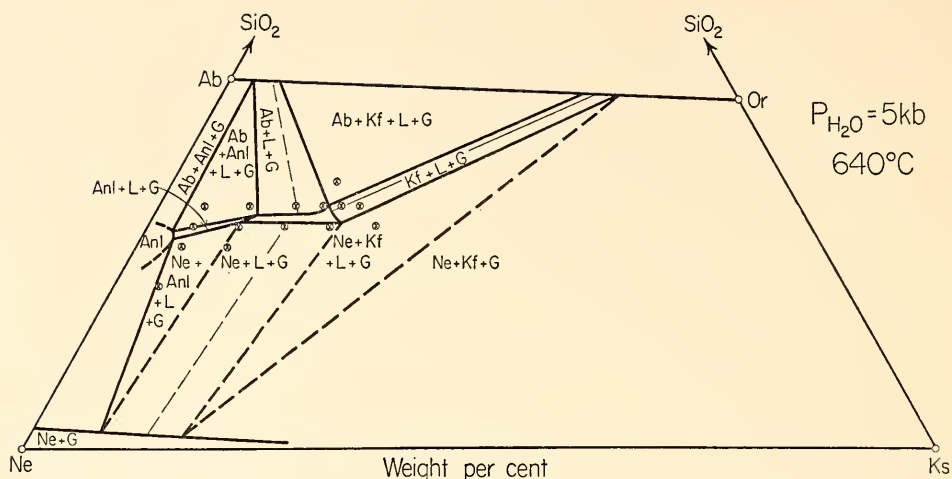


Fig. 24. Section at 640°C, 5 kb. Most of the tie lines are schematic (dashed). The section depicts the narrow field of analcite + *L* + *G* that prohibits the assemblage Ne + Ab at this pressure. Kf, K feldspar.

on a maximum relative to nepheline syenite and granite throughout the range of geologically reasonable water pressures, as well as at 1 atm. Water pressure has a more severe effect on the beginning of melting of nepheline syenite

than on that of granite, but there is no reason to believe that a water-under-saturated condition would raise the melting minimum of either of these above that of syenite. It seems clear that the syenite problem cannot be resolved

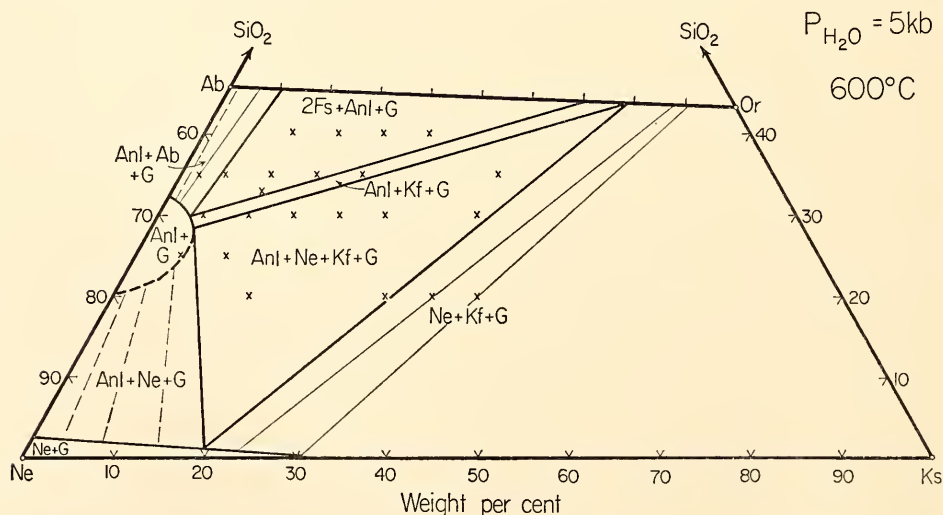


Fig. 25. Section at 600°C, 5 kb. Tie lines are schematic where dashed. The extent of the analcite field on Ne-Ab is taken from Peters, Luth, and Tuttle (1966). This essential configuration persists up to the beginning of melting at $635^\circ \pm 3^\circ\text{C}$, which takes place within the Anl + Ne + Kf + *G* field. Between 635° and 640°C the Anl + Kf tie line is broken by Ab + *L*; Ne + Ab never occurs at 5 kbs. Fs, feldspar; Kf, K feldspar.

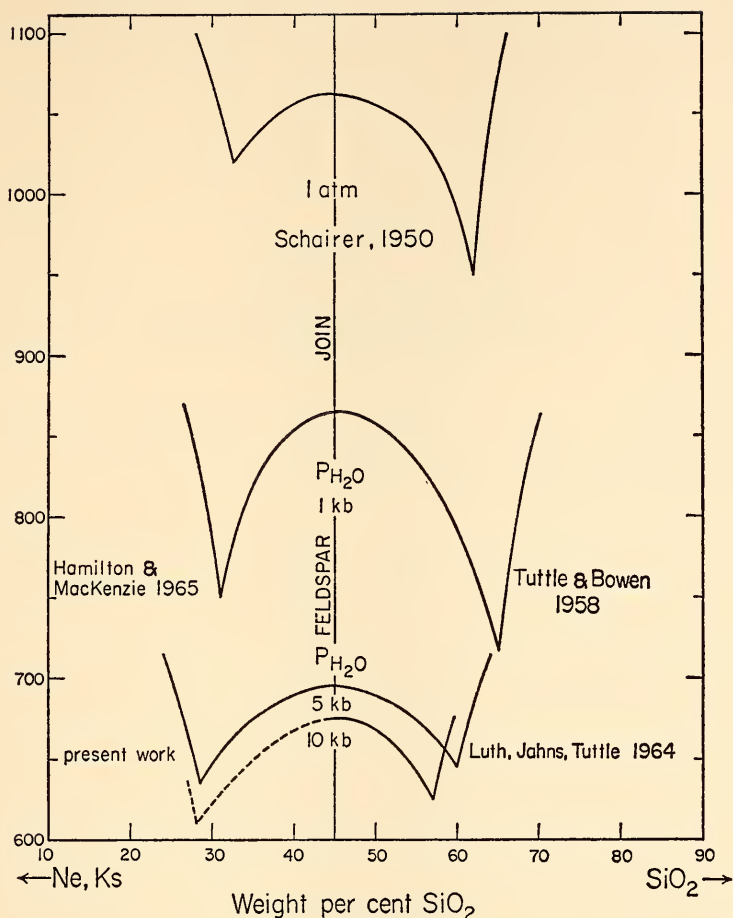


Fig. 26. Profiles along minima in petrogeny's residua system, projected parallel to lines of equal SiO_2 content onto the line $\text{Ne/Ks} = 1$. Syenites (on the feldspar join) always appear to lie on maxima relative to nepheline syenites and granites.

without consideration of the mafic components.

Diopside-albite-orthoclase at atmospheric pressure and at 5 kb $P_{\text{H}_2\text{O}}$. The addition of diopside to the alkali feldspars is a logical first step in assessing the effect of mafic components on syenites, since thereby calcium is automatically introduced to the feldspar (the plagioclase effect of Bowen, 1945). On the other hand, the exchange of Ca and Al between feldspar and diopside renders this a nonternary join in a higher-order system, and so it is difficult to treat.

The join forms a basis, however, for eventual studies including FeO , which may be expected to exert a feedback effect by consumption of excess silica to form olivine.

Glasses in Di-Ab-Or were prepared with J. F. Schairer, who also carried out the 1-atm experiments. The compositions chosen for study so far are shown in Fig. 27. On the basis of preliminary work, it can be reported that the maximum observed by Schairer and Yoder (1960) on the Di-Ab join persists well into the "syenitic" region of the Di-

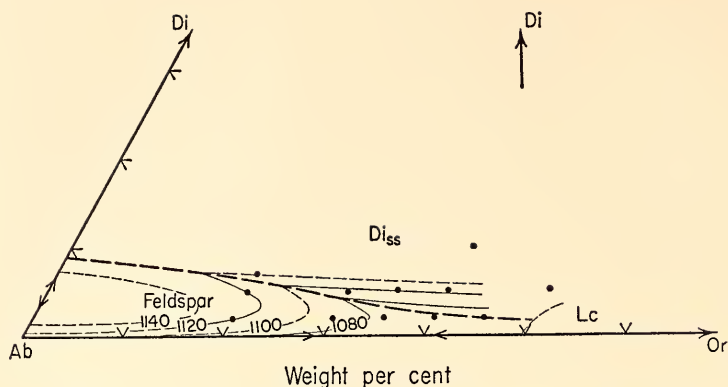


Fig. 27. A portion of the join Di-Ab-Or, showing compositions selected for study, a preliminary field boundary, and isotherms. Data are incorporated for Di-Ab from Schairer and Yoder (1960) and for Ab-Or from Schairer (1950).

Ab-Or plane. The beginning of melting at 1 atm is not far from 1020°C, which is about the temperature of the nepheline syenite minimum at 1 atm and about 40° below the alkali feldspar minimum at 1 atm. This does not reverse the thermal relations between nepheline syenite and syenite, since a comparable lowering of the beginning of melting is to be expected with addition of diopside to nepheline-syenite mixtures. The beginning of melting at 5 kb P_{H_2O} lies above 650°C, still well above the $635^\circ \pm 3^\circ\text{C}$ nepheline syenite eutectic in the residua system.

FELDSPARS

S. A. Morse

Alkali Feldspar-Water at 5 kb

The solvus in the alkali feldspar system ($\text{NaAlSi}_3\text{O}_8$ - KAlSi_3O_8) is of potential importance in unraveling the P - T history of many rocks and forms the basis of our understanding of the even more complex and useful ternary feldspar solvus. Repeated investigations at elevated water pressures (such as those of Bowen and Tuttle, 1950; Orville, *Year Book 58*, pp. 118-121; Yoder, Stewart, and Smith, *Year Book 56*, pp. 206-214; and Luth and Tuttle, 1966) have given somewhat diverse results.

In the present study the liquidus was determined with 3-day runs to ensure nucleation. Repeated runs were made at 5° intervals over much of the critical region from Ab to Or_{40} (wt %). The shape of the liquidus bears on whether the beginning of melting occurs at an isobaric minimum or a eutectic, which in turn bears on whether the solvus straddles that composition (in projection) which has no melting interval. Substantial melting intervals were found (Fig. 28) for all compositions studied, and the liquidus slopes imply a eutectic rather than a minimum, as found by Yoder, Stewart, and Smith (*Year Book 56*, p. 208, Fig. 38). The eutectic falls at $\text{Or}_{28.5 \pm 0.5}$.

During runs of 3 days or even longer, equilibrium is not achieved within the crystal+liquid+gas loops. The composition of feldspar, as determined by the 20I spacing, is sensitive to the bulk composition at a given temperature, being near the correct solidus composition only for the bulk composition nearest the solidus, and progressively nearer the liquid composition as the bulk composition approaches that of the liquidus. The ratio of crystals to liquid is simultaneously deranged, and the lever rule cannot be used reliably. Knowledge of this effect is important in interpretation of solvus

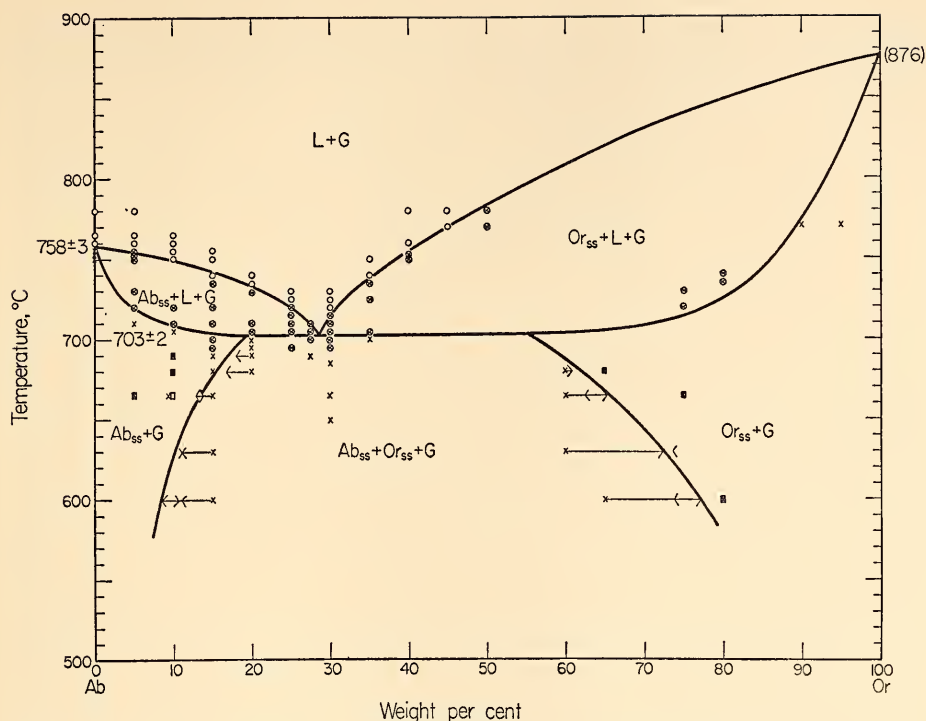


Fig. 28. Revised equilibrium diagram of the water-saturated alkali feldspar join at 5 kb. The diagram is a *projection* from H_2O . The K-rich liquidus and solidus portions incorporate results of Yoder, Stewart, and Smith (*Year Book 56*). Arrowheads along the Ab solvus limb indicate X-ray feldspar compositions of reactions from homogeneous Or_{15} glass (outward) and mixtures of Ab + Or_{75} in Or_{15} bulk composition (inward). Squares denote bulk compositions of runs outside the solvus that give feldspar compositions indicated by a large X. These runs were used as calibrations for X-ray compositions. Kf-limb arrowheads pointing outward are from initial glasses of Or_{80} , Or_{85} , Or_{70} , and Or_{75} compositions.

runs as well, since sensitivity of feldspar compositions to bulk compositions persists below the solidus.

In order to confirm the melting intervals observed initially, it was necessary to establish accurately the beginning of melting, with starting materials crystallized at 5 kb in the range 600°–680°C. It is possible to detect very small traces of glass in well-crystallized feldspar, and these appeared first at 695°C in bulk compositions Or_{15} , Or_{25} , and Or_{30} . The compositions Or_{20} and Or_{35} showed no sure signs of melting until 705°C. Compositions that exhibited premature beginning of melting all showed quartz when crystallized below about 650°C

and no quartz above that temperature; apparently the initial liquid lay in the ternary system $Or+Ab+Qz+H_2O$, not on the feldspar join. Significantly, at least two of the low-melting starting materials (Or_{15} and Or_{30}) had been ground for 1 hour in agate, and this very likely accounts for the excess silica. The beginning of melting in the alkali-feldspar join at 5 kb P_{H_2O} is taken as $703^\circ \pm 2^\circ C$.

Melting relations and solvus both derive support from concurrent studies in the nepheline syenite portion of petrogeny's residua system, nepheline-kalsilite-silica, discussed elsewhere in this report. The liquidus surface in the residua

system must, of course, be continuous with that of the feldspar join itself. The liquidus curves from the hydrous quaternary system are shown in Fig. 29 as serial sections through the silica-under-saturated liquidus surface at 5% increments of silica content and are compared with the feldspar liquidus from Fig. 28. The slopes are consistent with the liquidus slopes suggested for the join.

Determination of the albite-rich limb of the solvus is difficult, owing to slow reaction rates, metastability, and possibly local equilibrium in the form of zoning of crystals. Because reaction rates are presumably enhanced in the presence of liquid, present studies were made initially in the feldspar+liquid+gas portions of the residua system. These results consistently gave a more sodic albite-rich limb than previous determinations, except the alkali-excess run of Luth and Tuttle (1966). Moreover, it was noted in a detailed study of the 5 kb, 665°C section in the residua system that bulk compositions nearer the soda feldspar termination of the four-phase Na feldspar+K feldspar+liquid+gas field gave more Ab-rich values than those bulk compositions richer in K, just as in the melting loop of the feld-

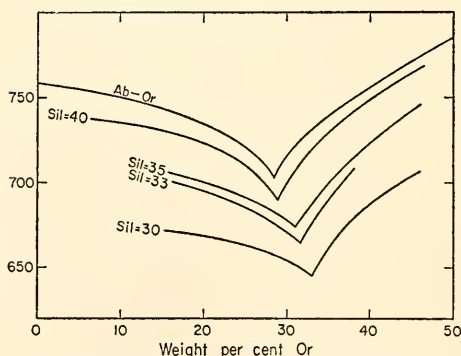


Fig. 29. Traces of liquidus surface at 5 kb P_{H_2O} of the alkali feldspar join (top) and the nepheline syenite region at various silica levels in Ne-Ks-Sil. The latter four curves are projected back onto the alkali feldspar join at constant Ks content.

spar join. This result suggested a principle, borne out by subsequent experience: in determining a solvus by synthesis from glass, those bulk compositions nearest the limb to be determined give the best approximations to the stable (binodal) solvus, determined by the X-ray composition method.

This principle was carried over to studies in the feldspar join to test whether the excess alkali produced different results because of solid solution off the feldspar join—or nonstoichiometry—or perhaps because of improved reaction rates. The problem was approached in several ways. Starting materials of various bulk compositions were made up of mechanical mixtures of pure Ab glass and Or₉₅ glass, on the theory that conversion from soda-rich glass to crystals should not overstep the stable solvus in the direction of K. If this assumption were correct, the runs made with these mixed glasses should define the Na limit of the possible positions of the stable solvus. Results of such runs are shown in Fig. 28 as arrows, indicating reaction of Ab glass+Or₉₅ glass to feldspar. Arrows pointing outward from inside the solvus indicate the X-ray composition of feldspar (Orville, 1963) formed from homogenous glass of the composition Or₁₅. The difference between feldspar composition and bulk composition was calibrated at several temperatures from runs outside the solvus. The combined arrows form a synthesis bracket, and the resulting solvus limit is consistent with both the eutectic-like liquidus surface and results in the presence of alkali-excess liquids in the residua system. It is also consistent with the 5-kb alkali-excess experiments of Luth and Tuttle (1966) and, by extrapolation, with those of Orville (1963) at 2 kb. Similar synthesis brackets are being obtained for the K-rich limb of the solvus.

It is noteworthy that in certain experiments the results from mechanical mixtures of Ab glass and Or₉₅ glass over-

lap those from homogeneous starting materials of the same composition, showing that reaction from end-member glasses does not reliably suggest the maximum breadth of the solvus. Both mechanical mixtures and homogeneous glasses having bulk compositions further inside the two-feldspar region gave feldspars that also lay further inside. An example of this dependence of feldspar composition on bulk composition is illustrated in Fig. 30. This suggests (1) that only those bulk compositions lying very closely inside a solvus limb will give feldspar compositions approaching the stable value and (2) that reactions from pure Ab glass or Or₉₅ glass to feldspar cannot be regarded as reversals in the rigorous sense. Reversals with the use of crystalline starting materials are in progress.

Although the melting relations of feldspar under water-saturated conditions at 5 kb may rarely be relevant to the crystallization of natural magmas, the subsolidus relations, barring appreciable effects of leaching, should correspond to natural water-undersaturated conditions at 5 kb. Thus the effect of pressure on the solvus can be qualitatively evalu-

ated from inspection of the present work and the various 2-kb studies cited above. Estimation of the critical temperature, however, has proved difficult at 5 kb, since it requires data on the water-deficient crystal+liquid region. Runs with crystalline starting materials suggest a critical temperature of $730^{\circ} \pm 10^{\circ}\text{C}$.

Feldspar Stoichiometry

Quartz has been observed in runs at 630° and 600°C from some starting materials in the alkali feldspar-water system at 5 kb. Runs at and above 665°C on the same starting materials show only feldspar. It is therefore possible that the feldspars from two different temperature regions contain different amounts of silica and, more specifically, that the feldspars found in the presence of quartz are saturated with silica but those synthesized at higher temperatures are not demonstrably saturated. This possibility, once again, raises serious questions regarding the stoichiometry of feldspars. The subject has been discussed recently by Luth and Tuttle (1966), and Carman and Tuttle (1968) have offered evidence suggesting the presence of excess silica in sanidines from natural rhyolite.

The experimental results are open to a number of interpretations. Leaching cannot be the sole cause of the quartz, unless the absence of quartz in higher-temperature runs is due to increased solubility of silica in the vapor. This explanation is unlikely, since nothing resembling quench-quartz or alkali-silicate glass balls was found in the charges, and since experiments made with purposely introduced quartz (4%) show quartz at 680°C . An alternative explanation is that the starting materials are off composition, owing either to loss of alkalis during preparation or to lengthy grinding in agate, and therefore lie in the ternary system Ab-Or-Q instead of the feldspar join. The fact that some glasses, ground only for short periods in agate,

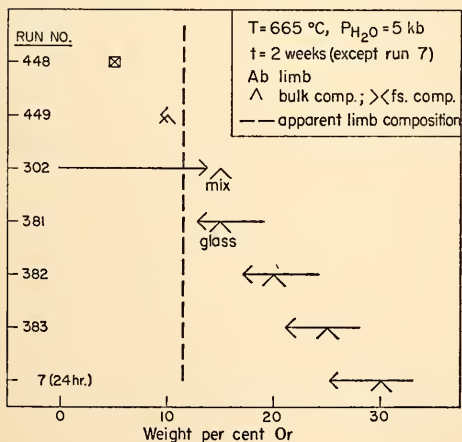


Fig. 30. X-ray compositions of feldspars at 665°C , 5 kb $P_{\text{H}_2\text{O}}$, produced from different starting materials, showing effect of bulk composition on the apparent solvus limb composition.

do not produce quartz at 600°C strongly suggests that this is the correct explanation and that the quartz seen at low temperatures is indeed dissolved in the feldspar at higher temperatures.

If the feldspars in the residua system do indeed lie off the feldspar join at sub-solidus temperatures, some interesting consequences follow. Pure feldspars would exist only at the liquidus of the Ab-Or system. The solvus reported here for the "pure" system would in fact be that applicable to silica-saturated granitic rocks. The true solvus for ideally stoichiometric feldspars would be somewhat narrower than depicted here. Co-existing alkali feldspars in undersaturated rocks would have compositions differing (perhaps only slightly) from those in oversaturated rocks at the same T and P of formation. Data from this study and from the silica-undersaturated portion of petrogeny's residua system (elsewhere in this report), as well as the two alkali-excess experiments of Luth and Tuttle (1966) at 5 kb, provide an inconclusive test of these possibilities. For virtually every alkali-excess run that can be compared with the presently determined solvus in the "pure" join, the alkali-excess points fall inside the solvus rather than outside. The results are nearly identical for 600° and 665°C on the Na-rich limb, and for 665° and 680°C on the K-rich limb. The deviations at 680°C for the Na-rich limb and 600°C for the K-rich limb may be due to bulk composition effects similar to those found in the join: in the residua system it is not possible to choose compositions in the two-feldspar+liquid field with Na:K ratios as near those of the feldspars as in the join itself. The 600°C equilibria in the undersaturated portion of the residua system are further complicated by the presence of analcite. As a result, the solvus deduced from the undersaturated part of the residua system and that determined for compositions ostensibly in the join, but con-

taining a slight excess of silica, are not demonstrably different.

Ternary Feldspars

As shown schematically by Yoder, Stewart, and Smith (*Year Book 56*, Fig. 46, p. 213), the height and configuration of the feldspar solvus change drastically with addition of anorthite. The solvus crest rises very steeply with increasing An until it intersects the ternary feldspar solidus. The shape of the solvus in the ternary T - X prism is known as yet only inexactly, however, and chiefly from study of natural feldspar chemical analyses. The experimental study of selected natural material offers certain advantages in assessing the effects of temperature and water pressure simultaneously.

During the past year, long runs made on a natural mesoperthite at 500 bars water pressure showed a solvus crest at about 920°C, a temperature decisively of interest for the origin of mesoperthite-bearing rocks and their hypabyssal equivalents, anorthoclase-bearing rocks. The sample studied was an analyzed bulk feldspar separate from a ferro-syenite of the Kiglapait layered intrusion, Labrador. The separate consists largely of mesoperthite, with small amounts of discrete oligoclase and K feldspar; the bulk analysis gives $Or_{29.6}Ab_{62.2}An_{8.2}$. The mesoperthite consists of sharply bounded, subparallel-to-tapering lamellae of oligoclase and K feldspar, about 2 μ wide. Textures in the rock indicate that this feldspar crystallized as a subhedral, homogeneous single phase, which subsequently exsolved. The slow cooling of this relatively deep-seated layered intrusion permitted a striking degree of internal equilibration within the former single crystals: X-ray compositions (projected from An) for the present lamellae are Or_0 and Or_{89} , although of course the Or_0 is not pure albite, but around An_{12} , if it is assumed that the K phase is essentially An free.

Mesoperthite appears to be a good example of a macroscopically single phase that is internally and microscopically a mixed-layered type of two-phase intergrowth. Further unmixing to discrete granules is apparently prevented by the large activation energy needed to break bonds across the phase interface region.

When the material was heated for 1 month with excess water at 500 bars, 910°C, the X-ray compositions converged to Or₂₃ and Or₄₀; essentially no further change was observed after a second month. At 930°C, small networks of glass were observed locally, indicating beginning of melting at 925° ± 5°C. At 935°C, a broadened peak indicated the persistence of two feldspars, again in the presence of a small amount of glass, which increased to only about 5%

at 950°C, in the presence of two feldspars, Or₂₁ and Or₅₄. The results are summarized in Fig. 31, which is a projection from anorthite. The figure shows the most likely interpretation of the data, i.e., that the solvus crest lies very slightly below the solidus in projection. The beginning of melting of 925° ± 5°C is in agreement with the alkali feldspar diagram of Tuttle and Bowen (1958, Figs. 17 and 26) but some 30° higher than implied by their text (p. 41) and run data (Bowen and Tuttle, 1950, Table 1).

Because the solvus crest rises with total pressure and the solidus is lowered with water pressure, the implication is clear that the Kiglapait rock from which this initially homogeneous feldspar was taken formed at an effective P_{H_2O} at least

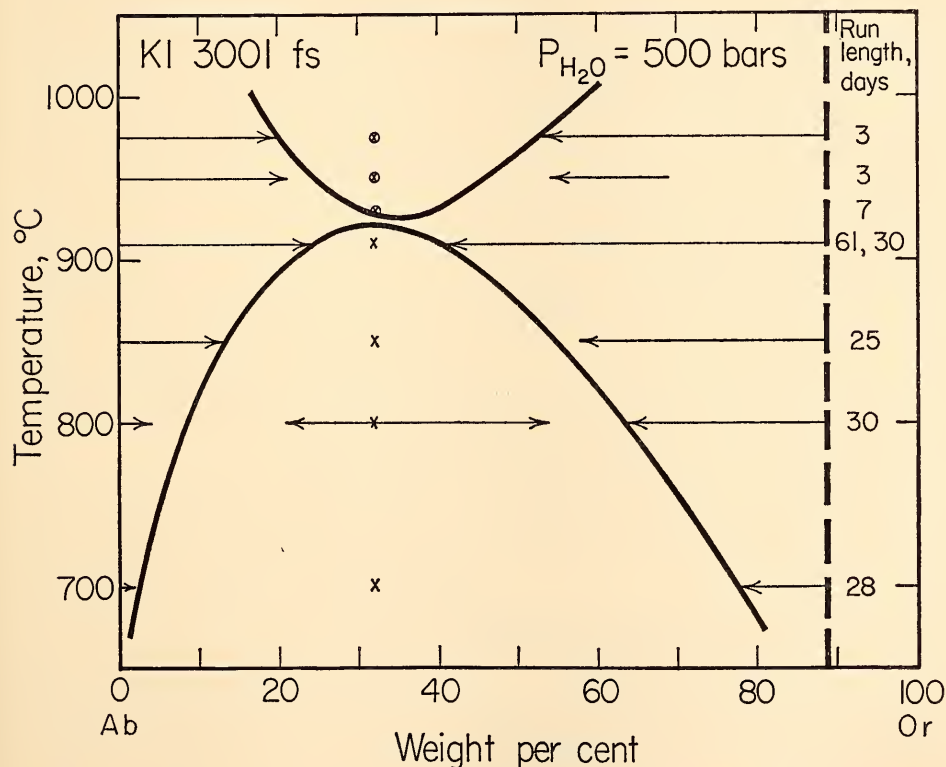


Fig. 31. Projection from anorthite of X-ray composition of mesoperthite from Kiglapait intrusion sample KI 3001 at 500 bars P_{H_2O} .

as low as 500 bars, and probably much lower. If the magma had been saturated with water vapor at the pressure of formation (perhaps as much as 5 kb), a two-feldspar rock would surely have resulted. These observations are in accord with the essentially anhydrous aspect of the rocks as observed in thin section. Hydrous rocks that contain mesoperthite would be expected to show a less calcic (or more sodic) feldspar than the Kiglapait sample studied; otherwise the origin of the hypersolvus feldspar would be difficult to explain.

The occurrence of mesoperthite in granulite facies rocks of the Adirondack region of New York has been used by de Waard (1967) as a lower limiting condition of the temperature of granulite facies metamorphism, based on the behavior of the alkali feldspar solvus with pressure, deduced by Orville (1963). Extrapolation of the present results for *calcic* mesoperthite would lead to the very high temperature of 1000°C at a pressure between 4 and 7 kb, allowing for uncertainty in the effect of anorthite on the dT/dP of the solvus crest. Clearly, therefore, the curve shown by de Waard (1967, Fig. 3) is even more stringently a minimum condition for granulite temperatures than he suggests, and again the An content of granulite mesoperthites would be expected to be low.

Many more experimental data on the solvus and solidus of the ternary feldspars are needed, since a number of unexpectedly rigorous bounding conditions appear to be imposed on some rocks as a result of the An content of their hypersolvus feldspars.

ANNEALING CHARACTERISTICS OF DENSE FELDSPAR GLASS

E. C. T. Chao and P. M. Bell*

Coesite, stishovite, and dense feldspar glasses have been found in ejecta from terrestrial meteorite craters. Their pres-

ence is evidence of a history that involves shock waves with associated pressures far greater than those seen in tectonic or volcanic events. Collisions between comets or meteorites, and between them and either the earth or the moon, could generate shock pressures ranging up to several megabars. The study of impact products, in the form of abundant dense feldspar glasses, should be helpful in investigating the origin of terrestrial and lunar structures that have the morphological characteristics of impact or explosive craters. Such a study is timely, particularly in light of the need for information to aid in the interpretation of lunar samples scheduled to be returned to the earth in the forthcoming Apollo project in the fall of 1969.

At present the identification of dense feldspar glass is based on measurement of index of refraction and the change to a lower index as a result of annealing at atmospheric conditions. It is necessary to correlate the density of the glasses with their pressure of formation. In the present work, several feldspar glasses were formed from the analyzed natural crystals by exposure to elevated temperatures and pressures in the range 1–45 kb, in the solid-media, piston-cylinder apparatus. The natural crystals used for starting materials in the high-pressure experiments were orthoclase (Or₉₆, Benson Mines, New York), oligoclase (An₂₀, Muskwa Lake, Ontario), and calcic labradorite (An₆₈, Lake County, Oregon).

The synthetic glasses produced from the high-pressure experiments were then studied in a series of annealing experiments in which relaxation of density and change in compressibility were followed by monitoring the index of refraction.

In Fig. 32 is seen a linear increase of refractive index of the three feldspar glasses as a function of the pressure at which they were run. The precision of measurement was ± 0.0002 with an accuracy of ± 0.001 . The indices were monitored on the experimental products

* U. S. Geological Survey.

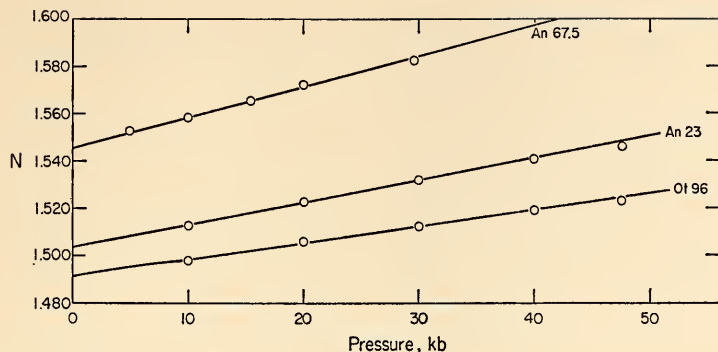


Fig. 32. Index of refraction of three feldspar glasses (An_{68} , An_{20} , Or_{10}) at the pressures at which they were quenched from liquid.

for 6 months after culmination of the experiments, and no index change was observed. Therefore, the index of refraction of a glass rapidly quenched from high pressures and temperatures could be used as a secondary calibration for pres-

sure and temperature. The quenched glasses are also useful in annealing studies.

After a few exploratory experiments it became evident that there are three distinct parts of a synthetic annealment:

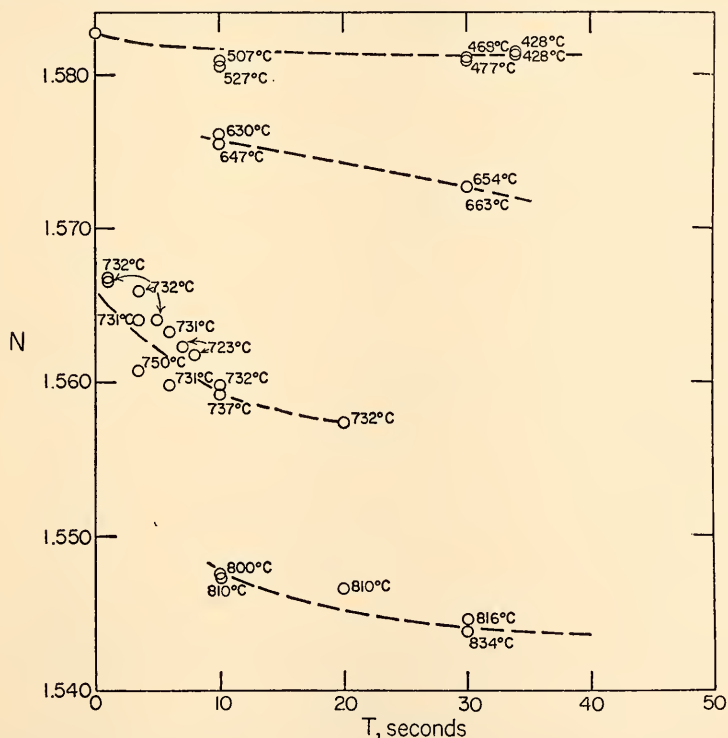


Fig. 33. Annealing experiments on An_{68} glass that had been prepared by quenching at 29.6 kb. Timing began as the glass reached the temperature indicated at each point. No measurements were made during the approach to annealing temperature.

change of index during heating, change of index during a period of constant temperature, and change of index during cooling. It was not feasible for us to duplicate the initial stage of the natural annealing process; however, it was possible to conduct meaningful studies of the second and third stages of the process. Experiments lasting up to 90 seconds were performed, and changes in refractive index were followed during the various parts of the annealing cycle. Fig. 33 shows the lowering of index at various temperatures and heating periods. For example, there is a negligible change as a result of heating at 400°–500°C, whereas a drop in index to the 1-atm value occurs at 850°C in 30 seconds. In these experiments the dense glass starting material (An_{68} , synthesized at 29.6 kb) was raised to the temperature indicated and rapidly quenched; the total time and index measured after the experiment are

plotted in Fig. 33; that is, the three parts of the annealing cycle are not distinguished.

In order to evaluate the annealing effects during heating, namely, the first part of the annealing cycle, rapid quenching (less than 2 seconds) was applied to two glasses of An_{68} composition, one previously synthesized at 29.6 kb and the other previously synthesized at 15 kb. The results are plotted in Fig. 34, each point indicating the maximum temperature achieved. A significant part of the annealing cycle occurs during the first few seconds of heating, and the glass of higher density anneals approximately twice as fast as the glass of lower density, even though the heating rate is the same for both.

A different type of annealing experiment from those previously mentioned was made at high pressures. The An_{68} glass was treated by the following procedure. (1) The glass was quenched

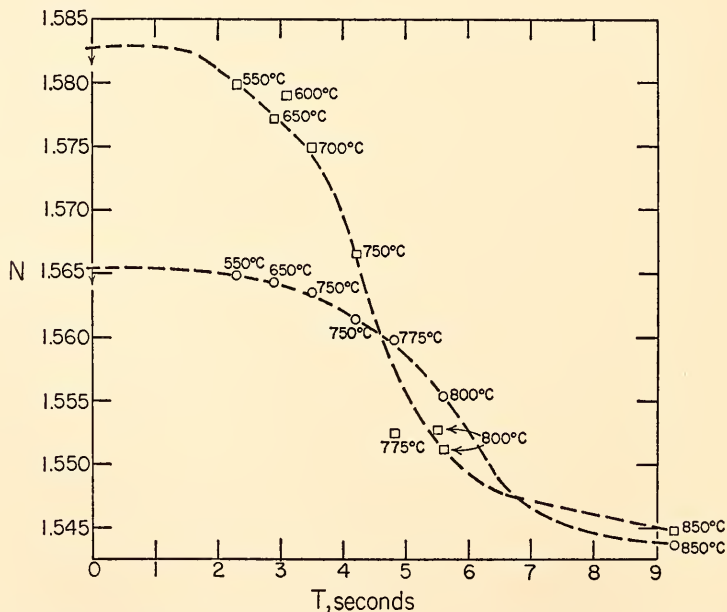


Fig. 34. Annealing experiments with two samples of An_{68} glass, one prepared at 15 kb and the other at 29.6 kb. The annealing furnace was set at 850°C. Temperatures indicated are the highest temperatures reached before quenching. Note that the glass prepared at 29.6 kb (open squares) anneals approximately twice as fast as the one prepared at 15 kb (open circles).

from above the liquidus temperature at 10 kb; (2) the pressure was raised to 20 kb in one set of experiments and to 40 kb in another set of experiments; (3) the temperature was raised to various values below the liquidus up to 1100°C and held for 10 minutes; (4) the experiment was quenched. Here the purpose was to investigate the densification process under static conditions. The results for the two sets of experiments, at 20 kb and 40 kb, are given in Fig. 35. A number of distinct features can be noted. The glasses do not undergo densification below 200°C, even if the pressure is 40 kb. There is a steep rise in density at both pressures up to 800°C, at which point the maximum index of refraction seems to decrease slightly with further

increase in temperature. This decrease is especially marked for the 20-kb experiments.

Our purpose has been to model the various parts of the shockwave process for careful observation by using static techniques. It is not possible to evaluate the actual rate process, since natural shock events probably last only a few microseconds to seconds and the actual characteristics of meteoritic impact ejecta will be influenced by many factors, for example the characteristics of the shock-wave, the release adiabat, and the particle size. It is evident from the present experiments that glasses produced at high pressures have a density reflecting the formation pressure. During annealing the high-pressure density will

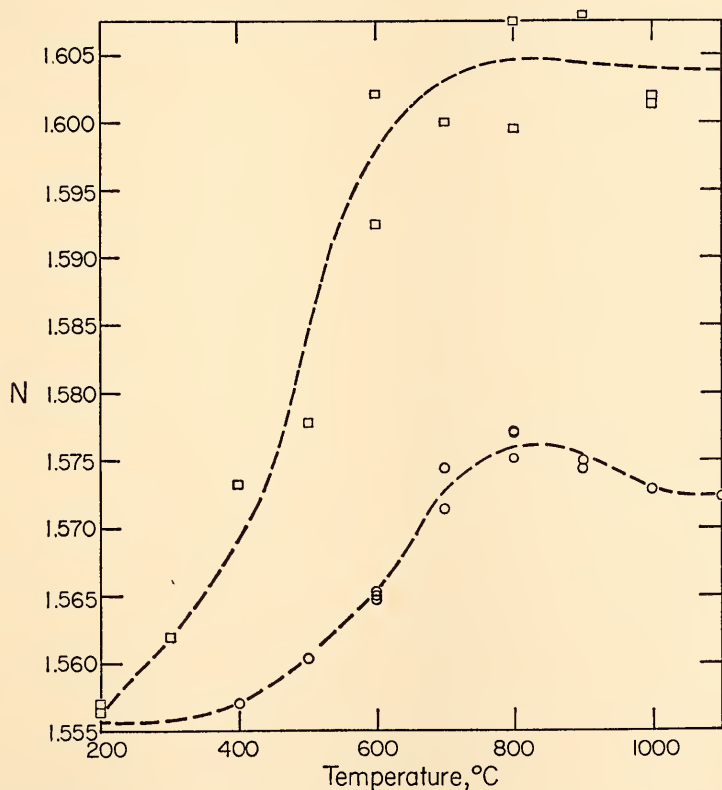


Fig. 35. Samples of An_{83} were melted and quenched at 10 kb, then raised to 20 or 40 kb (upper curve—40 kb, open squares; lower curve—20 kb, open circles) and held at the indicated temperatures for 10 minutes, then quenched.

be lowered at a rate that is a function of temperature. The curves plotted in Fig. 34 have a reverse *S* shape, which should prove useful in projecting back to the conditions of formation of high-density glasses. These curves cannot be used to describe the high-pressure, high-temperature history of shock-produced glasses with great accuracy, but will be useful in providing clues to the conditions of their formation. By analyzing dense glasses extracted from crater ejecta it should be possible to distinguish craters that have been produced by meteorite impact from those produced by volcanic or tectonic processes.

DIAMOND INCLUSIONS, ALUMINUM SILICATES, β -QUARTZ, ANDRADITE

MINERAL INCLUSIONS IN DIAMONDS

H. O. A. Meyer and F. R. Boyd

A unique method to obtain geochemical and mineralogical data on the phases that form the rocks of the upper mantle is to study the mineral inclusions found in natural diamonds. The conditions of high temperature and pressure required for the stable formation of diamond are such that coarse-grained natural diamonds (as distinguished from those formed in meteorite impacts) have most likely come from depths below 100 km, far below the base of the earth's crust.

It is of primary interest to determine the chemical compositions of these inclusions. In materials thus far made available for study, the inclusions are very small, the largest being only several hundred micrometers in longest dimension. This size is far too small to permit study by the classical methods of analytical chemistry, but the compositions can be determined accurately with an electron probe. The quantitative analyses reported here are the first to have been made of inclusions in diamond.

Most primary inclusions thus far found in natural diamonds are euhedral, and they are invariably single crystals.

The olivine inclusions especially may show particular crystallographic orientations with respect to their diamond hosts (Mitchell and Giardini, 1953; Meyer, *Year Book* 66). In some diamonds more than one inclusion is present, and occasionally more than one phase is found in a group of individually isolated inclusions. Nevertheless, in such cases each individual inclusion is monomineralic. This fact is curious, and its interpretation is at present not entirely clear but it suggests that the diamonds have formed by a solid-state process rather than by crystallization from a magma. In the latter event, the diamonds might be expected to have incorporated droplets of magma that would have crystallized as polymineralic inclusions.

Because of the monomineralic nature of the inclusions, it is impossible to be certain whether they are relics of one or more phase assemblages. The fact that two markedly different types of garnet have been found as inclusions suggests the latter possibility.

In a gross way the minerals that are found as inclusions are similar to the minerals of the nodules in kimberlite and to the individual primary crystals in the matrix of kimberlite. The electron-probe analyses, however, show that in detail there are some striking differences. Four of the five garnets analyzed are extremely rich in chrome pyrope, so much so that they contain about 30% of the $\text{Mg}_3\text{Cr}_2(\text{SiO}_4)_3$ end member. In this respect they are very distinctive garnets. The chromites analyzed are also unusually chrome rich. In contrast, the single diopside inclusion is notably low in R_2O_3 , particularly in Cr_2O_3 . In this regard, its composition contrasts with the chrome diopsides of the peridotite nodules and the omphacites of the eclogite nodules.

It is obviously very speculative at this stage to conclude that these facts are related. But it is known that in the system enstatite-pyrope high pressure favors the crystallization of pyrope

rather than aluminous enstatite. Possibly an analogous reaction exists in the system diopside-Mg₃Cr₂(SiO₄)₃. If so, it may develop that the inclusions reflect different, perhaps more deep-seated, pressure-temperature conditions than those under which the minerals of the nodules equilibrated. It is well established that diamonds have been found as primary phases in peridotite and eclogite nodules. It is possible that the monomineralic inclusions in diamond are armored relics of pressure-temperature events earlier than those reflected by the present phase assemblages of the nodules.

Mercy and O'Hara (1967) have noted that garnets from peridotites are rich in Cr and poor in Mn and Ti relative to garnets from eclogites. On this basis, the analytical data in Table 5 suggest that the chrome pyropes have a peridotite affinity whereas the pyrope-almandine could have been derived from an eclogite assemblage.

Method of Study

H. O. A. Meyer

The inclusions must be removed from their diamond hosts for study with the electron probe, and their removal is most easily and reliably accomplished by slowly burning the diamonds in air at about 800°C. At this temperature several hours are usually required to eliminate the diamond by oxidation. This treatment is destructive to sulfide inclusions, but on the silicates and oxides thus far recovered it appears to have little effect beyond slight oxidation of the olivines. Once removed, the inclusions are mounted on glass slides and lapped to produce flat surfaces suitable for electron-probe analysis. Because of the small size of the inclusions, areas available for analysis were usually restricted, and it was necessary to repolish an inclusion one or more times during analysis to remove contamination spots.

The analyses were made with a Ma-

terials Analysis Company Model 400 electron probe.* Standards used were predominantly those described by Boyd in *Year Book 66* (p. 329). The intensity ratios were reduced to chemical compositions and corrected for instrumental and matrix effects with the use of the computer programs described elsewhere in this report (Boyd, Finger, and Chayes). Results for the major elements are believed to be accurate to ± 2 relative %. Results for minor elements are somewhat less accurate, particularly where line interference (e.g., MnK α and CrK β) makes determination of background values uncertain. The ratio σ/\sqrt{N} , where σ is the standard deviation and N is the mean count, was calculated for the major elements in the analyses in Tables 4-7. This ratio is a useful indicator of inhomogeneity; a value greater than 3 is taken as evidence of inhomogeneity.

Olivines

H. O. A. Meyer

Five olivine inclusions were selected for analysis, and a sixth specimen, an olivine from the Stockdale kimberlite pipe, Kansas, supplied by D. G. Brookins, was analyzed for comparison. The results are given in Table 4.

The inclusions are markedly similar to olivines from ultramafic rocks (O'Hara and Mercy, 1963; Nixon, von Knorring, and Rooke, 1963; Ross, Foster, and Myers, 1954). Comparison of the inclusion analyses with that of the Stockdale olivine furthers this observation, although admittedly the latter is from a kimberlite and not an ultramafic nodule. The minor-element content of the olivine inclusions is identical with that of other forsterite-rich olivines. No analysis has yet been made for NiO, but qualitative results indicate it to be present in the range 0.2-0.3 wt %. Cobalt has been

* The assistance of the National Science Foundation in the purchase of this instrument under grant GP 4384 is gratefully acknowledged.

TABLE 4. Analyses of Olivine Inclusions

	9b	10c	11a	13c	23b	Stockdale
SiO ₂	40.7	40.8	40.4	41.0	40.7	40.8
TiO ₂	0.00	0.00	0.00	0.02	0.00	0.02
Al ₂ O ₃	0.07	0.02	0.02	0.06	0.02	0.02
Cr ₂ O ₃	0.17	0.06	0.08	0.06	0.04	0.00
FeO *	7.79	7.09	5.52	7.11	7.60	7.88
MgO	49.6	51.6	52.9	50.4	51.1	51.7
CaO	0.18	0.07	0.01	0.09	0.07	0.01
MnO	0.17	0.12	0.09	0.12	0.12	0.10
Totals	98.7	99.8	99.0	98.9	99.7	100.5
Number of Ions on the Basis of 4 Oxygens						
Si	1.001	0.991	0.982	1.003	0.992	0.987
Ti	0.000	0.000	0.000	0.000	0.000	0.000
Al	0.002	0.001	0.001	0.002	0.001	0.001
Cr	0.003	0.001	0.001	0.001	0.001	0.000
Fe ²⁺	0.161	0.144	0.112	0.145	0.155	0.159
Mg	1.821	1.868	1.918	1.839	1.887	1.863
Ca	0.005	0.002	0.001	0.002	0.002	0.001
Mn	0.003	0.003	0.002	0.003	0.003	0.002
End Members, mole %						
Forsterite	91.5	92.6	94.3	92.5	92.2	92.0
Fayalite	8.1	7.1	5.5	7.3	7.6	7.9
Larnite	0.3	0.1	0.0	0.1	0.1	0.0
Tephroite	0.1	0.2	0.1	0.1	0.1	0.1

* Total Fe as FeO.

Note: Numbers in italics are for the ratio σ/\sqrt{N} .

detected in two out of three inclusions in which it was sought; the concentration is of the order of 10 ppm.

Garnets

H. O. A. Meyer

Chrome-rich pyrope and pyrope-almandine occur as inclusions in the diamonds examined (Table 5). The chrome pyropes (Meyer, 1968) are the most magnesium-rich yet found in nature.

The large chromium content of the chrome pyropes is expressed in the end-member composition $\text{Mg}_3\text{Cr}_2(\text{SiO}_4)_3$. Because of the small calcium content in these inclusions it makes little difference whether the chromium is first assigned to uvarovite or to $\text{Mg}_3\text{Cr}_2(\text{SiO}_4)_3$. Previously, garnets containing $\text{Mg}_3\text{Cr}_2(\text{SiO}_4)_3$ in minor amounts were known only from olivine-bearing ultramafic rocks (Nixon, von Knorring, and Rooke, 1963; Fiala, 1965; O'Hara and Mercy, 1963). Re-

cently, Nixon and Hornung (1968) have discovered chrome-pyrope garnet, similar to the inclusions herein reported, in a heavy mineral concentrate from a kimberlite pipe in Lesotho (Basutoland). The stability field of $\text{Mg}_3\text{Cr}_2(\text{SiO}_4)_3$ garnet is unknown, although its synthesis at high pressure and temperature has been reported (Coes, 1955).

The pyrope-almandine inclusion (20f) is more iron rich than most garnets from kimberlite pipes (*cf.* Nixon, von Knorring, and Rooke, 1963; Bobrievich *et al.*, 1959). The small size ($10 \times 18 \mu\text{m}$) of this inclusion and the lack of repolishing between analyses undoubtedly contributed to the low total sum of the oxide weight percentages.

Chromites

H. O. A. Meyer

The three chromite inclusions analyzed (Table 6) are among the most chrome

TABLE 5. Analyses of Garnet Inclusions

	1		6		15e		15h		20f	
SiO ₂	42.3	3	42.8	2	41.8	3	42.2	2	37.8	4
TiO ₂	0.02	...	0.00	...	0.02	...	0.02	...	0.25	7
Al ₂ O ₃	17.2	1	18.2	2	15.7	2	15.7	2	20.3	3
Cr ₂ O ₃	8.93	1	7.9	1	10.9	1	10.7	1	0.06	...
FeO *	5.36	1	4.75	2	5.71	1	5.57	1	29.5	1
MgO	25.3	1	25.5	2	24.2	1	24.5	1	7.35	1
CaO	1.09	1	1.35	1	2.19	1	2.22	2	1.27	9
MnO	0.21	1	0.17	1	0.20	1	0.19	1	0.39	2
Totals	100.4		100.7		100.7		101.1		96.9 ‡	
Number of Ions on the Basis of 12 Oxygens										
Si	2.991	} 3.000	3.002	} 3.002	2.982	} 3.000	2.994	} 3.000	3.040	3.040
Ti	0.001		0.000		0.001		0.001		0.016	} 1.942
Al	0.008		...		0.017		0.005		...	
Al	1.424	} 2.000	1.506	} 1.997	1.300	} 2.000	1.304	} 2.000	1.922	} 3.000
Cr	0.499		0.438		0.617		0.601		0.004	
Fe ³⁺ †	0.077		0.053		0.083		0.095		...	
Fe ²⁺	0.240		0.226		0.258		0.235		1.982	
Mg	2.668	} 3.003	2.663	} 3.000	2.570	} 3.007	2.587	} 3.001	0.882	} 3.000
Ca	0.083		0.101		0.167		0.168		0.110	
Mn	0.012		0.010		0.012		0.011		0.026	
End Members, mole %										
Spessartite	0.4		0.3		0.4		0.4		0.9	
Andradite †	2.8		2.7		4.1		4.8		...	
Skiagite †	1.1		
Uvarovite	...		0.7		1.4		0.8		0.2	
Grossularite		3.6	
Mg ₃ Cr ₂ (SiO ₄) ₃	24.9		21.2		29.5		29.2		...	
Pyrope	63.9		67.7		56.2		57.0		30.3	
Almandine	6.9		7.4		8.4		7.8		65.0	

* Total Fe as FeO.

† Fe³⁺ calculated to satisfy charge requirements.

‡ See text.

Note: Numbers in italics are for the ratio σ/\sqrt{N} .

rich so far recorded (Irvine, 1967; Ross, Foster, and Myers, 1954; Nixon, von Knorring, and Rooke, 1963).

In two of the three inclusions examined (2 and 3b), exsolution lamellae were observed. Chromite inclusion 3b exhibited two different exsolution structures, believed to be possibly magnetite and ilmenite (A. El Goresy, personal communication). Similar but coarser ilmenite exsolution lamellae were present in chromite inclusion 2. Unfortunately, these lamellae could not be resolved by the microscope on the probe. In chromite 2, local increase in the FeK α count rate was believed to indicate the presence of an exsolution lamella. The analyses presented in Table 6 do not differentiate between the host or lamellae and are

thus bulk analyses approximating more closely the composition of the host than that of the lamellae.

The cell size of a third chromite from the same diamond as inclusions 3 and 3b was determined by X-ray diffraction to be 8.35 ± 0.02 Å. A second crystal structure evident in the X-ray photograph had an axis (repeat distance 8.5 ± 0.1 Å) parallel to [110] of the chromite host. This cell size and orientation are suggestive of magnetite and are in keeping with the above exsolution observations.

Diopside

F. R. Boyd

Both diopside and enstatite have been found as inclusions in diamond, but they

TABLE 6. Analyses of Chromites

	2		3		3b	
SiO ₂	0.13	3	0.29	7	0.43	8
TiO ₂	0.12	1	0.09	...	0.09	...
Al ₂ O ₃	5.12	3	3.20	2	3.26	19
Cr ₂ O ₃	67.2	2	61.4	2	62.1	2
FeO *	14.5	6	31.5	1	31.7	1
MgO	14.2	2	0.54	1	0.48	3
CaO	0.02	...	0.02	...	0.04	...
MnO	0.00	...	0.42	2	0.45	2
ZnO †	0.04	...	1.93	1	2.20	2
Totals	101.3		99.4		100.8	
Number of Ions on the Basis of 4 Oxygens						
Si	0.004	1.998	0.011	1.995	0.016	1.995
Ti	0.003		0.003		0.003	
Al	0.195		0.138		0.139	
Cr	1.716		1.781		1.776	
Fe ³⁺ ‡	0.080	1.000	0.062	1.000	0.061	1.000
Fe ²⁺	0.313		0.905		0.900	
Mg	0.685		0.029		0.026	
Ca	0.001		0.001		0.001	
Mn	0.000		0.013		0.014	
Zn	0.001		0.052		0.059	
End Members, mole %						
MnAl ₂ O ₄	...		1.3		1.4	
ZnAl ₂ O ₄	0.1		5.2		5.9	
MgCr ₂ O ₄	69.7		3.0		2.7	
FeCr ₂ O ₄	17.5		86.2		86.3	
FeAl ₂ O ₄	8.7		1.1		0.6	
FeFe ₂ O ₄	4.0		3.2		3.1	

* Total Fe as FeO.

† Matrix corrections calculated without aid of computer program.

‡ Fe³⁺ calculated from total iron as Fe²⁺ to satisfy charge requirements.Note: Numbers in italics are for the ratio σ/\sqrt{N} .

are uncommon. A diamond crystal in the collection of the Department of Chemistry, University College London, was discovered to contain two separate inclusions of diopside. They have been removed by fracturing the diamond, and one of them provided for electron-probe analysis through the courtesy of H. Judith Milledge.

The inclusion is tabular, parallel to (100), and measures about 200 μ m in its greatest dimension. There has been some alteration to kaolinite, presumably through cracks in the diamond host. When attempts were made to polish a flat surface on the crystal, it was found that only restricted, irregular areas would take a good polish. It appeared that the kaolinite alteration was more than surficial. Although the inclusion is

large in relation to the minimum-sized crystal that can be analyzed with a microprobe, the analysis was complicated because of the restricted areas of good polish.

Results of the analysis (Table 7) show that the inclusion differs in a number of ways from other diopsides from kimberlite nodules (Boyd, *Year Book 65* and *Year Book 66*). It is markedly inhomogeneous, particularly for Ti, Al, Fe, and Mn, as shown by high values for the ratio σ/\sqrt{N} . However, no regular pattern of zoning was found. The contents of Al₂O₃ and particularly Cr₂O₃ are notably low in comparison to other kimberlite diopsides. Al₂O₃ and Cr₂O₃ show wide ranges in these diopsides, but mean values of 42 analyses by Boyd (1968) are 0.9 wt % Cr₂O₃ and 1.6 wt % Al₂O₃.

TABLE 7. Analysis of Diopside Inclusion

Weight %			Number of Ions on the Basis of 6 Oxygens	
SiO ₂	52.8	<i>4</i>	Si	1.97
TiO ₂	0.43	<i>29</i>	Ti	0.012
Al ₂ O ₃	0.86	<i>74</i>	Al	0.018
Cr ₂ O ₃	0.09	...	Al	0.020
FeO *	5.89	<i>44</i>	Cr	0.003
MnO	0.71	<i>57</i>	Fe	0.183
CaO	20.9	<i>7</i>	Mn	0.022
MgO	16.1	<i>5</i>	Ca	0.834
Na ₂ O	1.38	<i>10</i>	Mg	0.895
K ₂ O	<0.004	...	Na	0.100
			K	...
Total	99.2			
Atomic %				
Ca		43.6		
Mg		46.8		
Fe		9.6		
Ca/(Ca + Mg)		48.2		

* Total Fe as FeO.

Note: Numbers in italics are for the ratio σ/\sqrt{N} .

On the other hand, FeO and particularly MnO are notably high in the diamond inclusion.

Solid solution toward enstatite is very restricted in this inclusion; its Ca/(Ca + Mg) ratio is 0.48. This is not outside the range found for other kimberlite diopside, but it would imply a temperature of equilibration of about 950°C if the inclusion were to have crystallized in equilibrium with enstatite. This temperature is low in comparison to the range in which diamonds have been synthesized in the laboratory.

THE ANDALUSITE-SILLIMANITE TRANSITION AND THE ALUMINUM SILICATE TRIPLE POINT

M. C. Gilbert, P. M. Bell, and
S. W. Richardson *

Our study of the stability relations of the three Al₂SiO₅ polymorphs, kyanite, sillimanite, and andalusite, is nearly completed. Experiments determining the kyanite-sillimanite and kyanite-andalu-

site univariant reactions were reported in *Year Book 66* (Richardson, Bell, and Gilbert, pp. 392-397). Subsequent analysis of those results yields the equation for the kyanite-sillimanite transition above zero pressure and 396°C:

$$P(\text{kb}) = 0.0243T(^{\circ}\text{C}) - 9.63$$

Similarly, the equation for the kyanite-andalusite transition, based on our work plus that of Newton (1966), is, above zero pressure and 110°C,

$$P(\text{kb}) = 0.0107T(^{\circ}\text{C}) - 1.173$$

The intersection of these curves at 5.5 kb and 622°C defines the triple point for the three polymorphs. Because of the low angle of intersection, a considerable region of uncertainty existed around this point. In order to reduce the uncertainty, we have studied the andalusite-sillimanite transition hydrothermally in cold-seal pressure vessels at 2, 3, and 4 kb.

Starting materials were equal mixtures of analyzed sillimanite from Brandywine Springs, Delaware (electron-microprobe analysis gave total Fe as Fe₂O₃ as 0.03 ± 0.015 wt %), and andalusite from Standish, Maine (total Fe as Fe₂O₃ is 0.4 ± 0.1 wt %). The sillimanite is fibrolitic and contains quartz. Experimental procedures and analysis of results are similar to those used in our kyanite-sillimanite study. An X-ray peak-height ratio, determined from diffractometer charts for andalusite (220)/sillimanite (120), was used to monitor the reaction. Average values of this ratio for many mounts of the starting material, determined by scanning each mount four times, ranged between 0.53 and 0.70, with values of all individual scans falling between 0.47 and 0.76. Reaction, if it has occurred, cannot be detected if mean values of the ratio fall in this range. But if the measured ratio of peak heights for a particular run product is less than 0.40, the change in ratio is ascribed to growth of andalusite; if 0.90 or more, to growth of sillimanite.

This reaction has proved particularly

* Grant Institute of Geology, University of Edinburgh.

sluggish, and run times of $2\frac{1}{2}$ to 4 months were necessary to demonstrate reaction. The runs were interrupted two or three times for measurement of the peak-height ratio and for regrinding. Runs meeting the direction-of-reaction criterion set forth above are shown in Fig. 36 and fix the transition within fair limits.

From the slopes of the kyanite-sillimanite and kyanite-andalusite transitions given by the equations above, and from application of the molar-volume data of Skinner, Clark, and Appleman (1961), the slope of the andalusite-sillimanite transition radiating from the triple point can be calculated by means of the equation

$$\left(\frac{dP}{dT}\right)_{A-S} = \frac{\left(\frac{dP}{dT}\right)_{K-S} \times \Delta\bar{V}_{K-S} - \left(\frac{dP}{dT}\right)_{K-A} \times \Delta\bar{V}_{K-A}}{\Delta\bar{V}_{A-S}}$$

where P is pressure in kilobars, T is temperature in degrees Celsius, and $\Delta\bar{V}$ is the change in volume across the appropriate Al_2SiO_5 transition. This results in an equation for the andalusite-sillimanite transition above zero pressure and 847°C of

$$P(\text{kb}) = -0.0243T(^{\circ}\text{C}) + 20.59$$

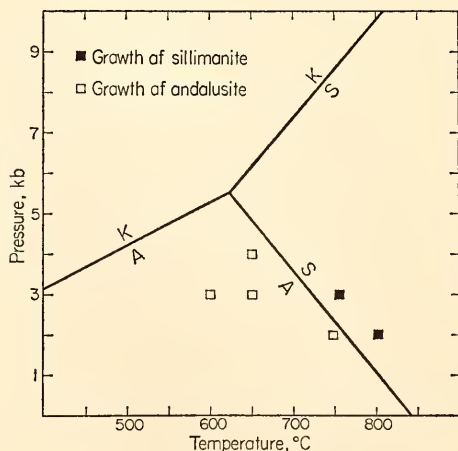


Fig. 36. Hydrothermal runs bracketing the andalusite-sillimanite transition. The kyanite-sillimanite, kyanite-andalusite, and andalusite-sillimanite curves are given by equations in the text.

which satisfies our run data very well (Fig. 36).

Figure 37 shows the limits of uncertainty around the triple point, based on the experimental data and determined by application of maximum and minimum slopes possible for each of the three curves.

The andalusite-sillimanite transition can be used as a fairly good geothermometer for a metamorphic facies series corresponding to relatively low-pressure conditions. Combination of information from this transition with that of dehydration reactions and/or with minimum melting curves of rock systems (Fig. 37) may also allow quantitative estimates of fugacity of H_2O during

metamorphism. Finally, the maximum pressure stability of andalusite (at the triple point) at about 5.5 kb provides a working minimum limit of pressure

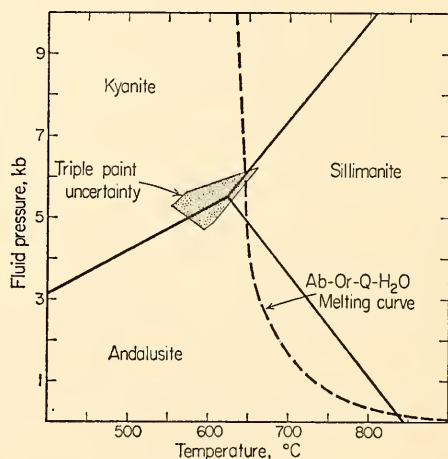


Fig. 37. Pressure-temperature uncertainty around the triple point determined by taking the maximum and minimum slopes permitted by the experimental data only. The Ab-Or-Q- H_2O ($\text{NaAlSi}_3\text{O}_8$ - KAlSi_3O_8 - SiO_2 - H_2O) curve modeling the minimum melting of granitic systems is taken from Luth, Jahns, and Tuttle (1964).

during kyanite-sillimanite metamorphism.

X-RAY PROPERTIES AND STABILITY RELATIONS OF β -QUARTZ SOLID SOLUTIONS ALONG THE JOIN $\text{LiAlSi}_2\text{O}_6\text{-SiO}_2$

J. L. Munoz

The most common polymorph of SiO_2 (α -quartz) is one of the purest natural compounds known. However, β -quartz, a nonquenchable, high-temperature polymorph of SiO_2 , can accommodate foreign ions with relative ease because of large holes in the structure adjacent to SiO_4 tetrahedra. One common example of this tendency is the addition of Li in tetrahedral sites, coupled by substitution of Al for Si in the tetrahedron ($\text{Li} + \text{Al} \rightleftharpoons \text{Si}$). A suitable Li+Al end member for this substitution is eucryptite, LiAlSiO_4 , which crystallizes at high temperatures in a structure of the β -quartz type, except that in β -eucryptite the c axis is doubled compared with the c axis of β -quartz (Winkler, 1948). At low pressures, however, extensive solid solution of eucryptite in SiO_2 is interrupted by the existence of a broad band of tetragonal solid solutions (β -spodumene solid solution). This report describes the effect of pressure on greatly expanding the field of β -quartz solid solution.

Above 10 kb, β -spodumene ($\text{LiAlSi}_2\text{O}_6$) becomes unstable and is replaced by a hexagonal phase (Year Book 66, p. 370). On the basis of powder diffractometer data only, this high-pressure phase was called " β -eucryptite_{ss}." Recently, however, X-ray precession photographs taken of a single crystal of this hexagonal phase, which had been quenched from 10 kb and 1350°C, demonstrated that the c axis of this phase is not the doubled c axis of β -eucryptite but rather the 5.5-Å c axis of β -quartz, as previously indicated by Li (1967). Thus, the high-pressure, high-temperature polymorph of $\text{LiAlSi}_2\text{O}_6$ is isomorphous with β -quartz.

In an attempt to find out whether the

β -quartz solid solution that formed on $\text{LiAlSi}_2\text{O}_6$ composition would extend continuously toward SiO_2 composition at high pressures, a number of glasses on the join $\text{LiAlSi}_2\text{O}_6\text{-SiO}_2$ (generously donated by David B. Stewart) were crystallized at 15 kb and 1350°C. Cell-dimension and molar-volume data (Fig. 38) were obtained from quenched charges crystallized in this way. Note that values obtained for a , c , and V_m from composition $\text{Spod}_{9.5}\text{Q}_{90.5}$ lie very far from the extrapolated trends and have not been considered in curve-plotting. These points are probably the result of one of two effects: either the molar volume curve itself may be strongly inflected near SiO_2 composition, or phases that closely approach SiO_2 composition cannot be quenched to room temperature in the β -quartz structure, as is the case with pure SiO_2 . Inasmuch as we cannot measure the molar volume of SiO_2 in the β -quartz structure at 25°C, no end points for these curves are available, and hence we cannot decide between the two possibilities at this time. Direct measurements of the cell parameters of these phases in their own stability fields with a high-pressure, high-temperature X-ray camera would resolve the ambiguity.

The β -eucryptite solid solutions along part of the join $\text{LiAlSiO}_4\text{-SiO}_2$ readily crystallize metastably at low pressures. Accordingly, it was necessary to perform a number of experiments on β -quartz solid solutions to determine whether they are stable at 15 kb or whether they might be metastable—either with respect to a two-phase assemblage (e.g., two coexisting β -quartz solid solutions) or to a completely different single phase (e.g., β -spodumene solid solution). The present interpretation of these experiments is that β -quartz solid solutions are stable at 15 kb and 1350°C for all compositions on the join $\text{LiAlSi}_2\text{O}_6\text{-SiO}_2$, but data sufficient for construction of T - X diagrams, including temperatures above and below the sta-

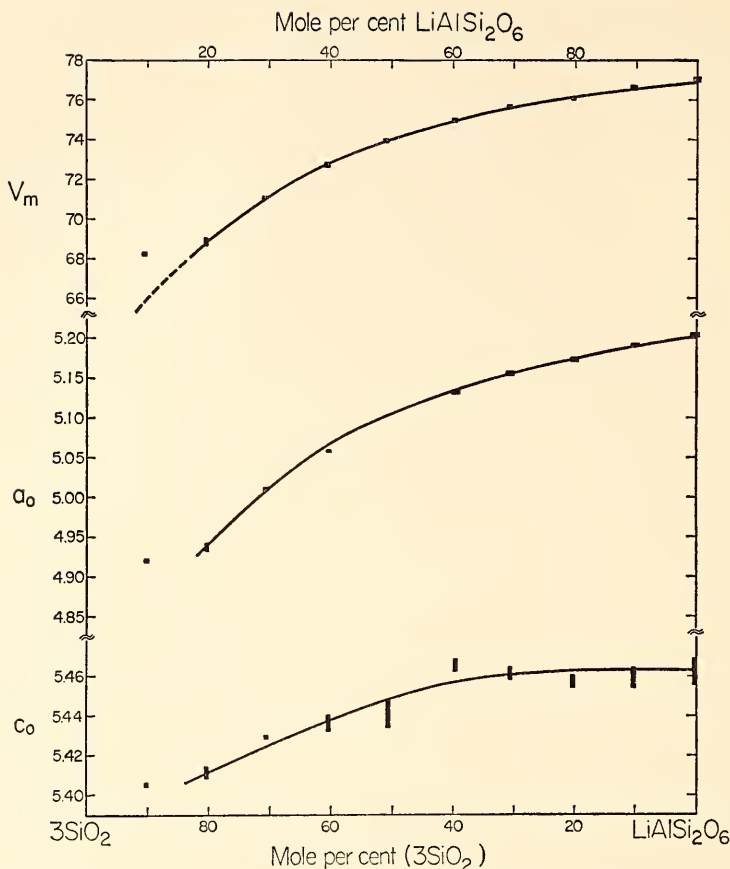


Fig. 38. Cell dimensions and molar volume for β -quartz solid solutions on the join $\text{LiAlSi}_2\text{O}_6$ - SiO_2 synthesized at 15 kb, 1350°C . Reflections were indexed according to the unit cell of β -quartz and were measured from diffractometer powder patterns, with CaF_2 as an internal standard. Data were refined with the use of the lattice-constant least-squares refinement program of Burnham (*Year Book 61*, p. 132).

bility field of these β -quartz solid solutions, are not yet available. Results of the experiments may be summarized as follows: (1) At 10, 15, and 20 kb, single-phase β -quartz solid solutions show no evidence of breaking down when run for 6 hours at 1500°C . (Contamination of the thermocouple precludes longer runs at this temperature.) (2) Two-phase mixtures consisting of $\text{SiO}_2 + \text{LiAlSi}_2\text{O}_6$ (β -quartz_{ss}) can be homogenized to single-phase hexagonal solid solutions of compositions $\text{Spod}_{39}\text{Q}_{61}$ at 15 kb and $\text{Spod}_{30}\text{Q}_{70}$ at 20 kb; the homogenization

reaction is extremely sluggish, however. (3) At 15 kb and very high temperatures (1650° – 1800°C) compositions in the range $\text{Spod}_{50}\text{Q}_{50}$ – $\text{Spod}_{30}\text{Q}_{70}$ crystallize in part as two hexagonal phases; in these experiments glass is invariably present (varying from about 5 to 30%) as an additional run product. The presence of glass—obviously representing a quenched liquid coexisting with two crystalline phases at temperature and pressure—may indicate the onset of nonbinary phase relations at these high temperatures. (4) At all pressures above 10 kb,

and for all compositions along the join, runs initially containing β -spodumene or a β -spodumene solid solution produced a single hexagonal phase in the run product.

The interpretation of these results provides a model for the phase relations along the join $\text{LiAlSi}_2\text{O}_6\text{-SiO}_2$ as a function of pressure. At low pressures, extensive substitution of Li+Al for 2Si in β -quartz is prevented by the presence of a wide field of tetragonal β -spodumene solid solutions. With increasing pressure this field contracts until, at about 10 kb, β -spodumene solid solutions disappear completely and are replaced by a continuous series of hexagonal phases. At still higher pressures (about 25 kb) this continuous series will ultimately be interrupted by the rapidly increasing stability of spodumene (*cf. Year Book 66*, p. 372).

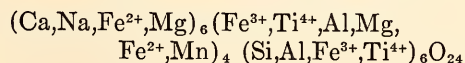
SYNTHESIS AND STABILITY OF Ti-ANDRADITE

H. G. Huckenholz

Andradite, $\text{Ca}_3\text{Fe}_2^{3+}\text{Si}_3\text{O}_{12}$, and its titanium-rich varieties, melanite, schorlomite, and iiaavarite, are common garnets in alkaline igneous rocks and in thermally metamorphosed, impure limestone and skarn deposits. The origin of Ti-bearing andradites has been the subject of much discussion because the structural positions of Ti and its valency states remain problematical. Zedlitz (1933) suggested that a part of Ti is present in the trivalent state, but optical absorption spectra of a melanite specimen from San Benito County, California, obtained by Manning (1967) do not appear to adequately prove this assumption. Suitable ion distribution may be achieved in Ti-rich andradites by substituting Ti^{4+} for Fe^{3+} and Si. Infrared spectra of titaniferous garnets (Tarte, 1960) and the synthesis of germanate, rare-earth iron, and rare-earth gallium garnets (Espinosa, 1964; Ito and Frondel, 1967; Geller, 1967) have

demonstrated that Ti^{4+} prefers a six-fold position in the garnet structure but may also enter a four-fold position. Most analyses of Ti-rich grandite garnets show an excess of tetravalent and divalent cations but a deficiency of the trivalent group. This fact indicates that 2R^{3+} cations (Fe^{3+} , Al) may also be replaced by $\text{R}^{4+}\text{R}^{2+}$ (Ti^{4+} and $\text{Mg, Fe}^{2+}, \text{Mn}$), as demonstrated by Geller, Miller, and Treuting (1960) for germanate garnets having Ti^{4+}Mg , Ti^{4+}Ni , and Ti^{4+}Co for 2R^{3+} . Some of the Ti-garnet analyses report alkalies, and if they are not attributable to impurities, a minor substitution of NaTi^{4+} for CaFe^{3+} may be possible too.

In dealing with garnet analyses, one has to keep in mind the great analytical and separatory difficulties, particularly if minute inclusions are involved and if the ferric iron content is high compared with the ferrous iron. However, chemical analyses of Ti-garnets may be balanced ionically within the limit of error. (In some older analyses that show an excess of R^{4+} cations, a conversion of Ti^{4+} to Ti^{3+} would have been necessary but a change of Fe^{3+} to Fe^{2+} would have the same balancing effect. Such analyses have been neglected here.) The generalized formula of Ti-rich grandite garnets as considered in this study may be expressed on the basis of 24 oxygens as



As a first approximation, reliable chemical analyses of Ti-rich grandites from both igneous (48) and metamorphic rocks (12) plot with their molecular norm in the enstatite ($\text{MgO} \cdot \text{SiO}_2$)-wollastonite ($\text{CaO} \cdot \text{SiO}_2$)-hematite (Fe_2O_3)-perovskite ($\text{CaO} \cdot \text{TiO}_2$) system on or below the plane wollastonite-hematite-perovskite (Fig. 39) and close to the join andradite ($3\text{CaO} \cdot \text{Fe}_2\text{O}_3 \cdot 3\text{SiO}_2$)-Ti-garnet ($3\text{CaO} \cdot \text{Fe}_2\text{O}_3 \cdot 3\text{TiO}_2$), correcting for a minor content of alkalies as a $\text{Na}_2\text{O} \cdot \text{CaO} \cdot 2\text{TiO}_2 \cdot 3\text{SiO}_2$ component. Hypothetical garnet components may be

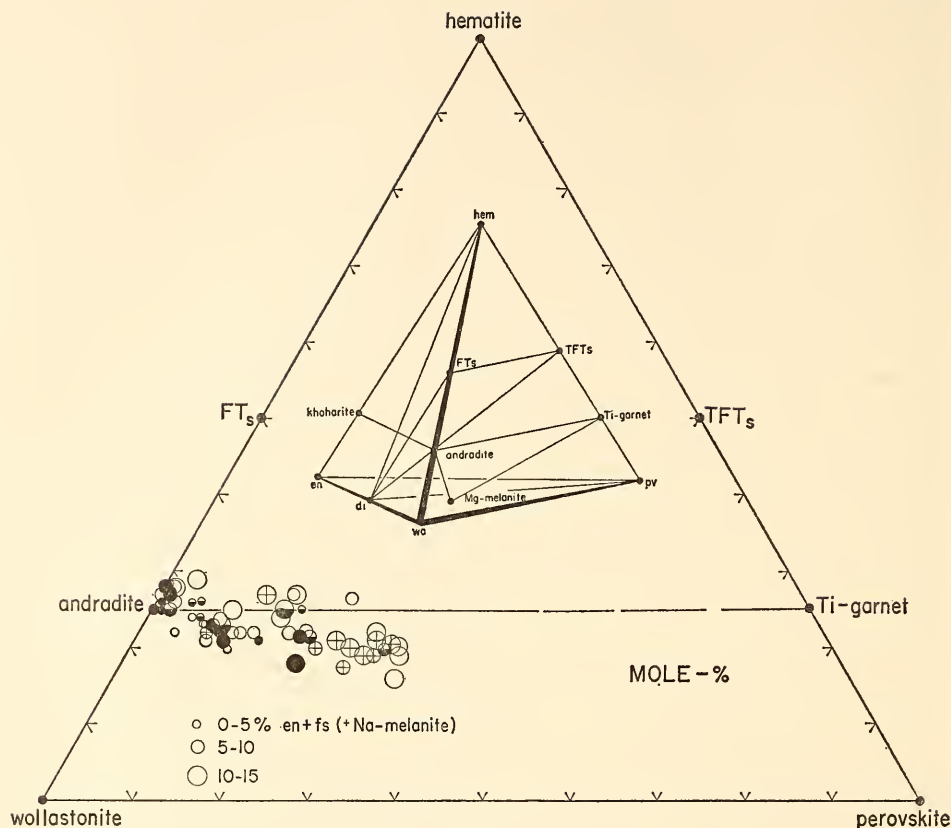
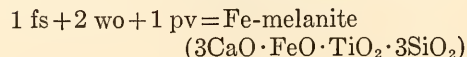
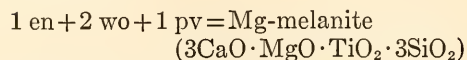
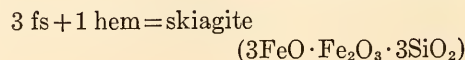
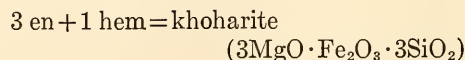
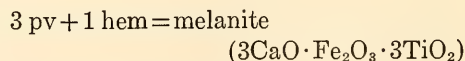


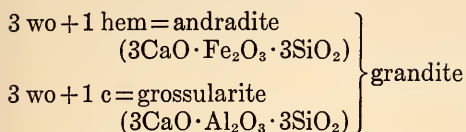
Fig. 39. The quaternary system en-wo-pv-hem, which includes the join wollastonite-perovskite-hematite with a plot of analyses of Ti-bearing garnets from metamorphic (solid circles), alkaline plutonic (open circles), alkaline volcanic (half-shaded circles), and alkaline pegmatitic rocks (circles with crosses). Data were taken from 60 published analyses; complete citations will be given in a forthcoming paper. Abbreviations and compositions of phases encountered: hem, Fe_2O_3 ; TFTs, $\text{CaO} \cdot \text{Fe}_2\text{O}_3 \cdot \text{TiO}_2$; FTs, $\text{CaO} \cdot \text{Fe}_2\text{O}_3 \cdot \text{SiO}_2$; pv, $\text{CaO} \cdot \text{TiO}_2$; wo, $\text{CaO} \cdot \text{SiO}_2$; di, $\text{CaO} \cdot \text{MgO} \cdot 2\text{SiO}_2$; en, $\text{MgO} \cdot \text{SiO}_2$; khoharite, $3\text{MgO} \cdot \text{Fe}_2\text{O}_3 \cdot 3\text{SiO}_2$; andradite, $3\text{CaO} \cdot \text{Fe}_2\text{O}_3 \cdot 3\text{SiO}_2$; Ti-garnet, $3\text{CaO} \cdot \text{Fe}_2\text{O}_3 \cdot 3\text{TiO}_2$; and Mg-melanite, $3\text{CaO} \cdot \text{MgO} \cdot \text{TiO}_2 \cdot 3\text{SiO}_2$; as well as fs, $\text{FeO} \cdot \text{SiO}_2$ and Na-melanite, $\text{Na}_2\text{O} \cdot \text{CaO} \cdot 2\text{TiO}_2 \cdot 3\text{SiO}_2$.

calculated on the basis of en, wo, hem, and pv. After deduction of $\text{Na}_2\text{O} \cdot \text{CaO} \cdot 2\text{TiO}_2 \cdot 3\text{SiO}_2$ (Na-melanite) the remaining sum of wo+en+fs+pv is equal to or larger than $3(\text{hem} + \text{c})$ in acceptable analyses, and may be expressed as a mixture of



if $\text{wo} + \text{en} + \text{fs} + \text{pv} > 3(\text{hem} + \text{c})$. If $\text{wo} + \text{en} + \text{fs} + \text{pv} = 3(\text{hem} + \text{c})$ the following additional components may be formed:





Ti-rich grandites from the Kaiserstuhl volcanic area, Germany, and from Magnet Cove, Arkansas, have the composition given in Table 8.

The Join Andradite-Ti-Garnet

In order to obtain information about the nature of the incorporation of titanium (calculated as tetravalent) in andradite, a series of nineteen compositions in the plane wollastonite-perovskite-hematite was prepared along the join andradite-Ti-garnet and for four additional compositions in this plane. DeVries, Roy, and Osborn (1956) examined the join wollastonite-perovskite at 1 atm. Ito and Frondel (1967) studied parts of the join andradite-Ti-garnet from $\text{andr}_{100}\text{Ti-gar}_0$ to $\text{andr}_{31}\text{Ti-gar}_{69}$ at 1050°C and 1 atm, using gel techniques. The latter authors reported a maximum heating time of 20 hours for the formation of a garnet solid solution, far short of the time required to attain equilibrium

in the present study, in which glasses and crystallized glasses were used. At least 50 days at 1050°C are necessary with ten thorough grindings in the crystallizing period for a complete solution of all metastably formed wollastonite in the garnet_{ss}, even when the starting material is a very fine powdered glass (Fig. 40). No wollastonite and pseudowollastonite (or only traces) were formed metastably from a starting material that was prepared in this way when treated under subsolidus conditions at temperatures between 1000° and 1268°C. The data in the present investigation were obtained at 1 atm pressure from quenching mixtures that had been held between 1000° and 1400°C. Results are presented in a *T-X* diagram (Fig. 41) and in seven critical and unique isothermal sections of the wollastonite-perovskite-hematite plane.

The stable phases crystallizing on the join andr-Ti-gar (Fig. 41) are garnet solid solution (gar_{ss}), pseudowollastonite (pwo), hematite (hem), and perovskite solution (pv_{ss}). Garnet solid solutions have compositions that correspond to the join andr-Ti-gar ; perovskite solid solu-

TABLE 8. Chemical Composition, Molecular Norm, and Hypothetical Garnet Components in Mole % from Two Ti-Bearing Garnets

1		2		1		2	
Chemical Composition			Garnet Components				
SiO ₃	27.94	27.89	Na-melanite	3.4	...		
TiO ₂	12.10	15.51	Mg-melanite	3.6		16.0	
Al ₂ O ₃	5.17	2.12	Fe-melanite	12.4		15.3	
Fe ₂ O ₃	17.47	18.32	Melanite	16.9		22.7	
FeO	3.26	2.91	Khoharite	
MnO	0.27	0.57	Skiagite	3.6		3.1	
MgO	0.31	1.22	Andradite	36.0		32.5	
CaO	31.90	31.79	Grossularite	24.1		10.4	
Na ₂ O	0.52	...	Molecular Norm				
K ₂ O	0.14	...	Na-melanite	3.4	...		
H ₂ O	0.59	...	hem + c	19.2		17.3	
Totals	99.93	100.33	pv	17.6		24.8	
			en	0.9		4.0	
			fs	6.1		6.1	
			wo	52.8		47.8	

1. Melanite from phonolite, Oberrotweil, Kaiserstuhl volcanic area, Germany (Zedlitz, 1933).

2. Melanite from biotite-garnet ijolite, alkaline igneous complex, Magnet Cove, Arkansas (Erickson and Blade, 1963).

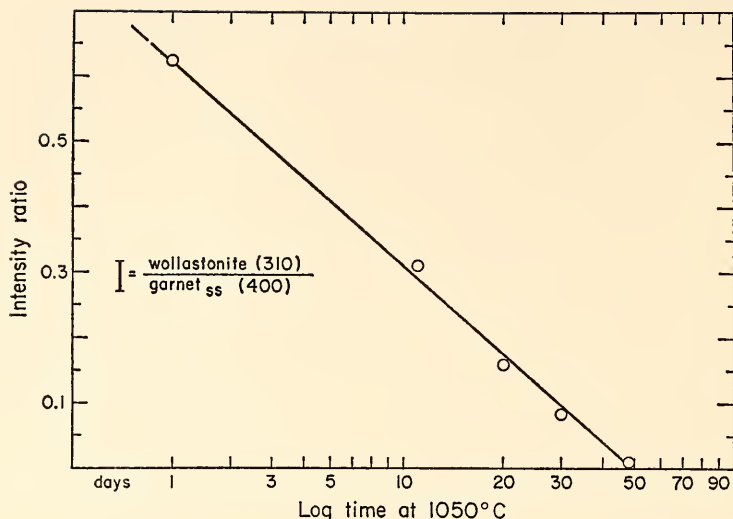


Fig. 40. The solution of metastably formed wollastonite in the garnet solid solution of andradite₉₀Ti-garnet₁₀ as a function of time, based on relative intensities of the (310) and (400) reflections, respectively.

tion, pseudowollastonite, hematite and, above 1268°C, even the liquid are on the ternary join wo-pv-hem.

The maximum degree of solid solution of $3\text{CaO} \cdot \text{Fe}_2\text{O}_3 \cdot 3\text{TiO}_2$ in the stable garnet is 54.5 wt % at a temperature of 1137°C. A composition of $3\text{CaO} \cdot \text{Fe}_2\text{O}_3 \cdot 1.5\text{TiO}_2 \cdot 1.5\text{SiO}_2$ is obtained close to 1000°C. Above 1137°C pure andradite is no longer stable as a single phase (Huckenholz, Schairer, and Yoder, *Year Book 66*), and garnet_{ss} of compositions ranging from andr₁₀₀Ti-gar₀ to andr₈₀Ti-gar₂₀ yield the assemblage pwo + gar_{ss} + hem and pwo + hem before they begin to melt at $1268^\circ \pm 2^\circ\text{C}$. Ti-garnet_{ss} melts incongruently to perovskite_{ss} + liquid at $1315^\circ \pm 2^\circ\text{C}$ and at a composition greater than 46.5 but less than 50 wt % $3\text{CaO} \cdot \text{Fe}_2\text{O}_3 \cdot 3\text{SiO}_2$. The composition with the maximum thermal stability is believed to be close to 48%, as depicted in Fig. 40. It was not possible to synthesize an andradite_{ss} containing 69% of the Ti-garnet component, believed by Ito and Frondel (1967) to have been synthesized by them. The Ti-garnet component in the garnet_{ss} does

not exceed 55 wt %, and at compositions greater than 55% the polyphase assemblages of pv_{ss} + gar_{ss} + hem or pv_{ss} + hem are formed. The latter assemblage is restricted to a composition less than andr₇Ti-gar₉₃.

In order to set up suitable determinative procedures for Ti-andradite_{ss}, the unit-cell parameter a_0 was measured on garnets along the join andr-Ti-gar with the use of material that had been held at temperatures of 1100°, 1175°, 1225°, 1280°, and 1300°C for periods of time required to obtain equilibrium (Fig. 42). The high-angle reflections (640) and (642) of the garnet_{ss} were measured against (300) and (024) reflections of KBrO₃, which are located at 52.723° and 57.391° 2θ CuK α for the entire range of the Ti-andradite_{ss} obtained in this study. Two patterns were run for a single garnet composition, and the diffraction chart was read ten times for every peak. The readings are reproducible to better than 0.01° 2θ , and the difference between a_0 calculated from (642) and (640) is rarely larger than 0.003 Å.

The cell parameter for pure andradite

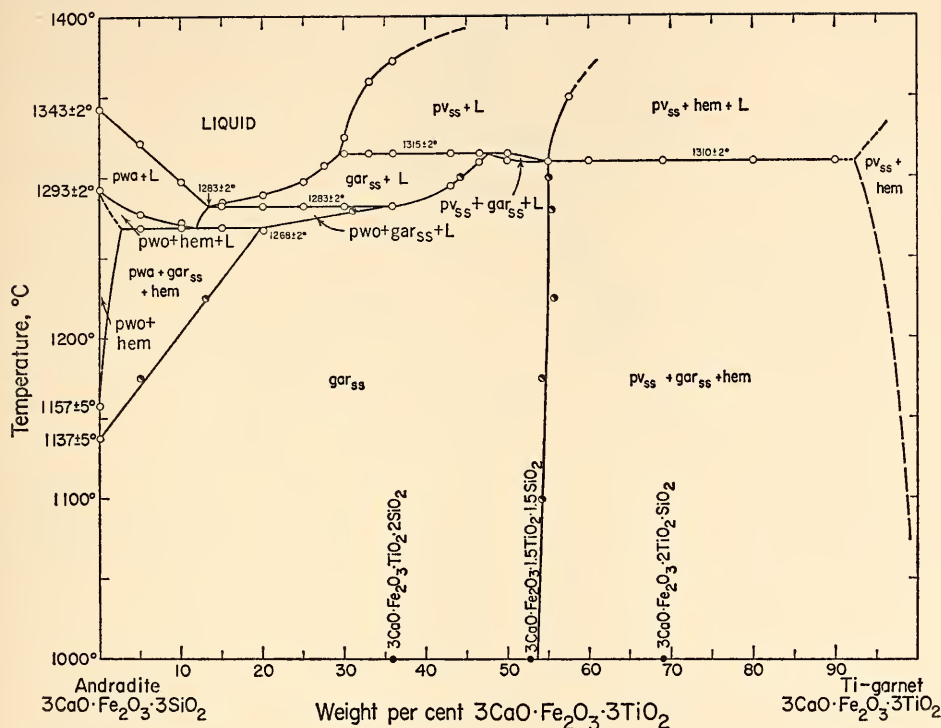


Fig. 41. Temperature-versus-composition plot of data obtained on the join andradite-Ti-garnet at 1 atm pressure. Abbreviations for phases encountered: gar_{ss}, garnet solid solution; pwo, pseudowollastonite; hem, hematite; pv_{ss}, perovskite solid solution. Open circles represent data obtained by optical and X-ray determinations; half-shaded circles represent data obtained by the determination of the unit-cell parameters of garnet_{ss} (illustrated in Fig. 42).

synthesized at 1 atm and at 1137°C was recently determined by Huckenholz, Schairer, and Yoder (*Year Book 66*) as 12.053 ± 0.003 Å, using reflections (642), (640), (611), (521), (510), (422), (420), and (400), with silicon as an internal standard. The increase of the cell parameter from andr₁₀₀Ti-gar₀ to andr₄₅Ti-gar₅₅ is 0.038 ± 0.002 Å per 10 wt % and 0.040 ± 0.002 Å per mole %. The cell dimensions reported by Ito and Frondel (1967) for five Ti-andradites synthesized along the join andr-Ti-gar at 1050°C lie close to the 1100°C unit-cell curve of this study (Fig. 42) within the limits of error. Their cell dimensions indicate, on the basis of the present interpretation, a termination of the garnet solid solution between 56 and 59 wt % (=84 to

88 mole % of Ito and Frondel's scale).

Determination of cell parameters is a very helpful means of obtaining garnet compositions in polyphase assemblages, and the cell parameter a_0 has been used in mapping field boundaries on the binary join andr-Ti-gar as well as in the ternary system wo-pv-hem. At compositions more Ti-rich than andr₄₅Ti-gar₅₅ and in the assemblage pv_{ss}+gar_{ss}+hem in which hematite is present in larger amounts, however, the (640) reflection of the garnet cannot be read with great precision. The hematite reflection ($11\bar{2}6$) at $53.88^\circ 2\theta$ coincides with that of the garnet_{ss} (640). In these determinations the (642) reflection of the garnet has been measured four times.

The liquidus phases on the join andr-

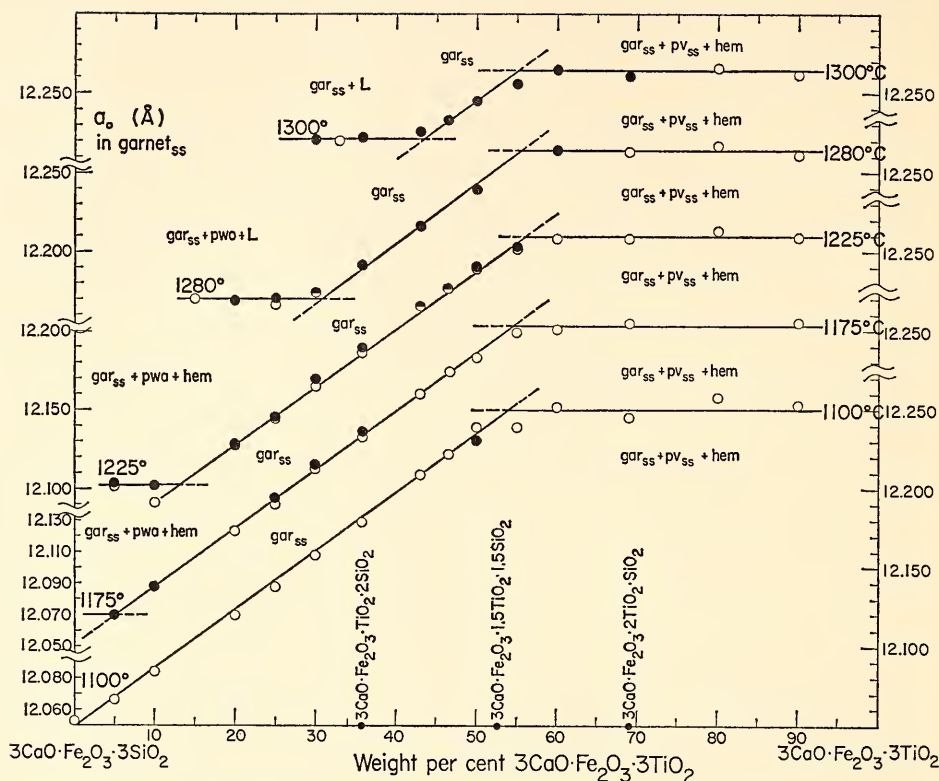


Fig. 42. Unit-cell parameters of garnets from compositions along the join andradite-Ti-garnet treated at temperatures as indicated in the diagram. Starting materials used are garnets crystallized at 1050°C (open circles) or finely powdered glasses (solid circles). Abbreviations as in Fig. 41.

Ti-gar are pseudowollastonite, garnet_{ss}, and perovskite_{ss}. The composition of the garnet that appears on the liquidus is restricted between andr₈₆Ti-gar₁₄ and andr₇₁Ti-gar₂₉. Garnet_{ss} reacts at temperatures higher than 1315° ± 2°C to pv_{ss} + liquid when the time is sufficient (>2 hours) to obtain equilibrium. The primary perovskite contains small amounts of silicon and traces of iron, as determined qualitatively by microprobe analyses, indicating a limited solid solution of CaO·SiO₂ in the perovskite. Above 1315°C the amount of perovskite_{ss} in the glass is small; below that temperature garnet_{ss} is very abundant, and the amount of glass becomes considerably smaller approaching the solidus of the garnet_{ss}. A quaternary univariant

line pierces the join andr-Ti-gar at 1310° ± 2°C and 55 wt %. The piercing point may be considered as a ternary invariant point because perovskite_{ss}, garnet_{ss}, hematite, and liquid are in equilibrium, assuming that all compositions lie on the join wo-pv-hem.

Isothermal Sections

In order to elucidate the phase relationships in the ternary system wollastonite (CaO·SiO₂)-perovskite (CaO·TiO₂)-hematite (Fe₂O₃), a series of isothermal sections at 1320°, 1312°, 1300°, 1280°, 1225°, 1175°, and 1100°C are presented. At 1320°C (Fig. 43) the stable phase assemblages on the join wo-pv-hem are *L*, hem + *L*, hem + pv_{ss} + *L*,

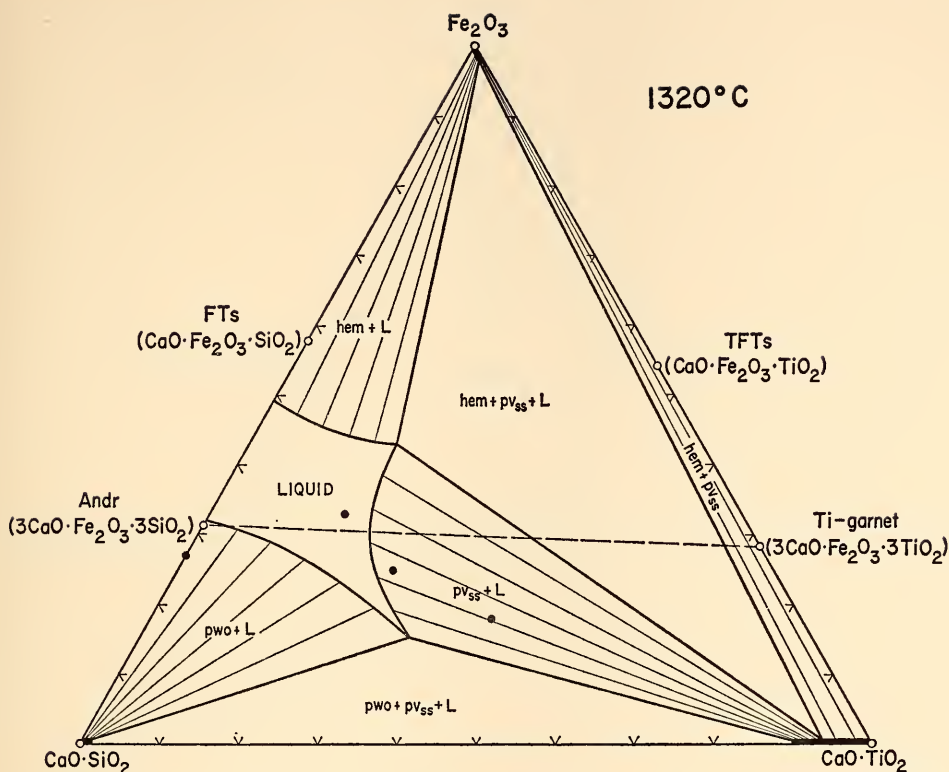


Fig. 43. Isothermal section of the wollastonite ($\text{CaO} \cdot \text{SiO}_2$)-perovskite ($\text{CaO} \cdot \text{TiO}_2$)-hematite (Fe_2O_3) join at 1320°C .

hem + pv_{ss} , $\text{pv}_{\text{ss}} + L$, $\text{pwo} + \text{pv}_{\text{ss}} + L$, and $\text{pwo} + L$. Garnet_{ss} appears on the join by the reaction $\text{perovskite}_{\text{ss}} + L \rightarrow \text{garnet}_{\text{ss}}$ at $1315^\circ \pm 2^\circ\text{C}$. Figure 44 depicts a condition slightly below this temperature. As can be seen, perovskite_{ss} is in equilibrium with a liquid either rich or poor in Fe_2O_3 . At 1300°C (Fig. 45) phase assemblages occur of gar_{ss} with either hem or pv_{ss} , or both, because perovskite_{ss} is no longer in coexistence with the liquid rich in Fe_2O_3 . The temperature for this reaction is $1310^\circ \pm 2^\circ\text{C}$, and at this temperature the liquid, garnet_{ss}, and perovskite_{ss} lie on or very close to a straight line. The three solid phases gar_{ss}, pv_{ss} , and hem, as well as the liquid, are in equilibrium, and a ternary invariant point appears in Fig. 41. The assem-

blages $\text{pv}_{\text{ss}} + L$ (Fe_2O_3 -poor) and $\text{pv}_{\text{ss}} + \text{gar}_{\text{ss}} + L$ (Fe_2O_3 -poor), still present at 1300° and 1290°C , have disappeared before the liquid reaches the binary join andr-Ti-gar at $1283^\circ \pm 2^\circ\text{C}$. $\text{Pwo} + \text{gar}_{\text{ss}} + \text{pv}_{\text{ss}}$ and $\text{pwo} + \text{gar}_{\text{ss}}$ become the stable phase assemblages, and the liquid region lies wholly on the Fe_2O_3 -rich side of the binary join andr-Ti-gar (Fig. 46). The liquid disappears from the ternary join wollastonite-perovskite-hematite between 1280° and 1225°C . The temperature was fixed in Fig. 41 at $1268^\circ \pm 2^\circ\text{C}$. From 1225°C (Fig. 47) there is a substantial increase of the garnet_{ss} series, which almost reaches the join wo-hem in the 1175°C section (Fig. 48). The garnet_{ss} has closed the gap at 1100°C

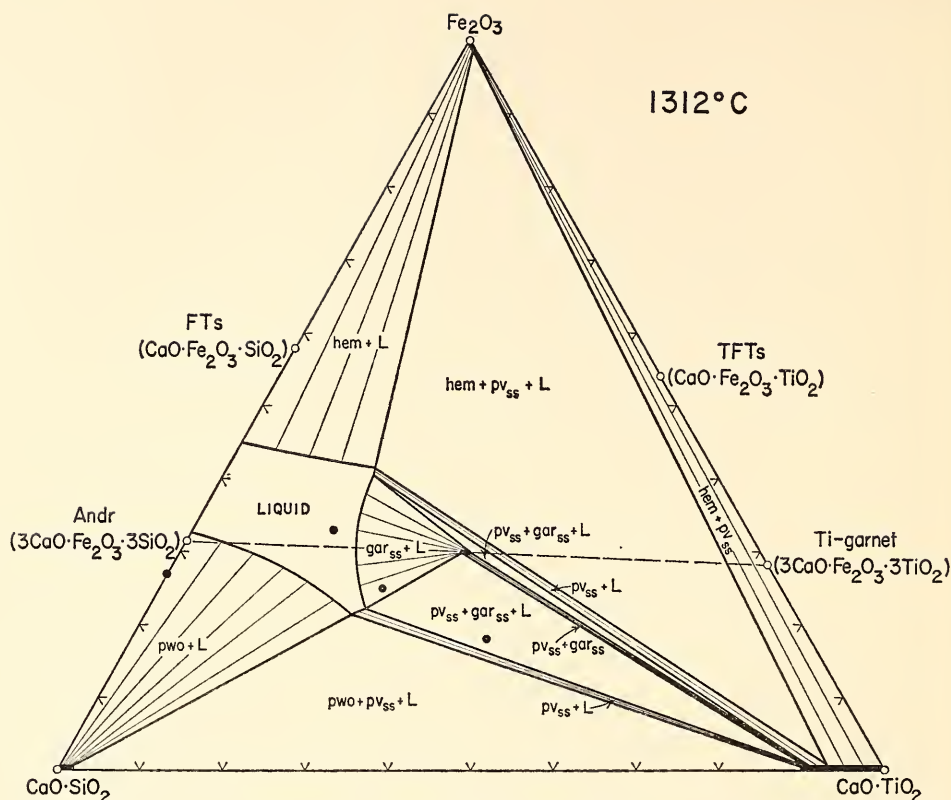


Fig. 44. Isothermal section of the wollastonite ($\text{CaO} \cdot \text{SiO}_2$)-perovskite ($\text{CaO} \cdot \text{TiO}_2$)-hematite (Fe_2O_3) join at 1312°C .

(Fig. 49). The temperature for this closure is the upper stability of pure andradite (Huckenholz, Schairer, and Yoder, *Year Book* 66).

The Join Diopside-Titanium Ferri-Tschermak's Molecule

In addition to the ternary join wollastonite-perovskite-hematite, a series of compositions were studied along the binary join diopside ($\text{CaO} \cdot \text{MgO} \cdot 2\text{SiO}_2$)-titanium ferri-Tschermak's molecule ($\text{CaO} \cdot \text{TiO}_2 \cdot \text{Fe}_2\text{O}_3$) on the plane diopside-perovskite-hematite, within the enstatite-wollastonite-perovskite-hematite system (Fig. 39), in order to obtain information about the phase relationships of clinopyroxene and garnet. The

stable phases along the join diopside (di)-titanium ferri-Tschermak's molecule (TFTs) are clinopyroxene solid solution (cpx_{ss}), garnet solid solution (gar_{ss}), hematite (hem), and perovskite solid solution (pv_{ss}) (Fig. 50). From the results obtained, clinopyroxene_{ss} and magnetite_{ss} appear on the liquidus in the di-rich part of the join. There is a very limited range of solid solution of TFTs in the diopside. The solid solution is less than 5 wt % TFTs and is believed to be of the order of 2% at temperatures between 1000° and 1150°C . Beyond 2% TFTs, clinopyroxene_{ss} is no longer stable as a single phase, and assemblages of $\text{cpx}_{\text{ss}} + \text{gar}_{\text{ss}}$, $\text{cpx}_{\text{ss}} + \text{gar}_{\text{ss}} + \text{hem}$, $\text{cpx}_{\text{ss}} + \text{gar}_{\text{ss}} + \text{hem} + \text{pv}_{\text{ss}}$, $\text{gar}_{\text{ss}} +$

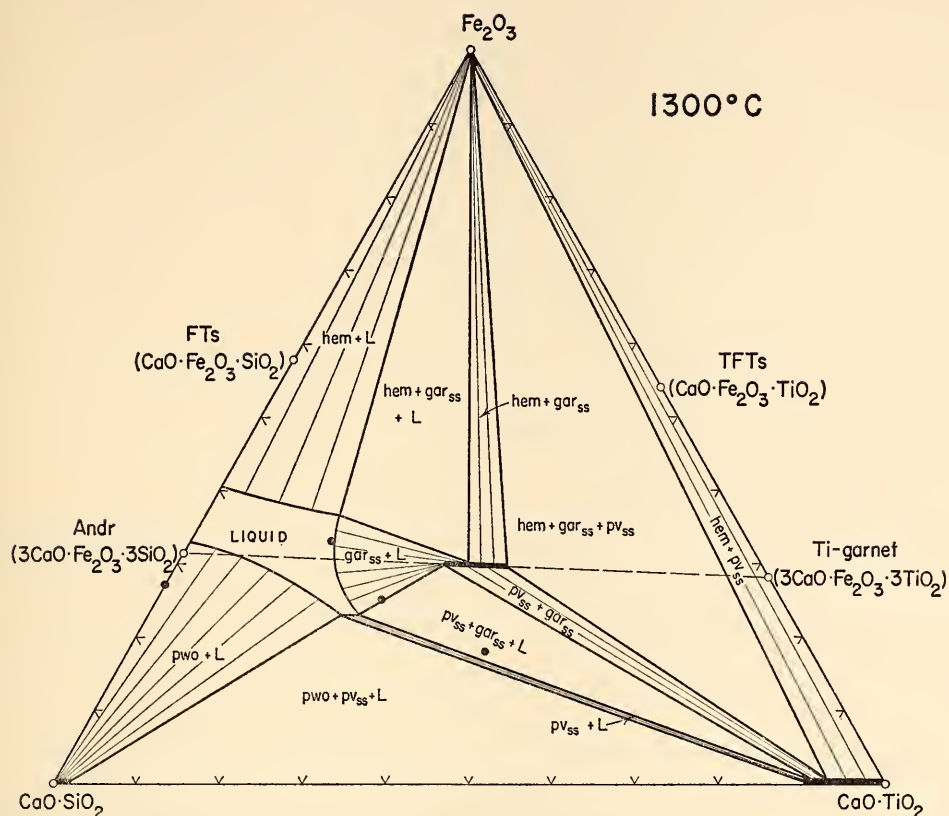


Fig. 45. Isothermal section of the wollastonite ($\text{CaO} \cdot \text{SiO}_2$)-perovskite ($\text{CaO} \cdot \text{TiO}_2$)-hematite (Fe_2O_3) join at 1300°C .

$\text{hem} + \text{pv}_{\text{ss}}$, and $\text{hem} + \text{pv}_{\text{ss}}$ are intersected by the join di-TFTs.

The cpx_{ss} in the polyphase assemblages cannot lie on the plane di-pv-hem, because tie lines from garnet solid solutions on or close to the plane wo-pv-hem in the en-wo-pv-hem system to diopside do not intersect the plane di-pv-hem. For this reason the cpx_{ss} composition must contain the enstatite component. A least-squares refinement of X-ray diffraction measurements was carried out on the composition $\text{di}_{50}\text{TFTs}_{20}$, which was treated at 1150°C for 8 days. The cell parameters ($a = 9.78 \pm 0.02 \text{ \AA}$, $b = 8.94 \pm 0.01 \text{ \AA}$, $c = 5.29 \pm 0.02 \text{ \AA}$, $V = 443.7 \pm 1.4 \text{ \AA}^3$) agree with those obtained for ferri-diopside_{ss} (Huckenholz, Schairer,

and Yoder, *Year Book 66*) within the limits of error. The angle β ($106.08^\circ \pm 0.16^\circ$) indicates, however, that the clinopyroxene is not simply ferri-diopside but is also a member of the diopside-enstatite solid solution series (Clark, Schairer, and de Neufville, *Year Book 61*). The substitution of Mg for Ca in eight-fold positions is indicated by an increase of β compared with pure diopside and ferri-diopside. Therefore, the clinopyroxene_{ss} in coexistence with garnet_{ss} is considered to be of diopside composition, containing both ferri-Tschermak's and enstatite molecules in solid solution.

The cell edges of the garnet along the join di-TFTs are 12.170 and 12.180 \AA in the two-phase volume $\text{cpx}_{\text{ss}} + \text{gar}_{\text{ss}}$; and

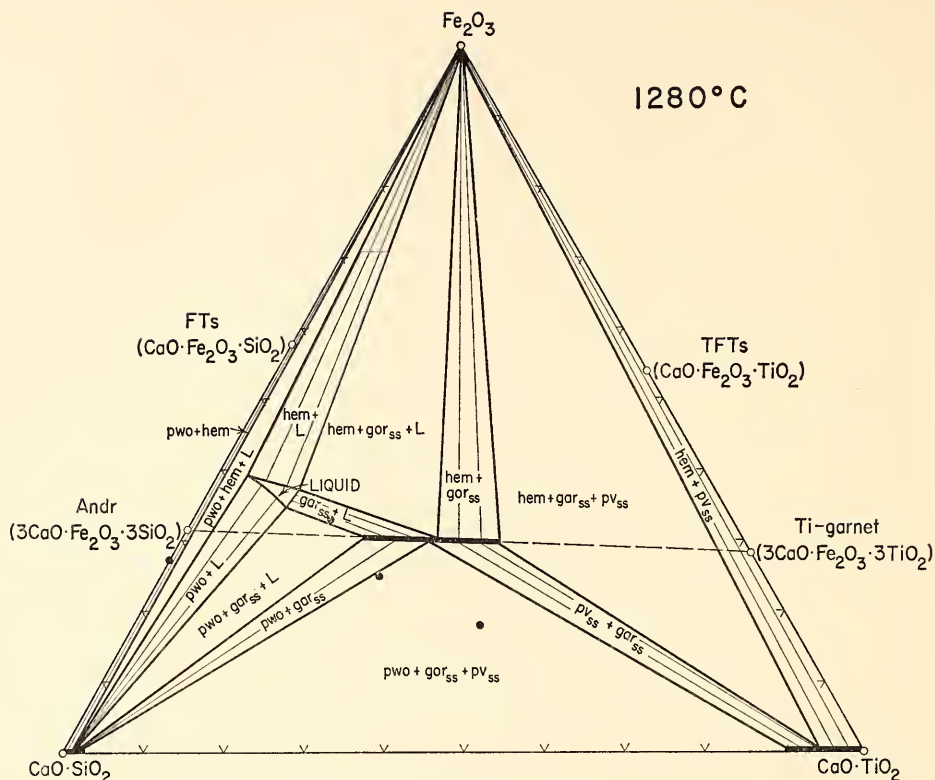


Fig. 46. Isothermal section of the wollastonite ($\text{CaO} \cdot \text{SiO}_2$)-perovskite ($\text{CaO} \cdot \text{TiO}_2$)-hematite (Fe_2O_3) join at 1280°C .

12.207, 12.208, and 12.201 \AA in the three-phase volume $\text{cpx}_{\text{ss}} + \text{gar}_{\text{ss}} + \text{hem}$, respectively. These cell edges refer to the solid solution series of andradite-Ti-garnet. The relationship will probably change, however, if Mg enters the andradite structure. There is a very limited substitution for andradite ($3\text{CaO} \cdot \text{Fe}_2\text{O}_3 \cdot 3\text{SiO}_2$) of khoharite ($3\text{MgO} \cdot \text{Fe}_2\text{O}_3 \cdot 3\text{SiO}_2$), as demonstrated by Huckenholz, Schairer, and Yoder (*Year Book 66*). The substitution of MgTi^{4+} for 2Fe^{3+} was tested for this investigation along the join andradite ($3\text{CaO} \cdot \text{Fe}_2\text{O}_3 \cdot 3\text{SiO}_2$)-Mg-melanite ($3\text{CaO} \cdot \text{MgO} \cdot \text{TiO}_2 \cdot 3\text{SiO}_2$) (Fig. 39). Compositions of $\text{andr}_{66.7}\text{Mg-mela}_{33.3}$ and $\text{andr}_0\text{Mg-mela}_{100}$ were treated at temperatures of 1050° , 1150° , and 1200°C . Polyphase assemblages of

$\text{garnet}_{\text{ss}} + \text{wollastonite} + \text{melilite}_{\text{ss}}$ and of $\text{clinopyroxene}_{\text{ss}} + \text{perovskite}_{\text{ss}} + \text{melilite}_{\text{ss}}$, respectively, were obtained under the applied conditions. The garnet of the $\text{andr}_{66.7}\text{Mg-mela}_{33.3}$ composition treated at 1150°C has a cell edge of $12.129 \pm 0.003 \text{ \AA}$. It cannot be unambiguously ascertained whether this $\text{garnet}_{\text{ss}}$ belongs to the solid solution series of andradite-Ti-garnet or of andradite-Ti-garnet-Mg-melanite. The substitution of MgTi^{4+} for 2Fe^{3+} will not substantially change the cell edge of the $\text{garnet}_{\text{ss}}$ because the interatomic distances of O to Fe^{3+} ($\text{Fe}^{3+}\text{-O} = 2.01 \text{ \AA}$), Mg ($\text{Mg-O} = 2.07 \text{ \AA}$), and Ti^{4+} ($\text{Ti}^{4+}\text{-O} = 2.01 \text{ \AA}$) for six-fold coordination are very similar. At present, the garnets stable on the join andradite-Mg-

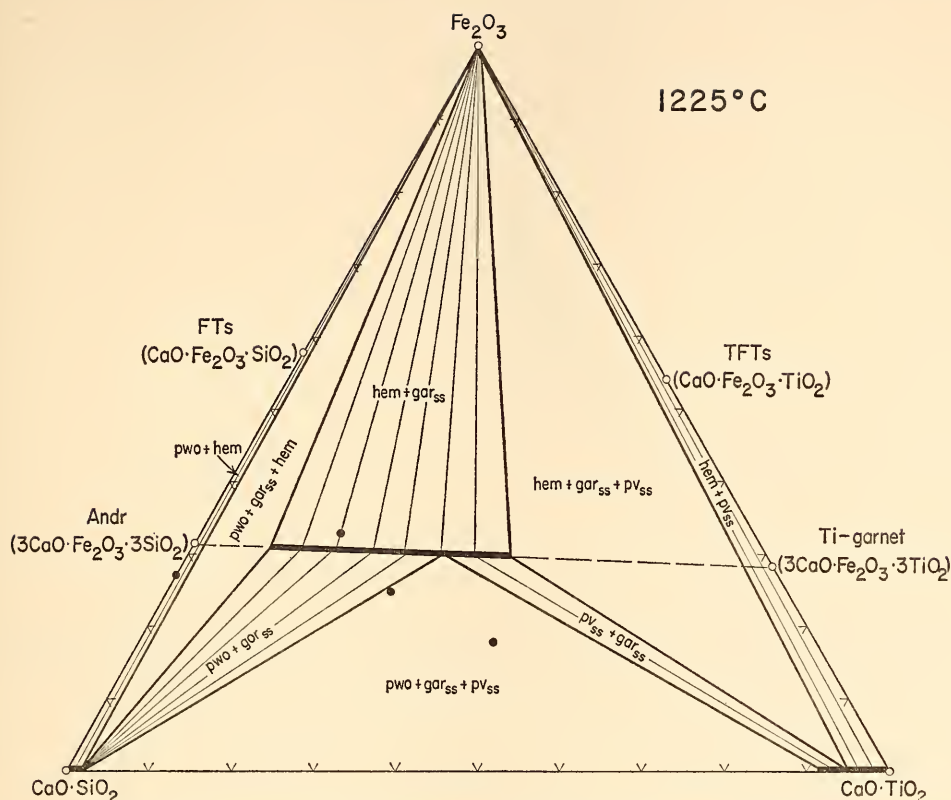


Fig. 47. Isothermal section of the wollastonite ($\text{CaO} \cdot \text{SiO}_2$)-perovskite ($\text{CaO} \cdot \text{TiO}_2$)-hematite (Fe_2O_3) join at 1225°C .

melanite and on the join di-TFTs are considered to be members of an andradite-Ti-garnet-Mg-melanite solid solution series containing less than 33.3 wt % of an Mg-melanite component. However, the Mg-melanite component does not appear to exceed 20 wt % in natural Ti-rich garnets.

Geologic Discussion

The most common rock types in which Ti-bearing garnets are abundant minerals belong to the nepheline syenite and ijolite families. They are often directly related to carbonatites and their alteration products, the fenites. The main feature of these rocks is the presence

of the mafic mineral association of clinopyroxenes and of Ti-bearing garnets (reported as melanite, schorlomite, and iiaavarite). Wollastonite, perovskite, and iron ores (magnetite, titanomagnetite, ilmenite, and occasionally hematite) are sometimes abundant phases too. Biotite, amphibole, and sphene may also occur.

The composition of the clinopyroxene varies from aegirine or aegirine-augite to diopside, sometimes rich in ferri-Tschermak's molecule. Even pigeonitic augites that contain melanite are reported from a pyroxenite and foyaite-porphyrite dike, from Alnö, Sweden (von Eckermann, 1948, 61 and 91). The associated garnet is andraditic in composition in most cases and contains in

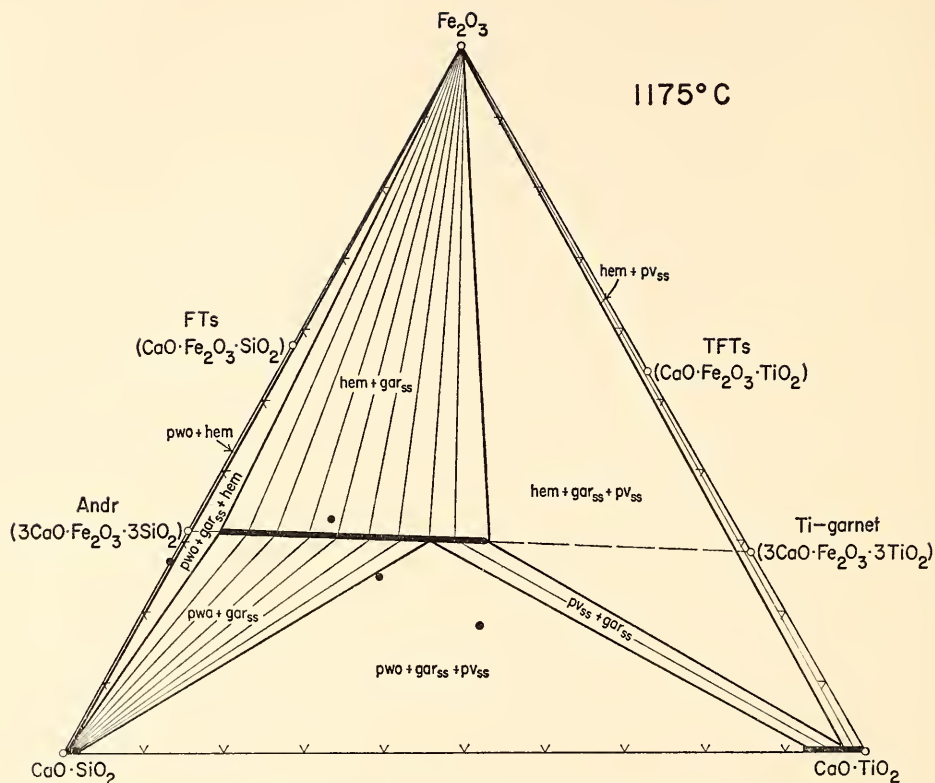


Fig. 48. Isothermal section of the wollastonite ($\text{CaO} \cdot \text{SiO}_2$)-perovskite ($\text{CaO} \cdot \text{TiO}_2$)-hematite (Fe_2O_3) join at 1175°C .

addition other components, as illustrated in Table 8. In 60 analyses of Ti-bearing garnets a relatively high Ti content in addition to Fe^{3+} is always related to a low Al content. This is in direct contrast to the associated pyroxenes: their Ti-content increases with increasing Al, a behavior outlined in general for clinopyroxenes by Kushiro (1960). Unfortunately, data about coexisting clinopyroxenes and garnets from alkaline igneous rock are rare. Examples are known from ijolites from Iron Hill, Colorado (Lar-

sen, 1941), the Napak volcanoes, Uganda (King, 1949), and the alkalic igneous complex at Magnet Cove, Arkansas (Erickson and Blade, 1963), and from a wollastonite-melanite melteigite from the alkaline complex at Oka, Quebec (Gold, 1966). The coexisting minerals or minerals from different hand specimens of similar rocks were plotted on an atomic Ti- Fe^{3+} -Al basis in Fig. 51. It can be seen that the Napak garnet, relatively high in Al, has a very low Ti content. The Magnet Cove garnet is low

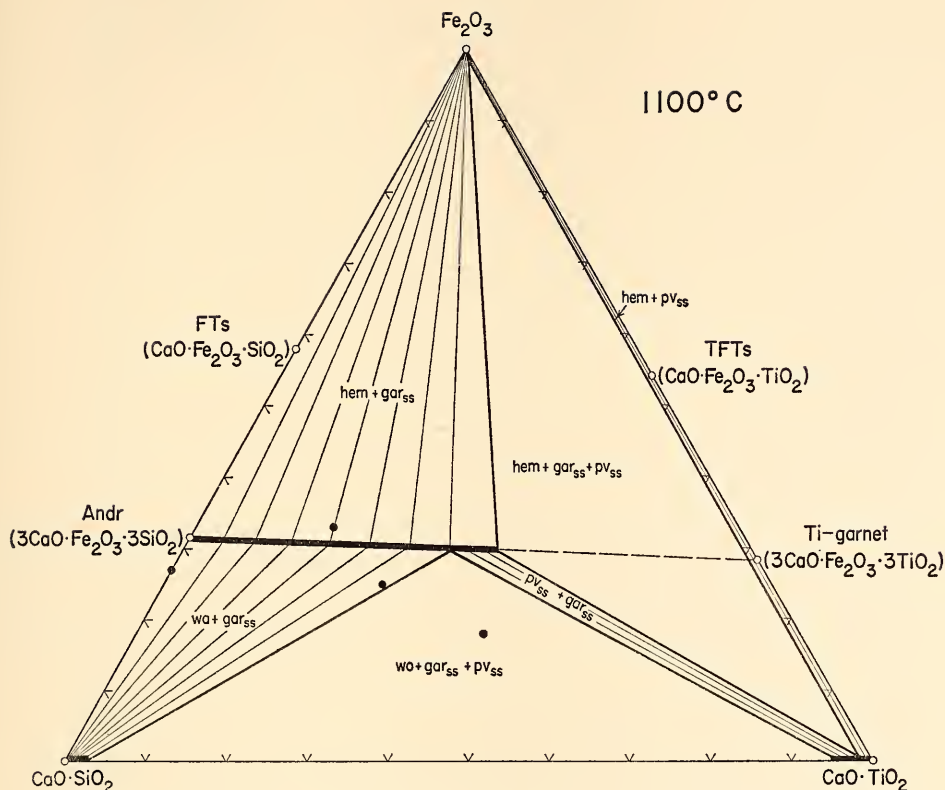


Fig. 49. Isothermal section of the wollastonite ($\text{CaO} \cdot \text{SiO}_2$)-perovskite ($\text{CaO} \cdot \text{TiO}_2$)-hematite (Fe_2O_3) join at 1100°C .

in Al but is very high in Ti. An intermediate position is held by the garnet from Iron Hill. The Oka garnet is almost a pure andradite, having only traces of Al and a low Ti content. It can be concluded, therefore, that Al-rich granulites are not expected to be rich in Ti.

The phase relationships in the ternary joins diopside-wollastonite-hematite (Huckenholz, Schairer, and Yoder, *Year Book 66*, p. 344), wollastonite-perovskite-hematite, and diopside-perovskite-hematite, and the binary join andradite-Mg-

melanite, as well as the behavior of natural clinopyroxenes under oxidizing conditions (Huckenholz, elsewhere in this report), bear directly on the formation of andradite and its Ti-rich varieties under magmatic conditions. The results of these studies suggest the concept that the appearance of Ti-bearing garnets and ferri-diopsides is the natural consequence of crystallization at or near atmospheric conditions and is not necessarily the result of unique deep-seated processes.



Fig. 50. Temperature-versus-composition plot of data obtained on the join diopside-titanium ferri-Tschermak's molecule at 1 atm. Abbreviations of phases encountered: cpx_{ss} , clinopyroxene solid solution; gar_{ss} , garnet solid solution; hem , hematite; mt_{ss} , magnetite solid solution; and pv_{ss} , perovskite solid solution. Numbers refer to unit-cell parameters of the coexisting garnet solid solutions.

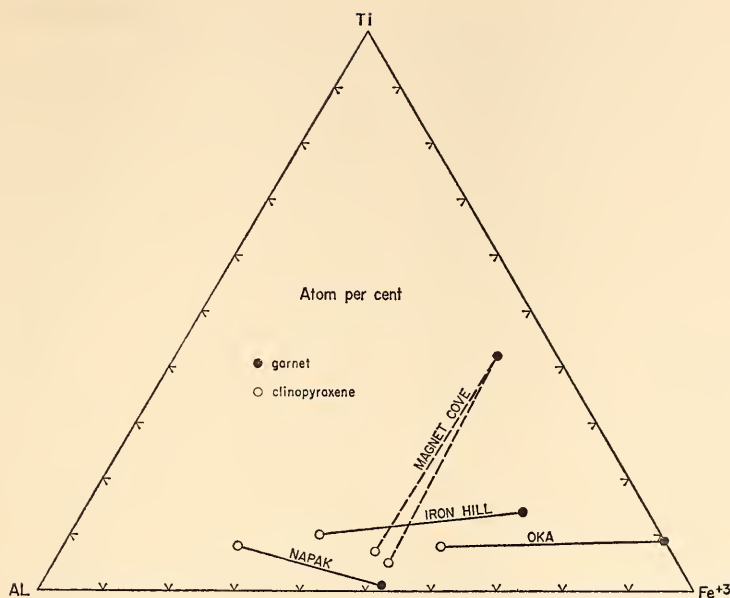


Fig. 51. Coexisting clinopyroxenes and Ti-bearing garnets from alkaline igneous complexes: (1) Iron Hill, Colorado; sodian augite and melanite from ijolite IH-129 (Larsen, 1941). (2) Napak, Uganda; aegirine augite and melanite from ijolite K.352 and K.372, respectively (King, 1949). (3) Magnet Cove, Arkansas; diopside from biotite-garnet ijolite L-123-6 and L-123-7, garnet from biotite-garnet ijolite MC-216-8 (Erickson and Blade, 1963). (4) Oka, Quebec; sodian augite and melanite from wollastonite-melanite melteigite DDH G 15, 330 feet (Gold, 1966).

SILICATE SYSTEMS INCLUDING A VAPOR PHASE

MELTING OF FORSTERITE AND ENSTATITE AT HIGH PRESSURES UNDER HYDROUS CONDITIONS

I. Kushiro and H. S. Yoder, Jr.

The effects of water on the melting behavior of forsterite (Mg_2SiO_4) and enstatite (MgSiO_3), the main constituents of peridotites, have been studied in the pressure range of 2 to 30 kb. The modified gas-media apparatus designed by Yoder (1950) was used for runs conducted at and below 10 kb, and a piston-cylinder, solid-media apparatus similar to that designed by Boyd and England (1960) was used for runs above 10 kb. Sealed platinum capsules with an outside diameter of 3.0 mm were used for the gas-media apparatus, and sealed platinum capsules with an outside diameter of 1.8 mm were used for the piston-

cylinder apparatus. The water content ranged from 3.8 to about 50 wt %. In the piston-cylinder apparatus, the vacant space between the capsule and the ceramic sleeve was filled with powdered crushable alumina in order to reduce the deformation of the capsule. Starting materials were MgSiO_3 glass made by the late Dr. N. L. Bowen, orthoenstatite crystallized from the MgSiO_3 glass at 10 kb, and pure forsterite synthesized with the help of Dr. J. F. Schairer.

Melting of Forsterite

The beginning of melting of forsterite under hydrous conditions is considerably lower than under anhydrous conditions at the same pressure. At 10 kb, clear granular crystals of forsterite (0.03–0.15 mm in diameter) were obtained from finely ground forsterite exposed to H_2O at temperatures between 1350° and

1500°C. On the other hand, opaque-looking, irregular crystals of forsterite containing numerous fine bubblelike inclusions, sometimes arranged regularly to form a herringbonelike texture, were obtained when the same starting materials were held at 1525°C. The inclusions are glass and liquid with or without gas bubbles and are probably formed from liquid and vapor that existed at the pressure and temperature of the runs and was trapped in rapidly grown forsterite crystals during the quenching. The relatively opaque-looking forsterite crystals with numerous inclusions are, therefore, interpreted to be quench crystals. In some liquid inclusions, a bubble exists and is observed moving rapidly, probably due to the Brownian action of the liquid. Because of the distinct difference between the melted and the unmelted textures of forsterite, the temperature of the beginning of melting of forsterite can be located with precision between 1500° and 1525°C at 10 kb.

At 20 kb the same distinct difference in texture was observed between the runs made at 1400° and 1425°C for H₂O contents greater than at least 23 wt %. In runs with H₂O contents of about 12 and 15 wt %, however, clear granular forsterite crystals coexist with quench forsterite crystals at 1425° and 1450°. Theoretically, complete melting occurs in the vapor-present region (excess water region), whereas forsterite crystals can exist stably at temperatures above the beginning of melting in the vapor-absent region (water-deficient region), although the temperatures of the beginning of melting are the same for both the water-deficient and excess-water regions. The experiments with 12 and 15 wt % H₂O are interpreted, therefore, as being in the water-deficient region. The maximum content of water that dissolves in a forsterite melt is, therefore, between 15 and 23 wt % at 20 kb. At 10 kb the run with 10.0 wt % H₂O does not contain primary forsterite at a temperature just above the melting temperature, and thus

the maximum water content in the liquid is less than 10 wt %.

Fig. 52 shows the beginning of melting of forsterite determined on the basis of the runs in the excess-water region. As shown in the figure, the melting temperature drops greatly with increasing pressure under hydrous conditions. The temperature of melting of forsterite at 20 kb under hydrous conditions, determined by Sclar, Carrison, and Stewart (1968a) by a belt apparatus, is about 80°C lower than the present data. The temperature difference between the melting curve under anhydrous conditions determined by Davis and England (1964) and that under hydrous conditions is about 450°C at 10 kb and about 670°C at 30 kb. The dT/dP of the melting curve probably becomes smaller with further increase of pressure. This results from the smaller volume difference between forsterite + vapor and liquid with increasing pressure due to the larger compression of vapor relative to liquid at high pressures.

Melting of Enstatite

Sixty runs have been carried out on the MgSiO₃ composition with various amounts of water in the pressure range 2 to 30 kb. The detailed results are given in a separate paper (Kushiro, Yoder, and Nishikawa, 1968), and a brief summary is reported here.

The temperatures of the beginning of melting of enstatite are 1360° ± 15° at 10 kb, 1280° ± 15° at 20 kb, and 1270° ± 15°C at 30 kb, as shown in Fig. 53. Just above these temperatures, euhedral to subhedral crystals of forsterite, as well as herringbonelike and radially grown crystals with or without patches of glass, glass globules, and glass coatings on very thin needlelike crystals, which may be enstatite, were obtained in the pressure range 10 to 30 kb. The herringbone-like and radially grown crystals are considered to be quench crystals; that is, they were formed from liquid during the quenching. The quench crystals consist

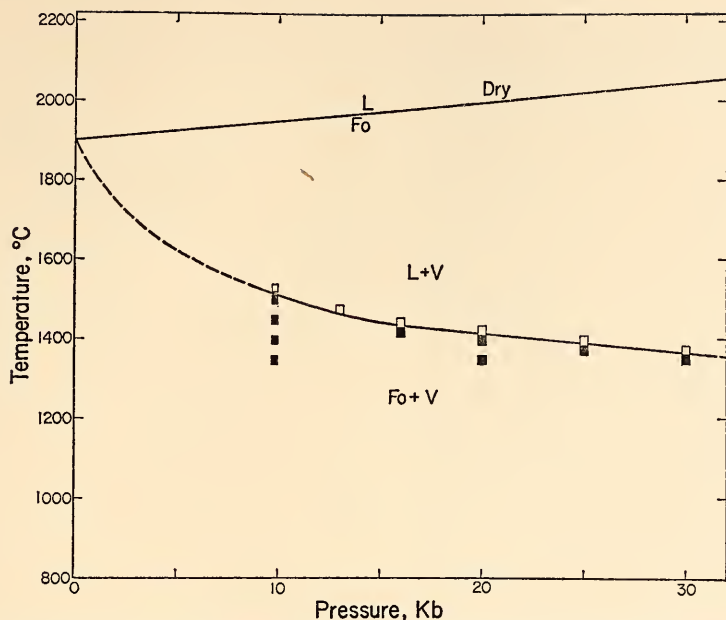


Fig. 52. Melting curve of forsterite under water-saturated conditions. Melting curve of forsterite under anhydrous conditions is from Davis and England (1964). Fo, forsterite; L, liquid; V, vapor.

of orthoenstatite or orthoenstatite separating forsterite and quartz. The presence of forsterite and quartz, although not in contact, clearly represents a metastable assemblage. The glass globules and coatings are concentrated more along the inner surface of capsules and have refractive indices lower than those of patches of glass quenched from liquid. They are considered to be quenched vapor; that is, they were formed directly from the materials in the vapor that existed during the runs.

Formation of the forsterite+liquid+vapor assemblage from $\text{MgSiO}_3 + \text{H}_2\text{O}$ composition indicates the incongruent melting of enstatite in the presence of water vapor. The temperature interval where forsterite and liquid coexist depends on the water content, and these relations are shown on the $\text{MgSiO}_3\text{-H}_2\text{O}$ join at 10 kb (Fig. 54). For H_2O contents less than 11 wt %, forsterite coexists with enstatite and liquid or with liquid only, whereas for H_2O contents greater

than 11 wt %, forsterite coexists with liquid and vapor. The upper temperature limit of the presence of forsterite ranges from about 1400° to about 1540°C in the water-deficient region, and from about 1400°C to somewhat higher temperatures ($+10^\circ$ to $\sim 20^\circ$) in the excess-water region for H_2O contents of 11 to 30 wt %. The upper temperature limit of the forsterite+liquid+vapor region in Fig. 53 is for limited H_2O saturation (less than 50 wt % H_2O). Above the forsterite+liquid+vapor region, liquid and vapor coexist, as shown by the evidence of quench crystals and materials quenched from vapor.

At temperatures below the beginning of melting and above 1000°C , prismatic enstatite (0.01–0.1 mm in length) with small amounts of round forsterite and glass globules and coatings on very thin needlelike crystals is obtained in most of the runs. The glass globules and coatings are considered to be materials quenched from vapor. The presence of

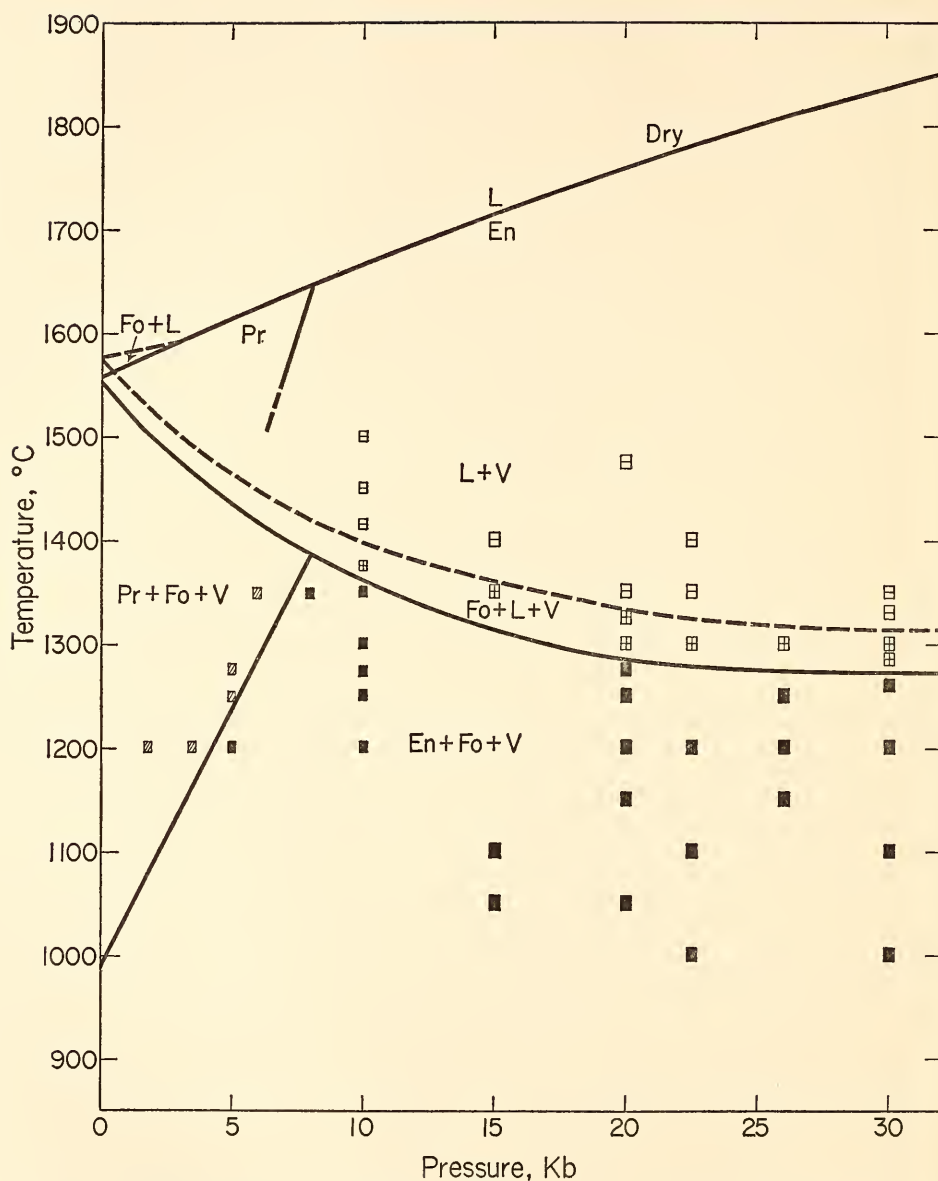


Fig. 53. Melting relations for MgSiO_3 composition under water-saturated conditions. The upper limit of the $\text{Fo} + \text{L} + \text{V}$ field is a projected liquidus for limited excess water (<50 wt %). The melting relations under anhydrous conditions are from Boyd, England, and Davis (1964). The inversion point between orthoenstatite and protoenstatite at 1 atm is from Atlas (1952). En, orthoenstatite; Pr, protoenstatite; other abbreviations as in Fig. 52.

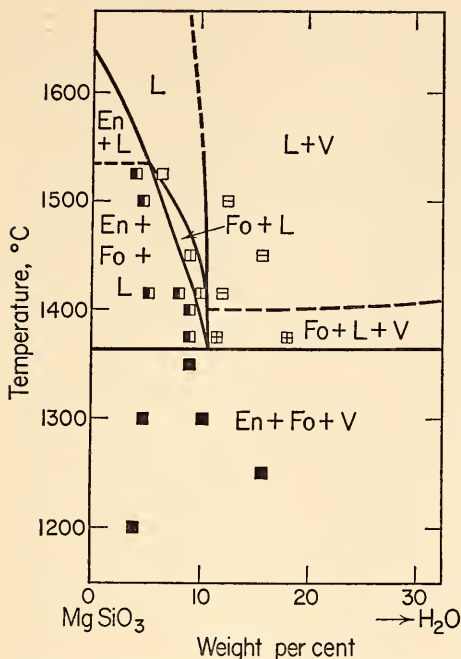


Fig. 54. Phase-equilibrium relations on the join $\text{MgSiO}_3\text{-H}_2\text{O}$ at 10 kb. Abbreviations as in Figs. 52 and 53.

a small amount of forsterite indicates that the vapor dissolves excess silica (that is, silica in excess of the proportionate amount in MgSiO_3).

Application of Results

The most important result of the present experiments is that enstatite melts incongruently to forsterite and liquid in the presence of water in the pressure range of at least 10 to 30 kb. Under anhydrous conditions, the incongruent melting of enstatite terminates at pressures higher than about 5 kb (Boyd, England, and Davis, 1964). Even if the water content is small (in the vapor-absent or water-deficient region), enstatite still melts incongruently to form enstatite, forsterite, and liquid. The liquids coexisting with forsterite in the water-deficient region are silica saturated or more silica rich than the proportion for the MgSiO_3 composition. This

is an important conclusion, which bears on the origin of silica-saturated magmas, such as quartz-tholeiite magma.

If partial melting of a rock consisting of enstatite and forsterite with a small amount of uncombined water takes place at pressures up to at least 30 kb, the first liquid to form is silica saturated and water saturated, containing 11 wt % water or more. With increasing temperature the amount of liquid increases, the water content in the liquid decreases, and the degree of silica saturation decreases; however, the liquids are still silica saturated. The presence of diopside does not change this conclusion (Kushiro, elsewhere in this report). Although the present system is far simpler than natural rocks, it is suggested that silica-saturated magmas could be generated by partial melting of the upper-mantle material, believed to be olivine-rich lherzolite, in the presence of a small amount of uncombined water at depths at least down to 100 km.

The present results also may be applicable to the formation of silica-saturated magmas by fractional crystallization of basaltic magmas containing water at high pressures. If crystallization of a magma, just silica saturated and containing a small amount of water, takes place at high pressures, forsterite will crystallize with enstatite with lowering temperature, and residual liquids will become silica saturated. With further decrease of temperature, the degree of silica saturation will increase.

As shown in Figs. 52 and 53, the temperatures of the beginning of melting of forsterite and enstatite, which have been determined in the presence of excess vapor ($P_{\text{H}_2\text{O}} = P_{\text{total}}$), are surprisingly low at high pressures. Some of the possible geotherms (e.g., oceanic geotherm, Clark and Ringwood, 1964) approach closely even to the beginning of melting of forsterite under hydrous conditions (Fig. 52) at pressures higher than 30 kb. For a mixture of forsterite and enstatite, melting begins to take

place at temperatures on the curve shown in Fig. 53, when the water pressure is equal to total pressure. It is suggested, therefore, that if the water pressure is equal to or close to total pressure at depths near 100 km or deeper in the upper mantle, melting of these parts may begin to take place. Water pressure in the upper mantle may be equal to or close to total pressure if water vapor or fluid exists as a separate phase in the upper mantle, regardless of its amount.

LIQUIDUS RELATIONS IN THE SYSTEM FORSTERITE-DIOPSIDE-SILICA-H₂O AT 20 KB

I. Kushiro

The system forsterite-diopside-silica, one of the most important systems for the understanding of the crystallization of basaltic magmas, has been studied at 20 kb under hydrous conditions in order to determine the effect of water on the course of crystallization of basaltic magmas at high pressures.

All the runs were carried out with a piston-cylinder, solid-media apparatus similar to that designed by Boyd and England (1960). Sealed platinum capsules with water contents of 25 to 50 wt % were used, and all the charges were wet after the runs. A small vacant space between the capsule and the ceramic sleeve was filled with powdered crushable alumina to reduce the deformation of the capsule. Twenty-two compositions were selected in the system forsterite-diopside-silica. The starting materials for fifteen compositions were crystallized glass prepared by Schairer and Yoder (*Year Book 61*, pp. 75-82), Kushiro and Schairer (*Year Book 62*, pp. 95-103), and Boyd and Schairer (1964). Mechanical mixtures of cristobalite, clinoenstatite, and diopside were used for seven compositions.

The System Forsterite-Silica-H₂O

The results of the runs on the system forsterite-silica-H₂O at 20 kb are shown

in Fig. 55, which is a projection of the ternary system onto the join forsterite-silica from the H₂O apex. The mixtures of compositions more silica rich than Fo₄₀Qz₆₀ are mechanical mixtures of clinoenstatite and cristobalite. The results on the Mg₂SiO₄ and MgSiO₃ compositions are from Kushiro and Yoder (elsewhere in this report). As shown in Fig. 55, the melting temperature of silica (quartz) is greatly lowered as compared with that of enstatite; consequently, the primary phase field of enstatite is greatly expanded toward silica and the primary phase field of quartz is greatly reduced, as compared with those at 1 atm given by Bowen and Andersen (1914) and Greig (1927). The forsterite liquidus extends beyond enstatite composition to about Fo₆₁Qz₃₉, where forsterite reacts with liquid to form enstatite in the presence of vapor. The "eutectic point" between enstatite and quartz, which is a projection of a point on the four-phase curve En + Qz + V + L (or an isobaric invariant point) exists at about Fo₁₄Qz₈₆ composition.

All the runs quenched from temperatures above the solidus contain glass that has numerous bubble inclusions. Glass globules, which are probably quenched vapor (Kushiro and Yoder, this report), were also obtained, except for compositions close to silica (>85 wt % SiO₂), indicating that vapor was present during the runs. It is not certain, however, whether both vapor and liquid or only a supercritical fluid existed above the solidus for compositions close to silica. In the En + L + V region, orthoenstatite crystals are prismatic and euhedral, and are most likely stable. It is possible, however, that metastable enstatite persists even above the solidus. To test this possibility, the mixture of composition Fo₂₆Qz₈₀ was held at 1250°C (well above the liquidus) for 45 minutes and then at 1100°C (just below the liquidus) for 90 minutes. In this run a small amount of large crystals of euhedral enstatite was obtained. It is

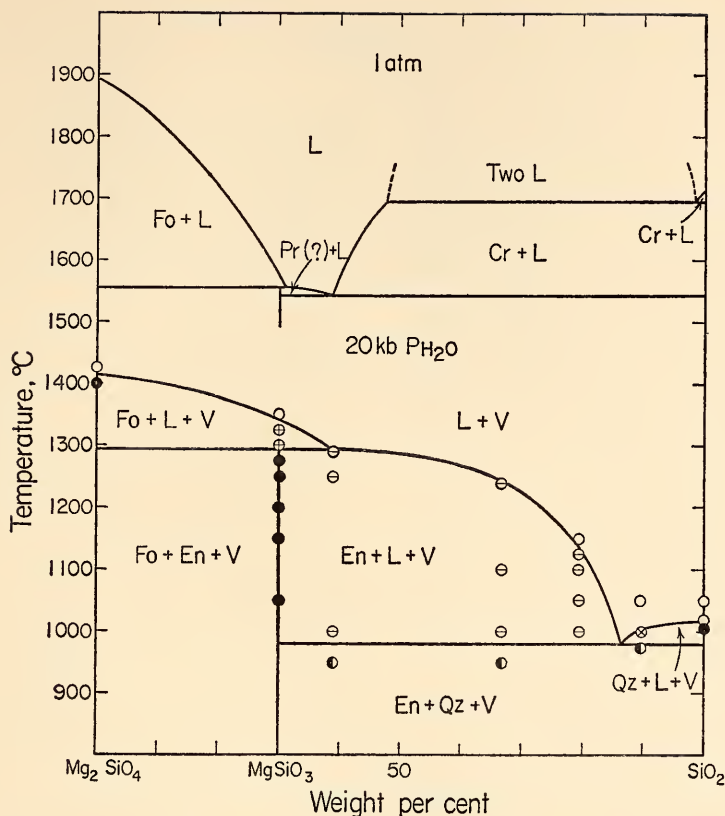


Fig. 55. Projection of the system forsterite (Mg_2SiO_4)-silica-water at $P_{\text{H}_2\text{O}} = 20$ kb. Phase relations at 1 atm are from Bowen and Andersen (1914) and Greig (1927). Cr, cristobalite; En, orthoenstatite; Fo, forsterite; L, liquid; Pr, protoenstatite; Qz, quartz; V, vapor.

concluded that the liquidus of enstatite shown in Fig. 55 is not metastable.

Quartz crystals in the $\text{Qz} + \text{L} + \text{V}$ region showed round or square forms and appeared to be high quartz, although those with double terminated pyramids were rarely observed.

The System Forsterite-Diopside-Silica- H_2O

The liquidus boundaries between the fields of forsterite, diopside, and enstatite solid solutions and quartz at 20 kb under hydrous conditions are shown in Fig. 56. They have been determined in the presence of excess vapor ($P_{\text{H}_2\text{O}} = P_{\text{total}}$) and are projections of the bound-

aries between the primary, solid-phase volumes in the quaternary system onto the forsterite-diopside-silica plane from the H_2O apex.

As shown in Fig. 56, the liquidus fields of both enstatite and diopside solid solutions are greatly expanded toward silica and the liquidus field of quartz is much reduced as compared with those at 1 atm. The forsterite field covers the enstatite-rich part of the diopside-enstatite join, as at 1 atm, indicating that forsterite reacts with an array of liquids to form enstatite solid solution in the presence of water vapor. The forsterite-enstatite_{ss} liquidus boundary is more silica rich than at 1 atm, whereas the forsterite-diopside_{ss} liquidus boundary is, for the

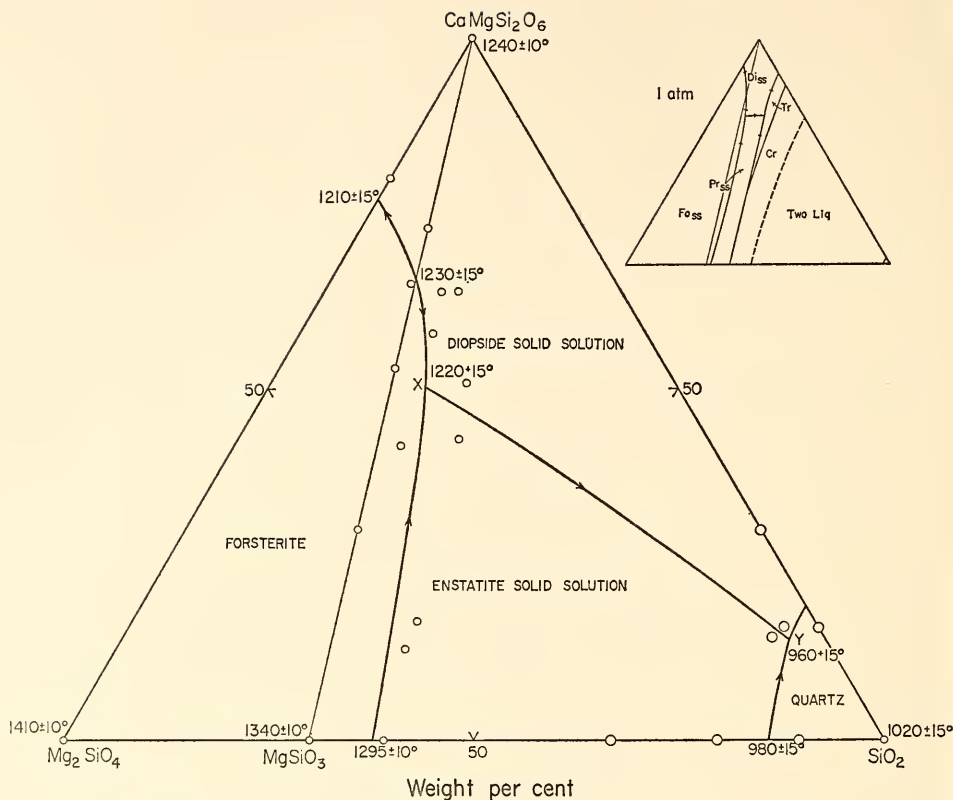


Fig. 56. Projection of the liquidus boundaries in the system forsterite (Mg_2SiO_4)-diopside ($\text{CaMgSi}_2\text{O}_6$)-silica-water at $P_{\text{H}_2\text{O}} = 20$ kb. Liquidus diagram of the system forsterite-diopside-silica at 1 atm shown in the upper right is from Bowen (1914), Schairer and Yoder (*Year Book 61*, pp. 75-82), and Kushiro and Schairer (*Year Book 62*, pp. 95-103).

most part, more forsterite rich than at 1 atm. Forsterite crystallizing near the liquidus temperature at 20 kb $P_{\text{H}_2\text{O}}$ is essentially pure forsterite, as inferred from the reflections in the X-ray powder diffraction pattern.

On the forsterite-pyroxene liquidus boundary is a projection of a point on the five-phase curve $\text{Fo} + \text{En}_{\text{ss}} + \text{Di}_{\text{ss}} + L + V$ (X in Fig. 56) (or an isobaric invariant point), which is a reaction point where forsterite reacts with liquid to form enstatite_{ss} and diopside_{ss} in the presence of vapor. The forsterite-diopside_{ss} liquidus boundary probably has a temperature maximum between the joins diopside-enstatite and forsterite-diopside, and its temperature probably drops

continuously from this maximum to a critically silica-undersaturated composition lying on the other side of the forsterite-diopside join, as at 1 atm. The join forsterite-diopside is not binary, because diopside crystallizing from this join is not pure diopside but a solid solution containing a small amount of enstatite, as inferred from the $2\theta(311)-2\theta(310)$ value in the X-ray powder diffraction pattern (Kushiro and Schairer, *Year Book 62*, p. 99).

The projection of another isobaric invariant point, $\text{En}_{\text{ss}} + \text{Di}_{\text{ss}} + \text{Qz} + L + V$, exists close to SiO_2 (Y in Fig. 56). In the present experiments, it was not determined whether this is a reaction point or a eutectic point. The temperature of

the diopside_{ss}-enstatite_{ss} liquidus boundary drops from $1220^{\circ} \pm 15^{\circ}\text{C}$ at *X* to $960^{\circ} \pm 20^{\circ}\text{C}$ at *Y*

The system forsterite-diopside-silica-H₂O includes the following common rock-forming hydrous minerals: serpentine [$\text{Mg}_3\text{Si}_2\text{O}_5(\text{OH})_4$], talc [$\text{Mg}_6\text{Si}_8\text{O}_{20}(\text{OH})_4$], anthophyllite [$\text{Mg}_7\text{Si}_8\text{O}_{22}(\text{OH})_2$], and tremolite [$\text{Ca}_2\text{Mg}_5\text{Si}_8\text{O}_{22}(\text{OH})_2$]. In the present experiments, conducted at temperatures above 950°C , however, none of these hydrous minerals was encountered. Tremolite is stable up to the highest temperature, about 880°C at 2 kb (Boyd, 1959). The volume change (ΔV) of the reaction tremolite = 2 diopside + 3 enstatite + quartz + H₂O can be expressed as $\Delta V = -24.9 + V_{\text{H}_2\text{O}}$ (cc) and can be calculated by the use of the molar volume of water ($V_{\text{H}_2\text{O}}$) given by Rice and Walsh (1957) for a wide pressure-temperature range. It was found that the ΔV has a negative value at pressures above about 6 kb $P_{\text{H}_2\text{O}}$, indicating that the breakdown curve of tremolite has a negative slope at these pressures. On the basis of the experimental data at low pressures and the calculated volume change, it is expected that the upper limit of the stability field of tremolite at 20 kb $P_{\text{H}_2\text{O}}$ is near 850°C , which is below the temperatures of the present experiments.

The present experimental results may have an important bearing on the origin of silica-rich magmas such as andesite, dacite, and rhyolite, which commonly occur in orogenic regions. From the liquidus relations given in Fig. 56, it is expected that liquid undersaturated with silica can produce silica-rich magmas by fractional crystallization. By maximum fractionation at 20 kb $P_{\text{H}_2\text{O}}$, the residual liquids attain the isobaric invariant point *Y*, the silica content of which is about 80 wt %. It is suggested that if fractional crystallization of olivine tholeiitic magmas containing water takes place at pressures up to at least 20 kb, magmas more silica rich than basalts, such as andesite, dacite, and

rhyolite magmas, will be produced. Even if the water content of the original magma was small, the same conclusion would be obtained in the light of the results on the melting of enstatite (Kushiro and Yoder, this report). It should be noted that high pressure is not necessarily required for the formation of silica-rich magmas, which can be produced by the fractional crystallization of water-bearing basaltic magmas at pressures of 5 kb or even less. In natural water-bearing basalt magmas the crystallization of amphibole may affect the course of fractional crystallization.

The present experimental results may also have a bearing on the generation of silica-saturated basaltic magmas in an upper mantle composed of olivine-rich lherzolite. In this model, under anhydrous conditions silica-saturated magmas can be formed only at pressures below 6 and 7 kb either by the partial melting of the lherzolite or by the fractional crystallization of olivine tholeiitic magmas (Kushiro, 1968b). Under hydrous conditions ($P_{\text{H}_2\text{O}} \simeq P_{\text{total}}$), however, the first liquid to form by the partial melting of a material consisting of forsterite and diopside and enstatite solid solutions (simple lherzolite) at 20 kb has the composition *X* (Fig. 56), which is silica saturated. On the basis of the experiments on the melting of enstatite, it is expected that silica-saturated liquids can be formed at pressures up to at least 30 kb in the presence of even small amounts of water. It is suggested from these considerations that some quartz tholeiites and quartz gabbros, particularly those of the calcalkali rock series, may have been formed in the upper mantle in the presence of water.

MELTING OF A HYDROUS PHASE: PHLOGOPITE

H. S. Yoder, Jr., and I. Kushiro

Understanding of the melting character of a hydrous phase is essential for predicting explosive volcanism, estimat-

ing the water content of the mantle, and outlining magma trends in which hydrous phases are involved. The beginning-of-melting curves for some simple and complex amphiboles, zeolites, and micas have previously been studied in the presence of what was believed to be an excess of water. The beginning-of-melting curves originate at an invariant point at elevated pressure where the anhydrous breakdown products, the hydrous phase, liquid, and gas are presumed to be in equilibrium. Only a few experiments have been made in which the water content is insufficient to saturate the liquid with gas, the most likely natural condition of a magma at generation (Yoder, *Year Book 64*, pp. 82-89). The principal problem now at hand is to account for the large amounts of water observed in water-saturated silicate liquids in laboratory experiments, whereas field deductions suggest that most natural magmas are low in water and water-undersaturated under the conditions of generation. Experiments in the gas-absent region were therefore undertaken in the hope of resolving this apparent disagreement in the water content of silicate liquids and to ascertain the behavior of hydrous minerals in the gas-absent region.

Phlogopite stability fields have been studied by Yoder and Eugster (1954), Crowley and Roy (1964), Wones (1967a), Luth (1967), and Kushiro, Syono, and Akimoto (1967). Luth (1967) examined phlogopite in the broader scope of the K_2O - MgO - Al_2O_3 - SiO_2 - H_2O system. The invariant point marking the onset of melting for phlogopite was examined in particular by Luth, and the sequence of curves *immediately* around that point was presented. The phases involved are phlogopite (Ph), forsterite (Fo), leucite (Lc), orthorhombic kalsilite (Ok), liquid (L), and gas (G), which produce six univariant reactions (indicated below by the absent phase). The sequence of univariant curves illustrated by Luth is similar to that shown in Fig.

57, with the exception that (G) and (Lc) are reversed in position. His sequence was based on the assumption that $Ph = Fo + Ok + L + G$, which requires that the water content of the liquid be less than that of those possible liquids that lie on a plane passing through the compositions of Fo-Ok-Ph. He obtained no data in the water-undersaturated region. The phases reported for his several runs on the phlogopite-water join (black dots of Fig. 58) support for the most part the sequence of curves either as drawn by him or as illustrated in Fig. 57, where the breakdown of phlogopite is $Ph = Fo + Ok + Lc + L$, no gas being involved. The issue of singular import is the water content of the liquid or liquids involved in the melting of phlogopite.

The first step was to determine the melting of phlogopite in the presence of an excess of water over a wide range of pressures, including those believed to exist in the region of magma generation. The results up to 37.5 kb are shown in Fig. 58. The invariant point and the curves extending to pressures lower than that of the invariant point are those of Luth (1967). The garnet-bearing assemblage of Kushiro, Syono, and Akimoto (1967) was not encountered at the highest pressure investigated. A singular point arises on the (G) curve of Fig. 57, marking the reaction $Ph = Ok + Fo + Lc + L$, which then becomes $Ph + Ks + Lc = L + Fo$ and $Ph = Fo + L$, as shown by (b) and (c), respectively, in Figs. 58 and 60. Two curves and the related singular points that describe the consumption of Lc and Ok in the water-saturated melt are not shown; the curves lie below about 2 kb and above the Ph-absent univariant curve, however, as illustrated by Luth (1967, p. 393, Fig. 4). Forsterite is the liquidus phase throughout the range studied and at 1 atm, where Schairer (1954) observed a liquidus of 1628°C. The appearance of spinel at lower temperatures at 1 atm, however, indicates that loss of alkalis may have occurred at the very high

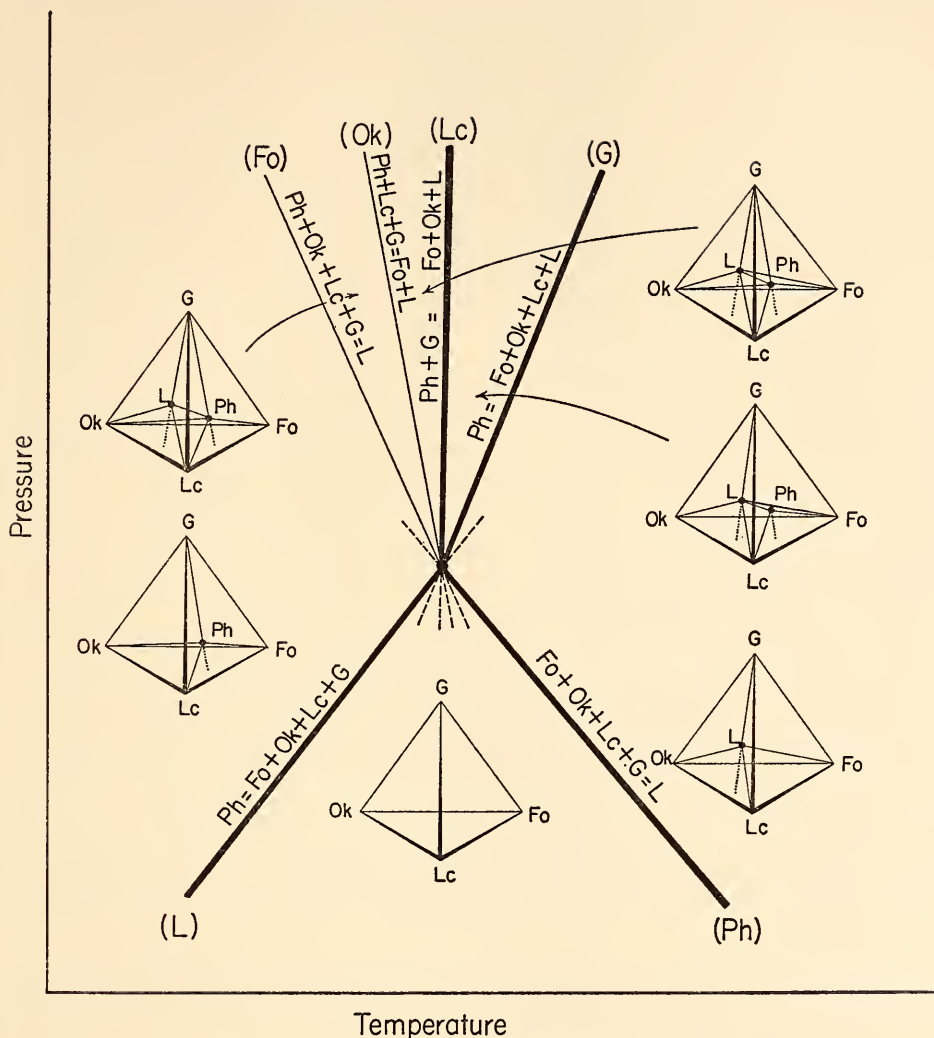


Fig. 57. Sequence of invariant curves immediately about the invariant point involving phlogopite (Ph), forsterite (Fo), leucite (Lc), orthorhombic kalsilite (Ok), liquid (L), and gas (G). Each curve is indicated by the absent phase. Beginning of melting in the presence of gas is given by curves (Fo) and (Ph). Heavy lines are those reactions exhibited by compositions on the join $\text{K}_2\text{O} \cdot 6\text{MgO} \cdot \text{Al}_2\text{O}_3 \cdot 6\text{SiO}_2 \cdot \text{H}_2\text{O}$, which includes phlogopite composition.

temperatures, and thus the liquidus of the ideal bulk composition may be somewhat lower.

The second step was to study the $\text{K}_2\text{O} \cdot 6\text{MgO} \cdot \text{Al}_2\text{O}_3 \cdot 6\text{SiO}_2 \cdot \text{H}_2\text{O}$ join at a temperature above the melting of phlogopite in the presence of an excess of water, 1225°C, and 10 kb. The results of that

study are shown in Fig. 59 in the broad view of the plane $\text{Fo}-\text{H}_2\text{O}-\text{Lc}:\text{Ks}$ (1:1 mole). The region marked $\text{Fo}+L+G$ is based on those run products that appeared after quenching as: euhedral or subhedral forsterite crystals ($=\text{Fo}$); clear glass ($=L$), usually highly vesiculated; balls or coatings of a pinkish glass, having a

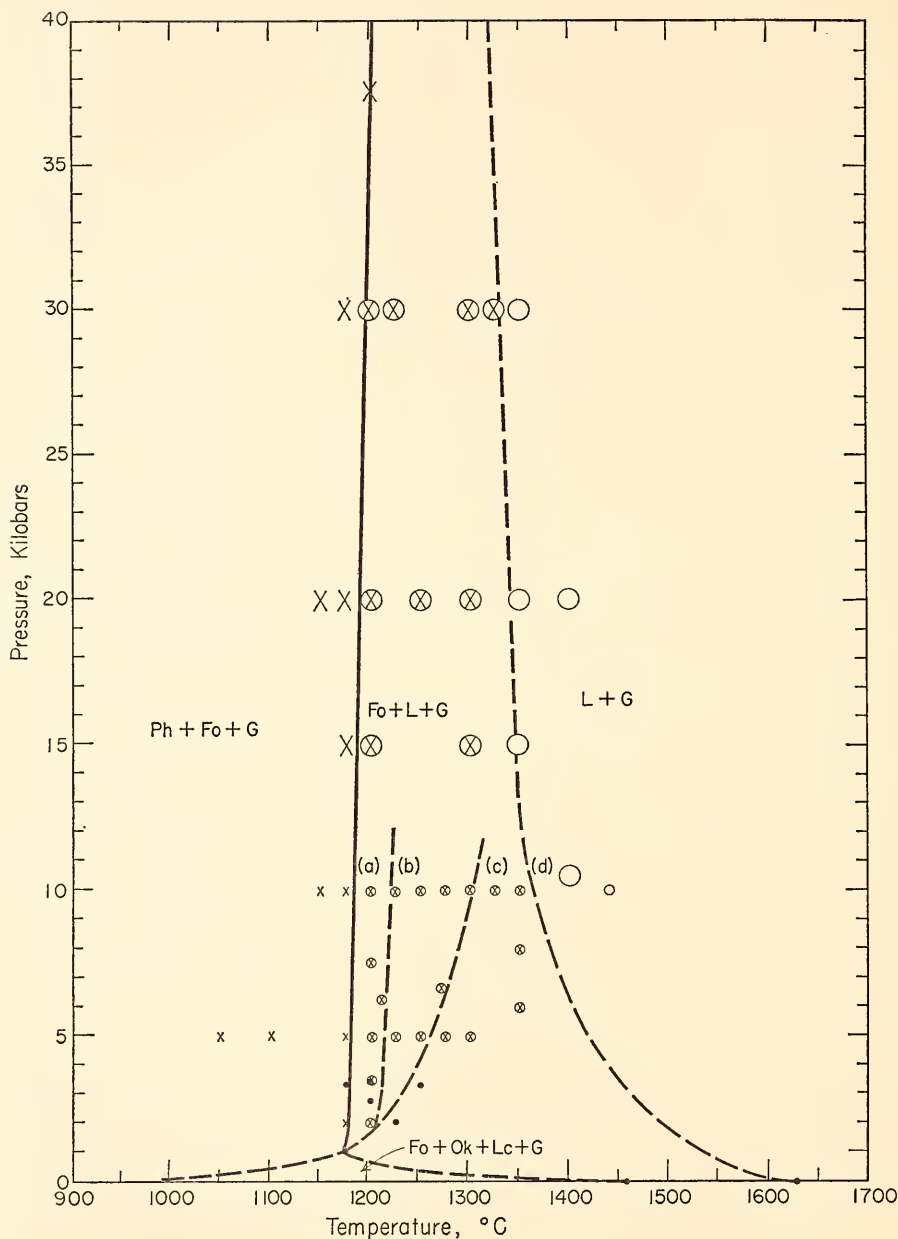


Fig. 58. Pressure-temperature diagram for compositions on the join $K_2O \cdot 6MgO \cdot Al_2O_3 \cdot 6SiO_2 - H_2O$. Lettered points appear in the 10-kb section presented in Fig. 60. The four univariant curves presented as heavy lines in Fig. 57 appear around the invariant point at about 1 kb and 1175°C. Curve on which point (a) lies is the upper stability limit of phlogopite in the presence of an excess of gas. Dashed curve on which point (b) lies represents the beginning of melting of the assemblage $Ph + Fo + Lc + Ks$. Dashed curve on which point (c) lies represents the locus of maximum melting points of phlogopite in the water-deficient region. Dashed curve on which the point (d) lies is the water-saturated liquidus.

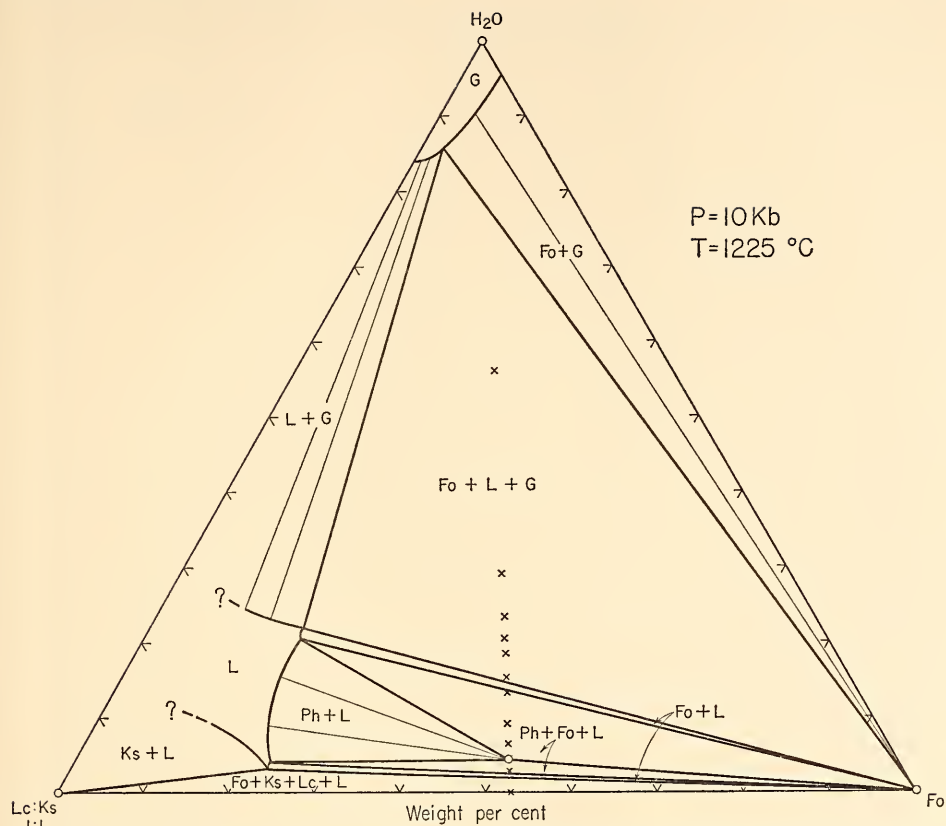


Fig. 59. Pseudoternary section at $P_T = 10$ kb and 1225°C for the system $\text{Fo}-\text{H}_2\text{O}-\text{Lc}:\text{Ks}$ (1:1 mole). Compositions investigated, marked with an X, lie on the join $\text{K}_2\text{O}\cdot 6\text{MgO}\cdot \text{Al}_2\text{O}_3\cdot 6\text{SiO}_2-\text{H}_2\text{O}$, and are the basis of this schematic construction.

variable and very much lower index of refraction ($=G$ in part); a milky fluid, often exuded when the container was punctured ($=G$ in part); and needles of mica, considered to have formed during the quenching process, not being stable during the run. The $\text{Ph}+\text{Fo}+\text{L}$ regions exhibited faceted crystals of phlogopite, often in books $10\ \mu$ thick, as well, but did not have any of the above-named products attributed to the gas phase, nor was the glass highly vesiculated. The anhydrous composition produced crystals of forsterite+leucite+kalsilite. (The anhydrous composition crystallized at 1 atm consisted of forsterite+leucite+orthorhombic kalsilite.)

The third step taken was a study of the $\text{K}_2\text{O}\cdot 6\text{MgO}\cdot \text{Al}_2\text{O}_3\cdot 6\text{SiO}_2-\text{H}_2\text{O}$ join at a series of temperatures at 10 kb. The results are presented in Fig. 60. Attention is called to the fact that the system is indeed quinary, and only those fields cut by part of the join are illustrated. The critical observation is that phlogopite is stable in the water-deficient region at temperatures (c) well above the beginning of melting (a) of the silicate-rich portion of the join. Furthermore, the initiation of melting in the gas-free assemblage, $\text{Ph}+\text{Fo}+\text{Lc}+\text{ks}$, is at a somewhat higher temperature (b) than that for the gas-present region (a). It is the former region which is of great im-

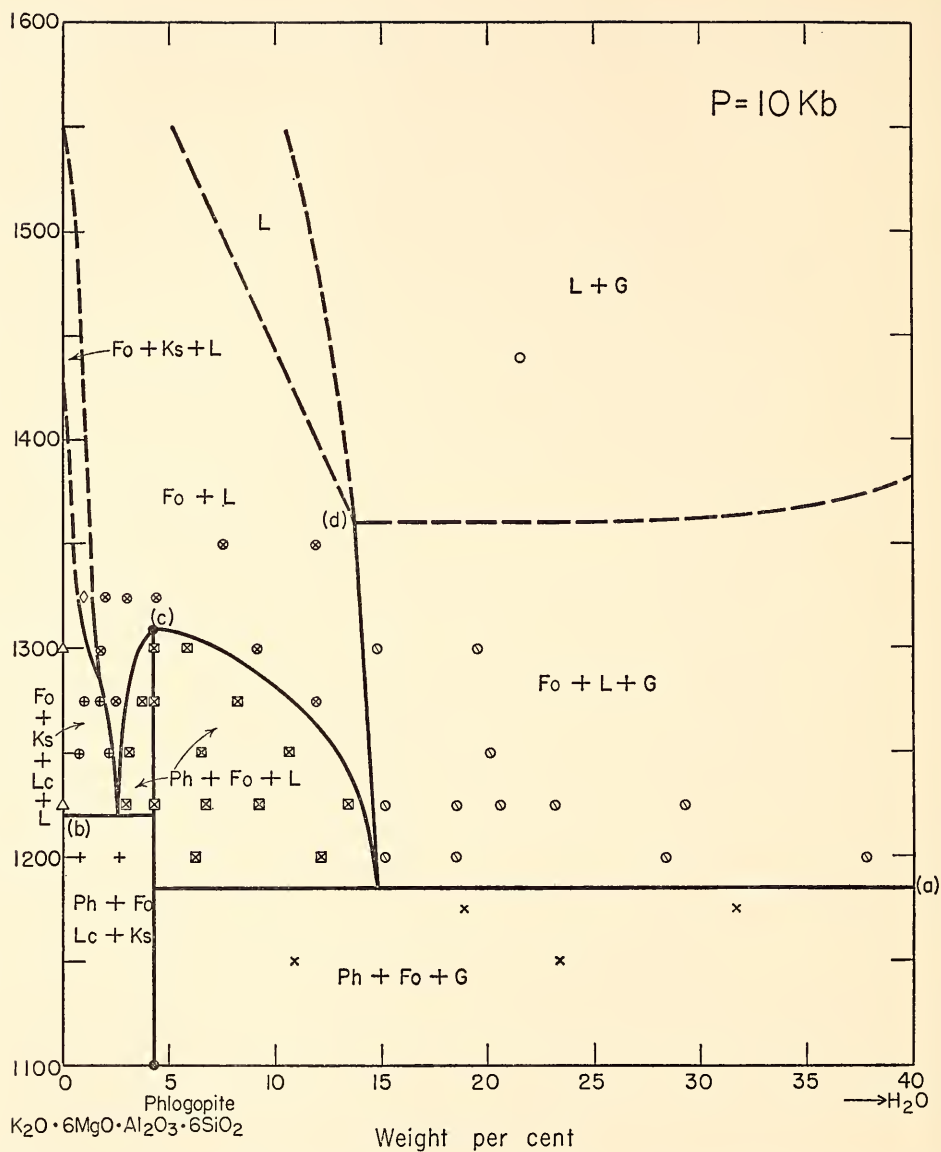


Fig. 60. The temperature-composition section at 10 kb for the silicate-rich portion of the $\text{K}_2\text{O} \cdot 6\text{MgO} \cdot \text{Al}_2\text{O}_3 \cdot 6\text{SiO}_2\text{-H}_2\text{O}$ join. The lettered points and lines are also indicated in Fig. 58, and the data at 1225°C are exhibited in Fig. 59.

port in the partial melting process of the mantle and lower continental crust.

Water is no doubt stored in the upper mantle, not as free gas but in hydrous phases, a large number of which have been shown to be stable to exceedingly

high pressures. In the absence of a gas phase, the melting of a mixture of hydrous and anhydrous phases will probably take place under conditions illustrated by the undersaturated region of Fig. 60. The water contents of the initial

melt will be of the order of a few percent (≈ 4 wt %, Fig. 59), not the large amounts of water (≈ 22 wt %, Fig. 59) in magmas formed in the presence of an excess of water. With increase of partial melting, two possible types of behavior may occur. If the mantle rock has mostly hydrous phases, then the water content of the liquid will increase. If the mantle rock consists mostly of anhydrous phases, the water content of the liquid will decrease with further rise in temperature. In each behavior the magma will remain undersaturated, even at temperatures at which all the hydrous phases are consumed. In the event that the hydrous mineral breaks down in the solid state, that is, before melting begins, a gas will be released, and the melting behavior is as outlined by Yoder (*Year Book 64*, pp. 82-89)—a water-undersaturated magma is produced on partial melting.

The results obtained are believed to apply, in general, to the melting of hydrous phases. The results of Ernst (1961), for example, on the melting of the amphibole glaucophane support this view, even though he chose a composition of liquid too low in water in determining the sequence of curves about the relevant invariant point. The water content of liquid (5 ± 2 wt %) reported by him is not in accord with the sequence of curves presented (Ernst, 1961, p. 755, Fig. 6). Glaucophane (Gl) would be stable in the gas-absent region at temperatures above the melting curve illustrated as $Gl = Fo + En + L + G$, which was actually observed by him to be $Gl + G = Fo + En + L$.

Extrapolation of the curve on which the point (c) lies to the gas-absent liquidus in Fig. 60 indicates that phlogopite, if stable, may melt congruently at pressures above the limit of these experiments. Possible solid solutions of phlogopite were not investigated. Substitution of 2Al for 3Mg would be possible within the system, as well as $H^+ \rightarrow K^+$, leading to an alkali-deficient hydrophlogopite.

In addition to outlining the behavior of a hydrous mineral in the gas-absent region, the principal conclusions drawn from this simple study are the following: (1) Partial melting at high pressures of forsterite-rock assemblages containing hydrous phases may yield water-undersaturated magmas having a low water content in the absence of a gas phase. (2) Continued melting of a hydrous mineral-bearing assemblage at high pressures yields either an undersaturated magma or a water-saturated magma, depending on whether the hydrous mineral melts incongruently or congruently. (3) Extremely water-rich magmas may be produced at high pressures from the melting of hydrous mineral-bearing assemblages when free water is present or becomes present on the breakdown of the hydrous mineral in the solid state.

It is thus demonstrated by experiment that liquids low in water content can be achieved in the laboratory even in the presence of a hydrous phase. The apparent disagreement between field deduction and previous laboratory studies in the presence of excess water is resolved.

RECONNAISSANCE STUDY OF THE STABILITY OF AMPHIBOLES AT HIGH PRESSURE

M. C. Gilbert

It is generally accepted that the hydrosphere has been generated throughout the history of the earth by degassing of the mantle, principally through vulcanism (Rubey, 1951). All indications are that this process has not been completed, and we are faced with the question of how H_2O is and has been held in the mantle. Answers are crucially important to understanding the origin of magmas because of the strong effect of H_2O on the melting of silicates.

H_2O would occur in the mantle (1) as an H_2O -rich fluid phase, (2) adsorbed on the grain boundaries, or (3) bound in hydrous mineral phases. Amphiboles

and micas are the most promising of the hydrous phases because of their relatively high upper thermal stability limits at low pressure. (See Ernst, 1968, for a summary of the stability relations of amphibole, and Wones, 1967*b*, for a summary of the stability relations of mica). The role of the hydroxylated pyroxene reported by Selar, Carrison, and Stewart (1967) is not clear at present.

The question arises as to what happens to these hydrous phases at high pressure. Mica can be stable to temperatures of 1200° to 1300°C near 40 kb (Kushiro, Syono, and Akimoto, 1967; Yoder and Kushiro, this report), but experiments bearing on the upper thermal stability limit of amphiboles above 10 kb have not previously been reported. Yoder and Tilley (1962) and T. H. Green and Ringwood (1967) have indicated that amphiboles may be stable up to about 1000°C at 10 kb in systems of basaltic composition plus H₂O. Ernst (1963) studied the polymorphism of alkali amphiboles at pressures up to 40 kb but did not investigate the decomposition boundaries at this pressure. Greenwood (1963) calculated that anthophyllite would not be stable at pressures much higher than 20 kb at any temperature. D. H. Green and Ringwood (1967) suggested that amphibole breakdown curves would have negative slopes at pressures higher than 10 to 20 kb because the large decrease in the specific volume of water at high pressure would change the ΔV of the reaction amphibole \rightleftharpoons breakdown products from positive to negative. Kushiro (1968*a*) has considered in detail the breakdown of hydrous minerals at

high pressures and calculates that practically all known amphibole species have negative slopes at higher pressure.

Reconnaissance experiments on a number of amphibole compositions in the presence of excess H₂O confirm these suggestions and calculations. Starting materials for the Mg-bearing compositions were glasses and oxide prepared by F. R. Boyd. Amphibole-bearing assemblages synthesized from these materials were also used as charges for some of the runs. Sealed platinum capsules were run in a 3/4-inch bore piston-cylinder apparatus with a talc pressure medium. The uncorrected nominal pressure is reported.

The amphibole compositions and nomenclature employed are given in Table 9. Some of the experimental results so far obtained are given in Table 10. Tremolite₅₀ tschermakite₅₀ has been synthesized at 800°C and 10 kb, confirming the earlier report of Boyd (*Year Book* 53, p. 110). He attempted the synthesis of tschermakite but was not confident that the amphibole obtained was on composition. An amphibole has been synthesized at 800°C and 10 kb from a starting material of tschermakite bulk composition with about an 85 to 90% yield. It is tentatively identified as tschermakite. Boyd had originally suggested that this phase might be stable at high pressure. It appears to be stable up to at least 20 kb, but significantly, tschermakite, tremolite, and tremolite₅₀ tschermakite₅₀ all seem not to be stable at 800°C and 30 kb. The decomposition assemblage is dominated by pyroxenes at the tremolite end (alumina-free, silica-

TABLE 9. Amphibole Nomenclature and Compositions Employed

Abbreviation	Name	Composition
Tr	Tremolite	$^{\circ}\text{Ca}_2\text{Mg}_5\text{Si}_3\text{O}_{22}(\text{OH})_2$
TT	Tremolite ₅₀ tschermakite ₅₀	$^{\circ}\text{Ca}_2\text{Mg}_4\text{AlSi}_7\text{AlO}_{22}(\text{OH})_2$
T	Tschermakite	$^{\circ}\text{Ca}_2\text{Mg}_3\text{Al}_2\text{Si}_6\text{Al}_2\text{O}_{22}(\text{OH})_2$
Ed	Edenite	$\text{NaCa}_2\text{Mg}_3\text{Si}_7\text{AlO}_{22}(\text{OH})_2$
Pa	Pargasite	$\text{NaCa}_2\text{Mg}_4\text{AlSi}_6\text{Al}_2\text{O}_{22}(\text{OH})_2$
Ha	Hastingsite	$\text{NaCa}_2\text{Fe}_4^{2+}\text{Fe}^{3+}\text{Si}_6\text{Al}_2\text{O}_{22}(\text{OH})_2$

TABLE 10. Some Results of High-Pressure Hydrothermal Runs for Amphibole End Members Studied

Condensed Reactants *	T, °C	P, kb	Duration, hours	Condensed Run Products
*Ca₂Mg₅Si₈O₂₂(OH)₂ + SiO₂ †				
Oxide mix	800	10	15¾	Tr + Qtz
Tr + Qtz	800	30	71	Tc + Opx + Qtz
*Ca₂Mg₄AlSi₇AlO₂₂(OH)₂				
gl	800	10	65	TT + Cpx + Opx? + G?
gl	900	10	17	TT + Cpx + Opx? + G?
gl	700	20	146	TT + Tc + Cpx + Opx + G?
TT + Cpx + Opx? + G?	800	20	75	TT + (Cpx + Opx? + G?)
gl	900	20	97	Cpx + Opx + G
TT + Cpx + Opx? + G?	800	30	71	Cpx + Opx + G
*Ca₂Mg₃Al₂Si₆Al₂O₂₂(OH)₂				
gl	800	10	65	T + G
T + Opx + G + tr Cpx	800	10	143	No change
gl	900	10	17	T + Opx + G + tr Cpx
T + Opx + G + tr Cpx	800	20	75	T + (G)
gl	900	20	16	G + Cpx
T + G	800	30	71	G + ?
T + G	900	38.7	21½	G + ?
NaCa₂Mg₅Si₇AlO₂₂(OH)₂				
Oxide mix	900	20	~25	Ed + Cpx + Fo + tr gl
Ed + Cpx + Fo + tr gl	950	28.2	20½	(Ed) + Cpx + Fo + gl
Ed + Cpx + Fo + tr gl	900	38.7	21½	Cpx + Fo + gl
NaCa₂Mg₄AlSi₆Al₂O₂₂(OH)₂				
Oxide mix	800	10	143	Pa + Cpx
Pa + Cpx	800	20	75	Pa + (Cpx)
Oxide mix	900	20	~25	Pa + Cpx
Pa + Cpx	800	30	71	Sheet silicate + G + Cpx + gl
Pa + Cpx	950	28.2	20	G + Cpx + Fo + gl
Pa + tr Cpx	900	38.7	21½	G + Cpx + Fo + gl
NaCa₂Fe₄²⁺Fe³⁺Si₆Al₂O₂₂(OH)₂				
Ha + Mt + Cpx + tr G + Pc	700	11.8	168	G + Mt + Cpx [FMQ] ‡
Ha + Mt + Cpx + tr G + Pc	750	12	97	G + Mt + Cpx [FFsM]
Ha + G + Mt + Cpx	650	19.9	237	G + Mt + Cpx [FFsM]
Ha + G + Mt + Cpx	700	20.9	93	G + Mt + Cpx [FFsM]

* Amphibole abbreviations are given in Table 9. Qtz, quartz; Tc, talc; Opx, orthopyroxene; Cpx, clinopyroxene; G, garnet; Fo, forsterite; Mt, magnetite; gl, glass; ?, presence not confirmed, or unidentified phase or phases; tr, trace; parentheses indicate metastable phases; bold-face type indicates dominant phase.

† Bulk compositions of the runs expressed in terms of amphibole end-member formulas. Only tremolite composition was silica excess.

‡ Oxygen fugacity buffers: FMQ denotes fayalite-magnetite-quartz assemblage; FFsM denotes fayalite-orthoferrosilite-magnetite assemblage.

rich end) of the tremolite-tschermakite join and by garnet at the tschermakite end (alumina-rich, silica-poor end). A run with anhydrous tschermakite composition at 1200°C and 30 kb also gave a breakdown assemblage consisting almost entirely of garnet. These nonsodium-bearing calcic amphiboles appear to have

comparable upper thermal stability limits, but their stability limits are lower than those of the sodium-bearing calcic amphiboles, the hornblendes.

The amphibole with the highest thermal stability limit is pargasite, reaching 1040°C at 1 kb (Boyd, 1959). Illustration of the possible stability limits of

intermediate members of the pargasite-hastingsite group was shown in the studies of Yoder and Tilley (1962) and T. H. Green and Ringwood (1967), mentioned earlier. From the work reported here, edenite and paragasite both appear to be unstable at 950°C and higher, near 30 kb, or at 900°C and higher, near 40 kb. Sodium-bearing, purely magnesian, calcic amphiboles appear to continue to melt incongruently, whereas those that are nonsodium-bearing break down in the solid state. In either case, the upper thermal stability limits are lower at higher pressures and must have negative slopes over all or part of the pressure range studied.

To determine the effect of pressure on the stability of one of the purely iron end members of the hornblendes, hastingsite was studied at 12 and 20 kb under conditions of controlled oxygen fugacity (f_{O_2}). The assemblages fayalite-magnetite-quartz (FMQ) and fayalite-orthoferrosilite-magnetite (FFsM) were used to fix f_{O_2} in the standard double-capsule method. The FFsM assemblage is stable to higher oxygen fugacities than FMQ (Lindsley, Speidel, and Nafziger, 1968).

Although the iron-amphibole stability field at high pressure has not been delineated, conditions of instability are known and place maximum temperature limits on stability. Thus hastingsite is not stable at 650°C and higher at 20 kb, or at 700°C and higher at 12 kb when f_{O_2} is defined by FFsM; or at 750°C at 12 kb when f_{O_2} is defined by FMQ.

Hastingsite dehydrates at low pressure (3 kb) to a plagioclase-bearing assemblage. At 12 and 20 kb, plagioclase disappears as a breakdown product, giving one more indication that the plagioclase \rightleftharpoons garnet + pyroxene reaction, in chemically complex systems, occurs at pressures suggestively close to those to be found at the crust-mantle transition.

If 950°C is a maximum temperature of stability at 30 kb, then depending on the geothermal gradient, no amphibole would be stable below about 70 to

100 km depth. Amphiboles may thus play a significant role in the petrology of the lower crust and uppermost mantle but cannot be the water containers at greater depths. It may be significant that no amphibole has ever been reported as a primary inclusion in diamond (Meyer, *Year Book 66*, pp. 446-450). It seems possible that some amphibole stability fields may be pinched out entirely at high pressure between expanding stability fields for sheet silicate-bearing assemblages from the low-temperature side and garnet- and pyroxene-bearing assemblages from the high-temperature side. The fact that phlogopite is stable to about 1300°C near 40 kb and pargasite is unstable at 900°C at 40 kb suggests that a depth-facies classification could be devised for the upper mantle based on amphibole/mica occurrence.

CONTROL OF FUGACITIES IN FLUORINE-BEARING HYDROTHERMAL SYSTEMS

J. L. Munoz

Fluorine is a common constituent of many rock-forming minerals, especially micas and amphiboles. Fluorine substitutes for the hydroxyl group in these minerals, and this substitution considerably affects their thermal stability. Thus, both the compositions and the stability relations of these minerals are partly dependent upon the magnitudes of the H_2O and HF fugacities of their environment. In order to calibrate these effects in synthetic systems, it is necessary to develop methods that permit control of the fugacities at elevated pressures and temperatures in a quantitative manner. The most simple and direct method is to vary the bulk composition of the gas phase. This approach is unsatisfactory for fluorine-bearing systems because of the high solubility of silicates in aqueous HF at low temperatures, analytical difficulties, and inadequate knowledge of the P - V - T and fugacity relations in the system O - H - F under the conditions of experimental interest. Alternatively, the

composition of the gas phase and its fugacities may be buffered by appropriate assemblages of crystalline phases. With this technique, the composition and fugacities of the equilibrium gases as functions of total P and T are calculated from the equilibrium constants and fugacity coefficients for all the important molecular species present (assuming ideal mixing) and from the free-energy data for the solid buffer phases.

Figure 61 shows the experimental arrangement. The charge is contained in gold foil and is surrounded by the fluorine buffer assemblage and a gas of composition O-H-F or C-O-H-F, depending on whether graphite is present as a buffer phase. This charge-buffer system is sealed in a Pt membrane. Because the fluorine buffer fixes only a fugacity ratio (e.g., $f_{\text{H}_2\text{O}}/f_{\text{HF}}$ or $f_{\text{O}_2}/f_{\text{F}_2}$), it is necessary to fix independently one additional fugacity within the system. This can be done by externally fixing the hydrogen fugacity, either by using a Shaw bomb, a standard oxygen buffer, or the methane buffer (see Eugster and Skippen, 1967).

Calculations have been performed for the following fluorine buffers over a wide range of P_{total} , T , and f_{H_2} :

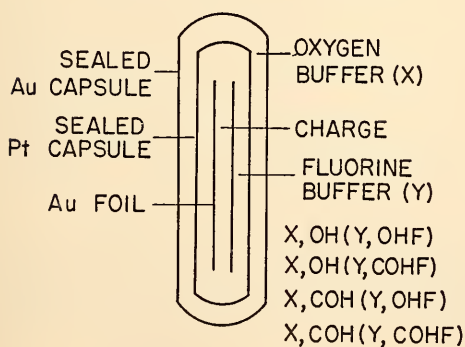
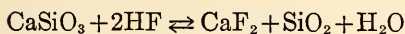
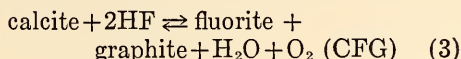
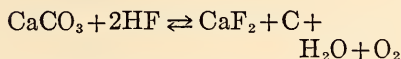
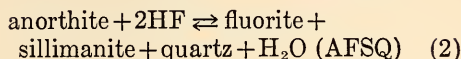
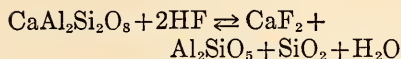
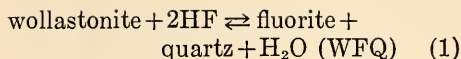


Fig. 61. Diagram of triple capsule arrangement used for fluorine buffer experiments. Notation: The charge-buffer system is enclosed by parentheses, together with the elemental composition of the gas phase. The external oxygen buffer and its gas components are written to the left of the parentheses.



Buffer notation is given as O_B , OH or COH (F_B , OHF or COHF) where O_B represents the external buffer assemblage, F_B represents the fluorine buffer, and the letters OHF or COHF refer to the components present in the gas phase. Details regarding the equations used in the calculations, and results for a number of different sets of conditions will appear in a forthcoming paper. As an example, Fig. 62 shows the dependence of the fugacity of HF on temperature, fluorine buffer, and f_{H_2} for a total pressure of 2 kb.

An alternative approach to controlling the fugacities of H_2O and HF is to control the activities of H^+ and F^- . Assuming that only monovalent ions are present, these two approaches can be related through the equations for the ionic dissociation of HF and H_2O :

$$K_{\text{HF}} = \frac{a_{\text{H}^+} a_{\text{F}^-}}{a_{\text{HF}}} \quad \text{and} \quad K_{\text{H}_2\text{O}} = \frac{a_{\text{H}^+} a_{\text{OH}^-}}{a_{\text{H}_2\text{O}}}$$

Combining these two equations with the restriction that the sum of the moles of positive ions must equal the sum of the moles of negative ions, we obtain

$$a_{\text{H}^+} = (\gamma_{\text{H}^+}) \left[\frac{K_{\text{HF}} a_{\text{HF}}}{\gamma_{\text{F}^-}} + \frac{K_{\text{H}_2\text{O}} a_{\text{H}_2\text{O}}}{\gamma_{\text{OH}^-}} \right]$$

where γ_{H^+} , γ_{F^-} , and γ_{OH^-} represent the activity coefficients for the respective ions. This equation shows that if the activities of the molecular species are independently defined, the pH , and hence the activities of the other ions in the gas phase, are fixed. Conversely, fixing the

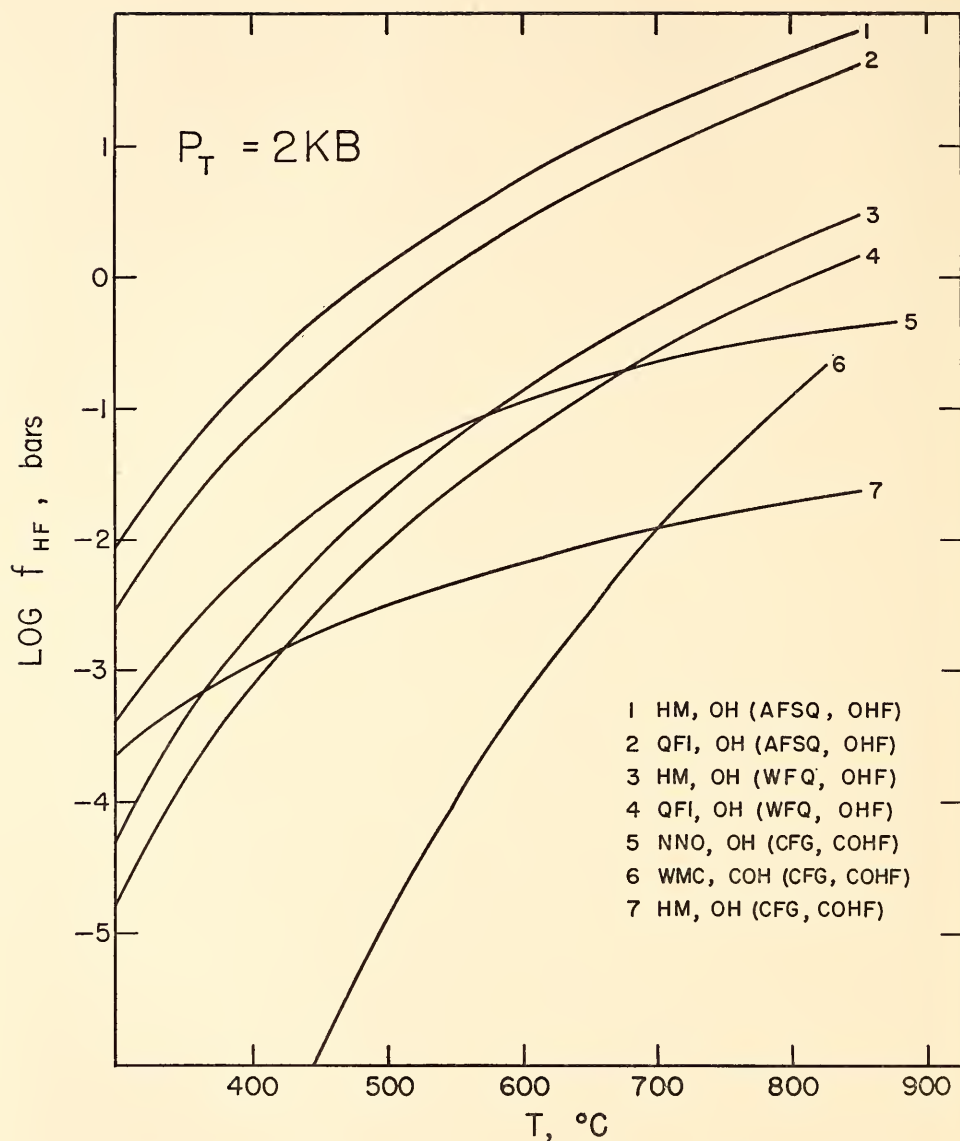


Fig. 62. Variation of HF fugacity with temperature calculated for a number of fluorine buffers at 2 kb. Buffer assemblages (neglecting gas) are HM, hematite + magnetite; NNO, nickel + nickel oxide; QFI, quartz + fayalite + iron; WMC, wustite + magnetite + graphite; AFSQ, anorthite + fluorite + sillimanite + quartz; WFQ, wollastonite + fluorite + quartz; CFG, calcite + fluorite + graphite.

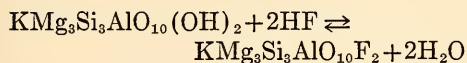
activities of the ions defines the fugacities of the molecular species. The molecular approach has been chosen only because this method creates fewer technical and

experimental difficulties; results obtained from both methods should, however, be identical.

To demonstrate the feasibility of fluo-

rine buffers, a number of experiments were performed equilibrating phlogopite $[\text{KMg}_3\text{Si}_3\text{AlO}_{10}(\text{F}, \text{OH})_2]$ with gases that were equilibrated with different fluorine buffer assemblages. Phlogopite was chosen because it exhibits complete solid solution between the F and OH end members; also, it is possible to prepare both end members in a pure state. By using both pure fluorophlogopite and pure hydroxyphlogopite as starting materials, the exchange reaction was approached from both sides, and equilibrium with the buffer was thus demonstrated (Table 11). Compositions of the phlogopites were determined by X rays to ± 2 mole % fluorophlogopite on the basis of the $d(005)$ value measured against $\text{CaF}_2(220)$ with copper $\text{K}\alpha_1$ radiation.

The phlogopite exchange reaction studied can be represented by the equation



for which we may write an equilibrium constant in terms of the fugacities of H_2O and HF, $K = f_{\text{H}_2\text{O}}^2 / f_{\text{HF}}^2$. Fluorine buffer curves, when plotted in terms of the log of this equilibrium constant versus reciprocal temperature, yield straight lines that show the calculated $f_{\text{H}_2\text{O}}/f_{\text{HF}}$ ratios for each buffer (Fig. 63). For a fixed temperature, these four curves are arranged in order of increasing fluorination (from top to bottom).

The compositions of the phlogopites as a function of temperature are shown in Fig. 64(A). Only one temperature was run for the buffer HM, OH (CFG, COHF); note that the composition of this mica is nearly pure fluorophlogopite, in contrast with the much more hydroxylated mica obtained by using NNO, OH (CFG, COHF). The large differences in mica composition also serve to demonstrate communication between the external oxygen buffer and the fluorine buffer, since the fluorine buffer was identical in both cases. Moreover, these differences in composition are consistent with relative fugacity ratios shown in Fig. 63 for these two buffers. Note also that the composition of the phlogopite equilibrated with the NNO, OH (ASFQ, OHF) buffer at 700°C is very close to that of the extremely fluorinated phlogopite equilibrated with the HM, OH (CFG, COHF) buffer at the same temperature (Table 11, Fig. 64A). This is precisely what the calculations predict, inasmuch as the values for the equilibrium constants for these buffers nearly overlap (Fig. 63).

A calibration problem was discovered between the CFG and WFQ buffers, however, as shown in Fig. 64(B). At all temperatures studied, phlogopites equilibrated with the WFQ buffer are more fluorine rich than those equilibrated with the CFG buffer, whereas calculated $f_{\text{H}_2\text{O}}^2/f_{\text{HF}}^2$ values predict the opposite

TABLE 11. Final Compositions of Phlogopite Solid Solutions Equilibrated with Various Fluorine Buffers at 700°C , 2 Kb *

Buffer	Starting Composition	Final Composition, $\pm 2\%$
NNO, OH (CFG, COHF)	OHPH	FPh ₅₅ OHPH ₄₂
NNO, OH (CFG, OHF)	FPh	FPh ₅₆ OHPH ₄₄
HM, OH (CFG, COHF)	OHPH	FPh ₅₆ OHPH ₄₄
HM, OH (CFG, OHF)	FPh	FPh ₅₅ OHPH ₄₅
NNO, OH (WFQ, OHF)	OHPH + FPh	FPh ₇₁ OHPH ₂₉
NNO, OH (ASFQ, OHF)	OHPH	FPh ₅₅ OHPH ₄₅

* Run times ranged between 20 and 40 days.

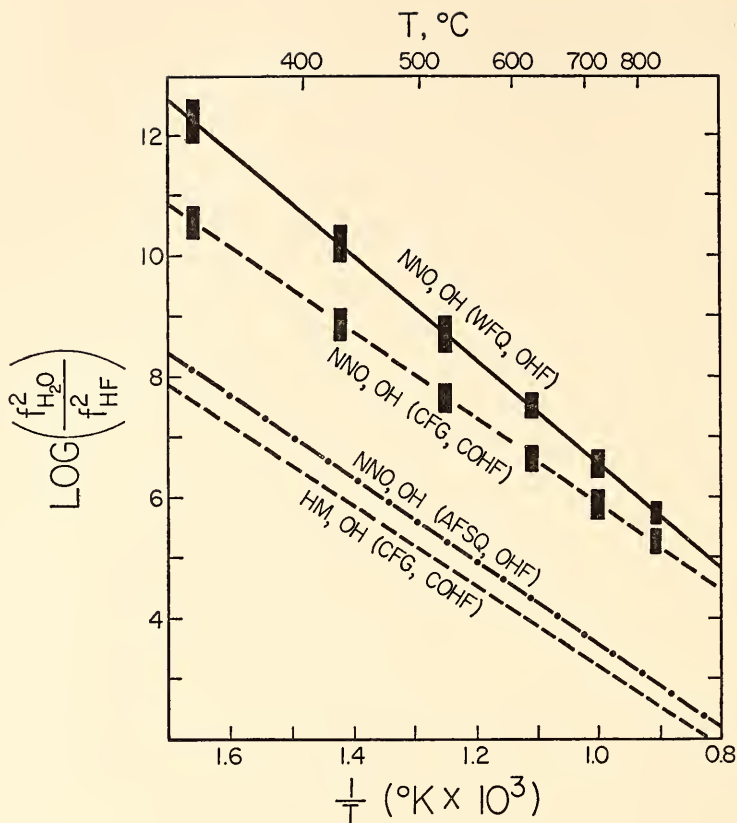


Fig. 63. $\log K (= f_{\text{H}_2\text{O}}^2 / f_{\text{HF}}^2)$ versus reciprocal temperature for four fluorine buffers. Height of solid bars represents the amount of uncertainty in the K that can be attributed to uncertainties in the ΔG values for the solid phases involved. For symbols, see Fig. 62.

result. This difficulty is most likely related to either (1) inadequately known ΔG° data for the buffer phases or (2) nonideal mixing in the gas phase. The rectangles in Fig. 63 represent the estimated maximum error in $f_{\text{H}_2\text{O}}^2 / f_{\text{HF}}^2$ due to uncertainties in the available free-energy data (Robie, 1962); the differences are not enough to account for the discrepancy. Fugacity coefficients for a number of the molecular species (including HF) are approximations and could well introduce a considerable source of error. Compounding this problem, however, the assumption of ideal mixing in the gas phase may not apply in the

presence of such a chemically reactive component as fluorine. A solution to the problem may be apparent when a number of different fluorine buffers are tested against one another; ultimately a systematic study of the system O-H-F may be necessary. In the meantime, these phlogopite experiments have demonstrated that the fluorine buffers function well experimentally even though some calibration problems are present. Moreover, knowledge of the compositions of these phlogopite F, OH solid solutions now provides a sensitive sliding scale, which will be useful in determining $f_{\text{HF}} / f_{\text{H}_2\text{O}}$ ratios in future experiments.

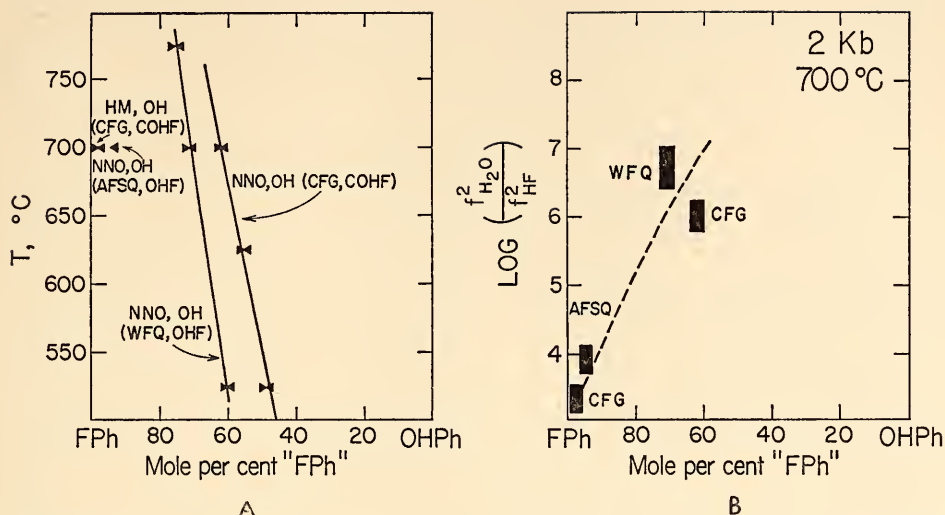


Fig. 64. (A) Compositions of phlogopites in equilibrium with four different fluorine buffers as a function of temperature at 2 kb. Compositions are precise to ± 2 mole % FPh (fluorophlogopite). Arrows show direction from which equilibrium was approached. (B) Compositions of phlogopites equilibrated with four fluorine buffers at 700°C (Fig. 64A) plotted as a function of the log of the equilibrium constant. The relative compositions of the micas equilibrated with NNO, OH (CFG, COHF) and NNO, OH (WFQ, OHF) buffers are in the opposite direction from that predicted by the equilibrium constant.

SULFIDE MINERALOGY AND PHASE-EQUILIBRIA STUDIES

ORE MINERALS THE Fe-Se SYSTEM

G. Kullerød

The Fe-Se system has been studied by quenching and differential thermal analysis (DTA) experiments. The phase relations at this point have been clarified above 400°C, as shown in Fig. 65. The solubility of Se in Fe is slight (less than 0.5 atomic % even at 900°C). A eutectic exists at 940°C and 5.5 atomic % Se, where the four phases Fe + FeSe + L + V coexist. DTA experiments on fifteen different compositions in the Fe-FeSe range all show a distinct thermal effect at this temperature.

Monotectic conditions exist at 962°C and 46.0 atomic % Se. At this point the four phases FeSe + L (containing 6.5 atomic % Se) + L (containing 46 atomic

% Se) + V coexist. Thus a wide field of liquid immiscibility exists above 962°C in the Fe-FeSe portion of this system. The high-temperature boundary curves of this field were not detected in DTA experiments.

The melting relations of the monoselenide phase are very similar to those of a number of monosulfides, such as Fe_{1-x}S, Ni_{1-x}S, and Co_{1-x}S. The maximum temperature on the monoselenide liquidus curve is 1065 \pm 5°C. The composition of the only monoselenide that melts directly to a liquid is about Fe₄₇Se₅₃ (corresponding to $x = 0.113$ in the Fe_{1-x}Se formula). Beyond this composition, the liquidus curve slopes steeply toward lower temperatures, as shown in Fig. 65, and reaches 790°C at 71.5 atomic % Se. A distinct thermal effect was recorded at this temperature in all DTA experiments containing 57.5 atomic % Se or

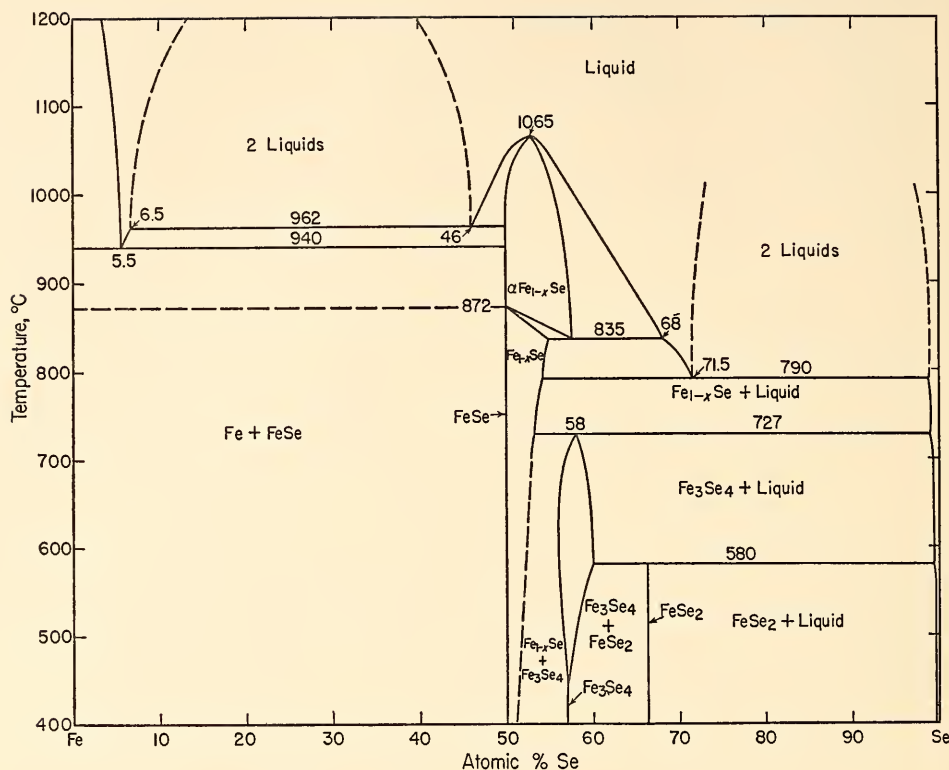


Fig. 65. Phase relations in the Fe-Se system above 400°C. Three compounds occur: Fe_{1-x}Se , Fe_3Se_4 , and FeSe_2 .

more. It was detected even in an experiment containing 98 atomic % Se. These results show that a liquid immiscibility field exists above 790°C. It spans the compositional region from a monotectic point (at 71.5 atomic % Se) to more than 98 atomic % Se. The presence of this monotectic, where the four phases $\text{Fe}_{1-x}\text{Se} + L$ (with 71.5 atomic % Se) + L (of essentially Se composition) + V co-exist, was demonstrated by an experiment containing 71.5 atomic % Se. When viewed by eye at 800°C a homogeneous liquid is observed; on cooling below 790°C growth of Fe_{1-x}Se and generation of brownish liquid Se are clearly noted to take place simultaneously. In the DTA experiments containing from 56 to 68 atomic % Se, distinct thermal effects were recorded at 835°C. The solidus

curve on the iron-deficient side of the Fe_{1-x}Se solid solution intersects the 835°C horizontal line at about 57.5 atomic % Se. Experiments with 49 atomic % Se give a thermal effect at 872°C, and those with 56 atomic % Se give thermal effects at 835° and 845°C. Combined, these data indicate that an inversion takes place in the Fe_{1-x}Se phase. The inversion temperature of stoichiometric FeSe is 872°C. Fe_{1-x}Se with maximum Fe deficiency (7.5 atomic % Fe) inverts at 835°. We shall refer to this high-temperature phase as $\alpha\text{Fe}_{1-x}\text{Se}$ to distinguish it from previously reported polymorphs stable at lower temperatures. Below this inversion, Fe_{1-x}Se has hexagonal NiAs-type structure down to 335°C for stoichiometric FeSe and to about 380°C for Fe_{1-x}Se (with $x=0.13$), as

indicated by DTA and quenching experiments. Below this second inversion, Fe_{1-x}Se is reported to have tetragonal structure.

In DTA experiments containing 58 to 98 atomic % Se, distinct thermal effects were recorded at 727°C. Below this temperature the Fe_3Se_4 compound is stable. The temperature of 727°C is taken as its incongruent melting point, where the four phases $\text{Fe}_3\text{Se}_4 + \text{Fe}_{1-x}\text{S} + L + V$ coexist. When it first crystallizes the Fe_3Se_4 compound contains about 58 atomic % Se, which is 1% more than indicated by the stoichiometric formula. The Fe_3Se_4 compound forms solid solution on both sides of the stoichiometric composition. This solid solution apparently reaches a maximum at 580°C, where the Fe_3Se_4 phase spans the region from about 56.0 to 60.0 atomic % Se.

At high temperatures, Fe_3Se_4 has a hexagonal crystal structure, which cannot be quenched. During cooling to some temperature below 600°C, an inversion takes place that results in prominent twinning. The low-temperature form is monoclinic. The structure and cell dimensions were determined by Morimoto and Kullerud (*Year Book* 58, pp. 199–201, 1959). The solvi defining coexisting compositions of the Fe_{1-x}Se and Fe_3Se_4 phases have not been determined accurately. Phase relations at elevated temperatures in the 50–60 atomic % composition range cannot be studied successfully by quench-type experimentation because even the fastest chilling will not freeze the equilibria achieved during the heating period. Constant heating and cooling rates are not readily achieved in DTA experiments at temperatures below 400°C, and the magnitude of most low-temperature heat effects in this critical region of the system appears to be near the limit of detection by our method.

The FeSe_2 phase melts incongruently at 580°C, where the four phases $\text{Fe}_3\text{Se}_4 + \text{FeSe}_2 + L + V$ coexist. Distinct thermal effects were recorded at this temperature

in all DTA experiments containing 61 to 98 atomic % Se. This compound, which is analogous with the mineral ferrosilite, is orthorhombic (Kullerud and Donnay, 1958).

THE Cu-Zn-S SYSTEM

J. R. Craig and G. Kullerud

Although copper and zinc sulfides are common, mineral assemblages containing coexisting copper sulfides and zinc sulfide are not common. Under natural conditions the almost ubiquitous presence of elements such as iron in addition to copper and zinc complicates the mineralogy. Knowledge of phase relations in the pure Cu-Zn-S system, however, serves to outline the stability limits of coexistence of the pure Cu and Zn sulfides and is a necessary prerequisite to investigation of complex systems like Cu-Fe-Zn-S, Cu-Pb-Zn-S, and Cu-Fe-Pb-Zn-S.

The phase relations in the Cu-Zn-S system were studied with the use of silica-tube reaction vessels for quenching and DTA experiments, with principal efforts on the 800° and 500°C isotherms. As shown in Fig. 66, tie lines exist between ZnS (sphalerite) and the Cu_2S - Cu_9S_5 solid solution at 800°C. ZnS is also noted to coexist with a CuZn alloy (α), which is stable over a composition range extending from nearly pure Cu to about 35 wt % Zn. Two additional CuZn alloys, referred to as β and γ , coexist with the ZnS phase. Pure Zn melts at about 419°C, and at 800°C liquid is present from the Zn composition corner to about 30 wt % Cu. As seen in Fig. 66, ZnS also coexists with this liquid phase. The phase relations on the Cu-Zn join were taken from Hansen and Anderko (1958). It is noted that in the phase diagram of Fig. 66 sphalerite and metallic copper form a stable assemblage, which occasionally is represented in ores, whereas coexistence of chalcocite-digenite solid solution with metallic zinc is prohibited by three different sets of tie lines. At 800°C the

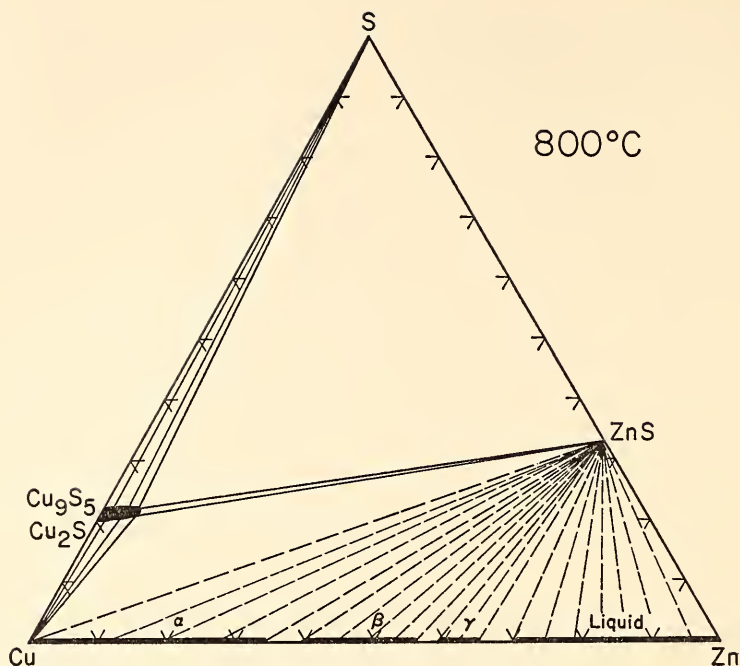


Fig. 66. Phase relations in the Cu-Zn-S system at 800°C. All phases and phase assemblages coexist with vapor.

solid solution of ZnS in Cu_2S ss is 7 ± 1 wt %. The solid solution of Cu_2S ss in ZnS is much less than 1 wt % at the same temperature but is sufficient to alter the color from the snow white of pure ZnS to a resinous yellowish brown. The ZnS in all experiments at 800°C had the cubic sphalerite structure. The unit-cell dimension of ZnS, whether present as the only phase or in equilibrium with any of the other phases shown in Fig. 66, is always within the limits of experimental error of $a = 5.409 \pm 0.003$ Å.

At 500°C the phase relations (shown in Fig. 67) are basically the same as those at 800°C. The solid solution of ZnS and Cu_2S ss has decreased to 3 wt %; the solid solution of Zn in the αCuZn alloy has increased to almost 40 wt %; the solubility of Cu in the Zn liquid has decreased to about 5 wt %; and a third CuZn alloy (ϵ) has appeared. The covellite (CuS) phase becomes stable in the pure Cu-S system at 507°C (Kullerud,

1965). Tie lines between ZnS and CuS are already established at $503^\circ \pm 2^\circ\text{C}$. The ZnS in all the experiments conducted at 500°C was found to have the sphalerite structure. Measurements of the cell edge were performed on ZnS from all stable assemblages containing this phase. As in the 800°C experiments, it was always found to lie within the limits of $a = 5.409 \pm 0.003$ Å.

Differential thermal analyses on Cu_2S ss saturated in ZnS indicate that the temperature of inversion is influenced by ZnS. Pure Cu_2S inverts on heating from hexagonal to cubic symmetry at 430°C, whereas the inversion takes place at $419^\circ \pm 3^\circ\text{C}$ when maximum solid solution of ZnS exists. Pure Cu_9S_5 (digenite) inverts at $73^\circ \pm 3^\circ\text{C}$ (Morimoto and Kullerud, 1963), but digenite with maximum ZnS in solid solution inverts at $79^\circ \pm 2^\circ\text{C}$.

Moh (1960) reported the presence of two or possibly three ternary phases in the Cu-Zn-S system at 400°C. We have

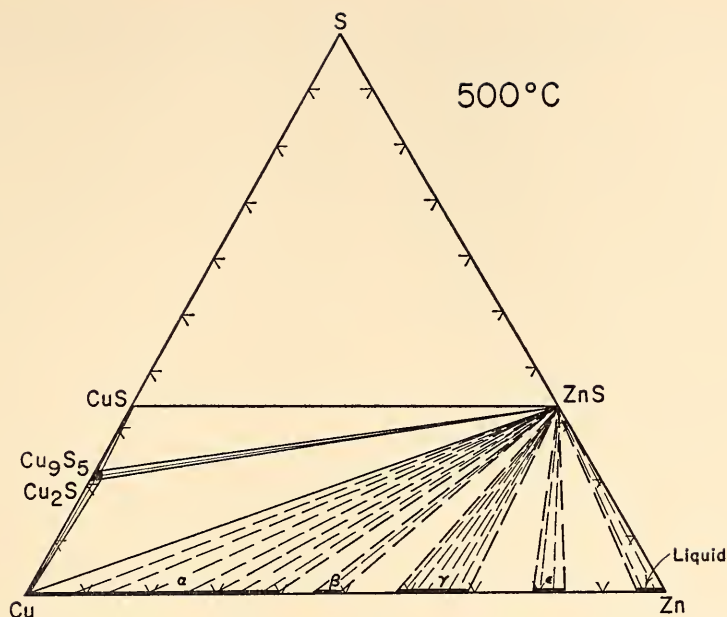


Fig. 67. Phase relations in the Cu-Zn-S system at 500°C. All phases and phase assemblages coexist with vapor.

not been able to synthesize any of the reported ternary compounds by heating, at 400° and 500°C, mixtures of the elements in some experiments, and mixtures of presynthesized ZnS and copper sulfides in others, for periods up to 8 months. Experiments recently performed by Moh at our request, using the same starting materials he employed earlier (Moh, 1960), produce small amounts of idaite, bornite, chalcopyrite, and copper oxides in addition to our reported binary phases. The compounds reported by Moh (1960) are not ternary phases in the Cu-Zn-S system. They are probably due to impurities, mostly Fe, in his starting materials.

CUBIC \rightleftharpoons HEXAGONAL INVERSIONS IN SOME M_3S_4 -TYPE SULFIDES

G. Kullerud

A number of sulfide-type compounds have the spinel structure. These compounds, which contain metals of the transition elements and sulfur, selenium,

or tellurium in the 3:4 atomic ratio, are of considerable interest, not only because many of them are minerals, but also because they display a large variation in electrical and magnetic properties. Some of these compounds are semiconductors, and others are metallic conductors. In contrast, the corresponding oxyspinels are all semiconductors.

Studies of the thermal stabilities of the M_3S_4 -type compounds show that most of them decompose to a mixture of monosulfides and disulfides; for instance, Ni_3S_4 produces $Ni_{1-x}S + NiS_2$ when decomposing. Some, such as $FeCr_2S_4$ (daubréelite), are reported to melt congruently.

During an investigation of the Ni-S system, Kullerud and Yund (1962) determined the temperature (356°C) of the invariant point where Ni_3S_4 breaks down to $Ni_{1-x}S + NiS_2$ in the presence of vapor. In another study (Year Book 60, pp. 176-178) they determined the upper stability curve of the Ni_3S_4 compound up to 2 kb confining pressure. This curve has a

positive slope of about $6^{\circ}\text{C}/\text{kb}$. The unit-cell dimensions of cubic spinel-type Ni_3S_4 as well as of the breakdown products, hexagonal Ni_{1-x}S (with $x=0.05$) and cubic NiS_2 , were determined, and the ΔV for the balanced equation was calculated. The calculation showed that the volume of the breakdown products is actually smaller than that of the cubic Ni_3S_4 . The curve describing the reaction $(1-2x)\text{Ni}_3\text{S}_4$ (cubic) $\rightleftharpoons 2\text{Ni}_{1-x}\text{S}$ (hexagonal) + $(1-4x)\text{NiS}_2$ (cubic) accordingly should have negative slope.

A number of pressure experiments on cubic Ni_3S_4 , which was synthesized in silica tubes below 350°C , showed that an inversion takes place in the Ni_3S_4 compound at low temperatures and low pressures. The schematic P - T diagram illustrating the behavior of the Ni_3S_4 compound is shown in Fig. 68. At the invariant point c (at 356°C) the four phases Ni_3S_4 (cubic) + Ni_{1-x}S (hexagonal) + NiS_2 (cubic) + V coexist. The univariant curve Ni_3S_4 (cubic) + Ni_{1-x}S (hexagonal) + NiS_2 (cubic) has a small negative slope between point c and its termination at about 400 bars and 353°C . At pressures exceeding 400 bars, cubic Ni_3S_4 is no longer stable; a high-pressure nonquenchable polymorph occurs instead. The inversion from the high-pressure to the low-pressure cubic symmetry is accompanied by twinning, which can be observed in appropriately etched polished sections. The approximate position of the P - T curve of the high-low inversion in the Ni_3S_4 compound is shown in Fig. 68. Appearance or lack of twinning in cubic Ni_3S_4 was used to bracket the curve in successive experiments.

This study shows that the field of stability of cubic Ni_3S_4 , which is represented in nature by the mineral polydymite, is very limited. In ores this mineral can have formed only at temperatures below 356°C , and in addition, if untwinned, it cannot have been exposed to pressures exceeding 400 to 500 bars. Since polydymite is cubic and

opaque, twinning is not readily observed, even in the best of polished sections, unless they are carefully etched. Etching shows that twinning is very common in this mineral in many localities; in others, twinning is entirely lacking. Its typical twinning gave this mineral its name polydymite, meaning many twins. The new experimental data provide a tool that can be used to obtain important information, not only on the maximum temperature prevailing during and after formation of this mineral, but on the pressure conditions as well.

The Co_3S_4 compound, which also has the spinel structure, is stable below 664°C in the condensed Co-S system. At this temperature it breaks down to hexagonal Co_{1-x}S and cubic CoS_2 .

Pressure experiments show that the stability curve of Co_3S_4 has a negative slope, which is in agreement with the calculated ΔV of the balanced reaction $(1-2x)\text{Co}_3\text{S}_4 \rightleftharpoons 2\text{Co}_{1-x}\text{S} + (1-4x)\text{CoS}_2$. At about 2.5 kb and 640°C the Co_3S_4 compound goes through an inversion similar to that observed for Ni_3S_4 . Albers and Rooymans (1965) have shown that the FeCr_2S_4 compound occurs in two polymorphs: a low-temperature, low-pressure, cubic spinel-type structure analogous to the mineral daubréelite, and a high-temperature, high-pressure form with a NiAs-derivative type structure. In DTA experiments the inversion in this compound is observed at about 1060°C in the presence of vapor. The morphology of single crystals grown in silica tubes above 1060°C is preserved on quenching and indicates a hexagonal symmetry for the high-temperature polymorph. With increasing pressure, the temperature of inversion decreases markedly. A series of synthetic compounds have also been found to invert from cubic spinel to NiAs-derivative structures when exposed to high pressures—examples are CuCr_2Se_4 , CuCr_2Te_4 , and CoCr_2S_4 . It is assumed by analogy that the high-pressure forms of spinel-type minerals, such as polydymite and lin-

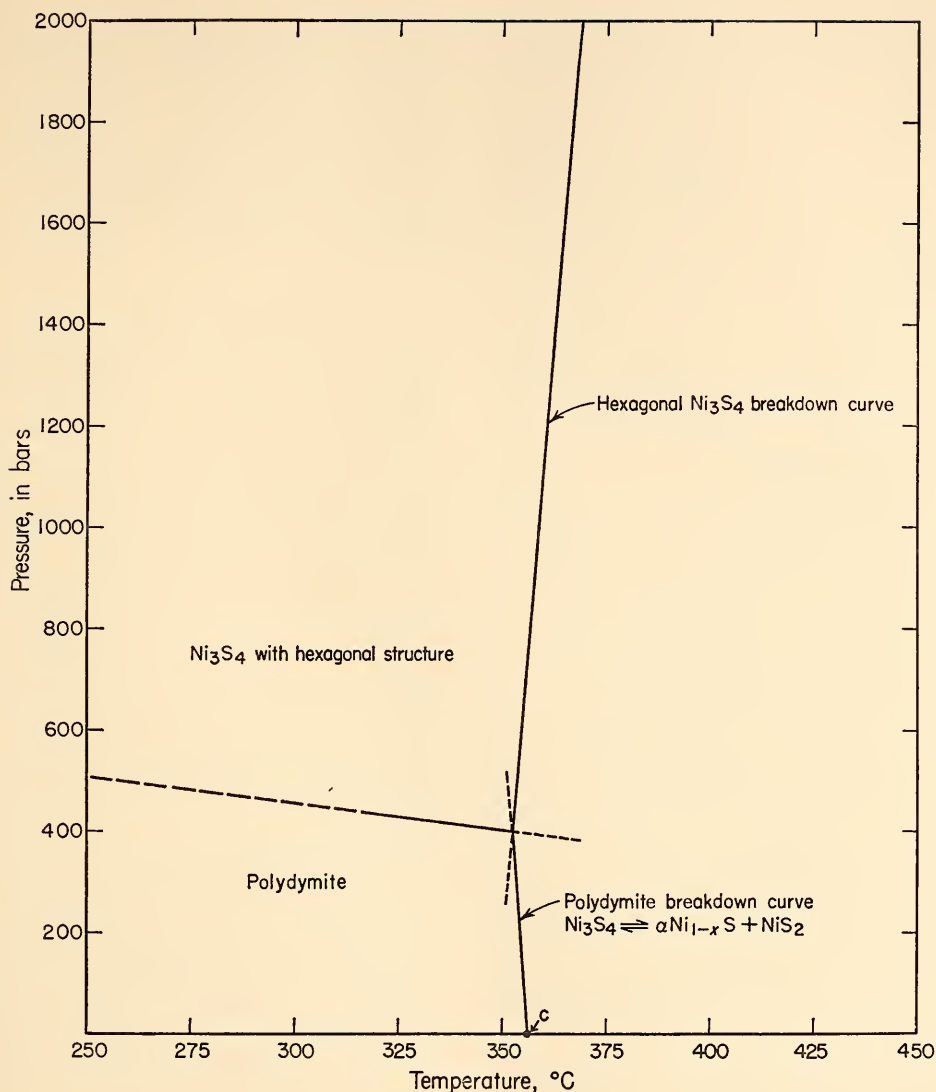


Fig. 68. The stability field of polydymite is limited to 356°C along the temperature axis and to about 500 bars along the pressure axis. Twinning, responsible for the mineral name polydymite (many twins), takes place when Ni_3S_4 with hexagonal structure inverts to the cubic polydymite form.

naeite, also have structures of the NiAs type.

The Fe_3S_4 compound is stable at low temperatures. On heating it decomposes below 100°C to monoclinic pyrrhotite of about Fe_7S_8 composition and to pyrite (FeS_2). This compound occurs in two

polymorphic forms: greigite, which has cubic spinel-type structure, and smythite, which has a NiAs -derivative type structure. The densities of the two polymorphs are nearly equal—Erd, Evans, and Richter (1957) gave 4.06 for smythite; and Skinner, Erd, and Grimaldi (1964)

give 4.08 for greigite. The effect of pressure on the greigite-smythite inversion, therefore, appears to be very small. Evidently, temperature is the main factor in deciding whether smythite or greigite forms. By analogy with the behavior of such minerals as polydymite, linnaeite, and daubréelite, smythite should be the high-temperature Fe_3S_4 polymorph, and greigite should be stable at low temperatures.

Preliminary studies on violarite (FeNi_2S_4), carrollite (CuCo_2S_4), siegenite [$(\text{Co,Ni})_3\text{S}_4$], bornhardtite (Co_3Se_4), and trüstedtite (Ni_3Se_4) indicate that these minerals, which all have cubic spinel-type structures, invert to polymorphs with NiAs-derivative hexagonal structures when exposed to elevated temperatures and pressures. A number of other sulfides, such as bornite (Cu_5FeS_4), chalcocite (Cu_2S), and digenite (Cu_9S_5), have $Fd3m$ (spinel)-type structures at elevated temperatures. Bornite has this structure above 248°C , chalcocite above 430°C , and digenite above 73°C . In accordance with the observations discussed above, it is to be expected that under pressure these spinel-type structures will become unstable and invert to a NiAs-derivative symmetry.

The NiAs-type structure is stable to very high pressures, as indicated by experiments of Kullerud, Bell, and England (*Year Book 64*, pp. 197–199) on FeS and Fe_{1-x}S , which have this structure.

METEORITE MINERALS

THE Cr-S AND Fe-Cr-S SYSTEMS

A. El Goresy and G. Kullerud

The purpose of the present study was to determine the phase relations in the Cr-S and Fe-Cr-S systems. Two new minerals have recently been reported to occur in the Cr-S system: Cr_2S_3 (mineral A; Ramdohr, 1964) and CrS (El Goresy, 1965). The study of the Cr-S system delineates the pressure-temperature fields of formation of the new minerals and

is a prerequisite to investigation of the complex Fe-Cr-S system. Daubréelite (FeCr_2S_4) is the only ternary phase. It is a common constituent of iron meteorites, enstatite chondrites, and achondrites, but is absent in all other types of meteorites. Troilite (FeS), the most common mineral in the ternary system, occurs in meteorites of all types.

The Cr-S System

Figure 69 shows the Cr-S phase diagram, based on data by previous investigators and on our studies at 500° , 600° , 700° , and 800°C .

$\text{Cr}_{1.03}\text{S}$. This compound, which apparently occurs only in one crystallographic modification, was observed in all experiments conducted with less than 39.61 wt % S. In polished sections it is seen as lenticular lamellae occurring parallel to at least four crystallographic directions in $\beta\text{Cr}_{1-x}\text{S}$. This type of intergrowth indicates an exsolution during quenching from a high-temperature homogeneous $\beta\text{Cr}_{1-x}\text{S}$ phase. The $\alpha\text{Cr}_{1.03}\text{S}$ phase is strongly reflecting (reflectivity similar to arsenopyrite) with weak birefringence and whitish color. The X-ray powder diffraction pattern of $\alpha\text{Cr}_{1.03}\text{S}$ was indexed by Jellinek (1957) as probably monoclinic. The X-ray powder diffraction pattern of this phase obtained by us agrees closely with that of Jellinek.

Cr_{1-x}S . This compound occurs in three crystallographic forms: a NiAs-type hexagonal (β) form, a hexagonal form with NiAs supercell, and a monoclinic, low-temperature modification.

$\beta\text{Cr}_{1-x}\text{S}$ was observed in all experiments containing less than 41.74 wt % S ($\text{Cr}_{0.86}\text{S}$). In quench products of experiments containing 37.62 wt % S or less, it occurs together with $\alpha\text{Cr}_{1.03}\text{S}$ and Cr, and in quench products of experiments containing 39.61 wt % S or less it occurs with $\alpha\text{Cr}_{1.03}\text{S}$ only. In polished sections, $\beta\text{Cr}_{1-x}\text{S}$ is brownish in color, with reflectivity similar to that of pyrrhotite. The X-ray powder diffraction pattern of

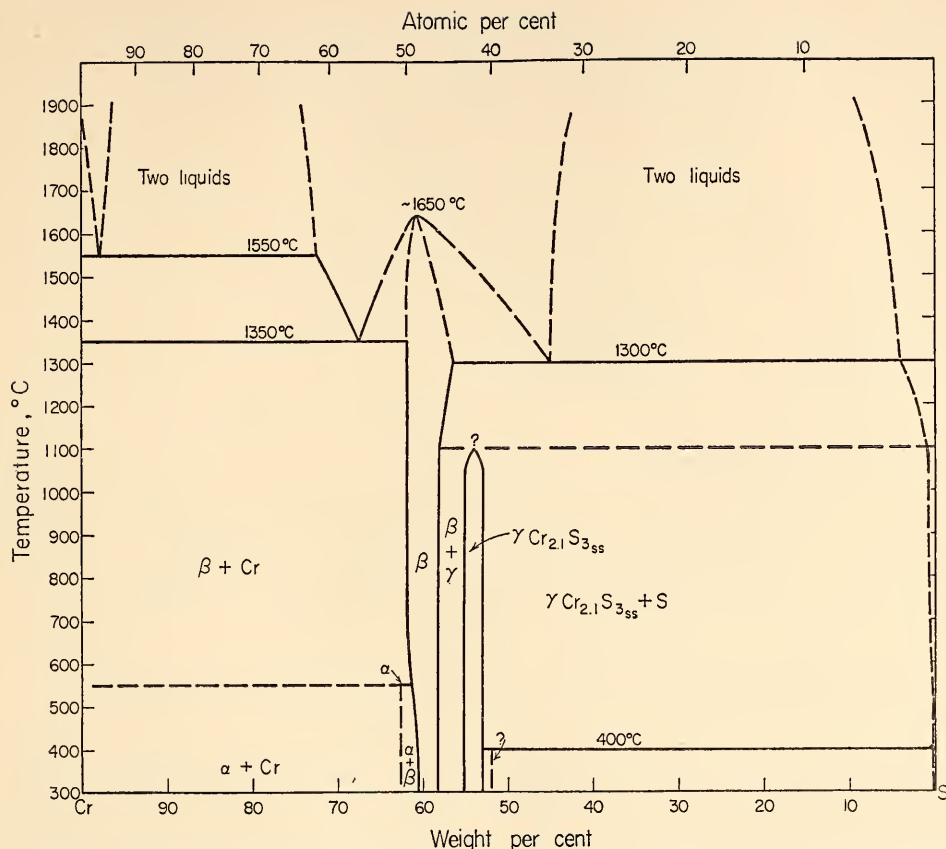


Fig. 69. A partially schematic T - X diagram of the system Cr-S. Dashed lines represent earlier work or relations which were not accurately determined.

$\beta\text{Cr}_{1-x}\text{S}$ is identical with that of Cr_7S_8 , as given by Jellinek (1957), but its stability field is not so narrow as reported by Jellinek. The approximate compositional stability limits of $\beta\text{Cr}_{1-x}\text{S}$ are shown in Fig. 69.

X-ray studies on $\beta\text{Cr}_{1-x}\text{S}$ mix-crystals containing 41.74 to 39.37 wt % S ($\text{Cr}_{0.86}\text{S}$ to $\text{Cr}_{0.93}\text{S}$), synthesized at 700°C and quenched, revealed that the d_{102} value may vary considerably. Fig. 70 illustrates the variation of d_{102} with composition, indicating that the d_{102} curve slopes steeply between $\text{Cr}_{0.93}\text{S}$ and $\text{Cr}_{0.89}\text{S}$ compositions but its slope is gentle in the $\text{Cr}_{0.89}\text{S}$ to $\text{Cr}_{0.86}\text{S}$ composition range. The curve offers a convenient method for

determining the composition of $\beta\text{Cr}_{1-x}\text{S}$ mix-crystals.

Hexagonal Cr_{1-x}S with superstructure was observed only in experiments with sulfur ranging from 42.04 to 43.53 wt % S. In polished section this phase cannot be distinguished from $\beta\text{Cr}_{1-x}\text{S}$. The X-ray powder diffraction patterns are distinctly different, however, with the superstructure, hexagonal Cr_{1-x}S phase displaying two characteristic reflections at low 2θ angles ($d=5.7759$ Å and $d=4.7374$ Å).

The monoclinic Cr_{1-x}S phase was observed in experiments containing 44.79 to 43.53 wt % S. It occurs with rhombohedral $\gamma\text{Cr}_{21}\text{S}_{3\text{ss}}$. In polished sections it can be recognized because it contains

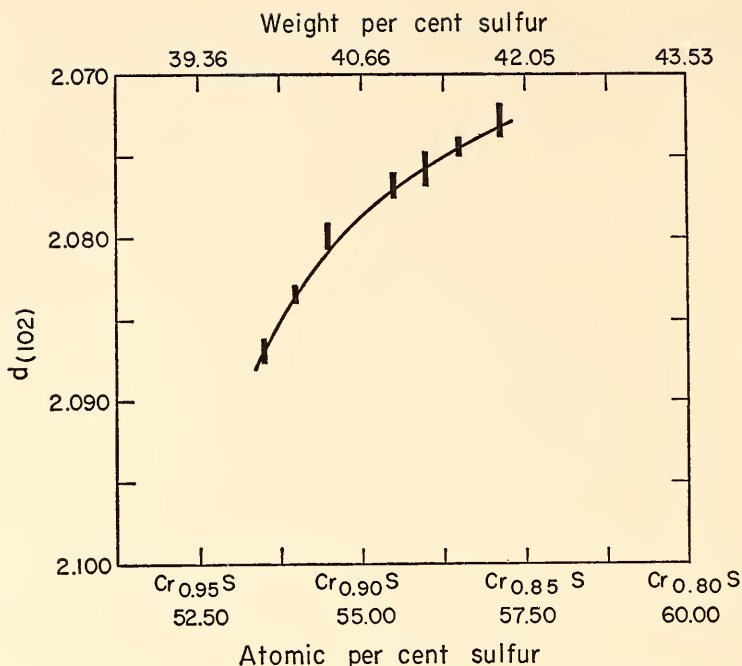


Fig. 70. Plot of d_{102} versus sulfur content for compounds of $\beta\text{Cr}_{1-x}\text{S}$ ss series.

inversion twin lamellae similar to those produced when chalcopyrite inverts from a high-temperature cubic to a low-temperature tetragonal form. The X-ray powder diffraction pattern has two reflections in the region of the 102 reflection of the hexagonal β pattern and an additional reflection at $d=5.2430$ Å. The X-ray powder diffraction pattern given by Jellinek for monoclinic Cr_3S_4 ($\text{Cr}_{0.75}\text{S}$ to $\text{Cr}_{0.76}\text{S}$) is identical with that of a composite of reflections produced from a mixture of monoclinic Cr_{1-x}S and $\gamma\text{Cr}_{2.1}\text{S}_3$ ss.

Cr_2S_3 . Jellinek (1957) reported two forms of Cr_2S_3 , a rhombohedral (γ) form with a narrow compositional range ($\text{Cr}_{0.67}\text{S}$) and a trigonal form with $\text{Cr}_{0.69}\text{S}$ composition. In the present investigation, only the rhombohedral form was observed in runs with sulfur content ranging from 46.84 to 45.12 wt %, indicating a wide range of compositional stability. In polished sections $\text{Cr}_{2.1}\text{S}_3$ ss cannot easily be distinguished from

other chromium sulfides. This compound does have a low-temperature form, as evidenced by twinning displayed in some polished sections. X-ray powder diffraction patterns of the twinned material show that the low-temperature form contains two reflections in the general region of the 114 reflection of the original rhombohedral $\gamma\text{Cr}_{2.1}\text{S}_3$ ss. This pattern, however, does not coincide with that of the trigonal Cr_2S_3 reported by Jellinek.

The Cr-Fe-S System

Experiments were performed with compositions lying in the monosulfide solid solution field at 700° and 600°C with mixtures of previously synthesized stoichiometric FeS and CrS as starting material, and in the sulfur-rich portion of the system with previously synthesized stoichiometric Cr_2FeS_4 and elemental sulfur. Fig. 71 shows the phase relations in the Cr-Fe-S system at 700°C. Above this temperature, complete solid solu-

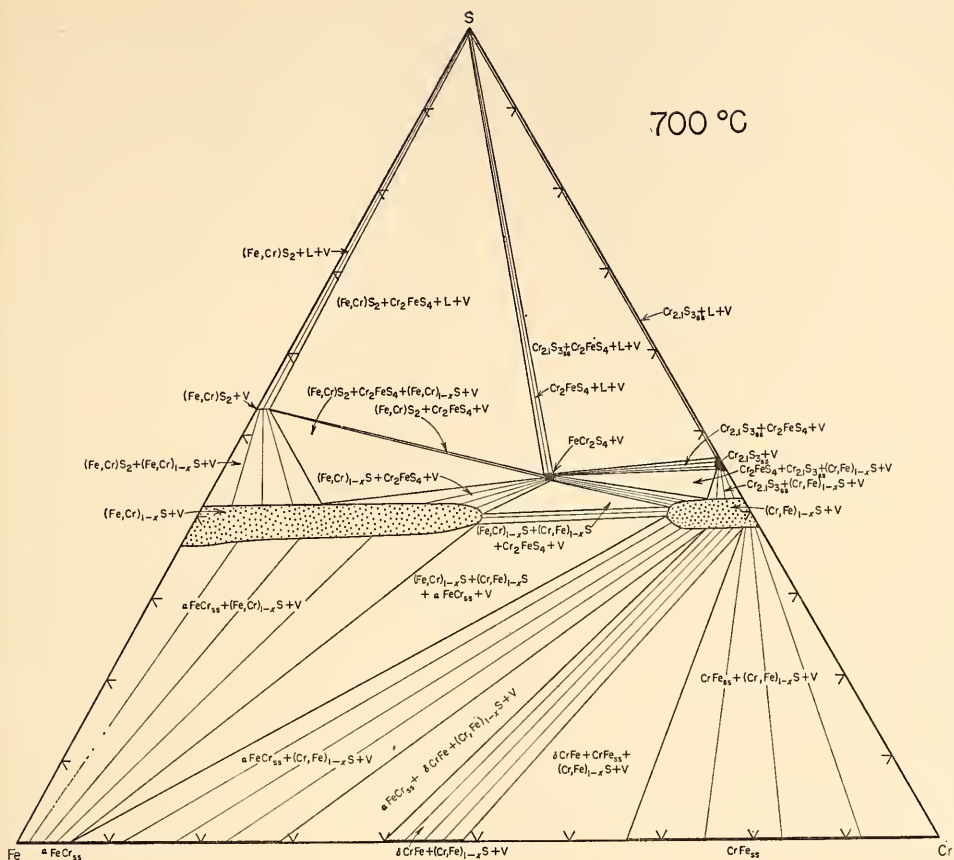


Fig. 71. Phase relations in the Cr-Fe-S system at 700°C. All assemblages are in equilibrium with vapor.

tion exists between Fe_{1-x}S and Cr_{1-x}S . At 700°C, two monosulfide solid solutions produced through breakdown of the Mss phase coexist: $(\text{Fe,Cr})_{1-x}\text{S}$ (Mss_I), extending from the Fe-S boundary, and $(\text{Cr,Fe})_{1-x}\text{S}$ (Mss_{II}), extending from the Cr-S boundary. These monosulfide solid solutions are separated by a divariant region containing Mss_I and Mss_{II}+V. At 700°C the ternary system contains eight univariant fields. The composition of αFeCr ss coexisting with Mss_I and Mss_{II} was determined with the electron microprobe and found to be 93.8–95.7% Fe and 4.3–6.2% Cr. Fig. 72 shows the phase relations at 600°C. Figs. 71 and 72 show that extensive changes take place

in the system between 700° and 600°C. The solid solution of Cr in Mss_I decreases markedly, whereas the solid solution of Fe in Mss_{II} decreases only slightly. In the metal-rich portion of the system, the solubilities of Cr in αFeCr ss and of Fe in CrFe ss decrease considerably and the sizes of the divariant regions $\text{CrFe ss} + (\text{Cr,Fe})_{1-x}\text{S} + V$ and $\alpha\text{FeCr ss} + (\text{Cr,Fe})_{1-x}\text{S} + V$ narrow markedly. Our experiments demonstrate that at $650^\circ \pm 50^\circ\text{C}$ an invariant reaction takes place: $(\text{Fe,Cr})_{1-x}\text{S} + (\text{Cr,Fe})_{1-x}\text{S} (\text{Mss}_\text{I} + \text{Mss}_{\text{II}}) + V \rightleftharpoons \text{Cr}_2\text{FeS}_4 + \alpha\text{FeCr ss}$. As a result, two new univariant fields appear in the system: $\text{Cr}_2\text{FeS}_4 + (\text{Fe,Cr})_{1-x}\text{S} + \alpha\text{FeCr ss} + V$ and $\text{Cr}_2\text{FeS}_4 + (\text{Cr,Fe})_{1-x}\text{S} + \alpha\text{Fe}$.

served vary considerably from one meteorite to another, and the daubréelite content may even vary from $\approx 5\%$ to more than 60% by volume in different parts of the same meteorite. This variation in mineral concentration corresponds to a range of 1 to 25% Cr, 20 to 30% S, and 60 to 70% Fe. Our experiments demonstrate that bulk compositions ranging from 50FeS+50CrS to 25FeS+75CrS (mole %) are accounted for by $\text{Mss}_I + \text{Mss}_{II} + \alpha\text{FeCr ss}$ assemblages at 700°C. Compositions with 50 to 75 mole % FeS will form one homogeneous phase (Mss_I), whereas compositions with more than 75 mole % CrS will form another homogeneous phase (Mss_{II}). In a cooling meteorite parent body containing (Fe, Cr)_{1-x}S mix-crystals with compositions in the range 50 to 75 mole % Cr_{1-x}S, the invariant reaction $\text{Mss}_I + \text{Mss}_{II} + V \rightleftharpoons \text{db} + \alpha\text{FeCr ss}$ takes place at $650^\circ \pm 50^\circ\text{C}$. Mix-crystals with more than 50% CrS will give the assemblage daubréelite + $\text{Mss}_{II} + \alpha\text{FeCr ss} + V$, whereas those with less than 50% CrS result in the assemblage daubréelite + $\text{Mss}_I + \alpha\text{FeCr ss} + V$. With decreasing temperature, the solubility of Cr in Mss_I diminishes considerably, the solubility of Fe in Mss_{II} decreases only slightly, and the univariant field $\text{Cr}_2\text{FeS}_4 + \text{Mss}_I + \alpha\text{FeCr ss} + V$ widens markedly. The crystallization of daubréelite and $\alpha\text{FeCr ss}$ from Mss_I mix-crystals with ~ 25 mole % CrS takes place below 600°C, and the $\alpha\text{FeCr ss}$ separating from these mix-crystals contains less than 0.5 wt % Cr. In iron meteorites the $\alpha\text{FeCr ss}$ tends to react with kamacite during the long cooling periods. Thus Cr is distributed in the major metallic phase. Under these conditions, minor amounts of Cr in the metallic phase of iron meteorites would not be detectable with microprobe techniques. Enstatite chondrites and achondrites contain much less kamacite than iron meteorites, and hence Cr might be detected in the reequilibrated kamacite of the latter.

The present study demonstrates that

the assemblage daubréelite + $\text{Mss}_I + \alpha\text{FeCr ss}$ originates at relatively low temperatures from Cr-poor monosulfide mix-crystals. The presence of $\text{Mss}_I + \text{Mss}_{II}$ in the 40:60% ratio—as in the Bethany, Obernkirchen, and Russel Gulch meteorites—may indicate rapid cooling to temperatures below 700°C. The presence of Ni in solid solution, forming (Cr,Fe,Ni)_{1-x}S mix-crystals, however, may prevent the establishment of the daubréelite + $\alpha\text{FeCr ss}$ assemblage, since Fe_{1-x}S-Ni_{1-x}S solid solution is complete down to 300°C (Naldrett, Craig, and Kullerud, 1967).

SULFIDE ASSEMBLAGES IN THE ODESSA METEORITE

G. Kullerud and A. El Goresy

Applications of pertinent phase diagrams, produced by experimental studies on synthetic systems, have shown that lack of equilibrium between minerals in one and the same assemblage is not a rare occurrence in meteorites and that equilibrium between different assemblages, often only a few millimeters apart, is usually not achieved. It appears, as we shall see below, that some of the nonequilibrium assemblages found in meteorites may be explained as effects of shock.

To investigate this phenomenon we have chosen to make a detailed examination of mineral associations occurring in the Odessa meteorite. This meteorite, which was found near Odessa, Texas, in 1922, weighed more than 1 ton and is classified as an iron meteorite. In the Odessa iron meteorite small troilite nodules, usually rimmed by graphite, are distributed throughout an FeNi matrix. Studies of polished sections of these nodules reveal that they are polymineralic, although troilite is always by far the most abundant phase. Some of the troilite spherules in the Odessa meteorite contain assemblages of heazlewoodite (Ni_3S_2), daubréelite (FeCr_2S_4), and sphalerite [(Zn,Fe)S], in addition to

troilite (FeS). Others contain assemblages of awaruite (Ni_3Fe), daubréelite, sphalerite, and troilite.

We have some knowledge of the behavior of the FeCr_2S_4 and $(\text{Zn,Fe})\text{S}$ compounds and have detailed information on the Fe-Ni-S system. Neither troilite and heazlewoodite nor troilite and awaruite coexist stably at any temperature in the condensed Fe-Ni-S system. At elevated pressures, troilite becomes stable with heazlewoodite over a relatively large temperature range and with awaruite over a much more restricted range. To provide a background for interpreting observations on minerals in meteorites, we present a discussion of some of the physical chemistry of the pertinent constituents.

Troilite (FeS) has a simple NiAs-type structure above 139°C and forms a superstructure below this temperature. The high-temperature form cannot be quenched, but the inversion can readily be detected by DTA experiments. Pressure decreases the inversion temperature to about 90°C at 20 kb (Kullerud, Bell, and England, *Year Book 64*, pp. 197–199). In other words, pressure lowers the inversion temperature by about $2.5^\circ\text{C}/\text{kb}$.

The Ni_3S_2 compound occurs in two crystalline modifications. The low-tem-

perature form is hexagonal and is represented in nature by the mineral heazlewoodite. This form is stoichiometric (Kullerud and Yund, 1962) and takes less than 1 wt % Fe in solid solution. At 556°C it inverts to a high-temperature pseudocubic (α) modification that exhibits extensive solid solution toward both Ni and S (Kullerud and Yund, 1962) and may also take as much as 5 wt % Fe in solid solution, lowering the inversion temperature to about 525°C . Kullerud, Bell, and England (*Year Book 64*, pp. 197–199) found that pressure increases the inversion temperature of pure stoichiometric Ni_3S_2 by about $1.7^\circ\text{C}/\text{kb}$ and that of iron-saturated $\alpha(\text{Ni,Fe})_{3\pm x}\text{S}_2$ by about $0.3^\circ\text{C}/\text{kb}$.

Taenite ($\gamma\text{Fe,Ni}$) is a high-temperature cubic Fe-Ni solid solution. Awaruite is a cubic Ni_3Fe phase, which is stable below 503°C in the condensed Fe-Ni-S system. The phase relations at 500°C in the pertinent portion of the condensed Fe-Ni-S system are shown in Fig. 73. The cubic pentlandite $(\text{Fe,Ni})_9\text{S}_8$ phase in the presence of vapor is stable below 610°C (Kullerud, 1963). Above this temperature it decomposes to the hexagonal $(\text{Fe,Ni})_{1-x}\text{S}$ -type phase and $\alpha(\text{Ni,Fe})_{3-x}\text{S}_2$. Bell, England, and Kullerud (*Year Book 63*, pp. 206–207) showed that the temperature at which pentland-

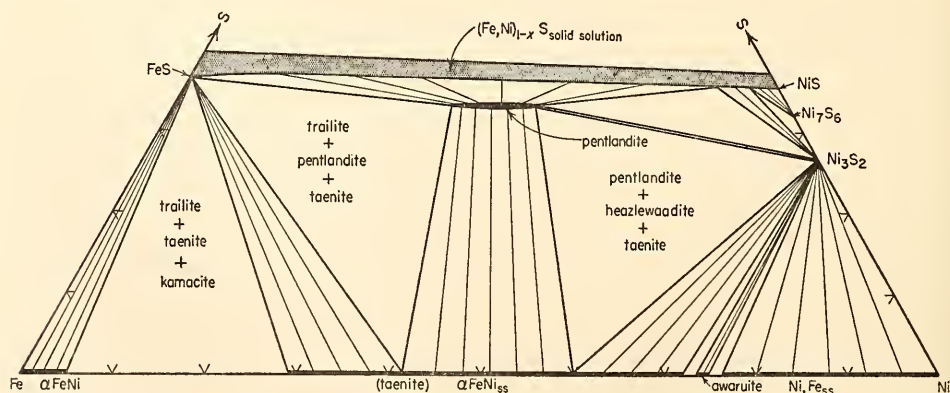


Fig. 73. Phase relations at 500°C in the metal-rich portion of the condensed Fe-Ni-S system. On cooling to about 450°C the $\gamma\text{FeNi ss}-\text{Ni}_3\text{S}_2$ tie lines are replaced by awaruite-pentlandite tie lines.

ite decomposes decreases markedly with increased pressures; for instance, at 25 kb pentlandite decomposed at 425°C. The pentlandite-taenite tie lines shown in Fig. 73 exist below about 580°C, prohibiting stable coexistence of troilite and heazlewoodite. It is shown in this figure that at 500°C tie lines exist between taenite and heazlewoodite; thus troilite-awaruite coexistence is prohibited by two sets of tie lines (taenite-pentlandite and taenite-heazlewoodite). At about 450°C, however, the taenite-heazlewoodite assemblage becomes unstable in the condensed system, and below this temperature awaruite is stable with pentlandite.

The reaction rates in the central portion of the system are extremely rapid. For instance, it is not possible to preserve troilite + $\alpha(\text{Ni,Fe})_3\text{S}_2$ assemblages in the condensed system, even by the most rapid chilling. On cooling, pentlandite always forms at 610°C, taenite appears at 580°C, and the $\alpha(\text{Ni,Fe})_3\text{S}_2$ phase inverts to the heazlewoodite form at about 525°C.

Troilite-Heazlewoodite-Daubréelite-Sphalerite Assemblages

Some nodules of the Odessa meteorite contain troilite, heazlewoodite, daubréelite, and sphalerite in physical contact (El Goresy, 1967). Examination of fine textures displayed in the heazlewoodite reveals that originally an $\alpha(\text{Fe,Ni})_3\text{S}_2$ phase formed. It later broke down to heazlewoodite and a few percent of troilite, which form exceedingly fine myrmekitic intergrowths.

By electron probe analyses the heazlewoodite was found to contain 65.3 Ni, 4.6 Fe, 0.2 Co, and 27.4 S (wt %). The composition corresponds closely to that of the $\alpha(\text{Ni,Fe})_{3\pm x}\text{S}_2$ phase when coexisting with troilite above 610°C (Kullerud, *Year Book 62*, pp. 175-189). Apparently, the heazlewoodite is the product of breakdown of a homogeneous $\alpha(\text{Ni,Fe,Co})_{3\pm x}\text{S}_2$ phase, which had a metal-to-sulfur ratio of 2.80:2, as calculated from

the analysis given above. The P - T curve (I) for this breakdown is shown in Fig. 74. The $\alpha(\text{Ni,Fe,Co})_{2.8}\text{S}_2$ phase formed in the P - T field on the right side of curve I. Since it coexisted with troilite, and pentlandite did not form, the P - T conditions must have exceeded those of curve II. Above this curve, troilite + $\alpha(\text{Ni,Fe,Co})_{3\pm x}\text{S}_2$ coexist stably; below this curve pentlandite is stable. The $\alpha(\text{Ni,Fe,Co})_{2.8}\text{S}_2 \rightleftharpoons$ heazlewoodite breakdown must have taken place at pressures exceeding 14 kb; otherwise heazlewoodite + troilite would have reacted to produce pentlandite.

The reactions on curves I and II are so rapid that Bell, England, and Kullerud (*Year Book 63*) were able to determine these curves by DTA experiments. Even at 425°C the reaction is sufficiently rapid to be detected by DTA.

Preservation of the troilite-heazlewoodite mineral assemblage in a meteorite, therefore, necessitates that cooling take place under pressures above curve II, to low temperatures, at which the reaction to form pentlandite is very sluggish. Reaction-rate studies conducted in silica tubes at 200°, 250°, and 300°C on synthetic mixtures of FeS and Ni_3S_2 , showed no reaction even after 6 months at 200°C, beginning reaction at 250°C, and a high percentage of pentlandite at 300°C.

Although reaction rates in silica tubes are not directly comparable with those attained under high confining pressures, these experiments indicate that preservation of the troilite-heazlewoodite assemblage in meteorites requires maintenance of pressure in excess of 40 kb down to a temperature of about 250°C. The study of polished sections also reveals that the FeCr_2S_4 compound was not cubic when originally formed, but apparently hexagonal. It inverted to daubréelite at a later stage in the history of the meteorite. Albers and Rooymans (1965) found that FeCr_2S_4 exists in two polymorphs, daubréelite and a hexagonal form with NiAs-type structure. They

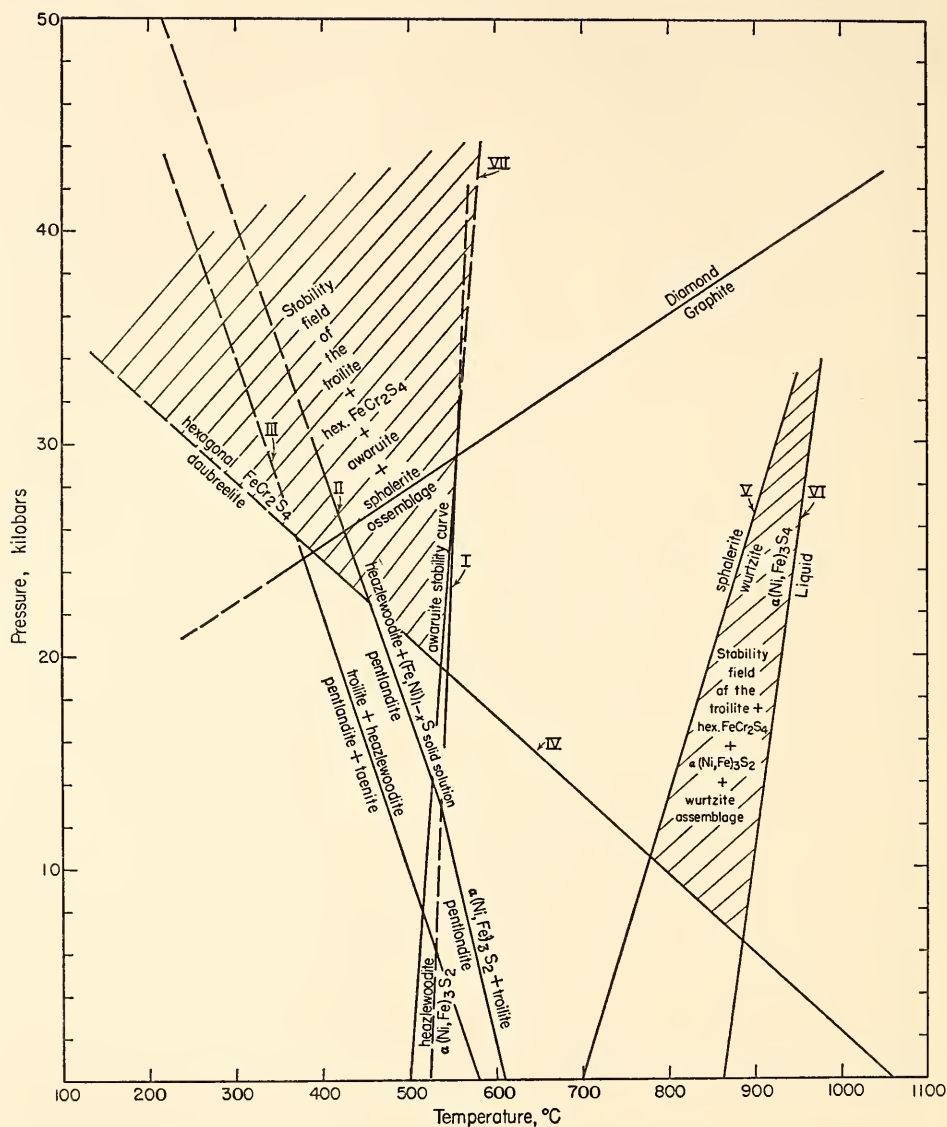


Fig. 74. Stability fields of the assemblages troilite + hexagonal FeCr_2S_4 + awaruite + sphalerite and troilite + hexagonal FeCr_2S_4 + $\alpha(\text{Ni,Fe})_{3-2}\text{S}_2$ + wurtzite.

determined the P - T curve of this inversion (curve IV in Fig. 74).

Fine textures in polished sections also show that the zinc sulfide when originally deposited did not have the cubic sphalerite structure, as evidenced by its morphology. Pure ZnS , which is cubic at low temperatures, inverts to hexagonal

wurtzite when heated to about 1020°C . Zinc sulfide forms extensive solid solutions with FeS and MnS (Kullerud, 1953), both of which depress the temperature of the cubic \rightleftharpoons hexagonal inversion. Electron probe analyses of the sphalerite in the Odessa meteorite show that it consists of 50.8 ZnS , 38.2 FeS , and

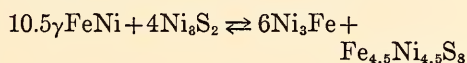
11.0 MnS (mole %). The P - T curve for the sphalerite-wurtzite transition for this composition is not known. It is estimated that the inversion takes place at $700^\circ \pm 50^\circ\text{C}$ at 1 atm, from the work on the FeS-ZnS and MnS-ZnS joins by Kullerud (1953), and that the slope of the P - T curve is 5° to 10°C/kb . This curve is labeled V in Fig. 74.

The original assemblage troilite + $\alpha(\text{Ni,Fe})_{3-x}\text{S}_2$ + hexagonal FeCr_2S_4 + wurtzite must have formed at a temperature limited downward by the sphalerite-wurtzite curve and upward by the melting curve of $\alpha(\text{Ni,Fe})_3\text{S}_2$. This curve (labeled VI in Fig. 74) starts at 862°C in the condensed system (Kullerud, 1963) and is expected to have a steep slope ($\approx +3^\circ\text{C/kb}$). The pressure when the above assemblage formed exceeded the FeCr_2S_4 inversion curve. On cooling, the $\alpha(\text{Ni,Fe})_3\text{S}_2$ phase decomposed to heazlewoodite and troilite at about 550°C under pressure exceeding about 20 kb. Troilite and heazlewoodite did not react to form pentlandite. The pressure, therefore, must have been maintained above curve III to at least 250°C . Reaction rates in the Fe-Ni-S system are sluggish below this temperature, and a release of pressure would not result in pentlandite formation during subsequent cooling. The inversion from hexagonal FeCr_2S_4 to daubréelite apparently took place when pressure was released below about 250°C .

Troilite-Awaruite-Daubréelite-Sphalerite Assemblages

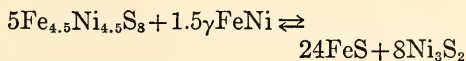
Studies of the fine textures displayed in some troilite nodules in polished sections reveal that hexagonal FeCr_2S_4 , cubic sphalerite, troilite, and awaruite originally coexisted (El Goresy, 1967). At the time of formation of this assemblage the pressure must have exceeded that of the FeCr_2S_4 hexagonal \rightleftharpoons cubic inversion curve. The temperature must have been below that of the sphalerite \rightleftharpoons wurtzite inversion curve. The awaruite

phase is stable below 503°C in the condensed Fe-Ni system. Pressure will influence its stability at the rate of 1° – 3°C/kb . The temperature could not have exceeded the awaruite stability curve (VII in Fig. 74). Coexistence of troilite and awaruite requires changes in two sets of tie lines, those connecting taenite and heazlewoodite and those connecting taenite and pentlandite. In the condensed Fe-Ni-S system the reaction taenite + heazlewoodite + V \rightleftharpoons awaruite + pentlandite takes place at about 450°C , awaruite + pentlandite being stable together below this temperature. Under high confining pressures the balanced reaction can be written



Calculations of the volumes involved demonstrate that the awaruite-pentlandite assemblage is favored by pressure. The awaruite + pentlandite mineral pair is stable at increasing temperatures (beyond 450°C) with increasing pressure.

Kullerud (*Year Book 62*) showed that pentlandite-taenite tie lines exist below about 580°C in the condensed Fe-Ni-S system. The balanced equation for the upper stability curve for the pentlandite-taenite assemblage can be written



Calculations of the volumes of the phases involved demonstrate that the assemblage of troilite + heazlewoodite is favored by pressure, and the upper stability curve of the pentlandite-taenite assemblage has a negative slope. This reaction is similar to that involving breakdown of pentlandite to heazlewoodite + $\alpha(\text{Fe,Ni})_{1-x}\text{S}$. The P - T curve of pentlandite was shown by Bell, England, and Kullerud (*Year Book 63*) to have a pronounced negative slope. In Fig. 74 the curves pentlandite + taenite \rightleftharpoons heazlewoodite + troilite (III) and pentlandite \rightleftharpoons heazlewoodite + $\alpha(\text{Fe,Ni})_{1-x}\text{S}$ have been assumed to be essentially parallel.

It is seen from this discussion and from Fig. 74 that troilite-awaruite assemblages are stable in the P - T region bounded upward in temperature by the upper stability curve of the awaruite phase and downward in pressure by the troilite + heazlewoodite \rightleftharpoons pentlandite + taenite curve.

Formation and preservation of the assemblages troilite + hexagonal FeCr_2S_4 + $\alpha(\text{Ni,Fe})_3\text{S}_2$ + wurtzite and troilite + hexagonal FeCr_2S_4 + awaruite + sphalerite require pressures of at least 40 kb. The first assemblage, however, requires an initial temperature of at least 750°C, whereas the second assemblage is not stable beyond about 550°C. If these assemblages formed more or less simultaneously in adjacent spherules, perhaps only a few millimeters apart, a very strong temperature gradient must have existed. Such a gradient could not have persisted for long in an iron-nickel mass, which is an excellent heat conductor.

Graphite is associated with all troilite nodules. The graphite-diamond P - T curve is shown in Fig. 74. It is noted that preservation to low temperatures of the mineral assemblages discussed above requires pressures in the diamond stability field. Maintenance of such pressures over an extended period of time would have converted the graphite to diamond.

The metal phase of the Odessa meteorite contains small amounts of almost pure albite and orthoclase (El Goresy, 1967). Under the P - T conditions indicated by the sulfide assemblages, albite under equilibrium conditions reacts to give jadeite + SiO_2 . The P - T curve for albite \rightleftharpoons jadeite + SiO_2 , therefore, could not have been exceeded for very long.

The mineral assemblages discussed above collectively present strong evidence of shock. Because of the rapid reaction rates displayed by sulfides, these minerals responded to the shock, whereas slowly reacting minerals, such as albite, did not.

The shock evidently produced very

inhomogeneous temperatures. The maximum temperature did not result in melting of the $\alpha(\text{Ni,Fe})_{3-2}\text{S}_2$ phase and therefore did not exceed about 900°C. The pressure of the shock must have exceeded 40 kb but was not sufficient to produce maskelynite, since the orthoclase phase remains.

SULFUR-ISOTOPE FRACTIONATION IN MINERALS

H. Puchelt

The $\text{S}^{34}/\text{S}^{32}$ ratios of minerals from different geological settings vary considerably. A number of geochemical processes are believed to have caused this phenomenon. Isotope fractionation in biogeochemical processes is substantial and has received much attention, but comparatively few efforts have been made to determine sulfur-isotope fractionation accompanying inorganic reactions of metallic sulfides under controlled conditions. During the past year, such experiments have been carried out in well-known, simple sulfide systems.

Analytical Procedure

The method of Sabels and Hoering (*Year Book 62*, pp. 238-239) for the preparation of sulfur hexafluoride and its subsequent introduction into the mass spectrometer for isotope analysis was improved and developed into a routine procedure. The main simplifications were the dispensing of the fluorinating agent, BrF_3 , into the reaction vessels as a liquid and the quantitative recovery of the reaction product. A fiftyfold excess of BrF_3 was reacted with sulfides at 230°C for at least 1 hour. A quantitative yield of SF_6 was obtained from pyrite, galena, sphalerite, covellite, chalcopyrite, cinnabar, cadmium sulfide, and elemental sulfur. Pyrrhotite, troilite, and digenite do not react completely but could be converted to cadmium sulfide first and then fluorinated.

The method has been used for over 350 samples. An interlaboratory check

was carried out with the Zentrallaboratorium für die Geochemie der stabilen Isotope, Göttingen, Germany, which uses a completely different system of sample preparation, sulfur dioxide being the gas employed for mass spectrometry. The results of both laboratories agreed to within 0.2 ‰ for a suite of four sulfide samples.

Results are expressed in parts per thousand difference of the S^{34}/S^{32} ratios as compared with a standard sulfur

$$\delta S^{34} = \frac{(S^{34}/S^{32})_x - (S^{34}/S^{32})_s}{(S^{34}/S^{32})_s} \times 1000$$

where the subscript x refers to the sample under investigation and the subscript s refers to the standard sulfur, which in this study was troilite from the Canyon Diablo meteorite.

Sulfur-Isotope Fractionation in the Reactions of Metallic Sulfides

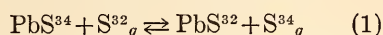
Formation of sulfides from the elements. Fifty mg of lead and a 50% excess of sulfur were sealed in evacuated quartz tubes and heated to 300°C. Likewise, copper, lead, and excess sulfur were reacted, with the metal powders kept separated in open gold tubes. Metallic sulfides formed rapidly. The runs were quenched, and the excess sulfur was extracted with trichloroethylene. The relative abundance of the sulfur isotopes in the separated phases was measured.

Table 12 shows the difference in δS^{34} of the lead sulfide and sulfur as a function of reaction time. During the

TABLE 12. Isotopic Composition of the Sulfur in Galena, and Sulfur during the Reaction of Lead and Sulfur at 300°C

$\delta S^{34}(\text{sulfur}) - \delta S^{34}(\text{galena}),$ ‰	Reaction Time, hours
4.8	0.08 ₃
7.6	0.25
10.8	0.42
7.5	1
6.1	5
4.6	16
3.9	96
2.8	240

initial reaction, the light isotope concentrated in the lead sulfide. Then, a slow exchange of sulfur atoms between sulfur vapor and the sulfide took place:



Extrapolation of the data to long periods of time indicates that the equilibrium constant for reaction 1 may be 1.002 at 300°C. Table 13 shows the results for the combined copper-lead sulfur system. Digenite, an intermediate phase in the reaction, was found in both runs, the larger proportion being found in the shorter run. During the initial sulfide formation, S^{34} concentrated in the copper sulfides and S^{32} in the lead sulfide. Following this, isotopic exchange between the sulfides and sulfur vapor took place, tending toward the equilibrium state.

In contrast to the rapid exchanges of sulfides and sulfur, no measurable change in sulfur-isotope ratios occurred when BaSO_4 and galena were heated to 500°C for 240 hours.

Sulfur-isotope exchange between sulfides and sulfur. Fifty-mg samples of a natural galena were heated with an equivalent amount of sulfur at 400° and 500°C for periods up to 96 hours. The initial difference in the S^{34} content was 18 ‰. Isotopic exchange took place, reducing the difference in δS^{34} to 0.8 ‰ in 24 hours at 500°C and to 4.1 ‰ in 96 hours at 400°C (Fig. 75). Extrapolation of the data in Table 12 indicates that at 300°C an initial difference of 10.8 ‰ decreased to 4.6 ‰ in 16 hours. The sulfide prepared from pure materials

TABLE 13. Sulfur-Isotope Fractionation between Copper Sulfide, Lead Sulfide, and Sulfur Vapor at 300°C

Phase	$\delta S^{34}, \text{‰}$	Reaction Time, hours
Sulfur	2.6	24
Covellite	4.3	
Galena	-1.4	
Sulfur	6.5	192
Covellite	1.6	
Galena	-1.1	

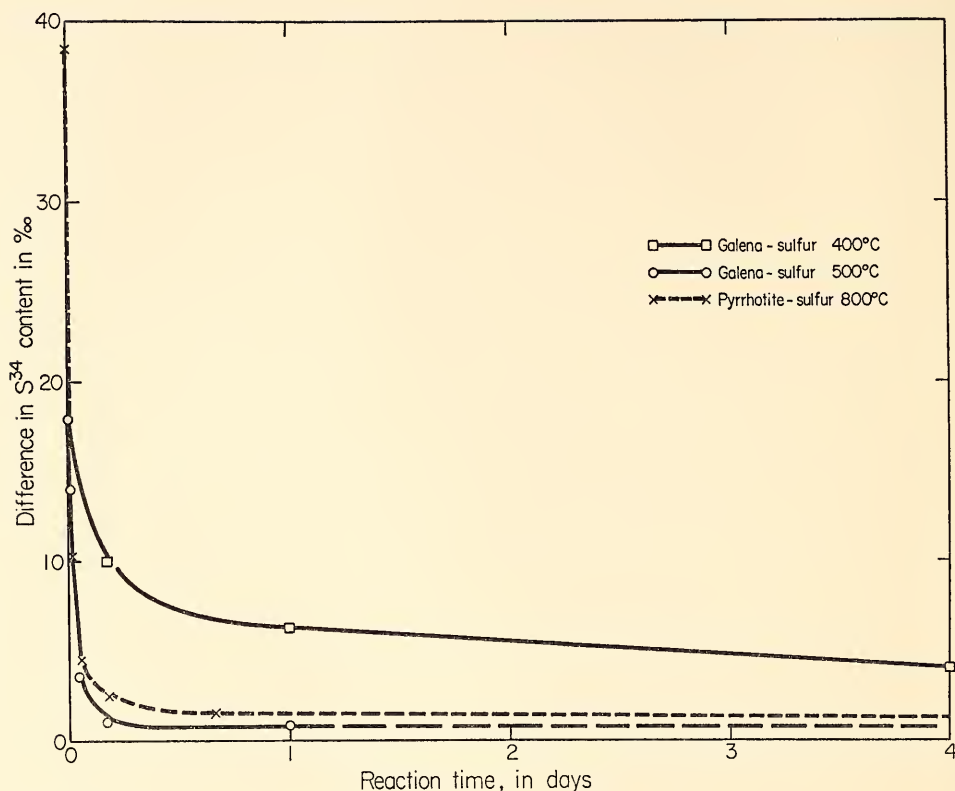


Fig. 75. Sulfur-isotope exchange between sulfides and sulfur.

seems to exchange more rapidly than the natural one.

The same reaction was brought about with pyrrhotite and sulfur at 800°C (above the pyrite invariant point). Here, the initial difference in δS^{34} of 38.4 ‰ decreased to 1.5 ‰ in 16 hours.

Some geological consequences are implied by these results. A sulfur vapor phase, generated by the breakdown of incongruently melting sulfides or by solfataric volcanic activity, may react with existing sulfides, causing exchange of their sulfur isotopes. A complete alteration of the original sulfur-isotope ratio in the sulfides may take place. A change in the isotope ratio of the sulfur vapor may also occur.

Isotope homogenization between sulfides. In a series of experiments, two samples of a mineral of natural origin

with different sulfur-isotope ratios were placed separately in gold tubes contained in a quartz vessel. The evacuated, sealed vessel was heated, the reaction was quenched, and the isotopic composition of the minerals was redetermined.

Two galena samples (50 mg each; differing by 27.9 ‰) were heated at 500° and 600°C. The difference in sulfur-isotope ratio as a function of time is plotted in Fig. 76. After 264 hours at 500°C, the samples had exchanged and had a difference of 2.4 ‰. At 600°C the same degree of homogenization was reached in only 12 hours. The minerals, which were initially fine powders (less than 150 mesh), were considerably recrystallized at the end of the run. Equal weights of two sphalerites showed a much lower rate of exchange. Heating for 96 hours at 600°C produced no appreciable change

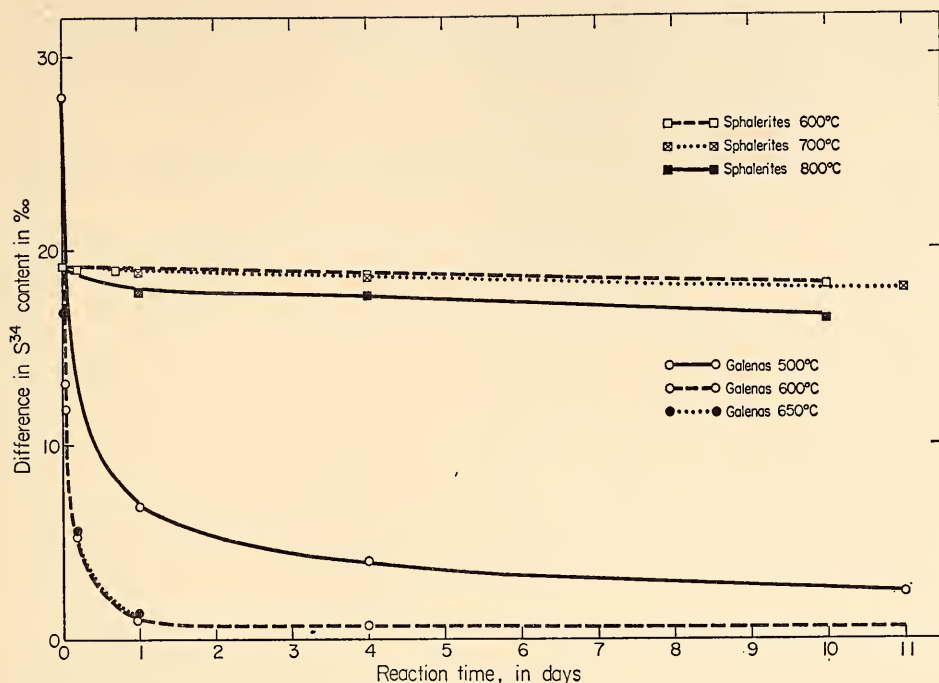


Fig. 76. Sulfur-isotope homogenization between galenas and sphalerites.

in isotopic ratios; 240 hours at 800°C caused the initial difference of 19.2 ‰ to change to 16.4 ‰. Pyrites reacted very slowly at 500°C. The data at 650°C in Fig. 77 show that after 39 days the initial difference in δS^{34} values had decreased from 56.7 ‰ to 45.6 ‰. The experiments establish a trend in the rates of reactions of isotope homogenization in mineral sulfides: galena is more rapid than pyrite, which is more rapid than sphalerite.

Breakdown Experiments

A sulfur-isotope fractionation has been reported during the incongruent melting of sulfides such as pyrite and covellite (Thode, 1963). This has been investigated further by analysis of S generated by heating pyrite, marcasite, and covellite for 15 minutes above their invariant points. The pyrite and marcasite showed little or no isotope effect during breakdown under these conditions. Covellite

showed a slight isotope effect; the sulfur was +2.9 ‰ different from the starting material.

The breakdown of pyrite below the invariant point was studied in a tube with a temperature gradient. The sample was kept at 600°C, and the sulfur distilled to the cold end. Table 14 shows the results of such an experiment where the sulfur has a relatively large isotopic difference from the pyrite. Presumably this is due to the lack of exchange of sulfur vapor with the remaining pyrite. In a natural, open system, such a process might cause considerable isotope variations.

Sulfur-Isotope Ratios in Minerals of the Bodenmais, Germany, Deposit

The results discussed above suggest that homogenization of sulfur-isotope ratios in sulfide minerals may take place at elevated temperatures in nature. This process may utilize a vapor of elemental

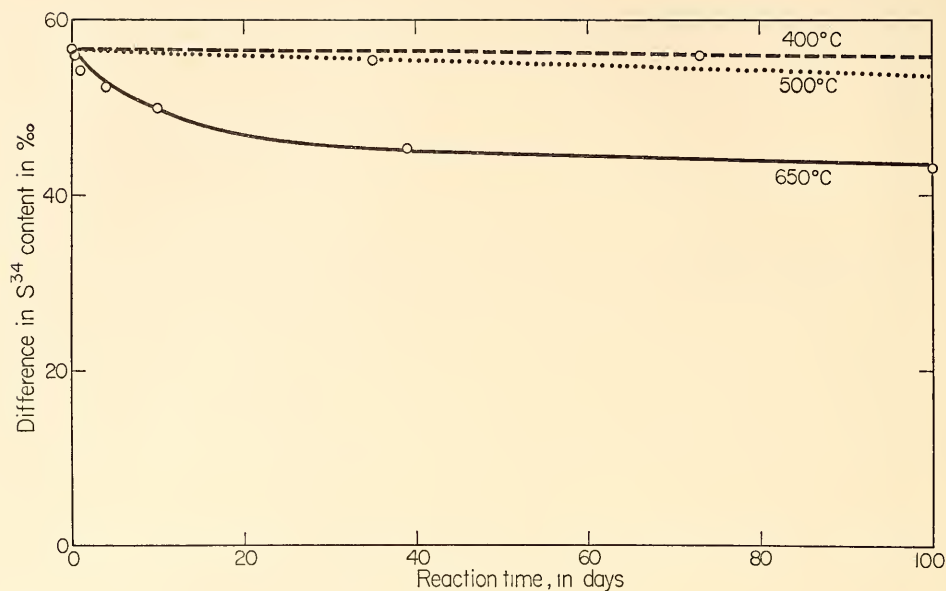


Fig. 77. Sulfur-isotope homogenization between pyrites.

sulfur. Conditions of this kind occur in sulfide ore deposits that have undergone thermal metamorphism. The conditions of metamorphism of the Bodenmais, Germany, ore deposit have been studied by Schreyer, Kullerud, and Ramdohr (1964), who showed that temperatures as high as 730°C and pressures of as much as 3000 bars prevailed.

The sulfides from 23 hand specimens of this deposit have been analyzed for their sulfur-isotope compositions, and the distribution of the results is shown in Fig. 78. The results fall in a relatively narrow range of ratios (+10.3 to 14.7 ‰), with a mean value for δS^{34} of +12.2 ‰. The samples were taken from

a number of levels in the mine, over a vertical distance of several hundred meters.

Two or more coexisting sulfides in 18 hand specimens were separated and analyzed for sulfur-isotope ratios. A trend in the enrichment of sulfur isotopes between coexisting minerals was observed. In 7 out of 10 coexisting pyrrhotite-pyrite pairs, δS^{34} (pyrite) was equal to or greater than δS^{34} (pyrrhotite). In 7 out of 8 examples, δS^{34} (sphalerite) was less than δS^{34} (pyrrhotite). In 4 out of 5 pairs δS^{34} (sphalerite) was less than δS^{34} (pyrite). Thus the minerals seem to show a tendency for concentrating S^{32} in the order sphalerite > pyrrhotite > pyrite.

Hegemann and Maucher (1933) have shown that the ore in Bodenmais was probably originally sedimentary. One of the characteristics of many sedimentary sulfide ore deposits is their wide range of sulfur-isotope ratios. Ore from a magmatic or magmatic-hydrothermal source, on the other hand, is characterized by a narrow range of sulfur isotope, with δS^{34} commonly near zero on our scale.

TABLE 14. Isotope Effect in the Breakdown of Pyrite

Heating Time, days	% S Released from the Possible Amount	Δ ‰ δS^{34} (sulfur) - δS^{34} (initial pyrite)
1	5	-9.2
2	7	-3.4
3	7	-1.2
10	81	-0.6

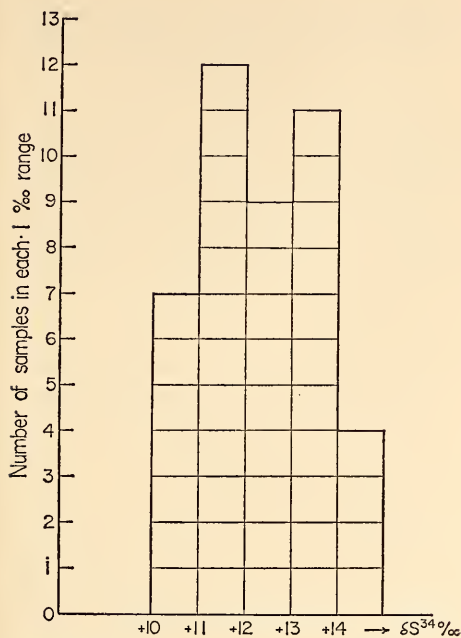


Fig. 78. Sulfur-isotope composition in Bodenmais, Germany, sulfide samples.

The isotopic composition of the Bodenmais ores indicates that the sulfur had at least one process that fractionated isotopes. A bacteriogenic sulfate reduction, with an isotope effect, may have taken place but the metamorphic event that followed destroyed the heterogeneous distribution.

The results of sulfur-isotope measurements on Bodenmais may be most easily explained in terms of an originally sedimentary sulfide deposit that suffered thermal metamorphism. A sulfur vapor phase, generated from the breakdown of pyrite, caused the homogenization of the isotope ratios between the minerals. These conclusions are consistent with the geological situation, petrography, and microscopic studies of the ore minerals.

SYNTHESIS OF $\beta\text{Cr}_2\text{FeS}_4$ AT 35 KB

A. El Goresy, P. M. Bell, and J. L. England

In the condensed Cr-Fe-S system, Cr_2FeS_4 is a stable compound below

1350°C at 1 atm. It occurs naturally as a low-temperature spinel-type mineral known as daubréelite ($\alpha\text{Cr}_2\text{FeS}_4$), a common accessory in enstatite chondrites, achondrites, and iron meteorites.

The textural relations of daubréelite-bearing meteorites suggest that Cr_2FeS_4 formed as a high-pressure β phase that inverted to the α form on cooling. A high-pressure hexagonal polymorph with a structure analogous to that of NiAs, reported by Rooymans and Albers (1967), is stable at 1 atm above 1060°C. These investigators studied the stability relations of Cr_2FeS_4 and showed that the P - T curve for the inversion has a strongly negative slope. It was not possible for them to recover the stoichiometric high-pressure form or produce its X-ray powder diffraction pattern because they used a squeezer apparatus of limited temperature range.

In the present study, synthesis of the high-pressure form of daubréelite was accomplished with a solid-media, piston-cylinder apparatus. Pure synthetic daubréelite ($a_0 = 9.996 \pm 0.002$ Å) was used as starting material.

Syntheses were conducted at 300° and 750°C, for 48 hours at 35 kb. These runs were quenched to 100°C in 10 to 15 seconds under pressure. From the 300°C run, only cubic $\alpha\text{Cr}_2\text{FeS}_4$ was recovered. At 750°C, however, complete conversion of $\alpha\text{Cr}_2\text{FeS}_4$ to a high-pressure phase ($\beta\text{Cr}_2\text{FeS}_4$) took place. This is the first time that the β form has been synthesized. Electron-microprobe analyses were carried out on the recovered high-pressure phase with stoichiometric Cr_2FeS_4 as a standard. No compositional differences between the standard and most of the high-pressure phase were observed. Only one grain of the $\beta\text{Cr}_2\text{FeS}_4$ was found to contain small domains (2 to 3 μ wide) with higher Cr and lower Fe and S contents. The density of the high-pressure form was 4.15.

$\beta\text{Cr}_2\text{FeS}_4$ is considerably harder to abrade and more strongly reflecting than cubic $\alpha\text{Cr}_2\text{FeS}_4$. In crossed nicols all

medium- and large-sized grains (50 to 100 μ) show one set of twin lamellae parallel in one direction (presumably basal).

The material was subjected to high-pressure differential thermal analysis (*Year Book 63*, p. 176) at 9 kb, 367° to 818°C; 11 kb, 579° to 818°C; 18 kb, 509° to 697°C; and 20 kb, 509° to 649°C. No thermal effects were observed.

The X-ray powder diffraction pattern (Table 15) of $\beta\text{Cr}_2\text{FeS}_4$ consists of 28 reflections of varying quality. It is characterized by two reflections ($d=2.041$ and $d=1.993$ Å) in the region of 102 of the hexagonal NiAs type. $\beta\text{Cr}_2\text{FeS}_4$ may be either monoclinic or hexagonal with a structure related to that of NiAs.

TABLE 15. d values of $\beta\text{Cr}_2\text{FeS}_4$ *

No.	d value	I
1	6.695	v.w.
2	5.648	m.
3	5.205	m.
4	4.120	st.
5	3.711	m.
6	3.293	m.
7	2.944	m.
8	2.612	st.
9	2.532	w.
10	2.041	v.st.
11	1.993	m.
12	1.930	m.
13	1.7100	st.
14	1.589	m.
15	1.432	w.
16	1.418	w.
17	1.303	m.
18	1.182	w.
19	1.158	w.
20	1.100	m.
21	1.093	m.
22	1.085	m.
23	1.046	st.†
24	0.9917	st.
25	0.9039	m.
26	0.8765	st.†
27	0.8405	st.†
28	0.8164	st.†

* Ni-filtered CuK α radiation.

† Broad line.

Note: v.st., very strong; st., strong; m., medium; w., weak; v.w., very weak.

MELTING RELATIONS IN THE Fe-RICH PORTION OF THE SYSTEM Fe-FeS AT 30 KB PRESSURE

P. R. Brett and P. M. Bell*

The Fe-rich portion of the system Fe-FeS has been thoroughly studied at 1 atm, and the main features of the phase relations have been reviewed by Hansen and Anderko (1958). The system has now been studied at 30 kb since (1) sulfur may occur with iron as a constituent of the earth's core and mantle and (2) iron sulfides commonly occur in meteorites. If sulfur is a constituent, its effect on the melting point of iron may prove to be a significant geophysical parameter (Clark, 1963; Birch, 1964; Mason, 1966).

Mixtures of Fe and FeS were loaded into small capsules of MgO and subjected to high-pressure, high-temperature conditions in the piston-cylinder, solid-media apparatus. The presence of liquid was determined on the basis of quench textures. Compositions were checked by the phase appearance-disappearance method, by electron probe, and by X-ray diffraction. The results of the probe analyses checked with each other to

* U. S. Geological Survey.

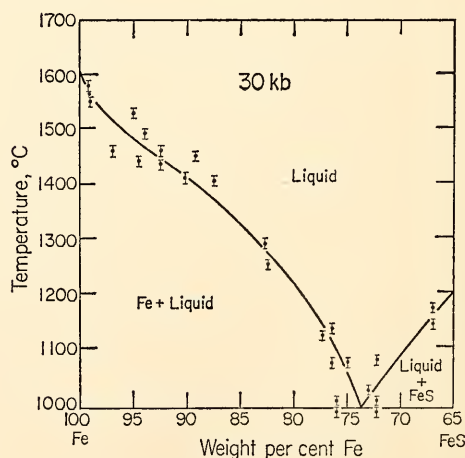


Fig. 79. Temperature-composition section for the system Fe-FeS at 30 kb.

better than ± 2 wt % of the amount present.

A binary eutectic similar to that observed at 1 atm was discovered at 30 kb, and is shown in Fig. 79. The eutectic temperature at 30 kb is $990 \pm 5^\circ\text{C}$. This temperature is nearly identical with that for the 1 atm results (988°C). There is no possible confusion in the interpretation of the present results, however, be-

cause all experiments were quenched at 30 kb pressure. The eutectic composition has moved from 31 wt % sulfur at 1 atm to 26.5 wt % sulfur at 30 kb.

The results shown in Fig. 79 suggest that, even if only a small percentage of sulfur is present in the earth's core, the effect on the melting of iron may be significant.

BIOGEOCHEMISTRY

REACTIONS OF THE ORGANIC MATTER IN A RECENT MARINE SEDIMENT

T. C. Hoering

Some of the chemical reactions produced by elevated temperatures in a short time in the organic matter in a Recent marine sediment from the San Nicholas Basin are the same as those that occur slowly at lower temperatures in nature. Thus the nature of organic geochemical processes can be investigated in the laboratory. A first report of our experiments was given last year (*Year Book 66*), and the experiments have been continued. Several new results are reported here.

If a dried sediment is exposed to an excess of deuterium oxide, redried, and then heated to 225°C for 1 week under an inert atmosphere, new hydrocarbons are produced with deuterium atoms substituted for hydrogen. A number of such hydrocarbons have been separated by preparative gas-liquid chromatography, and the amount of deuterium substitution has been determined by mass spectrometry. Table 16 shows a result determined for $n\text{-C}_{25}\text{H}_{52}$. Molecules with at least eight deuterium atoms are present. The results for a number of other normal and isoprenoid hydrocarbons are similar.

The extent of the deuterium exchange of the normal fatty acids that exist in the sediment is shown in Table 16. Much less deuterium is present in them than in the newly formed alkanes. The results

for the acids are most easily explained in terms of exchange of the hydrogens on the β carbons of the acid with water. Simple homogeneous exchange of water with the hydrogens on long, saturated alkyl groups is not likely.

The multiple deuteration of the alkanes is unexpected and indicates that the reaction mechanism of hydrocarbon production is complex. It is known that surface-catalyzed reductions of organic compounds in the presence of deuterated

TABLE 16. Relative Concentrations of Deuterated Species of n -Pentacosane and Hexadecanoic Acid from Deuterated Tanner Basin Sediment Heated to 225°C for 1 Week

Species	Normalized Abundance
<i>n</i> -Pentacosane	
$\text{C}_{25}\text{H}_{52}$	100
$\text{C}_{25}\text{H}_{51}\text{D}$	28
$\text{C}_{25}\text{H}_{50}\text{D}_2$	16
$\text{C}_{25}\text{H}_{49}\text{D}_3$	12
$\text{C}_{25}\text{H}_{48}\text{D}_4$	10
$\text{C}_{25}\text{H}_{47}\text{D}_5$	7
$\text{C}_{25}\text{H}_{46}\text{D}_6$	4
$\text{C}_{25}\text{H}_{45}\text{D}_7$	2
$\text{C}_{25}\text{H}_{44}\text{D}_8$	1
<i>n</i> -Hexadecanoic Acid	
$\text{C}_{16}\text{H}_{32}\text{O}_2$	85
$\text{C}_{16}\text{H}_{31}\text{DO}_2$	100
$\text{C}_{16}\text{H}_{30}\text{D}_2\text{O}_2$	37
$\text{C}_{16}\text{H}_{29}\text{D}_3\text{O}_2$	5
$\text{C}_{16}\text{H}_{28}\text{D}_4\text{O}_2$	1

Note: The data from the mass spectra have been corrected for contributions of C^{13} -containing species. The concentration of deuterium-substituted compounds arising from the natural abundance of deuterium is negligible.

substances often lead to extensive deuterium replacement at positions away from the immediate reaction site. Investigations with the use of this tracer technique may give some information on the role of mineral surfaces during the diagenesis of organic matter.

When the Recent marine sediment is heated to 225°C for a few days in an inert atmosphere, porphyrins are generated from the chlorophyll and chlorophyll residues present in it. The mass spectrum of the demetallated etioporphyrins and deoxophylloerythroetioporphyrins generated by such thermal treatment is shown in Fig. 80. The porphyrins are a complex mixture of homologues of the two classes. The spectrum is similar to that reported for the petroporphyrins in ancient sediments.

The presence of a regular series of

porphyrins with molecular weight $310 + 14n$, where n is an integer, indicates that alkyl-substituted etioporphyrins are present, since 310 is the molecular weight of the unsubstituted tetrapyrrole ring and 14 is the molecular weight of the added methylene substituents. Likewise, a series of porphyrins with molecular weights $308 + 14n$ must indicate a homologous series of alkyl-substituted deoxophylloerythroetioporphyrins with an isocyclic ring fused to the tetrapyrrole ring.

Chlorophyll is the major pigment present in the system, and it is the most likely precursor of the porphyrins. If so, there must have been alkylation and transalkylation of peripheral positions of the tetrapyrrole ring during the heating experiments to account for the mass spectra with molecular weight appear-

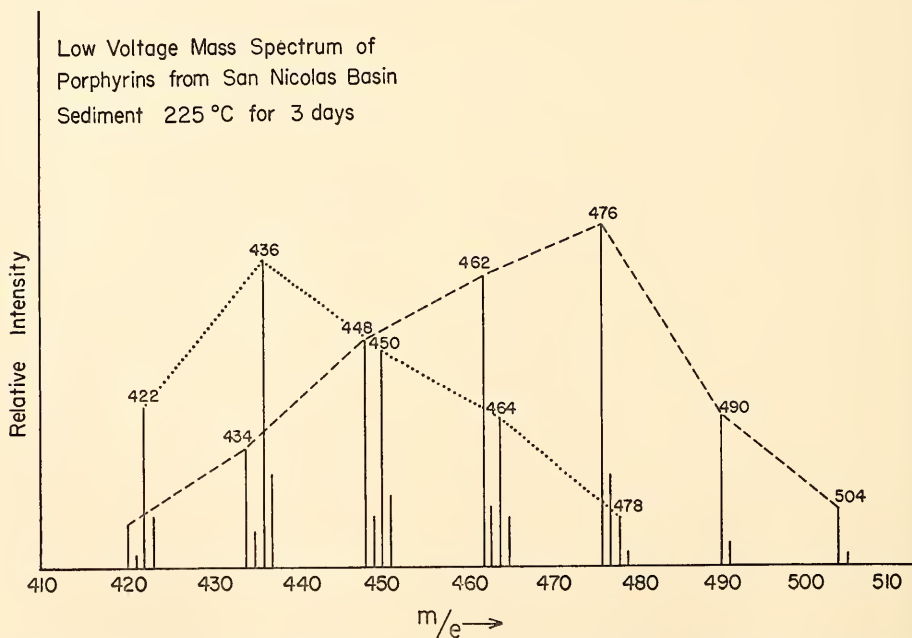


Fig. 80. Parent ion mass spectrum of porphyrins from heated San Nicolas Basin sediment. The spectrum was measured by West Coast Analytical Service Company, San Gabriel, California, on a Hitachi RMU-6D mass spectrometer. The porphyrins were volatilized into the ion source from a direct insertion probe at a temperature of 170°C. Electrons with an energy of 10 ev were used for ionization. Virtually no fragment peaks appeared in the mass spectrum. The dashed lines define the envelope of parent peaks due to deoxophylloerythroetioporphyrins. The dotted lines connect the parent peaks of etioporphyrins.

ing at increments of 14 units. Migration and transfer of alkyl groups may be an important organic reaction that occurs in sedimentary rocks, in addition to hydrogenation, dehydrogenation, cyclization, and hydrolysis.

Our laboratory heating experiments indicate that a study of the thermal reaction of sedimentary rocks gives important clues to the nature of the organic matter in them and to the organic reac-

tions that occur over geological lengths of time.

BRANCHED-CHAIN FATTY ACIDS IN RECENT SEDIMENTS

T. C. Hoering

Normal fatty acids predominate in Recent sediments, but there is an appreciable concentration of acids with branched carbon chains. The mass spec-

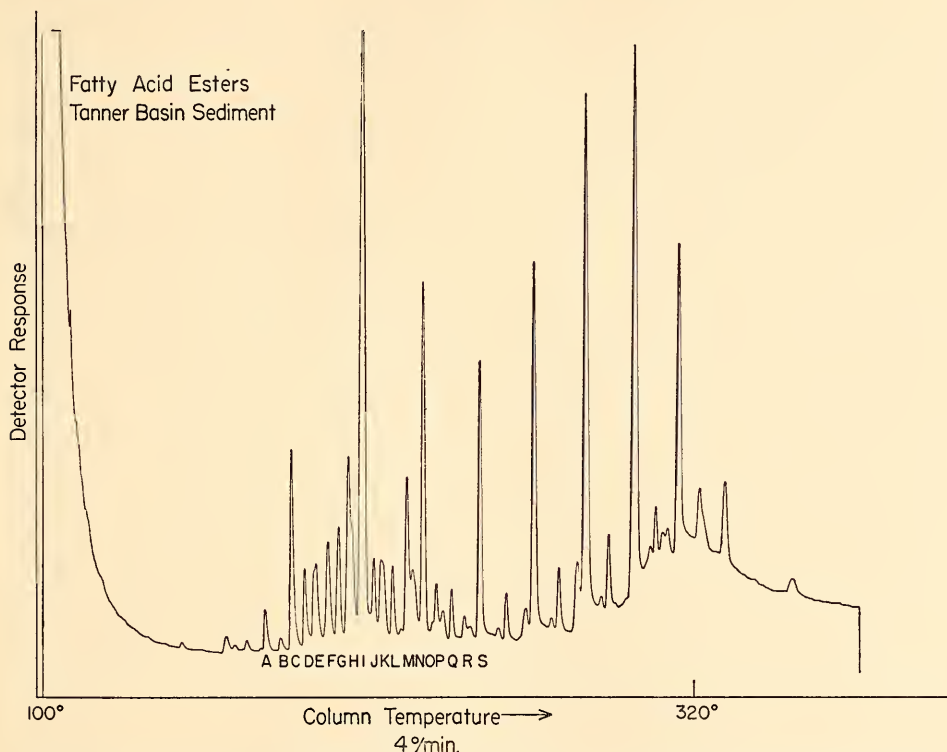
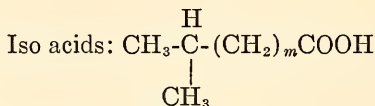


Fig. 81. Gas-liquid chromatogram of esters of free fatty acids from Tanner Basin sediment. Ten-foot by $\frac{1}{8}$ -inch column with 5% Apiezon L. Helium flow 40 cc/minute. Temperature programmed from 100° to 320°C at rate of 4°/minute. Identification of separated peaks by mass spectrometry. Peak symbols: (A) Methyl 3,7,11 trimethyl dodecanoate. (B) Methyl isotetradecanoate and methyl anteisotetradecanoate. (C) Methyl *n*-tetradecanoate. (D) Methyl 4,8,12 trimethyl tridecanoate. (E) Methyl isopentadecanoate and methyl anteisopentadecanoate. (F) Methyl *n*-pentadecanoate. (G) Methyl 5,9,13 trimethyl tetradecanoate plus a compound, not a methyl ester of fatty acid. (H) Methyl isohexadecanoate, methyl anteisohexadecanoate, methyl palmitoleate, and nonmethyl ester. (I) Methyl *n*-hexadecanoate. (J) Methyl 2,6,10,14 tetramethyl pentadecanoate. (K) Methyl isoheptadecanoate, methyl anteisoheptadecanoate and nonmethyl ester. (L) Methyl *n*-heptadecanoate. (M) Methyl 3,7,11,15 tetramethyl hexadecanoate. (N) Complex unresolvable mixture of esters. (O) Methyl *n*-octadecanoate. (P) Methyl ester of cyclic acid. (Q) Methyl *n*-nonadecanoate. (R) Methyl ester of cyclic acid. (S) Methyl *n*-eicosanoate.

trometric facilities put into operation during the last year make it possible to identify them. The molecular structure of pertinent species is as follows.

Normal acid: $\text{CH}_3-(\text{CH}_2)_m\text{COOH}$



Anteiso acids:

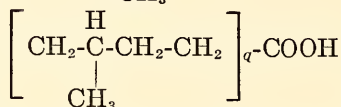
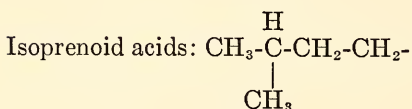
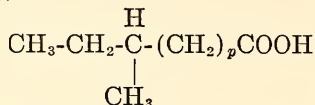


Figure 81 shows a gas-liquid chromatogram of the methyl esters of fatty acids extracted from a surface sediment of the Tanner Basin in the continental shelf off southern California. The normal fatty acids form the major peaks, but between them, especially in the region of C_{14} to C_{19} , are peaks due to the branched-chain acids.

Individual pure esters were isolated by multiple, preparative gas-liquid chromatography with the use of polar and nonpolar substrates. The individual peaks were complex, some having as many as four components. The mass spectrum of each pure compound was measured; the components are identified in Fig. 81.

The molecular structure of branched-chain fatty acid esters can be determined readily from the fragmentation pattern obtained by electron bombardment in the mass spectrometer ion source. The mass spectra of a number of such compounds have been correlated with their molecular structure.

The presence of iso and anteiso acids

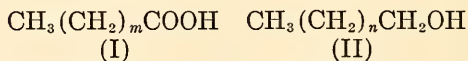
is not surprising, for they are known constituents of the lipides of living organisms, especially marine bacteria. The high concentration and variety of isoprenoid acids are somewhat unexpected. Such acids are known in lipides but are usually considered to be relatively rare. Whether the isoprenoid acids are primary products of the living biota or the products of diagenesis of chlorophyll and its degradation products is not known. Chlorophyll is a major organic constituent of the sediment and has a phytol side-chain with an isoprenoid structure.

FATTY ALCOHOLS IN SEDIMENTARY ROCKS

T. C. Hoering

Living organisms synthesize many lipides with long, normal chains of carbon atoms. Molecules of this structure are important constituents of sedimentary rocks. Last year's report described the unexpected occurrence in Recent marine sediments of normal fatty acids having more than twenty carbon atoms. It was shown that the chemical oxidation of the non-acidic "polar molecule" fraction of an extract of the Recent marine sediment produced normal fatty acids. It has been shown that mild thermal treatment of unextracted Recent sediment produced a good yield of the normal alkanes $n\text{-C}_{22}\text{H}_{46}$ and $n\text{-C}_{24}\text{H}_{50}$ and that under the same conditions Recent sediment will reduce a fatty alcohol to an alkane.

These considerations suggest that fatty alcohols in the form of wax esters may be present in sedimentary rocks. Plant waxes are esters of fatty acids (I) and fatty alcohols (II)



where m and n are integers that typically run from 12 to 30.

Waxes have been identified in lignite coals and peats. Although the ester linkage is hydrolyzed readily, waxes because

of their hydrophobic nature, can persist in relatively young sedimentary rocks. This report describes their occurrence in a Recent marine sediment from the Tanner Basin in the continental shelf off southern California and in the Green River shale of Colorado.

The alcohols were isolated as their acetates from benzene-methanol extracts of the sediments. The standard methods of lipide chemistry were modified to take into account the interfering substances found in rocks. A tracer of C^{14} -tagged *n*-octadecanol was added to the initial extract. A yield of about one-fourth of the added radioactivity was obtained in the final acetate preparation.

The acetates of the fatty alcohols were separated and analyzed by gas-liquid chromatography. Identification of the compounds is based on a comparison of retention times with those of pure standard compounds and on the mass spectra of individual pure compounds separated by preparative gas-liquid chromatography. Table 17 gives a quantitative analysis of normal fatty alcohols in the two rocks.

Fatty alcohols, presumably present in the form of wax esters, make a small but

significant contribution to the inventory of normal alkyl groups found in sedimentary rocks. Branched-chain alcohols are present too, but their mass spectra are not well suited for exact structure determination. Analogy with structures of the branched-chain fatty acids given in another part of this report suggests that they may be isoprenoid alcohols, but firm identification will require preparation of derivatives more suitable for mass spectrometry. There was no indication of the unsaturated alcohol phytol, which could be derived from the hydrolysis of chlorophyll initially present in the sediment.

The normal fatty acids in living organisms and in Recent sediments have predominantly an even number of carbon atoms. In ancient sediments, the ratio of acids with an even number of carbon atoms to those with an odd number approaches 1. On the other hand, the normal alkanes of living organisms and Recent sediments have predominantly an odd number of carbon atoms, and in ancient sediments the ratio of even to odd approaches 1. Table 17 indicates that the same thing is happening to the normal fatty alcohols, which have predominantly an even number of carbon atoms in cells and the Recent sediment from the Tanner Basin but a much higher relative abundance of odd-carbon-numbered molecules in the older Green River shale.

It may be speculated that the alcohols observed in the Tanner Basin sediment originated as waxes from land-based, higher plants, in which they form protective coatings. Waxes, containing alcohols in this molecular weight range, are not conspicuous constituents of marine organisms.

FICHTELITE HYDROCARBONS IN FOSSIL WOOD

T. C. Hoering

The mineral called fichtelite is one of the few naturally occurring crystalline organic substances found in sedimentary

TABLE 17. Fatty Alcohols in Extracts of Sedimentary Rocks*

Carbon No., Alcohol	Tanner Basin	Green River Shale
16	20	2.0
17	0.8	0.8
18	8.2	1.5
19	0.5	0.8
20	12	1.2
21	0.5	0.9
22	22	2.4
23	2	0.7
24	12	0.5
25	1	0.3
26	5	0.1
27	0.7	...
28	4	...
Totals	88.7	11.3

*The values are in parts per million of the individual alcohols per gram of organic carbon in the sample. Values have been corrected for yield of octadecanol tracer added to initial extract.

formations. It occurs in fossil conifer wood in the Fichtelgebirge area of southern Germany and is of Quaternary age. Fichtelite has been known for 140 years, but only in the past 30 years has the molecular structure of its major components been rigorously established. The saturated hydrocarbon 1,4a-dimethyl-7-isopropyl perhydrophenanthrene (given the chemical name fichtelite) (I) and the aromatic hydrocarbon 1-methyl-7-isopropyl phenanthrene (retene) (II) are present. Abietic acid (III) is one of the important resin acids of living conifers (Fig. 82).

The similarities in the carbon skeletons of the first three compounds is obvious. Apparently, abietic acid is readily saturated with hydrogen and decarboxylated in the sedimentary environment to give fichtelite. It is well known that elemental sulfur converts both abietic acid and fichtelite to retene.

In view of the rarity of pure crystalline organic substances in sediments, two specimens of fichtelite from the type locality were obtained from the Division of Mineralogy, U. S. National Museum (Museum Nos. C-3897 and R-7270). The specimens were tough, compact pieces of wood with no visible crystalline material. The wood was carved into small pieces and extracted in a Soxhlet extractor with benzene-methanol. Sulfur was removed with metallic copper. The mahogany-colored extract was separated by silica-gel chromatograph. Sample R-7270 yielded 1.2 wt % of a colorless,

saturated hydrocarbon oil and 4.3 wt % of a crystalline aromatic hydrocarbon. Gas-liquid chromatography, infrared spectrometry, and mass spectrometry showed that the aromatic hydrocarbon was pure retene. A gas-liquid chromatograph of the saturated hydrocarbons contained three closely spaced peaks, in the ratio of 30:100:28. The major component was identified as fichtelite (I). The other peaks are tentatively identified as iosine (IV) and a methyl-substituted iosine. Iosine is a known component of some lignite coals.

There were at least two stages in the diagenesis of the fossil wood. One was in a highly reducing environment, producing saturation of the resin acid to yield fichtelite and causing cyclization to give iosine. The second was in a sulfur-rich, dehydrogenating environment, producing retene.

Studies of fichtelite present an opportunity to investigate geochemical hydrogenation and dehydrogenation of organic substances. Such processes are important in generating hydrocarbons in bulk sediments, but the sequence of events there is difficult to unravel. In fossil wood the problem is less complex; the starting compounds seem to be known, the products are simpler, and the types of organic reactions are more straightforward. A search was made for fichtelite and retene in extracts of the Green River shale of Colorado, Chattanooga shale of Tennessee, tasmanite oil shale from Tasmania, and

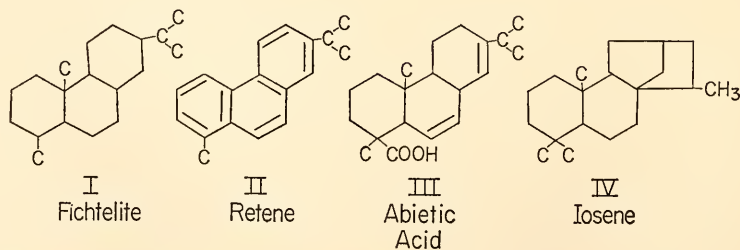


Fig. 82. Structures of hydrocarbons in fossil wood.

a lignite coal from North Dakota. The results were negative. Fichtelite seems to be limited to fossil wood.

LABORATORY SIMULATION OF AMINO-ACID DIAGENESIS IN FOSSILS

P. E. Hare and R. M. Mitterer

Changes in the amino-acid content of fossil shells with passage of time have been found to be consistent with deductions based on the order of stability of free amino acids heated in dilute aqueous solutions, as shown first by Abelson (*Year Book 53*, pp. 97-101; and 1959) and more recently by Vallentyne (1964).

Amino acids found stable in such heating tests included alanine, glycine, glutamic acid, valine, and the leucines (Abelson, 1959); these are the amino acids that are primarily found in fossils older than Pleistocene. Amino acids unstable to heating, such as serine and threonine, and therefore not expected in older fossils, have been reported (e.g. Degens, 1965, pp. 202-280) in older sediments. Amino-acid stabilization by surrounding matrix has been suggested (Prashnowsky and Schidlowski, 1967) to explain the apparent anomaly of unstable amino acids in ancient deposits.

In addition, experiments at this laboratory on heating free amino acids in solutions indicate that pH can be a significant factor in the stability of some amino acids. Samples of a standard mixture of amino acids buffered at pH 2.0, 4.6, and 9.4 (as measured at 25°C) were heated in sealed tubes under nitrogen for 4 days at 140°C. Arginine disappeared completely at pH 9.4 to form ornithine, whereas at pH 2.0 and 4.6 no appreciable amount of arginine was converted to ornithine. Cystine was stable only at pH 2.0, virtually disappearing at both other pH values. The alloseucine-to-isoleucine ratio observed after incubation was 0.05 at pH 2.0 but 0.2 at pH 9.4. Aspartic acid was less stable at pH 4.6 than at pH 2.0 or 9.4. At pH 9.4 the serine-to-threonine ratio

was 10 after heating. At pH 4.6 the serine-to-threonine ratio was 1.5, and at pH 2.0 it was reversed at 0.3.

In view of this pH effect and the possibility of a matrix effect on amino-acid stability, we have attempted to simulate more closely the diagenesis of amino acids in fossils by subjecting fragments of modern shells to incubation under a variety of temperatures and environments. A first series of experiments tested the role of water in the environment, allowing for the fact that in nature water is usually present. Modern shell fragments of *Mercenaria* were heated to 160°C for 10 hours in varying amounts of water or water vapor. The sample heated dry showed little or no reaction, in contrast to the samples heated in the presence of water or water vapor.

In subsequent experiments shell fragments of about 100 mg were heated in 1 ml of water sealed in a tube under nitrogen. The changes observed upon heating Recent shell fragments in the presence of water are analogous to and duplicate those changes found in the natural series of fossils. With continued heating the unstable amino acids virtually disappeared, the remaining amino acids racemized, and the mixture of amino acids approached that found in the oldest fossils examined.

Evidence that we are dealing with the same mechanisms and changes that take place in the natural environment is found in the data from a series of Recent and fossil shells heated for 1 day at 185°C. The results are shown in Table 18.

In the oldest shell, a sample from the Miocene St. Mary's formation, relatively few changes took place. Serine and threonine were already absent; the ratio of alloseucine to isoleucine was already the equilibrium ratio, so that heating for 1 day at 185°C in the presence of water changed the pattern very little. Similar treatment of a specimen from Wailes Bluff, of Upper Pleistocene age, caused much more extensive changes, but the final mixture resembled that ob-

TABLE 18. Amino-Acid Composition for Inner Layer of *Mercenaria* Shells Before and After Heating to 185°C for 24 Hours, nM/g shell

	Recent		Upper Pleistocene		Miocene	
	Unheated	Heated	Unheated	Heated	Unheated	Heated
Aspartic acid	1960	80	865	78	35	12
Threonine	1170	0	306	0	0	0
Serine	1430	0	247	0	0	0
Glutamic acid	1400	575	709	363	140	140
Proline	1790	570	767	375	120	120
Glycine	1500	735	572	325	104	99
Alanine	1210	850	715	523	166	165
Cystine	403	0	26	0	0	0
Valine	740	290	423	198	127	114
Methionine	225	77	85	35	10	10
Alloisoleucine	0	100	52	69	42	42
Isoleucine	370	80	163	55	34	34
Leucine	515	190	280	115	78	74
Tyrosine	515	134	286	94	38	38
Phenylalanine	354	147	202	84	52	47
Ornithine	0	97	52	62	9	5
Lysine	1143	155	442	81	46	20
Histidine	338	0	65	0	0	0
Arginine	612	0	241	0	0	0
Ratio allo/iso	0	1.25	0.32	1.25	1.25	1.25

tained in the previous experiment. When a Recent shell was heated, profound changes were observed, the final pattern again approaching that obtained in the other two heated samples.

To study the kinetics of the reactions in more detail, fragments of modern shells were heated at temperatures of 165°, 140°, 125°, 105°, and 90°C for periods of time ranging from 1 hour to over 3 months. The shell fragments were heated in water in tubes sealed under nitrogen. The total amount of amino acids decreased with time of heating. Amino-acid ratios changed systematically with time of heating, in a fashion analogous to that found in fossil shells.

Comparison of data on free amino acids and shell fragments showed that free amino acids reacted more slowly. For example, in 4 days at 140°C, serine decreased only to 80% of its original value (at pH 9.4), whereas in the shell fragments it decreased to less than 10%. This apparent decrease in stability in the shell matrix seemed to be true for all the amino acids.

Isoleucine racemizes to alloisoleucine by a first-order reaction. This reaction is

reversible, and by heating the two separately we have shown that the isoleucine-to-alloisoleucine reaction is approximately 25% faster than the reverse reaction, so that at equilibrium the ratio of alloisoleucine to isoleucine is about 1.25.

The Arrhenius equation used in Fig. 83 relates the rate constant of a reaction to the absolute temperature. A plot of the time necessary for a given amount of isoleucine to diminish to $1/e$ of its initial value at a particular temperature is shown. It is seen that extrapolation of data based on the laboratory treatment checks well with data from a series of radiocarbon-dated fossil-shell material from areas with average temperatures of 23° to 24°C. These data were obtained from the middle shell layer of *Mercenaria*. There is evidence that other shell structures in *Mercenaria* react at somewhat different rates.

Point A represents data from *Foraminifera* tests from an Antarctic deep-sea core (core 15-16 of Goodell and Watkins, 1968) supplied by Florida State University. Sedimentation rates are based on recognized magnetic reversals. Agree-

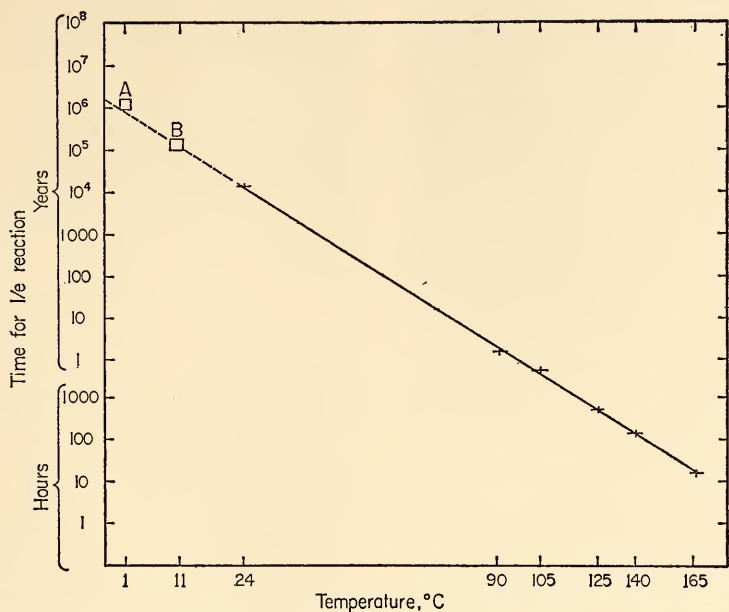


Fig. 83. Arrhenius plot of time ($1/e$ of reaction) as a function of temperature⁻¹.

ment with extrapolated values is good and gives us confidence that the reactions occurring in the laboratory treatment are similar to those occurring in fossils.

Point *B* represents data from the Upper Pleistocene Wailes Bluff locality. Radiocarbon dating shows that this deposit is older than 40,000 years. Amino-acid ratios suggest that it is probably around 60,000 years old if the temperature has been around 11° to 12°C.

The agreement between the values found in these Pleistocene samples and the Arrhenius plot suggests potential uses of amino-acid ratios in fossils. If the temperature is known precisely, an approximate age can be calculated. Alternatively, effective incubation temperature can be inferred on well-dated material. Still another potential use is for stratigraphic correlation, which should be particularly useful in deep-sea cores, since the temperatures are uniform and constant.

In addition to providing quantitative information on reaction rates, the heat-

ing experiments afforded an opportunity to study contamination of the shell and loss of amino acids from it. Amino acids were found in the water surrounding the heated shell fragment. The concentration of amino acids in the water varied directly with time of heating and temperature. With prolonged heating at higher temperatures, the amounts of amino acids outside the shell were approximately equal to those within the shell.

In another experiment, to test for the possibility of amino acids migrating into the shell, two shell fragments were placed in a 1-ml solution containing 10 μ M of the nonprotein amino acid norleucine, which is not found in modern or fossil shells. The sealed tube containing the shell fragments was heated for 4½ days at 165°C under the usual conditions. After the tube was opened, one fragment was removed, thoroughly washed, and prepared for amino-acid analysis. The other fragment was washed and dried, and surface material was removed with a dental tool. The fragment was then

acid-washed to remove more of the outer surface and analyzed. In the water-washed sample, norleucine amounted to 1.3% of the total amino acids. In the sample that was abraded and acid-washed, norleucine was about 0.5% of the total acids.

The results suggest that young intact fossil shells are probably not contaminated to a significant degree by amino acids in groundwater and sediment. On the other hand, older fossil specimens, having lost much of their amino acids and having been continuously subjected to contamination over a long period of time, might contain some adventitious amino acids.

The results of this study indicate that it is possible to simulate the diagenetic reactions occurring in nature by simple heating of shell fragments in water. Furthermore, when the data from calcareous fossils were compared with those from free amino acids heated in aqueous solutions, it was found that there is indeed a matrix effect. The matrix effect resulted in faster reaction in the shell than for free amino acids, however, in contrast to a stabilizing matrix effect that has been postulated for sediments.

RECENT AMINO ACIDS IN THE GUNFLINT CHERT

P. H. Abelson and P. E. Hare

Organic chemicals surviving for billions of years in sedimentary rocks are potential sources of evidence concerning the nature of ancient life. The quantities of original chemicals now present in many old rocks, however, are not much larger than those ubiquitously present as adventitious contaminants. Consequently, in organic geochemistry there is a substantial possibility that many interesting but illusory discoveries will be made. Rarely can a second investigator obtain specimens identical with those on which the original work was performed, and exact duplication of earlier work is usually not feasible. Moreover,

once a fictive result appears in the geochemical literature, the error is difficult to erase.

Work performed this year in examining the possible amino-acid content of the Gunflint chert illustrates an approach that often might be usefully employed. In the 1.9-billion-year-old Gunflint iron formation near the town of Schreiber, Ontario, Tyler and Barghoorn (1954) discovered a rich fauna of microfossils embedded in a flinty chert. Thin sections of this chert have been examined by a number of paleontologists, and there is general agreement that the forms noted are of biological origin.

Recently, Schopf, Kvenvolden, and Barghoorn (1968) reported finding amino acids in the chert that they believe have remained there 1.9 billion years. We questioned the finding, however, since some of the amino acids reported as present, notably serine and threonine, are not very stable chemically. Consequently, we have conducted a series of tests, which show that although specimens of the Gunflint chert examined by us contained small amounts of recent amino acids, they did not contain significant amounts of ancient amino acids.

Since it could be argued that the chert matrix might have a stabilizing effect on amino acids, we have conducted thermal tests on the chert similar to those employed with shells and described previously in this report. Samples of chert thought to contain ancient amino acids were heated at 165°C for 1 to 3 days. If the chert matrix confers special stability on serine, that amino acid and others should be affected little if at all by the treatment.

The specimens employed came from the type locality at Schreiber. Chemically they were about 99% SiO₂. They also contained organic carbon, pyrite, and CaCO₃. The setting and the appearance of the specimens testify to the possibility of contamination. The type locality is on the shore line of Lake Superior, and lichens abound on the sur-

face of the chert. When a cobble is bisected and etched much structure and some cracks may be seen. Schopf, Kvenvolden, and Barghoorn employed procedures well designed to guard against adventitious contamination. However, the amounts of amino acids that they found are tiny in comparison with the amounts present in the environment and available as possible contaminants.

Method

Special efforts were made to avoid contamination, and all reagents were tested repeatedly. Glassware was routinely heated to 500°C before use to destroy possible contaminants. Water was deionized, filtered through 0.2- μ membrane filters, and distilled. We have found that distillation without filtration does not eliminate dust contamination. HCl was redistilled and yielded a very low level of amino acids. HF was redistilled in a platinum still.

Cobbles of Gunflint chert were treated with boiling 6 *N* HCl and chromic acid to remove surface contamination of amino acids. HF was used to remove the outer 10% of the sample before size reduction.

An aliquot (*a*) of powdered Gunflint chert was compared to other aliquots treated as follows: One aliquot of powdered sample (aliquot *b*) was heated to 400°C for 2 hours to destroy any amino acids present. Analysis of this sample provides a measure of reagent and laboratory contamination. Another aliquot (*c*) was heated in the presence of water at 165°C for 3 days. To check recovery of amino acids in the procedure a standard amino-acid mixture was added to still another aliquot (*d*), which had previously been heated to 400°C to destroy the contained amino acids.

After the above pretreatments, all aliquots were extracted in Soxhlet extractors with water for 1 day, followed by 6 *N* HCl for 1 day. The residue from this treatment was reacted with HF to

volatilize off SiO₂. Later HCl was added to decompose resistant materials.

Desalting was accomplished by precipitating the interfering ions. HF was used to remove calcium. Iron was removed by adding NaOH to make the solution alkaline, thus precipitating iron hydroxides. Sodium ion was removed from a saturated HCl solution made by passing in HCl gas in the cold. The supernatant solution was dried *in vacuo*.

Results

Water extraction of the chert alone was not very effective. When standard amino-acid mixtures were added to finely ground chert, recovery of the hydrophilic acids was fair (~50%) and that of the more hydrophobic amino acids was poor (~20%). Recovery with HCl extraction, however, was excellent (90 to 100%). Recoveries of added standard amino acids were also poor following the treatment of chert with HF. The residue from this treatment included organic matter and pyrite. Even when this residue was cautiously taken to dryness, irreversible loss of hydrophobic amino acids was noted.

The use of tracer amino acids, including norleucine, gave us assurance that we were isolating most of the amino acids present in the samples of chert. Nevertheless, the total amounts isolated from unheated chert by H₂O+HCl extraction were less than those reported by Schopf *et al.* For example, they found the following (expressed in 10⁻⁹ *M*/g chert): glycine, 11.6; alanine, 2.8; serine, 1.5. In one of our cobbles we found, correspondingly, glycine, 1.2; alanine, 0.79; and serine, 0.80. In another cobble we found glycine, 1.08; alanine, 0.48; and serine, 0.47. Other specimens yielded even smaller amounts. The amino-acid content of one chert specimen was indistinguishable from the reagent background, which for that particular experiment was equivalent to 10⁻¹¹ *M*/g chert.

In contrast, HCl treatment of the

outer surface of the chert yielded substantial amounts of amino acids. From the surface of a 400-g cobble was isolated glycine, 1030 nM; alanine, 270; and serine, 630; and of course, the other usual amino acids.

Treatment of ground chert with water and HCl extracted essentially all the amino acids associated with the chert while leaving behind more than 99% of the weight of the original sample. The amounts of amino acids found after HF treatment to volatilize SiO₂ were about those of our reagent blanks. For example in one instance we found glycine, 0.038 nM/g chert; alanine, 0.014; and serine, 0.017; and this was indistinguishable from the blank.

It seems significant that the water and HCl treatments collected most, if not all, of the amino acid present in the chert while leaving behind the main body of the chert. Either the main part of the chert is readily pervious to extraction or it did not contain amino acids. If the chert is so permeable that amino acids can be completely extracted in 1 day, then amino acids from modern lichens would probably contaminate the chert after a few thousand years.

The heating experiments showed that amino acids associated with the chert were degraded in much the same way as amino acids in fossil shells. Exposure of chert to 165°C for 3 days resulted in a marked degradation of serine and

threonine and in the conversion of half of the isoleucine to alloisoleucine. In three unheated specimens the ratios of serine to glycine found were 0.90, 0.48, and 0.41. After 1 day of heating at 165°C the ratios were 0.38, 0.20, and 0.20.

Our observations on the stereo-isomers alloisoleucine and isoleucine seem particularly significant. As pointed out elsewhere in this report, the biologically produced isoleucine, in nature, is partially converted into alloisoleucine, and after a few million years an equilibrium is established in which 1.25 parts of alloisoleucine and 1.0 part isoleucine co-exist. We have examined the amino acids in eight different specimens of Gunflint chert and have found isoleucine in all of them. However, in no unheated specimen have we found any alloisoleucine. In specimens heated to 165°C for 1 day or more, alloisoleucine is readily detectable, showing that the chert matrix does not interfere with isomerization. Thus the absence of alloisoleucine in the chert is a strong indication that the isoleucine present is of recent origin.

In another experiment, designed to examine the antiquity of the amino acid, *L*-amino acid oxidase was used to determine the optical configuration of the amino acids in the chert. All the amino acids that reacted with this enzyme were of the *L* configuration. This result is also suggestive of amino-acid material of recent origin.

COMPUTER REDUCTION OF ELECTRON-PROBE DATA

F. R. Boyd, L. W. Finger, and F. Chayes

Reducing X-ray intensity measurements determined with an electron probe to estimates of chemical composition requires performance of a large number of simple mathematical operations. In addition to averaging groups of counts and forming intensity ratios, it is necessary to correct the observed intensities for instrumental factors and matrix effects. A complete correction procedure

includes corrections for drift, background, deadtime, absorption, fluorescence, and atomic number effects. Preliminary estimates of the composition are usually the basis for calculating matrix effects, and the correction elements are refined by iteration. Moreover, the investigator usually wishes to calculate statistical parameters to evaluate homogeneity, and if the analysis includes trace

elements, calculations of significance of small signals may also be required. To make such a complete set of calculations with a desk calculator for an analysis of a natural mineral containing eight to twelve elements would require at least weeks of work. Fortunately, the correction calculations can be programmed for a large computer, and this can be done in a way that leaves the investigator with considerable flexibility in his approach to an analytical problem. Other electron-probe laboratories, including those at the Scripps Institution of Oceanography, the U. S. Geological Survey at Menlo Park and the Goddard Space Flight Center, have developed computer programs for reducing probe data, and we have benefited from their experience in writing the programs described in this report.

The convenience with which a program can be used depends on the number of control cards that must be prepared for each analysis. These can be greatly reduced by providing for automatic printout of code numbers that identify the elements being analyzed, the standards used, and the type of measurement being made. Table 19 shows a line of out-

put from our electron probe. Ten control digits are followed by the counting interval, the counts obtained from the three channels, and the specimen current. These control digits are conveniently set by switches mounted on the data translator. The first digit specifies the type of measurement, i.e., whether a count is on peak or on background and whether it is for a standard or the unknown. The remaining digits, which specify the elements being analyzed and identify the standards, can be set at the beginning of an analysis and need not be changed. Output is recorded simultaneously on an automatic typewriter and a card punch.

We have found it convenient to set up the data-reduction procedure in two programs. The first, program CONE, averages counts, evaluates statistical parameters, and makes the instrumental corrections. The output of CONE is the initial approximation to the composition. A second program, ABFAN, calculates the matrix corrections and, if required, corrects the initial composition by iteration. These programs are written

TABLE 19. Line of Output from the Electron Probe

Data categories (see below)												
Standard numbers (spectrometers 1-3)												
Atomic numbers (spectrometers 1-3)												
Time (050.00 sec)												
1	159	14	20	12	05000	10028	1	61299	1	26255	1	0571
						Observed counts with scale factors (1:1, 2:10, 3:100)					Specimen current (0.0571 μ a)	

Data Categories

1. Standard peak (1)
2. Standard peak (2)
3. Standard background
4. Unknown peak
5. Unknown background (1)
6. Unknown background (2)

Any combination of categories that includes 1, 2, and 4 is permissible.

in Fortran IV for a Univac 1108 computer.

A sample sheet of output from program CONE is shown in Table 20. CONE can be used to calculate simple intensity ratios relative to any standard, but in the event that data on the compositions of the standards used are in the program's block data storage, the output will include analyses in weight percentages of the elements and oxides. Standard compositions are stored in a two-dimensional array for elements up to atomic number 28 (Ni) and with up to nine standards for each element. The drift calculated from counts on the standards taken before and after analysis of the unknown is also printed. Printout of the peak-to-background ratio provides a control on whether the background has been adequately evaluated.

The homogeneity index is the ratio of the observed standard deviation to the standard deviation predicted from counting statistics, and CONE calculates these indices for each group of counts before reducing their average to counts per second. A sample is considered inhomogeneous if its index is greater than 3. In the example shown, which is an analysis of a diopside inclusion from diamond,

it can be seen that Al and Ti have extremely inhomogeneous distributions. The index loses its sensitivity, however, at low peak-to-background ratios. Standards will normally be homogeneous, and printout of homogeneity indices for them is intended only to inform the user when counts are erratic for instrumental reasons.

Program CONE permits much flexibility with regard to the measurement of background. It can be determined on the standard, on the unknown, on both, or not at all. Background may be measured on the unknown both before and after analysis, and if this is done the printout will contain a calculation of background drift. If in a given analysis, background is measured on either the standard or the unknown, but not both, calculations are made on the assumption that the backgrounds of standard and unknown are equal. In the analysis of trace constituents, we have adopted the practice of scanning a peak and forming a ratio between background measured at some arbitrary wavelength (usually 0.050 Å above the peak) and the true background beneath the peak. During analysis the background is measured at this arbitrary wavelength and then corrected by the

TABLE 20. Example of CONE Printout

Weight %		Weight %		Intensity Ratio U/S	Standard Drift, %	Peak to Background
Al ₂ O ₃	0.93	Al	0.49	0.1852-00	1.4	8.53
K ₂ O	0.00	K	0.00	0.1395-03	2.6	1.03
TiO ₂	0.43	Ti	0.26	0.2140-00	2.3	2.89
Homogeneity Indices						
	Standard (1)		Standard (2)		Unknown	
Al	0.3		0.8		73.7	
K	0.9		0.7		2.3	
Ti	0.4		1.2		29.3	
Backgrounds						
	Unknown cps		Drift, %		Standard cps	
Al	23.12		0.0		23.12	
K	20.12		0.0		20.02	
Ti	75.55		0.0		75.55	
	Concentration, ppm	Student's <i>t</i>		Number of Counts		Detectability Limit, ppm
K	17	1.935		10		22

predetermined ratio. If such background factors are entered on a control card, program CONE will apply them.

Calculation of Student's t with a detectability limit provides a convenient test of the significance of peaks that are very small in relation to background. If an observed concentration is less than 0.1%, program CONE prints the result in ppm and a detectability limit for a confidence level of 99%. The detectability limit (Ziebold, 1966) is a function of the variance of a particular analysis, the number of counts taken, and the chosen confidence level. In the example shown in Table 20 the detectability limit for potassium is slightly greater than the concentration found. Hence, the presence of potassium in this sample has not been established at a confidence level of 99%.

Theoretical and empirical development of matrix corrections have advanced to the point where they can be used very successfully for silicates, provided the absorption corrections are kept below about 10 relative %. The absorption correction of Philibert (1963) with the over-voltage modification of Duncumb and Shields (1963) has been used in program ABFAN. K. F. J. Heinrich (personal communication) has recently suggested a change in the constants for the Leonard coefficient (σ).^{*} Heinrich's constants are used in ABFAN, and their use makes a substantial improvement in the analytical totals. ABFAN corrects for fluorescence of K lines by K lines with

^{*} With Heinrich's constants $\sigma = 4.25 \times 10^6 / (V\sigma^{1.65} - V_e^{1.65})$.

Reed's (1965) modification of the Castaing equation. Reed's simplifications for calculating the term $(r_A - 1)/r_A$ and for the fluorescence yield, $W_k(B)$, have been followed.

Atomic number effects are a combination of differences between standard and unknown in electron backscatter and stopping power. A recent treatment of these effects by Duncumb and Reed (unpublished manuscript) is promising, at least for heavy elements in a light matrix. Their treatment is used in ABFAN, including an equation adapted for computer calculation of the backscatter term made available by Duncumb.

Table 21 shows analyses that were made to test the Duncumb and Reed atomic number corrections. The materials analysed are themselves standards, either synthetic compositions or natural minerals whose compositions have been well established by wet-chemical analyses. These materials have been analysed with the probe relative to pure elements, and the individual corrections as well as the results are shown. Atomic number effects are large, with stopping-power corrections in the range 12–24 relative %. Results for Fe and Cr agree with expected compositions to ± 2 relative %, but the Ti analyses appear to be overcorrected by 3 to 5 relative %. These results are encouraging, particularly inasmuch as synthetic standards containing the transition elements are very difficult to synthesize.

ABFAN stores Heinrich's (1966) constants for calculation of mass absorp-

TABLE 21. Analyses of Various Materials, with Pure Elements as Standards

Material Analyzed	Element	Absorption Correction	Fluorescence Correction	Atomic Number Effects		Weight % Element	
				Stopping Power Correction	Backscatter Correction	Corrected Probe Result	Expected Composition
Chromite	Fe	1.055	1.000	1.131	0.965	17.0	17.17
Glass	Fe	1.021	1.000	1.189	0.957	13.7	13.99
Olivine	Fe	0.997	1.000	1.235	0.944	5.76	5.66
Chromite	Cr	1.001	0.967	1.125	0.966	30.7	30.45
Glass	Cr	1.033	1.000	1.222	0.949	1.28	1.3
Glass	Ti	1.052	0.987	1.125	0.975	11.4	10.89
Glass	Ti	1.051	1.000	1.198	0.965	1.24	1.20

tion coefficients. Other constants, such as wavelengths for $K\alpha$ lines and K edges, atomic weights, etc., are also stored. It would be possible to compute matrix elements for the standards as well as the unknown in each problem. But our analytical method uses relatively few standards, and it is simpler to store them in a data block. The matrix elements are dependent on kv, and handling them in this way requires the user to make analyses at the same kv values as those used in calculation of the standard constants. Normally this is not a severe restriction, but in the event a user wishes to employ some kv-standard combination different from those used in calculation of the values in the program, the required matrix constants can be read in with the data cards.

Program ABFAN can be used in two ways. It will calculate and print out matrix elements for an input composition. Alternatively it will correct an input composition, refining the matrix corrections by iteration with reference to standards. Table 22 shows an example of the first application. Use of ABFAN in this way provides constants for stan-

dards, which are then stored in data statements. It may also be used, in setting up an analytical program, to run trial compositions so that standards can be selected that will minimize absorption corrections.

Table 23 shows an example of a problem in which ABFAN is used to correct an input composition by iteration. ABFAN prints out the number of iterations required to produce a composition that differs from the composition on the previous cycle by less than 0.1 relative % of any of the elements present. Normally three or four iterations are sufficient and more than five have never been required.

An array of values of Reed's gamma function (Reed, 1965) is also printed (Table 22), a feature useful in locating fluorescence effects. In the example shown, only the fluorescence of $KK\alpha$ by $CaK\alpha$ is significant.

Oxygen contents of silicates and other oxides cannot readily be determined with an electron probe. ABFAN estimates the oxygen content of an unknown by summing the weight fractions of the analyzed elements, subtracting the sum

TABLE 22. Output of Program ABFAN for E-11 Diopside, No Iteration

	Weight %	Kv	$F(\chi)$	Fluorescence Factor *	Stopping Power Factor	Backscatter Factor
Ca	13.95	15	0.9194	0.9985	2.0675	0.9303
Mg	10.43	15	0.5585	0.9953	2.0675	0.9303
Al	1.60	15	0.6063	0.9913	2.0675	0.9303
Fe	2.02	20	0.9533	1.0000	2.1988	0.9264
Cr	0.99	20	0.9268	0.9950	2.1988	0.9264
Si	25.33	15	0.7012	0.9988	2.0675	0.9303
Na	1.34	15	0.4246	0.9961	2.0675	0.9303
Ti	0.25	15	0.9275	0.9969	2.0675	0.9303
Mn	0.07	20	0.9428	1.0000	2.1988	0.9264
K	0.01	15	0.8917	0.9794	2.0675	0.9303

Note: Mean atomic weight = 21.70; mean atomic no. = 10.78; $H = 0.224$.

Values of Reed's Gamma Function *

	Ca	Mg	Al	Fe	Cr	Si	Na	Ti	Mn	K	O
Ca	0.0000	0.0000	0.0000	0.0006	0.0006	0.0000	0.0000	0.0002	0.0000	0.0000	0.0000
Mg	0.0003	0.0000	0.0003	0.0000	0.0000	0.0041	0.0000	0.0000	0.0000	0.0000	0.0000
Al	0.0005	0.0000	0.0000	0.0000	0.0000	0.0082	0.0000	0.0000	0.0000	0.0000	0.0000
Fe	0.0000	0.0000	0.0000	0.0000	0.0000	0.0000	0.0000	0.0000	0.0000	0.0000	0.0000
Cr	0.0000	0.0000	0.0000	0.0050	0.0000	0.0000	0.0000	0.0000	0.0000	0.0000	0.0000
Si	0.0011	0.0000	0.0000	0.0000	0.0000	0.0000	0.0000	0.0000	0.0000	0.0000	0.0000
Na	0.0001	0.0017	0.0002	0.0000	0.0000	0.0019	0.0000	0.0000	0.0000	0.0000	0.0000
Ti	0.0000	0.0000	0.0000	0.0016	0.0014	0.0000	0.0000	0.0000	0.0001	0.0000	0.0000
Mn	0.0000	0.0000	0.0000	0.0000	0.0000	0.0000	0.0000	0.0000	0.0000	0.0000	0.0000
K	0.0202	0.0000	0.0000	0.0004	0.0003	0.0000	0.0000	0.0002	0.0000	0.0000	0.0000

Note: Row headings are analyzed elements; column headings are fluorescing elements.

* Fluorescence factor = $1/(1 + \gamma_1 + \gamma_2 + \gamma_3 + \dots \gamma_n)$.

TABLE 23. Output of Program ABFAN for E-11 Diopside Iterated with Reference to Standards

	Kv	Absorption Correction	Fluorescence Correction	Backscatter Correction	Stopping Power Correction	Initial Composition	Corrected Composition		
Ca	15	1.0024	0.9985	0.9997	0.9970	13.98	13.95	CaO	19.51
Mg	15	1.0328	1.0001	0.9997	0.9970	10.13	10.43	MgO	17.29
Al	15	0.9397	0.9990	1.0060	0.9809	1.73	1.60	Al ₂ O ₃	3.03
Fe	20	1.0184	1.0000	1.0049	0.9898	1.99	2.02	FeO	2.59
Cr	20	1.0013	0.9950	1.0014	0.9948	1.00	0.99	Cr ₂ O ₃	1.45
Si	15	1.0241	1.0004	0.9997	0.9970	24.81	25.33	SiO ₂	54.18
Na	15	0.9848	0.9987	1.0017	0.9936	1.37	1.34	Na ₂ O	1.81
Ti	15	0.9931	0.9969	0.9993	0.9988	0.25	0.25	TiO ₂	0.41
Mn	20	1.0200	1.0000	1.0053	0.9916	0.07	0.07	MnO	0.09
K	15	0.9950	0.9794	1.0016	0.9971	0.01	0.01	K ₂ O	0.01
Totals						55.34	55.99		100.38

Note: Number of iterations = 3.

from 1.0, and assigning the difference to oxygen. ABFAN will correct for the presence of any two elements by difference if their atomic numbers and atomic proportions are read in with the data cards. This feature is most useful in

analysis of carbonates and nitrates, for the concentrations of C and N cannot be determined with an accuracy comparable to that possible with heavier elements. It can also be used for silicates if the ratio of Si to O is well established.

CRYSTALLOGRAPHY

A NEW HEXAGONAL FORM OF CARBON FROM THE RIES CRATER

A. El Goresy and G. Donnay

The mineralogy and textural relations of shocked graphite gneisses from the Ries Crater were studied in polished sections. Several graphite grains contain a new phase. X-ray diffraction and electron-microprobe investigations of these grains reveal the presence of a new hexagonal form of carbon, which occurs in relatively thin lamellae (3 to 15 μ wide) alternating with graphite and perpendicular to the 0001 face of graphite. The new phase is much more strongly reflecting ($R \approx 40\%$) than hexagonal graphite and shows no sign of bireflection. It is slightly harder than graphite, and its reflection color is metallic gray to white. No anisotropism was observed, probably on account of the extremely small grain size. Electron-microprobe analysis of the new phase indicated carbon as the only major element; small amounts of Cl and Si ($<0.5\%$) were also detected. They

appear to be due to contamination by the glass matrix and the araldite mounting material in which the sample is embedded.

A grain containing more than 60% of the new phase, as estimated under the reflecting microscope, was carefully isolated mechanically from the polished section and mounted without crushing in a Debye-Scherrer camera (114.6 mm radius). The patterns made with FeK α and CuK α radiations ($\lambda_{\text{Fe}}=1.9373$, $\lambda_{\text{Cu}}=1.51418$ Å), consisted of 22 sharp lines (Table 24) in addition to the eleven strongest lines of hexagonal graphite. There is no evidence of preferred orientation. No rhombohedral graphite lines were observed.

A primitive hexagonal cell with cell dimensions $a=8.948 \pm 0.009$, $c=14.078 \pm 0.017$ Å, permits the indexing of all observed lines (Table 24). The least-squares program LCLSQ of C. W. Burnham (*Year Book 61*, pp. 131–135) was used to obtain the above refined cell dimensions. Note that although no 0001

TABLE 24. X-ray Powder Pattern of Chaoite

No.	$d_{obs.}$	$d_{calc.}$	I	hkl
1	4.47	4.465	v.v.st.	11·0
2	4.26	4.256	v.v.st.	11·1
3	4.12	4.014	v.st.	10·3*
4	3.71	3.728	m.	20·1
5	3.22	3.206	m.	10·4
6	3.03	2.985	st.	20·3
7	2.94	2.923	w.	21·0
8	2.55	2.536	st.	30·1
9	2.46	2.482	m.	21·3
10	2.28	2.277	st.	20·5
11	2.24	2.232	m.	22·0
12	2.10	2.080	m.	30·4
13	1.983	2.007	w.	20·6
14	1.910	1.915	w.	40·1
15	1.496	1.495	w.	22·7
16	1.370	1.370	w.	41·6, 22·8
17	1.289	1.289	w.	60·0, 50·6
18	1.26	1.257	w.	33·6
19	1.197	1.197	m.	33·7, 52·3
20	1.184	1.183	m.	42·7
21	1.080	1.0815	w.	41·10
22	0.8642	0.8643	w.	41·14

* Possibly the strongest line of an impurity, since the disagreement of observed and calculated d values, 2.7%, is considerably greater than for the next poorest reflection, 20·3, where it is 1.6%.

Note: v.v.st., very very strong; v.st., very strong; st., strong; m., medium; w., weak.

reflections are observed, so that a layer structure is excluded, the nature of the principal axis of symmetry is undetermined. If the holohedral space group $P6/mmm$, which has a 24-fold general position, is assumed, a reasonable calculated density of 3.43 g/cm³ is obtained by filling the general position seven times, leading to 168 atoms per cell. Not enough of the pure, new phase has yet been isolated for density measurement.

The name chaoite is proposed for this mineral to honor Dr. Edward C. T. Chao, of the U. S. Geological Survey, who contributed greatly to the recognition and discovery of meteorite craters and the shock-induced metamorphic processes that accompany meteoritic impacts.

DETERMINATION OF CATION DISTRIBUTIONS BY LEAST-SQUARES REFINEMENT OF SINGLE-CRYSTAL X-RAY DATA

L. W. Finger

The ordering of cations in the crystal structure of a material belonging to a

solid solution series greatly affects its thermochemical properties and its stability. Substitutions, such as of aluminum for silicon, in tetrahedra in which the variation in site chemistry changes the average cation-anion bond distance have been successfully rationalized by many investigators in terms of ordering parameters. For many octahedrally coordinated cations there is no reliable correlation between site chemistry and bond distance, and the difference in X-ray scattering power between cations has been used to allocate the different elements among the possible sites. Ghose and Hellner (1959) used this difference implicitly by noting that if the Fe/Mg ratio for a site in their model of grunerite were wrong, the least-squares treatment would change the scattering power in each site by adjusting the temperature factor. Their procedure assumes that the temperature factors for all the octahedral sites are equal, but one of the amphibole sites in fact has a much different environment than the others, and will therefore probably have a different temperature factor. Accordingly, a solution not involving this assumption was used by Fischer (1966) in refining the cation distributions in a cummingtonite by a direct least-squares treatment, applying no physical or chemical constraints to the solutions. Occupancy constraints are developed here, and their application is shown.

The first constraint is purely physical and limits the maximum occupancy of the site. If we define a_{mn} as the fractional occupancy of the m th site by the n th chemical species, then the equation

$$\sum_n a_{mn} \leq 1 \quad (1)$$

must be satisfied. If there are no vacancies, then the equality in (1) holds. Another requirement of the solution for the a_{mn} 's is that the site chemistry must agree with the bulk chemistry. Mathematically this may be written as

$$\sum_m b_m a_{mn} = c_n, \quad (2)$$

where c_n is the total number of atoms of species n per unit cell and b_m is the multiplicity of the position in which the m th atom is located. This latter constraint is usually handled implicitly by subjecting each atom in the asymmetric unit to the first condition while refining the coefficients and then checking that the chemical formula is confirmed. However, in at least one structure refinement, that of a grunerite by Finger and Zoltai (1967), this procedure did not work. This Mg-Fe amphibole had a value for the ratio $\text{Mg}/(\text{Fe}+\text{Mg})$ of 0.12, according to the chemical analysis of Klein (1964), and a total of 1.68 Mg atoms per cell, but the least-squares result led to a ratio of 0.33. The chemical equivalence of the material studied by Klein and the single crystal used in this work is reasonably certain, since both investigators determined the same value for the unit-cell volume, a parameter shown to be very sensitive to composition by Klein and Waldbaum (1967). The discrepancy in the chemical composition was initially resolved by a very complicated series of refinement steps. The final solution was checked with a difference Fourier synthesis, which showed very little discrepancy in the electron density at the locations of the cations. When the above refinement description was presented, C. T. Prewitt (personal communication) suggested that the constraint of (2) should be applied explicitly to this structure. If magnesium is chosen as species 1 and the amphibole cation positions M_1 to M_4 , as positions 1 to 4, respectively, the second constraint may be written as

$$4a_{11} + 4a_{21} + 2a_{31} + 4a_{41} = 1.68 \quad (3)$$

for this structure and composition. Note that the similar equation relating the iron contents of the sites is not independent, since it may be found from a linear combination of (3) and (1) because, in this case, (1) is an equality. Thus, for this structure, (2) contributes one equation to the eight needed to de-

termine the eight coefficients of occupancy. Four equations are supplied by (1), and there are three parameters to be fitted by least-squares analysis.

When the occupancy coefficients are fitted by refinement, the derivatives of the structure factors with respect to the parameters being varied must be computed. If the changes in the model are to be calculated properly, however, the constraints must be used in the calculation of the derivatives. The nature of the relationships introduced by (1) is well known and will not be covered here. The relationships for (2), although just as obvious, have not been described. In general, if parameter s is dependent on parameter r , this dependency must be applied to the least-squares equations as a modification to the derivatives of the structure factor with respect to the refined parameter. In addition, s must not be varied as a least-squares parameter. The derivatives are modified with the use of the chain rule to yield equations of the form

$$\left(\frac{\partial F}{\partial r}\right) = \left(\frac{\partial F}{\partial r}\right)_i + \left(\frac{\partial F}{\partial s}\right)_i \left(\frac{\partial s}{\partial r}\right) \quad (4)$$

where F is the calculated structure factor for the observation in question, the subscript i refers to the derivatives computed as if the parameters were independent, the quantity on the left being the derivative needed for the least-squares analysis. If the dependent occupancy parameter is a_{pn} , then (4) may be rewritten as

$$\left(\frac{\partial F}{\partial a_{mn}}\right) = \left(\frac{\partial F}{\partial a_{mn}}\right)_i - \frac{b_p}{b_m} \left(\frac{\partial F}{\partial a_{pn}}\right)_i \quad (5)$$

with one equation of this form for each of the three refined occupancies.

When the data on the grunerite mentioned above were subjected to least-squares analysis with the use of (5), the occupancy parameters converged in two cycles to the values obtained by the very laborious procedure referred to above.

MAGNETIC SUSCEPTIBILITY AND
EXCHANGE COUPLING IN
ARDENNITE *

F. E. Senftle,† A. Thorpe,† and G. Donnay

The highly distorted oxygen octahedra about Mn^{2+} and (Mn^{2+}, Ca) in ardenite were suspected to result in abnormal magnetic behavior (*Year Book 66*, p. 485). Magnetic susceptibility measurements were made along different crystallographic directions from room temperature down to 5°K. They showed anisotropic behavior along the short b axis (5.81 Å) and isotropic behavior in the (010) plane. The variation of the magnetic susceptibility with temperature can be described, according to Earnshaw and Lewis (1958, 1960), as follows:

$$\chi_T = \frac{1}{T} [A + B \cdot G(\theta)] + N(\alpha)$$

where A and B are constants, $G(\theta)$ is an exponential term, and $N(\alpha)$ is a temperature-independent term. Computer calculations give the best fit for $A=17.5$, $B=4.5$ emu/°K/g, and for the exponential term, $\theta=1.35$ to 1.60 depending on the direction with respect to the b axis. The data so obtained can be interpreted if, in addition to the normal paramagnetic contribution of manganese, there exists an antiferromagnetic contribution due to exchange coupling between adjacent manganese atoms through an intervening oxygen atom. Manganese atoms in both crystallographic positions participate in this exchange coupling. The effect appears to be due to the short Mn-Mn distance in the structure, rather than the distortion of the oxygen octahedra about the manganese atoms.

"MCKELVEYITE," A SYNTACTIC INTER-
GROWTH OF TWO PHASES

G. Donnay and J. D. H. Donnay

The first publication on mckelveyite (Milton *et al.*, 1965) attracted the atten-

tion of one of us because the reported space group $P\bar{3}$ and the development of the crystals shown on photographs (Milton *et al.*, 1965, Figs. 1b and 3) did not jibe. A second paper (Desautels, 1967), specifically treating the morphology of mckelveyite, assigned it to space group $P3m1$ or $P3$, still not in agreement with the symmetry observed on inspection (Desautels, 1967, Fig. 1). We were sufficiently intrigued by then to ask the authors for type material that we might study. We wish to thank Dr. Charles Milton for a most informative discussion and for his generous cooperation in presenting us with all the specimens of his collection.

The samples represent an example of "polycrystals" (Donnay, 1953) strikingly similar to the ones formed by the bastnaesite, parisite, roentgenite, synchisite series, $mCaFeCO_3 \cdot nCaCO_3$ (Donnay and Donnay, 1953). Two distinct phases are intergrown, one of which has the cell dimensions reported by Milton *et al.* (1965) but with space group $P31m$, the absence of the center of symmetry being indicated by morphology. The other phase is also hexagonal; it controls the morphology of the polycrystals studied by Desautels. We propose for it the name ewaldite in honor of Professor P. P. Ewald (pronounced *āvald*, *ā* as in able, *a* as in act). Its space group is $P6_3mc$, again taking into account the morphological evidence for the absence of center and horizontal mirror on crystals of the second phase. The a axes of the two phases are turned 30° with respect to each other about the common c axis. The cell dimensions of ewaldite (a_e , c_e) are related to those of mckelveyite (a_m , c_m) as follows:

$$a_e = 5.291 \pm 0.006 \text{ Å} = a_m / \sqrt{3} = 9.164 / \sqrt{3} \pm 0.010 \text{ Å},$$

$$c_e = 12.751 \pm 0.012 \text{ Å} = 2c_m / 3 = 2 \times 19.126 / 3 \pm 0.018 \text{ Å},$$

$$V_e = 2V_m / 9 = 2 \times 1391 / 9 \pm 4 \text{ Å}^3$$

* Publication authorized by the Director, U. S. Geological Survey, Washington, D. C.

† U. S. Geological Survey, Washington, D. C.

The syncrystallization of the two species is thus explained by the syntactic relations: $3c_e = 2c_m$, $a_e = a_m/\sqrt{3}$ (in the xyu plane, the ewaldite net "H-centers" the mckelveyite net). These data were obtained from back-reflection Weissenberg photographs taken at 21°C with $\text{CuK}\alpha$ radiation ($\lambda\alpha_1 = 1.54051 \text{ \AA}$, $\lambda\alpha_2 = 1.54434 \text{ \AA}$).

X-ray studies of some twelve specimens showed that the shiny black crystals consist exclusively of mckelveyite, whereas the dull light bluish-green to dark green individuals are polycrystals of ewaldite and mckelveyite. Only one crystal of pure ewaldite has so far been discovered. Its color is deep green. The quickest method of determining the relative amounts of the two phases present in a specimen consists in taking a cone-axis precession photograph with the c direction along the X-ray beam (Plate 1). Since there is no difficulty in identifying the c direction and adjusting the (0001) face in prism position on the two-circle goniometer, it takes only a few hours to obtain the desired information.

As would be expected, the black mckelveyite crystals frequently show twinning (by merohedry) on $2\bar{1}.0$ (Milton *et al.*, 1965, Fig. 3), with twin symmetry to be written $6'm'm$ in black-white symbolism. Ewaldite, contrary to expectation, has not been observed to twin. Another feature characteristic of mckelveyite consists of continuous and near-uniform diffraction streaks in reciprocal space running parallel to c^* for all those $hk \cdot l$ values that obey $k \neq 3p + h$, $l \neq 3r - h$, where p and r are any integers. Reflections of the type $h \cdot (3p + h) \cdot (3r - h)$ give the usual sharp Bragg reflections. About 250 of the latter have been recorded for a pure mckelveyite crystal, whose structure determination is now under way.

Ewaldite shows only sharp reflections. In addition to the space-group absences, we observe structural extinctions $hk \cdot l$ absent for $l = 2n + 1$ and $h - k = 3n$. This

is an absence criterion for position 2(b) in $P6_3mc$ and thus indicates that the heavy atoms, barium, rare earths, uranium, must occupy this position with site symmetry $3m$.

Electron-probe studies of four polycrystals showed no evidence of chemical differences in heavy atom and calcium content between mckelveyite and ewaldite. They could be different hydrates, of course. Dr. Max Hey is performing microchemical analyses on crystals studied by X rays, to give further information on the compositions. The Fe_2O_3 content reported by Milton *et al.* (1965) can be ascribed to iron-rich inclusions, which show up strikingly on an X-ray image of $\text{FeK}\alpha$ radiation (Plate 2) taken by Mr. C. Hadidiacos. The inclusion was identified under the reflecting microscope by Dr. A. El Goresy as hematite pseudomorphous after magnetite. For the time being we are using, for mckelveyite, an idealized cell content based on the published analysis (Milton *et al.*, 1965):



The density measured for several pure mckelveyite crystals on the Berman balance at 24°C is $3.25 \pm 0.05 \text{ g/cm}^3$, considerably less than the calculated value of 3.54 g/cm^3 obtained for the above cell content.

CRYSTALLINE HETEROGENEITY

Evidence from Electron-Probe Study of Brazilian Tourmaline

G. Donnay

The concept of "single crystal" defined in the conventional way as a "homogeneous edifice" is in need of critical reexamination when applied to minerals. We began this study with thin plates showing drastic color changes, cut from tourmaline crystals of Brazilian origin. Mr. Earl Williams of The Johns Hopkins University kindly supplied the crystals and cut the plates. The cuts were placed nearly perpendicular to the

boundary zone of the differently colored regions. Some crystals show color variation along the c axis; they were cut parallel to $(\bar{1}210)$. Others show color changes perpendicular to the c axis; they were cut parallel to (0001) . An elbaite crystal (U. S. National Museum R-17011) that looks uniformly pink to the naked eye was also studied. Its manganese content, which is mainly responsible for the pink color, varies continuously through a range down to 43% of the maximum over a distance of 0.45 mm. This was an unexpected finding. The sharp changes that we observed in Mg, Fe, and Al concentrations at the color boundaries of the multicolored plates were expected, but they too were preceded and followed by gradual, continuous changes in concentrations. The electron-probe results by themselves thus invalidate the assumption that a one-color chip picked from such a tourmaline crystal can be considered a "single crystal"; it is *not* chemically homogeneous.

The same thin tourmaline plates were oriented normal to the X-ray beam on the precession camera. We obtained diffraction patterns of differently colored regions on the same film by raising the cassette slightly when, with the help of the translation movement of the goniometer head, a differently colored region was brought into the beam. On such doubly and triply exposed films, very small changes in cell dimensions and axial orientations can be observed. The maximum differences that we measured were of the order of 0.7% in a , 0.3% in c , and a $0^\circ 10'$ rotation of the a axes about a constant c -axis direction. From three chips from the one elbaite crystal R-17011 cell dimensions were refined by a least-squares treatment of back-reflection Weissenberg data ($\text{CuK}\alpha_1 = 1.54051$ Å), with the following results: $a_1 = 15.836 \pm 0.002$, $c_1 = 7.0986 \pm 0.0005$; $a_2 = 15.846 \pm 0.004$, $c_2 = 7.1020 \pm 0.0008$; $a_3 = 15.838 \pm 0.001$, $c_3 = 7.1032 \pm 0.0002$ Å. This agreement would be considered good enough to warrant the conventional as-

sumption of constant chemical composition throughout the crystal if the electron-probe results had not warned us. Bragg reflections give the combined diffraction contribution of millions of unit cells and do not tell us whether or not the solid solutions present show short- or long-range order. If then we use the intensities from such a chip to refine the elbaite crystal structure, i.e. the atomic coordinates, temperature factors, and chemical occupancies, implicitly letting the chemical composition be constant throughout the crystal, we are misinterpreting the diffraction data. We shall, probably with the help of least-squares refinement, arrive at a structure that gives a small residual R , but the refined structure may have limited physical significance.

Careful testing of the crystal to be used for X-ray structure determination appears to be a necessity. Assurance of constant concentration of the major chemical constituents in a mineral crystal should be a prerequisite for using the crystal in a structure refinement.

Evidence from Source-Image Distortion

R. A. Young,* C. E. Wagner,* C. O. Pollard,*
and G. Donnay

Seven of the multicolored Brazilian tourmaline plates mentioned above were examined for variations in macromosaic texture by an X-ray diffraction technique described by Young and Wagner (1966). Five of the plates came from different crystals, were 0.7 mm thick, and were cut parallel to (0001) . Two thinner ones, 0.2 mm across, came from the same crystal; one was cut parallel to the basal plane, and the other was cut parallel to $(\bar{1}210)$.

In the arrangement used for SID studies, a diverging $\text{CuK}\alpha$ X-ray beam from a spot source (angle of divergence equals $13'$ of arc) impinges on the crystal plate at a distance of 134 cm from the

* Physical Sciences Division, Georgia Institute of Technology.

X-ray source; a 5-mm-wide slit is placed in the incident beam, 4 cm from the sample. The plate is oriented so that one of the Bragg reflections is in diffracting position. The diffracted beam is recorded for about 10 minutes on Ultra-Speed dental film, placed perpendicular to the diffracted beam, about 3 cm from the crystal (Plate 3).

An X-ray radiograph of the exposed section of the same crystal plate (Plate 4) shows a less-absorbing ring on the outside; it is colorless. A more-absorbing inside field is blue. Cell dimensions obtained from X-ray precession films indicate that the composition of the plate is on the dravite-schorl solid solution range, near the halfway point. The differences in a and c axes for the differently colored regions are both close to 0.2%.

On all samples studied, we observe a striking, abrupt change in macromosaic texture (Plate 3). It coincides with the color change but is more sharply delineated. The outside region of all the plates studied so far is light pink or colorless. It is always composed of small elongated grains in which the direction of elongation serves as the line about which lattice misalignments of the order of several minutes of arc occur. The central, darker, more iron-rich regions consist of larger grains, with only small misalignments in lattice directions between grains. Texturally, the central region would be described as a nearly perfect single crystal, the outside region as an exceedingly imperfect crystal.

We are led to the questions: Are the changes in texture a result of the chemical change, or are they due to drastic changes in the conditions of crystallization, such as temperature and pressure, that may be accompanying the chemical changes? Do other mineral crystals also show more than one texture type? What will synthetic crystals show? There is need for further extensive work along these lines.

STRUCTURE REFINEMENT OF ELBAITE

*G. Donnay and R. Barton**

The refinement of buergerite, $\text{NaFe}_3^{3+}\text{Al}_6\text{B}_3\text{Si}_6\text{O}_{30}\text{F}$ (Barton, 1967), shows no significant changes in fractional coordinates from those determined by Buerger, Burnham, and Peacor (1962) for dravite, the magnesium tourmaline variety. This was a surprising find, because chemical as well as physical properties of the two varieties differ markedly. We must now investigate the Li,Al end member, elbaite, to see whether its fractional coordinates are also the same. There appears to be no natural solid solution between elbaite and dravite, and the two minerals therefore may be expected to show some significant differences in crystal structure.

If, as results so far obtained suggest, elbaite proves to have the same fractional coordinates as buergerite and dravite, we could, of course, calculate interatomic distances and angles in all tourmalines from knowledge of cell dimensions alone. This seems highly unlikely.

Elbaite was claimed to have been the tourmaline studied by Ito and Sadanaga (1951). When plotting the given cell dimensions, $a=16.0$, $c=7.17$ Å on the diagram of cell dimensions c versus a (Mason, Donnay, and Hardie, 1964, Fig. 1), however, we were impressed by the fact that these dimensions placed the composition on the schorl-dravite solid solution join about one third of the way from schorl. The "probable atomic ratios $\text{Na}:\text{Ca}=7:1$, $\text{Li}:\text{Al}=1:2$, $\text{Al}:\text{Fe}:\text{Mn}=6:0.1:0.1$ " (given by Ito and Sadanaga, 1951) are identical with those given in *Dana's System of Mineralogy* (sixth edition, p. 555) for Brazilian rubellite. We asked Professor Sadanaga for the crystal he had used and were told in his answer of December 9, 1967, "In fact, I did not even see the specimen, only being informed that it was a Brazilian rubellite. I therefore carried out a

* Carothers Laboratory, E. I. du Pont de Nemours and Company, Wilmington, Delaware.

structure determination by assuming the composition as identical with those described in Dana's System." Unfortunately, the crystal itself has been lost.

We therefore decided to carry out an elbaite study on a single crystal large enough so that the chemical analysis, electron-probe tests, crystal optics, and infrared and ultraviolet spectroscopy (to be done by Dr. R. W. T. Wilkins at Harvard University), as well as the structure refinement, could be performed on material from the one crystal. Dr. G. Switzer, of the U. S. National Museum, kindly supplied a large, gem-quality, pink crystal (USNM R-17011) from San Diego County, California. Dr. B. Wiik has performed a wet-chemical analysis, which shows it to be a nearly pure Li_2Al composition, with only 0.24 wt % FeO and 0.02 wt % MgO. As mentioned above in the section on "Crystalline Heterogeneity, Electron-Probe Evidence," we tested several chips of this crystal for constancy of chemical composition and found especially that the Mn content was variable. Wiik found 2.36 wt % of MnO, an unusually high value. One circular traverse with the electron probe gave nearly constant concentrations of Si, Al, Mn, and Ca. This encircled region was chosen for X-ray study. Although there is the danger of heterogeneity in the specimen, we do not dare probe it until the structure refinement reaches a final stage so we can be sure that no further intensity measurements will be needed. This precaution is necessary because electron-probe scanning alters the chemical composition; especially, it removes alkali-metal ions from the specimen.

A complete set of intensities has been collected with $\text{MoK}\alpha$ radiation on the Supper-Pace automated diffractometer, and refinement is under way.

IMPROVEMENTS OF CRYSTALLOGRAPHIC EQUIPMENT

G. Donnay

The Optical Analyzer

The optical analyzer (Donnay and Donnay, 1957, 1966) is mounted on the stage of the microscope. When making the necessary adjustments of the goniometer head on which the crystal is mounted, one would like to have the analyzer stationary, not sliding about. Transfer tape has been used but has proved unsatisfactory. Instead, three magnets have now been mounted in the base of the analyzer, and whenever the analyzer is being used, the glass plate of the microscope is replaced by a metal plate in which a circular hole has been cut in the center, the same size as the hole in the optical analyzer, permitting light from below to pass through the specimen. The magnets hold the analyzer with sufficient strength to prevent sliding yet permit easy removal of the instrument. The arrangement has proved highly satisfactory.

Precision Film-Measuring Device

Back-reflection Weissenberg as well as powder films should be measured with the highest possible precision whenever a least-squares refinement of the data they furnish is to be carried out. A recently developed film-measuring device of Picker Corporation (catalog no. 684-813) permits readings to be made to 0.01 mm with a dial indicator, a precision greater than is warranted by the size of most diffraction spots and lines. The instrument does not provide, however, for movement of the film in a direction normal to the reading scale, so that a powder film cannot be readily centered before the measurements are begun and the Weissenberg film, which has to be translated parallel with itself during measurements, cannot be read at all.

The instrument has been rebuilt so that the frame holding the reading scale can be moved up and down over a distance of $1\frac{1}{2}$ inches in carefully machined grooves. The film remains stationary during the measurement, while an adjusting screw moves the scale parallel to itself.

SONORAITE

Richard V. Gaines,* G. Donnay, Max H. Hey,† and J. Zemann‡

A new iron tellurite mineral, $\text{Fe}_2^{3+}\text{Te}_2^{4+}\text{O}_7 \cdot x\text{H}_2\text{O}$, has been discovered by the senior author in the oxidized zone of the Moctezuma tellurium-gold mine in the state of Sonora, Mexico. It consists of highly lustrous, yellowish-green rosettes, usually associated with emmonsite, $\text{Fe}_2^{3+}\text{Te}_3^{4+}\text{O}_9 \cdot 2\text{H}_2\text{O}$, and has been found so far only in very small amounts. The chemical analysis was carried out (by Hey) on only 890 μg of material, and the water content is therefore not firmly established.

The space group $P2_1/c$ is uniquely given by the observed systematic absences: $0k0$ absent with k odd, $h0l$ absent with l odd. The cell dimensions at 21°C obtained from a least-squares refinement (Program LCLSQ of C. W. Burnham, *Year Book 61*, pp. 132–135) of back-reflection Weissenberg photographs with $\text{CuK}\alpha$ radiation ($\lambda\alpha_1 = 1.54051$, $\lambda\alpha_2 = 1.54434$ Å) are $a = 10.984 \pm 0.002$, $b = 10.268 \pm 0.001$, $c = 7.917 \pm 0.002$ Å, $\beta = 108.49 \pm 0.02^\circ$, $V = 846.8 \pm 0.5$ Å³. For $4(\text{Fe}_2\text{Te}_2\text{O}_7 \cdot 2\text{H}_2\text{O})$ per cell, the calculated density is 4.04 g/cm³, in good agreement with the measured value of 3.95 ± 0.01 g/cm³ obtained by the flotation method in Clerici solution.

The thin platy habit of sonoraite crystals shows little variation. The dominant form is the pinacoid (100); rhombic prisms (110) and (011) border the plate in the order of importance predicted by

the Generalized Law of Bravais (Donnay and Harker, 1937). Striations parallel to c appear on (100) and (110).

The crystals are soft ($H \sim 3$). They show biaxial negative optical character, with $\alpha = 2.018 \pm 0.003$, $\beta = 2.023 \pm 0.003$ and $\gamma = 2.025 \pm 0.003$, determined in Cargille oils. $2V$ is in the range 20° to 25° . No pleochroism is observed.

The mineral has been approved by the Commission on New Minerals and Mineral Names of the International Mineralogical Association.

THE CRYSTAL STRUCTURE OF SONORAITE, $\text{Fe}_2\text{Te}_2\text{O}_5(\text{OH})_4 \cdot \text{H}_2\text{O}$

G. Donnay, J. Stewart,* and J. Zemann

We recorded 1895 observable, symmetry-independent reflections on the automated Supper-Pace diffractometer with $\text{MoK}\alpha$ radiation. The "X-ray 67 phase program" (Technical Report 67-58 of the Computer Science Center, University of Maryland) led to the placement of Te and Fe atoms, which were then used for sign calculations for a first three-dimensional electron density, which gave ten oxygen locations ($R = 11.9\%$). All atoms are in general 4-fold position. Refinement by the least-squares method is in progress.

Of the ten oxygens present, one or two belong to water molecules. The presence of at least two hydroxyl ions is indicated by the Pauling bond strength distribution. We may picture the structure as composed of stepped chains of anion octahedra about ferric ions extending along [101]. The average iron-anion distance is 2.05 Å. There are two such chains per cell, related to each other by the c glide plane. The four octahedra per cell in each chain form two edge-sharing pairs with a center of symmetry bisecting the shared edge; these pairs are joined by one shared corner. The Fe-Fe distances within the pairs are 3.12 and 3.28 Å, whereas the distance between

* Universidad Nacional Autónoma de México.

† British Museum (Natural History).

‡ University of Vienna.

* University of Maryland.

symmetry-independent iron atoms in the chain is 3.70 Å. Both tellurium ions are tetrahedrally coordinated by three oxygens and the unshared electron pair of Te^{4+} . The average Te-O distance is

1.92 Å, the average O-O distance in the triangles bonded to Te is 2.75 Å. The oxygen triangles connect the chains of iron octahedra into a three-dimensional framework.

GEOCHRONOLOGY AND GEOCHEMISTRY

G. L. Davis, T. E. Krogh, S. R. Hart, and L. T. Aldrich,* with S. A. Morse and Kyoichi Ishizaka **

The time of formation of the rocks in the Grenville structural and lithologic province, an area of high-grade metamorphic rocks in the Canadian shield, has been a subject of controversy since the earliest geological investigations. The vastness of the area and its obvious boundary with the older Superior province rocks to the northwest make it a key to theories regarding the continental development of North America. About a decade ago several workers on geochronology concluded that these rocks were formed shortly before 900 m.y. ago, the age value obtained by the K-Ar method on micas in the area. Those characteristics of the rocks that indicated intense metamorphism and plastic deformation were assumed to have developed during the time of last heating, 900 m.y. ago. Our current results demonstrate that these conclusions are largely incorrect.

Earlier studies by Krogh showed that intrusion and metamorphism occurred in the Grenville in southeastern Ontario between 1300 and 900 m.y. ago. Our recent studies in the northwest Grenville area of Ontario show that certain rocks in this area were metamorphosed and intruded between 1500 and 1800 m.y. ago. The whole-rock Rb-Sr method made it possible to look behind the younger event that reset all mineral Rb-Sr or K-Ar ages. We thus found a bimodal whole-rock age pattern. In the northwest Grenville area of Ontario extensive plutonism and regional metamorphism occurred between 1500 and 1800 m.y. ago

and again between 1300 and 900 m.y. ago. Furthermore, it is probable that the Grenville Front existed as an active structural entity as early as 1700 m.y. ago, and was again the locus of movement between adjacent continental blocks about 1000 m.y. ago.

In this report the results of our current studies are combined with some of those from the past 2 years. Last year's study of a single outcrop of paragneiss demonstrated that the chemical interactions that accompanied the formation of the gneiss took place between 1500 and 1800 m.y. ago. We have verified this conclusion and extended the area to which it applies by examining paragneiss in other parts of the region. These recent studies, although less detailed, are more reliable because of the large variation in the Rb/Sr ratios discovered in adjacent paragneiss layers.

Specific times of emplacement of granite at 1500 and 1725 m.y. were established by detailed whole-rock isochron studies presented last year. Other granites in the region are now known to have been formed at these same times.

GEOCHRONOLOGY OF THE GRENVILLE PROVINCE

T. E. Krogh and G. L. Davis

Paragneiss in the Northwest Grenville Area

The geochronology report in *Year Book 66* included a detailed discussion of Rb-Sr isotopic studies of a single block from a paragneiss outcrop in the French River area, location 10. Closely spaced

* Department of Terrestrial Magnetism.

samples of this compositionally layered rock were not isotopically similar during the 1000-m.y. event that caused isotopic mixing among certain coexisting minerals analyzed. Considering the large amount of metamorphic chemical interaction between certain layers, it seemed likely that the paragneiss formed during an earlier metamorphic event, a conclusion supported by the fact that an apparently syntectonic and synmetamorphic granite sill nearby yielded an isochron age of 1730 m.y.

To determine the regional extent of the metamorphism of paragneisses, we collected samples at locations 11, 12, 13, and 14 on Fig. 84. The diagrams on Figs. 85 and 86 show the variation in the concentrations of rubidium and strontium in sections normal to the layering. The dashed and crosshatched portions repre-

sent felsic gneiss and biotite amphibolite, respectively. Concentrations estimated by X-ray fluorescence differ from isotope dilution values by less than 5%. As noted previously in *Year Book 66* (p. 531), plagioclase-quartz layers commonly occur between quartz-microcline-plagioclase gneiss and plagioclase-hornblende-biotite amphibolite. The variations in plagioclase and microcline content, and concomitant Sr and Rb concentration, cause large variations in the Rb/Sr ratio.

Limited isotopic data for small, single whole-rock slices taken near steep gradients in the Rb/Sr ratio generally cannot give precise ages. They are, however, sensitive indicators of isotopic mixing. For example, the two samples from section 12 subjected to isotope analyses were separated by 3 cm of rock. If the isotopic composition became similar over

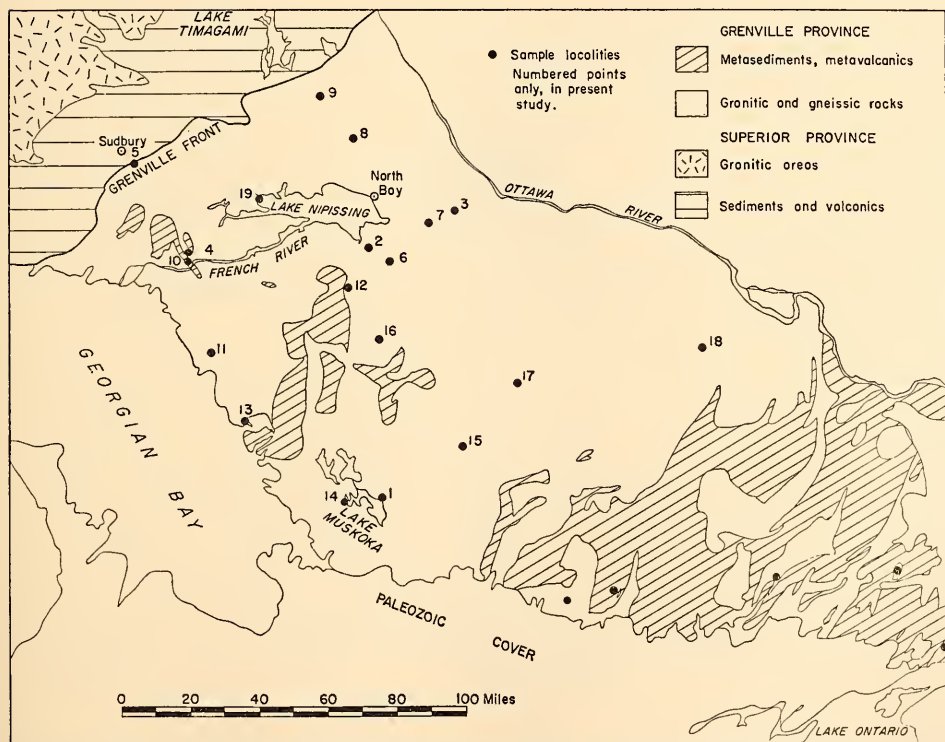


Fig. 84. Map of northwest Grenville area in Ontario, showing sample locations. Sample location numbers are used to identify analyzed specimens on the isochron diagrams.

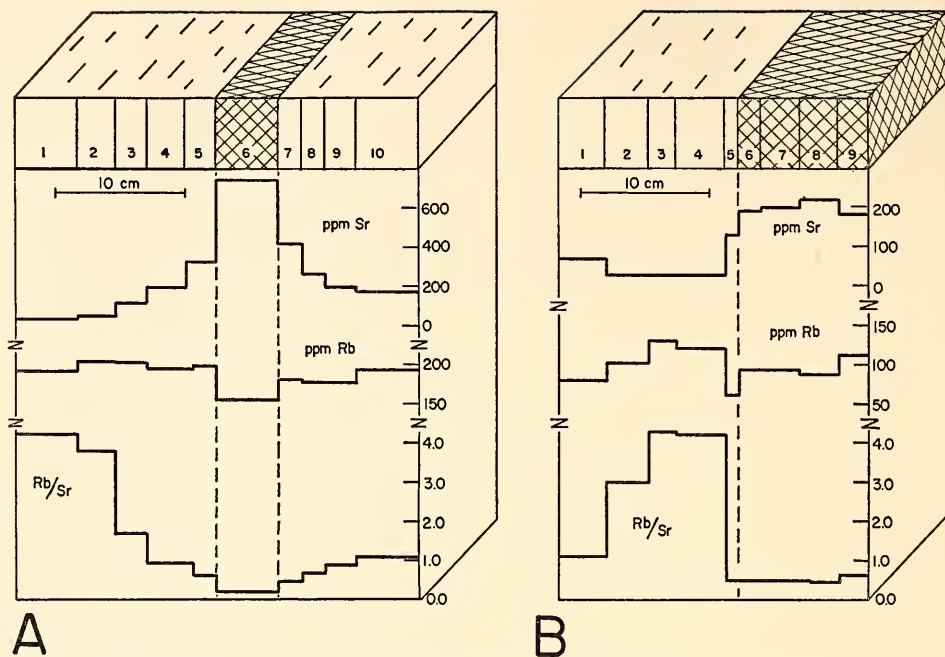


Fig. 85. (A) Paragneiss, location 14; analyzed samples 14-7 and 14-10. (B) Paragneiss section, location 12; analyzed samples 12-1 and 12-3.

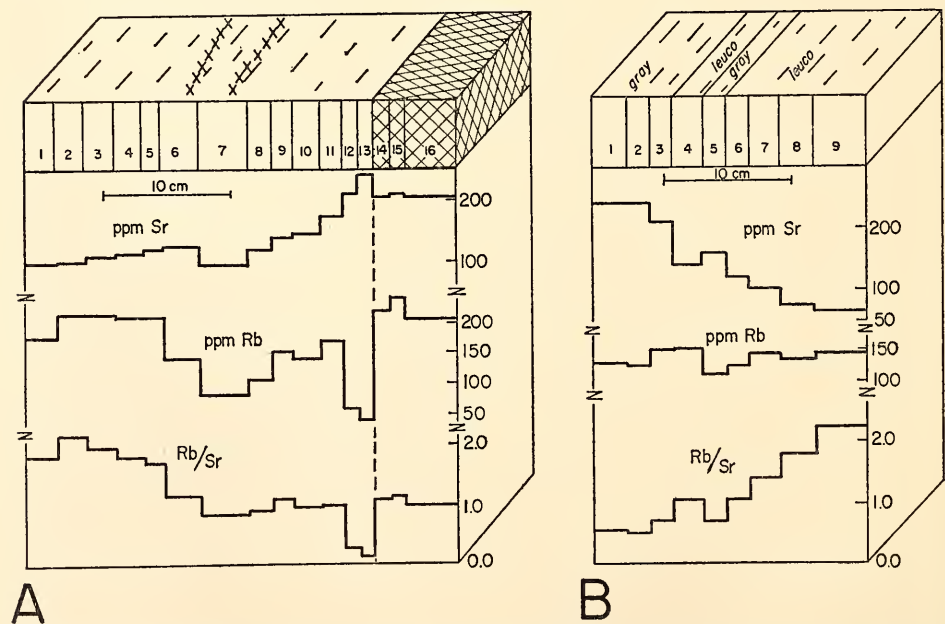


Fig. 86. (A) Paragneiss, location 13; analyzed samples 13-3 and 13-10. (B) Paragneiss, location 11; analyzed samples 11-2, 11-9, and 11-10, the latter collected 2 meters to the right of the section.

these limited distances during the 1000-m.y. thermal event, a 1000-m.y. isochron slope would have resulted. Data for section 12 on Fig. 87 indicate an apparent age of 1560 m.y., demonstrating that iso-

topic equilibration did not take place at 1000 m.y.

Data for three samples from section 11 are colinear on the isochron diagram (Fig. 87) and probably specify a time

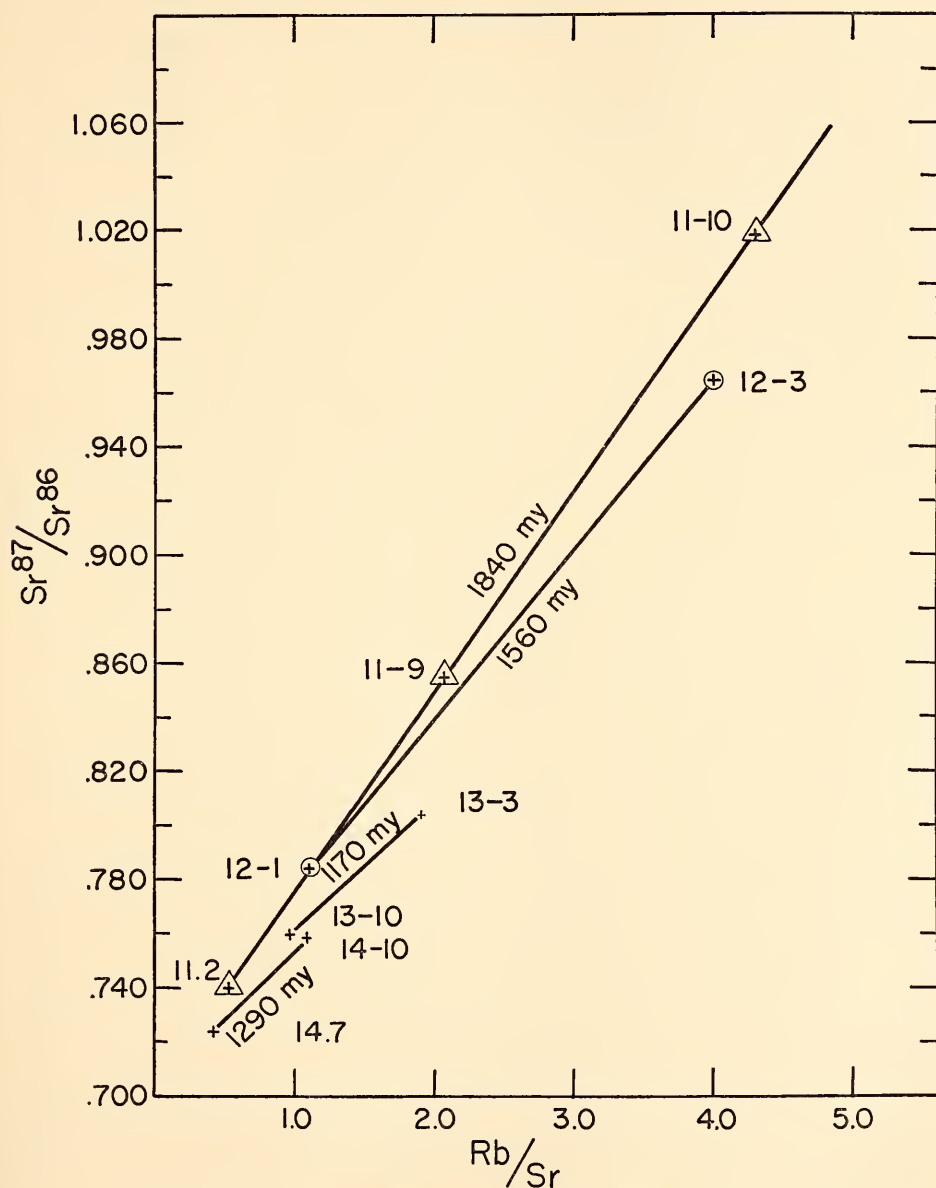


Fig. 87. Isochron plot for paragneiss samples. Sample numbers specify locations on Fig. 84. Projected initial strontium ratios for related samples are 0.704 for location 11, 0.715 for location 12, 0.716 for location 13, and 0.703 for location 14.

1840 m.y. ago when the isotopic composition of strontium was identical in all parts of the section. These samples and those in section 12 are especially significant because their unusually high Rb/Sr ratios allow a more accurate determination of the slope of the isochron. The paragneisses in sections 13 and 14 yield apparent isochrons for 1170 and 1290 m.y., respectively, suggesting that these gneisses either formed or underwent isotopic mixing at these times.

These studies confirm and extend the earlier conclusions, based on the French River paragneiss, that much of the paragneiss in the northwest Grenville area formed from its sedimentary parent between 1500 and 1900 m.y. ago. A regional metamorphism in this time interval is indicated. Other paragneisses in this region either formed or were isotopically equilibrated about 1300 and 1100 m.y. ago.

Granitic Rocks in the Northwest Grenville Area

French River granite and coeval granitic rocks. An isochron obtained for a granitic layer in a major northwest-trending syncline in the French River area (location 4, Fig. 84) was presented last year (*Year Book 66*). This isochron, with a slope of 1725 m.y., is shown without the data points on Fig. 88. Isotopic data for biotite and apatite in one sample of granite indicated isotopic mixing among minerals in the rock about 1000 m.y. ago. Two sphene samples from this granite, analyzed by Tilton and Grönerfelder (1968), gave concordant U-Pb ages very close to 1100 m.y., indicating a younger thermal event.

Data for whole-rock samples of other foliated leucogranites at locations 2 and 3 (Fig. 84) are shown on Fig. 88. Incomplete isochrons for 1730 and 1820 m.y. are apparent. The country rocks in these widely spaced localities must be at least as old as these intrusives.

Lake Muskoka granite and similar

granitic rocks. In *Year Book 66* we presented a Rb-Sr isochron study of an intensely metamorphosed and deformed granitic body situated approximately 150 km southeast of the Grenville Front (location 1, Fig. 84). The isochron obtained from ten analyzed samples is shown as a reference isochron without data points on Fig. 88. Isotopic mixing about 800 m.y. ago is indicated by mineral analyses. Our previous study also included the analysis of small, intensely recrystallized whole-rock volumes situated 10 cm apart on the outcrop, with very different Rb/Sr ratios. These samples showed no evidence of gain or loss of the dating elements during the past 1500 m.y.; accordingly, the metamorphism recorded in the rocks very likely occurred at about this time.

Data for two samples from a similarly deformed granitic body at location 18 (Fig. 84) lie on the reference 1500-m.y. isochron. In the same way, single whole-rock samples from locations 15, 16, 17, and 19 lie on or above this isochron, inferring that they too are at least 1500 m.y. old. Certainly country rocks older than about 1500 m.y. must occur over a very large portion of the northwest Grenville area (Fig. 84).

Because the Muskoka granite is intensely recrystallized and deformed, the possibility exists that the isochron age indicates only the time since the rock underwent extensive metamorphism. A short pre-1500-m.y. history is implied, however, by the low initial $\text{Sr}^{87}/\text{Sr}^{86}$ ratio and the high degree of fit of the isotopic data to a single isochron. We hope to elucidate this problem by a zircon study now in progress. To date analyses of zircons from three whole-rock strontium samples have been completed. These define a chord on the concordia diagram with intercepts at 1440 and 260 m.y. Significantly, the chord does not yield an intercept at the 800–1000 m.y. thermal event that produced isotopic mixing of strontium between coexisting mineral phases. Indeed, the three zircon points

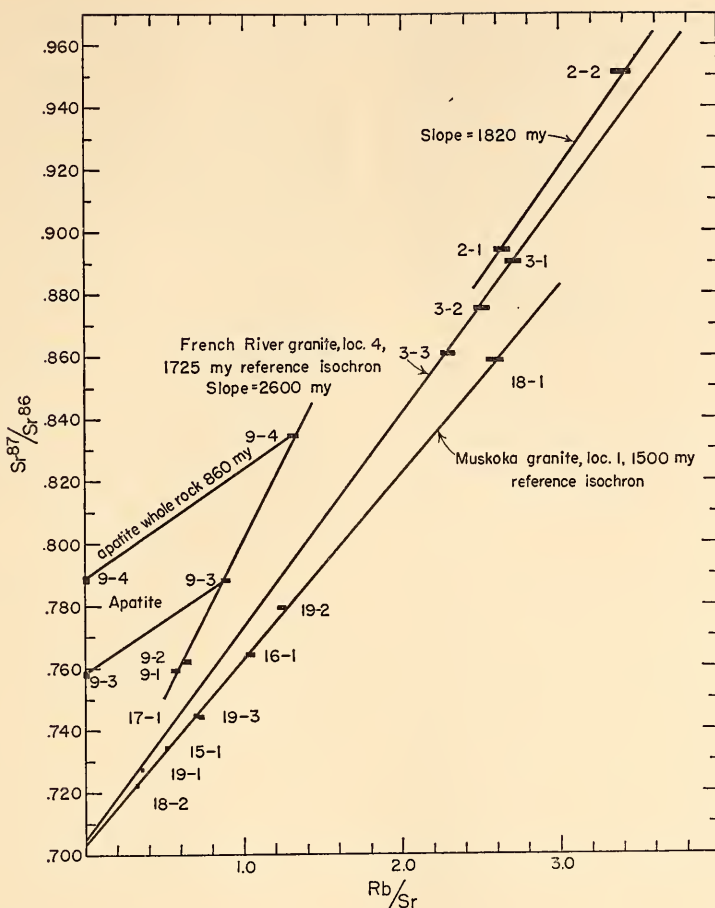


Fig. 88. Isochron plot for granitic rocks. Reference isochrons shown here without data points are from previous report. French River granite occurs at location 4; Muskoka granite, at location 1. Sample numbers specify locations on Fig. 84.

lie on a continuous diffusion curve drawn from 1440 m.y.

North Bay trondhjemite and younger granites. As examples of the younger intrusives we have studied garnetiferous trondhjemites in the North Bay area. Several samples collected at locations 6 and 7 (Fig. 84) yield an isochron for 1330 m.y. (see *Year Book 65*). Field work by S. B. Lumbers, of the Ontario Department of Mines, indicates that these bodies are generally large, 15 to 30 km across, intensely deformed on their margins, and recrystallized but not strongly lineated or foliated in their

cores. These bodies of metamorphosed igneous rocks may be useful in determining the post-1300-m.y. metamorphism and deformation in the region. Two samples from a foliated granite body at location 8 (Fig. 84) yielded an approximate maximum whole-rock age of 1200 m.y.

Age Relationships along the Grenville Front

Sudbury area, Grenville Front granite. A previous report (*Year Book 65*) contained data for analyzed whole-rock

samples from a granite situated along the Grenville Front south and west of Sudbury, Ontario. A tentative isochron for 1750 m.y. was shown, but several of the analysed samples plotted below the isochron. Since that time, further samples and encouragement to renew our investigation were provided by Jack Henderson, of McMaster University, who recently completed a Ph.D. study on the structure and petrology of this portion of the Grenville Front.

Data for four of the five whole-rock samples provided by Henderson lie on our previous 1750-m.y. isochron. The pre-Grenville age of this granite was confirmed by a muscovite Rb-Sr age of about 1600 m.y. and a zircon Pb-Pb age of 1655 m.y. These minerals are from a small northeast-trending granite dike that intrudes the Huronian section along the northwest margin of the granite.

A dominant characteristic of this granite is the pervasive evidence of both plastic and brittle deformation. Henderson has shown that the structural elements in the granite, in the plastically deformed migmatites on the southeast margin, and in the brittlely deformed Huronian rocks to the northwest, formed in response to a single stress pattern. A single Rb-Sr age of 1450 m.y. on muscovite from a strongly foliated granite sample indicates that some of the foliation developed prior to the 1000-m.y. event.

This granite was formerly considered to be a part of the Grenville structural province and to have been emplaced and deformed during the formation of the Grenville Front, 1000 m.y. ago. Later, after we discovered evidence for a 1750-m.y. age, all the deformation features were believed to have formed 1000 m.y. ago. Considering our isotopic data, it is probable that the northeast-trending granite mass with its parallel satellite dikes was intruded into the "Grenville Front" 1700 m.y. ago and that it underwent plastic and brittle deformation then

or at some time earlier than 1450 m.y. ago.

North Bay area, Grenville Front granite. Data for several samples from a granitic body situated 14 km south of the biotite isograd along the Grenville Front, north of North Bay, Ontario, yield an apparent isochron age of 2600 m.y. (Fig. 88). The isotopic composition of apatite from two of the analyzed samples is identical with that present in each host rock 860 m.y. ago (Fig. 88). A single biotite sample from this granite has a Rb-Sr isotopic age of 960 m.y.

To date, this granite comprises the maximum southward extension of the Superior Province into the region affected by the so-called Grenville orogeny about 1000 m.y. ago.

Chibougamou area, Grenville Front at Surprise Lake, Quebec. A metamorphic transition situated along the boundary between the Superior and Grenville provinces has been mapped and studied in detail by Deland (1956). In this area fine-grained metasediments and basic volcanics can be observed in various stages of recrystallization at progressively higher temperatures as one proceeds along the regional strike from west to east. Migmatites and gneisses typical of the Grenville province occur beyond this transition to the south and east.

In our investigation of age relationships along the Grenville Front, we selected muscovite samples from the edge of the transition zone, as well as 6 and 12 km to the southeast. A Rb-Sr isotopic age between 2600 and 2700 m.y. at each location demonstrates that this metamorphic transition developed about 2700 m.y. ago. A coexisting biotite from the sample at the edge of the transition has a Rb-Sr age of 2100 m.y., and another biotite collected 15 km to the southwest has an age of 880 m.y. These ages on biotites, which are more responsive to thermal events than muscovite, demonstrate the existence of the younger metamorphism in part of this area.

FRACTIONATION OF POTASSIUM AND RUBIDIUM IN A LAYERED INTRUSION

S. A. Morse and G. L. Davis

The ratio of potassium to rubidium in igneous rocks is known to vary through approximately two orders of magnitude, i.e., from ~ 30 to ~ 3000 . It may be inferred from this that the K/Rb ratio is potentially an indicator of igneous fractionation or of the source regions of magmas. Such an inference has underlain main interpretations of K/Rb variation, although detailed examination of the partitioning of these two alkali elements between crystals and liquids is lacking. The evidence, largely from volcanic rocks, points to decrease of K/Rb with increased fractionation, particularly in late stages (e.g., Lessing, Decker, and Reynolds, 1963; Gast, 1965).

We have found in the Kiglapait layered intrusion, Labrador, an exception to the supposed normal trend (Morse and Davis, 1968). According to Morse (1968), the intrusion provides an excellent natural example of *in situ* fractionation of basaltic magma under plutonic conditions, several lines of evidence indicating that the magma was virtually a closed system throughout its fractionation history. We have analyzed K and Rb by stable-isotope dilution techniques for 19 whole rocks and for several separated feldspars and mafic minerals. Figure 89 shows a K/Rb versus K plot for the whole-rock data, along with the approximate fields of abyssal tholeiites, some meteorites, and ultramafics. Many of the Kiglapait whole-rock ratios in Fig. 89 fall far from the previously determined fields, and although a valid trend cannot be established from this figure, a gentle increase in K/Rb with fractionation is suggested by study of a K versus Rb plot and by Fig. 90.

In Fig. 90 the whole-rock values of K and Rb are plotted against the fraction of liquid remaining, which is computed on a geometrical basis from the form and internal structure of the intrusion

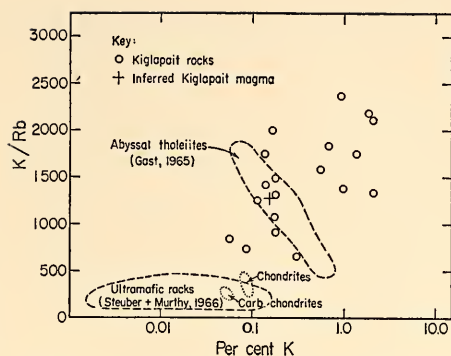


Fig. 89. K/Rb versus K plot for Kiglapait intrusion whole rocks and the inferred initial magma compared with ultramafic rocks, abyssal tholeiites, and chondritic meteorites. The Kiglapait magma is derived by a numerical summation of K and Rb over the volume of the intrusion.

(Morse, 1968). The scatter of these points is due largely to variation in the modal amount of mafics in the rocks. Data for separated feldspars probably define a smoother trend and are indicated by special symbols. The central portion of Fig. 90 shows that K/Rb surely does not decrease with fractionation and probably increases slightly.

Both K and Rb increase with fractionation. Both are concentrated in feldspar relative to the whole rock, but the early plagioclases have consistently higher K/Rb ratios than their host rocks and their calculated parent liquids. There is little doubt that plagioclase discriminates against Rb relative to K in slow magmatic processes. It would be expected, therefore, that Rb would be concentrated in the liquid and that the K/Rb ratio of the liquid and later crystals would tend to fall. The role of the mafics may be to suppress this tendency. Olivine and augite in the Kiglapait clearly have low K/Rb ratios as well as low alkali contents, if not for crystal-chemical reasons, then simply because they reflect the ratio of the nearby liquid. It is possible to generate numerical closed-system models of Kiglapait frac-

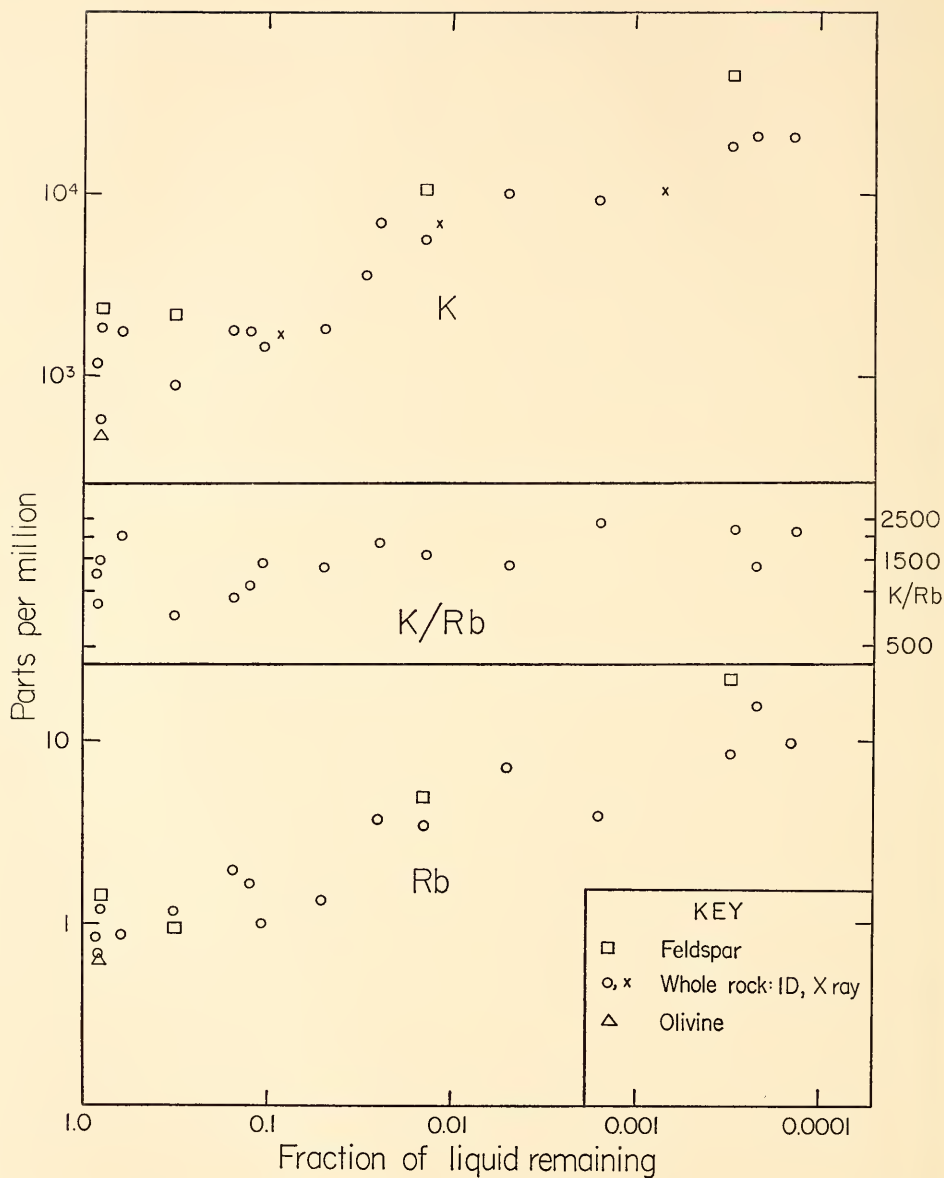


Fig. 90. Values of K and Rb for whole rocks and separated minerals as well as K/Rb for whole rocks of the Kiglapait layered intrusion, plotted against the fraction of liquid remaining, derived from geometrical analysis of the intrusion structure.

tionation that mimic the observed effects and culminate in high K/Rb ratios.

Assuming a closed system, a numerical summation of K and Rb for the Kiglapait yields $K=1530$, $Rb=1.2$ ppm,

$K/Rb=1270$ for the whole intrusion and thus the initial magma. In this respect, the Kiglapait belongs to a group of high K/Rb rocks, typified by the abyssal tholeiites and including anorthosite

(Reynolds, Whitney, and Isachsen, 1968; Gill, 1968), amphibolite (Hart and Aldrich, 1967), and parts of the Bushveld complex (Erlank, Danchin, and Fullard, 1968).

It is difficult to ascribe such high K/Rb ratios to mineralogical control in the source regions of basalt, since the only two major rock-forming minerals known to have high ratios are plagioclase and amphibole, and they probably have limited stability in the upper mantle. It may be profitable to consider prior stripping of alkalis, especially Rb, by limited partial fusion in the upper mantle. A more extensive later fusion might then produce basic magmas showing high K/Rb, provided some mineral with high K/Rb remained from the first event. Such stripping processes, if they did occur, would have important implications for models of heat flow, crustal

evolution, and the geochemistry of K and Rb and their radiogenic daughters.

The evidence from the Kiglapait intrusion emphasizes our need to understand the fundamental controls on element partitioning between crystals and liquid in magmatic processes. It is clear that we could have neither predicted the Kiglapait trend nor made intelligent geochemical guesses about the source of the Kiglapait magma from a knowledge of the initial K and Rb values alone, using volcanic rocks as a model. Yet many volcanic rocks presumably owe some portion of their evolution to fractionation in subjacent chambers that resemble layered intrusions in principle, and an understanding of plutonic-element partitioning is therefore essential to correct geochemical interpretation of many volcanic suites.

PETROLOGY

STATISTICAL PETROGRAPHY

The work in statistical petrography has ranged over such a broad subject-matter spectrum that it is difficult to present a coherent résumé or single out particular projects for detailed review. A long manuscript on petrographic ratio correlation, integrating results obtained over nearly 20 years of intermittent study of the percentage data that form the core of chemical petrography, has been completed. As might almost have been guessed, the attempt to present a unified, consistent development of old material has led to discoveries of previously unsuspected relationships; two of these are described below. In the first it is shown that, for the particular null model in question, the correlations expected between the variables of the recently proposed and so far unused "remaining-space" transformation are identical, to the limits of approximation, with those between the "Niggli numbers" so well known and widely used in petro-

graphy. As shown in last year's report, however, it will usually be impossible to calculate either set of expectations, for the reason that the hypothesized "open" parent is numerically impossible, the sample estimates of certain parent variances proving consistently negative. *Year Book 66* reported preliminary work on transformations aimed at eliminating the negative elements of the open variance vector. The transformations described there performed rather unevenly, however, often either introducing new negative elements in the course of eliminating the original ones or failing to eliminate the latter. The transformation described below operates satisfactorily on all data so far tested.

As an outgrowth of work on the "remaining-space" transformation (see *Year Book 65*, p. 376) attention was directed to a transformation that may often linearize ternary closed data that appear to follow some gently nonlinear trend. The potential importance of this and

similar transformations arises from the fact that the variables of a closed array are interdependent, so that conventional regression analysis, which requires identification of one of the variables as independent and the other as dependent, is inapplicable. Where linear fitting is sufficient, the "reduced major axis" or "line of organic correlation" may be used, but this is not defined for nonlinear interdependence. Accordingly, a transformation eliminating systematic departure from linearity in ternary data might prove very useful. The "binary ratio" transformation described below appears to have this effect on the data for the calciferous pyroxenes of the layered series of Skaergaard.

A much simpler and more conventional examination of interdependence seems to establish beyond any reasonable doubt the existence of marked interlaboratory bias in the analysis of silicates. Paired analyses of the well-known granite (G1) and basalt (W1) reference materials distributed by the U. S. Geological Survey are the subject of this study. If there were no systematic differences between laboratories one would expect no correlation between results obtained by an individual analyst for the same oxide(s) in the two rocks. In fact, there is very strong positive correlation between paired values of SiO_2 , MgO , Na_2O , K_2O , Al_2O_3 , and FeO , the observed values of four of these correlations being significant at the 1%-level and the other two at the 5%-level.

A carefully designed test (Flanagan, in Stevens *et al.*, 1960) has failed to detect inhomogeneity with regard to Pb content. Despite this evidence, complaints about the alleged heterogeneity of the two (powdered) materials are not infrequent. The present examination of already published data strongly supports Flanagan's position, in the sense that the combined effect of random analytical error with whatever sample inhomogeneity exists is obviously insufficient to obscure interlaboratory bias. The popu-

larity of powdered reference materials among geochemists is now such that allegations of sample inhomogeneity should be neither casually brought nor casually dismissed. But the burden of proof is surely on the plaintiffs in the present instance. With regard to major constituents, what evidence there is strongly suggests a considerable interlaboratory bias. Unless this bias is eliminated, or data are obtained in a pattern that permits its isolation and estimation, no collection of analyses will throw much light on the vexed and vexing question of sample inhomogeneity.

Turning now from the criticism of chemical analyses to their use and appreciation, speculation on the petrological significance of crystal-melt fractionation often relies heavily on demonstrations of "gradual transitions" as illustrated by "trend lines" in variation diagrams. Studies of this kind are all too rarely accompanied by demonstration that a proposed fractionation scheme could in fact produce the observed or inferred variation trends. Graphical methods have been employed to test the effects of adding or subtracting various combinations of mineral phases or xenoliths, an excellent example being the study by Wilcox (1954) of the variation in the lavas of Parícutin volcano. Although feasible where the number of variables is small, the graphical method is slow, cumbersome, and subject to plotting and reading errors; with more than three variables it usually requires a series of trial and error approximations and often yields no useful result at all. In an effort to improve on the present state of the art, part of the work during the report year was devoted to the development of a computational procedure that requires no intermediate approximations and processes up to ten variables simultaneously. In principle, any petrological problem that can be restated as a problem in linear combination can be formulated for this type of calculation. The method is illustrated here in three

calculations based on the Parícutin data of Wilcox.

During the last part of the report year the Laboratory took delivery on a medium-speed data terminal which, when it is operating routinely, will transmit information at a rate making it practical to resume pilot operations on storage and retrieval of rock analyses. This extremely productive work, results of which have been presented in numerous journal articles and summarized in *Year Books 61-64*, was brought to a tempo-

the remaining space occupied by some one of the others. The null value against which the observed correlation is to be tested, following the general approach outlined in *Year Book 65*, is the correlation expected between $V_1=Y_1$ and $V_j=Y_j/(1-Y_1)$ on the assumption that each \mathbf{Y} has been formed by closure of a randomly drawn sample of \mathbf{X} , whose elements are by definition open and uncorrelated. The required approximate expectation, not available at the time of the earlier writing, is

$$\rho_{V_1 V_j} = \frac{\text{cov}(V_1, V_j)}{\sqrt{\text{var}(V_1) \cdot \text{var}(V_j)}} \cong \frac{p_1 q_j \sigma_\omega^2 - p_1 \sigma_j^2}{\sqrt{[p_1^2 \sigma_t^2 + (1-2p_1) \sigma_1^2] [q_j^2 \sigma_\omega^2 + (1-2q_j) \sigma_j^2]}}, \quad (1)$$

any halt when we lost ready access to a high-speed computation facility. The limited capacity of the new terminal forces us to a difficult decision that should have been made long ago. The entire library of analyses and all the longer programs must be held on tape at the central processor, reserving the terminal, as far as possible, for the transmission of commands and the printing of output. Our first major task will be preparation of programs for the generation and maintenance of the tape containing the library of rock analyses. A preliminary tape generator is already operating, but at the present writing the circuits that permit modification of an existing tape—i.e., the editing and updating functions that will be in frequent demand during reorganization and expansion of the punch-card library—have not been fully tested.

IDENTITY OF EXPECTED INTERDEPENDENCE BETWEEN PAIRS OF NIGGLI NUMBERS AND PAIRS OF ANALOGOUS REMAINING-SPACE VARIABLES

F. Chayes

In the remaining-space transformation (see *Year Book 65*, p. 376) attention is directed to detecting nonrandom association of some one of a set of proportions, say Y_1 , with the proportion of

where σ_k^2 is the variance of the k th element of \mathbf{X} , $\sigma_t^2 = \Sigma(\sigma_k^2)$, $\sigma_\omega^2 = \sigma_t^2 - \sigma_1^2$, $p_k = X_k/\Sigma(X)$, $q_k = p_k/(1-p_1)$, and $j > 1$.

If the elements of \mathbf{Y} are molar proportions and we denote SiO_2 by subscript 1, the well-known Niggli numbers are sums of quantities of the form $N_j = Y_j/\Sigma(Y_k)$, $k > 1$. For $j > 1$ any N_j is thus a remaining-space variable, so that $\text{var}(N_j) = \text{var}(V_j)$. N_1 , however, is not simply Y_1 under a new name, as was the case with V_1 , for in the Niggli transformation the molar proportion of SiO_2 is also divided by the sum of the other molar proportions. Under this condition, and after considerable algebraic manipulation, the approximation procedure reviewed in *Year Book 65* leads to

$$\text{var}(N_1) \cong (1-p_1)^{-4} \text{var}(V_1), \quad (2)$$

and

$$\text{cov}(N_1, N_j) \cong (1-p_1)^{-2} \text{cov}(V_1, V_j). \quad (3)$$

Since (3) appears in the numerator and the square root of (2) in the denominator of $\rho_{N_1 N_j}$, it follows at once that $\rho_{N_1 N_j} = \rho_{V_1 V_j}$ for $j > 1$, and thus that $\rho_{N_j N_k} = \rho_{V_j V_k}$ for all $j \neq k$.

Given the null model basic to this discussion, the effects of the remaining-space and Niggli-number transformations on interdependence generated by closure are identical, to the limits of approximation.

TRANSFORMATIONS DESIGNED TO ELIMINATE
NEGATIVE ELEMENTS FROM SAMPLE
ESTIMATES OF THE VECTOR OF
OPEN VARIANCES

F. Chayes

The results of the preceding section would find wide application if, in situations of practical petrographic interest, realistic estimates of the parameters of the hypothetical open parent could be obtained from the data. For one very common type of data this will nearly always be impossible. In every Harker array so far examined, one or two of the calculated variances of the open variables prove to be negative; the variance of the open equivalent of Al_2O_3 is always one of these, and where there are two the second is that for the open equivalent of Na_2O . As suggested earlier, this may reflect unsatisfactory or inadequate sampling, may indicate that the underlying statistical model is unrealistic, or may be the consequence of an unwise choice of variables. In *Year Book 66* the latter possibility was discussed at considerable length. It was argued that the oxides as reported by the analyst may indeed be an unwise "choice" of variables, and reasons were given for preferring a number of sets of synthetic variables obtained as linear combinations of the original oxides. Seven such combinations were proposed, of which none completely eliminated negative elements from the open variance vectors of the trial arrays. The transformation of Na_2O to *ab* was the most nearly successful, eliminating both negative elements in the open variance vectors of five of the six test arrays, but failing to eliminate a negative variance for the open equivalent of Na_2O in the sixth. Transformations of K_2O to *or* or of Na_2O and K_2O to *ab* and *or* were ineffective. It has since been found that the combined transformation of Na_2O to *ab* and K_2O to KAlO_2 is completely successful in the original test data (for identification of which see *Year Book 66*), as

well as in a large number of other suites of analyses to which it has been applied.

At the present writing the bearing of this finding on the work of the preceding section is not clear. At first glance, no further manipulation of the data would appear to be either necessary or desirable if, as appears to be the case, a reasonable choice of variables makes possible a direct test of the announced null hypothesis.

CURVE-FITTING IN THE TERNARY
DIAGRAM

F. Chayes

The relation between the variables in a ternary diagram is necessarily one of mutual interdependence rather than the dependence-independence essential to a conceptually sound regression analysis. It is always possible to compute two (linear) regression lines from the data of a ternary array, but since no variable is independent there is no objective reason for preferring one of these lines to the other. This is not likely to be a serious handicap if the correlation is very strong. If the residual dispersion is more than trifling, however, the regression lines will be separated by a considerable angle, and even as a sample description the conventional regression calculation will be of little use.

When the relation between two variables is one of interdependence the "reduced major axis" (Kermack and Haldane, 1950)—also called the "diagonal line of organic correlation" (Kruskal, 1953)—should be fitted in preference to the conventional regression line(s). This is a line passing through the mean of the distribution with a slope whose absolute value is the ratio of the standard deviations and whose sign is that of the covariance. For any set of data there is only one line of organic correlation; it can be shown that it always lies in the acute angle between the regression lines, that it bisects this angle when the variances are equal, and that it is the line

toward which the regression lines rotate with increase in correlation, means and variances remaining unchanged. (From these properties it is clear that when $\rho^2=1$ the line of organic correlation coincides with the regression lines.)

The probability of correctly predicting the value of either of two normally distributed interdependent variables from a given value of the other is maximized if the predicting line is the diagonal line of organic correlation (Kruskal, 1953, p. 55). As a descriptor, this line has the intuitively appealing property of minimizing the sum of squares of deviations taken normal to it, a characteristic which, like the analogous minimizing property of the conventional regression line, is distribution free.

In the absence of a tendency toward systematic departure from linearity in the data, the diagonal line of organic correlation would seem to be admirably suited for use in the ternary diagram. When there is a strong tendency toward curvilinear variation, however, the lack of an independent variable again makes trouble, for the only additional variables available are logs, roots, powers, products or other transformations of those already given. There is no systematic way in which to decide which variable in a ternary array is to be chosen for this special treatment.

A linearizing transformation might sometimes provide an escape from the dilemma; if desired, the line of organic correlation computed from the transformed data could be drawn in the original ternary. The rather gentle curvature characteristic of the lines in many published ternary diagrams may sometimes be materially reduced by transformation from the original ternary coordinates, X_1 , X_2 , and $X_3=1-X_1-X_2$, to $Y_i=X_1/(X_1+X_2)$ and $Y_j=X_1/(X_1+X_3)$, referred to below as the "binary ratios." The diagonal line of organic correlation is then

$$Y_j - \bar{y}_j = \text{sgn}(\sigma_{ij}) \frac{\sigma_j}{\sigma_i} (Y_i - \bar{y}_i), \quad (1)$$

where $\text{sgn}(\sigma_{ij})$ is the sign of the covariance, \bar{y} denotes a mean, and σ a standard deviation. A straight line in rectangular coordinates, equation 1 is in general nonlinear in the trilinear coordinate system.* Depending on the values of σ_i , σ_j , \bar{y}_i and \bar{y}_j , in fact, its curvature in trilinear coordinates may be quite pronounced.

The transformation to binary ratios is not to be regarded as a panacea which will automatically eliminate systematic departure from linearity in ternary closed data. Indeed, if the relation between any two ternary variables is already linear, then in general its transformation to binary ratios will *not* be linear in rectangular coordinates. The only exceptions to this rule are equations that plot as straight lines either parallel to an edge or terminating in an apex of the triangle, i.e., relations in which some one of the ternary variables or the ratio of some pair of them is constant. The need for a transformation only arises, however, when there seems to be a systematic *departure* from linearity in the ternary diagram. When nonlinearity is apparent in the ternary diagram it is worth inquiring whether it can be reduced by transformation to binary ratios, for, in general, linear relations between binary ratios will plot as curves in trilinear coordinates.

In principle, a point may be located as readily in the ternary diagram by its binary ratios as by its trilinear coordinates. For any pair of values (Y_i, Y_j) the desired point is the intersection of the lines drawn from each marginal Y to the opposite apex of the triangle. If a desk calculator is available, however, it may be more convenient, and will usually be more accurate, to revert to the original coordinate system before plotting.

* This is readily shown by substituting the trilinear definitions of Y_i, Y_j into (1), solving explicitly for X_1 , and then differentiating; in general the derivatives of X_1 with regard to X_2 and X_3 are not constants.

From the definitions of (Y_i, Y_j) it is evident that

$$X_2 = \left(\frac{1 - Y_i}{Y_i} \right) X_1, \text{ and } X_3 = \left(\frac{1 - Y_j}{Y_j} \right) X_1. \quad (2)$$

Recalling that $X_1 + X_2 + X_3 = 1$, we have at once that

$$\left(1 + \frac{1 - Y_i}{Y_i} + \frac{1 - Y_j}{Y_j} \right) X_1 = 1,$$

or

$$X_1 = Y_i Y_j / (Y_i + Y_j - Y_i Y_j). \quad (3)$$

Any X_1 found from Y_i and Y_j satisfying (1) is one of the trilinear coordinates of a point on the desired curve. For any

such point a second coordinate may then be found by substitution in either of the definitions given in (2).

Figure 91(A) is a plot of $Y_i = \text{Ca}/(\text{Ca} + \text{Fe})$ against $Y_j = \text{Ca}/(\text{Ca} + \text{Mg})$ for the CaO-rich pyroxenes of the layered series of Skaergaard (data from Brown, 1957, and Brown and Vincent, 1963). There is little doubt of the basically linear character of the variation; r_{ij} is -0.94 for the diopside "trend" and -0.99 for the hedenbergite "trend." The equations of the "diagonal lines of organic correlation" are:

$$di; Y_j = 51.88 - 0.061 Y_i \quad (4)$$

$$hd; Y_i = 64.21 - 0.022 Y_j \quad (5)$$

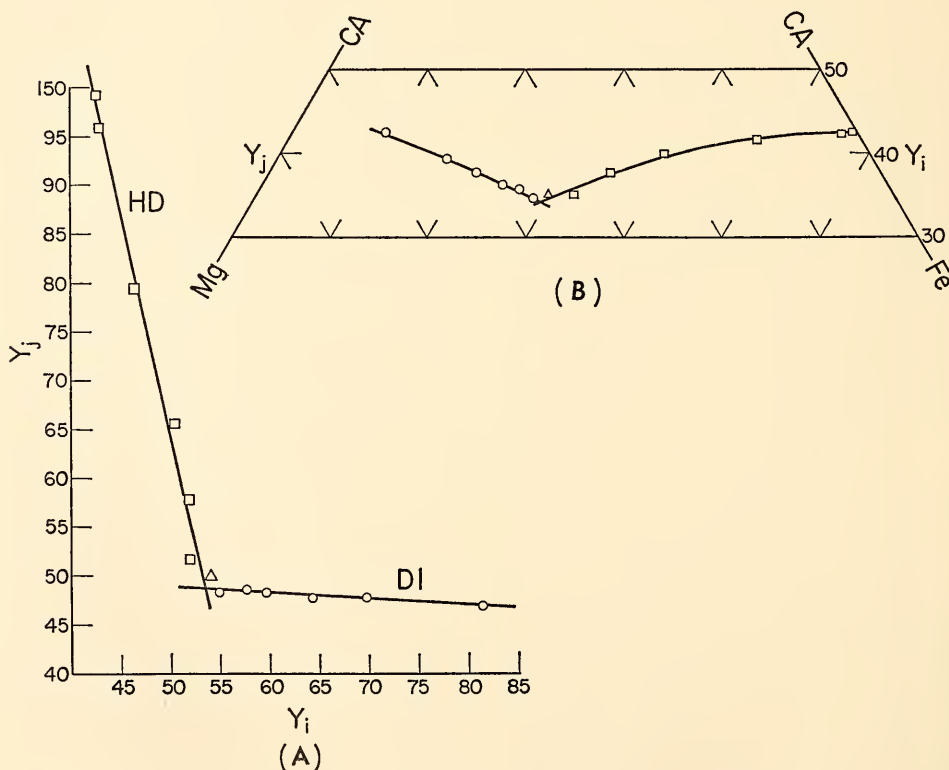


Fig. 91. Calciferous pyroxenes of the layered series of Skaergaard. Circles, data points used in computing equation (4); squares, data points used in computing equation (5); triangle, datum point not used in either set of calculations. The coordinates are the binary ratios $Y_i = (\text{Ca} + \text{Fe})$, $Y_j = \text{Ca}/(\text{Ca} + \text{Mg})$ in (A), and the ternary ratios $\text{Ca}/(\text{Ca} + \text{Mg} + \text{Fe})$, $\text{Fe}/(\text{Ca} + \text{Mg} + \text{Fe})$ in (B). The lines are traces of equations (4) and (5) in the two reference systems.

In Fig. 91(B) the data and these equations are plotted in the original ternary coordinates (Ca,Mg,Fe). In this reference system equations (4) and (5) are *not* straight lines; the curvature of (4) is trifling, but (5) closely follows the rather marked departure from linearity shown by the data.

Except for the implication of a central discontinuity, the plots of equations (4) and (5) in Fig. 91(B) are virtually indistinguishable from the line shown in one of the source references (Brown and Vincent, 1963, Fig. 3), so that the effect of the calculations in this case is essentially to "numericalize" a relationship already found by other means. This is a useful but not particularly profound result and there are other, and perhaps simpler, ways in which it could have been reached. These other methods, however, are scarcely appropriate unless discrepancies from the proposed relations are trifling, for they provide no measure of the adequacy, as sample descriptions, of either the original graph or the equation derived directly from it. If the proposed (or any) transformation does indeed eliminate a tendency toward systematic departure from linearity, on the other hand, the quantity r_{ij}^2 has its usual meaning as a measure of the strength of the interdependence between the (transposed) sample statistics.

A LAST LOOK AT G1-W1

F. Chayes

After a detailed initial test whose results were summarized in *U.S. Geological Survey Bulletin 980* (Fairbairn *et al.*, 1951), the U. S. Geological Survey generously distributed, upon request, samples of two now well-known reference materials, a granite from Westerly, Rhode Island (G1), and a diabase from Centerville, Virginia (W1). *Bulletin 980* reported 30 paired analyses of these materials (i.e., analyses of both materials by the same analyst), and an additional 20 pairs were given in *Bulletin 1113*

(Stevens *et al.*, 1960). Distribution of the samples continued for some time after the appearance of *Bulletin 1113* but the supply of G1 is now exhausted; hence the title of this note.

The ready accessibility of reference materials presumed to be reasonably uniform in composition proved so useful that similar distribution schemes were established elsewhere—notably in Canada and France—and our own Survey was led to materially expand its activity in this field.* From the beginning of the program there have nevertheless been persistent suggestions that the very property which made the reference materials so useful, their alleged uniformity, was open to serious doubt. These doubts were thoroughly aired in the deliberations of the Standards Committee of the Geochemical Society, charged with obtaining a successor to G1. There is no published record of a soundly designed experiment substantiating the charge of heterogeneity in either G1 or W1, and in fact a small but well-designed experiment (*cf.* Flanagan in Stevens *et al.*, 1960) failed to establish significant heterogeneity in the distribution of Pb. But Pb is present only in trace amounts, the experiment led to a sharp revision of the previously "preferred" values, and the residual fear of heterogeneity was sufficient to persuade the committee to overrule a suggestion that the successor of G1 should be coarse enough to permit preparation of reasonably pure monomineralic separates. (No one, to my knowledge, has successfully separated pure mineral fractions from G1 in more than micro amounts.)

Now, of course, the possibility of heterogeneity in any powdered material cannot be denied, and the temptation to ascribe embarrassingly large discrepan-

*The number and variety of Survey specimens available for general distribution is continually increasing. Interested analysts should address requests to the Liaison Officer, Analytical Laboratories, U. S. Geological Survey, Washington, D. C.

cies to this source is sometimes difficult to resist. Indeed, in connection with the work on G1 and W1, the only alternative appears to be to accept what seem utterly unrealistic estimates of interlaboratory differences. The structure of the published work on G1 and W1 is such that if one considers the results for either rock separately, the decision between these alternatives must be made quite independently of the evidence. Considering the results for G1 and W1 jointly, however, it is easy to show that there is indeed a very strong interlaboratory effect, an effect so strong as to be readily perceptible despite the masking countereffects of random analytical error and the supposed sample heterogeneity.

If there were no consistent interlaboratory bias, one would expect only insignificant correlation between the result an analyst obtained for a particular oxide in G1 and the result he obtained for the same oxide in W1. The correlations computed from the paired analyses published in *Bulletins 980* and *1113* are shown in Table 25. In the data from *Bulletin 980* the correlations for SiO_2 , MgO , Na_2O , and K_2O are easily significant at the 0.01 point and those for Al_2O_3 and FeO at the 0.05 point. The correlations are by no means strong enough so that an analyst's result for a particular oxide in one rock can be precisely predicted from his result for the

same oxide in the other rock. In general, however, a man reporting appreciably high (or low) values for SiO_2 , MgO , Na_2O , K_2O , FeO , or Al_2O_3 in either rock usually reported high (or low) values for these oxides in the other rock as well; indeed, something between a quarter and a half of the total variation exhibited by these oxides may be "accounted for" in this fashion.

Even in a sample of 30 pairs, the effect of occasional extreme outliers on calculations of this sort may be considerable. It is therefore of some interest that deletion of one pair rendered suspect by an Al_2O_3 value differing from the group mean by more than 4σ materially *strengthens* the correlations for Al_2O_3 , CaO , and K_2O and does not reduce the other correlations by more than trifling amounts; the results are shown in column *B* of the table. Clearly the interdependence of the sheep is not to be attributed to the presence of an occasional goat. Example may be more persuasive than argument, but the result of this recalculation is not to be considered particularly unexpected. Bona fide incompetence should not in general lead to *systematic* differences of the kind in question; we are almost certainly concerned here with unsuspected differences between reasonably competent analysts whom the uninitiate, at least, presume to be using reasonably standardized techniques.

Does the final column of the table suggest substantial improvement in the course of the next 10 years? The shockingly large correlations are no longer in evidence; against the hypothesis that $\rho=0$, only one correlation in column *C* exceeds the 0.01 point and only three others exceed the 0.05 point. But it hardly seems legitimate to test the entries in column *C* against this hypothesis. The work summarized in column *C* was done in the shadow of that summarized in column *A*. The meaningful query is not whether an entry in column *C* differs

TABLE 25. Correlation between Results for Essential Constituents of G1 and W1 †

Oxide	<i>A</i>	<i>B</i>	<i>C</i>
SiO_2	0.724**	0.725**	0.545
Al_2O_3	0.444*	0.579**	0.304
Fe_2O_3	0.250	0.243	0.352
FeO	0.430*	0.428*	0.515
MgO	0.708**	0.720**	0.198
CaO	0.136	0.506**	0.156
Na_2O	0.685**	0.684**	0.459
K_2O	0.568**	0.706**	0.655

† *A*, for 30 pairs from *U. S. Geol. Surv. Bull. 980*; *B*, for data of *Bull. 980* less pair no. 26; *C*, for 20 pairs from *Bull. 1113*. Against the alternative that $\rho=0$, * indicates significance at the 0.05 and ** at the 0.01 level.

significantly from zero but whether it differs significantly from the analogous entry in column *A* or *B*. The only entry in column *C* that is significantly smaller than its analogue in column *A* is that for MgO. For SiO₂, Al₂O₃, FeO, Na₂O, and K₂O no significant improvement is indicated. The combination of random analytical error and sampling variation is insufficient to obscure a powerful interlaboratory bias affecting these constituents.

The bearing of this discussion on the question of sample inhomogeneity is evident. The 50 paired analyses so far published suggest a quite different explanation for the observed dispersion and in fact contain no direct or useful information about sample inhomogeneity. If we want to know whether powdered rock samples are sufficiently uniform in composition for use in interlaboratory calibration, we shall have to conduct an experiment designed to answer this question. In such an experiment each of a group of analysts would analyze each—or a considerable number—of a series of (supposedly identical) powders. Given appropriate prior agreement about a common set of analytical procedures to be followed throughout the experiment, it would then be possible to isolate a sum of squares associated with differences between analysts and another generated by differences between powders. The mean square for discrepancy would provide a sound estimate of random analytical error—now quite unknown—against which the significance of the nonrandom effects could be tested.

Although it is too late to conduct this experiment with G1, the work on G1 and W1 makes it abundantly clear that much could be learned in this fashion. The increasing popularity of powdered reference materials makes a careful partition of analytical variance into sample, systematic, and random components virtually indispensable.

MATERIALS BALANCE IN IGNEOUS ROCK SUITES

W. B. Bryan

In order to improve upon the traditional graphical methods of testing effects of addition and subtraction of mineral phases in igneous rock suites, it is reasonable to seek a computational procedure which is a numerical equivalent of the graphical method. One thinks naturally of expressing the composition vectors as linear equations, in which the known values are the weight percentages of the individual cation oxides in each mineral or rock analysis, and the unknowns are the weight fractions of each mineral or rock to be combined in order to obtain some given composition.

An appropriate working model can be formulated from consideration of the nature of the data that usually emerge from the study of an intrusive igneous rock suite. Field and petrographic studies represent a search for all the physically independent phases that may have been added to or subtracted from the original parent magma, or that remain as liquid residua after successive modifications of the parent magma. The resulting collection of phases represents a complete system of variables that is closed with respect to composition. An igneous intrusion that has solidified without reaction with the enclosing rock is the simplest example of such a closed system, its bulk composition being identical to that of the parent magma. Individual minerals and rocks contained within this intrusion will differ appreciably in composition from the parent liquid, but the chemical components of the parent magma must be distributed in such a way that the sum of the products of the weight fraction of each phase and its composition equals the composition of the parent magma. This will seem intuitively obvious to petrographers who have calculated chemical compositions of rocks from their modes. If the magma has assimilated a portion of the enclosing coun-

try rock, it will be necessary to extend the system to include the country rock, and the weight fraction of country rock assimilated must be subtracted from the summation to arrive at the parent magma composition.

It is evident then that problems of this sort have associated with them an implicit materials balance that may be used as a check on the genetic model in-

ferred from the text discussion, it is possible to estimate the weight fractions from the compositional data.

The procedure is best summarized in matrix notation, where a_{ij} , for $i=1, k$ and $j=1, n$, is the weight percentage of oxide i in phase j , x_j is the unknown weight fraction of each phase, and p_i is the weight percentage of oxide i in the assumed parent composition. Then,

$$\begin{bmatrix} a_{11} & a_{12} & a_{13} & \dots & a_{1n} \\ a_{21} & a_{22} & a_{23} & \dots & a_{2n} \\ a_{31} & a_{32} & a_{33} & \dots & a_{3n} \\ \vdots & \vdots & \vdots & \ddots & \vdots \\ a_{k1} & a_{k2} & a_{k3} & \dots & a_{kn} \end{bmatrix} \begin{bmatrix} x_1 \\ x_2 \\ x_3 \\ \vdots \\ x_n \end{bmatrix} = \begin{bmatrix} p_1 \\ p_2 \\ p_3 \\ \vdots \\ p_k \end{bmatrix} \quad (1)$$

ferred from field and petrographic data. Thus, one might proceed by multiplying the composition of each rock or mineral phase by its measured weight fraction with appropriate regard to sign, summing the products, and comparing the result with the parent-magma composition. A close correspondence between the two would be expected if all phases have been accounted for, if their compositions are accurately determined, if the rock representing the parent magma has been correctly specified, and if the correct amount of each phase has been added into or subtracted from the system according to a properly conceived petrological hypothesis. But it may be much easier to determine the composition of a rock or mineral than to measure its absolute quantity in volume or weight percent. The exact size and shape of rock bodies are often obscured by vagaries of erosion and exposure, and modal analysis of thin sections becomes impractical for rocks that are either very coarse or very fine in grain size. The density measurements necessary to convert volume to weight fractions are also frequently subject to serious difficulties. Where the composition of the presumed parent is known or can reasonably be

Ordinarily the subscript k will be not more than 10, the usual number of essential elements reported in a standard chemical analysis, and n is much less than 10, as one would indeed expect from phase-rule considerations. Barring singularity, which should be very uncommon, any n equations selected from (1) will yield a solution for the x 's. The final step in the calculation is to sum for each unused row, i , the products $(a_{ij}x_j)$, to yield an estimate, say \hat{p}_i . It is then a matter of judgment whether the differences $[\hat{p}_i - p_i]$ are small enough to justify belief that all the positively signed phases were in fact derived from the parent. One would also expect the sign and magnitude of the coefficients to agree with field or petrographic data such as estimated rock volumes or modal proportions, with a negative sign implying removal of a phase to obtain the desired parent composition.

Table 26 gives the results of three calculations based on the data for Parícutin (Wilcox, 1954). Andesite P-10 was used by Wilcox as a starting composition from which to test other members of the series, and SiO_2 , MgO , and Al_2O_3 were the "oxide controls" he selected for the graphical solution. These and FeO were

TABLE 26. Parícutin Volcano, Mexico: Calculated and Observed Compositions, and Fractions of Inferred Components

	P-1		P-15		P-21	
	1	2	1	2	1	2
SiO ₂	55.00*	55.00	58.63*	58.63	60.50*	60.50
Al ₂ O ₃	18.81*	18.81	17.85*	17.85	17.30*	17.30
FeO	7.41*	7.41	6.22*	6.22	5.66*	5.66
MgO	5.68*	5.68	4.05*	4.05	3.60*	3.60
CaO	8.04	7.16	6.76	6.78	6.05	6.17
Na ₂ O	4.03	3.88	4.06	3.88	4.02	3.90
K ₂ O	0.80	0.85	1.42	1.31	1.73	1.69
MnO	0.13	0.07	0.12	0.12	0.11	0.10
TiO ₂	1.12	0.94	0.98	0.86	0.89	0.80
P ₂ O ₅	0.36	0.21	0.32	0.30	0.28	0.28
Totals	101.38	100.01	100.41	100.00	100.14	100.00
Andesite P-10		1.2538		1.0480		0.9066
Average xenolith		-0.1954		0.0399		0.1726
Plagioclase An ₇₀		-0.0149		-0.0387		-0.0384
Olivine Fo ₈₀		-0.0297		-0.0452		-0.0394
Totals		1.0138		1.0040		1.0014

* Oxide used as control.

1. Calculated composition.

2. Observed composition, recalculated to 100% minus CO₂, H₂O, all iron as FeO. Data from Wilcox (1954, Table 2, columns 1, 15, and 21).

also used for the numerical solution, which requires four equations. Calculations are presented only for analyses 1, 15, and 21, which adequately represent the full range of compositions erupted at Parícutin. However, by repeating the calculation for each analysis in turn entered into the final column of the augmented matrix, it is possible to simulate the complete set of variation curves. As in the original paper, all data were recalculated anhydrous, with total Fe expressed as FeO.

Using only the major cation oxides, Wilcox (1954) was able to show that simultaneous addition of xenolith material and removal of plagioclase and olivine appearing as phenocrysts could duplicate the bulk variation trends of the Parícutin lavas. The computer-generated compositions (Table 26) based on this hypothesis are in excellent agreement with the bulk analyses of the Parícutin lavas, even when extended to alkalis and minor elements not included in the original graphical solution. The somewhat less satisfactory agreement at the

low-silica end of the series, represented by analysis 1, was also noted by Wilcox (1954) and is illustrated in his Fig. 106.

A LEAST-SQUARES APPROXIMATION FOR ESTIMATING THE COMPOSITION OF A MIXTURE

W. B. Bryan, L. W. Finger, and F. Chayes

The procedure described in the preceding section is an exact numerical analogue of graphical devices widely employed by petrographers. Much quicker and more precise than the graphical procedures, it is nevertheless subject to the same general restrictions. Chief among these, in the notation used on page 242, is the circumstance that if $k < n$ there is no solution at all, whereas if $k > n$ there are in principle $k!/n!(k-n)!$ solutions, each of which uses only n/k of the data. If, for instance, $k=9$ and $n=5$, each of the 126 different sets of n simultaneous equations that may be drawn from (1) of page 242 yields either a solution or a singular matrix. If some of these sets are soluble and others are

not, there would appear to be no rational interpretation of the result, but even in the absence of singularity the situation may sometimes be little better. If the entire body of data is worth having in the first place, one feels intuitively that a single solution using all the information would be preferable to a large number of solutions each of which ignores $(1-n/k)$ of the information.

Now such a solution is in fact available if, in the fashion long adopted in other fields of inquiry (see, for instance, Legendre, 1805), one is prepared to accept as preferable that result which minimizes the sum of squares of the residuals. Letting \mathbf{A} and \mathbf{X} denote, respectively, the matrix and vector on the left side, and \mathbf{P} the vector on the right side, of (1), the equations of condition may be restated as

$$\mathbf{AX}=\mathbf{P}. \quad (2)$$

Premultiplication of (2) by the transpose of \mathbf{A} then gives the normal equations

$$\mathbf{A'AX}=\mathbf{A'P}, \quad (3)$$

and, finally, premultiplication of (3) by the inverse of $[\mathbf{A'A}]$, yields the desired solution,

$$\mathbf{X}=[\mathbf{A'A}]^{-1}\mathbf{A'P}. \quad (4)$$

There is only one such solution, and all of the available information contributes to it.

If we now substitute \mathbf{X} from (4) into the left side of (2) and perform the indicated multiplication, we obtain a vector, say, $\hat{\mathbf{P}}$, each element of which is the least-squares estimate of the analogous element of \mathbf{P} , i.e., the solution obtained from (4) is the one which minimizes the quantity $\sum_j (\hat{p}_j - p_j)^2$. This solution exists when $k \geq n$, the inequality denoting the common situation, in which, incidentally, graphical procedures and their numerical analogues fail to yield unique solutions.

CHEMICAL AND OPTICAL PETROGRAPHY

W. B. Bryan

During the report year, work has centered on the petrography and mineralogy of basalts and associated volcanic and intrusive rocks from the Bunya Mountains and Carnarvon Range, Australia. The Bunya Mountains lavas, for which chemical and mineralogical data are being prepared for later publication, illustrate well the compositional characteristics and resulting problems of classification that appear typical of many basaltic lavas from eastern Australia. Although intermediate compositions appear to be as rare among the volcanic rocks of eastern Australia as among the lavas of oceanic islands summarized by Chayes (1963), the six analyzed samples from the Bunya Mountains discussed below include one sample of trachyandesite (benmoreite), indicating that liquids of this composition are not entirely lacking among the volcanic rocks of southeast Queensland.

The extrusive rocks from the Carnarvon Range are discussed only briefly here, as the data are being prepared for publication in the near future. In spite of an apparently extreme compositional hiatus between basalt and trachyte in this area, these two compositions are intimately associated in a composite olivine gabbro-microsyenite intrusion, suggesting a close genetic relation between basaltic and trachytic magmas. The occurrence provides a rare opportunity to examine mineral paragenesis and crystal-melt equilibria relevant to the basalt-trachyte problem.

VOLCANIC ROCKS FROM THE BUNYA MOUNTAINS, QUEENSLAND, AUSTRALIA

The Bunya Mountains form a high, domelike plateau located about 80 miles northwest of Brisbane, in the southeast corner of Queensland, Australia. Samples from the Bunya Mountains were not included in the pioneering work of

Richards (1916) on the volcanic rocks of southeast Queensland, and although the mountains are readily accessible they have continued to escape the attention of petrographers. The six analyzed samples discussed here are the first to be described from this area, which appears to be a distinct volcanic center, probably the remnant of a once more extensive shield volcano. The rocks are of special interest because the basalts fall in the composition field termed olivine tholeiite by Yoder and Tilley (1962, p. 352) and lie close to the quadratic discriminant function proposed by Chayes

(1966, pp. 137-144) for distinguishing between alkaline and subalkaline basalts in the normative diopside-olivine-hypersthene ternary (Fig. 92). As demonstrated previously by Chayes (*Year Book 64*, p. 155), basalt analyses yielding neither normative quartz nor normative nepheline are relatively uncommon, although the majority of those recently dredged from the submarine ridges are in this category. Basalts of this type are evidently also common in eastern Australia. Similar rocks from the Mt. Warning shield volcano south of Brisbane were called "subtholeiitic" by Green (1964)

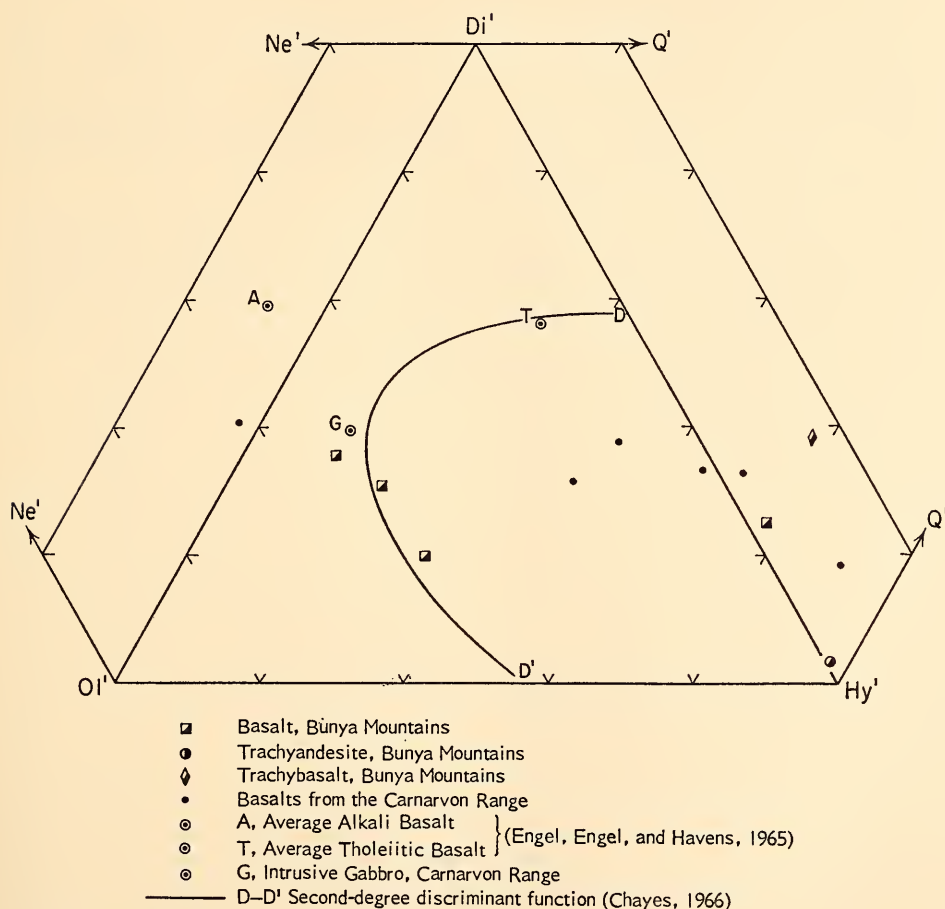


Fig. 92. Lavas from the Bunya Mountains, Carnarvon Range, and averages of oceanic alkaline and tholeiitic basalt, projected in the ternary fields *ne-ol-di*, *ol-di-hy*, and *hy-di-Q*. Two strongly oxidized Carnarvon basalts, included in Figs. 93 and 94, are excluded from this figure.

and more recently, "transitional" (Green, 1968); and McDougall and Wilkinson (1967, pp. 229-230) have described others from northern New South Wales as "mildly alkaline," "transitional," and "mildly tholeiitic." It will be evident from Fig. 92 that basaltic rocks from the Carnarvon Range, Queensland (Bryan, 1968), are also in this category.

Other graphical plots that have been used to distinguish alkaline and tholeiitic basalts confirm the ambiguous nature of these rocks. Figure 93 is essentially that used by Yoder and Tilley (*Year Book 64*, p. 75), except that total iron is expressed as FeO. The Bunya Mountains lavas show the initial iron-enrichment trend regarded as typical of tholeiitic suites, but the more siliceous rocks revert to the iron-depletion trend typical of alkaline lavas. The Carnarvon lavas show the same initial iron-enrichment trend, but the data do not extend over a sufficient composition range to indicate whether reversal to an alkaline trend is to be expected. In the familiar alkali-silica plot (Fig. 94), with the alkali

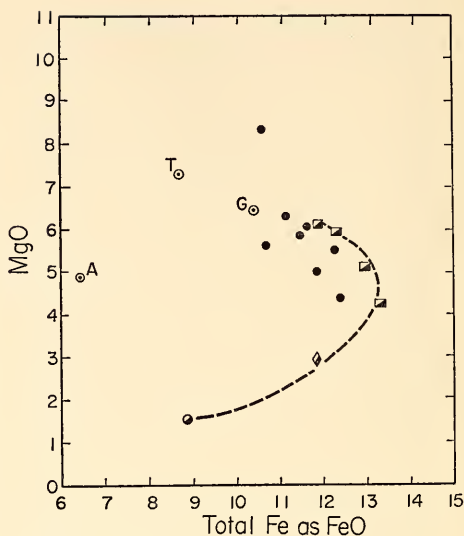


Fig. 93. Variation of MgO versus total iron as FeO. All symbols as in Fig. 92. Dashed line connects lavas of Bunya Mountains.

basalt-tholeiite boundary as defined by Macdonald and Katsura (1964), the Queensland basalts tend to fall within the alkaline field between the averages

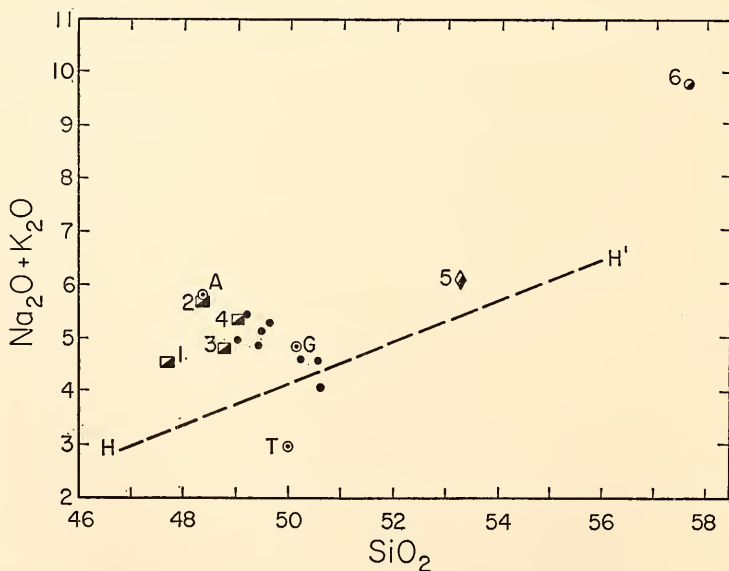


Fig. 94. Variation of $(\text{Na}_2\text{O} + \text{K}_2\text{O})$ versus SiO_2 . All symbols as in Fig. 92; dashed line $H-H'$ is boundary between alkali basalt field (upper) and tholeiite field (lower) as defined by Macdonald and Katsura (1964).

of oceanic alkaline and tholeiitic basalt, with the trachybasalt and trachyandesite also in the alkaline field at higher silica percentages.

The basalts contain phenocrysts of olivine (Fo_{65-70}) and, in the groundmass, pink augite with optical properties suggesting a composition approximately $\text{Ca}_{35}\text{Mg}_{30}\text{Fe}_{35}$, minerals generally regarded as typical of alkaline basalts. The glassy groundmass of the trachybasalt contains a few granules of olivine but no pyroxene. The trachyandesite, the most alkaline rock in Figs. 93 and 94, contains two pyroxenes, a hypersthene pleochroic in pale pink and green, and a pale green augite zoned outward to a rim of dark green. Optical properties of the latter mineral suggest ferroaugite zoned to ferrohedenbergite rather than a sodic pyroxene. These pyroxenes are suggestive of a tholeiitic rather than an alkaline affinity, although ferrohedenbergite is common in supposedly alkaline trachytes and rhyolites.

Analyses projecting well toward the diopside-hypersthene boundary or into the quartz field of Fig. 92 are perhaps best regarded as siliceous derivatives of the more mafic basalts. One of the olivine basalts falls in this region, owing to a relatively high content of ferric iron and low magnesia. The trachybasalt is similar in composition to the type tholeiite from the Tholey sill (Jung, 1958), as are equivalent rocks from New South Wales described as "potassic tholeiitic andesite" by McDougall and Wilkinson (1967, p. 230). The trachyandesite analysis resembles closely the sodic intermediate rocks called benmoreite by Tilley and Muir (1964). In view of the interest in analyzed rocks of intermediate composition since their scarcity in the ocean basins was publicized by Chayes (1963), it must be emphasized that this specimen is the most leucocratic of the nineteen basaltic rocks collected in a traverse of the Bunya Mountains, during which special effort was made to include rocks thought to be of intermediate com-

position. Equivalent rocks were not discovered on a traverse of the southern end of the Carnarvon Range, nor were they found by Green (1964) in a thorough sampling of part of the Mt. Warning shield volcano south of Brisbane. Rocks called mugearite were included in a summary of volcanic rocks from the Main Range, southwest of Brisbane (Stevens, 1965), where they are apparently common, though volumetrically subordinate to the basalts (Stevens, 1966, personal communication).

AN OLIVINE GABBRO-MICROSYENITE INTRUSION FROM THE CARNARVON RANGE, QUEENSLAND, AUSTRALIA

An unusual volcanic neck, located just north of the divide between the headwaters of Marlong Creek and Meteor Creek in the southern part of the Carnarvon Range, provides good geologic evidence of a genetic relation between basaltic and trachytic magma. The neck is circular in plan, about $\frac{1}{4}$ mile in diameter, and consists of a coarsely crystallized gabbro core surrounded by a ring-dike of microsyenite. Geologic and topographic relations indicate that the neck was intrusive into at least the lower half of the sheet of basaltic lavas capping the adjacent peaks. The gabbro is similar in bulk chemical composition to the uppermost lavas of the sheet, and it seems likely that the neck originally served as a conduit for these lavas. The gabbro evidently pulled away from the steeply dipping sides of the conduit shortly after consolidation, and settled downward into the underlying partly consolidated magma, allowing residual trachytic liquid generated at depth to rise into the circular void thus created.

The gabbro is composed of plagioclase (An_{50}) zoned outward through narrow rims of oligoclase to overgrowths of alkali feldspar, the crystals being 3 to 6 mm in length. Olivine (Fo_{53}) occurs as rounded grains, 1 to 2 mm in diameter;

both olivine and plagioclase are optically enclosed by large patches of optically continuous pink augite. Minor constituents include ilmenite, apatite, and rare flakes of red-brown biotite. Quartz appears in small areas of micropegmatite interstitial to the alkali feldspar overgrowths. An iddingsitelike brown alteration product penetrates fractures in many olivine crystals. The microsyenite is composed primarily of alkali feldspar, with conspicuous rounded phenocrysts of anorthoclase, 1 to 2 mm in diameter, and scattered microphenocrysts of ferrohedenbergite. The groundmass consists of flow-oriented laths of alkali feldspar with interstitial granules of magnetite, ferrohedenbergite, and cryptocrystalline feldspar. There are rounded brown iddingsitelike pseudomorphs, 0.5 to 1.0 mm in diameter, which may originally have been olivine. Many of the anorthoclase phenocrysts show patchy extinction, traces of perthitic lamellae, and grid twinning, and have a few tiny inclusions of ferrohedenbergite. The chemical compositions of the rocks and of some major mineral phases are given in Tables 27 and 28. The esti-

mated composition of olivine is Fo_{53} ($D=3.737$, $\alpha=1.725\text{--}1.727$, $d_{130}=2.802$). Ilmenite was identified in polished section and by X-ray diffraction; no magnetite was detected optically or in the diffraction pattern. Apatite is evidently a fluorapatite ($\omega=1.638\text{--}1.645$).

Thin sections of the gabbro provide the usual, not entirely unambiguous evidence for the sequence of crystallization. Olivine may be enclosed by all minerals, although it tends to be crowded into areas between the large plagioclase laths rather than to be enclosed by them, suggesting that the crystallization of plagioclase began later than that of olivine. Ilmenite is interstitial to plagioclase and olivine, but tends to be intergrown with augite, indicating essentially simultaneous crystallization of these minerals. Apatite is imbedded in the outer zones of plagioclase but is especially conspicuous in the alkali feldspar overgrowths, with which it is evidently in part contemporary. Such overgrowths are present only on those portions of plagioclase laths not optically enclosed by augite. Quartz occurs only as intergrowths with alkali feldspar interstitial to plagioclase. Carbonate, traces of biotite, and marginal replacement of olivine by hypersthene or "iddingsite" are also restricted to these areas.

The calculated mineral proportions of the microsyenite are given in Table 29. Table 30, column *A*, shows the measured modal proportions of the gabbro with the chemical analysis recalculated anhydrous, and column *B* shows the modal minerals expressed as weight percentages, with the corresponding calculated chemical composition as a check on the modal mineral data. In column *C*, Table 30, alkali feldspar is replaced by the microsyenite, with the equivalent amount of plagioclase, augite, and iron-titanium oxide in the microsyenite subtracted from the modally determined weight fractions. The corresponding chemical composition and density calculated from this adjusted mode agree well with those

TABLE 27. Chemical Composition of Gabbro and Microsyenite, Carnarvon Range, Queensland

	1	2		1a	2a
SiO ₂	49.19	63.94	Q	...	8.07
TiO ₂	1.87	0.20	Or	6.86	31.50
Al ₂ O ₃	16.83	16.74	Ab	29.87	45.10
Fe ₂ O ₃	1.72	2.67	An	26.65	6.01
FeO	8.66	2.41	Di	10.97	2.17
MnO	0.14	0.12	Hy	3.79	1.59
MgO	6.30	0.24	Ol	13.29	...
CaO	8.45	1.78	Mt	2.49	3.87
Na ₂ O	3.53	5.33	Il	3.55	0.38
K ₂ O	1.16	5.33	Ap	0.70	0.11
P ₂ O ₅	0.32	0.05			
H ₂ O ⁺	1.45	0.26			
H ₂ O ⁻	0.51	1.18			
Totals	100.13	100.25			
D	2.899	2.657			

1. Olivine gabbro C16-64; J. R. Dickson, analyst.

1a. Normative composition of olivine gabbro.

2. Microsyenite C17-64; J. R. Dickson, analyst.

2a. Normative composition of microsyenite.

TABLE 28. Chemical Composition of Minerals from Gabbro and Microsyenite

	1	2	3	4	5	6	7
SiO ₂	51.12	48.00	66.45	66.36	54.70
TiO ₂	0.72	0.31	nil	48.86	14.22
Al ₂ O ₃	3.04	1.26	19.06	19.37	28.81
Fe ₂ O ₃	0.44	2.97	0.52	3.79	41.40
FeO	8.66	25.59	0.43	47.36	44.30
MnO	0.22	0.59	nil
MgO	15.22	1.40	0.10
CaO	20.26	18.16	0.55	0.50	11.00
Na ₂ O	0.18	1.17	6.80	6.35	5.08
K ₂ O	tr.	0.34	5.77	7.41	0.40
P ₂ O ₅	0.06	n.d.	n.d.
H ₂ O ⁺	0.15	0.20	0.10
H ₂ O ⁻	0.10		
Totals	100.17	99.99	99.78	99.99	99.99	100.01	99.92
α	1.689	1.738	1.525	...	1.558-1.560
β	1.701	1.746	1.530
γ	1.720	1.765	1.533
2V	(+)49°	(+)55° ± 5	(-)57°
D	3.276	3.639	2.572	<2.570	>2.682	4.736	5.03

1. Augite, olivine gabbro C16-64; J. R. Dickson, analyst.
2. Ferrohedenbergite, microsyenite C17-64; L. J. Sutherland, analyst.
3. Anorthoclase, microsyenite C17-64; L. J. Sutherland, analyst.
4. Alkali feldspar, olivine gabbro C16-64, calculated from Na,K,Ca analysis by electron microprobe; SiO₂ and Al₂O₃ by difference, assuming ideal formula.
5. Plagioclase feldspar (cores), olivine gabbro C16-64, calculated from Na,K,Ca analysis by electron microprobe; SiO₂ and Al₂O₃ by difference, assuming ideal formula.
6. Ilmenite, olivine gabbro C16-64, calculated from Fe,Ti analysis by electron microprobe, assuming ideal ilmenite-hematite solid solution.
7. Titaniferous magnetite, microsyenite C17-64, calculated from Fe,Ti analysis by electron microprobe, assuming ideal magnetite-ulvöspinel solid solution. Density calculated for 60% magnetite, $D = 5.20$; 40% ulvöspinel, $D = 4.78$.

TABLE 29. Calculated Modal Proportions and Chemical Analysis of Microsyenite

	Volume %	Weight %		A	B
Anorthoclase *	91.08	88.15	SiO ₂	64.71	64.71
Ferrohedenbergite *	4.97	6.80	Al ₂ O ₃	16.94	16.94
Quartz †	2.96	2.68	Fe ₂ O ₃	2.17	2.70
Apatite ‡	0.10	0.12	FeO	2.68	2.44
Magnetite §	0.67	1.27	MgO	0.19	0.24
Hematite §	0.50	0.98	CaO	1.79	1.80
			Na ₂ O	6.09	5.39
			K ₂ O	5.12	5.39
			TiO ₂	0.20	0.20
			P ₂ O ₅	0.05	0.05
			MnO	0.04	0.12
			Totals	99.98	100.00
			D	2.658	2.657

* Weight fraction computed from simultaneous solution for Al₂O₃ and CaO, after subtracting CaO in apatite, and using microsyenite analysis recalculated anhydrous.

† Excess SiO₂ after subtracting anorthoclase and ferrohedenbergite; ideal formula and density assumed.

‡ Weight fractions estimated from P₂O₅ and TiO₂ in bulk analysis; ideal formula and density assumed.

§ Weight fraction is that required to bring sum of weight fractions to 1.000; ideal formula and density assumed.

A, Composition and density calculated from mode.

B, Actual analysis recalculated anhydrous, and measured density.

TABLE 30. Measured and Adjusted Mode of Gabbro C16-64, with Corresponding Observed and Calculated Chemical Composition and Absolute Density *

	A	B	C
	Modal Volume %	Modal Weight %	Adjusted Modal Weight %
Alkali feldspar and micropegmatite	17.07	14.92	...
Microsyenite	18.49
Plagioclase	52.34	47.76	45.84
Augite	15.01	16.93	15.68
Olivine	10.72	13.79	13.79
Ilmenite	2.15	3.51	3.11
Iddingsite †	2.70	2.32	2.32
Apatite ‡	...	0.76	0.72
SiO ₂	50.11	50.23	50.61
Al ₂ O ₃	17.14	17.34	16.99
Fe ₂ O ₃	1.75	1.05	1.53
FeO	8.82	8.72	8.87
MgO	6.42	6.46	6.32
CaO	8.61	9.23	9.02
Na ₂ O	3.60	3.41	3.36
K ₂ O	1.18	1.30	1.19
TiO ₂	1.90	1.85	1.69
P ₂ O ₅	0.33	0.34	0.35
MnO	0.14	0.04	0.06
Totals	100.00	99.97	99.99
Absolute density	2.899	2.904§	2.913§

* All chemical analyses used in calculations have been recalculated to 100%, minus H₂O.

† Composition from Gay and LeMaitre (1961, p. 106, Table 3, column 5).

‡ Ideal formula and density of 3.21 assumed, weight fraction inferred from P₂O₅ in bulk rock analysis, and an equivalent weight subtracted from the feldspars.

§ Calculated.

A, Measured modal volume % (average of three thin sections), chemical analysis of gabbro recalculated to 100% anhydrous, and measured absolute density.

B, Mineral weight percentages and bulk chemical composition calculated from modal data.

C, Adjusted weight percentages, substituting microsyenite for alkali feldspar, and calculated bulk chemical composition.

of the gabbro. The compositions and modal proportions of the minerals of the gabbro are thus compatible with geological evidence suggesting derivation of the microsyenite liquid from the gabbro. The residual liquid would apparently have had the appropriate composition when the gabbro was 81.5 wt % crystallized. It is interesting that the liquid remaining after more than 80% crystallization of the gabbro is only slightly oversaturated with respect to silica (Table 27, column 2a). A slight further

crystallization of remaining plagioclase, augite, and oxide components would leave a residual liquid having essentially the composition of the interstitial alkali feldspar of the gabbro (Table 28, column 4) with a small amount of quartz. In this example at least, which is representative of low-pressure crystal-melt equilibria, a basaltic liquid lying near the *ol-di* join in the ternary *ol-di-hy* (G, Fig. 92) yields a slightly oversaturated residual liquid, which is ultimately enriched in potash relative to soda.

STRUCTURAL GEOLOGY

EXPERIMENTS IN FLOW DEFORMATION

William H. Scott

In most geologic experiments designed to reproduce natural folds, particular attention is given to scaling the physical properties of rock bodies and the time and size of the natural process, so that the experiment more closely reproduces geologic deformation. It is probable that the three-dimensional conditions of flow—whether convergent, divergent, or parallel; whether velocity gradient or not—are factors as important as the physical properties of the rock body in controlling the geometry and style of the folds produced (Hansen, 1963, 1968). The experiments described below are the first in a series designed to test the relationships between the conditions of flow and the resultant plastic strain seen as folds in anisotropic fluids.

Design of the Apparatus

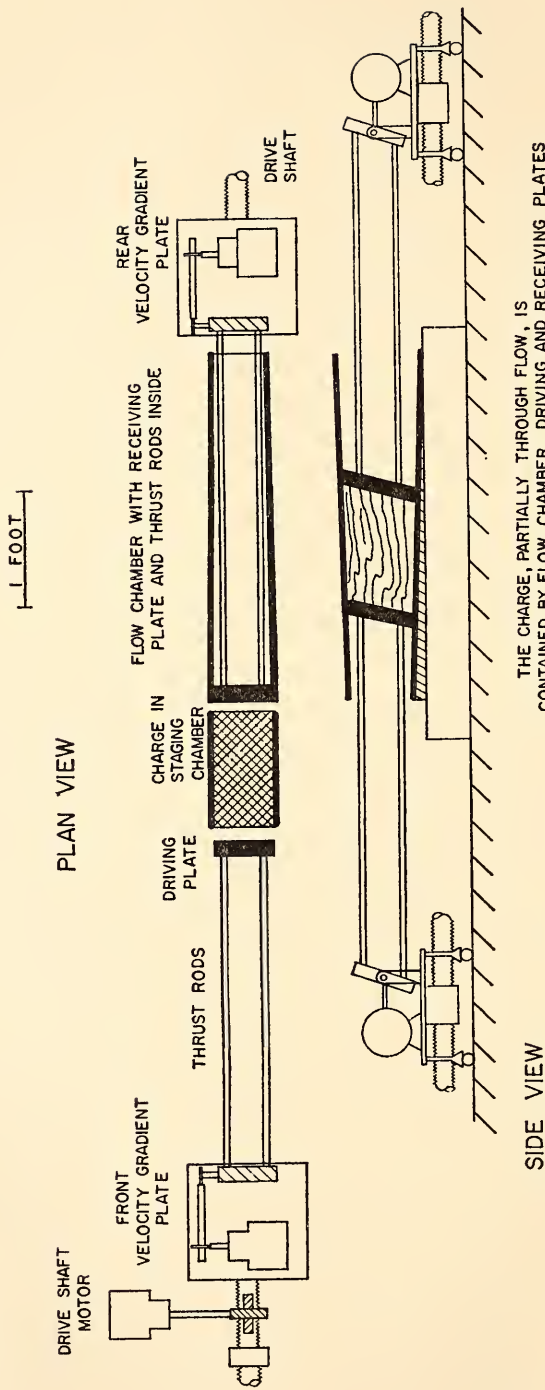
Fig. 95 is a schematic diagram of the experimental apparatus. A charge of low-viscosity fluids is forced through a chamber under conditions of controlled flow. The charge, measuring $5 \times 5 \times 12$ inches, is composed of alternating layers of two petroleum-based materials of different viscosities. It is built in a staging chamber, open at each end. Confining the charge at the ends are two expandable plates, the driving and receiving plates, which are connected by thrust rods and velocity-gradient assemblies to a common drive shaft. This shaft, driven at 2.9 rpm, translates the driving and receiving plates at 18 inches/hour. The charge is thus forced to flow through the staging and flow chambers at that rate, confined at all times by the chamber walls and the expandable plates. The flow chambers are 36 inches long; they are detachable and can be replaced by others that provide for any one of a variety of flow conditions. In order to

maintain constant volume in chambers with progressively changing cross sections, the rear velocity-gradient plate is spring-loaded on a spline (not shown in Fig. 95), as well as attached to the driveshaft, allowing the receiving plate to move at a variable rate that will just maintain equal-volume flow. Motor-driven gear trains on the velocity-gradient plates rotate the driving and receiving plates 15° /hour. Besides translating the charge through the chamber, therefore, the velocity-gradient plates produce a velocity gradient in the vertical plane by forcing the top of the charge to move faster than the bottom of the charge. Thus, at constant volume, the apparatus can impose variable conditions of convergent, divergent, parallel, and velocity-gradient flow on charges of anisotropic fluids.

Experimental Conditions

A series of experiments has been run with interlayered stitching wax ($\eta \approx 10^6$ poises at 25°C , layers 0.075 to 0.100 inch thick) and Vaseline ($\eta \approx 10^3$ poises at 25°C , layers 0.200 to 0.300 inch thick). Charges were made to flow through a compound flow environment, converging 8° in the horizontal plane and diverging 16° in the vertical plane, during 36 inches of translation in 2 hours (see Fig. 95). In addition, 30° rotation of the driving and receiving plates imposed a vertical velocity gradient by cumulative relative slip of 4 inches between the layers. ϵ_1 and ϵ_3 for the total strain of the charges are located in the vertical plane containing the direction of translation; ϵ_1 , vertical at the beginning of flow, plunges 60° back toward the driving plate at the end of flow. ϵ_2 is horizontal and perpendicular to the direction of translation. Strain rates for total strain are of the order of 10^{-5} /second.

Translation of a charge during an experiment was horizontal and parallel to



THE CHARGE, PARTIALLY THROUGH FLOW, IS CONTAINED BY FLOW CHAMBER, DRIVING AND RECEIVING PLATES

Fig. 95. Flow-deformation apparatus. Horizontal convergent, vertical divergent, and velocity-gradient flow illustrated.

the imposed velocity gradient. The major component of slip between the layers, therefore, was parallel to the velocity gradient and to the direction of translation. The layers were also constricted in the horizontal plane, shortening both parallel and perpendicular to translation.

Wall friction during flow was considerable, noticeably deflecting the wax layers within 2 cm of the walls. No structural data are reported from this region, but it is not known how far the shear

from this friction penetrated into the charge. Succeeding experiments are expected to include modifications that effectively eliminate wall friction.

Initial Results

1. The layers of stitching wax were deformed into folds during flow. The folds are concentric in profile and disharmonic, and display curved hinge lines.

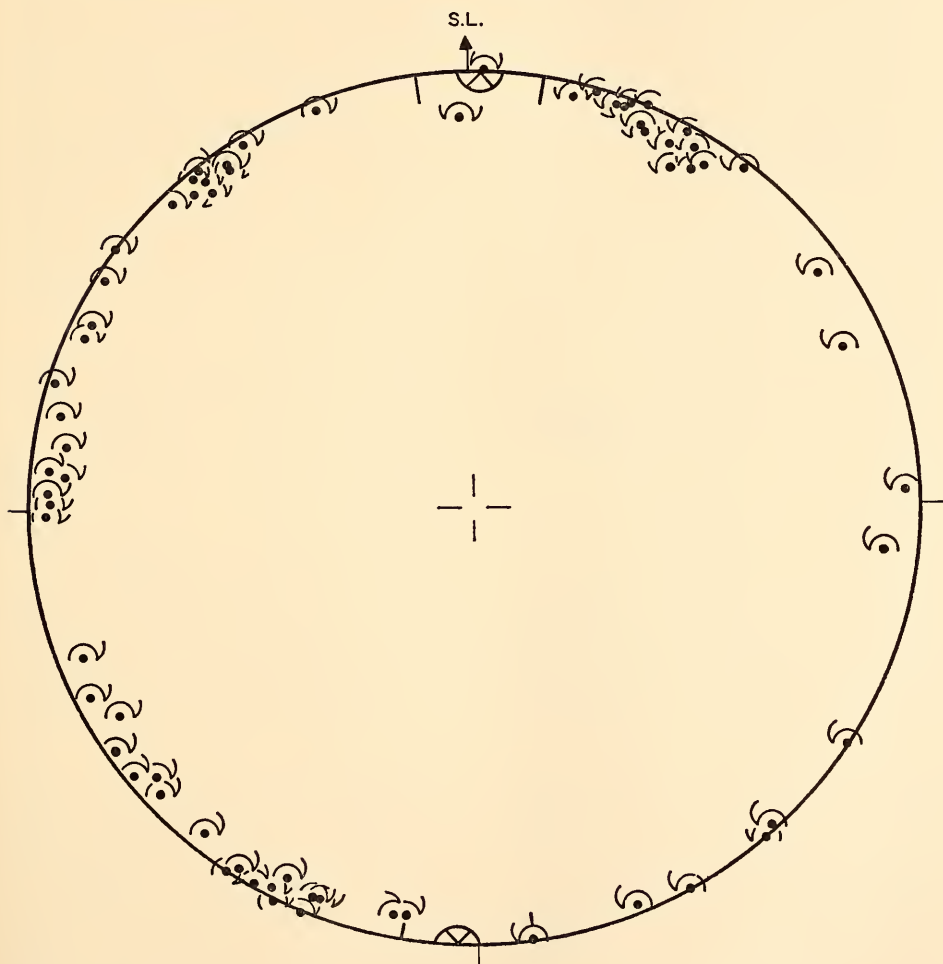


Fig. 96. Orientation of, and asymmetry about, fold axes formed during experimental flow (8° horizontal convergence perpendicular to the direction of transport, 16° vertical divergence, and velocity-gradient flow). The separation angle (bold arc of horizontal great circle) includes the slip line, *S.L.*

2. In all layers, the folds display a planar preferred orientation of fold axes. The planes so described are horizontal and parallel to the wax layers ("bedding").

3. Most of the folds are asymmetrical. The sense of overturning is consistently top-over-bottom in the sense and direction of the shear couple imposed by the velocity gradient.

4. The orientation of the fold axes and the asymmetry of the folds in a single, deformed charge are shown in spherical projection in Fig. 96; folds in the eastern portions of the net are counterclockwise, and in the western portions, clockwise. The 18° separation angle, which separates the clockwise axes from the counterclockwise axes (Hansen *et al.*, 1961; Hansen, *Year Book 65*, pp. 390–405), includes the line of slip (S.L.) produced by the velocity gradient between the layers. Hansen (*Year Book 65*, pp. 390–397) showed by geometric analysis of folds in a tundra landslide that the separation angle contains the slip line for folding. These experiments reproduce nearly identical fold fabrics, independently confirming his conclusions.

MOVEMENT DIRECTIONS AND THE AXIAL-PLANE FABRICS OF FLEXURAL FOLDS

William H. Scott and Edward Hansen

It was predicted from theoretical considerations in an earlier report that the axial planes of a group of flexures or flexural-slip folds would be found to share a common axis (Hansen, *Year Book 65*, pp. 393–398). Subsequently a common axis, or zone axis, has been observed in the axial-plane fabrics of these types of folds in several localities. Two field examples are described here that illustrate the relationship between the zone axis and the movement history of the folds. These examples indicate that the zone axis can be used as another independent means of deducing movement directions, or slip-line orientations,

that obtained during flexural and flexural-slip folding.

"Slip-line orientations" of flexures and flexural-slip folds, as meant here, does not refer to the directions of slip between layers within the limbs of flexural-slip folds. Instead it refers to the orientations of the lines of relative slip between the layer(s) that undergoes folding and the adjacent layers that do not fold.

Flexures in Lava

Flexural folds displaying a zone axis of axial planes occur on a small volcanic spattercone near Reykjavik, Iceland. The cone is the subject of a study of the relationships between folds and the flow in lava (Scott, 1968). In the study, fabric data were collected from nine small areas on the sides of the cone. Data from one representative area serve here to illustrate the relationship between the axial-plane fabric and the movement direction of the lava.

Ejected lava bombs, after falling onto the cone surface, flattened into plates and flowed several inches downslope. The lava plates deformed plastically into concentric, disharmonic folds, consistently overturned in the downslope direction. Fold axes of 14 folds are shown in spherical projection in Fig. 97(A). Semicircular arrows modifying the axes indicate the asymmetry of the folds (Hansen *et al.*, 1961). The plane that best fits the distribution of axes has been calculated as the plane whose pole is axis 1 of the Dimroth ellipsoid for the distribution (Dimroth, 1962a, 1962b, 1963); it is shown as the dashed great circle, *S*, which approximates the slope of the spattercone. Flow of the lava plates under gravity was downslope. Orientation of the downslope direction—the slip-line orientation for the area—is shown as a square in Fig. 97(A). It is oriented between the group of six clockwise axes and the group of eight counterclockwise axes, within the separation angle (solid

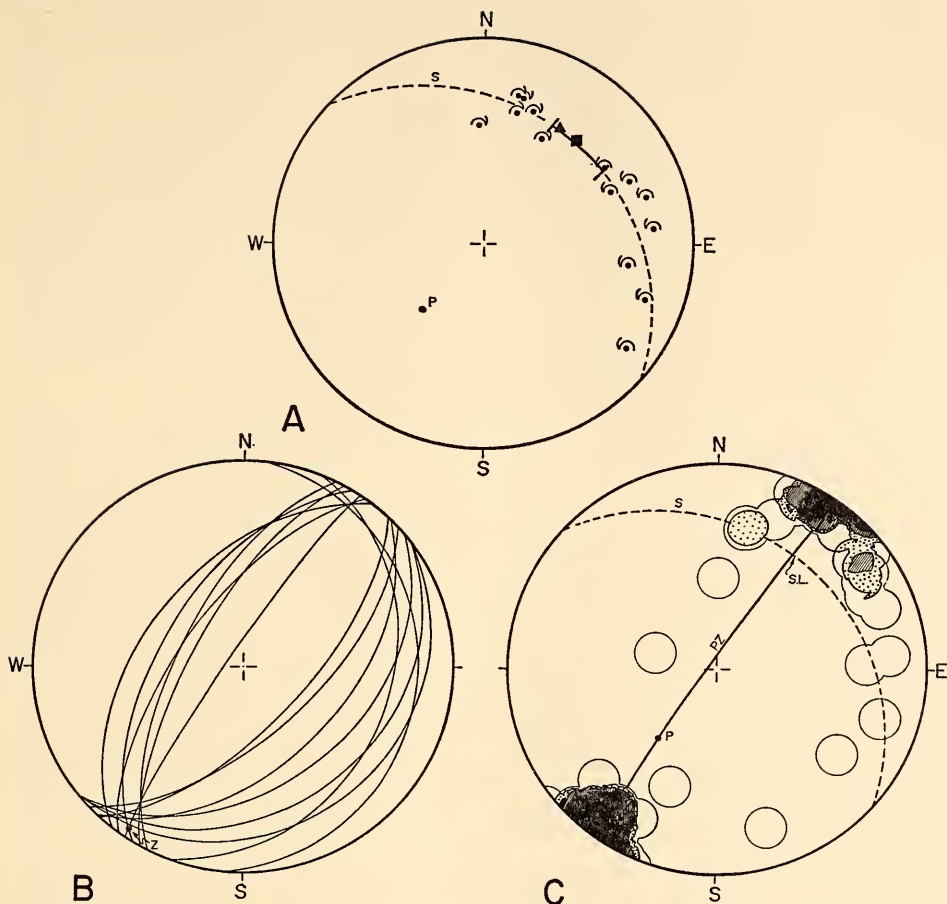


Fig. 97. Orientation data of 14 flexures in lava on a small spattercone, Iceland. (A) Fabric data: Dots represent fold axes, semicircular arrows show asymmetry patterns, S is the best-fitting plane to the fold axes, and P is the pole to S . Slip-line solutions: The square represents the downslope direction, the solid arc represents the separation angle, and the triangle is the solution from the zone axis in diagram C. (B) Axial planes of folds in diagram (A). Z represents the zone axis. (C) Contour diagram of the 91 intersections of the axial planes in diagram (B). SL is the slip-line solution from the zone axis. Contours: 1.1, 3.3, 5.5, 9.9% per 1% area; maximum, 51%.

arc in Fig. 97A; Hansen *et al.*, 1961; Hansen, *Year Book 65*, pp. 390–405).

Axial planes of the 14 folds are shown in Fig. 97(B). They intersect in a strong point maximum in the southwest quadrant of the diagram. The pole to the plane that best fits the poles to the 14 axial planes is labeled Z ; it approximates the center of gravity of the maximum. The maximum is emphasized by con-

touring of the 91 intersections in Fig. 97(C).

The slip-line orientation of flexural folds is contained in the plane of layering (S in Fig. 97A). It follows from the discussion of Fig. 108 (p. 395) in *Year Book 65* that the pole to layering (P , Fig. 97A) and the zone axis (Z , Fig. 97B) define a plane that also contains the slip-line orientation. The plane is shown as a solid

great circle in Fig. 97(C). Its intersection with S , therefore, should parallel the slip line ($S.L.$, Fig. 97C). The orientation of the intersection, which is a solution for the slip-line orientation, is plotted in Fig. 97(A) as a triangle. It is included in the separation angle and oriented 5° from parallelism with the downslope direction. All three solutions are compatible.

Flexural-Slip Folds in Migmatite

The best set of flexural-slip folds found during a reconnaissance of several mountain chains occurs in granite migmatite in Lilledalen, southern Norway, deep within the metamorphic core of the Caledonides (Hansen, Scott, and Stanley, *Year Book 65*, p. 407, Fig. 117, area 6). Fold axes and the asymmetry patterns of 45 of these concentric, disharmonic folds are shown in projection in Fig. 98(A). The plane that best fits the axes is shown as the dashed great circle, S , which parallels the general attitude of compositional layering in the area. The solid arc within S is the separation angle between the groups of clockwise and counterclockwise axes. It is a solution for the slip-line orientation that obtained during the development of the folds.

Axial planes of 11 folds are shown in Fig. 98(B). Their intersections cluster in the eastern part of the diagram; the point of highest density in the cluster is labeled Z . In Fig. 98(C), which contains the contoured intersections of the axial planes, the planes PZ (solid) and S (dashed) are shown. Their intersection ($S.L.$) is a solution for the slip-line orientation. It is plotted as a triangle in Fig. 98(A) for comparison with the separation angle. The two solutions are compatible.

Use of the Axial-Plane Fabrics to Deduce Slip-Line Orientations

These examples indicate that the zone axes of the axial planes of flexural folds can be used to deduce slip-line orientations. To do so, it is necessary (1) to

measure the fold axes, find the plane (S) that best fits the axes, and find its pole (P); (2) to measure the axial planes and find their zone axis (Z); and (3) to construct the plane PZ . The intersection of PZ with S is a solution for the slip-line orientation. It should be noted, however, that any solution obtained by this method is based upon the same assumption of the intermediate principal stress axis (σ_2) being parallel to S as any solution obtained from the separation angle (*cf.* Hansen, *Year Book 65*, pp. 396–397).

For any group of folds under consideration, the zone axis can be taken as either (1) the pole (π) to the plane that best fits the poles to the axial planes or (2) the highest density (β) of intersections of the axial planes (Turner and Weiss, 1963, pp. 83, 154). Although π was used for the zone axis in the lava plates (Fig. 97C) and β for the zone axis in the migmatite (Fig. 98C), it is not clear which of the two will prove more accurate or more useful.

Perhaps it should be made explicit that the kind of zone axis used here to deduce slip-line orientations is found in originally nonparallel axial planes of a single generation of flexural folds that display a planar distribution of fold axes. This kind of zone axis should not be confused with other kinds, such as those produced by the subsequent rotation of originally parallel axial planes in areas of superposed folding.

An Explanation of the Spread of Zone Axes

The contours around the major point maximum that represents the zone axis in Fig. 97(C) describe a V pattern. The V points away from the plane of axes (S) and opens toward that plane. Although a V pattern is not obvious in Fig. 98(C), it has been observed in many diagrams of this type and appears to be characteristic. It is interpreted to mean that the folds formed consecutively

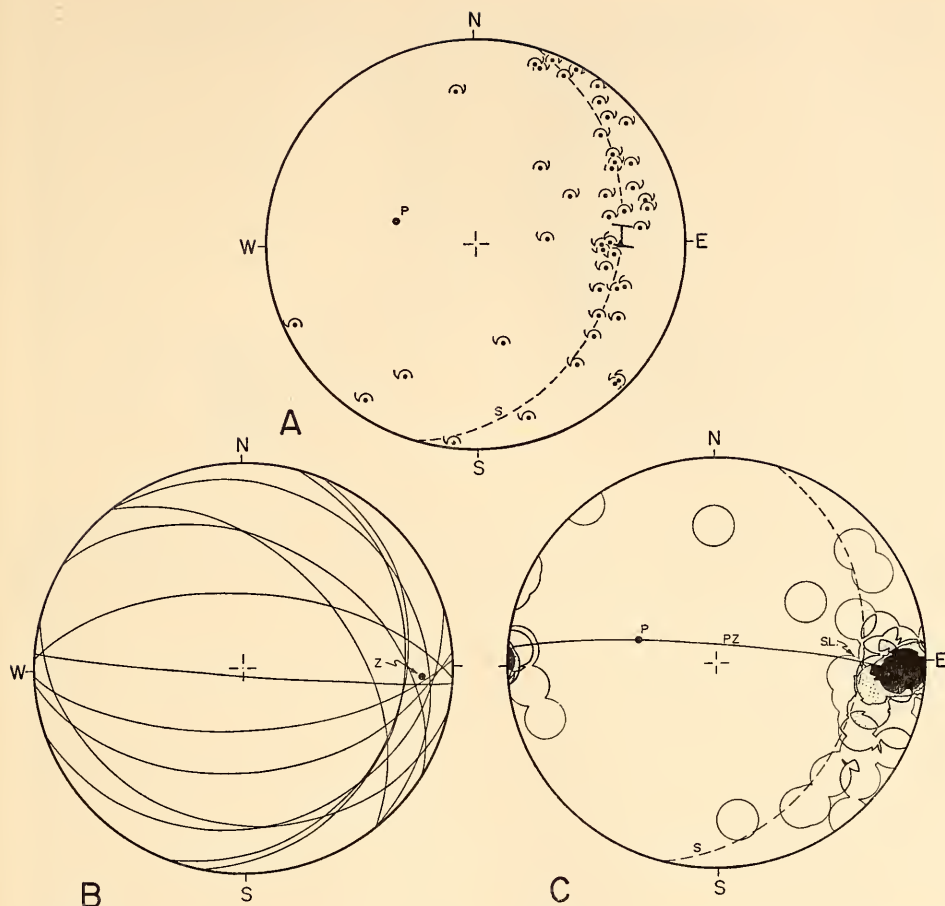


Fig. 98. Orientation data of flexural-slip folds in magmatite, Lilledalen, Norway. (A) Fabric data: Dots represent fold axes ($n=45$), semicircular arrows show asymmetry patterns, S is the best-fitting plane to the fold axes, and P is the pole to S . Slip-line solutions: The solid arc represents the separation angle, and the triangle is the solution from the zone axis in diagram (C). (B) Axial planes of 11 folds in diagram (A). Z represents the zone axis. (C) Contour diagram of the 55 intersections of the axial planes in diagram (B). $S.L.$ represents the slip-line solution from the zone axis. Contours: 1.8, 5.5, 9.1, 12.7% per 1% area; maximum, 34.6%.

under rotation due to a shear couple (i.e., under drag). This interpretation is supported by the following geometrical demonstration that such a pattern can be produced in this manner.

Suppose that four flexural-slip folds with fold axes b'_1, b'_2, b'_3, b'_4 (Fig. 99A) develop in bedding S under compression (σ_2/S ; cf. Hansen, *Year Book* 65, pp. 393-396); their axial planes (S'_1, S'_2, S'_3, S'_4) intersect at Z . Under the influence of the maximum resolved shear stress on

S (open circle), the axial planes are rotated toward parallelism with S , and the zone axis is rotated toward parallelism with the line of relative slip, or drag, between beds. If we assume that slip can occur with equal ease in any direction within S , the slip line parallels the maximum resolved shear stress (open circle). New orientations of the axial planes ($S'_{1r}, S'_{2r}, S'_{3r}, S'_{4r}$) and the zone axis (Z_r) after rotation are shown in the figure. Suppose now that four additional

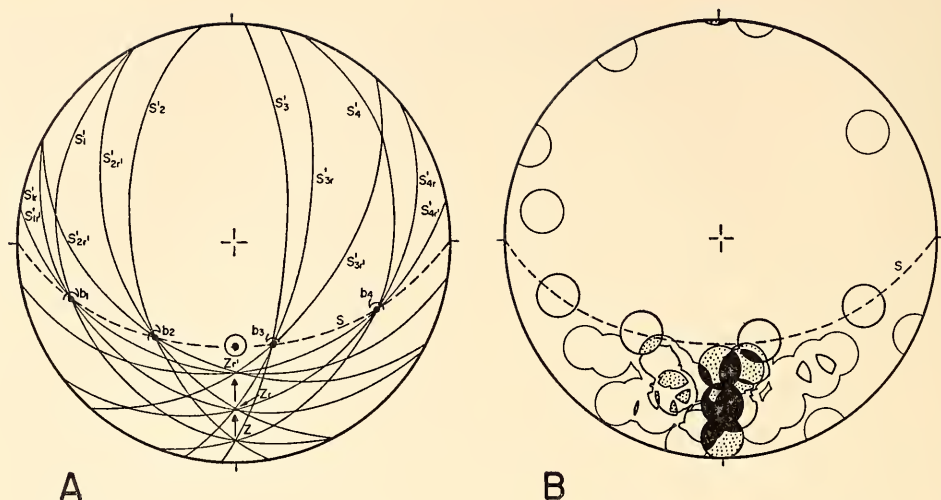


Fig. 99. Hypothetical development of a set of twelve flexural folds during rotation by drag. (A) Orientation of bedding (S), fold axes (b'), axial planes (S'), and zone axes (Z); the open circle represents the slip-line orientation. (B) Contour diagram of 66 intersections of the twelve axial planes in diagram (A). Contours: 1.5, 4.5, 7.6, 10.6% per 1% area; maximum, 25.8%.

folds develop in the same manner as the first four folds and, for simplicity, in the same orientations as the first folds before rotation (i.e., $b'_1, b'_2, b'_3, b'_4, S'_1, S'_2, S'_3, S'_4, Z$, Fig. 99A). Under the same shear that rotated the first set of folds, the axial planes of the second set are rotated in the same direction as the first, so that their common axis at Z is rotated to Z_r . At the same time, the common axis of the first set at Z_r is rotated to $Z_{r'}$. Finally, let us suppose that a third set of four folds develops and, again for simplicity, that they have the initial orientations ($b'_1, b'_2, b'_3, b'_4, S'_1, S'_2, S'_3, S'_4, Z$). At this point, the stress is dissipated, and folding and rotation stop. The fold axes b'_1, b'_2, b'_3, b'_4 are shared by all three fold sets, but the orientations of the axial planes are unique; the zone axis of the first set is at $Z_{r'}$, the zone axis of the second set is at Z_r , and the zone axis of the third set is at Z (Fig. 99A).

Mutual intersections of the twelve axial planes in Fig. 99(A) are contoured in Fig. 99(B). The higher contours around the most important maximum show an irregular V pattern, which points

away from S . Therefore, the V pattern in this diagram is similar to that in Fig. 97(C).

It is expected that in the natural formation of a group of folds their development and the rotation of their axial planes would occur as one continuous process. Hence, the development of multiple, discrete zone axes, as illustrated in Fig. 99(A), probably would not occur in nature. The unusual coincidence of some of the contours of different levels in Fig. 99(B) is the product of restricting the folds to four axial orientations and the zone axes to three discrete orientations. Nevertheless, the spread of the zone axis into a V pattern as contoured in Fig. 99(B) is the product of the rotation of some of the axial planes with respect to the others; it is not the product of the simplifications and restrictions.

ON THE "DRAG FOLDS" OF VAN HISE AND LEITH (1911)

Edward Hansen and William H. Scott

In his recent text, Whitten drew attention to the apparent introduction into the

structure literature of the term "drag fold" by Van Hise and Leith (1911) for a distinct type of fold seen in the Soudan formation, Vermillion iron district, Minnesota. Three descriptive properties of this fold type were given (Van Hise and Leith, 1911, p. 123; Whitten, 1966, pp. 164–165): (1) The folds display a planar distribution of fold axes parallel with bedding. (2) The folds, though locally complex, do not alter the general trend of the beds. (3) The profile geometry is concentric but somewhat flattened (observed in Fig. 12 of Van Hise and Leith). In addition, the authors mentioned that the folding involved buckling of the beds.

Since the time of Van Hise and Leith, the name "drag fold" has been used by many geologists for most of the minor or small-scale folds encountered in the field, whether or not they shared the descriptive properties of the original "drag folds." The planar distribution of fold axes was forgotten, and even the concentric profile section, flattened or not, was not characteristic of all so-called drag folds. Rather, the basis for using the name was apparently genetic—the idea that small folds are produced by the drag generated between beds on the limbs of larger folds undergoing flexural slip (*cf.* Knopf and Ingerson, 1938, pp. 159–160). However, the difficulty of ascertaining that any natural fold was actually produced or even modified by drag, as well as the recognition that many so-called drag folds occur in hinge areas of larger folds where no drag is generated during flexural slip, has placed the term "drag fold" in general disrepute (de Sitter, 1956, p. 226; Whitten, 1966, pp. 164–168; Ramsay, 1967, pp. 396–397).

Nevertheless, the folds that Van Hise and Leith described are of interest because they are the "type" folds for which one of the important dynamic concepts of folding was introduced—folding by drag. In particular, these folds are of interest here because of their similarity on all three counts, above, to the folds

that the present writers and Stanley studied rather extensively in reconnaissance (*Year Book 65*, pp. 406–410). Consequently, a trip was made to the area where the folds are reportedly well developed (secs. 13 and 14, T.62N., R.13W., Minn.) in the vicinity of Mitchell Lake and Twin Lakes, between Tower and Ely. The relationships noted during the trip are reported here.

Three sets of folds are described for the Soudan formation (Van Hise and Leith, 1911, pp. 123–124). From the original descriptions, all three are easily recognizable in the outcrops near Mitchell and Twin Lakes: an early set of isoclinal "longitudinal folds" with nearly horizontal fold axes, a later set of more open "cross folds" with axes that commonly plunge 50° to 60° , and a set of "drag folds" with axes in all orientations within the compositional layering. The relative age of the "drag folds" is unclear, but they seem to be intermediate between the "longitudinal folds" and the "cross folds." The geometry of the rocks is complex.

The best group of "drag folds" uncomplicated by folds of the other generations was found on the southern shore of the eastern Twin Lake, in a frost-heaved block (2 m \times 2 m) that had rotated about 20° from its original orientation in outcrop. However, because our interest was not in the relationship of the folds to the regional geology but in the nature of the folds themselves, this group was satisfactory. The rock types are interlayered greenstone and jasper. The folds are contained in an incompetent layer 3 cm thick with internal competent layers approximately 1 mm thick. The folds are seen better in the competent layers, where most of the orientation data were collected. The portion of the layer in which the folds occur is about 40 cm long; it is part of a long limb of a "cross fold" that is nearly two orders of magnitude larger than the "drag folds."

Fold-Axis and Axial-Plane Fabrics

The folds are concentric in profile geometry, but somewhat flattened, very much like the one illustrated by Van Hise and Leith (1911, Fig. 12). Fold axes and asymmetry patterns of eight folds are shown in Fig. 100(A). The best-fitting plane (S) to the fold axes parallels the compositional layering. A separation angle of 39° is defined in S by the re-

versal in asymmetry in the southwestern quadrant of the diagram. Therefore, the folds are compatible with a single shear couple acting parallel with S and within the separation angle, in the sense of top downward (Hansen, *et al.*, 1961; Hansen, *Year Book 65*, pp. 390-405). The concentric profile geometry, the planar distribution of fold axes, and the distribution of asymmetry patterns com-

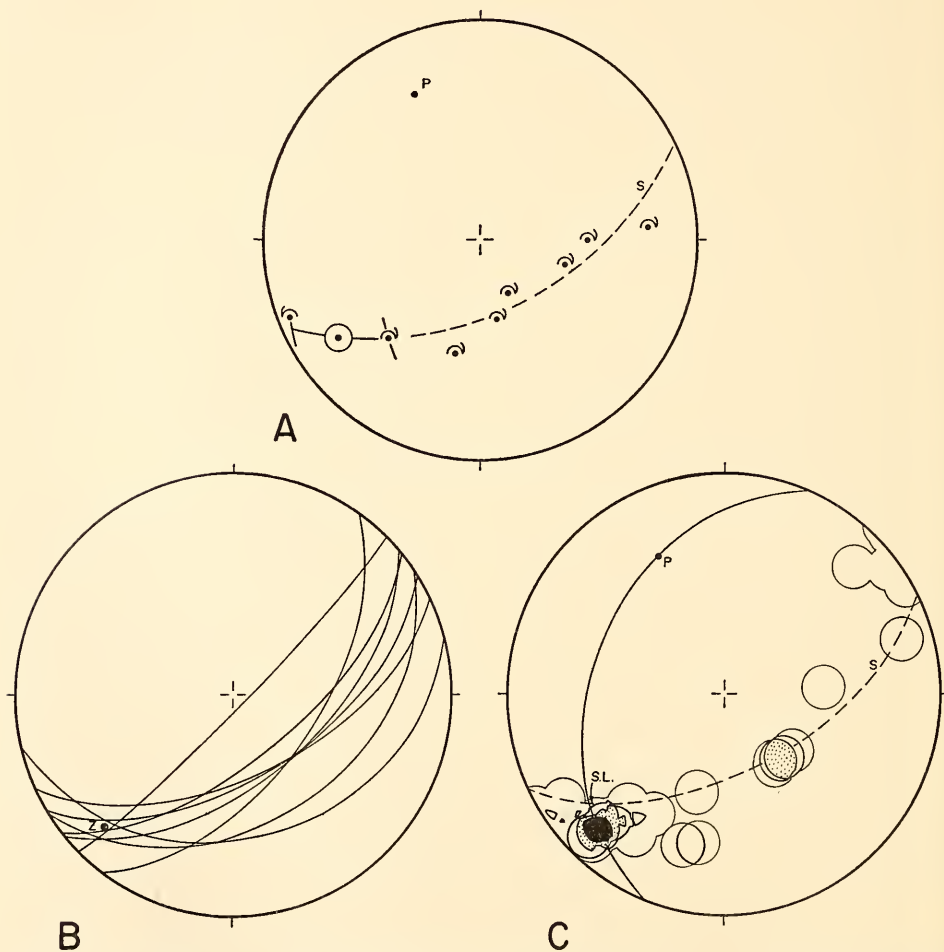


Fig. 100. Orientation data of eight "drag folds" in the Soudan formation, Twin Lakes, Minnesota. (A) Dots represent fold axes, semicircular arrows show asymmetry patterns, S is the best-fitting plane to the fold axes, and P is the pole to S . The arc with the open circle within S represents the separation angle. (B) Axial planes of the folds in diagram (A). Z represents the zone axis. (C) Contour diagram of the 28 intersections of the axial planes in diagram (B). $S.L.$ is the slip-line solution from the zone axis. Contours: 3.6, 10.7, 17.8, 25% per 1% area; maximum, 32%.

patible with a single shear couple indicate that these "drag folds" are the same kind of fold as the so-called drag folds described in *Year Book 65* (pp. 406–410).

Axial planes of the eight folds in diagram (A) are shown in diagram (B). The intersections of the axial planes are contoured in diagram (C). They define two major point maxima 70° apart, the most important of which is located in the southwestern quadrant. The highest density of intersections is labeled *Z* (Fig. 100B). *Z* can be considered a zone axis of the axial planes and can be used to get a solution for the slip-line orientation that obtained during folding (*cf.* preceding report on axial-plane fabrics of flexural folds). The intersection of *S* with the plane containing *Z* and the pole (*P*) to *S* is the slip-line solution, labeled *S.L.* in Fig. 100(C). This solution is compatible with the separation angle, which it bisects. Therefore, the axial planes of the "drag folds," though less regular, display the same relationships of fabric and kinematics as the axial planes of other groups of folds of the same type (Figs. 97 and 98, this report).

Height-Width and Depth-Width Ratios

Where folds are asymmetric, two adjacent hinges are commonly coupled by an intervening short limb. The form of such a coupled fold can be described

by various ratios of absolute measurements. The measurements used in this study are the height (Matthews, 1958), width, and depth (Hansen, 1963, pp. 17–20; 1968). All three distances are measured in the profile section of a fold (Fig. 101). The height (*H*) is the distance between the two hinges coupled by the short limb, measured parallel to the trace of the axial surfaces (*AT*, Fig. 101). Two lines can be constructed perpendicular to the axial traces, each tangent to the fold at a hinge and intersecting a long limb; the width (*W*) is the projected distance between the points of intersection of these lines with the long limbs, measured perpendicular to the axial traces. The width is measured at maximum height. The depth (*D*) is the length of the axial surface in profile (Fig. 101).

These distances were measured on seven of the eight folds of Fig. 100. (The eighth fold was not exposed well enough for this purpose.) The heights range from 2 to 7 mm; the mean value is 4.4 mm. The widths vary from 3 to 6 mm; the mean is 4.3 mm. And the depths vary from 2.5 to 5 cm; the mean is 3.9 cm. Height-width ratios range from 0.67 to 1.33, and their mean is 1.0; depth-width ratios range from 6.3 to 13.3, and their mean is 9.7. These values show that an average "drag fold" in this group is near the boundary between open and isoclinal ($H/W=1.0$), and that

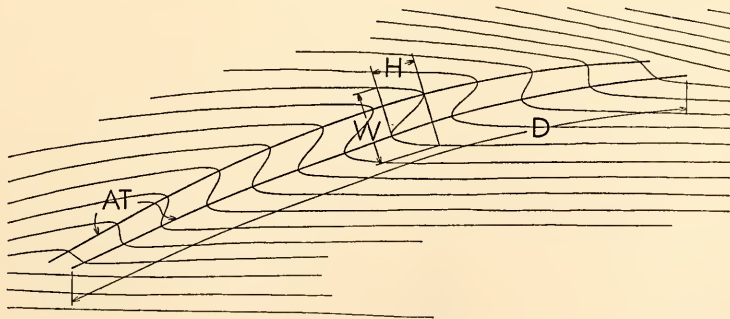


Fig. 101. Profile section of a hypothetical, coupled similar fold. *AT* are traces of the axial surfaces. *H* is the height, *W* the width, and *D* the depth.

it is an order of magnitude deeper than it is high.

To see if the form of the folds varies as a function of the angle between the fold axis and the slip-line orientation (kinematic a), the height-width ratios are plotted in Fig. 102(A) against the angle measured in S , between the fold axes and the nearest end of the separation angle (cf. Fig. 100A). A line has been fitted to the points by the method of least squares, and a correlation coefficient of 0.92 indicates that, for $(n-2)$ degrees of freedom, the correlation is significant at the 0.005 level. It is apparent from the diagram that the height of the folds increases relative to the width as the fold axis diverges from parallelism with the slip-line orientation. Thus the folds in which the fold axes are nearly parallel to the slip-line orientation are relatively open, and the folds in which the axes are nearly perpendicular to the slip-line orientation are relatively isoclinal.

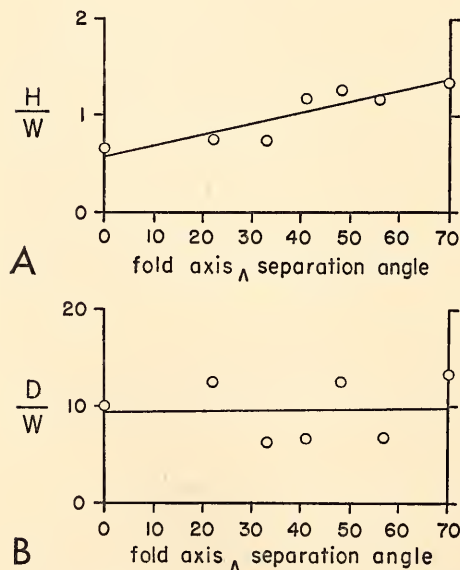


Fig. 102. Height-width ratios (A) and depth-width ratios (B) of seven "drag folds" in Fig. 100 plotted against the angle, measured in S , between the fold axes and the nearer end of the separation angle.

Ratios of depth to width are plotted in a similar fashion in Fig. 102(B). A line has been fitted to the points by the method of least squares. There appears to be no significant correlation between depth-width ratio and divergence between fold axis and slip-line orientation.

Dynamic Models

The relationships observed in the "drag folds" under consideration appear to be compatible with several modes of development, of which drag is one possibility. Three models are outlined in the following paragraphs. Primarily they seek to explain the relationship between height-width ratio and divergence between fold axis and slip-line orientation. The zone axis of axial planes and the separation angle defined by the patterns of asymmetry have been discussed previously (Hansen, *Year Book 65*, pp. 393-397). It is assumed that the "drag folds" developed by flexural slip, as inferred from their concentric profile sections and their nonparallel axial planes sharing a common axis.

1. Let us suppose that the folds develop only under drag—the traction produced on an active layer by another layer moving past it. This physical situation can be described dynamically by a single shear couple, or kinematically by a single slip-line orientation, acting parallel to the plane of layering. Depending upon the disposition of inhomogeneities that can serve as triggers within the layer, potential flexural-slip folds could develop with axes in any orientation within the plane of layering. However, the layer can only be dragged into folds about the axial orientations that the shear couple acts across; thus, potential folds with axes parallel to the shear couple (or slip-line orientation) do not develop. If the layer were dragged about all the fold axes the same distance parallel with the shear couple, the distance that the layer would become folded over itself, which is measured as the height

of a fold, would be directly proportional to the sine of the angle between the fold axis and the line of action of the shear couple. Therefore, the height would attain a maximum value in folds with axes perpendicular to the shear couple, and it would grade down to a minimum value in folds with axes nearly parallel to the couple. The height-width ratios would probably show a similar relationship (Fig. 102A) because the width of a fold appears to be more a function of the strength of the layer relative to its surroundings, which remains constant, than a function of the relative orientation of the fold to the shear couple. Of course, in nature, the layer would not be dragged exactly the same amount in every fold, and some "noise" in the relationship should be expected.

2. Suppose that the folds develop in response to a triaxial stress field ($\sigma_1 > \sigma_2 > \sigma_3$) such that σ_2 parallels the plane of layering, σ_1 makes a small angle with the layering, and the layer to be folded is under constriction. In response to the constriction, flexural-slip folds develop with fold axes in all orientations within the layering. Let us stipulate that the two principal stress directions within the layering (σ_2 and σ_{1-3} , which is the intersection of the σ_1 - σ_3 plane with the layering) are different such that $\sigma_{1-3} > \sigma_2$. If the folds develop in equal numbers in all orientations within the layering and if the strain manifested as folds is proportional to stress, it is expected that the height of the folds would attain a maximum value where fold axes are perpendicular to the direction of major compression (σ_{1-3}) and would grade down to a minimum value where fold axes are perpendicular to the direction of minor compression (σ_2). If the width of the folds did not respond in this manner but remained fairly constant as a function of the relative strength of the layer, the height-width ratios would also attain a maximum value where fold axes are perpendicular to σ_{1-3} and grade down to a minimum value where fold axes are

perpendicular to σ_2 . The maximum resolved shear stress on the plane of layering parallels σ_{1-3} ; on the assumption that slip can occur with equal ease in all directions within the layering, the maximum resolved shear stress also parallels the slip-line orientation for the whole domain. Thus, the height-width ratios should bear the same relationship to the maximum resolved shear stress and the slip-line orientation as suggested for σ_{1-3} .

3. A combination of the two models just outlined could also be proposed in which the folds develop as compressional folds under the influence of a stress field similar to the one described for model 2, but were subsequently dragged and/or flattened into the present forms under the influence of the resolved shear stresses on the layer(s). This model has been described elsewhere in detail (Hansen, *Year Book 65*, pp. 393-395).

SLIP FOLDS IN PLANES OF UNSYSTEMATIC ORIENTATION

Edward Hansen

Part of the past field season was spent working on the compound problem of the strain involved in, and the directions of flow that obtained during, the development of the earliest generation of folds in the metamorphic core of the Norwegian Caledonides. These folds are important to an understanding of orogeny because, as in most orogenic belts, they appear to involve the greatest amount of strain of all orogenic folds. Nevertheless, they are difficult to interpret because they have formed in a geosynclinal sequence practically devoid of preexisting penetrative structures providing reference to the original unstrained state and because they are superimposed by two or more subsequent generations of folds. In an attempt to minimize the former difficulty, these folds are being studied in a pre-Caledonide metamorphic terrane between Grotli and Geiranger, southern Norway (Strand, 1966; Brueckner,

1968), where they themselves may be observed superimposed upon structures of an earlier orogeny. The rocks in this area are predominantly gray gneisses and schists that are locally cut by granite veins in virtually all orientations. The most obvious folds are seen in the granite veins and are apparently slip folds. The initial problem in this study is whether the asymmetry patterns of a single system of slip folds in planes of unsystematic orientation can be used to deduce part of the movement history of the folds.

The problem can be solved by using the kind of analysis of asymmetry that has been reported earlier (*Year Book 65*, pp. 393-405). For this purpose, let us consider the hypothetical situation summarized in Fig. 103. Six planes (S_1, S_2, \dots, S_6) are intersected by a family of slip planes (S'); the orientation of the slip lines within S' is indicated by an open circle. Slip along S' is such as to

produce folds within the six planes. The axes (b'_1, b'_2, \dots, b'_6) of the resulting folds parallel the intersections of S' with the six planes. The dashed arrows drawn from the poles of S_1, S_2, \dots, S_6 to the pole of the slip planes (S') indicate the asymmetry patterns of the folds, shown by the semicircular arrows modifying the fold axes (*cf. Year Book 65*, p. 394, Fig. 107). It is clear from the resulting diagram that the asymmetry patterns of the six folds are mixed, both clockwise and counterclockwise, within the slip planes and bear no systematic relationship to the slip-line orientation. In conclusion, the asymmetry of slip folds in unsystematically oriented planes has no kinematic significance.*

* We can also regard the six planes (S_1, S_2, \dots, S_6) as different attitudes of a single surface folded about several axes, represented in the diagram by some of the mutual intersections of the planes. The conclusion also applies, therefore, to the asymmetry of slip folds in non-coaxially folded surfaces.

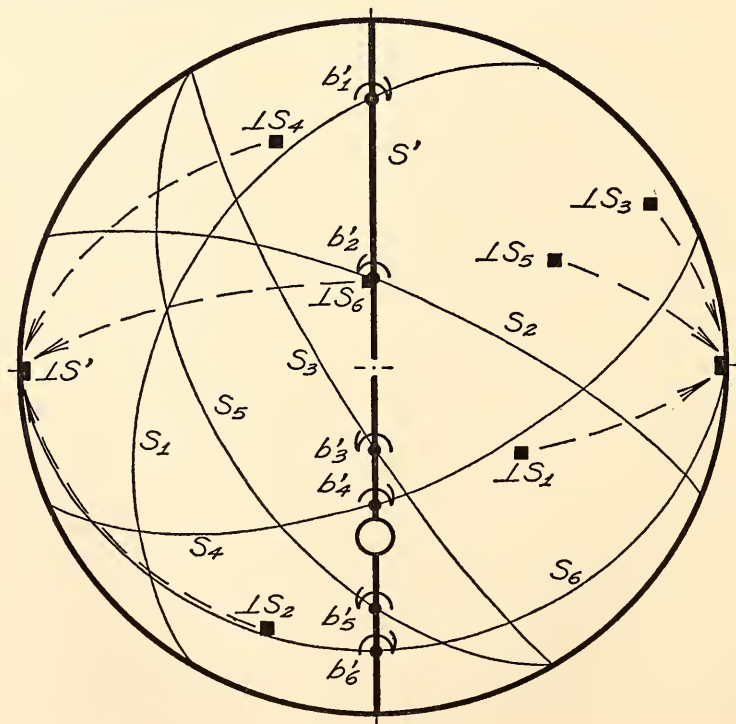


Fig. 103. Lower-hemisphere, equal-area projection of structural elements of six planes superimposed by a system of slip folds.

Nevertheless, the preceding section of this report suggests that the height-width ratios of folds might be used instead to determine the slip-line orientation that obtained during folding. The height (H) of a slip fold is proportional to the sine of the angle α between the fold axis and the slip-line orientation (*Year Book 66*, p. 539, Fig. 104*). The spacing (S) between the axial planes of slip folds coupled by a short limb is completely independent of the angle α , and the width (W) is practically independent. Therefore, we can expect the height-spacing and height-width ratios of slip

* With regard to Fig. 104 in *Year Book 66*, the height was loosely termed "amplitude (H).\" Although the amplitude (A) of a fold may, in the usage of a few workers, be equal to the short-limb height (H) of a fold (Matthews, 1958), A is best considered roughly equal to $H/2$ (cf. Ramsay, 1967; Hansen, 1968).

folds to be proportional to $\sin \alpha$, attaining their maximum values where the slip lines are perpendicular to the fold axes ($\alpha=90^\circ$) and their minimum values where the slip lines approach parallelism to the fold axes ($\alpha=0^\circ$). It follows that, in a group of slip folds with a planar distribution of fold axes, we can measure a set of either of these ratios, plot the ratios against the orientation of the fold axes, and take the minimum in the curve as the orientation of the slip lines by which the folds developed (cf. Fig. 102A).

This relationship applies to the folds in planes of random orientation in the Grotli-Geiranger area, which are the immediate concern here, and should apply also to groups of slip folds with planar distributions of fold axes in any geological situation.

STAFF ACTIVITIES

Aluminum Silicate Conference

A conference on the experimental relationships and field occurrences of the aluminum silicate minerals, kyanite, andalusite, and sillimanite was held jointly by the Geophysical Laboratory and Yale University at the Klein Geology Laboratory, New Haven, Conn., May 20-22, 1968. P. M. Bell, of the Geophysical Laboratory, and S. P. Clark, Jr., and B. J. Skinner, of Yale University, planned the conference for the purpose of analyzing recent experimental and field observations that are highly significant in interpreting the pressures and temperatures of the earth's crust.

Papers were presented by the following participants: A. Albee (California Institute of Technology), E. Althaus (Yale University), P. M. Bell (Geophysical Laboratory), C. W. Burnham (Harvard University), G. A. Chinner (Cambridge University), M. C. Gilbert (Geophysical Laboratory), H. J. Greenwood (University of British Columbia),

S. S. Hafner (University of Chicago), A. Hietanen (United States Geological Survey), M. J. Holdaway (Southern Methodist University), L. S. Hollister (University of California at Los Angeles), G. C. Kennedy (University of California at Los Angeles), O. J. Kleppa (University of Chicago), R. C. Newton (University of Chicago), S. W. Richardson (University of Edinburgh), P. Robinson (University of Massachusetts), J. L. Rosenfeld (University of California at Los Angeles), W. Schreyer (University of Kiel), R. D. Schuilling (University of The Utrecht), J. B. Thompson (Harvard University), E. Zen (United States Geological Survey). The last day of the conference included a field trip to the unusual occurrences of aluminum silicate minerals in Connecticut, led by John Rodgers of Yale University. Several papers presented at the conference will be published in the fall of 1968 in a special issue of *The American Journal of Science*, devoted to the aluminum silicates.

Journal of Petrology

The *Journal of Petrology*, aided by the careful work of an internationally renowned group of reviewers and a co-operative printer, continues to offer an outlet for definitive researches based on extensive new data bearing on major petrological problems. Volume 8 for 1967 consisted of 531 pages with contributions, by, among others, one Staff Member, one Fellow, three alumni, and one guest investigator. Professor C. E. Tilley, Research Associate, and Dr. H. S. Yoder, Jr., Staff Member, continue to serve as Editors. Professor G. M. Brown, a recent Fellow, is the Senior Managing Editor.

Lectures

During the report year staff members and fellows were invited to present lectures as follows:

P. H. Abelson made a total of 20 invited public appearances. He made speeches in the following capacities: As opening speaker ("How Man Shapes His Environment") at a special session on man-made environmental hazards at the Annual Meeting of the American Public Health Association at Miami Beach; as Distinguished Lecturer ("Chemical Events on the Primitive Earth") at the Department of Geology and Dana Club, Yale University; as a participant in a Panel on Environmental Pollution at the annual meeting of the American Association for the Advancement of Science, New York City; as the keynote speaker ("The Future of Science and Its Effects on Society") at the Southern Regional Science Seminar for University Information Officers at the College of Journalism and Communications, University of Florida, Gainesville; as 1968 Henry Darwin Rogers Lecturer ("Organic Chemicals in Rocks and Fossils") at the Department of Geology, University of Pennsylvania, Philadelphia; as a banquet speaker ("The Changing Role of Science in Our Society") at the 49th Annual Meeting of the American

Geophysical Union, Washington, D. C.; and as a speaker ("Can Man Learn to Live with Technology" at the dedication of a new science complex at the University of Puget Sound, Tacoma, Washington, where he received an Honorary Doctor of Humane Letters degree.

P. M. Bell lectured at the Department of Geology, University of Pennsylvania and gave a series of lectures at the Department of Geology, Johns Hopkins University.

On a visit to the Department of Geology of the University of Illinois, Urbana, W. B. Bryan lectured on the use of materials balance computations in the testing of petrologic hypotheses.

F. Chayes spent a month in residence at the Department of Geology of the University of Toronto and two weeks in residence at the Department of Geology of the University of Bologna, during which periods he lectured on various topics in statistical petrology and conferred extensively with faculty and students. He also delivered guest lectures at the Universities of Padua, Florence, and Rome and visited briefly with geochemists and petrologists in the universities of Cambridge, Oxford, Reading, and London (King's College). His presidential address to the annual meeting of the Mineralogical Society of America, in New Orleans, was "On locating field boundaries in simple phase diagrams by means of discriminant functions."

Gabrielle Donnay gave an invited lecture on "Solid Solutions in Mineralogy" at the Eleventh Annual Micromount Symposium in Baltimore.

A. El Goresy addressed the Department of Geology at Lehigh University.

L. W. Finger and M. C. Gilbert gave papers at the Amphibole Conference held at the University of Massachusetts.

E. Hansen addressed the Geological Society of Washington.

P. E. Hare gave invited lectures at the Marine Biology Seminar at The Lamont Geological Observatory of Columbia

University, the Biology Department of York University, Toronto, the Virginia Institute of Marine Sciences of William and Mary College, and the Geology Department at the Massachusetts Institute of Technology. He also addressed a joint seminar on paleontology at McMaster University, Canada.

T. E. Krogh lectured at the Lamont Geological Observatory of Columbia University.

G. Kullerud continued as Adjunct Professor in Geochemistry at Lehigh University where he supervised the sulfide research program and lectured three hours per month. He also served as a Visiting Professor at Heidelberg University and delivered five lectures and conducted seminars in the Mineralogisch-Petrographisches Institut of that University. In addition, he served as a Consulting Professor to the Department of Geosciences, Texas Technological College, Lubbock, Texas. He conducted a five-week lecture series on sulfide phase equilibria at the Department of Geology at the University of Colorado. He also gave an invited lecture at the symposium on "Experimental Methods in Petrology and Ore Genesis" at the University of Western Ontario, London, Canada. Dr. Kullerud lectured in the Mineralogisches Institut der Universität Frankfurt, the Geologisches Institut der Universität zu Köln, the Mineralogisches Institut der Universität Saarbrücken and the Institut für Mineralogie und Kristallographie der Universität Stuttgart. He also presented a lecture on "Current Research in the Field of Sulfide Mineralogy" at a meeting of the Lubbock Geological Society.

D. H. Lindsley presented an invited paper at a Symposium on Experimental Methods in Petrology and Ore Genesis at the University of Western Ontario. He also gave lectures at the geology departments at Johns Hopkins University, McGill University, Princeton University, and the State University of New York at Stony Brook.

J. L. Munoz lectured at the Department of Geology at Johns Hopkins University.

H. R. Puchelt gave invited lectures at the departments of geology at Rensselaer Polytechnic Institute and Lehigh University and at the Department of Geochemistry and Mineralogy at the Pennsylvania State University.

J. F. Schairer gave a series of three lectures each at the Department of Geology, Memorial University of Newfoundland, and the Department of Geology at the University of New Brunswick, Canada. He also presented a paper at the symposium on "Experimental Methods in Petrology and Ore Genesis" at the University of Western Ontario.

W. H. Scott lectured at the Department of Geology at the University of Minnesota.

H. S. Yoder, Jr., gave four lectures at the Department of Geology, University of Witwatersrand, Republic of South Africa. Fifteen lectures on experimental results bearing on major petrological problems were presented at the Department of Geology, University of Cape Town, Republic of South Africa. Both visits in South Africa were sponsored in part by the Students' Visiting Lecturers' Organization.

Petrologists' Club

Six meetings were held during the 57th year of the Petrologists' Club, and the following lectures were presented:

"Feldspar crystallization in trachytes from Ischia," by W. S. MacKenzie (University of Manchester), November 16, 1967.

"Petrology of the Kiglapait layered intrusion, Labrador," by Stearns A. Morse (Geophysical Laboratory), December 5, 1967.

"Large gravity slides in the Mediterranean and Appalachian regions," by John Rodgers (Yale University), December 18, 1967.

"Strontium isotopic composition and petrogenesis of potassic rocks," by James L. Powell (Oberlin College), March 19, 1968.

"Applications of optical and infrared spectroscopy in mineralogy," by William

White (Pennsylvania State University), April 2, 1968.

"Conditions of garnet genesis from elastic effects around inclusions," by John Rosenfeld (University of California at Los Angeles), April 16, 1968.

BIBLIOGRAPHY

- Abelson, P. H., Conversion of biochemicals to kerogen and *n*-paraffins, in *Researches in Geochemistry*, Vol. 2, P. H. Abelson, ed., John Wiley and Sons, Inc., New York, 63-86, 1967.
- Allmann, R., *see* Donnay, G.
- Bell, P. M., Geophysical research at pressures above 30 kilobars, *Trans. Am. Geophys. Union*, 48, 666-671, 1967.
- Bell, P. M., and J. L. England, High-pressure experimental techniques, in *Researches in Geochemistry*, Vol. 2, P. H. Abelson, ed., John Wiley and Sons, Inc., New York, 619-638, 1967.
- Boyd, F. R., Petrological problems in high-pressure research, in *Researches in Geochemistry*, Vol. 2, P. H. Abelson, ed., John Wiley and Sons, Inc., New York, 593-618, 1967.
- Burnham, C. W., *see* Güven, N.
- Carmichael, I. S. E., *see* Lindsley, D. H.
- Chayes, F., On the graphical appraisal of the strength of associations in petrographic variation diagrams, in *Researches in Geochemistry*, Vol. 2, P. H. Abelson, ed., John Wiley and Sons, Inc., New York, 322-339, 1967.
- Chayes, F., On locating field boundaries in simple phase diagrams by means of discriminant functions, *Am. Mineralogist*, 53, 359-371, 1968.
- Coleman, L. B., *see* Donnay, G.
- Cowan, D. O., N. G. Krieghoff, and G. Donnay, Reinvestigation of the reaction of trimethylplatinum (IV) iodide with methylsodium, *Acta Cryst.*, B24, 287-288, 1968.
- Cowan, D. O., *see also* Donnay, G.
- Craig, J. R., and G. Kullerud, Phase relations and mineral assemblages in the copper-lead-sulfur system, *Am. Mineralogist*, 53, 145-161, 1968.
- Craig, J. R., *see also* Naldrett, A. J.
- Davis, G. L., *see* Wetherill, G. W.
- Donnay, G., and R. Allmann, Si_2O_{10} groups in the crystal structure of ardeninite, *Acta Cryst.*, B24, 845-855, 1968.
- Donnay, G., L. B. Coleman, N. G. Krieghoff, and D. O. Cowan, Trimethylplatinum (IV) iodide and its misrepresentation as hexamethylidiplatinum, *Acta Cryst.*, B24, 157-159, 1968.
- Donnay, G., *see also* Cowan, D. O.
- England, J. L., *see* Bell, P. M.
- Güven, N., and C. W. Burnham, The crystal structure of 3T muscovite, *Z. Krist.*, 125, 163-183, 1967.
- Hoering, T. C., The organic geochemistry of Precambrian rocks, in *Researches in Geochemistry*, Vol. 2, P. H. Abelson, ed., John Wiley and Sons, Inc., New York, 87-111, 1967.
- Krieghoff, N. G., *see* Cowan, D. O.; Donnay, G.
- Kullerud, G., Sulfide studies, in *Researches in Geochemistry*, Vol. 2, P. H. Abelson, ed., John Wiley and Sons, Inc., New York, 286-321, 1967.
- Kullerud, G., *see also* Craig, J. R.; Naldrett, A. J.
- Lee-Hu, C., *see* Wetherill, G. W.
- Lindsley, D. H., I. S. E. Carmichael, and J. Nicholls, Iron-titanium oxides and oxygen fugacities in volcanic rocks: A correction, *J. Geophys. Res.*, 73, 3351-3352, 1968.
- Lindsley, D. H., D. H. Speidel, and R. H. Nafziger, *P-T-f_{O2}* relations for the system Fe-O-SiO₂, *Am. J. Sci.*, 266, 342-360, 1968.
- Meyer, H. O. A., Chrome pyrope: An inclusion in natural diamond, *Science*, 160, 1446-1447, 1968.
- Nafziger, R. H., *see* Lindsley, D. H.
- Naldrett, A. J., J. R. Craig, and G. Kullerud, The central portion of the Fe-Ni-S system and its bearing on pentlandite exsolution in iron-nickel sulfide ores, *Econ. Geol.*, 62, 826-847, 1967.
- Naldrett, A. J., and G. Kullerud, A study of the Strathcona Mine and its bearing on the origin of the nickel-copper ores of the Sudbury District, Ontario, *J. Petrol.*, 8, 453-531, 1967.
- Nicholls, J., *see* Lindsley, D. H.
- O'Hara, M. J., and H. S. Yoder, Jr., Formation

and fractionation of basic magmas at high pressures, *Scot. J. Geol.*, **3**, 67-117, 1967.

Schairer, J. F., Phase equilibria at one atmosphere related to tholeiitic and alkali basalts, in *Researches in Geochemistry*, Vol. 2, P. H. Abelson, ed., John Wiley and Sons, Inc., New York, 568-592, 1967.

Speidel, D. H., see Lindsley, D. H.

Stewart, D. B., Four-phase curve in the system

$\text{CaAl}_2\text{Si}_2\text{O}_8\text{-SiO}_2\text{-H}_2\text{O}$ between 1 and 10 kilobars, *Schweiz. Mineral. Petrog. Mitt.*, **47**, 35-59, 1967.

Wetherill, G. W., G. L. Davis, and C. Lee-Hu, Rb-Sr measurements on whole rocks and separated minerals from the Baltimore gneiss, Md., *Geol. Soc. Am. Bull.*, **79**, 757-762, 1968.

Yoder, H. S., Jr., see O'Hara, M. J.

REFERENCES CITED

- Abelson, P. H., Geochemistry of organic substances, in *Researches in Geochemistry*, Vol. 1, P. H. Abelson, ed., John Wiley and Sons, Inc., New York, 79-103, 1959.
- Akimoto, S., H. Fujisawa, and T. Katsura, Synthesis of FeSiO_3 pyroxene (ferrosilite) at high pressures, *Proc. Japan Acad.*, **40**, 272-275, 1964.
- Akimoto, S., T. Katsura, Y. Syono, H. Fujisawa, and E. Komada, Polymorphic transition of pyroxenes FeSiO_3 and CoSiO_3 at high pressures and temperatures, *J. Geophys. Res.*, **70**, 5269-5278, 1965.
- Albers, W., and C. J. M. Rooymans, High-pressure polymorphism of spinel compounds, *Solid State Communications*, **3**, 417-419, 1965.
- Alexandrov, K. S., and T. V. Ryzhova, The elastic properties of rock-forming minerals, *Izv. Acad. Sci. USSR, Geophys. Ser. (English Transl.)*, **9**, 871-875, 1961.
- Atlas, L., The polymorphism of MgSiO_3 and solid state equilibria in the system $\text{MgSiO}_3\text{-CaMgSi}_2\text{O}_6$, *J. Geol.*, **60**, 125-147, 1952.
- Barton, R., Jr., Refinement of the crystal structure of buergerite and the absolute orientation of tourmalines, unpublished Ph.D. thesis, The Johns Hopkins University, 1967.
- Birch, F., Density and composition of the mantle and core, *J. Geophys. Res.*, **69**, 4377-4888, 1964.
- Birch, F., Compressibility: Elastic constants, in "Handbook of Physical Constants," revised ed., *Geol. Soc. Am. Mem.* **97**, 97-173, 1966.
- Birch, F., and P. LeComte, Temperature-pressure plane for albite composition, *Am. J. Sci.*, **258**, 209-217, 1960.
- Bobrievich, A. P., M. N. Bondarenko, M. A. Gnevushev, L. M. Krusov, G. I. Smirnov, and R. K. Yurkevich, *Diamond Deposits of Yakutia*, State Sci.-Techn. Publ. Lit. on Geol. and Prot. Min. Res., Moscow, 1959.
- Bowen, N. L., The melting phenomena of the plagioclase feldspars, *Am. J. Sci.*, **35**, 577-599, 1913.
- Bowen, N. L., The ternary system diopside-forsterite-silica, *Am. J. Sci.*, **38**, 207-264, 1914.
- Bowen, N. L., Phase equilibria bearing on the origin and differentiation of alkaline rocks, *Am. J. Sci.*, **243A**, 75-89, 1945.
- Bowen, N. L., and O. Andersen, The binary system MgO-SiO_2 , *Am. J. Sci.*, **37**, 487-500, 1914.
- Bowen, N. L., and J. F. Schairer, The system MgO-FeO-SiO_2 , *Am. J. Sci.*, **29**, 151-217, 1935.
- Bowen, N. L., J. F. Schairer, and E. Posnjak, The system CaO-FeO-SiO_2 , *Am. J. Sci.*, **26**, 193-284, 1933.
- Bowen, N. L., and O. F. Tuttle, The system $\text{NaAlSi}_3\text{O}_8\text{-KAlSi}_3\text{O}_8\text{-H}_2\text{O}$, *J. Geol.*, **58**, 489-511, 1950.
- Boyd, F. R., Hydrothermal investigations of amphiboles, in *Researches in Geochemistry*, Vol. 1, P. H. Abelson, ed., John Wiley and Sons, Inc., New York, 377-396, 1959.
- Boyd, F. R., Electron-probe studies of diopsides from kimberlite, *Am. J. Sci.*, *Schairer Vol.*, in press, 1968.
- Boyd, F. R., and J. L. England, Apparatus for phase-equilibrium measurements at pressures up to 50 kb and temperatures up to 1750° C, *J. Geophys. Res.*, **65**, 741-748, 1960.
- Boyd, F. R., and J. L. England, Effect of pressure on the melting of diopside, $\text{CaMgSi}_2\text{O}_6$, and albite, $\text{NaAlSi}_3\text{O}_8$, in the range up to 50 kb, *J. Geophys. Res.*, **68**, 311-323, 1963.
- Boyd, F. R., J. L. England, and B. T. C. Davis, Effects of pressure on the melting and polymorphism of enstatite, MgSiO_3 , *J. Geophys. Res.*, **69**, 2101-2109, 1964.
- Boyd, F. R., and J. F. Schairer, The system $\text{MgSiO}_3\text{-CaMgSi}_2\text{O}_6$, *J. Petrol.*, **5**, 275-309, 1964.
- Brown, G. M., Pyroxenes from the early and middle stages of fractionation of the Skaergaard intrusion, east Greenland, *Mineral. Mag.*, **31**, 511-543, 1957.
- Brown, G. M., and E. A. Vincent, Pyroxenes from the late stages of fractionation of the Skaergaard intrusion, east Greenland, *J. Petrol.*, **4**, 174-196, 1963.

- Brueckner, H. K., Relations of anorthosite, eclogite, and ultramafic rock to the country rock, Tafjord area, Norway, unpublished Ph.D. thesis, Yale University, 1968.
- Bryan, W. B., Mineralogy and petrochemical relations of volcanic rocks from the Carnarvon Range, Queensland, Australia, *Bull. Volcanol.*, in press, 1968.
- Buerger, M. J., C. W. Burnham, and D. R. Peacor, Assessment of the several structures proposed for tourmaline, *Acta Cryst.*, **15**, 583-590, 1962.
- Carman, J. H., and O. F. Tuttle, Experimental verification of solid solution of excess silica in sanidine from rhyolites (abstract), *Geol. Soc. Am. Spec. Paper*, in press, 1968.
- Chayes, F., Relative abundance of intermediate members of the oceanic basalt-trachyte association, *J. Geophys. Res.*, **68**, 1519-1534, 1963.
- Chayes, F., Alkaline and subalkaline basalts, *Am. J. Sci.*, **264**, 128-145, 1966.
- Clark, S. P., Jr., Variation of density in the earth and the melting curve in the mantle, in *Earth Science: Problems and Progress in Current Research*, T. W. Donnelly, ed., University of Chicago Press, 1963.
- Clark, S. P., Jr., and A. E. Ringwood, Density distribution and constitution of the mantle, *Rev. Geophys.*, **2**, 35-88, 1964.
- Coes, L., Jr., High-pressure minerals, *J. Am. Ceram. Soc.*, **38**, 298, 1955.
- Coleman, R. G., O. E. Lee, L. B. Beatty, and W. W. Brannoch, Eclogites and eclogites: Their differences and similarities, *Geol. Soc. Am. Bull.*, **76**, 483-508, 1965.
- Crowley, N. S., and R. Roy, Crystalline solubility in the muscovite and phlogopite groups, *Am. Mineralogist*, **49**, 348-362, 1964.
- Davis, B. T. C., and F. R. Boyd, The join $Mg_2Si_2O_6$ - $CaMgSi_2O_6$ at 30 kb pressure and its application to pyroxenes from kimberlites, *J. Geophys. Res.*, **71**, 3567-3576, 1966.
- Davis, B. T. C., and J. L. England, The melting of forsterite up to 50 kb, *J. Geophys. Res.*, **69**, 1113-1116, 1964.
- Degens, E. T., *Geochemistry of Sediments*, Prentice-Hall, Englewood Cliffs, N. J., 1965.
- Deland, A. N., The boundary between the Timiskaming and Grenville subprovince in the Surprise Lake area, Quebec, *Proc. Geol. Assoc. Can.*, **8**, 127-141, 1956.
- Desautels, P. E., The morphology of mckelveyite, *Am. Mineralogist*, **52**, 860-864, 1967.
- DeVries, R. C., R. Roy, and E. F. Osborn, Phase equilibrium in the system CaO - TiO_2 - SiO_2 , *J. Am. Ceram. Soc.*, **38**, 153-171, 1956.
- Dimroth, Erich, Untersuchungen zum Mechanismus von Blastesis und Syntexis in Phylliten und Hornfelsen des südwestlichen Fichtelgebirges, *Tschermaks Mineral. Petrog. Mitt.*, 3rd Ser., **8**, 248-274, 1962a.
- Dimroth, Erich, Eine Theorie der Korngestügestatistik, *Neues Jahrb. Mineral., Monatsh.*, 218-229, 1962b.
- Dimroth, Erich, Fortschritte der Gefügestatistik, *Neues Jahrb. Mineral., Monatsh.*, 186-192, 1963.
- Donnay, G., The "polycrystal," a product of syntaxial intergrowth (abstract), American Crystallographic Association Meeting, Program and Abstracts, Abstract 16, June 1953.
- Donnay, G., and J. D. H. Donnay, Crystallography of bastnaesite, parisite, roentgenite, and synchisite, *Am. Mineralogist*, **38**, 932-963, 1953.
- Donnay, G., and J. D. H. Donnay, Optical analyzer, *Rev. Sci. Instr.*, **28**, 145, 1957.
- Donnay, G., and J. D. H. Donnay, The theory of the optical analyzer (abstract), American Crystallographic Association, Austin Meeting, Program and Abstracts, p. 44, 1966.
- Donnay, J. D. H., and D. Harker, A new law of crystal morphology extending the Law of Bravais, *Am. Mineralogist*, **22**, 446-467, 1937.
- Duncumb, P., and P. K. Shields, The present state of quantitative X-ray microanalysis, Part I, Physical basis, *Brit. J. Appl. Phys.*, **14**, 617-625, 1963.
- Earnshaw, A., and J. Lewis, Magnetic properties of some binuclear complexes of chromium and iron, *Nature*, **181**, 1262-1263, 1958.
- Earnshaw, A., and J. Lewis, Polynuclear compounds, Part I, Magnetic properties of some binuclear complexes, *J. Chem. Soc.*, 396-404, 1960.
- Eckermann, H. von, The alkaline district of Alnö Island, *Sveriges Geol. Undersökn., Ser. Ca, Avhandl. Uppsat.*, no. 36, 1948.
- El Goresy, A., Mineralbestand und Strukturen der Graphit- und Sulfideinschlüsse in Eisenmeteoriten, *Geochim. Cosmochim. Acta*, **29**, 1131-1151, 1965.
- El Goresy, A., Quantitative electron microprobe analysis of coexisting sphalerite, daubréelite and troilite in the Odessa iron meteorite and their genetic implications, *Geochim. Cosmochim. Acta*, **31**, 1667-1676, 1967.
- Emslie, R. F., The Michikamau anorthositic intrusion, Labrador, *Can. J. Earth Sci.*, **2**, 385-399, 1965.
- Emslie, R. F., Crystallization and differentiation of the Michikamau intrusion, in *Origin of Anorthosite and Related Rocks*, Y. Isachsen, ed., New York State Museum and Science Survey Memoir 18, in press, 1968.
- Engel, A. E. J., C. G. Engel, and R. G. Havens, Chemical characteristics of oceanic basalts

- and the upper mantle, *Geol. Soc. Am. Bull.*, **76**, 719-734, 1965.
- Epstein, S., and H. P. Taylor, Jr., Variation of O^{18}/O^{16} in minerals and rocks, in *Researches in Geochemistry*, Vol. 2, P. H. Abelson, ed., John Wiley and Sons, Inc., New York, 29-62, 1967.
- Erd, R. C., H. T. Evans, Jr., and D. H. Richter, Smythite, a new iron sulfide, and associated pyrrhotite from Indiana, *Am. Mineralogist*, **42**, 309-333, 1957.
- Erickson, R. L., and L. V. Blade, Geochemistry and petrology of the alkalic igneous complex at Magnet Cove, Arkansas, *U. S. Geol. Surv. Prof. Paper*, **425**, 1963.
- Erlank, A. J., R. V. Danchin, and C. C. Furlard, High K/Rb ratios in rocks from the Bushveld igneous complex, South Africa, *Earth and Planetary Sci. Letters*, **4**, 22-29, 1968.
- Ernst, W. G., Stability relations of glaucophane, *Am. J. Sci.*, **259**, 735-765, 1961.
- Ernst, W. G., Polymorphism in alkali amphiboles, *Am. Mineralogist*, **48**, 241-260, 1963.
- Ernst, W. G., *Amphiboles*, Springer-Verlag, New York, 1968.
- Espinosa, G. P., A crystal chemical study of titanium and chromium substituted yttrium iron and gallium garnets, *Inorg. Chem.*, **3**, 848-850, 1964.
- Eugster, H. P., and G. B. Skippen, Igneous and metamorphic reactions involving gas equilibria, in *Researches in Geochemistry*, Vol. 2, P. H. Abelson, ed., John Wiley and Sons, Inc., New York, 492-520, 1967.
- Fairbairn, H. W., and others, A cooperative investigation of precision and accuracy in chemical, spectrochemical, and modal analysis of silicate rocks, *U. S. Geol. Surv. Bull.*, **980**, 71 pp., 1951.
- Fiala, J., Pyrope of some garnet peridotites of the Czech massif, *Krystalinikum*, **3**, 55-74, 1965.
- Finger, L. W., and T. Zoltai, Cation distribution in grunerite (abstract), *Trans. Am. Geophys. Union*, **48**, 233-234, 1967.
- Fischer, K., A further refinement of the crystal structure of cummingtonite, $(Mg,Fe)_7(Si_4O_{11})_2(OH)_2$, *Am. Mineralogist*, **51**, 814-818, 1966.
- Foster, W. R., The system $NaAlSi_3O_8$ - $CaSiO_3$ - $NaAlSiO_4$, *J. Geol.*, **50**, 152-173, 1942.
- Foster, W. R., High-temperature X-ray diffraction study of the polymorphism of $MgSiO_3$, *J. Am. Ceram. Soc.*, **34**, 255-259, 1951.
- Gast, P. W., Terrestrial ratio of potassium to rubidium and the composition of the earth's mantle, *Science*, **147**, 858-860, 1965.
- Gay, P., and R. W. LeMaitre, Observations on iddingsite, *Am. Mineralogist*, **46**, 92-111, 1961.
- Geller, S., Crystal chemistry of the garnets, *Z. Krist.*, **125**, 1-47, 1967.
- Geller, S., C. E. Miller, and R. G. Treuting, New synthetic garnets, *Acta Cryst.*, **13**, 179-186, 1960.
- Ghose, S., and E. Hellner, The crystal structure of grunerite and observations on the Mg-Fe distribution, *J. Geol.*, **67**, 691-701, 1959.
- Gill, J. B., Some implications of the abundance of K, Rb, Ba, and Sr in the Nain anorthosite, Labrador, M.Sc. thesis, Franklin and Marshall College, 1968.
- Gold, D. P., The minerals of the Oka carbonate and alkaline complex, Oka, Quebec, *Papers Proc. Intern. Mineral. Soc., 4th Gen. Meeting, New Delhi*, 109-125, 1966.
- Goodell, H. G., and N. D. Watkins, The paleomagnetic stratigraphy of the southern ocean, *Deep-Sea Res.*, **15**, 89-112, 1968.
- Green, D. C., The volcanic rocks of Mt. Tamborine, S. E. Queensland, Unpublished M.Sc. thesis, University of Queensland, 1964.
- Green, D. C., Further evidence for a continuum of basaltic compositions, from southeast Queensland, *J. Geol. Soc. Australia*, in press, 1968.
- Green, D. H., and A. E. Ringwood, An experimental investigation of the gabbro to eclogite transformation and its petrological applications, *Geochim. Cosmochim. Acta*, **31**, 767-833, 1967.
- Green, T. H., High pressure experiments on the genesis of anorthosites, in *Petrology of the Upper Mantle*, Publication no. 444, Department of Geophysics and Geochemistry, Australian National University, 206-233, 1966.
- Green, T. H., and A. E. Ringwood, Crystallization of basalt and andesite under high pressure hydrous conditions, *Earth and Planetary Sci. Letters*, **3**, 481-489, 1967.
- Greenwood, H. J., The synthesis and stability of anthophyllite, *J. Petrol.*, **4**, 317-351, 1963.
- Greig, J. W., Immiscibility in silicate melts, *Am. J. Sci.*, **13**, 1-44, 1927.
- Hamilton, D. L., and W. S. MacKenzie, Nepheline solid solution in the system $NaAlSiO_4$ - $KAlSiO_4$ - SiO_2 , *J. Petrol.*, **1**, 56-72, 1960.
- Hamilton, D. L., and W. S. MacKenzie, Phase equilibrium studies in the system $NaAlSiO_4$ (nepheline)- $KAlSiO_4$ (kalsilite)- SiO_2 - H_2O , *Mineral. Mag.*, **34**, 214-231, 1965.
- Hansen, E., Strain facies of the metamorphic rocks in Trollheimen, Norway, unpublished Ph.D. thesis, Yale University, 1963.
- Hansen, E., *Strain Facies*, Springer-Verlag, New York, in press, 1968.

- Hansen, E., S. C. Porter, B. A. Hall, and A. Hills, Décollement structures in glacial-lake sediments, *Geol. Soc. Am. Bull.*, **72**, 1415-1418, 1961.
- Hansen, M., and K. Anderko, *Constitution of Binary Alloys*, McGraw-Hill Book Co., Inc., New York, 2nd ed., 1958.
- Hart, S. R., and L. T. Aldrich, Fractionation of potassium/rubidium by amphiboles: Implications regarding mantle composition, *Science*, **155**, 325-327, 1967.
- Hays, J. F., Stability and properties of the synthetic pyroxene $\text{CaAl}_2\text{SiO}_6$, *Am. Mineralogist*, **51**, 1524-1529, 1966.
- Heath, S. A., $\text{Sr}^{87}/\text{Sr}^{86}$ ratios in anorthosites and some associated rocks, in *M.I.T. 14th Annual Progress Report for the U. S. Atomic Energy Commission*, 151-155, 1966.
- Hegemann, F., and A. Maucher, Die Bildungsgeschichte der Kieslagerstätte im Silberberg bei Bodenmais, *Abhandl. Geol. Landesunters. Bayer. Oberbergamt*, **11**, 4-36, 1933.
- Heinrich, K. F. J., X-ray absorption uncertainty, in *The Electron Microprobe*, T. D. McKinley, K. F. J. Heinrich, and D. B. Wittry, eds., pp. 296-377, John Wiley and Sons, Inc., New York, 1966.
- Hess, H. H., Chemical composition and optical properties of common pyroxenes, Part I, *Am. Mineralogist*, **54**, 621-666, 1949.
- Hsu, L. C., Melting of fayalite up to 40 kb, *J. Geophys. Res.*, **72**, 4235-4244, 1967.
- Irvine, T. N., Chromian spinel as a petrogenetic indicator, Part 2, Petrologic applications, *Can. J. Earth Sci.*, **4**, 71-104, 1967.
- Ito, J., and C. Frondel, Synthetic zirconium and titanium garnets, *Am. Mineralogist*, **52**, 773-781, 1967.
- Ito, T., and R. Sadanaga, A Fourier analysis of the structure of tourmaline, *Acta Cryst.*, **4**, 385-390, 1951.
- Jellinek, F., The structures of the chromium sulphides, *Acta Cryst.*, **10**, 620-628, 1957.
- Jung, D., Untersuchungen am tholeyt von Tholey (Saar), *Beitr. Mineral. Petrog.*, **6**, 147-181, 1958.
- Kermack, K. A., and J. B. S. Haldane, Organic correlation and allometry, *Biometrika*, **37**, 30-41, 1950.
- King, B. C., The Napak area of southern Karamoja, Uganda, *Geol. Surv. Uganda Mem.*, **5**, 1949.
- Klein, C., Jr., Cummingtonite-grunerite series: A chemical, optical and X-ray study, *Am. Mineralogist*, **49**, 963-982, 1964.
- Klein, C., Jr., and D. R. Waldbaum, X-ray crystallographic properties of the cummingtonite-grunerite series, *J. Geol.*, **75**, 379-392, 1967.
- Knopf, E. B., and E. Ingerson, Structural petrology, *Geol. Soc. Am. Mem.*, **6**, 1938.
- Kraut, E. A., and G. C. Kennedy, New melting law at high pressures, *Phys. Rev. Letters*, **16**, 608-609, 1966a.
- Kraut, E. A., and G. C. Kennedy, New melting law at high pressures, *Phys. Rev.*, **151**, 668-675, 1966b.
- Kruskal, W. H., On the uniqueness of the line of organic correlation, *Biometrics*, **9**, 47-58, 1953.
- Kullerud, G., The FeS-ZnS system; a geological thermometer, *Norsk Geol. Tidsskr.*, **32**, 61-147, 1953.
- Kullerud, G., Thermal stability of pentlandite, *Can. Mineralogist*, **7**, 353-366, 1963.
- Kullerud, G., Covellite stability relations in the Cu-S system, *Freiberger Forschungsh.*, **C**, **186**, 145-160, 1965.
- Kullerud, G., and G. Donnay, Natural and synthetic ferrosilite: A roentgenographic mimesis of rammelsbergite, *Geochim. Cosmochim. Acta*, **15**, 73-79, 1953.
- Kullerud, G., and R. A. Yund, The Ni-S system and related minerals, *J. Petrol.*, **3**, 126-175, 1962.
- Kuno, H., Review of pyroxene relations in terrestrial rocks in the light of recent experimental works, *Mineral. J. (Tokyo)*, **5**, 21-43, 1966.
- Kushiro, I., Si-Al relation in clinopyroxenes from igneous rocks, *Am. J. Sci.*, **258**, 548-554, 1960.
- Kushiro, I., State of H_2O in the upper mantle, Sobolev Vol., USSR, in press, 1968a.
- Kushiro, I., Compositions of magmas formed by partial zone melting in the earth's upper mantle, *J. Geophys. Res.*, **73**, 619-634, 1968b.
- Kushiro, I., Y. Syono, and S. Akimoto, Stability of phlogopite at high pressures and possible presence of phlogopite in the earth's upper mantle, *Earth and Planetary Sci. Letters*, **3**, 197-203, 1967.
- Kushiro, I., and H. S. Yoder, Jr., Anorthite-forsterite and anorthite-enstatite reactions and their bearing on the basalt-eclogite transformation, *J. Petrol.*, **7**, 337-362, 1966.
- Kushiro, I., H. S. Yoder, Jr., and M. Nishikawa, Effect of water on the melting of enstatite, *Geol. Soc. Am. Bull.*, **79**, 1685-1692, 1968.
- Larsen, E. S., Alkaline rocks of Iron Hill, Gunnison County, Colorado, *U. S. Geol. Surv. Prof. Paper*, **197A**, 1941.
- Legendre, A. M., Méthodes pour la détermination des orbites des comètes, Paris, 1805.
- Lessing, P., R. W. Decker, and R. C. Reynolds, Jr., Potassium and rubidium distribution in

- Hawaiian lavas, *J. Geophys. Res.*, **68**, 5851-5855, 1963.
- Li, C.-T., The crystal structure of $\text{LiAlSi}_2\text{O}_6$ -III (abstract), Program, Summer Meeting, American Crystallographic Association, August 20-25, Minneapolis, Minn., 1967.
- Lindsley, D. H., Melting relations of KAlSi_3O_8 : Effect of pressure up to 40 kb, *Am. Mineralogist*, **51**, 1793-1799, 1966.
- Lindsley, D. H., B. T. C. Davis, and I. D. MacGregor, Ferrosilite (FeSiO_3): Synthesis at high pressures and temperatures, *Science*, **144**, 73-74, 1964.
- Lindsley, D. H., D. H. Speidel, and R. H. Nafziger, P - T - f_{O_2} relations for the system Fe-O-SiO_2 , *Am. J. Sci.*, **266**, 342-360, 1968.
- Luedemann, H. D., and G. C. Kennedy, Melting curves of lithium, sodium, potassium, and rubidium to 80 kb, *J. Geophys. Res.*, **73**, 2795-2805, 1968.
- Luth, W. C., Studies in the system $\text{KAlSiO}_4\text{-Mg}_2\text{SiO}_4\text{-SiO}_2\text{-H}_2\text{O}$: I, Inferred phase relations and petrologic applications, *J. Petrol.*, **8**, 372-416, 1967.
- Luth, W. C., R. H. Jahns, and O. F. Tuttle, The granite system at pressures of 4 to 10 kb, *J. Geophys. Res.*, **69**, 759-773, 1964.
- Luth, W. C., and O. F. Tuttle, The alkali feldspar solvus in the system $\text{Na}_2\text{O-K}_2\text{O-Al}_2\text{O}_3\text{-SiO}_2\text{-H}_2\text{O}$, *Am. Mineralogist*, **51**, 1359-1373, 1966.
- Macdonald, G. A., and T. Katsura, Chemical composition of Hawaiian lavas, *J. Petrol.*, **5**, 82-133, 1964.
- Manning, P. G., The optical absorption spectra of some andradites and the identification of the ${}^6\text{A}_1 \rightarrow {}^4\text{A}_1$ ${}^4\text{E}(\text{G})$ transition in octahedrally bonded Fe^{2+} , *Can. J. Earth Sci.*, **4**, 1039-1047, 1967.
- Mason, B., Composition of the earth, *Nature*, **211**, 616-618, 1966.
- Mason, B., G. Donnay, and L. A. Hardie, Ferrie tourmaline from Mexico, *Science*, **144**, 71-73, 1964.
- Matthews, D. H., Dimensions of asymmetrical folds, *Geol. Mag.*, **95**, 511-513, 1958.
- McDougall, I., and J. F. G. Wilkinson, Potassium-argon dates on some Cainozoic volcanic rocks from northeastern New South Wales, *J. Geol. Soc. Australia*, **14**, 225-233, 1967.
- Mercy, E. L. P., and M. J. O'Hara, Distribution of Mn, Cr, Ti, and Ni in coexisting minerals of ultramafic rocks, *Geochim. Cosmochim. Acta*, **31**, 2331-2341, 1967.
- Meyer, H. O. A., Chrome pyrope: An inclusion in natural diamond, *Science*, **160**, 1446-1447, 1968.
- Milton, C., B. Ingram, J. R. Clark, and E. J. Dwornik, Mckelveyite, a new hydrous sodium barium rare-earth uranium carbonate mineral from the Green River formation, Wyoming, *Am. Mineralogist*, **50**, 593-612, 1965.
- Mitchell, R. S., and A. A. Giardini, Oriented olivine inclusions in diamond, *Am. Mineralogist*, **38**, 136-138, 1953.
- Moh, G. H., Experimentelle Untersuchungen an Zinnkiesen und analogen Germaniumverbindungen, *Neues Jahrb. Mineral., Abhandl.*, **94**, 1125-1146, 1960.
- Morimoto, N., and G. Kullerud, Polymorphism in digenite, *Am. Mineralogist*, **48**, 110-123, 1963.
- Morse, S. A., The Kiglapait layered intrusion, Labrador, *Geol. Soc. Am. Mem.*, **111**, in press, 1968.
- Morse, S. A., and G. L. Davis, K/Rb fractionation in the Kiglapait layered intrusion (abstract), *Geol. Soc. Am. Spec. Paper* **101**, 145, 1968.
- Morse, S. A., and R. E. Stoiber, Preliminary report on Fe-Ti oxides from the Kiglapait layered intrusion (abstract), *Trans. Am. Geophys. Union*, **47**, 210, 1966.
- Muir, I. D., The clinopyroxenes of the Skaergaard intrusion, eastern Greenland, *Mineral. Mag.*, **29**, 690-714, 1951.
- Munro, M., Errors in measurement of $2V$ with the universal stage, *Am. Mineralogist*, **48**, 308-323, 1963.
- Naldrett, A. J., J. R. Craig, and G. Kullerud, The central portion of the Fe-Ni-S system and its bearing on pentlandite exsolution in iron-nickel sulfide ores, *Econ. Geol.*, **62**, 826-847, 1967.
- Newton, R. C., Kyanite-andalusite equilibrium from 700° C to 800° C, *Science*, **153**, 170-172, 1966.
- Newton, R. C., and J. V. Smith, Investigations concerning the breakdown of albite at depth in the earth, *J. Geol.*, **75**, 268-286, 1967.
- Nixon, P. H., and L. Clark, The alkaline centre of Yelele and its bearing on the petrogenesis of other eastern Uganda volcanoes, *Geol. Mag.*, **104**, 455-472, 1967.
- Nixon, P. H., and G. Hornung, A new chromium garnet end member, knorringite, from kimberlite, *Am. Mineralogist*, in press, 1968.
- Nixon, P. H., O. von Knorring, and J. M. Rooke, Kimberlites and associated inclusions of Basutoland: A mineralogical and geochemical study, *Am. Mineralogist*, **48**, 1090-1132, 1963.
- O'Hara, M. J., and E. L. P. Mercy, Petrology and petrogenesis of some garnetiferous peridotites, *Trans. Roy. Soc. Edinburgh*, **65**, 251-314, 1963.

- Orville, P. M., Alkali ion exchange between vapor and feldspar phases, *Am. J. Sci.*, **261**, 201-237, 1963.
- Osborn, E. F., Role of oxygen pressure in the crystallization and differentiation of basaltic magma, *Am. J. Sci.*, **257**, 609-647, 1959.
- Peters, Th., W. C. Luth, and O. F. Tuttle, The melting of analcite solid solutions in the system $\text{NaAlSiO}_4\text{-NaAlSi}_3\text{O}_8\text{-H}_2\text{O}$, *Am. Mineralogist*, **51**, 736-753, 1966.
- Philibert, J. A., A method for calculating the absorption correction in electron-probe microanalysis, in *Third International Symposium on X-ray Optics and Microanalysis*, H. H. Pattee, Jr., V. E. Cosslett, and A. Engström, eds., pp. 379-392, Academic Press, New York, 1963.
- Prashnowsky, A. A., and M. Schidlowski, Investigation of Pre-Cambrian thucholite, *Nature*, **216**, 560-563, 1967.
- Ramdohr, P., The opaque minerals in stony meteorites, *J. Geophys. Res.*, **68**, 2011-2036, 1963.
- Ramdohr, P., Einiges über die Opakerze in Achondriten und Enstatitichondriten, *Sitzber. Akad. Wiss. Berlin, Kl. Chem., Geol., Biol.*, **5**, 40 pp., 1964.
- Ramsay, J. C., *Folding and Fracturing of Rocks*, McGraw-Hill Book Co., Inc., New York, 1967.
- Reed, S. J. B., Characteristic fluorescence corrections in electron-probe microanalysis, *Brit. J. App. Phys.*, **16**, 913-926, 1965.
- Reynolds, R. C., Jr., P. R. Whitney, and Y. W. Isachsen, K/Rb ratios in Adirondack meta-anorthosites and associated charnockitic rocks, and their petrogenetic implications, *N. Y. Geol. Surv. Mem.*, in press, 1968.
- Rice, J. M., and J. M. Walsh, Equation of state of water to 250 kb, *J. Chem. Phys.*, **26**, 824-830, 1957.
- Richards, H. C., The volcanic rocks of south-eastern Queensland, *Proc. Roy. Soc. Queensland*, **28**, 105-204, 1916.
- Riecker, R. E., and T. P. Rooney, Deformation and polymorphism of enstatite under shear stress, *Geol. Soc. Am. Bull.*, **78**, 1045-1054, 1967.
- Robertson, E. C., F. Birch, and G. J. F. MacDonald, Experimental determination of jadeite stability relations to 25,000 bars, *Am. J. Sci.*, **255**, 115-137, 1957.
- Robie, R. A., Thermodynamic properties of minerals, *U. S. Geol. Surv. Open-File Rept.*, Te 1-816, 1962.
- Rooymans, C., and W. Albers, High-pressure polymorphism of Cr_2FeS_4 and related compounds, preprint, pp. 63-66, 1967.
- Ross, C. S., M. D. Foster, and A. T. Myers, Origin of dunites and olivine-rich inclusions in basaltic rocks, *Am. Mineralogist*, **39**, 693-737, 1954.
- Rubey, W. W., Geologic history of sea water: An attempt to state the problem, *Geol. Soc. Am. Bull.*, **62**, 1111-1147, 1951.
- Schairer, J. F., The alkali feldspar join in the system $\text{NaAlSiO}_4\text{-KAlSiO}_4\text{-SiO}_2$, *J. Geol.*, **58**, 512-517, 1950.
- Schairer, J. F., The system $\text{K}_2\text{O-MgO-Al}_2\text{O}_3\text{-SiO}_2$: I, Results of quenching experiments on four joins in the tetrahedron cordierite-forsterite-leucite-silica and on the join cordierite-mullite-potash feldspar, *J. Am. Ceram. Soc.*, **37**, 501-533, 1954.
- Schairer, J. F., Melting relations of the common rock-forming oxides, *J. Am. Ceram. Soc.*, **40**, 215-235, 1957.
- Schairer, J. F., and H. S. Yoder, Jr., The nature of residual liquids from crystallization, with data on the system nepheline-diopside-silica, *Am. J. Sci.*, **258A**, 273-283, 1960.
- Schopf, J. W., K. A. Kvenvolden, and E. S. Barghoorn, Amino acids in Precambrian sediments: An assay, *Proc. Natl. Acad. Sci. (U.S.)*, **59**, 639-646, 1968.
- Schreyer, W., G. Kullerød, and P. Ramdohr, Metamorphic conditions of ore and country rock of the Bodenmais, Bavaria, sulfide deposit, *Neues Jahrb. Mineral. Abhandl.*, **101**, 1-26, 1964.
- Scar, C. B., L. C. Carrison, and C. M. Schwartz, High-pressure stability field of clinoenstatite and the orthoenstatite-clinoenstatite transition (abstract), *Trans. Am. Geophys. Union*, **45**, 121, 1964.
- Scar, C. B., L. C. Carrison, and O. M. Stewart, High-pressure synthesis of a new hydroxylated pyroxene in the system $\text{MgO-SiO}_2\text{-H}_2\text{O}$ (abstract), *Trans. Am. Geophys. Union*, **48**, 226, 1967.
- Scar, C. B., L. C. Carrison, and O. M. Stewart, Effect of water vapor on the melting of forsterite and enstatite at 20 kb (abstract), *Trans. Am. Geophys. Union*, **49**, 355-356, 1968a.
- Scar, C. M., L. C. Carrison, and O. M. Stewart, High-pressure synthesis and stability of hydroxylated orthoenstatite in the system $\text{MgO-SiO}_2\text{-H}_2\text{O}$ (abstract), *Trans. Am. Geophys. Union*, **49**, 356, 1968b.
- Scott, W. H., Kinematic significance of folds on a volcanic spatter-cone (abstract), *Trans. Am. Geophys. Union*, **49**, 305, 1968.
- Sitter, L. U. de, *Structural Geology*, McGraw-Hill Book Co., Inc., New York, 1956.
- Skinner, B. J., S. P. Clark, and D. E. Appleman, Molar volumes and thermal expansions

- of andalusite, kyanite, and sillimanite, *Am. J. Sci.*, 259, 651-668, 1961.
- Skinner, B. J., R. C. Erd, and F. S. Grimaldi, Greigite, the thio-spinel of iron; a new mineral, *Am. Mineralogist*, 49, 543-555, 1964.
- Steuber, A. M., and V. R. Murthy, Potassium: rubidium ratio in ultramafic rocks: Differentiation history of the upper mantle, *Science*, 153, 740-741, 1966.
- Stevens, N. C., The volcanic rocks of the southern part of the Main Range, southeast Queensland, *Proc. Roy. Soc. Queensland*, 77, 37-52, 1965.
- Stevens, R. E., and others, Second report on a cooperative investigation of the composition of two silicate rocks, *U. S. Geol. Surv. Bull.*, 1113, 126 pp., 1960.
- Strand, Trygve, Geological investigations around Grotli, central S. Norway, *Norsk Geol. Tidsskr.*, 46, 259-260, 1966.
- Tarte, P., Infrared spectra of garnets, *Nature*, 186, 234, 1960.
- Thode, H. G., Sulphur isotope geochemistry, *Roy. Soc. Can. Spec. Publ.*, 6, 25-41, 1963.
- Tilley, C. E., and I. D. Muir, Intermediate members of the oceanic basalt-trachyte association, *Geol. Foren. Stockholm Forh.*, 85, 434-443, 1964.
- Tilton, G. R., and M. H. Grünenfelder, Sphene: Uranium-lead ages, *Science*, 159, 1458-1461, 1968.
- Tobi, A. C., A chart for measurement of optic angles, *Am. Mineralogist*, 41, 516-519, 1956.
- Turner, F. P., and L. E. Weiss, *Structural Analysis of Metamorphic Tectonites*, McGraw-Hill Book Co., Inc., New York, 1963.
- Tuttle, O. F., and N. L. Bowen, Origin of granite in the light of experimental studies in the system $\text{NaAlSi}_3\text{O}_8\text{-KAlSi}_3\text{O}_8\text{-SiO}_2\text{-H}_2\text{O}$, *Geol. Soc. Am. Mem.*, 74, 153 pp., 1958.
- Tyler, S. A., and E. S. Barghoorn, Occurrence of structurally preserved plants in Pre-Cambrian rocks of the Canadian shield, *Science*, 119, 606-608, 1954.
- Vallentyne, J. R., Biogeochemistry of organic matter, II, Thermal reaction kinetics and transformation products of amino compounds, *Geochim. Cosmochim. Acta*, 28, 157-188, 1964.
- Van Hise, C. R., and C. K. Leith, The geology of the Lake Superior region, *U. S. Geol. Surv. Monogr.*, 52, 1911.
- Waard, D. de, Absolute *P-T* conditions of granulite-facies metamorphism in the Adirondacks, *Koninkl. Ned. Akad. Wetenschap., Proc., Ser. B*, 70, 400-410, 1967.
- Wager, L. R., and G. M. Brown, *Layered Igneous Rocks*, Oliver and Boyd, London, 1968.
- Watt, W. S., Chemical analyses from the Gardar igneous province, south Greenland, *Grønlands Geol. Undersøgelse Rept.* 6, 1966.
- Whitten, E. H. T., *Structural Geology of Folded Rocks*, Rand McNally, Chicago, 1966.
- Wilcox, R. E., Petrology of Parícutin volcano, Mexico, *U. S. Geol. Surv. Bull.*, 965-C, 281-353, 1954.
- Winkler, H. G. F., Synthese und Kristallstruktur des Eukryptits, LiAlSiO_4 , *Acta Cryst.*, 1, 27-34, 1948.
- Wones, D. R., A low-pressure investigation of the stability of phlogopite, *Geochim. Cosmochim. Acta*, 31, 2248-2253, 1967a.
- Wones, D. R., Compositional variations and phase equilibria of some layer silicates, DRW-1 to 45; Phase equilibria of the micas, DRW-79 to 142, in "Layer Silicates," *American Geological Institute Short Course Lecture Notes*, 1967b.
- Wyckoff, R. W. G., H. E. Merwin, and H. S. Washington, X-ray diffraction measurements upon the pyroxenes, *Am. J. Sci.*, 10, 389-397, 1925.
- Wys, E. C. de, and W. R. Foster, The binary system anorthite ($\text{CaAl}_2\text{Si}_2\text{O}_8$)-akermanite ($\text{Ca}_2\text{MgSi}_2\text{O}_7$), *J. Am. Ceram. Soc.*, 39, 372-376, 1956.
- Yoder, H. S., Jr., High-low quartz inversion up to 10,000 bars, *Trans. Am. Geophys. Union*, 31, 827-835, 1950.
- Yoder, H. S., Jr., and H. P. Eugster, Phlogopite synthesis and stability range, *Geochim. Cosmochim. Acta*, 6, 157-185, 1954.
- Yoder, H. S., Jr., and C. E. Tilley, Origin of basalt magmas: An experimental study of natural and synthetic rock systems, *J. Petro.*, 3, 342-532, 1962.
- Young, R. A., and C. E. Wagner, X-ray source-image distortion technique for the study of crystal distortion and vibration, *J. Appl. Phys.*, 37, 4070-4076, 1966.
- Zedlitz, O., Über titanreichen Kalkeisengranat, *Centr. Mineral. Geol. Paleontol., Abt. A, Mineral. Petrogr.*, 225-239, 1933.
- Ziebold, T. O., editor, The electron micro-analyzer and its applications: Lecture notes for a course in electron-probe analysis given at the Massachusetts Institute of Technology, July 1966.

PERSONNEL

Scientific Staff

Director: P. H. Abelson

Emeritus Research Associate: E. G. Zies,
Chemist

Physical Chemists: F. R. Boyd, T. C. Hoering, J. F. Schairer

Petrologists: F. Chayes, D. H. Lindsley, H. S. Yoder, Jr.

Geochemists: G. L. Davis, T. E. Krogh, G. Kullerud

Organic Geochemist: P. E. Hare

Geophysicist: P. M. Bell

Physicist: J. L. England

Crystallographer: Gabrielle Donnay

Fellows: G. M. Brown, Oxford University; ¹ W. B. Bryan, University of Queensland, Brisbane, Australia; ² J. R. Craig, Lehigh University; ³ A. El Goresy, Max Planck Institut für Kernphysik, Heidelberg, Germany; ⁴ L. W. Finger, University of Minnesota; ⁴ M. C. Gilbert, University of California at Los Angeles; N. Güven, Columbia University; ⁵ S. E. Haggerty, Imperial College of Science and Technology, University of London, England; ⁶ E. Hansen, Yale University; H. G. Huckenholz, University of Cologne, Germany; ⁷ J. E. Kalb, American University; ⁸ I. Kushiro, University of Tokyo; ⁹ H. O. A. Meyer, University College, London; R. M. Mitterer, Florida State University; ¹⁰ S. A. Morse, Franklin and Marshall College; ⁴ J. L. Munoz, Johns Hopkins University; ¹¹ A. J. Naldrett, Queen's University, Canada; ¹² H. R. Puchelt, University of Tübingen, Germany; ² S. W. Richardson, Oxford University, England; ¹³ W. H. Scott, Yale University.

Guest Investigators: M. Bird, U. S. Geological Survey; E. Chao, U. S. Geological Sur-

vey; J. de Villiers, University of Illinois; J. D. H. Donnay, Johns Hopkins University; R. F. Emslie, Geological Survey of Canada; P. Geiser, Johns Hopkins University; H. G. Huckenholz, University of Cologne, Germany; J. T. Iiyama, Ministry of National Education of France; A. Long, Smithsonian Institution; E. A. Magnusson, Avondale College, Australia; R. M. Mitterer, Southwest Center for Advanced Studies; G. Moh, University of Heidelberg, Germany; R. G. Platt, University of Western Ontario, Canada; D. C. Presnall, Southwest Center for Advanced Studies; L. A. Taylor, Lehigh University; C. E. Tilley, Cambridge University, England; J. F. Wehmler, Lamont Geological Observatory; R. Wheeler, Princeton University; J. Zemann, University of Vienna, Austria.

Operating and Maintenance Staff

Executive Officer: A. D. Singer

Accountant: C. B. Petry

Editor and Librarian: Dolores M. Thomas

Stenographers: Patricia S. Garrett, Marjorie E. Imlay

Clerk: H. J. Lutz

Electronic Technician: C. G. Hadidiacos

Research Assistant: J. F. Kocmanek

Chief Mechanician: F. A. Rowe

Instrument Makers: C. A. Batten, L. C. Garver, W. H. Lyons, O. R. McClunin,¹⁴ G. E. Speicher

Mechanic and Carpenter: E. J. Shipley

Electrician: E. C. Huffaker¹⁵

Machinists: W. R. Reed,¹⁶ J. R. Thomas

Building Engineer: R. L. Butler

Mechanic's Helper: M. Ferguson

Janitor: A. T. Lewis¹⁷

¹ Appointment terminated August 31, 1967, to accept position as Professor and Chairman of the Department of Geology, University of Durham, England.

² Appointment from July 1, 1967.

³ Appointment terminated September 15, 1967, to accept position as Assistant Professor of Geosciences, Texas Technological College, Lubbock, Texas.

⁴ Appointment from September 1, 1967.

⁵ Appointment terminated August 31, 1967, to accept position as Visiting Assistant Professor of Geology, University of Illinois, Urbana, Illinois.

⁶ Appointment from June 1, 1968.

⁷ Appointment from March 1 through April 30, 1968.

⁸ Appointment from February 1, 1968.

⁹ Appointment from January 1, 1968.

¹⁰ Appointment terminated August 31, 1967, to

accept position as Assistant Professor of Geosciences, Southwest Center for Advanced Studies, Dallas, Texas.

¹¹ Appointment terminated June 30, 1968, to accept position as Assistant Professor, Department of Geological Sciences, University of Colorado, Boulder, Colorado.

¹² Appointment terminated August 31, 1967, to accept position as Assistant Professor, Department of Geology, University of Toronto, Canada.

¹³ Appointment terminated September 30, 1967, to accept position as National Environment Research Council Research Assistant, Grant Institute of Geology, University of Edinburgh, Scotland.

¹⁴ Died November 14, 1967.

¹⁵ Died March 2, 1968.

¹⁶ Appointment from March 1, 1968.

¹⁷ Appointment terminated June 30, 1968.

PLATES

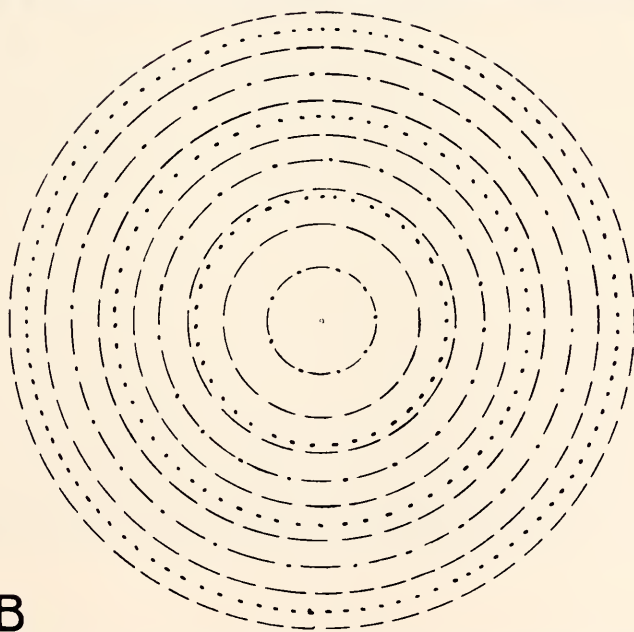
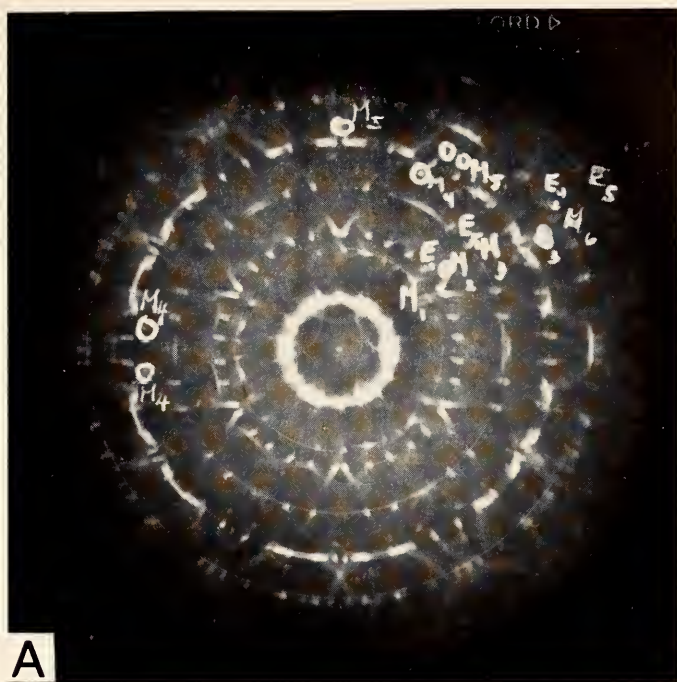
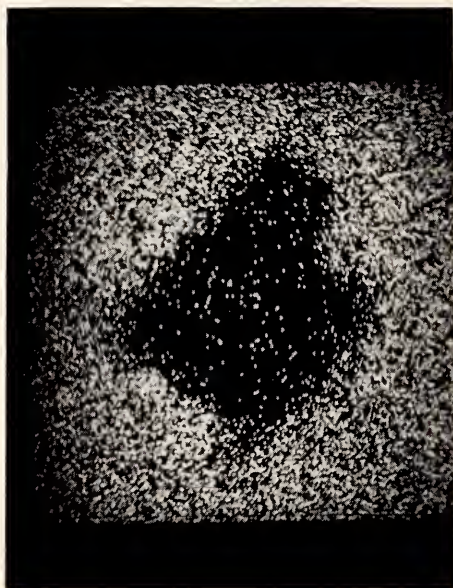


Plate 1 (A) Cone-axis precession photograph along c of polycrystal ewaldite-mckelveyite. $\text{MoK}\alpha$, $\mu\text{m} = 10^\circ$, $s = 4.0$ cm, 5.0 hours. (B) Drawing of predicted c cone-axis film for $\text{MoK}\alpha$, $\mu\text{m} = 10^\circ$, $s = 4.0$ cm. Dotted lines, ewaldite; dashed lines, mckelveyite; dash-dot lines, both phases superposed.



A



B

Plate 2. X-ray images of iron-rich inclusions in ewaldite-mckelveyite polycrystal. Horizontal distance across inclusion about $30\text{ }\mu\text{m}$. (A) FeK α image. (B) CaK α image.



Plate 3. X-ray diffraction of 0003 Bragg reflection from two-color tourmaline plate, *D3*, showing source-image distortion.

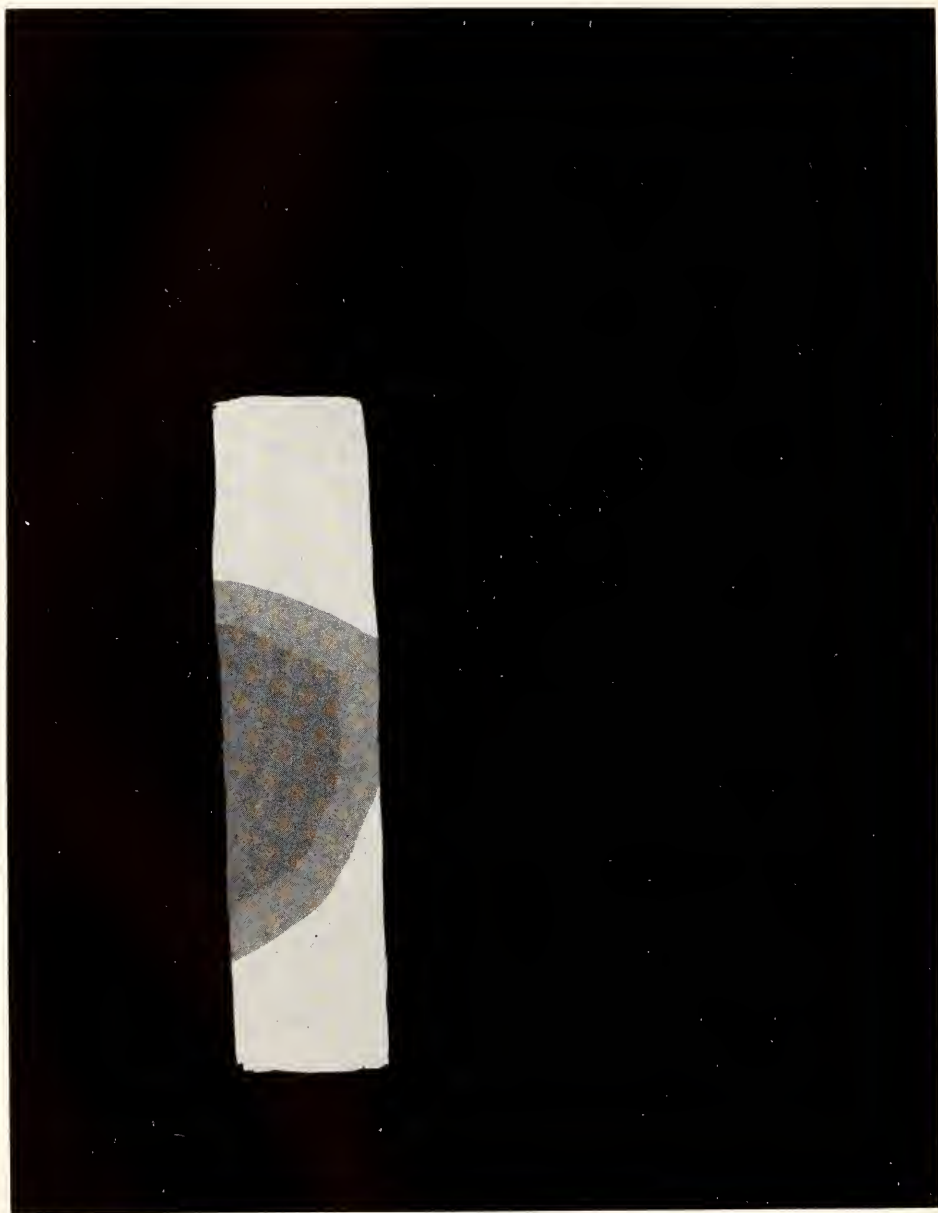


Plate 4. X-ray radiograph of tourmaline plate *D3*. Central region is blue; outside ring is colorless.

Department of Terrestrial Magnetism

Washington, District of Columbia

Ellis T. Bolton
Director

L. Thomas Aldrich
Associate Director

Contents

Introduction	285
Astrophysics	286
Optical astronomy	286
Radio astronomy	290
Nuclear physics	294
Reactions ${}^7\text{Li}(p, \alpha){}^4\text{He}$ and ${}^6\text{Li}(p, {}^3\text{He}){}^4\text{He}$	295
Elastic scattering of polarized protons on spin-one nuclei	297
Optical model applied to ${}^4\text{He}(p, p){}^4\text{He}$	298
Atomic physics	299
Biophysics	300
Bacterial and viral DNA reactions	301
Isolation and characterization of bacterial ribosomal RNA cistrons	310
Genetic expression of nonrepeated DNA sequences in the mouse	320
Search for saltatory replication	325
Repeated sequences in human DNA	327
Reassociation of nonrepeated DNA	330
The arithmetic of nucleic acid reassociation	332
Brain function	335
Theory	335
Experimental work	337
Geophysics	339
Earthquake seismology	339
Distribution of absorption of shear waves in South America and its tectonic significance	339
On locating local earthquakes using small station networks	344
Upper mantle structure beneath western South America	353
A study of the crust and upper mantle of northern Chile	357
Heat flow	360
Geomagnetism	367
Cosmic-ray program	367
Studies of conductivity anomaly under the Andes	369
The equatorial electrojet and the solar eclipse of November 12, 1966	372
Isotope studies	376
Zircon ages of Hida and Ryoke metamorphic terrains, Japan	376
References cited	377
Bibliography	379
Personnel	381



Dr. Winifred G. Whitman (Mrs. Merle A. Tuve) at her microscope in the DTM attic—Biophysics nearly 40 years ago.

INTRODUCTION

The process by which the boundaries of knowledge are advanced, and the structure of organized science is built, is a complex process indeed.

VANNEVAR BUSH—"The Builders," 1945

The reader of this report will appreciate Dr. Bush's remark, as he reads the words of those who play a part in unfolding the universe to comprehension.

In this report we deal with the diverse fields of astrophysics, biophysics and geophysics. These are not new areas of our endeavor. As our name indicates, geophysics is our oldest subject—but it is still virile, although it has lost some of its "magnetic" personality of earlier days. Earthquakes, heat flow, and earth dating are now nearer the center of our interest. Biophysics is the youngest field of interest, but nevertheless mature. The frontispiece shows Dr. Winifred G. Whitham (Mrs. Merle A. Tuve) in 1931 observing rats which had been irradiated by gamma rays from six grams of radium furnished by the U. S. Bureau of Standards. The Tuves also studied the effects of high-energy, high-frequency (for those days!) radio waves produced by Dr. Merle Tuve's transmitters for studies of the "Kennelly-Heaviside Layer" in the upper atmosphere. Even then there was a keen awareness of the potentialities in the relationship between physics and biology. And so with astrophysics—an awareness of the common ground between astrophysics and earth-bound physics, especially in magnetic and electrical studies, and its implications for understanding the stars and the cosmos was clear and overt. Indeed, Dr. Louis Bauer, the first DTM Director, in about 1916, called an extraordinary session of experts to discuss, especially with Dr. Ellery Hale, the magnetic properties of the sun. Clearly, the DTM and its activities have roots buried very firmly in a fertile soil tirelessly prepared by men

of vision and wisdom. The following anecdote will illustrate how far these roots extend.

This report appears thirty years from the time that nuclear fission was made known to the world during a few days in January 1939. The occasion was the Fifth Washington Theoretical Physics Conference, whose subject was, innocently enough, "Magnetic, Electrical and Mechanical Properties of Matter at Very Low Temperatures" and was, as was the custom, jointly sponsored by the Carnegie Institution of Washington and the George Washington University. The sessions were quite informal and were conducted rather like a Quaker meeting. Bohr opened the scientific session with a statement of the Hahn-Strassman experiments (in which they chemically isolated barium after neutron irradiation of uranium) and of the Meitner-Frisch interpretation (which indicated the release of huge amounts of energy during the process). Both he and Fermi speculated upon and suggested the kinds of experiments which might be done. During Fermi's lucid exposition, Tuve leaned over to Lawrence Hafstad and said, "Larry, you better put a new filament in the Van de Graaff!" (The same device is still being effectively used, as reported below.) Immediately upon Fermi's conclusion Hafstad, R. B. Roberts, and Robert Meyer left the hard, slatted chairs and motored from the University to the DTM to begin work on the experimental demonstration of the fission of uranium. Meanwhile, the conference continued much as planned, with, of course, a good deal of discussion of Bohr's announcement during the tea

breaks and lunches. Roberts, Hafstad, and Meyer worked hard and unceasingly to get the Van de Graaff accelerator "on the air." Finally, on Saturday, January 28, 1939, at 4:30 p.m. Roberts entered into the logbook:

Set up ionization chamber to try to detect
 $U_{92}^{238} + n \rightarrow U_{92}^{239} \rightarrow Ba_{56}^? + Kr_{36}^?$

Neutrons from Li+D

Maximum size neutron recoil 4 mm on
 oscillograph

With uranium lined I.C. [i.e., ionization
 chamber] observed α 's ~1-2 mm and
 occasional 35 mm kicks. (Ba=Kr?)

At 9:00 p.m. his entry reads: "Ran
 machine and demonstrated large kicks
 to Bohr, Fermi, Breit, Rosenfeld and
 Teller."

The story is simple, exciting, dramatic, and the events helped to begin a new scientific age. It was not known at the time that Frisch had successfully demonstrated fission in Copenhagen on January 16, and Dunning and his colleagues at Columbia on the 25th, the evening before the Conference began. And there is a touch of pathos as seen in these words written by Niels Bohr in a letter to

his wife Margrethe: "I had to stand and look at the first experiment without knowing certainly if Frisch had done the same experiment and sent a note to *Nature*."

This introduction acknowledges an event of thirty years ago which had tap roots extending deeper still in time; nuclear physics was being investigated at the DTM even in the early 1920's. The brief narrative illustrates also an abiding quality of the Institution: the capacity to respond to evident challenge within our grasp. That same capacity will be noted in the pages to follow. It illustrates the flexibility which allows for personal expression in personal research and illuminates the virtue of diversity of interest—a Department which once gloried in sailing ships or camel caravans could also glory in atom smashers. We still do. And we continue in attitudes fostered by an Institution which truly believes that "The Institution is its Staff." The reports of the several sections of the Department follow. They are expressions of individuals interacting and intellectually cross-fertilizing, and the resultant vigor is as evident today as it was thirty years and more ago.

ASTROPHYSICS

L. Brown, W. K. Ford, Jr., C. Petitjean, Vera C. Rubin, W. Trächslin, K. C. Turner, M. A. Tuve, and C. M. Varsavsky

The results reported here have been obtained with equipment as diverse as image intensifier spectrographs on optical telescopes, radio telescopes, and a Van de Graaff accelerator. With such devices we are able to study the distant galaxies and atomic nuclei—in short, to span the dimensions of the universe. These studies are leading to a better understanding of the internal gaseous motions of galaxies, of the relative motions and past history of motion of the nearby galaxies, and of the nature of the nuclear force.

OPTICAL ASTRONOMY

W. K. Ford, Jr., and Vera C. Rubin

The DTM image tube spectrograph has been used on the 72-inch Perkins Telescope of the Ohio State and Ohio Wesleyan Universities at Lowell Observatory, and on the 84-inch telescope at the Kitt Peak National Observatory for observations of galaxies. Ford made two visits to Mt. Stromlo Observatory, Australia, to install and work with a DTM image tube spectrograph at the Cassegrain focus of the 74-inch telescope. On

both visits, spectra of southern quasi-stellar objects and galaxies were obtained. Observations were continued at Lowell Observatory in collaboration with Rev. M. F. McCarthy, S. J., of the Vatican Observatory, to obtain spectra of suspected M dwarfs in the Pleiades cluster. Details of these programs follow:

M 31. Because M 31 is one of the brightest spiral galaxies, individual emission regions in that galaxy can be observed spectroscopically. Little such work has been carried out since the classic study of Mayall (1951).¹ At present the increase in speed offered by the use of an image tube, coupled with the exact information obtained by radio observation, makes such a study both feasible and rewarding. Spectra have been obtained for fifty emission regions in the spiral arms of M 31 that were identified many years ago by Baade. The distances of these regions from the nucleus of the galaxy range from $r=17'$ to $r=118'$. Some examples are shown in Plate 1. All spectrograms are calibrated so that both line intensities and radial velocities can be determined. The dispersion is 132 Å/mm and typical exposure times are about one hour. For the brighter regions, lines of $H\beta$; [O III] $\lambda\lambda$ 5007, 4959; [N II] λ 5755; He I 5875; [O I] $\lambda\lambda$ 6300, 6364; [N II] λ 6583; He I λ 6678; [S II] λ 6717 and λ 6731 are recorded. The ratio of the intensity of [O III] λ 5007 to $H\alpha$ indicates a large spread in excitation class, with a tendency for regions of higher excitation to occur at greater distances from the center. The intensity ratio of $H\alpha$ to [N II] λ 6583 is greater than unity except for regions near the nucleus. The He I line λ 5875 is strong on only 10 plates; for these regions the strength of the line decreases by a factor of 4 with increasing distance from the center ($20' < r < 75'$). Observations will continue through the next observing season.

Spectra were also obtained of the nuclear regions out to a distance of 2.5.

Emission lines are observed superimposed upon the continuous spectrum from the integrated stellar background. In the region 2.5 to 1' from the nucleus, [N II] λ 6583 and He λ 5875 are seen clearly over the entire region while $H\alpha$ is observed only in a few discrete regions. [N II] λ 6583 is present in emission as close as 3" to the nucleus. Thus M 31 falls into that class of galaxies in which the intensity ratio of the emission lines of hydrogen to [N II] is greater than unity far from the nucleus, but becomes less than unity near the nucleus.

Southern galaxies. From the Mt. Stromlo plates obtained by Ford at a dispersion of 185 Å/mm, the observed lines and measured velocities are as follows:

NGC 6699: Sharp, narrow $H\alpha$ emission is observed over a region about 9 arc sec. Weak Na D absorption is also present. $V_0=3454$ km/sec.

NGC 6754: Sharp, narrow $H\alpha$ emission is observed over a region of 35 arc sec. The central velocity is $V_0=3274$ km/sec but an almost linear rotation curve is derived, with $V_{\min}=2970$ km/sec. No other lines are seen.

NGC 6851: A strong continuum with deep Na D absorption and weak $H\alpha$ absorption is seen. $V_0=2988$ km/sec, measured from the Na D lines.

IC 4622: The strongest lines are $H\alpha$ [O III] $\lambda\lambda$ 5007, 4959. $H\beta$ and He λ 5875 are moderately strong. [S II] $\lambda\lambda$ 6717, 6731 are weak, and [N II] $\lambda\lambda$ 6548, 6583 are almost absent. $V_0=246$ km/sec. ($V_0=237$, Evans 1963).

Faint nebulosity SW of IC 4662: $H\alpha$, [O III] λ 5007 are strong and I ($H\beta$) > I([O III] λ 4959). [S II] $\lambda\lambda$ 6717, 6731 are weak; [N II] $\lambda\lambda$ 6548, 6583 are absent. $V_0=307$ km/sec.

Southern quasi-stellar objects. Velocities have been determined for two southern quasi-stellar objects.

PKS 1233-24: Strong, narrow ($<10\text{\AA}$) lines of [O III] $\lambda\lambda$ 5007, 4959; weaker lines of [Ne III] λ 3869 and [O II]

λ 3727 and a weak continuum are observed; $\Delta\lambda/\lambda=0.3552$.

PKS 1417-19: Strong, narrow ($<10\text{\AA}$) lines of [O III] $\lambda\lambda$ 5007, 4959, and $H\beta$; weaker lines of He II λ 4686, [O III] λ 4363, and a weak continuum are present; $\Delta\lambda/\lambda=0.1201$.

Virgo cluster objects. Observations are continuing on the program to obtain (1) spectra of galaxies in the Virgo cluster, and (2) spectra of compact blue objects in the field of the Virgo cluster. We have spectra of 26 blue objects from the list of Rubin *et al.* (1967).² For seven of these objects with sharp emission lines, velocities have been determined and are listed in Table 1. Work is in progress to attempt to determine the nature of these objects.

NGC 3227. NGC 3227 is one of the galaxies originally listed by Seyfert (1943)^{2a} because its spectrum shows broad, high-excitation emission lines superimposed upon a solarlike continuum. In the nucleus of NGC 3227, we observe emission lines of [O III] λ 4363; $H\beta$; [O III] $\lambda\lambda$ 4959, 5007; [NI] λ 5198; [O I] $\lambda\lambda$ 6300, 6364; [N II] λ 6548; $H\alpha$; [N II] λ 6583; [S II] $\lambda\lambda$ 6717, 6731; and [O II] λ 7330. He II λ 4686 is not observed. In the absorption line spectrum, the sodium D lines are most prominent, but $\lambda\lambda$ 4174 (Fe II + Ti II), 4227 (Ca I), the G-band, 5176 (Mg I) are also strong.

Line strengths and velocities have been measured. In the nucleus ($r<200$ pc) the hydrogen emission lines are about 6000 km/sec broad and consist of multiple components. With respect to the central

velocity, $V=1175$ km/sec, all components show negative velocities which are attributed to discrete gas clouds expanding from the nucleus. Although some clouds are moving with velocities in excess of the escape velocity, some are not, and may be moving out from the center but still remaining in bound orbits.

Outside of the nucleus, sharp $H\alpha$ and [N II] λ 6583 lines are observed to $r=600$ pc, and exhibit a linear velocity curve. Emission is also observed from a region at $r=3900$ pc, as well as from the connecting arm between NGC 3227 and NGC 3226. A mass of $M=3\times 10^9 M_\odot$ is determined for the nucleus, and $M=3\times 10^{10} M_\odot$ for the region $r<3900$ pc. The mass/luminosity ratio is 10. From the intensity ratio I ([O III] λ 5007 + λ 4959) / I ([O III] λ 4363) a temperature of 15,000–20,000° K is determined. The electron density is low, of the order of 200/cc, as determined from the I ([S II] λ 6717 / I [S II] λ 6731) ratio. $H\alpha$ is about twice as strong as [N II] λ 6548 + 6583, in the nucleus, the disc, and the distant emission region. In the nucleus of NGC 3227, the ratio of $H\alpha/H\beta$ is about 17/1, very much higher than the 3/1 ratio predicted by recombination theory. This observation, plus the rather large M/L ratio, the similar low velocities from the Na D absorption lines and the broad emission lines, and the excess negative velocities in the nucleus, all could indicate that large amounts of absorbing material are present in the nucleus of the galaxy.

The spectrum of the elliptical com-

TABLE 1. Velocities of Blue Objects in Virgo

Object	Lines Measured	Angular Extent of Emission	Velocity Reduced to Sun
RMB 46	$H\alpha$, [O III] λ 5007	Small	+452
RMB 56	$H\alpha$, $H\beta$, [O III] $\lambda\lambda$ 4959, 5007	7"	—200
RMB 77	$H\alpha$, [O III] λ 5007	8"	+12990
RMB 132	$H\alpha$, $H\beta$, [O III] $\lambda\lambda$ 4959, 5007	5"	+1240
RMB 159	$H\alpha$, [O III] $\lambda\lambda$ 4959, 5007	6"	+12830
RMB 169	[O III] λ 5007	7"	+262
RMB 175	$H\alpha$, $H\beta$, [O III] $\lambda\lambda$ 4959, 5007	6"	+34

panion NGC 3226 has emission lines of $H\alpha$, $H\beta$, $[N II] \lambda\lambda 6548$ and 6583 , with $[N II]$ about twice as strong as $H\alpha$.

X-ray stars. During the report year, astronomers have been studying spectra of the two optical stars identified as sources of strong X-ray emission. These observations have been in the ultraviolet and blue regions of the spectrum. We have obtained spectra of Sco X-1 and Cyg X-2 which extend in the red past $H\alpha$, at a dispersion of 135 \AA/mm . A record of observations made with the 72-inch Perkins Telescope of Ohio State and Ohio Wesleyan Universities at Lowell Observatory is contained in Table 2. Only the strongest lines have been measured, and the velocities are accurate to about $\pm 25 \text{ km/sec}$. A few weaker lines are also seen.

On the September 7 plate of Sco X-1, $H\alpha$ appears broad (35\AA), probably double, with two maxima separated by 4\AA (180 km/sec). The tabulated velocity refers to the center. $H\beta$ is narrower, with no sign of complex structure. He II $\lambda 4686$ and Fe I (?) $\lambda 5167$ are present in emission, as well as the emission blend $\lambda\lambda 4628-4660$, with maxima at $\lambda\lambda 4635$, 4646 , and 4655 . Line intensities relative to $H\alpha$ have been determined as follows: $H\alpha=10$, $H\beta=2.3$, He I $\lambda 5876=0.98$, He II $\lambda 4686=0.68$.

From the two plates of Sco X-1 it appears that the $H\alpha$ velocity is variable. The March 23 spectrum is time resolved, with measured velocities $V=-208$, -151 , -152 , -149 , -135 km/sec each 10 minutes. This variation is close to the

uncertainty in each velocity, and hence must be considered tentative.

The variation of radial velocity of the Cyg X-2 object has been discussed by Kraft and Demoulin (1967)³ and others from lines other than $H\alpha$. For the two plates on October 11, a velocity change of about 100 km/sec in one hour is measured in $H\alpha$, in good agreement with variations of the same amount obtained by Kraft and Demoulin on October 8, 1967, for other hydrogen lines. The $H\alpha$ profile has also changed noticeably in one hour. On the earlier plate, it is single; on the later plate it is broader (17\AA) and double, with a separation of about 5\AA between maxima. It is not as broad as the complex $H\beta$ absorption feature seen on all plates except on that of September 5. The velocity measured for the He I $\lambda 6678$ line on October 11 indicates that its velocity is not varying in phase with $H\alpha$. A strong He II $\lambda 4686$ emission line is seen on all plates except on that of September 5.

The interpretation of the spectra of both of these X-ray stars remains a puzzle. The presence of emission lines of hydrogen, He I and He II, suggests old novae. The rapid variation of velocity of a single line, and the spread in velocities of the lines at a given time, suggests a multiple star system. It may be that both of these resemblances are only superficial and that only continuing observations and accurate velocity measures will lead us toward the correct interpretation.

Pulsars. Early in 1968, Cambridge radio astronomers announced the dis-

TABLE 2. Emission Line Velocities of X-ray Stars

Object	Date, UT	Velocities with Respect to Sun (km/sec)			
		$H\beta$	He I $\lambda 5876$	$H\alpha$	He I $\lambda 6678$
Sco X-1	Sept. 7.179, 1967	+28	-192	-64	
Sco X-1	March 23.509, 1968			-159	
Cyg X-2	Sept. 5.285, 1967			-188	
Cyg X-2	Oct. 4.160, 1967			-187	
Cyg X-2	Oct. 11.203, 1967			-234	-117
Cyg X-2	Oct. 11.251, 1967			-127	

covery of objects which emit bursts of radio radiation with periods near 1 second. At the position of one of these pulsars, CP 1919, Ryle and Bailey (1968)⁴ have identified an 18th magnitude star. We obtained spectra of this star on March 28 and 29, 1968, extending from 4000Å to 7000Å. There is an essentially featureless continuum, with possible weak absorption from λ 5640 to λ 5654, and at λ 5859. The most interesting feature is weak $H\alpha$ in emission, not in the stellar spectrum, but surrounding the object, visible on the March 28 plate. The plate of March 29 was taken with a wider slit, so weak night sky features complicate the region near $H\alpha$. The spectra were taken with the slit of the spectrograph in position angle 124° , so that both Ryle's star and a fainter red star were on the slit. The separation of the two stars is about 9 arc sec. In this position angle, the emission extends from 21 arc sec SE of the pulsar to 4 arc sec NW of the pulsar toward the red star. The radial velocity of the emitting hydrogen is $V = -110$ km/sec. At the position of the pulsar, the effects of galactic rotation will produce positive radial velocities, so the large negative velocity is a curiosity. There is no conclusive evidence that the gas is associated with the pulsar. However, radio astronomers believe that there is a small ionized region surrounding the pulsar (Drake, *et al.*, 1968)⁵ which could be the region giving rise to the $H\alpha$ emission.

RADIO ASTRONOMY

*K. C. Turner, C. M. Varsavsky, and
M. A. Tuve*

Observations. Extensive observations of neutral hydrogen in the region between the Magellanic Clouds were made this year. During an expedition in July and August the low-noise parametric amplifier which had been constructed at the DTM, was installed on the 100-foot radio telescope at the Carnegie-Argentina southern station. A complete digital data

acquisition system was also shipped down and installed. It is now possible to have a complete hydrogen-line profile automatically punched on IBM cards for each observation. A preliminary survey of the region between the two Magellanic Clouds was carried out. Observations were made over a grid spaced every 2.5° perpendicular to the line between the rotational center of the two clouds and every 5° parallel to that axis. A few areas were observed at closer spacing, and observations were made with a spacing of 1° (2 beam widths) along the axis between the rotational centers of the two clouds. A velocity-distance contour diagram of this region is shown in Fig. 1. It can be seen that the "neutral hydrogen envelope" of Kerr, Hindman, and Robinson⁶ has been resolved into discrete clouds.

In October and November observations were made spaced on a 1° grid, over a $10^\circ \times 20^\circ$ region between the two clouds. Analysis of the data is still in progress.

Equipment. Our hydrogen-line receiver at the Derwood Observatory is once again on the air after extensive modernization of the telescope control room. This has provided a more pleasant and efficient place in which to work. An improved Klystron power supply for the parametric amplifier has markedly increased the gain stability of the system.

New solid-state versions of our multi-channel square-wave driver and the high-frequency section of our local oscillator system have been completed and are ready for installation.

The Derwood-Avery Road interferometer should come into operation this year. Simple Shottky diode mixer-cascades with noise temperatures of about 300°K have been developed, and a complete front end is being installed on the Avery Road telescope. A newly designed movable feed will permit a source to be observed for almost 2° on either side of the meridian. This allows integration for about 20 minutes at declinations near the zenith.

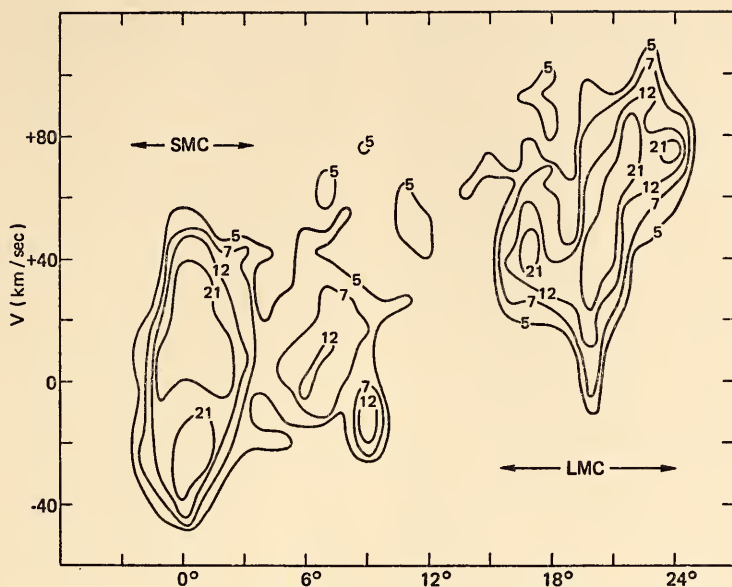


Fig. 1. Velocity intensity contours for the Magellanic Cloud system. Contour units are in degrees Kelvin antenna temperature. Observations are along the line connecting the rotational centers of the two clouds.

Data reduction and theory. The preparation of a 234 Mc source catalog from our NRAO 300-foot survey of 1964 has proceeded slowly. The analogue records from that part of the survey south of declination 10° have been examined, and pertinent data punched into IBM cards for further analysis. About one third of the remaining analogue material has been read, but not yet entered on cards.

The large amount of material between the Magellanic Clouds has prompted an investigation of the dynamical history of the Galaxy-Magellanic Cloud system. Programs have been written for our IBM 1130 which integrate the equations of motion of as many as 10 gravitationally interacting point masses.

Histories of the Galaxy and the Magellanic Clouds, together with the material between the clouds, have been calculated with several different assumed velocities perpendicular to the line of sight. The masses and distances of the objects have also been varied.

Figure 2 shows the geometry of the system. The plane of the page is the plane in which the mass centers of the Galaxy and the Magellanic Clouds now lie. The observed radial velocities are indicated. Several general conclusions may be drawn from these studies. With the exception of the small feature 9° from the

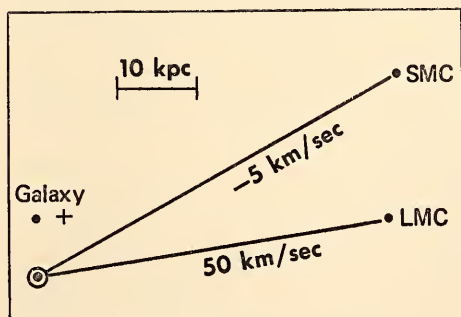


Fig. 2. Geometry of the Galaxy-Magellanic Cloud system. Points are shown in the plane in which the three objects lie. Radial velocities are indicated after correction for 250 km/sec solar galactic rotation.

Small Cloud in Fig. 1, the radial velocities of the material between the two clouds are consistent with an explosive origin for these objects. If one assumes zero velocity perpendicular to the line of sight, one finds that the object 8° from the Small Cloud was ejected from it about 360 million years ago, and the object 11.5° from the Small Cloud was ejected from the Large Cloud about 160 million years ago. The object 9° away from the Small Cloud is in orbit around it with a period of about 470 m.y.

The question of the permanence of the Magellanic Cloud pair depends very sensitively on the transverse velocities assumed for the clouds. Figure 3 shows the distance between the two clouds in the past if they each have a velocity perpendicular to the line of sight of 100 km/sec. The two curves correspond to oppositely directed velocities lying in the plane of Fig. 1. There seem to be no considerations other than aesthetic ones which require the clouds to be a permanent pair.

Continuing program of surveys. There are reasons to be less than fully confident that radio astronomy is a field for the highly personal endeavor of one or two men working together, as distinguished from the comprehensive "research team" approach, in which groups of engineers and technicians, working in shifts, undertake to construct, revise, maintain,

calibrate, and make extensive observations with large and expensive equipment. In this "team" pattern specialized operators carry out programs on the sky which are specified from their desks by a staff of astronomers, whose assigned task is to extract the maximum of information from the sky at the earliest moment. The old-fashioned research pattern of giving a highly interested individual freedom and tools to measure and study some interesting aspect of the world around us, perhaps with the help of an assistant and, if possible, with a professional associate, is still the general pattern at the Carnegie Institution. The "team" approach, in contrast, is utilized at most of the radio astronomy observatories in the world, at least at those where comprehensive surveys and the rapid follow-up of the new discoveries are accomplished.

There are some frustrations for the individual investigator, and also some very real shortcomings or limitations in his observational results, when design, test, modification, maintenance, and detailed calibration and observation routines are all pretty much restricted to the dimensions of his own time and energy. Nevertheless, when the qualitative nature and the system dimensions of the astronomical objects so conspicuous in the radio recordings are kept in the foreground of his thinking, with some deliberate de-emphasis of the electronic and other technical questions, an individual observer finds a deep satisfaction in measuring and interpreting these objects, which were previously seen only by a very few astronomers at only one or perhaps two other observatories. The vast clouds of atomic hydrogen whose densities and Doppler velocities are shown by the hydrogen line at 1420 megacycles (21-cm wavelength) are not individually impressive, being somewhat vague and indefinite in location and size, but all of these clouds, viewed as an ensemble, sketch out the vast wheel of our whole Galaxy, revolving at different rates at

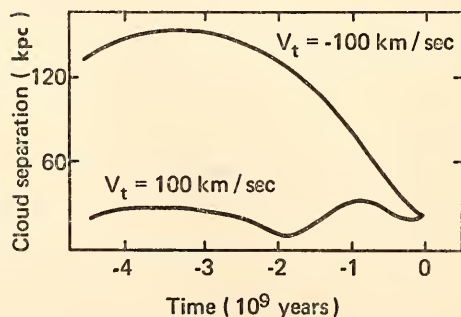


Fig. 3. Past history of the Magellanic Cloud separation for two choices of velocity perpendicular to our line of sight.

different distances from the center, but roughly once in 200,000,000 years at the sun's distance of about 30,000 light years from the galactic center in Sagittarius. With his thoughts and his working hours focused in a world of such dimensions, steering the antenna himself, making and computing his own radio observations, the question whether he is the first or the second or the fifth human being to "see" a given object in the sky, or to perceive a large-scale regularity of motion or other pattern in his assembly of data, fades into triviality. He himself sees it, and there it clearly is exposed and preserved in the records of his work, and that is enough. This is a greatly satisfying experience, and it is perhaps more poignant for the individual who carries a whole observing project through from start to finish than it is for the "team" participant who does an assigned part of a more comprehensive project, even when that is done to higher standards of precision or detail.

These remarks may give some clue to the kinds of questions concerning research patterns and direction toward which the DTM efforts, in radio astronomy and also in other fields, have been directed. Only by sustained examples of different patterns of research activity can the values of each, especially in human terms, be assessed.

The Carnegie 60-channel receiver for hydrogen-line observations, first built in 1954-1955 for use with the 8-meter Wurzburg antenna, has been modified from time to time, in various efforts to improve the base line (cold sky zero line), the constancy of gain (which varies with equipment temperatures, line voltage, input level, noise, etc.), the "noise figure" (statistical fluctuation), and many other basic instrumental characteristics. However, a choice must always be made between technical busywork and astronomical observing. During the years before the 60-foot steerable parabolic antenna was installed at Derwood most of the sky visible from Washington was

observed in an open grid of points. Profiles for the high latitude positions 20° to 90° and -20° to -90° were published (Helfer and Erickson, 1959). The profiles for the Milky Way were much more complex; a reasonably complete survey in and near the plane of the Galaxy was made with the Wurzburg (beam width about 2.3° between half power points) using channels of 10-kc width (between half power points). These profiles were assembled and reduced to "maps" for the regions outside of the circular galactic path of the sun, but maps were not attempted for the regions nearer the galactic center, where arbitrary assignments of location must be made because the rotating galactic model gives two possible positions for each value of the Doppler shift (to the red). After moving to the 60-foot steerable Carnegie antenna at Derwood, Maryland, in 1960 numerous partial surveys and studies of individual regions were carried out with the new and sharper beam with $3/4^\circ$ between half-power points. Most of these were in connection with revisions of the receiver and in preparations for special studies elsewhere, such as studies of the galactic center, of the Orion region, and of the Andromeda nebula prior to using our receiver on the 300-foot transit parabola at the National Radio Astronomy Observatory, Greenbank, West Virginia, as indicated in previous *Year Books*. Many frustrating months of effort and discarded observations at intervals over the past six or seven years have been spent on the vagaries of parametric amplifiers, and only during the past report year has this technique been reasonably satisfactory in use both at Derwood and with the receiver we have supplied to our Villa Elisa Station near Buenos Aires which we operate jointly with the Instituto Argentino de Radioastronomía.

A rather comprehensive series of observations has been made with the 60-foot Derwood parabola and 60-channel receiver. For example, from February 1968 through the report year, observa-

tions resulting in repeated Doppler velocity "profiles" were drawn by the pen recorder of the receiver for more than 1700 selected sky positions. These also resulted in more than 22,000 IBM cards punched at the receiver, each separate profile yielding 60 4-digit observations, for a grand total of 320,000 independent data points. It is easy to understand that any really comprehensive reduction of so many observations to uniform intensity scales and their resolution into (assumed) Gaussian cloud components requires a computer. The IBM 1130 computer purchased and installed at the Department two years ago is a most useful and important addition to the resources now available to our individual staff members.

These recent observations, made rather intensively because the parametric amplifier (constructed at Derwood) has been, along with the rest of the complex equipment, in a long period of relatively good behavior, together with a reduced level of local radar interference, have included a re-survey of the plane of the Galaxy at intervals of 4° in longitude, at latitudes of 0° , -2° , $+2^\circ$ and also -4° and $+4^\circ$ (incomplete), a detailed grid in the longitude region 40° to 60° from $+6^\circ$ to -14° latitude, three rather extensive grids in the vicinity of the anti-center, longitude 180° , also networks in the Taurus and Orion regions, below the equator at longitudes 210° to 240° , and grids in the vicinity of 90° and 130° longitude. In addition, a considerable number of profiles were recorded in searches for residual clouds (at the Trojan points) possibly related to the Magellanic Clouds, and in efforts to search for molecular hydrogen. Since these surveys have to date been only visually scanned and not thoroughly reduced and analyzed, this listing represents an expression of interest and satisfying efforts, not a presentation of scientific results.

NUCLEAR PHYSICS

L. Brown, C. Petitjean, and W. Träichslin

Reactions ${}^7\text{Li}(p, \alpha){}^4\text{He}$ and ${}^6\text{Li}(p, {}^3\text{He}){}^4\text{He}$

During the past year we investigated transmutation reactions for the first time with our polarized proton beam, selecting two that have long histories in nuclear research at DTM and elsewhere. The reaction ${}^7\text{Li}(p, \alpha){}^4\text{He}$ was the first induced with accelerated particles,⁷ and its differential cross section was first measured as a function of energy⁸ here in 1948; the reaction ${}^6\text{Li}(p, {}^3\text{He}){}^4\text{He}$ was first observed⁹ ten years earlier at this laboratory. In the two preceding *Year Books* we have discussed briefly how phase shifts, which are deduced from polarization measurements in elastic scattering, can be used to determine the structure of the intermediate nucleus and the potential of the nuclear force. If a transmutation reaction or inelastic scattering occurs, it is clear that phase shifts cannot describe the process because the de Broglie wavelength of the outgoing particle is different from the incident one. For such processes the measurements of cross section and polarization can be expressed in terms of the matrix elements of the various transitions that take place. A deduction of matrix elements directly from experiment, which is analogous to the determination of phase shifts in elastic scattering, is difficult, and it is better to describe the angular distributions of cross section and polarization with a series of Legendre functions, the coefficients of which can be calculated under a variety of assumptions.

The differential cross section for unpolarized protons can be written

$$\sigma_0(E, \theta) = \frac{\sigma_{\text{tot}}}{4\pi} [1 + B_1(E)P_1(\cos \theta) + B_2(E)P_2(\cos \theta) + \dots] \quad (1)$$

where θ is the reaction angle, B_1 and B_2 are energy-dependent coefficients and σ_{tot} is the total reaction cross section. If

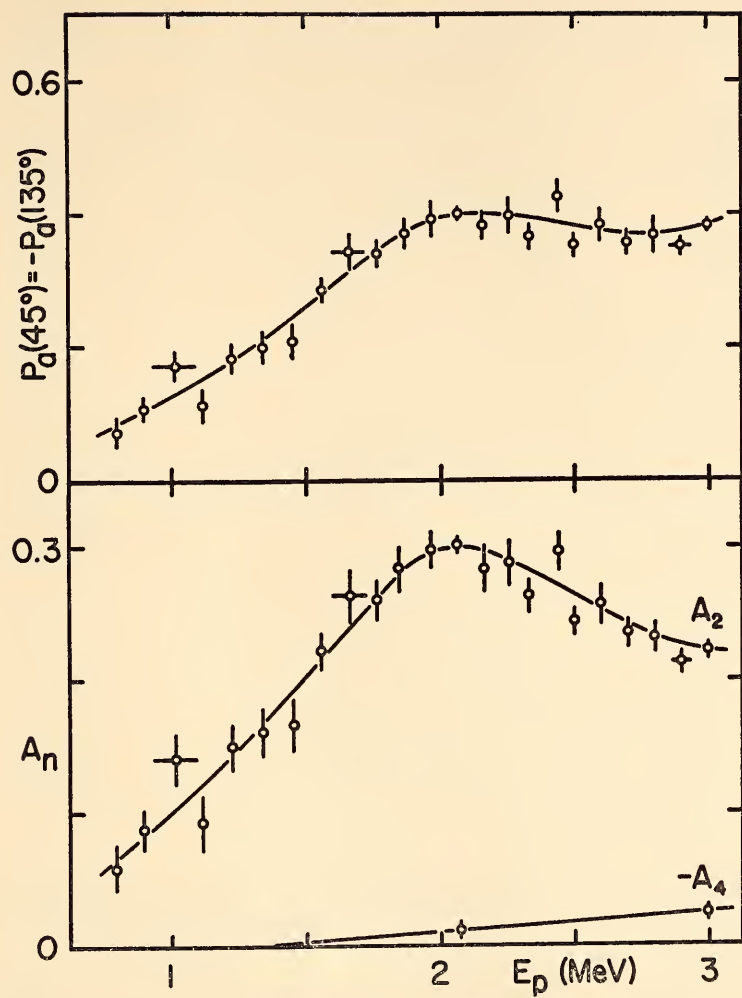


Fig. 4. Coefficients A_n , as defined in equation 3, that describe the angular distribution of the polarization efficiency of the reaction ${}^7\text{Li}(p, \alpha){}^4\text{He}$ plotted against the incident proton energy. For this reaction only even order Legendre functions can be present because both outgoing particles are identical.

the incident protons are polarized, the expression has to be enlarged to

$$\sigma_p(E, \theta, \phi) = \sigma_0(E, \theta) [1 + P_b P_a(E, \theta) \cos \phi] \quad (2)$$

where P_b is the incident proton polarization perpendicular to the direction of the beam, ϕ is the azimuthal angle between the normal to the reaction plane, defined according to the Basel sign convention,

and the axis of polarization and P_a is the analyzing efficiency of the reaction, which can be written

$$P_a = \frac{A_1(E)P_1^1(\cos \theta) + \frac{A_2(E)P_2^1(\cos \theta) + \dots}{B_2(E)P_2(\cos \theta) + \dots}}{1 + B_1(E)P_1(\cos \theta) + \dots} \quad (3)$$

Our experimental results can thus be given as the coefficients A_i .

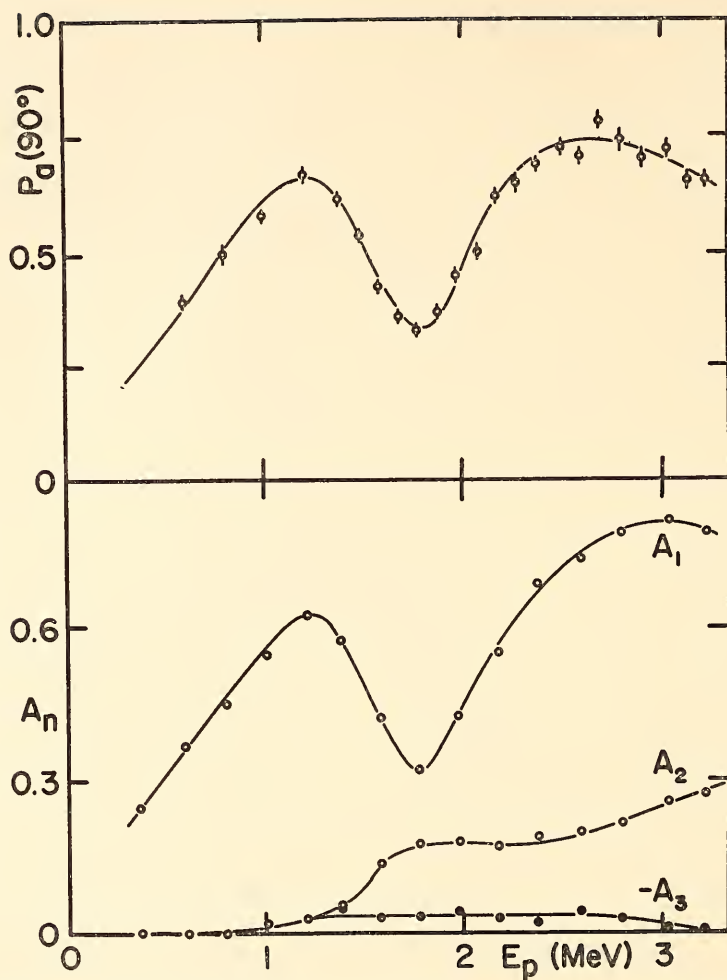


Fig. 5. Coefficients A_n , as defined in equation 3, that describe the angular distribution of the polarization efficiency of the reaction ${}^6\text{Li}(p, {}^3\text{He}){}^4\text{He}$ plotted against the incident proton energy.

The two reactions ${}^7\text{Li}(p, \alpha){}^4\text{He}$ and ${}^6\text{Li}(p, {}^3\text{He}){}^4\text{He}$ are strongly sensitive to polarization, as shown by our measurements, which are now complete for the available range of energy and reaction angle. The energy range covers a region where the structure of the intermediate nuclei ${}^8\text{Be}$ and ${}^7\text{Be}$ is still uncertain after 30 years of research with unpolarized protons. Obviously, complete knowledge of the energy levels of these nuclei is needed before a theoretical explanation of them can succeed. Two theorists,

Dr. R. G. Seyler of Ohio State University and Prof. G. S. Mani of the University of Manchester, are attempting to explain our results in terms of a compound nucleus with two or three interfering levels. A pure compound nuclear state, e.g., a single isolated level, must have fore and aft symmetry in the distribution of reaction products and no sensitivity to polarization, since the decaying nucleus can only remember the orientation of the orbital angular momentum, a vector perpendicular to the direction of the incident

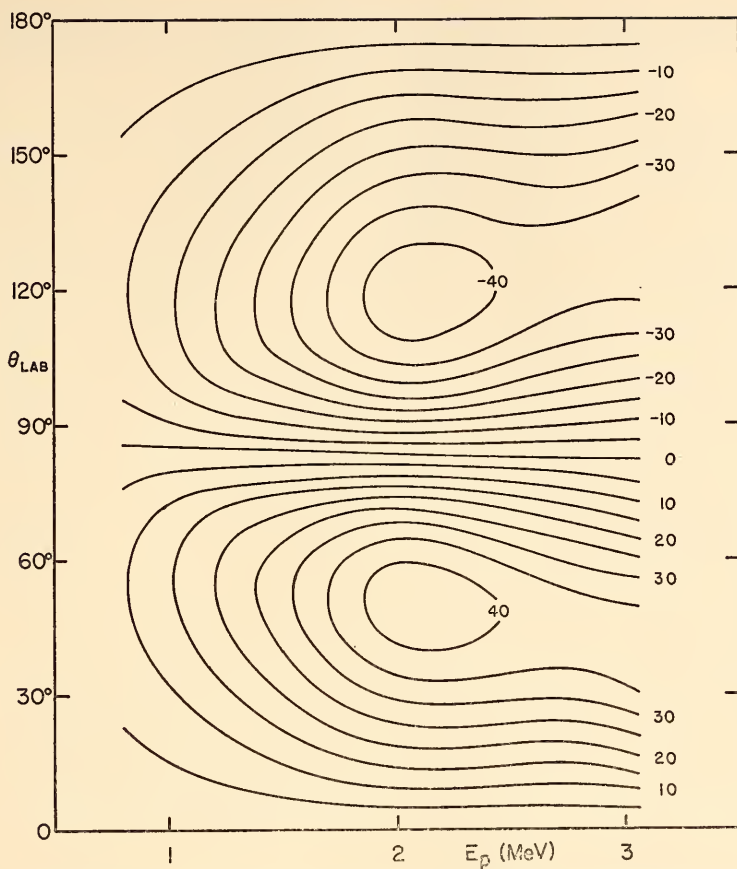


Fig. 6. Polarization contour map for the reaction ${}^7\text{Li}(p, \alpha){}^4\text{He}$. The polarization efficiency is shown in contours of equal value in units of 0.01 with contour intervals of 0.05.

proton. Two or more interfering states, e.g., levels that overlap, can remember because they were excited coherently. Polarization and lack of fore and aft symmetry can also result, if no compound nucleus is formed.

The results of these two experiments are shown in Figs. 4 through 7 as plots of the coefficients A_i and as polarization contour maps. Because the bombardment of ${}^7\text{Li}$ with protons yields two α -particles, only even order Legendre functions can occur for that reaction, i.e., only A_2, A_4, A_6 , etc., can be different from zero. No such restriction applies to the other reaction.

Elastic Scattering of Polarized Protons on Spin-One Nuclei

Our phase shift analysis of the elastic scattering of protons on nuclei of spin-one (see *Year Book 66*, p. 64) was intended not only to describe our measurements of proton-deuteron scattering but to suggest measurements of the change of polarization resulting from scattering. Such measurements require us to scatter the polarized beam from deuterium and measure the polarization of the scattered protons, an experiment that is difficult, though possible. To our surprise the calculations indicate a meager return from such an experiment, and we set about

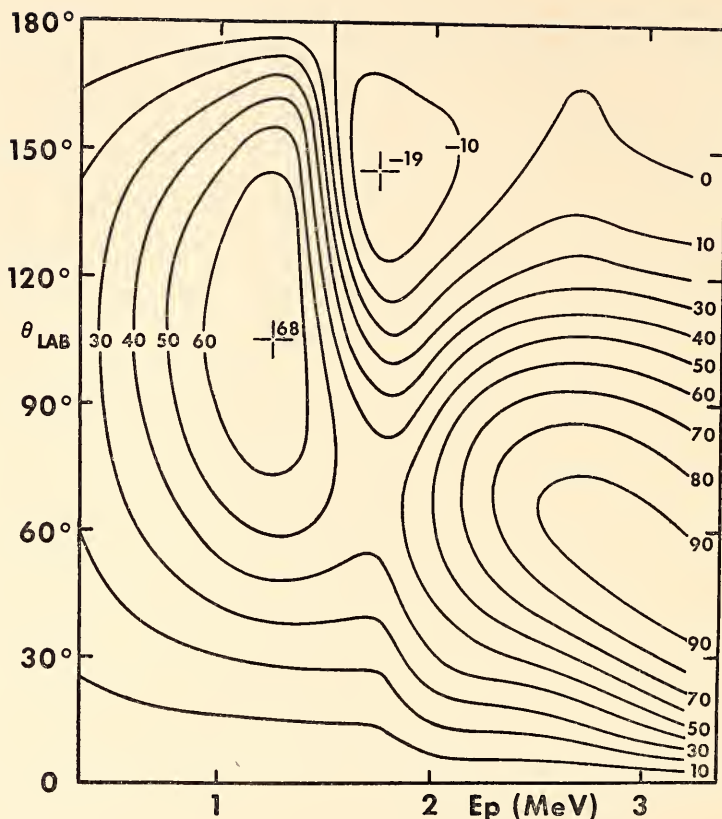


Fig. 7. Polarization contour map of the reaction ${}^6\text{Li}(p, {}^3\text{He}){}^4\text{He}$. The polarization efficiency is given in units of 0.01 with contour intervals of 0.1.

measuring the polarization effects in ${}^6\text{Li}(p, p){}^6\text{Li}$, which can be analyzed with the same computer program. The cross section for this simple interaction has just recently been measured with unpolarized protons¹⁰ to an accuracy suitable for a phase shift analysis,* so our additional polarization data may allow a unique set of phases to be established. The measurements are possible only because of the high energy resolution of solid state charged particle detectors, since protons must be distinguished according to whether they were scattered

from the nickel target backing, the carbon and oxygen contamination and the ${}^6\text{Li}$. The data are complete, and the analysis will begin shortly.

Optical Model Applied to ${}^4\text{He}(p, p){}^4\text{He}$

The nucleus often shows itself to be simpler than expected. Considering our ignorance of the nuclear force and the large number of interactions to which a nucleon is subjected, one would hardly expect simple, phenomenological models to describe nuclear events satisfactorily, but such has been the case. The structure of nuclei with the number of protons or neutrons near "magic" values for closed shells is given to good approximation by the *single particle model*, the structure of heavy nuclei by the *collective model*, and

* Cross-section measurements are very difficult for lithium because of the uncertainty in determining the thickness of the target, which reacts strongly with air. Hence the long delay in gaining this important information.

nuclear scattering at high energies on medium and heavy nuclei is described by the *optical model*.¹¹ These models are useful as intermediate steps in gaining knowledge of nuclear forces and interactions. Until now the optical model has been applied only to nuclei where the structure is lost in the complexities of many overlapping levels. A group of theorists led by Dr. G. R. Satchler of Oak Ridge National Laboratory has applied¹² with considerable success the optical model to our measurements of $^4\text{He}(p, p)^4\text{He}$, an interaction that has no sharp structure at energies below 20 MeV. The fit of theory to data is not only very good but had to be made with a reduced number of parameters, since the usual complex potentials must be replaced with real ones because no inelastic processes are possible.

ATOMIC PHYSICS

L. Brown, W. K. Ford, Jr., V. C. Rubin, and W. Trüchslin

Our first experiment in foil excitation spectroscopy was described in *Year Book 66* (pp. 66-68) where we also described the confusing nature of the results: seventy-seven spectral lines were observed, only five of which had been observed previously and only three of these were from known transitions. Conventional spectroscopic excitation also produces spectral lines that cannot be classified, which are referred to as anomalous and which are generally discarded from further consideration; most of them are thought to result from multi-electron excitation. For us to throw out the anomalous lines would mean to discard virtually all the results of the experiment! A recent discovery¹³ by W. Brandt and R. Laubert of New York University of a new kind of excitation mechanism for the production of X rays when heavy ions impinge on a solid suggested a new approach to the problem. Prof. Brandt subsequently proposed the application of the statistical theory of

spectra¹⁴ to the strange sodium lines, and it appears that this may be the key to understanding the matter.

Excitation occurs during the collision of a moving atom and a target atom; in this case the moving atom is sodium of the beam and the target atom is carbon of the foil. The electron clouds of the two atoms interpenetrate, and exchange-forces cause rearrangement in accordance with the Pauli principle as applied to an "atom" of nuclear charge $+6e$ and $+11e$. On separation the two atoms are left with holes throughout their electronic shells and hence are highly excited. Little is known of the structure of atoms in such high degrees of excitation, but one would suspect that the density of states is very high and that transitions between them would give rise to photons over a wide range of wavelength, of which we see only a small fraction. In contrast to the spectrum of an atom that has its single valence electron excited, no systematic relationship is expected; the spectral lines should be randomly spaced relative to one another.

We define a mean line density D for n lines as

$$D = \frac{\Delta E}{n-1} \quad (4)$$

where ΔE is the energy range of the lines in electron volts. If the spacing between any two adjacent lines is S , then a convenient reduced variable can be defined

$$x = S/D. \quad (5)$$

The number of lines between x and $x + \Delta x$ is plotted in Fig. 8 for the foil-excited spectrum. The instrumental resolution precludes the recording of lines if $x < 0.24$. Also included are plots of the Poisson distribution

$$P_a = \exp(-x), \quad (6)$$

which indicates a random spacing of the lines, and the Wigner distribution,

$$P_w = \frac{\pi x}{2} \exp\left(-\frac{\pi x^2}{4}\right) \quad (7)$$

which indicates a repulsion between

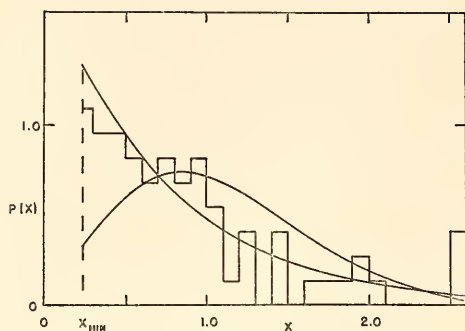


Fig. 8. Number of lines between x and $x+\Delta x$ for the foil-excited spectrum of sodium. Instrumental resolution precludes observation of lines if $x < 0.24$. The theoretical curve with the higher value at the left is a Poisson distribution and indicates random spacing of adjacent lines; the curve with the lower value at the left is a Wigner distribution and indicates repulsion between lines.

lines. The curves differ from equations 6 and 7 in that they are normalized to unity by integrating from $x=0.24$ rather than $x=0$.

We conclude on the basis of our first observations that the foil-excited spectrum of sodium is best described as consisting of randomly distributed emission lines. Only extended investigation can shed light on the detailed nature of the atomic states excited in this way and on the excitation mechanism itself.

No experiments have been performed since the original work with sodium because of limitations of the accelerator for handling heavy ions. Within the next few months a new deflecting magnet will be installed that should allow us to observe atoms throughout the periodic table.

BIOPHYSICS

E. T. Bolton, D. J. Brenner, R. J. Britten, D. B. Cowie, D. E. Kohne, A. V. Rake, and R. B. Roberts

The investigation of the nucleic acids of a wide range of organisms continues to be the focal point of interest of the Biophysics Section. The results of these studies permit several broad conclusions concerning the DNA of both primitive and higher organisms. For example, in the bacteria and viruses studied DNA consists for the most part of nonrepetitive (unique) nucleotide sequences. Conversely, the DNA composition of higher organisms is vastly more complex, a large portion being contained in many different families of repeated nucleotide sequences and the remainder being nonrepetitive in its composition.

Such generalizations, however, serve only as broad guidelines for DNA characterization. The experience in handling reassociated nucleic acids was exploited to provide methods for the isolation and analysis of specific nucleotide sequences, and the study of some of these specific nucleic acid segments will be described below.

While most of the bacterial DNA is

unique a few repeated nucleotide sequences have been isolated—those which code for ribosomal RNA. This specific DNA appears to have been more strongly conserved (i.e., to have changed less) during bacterial evolution than the great majority of the unique nucleotide sequences present. This is a clear example of repeated nucleotide sequences which are strongly conserved in bacterial population.

Specific portions of the unique DNA of bacteria also show relationships that are strongly conserved. These regions, less than 1% of the bacterial genome, are those homologous to the DNA of certain lysogenic viruses. The high degree of precision of matched base pairing observed among these reacting DNA segments implies common origin and an active mechanism for conserving precise viral-bacterial genetic elements.

Another example of unusual genetic stability also concerns the lysogenic state. Several lysogenic viruses are genetically related to each other, their DNAs

containing common nucleotide sequences. The thermal stability of the product of the cross-reactive segments of the DNAs of these viruses is as high as that observed with reactions using identical virus DNAs. It is again apparent that a mechanism exists for the conservation of these various genetic elements. Though the relationship remains precise, the experiments do not indicate whether the DNA remains unchanged or whether there is a rapid exchange of genetic elements among the organisms.

Evolutionary divergence has been recognized from studies of the unique portions of bacterial DNAs. On the other hand, the very presence of families of repeated sequences in the DNA of higher organisms is a strong indication of divergence by relatively sudden genetic events (saltatory replication). A search for evidence for such an event was carried out by comparing the pattern of repeated sequences contained in the DNA of transformed cells (rat hepatoma and mouse L cells) with normal mammalian cells.

Another question concerning specific portions of mammalian DNA relates to the expression of the nonrepeated sequences. This report demonstrates that in mice the unique DNA is expressed. An estimate is given of the fraction of the DNA transcribed as well as the percentage of rapidly labeled RNA which is derived from the unique DNA.

A further study reports the measurement of the frequency of repetition and the quantity of repeated nucleotide sequences in human DNA. As in other mammals, almost half of the human DNA is made up of repeated nucleotide sequences. This is an example of the detailed analysis which is required just to measure this aspect of the organization of complex genetic systems.

BACTERIAL AND VIRAL DNA REACTIONS

Dean B. Cowie and Don J. Brenner

Bacterial-bacterial DNA reactions.
The presence of genetic material held in

common among organisms serves as a means for investigating taxonomic relationships and as an indicator of probable evolutionary patterns. Thus, nucleotide sequence homologies among certain enterobacteria were investigated by Bolton and McCarthy¹⁵ using the DNA-agar technique, as shown in Table 3. These early studies clearly demonstrated the value of the method, the quantity of *E. coli* DNA reacting with the DNA of the other enterobacteria serving as a measure of the similarities of their genomes. Left unanswered by such experiments was the question of the degree of precision of base pairing occurring in these binding reactions.

One means of estimating this precision is to compare the thermal stabilities of the reaction product formed between DNA from two species with that of the product of the reassociation of a given DNA.

Several methods have been employed to measure the thermal stability of the reassociation products. Thermal elution profiles, each characteristic of a specific DNA-DNA reaction, have been obtained from studies involving labeled DNA fragments reacting with identical or heterologous DNA-agar preparations.¹⁶ Similar studies are possible using DNA bound

TABLE 3. Binding of λ DNA Fragments to Various DNA-agar Preparations

Organism	<i>E. coli</i> DNA Bound,* Relative %	Total λ Bound,† %
<i>E. coli</i> B	100	6.8
<i>E. coli</i> K12(λ)	101	9.5
<i>Shigella dysenteriae</i>	71	13.5
<i>Aerobacter aerogenes</i>	48	11.1
<i>Salmonella typhimurium</i> *	42-35	8.2
<i>Klebsiella pneumoniae</i>	25	0.7
<i>Proteus vulgaris</i>	14	0.2
<i>Serratia marcescens</i>	7	0.3
T ₄ bacteriophage	1	0.1

* Data from Bolton and McCarthy¹⁵ except for *Salmonella* values which are from Year Book 66, p. 110.

† 0.4 μ gm fragmented labeled λ DNA added to approximately 30 μ g DNA-agar.

to membrane filters in place of the DNA-agar.¹⁷ The effectiveness of hydroxyapatite columns for the fractionation of native and denatured DNA has been demonstrated by Bernardi¹⁸ and Miyazawa and Thomas¹⁹ and a modification of this procedure has been employed to study a variety of DNA-DNA reactions by Britten and Kohne.²⁰ Brenner, *et al.*²¹ have shown that the quantity of *E. coli* DNA which would react with *Salmonella* DNA is dependent upon the temperature of incubation. The amount of binding decreases as the incubation temperature is raised. Control experiments using *E. coli* DNA fragments reacted with *E. coli* DNA-agar incubated at 60°C and 66°C showed that the extent of reassociation is only slightly affected by these incubation temperature differences. However, as reported last year (*Year Book 66*, p. 109), the double-stranded molecules resulting from the reassociation of *E. coli* DNA with *S. typhimurium* DNA have a markedly lower thermal stability than reassociated *E. coli* DNA.

A reasonable explanation for these results is that a significant portion of the nucleotide sequences held in common between species either (1) contain unmatched base pairs or (2) are richer in adenine+thymine (A+T) than intraspecies duplexes, or (3) a combination of both (1) and (2) above. Studies investigating the thermal stability of DNA-DNA reaction products have been extremely useful in distinguishing between these alternatives.

Thermal stability of E. coli DNA fragments recovered from S. typhimurium DNA-agar. If the decreased thermal stability seen in the reaction between *E. coli* and *S. typhimurium* DNAs were due to unpaired bases, *E. coli** fragments, recovered from this interspecies reaction and subsequently reacted with *E. coli* DNA, should have a stability pattern typical of a reassociation reaction between *E. coli* DNAs. Conversely, a preponderance of A+T base pairs in the interspecies DNA duplex should result in

recovered *E. coli** fragments having a diminished stability when reassociated again with either *E. coli* or *Salmonella* DNAs. If both factors are involved, the thermal stability of the reisolated *E. coli** fragments reacting with *E. coli* DNA should have a stability pattern somewhere between that of a typical *E. coli**-*E. coli* reaction and that of an *E. coli**-*Salmonella* reaction.

Such an experiment was carried out as shown in Fig. 9. The results seen in this figure show that both unpaired bases and possibly a preferentially high percentage of A+T base pairs are present in the *E. coli*-*Salmonella* duplex.

A study of reactions among other enterobacterial DNAs is currently in progress. Preliminary experiments indicate that the reassociation products formed from the more closely related strains, *Shigella flexneri* and *E. coli*, have the same thermal stability as *E. coli*-*E. coli* duplexes.

Both the degree of reassociation and the thermal stability of the DNA-DNA reaction products are indicative of genetic relationships. Homology among family members indicates common origin and the degree of reduction of the thermal stability is another measure of the degree of genetic divergence.

Viral-bacterial DNA reactions. The demonstration that a third of the bacteriophage λ DNA was homologous to the DNA of its lysogenic host²² led to further studies of virus-host interrelationships. An initial concept was the belief that lysogeny and the high frequency of transduction of host genetic markers with lysogenic bacteriophages was probably due to some DNA homology between virus and host DNA. Schildkraut and co-workers²³ had reported no homology between the DNA of the T-even and the T-odd bacteriophages (all considered as being unable to lysogenize *E. coli*) and the *E. coli* DNA. Where no homology exists, bacteriophage infection

* P³² labeled

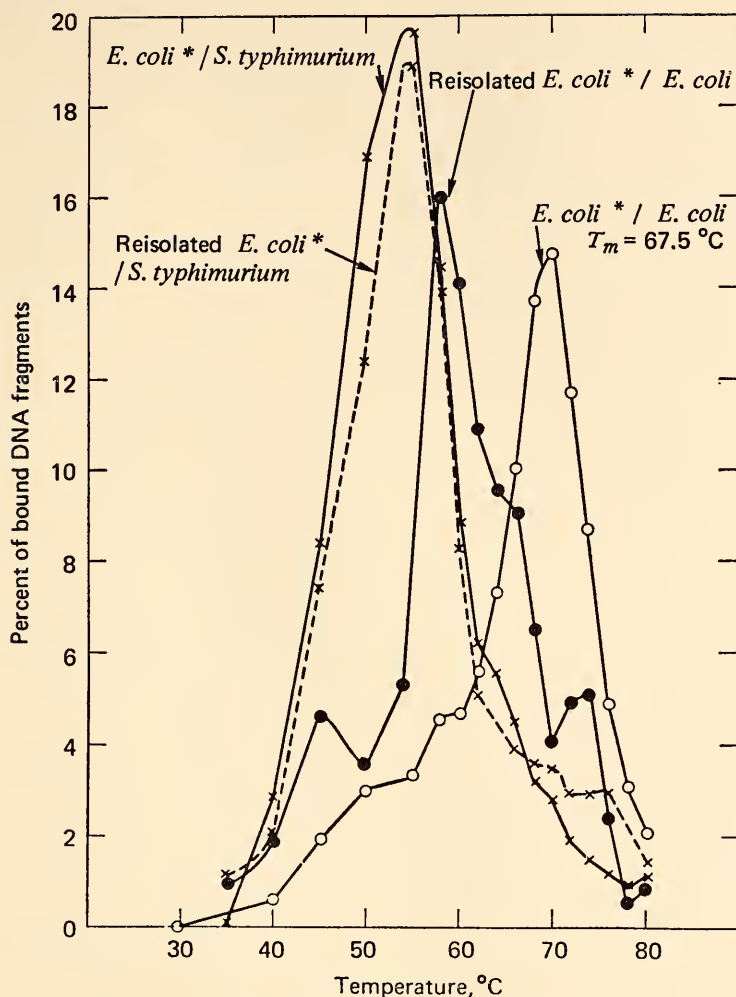


Fig. 9. Thermal elution profiles of *Escherichia coli** DNA fragments. *E. coli** DNA fragments (0.2 μ g in 0.2 ml) were reacted with 0.2 g of agar containing 32 μ g of *Salmonella typhimurium* DNA. The fragments were eluted and reisolated. The fragments were then reincubated with *E. coli* and *Salmonella typhimurium* DNA-agar, and the bound fragments were removed by a series of thermal elutions. *E. coli**-*E. coli* DNA-agar (open circles on line); *E. coli**-*Salmonella typhimurium* DNA-agar (x's on line); reisolated *E. coli**-*E. coli* DNA-agar (closed circles on line); reisolated *E. coli**-*Salmonella typhimurium* DNA-agar (x's on broken line).

results only in virulence and the lysis and death of the cell.

A second enterobacterial lysogenic system was therefore examined for virus-host DNA relationships. P₂₂ bacteriophage DNA was found to contain nucleotide sequences which would react

with the DNA of its lysogenic host *Salmonella typhimurium*.

Despite the success in these early experiments, it has not yet been demonstrated that DNA-DNA homologies play a direct role in lysogeny, transduction or the specificity of attachment to the host

chromosome. The problem became more complicated when it was observed that the DNA of bacteriophage λ was also homologous to the DNA of a λ sensitive strain of *E. coli* and to the DNA of three other enterobacteria (Table 3). None of these bacteria is normally considered to be a lysogenic host for phage λ . It is of interest that the three enterobacteria having the highest proportion of DNA homology with *E. coli* DNA are also homologous with phage λ DNA. Those enterobacteria showing lesser degrees of homology with *E. coli* DNA (Table 3) did not react with λ DNA fragments. Similarly P₂₂ bacteriophage DNA was found to be homologous to *E. coli* DNA.

In the hope of precisely locating the region of the λ genome containing the base sequence homology with *E. coli* DNA, Cowie and Hershey²⁴ examined left and right ends of λ and a segment of (b_2^+) defined by a genetic deletion. All three parts of the λ DNA molecule interacted with the *E. coli* DNA. Furthermore, Ingraham, Ehring and Hershey confirmed these findings and demonstrated that the strongest reaction occurs with fragments containing 46% guanine + cytosine (G+C), derived from the right half of the molecule (*Year Book 65*, p. 563). These authors also concluded that not more than eight sections, homologous to *E. coli* DNA, together spanning a third of the molecular length, are unequally distributed throughout the λ DNA.

The results described above do not

throw much light upon the function of the homology between λ DNA and the DNA of its host. The inference is, however, that there are three, and probably more, regions that can interact with the *E. coli* DNA. Which region, or regions, are involved in the lysogenic process, however, still remains obscure.

Table 4 indicates that virus-host DNA homology probably is a feature common to lysogenic systems. The first five temperate bacteriophages, despite differences in attachment sites, base compositions, and serological responses, all show base sequence interactions with *E. coli* DNA. Mutants of T₃ bacteriophage have been shown to be semitemperate, forming "lasting complexes" in which cellular lysis is long delayed following phage infection.²⁵ *Salmonella* is the bacterial host for the lysogenic P₂₂ bacteriophage. On the other hand T₄ bacteriophage does not lysogenize *E. coli*, and, in agreement with the results of Schildkraut *et al.*,²³ we find it has little or no capacity for interaction with *E. coli* DNA.

A study of the thermal stability of the products formed by the reaction of temperate bacteriophage DNAs with host DNA provided several significant results. Figures 10 and 11 are indicative of these findings.

The thermal elution profile shown in Fig. 10 shows the thermal stability of the reaction product of T₃ DNA fragments which have reacted with *E. coli* DNA. This profile should be compared to the control elution profiles where T₃ DNA

TABLE 4. Binding of Bacteriophage DNA Fragment to Bacterial DNA-agar Preparation

Bacteriophages	Bacteria	Homology, % *
λ	<i>E. coli</i>	33
$\phi 80$	<i>E. coli</i>	25
434	<i>E. coli</i>	46
434 hy	<i>E. coli</i>	38
15 (TAU)-	<i>E. coli</i>	6
T ₃	<i>E. coli</i>	7
P ₂₂	<i>Salmonella typhimurium</i>	26
T ₄	<i>E. coli</i>	0.1

* Approximately 0.2 μ g fragmented, P³²-labeled viral DNA was added to 0.2 gram agar containing bacterial DNA in excess of 100 μ g per 0.2 gram.

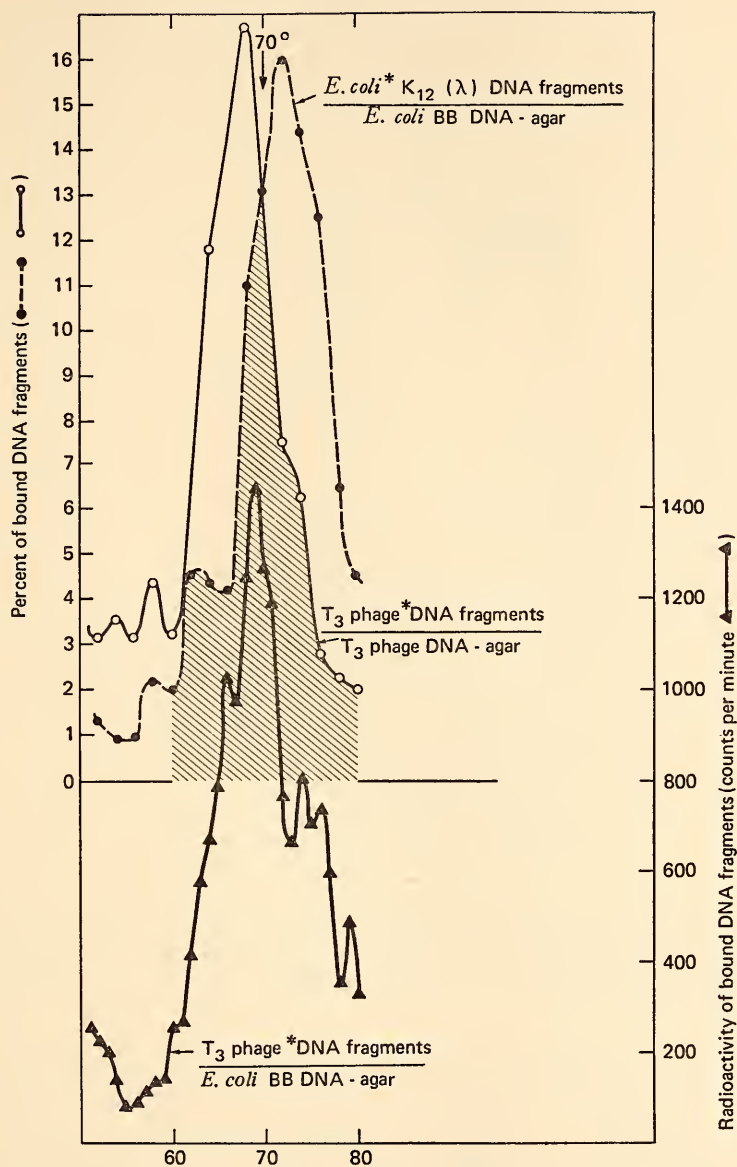


Fig. 10. Upper curves: Thermal elution profile resulting from a study of the reaction of *E. coli* K12(λ) DNA fragments with *E. coli*, BB DNA-agar (closed circles on broken line) and T_3 phage* DNA fragments with T_3 DNA-agar (open circles on line). Lower curve: Thermal elution profile obtained from a study of the reaction of 7 μ g T_3 phage* DNA fragments with 64 μ g *E. coli* BB DNA-agar (triangles on line). Approximately 3% of the T_3 phage DNA fragments were bound to the *E. coli* DNA-agar at these concentrations.

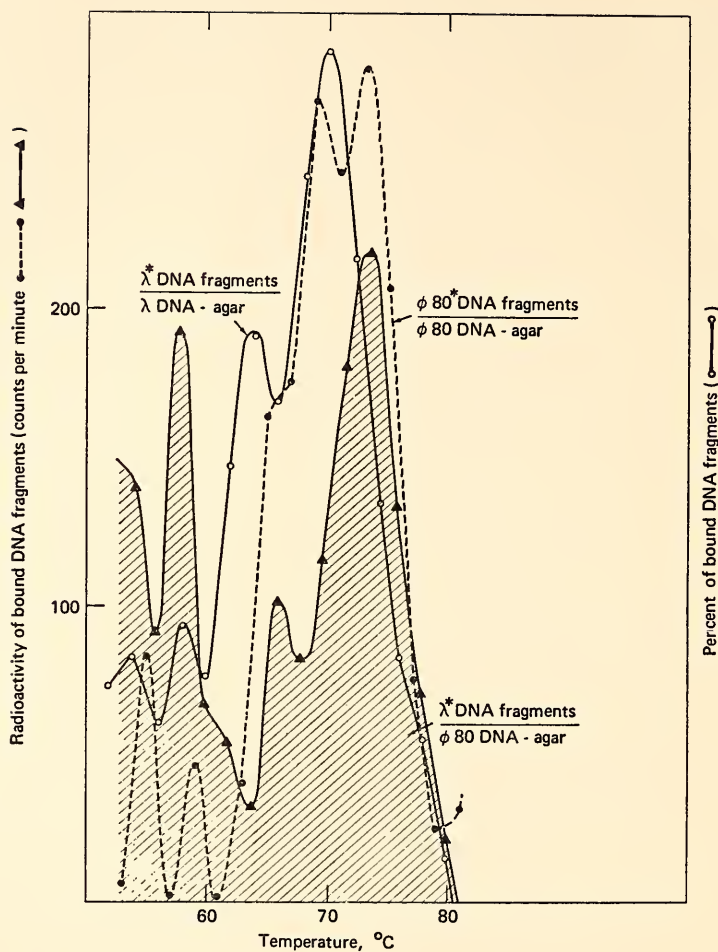


Fig. 11. Thermal elution profiles resulting from a study of the reaction of $\phi 80^*$ DNA fragments with $\phi 80$ DNA-agar (closed circles on broken line); *E. coli** DNA fragments with *E. coli* DNA-agar (open circles on line) and $\phi 80^*$ DNA fragments reacting with *E. coli* DNA agar (triangles on line).

fragments were reassociated with T_3 DNA-agar and *E. coli* DNA fragments with *E. coli* DNA-agar.

The virus-host DNA reaction shows a thermal elution maximum at 69°C , a value greater than that observed with the T_3 - T_3 DNA-agar control and lower elution maximum than that obtained for *E. coli* fragments reacting with *E. coli* DNA-agar. The elution maximum for the T_3 -*E. coli* reaction corresponds to the shaded area in Fig. 10 where maximum

overlapping of the two control elution profiles is observed. Since this is the region containing the largest amount of DNA with similar G+C compositions, one interpretation of the results shown is that T_3 DNA and *E. coli* DNA have reacted by almost perfect base-pair matching. Nevertheless, imperfect base sequence homology between the reacting portions of these heterologous DNAs has not yet been ruled out. If, however, imperfect matching of base pairs is occur-

ring in this reaction, then the fraction of unpaired nucleotides is much less than that observed between the reaction product obtained with the bacterial DNAs of *E. coli* and *Salmonella* (Fig. 9).

Figure 11 shows a similar virus-host elution profile obtained by reacting the DNA of bacteriophage $\phi 80$ with the DNA of its lysogenic host *E. coli*. In this case the reaction product has a higher elution temperature and therefore greater thermal stability than the average thermal stability of either of the two reacting DNAs. This example is indicative of almost perfect matching of nucleotide sequences. *It also indicates that the reaction must involve segments of both DNAs having a higher G+C content than the average content of either.*

Virus-virus DNA reactions. Since portions of the DNA of both lysogenic bacteriophages λ and P_{22} had been shown to be homologous to *E. coli* DNA, similarities between these phage DNAs might also have been expected. Table 5 demonstrates that approximately one fifth of the λ DNA can react with P_{22} DNA.

Right and left end quarters of the λ genome were tested to ascertain what portion (or portions) of the λ DNA contains nucleotide sequences which react with P_{22} DNA. Both ends were reactive, the right ends exceeding by a factor of two the capacity of the left ends to bind to P_{22} DNA.¹⁶

A similar result was obtained by Ingraham, Ehling, and Hershey²⁶ where the largest reaction of λ DNA with *E.*

coli DNA occurs with fragments containing 46% G+C, derived from the right half of the λ molecule.

These results suggest that λ and P_{22} might contain common DNA sequences which are also homologous to portions of the *E. coli* DNA. Table 5 confirms this hypothesis. Large quantities of unlabeled DNA fragments and labeled λ DNA fragments were added to P_{22} DNA-agar. The addition of unlabeled P_{22} DNA fragments produced the anticipated 60% reduction in the binding of the λ DNA fragments. Unlabeled *E. coli* fragments, added as the competing DNA, reduced the binding of the λ DNA by 25%. Even more reduction occurs when unlabeled *Salmonella* DNA is added.

A similar relationship exists among bacteriophages λ and $\phi 80$ and *E. coli*. Approximately 20% of the λ DNA will react with $\phi 80$ DNA; the addition of a large excess of unlabeled *E. coli* DNA reduces the quantity of λ DNA reacting with $\phi 80$ by 45%.

The interaction between the DNAs of two lysogenic viruses has never been completely eliminated by the addition of excess *E. coli* DNA as competitor material. This result implies that there are sequences held in common among the viruses which are not shared with the bacterium.

As an example of the relationships observed with lysogenic bacteriophage Table 6 shows the percentage of binding of λ DNA to other viral DNAs. It is evident from the above results that

TABLE 5. Effect of Bacterial and Viral DNA Fragments upon Binding of λ DNA to P_{22} DNA-agar

Preparation Number	Fragmented DNA Competitors	μg of DNA Competitors	Labeled λ DNA Fragments Bound, %
1	0	0	20.0
2	P_{22}	60	6.8
3	<i>Salmonella</i>	129	10.6
4	<i>E. coli</i>	108	15.4

Note: 0.01 μg λ^* DNA fragments was added to each agar preparation containing 24 μg P_{22} DNA together with unlabeled DNA competitor fragments. The P_{22} nonradioactive DNA control fragments diluted the P_{22} DNA (trapped in agar) by about two thirds.

TABLE 6. DNA Binding among Temperate Bacteriophages, %

Labeled DNA Fragments	434 hy	434	$\phi 80$	P ₂₂	Phage 15 (TAU) ⁻	T ₄
λ^*	69	67	22	20	0.1	0.1

among the temperate phage DNAs studied numerous viral-viral and viral-bacterial DNA homologies exist and that portions of the viral-viral homologous regions are also homologous to bacterial DNA.

The use of the thermal chromato-

graphic method has yielded significant information concerning the reaction products of interspecies DNA-DNA interactions. An elution profile characteristic of the reaction product formed in incubating λ DNA fragments with $\phi 80$ DNA-agar is shown in Fig. 12. Most of

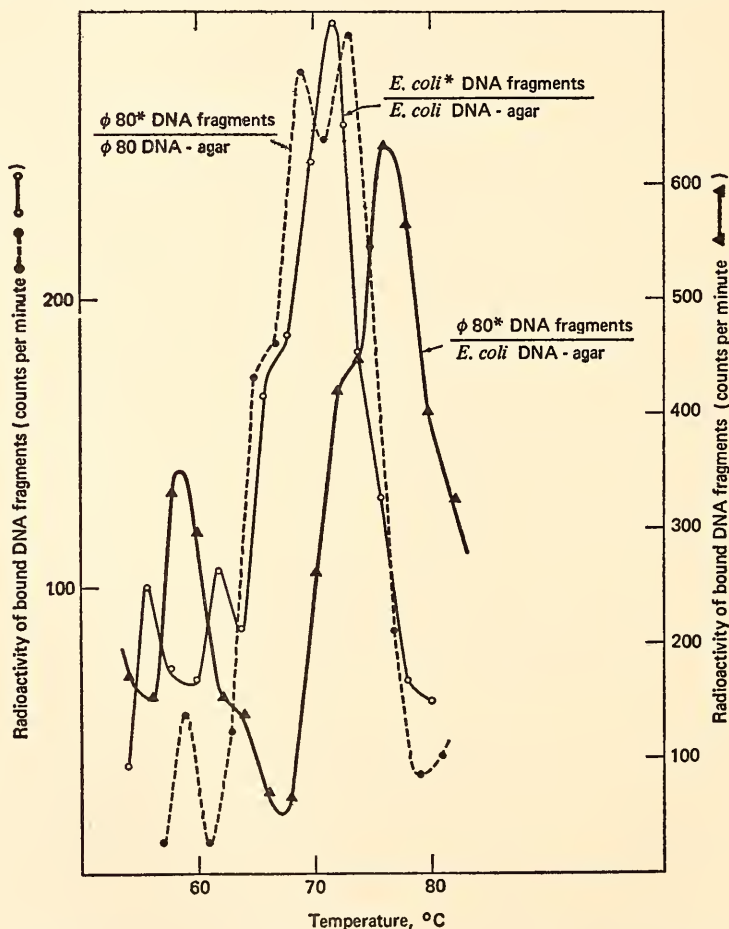


Fig. 12. Thermal elution profile resulting from a study of the reaction of $\phi 80^*$ DNA fragments with $\phi 80$ DNA-agar (closed circles on broken line); λ^* DNA fragments with λ DNA-agar (open circles on line) and λ^* DNA fragments reacting with $\phi 80$ DNA-agar (triangles on line, shaded area). The right-hand abscissa represents (for the λ - λ DNA reaction only) the percentage of the total bound material recovered in each elution fraction.

the reacting interspecies DNA duplexes are eluted at temperatures higher than those found to be characteristic of either the λ - λ or ϕ 80- ϕ 80 DNA reactions—also shown in Fig. 12. The λ DNA eluting at these higher temperatures presumably is contained in the left end of the λ molecule (56% G+C). Ingraham, Ehring and Hershey²⁶ independently arrived at the same conclusion with labeled λ fragments with known G+C values. The high thermal stability of this material also is indicative of precise matching of the reacting nucleotide sequences.

Summary. We have presented examples typical of DNA-DNA reactions that have been observed among enterobacteria and bacteriophages.

1. In contrast to the repetition observed in higher organisms repeated DNA sequences do not appear to be present in bacteria, except for a few sequences which code for ribosomal RNA (see p. 320).

2. Bacterial DNA-DNA reactions studied provide evidence that genetic similarities and differences among family members are distinguishable. Closely related bacteria show a high degree of similarity among their DNAs in quantity reacting and in the precision of base pairing.

3. Divergence among the bacteria can be estimated by the loss of the quantity of DNA capable of interaction and in the decrease in the thermal stability of the reactive segments.

Virus-bacterial DNA studies revealed several unexpected results.

1. Lysogenic bacteriophages have sizable portions of their DNAs which react with the DNA of their bacterial hosts. In the viral DNA these homologous segments appear to be numerous and scattered throughout the genome.

2. More of the lysogenic bacteriophage DNA is shared with the bacterial chromosome than would be needed for a single recognition site for lysogenization or for a specific attachment site. Perhaps sometime in their history these viruses

reacted with the bacterial chromosome at other than their present attachment site, or more than one attachment site is present.

3. Little evidence for base sequence divergence has been detected among the virus-host reacting DNA regions. The accuracy of base-pair matching in these regions appears to be nearly perfect.

This relatedness implies common origin and suggests that the presence of "hostlike" material is due to recurrent acquisition or to a single recent event, or to severe selection; that is, the homologous sequences are essential for the survival of the temperate virus. The lysogenization process appears to be a strong factor in the conservation of precise viral-bacterial genetic elements.

Very little is known concerning the evolutionary differentiation of the temperate bacteriophages.

1. The homologies which have been detected among the viral-viral DNA reactions show a curious pattern of evolutionary relationship; the thermal stability observable among the large number of interacting nucleotide sequences among the lysogenic viruses indicates perfect or almost perfect base-pair matching.

2. From these studies it is difficult to classify some bacteriophages infecting *E. coli*. Those which lysogenize appear to be closely interrelated. Little or no interaction is observable between these temperate phages and the virulent phages (like T_4) unable to lysogenize *E. coli*.

Once the extent of the genetic similarities has been recognized among the temperate viruses it is surprising that so little interaction is observable with other viruses which can only lyse the *E. coli* bacterium. At least 30 cistrons have been recognized in the viral genome, most of these presumably essential for specifying the enzymes which synthesize viral components. Different viruses which carry out similar functions might be expected to contain similar genetic se-

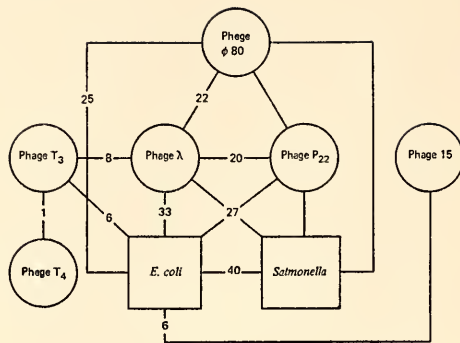


Fig. 13. Schematic diagram summarizing some of the genetic relationships observed among the bacteriophages and bacteria investigated. The percent homology is represented by the arrows linking the DNAs tested, the head of the arrow indicating the DNAs contained in the agars and the values shown representing the highest values observed in these studies.

quences. Apparently this is not generally true.

Figure 13 graphically summarizes some of the results of these studies. The conclusions reached provide some insight concerning genetic interrelationships among organisms having little repetitious DNA and should be useful in comparison of results observable among more evolutionarily advanced systems.

ISOLATION AND CHARACTERIZATION OF BACTERIAL RIBOSOMAL RNA CISTRONS

D. E. Kohne

In several bacterial species about 0.3% of the DNA has been shown to be complementary to R-RNA²⁷ which indicates that 4–5 ribosomal genes are present in each cell. This report describes the isolation of the rR-cistrons (ribosomal RNA cistrons), i.e., the fraction of DNA which codes for R-RNA. This is believed to be the first instance of the essentially complete purification of deoxyribonucleotide sequences characteristic for a specific gene function.

The isolation of the rR-cistrons was made possible by knowledge of the reas-

sociation kinetics of bacterial DNA and by the ability to separate specifically re-associated DNA from unreassociated DNA. The basic isolation procedure consisted of: (1) reacting nonradioactive R-RNA with radioactive DNA under conditions such that very little DNA:DNA reassociation occurred while virtually all of the DNA complementary to R-RNA formed R-RNA:DNA hybrids, and (2) separating the reassociated and unreassociated DNA by passing the incubation mixture through a hydroxyapatite column. Under the proper conditions reassociated DNA adsorbs to hydroxyapatite while unreassociated DNA passes through the column.

The basic technique of reacting labeled DNA with unlabeled RNA has broad application for RNA:DNA hybrid studies. It can be used to isolate any specific DNA sequence for which sufficient product RNA can be obtained. Although specific messenger RNA fractions are very difficult to isolate, R-RNA and transfer RNA are readily available. In addition, the method provides a very powerful tool for fractionating DNA on the basis of the expression of that DNA during the life cycle of a cell or an organism. This aspect will have great usefulness in the study of "differential gene expression" occurring in developing organisms.

Conditions for the formation and isolation of RNA-DNA hybrids. Knowledge of the reassociation kinetics of bacterial DNA made it possible to choose conditions for the reaction of R-RNA with DNA such that very little DNA:DNA reassociation occurred while all of the DNA complementary to R-RNA formed DNA:R-RNA hybrids. The hybrids could then be separated from the unreassociated DNA by using hydroxyapatite.

A convenient way to express the exposure of nucleic acids under reassociation conditions is the C_0t ²⁸ which is defined as the product of the nucleic acid concentration (C_0) and the time (t) of the reassociation incubation period. In this re-

port C_0t is conveniently calculated as the product of the nucleic acid concentration expressed as optical density at 260 $m\mu$ and the time of incubation expressed in hours, divided by two ($C_0t = \text{O.D.}/2 \times \text{hours}$). Incubation of a reassociation mixture with an optical density of 2 for one hour results in a $C_0t = 1$. The extent of reassociation of R-RNA with DNA complementary to it is controlled by the magnitude of the R-RNA C_0t . For these experiments a large enough R-RNA C_0t is used to ensure complete reaction of all DNA complementary to R-RNA.

DNA:DNA reassociation can occur in the incubation mixture as well as R-RNA:DNA hybrid formation. In order to minimize the extent of DNA:DNA reassociation the DNA C_0t is kept very low. It was impractical to utilize a DNA C_0t low enough to completely prevent DNA:DNA reassociation when R-RNA was reacted with whole DNA. Consequently, the reassociated fraction adsorbed to hydroxyapatite contained both DNA:DNA duplexes and R-RNA:DNA hybrids. In order to eliminate DNA which was not complementary to R-RNA it was necessary to pass the isolated fraction containing the R-RNA:DNA hybrids through two additional cycles of reassociation and isolation of the reassociated fraction. In each cycle of purification the DNA C_0t decreases greatly while the R-RNA C_0t is kept constant at a level which ensures complete reaction of the rR-cistrons with R-RNA.

Purification of DNA. The P^{32} -DNA used in these experiments was isolated by standard methods. Several additional steps were also necessary: The purified DNA was precipitated from 2-ethoxyethanol four times in order to eliminate P^{32} -labeled contaminants. The DNA was sheared at 50,000 psi, denatured in 0.14 M PB* and immediately passed through

a hydroxyapatite column equilibrated to 50°C and 0.14 M PB. Crosslinked DNA and any radioactive contaminants which adsorb to hydroxyapatite are removed from the bulk DNA in this step.

Isolation of rR-cistrons. The method used to isolate bacterial rR-cistrons is as follows:

1. Mix P^{32} -labeled (100,000 cpm/ μg), sheared, hydroxyapatite purified DNA (10 $\mu\text{g}/\text{ml}$) with unlabeled R-RNA (20 $\mu\text{g}/\text{ml}$) in 0.14 M PB.

2. Denature the mixture by heating at 100°C for 3–5 minutes in a water bath; incubate at 60°C for one hour (R-RNA $C_0t = 0.25$). Pass the incubation mixture through a hydroxyapatite column equilibrated to 60°C and 0.14 M PB. Wash all single-stranded DNA through the column. R-RNA adsorbs almost completely under these conditions. Recover the reassociated DNA from the column by heating the water-jacketed column to 100°C and washing the RNA and DNA off in 0.14 M PB.

3. Take the material recovered by the 100°C elution of the column and repeat step 2. The R-RNA C_0t should be the same for each cycle.

4. Take the high temperature elution material from step 3 and bring the solution to 0.2 M NaOH and incubate this solution at 60°C for 1 hour to hydrolyze the RNA. Cool the solution and neutralize the NaOH present. Dilute the solution to 0.035 M PB and pass it through a hydroxyapatite column equilibrated to 60°C and 0.035 M PB. At this phosphate ion concentration DNA adsorbs to hydroxyapatite while ribonucleotides pass through the column. Recover the DNA from the hydroxyapatite column in several milliliters by eluting the column at 100°C with 0.14 M PB.

5. React the P^{32} -DNA recovered in step 4 with R-RNA (100 $\mu\text{g}/\text{ml}$) for 12 minutes at 60°C in 0.14 M PB (R-RNA $C_0t = 0.25$) and separate the reassociated fraction on hydroxyapatite and recover it. Again treat the isolated fraction with NaOH and recover as in (4). The prod-

* Phosphate buffer, $\text{pH} = 6.8$, prepared by mixing equimolar volumes of Na_2HPO_4 and NaH_2PO_4 .

ucts of this procedure are purified rR-cistrons.

P³²-DNA which did not reassociate in the first cycle (2) was reacted again with R-DNA and only 0.02% of the P³²-DNA was recovered after two cycles of purification. This indicates that the rR-cistrons were essentially completely removed during the first purification cycle.

Characterization of isolated rR-cistrons. Table 7 presents data which show that in the presence of *E. coli* R-RNA the quantity of *E. coli* DNA adsorbing to hydroxyapatite did not fall below 0.27% during the cycles of purification described. Where no R-RNA was present the fraction of *E. coli* DNA recovered fell to 0.01% after only three cycles of purification. The reaction of chicken R-RNA with the *E. coli* DNA resulted in a level of recovery of DNA almost identical to the value obtained when R-RNA was absent. This demonstrates the specificity of the reassociation reaction. Control or blank values were determined for each different P³²-DNA preparation and varied from 0.01% to 0.02% of the input radioactivity.

Table 8 shows the quantity of DNA recovered with increasing R-RNA *C₀t*. These "saturation" experiments indicate that the quantity of DNA complementary to R-RNA under these conditions is about 0.27% for *E. coli* and about 0.35%

TABLE 8.

R-RNA <i>C₀t</i>		Original Input DNA Recovered, % (Corrected for Blank)
<i>E. coli</i>	0	0.00 (blank = 0.01)
	0.12	0.274
	0.25	0.266
	0.5	0.261
<i>Proteus mirabilis</i>	0	0.00 (blank = 0.018)
	0.11	0.36
	0.11	0.35
	0.38	0.36

Note: The fraction of original input P³²-DNA adsorbed to hydroxyapatite with increasing R-RNA *C₀t*. Each value represents the fraction adsorbed after three cycles of purification. The approximate one-half *C₀t* for the reaction of R-RNA with rR-cistrons is about 0.008.

for *Proteus mirabilis*. The value for the fraction of *E. coli* DNA which is complementary to R-RNA agrees well with the values obtained by other investigators using the reaction of labeled R-RNA with unlabeled DNA.²⁷

The data in Table 9 show that isolated rR-cistrons from *E. coli* and *Proteus mirabilis* reassociate almost completely with their respective DNAs and R-RNAs. Further, 94% of the *E. coli* rR-cistrons reassociates with a mixture of MAK purified 16S and 23S *E. coli* R-RNA subunits. This high percentage of reaction indicates that little if any DNA which codes for 5S or transfer RNA is present in the rR-cistron preparation.

TABLE 7.

Cycle		P ³² -DNA <i>C₀t</i>	R-RNA <i>C₀t</i>	Original Input P ³² -DNA Adsorbed, %
(A)	1	0.08	0.25 (<i>E. coli</i> RNA)	2.37
	2	0.0008	0.25 (<i>E. coli</i> RNA)	0.307
	3	1.5 × 10 ⁻⁵	0.25 (<i>E. coli</i> RNA)	0.276
	4	1.5 × 10 ⁻⁵	0.25 (<i>E. coli</i> RNA)	0.265
(B)	1	0.08	0	2.1
	2	0.0008	0	0.029
	3	7 × 10 ⁻⁶	0	0.01
(C)	1	0.033	0.3 (chicken RNA)	1.1
	2	0.0002	0.3 (chicken RNA)	0.038
	3	9 × 10 ⁻⁶	0.3 (chicken RNA)	0.017

Note: Data showing the fraction of original input P³²-*E. coli* DNA adsorbing to hydroxyapatite when reacted (A) with *E. coli* R-RNA; (B) in the absence of any R-RNA; (C) with chicken R-RNA.

TABLE 9.

Source of rR-cistrons	Reaction of rR-cistrons, % with		Mixture of Purified 16S and 23S R-RNA Subunits
	Homologous R-RNA	Homologous DNA	
<i>E. coli</i>	96	96.5	94
<i>Proteus mirabilis</i>	96	96.5	...

Note: The extent of reassociation of preparations of P^{32} -rR-cistrons with various preparations of unlabeled nucleic acids. The R-RNA *Cot* for these reactions was greater than 0.2. The DNA *Cot* utilized in each case was sufficient for the reassociation of greater than 95% of the unlabeled DNA. All reactions were carried out at 60°C in 0.14 M PB. *E. coli* R-RNA subunits were purchased from Miles Laboratories. Similar results were obtained using an alternate source of 16S and 23S R-RNA subunits.

The 6% of the radioactivity which did not reassociate has not been characterized. About 3% of the *E. coli* rR-cistron radioactivity adsorbed to hydroxyapatite when reacted with a R-RNA preparation which was first hydrolyzed in 0.2 N NaOH for 1 hour at 60°C. Approximately 3% of the rR-cistron radioactivity also adsorbs to hydroxyapatite when the preparation is denatured and passed through hydroxyapatite in the absence of R-RNA.

E. coli, with a DNA content of 2.8×10^9 daltons, contains enough DNA complementary to R-RNA for about 5 separate rR-cistrons. *Proteus mirabilis* also has a DNA content of about 2.8×10^9 daltons and apparently contains about 6 separate rR-cistrons per cell. These numbers are calculated using values of 1.1×10^6 and 0.55×10^6 daltons for the 23S and 16S R-RNA subunits. Moore and McCarthy²⁹ have reported that 0.18% of *E. coli* DNA is complementary to 23S R-RNA. This is enough DNA for 5 separate copies of the nucleotide sequence coding for 23S R-RNA. This value and data reported here and elsewhere²⁷ suggest that the number of 16S cistrons is equal to the number of 23S cistrons.

*Thermal stability of reassociated DNA.** The thermal stability of reasso-

ciated DNA indicates the accuracy of base-pair matching between component strands of DNA. Native DNA is assumed to have perfect base-pair matching. Since the thermal stability of reassociated and native DNA are virtually the same,²⁸ perfect or near-perfect base-pair matching should exist also between component strands of the reassociated DNA.

Hydroxyapatite has been utilized to measure the thermal stability of native and reassociated DNA. Figure 14 presents a hydroxyapatite thermal elution profile for *E. coli* R-RNA:DNA hybrids. These hybrids were formed by allowing radioactive rR-cistrons to reassociate with a mixture of unlabeled 16S and 23S R-RNA subunits. The T_m of the R-RNA:DNA hybrids is about 10°C lower than the T_m of reassociated bulk *E. coli* DNA measured under the same conditions (Fig. 15, dashed curve). *Proteus mirabilis* R-RNA:DNA hybrids have a similar T_m . Other investigators also have reported RNA:DNA hybrids to have a lower thermal stability than double-stranded DNA of the same base composition.²⁹

*The incubation mixtures were passed through a hydroxyapatite column equilibrated to 60°C and 0.14 M PB. After washing all of the single-stranded DNA off the column, the temperature of the column was raised in 5°C steps. After each 5°C temperature rise the

column was washed once with 20 ml of 0.14 M PB. After the 0.14 M PB wash at 100°C, 20 ml of 0.4 M PB were passed over the column to elute any remaining DNA. The column effluents (20 ml) were collected in a standard glass counting vial and assayed for radioactivity by Cerenkov counting. When necessary, the optical density (260 m μ) of the same solution was measured in a spectrophotometer.

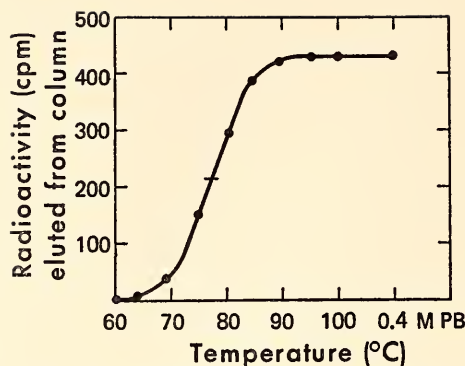


Fig. 14. Thermal stability profile of RNA:DNA hybrids formed between a mixture of 16S and 23S R-RNA subunits and P^{32} -labeled rR-cistrons. The R-RNA subunits were purchased from Miles Laboratory. A R-RNA C_{0t} of 0.3 (120 μ g R-RNA/ml incubated for 12 minutes at 60°C in 0.14 M PB) was utilized for this reaction. Ninety-four percent of the rR-cistrons reassociated with the R-RNA.

Figure 15 shows the thermal stability profile of reassociated *E. coli* rR-cistrons and bulk DNA. The T_m of the rR-cistrons is about one to two degrees lower than the T_m of the bulk DNA. A variety of factors influence the thermal stability of these reassociated rR-cistrons. *E. coli* R-RNA, and hence its DNA complement, has a slightly greater guanine-cytosine content than bulk *E. coli* DNA. Reassociated rR-cistrons (55% guanine-cytosine) should have a T_m one to two degrees higher than bulk DNA (52% guanine-cytosine). This assumes, however, that perfect base-pair matching occurs between component strands of the reassociated rR-cistrons as it does for bulk *E. coli* DNA.²⁸ Occurrence of base-pair mismatches in the reassociated rR-cistrons would reduce the T_m about 0.5–1°C per one percent mismatched bases.^{30, 31, 32} If the multiple rR-cistrons were not identical but were similar enough so that each cistron could react with another cistron's complement, the thermal stability of the reassociated rR-cistrons would be lower than that expected from their guanine-cytosine content.

In order to interpret properly the data of Fig. 15, a correction must be made for the fact that the rR-cistrons are slightly damaged during the isolation procedure. P^{32} -labeled bulk *E. coli* DNA, when put through the same processes of boiling, column fractionation, and alkaline hydrolysis, had a T_m 2–3°C lower than the T_m of untreated bulk DNA with which it was reassociated. If these data are used to adjust the data of Fig. 15, the corrected T_m of the rR-cistrons is slightly higher than the T_m of bulk *E. coli* DNA. Such a high thermal stability indicates that perfect or nearly perfect base-pair matching is present in the reassociated rR-cistrons. The present data cannot rule out, however, the existence of a

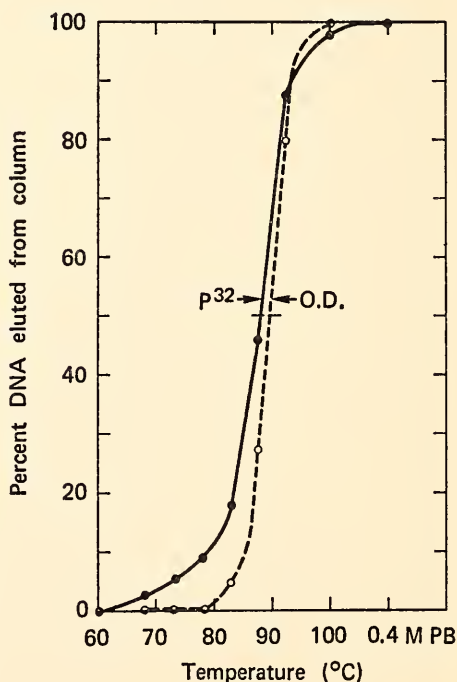


Fig. 15. Thermal stability profile of reassociated unlabeled bulk *E. coli* DNA (broken line) and reassociated radioactive *E. coli* rR-cistrons (solid line). A mixture of rR-cistrons (0.023 μ g) and unlabeled bulk DNA (530 μ g) was denatured and incubated in 0.5 ml for a DNA C_{0t} of 306. Ninety-four percent of the radioactivity and 96% of the bulk DNA adsorbed to hydroxyapatite.

small amount (1% or less) of base-pair mismatching.

Whole DNA from *Proteus mirabilis* has a guanine-cytosine content of about 39%, while its R-RNA contains about 54% guanine-cytosine. Thermal stability studies similar to those described above for *E. coli* show that reassociated *Proteus mirabilis* rR-cistrons exhibit a T_m 2–3°C higher than whole DNA (Fig. 16). This suggests that these isolated rR-cistrons have a higher guanine-cytosine content than does whole DNA. The high thermal stability of the R-RNA cistrons once again indicates that nearly all bases have paired properly with their complementary bases during reassociation. Again, the existence of a small amount of

base-pair mismatching cannot be ruled out.

Since multiple rR-cistrons are known to exist in each bacterial cell, the possible heterogeneity of R-RNA has been an open question of evident importance. Isolation of these rR-cistrons has made it feasible to examine the possibility of R-RNA heterogeneity. The thermal stability results presented here indicate that the population of rR-cistrons in a cell does not show the nucleotide sequence divergence typical of a "family" of repeated nucleotide sequences present in higher organism DNAs.²⁸ The rR-cistrons in bacterial cells should be either (1) completely different from one another; (2) all identical, or nearly identical, to one another; or (3) a situation intermediate between (1) and (2) where, for example, three of the R-RNA cistrons have identical nucleotide sequences and two are different. Reassociation kinetic studies make it possible to discriminate partially among these alternatives. These experiments are described in the next section.

Kinetics of reassociation of R-RNA cistrons.* Virtually all nucleotide sequences in bacteria occur only once per cell.²⁸ If the five separate rR-cistrons of *E. coli* each represent a different nucleotide sequence, occurring once per cell, such cistrons would be expected to reassociate at the same rate as bulk *E. coli* DNA. If, however, these separate rR-cistrons represent one nucleotide sequence repeated five times in each cell,

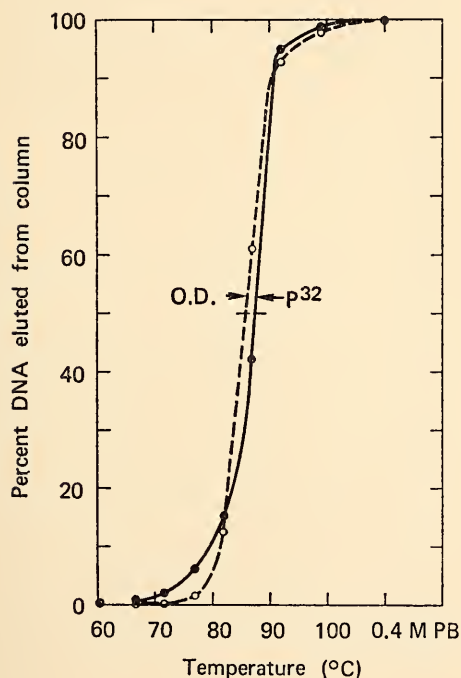


Fig. 16. Thermal stability profile of reassociated unlabeled *Proteus mirabilis* bulk DNA (broken line) and reassociated radioactive *Proteus mirabilis* rR-cistrons (solid line). A mixture of rR-cistrons (0.014 μ g) and bulk DNA (400 μ g) was denatured and then incubated in 0.3 ml for a C_0t of 277. Ninety-six percent of both the radioactivity and bulk DNA adsorbed to hydroxyapatite.

* Nucleic acids in 0.14 M PB were denatured at 100°C for 3–5 minutes and incubated at 60°C for specified times. At the end of the incubation period the sample (or a fraction of it) was passed through a hydroxyapatite column equilibrated to 60°C and 0.14 M PB. After washing single-stranded DNA from the column, the DNA adsorbed to hydroxyapatite could be recovered by thermal elution at 100°C in 0.14 M PB, or high salt (0.4 M PB) elution at 60°C. DNA recovered by high salt elution retains its double-stranded form. The amount of DNA in the reassociated and unreassociated fractions was then measured.

they would be expected to reassociate five times faster than bulk *E. coli* DNA. Intermediate cases, while more complex in nature, would fall between the two extremes. If, for example, four similar and one different rR-cistrons were present, they would reassociate somewhat less than four times faster than bulk *E. coli* DNA.

Hydroxyapatite has been utilized to determine the rate of reassociation of rR-cistrons relative to the rate of reassociation of bulk bacterial DNA. For these experiments radioactive rR-cistrons were mixed with nonradioactive whole bacterial DNA and the kinetics of reassociation of the two fractions determined. Measuring the reassociation kinetics of the mixture of rR-cistrons and bulk DNA should control the many variables which affect the rate of reassociation. It therefore should be possible to obtain a reasonably accurate value for the relative rates of reassociation. The reassociation data have been plotted using the C_0t method of presentation.²⁸

Figure 17 shows the reassociation kinetics of *E. coli* rR-cistrons and bulk *E. coli* DNA. The curves drawn are for ideal second-order reactions. The experimental points for the bulk DNA closely follow the ideal curve. *E. coli* rR-cistrons reassociate about 3.6 times faster than bulk *E. coli* DNA. Figure 18 presents a similar study on the reassociation of *Proteus mirabilis* rR-cistrons with unfractionated *Proteus mirabilis* DNA. In this case the rR-cistrons reassociate about 4.4 times more rapidly than bulk DNA.

The rate of reassociation of the rR-cistrons indicates that a large majority of the cistrons are sufficiently alike to reassociate together to form a stable double-stranded product. Thermal stability studies show that very nearly perfect base-pair matching exists between the component strands of the reassociated rR-cistrons. These results strongly indicate that the majority of the rR-cistrons in both *E. coli* and *Proteus mirabilis* are very similar to one

another and that a high degree of homogeneity exists in the R-RNA gene family.

The dashed curves on either side of the rR-cistron reassociation kinetic data (Fig. 17) are the theoretical second-order curves calculated for the reassociation of rR-cistrons when: (A) all are identical; (B) four are identical and one differs. The present data cannot discriminate between these and other alternatives. Measurements of the kinetics of reassociation of R-RNA and rR-cistrons should make it possible to discriminate between the various possibilities. Such studies are now in progress.

Other investigators have studied the question of the heterogeneity of R-RNA in bacteria,^{33, 34, 35} and have reported data which suggest that heterogeneous R-RNA might be present in a bacterial cell. In each case, however, heterogeneity of the R-RNA was only one of several possible interpretations of their data.

Comparison of R-RNA cistrons in different bacterial species. Isolation of rR-cistrons of *E. coli* made possible the direct comparison between these rR-cistrons and those which exist in other species of bacteria. This was accomplished by reassociating small quantities of labeled *E. coli* rR-cistrons with large amounts of unlabeled DNA from other bacterial species. A time period long enough to ensure greater than 90% reassociation of the unlabeled DNA was used. Reassociated DNA then was separated from single-strand DNA by using hydroxyapatite. Thermal stability profiles of both reassociated bulk DNA and reassociated rR-cistrons were obtained by thermally eluting DNA from hydroxyapatite and assaying for radioactivity and optical density at 260 m μ . Thermal stability profiles for the unlabeled DNA served as a useful internal marker for determining the relative T_m of the DNA: DNA "hybrid" molecules. The bacterial species examined showed over 90% relatedness between their rR-cistrons. In addition, thermal stability profiles indi-

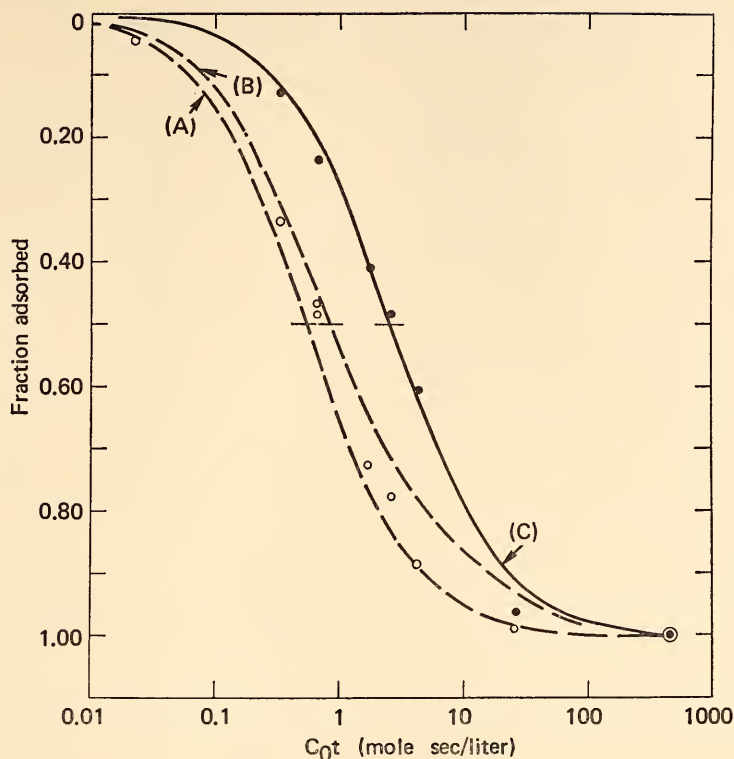


Fig. 17. Reassociation kinetics of a mixture of radioactive *E. coli* rR-cistrons and *E. coli* unlabeled bulk DNA. Open circles represent the reassociation of P^{32} -rR-cistrons while the closed circles represent the reassociation of bulk DNA. Curves A and B represent the theoretical second-order reaction curves calculated for situations where (A) all of the rR-cistrons are identical, (B) four of the rR-cistrons are identical and one is different. Curve C drawn through the bulk DNA reassociation points (closed circles) is the theoretical second-order reaction curve calculated for a homogeneous DNA with a C_{ot} at one half reassociation equal to that of the bulk DNA. Each point represents a separate incubation mixture which was denatured and incubated for a specific C_{ot} before passing it through hydroxyapatite. The lowest unlabeled DNA to rR-cistron ratio used for any incubation mixture was 6500/1. Incubation mixtures with a ratio of 30,000/1 or greater were used for the majority of points. Several different bulk DNA concentrations (18 $\mu\text{g/ml}$ to 880 $\mu\text{g/ml}$) were utilized for these experiments. Reassociation of the rR-cistrons was followed by monitoring the radioactivity. Reassociation of bulk DNA was followed by assaying for optical density at 260 $m\mu$. The maximum observed reassociation of the radioactivity was 95.5%, and that of the bulk DNA was 95.5%. At the C_{ot} utilized for this point ($C_{ot} = 484$) all of the DNA present in the reaction mixture should have reassociated. At zero time of incubation about 1.7% of the rR-cistron radioactivity adsorbed to hydroxyapatite. The data points on this curve have been corrected for the zero time adsorption and for the radioactive and optical density material which is incapable of reassociating.

cated a high precision of base-pair matching between component strands of the interspecies DNA:DNA hybrids (Figs. 15, 19, 20). Considerably less relatedness between these bacterial species was detected when the degree of related-

ness between the whole DNAs was measured under incubation conditions identical to those used here. There is about 40% relatedness between *Salmonella typhimurium* and *E. coli* DNAs³⁶ while only about 4% relatedness can be de-

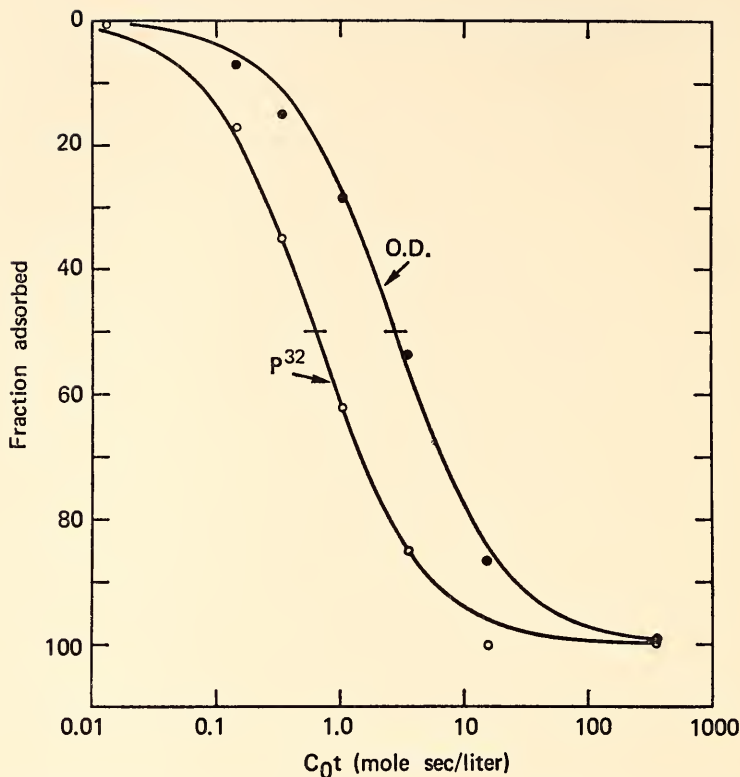


Fig. 18. Reassociation kinetics of a mixture of radioactive *Proteus mirabilis* rR-cistrons and unlabeled *Proteus mirabilis* bulk DNA. Each point represents a separate incubation mixture which was denatured and incubated for a specific *Col* before passing it through hydroxyapatite. The curves drawn through these points are ideal second-order reaction curves. The lowest ratio of unlabeled DNA to rR-cistrons used for any incubation mixture was 1000/1. Incubation mixtures with a ratio of 20,000/1 or greater were used for the majority of points. Several different bulk DNA concentrations (8 $\mu\text{g/ml}$ to 1240 $\mu\text{g/ml}$) were utilized for these experiments. Reassociation of the rR cistrons was measured by monitoring the radioactivity. Reassociation of bulk DNA was followed by assaying for optical density at 260 $m\mu$. The maximum observed reassociation of the radioactive DNA and bulk DNA was 96.5%. At zero time of incubation about 2% of the rR-cistron radioactivity adsorbed to hydroxyapatite. The data points on this figure have been corrected for zero time adsorption and for the fact that not all of the radioactive or optical density material is capable of reassociating.

tected between the DNAs of *E. coli* and *Proteus mirabilis*.³⁷ Further, thermal stability studies indicate that the nucleotide sequences which are held in common between these species are similar but not identical. The T_m of interspecies DNA: DNA hybrids formed between whole DNAs of *Salmonella typhimurium* and *E. coli* is about 9.0°C below that expected for perfect base-pair matching, while the

T_m of *E. coli*-*Proteus mirabilis* DNA: DNA hybrids is about 14°C lower than that of reassociated *E. coli* DNA.³⁷

These data suggest that rR-cistrons apparently have been strongly conserved during bacterial evolution and that the great majority of nucleotide sequences have diverged at a much faster rate than the rR-cistrons. Such a conclusion, while not new information, serves to confirm in

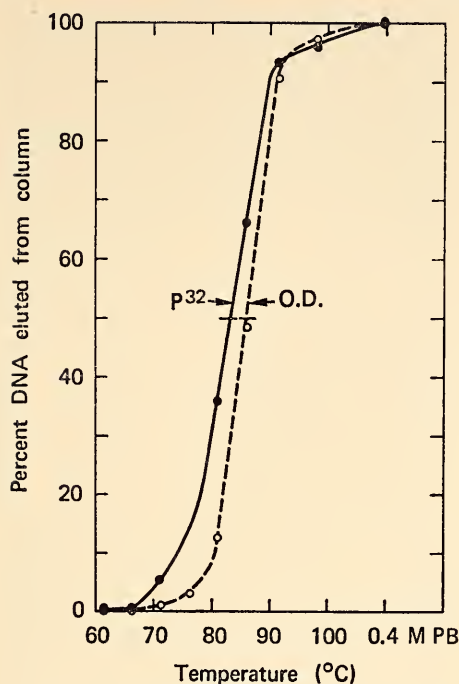


Fig. 19. Thermal stability profile of DNA:DNA interspecies "hybrids" formed between P^{32} -labeled *E. coli* rR-cistrons and unlabeled *Proteus mirabilis* bulk DNA. A mixture of rR-cistrons (0.006 μ g) from *E. coli* and *Proteus mirabilis* bulk DNA (400 μ g) was denatured and then incubated in 0.5 ml for a C_{ot} of 1350. Ninety-two percent of the radioactivity and 97% of the bulk DNA adsorbed to the hydroxyapatite. The percent relatedness of *E. coli* rR-cistrons to those of *Proteus mirabilis* is about 93% when normalized to the extent of reassociation of *E. coli* rR-cistrons with *E. coli* DNA.

an independent manner the previous findings of several other investigators.²⁹

The thermal stability data indicate that some divergence has occurred between the rR-cistrons of bacterial species. This is most striking in the case of the comparison of *E. coli* rR-cistrons with those of *Proteus mirabilis* (Fig. 19). Moore and McCarthy have more extensive data concerning this point.²⁹ Their data were obtained by reacting radioactive R-RNA from one species with unlabeled DNA from other species and

measuring the thermal stability profiles of the R-RNA:DNA hybrids formed.

Repeated nucleotide sequences in bacteria. The experiments described above demonstrate that small amounts of repeated nucleotide sequences occur in the bacterial genome. Further, the sequence which has been repeated is directly involved in a known physiological function, protein synthesis. It is not known, however, whether all of the member sequences in this family are utilized as templates for R-RNA synthesis. If all of the sequences are not used for transcrip-

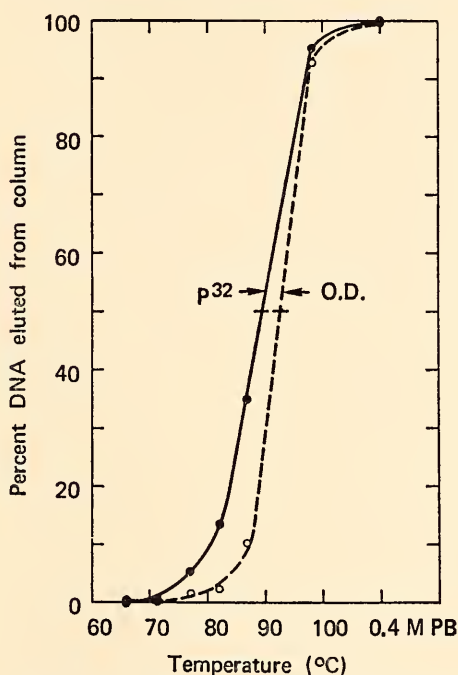


Fig. 20. Thermal stability profile of DNA:DNA interspecies "hybrids" formed between P^{32} -labeled *E. coli* rR-cistrons and unlabeled *Salmonella typhimurium* bulk DNA. A mixture of rR-cistrons (0.007 μ g) from *E. coli* and unlabeled *Salmonella typhimurium* bulk DNA (360 μ g) was denatured and then incubated in one ml for a C_{ot} of 511. Ninety-two percent of the radioactivity and 97% of the bulk DNA adsorbed to the hydroxyapatite. The percent relatedness of *E. coli* rR-cistrons to those of *Salmonella* is 96% when normalized to the extent of reassociation of *E. coli* rR-cistrons with *E. coli* DNA.

tion, the bacteria are carrying a minor fraction of DNA which is nonfunctional.

GENETIC EXPRESSION OF NONREPEATED DNA SEQUENCES IN THE MOUSE

A. H. Gelderman, A. V. Rake, and
R. J. Britten

The transcription of genetic information from the nucleotide sequences of DNA into complementary RNA has been studied fruitfully in many laboratories by hybridization of the RNA to DNA. None of the previous experiments which measured the RNA-DNA hybridization of higher organisms observed hybrids between RNA and nonrepeated DNA sequences. These earlier experiments were done at so low a concentration of either RNA or DNA that the observed hybridization was due to RNA reaction with the repeated DNA sequences (ERRF, or rapidly reassociating fraction). Thus, the following important questions concerning higher organisms have remained unanswered. Are nonrepeated sequences, i.e., unique DNA, expressed? How much of the unique DNA is expressed? How much of the rapidly labeled RNA, presumed messenger RNA (mRNA), is derived from unique DNA?

Three techniques using high concentrations of either mouse RNA or DNA were devised to study these questions of unique DNA expression.

1. The first employed a high concentration of unlabeled RNA and a small amount of labeled unique DNA to determine what fraction of the unique DNA was transcribed. The RNA-DNA hybrid was separated from unreacted DNA by hydroxyapatite fractionation. The DNA recovered from the hybrid was shown to be nonrepeated by its slow rate of reassociation with unfractionated mouse DNA.*

* *C¹⁴ DNA-RNA hybrid separation on hydroxyapatite.* Unlabeled RNA was extracted from whole newborn mice. Any contaminating DNA was removed by repeated digestion with DNase (50 μ gm/ml, 30 min. 37°C in

2. The second method used unlabeled unique DNA at a high concentration and a smaller amount of rapidly labeled RNA to determine the percentage of this RNA that was homologous to the unique DNA. RNase was used to digest the unhybridized RNA and the hybrids were isolated by Sephadex column chromatography.†

0.005 *M* MgCl₂, 2.0 *M* CH₃ COOK) and by repeated precipitation of the RNA (75% C₂H₅OH, -10°C, overnight).

The RNA was found to be free of contaminating nucleases by incubation of the solution for 50 hours at 70°C with P³²-labeled RNA. At the end of the incubation 9% of the labeled RNA was acid soluble; such a small amount of deterioration was not considered to be crucial.

Uniformly labeled C¹⁴ "L" cell DNA was prepared as described in the footnote on page 327. The C¹⁴ DNA was incubated to a point where 54% of the DNA was reassociated (*C₀t* $\sim 1.5 \times 10^9$) and the unreassociated unique DNA was separated from the reassociated DNA by hydroxyapatite fractionation and re-concentrated by adsorption to a nitrocellulose filter and eluted in a small volume.

To hybridize the RNA with the unique C¹⁴ DNA a solution of 14 μ gm and 67 mg of RNA in 1.0 ml of 0.24 *M* phosphate buffer was thermally denatured (100°C for 3 min.) and incubated at 70°C for 50 hours. The solution was then diluted to 0.12 *M* phosphate buffer and the RNA-DNA hybrids were collected by hydroxyapatite fractionation at 70°C. The bound fraction was eluted with 0.48 *M* phosphate buffer so that the DNA in the hybrid could be rendered single stranded again by RNase and could be further analyzed.

† *RNA-DNA hybrid separation by Sephadex:* Mouse DNA was purified, sheared at 50,000 psi and passed through Dowex-50 to remove RNase and Sephadex G-100 to remove salt. The DNA was then denatured (3 min. 100°C) incubated (60°C, 0.12 *M* phosphate buffer) to a *C₀t* of 100 and the unreacted DNA separated by hydroxyapatite. The reassociation curve of this DNA in $6 \times$ SSC is shown on Fig. 29. (Reassociation of nonrepeated DNA). This unreassociated DNA, the unique fraction, was then dried by lyophilization and buffer ($9 \times$ SSC pH 5.5) was added so that the solution was 10.0 mg/ml.

Mice that had been pregnant for about 17 days were injected interperitoneally with 10 mc P³², sacrificed at the end of one hour, and the embryos removed. The P³²-labeled RNA was extracted from the embryos and the acid

3. The third method employed a high concentration of unlabeled DNA, small amounts of rapidly labeled RNA and uniformly labeled DNA to assay both the reassociation of DNA and the hybridization of RNA to DNA. The unhybridized RNA was digested with RNase and the DNA strand pairs and the RNA-DNA hybrids were collected on hydroxyapatite.*

These techniques present special problems. The requirement to be free of nucleases is unusually stringent because, even at high concentrations of either RNA or DNA, long incubations (up to

soluble contamination was removed by repeated Sephadex G-100 chromatography.

Varying concentrations of this rapidly labeled RNA were added to the unique DNA (10 mg/ml). The volume was 0.15 ml and the buffer concentration was $6\times$ SSC. The solution was denatured at 100°C , incubated at 60°C for 16 hours, and then incubated with RNase (5 $\mu\text{gm/ml}$ for 15 minutes at 37°C). When the solution was passed through a Sephadex G-100 column (25 by 1 cm) at a rate of 30 ml/hr, the hybridized RNA was in the front peak and the digested RNA in the back peak.

The P^{32} RNA was more than 90% precipitable. When unhybridized RNA was digested by RNase (5 $\mu\text{gm/ml}$, 15 min. 37°C), all of the labeled material appeared in the back peak when fractionated on the Sephadex G-100 column. There was no detectable hybridization of the rapidly labeled RNA with salmon DNA.

* *Hydroxyapatite fractionation of DNA-DNA and RNA-DNA hybrids:* Aliquots of a solution containing 6.85 mgm/ml unfractionated mouse DNA, 0.1 mg/ml rapidly labeled P^{32} RNA and 0.02 mg/ml of unfractionated uniformly labeled C^{14} "L" cell DNA were mixed, thermally denatured and incubated at 60°C for varying times in 0.36 M phosphate buffer. The solution was then cooled, diluted to 0.12 M phosphate buffer, and incubated with 5 $\mu\text{gm/ml}$ of RNase at 37°C for 15 min. The RNase was removed and the solution fractionated on hydroxyapatite. The P^{32} was counted by Cerenkov radiation. Samples were then precipitated with 10% TCA and the C^{14} DNA was collected on filters and its radioactivity determined.

As with the Sephadex method there was no detectable hybridization of the P^{32} -labeled RNA with salmon DNA.

100 hours) are required. The first technique, using high RNA concentration, required RNA free of contaminating DNA which would have caused a high background reaction of DNA-DNA reassociation. Also, the limited solubility of the concentrated RNA required the solution to be incubated at 70°C . In all three techniques it was necessary that the RNA remain intact during thermal denaturation and the long periods of incubation. We found that RNA in $2\times$ SSC became acid soluble in minutes at 100°C or long incubations at 60°C , but that RNA in phosphate buffer at pH 6.8 or $6\times$ SSC at pH 5.5 was stable. The use of hydroxyapatite presented other problems in that unhybridized RNA binds to hydroxyapatite to a certain extent. DNA, in the presence of RNase, can also bind to the column even in single-stranded form. These problems were overcome by digesting the unreacted RNA with RNase and then removing the RNase by pronase digestion, phenol and chloroform extraction, and finally passage through a Dowex-50 column.

Fraction of unique DNA transcribed. When RNA, in high concentrations, was incubated with labeled unique DNA, 8% of the DNA (3.7% of the total cell DNA) reacted with the RNA as shown by binding to the hydroxyapatite. This fraction was eluted from hydroxyapatite (0.48 M phosphate buffer, 70°C) so that the hybrids were retained in double-stranded form. Recovery of this fraction intact permitted the further testing of the hybrids which was required to show that they were RNA-DNA hybrids and that unique DNA was involved.

The melting temperature of the RNA-DNA hybrid was determined by binding another aliquot of the incubation mixture to a hydroxyapatite column at 70°C and determining the C^{14} eluted at 5° increments up to 100°C . (Fig. 21). The T_m of the hybrids was 77°C , which is about $5-7^{\circ}\text{C}$ below the T_m of DNA-DNA at that salt concentration (see section "Isolation

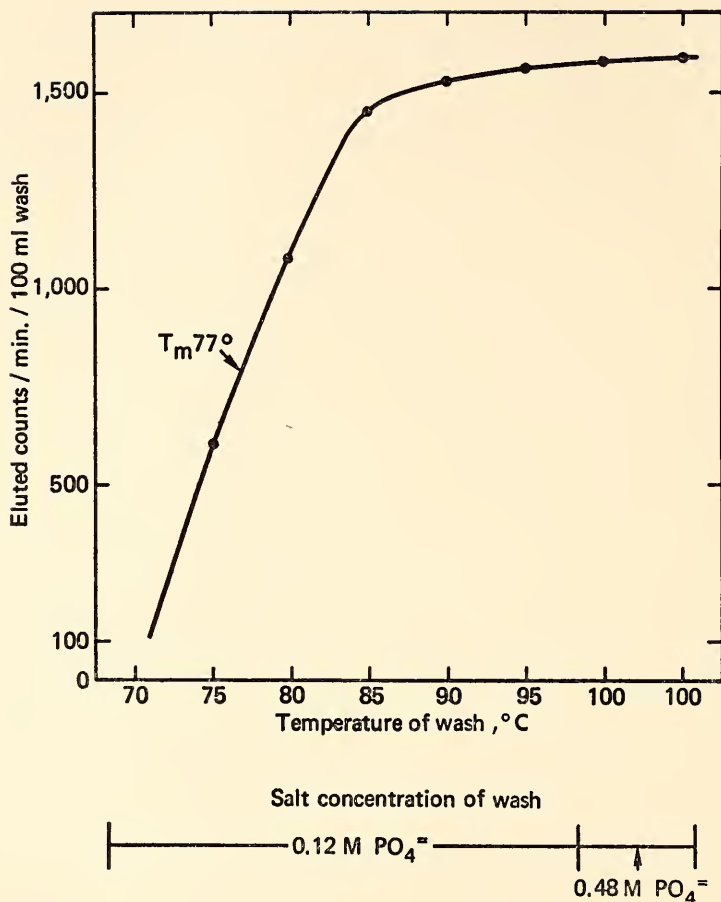


Fig. 21. Integral melting curve of DNA-RNA hybrids. C^{14} "L" cell DNA-mouse embryo RNA hybrids were bound to an hydroxyapatite column at 70°C in 0.12 M phosphate buffer. After washing to remove unreassociated DNA, the temperature was increased by 5°C increments and the dissociated C^{14} DNA was eluted at each temperature.

and Characterization of Bacterial Ribosomal RNA Cistrons"). There was very little melting above 85°C , where DNA-DNA would melt, indicating that most, if not all, of the DNA had been in hybrid form.

The recovered hybrid fraction was given prolonged treatment with RNase ($50\text{ }\mu\text{g/ml}$, 18 hours, 37°C , while being dialyzed against 0.03 M phosphate buffer) and the DNA was thus rendered single-stranded. After removal of the RNase, three quarters of the original 8% of C^{14} DNA which bound to the hydroxy-

apatite under standard conditions was no longer adherent to hydroxyapatite, thus indicating that at least this much DNA was truly in a hybrid form. When some of this DNA was reincubated with another sample of RNA from the same preparation and assayed under the same conditions as before, 37 percent was bound. This DNA, as expected, was enriched in the fraction that would hybridize with RNA. However, the fact that 100% of the DNA was not bound on the second hybridization indicated the incubation time and RNA concentration were

TABLE 10. Reassociation with Mouse DNA of the C^{14} DNA Released from RNA-DNA Hybrids

C_0t	DNA Bound to Column, %		Increment of DNA Bound, %	
	Unique C^{14}	Unfractionated Mouse	Unique C^{14}	Unfractionated Mouse
2×10^{-1}	5.3	(18)		
25	13.6	28	8.3	10
2.5×10^3	48.3	61	34.7	33

Note: The C^{14} DNA that formed hybrids with mRNA was released from the RNA by RNase, purified and concentrated in water. 0.08 ml of 1.2 M phosphate buffer was added to 0.675 ml of this C^{14} DNA solution (2.2 μ gm DNA/ml). A 0.225-ml aliquot of this solution was incubated at 60°C for 100 hours. 2 mg of unlabeled, unfractionated mouse DNA was added to the remaining solution and half was incubated for 10 hours and the other half for 100 hours. The amount of C^{14} and unlabeled DNA that bound to the hydroxyapatite column was determined. The value in parentheses was calculated from Fig. 23.

not sufficient to get complete hybridization of the transcribed unique DNA. Thus, the 8% value for the unique DNA hybridizable with RNA is a minimum estimate of the unique DNA that is transcribed.

Another portion of the recovered RNase-treated DNA was incubated with a high concentration of unfractionated-unlabeled mouse DNA. The rate of reaction of this C^{14} DNA was much slower than the mouse DNA at a low C_0t as expected since most of the C^{14} ERRF had been removed (Table 10). At a higher C_0t the C^{14} DNA that had been hybridized reacted at essentially the same rate as the total unique mouse DNA: 35% versus 33%. Thus, the majority of the hybridizing DNA was unique DNA.

Percentage of rapidly labeled RNA derived from unique DNA. The other set of experiments using rapidly labeled RNA

with large concentrations of DNA demonstrated that most of this RNA reacts with unique DNA. As indicated in Table 11, few sites on the unique DNA were occupied at the high concentration (10:1) of RNA.

The kinetics of both DNA-DNA and RNA-DNA reactions were determined by the hydroxyapatite technique (Fig. 22). The earliest sample was taken after most of the repeated sequences had reacted. Further samples were taken until most of the unique DNA had reacted. Under these conditions the RNA-DNA hybridization curve generally parallels that of the DNA-DNA reassociation curve. The unique DNA reassociation and the hybridization of the RNA to the unique DNA are half completed at the same time. Figure 22 shows that most of the rapidly labeled RNA is homologous to the unique DNA.

TABLE 11. The Reassociation of Unique DNA with Rapidly Labeled RNA

DNA C_0t ($6 \times$ SSC)	DNA:RNA Ratio	Estimated Ratio of DNA to mRNA	P^{32} RNA Reacted, %
1600	10	500	42
1600	1000	50,000	52.8

Note: Mouse DNA was fractionated to a point where 32% of the DNA had reacted and the resulting unique fraction was incubated with rapidly labeled P^{32} RNA. The unreacted RNA was removed by RNasing and the percentage of reassociating RNA was determined by Sephadex fractionation. The mRNA is estimated to be 2% of the total. These results probably underestimate the quantity of RNA homologous to the unique DNA because the reaction did not go to completion and possibly overestimate RNA homologous to the unique DNA because of ERRF contamination.

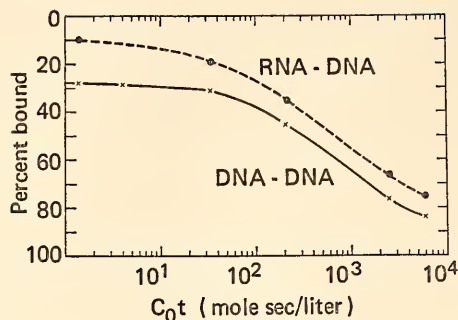


Fig. 22. Kinetics of reassociation of mouse DNA and rapidly-labeled RNA. Uniformly-labeled C^{14} "L" cell DNA (0.02 mg/ml) and rapidly-labeled P^{32} mouse embryo RNA (0.1 mg/ml) were incubated (60°C in 0.36 M phosphate buffer) with unlabeled mouse DNA (6.85 mg/ml). The unreacted RNA was digested by RNase and the reaction solution was fractionated on hydroxyapatite. The P^{32} was counted by Cerenkov radiation. The samples were then precipitated with 10% TCA and the C^{14} DNA was collected on filters and its radioactivity determined.

Discussion. Each of the three methods demonstrated that unique DNA was expressed. The method employing mRNA to determine the C_0t demonstrated the existence of RNA-unique DNA hybrids by showing (1) the RNA-DNA had a 5–7° lower melting temperature than DNA-DNA; (2) DNA which initially bound to the hydroxyapatite after reaction with RNA could be rendered single stranded again by prolonged RNase treatment, providing that the DNA was truly hybridized to RNA; (3) the C^{14} DNA released by RNase rehybridized more efficiently than the total DNA on reincubation with RNA; (4) this DNA, freed by RNase, was dominantly unique DNA. The method employing DNA to determine the C_0t demonstrated that over 70% of the rapidly labeled RNA is homologous to DNA and most of this RNA is homologous to the unique fraction.

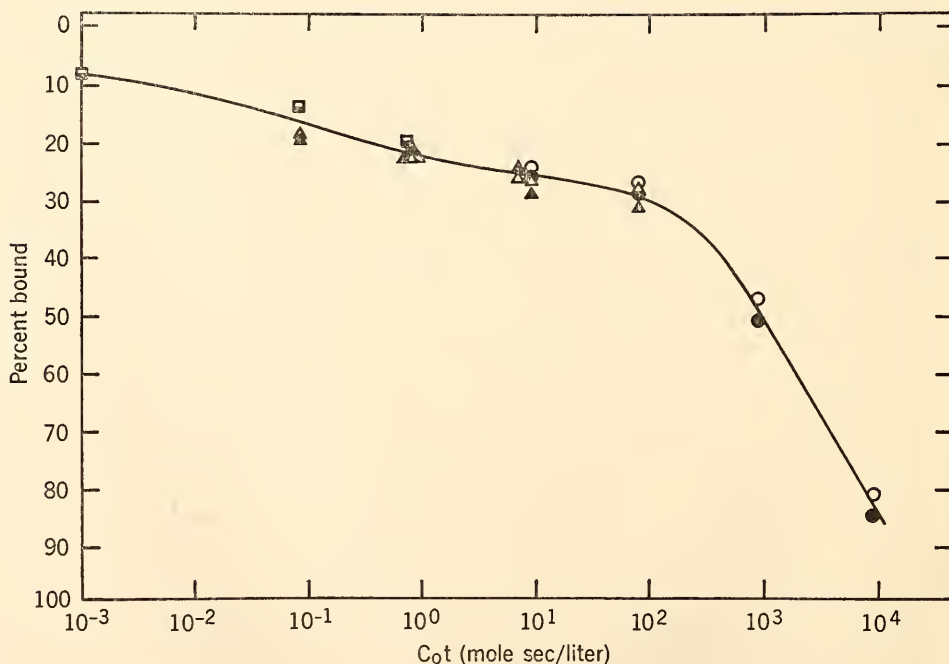


Fig. 23. Reassociation of labeled mouse "L" cell DNA mixed with normal mouse DNA. Data from Table 13. Filled symbols, C^{14} "L"-cell DNA. Open symbols, normal DNA. Squares, 0.66 micrograms/ml. Triangles, 66 micrograms/ml. Circles, 6600 micrograms/ml.

If various assumptions are made, it can be calculated that a rather large fraction of the unique DNA is probably expressed. If we assume that only 2% of the 67 mg/ml RNA represents mRNA and that the different mRNA molecules are present in equal numbers, incubation for 50 hours at this concentration of RNA would be sufficient to achieve a C_0t of only 800–1600 or a level where only 20–40% of the unique DNA would be expected to react (Fig. 23). Further, since the kinetic curve shown in Fig. 22 demonstrated that the RNA-DNA hybridization followed the DNA-DNA kinetics, more DNA could have been expected to react at a higher mRNA C_0t . Therefore, the experimental value of 37% rehybridization of enriched DNA to mRNA could be taken as a measure of the extent of the reaction. If one third of the recovered RNase treated DNA rehybridized under the same conditions as the first hybridization, then the 8% hybridizing during the first hybridization represents one third of that DNA that could have eventually hybridized. Thus, about 25% of the total unique fraction could have been expressed. We can assume one half of the mouse DNA will not hybridize because only one of the complementary strands can be transcribed, as in bacteria. Thus perhaps half of the transcribable unique DNA is actually being transcribed into mRNA in the mouse embryo.

SEARCH FOR SALTATORY REPLICATION

R. J. Britten and A. V. Rake

Present evidence indicates that families of repeated sequences in the DNA of higher organisms are produced in rather sudden events called *saltatory replications*. The probable steps leading to the appearance in a species of a family of repeated sequences have been summarized (*Year Book 66*, p. 85) as follows: "(1) Many copies must be made of a segment of DNA. (2) A number of these copies must be integrated into the genome in such a way that they are dupli-

cated and transmitted to progeny. (3) The resulting family must either determine a favorably selected phenotype or be associated with a favorable genetic element. (4) Sufficient time must pass for its dissemination throughout the population. (5) . . . the growth of the family must be terminated within a reasonably short time."

There is evidence that the whole process is not often completed. Perhaps only once in every one to ten million years does a new family of repeated sequences appear in individual vertebrate species. Nevertheless, since steps (2) and (3) might have a low probability, the first event—multiple copying of a sequence—may occur fairly often. A sudden occurrence—within the lifetime of an individual—might be observed in the way a somatic mutation can occasionally be observed. Certain tissues or cell lines might contain new families of repeated sequences. If so, how could such cells be identified? It is not easy to predict what effects would be seen. However, the karyotype might well be affected. If the karyotype has changed in a particular cell line the question arises whether the relative quantity of repeated sequences has remained unchanged.

These speculations have led to two sets of measurements of the pattern of repeated sequences in transformed cells. DNA from rat hepatoma (3924a) has been compared with rat liver DNA, and DNA from mouse "L" tissue culture cells has been compared with DNA from mouse tissues. In both of these cases the transformed cells show heteroploid karyotypes. In this work, however, no significant differences have been observed between their DNAs and the normal counterpart DNA.

Rat hepatoma DNA. The work with rat hepatoma DNA was a cooperative venture with Drs. William B. Looney and Lillie O. Chang of the University of Virginia Medical School, at Charlottesville. Hepatoma 3924a was grown sub-

cutaneously in rats. This tumor was selected because of its abnormal chromosome number as well as its major chromosomal changes. It has a chromosome number of 73 (compared to a normal complement of 42) with at least 8 abnormal chromosomes. It is a rapidly growing, undifferentiated tumor with a generation time of approximately 0.6 month. There are, in addition, gross changes in enzymatic activity involved in carbohydrate, amino acid, and lipid metabolism. Twelve days after implantation, C^{14} -thymidine was injected intraperitoneally three times daily for a period of 7 days, for a total dose of 4.5 μ c. DNA prepared from the hepatoma had a specific radioactivity of about 12 cpm per microgram which, while low, was adequate. DNA was also prepared from the livers of the same strain of rats (ACI).

The reassociation of the two DNAs was assayed after various times of incubation by adsorption to hydroxyapatite.*

*The details of the method are as follows: DNA was sheared by passing a solution through an orifice at 50,000 psi (50 k sheared), denatured (3 min. 100°C) and incubated in 0.12 M PB at 60° at the concentration and for the time shown on Table 12. For each measurement about 400 micrograms of DNA were incubated. The incubation solution was passed over a 10-ml column of hydroxyapatite (Bio-Gel HTP) at 60°C. The adsorbed DNA was eluted by raising the temperature to 100°C and eluting with 0.12 M PB. Recovery of DNA was uniformly excellent. The unbound and bound fractions were assayed by optical

Table 12 presents the results of the measurements. The hepatoma DNA reassociates to the same extent as the liver DNA, within the accuracy of such measurements. In the majority of cases the liver DNA is present at 14 times the hepatoma DNA and thus the liver DNA concentration principally determines the extent of reassociation. We may conclude that there are few, if any, repeated sequences in the hepatoma DNA which are not present in the liver DNA. A saltatory replication which had produced a family of repeated sequences amounting to only 1% or 2% of the hepatoma DNA would not have been detected in this experiment. It also may be concluded that the ratio of DNA contained in repeated sequences to unique DNA is about the same in the hepatoma as in the liver. Thus, the extra chromosomes in the heteroploid karyotype are not exceptional in their relative content of repeated sequences, or the frequency of repetition.

Mouse "L" cell DNA. The "L" cell is a tissue culture strain that was isolated from the mouse some 30 years ago and is heteroploid and transformed. It was of interest to determine whether "L cell" DNA differs from normal mouse DNA either by the introduction of new families of repeated sequences or by a change in the amount of repetitive DNA relative to unique DNA. The experiments were per-

density at 260 $m\mu$ and by counting TCA precipitated DNA on filters in a liquid scintillation counter.

TABLE 12. Reassociation of DNA from Rat Hepatoma and Rat Liver

Concentration μ g/ml		Hours of Incubation	C_{ot} *	DNA Bound to Hydroxyapatite, %	
Hepatoma	Liver			Hepatoma	Liver
13.0	...	0.092	0.0072	6.8	...
...	13.0	0.092	0.0072	...	7.8
67.0	...	0.186	0.075	15.1	...
8.0	111.0	0.10	0.072	15.9	14.9
8.3	116.0	0.125	0.087	11.1	14.3
6.6	94.0	1.25	0.74	25.0	23.6
66.0	890.0	1.1	15.6	29.8	30.0
66.0	890.0	16.8	464.0	40.6	38.4

* The C_{ot} is calculated for the total DNA present.

formed in very much the same way as those with rat hepatoma.*

The results are shown on Table 13 and Fig. 23. Again no significant difference is observed between the degree of reassociation of the normal tissue DNA and the DNA from the transformed heteroploid cells. The accuracy is a little better than $\pm 5\%$.

Further search for saltatory replications. It is clear that these experiments have only initiated the subject of saltatory replications in similar tissues. A greater sensitivity to minor differences is obviously required. An inexhaustible number of possible tissue combinations exists. Perhaps a stroke of luck or intuition will turn up the right one and we can then learn of a mechanism by which saltatory replications are produced. A suggestion was made by Dr. Van R. Potter of the University of Wisconsin (personal communication several years ago, well before these experiments were initiated) that "minimal deviation hepatomas" should be examined from this point of view. Perhaps minor changes in karyo-

type and aberrant chromosome morphology would be good clues to events of excessive replication of given DNA sequences.

In any case, it is likely that DNA sequence complementarity tests will contribute to future studies of the relationships between virus replication, transformation, karyotype changes, and patterns of repeated sequences.

REPEATED SEQUENCES IN HUMAN DNA

R. J. Britten

When the presence of repeated sequences in vertebrate DNA was established (*Year Book* 64) it seemed very likely that our own DNA shared this feature. The earlier measurements with DNA-agar had shown that a fraction of human DNA reassociated rapidly. Only in the past year, however, has any attempt been made to measure the frequency of repetition and quantity of repeated sequences in the human genome.

The methods used were successive hydroxyapatite fractionation and optical measurement of reassociation of the fractions. Thermal stability profiles of selected fractions have been measured both by optical hyperchromicity and elution from hydroxyapatite. Figure 24 shows diagrammatically the steps of incubation

* The normal DNA was derived from mixed mouse tissues. C^{14} -labeled DNA was prepared from "L" cells grown on glass 4-8 generations in the presence of C^{14} -thymidine. During purification this labeled DNA was adsorbed in a denatured state to nitrocellulose filters with a 20% loss, entailing some risk of fractionation.

TABLE 13. C^{14} "L" Cell DNA-Mouse DNA Reassociation

DNA Concentration $\mu\text{g/ml}$	Incubation Time, hrs	C_{ot}	Normal DNA, %	"L" Cell DNA, %	Ratio Column 4 Column 5
0.66	1	8×10^{-3}	7.2	7.14	1.01
0.66	10	8×10^{-2}	12.25	13.05	0.94
66.	1/10	8×10^{-2}	17.3	18.0	0.96
66.	1	8×10^{-1}	22.6	22.6	1.00
0.66	100	8×10^{-1}	18.9	19.5	0.97
66.	1	8×10^{-1}	22.0	20.3	1.08
66.	10	8	25.1	23.9	1.05
66.	10	8	25.3	28.4	0.89
6600.	1/10	8	23.1	24.9	0.93
66.	100	80	28.6	31.8	0.90
6600.	1	80	27.1	29.2	0.93
6600.	10	8×10^2	46.2	50.9	0.91
6600.	100	8×10^3	79.5	83.5	0.95

Note: In each incubation the amount of labeled "L" cell DNA present was 1/60 of the amount of the normal mouse DNA.

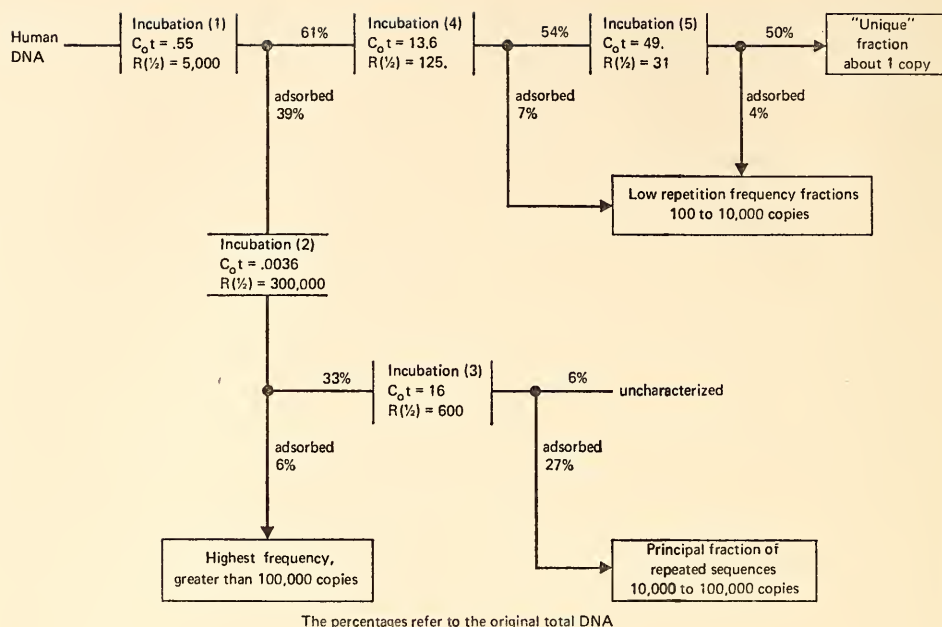


Fig. 24. Fractionation of human DNA—flow diagram. Initially the DNA was sheared at 50,000 psi and denatured. For each of the steps the particular fraction was incubated for an appropriate time and concentration at 60° in 0.12 *M* PB. The resulting C_0t is shown for each incubation. Each of the solid circles represents a separation with hydroxyapatite of double-stranded DNA (downward path) from single-stranded (path to the right). The DNA solutions were passed over the hydroxyapatite at 60°C in 0.12 *M* PB, and eluted with 0.12 *M* PB at 100°C. In no case did the bound DNA exceed 80 $\mu\text{g/ml}$ hydroxyapatite. $R(1/2)$ is the repetition frequency of a component which would be just half reassociated if all of it were present in a given incubation. Under these conditions it may be calculated by multiplying the fraction of the original DNA present by 2800 and dividing by the C_0t reached in the incubation.

and fractionation and the percentage of the total DNA carried through succeeding steps.

Such a procedure yields complete separation of rapidly and slowly reassociating DNA only if the rates of reassociation differ by a sufficiently large factor. For example, the first incubation ($C_0t = 0.55$) would give half reassociation for DNA with a repetition frequency of 5000. (Under these conditions nonrepeated human DNA requires $C_0t = 2800$ for half-reassociation). Thus, DNA with a repetition frequency of 50,000 or greater would be essentially completely reassociated and would be bound. DNA with a repetition frequency less than 500 would be very little reassociated and

would not be bound (moving to the right on Fig. 24). DNA between these degrees of repetition would appear in both fractions.

Follow, for example, on Fig. 24, the *principal* fraction of repeated sequences in human DNA. It appears to be predominantly made up of sequences with a repetition frequency between 10,000 and 100,000. Thus, in incubation (1) it is almost completely reassociated, binds and may be traced downward on the diagram at the first hydroxyapatite fractionation. At incubation (2) only the very fast components reassociate to any great extent. They may be traced downwards and the *principal* fraction traced to the right. Then after incubation (3)

the principal repetitive fraction reassociates nearly completely.

Such a procedure demonstrates the presence of rapidly reassociating components in certain ranges of rate constant and separates the classes of DNA for further characterization. The thermal stability was measured for the *principal* and the *highest frequency* fractions.

Figure 25 shows the results of the hydroxyapatite thermal chromatography after incubation at 50°C. The expected broad range of thermal stability is observed for both fractions. A sizable part of the high repetition frequency fraction, however, has a melting temperature approaching that of native DNA. These characteristics—high thermal stability and high frequency of repetition—suggest that recent saltatory replications have occurred in the human evolution-

ary line. It is probable that a part of this DNA has appeared since the divergence of the human line from the lines leading to the other higher primates. Corneo, Ginelli and Polli³⁸ have reported a "satellite" comprising 0.5% of human DNA, which reassociates rapidly with relatively high precision. Careful comparisons of the sequence homologies between such fractions of DNA among the higher primates and human races should supply new quantitative information about human evolution.

The conclusion that there is a large fraction of human DNA with repetition frequencies between a hundred and a million copies is also supported by a preliminary series of measurements of the kinetics of reassociation (assayed with hydroxyapatite). The resulting curve is similar to that published last year (*Year Book 66*) for calf DNA, except for the appearance of a little DNA with a repetition frequency between one hundred and ten thousand. The few mammals that have been examined—calf, mouse, rat, and human—all appear to have a great deal of similarity in *pattern* of repeated sequences. That is, they have about the same total quantity of repeated sequences and range of frequency of repetition. The mouse satellite is indeed an individual feature. Ten percent of the DNA results from a short sequence repeated a million times. In each of the other cases, however, a few percent of the DNA occurs in a very high frequency fraction which may approach a million copies. While the quantity of repeated DNA and the patterns of repetition frequency are similar among these mammals, the repeated DNA sequences themselves are—many of them—different. Between mouse, calf, and human, for example, only about 20% of the repeated sequences are similar enough to reassociate under the usual criterion of precision. During the last 50 to 100 million years many events of saltatory replication have apparently

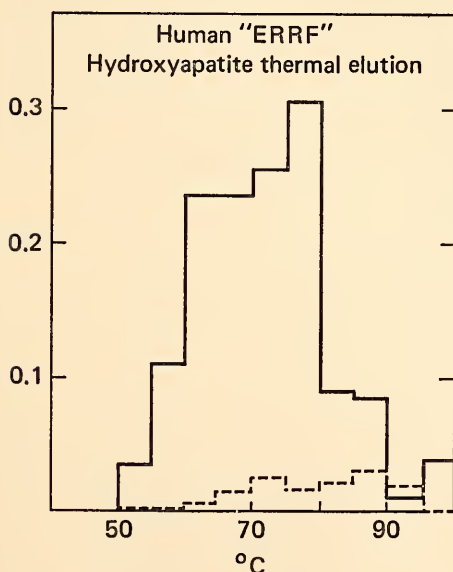


Fig. 25. The thermal stability profile of reassociated repeated fractions of human DNA. The upper curve (solid line) is the *principal* and the lower (broken line) the *highest frequency* fraction prepared as described in Fig. 24. Both fractions were incubated at 50°C and adsorbed at 50°C on hydroxyapatite in 0.14 M PB. Elution was done with 0.14 M PB at 5°C temperature intervals.

occurred in each of these evolutionary lines.

REASSOCIATION OF NONREPEATED DNA

R. J. Britten

Measurements of the reassociation of nonrepeated DNA continue to be of interest. They yield a measure of the genome size or DNA content per cell, and an accurate knowledge of the kinetics of reassociation of such DNA makes it possible to determine more accurately small quantities of repeated DNA. The physical chemistry of the process of reassociation is also of interest, *per se*. Figures 26, 28 and 29 show the reassociation of *Proteus mirabilis*, PPLO H-30, and mouse unique DNA, all measured in the spectrophotometer by optical hypochromicity.

Data were reduced and the figures plotted by the IBM 1130 computer. The

computer was also used to find the best fit between the data and ideal second-order reaction kinetics. Finally, the difference between the data and the best fitting second-order curve was plotted by the computer.

Figure 26 shows the reassociation of *Proteus mirabilis* DNA (sheared at 50,000 psi) at two salt concentrations traced from the computer plots. Table 14 gives the constants for the best fitting ideal second-order curve. The deviation of the data from this curve is shown by the curves on Fig. 27 on a tenfold expanded scale. The rate of reassociation is very similar to that for *E. coli* DNA (Year Book 65, Fig. 40, p. 84) measured under the same conditions. Thus the genome size is similar to that of *E. coli*.

The time course of reassociation of *Proteus mirabilis* DNA appears to deviate very slightly (perhaps 1% of the span of the reaction) from that expected for

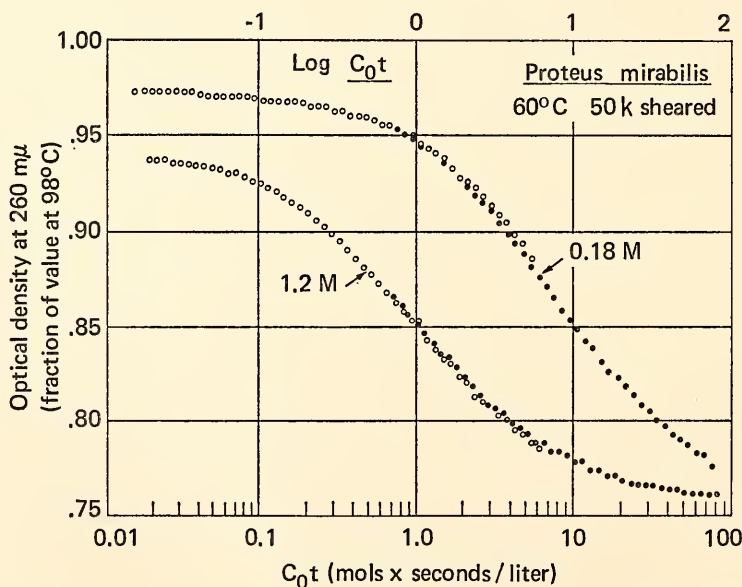


Fig. 26. Reassociation of *Proteus mirabilis* DNA, measured by optical hypochromicity, at two salt concentrations. Measured with a 1-cm path length, 18 micrograms/ml (open circles); 1-mm path length 377 $\mu\text{g/ml}$ (closed circles). For the upper curve the buffer was 0.12 *M* phosphate buffer, with a sodium ion concentration of 0.18 *M*. For the lower curve the buffer was 6 \times SSC with a sodium ion concentration of about 1.2 *M*. There is no measurable effect of DNA concentration on the rate of reassociation.

TABLE 14. *Proteus mirabilis* Reassociation

Solution	Reaction Constants	
	0.12 PB	6 × SSC
κ Mols/liter	0.18	1.2
C ₀ t at half reaction	7.001	0.949
Optical density, % below value at 98°C		
Initial	2.75	5.82
Final	23.7	23.9

a second-order reaction. The final absorbancy, however, is not that of native DNA. Thus, some processes retard the reassociation when only about 95% of the nucleotides are paired.

The intramolecular interactions that occur very rapidly during cooling from 98° to 60°C are responsible for the initial drop in optical density. This effect depends slightly on the nucleotide composition of the DNA and quite strongly on the cation concentration. The initial drop in optical density is of importance in the recognition of very rapidly reassociating fractions of complex DNA from higher organisms.

Figure 28 shows the reassociation of

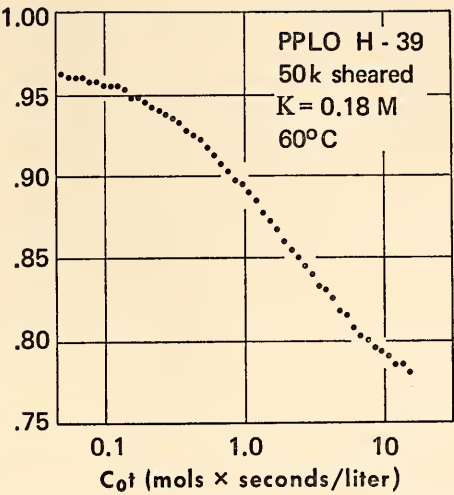


Fig. 28. Reassociation of mycoplasma (PPLO H-39) DNA measured by optical hypochromicity.

DNA from human mycoplasma H-39. The DNA was a gift from Dr. Harold Morowitz of Yale University. The measured values deviate only 1% of the span of the reaction (or $\pm \frac{1}{4}\%$ in optical density) from a second-order curve with

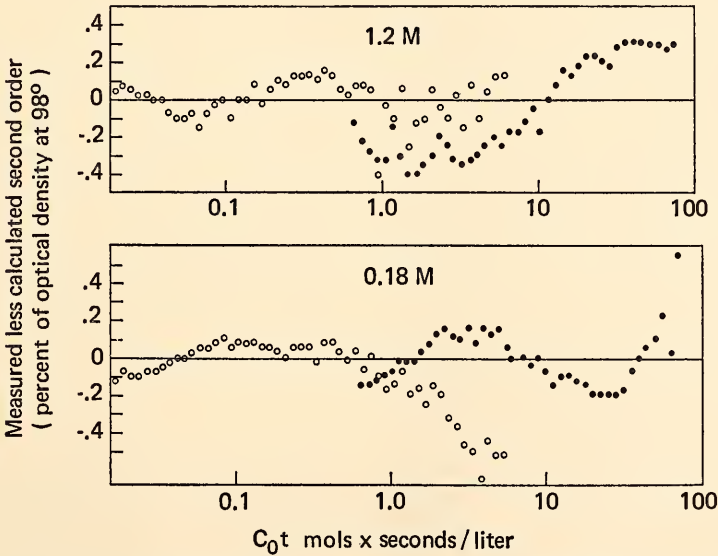


Fig. 27. Deviation from ideal second-order kinetics of the reassociation of *Proteus mirabilis* DNA. Shown on an expanded scale is the difference between the measurements described in Fig. 25 and an ideal curve with the constants listed in the text.

an initial value of 0.966, a final value of 0.764 and a C_0t for half reaction of 1.8. According to Bode and Morowitz,³⁹ the genome size is 500×10^6 daltons, or one sixth of that of *E. coli*. *E. coli* DNA of this fragment size under these conditions is half reassociated at a C_0t of about 6. Thus, the mycoplasma DNA would be expected to be half reassociated with a C_0t of about 1. It reassociates more slowly (C_0t for half reaction=1.8) and further measurements will be required to determine the source of this apparent discrepancy.

Figure 29 shows the reassociation of mouse unique DNA at high salt concentration. It reassociates at the expected rate, about 500 times more slowly than *E. coli* DNA would reassociate under the same conditions. An accurate figure for the reassociation rate constant can not be deduced from these measurements due to apparent slight heterogeneity and the lack of data defining the final optical density. It does supply a useful estimate of the reassociation rate for comparison with the

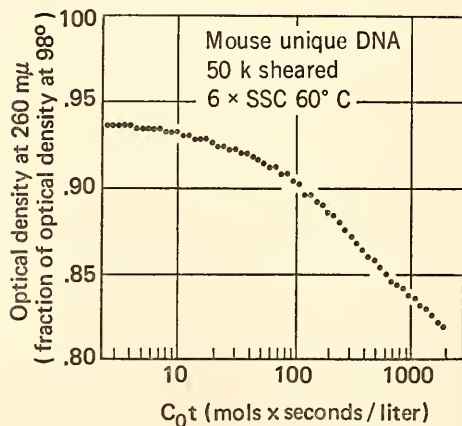


Fig. 29. Reassociation of the nonrepeated DNA of the mouse, measured by optical hypochromicity. Repeated sequences removed by previous hydroxyapatite fractionation. The salt concentration is the same as that for the lower curve of Fig. 25. Note the agreement in the initial drop in optical density between the mouse unique and *Proteus mirabilis* curves.

RNA-DNA reassociation studies described below which were carried out under the same salt conditions.

THE ARITHMETIC OF NUCLEIC ACID REASSOCIATION

R. J. Britten

Definition of segment concentration.

In a previous report (*Year Book 65*) a mathematical description of the reassociation of DNA was presented. It supplied the basic formulas for the calculation of the rates of reassociation of DNA in terms of genome size and repetition frequency. Here we introduce a useful parameter which simplifies the analysis and planning of both DNA-DNA and RNA-DNA reassociation experiments.

The segment concentration, χ , is defined as the molar concentration of *like sequences* in a suspension of nucleic acid molecules. Many paragraphs could be written on the meaning of *like sequences*. The degree of similarity and the length over which the similarity is present can not yet be exactly described except where sequences are perfectly identical. In practice the definition must be empirical and depends on a criterion of thermal stability in a particular experiment.

A simple example will clarify the way χ can be used. An organism containing double-stranded DNA and no repeated sequences (at our chosen criterion) has a genome size G , expressed in numbers of nucleotide pairs. If the DNA is suspended at a concentration C_0 (mols of nucleotides per liter), the segment concentration will be

$$\chi = \frac{C_0}{2G} \quad (8)$$

for all the different sequences present in the genome. χ is the molar concentration of each particular stretch of nucleotide sequence. Fragmentation of the DNA does not change the segment concentration.

The equations for DNA reassociation. A considerable amount of evidence indicates that, in solution, the reassociation of DNA follows almost exactly the time course of a second-order reaction. Examples are given above in this report. We expect the time course to be somewhat more complex, since the fragments terminate at many places in the sequence and a range of fragment lengths is present, but these effects appear to be small. For simplicity the following equations are written as though the second-order time course were exactly followed. If S is the segment concentration of DNA which has not yet reassociated,

$$\frac{dS}{dt} = -HS^2 \quad (9)$$

The solution of (9) can be written in terms of the fraction of the DNA remaining single stranded:

$$\frac{S}{\chi} = \frac{1}{1+H\chi t} = \frac{1}{1+HC_0 t/2G} \quad (10)$$

H is a reaction rate constant which does not depend on the genome size (nor on the repetition frequency in examples where repetition is present). It does depend on the ionic strength, temperature, and fragment size, as described below.

We now consider the reassociation of the DNA when families of repeated sequences are present. If a particular sequence is repeated N_i times in the genome (and C_0 is the total DNA concentration), the segment concentration for the sequence is:

$$\chi_i = \frac{N_i C_0}{2G} \quad (11)$$

The reassociation curve of the DNA will show a component for each family of repeated sequences. For each family the fraction remaining single stranded is:

$$\frac{S_i}{\chi_i} = \frac{1}{1+H\chi_i t} = \frac{1}{1+HN_i C_0 t/2G} \quad (12)$$

Thus, we have the familiar relation*:

$$C_0 t \left(\frac{\text{half}}{\text{reaction}} \right) = \frac{2G}{H N_i} \quad (13)$$

Numerical value of the rate constant. Recent measurements of the rate of reassociation of DNA under a variety of conditions^{40, 41, 42} make it possible to construct an empirical formula (see Fig. 30) from which the reassociation rate constant can be calculated (subject to the limitations listed below):

$$H = \frac{a F^{1/2} T^{-\kappa(b/\kappa)^c}}{\eta} \quad (15)$$

F is the fragment size (number of nucleotides), κ the monovalent cation concentration (mols/liter), T the absolute temperature and η the viscosity of the solution (centipoise). a has the value 1.19×10^3 , b is about 0.242, and c is about 0.417.

In current practice many reassociation experiments are carried out at 60°C in water with 0.2–1.0 M sodium ion concentration. Under these conditions a simpler formula applies:

$$H = 8.1 \times 10^5 F^{1/2} \kappa^{(0.24/\kappa)} \quad (16)$$

The following restrictions apply to the use of equations 15 and 16:

1. The constant a applies for hydroxy-apatite assay and will have about half this value for optical hypochromicity assay.

2. The equations are applicable at the optimum temperature which is $25 \pm 5^\circ\text{C}$ below the melting temperature. The relationships are not known for temperatures far from optimum.

3. The values for the constants are tentative and may not be realized in other work because of unidentified variables such as divalent ion contamination.

*It is worth noting that if a particular family of repeated sequences were isolated from the DNA in pure form it would reassociate more rapidly, because of its higher relative concentration:

$$C_0 t (\text{half reaction}) = 2 G \alpha / H N_i \quad (14)$$

where α is the fraction of the original DNA present in the family of repeated sequences.

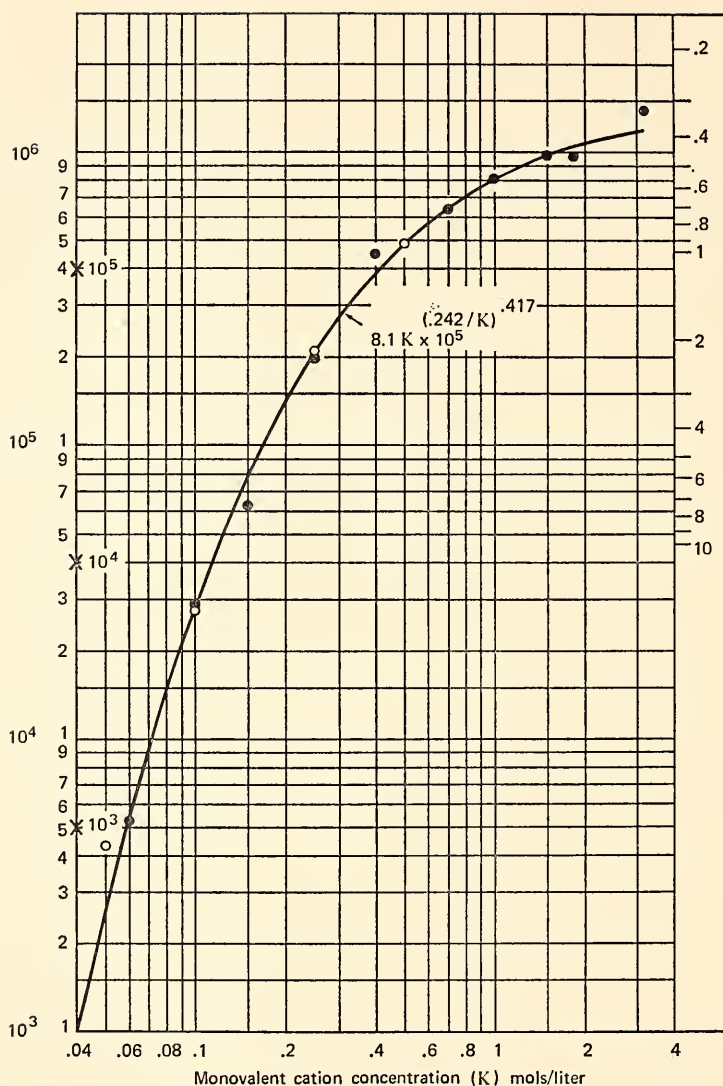


Fig. 30. Effect of salt concentration on the rate of reassociation of DNA. The ordinate on the left is H , the reaction rate constant defined in equation 9. On the right is a scale giving the expected Cot for half reaction for *E. coli* DNA measured with hydroxyapatite. The solid circles are calculated from Wetmur's measurements⁴⁰ of the rate of reassociation of T_4 DNA. The open circles are calculated from measurements⁴¹ of the rate of reassociation of poly U with poly A. The solid curve is calculated from equation 16. Using an 1130 computer the constants in the exponent were adjusted to give a curve of the shape dictated by Wetmur's data. The constant that determines the position of the curve (8.1×10^5) was set from our measurement of rate of reassociation of *E. coli* DNA (Cot for half reaction = 4.0, assayed by hydroxyapatite) assuming the genome size to be 4.5×10^9 and the fragment size to be 400 nucleotides.

Calibration with a reference DNA such as *E. coli* is always advisable.

4. There is probably a slight variation with the GC content of the DNA.

5. It is not known for certain that the equations for RNA reassociation or RNA-DNA hybrid formation have the same set of constants.

6. If only a small fraction of the nucleotides of a pair of fragments are complementary (because of short or imprecise regions of homology) a reduction in rate may occur.

7. For filter or agar-bound DNA the rate constant is very much reduced, and the proportionality to segment concentration does not necessarily hold.

Application to RNA-DNA hybridization. When the reassociation of RNA with DNA is examined the concentration of RNA complementary to different segments of the DNA will probably vary due to differences in transcription rate or RNA lifetime in the cell. Some concept equivalent to segment concentration is necessary for the analysis.

We write R_i as the RNA segment concentration complementary to a given DNA sequence having the segment concentration χ_i .

As a simple example we choose the condition that $R_i > \chi_i$ and thus the amount of RNA available to react remains essentially constant. RNA-DNA hybrids form in a pseudo-first order reaction and if S_i is the amount of single-stranded DNA remaining:

$$\frac{dS_i}{dt} = -H R_i S_i \quad (17)$$

The solution for (17) is

$$\frac{S_i}{\chi_i} = e^{-H R_i t} \quad (18)$$

Using equation 18 we may determine the segment concentration of the RNA transcribed from the family of DNA sequences. This information may be used to calculate, for example, the number of copies of the RNA sequences present per cell.

In most cases different DNA segments will be transcribed to various extents and a problem of resolution of a variety of rates of reassociation arises. Equations 17 and 18 are applicable to a variety of conditions where one component is in excess and the quantity available for reaction remains essentially constant. For example, if χ_i were the concentration of DNA ($R_i \ll \chi_i$) and ρ_i the quantity of unreacted RNA then:

$$\frac{\rho_i}{R_i} = e^{-H' \chi_i t} \quad (19)$$

BRAIN FUNCTION

A. V. Rake and R. B. Roberts

Theory

One question regarding the function of the brain concerns the mechanisms by which memories are established. What biochemistry is involved when the probabilities of different reactions to a stimulus change as a result of learning? This question is quite separate from the question of what elements participate. We can attempt to detect biochemical changes correlated with learning even though we are in complete ignorance as to what parts of the cells change and whether many or relatively few cells participate in the change. Similarly, drugs can be used to block the establishment or maintenance of memory even without knowledge of what patterns of neurones are involved. It is also possible that the answer to our question will not be useful in the larger problem: a determination of the composition of the solder used in connections would be of little use in understanding the circuits of a computer. We trust, however, that this will not be the outcome, and that an understanding of the biochemical basis of learning and memory will contribute significantly to our understanding of brain function.

The experimental work was initiated last year to supplement our long-stand-

ing collaboration with Drs. L. B. and J. B. Flexner, of the University of Pennsylvania. Their efforts and ours are based on the similarity of long-term memory and inherited behavior patterns. Since these behavior patterns are genetically controlled they must result from the expression of DNA. Accordingly, if learning can induce new patterns having stability comparable to inherited patterns, then the new patterns might well be the result of changes in the state of expression of the DNA. Such changes would be expected to involve changes in the kinds and quantities of RNA and protein synthesized by the cell. Moreover, permanent changes in the synthetic system would be anticipated, as the duration persists beyond the usual lifetime of molecules of protein or RNA in the brain.

Ten years ago this line of reasoning led the Flexners to measure the rate of protein synthesis in the brain of mice and then to observe the behavioral effects of injecting inhibitors of protein synthesis. Initially it appeared that puromycin could erase a newly formed memory. Much later it was found that the effects of puromycin in blocking the expression of memory could be reversed. Thus, the memory trace must have persisted but its expression was blocked. At present what has emerged clearly is that mice can learn and remember for a period of hours even though the synthesis of protein in the brain is severely inhibited. Thus, it appears necessary to postulate a form of memory which does not require the synthesis of proteins but which has a chemical basis because it persists beyond the time when memory (presumably held as electrical reverberation) can be disrupted by electroconvulsive shock. The requirement for protein synthesis is suggested only in tests of the long-term memory of animals given minimal training.

To summarize, there appear to be three forms of memory. (1) A *long-term memory* that persists throughout the lifetime

of the individual is postulated to have a basis similar to an inherited behavior pattern and thus to require protein synthesis in its formation and maintenance. This assumption is reasonable on theoretical grounds but there is no conclusive experimental evidence to prove it. (2) A *very short-term memory* lasting some seconds is postulated to be based primarily on electrical reverberation because the memory of an experience can be erased when electroconvulsive shock is applied very shortly after the experience.⁴³ (3) An *intermediate-term memory* lasting several hours is postulated to have a chemical basis excluding protein synthesis, since it is formed during inhibition of protein synthesis, yet persists beyond the period of susceptibility to electroconvulsive shock. The details of the chemical changes involved are unknown; possible changes include those of location or shape of existing macromolecules, movements of ions, synthesis of small molecules or the release of transmitter substance from vesicles. This type of memory (without formation of long-term memory) is often observed as a result of damage to the brain.

In the discussion below, the suggestion is made that forms 2 and 3 are intimately associated and together comprise a system having different properties from either type operating alone. The memory resulting from the interplay of electrical and chemical activity will be designated *short-term memory*.

The question then arises as to why a requirement for protein synthesis is so difficult to demonstrate if it really is important in the formation of long-term memory. One possible reason is that the short-term memory persists beyond the period of inhibition caused by the drugs. If so, a more prolonged inhibition might be effective. Alternatively, drugs acting to curtail the duration of short-term memory might enhance the effect of protein inhibitors.

A possibility exists that the short-term

memory might be sustained by an interplay of electrical and chemical factors. The original stimulus undoubtedly reaches the brain in the form of a pattern of electrical impulses. For a period of seconds the record of the experience is primarily an electrical reverberation. This reverberation might then cause chemical changes that facilitate further reverberation. Thus, there is a positive feedback between the electrical and chemical forms.

Such a system provides high sensitivity but is apt to break into sustained oscillation as exemplified by the howling of a public address system. An instability of this nature could not be tolerated in the brain as each incoming pattern would set off a sustained reverberation. The instability can be brought under control by periodic reduction of the gain as is done in the super-regenerative circuits of radio receivers. Thus, we can imagine a short-term memory in which an initial burst of reverberation caused chemical changes facilitating further reverberation and greater chemical change. At some later time the reverberation might be quenched by inhibition of the cells concerned. During periods of quenching the chemical traces would decay. Sporadically, however, an increase in the gain of the system might bring another burst of reverberation which would restore or increase the chemical trace. Thus, the duration of this type of memory would depend not only on the initial strength of the chemical trace and its rate of decay but also on the frequency of bursts of reverberation.

The plausibility of such a model gains support from several known features of learning. Strychnine, a central nervous system stimulant, enhances learning when given in subconvulsive doses.⁴⁴ Possibly it enhances the sensitivity of the cells and the frequency of reverberation. Similarly, the interest or importance of an event is a significant factor in its later recall *and* in the recall of associated tri-

vial details. Thus, the details of their activities on Pearl Harbor Day remain familiar to many. Possibly that day was a period of high sensitivity and frequent bursts of reverberation. Bursts of reverberation also seem essential in the transfer of an experience from one hemisphere of the brain to another at a time after the initial experience.⁴⁵ Transfer by chemical messengers would not provide the required specificity. Finally, the recurrence of a typical evoked response to a stimulus has been observed in cats when they were returned to the training cage even though the stimulus was not repeated.⁴⁶ This model of the early events of memory formation suggests the duration of short-term memory might be reduced by treating the animal with drugs that generally reduce the excitability of neurones.

Experimental Work

The experimental work suggested by the theoretical considerations above falls into two categories: attempts to observe biochemical changes correlated with learning, and attempts to affect learning and memory by injections of drugs.

Biochemical correlates of learning. Results in this category were uniformly negative. In last year's report we noted that intracranial injections of uridine gave erratic patterns of incorporation depending critically on the depth of injection. Intraperitoneal (i.p.) injections of the drug were then used, sacrificing efficiency of incorporation to gain greater reproducibility. With this technique there was no significant difference in the incorporation of C¹⁴/uridine into various areas of the brain in mice that had been trained to escape shock in a shuttle box compared to the controls that remained in their home cage.

Other mice were given i.p. injections of radioactive leucine and the proteins of their brains fractionated on DEAE cellulose. Again, there was no significant difference between trained animals and controls.

We realize that there are many differences between these experiments and similar experiments reported by others who found positive results. We would not, therefore, consider these experiments a negation of their more extensive work. Nevertheless, we were not encouraged to continue this line of experimentation as our original goal was to obtain enough of the material "specific" to the learning situation so that it could be characterized further.

Biochemical changes induced by learning will be extremely difficult to detect if only a few dispersed and indistinguishable cells are affected. A model system in which the cells could be reproducibly stimulated and then examined for change in their response and biochemistry would have many advantages to compensate for its lack of resemblance to a real brain. Some exploratory efforts were therefore made to culture separate neurones in such a way that they might link up into an interconnected functioning network. We have found that the nerve cells of one-day-old mice may be completely separated from each other in 10% Ficoll, 1.5mM tetraphenyl boron medium when the tissue is stirred for one half hour at 37°C. After removal of the boron and Ficoll medium the cells, neurones and glia, are 95% viable, as determined by vital stains, with little obvious disruption of cellular membranes and little contaminating cellular debris. Since these cells attach to the surface of glass very poorly, a bed of mouse plasma clot was used to give the cells better footing so that the cells were more firmly attached to the glass. The neurones uniformly died within 24 hours if they were cultivated in a synthetic growth medium with 15% new-born calf serum. In adult mouse serum at the same concentration, however, the cells remained viable indefinitely but the neurones did not divide. At present we are attempting to induce these neurones to link up into a neural network. The addition of mouse adult brain extract to these cultures ap-

pears promising; it seems to enhance outgrowth of neuronal processes.

Behavioral effects of drugs. The other line of experimental work has attempted to probe into the difficulty of demonstrating a requirement for protein synthesis in the establishment of a long-term memory. Mice are placed in a box divided into two regions by a barrier with a small "mouse hole." A buzzer is sounded and the mice are shocked through the feet if they do not move through the hole in 5 seconds. Trials are repeated until the mice respond to the buzzer at least 4 times in a set of 10 trials. Thirty to 50 trials are usually needed to attain this degree of learning. The mice learn equally well and retain the memory if injected subcutaneously with cycloheximide (100 mg/kg) one half hour before training. This dose is sufficient to inhibit protein synthesis to a level of 20% during the training, and for roughly 4 hours thereafter.

Reasoning that short-term memory might persist beyond the period of inhibition and then be transformed into a protein-based memory we gave repeated injections of the drug. Some mice tolerated 4 doses at this level given at one-day intervals, but their memory was not impaired. More frequent doses proved to be lethal.

We then turned to depressant drugs in an effort to reduce the reverberation (postulated above) and thereby shorten the duration of the short-term memory. Mice were injected with cycloheximide, trained and then injected with pentobarbital (50 mg/kg, repeated after one hour). With this procedure the memory of several groups of mice has been severely impaired though neither drug alone has shown such an effect. The present results are not yet conclusive but are sufficiently encouraging that these experiments are being continued. We hope that this line of experimentation will ultimately indicate the duration of the short-term memory and the time required for the establishment of a protein-based long-term memory.

GEOPHYSICS

S. E. Forbush, S. R. Hart, I. S. Sacks, J. S. Steinhart, T. J. Smith, L. T. Aldrich, M. A. Tuve, C. Brooks, K. Ishizaka, D. E. James, G. Saa, S. Suyehiro, M. Casaverde, R. Salgueiro, E. Lazo, P. Aparicio, A. Rodriguez, D. Simoni, L. Tamayo, A. A. Giesecke, Jr., E. Deza, R. Olea, J. Frez, A. Cisternas, E. Kausel, E. Gajardo, F. Volponi, J. Mendiguren, R. Cabre, L. Fernandez, S. del Pozo, J. Santa Cruz

In the short time the Department has been involved in the seismological investigation of the earth, many references to the "onion" model of the earth have been made. As investigations here and at other laboratories have progressed, the fallacy of this homogeneous, isotropic model has become increasingly evident. Variations in physical properties of the crust of different segments of continents are firmly established. As reported below, evidence for lateral variation deeper than 350 km below the surface is now almost certain. The "onion," if it is still the proper model, has a rough skin for at least 10% of its outer shell and may only be valid as a measure of our ignorance of the rest of the mantle of the earth.

In looking over reports of other years one finds many expressions of the staff's pleasure in the Carnegie association. Even among our "alumni" the Carnegie experience is a valued portion of their professional and personal lives. In looking at the group listed above as contributors to the continuing program of the Geophysics section, one of the reasons for the value of the Carnegie association may be evident. For each staff member, there are, on the average, four others who share his enthusiasm for his field of research. Fellows, Research Associates and Collaborators in many countries contribute greatly to the understanding and the obtaining of geophysical data about the problems studied. The resources of our colleagues in the U. S. government and in other governments are made completely available to our staff, thereby expanding considerably the range and intensity of experimental investigation of the planet on which we live. Some of the results of such opportunity follow.

EARTHQUAKE SEISMOLOGY

I. S. Sacks, D. E. James, M. A. Tuve, L. T. Aldrich, R. Cabre, S. J., A. Cisternas, L. Fernandez, S. J., J. Frez, P. Aparicio, E. Lazo, R. Olea, A. Rodriguez, and F. Volponi

*Distribution of Absorption
of Shear Waves in South America
and Its Tectonic Significance*

I. S. Sacks

The study of the anelasticity of various regions of the earth has been a major focus of the earthquake seismology section. The upper mantle beneath South America was the first region studied. The attenuation of shear waves due to anelasticity was found to be 160 for the upper 600 km. This determination was based on the comparison of spectra of ScS and SKP arrivals and was reported in *Year Book 62*. This value has been verified by other workers, notably Anderson and Kovach,⁴⁷ who compared the spectra of ScS and sScS.

It was realized, however, that a substantial part of the upper 600 km has a Q_s value substantially higher than 160, and that some zone must therefore have a substantially lower Q value. The Q_s for the upper 130 km, for instance, was determined to be 300 (*Year Book 66*). Figure 31 shows attenuation as a function of frequency for shear waves from a depth of 600 km observed at the surface. The relative amplitude of arrivals at a frequency of 2 cps is extremely small, and, in the case of an earthquake with a relatively flat source spectrum, arrivals at frequencies above 2 cps would probably not be detectable above noise. This has been confirmed by observation of the direct S arrival on the broad band large range seismographs (see *Year Book 66*). However, it was noted at the time that

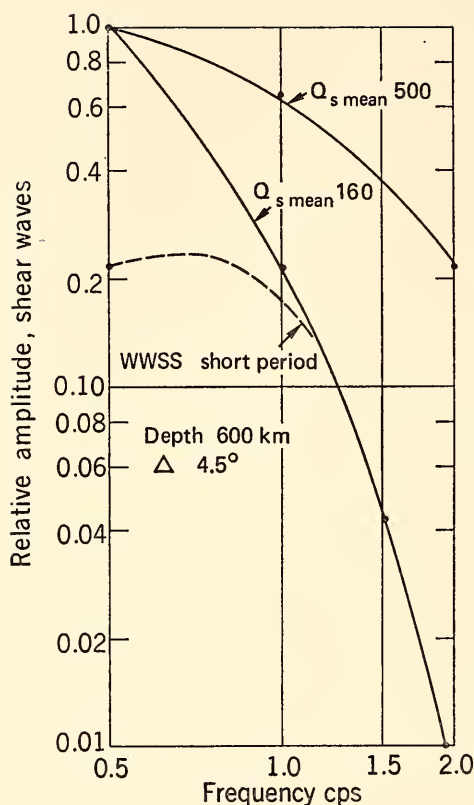


Fig. 31. Attenuation of shear waves from an earthquake at a depth of 600 km and a distance of 4.5° . The mean Q_s for the upper 600 km has been determined to be 160. Energy above 2 cps is very severely attenuated and the range 2–5 cps was therefore used as a criterion for the existence of a higher Q_s path.

there was high frequency shear energy arriving 15 seconds after the direct shear waves on the Toconce station from a source in Salta, northern Argentina. Since that time, deep earthquakes from other regions have been recorded on both the Toconce and the Cuzco broad band stations and three types of shear arrivals from deep earthquakes have been recognized. The first type of arrival is a simple low frequency shear wave compatible with a transmission medium with a Q of about 160 which has no direct high frequency paths reaching the station (Plate 2). The second type of arrival is the one

which was described in *Year Book 66* and is reproduced in Plate 3. It shows that the direct S wave has passed through a low Q path, but there is an indirect and slower path for the higher frequencies. Examples have been found where the delay between the direct S (low frequency) and indirect high frequency S waves, range between 4 and 20 seconds. The third type shows no evidence of low Q path. Seismograms at different frequencies of an arrival recorded at Cuzco from the Peru-Brazil deep earthquake region (Plate 4) show substantial high frequency shear wave energy arriving at the same time as the low frequencies (lower than 1 cps), i.e., the type of arrival expected from a simple high Q path. The indication from these results is that the previously considered upper mantle model which consisted of a thin layer with a very low Q in a relatively high Q mantle, was oversimplified because paths through this layer obviously exist. This low Q zone had been considered to be in the region between 350 and 520 km depth, which is earthquake-free (see Fig. 32). Since the Q for compressional waves (which can pass through liquids) is relatively high, it was conjectured that a low Q_s would be an indication of a low rigidity zone. A low rigidity zone would be unable to store the strain energy which is released by the earthquakes.

Recently there has been a substantial amount of data suggesting that the sea floors have been spreading away from the midoceanic ridges. It has been conjectured that upward convection currents diverge horizontally at these ridges, and move outwards away from the ridge. The Lamont group working in the Fiji area believe that the spreading sea floor plunges down at the Tonga Islands, reaching a depth of about 600 km below Fiji. Figure 33 shows the region and the flow paths. Earthquakes occur on the downward limb ranging from near crustal at Tonga to 600 km deep below Fiji. The fault plane solutions from first mo-

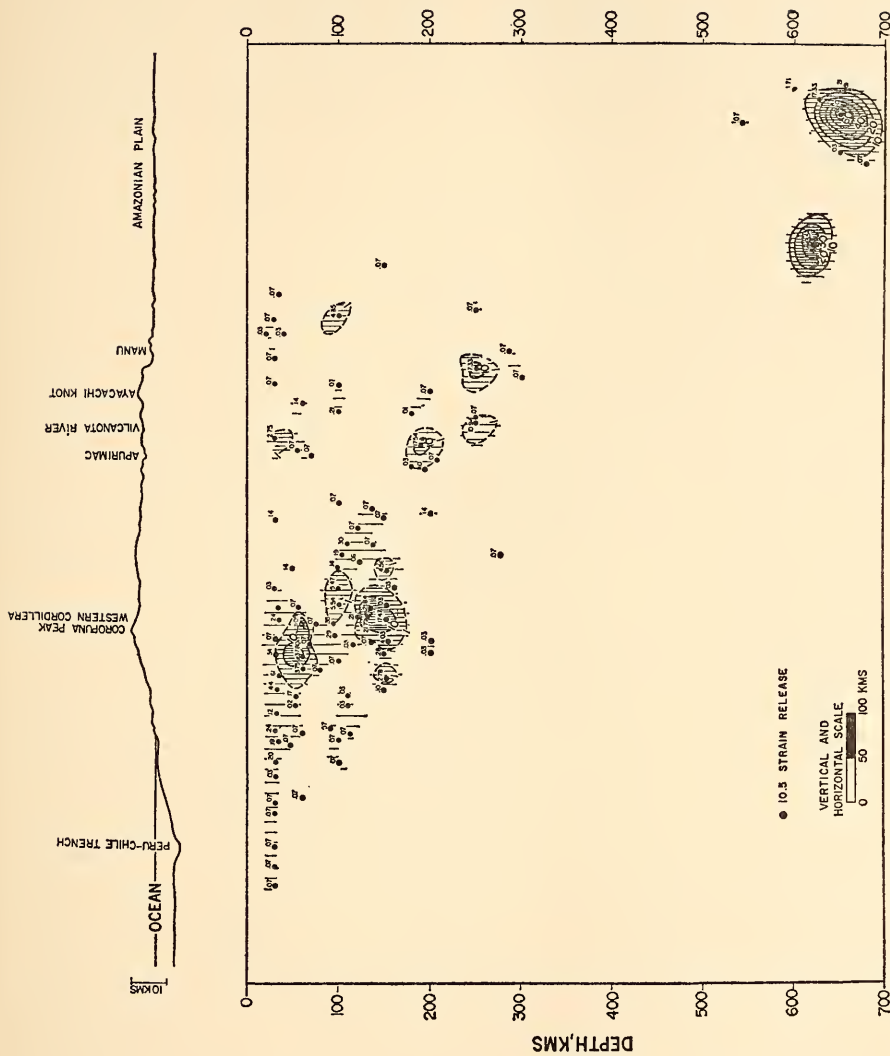


Fig. 32. Section through southern Peru and western Brazil, after Ocola, showing the earthquake occurrence. Deeper earthquakes occur away from the trench. Note the earthquake-free zone between about 350 and 520 km. N is a measure of energy. Contours in units of $\Sigma N_i^{1/2}$ per 20×20 km² per year.



Fig. 33. Hypothetical section through Fiji, Tonga and Rarotonga, assuming Q correlates with strength. The lithosphere and mesosphere are zones of significant strength, and the asthenosphere is a zone of vanishing strength on appropriate time scale. From Oliver and Isacks, *J. Geophys. Res.*, 72, 4273, 1967.

tion studies are consistent with a down-thrusting force system along the downward limb. The relative Q for shear waves from the deep earthquake source below Fiji to a seismograph in Tonga and in Fiji suggests that the downward limb is more rigid than the surrounding upper mantle material. High frequency shear waves are observed at Tonga but not at Fiji. There is considerable tectonic similarity between the Fiji-Tonga region and western South America. Both

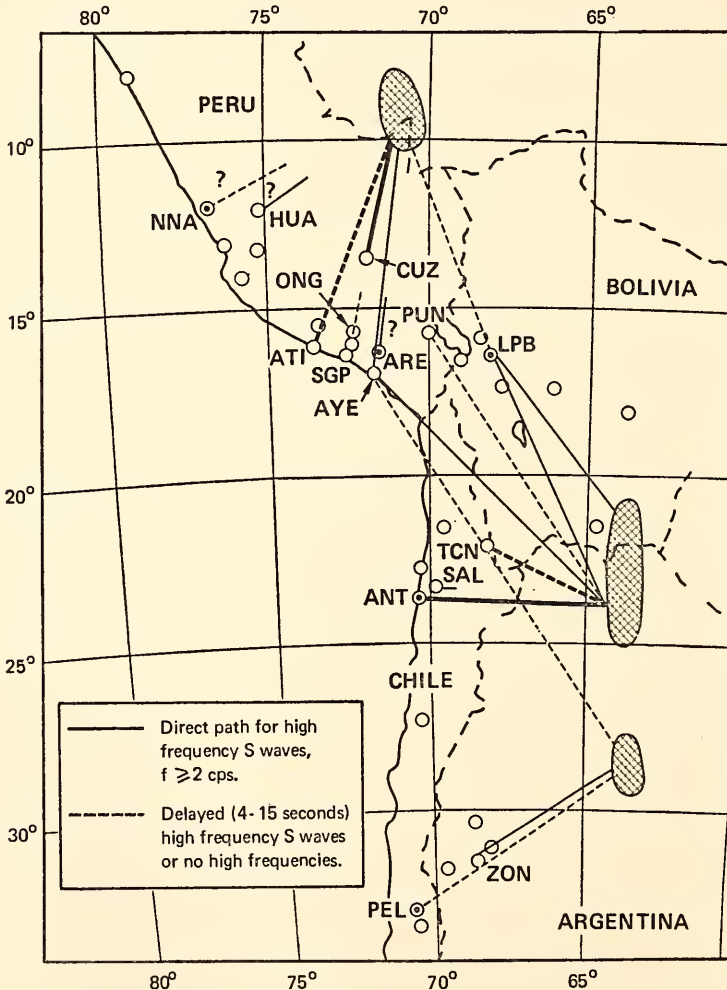


Fig. 34. Distribution of high Q_s (solid lines) and low Q_s (dashed lines) paths from deep earthquake regions (hatched) in South America. There is no simple pattern of these paths related to the tectonics.

have trenches near which shallow earthquakes occur and from which the earthquake zone dips into the upper mantle. The Lamont group suggests that all such regions, i.e., deep sea trenches, having deep earthquakes associated with them in a direction away from a midocean ridge may be the downward limb of a convection cell. This mechanism would produce a particular distribution of high Q_s and low Q_s regions. The stations on the coast, i.e., nearest to the trench, should receive high frequency shear waves, whereas stations farther from the coast nearer the deep sources would be expected to have a low Q_s path and receive only low frequency shear waves, as does the Fiji station. Preliminary results from earthquakes in the Peru-Brazil region contradict this pattern. Figure 32 shows the earthquake occurrence in southern Peru and western Brazil. As is the case in Tonga, earthquakes near the trench are shallow, and get deeper away from the trench. The station at the coast, ATI, which should have had a high Q_s path, shows a low Q direct S arrival with a later high frequency S (Plate 3), whereas the Cuzco station, which is near the source and should have had a low Q_s only, has a direct high Q_s path (Plate 4). A study was undertaken to delineate high Q_s paths in the South American region. The pass band of the Carnegie drum recorder stations fortunately covers the critical frequency range of 1–3 cps and seismograms from these stations were studied from all the South American deep sources. Data from other seismograms covering this frequency range were also used. Examples of shear arrivals are shown in Plates 2–6. S arrivals at the Puno station from the Salta source show no high frequencies either on time or delayed, whereas at AYE on the coast, (Plate 5) arrivals from the same earthquake show high frequency (greater than 2 cps) at S time. The deep source

at Santiago del Estero in Argentina has direct high Q path to the Zonda station east of the Andes, but the high frequencies arriving nearer the coast at PEL are delayed, (Plate 6).

Figure 34 shows some of the results. For simplicity, direct high Q paths are shown as solid lines and the two other classes, i.e., delayed high frequency and no high frequency, are indicated with dashed lines. No clear pattern of high Q paths has emerged from this study. This considerable body of data suggests rather that there are holes through a low Q zone which allow the passage of the high frequency shear waves, Fig. 35. Furthermore, these holes are not distributed in any systematic manner relative to the trench-mountain system.

It should be noted, moreover, that the earthquake occurrence also is "lumpy" even though some general trend is followed (See Fig. 32). The conclusions drawn from the study are:

1. The simple model of a downward limb of a convectional cell does not fit the data in South America.

2. A low Q zone which exists under the region has high Q pathways through it. The difference in Q between the low Q zone and the high Q pathway is con-

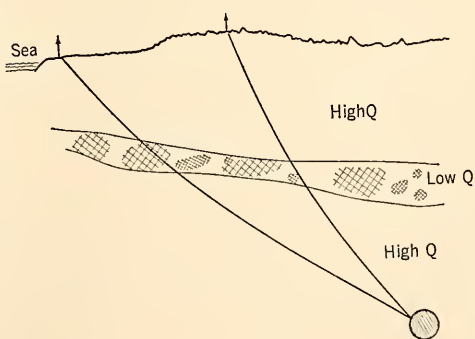


Fig. 35. A suggested model to explain the existence of high Q_s paths. There are holes in a low Q_s region. The low Q_s region is presumed to be caused by partial melting.

siderable, probably more than an order of magnitude.

On Locating Local Earthquakes Using Small Station Networks

*D. E. James, I. S. Sacks, E. Lazo and
P. Aparicio*

Introduction. A study of the reliability of the customary least squares technique of locating earthquake hypocenters was undertaken as a result of our attempts to locate local South American earthquakes using small (5–10 station) networks. The usual iterative least squares technique whereby origin time (T_0), latitude (ϕ), longitude (λ), and depth (z) are computed as independent parameters (e. g., Bolt, 1960;⁴⁸ Cisternas, 1964;⁴⁹ Engdahl and Gunst, 1966⁵⁰) was found to yield hypocenter solutions that depend in an important way upon the number and configuration of the observing stations, and possibly also upon the provisional (zeroth iteration) hypocenter location. This important instability in the hypocenter solutions led us to reevaluate computerized earthquake location techniques as they are presently formulated.

It is appropriate to enumerate some of the more common manifestations of instability in the four parameter least squares hypocenter location method.

1. The computed hypocenter varies markedly when different station subsets of a given station network are used for the calculation.

2. This variation has little dependence upon the model used or upon normal observational errors. Errors arising as the result of an inappropriate model (in practice, the J-B travel-times are commonly used), even when that model is known to be grossly in error, (e.g., a constant velocity mantle), are typically an order of magnitude less than those

arising as the result of varying station configuration.

3. The greatest variation is typically in T_0 and z ; commonly T_0 and z vary in such a way as to effect mutual compensation of errors.

4. When many stations, including teleseismic stations, are used in the location, a common manifestation of an error in location is the presence of large time residuals at local stations. This effect is especially common in South America where big earthquakes often are located by using observations predominantly from the North American continent. For some time we thought these large residuals to be the result of bizarre velocity structure in South America; it can easily be shown, however, that the residuals are much too large to be produced by structure alone.

Of course, workers who have seriously studied the problems inherent in earthquake location (e.g., Bolt, 1960;⁴⁸ Norquist, 1962;⁵¹ Cisternas, 1964;⁴⁹ and others) have been aware of the limitations on the least-squares procedure using only P -wave arrival times to determine T_0 , ϕ , λ , and z , and have laid down various conditions that must be met if reliable solutions are to be obtained. As it is difficult to meet these conditions (e.g., many stations, together with good azimuth and range control) in many parts of the world, especially South America, it has been necessary to seek another more stable method of location.

Examples of instability. Two well-observed earthquakes have been selected to illustrate the instability of four parameter solutions. The first example involves an earthquake that occurred just outside the Arequipa network on February 5, 1965, and which was observed by all nine stations within the network. The test for stability is based upon the simple procedure of locating the earthquake, using different subsets of the nine-station network. The results are shown in Fig. 36. The total change

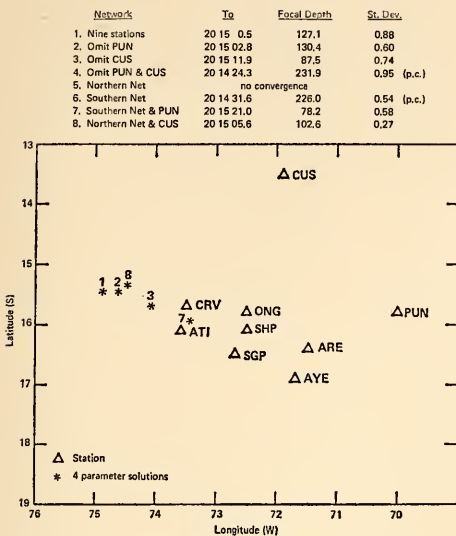


Fig. 36. Four parameter solutions for earthquake of February 5, 1965. Key: Northern net includes stations CRV, ATI, ONG, SHP, SGP; Southern net includes stations ONG, SHP, SGP, ARE, AYE. Standard elevation correction.

in origin time is more than 30 seconds, total spread in depth is 110 km, and total variation in epicenter is more than 200 km. It is important to note that the standard deviation (S. D.) in the travel time does not change significantly from one example to the next and gives no indication whatever as to the reliability of the solution.

The second example (Fig. 37) involves an earthquake whose epicenter is located on the outer boundary of the network. In this case, the instability is somewhat less than that exhibited in the previous example, although it is still so large as to render the solution unusable for most travel time or other studies requiring precise locations and origin times.

It is natural to inquire whether this instability is the result of mathematical instability inherent in the four parameter technique or is caused by the structural complexity and inappropriateness of the J-B model for this region of South

America. To test this possibility, we added station corrections found from teleseismic data (*Year Book 65*, p. 47) which provide some correction for both structure and model. The result is shown in Fig. 38. Other changes in the travel times and station corrections produce a similar result. One obtains some change in location, as expected, but the change due to adding or subtracting various station corrections is much smaller than the change in location and origin time resulting from different station configurations for those cases in which normal convergence is achieved. Thus, station corrections designed to accommodate structures and models different from those assumed produce only relatively small changes in location. Similar small differences in hypocenter result from errors in data. It appears that no reasonable model, structure, or data errors can produce the kinds of origin time and hypocenter changes observed.

Nonetheless, as a final test to exclude all effects of model, data, and structure, we undertook additional studies in which travel times were generated for a number

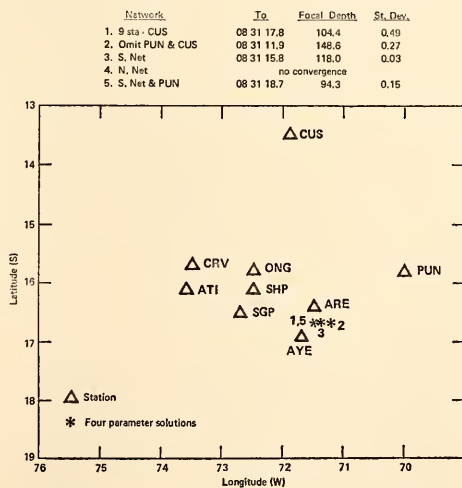


Fig. 37. Four parameter solutions for earthquake of January 26, 1965. Network key same as Fig. 36. The network "9 sta-CUS" includes all stations but CUS.

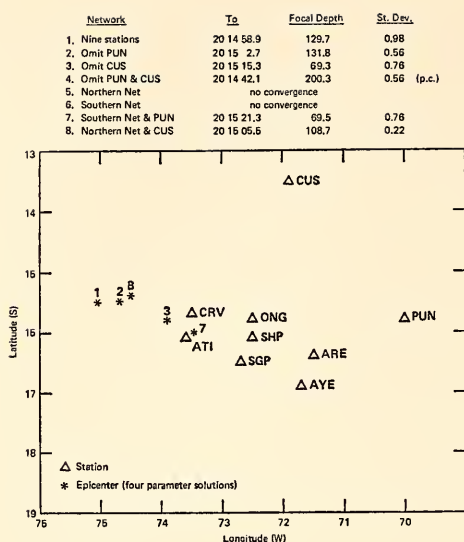


Fig. 38. Four parameter solutions for February 5, 1965 earthquake with empirical elevation correction added. Network key same as in Fig. 36.

of synthetic earthquakes in the vicinity of the Arequipa network. To do this we assumed various appropriate hypocenters and computed *P*-wave and *S*-wave arrival times at the stations on the basis of a J-B model. These arrival times were then used in the four parameter hypocenter program to ascertain under what conditions the four parameter technique fails to obtain a reliable solution. For the purposes of this study, synthetic earthquakes with locations near the actual earthquake examples given above were used. The generated *P*-wave travel times include random errors up to ± 0.5 second and generated *S*-wave travel times include random errors up to ± 1.0 second.

The two synthetic earthquake examples are shown in Figs. 39 and 40. It is apparent that much the same behavior found for actual earthquake examples obtains for the synthetic earthquakes. This instability cannot, of course, be attributed to model, structure, or data errors but must reside within the least squares procedure.

Sources of instability. It has been observed in the literature that in certain common circumstances the four parameter least squares technique may yield spurious results. In particular, some workers (e.g., Bolt, 1960;⁴⁸ Cisternas, 1964⁴⁹) have observed that a poor geometric distribution of the stations relative to the hypocenter (i.e., inadequate azimuthal or range control) can produce spurious solutions, especially if the number of observations is small. Norquist (1962)⁵¹ noted that focal depth can be traded for origin time even in instances where many stations provide good azimuthal and range control. It is this fact that leads to the crux of the instability; namely, that ϕ , λ , and z are not independent variables with respect to T_0 . This fact is of great importance because of the least-squares re-

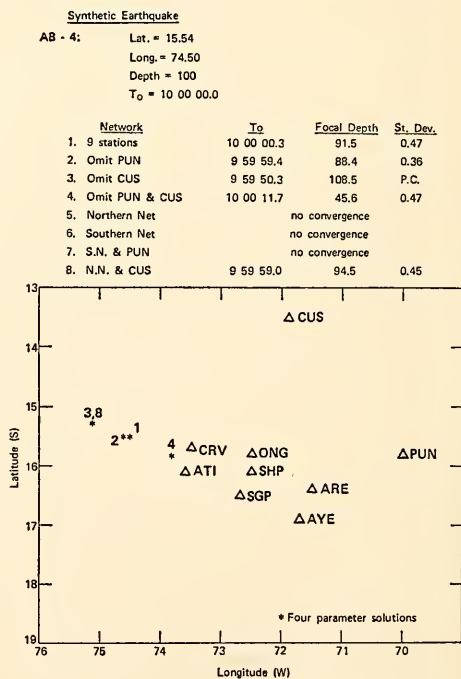


Fig. 39. Synthetic earthquake in location comparable to actual earthquake of February 5, 1965. For purposes of computation, all station elevations were taken to be zero. Code: S. N. = Southern net; N. N. = Northern net.

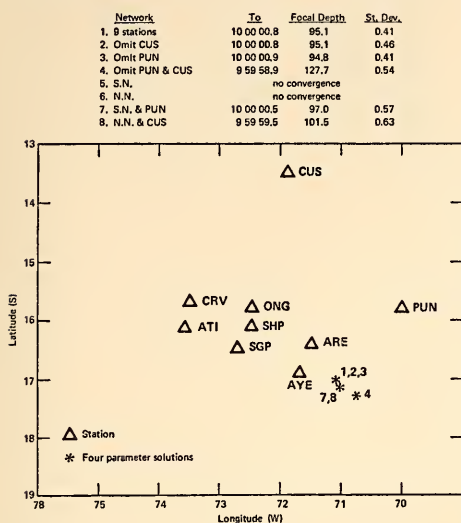


Fig. 40. Synthetic earthquake in location comparable to actual earthquake of January 26, 1965. Same code given in Fig. 39 caption applies here.

quirement that all variables be strictly independent. This lack of independence is shown particularly by the presence of pseudominima in the time residual surface. Thus, the minimum to which the solution converges need not be the true minimum and is dependent both upon the configuration of the observing network and upon the location of the provisional hypocenter.

It is clear, then, that if some independent means of calculating T_0 could be found, the mathematical instability would be removed and ϕ , λ , and z could be calculated by least squares. Because of the clear S -waves that are recorded for most South American earthquakes, we looked to them to provide a means of calculating T_0 .

Independent calculation of origin time. Origin time can be calculated for each station at which S is observed from the equation:

$$T_0 = T_p - \frac{(V_k)(T_{s-p})}{V_p} \quad (20)$$

where T_p = arrival time of P -wave

T_{s-p} = S - P travel time

$$V_k = S-P \text{ velocity} = \frac{T_s - T_p}{\Delta}$$

V_p = P -wave velocity

V_k and V_p are calculated for each provisional hypocenter (assuming a J-B model) and T_0 computed for each station and a suitable average origin time obtained. P -wave travel times are derived by subtracting the average origin time from the arrival time of each station. After the P -wave travel times are obtained, the computations follow the least-squares procedure described above, except that T_0 is not a least-squares parameter. T_0 is, however, recomputed after each iteration. The solutions obtained by this technique prove to be stable regardless of station configuration or provisional hypocenter location.

It is clear, of course, that use of this technique depends upon reliable S -wave readings for at least one station. Because of the difficulty in reading S accurately, it is desirable to have several S readings so that the origin time can be evaluated according to station-to-station consistency. It should be noted that the effectiveness of this means of calculating T_0 is made possible by the fact that calculated origin time varies little with depth or distance. Thus, an error of 5° in the provisional hypocenter for an earthquake 100 km deep produces an origin time error of less than 3 seconds. Moreover, because the model enters in only as a ratio of velocities, origin time varies little from model to model provided the ratio of velocities does not change significantly. For the remainder of this paper, the procedure whereby T_0 is independently computed, and ϕ , λ , and z are found by least squares, will be referred to as the "three parameter method" to distinguish it from the usual four parameter method.

Three parameter solutions. The three parameter technique was tested in pre-

cisely the same way and on the same earthquakes (real and synthetic) as the four parameter method. The results, showing hypocenter solutions for different station subsets, are presented in Figs. 41-44. Comparison can be made of the four parameter solutions shown in Figs. 36 and 37. The most striking difference between the three parameter and the four parameter solutions is the great stability shown in the three parameter solutions compared to the four parameter solutions. Of course some variation in the three parameter solutions remains, particularly in the case of the real earthquakes. These variations appear now, however, to be almost entirely a function of the consistency and precision of the data and the appropriateness of the model. In no solution of any of the hundreds of earthquakes located by this technique has there been any indication of the instability so commonly exhibited by the four parameter method. As mentioned above, the station-to-station consistency gives a measure not only of the reliability of T_0 , but also of the reliabil-

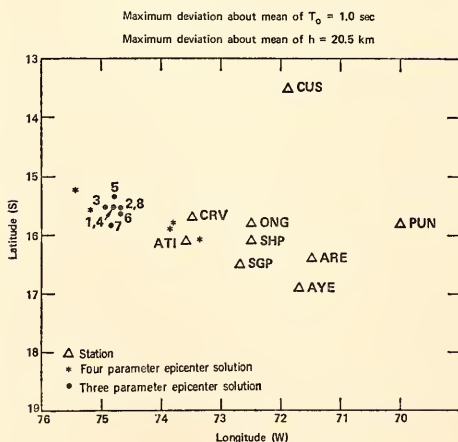


Fig. 41. Three parameter solutions for earthquake of February 5, 1965. Four parameter solutions are shown for comparison. Note that all station subsets provide convergent solutions in the three parameter procedure; the four parameter technique failed to provide convergent solutions in three cases for the same earthquake.

Network	To	Focal Depth	St. Dev.
1. 9 sta - CUS	08 31 19.4	87.2	0.70
2. Minus CUS & PUN	08 31 19.5	89.2	0.63
3. S. Net	08 31 18.8	93.5	0.16
4. N. Net	08 31 20.6	108.2	0.30
5. S. Net & PUN	08 31 19.0	90.9	0.18

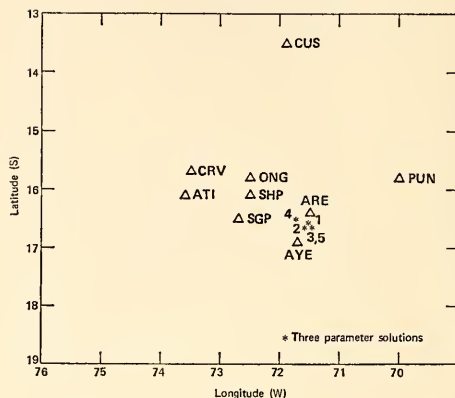


Fig. 42. Three parameter solutions for earthquake of January 26, 1965. Note that network 4 (N. net) yields a convergent solution whereas no solution was obtained using the four parameter technique.

ity of P and S times. In general, a variation of less than 2-3 seconds in origin time from station to station is considered to constitute a reliable solution.

The errors that persist for the syn-

Network	To	Focal Depth	St. Dev.
1. 9 stations	10 00 00.0	92.6	0.43
2. Omit PUN	10 00 00.2	86.3	0.34
3. Omit CUS	10 00 00.1	90.7	0.46
4. Omit CUS & PUN	10 00 00.4	86.2	0.37
5. Southern Net	no convergence		
6. Northern Net	10 00 00.0	91.7	0.46
7. S. Net & PUN	10 00 00.2	93.2	0.58
8. N. Net & CUS	10 00 00.0	92.3	0.37

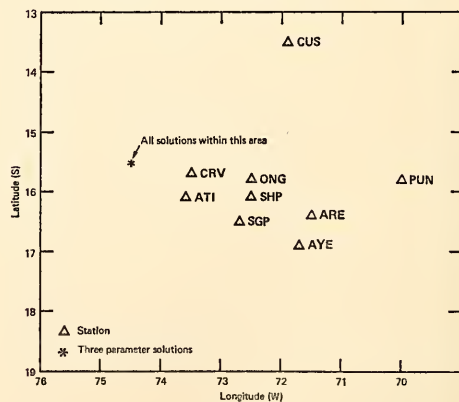


Fig. 43. Three parameter solutions for synthetic earthquake AB-4.

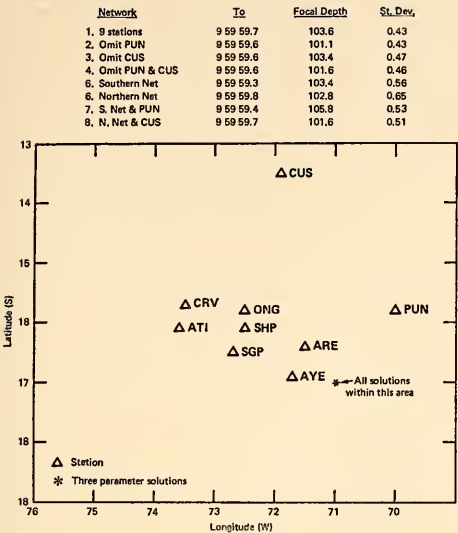


Fig. 44. Three parameter solutions for synthetic earthquake AB-11.

thetic earthquakes (beyond those uncertainties produced by the random errors introduced in the travel times) are a measure of the minimum uncertainty in the hypocenter location. This minimum uncertainty results from the nature of travel times and cannot be eliminated. We turn now to an examination of those factors which contribute to this uncertainty.

Remaining problems. Although the method of computing an origin time independent of the location parameters eliminates the mathematical instability that has been the primary focus of this paper, there remain a number of problems connected with earthquake location using small networks. Most of these problems relate to the particular nature of travel times within the earth and are not soluble within the framework of the location techniques that have been discussed. A model study was undertaken to ascertain the nature and magnitude of these problems. The station layouts and the epicentral locations are shown in Fig. 45. The station coordinates chosen were those of actual operating

seismograph stations involved in the hypocenter location examples discussed in earlier sections of this paper.

Theoretical arrival times were calculated for each station from each epicenter assuming a J-B earth model. At each epicentral location, source depths covering the range 30–600 km were considered. Random errors (up to ± 0.5 sec for *P* and ± 1.0 sec for *S*) were added to the arrival times in order to make this model study compatible with actual conditions. A gaussian distribution of errors was assumed, producing a standard deviation of 0.33 sec for *P* waves. Comparison of the residual of the standard deviation in the model with those of actual earthquakes suggests that the assumed errors are of the right order. The calculated arrival times, with added errors, were then used to locate hypocenters using the three parameter method. It was found that the errors in depth were generally about twice those in latitude or longitude, and the depth error was therefore used as a criterion for evaluation. Figure 46(A) and (B) shows the depth errors for profile *AB* which is parallel with the longer axis of the location network, and *CD* which is perpendicular to this axis.

It was found that the accuracy of the hypocenter was a function not only of epicentral distance but also of focal depth. The error of hypocentral determination as a function of depth for various positions relative to the network is shown in Fig. 47. The 20-km error contours have been drawn in Fig. 46 for the two station configurations considered. The 20-km contour was chosen because inspection of Fig. 47 reveals that at any distance the errors below the 20-km level decrease rapidly as the depth increases and conversely, errors above the 20-km level increase rapidly.

In the stable zone, i.e., below the contour lines in Fig. 46, the error in hypocenter is mainly a function of the magnitude of random errors added to arrival

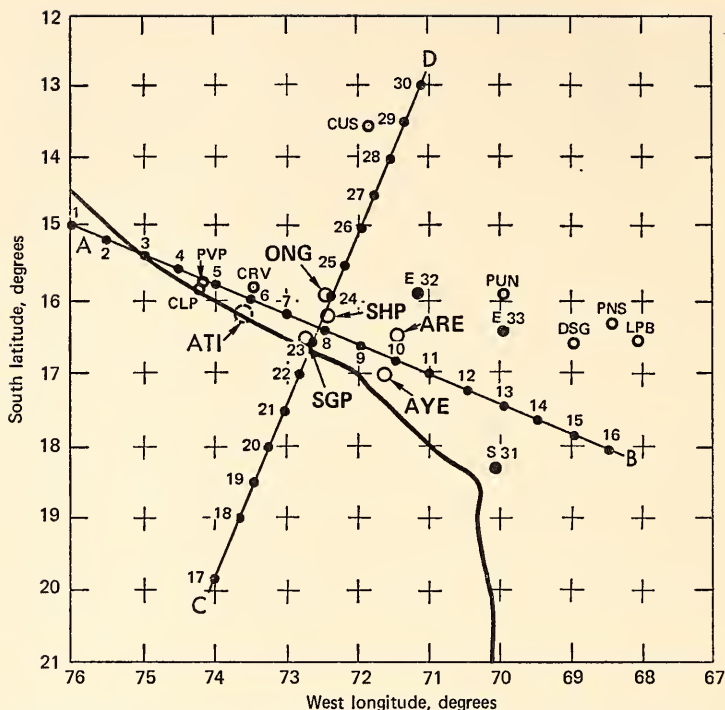


Fig. 45. Seismograph stations and epicenters used in the model study. The "small" net consists of ARE, AYE, SGP, SHP, and ONG. The epicenters lie along line *AB* parallel to, and *CD* perpendicular to, the longer axis of the net.

times. In this particular example for a five-station network (with a standard deviation of 0.33 sec in arrival times), the probable error in the stable region is about 7 km. The effect of the size of the network may be seen from the upper and lower contour sets in Fig. 46. The length of the network in the *AB* direction is approximately twice that in the *CD* direction and it can be seen that satisfactory locations along the line *AB* can be obtained to rather greater distance than is the case in the direction *CD*. The effect of one extra station added to increase the dimension in the *AB* direction substantially improves the networks' locating ability for relatively distant earthquakes. The effect is much smaller in the *CD* direction. It was also found that shallow earthquakes were very difficult to locate with accuracy

even when they were inside the network unless they were very close to a particular station such as *CD* 23 in Fig. 47. A rough rule is that focal depths less than half the average station separation will be inaccurately determined. This is, however, a function of the geometry of the network and each network should be evaluated by a method such as the one described here.

The above remarks apply to the determination of focal depth. Errors in epicenter are significantly smaller. In particular, epicenter solutions are reliable within the network even for shallow depths for which the error in depth determination may be very large.

One reason for the limitations in the networks' locating ability can be seen from Fig. 48. This shows the change in arrival time for various focal depths as

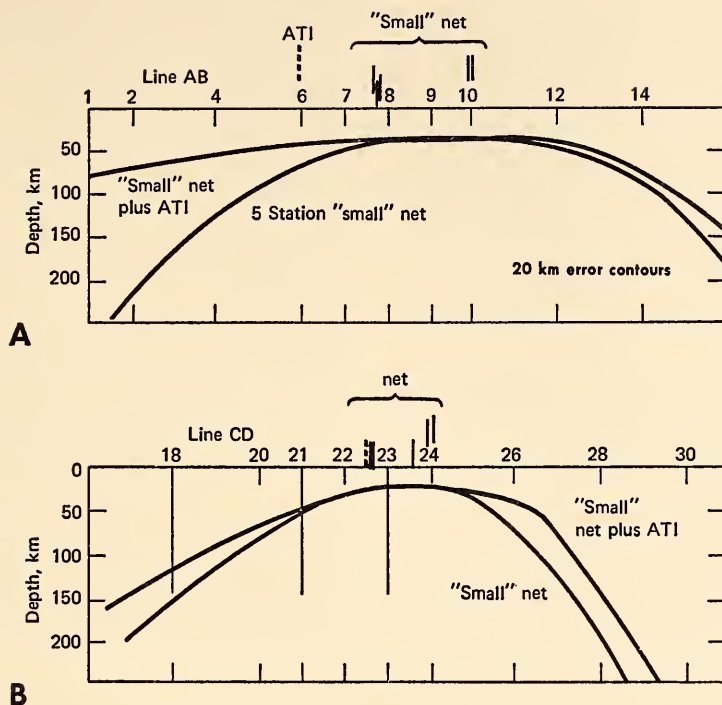


Fig. 46. (A) shows error contour for epicenters on line *AB*. (B) shows error contour for epicenters on line *CD*. Hypocenters lying on the contour line have probable errors of 20 km. Hypocenters below the contour line have smaller errors; those above, larger. The addition of station *ATI* improves the locating ability of the net greatly in the *A* (northwest) direction. The aperture of the net in the *AB* direction (A) and its ability to locate earthquakes outside the net is greater than in the *CD* direction (B).

a function of distance. It can be seen that the value is highest, i. e., the sensitivity to depth change is greatest, when the station is vertically above the source, and the value drops rapidly passing through zero at a relatively short distance for shallow earthquakes, e. g., travel times from an earthquake at a depth of 33 km will be virtually the same as the travel times from a 96-km deep event at a distance of 4° .

When the hypocenter is at such a distance from a network that some of the stations are in this low sensitivity region, the depth cannot be determined with accuracy. Timing errors of 0.33 sec would be equivalent to the depth change of 20 km at a distance of 2° and a mean

focal depth of 60 km. This is what was found in the random error study shown in *CD* 21, Fig. 47. If the size of the error is reduced, then at the particular location given above, the change in arrival time with depth is greater than the errors in arrival times, and a reliable depth may be determined. This effect is shown in Fig. 47, curves *CD* 18 with errors of 0.33 and 0.1 sec. The distance to the minimum in *DT* by *DZ* decreases as the focal depth decreases.

Teleseismic earthquakes. The significance and relevance of these results to teleseisms (large earthquakes) is largely in terms of limits that can be imposed on the hypocenter solutions by near station data. The problem of obtaining

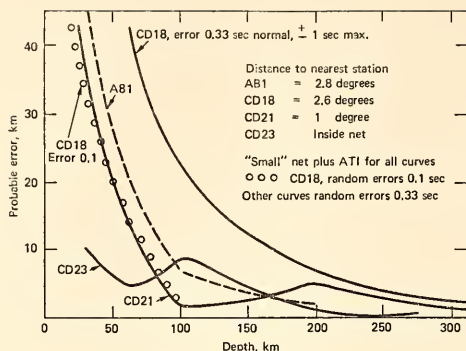


Fig. 47. Probable errors for various positions in Fig. 45 as a function of depth. *CD 18* and *AB1* are similar distances from the station network, but the longer dimension of the net in the *AB* direction gives a more accurate location for *AB1*. Note that if the errors in the data are reduced, (*CD 18*, open circles), the location accuracy is improved. This is explained in Fig. 48. Note also that deeper earthquakes (deeper than 100 km or so) can be located with good accuracy even 300 km outside the net.

reliable solutions for large earthquakes (particularly large shallow earthquakes) is one which we shall not discuss, except to note that it is a significantly more difficult problem than that of locating local smaller earthquakes. Nonetheless, it is informative to examine the reliability of these solutions in light of the demonstrated instability of the four parameter technique.

Many examples have been found of teleseismic determinations of South American hypocenters for which the standard deviation is low, but the hypocenter solution highly inaccurate. Hypocenter solutions for which depth is constrained (usually on the basis of *pP* arrivals) tend to be considerably more accurate, and patently unstable solutions are rare if the depth is constrained. The fundamental difficulties in obtaining reliable focal depths, for either the four

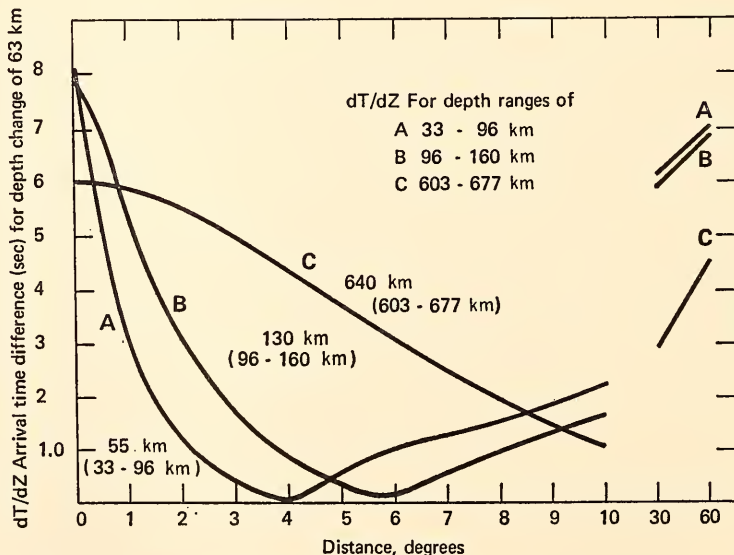


Fig. 48. Theoretical sensitivity of travel time to changes in depth of hypocenter, assuming a Jeffreys-Bullen earth model. Absolute values are shown. The minimum in sensitivity occurs at greater distances for hypocenters at greater depths. For a station to control the depth within same range, the errors in its time readings must be less than the variation in the arrival times for that depth range, i.e., station errors must lie below the curve for the relevant depth. Stations immediately above an earthquake have greatest sensitivity to its depth. The depth of shallow earthquakes is difficult to determine if there is no very close station because the minimum in sensitivity occurs at a small distance, possibly less than the network spacing.

parameter or three parameter method dictates that depths be determined independently whenever possible.

Because of the difficulty of determining the onset of S for large earthquakes at high gain stations, origin time cannot always be computed independently. This fact makes the three parameter method considerably less useful in the case of large earthquakes. The ${}_pP$ phase can, however, often be identified with some certainty, and constrained depth is a minimum requirement for reliable hypocenter solutions. Ideally, origin time should be determined from P wave and $S-P$ times at near stations, depth from ${}_pP$, and ϕ and λ determined by least squares.

Discussion. Several conclusions may be drawn from the study. Four parameter hypocenter location techniques such as the P -wave method in which X , Y , and Z , and the origin time are the parameters solved for, or the $S-P$ method in which X , Y , Z , and the apparent $S-P$ velocity are the parameters solved for, are unstable if used in networks consisting of few stations. It is difficult to define what minimum number of local stations are required for stability of these location methods, but experience with the Arequipa network in southern Peru suggests that nine stations or more are required and the earthquakes must be well within the network. This number of stations is, of course, affected by the geometry of the station layout and the position of the hypocenter relative to the stations. If the hypocenter is outside the network even nine stations are not enough. The three parameter solution described here has been found to be free of these instabilities. For any method, however, it is important to realize that the standard deviation of the result is not in any way an indication of the reliability or accuracy in the hypocenter.

The depth of shallow earthquakes less than about half the mean station spacing is difficult to determine accurately

even if the earthquake is inside the network, unless it occurs close to one of the stations. Deeper earthquakes, i. e., those at a depth greater than 100 km, may be located quite accurately more than 1° outside a net whose dimension is only $\frac{1}{2}^\circ$. The effect of the model used for the travel-time calculation is least severe inside the network but can be serious if some distant stations are used. In an area such as South America, travel times are known to depart substantially from J-B at distances less than 20° . A more reliable solution is therefore obtained by omitting stations much beyond 3° or 4° provided that there are at least five stations at lesser ranges.

Some of the above conclusions apply equally well to location of teleseisms; in particular, the standard deviation does not indicate the magnitude of uncertainty in the hypocenter solution (although a high standard deviation almost always means a poor location). Hypocenter solutions for which depth is constrained are significantly more reliable than those four parameter solutions for which depth is not constrained. In the absence of sufficiently good S -wave determinations with which to determine origin time, the independent determination of depth (usually from ${}_pP$) is a minimum requirement for stability in teleseismic hypocenter solutions.

Upper Mantle Structure Beneath Western South America

D. E. James and I. S. Sacks

As a first step in deriving velocity-depth relations beneath the various tectonic provinces of western South America, P -wave travel times were studied for rays whose paths were confined entirely to coastal and oceanic regions and in the distance range to 20° . Figure 49 is a map of South America showing the location of recording stations and of earthquakes used for this study. The earthquakes shown in Fig.

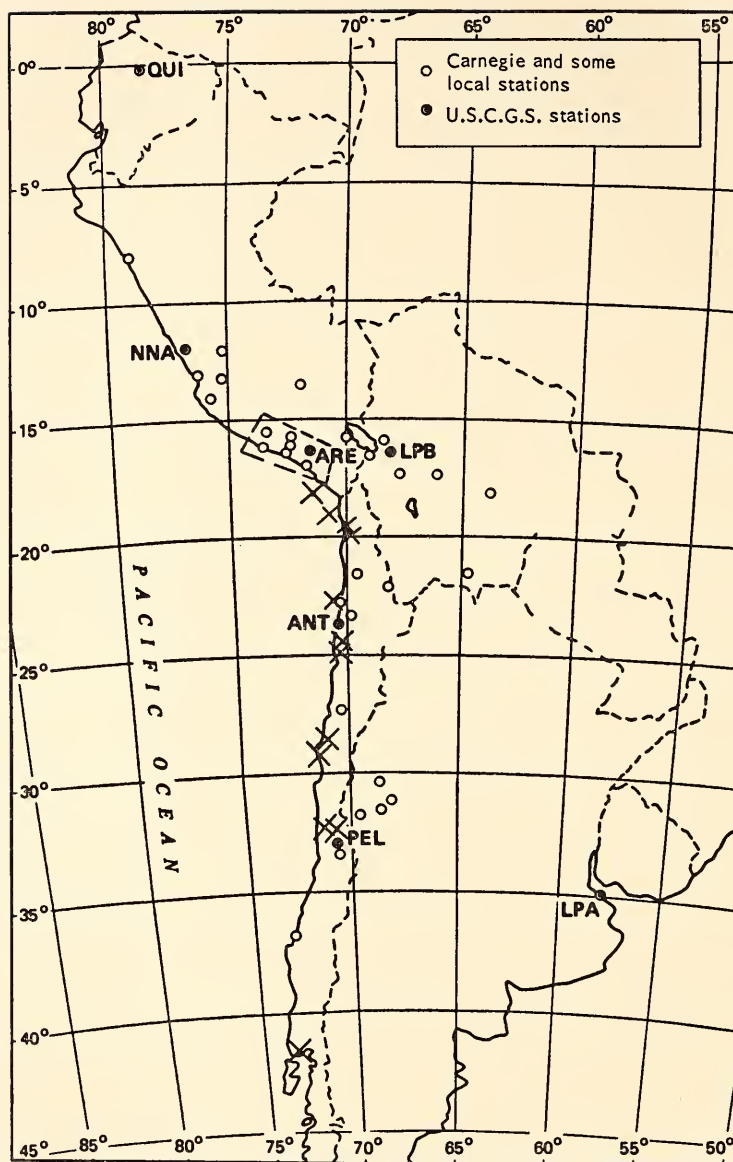


Fig. 49. Map showing station locations and epicenters. X's denote epicenters used in travel time determinations.

49 are all shallow and occur at depths of 50 ± 25 km. With few exceptions, only Arequipa network stations (see box in Fig. 49) were used for the final record section. The earthquakes involved in this report are among those selected by Kamitsuki (see *Year Book 65*, pp. 39-43),

who also read all first arrivals. This study is an extension of Kamitsuki's work.

The procedure followed for location of the hypocenters is similar to that outlined in the section above dealing with problems of locating hypocenters.

The technique has been modified somewhat, however, to achieve more accurate depth determinations and to permit determination of origin time for very large earthquakes where the S arrival cannot be reliably read on near-station records. Thus, all depths have been constrained on the basis of at least 5 pP readings. In most cases, the origin times were computed using the equation given in the above section; in those instances where fewer than 3 or 4 S -wave readings were obtained at near stations ($<5^\circ$), or where the origin times were inconsistent from station to station, the origin time was calculated using least squares, together with latitude and longitude. In most cases, however, only latitude and longitude were computed by least squares. As stated in the previous section, this least-squares method employs only P -wave arrivals and assumes a Jeffreys-Bullen (J-B) model.

The question of whether or not it is a valid procedure to use the same stations for locations and for travel times natu-

rally arises. As a means of avoiding the various problems inherent in this kind of "bootstrapping," we chose to use no arrivals in the 5 – 20° distance range (the interval in which major deviations from J-B occur) in hypocenter calculations.

Figure 50 shows all first arrivals from the earthquakes shown in Fig. 49. Corrections have been applied (on the basis of a J-B model) for the variation in focal depth and all times have been normalized to a 50-km focal depth. The error in this procedure due to inappropriate model is probably no more than a few tenths of a second. The scatter of points around the J-B curve at distances less than 500 km is a result of using these readings in the hypocenter location calculations. The "observed curve" is simply a curve fitted by eye through the first arrivals. Most of the large positive deviations off the observed curve in the distance range 5 – 20° are for a single station (NNA), which has a poor signal-to-noise ratio. The remaining deviations appear primarily to be due to hypocenter location errors. For the purpose of studying

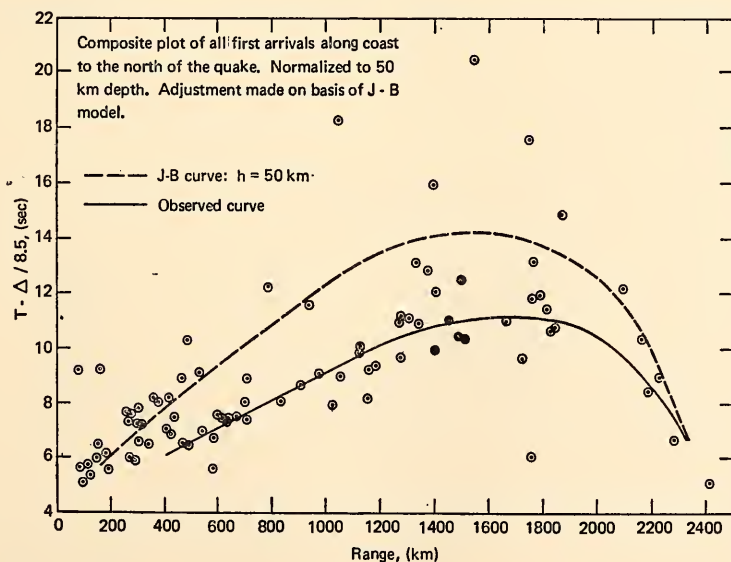


Fig. 50. First arrivals at coastal stations to north of epicenters shown in Fig. 49. Cluster of arrival times near J-B curve is a consequence of using stations at less than 5° for hypocenter location.

later arrivals, all first arrivals in Fig. 51 have been placed on the observed curve. This procedure is not entirely satisfactory because of the assumption that all first arrivals would fall on the observed curve if the hypocenters were perfectly located. This is necessary since scatter due to hypocenter location errors produces sufficiently large scatter in the secondary arrivals to make tracing of later phases even more difficult.

Figure 51 is a composite of a number of records, mostly from stations of the Arequipa network. For AYE station, with both high and low gain channels, the low gain channel is shown, although its relative position on the time axis is determined on the basis of the high gain channel, on which the first arrival is very clear. The dashed travel-time curve

shown is that produced by the velocity-depth model shown in Fig. 52. One important feature of the composite is the set of large later arrivals which begin at about 1450 km and proceed back to about 1200-km range. This particular branch of the travel-time curve is produced by the major low velocity zone shown in Fig. 52. Apparent lack of any significant triplication beyond 1450 km gives positive indication that the low velocity zone is narrow and its upper and lower boundaries sharp.

Although the data shown in Fig. 51 are too sparse in the distance range beyond 1900 km to permit tracing of triplication for the purpose of velocity-depth computations, there is strong indication of triplication and a possible cusp in the distance range 1600–1900 km. These ap-

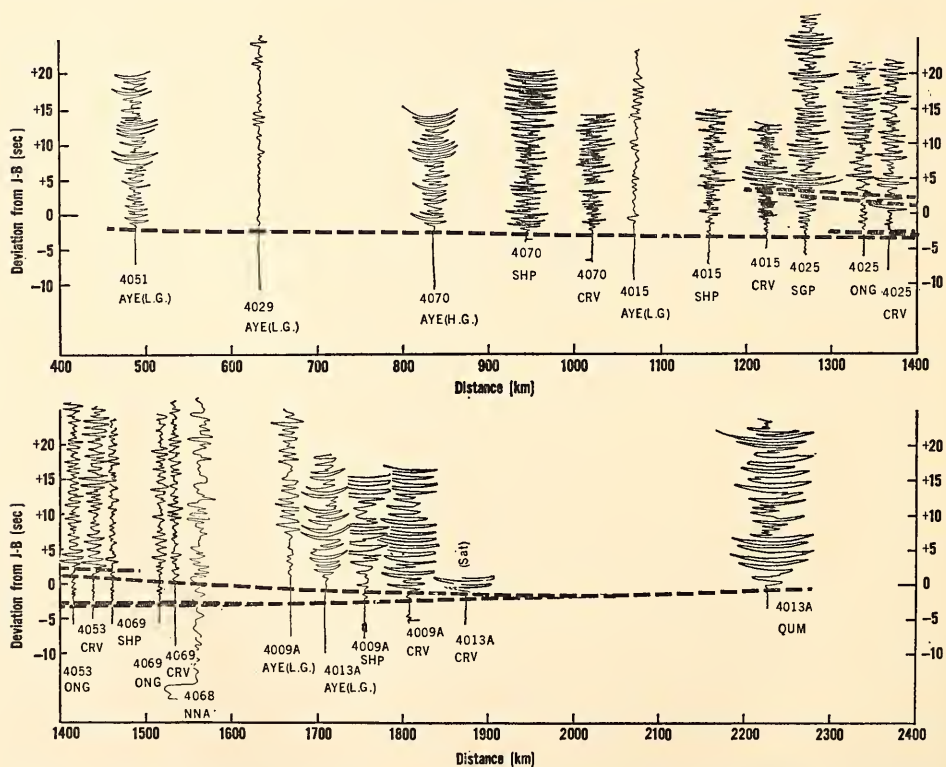


Fig. 51. Record section with travel-time curve produced by the "Carnegie" velocity-depth model shown in Fig. 52.

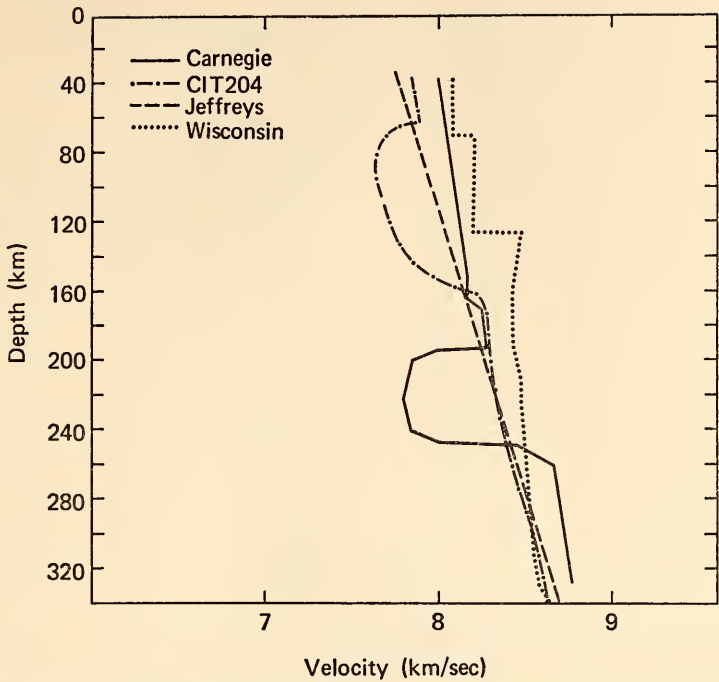


Fig. 52. Velocity depth model (solid line) for upper mantle beneath coastal and oceanic areas of western South America. The other velocity-depth curves are provided for comparison.

pear to be related to the 20° discontinuity which probably results from a velocity increase at a depth of 400–450 km. More on the nature of this discontinuity will be presented in future *Year Books*. See also *Year Book 66* for a discussion of this discontinuity.

For the velocity-depth model shown in Fig. 52, a crust of 36 km with a mean velocity of 6.29 km/sec has been assumed (Woollard, 1960).⁵² The petrologic significance of the low velocity zone is not entirely clear, although we speculate that it probably corresponds to a region of partial melting. The low velocity zone is consistent with the low velocity–low Q_s zone that is apparently present in the mantle beneath the Andes at a depth of 300–400 km. It is possible, though certainly not confirmed, that the low velocity zone beneath the coastal and oceanic areas is continuous with a similar but deeper zone beneath the Andes.

A Study of the Crust and Upper Mantle of Northern Chile

R. Olea M., A. Cisternas, and E. Kausel
Department of Geophysics,
University of Chile, Santiago

Using the network of five short-period stations supplied by the Department of Terrestrial Magnetism, and the worldwide station at Antofagasta, a group of 47 earthquakes and 4 explosions was

TABLE 15. Values of Seismic Parameters for Northern Chile

	Data from Tuve <i>et al.</i>	Data from this study
<i>P</i> (crustal)	6.2 km/sec	6.15 km/sec
<i>S</i> (crustal)	3.57 km/sec	3.55 km/sec
<i>P</i> (mantle)	8.00 km/sec	7.82 km/sec
<i>S</i> (mantle)	4.62 km/sec	4.52 km/sec
Dip angle of Moho	8.5° E	11.5° E
Depth of crust at 70°W latitude	30 km	36 km

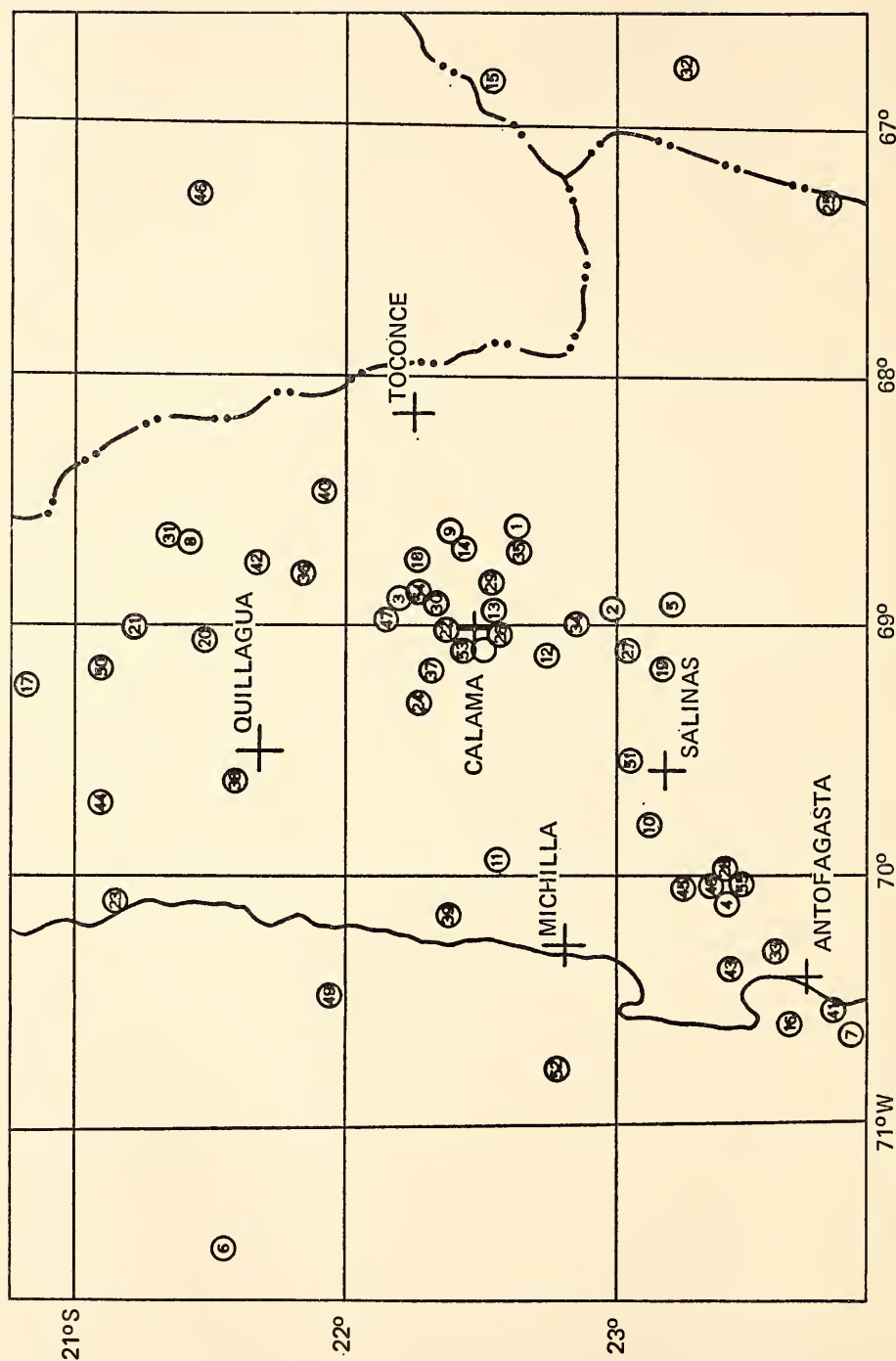


Fig. 53. Map of northern Chile showing locations of hypocenters used in determining model for the crust discussed.

TABLE 16. Epicentral Locations, Depths and Residual Times
for the Earthquakes Displayed in Figure 53

No.	1964	S. Latitude	W. Longitude	Depth (km)	Residual Time, sec
		° ' "	° ' "		
1	31 May	22 40 2.9	68 35 53.8	88	0.33
2	19 June	23 0 6.6	68 55 33.0	82	0.32
3	26 June	22 13 23.2	68 53 5.7	93	0.26
4	27 June	23 24 33.5	70 4 21.7	25	0.16
5	28 June	23 15 1.8	68 53 3.3	105	0.17
6	1 July	21 36 36.8	71 29 26.9	57	0.42
7	4 July	23 57 28.4	70 38 35.5	32	0.35
8	5 July	21 25 32.8	68 36 54.6	126	0.52
9	5 July	22 26 49.3	68 35 48.4	107	0.35
10	5 July	23 9 13.7	69 48 3.6	85	0.50
11	18 July	22 35 4.6	69 57 4.8	29	0.32
12	25 July	22 47 20.2	69 6 10.3	104	0.27
13	11 Aug.	22 33 7.6	68 58 21.9	96	0.39
14	14 Aug.	22 25 31.6	68 38 43.0	89	0.59
15	7 Sept.	22 34 8.5	66 48 1.1	301	0.54
16	7 Sept.	23 40 27.6	70 37 19.7	33	0.25
17	11 Sept.	20 49 19.1	69 13 44.2	120	0.59
18	12 Sept.	22 19 20.7	68 44 20.5	98	0.50
19	14 Sept.	23 13 19.6	69 11 38.5	87	0.40
20	17 Sept.	21 27 58.5	69 3 5.2	94	0.16
21	24 Sept.	21 14 11.3	68 59 19.8	105	0.30
22	26 Sept.	22 24 55.7	68 59 52.4	85	0.55
23	26 Sept.	21 9 54.4	70 5 32.9	73	0.45
24	27 Sept.	22 17 11.7	69 18 35.1	95	0.66
25	27 Sept.	23 51 52.8	67 13 0.7	236	0.20
26	27 Sept.	22 34 34.2	69 4 3.6	85	0.64
27	28 Sept.	23 5 50.7	69 6 37.7	80	0.53
28	28 Sept.	23 24 44.7	70 1 35.1	14	0.51
29	28 Sept.	22 33 51.3	68 47 34.5	97	0.28
30	16 Oct.	22 20 58.6	68 54 3.0	116	0.39
31	17 Oct.	21 12 40.6	68 37 53.0	164	0.67
32	18 Oct.	23 18 6.6	66 39 46.2	161	0.34
33	18 Oct.	23 39 12.4	70 19 20.2	35	0.39
34	23 Oct.	22 53 0.7	68 59 56.1	96	0.55
35	23 Oct.	22 39 5.4	68 39 35.2	101	0.49
36	7 Nov.	21 53 30.9	68 47 5.4	13	0.25
37	10 Nov.	22 18 57.1	69 10 3.8	87	0.38
38	11 Nov.	21 37 43.2	69 36 47.8	2	0.93
39	13 Nov.	22 23 16.0	70 8 00.0	27	0.56
40	13 Nov.	21 55 23.6	68 27 52.0	121	0.38
41	16 Nov.	23 55 8.0	70 32 49.2	72	0.19
42	19 Nov.	21 40 48.6	68 42 48.5	105	0.26
43	24 Nov.	23 27 30.5	70 21 9.7	23	0.49
44	25 Nov.	21 6 25.8	69 41 34.1	15	2.14
45	1 Dec.	23 18 11.9	70 4 47.5	60	0.32
46	12 Dec.	21 30 3.5	67 15 1.2	193	0.29
47	12 Dec.	22 12 57.2	68 56 43.1	—3	0.50
48	12 Dec.	23 24 14.3	70 2 53.9	—1	0.66
49	17 Dec.	21 56 20.1	70 28 16.6	49	0.37
50	21 Dec.	21 6 9.1	69 9 30.0	107	0.53
51	21 Dec.	23 5 47.9	69 32 44.1	82	0.22
52	21 Dec.	22 49 11.7	70 44 39.2	26	0.41
53	27 Dec.	22 29 45.2	69 6 53.3	105	0.37
<u>1965</u>					
54	11 June	22 17 36.3	68 53 35.5	—3	0.31
55	24 June	23 29 8.9	69 59 40.8	—1	0.30

selected from events recorded in the period May–December of 1965. These events were all well recorded on at least 4 of the stations and were chosen in part because their epicenters covered most of the area of the net. The epicentral distribution is shown in Figure 53. The events outside the net were well recorded at all stations and were examined to learn the problems of locating such events.

The hypocenters were located by the standard four parameter method using the model shown in column I of Table 15. Then each of the following parameters—crustal velocity, mantle velocity, crustal thickness, and dip angle between the crust and mantle—was varied one at a time until the calculated time residuals for the resulting hypocenters were a minimum. The values of the parameters initially used were those found from the data of Tuve *et al.* taken in 1957 (*Year Book 57*) as interpreted by Woolard. Column II of Table 15 gives the results of the minimizing procedure which are significantly different from those of column I. Table 16 gives hypocenter locations and residuals for the events of Figure 53 using the model found by the procedure described. It is planned to repeat the calculations using the technique described by James, Sacks, Lazo, and Aparicio earlier.

HEAT FLOW

J. S. Steinhart, S. R. Hart, and T. J. Smith

The regional heat flow survey of Lake Superior, started in 1966, was completed this past year. Working from the U. S. Coast Guard Cutter *Woodrush*, 95 heat flow sites were occupied in 1967, most of them in the eastern half of the lake. Sediment temperature gradients were measured with the Department's six-meter thermistor probe; thermal conductivities were determined on the core samples of sediment by both water content and needle-probe methods.

Operation in the eastern part of the lake differed from that in the western lake. Much of the eastern lake appears to be underlain by sediments of lower water content; this caused occasional incomplete penetration of the corer, lower temperature differences between thermistors because of the higher conductivities, and somewhat smaller attenuations of the annual bottom water temperature cycle. In addition, the bottom topography in the lake east of $86^{\circ}30'$ is characterized by a series of deep north-south valleys. A number of tests had to be made in this area to ensure that the effect of topography and increased sediment fill in the valleys was not seriously affecting the measured heat flow.

A number of sub-bottom seismic reflection profiles of this area were made available to us by R. Wold and N. Ostenso; with these it was possible to compare measurements in valleys with thick sediment fill and valleys with relatively less sediment fill. No detectable differences were found which could be attributed to this effect. For example, nine measurements were made on an east-west traverse at 47°N which included five values in valleys with variable sediment thickness, one in a broad basin, two on intervening ridges, and one on a local saddle in a troughlike area. Only one value differed from the mean of 1.10 hfu (1 heat flow unit = 1 hfu = 10^{-6} cal/cm²/sec) by more than 10%. (This one value has somewhat larger experimental uncertainty owing to above-average conductivity at this site.) This empirical finding is also in line with calculations of the topographic and sedimentation-rate effects.

For a typical Lake Superior valley, calculations suggest that there will be a 3–5% enhancement of heat flow due to the geometric or topographic effect, a reduction of a few percent due to the refraction effects of the sediment fill, and a reduction of 5–7% due to the deposition of a 50-meter sediment layer during, or

prior to, the last glacial period (10,000 years ago). Since these effects largely cancel each other, we would predict heat flow perturbations of less than 5% for the normal-type valleys in the eastern lake. Measurements in this part of the lake should thus be directly comparable to those in the central and western lake where the topography is broad and undulating. One possible exception to this is encountered in a sharp valley running along the northwest shore of the lake, which has been shown by drilling (Zumberge, 1962)⁵³ to have over 200 meters of sediment fill. Based on calculations similar to the above, it is probable that the heat flow values measured along the axis of this valley are about 30% too low. The measured heat flow in this area, which we will discuss further below, is in the range 0.50–0.60 hfu; approximate correction for the above effects raises these values to 0.7–0.8 hfu and they then become more comparable with adjacent measurements made away from the valley axis.

With the additional thermal conductivity measurements made during the 1967 field season, we are now able to confirm a difference in the water-content-needle-probe relationship between Lake Superior sediments and the oceanic sediments reported on by Ratcliffe (1960)⁵⁴. Figure 54 is a plot of the more than 600 samples of Lake Superior sediment analyzed by us; Ratcliffe's curve is shown for comparison. For samples above 50% water content, the difference between the two curves is only about 4%, and this may be attributed to the effect of salinity in the oceanic sediments. At water contents below 50% there is considerable divergence between the two curves, however, and there is also increased scatter in our results. These effects suggest that the actual mineralogy of the sediments is of some importance in determining total sediment conductivities, and that these lake sediments are not only variable in mineralogy but differ on the average

from the mineralogy of ocean sediments. Evidence for mineralogical variation was also found in the results of a number of wet-density determinations, where the inferred densities of the solid (mineral) fractions were greater in the low water content sediments than in the high water content sediments.

With the new results from the eastern lake we are now able to present a contoured heat flow map of some detail which covers most of Lake Superior (Fig. 55). This new map represents a significant advance in our understanding of regional heat flow patterns and permits for the first time regional correlation with other geophysical parameters such as gravity and magnetic field variations.

The range of heat flow values reported in Fig. 55 is surprisingly large, with a variation of almost a factor of three between 0.5 hfu and 1.45 hfu. Furthermore, these variations can occur within very short distances. In the northeastern part of the lake, for example, the heat flow drops from a plateau of about 1.45 hfu to values as low as 0.5 hfu in a lateral distance of only 23 km. More typically, the scale of the heat flow anomalies or variations appears to be larger, perhaps 50 km–100 km, and there are generally rather smooth and continuous changes from one anomaly to the next. Some regions show almost no variation in heat flow—the southwestern part of the lake contains only values within 10% of 1.15 hfu over an area exceeding 15,000 square kilometers. In the other areas there are also very few "erratic" values, i.e., single measurements which differ from the regional pattern by more than 10%; this suggests that the precision of individual measurements is better than 10% and that errors related to topography, sediment erosion or slumping, annual bottom water temperature cycle correction, ground water flowage, etc., generally contribute perturbations of less than 10% to the "real" heat flow component. The overall average of

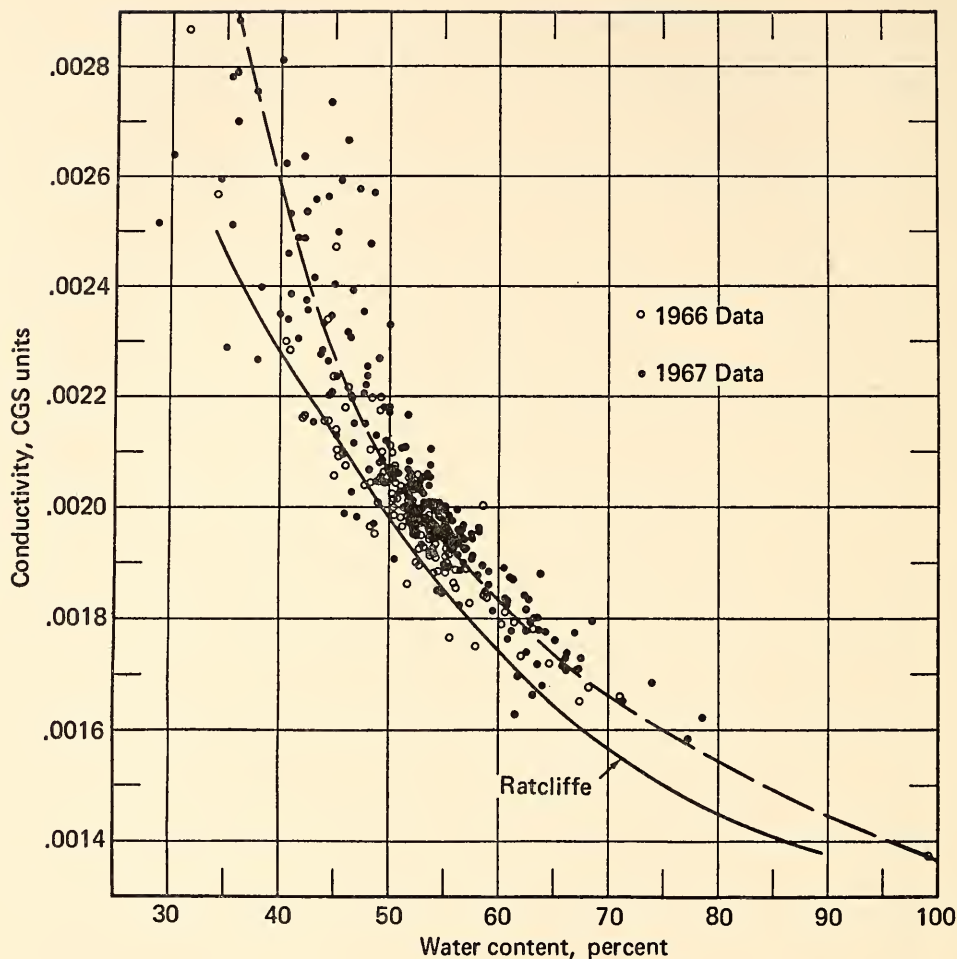


Fig. 54. Empirical curve relating water content and thermal conductivity of Lake Superior sediments. Ratcliffe's curve for ocean sediments shown for comparison.

the 145 measurements shown in Fig. 55 is 0.99 hfu.

The patterns of heat flow exhibited in Fig. 55 may be characterized in terms of anomalies as follows:

1. The "north shore low." A band of low heat flow values (0.5–0.9 hfu) parallel to the north shore of the lake, forming a horseshoe-shaped belt which runs essentially without break for almost 700 kilometers.

2. The "central high." A band just south of the north shore low, composed

of average and above average (1.0–1.45 hfu) heat flow values, also essentially of horseshoe shape. This belt widens on its eastern limb to form the large uniform area mentioned above.

3. The "central low." A broad low lying northeast of the Keewenaw Peninsula, with values between 0.8 and 1.0 hfu. This low occupies the center of the horseshoe formed by other belts. An onshore extension of this region may be represented by the Keewenaw Peninsula where borehole measurements of 0.93

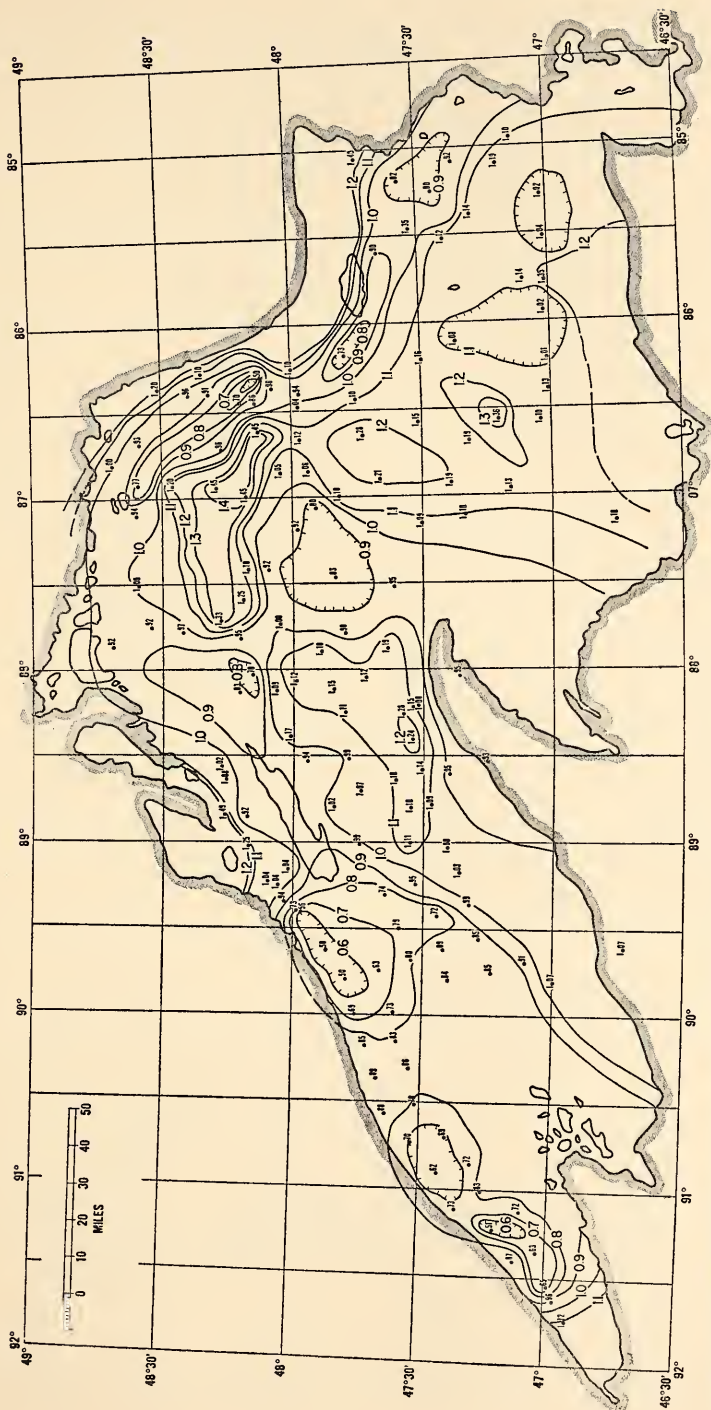


Fig. 55. Contoured heat flow map of the Lake Superior region. Heat flow anomalies may be compared with the features shown in Fig. 56.

and 0.95 hfu have been reported by Roy (1963).⁵⁵

The only measurements which are not included in these three general anomalies are a limited number of measurements close to the north shore, particularly north of Isle Royal, which give higher values than those in the "north shore low," and appear to mark the northern limit of this low belt. As these transitional values occur essentially at the edge of the lake, we are unable to say whether they represent another high belt or simply mark the beginning of a general region on the shield of average heat flow. Along the northwest shore, the "north shore low" widens considerably and appears to extend onshore without any intervening high values. This belt may in fact extend quite far inland, as on-land borehole measurements made by R. Roy about 60 km from shore give values of 0.8 hfu.

In a broad regional sense there is rather good correlation between the heat flow map (Fig. 55) and the known geologic, gravity, and magnetic features of the area. Figure 56 is a comparison of geologic, magnetic, and gravity maps of the Lake Superior region, emphasizing the main features and anomalies. Basically, the lake occupies the center of a large curved syncline of rocks of Keewenawan age (about 1 billion years). The lowest units of the Keewenawan sequence are mafic volcanics with a thickness estimated to be as great as 10 km (White, 1966).⁵⁶ These volcanics outcrop in and along the north shore of the lake and outline the northern limb of the Keewenawan syncline. The southern limb of the syncline is represented by the extensive volcanic exposures on the Keewenaw Peninsula. These volcanics have very clear expression on the magnetic map as shown by the horseshoe-shaped magnetic highs paralleling both shores of the lake; the gravity expression of the volcanics is a series of gravity highs which are not continuous but are never-

theless situated over the known and inferred trace of the volcanics. It seems rather certain that the "north shore low" heat flow belt is also a reflection of these volcanics, as it coincides rather closely with both the known outcrop exposures and with the magnetic and gravity highs.

Above the volcanics in the syncline lies a sequence of sedimentary rock, chiefly sandstone, of rather great thickness; White (1966)⁵⁶ estimates 5–6 km of thickness, while seismic work reported earlier (*Year Book* 64) is consistent with such a thickness. Presumably the axis of thickness sediment lies somewhere in the middle of the syncline, and is probably indicated on the magnetic map by the rather broad magnetic low which occurs along the central parts of the lake, lying between the magnetic highs produced by the volcanics. On the gravity map, with the exception of a gravity high running between Isle Royal and the Keewenaw Peninsula, the Keewenawan sediments appear to be characterized by gravity lows generally occurring along the central axis of the lake with the magnetic lows. In the central and eastern lake, the correlation of the "central high" heat flow belt with these magnetic and gravity expressions of the Keewenawan sediments is excellent. In the western lake the heat flow high correlates well with the magnetic low, but neither follows the gravity features particularly well. In cases such as this it is always possible to appeal to deeper features within or below the crust to explain correlation or lack of correlation of such parameters as gravity and heat flow.

It is more useful in the beginning, however, to try to explain the geophysical features on the simplest possible basis; namely, in terms of the near-surface (5–10 km) geologic sequence. For the volcanics this works admirably well—they are highly magnetic, dense, and relatively low in radioactivity. Thus a correlation of high magnetic and gravity anomalies with low heat flow is rea-

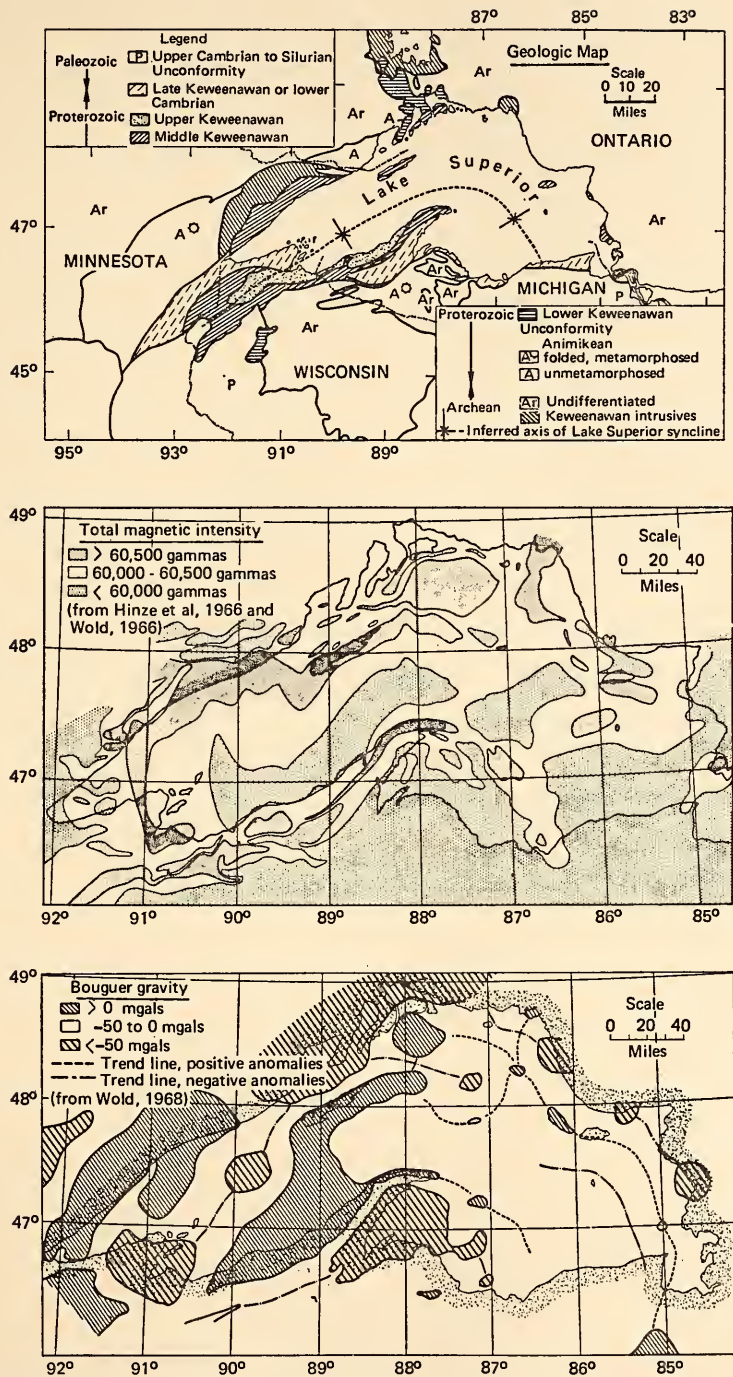


Fig. 56. Maps of the Lake Superior region showing the relationships between geologic features and measured magnetic and gravity anomalies.

sonable over areas underlain by the volcanics. Sediments are not so well characterized; they are usually low in density but may be either high or low in radioactivity and magnetic intensity. We can construct a model for sediments in the Lake Superior syncline which would produce the observed geophysical anomalies. This would involve relatively thick (10-km) sections of nonmagnetic, moderately dense (2.66 gm/cm^3) and quite radioactive sediments in the central and eastern lake to produce the heat flow highs and the gravity and magnetic lows. The western lake, particularly the area southwest of Isle Royal, would require non-radioactive and very light (2.3 gm/cm^3) nonmagnetic sediments in lesser thicknesses (5 km). Geologically, we would relate this western lake sedimentary sequence to the Bayfield Group, which makes up the surface of the Apostle Islands. These are light, relatively quartz-rich sandstones presumably deficient in radioactivity. The sediments east of $89^\circ 30'$, perhaps in fault contact with

the Bayfield Group, are probably Oronto Group. These are rather dense, impure sandstones and conglomerates possibly high in radioactivity (as judged from their known content of potassic minerals and uranium-thorium bearing heavy minerals).

This "near-surface" model involving basic volcanics and two types of sediment can qualitatively explain the main features of the gravity, magnetic, and heat flow maps in terms consistent with the known or inferred geology under the lake. Quantitatively, the only difficulty is in obtaining enough heat flow from the Oronto Group sediments. This would require that they have essentially the radioactivity of a granite, which is about twice the radioactivity of average sandstones and shales.

In comparing gravity and heat flow data, we have found a distinct relationship between density and heat production (radioactivity) of common rock types. Figure 57 presents this relationship, based on a compilation of data from the

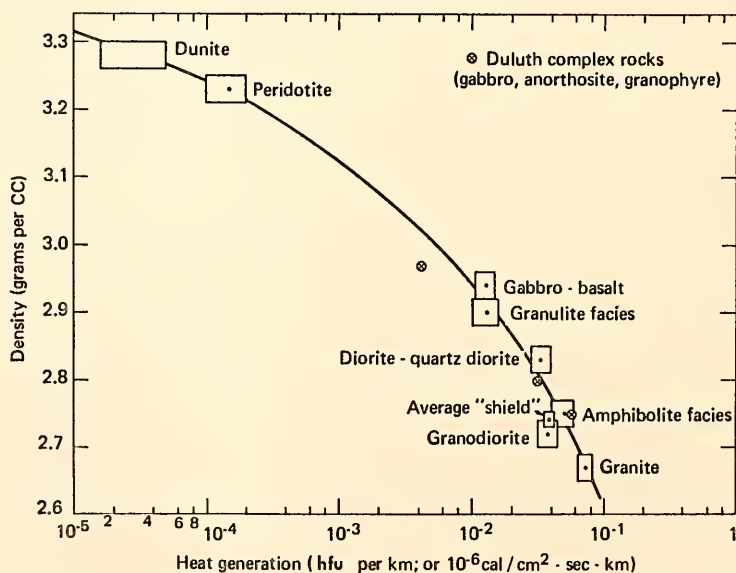


Fig. 57. Empirical relationship between the density of common rock types and their radioactivity or heat generation. Each point is based on a large number of analyses reported in the literature, and the size of the symbol represents the estimated uncertainty in the final average value.

literature. The heat production (sum of radioactivities of K^{40} , U^{235} , U^{238} and Th^{232}) is given in units of hfu per kilometer, so for any thickness of given rock type, the surface steady-state heat flow can be quickly computed. Since the trend line fits both igneous and metamorphic rocks, as well as the estimate for average Precambrian shield rocks, one might predict a close relationship between gravity and heat flow in areas composed mainly of crystalline rocks. Values for sedimentary rocks do not fit the trend, but scatter considerably in the region below the line. This is perhaps not surprising, as the density of sediments depends mainly on degree of lithification and depth of burial, whereas the heat generation is strongly influenced by very minor contents of highly radioactive minerals such as zircon, sphene, apatite, and magnetite.

The slope of the trend in the region between granite and gabbro-basalt is approximately linear and corresponds, in terms of equivalent anomalies, to -18 mgal (gravity) per 0.1 hfu. We have as yet been unable to test this relationship, mainly due to the lack of reasonable heat flow coverage in a suitable area. Our own Lake Superior data are unsuitable because of the known presence of thick sedimentary sequences. It is interesting to note, however, that the general "dynamic range" of gravity and heat flow values from older areas of crystalline rock is approximately in the ratio given by the relationship of Fig. 57; total range in gravity being ~ 200 mgal and in heat flow ~ 1.3 hfu (15 mgal per 0.1 hfu).

In dealing with the heat flow of Lake Superior in near-surface terms we are clearly ignoring complexities known to exist at deeper levels (*Year Books* 64, 66), such as the large variations in crustal thickness under different parts of the lake. Along the axis of the lake, the crust thickens from a minimum of 35 km off the Apostle Islands to over

50 km for most of the region east of 89° . If the mean radioactivity of the crust is constant along this trend, then the surface heat flow must necessarily change in proportion to the crustal thickness. Since undoubtedly some of the observed surface heat flow is generated below the crust, a change in crustal thickness of 40% will change the surface heat flow by no more than 40% . As the total variation in heat flow which we observe is almost a factor of three, we feel that changes in crustal thickness alone are not sufficient to explain the observed heat flow patterns. It seems most reasonable, in light of the general agreement of the heat flow patterns with the geologic, magnetic, and gravity features, to ascribe most of the heat flow variations to variations in the radioactivity of the upper (10 -km) crustal rocks.

GEOMAGNETISM

Cosmic-Ray Program

S. E. Forbush

Diurnal anisotropy from ionization chambers and from the IGY neutron monitor at Huancaayo. Last year's annual report described the newly found, well-determined wave, w , with a period of two solar cycles, in the cosmic-ray diurnal anisotropy from Carnegie Institution ionization chambers. It also described the correlation discovered between the cosmic-ray diurnal anisotropy, with w removed, and the U_0 measure of magnetic activity. It was shown how this correlation determined the total annual mean diurnal anisotropy from deviations of yearly means of the diurnal anisotropy from the average over a period of about 25 years. In these yearly deviations the relatively large atmospheric temperature effect was shown to be effectively eliminated.

It is most desirable to compare the diurnal anisotropy thus determined from ionization chamber data with that from neutron monitor data which are essen-

tially free of the atmospheric temperature effect, even though the longest sequence of neutron data available would have been inadequate to reveal the findings mentioned above. Fortunately, pressure-corrected diurnal variation data were kindly made available by John A. Simpson from his IGY-type neutron monitor at Huancayo for the period 1953–1966. For this period, deviations of annual means of the diurnal variation from the average for the 13 usable years were derived for the ion chamber at Huancayo. These deviation vectors, in a 24-hour harmonic dial, including the wave, w , were found to have their maxima, on the average, 1.6 hours earlier for the neutron data than for the ion chamber data at Huancayo. Thus, for the period 1953–1966, 1.6 hours were added to the observed time of maximum of the average neutron diurnal variation vector in the 24-hour harmonic dial. For the same period the “total” vector average was determined, as described earlier, from the ion chamber data. The time of maximum for these two vectors (both include w) agreed within a few minutes of time. Yearly values of the component, of the total diurnal anisotropy, with maximum at 18.0 hours local asymptotic time, were derived for the ion chamber and for the neutron monitor (after adding 1.6 hours to the times of maxima). Using the linear correlation ($r = +0.94$) between these values the variations in those from the ion chamber were shown to be 0.81 times those from the neutron monitor. This linear relation determined the value 0.019% for the component of the total diurnal anisotropy from the ionization chamber at Huancayo, corresponding to zero for that from the neutron monitor. For the 12 years used, the average of this component thus obtained was 0.126% from ion chamber data and 0.145% from neutron data, after multiplying the latter by the factor 0.81 derived as described above. Thus, at Huancayo the phase and amplitude of

the diurnal anisotropy derived from ion chamber data is in excellent agreement with that from the neutron monitor.

Barometric pressure corrections to the cosmic-ray ionization at Huancayo and the apparent change after about 1955 in sensitivity used to reduce ion chamber data. A detailed investigation was made to obtain an improved estimate for the barometric pressure coefficient for the cosmic-ray ionization at Huancayo. This involved a study of behavior of different barographs which had been used at Huancayo. The most reliable of these was that used by Simpson with his neutron monitor. The other barographs were shown to be affected by friction in the pen recording system. The investigation led to changing the barometric coefficient from -0.30% /mm Hg to -0.33% /mm Hg. The study provided reliable pressure corrections for the period after March 1958 when a microbarograph was installed by the Instituto Geofísico at Huancayo to replace the ordinary barograph. The microbarograph was found to be quite unreliable due to considerable friction which was also variable. In the course of the investigation an apparent change of 10% in the sensitivity used after about 1955 to reduce the ion chamber data was found and taken into account in the data used for the study described in the section above. Detailed results of the study are made available in copies of a memorandum on file at the Department.

Cosmic-ray ionization chamber for Christchurch, New Zealand. In retrospect it seems unfortunate that the cosmic-ray meter at Christchurch ceased operation after 1961, when the equipment was donated to the government of New Zealand, which is now using it for other purposes. To provide adequate data for a further investigation of the diurnal anisotropy and especially for a redetermination of w (see previous section) it is planned to install in Christchurch the Carnegie In-

titution ionization chamber that had been stored in Climax. This instrument was overhauled at the Department and the insulation and argon seals improved. A new control box was completed and AC-DC voltage supplies made to eliminate all batteries. This equipment has been operating at the Fredericksburg Magnetic Observatory since the latter part of April to obtain data for adequate comparison with the meter normally in use there. It will later be shipped to the Christchurch Magnetic Observatory which will cooperate in its operation. Voltage supplies to eliminate all batteries in the equipment have also been installed in the controls for the meters at Fredericksburg and at Huancayo.

Observations and reductions of data. Cosmic-ray ionization chambers were operated throughout the report year at Huancayo and at Fredericksburg, Virginia. Since the latter part of April 1968 a second meter has been operated at Fredericksburg (see section above). Scalings and reduction of records have been maintained current for both stations. The reductions have been greatly facilitated by the use of the IBM 1130 computer.

Cooperation in operation of cosmic-ray meters. Grateful appreciation is expressed to the U. S. Coast and Geodetic Survey and the staff of its magnetic observatory at Fredericksburg for efficient operation of the meters during the past report year, and to the Government of Peru and the Director and staff of the Instituto Geofísico del Peru for making cosmic-ray records from Huancayo available.

Studies of Conductivity Anomaly under the Andes

M. Casaverde, A. A. Giesecke, Jr., R. Salgueiro, S. del Pozo, L. Tamayo, M. A. Tuve, and L. T. Aldrich

Andean studies. The present report is an extension of previous ones as a result of a joint geomagnetic program of the

Department, the Instituto Geofísico del Peru, and the Instituto Geofísico Boliviano to study deep conductivity anomalies under the Andes, specifically the eastern side in southern Peru and Bolivia. For this purpose a permanent station was established at Arequipa (ARE) with new variometers built at the Department, and the installation of temporary field stations with Askania portable magnetographs during the last quarter of 1967 in Peru: at Unini (UNI), Quincemil (QML) and Iberia (IBE), and in Bolivia at Tarija (TAR) and Riberalta (RIB). The location of these stations can be seen on the map, Fig. 58. The measurements obtained at these stations complement the previous surveys made since late 1962 and also those obtained during the IGY. The installation of two additional temporary stations with DTM instruments at Huanuco (HUC) and Abancay (ABA), as references for future programs, was initiated.

Reductions of D , H , and Z for the present analysis have been made only for a single night-time event at each station, referred to Arequipa (ARE). More geomagnetic events have been recorded and are being studied. This analysis attempts to fill in the gap in previous reports for the eastern side of the Andes in Peru as well as in Bolivia in order to further delineate the nature of the conductivity anomaly. The geomagnetic bays listed in Table 17 have been used. The events as recorded at Arequipa all had the same general characteristics with periods of 1–2 hours.

The perturbation vectors have been computed using the anomalous X and Y components in the equation

$$\Delta B = \Delta X \cdot i + \Delta Y \cdot j \quad (21)$$

where i and j are unit vectors along true north and true east, respectively. These vectors give direction and relative strength of the anomalous horizontal variations. The numbers, each with a sign below the station, confirm the position of the anomaly ($\Delta Z = 0$) in Peru,



Fig. 58. Map showing locations of observed magnetic variations.

as shown in Fig. 58. In Bolivia the center of the anomaly seems to pass very close to La Paz and Tarija. It is observed that the heavy dashed line, which represents the shallowest part of the anomaly,

is located in northern Peru under the western Cordillera, and that it bends toward the east in central Peru and then to the southeast, coinciding with the eastern Cordillera in southern Peru, to

TABLE 17. Magnetic Events Used to Determine Perturbation Vectors at Newly Occupied Stations

Station	Date	Time, UT	
		h	m
Quincemil (QML)	Sept. 29, 1967	03	10
Iberia (IBE)	Sept. 29, 1967	03	10
Unini (UNI)	Dec. 31, 1967	23	10
La Paz (LAP)	Dec. 23, 1967	01	10
Riberalta (RIB)	Nov. 1, 1966	03	42
Tarija (TAR)	Dec. 23, 1967	01	10

continue into Bolivia, crossing the western side of the Altiplano.

Fig. 59 presents an observed cross section through the anomaly along the line PP' in Fig. 58 following the same model used previously. The h_p points represent the anomalous component of a horizontal transient surface field deduced from the magnetic bays mentioned above; the Z_p points, the anomalous vertical component also deduced from the same bays. The curves were calculated as indicated in *Year Book 65* for a model of the conductivity anomaly

having a semicylindrical shape (model B, Fig. 7, p. 25). The last observations made at QML, IBE, UNI, LAP, RIB and TAR fit the Z_p component of the model better than the h_p . This indicates the need for both a more careful study of additional events with a new survey using a closer spacing of stations along the profile PP' and a theoretical study of more models to help define the characteristics of this unusual geophysical phenomenon.

The cooperation of Dr. Anibal Rodriguez, Director of the Institute of Geophysics, Universidad Nacional de San Agustín, is noted with pleasure. The skills of W. F. Steiner in producing the DTM version of the Göttingen vario-graph were important to the success of this effort.

Related studies. The discovery of high electrical conductivity relatively near the surface (perhaps 60 km deep) along the eastern edge of the Andes Mountains several years ago (*Year Book 62*, p. 263, and *Year Book 63*, pp. 354-362) has

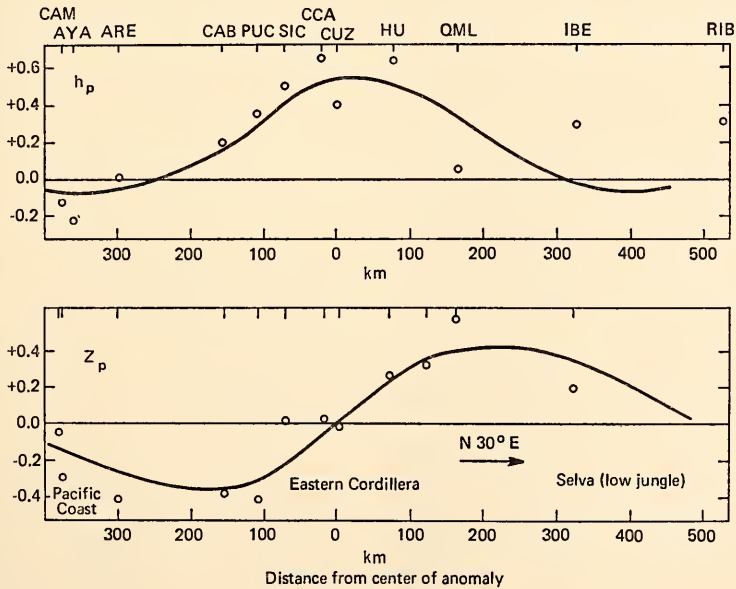


Fig. 59. Cross section A-A from Fig. 58 showing the anomalous horizontal component and vertical component of the magnetic field measured at the surface from the magnetic base observed.

reminded us that vast areas, even of the earth's land surface, have not been examined for possible buried regions of high conductivity much nearer to the surface than the "usual" depth of 300 to 400 kilometers, where high temperature and corresponding electrical conduction in the rock provides a conducting region in which eddy currents are induced by magnetic changes in the upper atmosphere overhead. Rapid changes in the "electrojet" in the high atmosphere above the Andes in the equatorial region gave us a relatively simple electrical current system for the magnetic detection of induced currents in any relatively shallow buried region of high conductivity, but qualitatively similar magnetic patterns are to be expected in other regions, such as the continental USA, if rather sharply defined structures of high electrical conductivity exist at shallow depths such as 30–60 kilometers. This is true because the electrical current sheets in the ionosphere are at heights of 90 kilometers and more and are spread out over relatively wide regions. If the magnetic "pattern" changes in 50 kilometers or so on the ground (as was found in Peru), the inducing edge of a current sheet must be at a distance of the same order or less.

Whether such effects occur or not cannot be known until a given region is examined by magnetometers which record the changes in the D , H , and Z magnetic components simultaneously for magnetic disturbances of suitable time-periods, usually 10 minutes to an hour or so. A large array of 6 or 8 magnetometers spread in two dimensions over several hundred kilometers makes efficient use of magnetic disturbances if they are rare, but in periods of high solar activity, as at present, even 2 or 3 magnetometers, with one at a fixed base station, can serve to survey a limited region. With this in mind, some initial observations have been made in Washington, D.C., and near Charlottesville, Virginia, and they have been compared to the Fredericksburg

magnetic station of the U. S. Coast and Geodetic Survey. Washington and Fredericksburg agree very well, but the ratio of $\Delta Z/\Delta H$ for disturbances in the period range of 10 to 25 minutes is much smaller (about 0.35) at Fan Mountain Observatory, 15 miles south of Charlottesville, where the Astronomy Department of the University of Virginia graciously provided a place for our magnetometer.

To date this unexpected observation must only be regarded as an interesting indication, but the effect is qualitatively what one expects if excess conductivity occurs below the edge of the Appalachians. Observations at added sites will be undertaken as manpower permits. We are grateful to Dr. A. L. Hales and Dr. John Reitzel, Southwest Center for Advanced Studies, Dallas, Texas, for supplying us with one of their magnetometers specially designed for field studies of this type, and to the Geophysical Institute, Göttingen, Germany, for a prototype of the Bartels-Schmucker magnetometer, as used in Germany in the middle 1950's for similar studies.

The Equatorial Electrojet and the Solar Eclipse of November 12, 1966

M. Casaverde, A. A. Giesecke, Jr., R. Salgueiro, and S. del Pozo

The experimental program and the preliminary results presented are part of the cooperative program of the Instituto Geofísico del Peru, the Instituto Geofísico Boliviano, and this Department. Professor Y. Kato of Tohoku University, Japan, joined us to make additional geomagnetic measurements during the eclipse.

Most of the measurements of the geomagnetic effect of the total solar eclipse of November 12, 1966, were recorded with Askania portable variographs in Peru and Bolivia. In Peru, the instruments operated at Ancon (ANC), Huanacayo (HUA), Santa Ines (STI), Velille (VEL), Puno (PUN), Arequipa (ARE),

all of them under the electrojet region. In Bolivia, records were obtained at La Paz (LAP) under the electrojet with a La Cour instrument, and at Tarija (TAR) south of the electrojet with an Askania variograph. In Argentina measurements were made at La Quiaca (LAQ) and Pilar (PIL), both far south of the magnetic equator. Table 18 shows the list of these stations and contains additional information. Figure 60 is a map of South America with the location at the time of the eclipse of all the magnetic stations of this table. This map also shows the path of the total eclipse (100% magnitude) estimated at 100 km in height, isolines of eclipse magnitude, and times of maximum eclipse.

Several workers have attempted to obtain definitive observations of the effect of a solar eclipse on the geomagnetic field. One of the first to obtain good results was Y. Kato (1960)⁵⁷ who observed the solar eclipse of October 12, 1958, at Suvarrow Island in the Pacific. Chapman and Bartels (1951),⁵⁸ Matsu-shita (1966)⁵⁹ and others have given the theoretical explanation of this effect on the basis of the conductivity decrease in the E region of the ionosphere. The phenomenon is due to the fact that transient geomagnetic variations are caused by the variations in the conductivity and current circulation in the E layer. Y. Kato

and Y. Mori (1968)⁶⁰ have made the study of the changes of the electron density and the effective conductivity in the E region for the particular event of November 12, 1966, with ionospheric measurements made at Huancayo and the geomagnetic measurements under the electrojet, taking into consideration the anisotropy of the electrical conductivity of the ionosphere. Figure 61 shows the Cowling, or effective, conductivity variation computed as a first approximation for Huancayo and Jicamarca, under the electrojet during the eclipse. This conductivity variation is responsible for the geomagnetic variation at the two stations. If we compare the maximum horizontal component depression at Huancayo (Fig. 61, B) with the minimum effective conductivity, we find a time delay of about 5–10 minutes. The slow recovery of the conductivity variation coincides with the description given by Kato and Mori (1968).⁶⁰

Figure 62 shows the sequence of the horizontal component depressions associated with the eclipse from the dip equator in Peru and Bolivia through Argentina. A perturbation beginning just before 13:15 hours (UT) is observed at all stations. This may be due to the eclipse crossing the electrojet or some other event which would confuse the observations at higher latitudes. Eclipse effects

TABLE 18. Magnetic Stations Recording the Eclipse and Their Relationship to the Eclipse

		Geog. South Lat.	Coord. West Long.	Dip Deg.	Time of Max. Eclipse at 100-km Height, UT	Magnitude of Eclipse at 100-km Height, %
		° ' "	° ' "		h m	
Jicamarca	(JIC)	11 57	76 52	1.9	13 01	100
Ancon	(ANC)	11 47	77 09	2.1	13 01	100
Huancayo	(HUA)	12 42	75 19	2.1	13 02	100
Santa Ines	(STI)	13 13	75 06	—0.1	13 04	99
Velille	(VEL)	14 31	71 54	—1.7	13 09	100
Puno	(PUN)	15 50	70 02	—3.8	13 14	100
Arequipa	(ARE)	16 28	71 29	—4.6	13 13	99
La Paz	(LAP)	16 32	68 10	—4.3	13 15	96
Tarija	(TAR)	21 36	64 40	—13.2	13 30	100
La Quiaca	(LAQ)	22 07	65 35	—15.0	13 35	95
Pilar	(PI)	31 40	63 53	—29.0	13 52	85

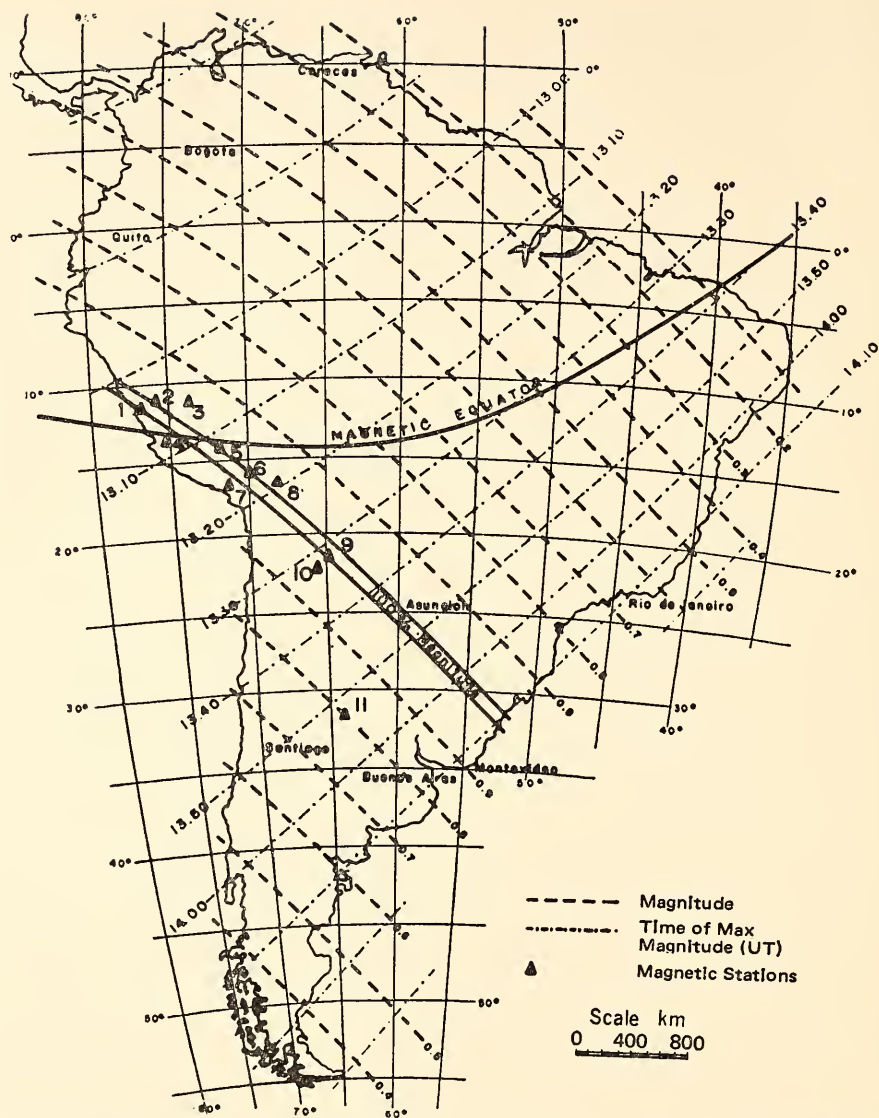


Fig. 60. Map of South America showing path, percent of the total, and time of passage of the eclipse of November 12, 1966. Also indicated are magnetic stations which recorded variations during the eclipse and the approximate position of the magnetic equator.

at temperate latitudes are usually small and difficult to identify unless the geomagnetic activity has a k -index equal to zero. Also, at the equatorial latitudes, on isolated stations, the same event can be very difficult to identify. The series of measurements at the locations of Fig. 60

shows clearly the effect of the November 12, 1966, total solar eclipse. The arrows in Fig. 62 indicate times of maximum magnitude of the eclipse, and show the time delay of the maximum effect as the eclipse moves approximately from north to south. In contrast, we can

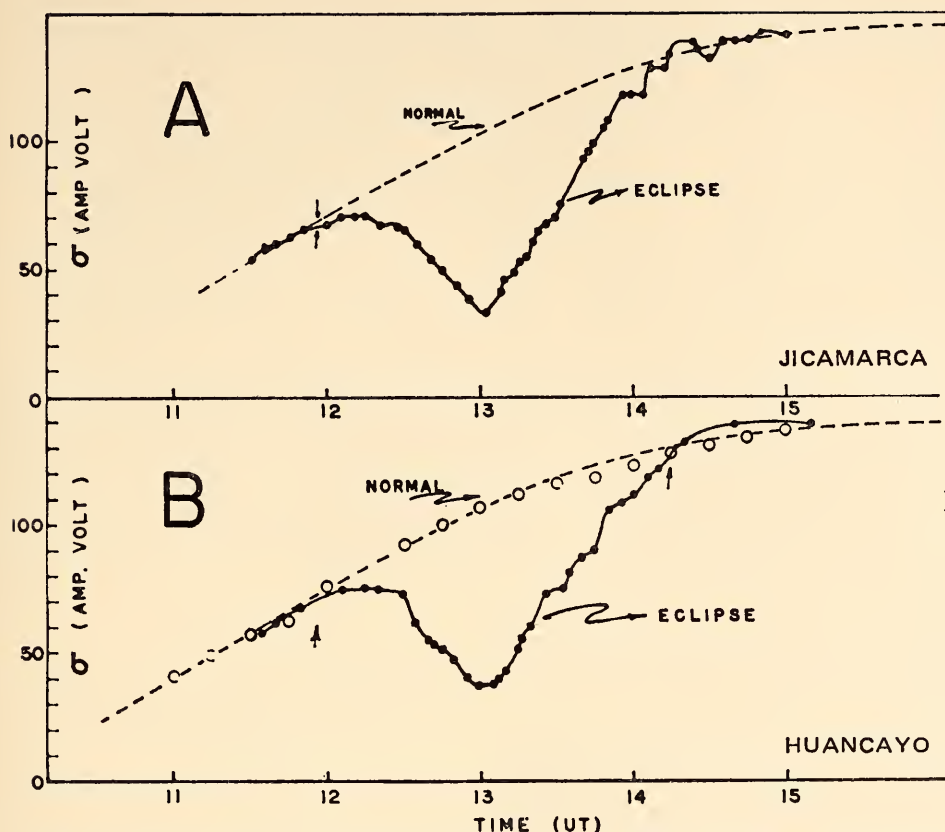


Fig. 61. The variation in the Cowling conductivity of the E region as measured at Jicamarca and Huancayo, November 12, 1966. The dashed curve is estimated at Jicamarca, and normal at Huancayo is the mean for this time of day as measured on November 9, 10, 11, 13, 14, 15, and 16. The conductivity values assume a 15-km thickness of the E region.

observe in the same figure a simultaneous event (sharp increase) around 14:15 hours at all the stations.

The horizontal component depressions of the geomagnetic field given in Fig. 62 show also the well-established distribution of H -amplitudes of low latitude day-time variations, greatly enhanced near the dip equator. The H -amplitude range is from 57 gammas at the dip equator (Santa Ines) to 19 gammas in the outskirts of the electrojet (La Paz). This is the so-called electrojet effect. This effect results from the fact that the ionospheric current systems at the E region heights of both hemispheres, converge within a

narrow latitude zone just above the dip equator.

Figure 63 shows the distribution with latitude of three measured amplitudes of the variation in H . R_1 is the maximum amplitude of this variation (which occurs usually at noon local time) on a normal day. R_2 is the amplitude on a normal day at the time that the eclipse passed the station, and R_3 is the amplitude measured on the day of the eclipse at the time of the eclipse. At the electrojet (Santa Ines) the normal maximum value R_2 is 120 gammas and that on the day of the eclipse, R_3 , is but 60 gammas, or 50% of normal. Following the model used by Schmucker *et al.* (1966),⁶¹ in

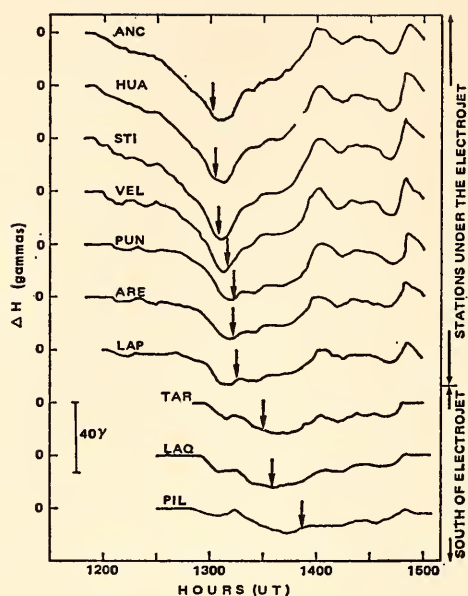


Fig. 62. Variation in the horizontal component of the earth's magnetic field, H , obtained by taking the difference between "normal value" of H and that measured November 12.

separating the external and internal fields of the normal solar daily variation known as S_q and the electrojet field, we have the following estimates: from the

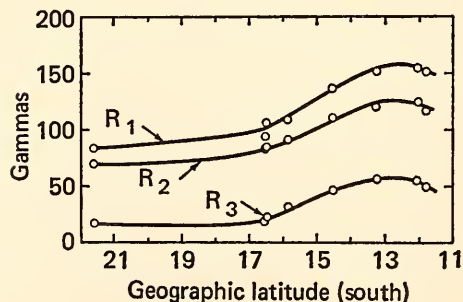


Fig. 63. Curves showing the maximum variation in the horizontal component, H , as a function of latitude. R_1 is pictured for a normal day at about noon local time. R_2 is the distribution for 1315 UT on the day of the eclipse found by taking the mean of the values at that time for three days before and three days after the eclipse. R_3 shows the distribution at the time the eclipse was a maximum at each station.

total 60 gammas of maximum depression at the center of the electrojet, deduced from Fig. 62, the normal S_q effect is about 23 gammas (external 16 gammas, internal 7 gammas) and the electrojet effect is about 37 gammas (external 30 gammas, internal 7 gammas). The total solar eclipse effect is the sum of the two external effects, or 46 gammas.

We wish to express our gratitude to the Directors of the magnetic observatories at La Quiaca and Pilar, and the Comision Nacional para el Eclipse of Argentina, for allowing us the use of their valuable magnetograms. We are also indebted to the Director and staff of the Instituto Geofísico de la Universidad de Arequipa for their continuous and valuable cooperation.

Isotope Studies

ZIRCON AGES OF HIDA AND RYOKE METAMORPHIC TERRAINS, JAPAN

K. Ishizaka

The ages of the metamorphism which produced the Hida and Ryoike metamorphic terrains have been the subject of recent investigation in Japan. In an attempt to get more information on these metamorphic terrains U-Th-Pb ages on zircons have been determined. The age data are presented in Table 19. The U content ranges 1400~678 ppm, 323~150 ppm for Th and 67~15 ppm for lead.

All zircons except Ryoike banded gneiss yield nearly concordant ages: the 180-m.y. age of Shimonomoto zircon is identical to the mica and some whole rock ages (Rb-Sr and K-Ar) which were obtained from many localities on Hida metamorphic terrain. However, the 240-m.y. age of Omi zircon is significantly greater than the 180-m.y. age of the Shimonomoto and less than the oldest K-Ar age on hornblende, i.e., 345

TABLE 19. Measured Ages of Zircons, m. y.

	$\frac{\text{Pb}^{206}}{\text{U}^{238}}$	$\frac{\text{Pb}^{207}}{\text{U}^{235}}$	$\frac{\text{Pb}^{206}}{\text{Th}^{232}}$	$\frac{\text{Pb}^{207}}{\text{Pb}^{206}}$
Hida, Omi Gneiss	237	229	241	
Hida, Shimonomoto Granodiorite	177	189	178	
Ryoke, Kiryu Granodiorite	88	93	72	
Ryoke, Kimigano Granite	94	97	82	
Ryoke, Kimigano Gneiss	535	841	569	1782

m.y. Yamaguchi (1967)⁶² also reported zircons having 240-m.y. age. No geological event has been found to have occurred 240 m.y. ago. Further study is required.

The zircon ages from Ryoke granite rocks are concordant with their cogenetic mica ages, i.e., 90~100 m.y., which indi-

cates that the metamorphism occurred 90~100 m.y. ago in this terrain. The zircon which comes from pelitic banded gneiss reveals discordant ages. This zircon is rounded and considered to be detritus. The original sedimentary rock which was metamorphosed is known to be Permo-Carboniferous in geologic age.

REFERENCES CITED

- Mayall, N. U., Symposium on the Structure of the Galaxy, *Publications of the Observatory of the University of Michigan*, vol. X, 19, 1951.
- Rubin, V. C., S. Moore, and F. C. Bertiau, *Astron. J.* 72, 59, 1967.
- Seyfert, C. K., *Astron. J.* 97, 28, 1943.
- Kraft, R. P., and M. H. Demoulin, *Astrophys. J. Letters* 150, 183, 1967.
- Ryle, M., and J. A. Bailey, *Nature* 217, 907, 1968.
- Drake, F. D., E. J. Gundermann, D. L. Jauncey, J. M. Comella, G. A. Zeissig, and H. D. Croft, Jr., *Science* 160, 503, 1968.
- Hindman, J. V. et al., *Australian J. Phys.*, 16, 552 ff., 1963.
- Cockcroft, J. D., and E. T. S. Walton, *Proc. Roy. Soc. A136*, 619, 1932; *A137*, 229, 1932.
- Heydenburg, N. P., C. M. Hudson, D. R. Inglis, and W. D. Whitehead, *Phys. Rev.* 73, 241 (1948); 74, 405, 1948.
- Rumbaugh, L. H., R. B. Roberts, and L. R. Hafstad, *Phys. Rev.* 54, 657, 1938.
- McCray, J. A., *Phys. Rev.* 130, 2034, 1963.
- Feshbach, H., C. E. Porter, and V. F. Weisskopf, *Phys. Rev.* 96, 448, 1954.
- Satchler, G. R., L. W. Owen, A. J. Elwyn, G. L. Morgan, and R. L. Walter, *Nuclear Phys.*, A112, 1-31, 1968.
- Brandt, W., and R. Laubert, in press, 1968.
- Porter, C. E., *Statistical Theories of Spectra: Fluctuations*, Academic Press, New York, 1965.
- Bolton, E. T., and B. J. McCarthy, *Proc. Natl. Acad. Sci. U. S.*, 48, 1390-1397, 1962.
- Cowie, D. B., and P. Szafranski, *Biophys. J.* 7, 567-584, 1967.
- Denhardt, D. T., *Biochem. Biophys. Res. Commun.* 23, 641-646, 1966.
- Bernardi, G., *Nature* 206, 779-783, 1965.
- Miyazawa, Y., and C. A. Thomas, *J. Mol. Biol.* 11, 223-237, 1965.
- Britten, R. J., and D. E. Kohne, *Science* 161, 529-540, 1968.
- Brenner, D. J., M. A. Martin, and B. H. Hoyer, *J. Bacteriol.* 94, 486-487, 1967.
- Cowie, D. B., and B. J. McCarthy, *Proc. Natl. Acad. Sci. U. S.* 50, 537-543, 1963.
- Schildkraut, C. L., K. L. Wierchowski, J. Marmur, D. M. Green, and P. Doty, *Virology* 18, 43-55, 1962.
- Cowie, D. B., and A. D. Hershey, *Proc. Natl. Acad. Sci. U. S.* 53, 57-62, 1965.

25. Fraser, D. K., *Virology* 3, 527-553, 1957.
26. Ingraham, L. J., R. Ehrling, and A. D. Hershey, *Carnegie Inst. Wash. Year Book* 65, 563, 1966.
27. Spiegelman, S., and S. A. Yankofsky, in *Evolving Genes and Proteins*, V. Bryson and H. J. Vogel, eds., Academic Press, New York, 1965.
28. Britten, R. J., and D. E. Kohne, *Carnegie Inst. Wash. Year Book* 65, 78, 1966.
29. Moore, R. L., and B. J. McCarthy, *J. Bacteriol.* 94, 1066, 1967.
30. Kotaka, T., and R. L. Baldwin, *J. Mol. Biol.* 9, 323, 1964.
31. Britten, R. J., *Carnegie Inst. Wash. Year Book* 64, 322, 1965.
32. Bautz, E., in *Evolving Genes and Proteins*, V. Bryson and H. J. Vogel, eds., Academic Press, New York, 1965.
33. Aronson, A. I., and M. A. Holowczyk, *Biochim. Biophys. Acta* 95, 217, 1965.
34. Doi, R. H., and R. T. Igarashi, *J. Bacteriol.* 92, 88, 1966.
35. Gould, H., Symposium on Sero and Chemotaxonomy at the Birmingham University, Birmingham, England, in press 1968.
36. Brenner, D. J., and D. B. Cowie, *J. Bacteriol.* 95, 2258-2262, 1968.
37. Brenner, D. J., personal communication, 1968.
38. Corneo, G., E. Ginelli, and E. Polli, *J. Biol.* 33, 331, 1968.
39. Bode, H. R., and H. J. Morowitz, *Biophys. Soc. Abstr.*, 109, 1965.
40. Wetmur, J. G., and N. Davidson, *J. Mol. Biol.* 31, 349, 1968.
41. Ross, P. D., and J. M. Sturtevant, *J. Am. Chem. Soc.* 84, 4503, 1962.
42. Britten, R. J., and D. Kohne, *Carnegie Inst. Wash. Year Book* 65, 78, 1966.
43. *Mechanisms of Memory*, p. 27, E. Roy John, ed., Academic Press, New York, 1967.
44. *Ibid.* p. 45.
45. *Ibid.* p. 25.
46. *Ibid.* p. 295.
47. Anderson, D. L., and R. L. Kovach, Attenuation in the mantle and rigidity of the core from multiple reflected core phases, *Proc. Natl. Acad. Sci. U. S. A.* 51, 168, 1964.
48. Bolt, B. A., Earthquake epicenters, focal depths, and origin times using a high-speed computer, *Geophys. J.* 3, 433-440, 1960.
49. Cisternas, A., Precision determination of focal depths and epicenters of earthquakes, CIT publication, AFOSR contract No. AF-49 (638) 1337, August, 1964.
50. Engdahl, E. R., and R. H. Gunst, Use of a high-speed computer for the preliminary determination of earthquake hypocenters, *Bull. Seis. Soc. Am.* 56, No. 2, 325-336, 1966.
51. Norquist, J. M., A special purpose program for earthquake location with an electronic computer, *Bull. Seis. Soc. Am.* 52, 431-437, 1962.
52. Woollard, G. P., Seismic crustal studies during the IGY. Part II: Continental program, IGY Bull. No. 34 in *Am. Geophys. Union Trans.* 41, No. 2, 351-355, 1960.
53. Zumberge, J. H., A new shipboard coring technique, *J. Geophys. Res.* 67 (6), 2529-2536, 1962.
54. Ratcliffe, E. H., *J. Geophys. Res.* 65, 1535-1541, 1960.
55. Roy, R. F., Heat flow measurements in the United States, Ph.D. Thesis, Harvard Univ., 1963.
56. White, W. S., Geologic evidence for crustal structure in the western Lake Superior basin, in *The Earth beneath the Continents*, Geophys. Mono. No. 10, p. 28, J. S. Steinhardt and T. J. Smith, eds., Wash., D. C., American Geophysical Union, 1966.
57. Kato, Yoshio, The effect on the geomagnetic field of the solar eclipse of October 12, 1958, The Science Reports of the Tohoku University Series 5, *Geophysics*, 12, No. 1, 1960.
58. Chapman, S., and J. Bartels, *Geomagnetism, Vol. II*. University Press, Oxford, 1951.
59. Matsushita, S., Effects of a solar eclipse on the equatorial geomagnetic field, *Ann. géophys.*, Juillet-Sept., 1966.
60. Kato, Yoshio, and Yohsuke Mori, The changes in the conductivity of the ionosphere on and near the dip equator during the solar eclipse of November 12, 1966. *Proceedings of Eclipse Symposium*, F. de Mendonça, ed., CNAE, Sao José dos Campos, Brasil, in press, 1968.
61. Schmucker, U., et al., Electrical conductivity anomaly under the Andes, *Carnegie Inst. Wash. Year Book* 65, 11, 1966.
62. Yamaguchi, M., *J. Geol. Soc. Japan* 73, No. 2, 71, 1967.

BIBLIOGRAPHY

- Baum, W. A., J. S. Hall, L. L. Marton, and M. A. Tuve, Report of the Committee on Image Tubes for Telescopes, *Carnegie Inst. Wash. Year Book* 66, 135-140, 1967.
- Brenner, D. J., and D. B. Cowie, Thermal stability of *Escherichia coli*-*Salmonella typhimurium* deoxyribonucleic acid duplexes, *J. Bacteriol.*, 95, 2258-2262, 1968.
- Brenner, D. J., D. B. Cowie, and S. Falkow, Thermal stability of interspecific enterobacterial DNA duplexes, (abstract), *Biophys. J.*, 8, Biophys. Soc., 12th Ann. Meeting, Pittsburgh, Pa., A-60, Feb. 19-21, 1968.
- Brenner, D. J., S. Falkow, and D. B. Cowie, Thermal stability of temperate phage DNA duplexes (abstract), *Phage Information Service*, 13, Bacteria Phage Meeting, Aug. 30-Sept. 3, 1967, Cold Spring Harbor, N. Y.
- Britten, R. J., and Margaret Chamberlin, The imprecisely redundant human DNA, (abstract), *Biophys. J.*, 8, Biophys. Soc., 12th Ann. Meeting, Pittsburgh, Pa. A-59, Feb. 19-21, 1968.
- Brown, L. Polarized ion source for an electrostatic accelerator (abstract), *Bull. Am. Phys. Soc.*, 12, 1170, 1967.
- Brown, L., and C. Petitjean, Polarization analyzing power of ${}^7\text{Li}(p, {}^4\text{He}){}^4\text{He}$ as function of angle and energy (abstract), *Bull. Am. Phys. Soc.*, 13, 565, 1968.
- Brown, L., see also Petitjean, C., and Trächslin, W.
- Chamberlin, Margaret, see Britten, R. J.
- Christy, J. W., see Rubin, Vera C.
- Clegg, T. B., see Trächslin, W.
- Cowie, D. B., and P. Szafranski, Thermal chromatography of DNA-DNA reactions, *Biophys. J.*, 7, 567-584, 1967.
- Cowie, D. B., see also Brenner, D. J.
- Falkow, S., see Brenner, D. J.
- Forbush, S. E., A variation, with a period of two solar cycles, in the cosmic-ray diurnal anisotropy, *J. Geophys. Res.*, 72, 4937-4939, 1967.
- Ford, W. J., Jr., see McCarthy, M. F., S. J., and Rubin, Vera C.
- Hall, J. S., see Baum, W. A.
- Hart, S. R., Radiogenic helium/argon ratios in oceanic ultramafic rocks (abstract), *Trans. Am. Geophys. Union*, 49, 358-359, 1968.
- Hart, S. R., see also Ohmoto, H., Steiger, R. H., and Steinhart, J. S.
- Holland, H. D., see Ohmoto, H.
- Hoyer, B. H., and R. B. Roberts, Studies of nucleic acid interactions using DNA-agar, in *Molecular Genetics, Pt. II*, 425-478, Taylor, J. H., ed., N. Y., Academic Press, 1967.
- James, D. E., and I. S. Sacks, Upper mantle structure beneath western South America: preliminary results (abstract), *Trans. Am. Geophys. Union*, 49, 291, 1968.
- James, D. E., T. J. Smith, and J. S. Steinhart, Crustal structure of the middle Atlantic States, *J. Geophys. Res.*, 73, 1983-2007, 1968.
- Ludwig, W. J., J. E. Nafe, E. S. W. Simpson, and S. Sacks, Seismic-refraction measurements on the southeast African continental margin, *J. Geophys. Res.*, 73, 3707-3719, 1968.
- McCarthy, M. F., S. J., P. J. Treanor, S. J., and W. K. Ford, Jr., Image tube spectra of late type stars, in *Colloquium on Late-Type Stars*, 100-108, Margherita Hack, ed., Trieste, Osservatorio Astronomico, 1966.
- Marton, L. L., see Baum, W. A.
- Nafe, J. E., see Ludwig, W. J.
- O'Brien, P. N. S., Lake Superior crustal structure—a reinterpretation of the 1963 seismic experiment, *J. Geophys. Res.*, 73, 2669-2689, 1968.
- Ohmoto, H., S. R. Hart, and H. D. Holland, Studies in the Providencia area, Mexico, II, K-Ar and Rb-Sr ages of intrusive rocks and hydrothermal minerals, *Econ. Geol.*, 61, 1205-1213, 1966.
- Petitjean, C., and L. Brown, ${}^7\text{Li}(p, \alpha){}^4\text{He}$ reaction with polarized protons from 0.8 to 3 MeV, *Nuclear Phys.*, A111, 177-183, 1968.
- Petitjean, C., and L. Brown, Polarization in the ${}^7\text{Li}(p, \alpha){}^4\text{He}$ reaction from 1 to 3 MeV (abstract), *Bull. Am. Phys. Soc.*, 12, 1176, 1967.
- Petitjean, C., see also Brown, L.
- Roberts, R. B., Critical points in evolution, *School Science and Mathematics*, 68, 369-376, 1968.
- Roberts, R. B., Memory and learning from the standpoint of computer model building, *Am. Scientist*, 56, 58-69, 1968.
- Roberts, R. B., Memory and learning from the standpoint of computer model building, *Proc. Am. Phil. Soc.*, 111, 352-358, 1967.
- Roberts, R. B., see also Hoyer, B. H.
- Rubin, Vera C., Optical observations of radio galaxies and quasi-stellar objects, *High Energy Astrophysics*, 1, 133-151, DeWitt, C., E. Schatzman, and P. Verón, eds., N. Y., Gordon and Breach, 1967.

- Rubin, Vera C., and W. K. Ford, Jr., The spectrum of the 1967 supernova in NGC 3339 and H-alpha velocities in the galaxy, *Publ. Astron. Soc. Pacific*, 79, 322-329, 1967.
- Rubin, Vera C., W. K. Ford, Jr., and J. W. Christy, Radial velocities from image tube spectra, in *Intern. Astron. Union Symp. No. 30*, 5-8, 1967.
- Sacks, I. S., Direct and indirect high Q paths for shear waves from deep earthquakes (abstract), *Trans. Am. Geophys. Union*, 49, 292, 1968.
- Sacks, I. S., The 400-km discontinuity in South America (abstract), *Trans. Am. Geophys. Union*, 49, 291-292, 1968.
- Sacks, I. S., see also Ludwig, W. J.
- Seyler, R. G., see Trächslin, W.
- Simpson, E. S. W., see Ludwig, W. J.
- Smith, T. J., Head waves, in *International Dictionary of Geophysics*, 1, 702-705, S. K. Runcorn, ed., N. Y., Pergamon Press, 1967.
- Smith, T. J., see also James, D. E., and Steinhart, J. S.
- Steiger, R. H., and S. R. Hart, The microcline-orthoclase transition within a contact aureole, *Am. Mineral.*, 52, 87-116, 1967.
- Steinhart, J. S., Explosion studies on the continents, *Trans. Am. Geophys. Union*, 48, 412-415, 1967.
- Steinhart, J. S., Mohorovičić discontinuity, in *International Dictionary of Geophysics*, 2, 991-994, S. K. Runcorn, ed., N. Y., Pergamon Press, 1967.
- Steinhart, J. S., S. R. Hart, and T. J. Smith, A regional heat flow survey in Lake Superior (abstract), in *Abstracts of Papers, Vol. 11a, International Heat Flow Committee*, p. B-15, Zurich, Switzerland, Intern. Union Geod. Geophysics, 14th General Assembly, Sept. 25-Oct. 7, 1967.
- Steinhart, J. S., S. R. Hart, and T. J. Smith, Heat flow in Lake Superior (abstract), in *Institute on Lake Superior Geology*, 37, East Lansing, Michigan, Michigan State University, 13th Annual Meeting, May 1-2, 1967.
- Steinhart, J. S., S. R. Hart, and T. J. Smith, The technique of heat flow measurement in lakes (abstract), in *Abstracts of Papers, Vol. 11a, International Heat Flow Committee*, C-9, Zurich, Switzerland, Intern. Union Geod. Geophysics, 14th General Assembly, Sept. 25-Oct. 7, 1967.
- Steinhart, J. S., see also James, D. E.
- Szafranski, P., see Cowie, D. B.
- Trächslin, W., and L. Brown, Polarization and phase shifts in $^{12}\text{C}(\text{p}, \text{p})^{12}\text{C}$ and $^{16}\text{O}(\text{p}, \text{p})^{16}\text{O}$ from 1.5 MeV, *Nuclear Phys.*, A101, 273-287, 1967.
- Trächslin, W., L. Brown, T. B. Clegg, and R. G. Seyler, Polarization and phase shifts in $\text{D}(\text{p}, \text{p})\text{D}$ at 3.00 MeV (abstract), *Bull. Am. Phys. Soc.*, 12, 1172, 1967.
- Trächslin, W., L. Brown, T. B. Clegg, and R. G. Seyler, Polarization and phase shifts in $\text{D}(\text{p}, \text{p})\text{D}$ at 3.00 MeV, *Phys. Letters*, 25B, 585-587, 1967.
- Treanor, P. J., S. J., see McCarthy, M. F., S. J.
- Turner, K. C., Neutral hydrogen features between Magellanic Clouds (abstract), *Astron. J.*, 73, S37-S38, 1968.
- Tuve, M. A., Citation for Dr. Lloyd Viel Berkner, Twenty-ninth award of the William Bowie Medal, April 19, 1967, *Trans. Am. Geophys. Union*, 48, 313-314, 1967.
- Tuve, M. A., John Adam Fleming, Biographical memoirs, *Natl. Acad. Sci. U. S.*, 38, 103-140, N. Y., Columbia Univ. Press, 1967.
- Tuve, M. A., Preface to crustal structure in coastal Alaska, in *The Earth beneath the Continents*, Geophysical Monograph 10, 420-422, J. S. Steinhart, and T. J. Smith, eds., Wash, D. C., American Geophysical Union, 1966.
- Tuve, M. A., Symposium on the years of the quiet sun-IGSY, Introductory remarks, *Proc. Natl. Acad. Sci. U. S.*, 58, 2131-2135, 1967.
- Tuve, M. A., See also Baum, W. A.
- Tuve, M. A., Lloyd Viel Berkner, Biographical memoirs, in *Year Book of the American Philosophical Society*, 109-116, 1967.

PERSONNEL

Director

ELLIS T. BOLTON

Associate Director

L. THOMAS ALDRICH

Staff Members

Roy J. Britten
 Dean B. Cowie
 Scott E. Forbush
 W. Kent Ford, Jr.
 Stanley R. Hart ¹

Richard B. Roberts
 I. Selwyn Sacks
 T. Jefferson Smith ²
 John S. Steinhart

Staff Associates

Louis Brown
 David E. Kohne

Vera C. Rubin
 Kenneth C. Turner

Distinguished Service Member of Carnegie Institution

M. A. Tuve

Section Chairmen

Astrophysics: W. Kent Ford, Jr.

Biophysics: Dean B. Cowie

Geophysics: L. Thomas Aldrich

Fellows

George E. Assousa, Florida State University,
 Tallahassee, Florida ³

Don J. Brenner, Fellow of U. S. Public
 Health Service, Bethesda, Maryland ⁴

Christopher Brooks, Australian National
 University, Canberra, Australia ⁵

J. Alfred Chiscon, Purdue University, La-
 fayette, Indiana ⁶

Kyoichi Ishizaka, Kyoto University, Kyoto,
 Japan ⁷

David E. James, Stanford University, Stan-
 ford, California

Peter N. S. O'Brien, British Petroleum Com-
 pany, Ltd., Sunbury-on-Thames, Middle-
 sex, England ⁸

Claude Petitjean, University of Basel, Basel,
 Switzerland

Adrian V. Rake, University of British Co-
 lumbia, Vancouver, B. C.

German Saa, S. J., Carnegie Seismic Analysis
 Center, Lima, Peru

Alan M. Stueber, Washington University, St.
 Louis, Missouri ⁹

Walter Trächslin, University of Basel, Basel,
 Switzerland ¹⁰

¹ On leave of absence to August 31, 1967.

² On leave of absence October 1, 1967–March
 31, 1968. Resigned June 30, 1968.

³ From June 1, 1968.

⁴ Through September 30, 1967.

⁵ From November 1, 1967.

⁶ From February 1, 1968.

⁷ From September 1, 1967.

⁸ Through August 31, 1967.

⁹ Through August 31, 1967.

¹⁰ Through July 31, 1967.

Research Associates

- Mateo Casaverde, Instituto Geofísico del
Peru, Lima, Peru
- Reynaldo Salgueiro, Instituto Geofísico Boli-
viano, La Paz, Bolivia
- Shigeji Suyehiro, Meteorological Research
Institute, Tokyo, Japan

Collaborators and Visiting Investigators

- Javier Aparicio, Observatorio San Calixto,
La Paz, Bolivia
- Pablo Aparicio, Carnegie Seismic Analysis
Center, Lima, Peru
- Arnold Bendich, University of Washington,
Seattle, Washington
- Werner Brandt, New York University, New
York, N. Y.
- Ramon Cabre, S. J., Observatorio San Ca-
lixto, La Paz, Bolivia
- Dorothy Canter, George Washington Uni-
versity, Washington, D. C.
- Armando Cisternas, Universidad de Chile,
Santiago, Chile
- Thomas B. Clegg, University of Wisconsin,
Madison, Wisconsin
- Salvador del Pozo, Instituto Geofísico Boli-
viano, La Paz, Bolivia
- Ernesto Deza, Instituto Geofísico del Peru,
Lima, Peru
- Dale Evertson, Defense Research Labora-
tories, University of Texas, Austin, Texas
- Stanley Falkow, Georgetown University,
Washington, D. C.
- Luis Fernandez, S. J., Observatorio San Ca-
lixto, La Paz, Bolivia
- Louis B. Flexner, University of Pennsyl-
vania, Philadelphia, Pennsylvania
- Josefa B. Flexner, University of Pennsyl-
vania, Philadelphia, Pennsylvania
- Jose Frez, Universidad de Chile—Zona
Norte, Antofagasta, Chile
- Enrique Gajardo, Universidad de Chile,
Santiago, Chile
- Albert Gelderman, National Institutes of
Health, Bethesda, Maryland
- Alberto A. Giesecke, Jr., Instituto Geofísico
del Peru, Lima, Peru
- Daniel Haapala, Georgetown University,
Washington, D. C.
- Bill Hoyer, National Institutes of Health,
Bethesda, Maryland
- Edgar Kausel, Universidad de Chile, San-
tiago, Chile
- Roman Laubert, New York University, New
York, N. Y.
- Eduardo Lazo, Universidad Nacional de San
Agustín, Arequipa, Peru
- Melezio Lazo, Universidad Nacional de San
Agustín, Arequipa, Peru
- William Losonsky, New York University,
New York, N. Y.
- Martin F. McCarthy, S. J., Observatorio
Astronomico Specola Vaticana, Italy
- Jorge Mendiguren, Universidad Nacional de
Cuyo, San Juan, Argentina
- Ricardo Olea, Universidad de Chile, Santiago,
Chile
- Jose Orruma, Universidad Nacional de Cor-
doba, Cordoba, Argentina
- Alois Th. Purgathofer, Universität Stern-
warte, Vienna, Austria
- Anibal Rodriguez, Universidad Nacional de
San Agustín, Arequipa, Peru
- Jaime Santa Cruz, Observatorio San Calixto,
La Paz, Bolivia
- Richard G. Seyler, Ohio State University,
Columbus, Ohio
- Diglio V. Simoni, Universidad Nacional de
San Agustín, Arequipa, Peru
- Lupe Tamayo, Universidad Nacional de San
Agustín, Arequipa, Peru
- Carlos Varsavsky, Instituto Argentino de
Radioastronomía, Villa Elisa, Argentina
- Fernando Volponi, Universidad Nacional de
Cuyo, San Juan, Argentina

Design Engineer

Everett T. Ecklund

*Electronic Research Specialists*Kenneth D. Burrhus
John B. Doak
Paul A. JohnsonCharles A. Little
Glenn R. Poe*Laboratory Assistants*Liselotte Beach
H. Lowell Belin ¹¹
Stephen J. Buynitzky ¹²Margaret E. Chamberlin
Neltje W. van de Velde*Office*Chief, Fiscal Section: Helen E. Russell
Office Manager: William N. Dove
Assistant Fiscal Officer: Niels M. Pedersen ¹³
Librarian: Lelah J. Prothro (part time)
Secretary: Claudine C. AtorStenographers: Dorothy B. Dillin, E. Kathleen Hill
Typist: Mary T. Sheahan ¹⁴
Accounting Assistant: Glenda J. Johnston ¹⁵*Shop*Shop Manager: John G. Lorz ¹⁶
Instrumentation Research Specialist:
Michael SeemannInstrument Makers: Robert Hoffmaster,
Carl M. Rinehart
Machinist: Francis J. Caherty*Buildings and Grounds*Carpenter and Maintenance Foreman: Leo J. Haber
Assistant Maintenance Foreman: Elliott M. QuadeCaretaker: Stanley Gawrys
Assistant Caretakers: Bennie Harris, Willis Kilgore, Jr.*Part Time and Temporary Employees*George F. Brigham, Jr.
Robert Cadmus
Allen Forsbacka
Stephen Nezezou
Milan PavichJerome Roddy
John Roddy
Martin Roddy
Doris Titus
Anne Unger¹¹ Through June 15, 1968.¹² Retired June 30, 1968.¹³ From December 1, 1967.¹⁴ Full time from June 1, 1968.¹⁵ Through October 15, 1967.¹⁶ Retired June 30, 1968.

PLATES

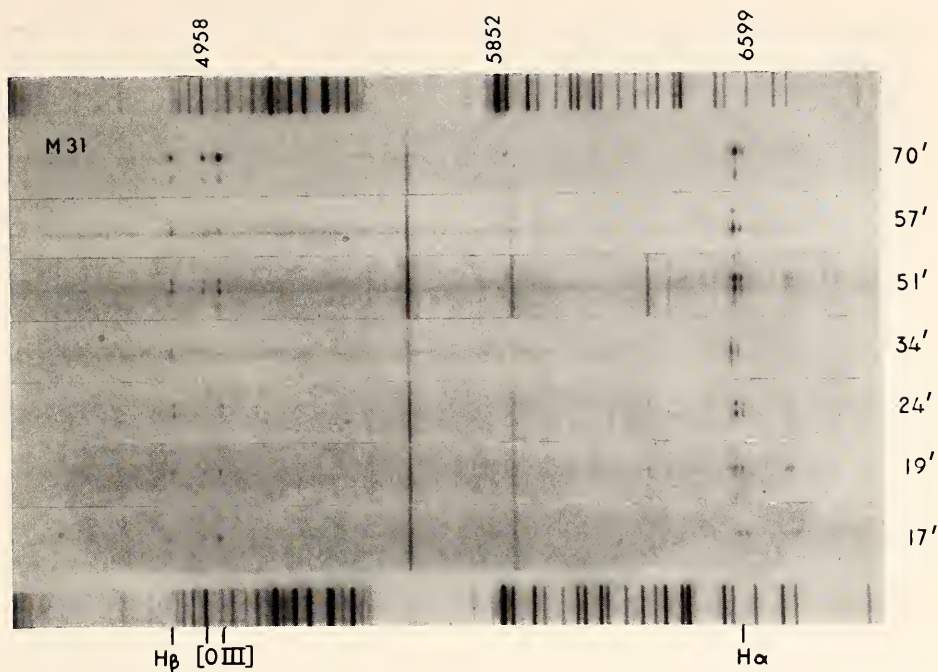


Plate 1. Spectra of seven emission regions in M 31. The distance from the nucleus for each region, in minutes of arc, is indicated on the right. The velocity variations within the galaxy can be seen by the displacement of the lines from region to region. This variation is not smooth because the regions are chosen from both the northeast and the southwest parts of the galaxy.

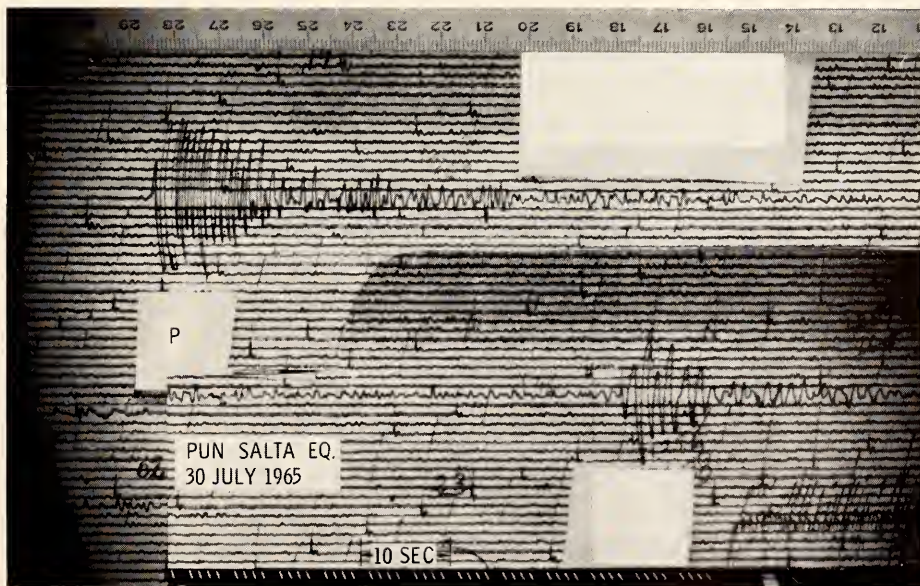


Plate 2. Puno seismogram of deep earthquake in Salta region, north Argentina. The *P* phase shows higher frequencies but the shear phase has no frequencies above 1 cps, or any delayed high frequencies. Type 1 arrival.

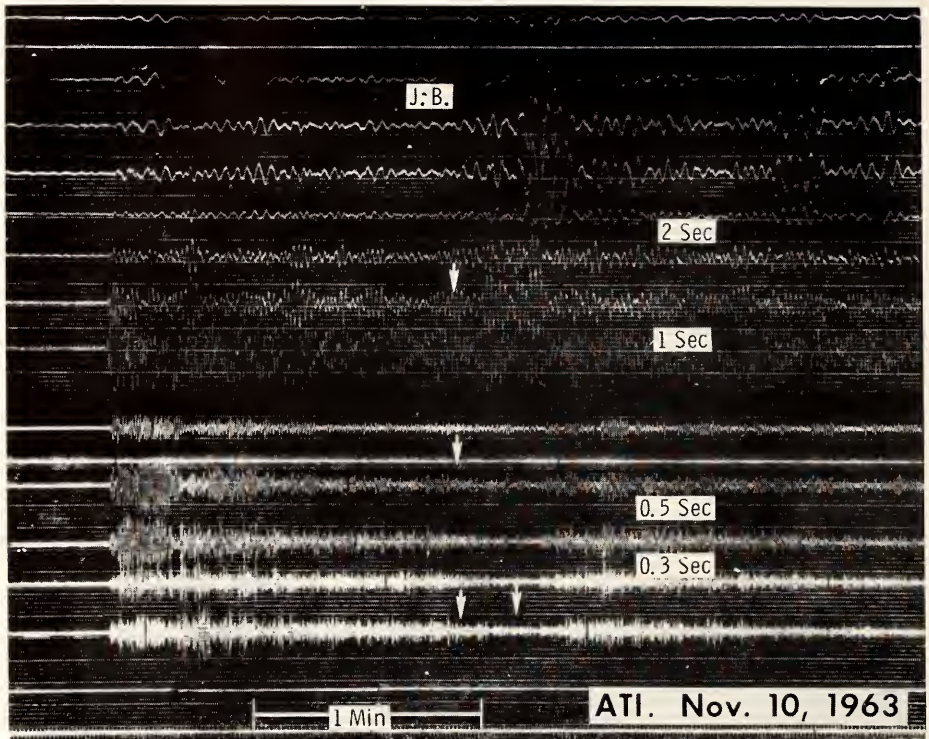


Plate 3. Filtered seismograms from the deep earthquake near the Peru-Brazil border, recorded at the west coast. The numbers indicate the dominant periods of the various traces. The line of arrows indicates the calculated arrival time of the direct shear wave. At periods longer than 1 sec, there is an arrival as expected. At short periods, however, there is no arrival at the expected time, but after 20 seconds higher frequency arrives. Type 2 arrival.

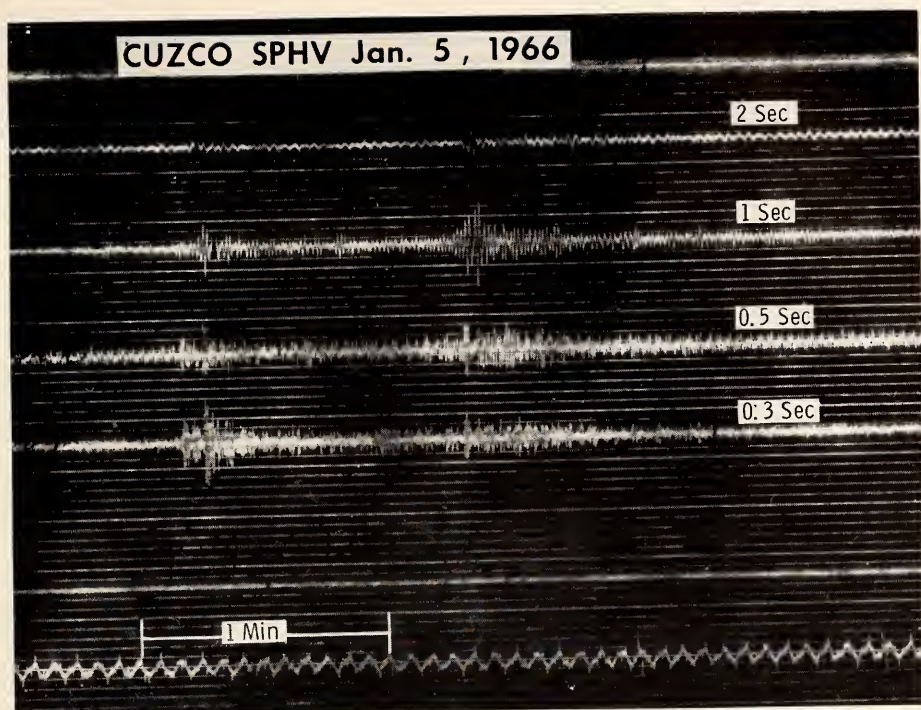


Plate 4. Filtered seismograms from the deep earthquake near the Peru-Brazil border. The shear waves arrive when expected at all periods. Type 3 arrival.

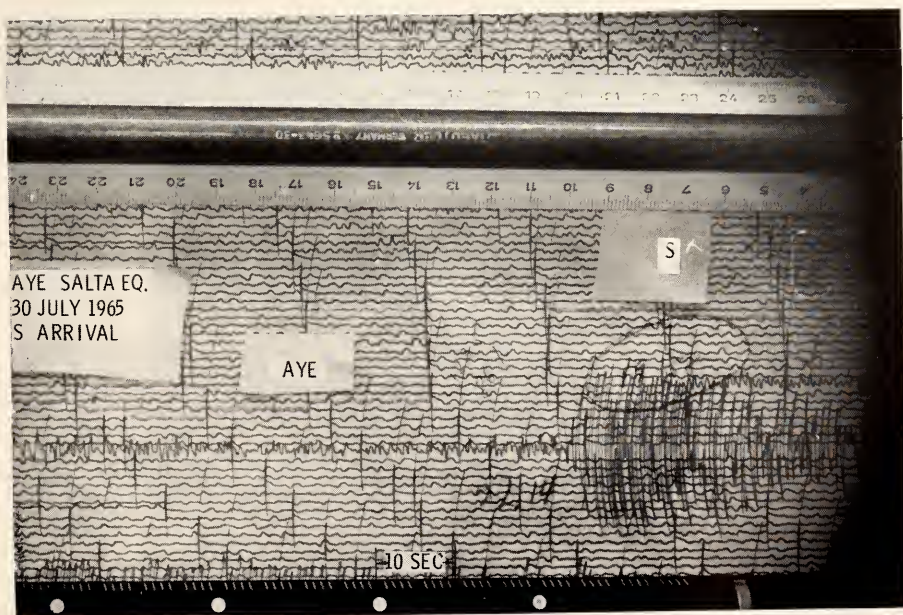


Plate 5. Shear arrival at station AYE on the coast from deep earthquake in Salta region. There are high frequencies in the shear wave, i.e., Type 3 arrival.

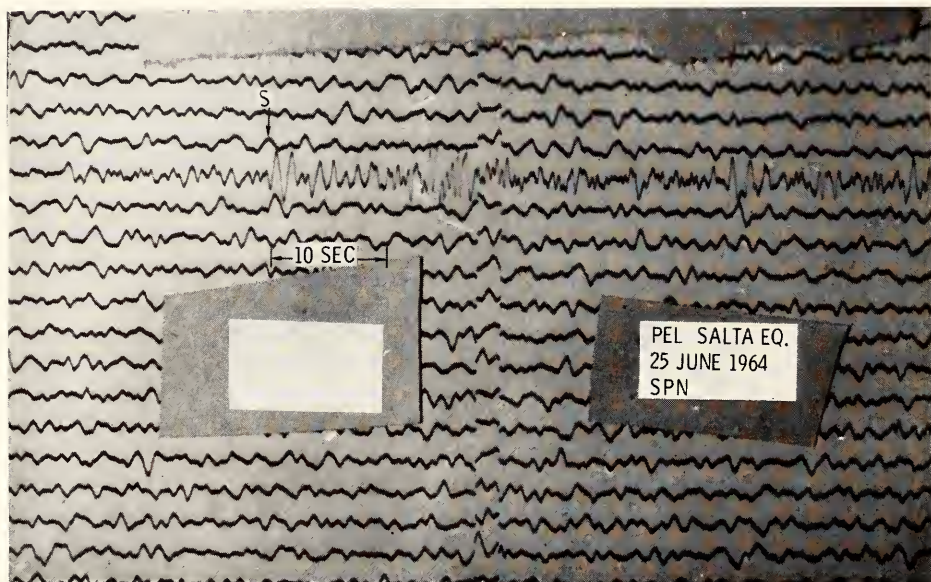


Plate 6. Shear arrival at the WWSS seismograph PEL, near Santiago, Chile. The direct shear wave (marked *S*) has only low frequencies, but there is a clear high frequency arrival 12 seconds after direct *S*. The deep earthquake occurred at Santiago del Estero, Argentina. Type 2 arrival.

Committee on Image Tubes for Telescopes

Cooperative Project of Mount Wilson and Palomar Observatories
Department of Terrestrial Magnetism, Lowell Observatory
National Bureau of Standards, and United States
Naval Observatory

W. A. Baum
Lowell Observatory

John S. Hall (*Chairman*)
Director, Lowell Observatory
Flagstaff, Arizona

L. L. Marton
National Bureau of Standards

M. A. Tuve
Department of Terrestrial Magnetism
Carnegie Institution

Contents

Introduction 389

Allocation of Intensifier Systems 389

Optical Problems Associated with Image Tubes 390

Improved Tubes 390

Acknowledgments 391

INTRODUCTION

The Carnegie Image Tube Project was initiated in February 1954 to explore the possible use of electronic techniques which would supplant or supplement present photographic methods in order to increase the capacity of optical telescopes. With the aid of a grant to the Carnegie Institution of Washington from the Carnegie Corporation of New York, several image orthicon and vidicon systems were evaluated for astronomical applications and an electronographic device was developed. The television-type tubes were found to be ill suited for low-light level photography, and the electronographic device, a barrier-film image converter, was a cumbersome and less-than-satisfactory approach.

In 1958 and 1959 several electrostatically focused mica-window converters and cascaded tubes were tested by the Carnegie Committee with financial support from the National Science Foundation. These tubes gave a satisfactory performance over a small (~ 4 mm in diameter) area and were relatively simple to operate and reliable. The main limitation was the small useful field, but magnetic rather than electrostatic focusing could alleviate this difficulty. Unfortunately, there was no operating prototype of even a simple-stage magnetic

tube that could be copied directly for astronomical purposes. Through the co-operation of industrial laboratories (especially RCA and ITT) with the Committee, and with the financial support of the National Science Foundation, the first successful two-stage cascaded tubes were available from RCA by the end of 1963.

In order that a sufficient number of these tubes could be manufactured to the high performance specifications required for astronomical work, the Committee undertook to purchase and distribute several dozen of these RCA cascaded tubes to observatories both in the United States and abroad. The first allocations were made early in 1965, and by the end of the last report year (June 1967) twenty-one tubes, along with the required focusing magnet, relay lens, voltage divider and hardware, had been distributed.

During this report year fourteen more of these systems have been distributed. Eleven of these have been allocated to observatories and three are on loan in connection with special projects. These image tube systems are producing important results in a striking variety of astronomical problems.

ALLOCATION OF INTENSIFIER SYSTEMS

Because the demand for the Carnegie image tube system has generally exceeded the available supply of sets, a joint National Science Foundation-Carnegie allocations committee was established to recommend priorities in distribution. At the close of this report period (June 1968) all available tubes have been allocated or, in a few cases, made available on a six-month or one-year loan. However, there is sufficient interest in the RCA tube (type C33011)

for other scientific purposes that a substantial number of tubes of this basic type are manufactured by the RCA Industrial Tube Division in Lancaster, Pennsylvania. These tubes meet the same high performance specifications as the tubes that have been made for the Carnegie Committee.

The basic equipment required to operate the cascaded tube has been assembled and tested at the Department of Terrestrial Magnetism. Fortunately,

there is now a small, capable firm that is manufacturing a complete image tube system based on the Carnegie design. This firm, Weiser Associates, at 949 Bonifant St., Silver Spring, Maryland, has already furnished several complete sets for astronomical use.

This year National Science Foundation-Carnegie image tube sets were allocated to: Dr. A. D. Code, University of Wisconsin; Dr. S. Sharpless, University of Rochester; Dr. L. W. Fredrick, University of Virginia (an S1 infrared tube had been supplied previously); Fr. M. F. McCarthy, S. J., Vatican Observatory; Dr. William Liller, Harvard College Observatory; Dr. L. H. Aller, University of California at Los Angeles; Dr. L. V. Kuhi, University of California at Berkeley; Dr. T. D. Kinman, Lick Ob-

servatory (this was a second set intended for the coude spectrograph); Dr. B. F. Peery, Goethe Link Observatory, University of Indiana; Dr. A. Elvius and Dr. P. O. Lindblad, Stockholm Observatory; Dr. J. F. Heard, David Dunlap Observatory, University of Toronto.

In addition, sets have been loaned to Dr. T. A. Mathews, University of Maryland, to aid in Fabry-Perot interferometry for radial velocity work; to Dr. J. P. Rodman, Mount Union College, for use in evaluating improved permanent magnet focusing arrays; and to Drs. A. G. Millikan and J. C. Marchant, Research Laboratories, Eastman Kodak, for evaluation of experimental photographic emulsions for possible use with cascaded tubes.

OPTICAL PROBLEMS ASSOCIATED WITH IMAGE TUBES

As the general quality and performance of image tubes have improved it has been necessary to give more attention to the optics associated with the tube. In the last report a highly successful Cassegrain-schmidt spectrograph camera designed by Dr. Bowen was described in some detail. This $f/2.25$ system is well suited for image tube work because of the 6-cm working distance that it provides.

The design of a somewhat faster system has been worked out by Dr. Bowen in collaboration with Dr. Baum. This system is an improved version of one

designed by Dr. Lynds at Kitt Peak for his image tube system. It is a zero-tilt system that is sufficiently small to fit inside a standard focusing magnet. One of these systems has been ordered from the Boller and Chivens Division of Perkin-Elmer. The transfer lens that is used in photographing the output phosphor screen is one of the elements limiting the resolution of the image tube system. The presently available systems are either too slow or, if fast enough, have too low resolution or too small a field. This problem is being reevaluated by Dr. Baum.

IMPROVED TUBES

An attempt to develop an improved version of the cascaded tube has been made at RCA. By a clever redesign of the accelerating electrodes, and by constructing the tube envelope of ceramic rather than glass, it has been possible to build two-stage tubes that should operate at 30 or 40 kilovolts overall

rather than at the usual 17 to 20 kilovolts. This promises to increase appreciably the available gain. The increased gain might permit the use of slower, fine-grain phosphor screens—and hence obtain increased resolution—or the use of slower, higher-resolution transfer lenses. In addition, the new electrodes provide

a more uniform electric field and a less distorted magnetic field. Consequently, there is less S-distortion of the image, and the edge resolution is improved. This development is very encouraging, but procedures for forming efficient photocathodes in the new bulb structure have not yet been worked out satisfactorily.

The same experimental tube structure has been incorporated in several single-stage tubes of double length. These devices operate quietly at 34 to 42 kV, but also have relatively low cathode sensitivities. These tubes, when perfected, may be adapted as prototypes for a Lenard-window tube.

ACKNOWLEDGMENTS

The Committee wishes to acknowledge and thank the National Science Foundation for the support that has been so necessary for the development of these image intensifying devices. The assembly and testing of the National Science

Foundation-Carnegie image tube systems has been carried out by Dr. W. Kent Ford, Jr., at the Department of Terrestrial Magnetism. We particularly thank Dr. I. S. Bowen for his assistance with many optical problems.

Department of Embryology

Baltimore, Maryland

James D. Ebert
Director

Contents

Introduction	397	The use of Sendai-assisted hybridization to make possible hybridization between unselectable cells: virus fusion as a partial selective agent	426
Nucleic Acid and Protein Synthesis during Oogenesis and Development . .	401	Loss of SV ₄₀ -Induced T-antigen from Somatic Hybrids between Mouse Cells and SV ₄₀ -Transformed Human Cells.	428
Ribosomal RNA and its Genes during Oogenesis and Development . .	401	Cell Differentiation and Viral Susceptibility	429
"molecular mapping" of the genes for the ribosomal RNAs	401	The Interactions of Rous Sarcoma Virus with Developing Muscle . .	429
Control of synthesis of ribosome components	401	RSV-RNA Hybridization with Avian and Mammalian DNA	431
The extra copies of ribosomal genes in oocytes	402	Hybridization technique	432
Comparative Studies of Genes for Ribosomal RNA in Eukaryotes . . .	404	Hybridization of RSV-RNA to chick DNA	432
Behavior of ribosomal DNA in CsCl gradients	405	Hybridization of RSV-RNA to DNA from several other avian and mammalian species.	435
Relative amounts of rDNA in different organisms	405	Additional Cell Culture Systems for Future Study	436
The extent of homology among the ribosomal genes of eukaryotes. .	407	Isolation and maintenance of sensory nerve cells	436
Synthesis of Ribosomal Proteins in <i>Xenopus laevis</i> Embryos	409	Aggregation techniques for culture of hepatocytes	438
Synthesis of Collagen during Embryogenesis in <i>Xenopus laevis</i>	413	Isolation and culture of cells from the chorioallantoic membrane .	439
Nucleic Acid Metabolism during Oogenesis and Embryogenesis in <i>Urechis caupo</i>	413	Studies employing HeLa cell-erythrocyte heterokaryons	439
Histone Synthesis during Development .	417	Cardiogenesis in the Chick Embryo . .	440
Studies on Mitochondrial Nucleic Acids.	417	Electrophysiological Impalement of Isolated Cells	440
A Size Difference between the Mitochondrial DNAs of Urodele and Anuran Amphibia.	417	Impalability	442
RNA in Frog Oocyte Mitochondria .	418	Properties of Heart Cells.	445
Clonal Culture of Differentiated Cells from Mammals: Rat Liver Cell Culture.	419	Mechanism of Enlargement of the Pericardial Space	447
An Established Cell Line of Fibroblasts from Goose Cells	421	Studies on Cell Interactions	452
Studies Using Somatic Cell Hybrids . .	424	Properties of Embryonic Heart Cells in Tissue Culture.	452
The Production of Cell Hybrids with UV-Inactivated Sendai Virus . .	424	Noncovalent interactions in adhesion	452
Sendai virus-assisted hybridization of the fully selectable cell lines A9 and Cl 1 D	424	Interaction of Blastomeres in Eggs of <i>Urechis caupo</i>	453
Sendai virus-assisted hybridization of a partially selectable cell system: Cl 1 D and normal rat liver cells	426	Ovulation and Germinal Vesicle Breakdown in Amphibian Oocytes: Gonadotrophic Hormone Specificity .	454

The Mammalian Embryo in its Relation to its Environment	455	The Collection of Human Embryos . .	462
The Uptake of Water by the Rabbit Blastocyst	455	The Development of the Epiphysis Cerebri and the Subcommissural Complex in Staged Human Em- bryos	462
Anatomy and Physiology of the Pla- centa	459	The Development of the Teeth and Oral Structures	462
Radioangiography of placental cir- culation in the rhesus monkey .	460	Staff Activities	462
Experimental production of hyper- tension	461	Bibliography	464
Incidence of single disc placentas in rhesus monkeys.	461	Personnel	466

INTRODUCTION

The past year was one of active and uninterrupted work in the several lines of research established at the Department of Embryology. There have been no changes in the permanent staff of the Department and no ebb in the tide of publication. In fact the year was marked by a large flow of published results. To say this, however, gives a misleading impression of the state of the Department as this report is being assembled, for more perhaps than in any recent year, Staff Members and Fellows have embarked upon exploratory studies aimed at opening up pathways for future investigation. Progress reports are never satisfying for either their authors or readers; this one is no exception, for it has been uncommonly difficult to summarize work already completed while conveying an idea of new directions. The problems encountered in reaching a proper balance of "old" and "new" are illustrated in the following samples of our activities.

Brown, Dawid, and their colleagues have shown that oocytes of five amphibian species as well as those of an echiuroid worm contain many extra copies of the genes for 28S and 18S ribosomal RNA. For example, an oocyte nucleus of *Xenopus laevis* has about 1000 times as many genes for 28S and 18S ribosomal RNA as does the nucleus of a somatic cell. The oocytes of these animals synthesize large quantities of ribosomes for storage and the extra gene copies act as templates in this synthesis. They are active only in oocytes and no longer function after meiosis and ovulation. Of primary importance is the mechanism of this replication. The specificity of the event is unusual, since about 0.1–0.2% of the germ cell's DNA has been singled out for repeated copying. Does this replication involve changes in the nucleotide sequence of the

genes for ribosomal RNA, or subtle cues in the structure of the nucleolar organizer sites of the chromosomes which presumably are copied? Alternatively, specific enzymes—polymerases—which function in DNA synthesis, and which recognize only the DNA involved in ribosomal RNA synthesis, might be involved. An important clue may lie in the finding reported by Brown, Dawid, and Ronald H. Reeder, a Fellow of the Helen Hay Whitney Foundation, that the extrachromosomal copies of rDNA are subtly different from the rDNA associated with the genome in somatic cells. The extra DNA copies (the "ribosomal DNA," or rDNA) in the germinal vesicle have a higher buoyant density than somatic-cell DNA. The explanation for this difference in buoyant densities between the extra copies of rDNA in oocytes and the rDNA in the chromosomes is a major question and is the major focus of interest of this group at the present time.

George Wald is reported to have defined a great question as one an intelligent child asks, and, getting no answer, stops asking. Thus it is reassuring to observe that one important step in solving this problem—the development of a method to isolate large amounts of ribosomal DNA from bulk DNA—has already been accomplished. The cesium chloride technique has been coupled with an initial precipitation with polylysine which precipitates the adenine–thymine-rich DNA before the guanine–cytosine-rich DNA. Over 90% of bulk *X. laevis* DNA can be precipitated with polylysine under conditions where at least 50% of the rDNA remains in solution. Using this method it has been possible to purify large amounts of pure rDNA from somatic-cell DNA. Experiments in progress are designed to analyze the two rDNAs in sufficient detail to explain the difference in their buoyant densities and to

obtain a complete understanding of the arrangement of the genes which comprise this DNA.

Previous reports have emphasized the patterns of synthesis of the ribosomal RNAs. Yet the RNAs make up only a part of the ribosomes, which contain many proteins. Are the controls operating in the synthesis of ribosomal RNAs and ribosomal proteins closely coordinated? Using techniques perfected over the past two years, Hallberg has studied the synthesis of ribosomal proteins both in normal *Xenopus* embryos and in the anucleolate mutant. It will be recalled that normally ribosomal RNAs are made in bulk during oogenesis, but that none are formed during cleavage. Moreover, none are formed during posthatching stages in the anucleolate mutant. If the synthesis of ribosomal RNAs and proteins were closely coordinated, then it would be expected that ribosomal proteins would not be synthesized during the same periods. Hallberg's findings thus far support this conclusion. Cleaving embryos which do not synthesize rRNA do not synthesize detectable amounts of ribosomal protein, nor do posthatching stages of anucleolate embryos.

In presenting these findings as part of his doctoral thesis at Johns Hopkins, Hallberg has emphasized that his conclusions must be tempered by several considerations. If incorporation of newly made ribosomal proteins into mature ribosomes involves some modification in their primary structure, newly synthesized "precursor" molecules would go undetected, since their chromatographic and electrophoretic properties would most likely be different from "mature" ribosomal proteins. Moreover, these conclusions are based on a select group of ribosomal proteins. Finally, the techniques are not sensitive enough to rule out synthesis and rapid degradation of these ribosomal proteins. The above criticisms notwithstanding, it appears that ribosomal protein synthesis is under close coordinate control with the synthesis of

ribosomal RNA. The mechanism of this control which would account for the coordination both during cleavage and in the 0-nu embryos is unknown.

Dawid's program on mitochondrial DNA has also taken a new direction. Although, in collaboration with Wolstenholme at the University of Chicago, he is still concerned with the structure of mitochondrial DNA in amphibian oocytes, he has now shifted part of his attention to its function. It has been suggested, and for two forms—yeast and *Neurospora*—demonstrated, that mitochondria contain ribosomes, and that these ribosomes differ from those in the rest of the cytoplasm. Dawid is currently examining this proposition in frog oocyte mitochondria using the technique of electrophoresis on polyacrylamide gel. The results thus far suggest that oocyte mitochondria do contain ribosomal RNAs of distinct properties. If this suggestion can be verified, it will lend important support to the concept that animal mitochondria possess distinct endogenous protein-synthesizing machinery.

Two Fellows, Yoshikawa-Fukada and Weiss, have centered their attention on the interactions of tumor viruses with the genome of the host cell.

Yoshikawa-Fukada, a Fellow of Carnegie Institution working in cooperation with Ebert, has continued to examine the interaction of Rous sarcoma virus with cells of the chick embryo. It will be recalled that during the differentiation of skeletal muscle, mononucleated myoblasts fuse to form multinucleated myotubes. After fusion, both DNA synthesis and nuclear division cease. When clones of chick embryonic leg muscle consisting of both myoblasts and myotubes are infected with Rous sarcoma virus (RSV), DNA synthesis (as measured by H^3 -thymidine incorporation) is induced in the nuclei of myotubes within 24 hours. Yoshikawa-Fukada has now initiated inquiries into the nature of the DNA synthesized and the mechanism whereby the virus induces its formation. Molecular

hybridization studies show a partial homology between the RNA of RSV and DNA, not only of normal and RSV-infected chick embryo cells, but DNAs of several other species as well. Moreover, the hybridized RNA, which is only a part of the viral RNA, presumably that portion which binds most firmly to cellular DNA, is characterized by a high content of adenylic acid. The significance of this homology is thus far obscure. However, the findings agree with the independent observations of Harel *et al.* Moreover, Kubinski and Rose have advanced evidence that oncogenic adenovirus DNA and SV₄₀ virus DNA contain more deoxy-adenosine-rich sequences than nononcogenic viruses. Do these special sequences somehow enhance the possibility of integration of viral DNA into the genome? If so, what might be the function of the high adenylic acid content of the RSV-RNA hybridizable moiety?

Weiss, a Fellow of the U. S. Public Health Service, working in cooperation with Ephrussi (Paris) and Scaletta (Case Western Reserve) has been concerned directly with the nature of the relations between the viral genome and the transformed cell. Is a tumor virus integrated into the genome or does it persist as an episomelike free particle? The technique of somatic hybridization has been used under conditions such that all the chromosomes of one "parent" are lost from the hybrid cells. In earlier experiments by Weiss and Green it had been shown that hybrids made between mouse and human cells undergo rapid and extensive segregation of human chromosomes with no concomitant loss of mouse chromosomes. It was reasoned that if hybrids were made between normal mouse cells and human cells transformed by a tumor virus, SV₄₀, and if all human chromosomes were lost, then if the viral genome were integrated into a human chromosome, it too would disappear. Such experiments have been performed; they show that a viral antigen (T) is absent only from hybrid cells which have lost

most or all of their human chromosomes, providing suggestive evidence that the viral genome is integrated into the chromosomes of transformed cells.

Weiss has also collaborated with another Carnegie Fellow, H. G. Coon, in a systematic study of the influence of inactivated Sendai virus upon hybridization of cells grown in medium which permits selective growth of hybrids, in the hope that artificial induction of fusion might substantially assist the formation of propagating hybrid strains. As described in the body of the report, "virus-assisted hybridization" does result in a substantial increase in the spontaneous mating rate of cells of lines A9 and Cl 1 D. Possibly of greater import is the high virus-assisted mating rate observed in combinations of Cl 1 D and normal rat liver cells. These hybrids should be of considerable interest.

The rat liver cells employed in this study themselves represent an important technical advance. During the year Coon has succeeded in cloning liver cells from infant rats. Typical epithelial pavement cells, showing phase-dense cytoplasm and tightly packed nuclei, appearing very similar to liver parenchymal cells have been serially subcultured. Individual cells do form colonies upon transfer.

It remains to be established by other criteria that these cells are, in fact, liver parenchymal cells. As reported below, they do produce some of the normal serum antigens, but whether they are capable of other complex liver functions is yet unknown.

R. J. Hay, who joined the Department as an Assistant Investigator, has taken up several questions arising out of the interactions of RSV and developing muscle. With a Carnegie Fellow, S. Yuyama, and in consultation with Ebert, he has been exploring several approaches to the problem of obtaining cultures of multinucleated myotubes free of their mononucleate precursor cells, the myoblasts. Thus far, limited success has been achieved with two methods: manipulation of the growth

medium with the aim of promoting synchronous fusion, and selective inhibition of dividing cells by antimitotic drugs. In addition he has been engaged in attempts to isolate and maintain cells from several additional chick embryonic tissues, planning ultimately to include studies of the effects of RSV on sensory nerve cells, liver cells, and cells of the chorioallantois at different stages of development and growth.

Robert DeHaan and several colleagues have continued to take a multilevel approach to the study of cardiogenesis in the chick embryo. In DeHaan's own words, however, "Overshadowing all else in our work during the past year is the breakthrough we have enjoyed in the electrophysiological analysis of heart cells in culture." This work is discussed in detail below; here it will suffice to say that DeHaan and Gottlieb have succeeded in the electrophysiological impalement and analysis of isolated embryonic heart cells.

Two experienced investigators spent a major part of the year in the Department, much to our advantage. Peter Tuft of the University of Edinburgh worked as a Carnegie Fellow on the uptake of water by the rabbit blastocyst. This work, carried out with the cooperation of B. G. Böving, is of special importance not just because the expansion of the blastocyst resulting from the accumulation of fluid in the blastocyst cavity is the stimulus for equidistant spacing of blastocytes in the uterus, but also because it exemplifies an important feature of embryogenesis, the formation of large, transient, liquid-filled intercellular cavities.

S. Shifrin, on leave from the National Cancer Institute for a period of training in developmental biology, undertook a preliminary study of the forces involved in cell surface interactions.

In addition to Reeder and Hallberg, three Fellows and students continued studies in cooperation with Brown: John

Sinclair, who will soon complete his second year as a Fellow of the U. S. Public Health Service and take up an appointment at Indiana University; Harold Kasinsky; and Merry Schwartz. Their contributions are to be found in the body of the report.

Other newcomers included H. R. Mienshimer, working in cooperation with E. M. Ramsey; Ronald Swanson, until recently at the University of Chicago, now with Dawid; and Douglas M. Fambrough.

Fambrough, a recent graduate of California Institute of Technology, joined the Department as a Carnegie Fellow early in 1968 to begin a long-range program dealing with the interaction of nerve and muscle. Although some progress has been made, it seemed premature to attempt a formal report. His objectives can be summarized briefly as follows:

When deprived of innervation, most mammalian skeletal muscles undergo profound changes in metabolism, contractile properties, and even morphology, leading eventually to muscle fiber degeneration. We wish to know how these changes are inhibited by maintenance of functional nerve-muscle connections and reversed by reinnervation of the denervated muscle. With the help of Arlyne Musselman, Fambrough is bringing the techniques of organ culture, electrophysiology, and biochemistry to bear on these problems.

A. W. Schuetz of the Johns Hopkins School of Hygiene and Public Health continued to work in the Department during a large part of the year, centering his attention on mechanisms involved in the induction of ovulation and completion of meiotic maturation in the amphibian oocyte. Other visitors, some of whose studies are reported, included John Bonica of the University of Washington School of Medicine; P. E. B. Calonijs, University of Helsinki and University of

Maryland; Martin Donner, Johns Hopkins; C. B. Martin, Jr., Medical College of Georgia; E. B. Nery, Cleft Palate

Center, University of Pittsburgh; and M. Wharton Young of Howard University College of Medicine.

NUCLEIC ACID AND PROTEIN SYNTHESIS DURING OOGENESIS AND DEVELOPMENT

ribosomal RNA and ITS GENES DURING OOGENESIS AND DEVELOPMENT

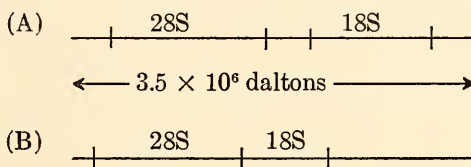
D. D. Brown, I. B. Dawid and R. Reeder

Our studies of the ribosomal RNAs (*Year Books* 64 through 66) have been extended to an analysis of their genes. The emphasis over the past year has been twofold. First, techniques of molecular hybridization have been developed which permit a kind of "molecular mapping" of these genes. Second, the process of specific amplification of these genes in oocytes has been quantitated and characterized in some detail. Gene amplification has emerged as a significant and novel mechanism in development. In the recent past, studies of mechanisms controlling development have focused on ways in which a constant, unaltered genome can be modified by repressor or activator substances which complex with specific regions of the DNA (or genome) permitting "differential gene action." A different mechanism is operating in the control of synthesis of 28S and 18S ribosomal RNAs in oocytes. The oocyte increases its synthesis of ribosomes by replicating specifically the genes for 28S and 18S ribosomal RNA at an early stage of oogenesis and subsequently using these extra genes as templates for massive rRNA synthesis.

"Molecular Mapping" of the Genes for the Ribosomal RNAs

We and others have obtained the following information about the genes for the three ribosomal RNAs in *Xenopus laevis*—28S, 18S, and 5S RNA. There are about 450 genes for 28S and 18S RNA, all of which are clustered together on one of the 16 chromosomes in the haploid set

along with some "spacer" DNA which has a nucleotide composition different from either 28S or 18S DNA. There are more than 20,000 genes for 5S RNA which appear to be partly clustered; these genes are not intermingled with the cluster of genes for 28S and 18S RNA. Gene arrangements which are compatible with our data and those of others suggest one of the following sequences which repeats 450 times. The sizes given below refer to the single-strand lengths of DNA.



In model A the 28S and 18S genes (1.4 and 0.7×10^6 daltons, respectively, as single-stranded DNAs) are separated by spacer DNA (a total of 1.4×10^7 daltons). In model B the spacer DNA separates adjacent pairs of 28S and 18S genes. At least part if not all of the 3.5×10^6 dalton unit is transcribed in vivo as a single high molecular weight RNA molecule which is a precursor of the mature 28S and 18S RNAs.

Control of Synthesis of Ribosome Components

As mentioned above, genes for 5S RNA are not included in the repeating sequence of rDNA which contains the 28S and 18S genes. 5S RNA must therefore be transcribed separately. Synthesis of 5S RNA is coordinated with the synthesis of 28S and 18S RNA as shown by the fact that deletion of only the 28S and 18S genes (the anucleolate mutation) causes cessa-

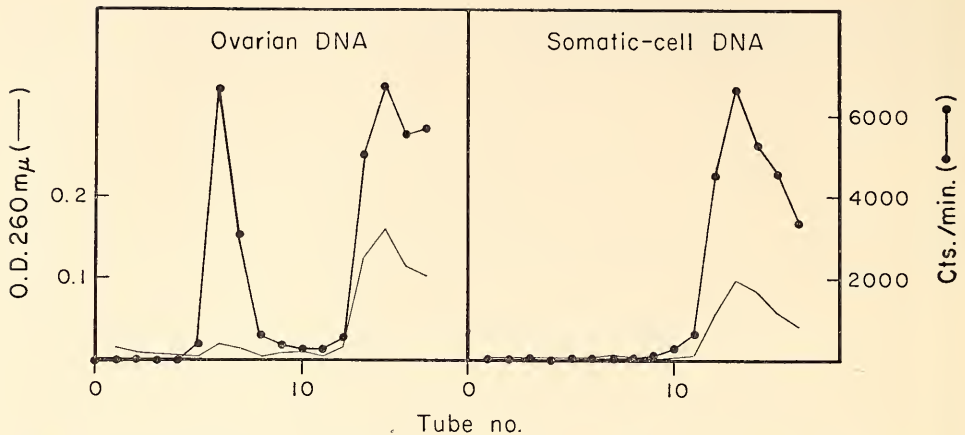


Fig. 1. CsCl centrifugation of DNA from ovaries and carcasses of *X. laevis* isolated 4 weeks after metamorphosis. The animals were injected with 50 μ c of (H^3)-thymidine twice a week for 2 weeks. As much high buoyant density ribosomal DNA has been synthesized in ovaries as bulk DNA.

tion of 5S RNA synthesis, whereas enrichment of only the 28S and 18S genes in the oocyte enhances 5S RNA synthesis. In addition we can now consider the multiple proteins which are part of the ribosome structure. The studies of Hallberg described elsewhere in this report show that these proteins are synthesized coordinately with the three RNA moieties of the ribosome.

The Extra Copies of Ribosomal Genes in Oocytes

We have demonstrated that an oocyte nucleus of *X. laevis* has about 1000 times as many genes for 28S and 18S ribosomal RNA as does the nucleus of a somatic cell. Gall has shown that these extra copies are synthesized during a relatively short interval of oogenesis, between 2 and 4 weeks after metamorphosis when most of the oocytes are in pachytene stage. Figure 1 demonstrates this high rate of rDNA synthesis relative to the synthesis of bulk DNA in ovaries from animals just after metamorphosis. Of primary importance is the mechanism of this replication. The specificity of the event is unusual, since about 0.1–0.2% of the germ cell's DNA has been singled out for repeated copying. Does this repli-

cation involve changes in the nucleotide sequence of the ribosomal DNA itself, or subtle cues in the structure of the nuclear

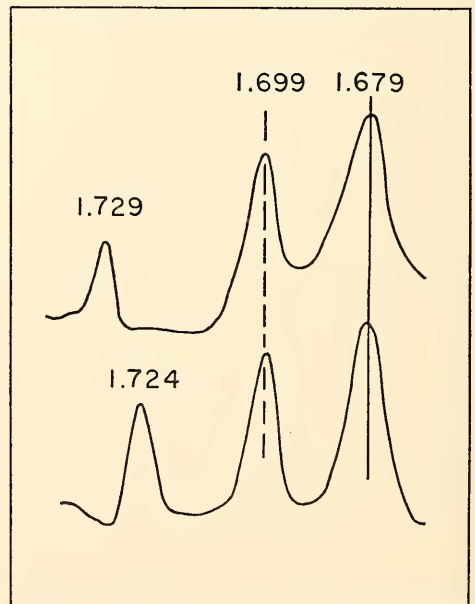


Fig. 2. Tracings of CsCl density-gradient experiments comparing the germinal-vesicle rDNA (top) and somatic-cell rDNA (bottom) of *X. laevis*. The two light DNA markers are bulk somatic-cell DNA of *X. laevis* (density 1.699) and deoxyadenylate-deoxythymidylate copolymer (density 1.679).

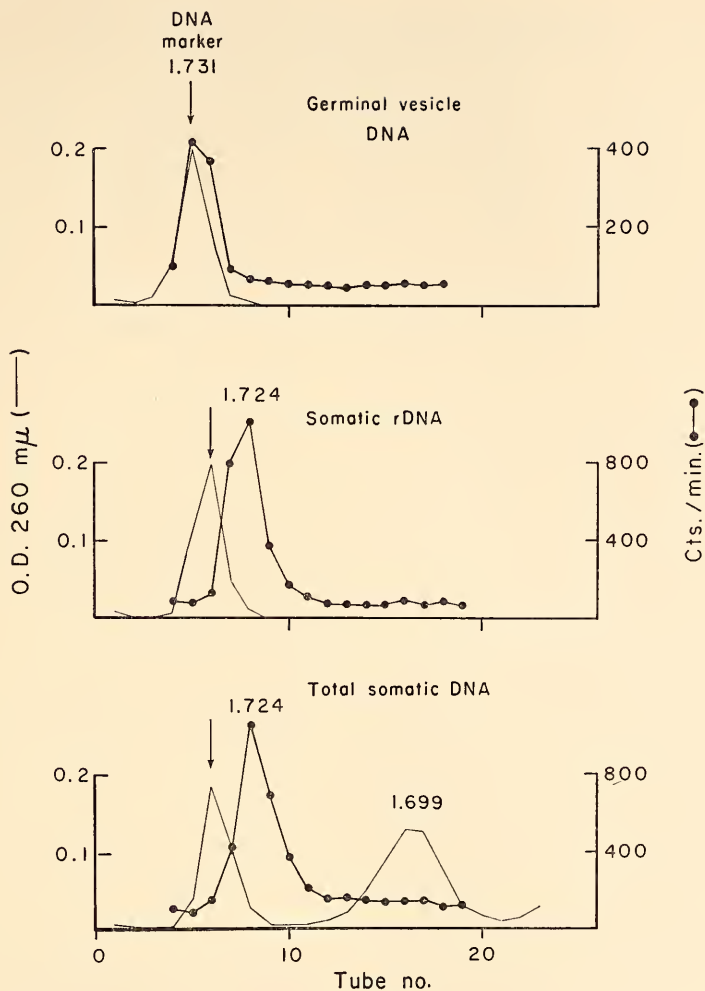


Fig. 3. The difference in buoyant density between germinal-vesicle and somatic-cell rDNA as shown by hybridization with (H^3)-rRNA of *X. laevis*. The marker is native *Micrococcus lysodeikticus* DNA (density 1.731). The DNAs were centrifuged in CsCl gradients in the 65-fixed angle rotor of a Spinco centrifuge at 33,000 rpm for 64 hours at 25°C. Each fraction was denatured with alkali, and the DNA was trapped on filters and hybridized with (H^3)-rRNA.

organizer site of the chromosomes which presumably are copied? Alternatively, specific DNA polymerase enzymes might be involved which only recognize rDNA. An important clue may lie in the discovery that the extrachromosomal copies of rDNA are subtly different from the rDNA associated with the genome in somatic cells. The extra DNA copies (germinal-vesicle rDNA) have a higher

buoyant density than somatic-cell rDNA. Figures 2 and 3 compare the buoyant densities of germinal-vesicle and somatic-cell rDNAs both by analytical ultracentrifugation in CsCl and hybridization methods. The buoyant densities of both rDNA preparations have been measured under a variety of conditions and in each case the difference persists (Table 1). The explanation for this difference in

TABLE 1. The Buoyant Densities and the Calculated Base Compositions of Somatic-Cell and Germinal-Vesicle rDNA of *X. laevis*

Centrifugation Condition	DNA State	Somatic-Cell DNA		Germinal Vesicle DNA	
		Density	% G + C	Density	% G + C
Neutral CsCl	Native	1.724	65	1.729	70
Neutral CsCl	Denatured	1.735	65	1.740	70
Alkaline CsCl	Denatured	1.779	67	1.785	72
Neutral CsSO ₄	Native	1.432	65	1.436	73

Note: Experiments were performed with purified rDNA in the Model E ultracentrifuge.

buoyant densities between the extra copies of rDNA in oocytes and the rDNA in the chromosomes seems to us to be of primary importance, and is our major focus of interest at the present time.

An important step in solving this problem has been the development of a method to isolate large amounts of rDNA from bulk DNA. It can be isolated by recycling the high buoyant density fraction of bulk DNA from CsCl density gradients. This CsCl method has been coupled with an initial precipitation with polylysine which precipitates the adenine-thymine-rich DNA before the guanine-cytosine-rich DNA. This selective action of polylysine had been shown by Felsenfeld with bacterial DNAs. Over 90% of bulk *X. laevis* DNA can be precipitated with polylysine under conditions where at least 50% of the rDNA remains in solution (Fig. 4). Using this method it has been possible to purify large amounts of pure rDNA from somatic-cell DNA. Experiments in progress are designed to analyze the two rDNAs in sufficient detail to explain the difference in their buoyant densities and to obtain a complete understanding of the arrangement of the genes which comprise this DNA.

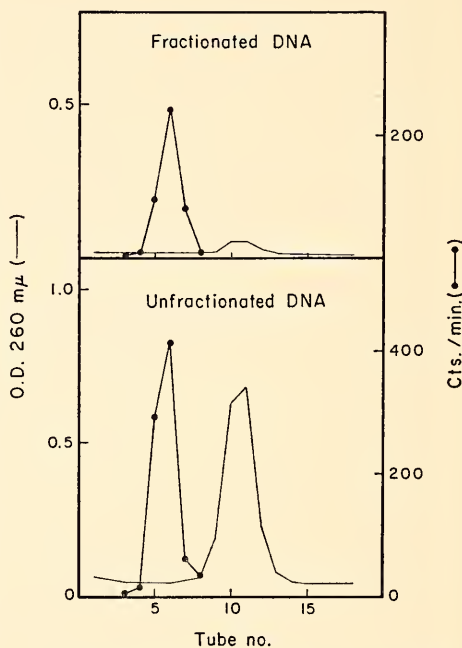


Fig. 4. Enrichment for r-DNA by polylysine precipitation. Polylysine was added to *X. laevis* DNA in 1 M NaCl until 90% of the DNA had been precipitated. The remaining DNA in the supernate was centrifuged to equilibrium in CsCl, fractionated and the DNA in each fraction hybridized with (H³)-rRNA from *X. laevis*. Unfractionated DNA was hybridized in the same way.

COMPARATIVE STUDIES OF GENES FOR RIBOSOMAL RNA IN EUKARYOTES

J. H. Sinclair and D. D. Brown

Except for *Xenopus* and *Drosophila*, little is known about the physical characteristics of the DNA which serves as templates for the ribosomal RNAs of

eukaryotes. We have studied the rDNA of a number of organisms by preliminary CsCl equilibrium centrifugation of the bulk DNA, fractionation of the gradients,

and hybridization of the DNA in each fraction with (^3H)-rRNA from *X. laevis*. Since rRNA of *Xenopus laevis* will hybridize with rDNA of most eukaryotes (see *Year Book 66*, Table 1, p. 586; reprint, p. 14), the banding profile and buoyant densities of rDNA have been determined for a variety of organisms. Evidence from molecular hybridization studies using competition methods is also presented, indicating that the degree of homology between the rRNA of distantly related organisms such as higher plants and animals may approach 50%.

BEHAVIOR OF RIBOSOMAL DNA IN CsCl GRADIENTS

The rDNA of most organisms as detected by molecular hybridization is a distinct and symmetrical satellite which separates from the bulk DNA in CsCl, indicating that the ribosomal genes are clustered. Occasionally there is a slope on the lower density side of the hybridization profile, suggesting either heterogeneity of rDNA itself or heterogeneity of the DNA attached to it. Although the buoyant densities of rDNA are consistently higher in some organisms such as mammals and birds, they may vary considerably even within a given class of organisms.

The base composition of rDNA has been calculated from its buoyant density and is expressed in Table 2 as % guanylic + cytidylic acid (% GC). Table 2 also includes the known base composition of rRNA from some of these organisms. Although the calculated % GC of rDNA for most organisms is similar to the measured % GC for its homologous rRNA, the rRNA base composition is usually slightly higher than that for the rDNA of the same organism, suggesting that other DNA of lower % GC is attached to the 28S and 18S genes or that the buoyant density does not reflect the actual base composition of rDNA for as yet unknown reasons.

A knowledge of the buoyant density of

the rDNA satellite has made it possible to isolate rDNA by preparative CsCl centrifugation and to examine it in the analytical ultracentrifuge (Fig. 5). The base composition of several rDNA preparations fractionated in this way is presented in the "sat-DNA" column of Table 2. The buoyant density of rDNA measured by hybridization after preparatory CsCl centrifugation agrees well with the measurements of rDNA satellite directly visualized in the analytical centrifuge.

RELATIVE AMOUNTS OF rDNA IN DIFFERENT ORGANISMS

Since rRNA of *X. laevis* hybridizes with DNA from a large number of organisms, it has been possible to use a single preparation of (^3H)-rRNA from cells cultured from adult *X. laevis* kidney to estimate the amount of rDNA in a variety of eukaryotes. Identical hybridization conditions were used for the DNA of each organism. Hybridization with DNA in the high density regions of CsCl gradients was scored. The extent of hybridization is a product of the fraction of the total DNA which codes for rRNA and the degree of homology between *X. laevis* RNA and the DNA of the organism. Since this homology must always be less than 100%, the amount of RNA hybridized gives a *minimal size* for the 28S and 18S ribosomal RNA genome for each organism.

The magnitude of the differences between *X. laevis*, HeLa cells, and barley is illustrated in Fig. 6. *X. laevis* rRNA hybridizes with HeLa DNA to about 20% the extent that it does with *X. laevis* DNA. Since about 0.06% of *X. laevis* DNA is known to be homologous with its homologous rRNA by saturation experiments, it is concluded that about 0.1% of HeLa hybridizes with *X. laevis* rRNA. The proportion of each of several heterologous DNAs which hybridize with *X. laevis* rRNA is summarized in the last column of Table 2. The DNAs from

TABLE 2. Physical Properties of Nucleolar DNA of Various Organisms

Class	Organism	Buoyant Density		Percent G + C			Amount of rDNA
		bulk DNA 1	rDNA 2	rDNA 3	sat-DNA 4	rRNA 5	
Mammalia	Man (HeLa)	1.699	1.719	59	...	65	0.15-0.45
	Monkey	1.700	1.720	60	
	Rat	1.699	1.711	51	...	60	
	Rabbit	1.699	1.718	58	...	63	
	Cow	1.699	1.719	59	...	63	0.8
Aves	Chicken	1.700	1.723	63	...	64	0.6-1.0
	Turkey	1.699	1.720	60	
	Goose	1.699	1.722	62	57	...	
Reptilia	Tortoise	1.703	1.719	59	1.0
Amphibia	<i>Amphiuma</i>	1.701	1.706	46	47	...	1.2
	<i>Necturus</i>	1.708	1.719	59	62	...	0.4
	Axolotl	1.703	1.714	54	1.5
	<i>A. tigrinum</i>	1.704	1.717	57	56	...	0.71
	<i>A. punctatum</i>	1.704	1.718	58	0.35
	<i>T. viridescens</i>	1.702	...	54, 59	...	59	0.6
	<i>B. americanus</i>	1.701	1.713	53	1.0
	<i>B. marinus</i>	1.704	1.717	57
	<i>R. sylvaticus</i>	1.701	1.719	59	2.0
	<i>R. pipiens</i>	1.702	1.723	63	0.9-1.1
	<i>R. palustris</i>	1.701	
	<i>R. clamitans</i>	1.701	1.721	61	
	<i>X. laevis</i>	1.699	1.722	62	63	62	
Osteichthyes	Toadfish	1.687	1.719	59
	<i>Fundulus</i>	1.699	1.711	51
	Salmon	1.700	1.705	45	1.3-1.6
Chondrichthyes	Shark	1.704	1.714	54	
Echinodermata	Starfish	1.697	1.722	62	63	...	1.0-1.4
	<i>Lytechinus</i>	1.696	1.722	62	
Arthropoda	Crab	1.703	1.706	46	2.0-2.5
	<i>Artemia</i>	1.695	...	45, 48	...	47	
	<i>Limulus</i>	1.693	1.712	52	54	...	
	<i>Drosophila</i>	1.701	...	38, 42	
Echiuroida	<i>Urechis caupo</i>	1.700	1.710	50	1.5
Mollusca	Squid	1.695	1.719	59	0.3-0.9
	Clam	1.696	1.713	53	
Coelenterata	<i>Metridium</i>	1.696	1.705	45	2.3
Protozoa	<i>T. pyriformis</i> , W.	1.690	1.698	38	...	44	0.2-0.6
	<i>Astasia longa</i>	1.709	
Eumycophyta	<i>Neurospora crassa</i>	1.710	1.715	55	5.0
	<i>S. cerevisiae</i>	1.695	44	47	7.0
	<i>S. carlsbergensis</i>	1.698	1.702	42	44
	<i>Hansenula anomala</i>	1.695	48
	<i>Debaromyces kloederi</i>	1.696	42
Chlorophyta	<i>C. reinhardi</i>	1.723	1.714	54	55
Tracheophyta	Barley	1.702	1.705	45	4.4
	Wheat	1.703	1.708	44	...	49	2.0-2.4
	Pea	1.695	1.704	44	...	49	

1. "Bulk DNA" refers to nuclear or main band DNA.

2. "rDNA buoyant densities" in this column were determined from the aliquot of a preparative gradient which hybridizes with radioactive *X. laevis* rRNA.

3. "rDNA percent G + C" was determined by subtracting 1.660 from the buoyant density.

4. "sat-DNA percent G + C" values were estimated from the buoyant density of isolated rDNA observed on the analytical ultracentrifuge.

5. rRNA values are from the literature and are an average of the 18S and 28S RNAs.

6. The "amount of rDNA" refers to the fraction of the DNA which hybridizes with radioactive rRNA of *X. laevis*. These values represent the true size of the 18S and 28S ribosomal RNA genome only with organisms which have nearly 100% homology with *X. laevis*, such as perhaps the *Rana* species. All other values are underestimated and, for distantly related organisms, the underestimation is probably quite large.

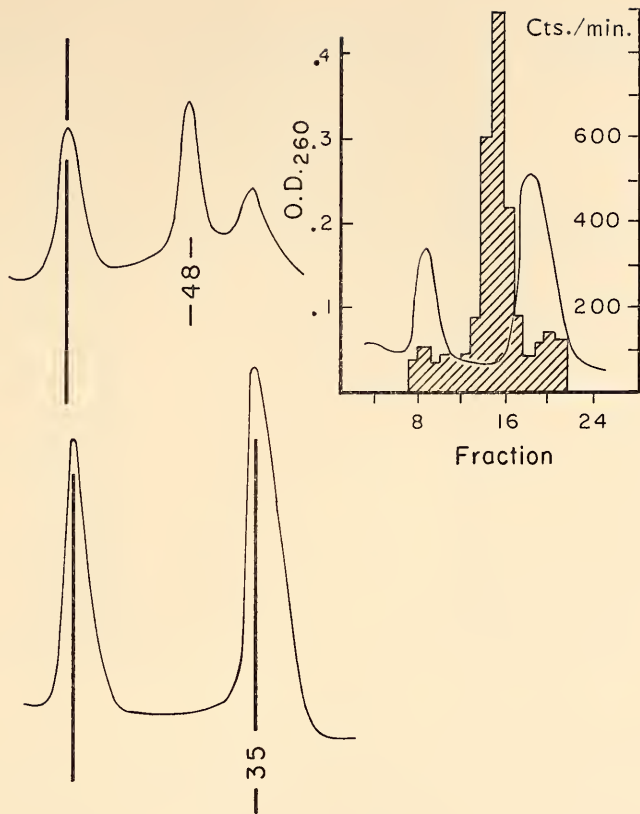


Fig. 5. Partial purification of *Artemia* rDNA by preliminary centrifugation of bulk native DNA in CsCl. Optical density (solid line) and hybridization (hatched area) profile for DNA centrifuged to equilibrium in the preparative centrifuge (Spinco angle rotor No. 65) (upper right). Densitometric tracings of an analytical ultracentrifuge photograph of DNA taken from fractions 14–16 of a preparative gradient such as shown. The enriched fraction has a buoyant density of 1.708 (48% GC) compared to the bulk DNA density of 1.695 (35% GC) (upper left). Densitometric tracings of unfractionated *Artemia* DNA showing no evidence of the rDNA satellite. Both analytical profiles include a density marker (*M. lysodeikticus* of $\rho = 1.731$) (lower left).

mammals and birds in general hybridize with the lowest amount of *X. laevis* rRNA. Most amphibian DNAs hybridize to about the same extent as *X. laevis* DNA, while the DNAs from invertebrates have in general a larger fraction of their genome homologous to rRNA than does *X. laevis* DNA. Of the organisms examined, fungi and higher plants appear to have the largest fraction of their genome present as rDNA, in some cases exceeding 1%.

THE EXTENT OF HOMOLOGY AMONG THE RIBOSOMAL GENES OF EUKARYOTES

Competition experiments have been carried out to determine the degree of homology between distantly related organisms. The effectiveness with which large excesses of cold heterologous rRNA can reduce the hybridization of (^3H)-rRNA with its homologous DNA is a measure of homology between the RNA preparations. The sensitivity of this assay is increased by preliminary centrif-

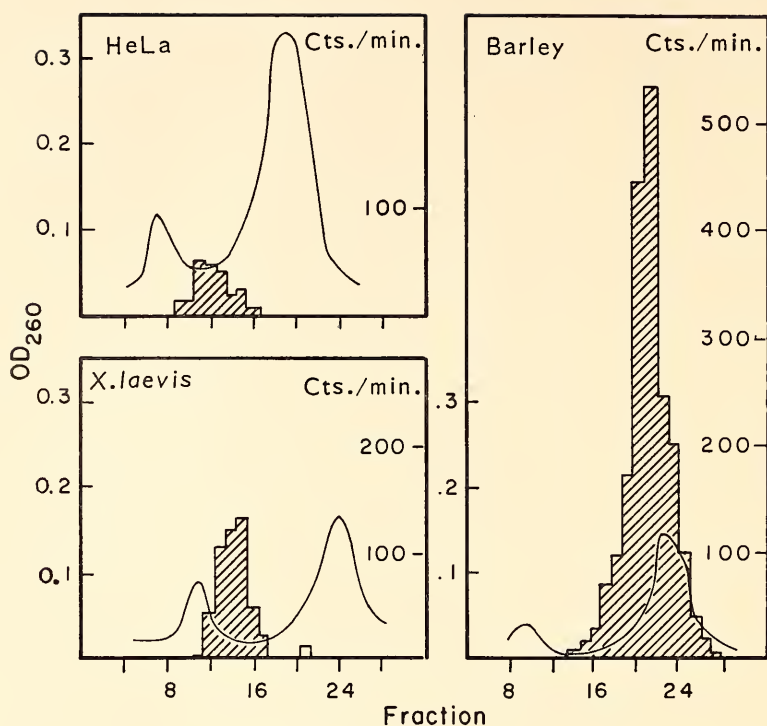


Fig. 6. Hybridization profiles of *X. laevis* rRNA with DNA of different organisms. The hybridization profile (hatched area) was determined by denaturing the DNA in each fraction with alkali, neutralizing the solution, trapping the DNA on Millipore filters by filtration, then incubating all of the filters with 0.1 $\mu\text{g}/\text{ml}$ of radioactive rRNA. The same concentration of *X. laevis* rRNA was used for the DNA of all organisms.

ugation of the DNA in CsCl and hybridization of the rRNA mixtures with the fractionated DNA on filters. Figure 7 illustrates the effectiveness with which mouse, yeast, and *M. lysodeikticus* rRNAs compete with (^3H)-*X. laevis* rRNA for *X. laevis* rDNA. Mouse rRNA is almost as effective as *X. laevis* rRNA in competitive ability. However, rRNAs from *Tetrahymena*, tobacco, and yeast compete with 37%, 52%, and 50% of the *X. laevis* rRNA, respectively. *M. lysodeikticus* rRNA does not compete in this reaction. Similar results have been obtained in competition experiments using other organisms as a source of both the

DNA and the radioactive rRNA. The results of these preliminary studies indicate that base sequences which exist in common between organisms as distantly related as higher plants and higher animals may be quite large. Competition experiments involving the rRNAs from more than one organism suggest that some sequence homologies may exist in common among most if not all eukaryotes. If this is true, then it seems likely that there are some sequences in ribosomal RNA which are sufficiently important to the functioning of the ribosome to have been retained throughout the evolution of eukaryotes.

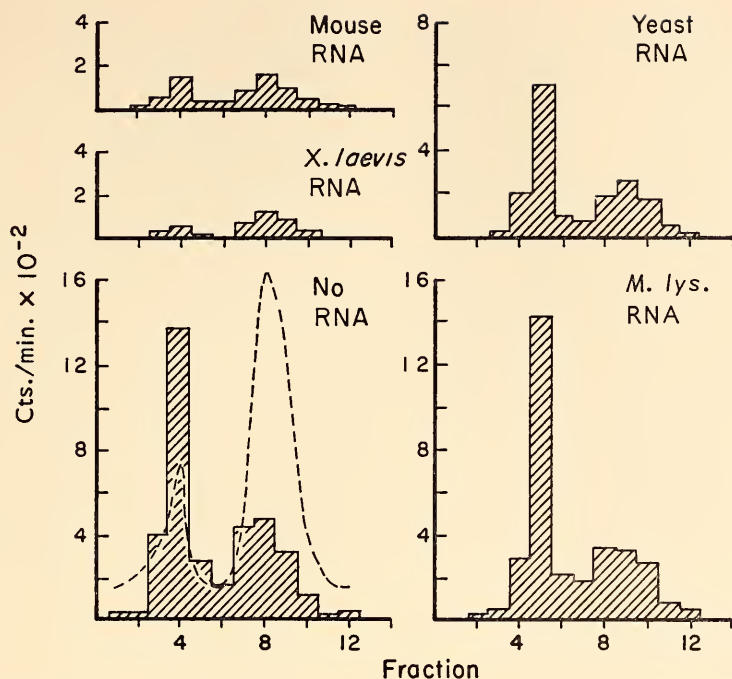


Fig. 7. Effectiveness with which heterologous rRNAs compete with radioactive homologous (*X. laevis*) rRNA for hybridization sites on *X. laevis* DNA. The dashed line in the "No RNA" treatment indicates the optical density profile of *M. lysodeikticus* marker and native *X. laevis* DNA. The profile is the same for each treatment and represents 50 μ g of DNA. Each of the gradients indicated was hybridized with an identical amount of radioactive *X. laevis* rRNA. Where indicated, 100 times the amount of radioactive rRNA was added as unlabeled competitor.

SYNTHESIS OF RIBOSOMAL PROTEINS IN *XENOPUS LAEVIS* EMBRYOS

R. L. Hallberg

In order to determine whether ribosomal proteins are being synthesized by *X. laevis* embryos when no new ribosomes are assembled, it was necessary to have an assay for ribosomal proteins which was independent of their presence in the ribosomal particle. In the past two annual reports (*Year Book 65*, pp. 515-517; *Year Book 66*, pp. 589-590; reprint pp. 17-18), we described techniques for characterizing ribosomal proteins from unfertilized eggs of *X. laevis*. These techniques now form the basis of an assay for these proteins which does not require the isolation of ribosomes or their subunits,

but rather permits the extraction and isolation of these proteins from the entire complement of cellular protein of embryos at any stage of development. This assay has been used to determine whether the proteins are synthesized at times when no ribosomal RNA is synthesized, namely, during early cleavage stages of normal embryos and during posthatching stages of anucleolate (0-*nu*) embryos.

To establish the assay conditions, the following experiment was performed to see how ribosomal proteins would behave when mixed with total embryo protein and then purified by methods devised for

isolated ribosomes (see *Year Book 66*, pp. 589-590; reprint pp. 17-18). Radioactive (^{14}C -leucine) large ribosomal subunits purified from extracts of cultured adult *Xenopus* kidney cells were cohomogenized with several hundred stage 44 *X. laevis* tadpoles in 8 M urea-2 M LiCl. The small amount of cultured cell ribosomes made up less than 5% of the total ribosome population. After removal of nucleic acids and lipids, and reduction of disulfide bonds, the remaining protein (80% of the embryo protein, 93% of the radioactive ribosomal proteins) was fractionated on a carboxymethyl cellulose (CMC) column. Figure 8 shows the degree of separation that is achieved between the bulk embryo protein (O. D.) and ribosomal proteins (cts/min). Calculations based on recovery values for

total protein and ribosomal proteins and on estimates of the amount of ribosomal proteins per embryo (about 4% of the total protein) indicate that about one third of the protein in the region of the gradient eluate marked D is ribosomal.

Fractions A-D from the CMC eluate were electrophoresed on acrylamide gels to identify individual ribosomal proteins. The gels were stained, sliced, dried, and autoradiographed according to the method of Fairbanks, Levinthal and Reeder. The amount of radioactive ribosomal protein added to the embryos was too low to be detected by stain on acrylamide gels. However, individual embryos at the stage of development used contain about 8-10 μg ribosomal protein. Since this represents about 4% of their total protein, there is sufficient "carrier" non-

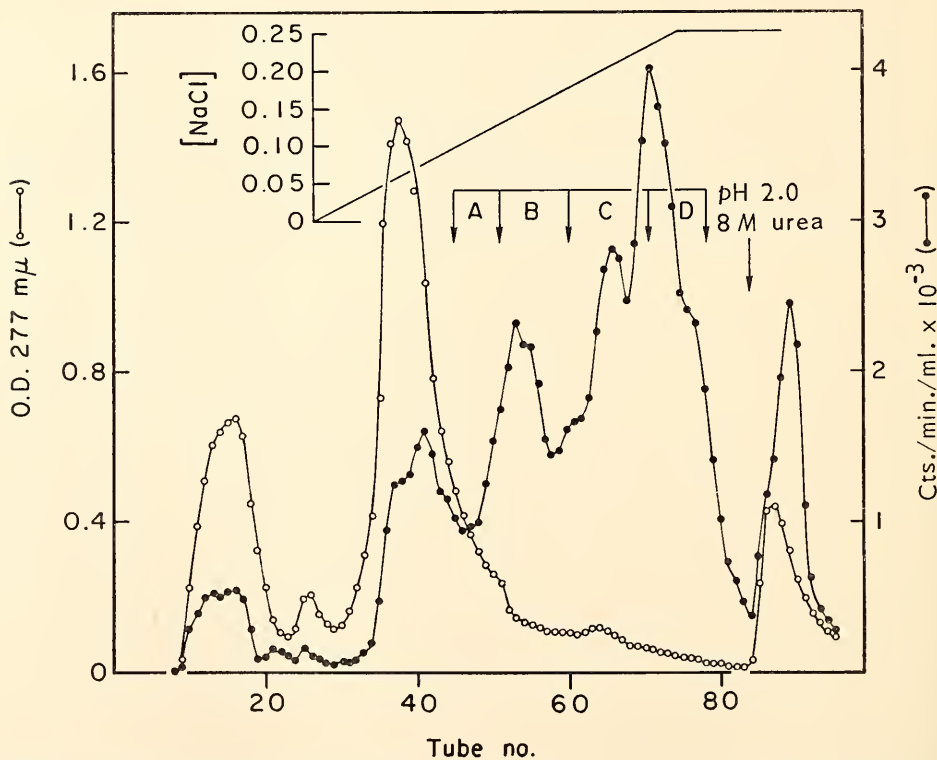


Fig. 8. Carboxymethyl cellulose (CMC) chromatography of radioactive protein derived from the large ribosomal subunit of *X. laevis* cultured kidney cells and total protein from *X. laevis* tadpoles. The purified subunits were mixed with whole tadpoles and the protein isolated together.

radioactive protein from the embryos themselves to give stainable bands on acrylamide gels. Plate 1 shows the stained gel patterns next to the autoradiograms obtained from each. In all 4 gels, stained bands are present which exactly coincide with the radioactive ribosomal proteins detected by autoradiography. In gel D a majority of the stained bands are radioactive. There are only two obvious exceptions (lines). The percentage of the total proteins applied to the gels which actually enters the gels and makes up the stainable band patterns seen in Plate 1 has not been measured. However, the radioactive bands consist of more than 95% of the radioactive protein which was applied to the gels. The identification of ribosomal proteins in these gels (especially those in gel D) serves as an assay for ribosomal proteins extracted directly from total cell homogenates.

The synthesis of ribosomal proteins was studied in cleaving embryos which had been labeled with $^{14}\text{CO}_2$ until they were late blastulae, before the onset of ribosomal RNA synthesis. The embryos were washed several times and then homogenized in 8 *M* urea-2 *M* LiCl and processed as before. Figure 9 is the CMC column elution profile of the cleavage proteins. The pattern of optical density is similar to patterns seen for later stage embryos with one noteworthy exception. Tadpole proteins show a small but reproducible optical density peak which elutes at about 0.19 *M* NaCl and which is not present in unfertilized eggs, cleavage, or gastrula stage embryos. However, the radioactivity profile of the cleavage gradient contains a large peak of radioactive protein which elutes at this same region (C) of the gradient.

Plate 2 shows the electropherograms

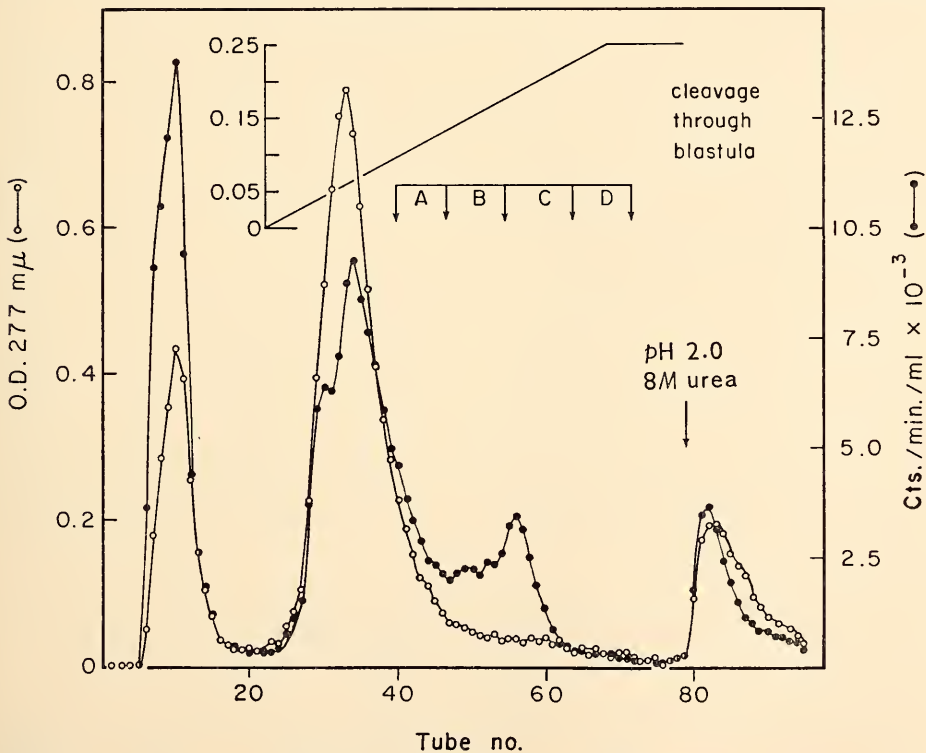


Fig. 9. CMC chromatography of total protein extracted from radioactive cleaving embryos.

and autoradiograms of the proteins from regions A–D of the cleavage fractionation. In the electropherogram of gel C the two darkly staining bands present in later stage embryos (see Plate 1) are missing. However, the autoradiogram shows that these two bands are very radioactive and represent about 80% of the total protein in region C. This represents at least 8% of the total protein being synthesized by the cleavage stage embryos. Although other bands are radioactive, 10 of the approximately 15 bands identified before as ribosomal proteins have little or no radioactivity associated with them. Our conclusion, based on quantitative measurements of autoradiograms, is that less than 0.05% of the protein synthesized during cleavage and blastulation in *X. laevis* embryos is ribosomal protein. This is to be contrasted with stage 44 embryos which synthesize 3–4% of their protein as ribosomal proteins.

Cleaving embryos which do not synthesize rRNA do not synthesize detectable amounts of ribosomal protein. However, would 0-*nu* embryos synthesize ribosomal protein at development stages when normal embryos are synthesizing these proteins and assembling ribosomes? Sibling embryos of mixed genotype were raised together and labeled twice with $^{14}\text{CO}_2$. One pulse was given for 6 hours at stage 35–36 when the 0-*nu* embryos appear normal. The second pulse was given for 8 hours at stage 39–40 when 0-*nu* can first be distinguished morphologically from the controls (1-*nu* and 2-*nu*). One day later the 0-*nu* embryos were identified by morphological criteria and separated from control embryos which had developed to stage 42.

About 500 0-*nu* and 500 control embryos were homogenized in small volumes of reticulocyte standard buffer (RSB). About 20% of each homogenate was used for an analysis of ribosomal subunits. The remainder of the homogenate was brought to a final concentration of 8 M urea–2 M LiCl and the resulting solutions

processed as described before. The analysis of the ribosomal subunits was carried out to determine if the 0-*nu* embryos were contaminated by 1-*nu* or 2-*nu* embryos. The upper limit of contamination of 0-*nu* embryos by 1-*nu* or 2-*nu* embryos was less than 3%. CMC chromatography was carried out by the remaining total protein of both 0-*nu* and control embryos. Although elution patterns differed quantitatively, there were no significant qualitative differences. Identical regions were pooled for electrophoresis. All samples were concentrated together and dialyzed in the same container. The radioactivity in each dialysate was measured, and electrophoresis was carried out on pool fractions of A–D of the two eluates using aliquots which contained identical amounts of radioactive protein. The electropherograms and autoradiograms of 0-*nu* and control proteins from regions C and D are shown in Plate 3. Whereas the bands identified previously as ribosomal proteins are radioactive from control embryos, their counterparts extracted from 0-*nu* embryos were not labeled. This is particularly striking in the gel containing the protein from region D of the CMC column. Quantitative measurements of autoradiograms of this gel show that 0-*nu* embryos could not have accumulated more than 5% of the specific ribosomal proteins synthesized by control embryos. In contrast the 0-*nu* embryos incorporated 70% as many counts as did the control embryos into the two darkly stained bands in gel C. Whether any of the marginally resolved or unresolved ribosomal proteins are synthesized is unknown. However, the 0-*nu* embryos do not accumulate and presumably do not synthesize at least 10 out of approximately 15 proteins which have been identified as components of the large ribosomal subunit.

Conclusions regarding the synthesis of ribosomal proteins must be tempered by the following considerations. If incorporation of newly made ribosomal proteins into mature ribosomes involved some

modification in their primary structure, newly synthesized "precursor" molecules would go undetected, since their chromatographic and electrophoretic properties would most likely be different from "mature" ribosomal proteins. Secondly, these conclusions are based on a select group of large subunit proteins. Finally, the techniques are not sensitive enough to

rule out synthesis and rapid degradation of these ribosomal proteins. The above criticisms notwithstanding, it appears that ribosomal protein synthesis is under close coordinate control with the synthesis of ribosomal RNA. The mechanism of this control which would account for the coordination both during cleavage and in the 0-*nu* embryos is unknown.

SYNTHESIS OF COLLAGEN DURING EMBRYOGENESIS IN *XENOPUS LAEVIS*

Merry C. Schwartz and Donald D. Brown

A study of the synthesis of collagen during embryogenesis in *Xenopus laevis*, which was initiated in 1965 in collaboration with Drs. Howard Green and Burton Goldberg at New York University, has now been concluded. At least a 700-fold increase in the differential rate of collagen synthesis occurs between early cleavage and the feeding tadpole stage (see *Year Book 66*, pp. 590-592). The first unequivocal synthesis of collagen was detected at gastrulation. Furthermore, the low counts then tabulated as hydroxyproline synthesis during cleavage now appear to be nonspecific contaminants, thus suggesting that the synthesis of collagen may be strongly repressed prior to gastrulation.

However, the collagen assay employed detects collagen polypeptides only after the addition of hydroxyl groups by collagen hydroxylase. In order to ascertain whether the developmental curve thus obtained reflects a change in the synthesis of collagen polypeptides or a progressive increase in collagen hydroxylase activity, the following experiments have been performed:

1. Extracts of unfertilized eggs, cleavage stage embryos, and tadpoles were all assayed directly for collagen hydroxylase activity using as substrate subhydroxylated collagen polypeptides which had been extracted from fibroblasts cultured in the presence of hydroxylase inhibitors. The previously observed increase in the differential rate of collagen synthesis can not be attributed to a change in collagen hydroxylase activity, since extracts from all stages showed comparable levels of this enzyme.

2. L-proline- H^3 -labeled cleavage stage embryos were assayed for the presence of nonhydroxylated collagen peptide chains using a collagen hydroxylase from cultured fibroblasts. No such precursors could be detected.

These additional experiments enable us to conclude that the developmental curve previously presented for collagen synthesis (*Year Book 66*, p. 591; reprint, p. 18) actually represents the dramatic increase in the differential rate of collagen synthesis during development.

NUCLEIC ACID METABOLISM DURING OOGENESIS AND EMBRYOGENESIS IN *URECHIS CAUPO*

Merry C. Schwartz

The embryogenesis of *Urechis caupo*, a marine echiuroid worm from the Pacific, was described by Newby in 1940.

Several features of oogenesis and embryogenesis make it of special value for biochemical studies. *Urechis* undergoes

spiral cleavage, a pattern which has been found to correlate with a mosaic type of egg. The sea urchin and the frog, both of which have been extensively studied, are samples of the regulative type of development. Therefore, the biochemical studies of *Urechis* development initiated in the past few years provide a further molecular comparison between mosaic and regulative development.

Moreover, gametogenesis in *Urechis* is nonseasonal, thus providing an uninterrupted supply of sperm and eggs at all stages of gametogenesis. Worms shipped by air approximately once a month from the coastal area north of Stanford, California, have been maintained in Instant Ocean synthetic seawater at 12–14°C. Greater than 90% normal development is obtained routinely. The oocytes and embryos at all stages take up radioactively labeled protein and nucleic acid precursors, and the application of standard nucleic acid extraction procedures meets with no special difficulties.

The oocytes mature while suspended in the coelomic fluid and free of any cellular associations. When mature they are collected and stored in three pairs of storage sacs from which they can be released via pores which open onto the surface of the worm. A mature female may contain

more than 25 milliliters of packed eggs (approximately 10^7 eggs) in these sacs, and these can be collected by dissection or by gently expanding the external pores with a blunt probe.

Our studies during the past year have characterized the nucleic acid synthesis throughout embryogenesis as well as in the mature oocyte. The mature oocytes (about 120 microns in diameter) are in arrested prophase of the first meiotic division and contain a large nucleus (germinal vesicle) with a single prominent nucleolus. The mature oocytes are metabolically active and continue to synthesize sRNA and rRNA (Fig. 10). They contain approximately 15 μg of RNA, and the ratio of 8–10 sRNA molecules per ribosome is similar to that of most somatic tissues.

Fertilization is followed by the meiotic reduction divisions which are characterized by the dissolution of the nuclear membrane and the nucleolus within fifteen minutes of fertilization, and the emission of both polar bodies within 45 minutes (18–20°C). We are currently seeking to characterize RNA synthesis during meiosis and first cleavage, as well as to determine the time at which the zygote's DNA is replicated for the first cleavage division.

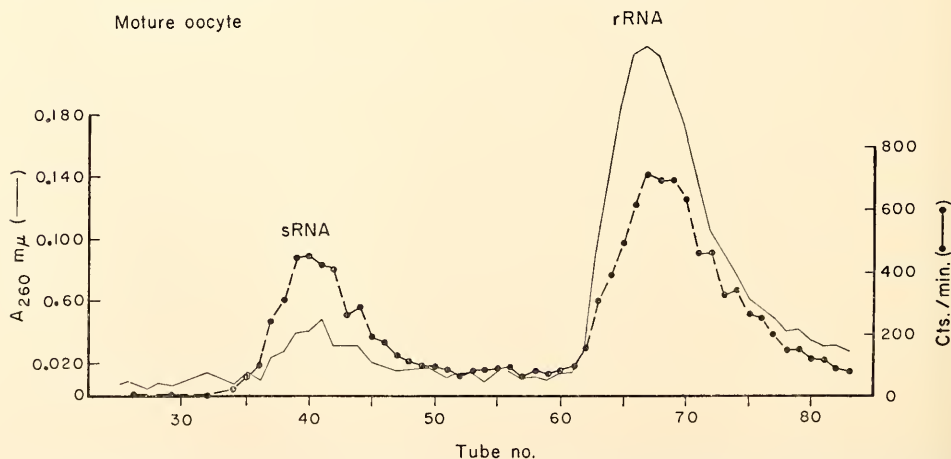


Fig. 10. Synthesis of sRNA and rRNA in mature oocytes of *Urechis caupo*. Oocytes were pulsed with guanosine- H^3 for 44 hours. The total nucleic acid fraction was applied to an MAK column and eluted with a linear salt gradient.

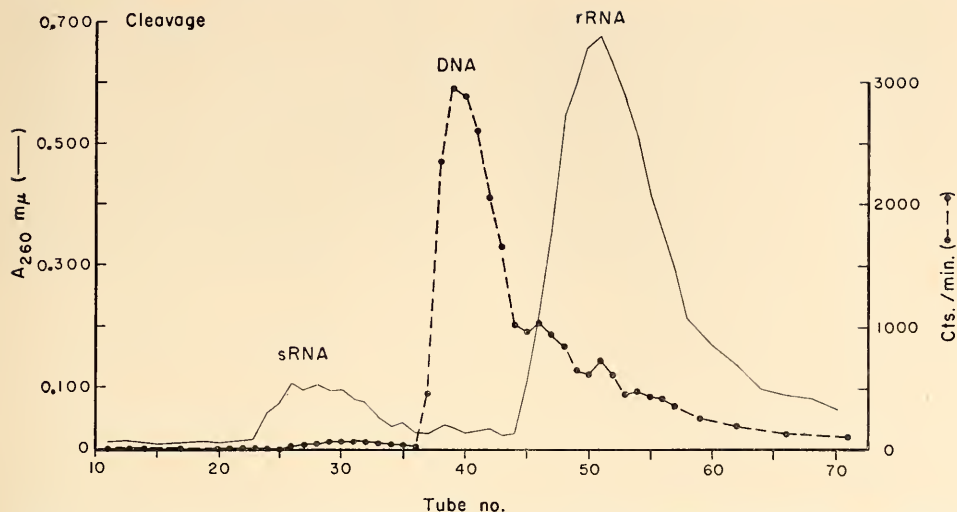


Fig. 11. Synthesis of nucleic acids in cleaving embryos. Embryos were pulsed in phosphate-free seawater with phosphoric acid- P^{32} from fertilization to four hours postfertilization (32-cell stage). The total nucleic acid fraction was treated as described for Fig. 10.

During cleavage the pattern of nucleic acid synthesis is virtually a reversal of that observed in the oocyte: i.e., the syn-

thesis of DNA predominates (Fig. 11). Seven to eight hours after fertilization the embryo is composed of 64 cells, and

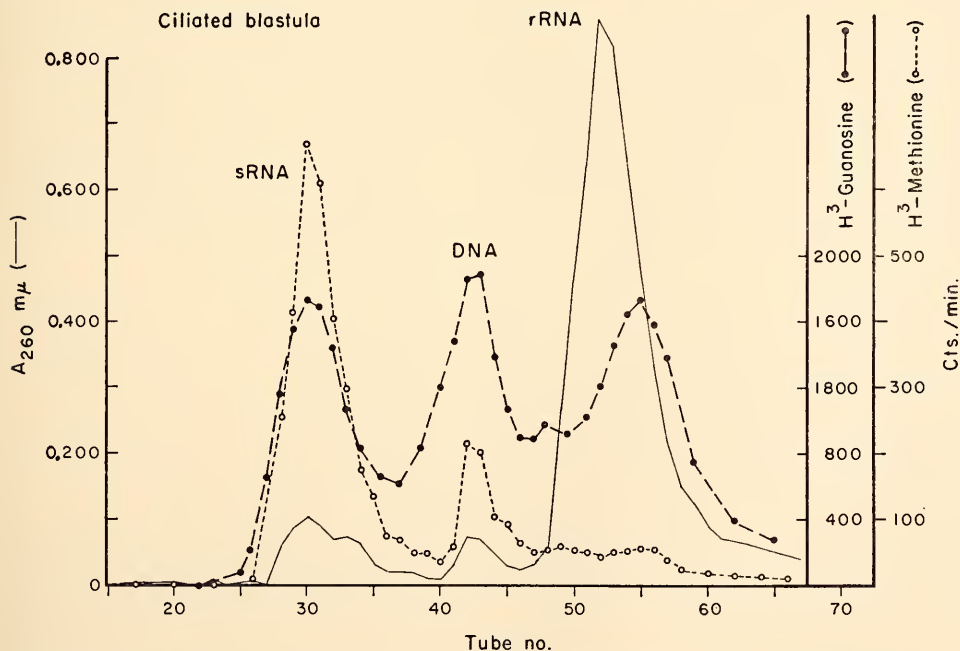


Fig. 12. Synthesis of nucleic acids in ciliated blastulae. Embryos were pulsed with either guanosine- H^3 or L-methionine-methyl- H^3 from 7 to 11 hours postfertilization (64 to 92 cells). The total nucleic acid fractions from each sample were extracted and fractionated separately, and the radioactivity profiles obtained have been superimposed.

hatches as a ciliated swimming blastula. While continuing DNA synthesis, the embryo first displays both the synthesis and methylation of sRNA in the absence of rRNA synthesis (Fig. 12). Considerable labeling occurs also in an RNA fraction which elutes from an MAK column at slightly higher salt concentration than does rRNA, i.e., in the same region as ribosomal precursor RNA. However, due to the absence of methylation in these molecules and their behavior in sucrose density gradient centrifugation, they are tentatively identified as heterogeneous DNAlike RNAs (dRNA).

Approximately 16 hours after fertilization when the 148-cell embryo has begun to gastrulate, the synthesis and methylation of rRNA resumes. Its synthesis increases relative to that of both DNA and sRNA as the embryo develops into a trochophore larva and begins to feed (Fig. 13).

Thus several features distinguish the patterns of nucleic acid metabolism in oocytes and embryos of *Urechis* from those previously described for *Xenopus*. First, unlike the amphibian oocyte, the *Urechis* oocyte does not become dormant, as evidenced by its continued RNA synthesis. In both organisms the synthesis of sRNA resumes at late blastula and is followed at gastrula by the onset of rRNA synthesis. The synthesis of considerable heterogeneous RNA is demonstrable in both systems throughout development before it is obscured by increased synthesis of rRNA in the larval stages.

However, once sRNA synthesis is initiated in a *Xenopus* embryo, the embryo doubles its sRNA content with each doubling of its cell number. This increase in sRNA content prior to any significant increase in the embryo's ribosome content serves to raise the sRNA per ribosome ratio from less than one in the egg to

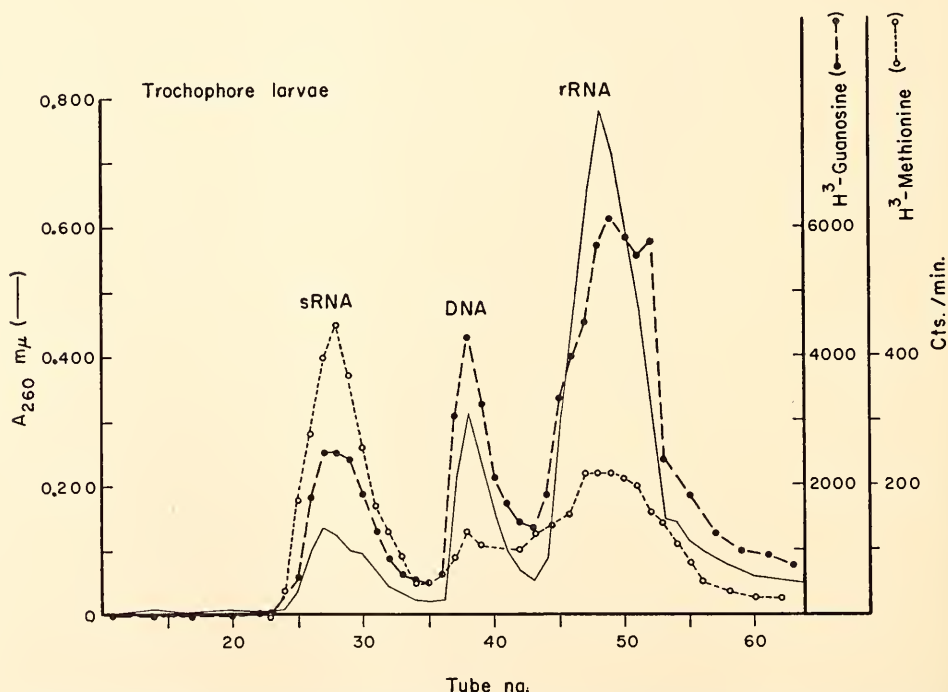


Fig. 13. Synthesis of nucleic acids in trochophore larvae. Trochophore larvae were pulsed and extracted as described in Fig. 12, from 26 to 30 hours postfertilization.

approximately 10. No such imbalance exists in the *Urechis* oocyte, and indeed it was found that the sRNA content of a *Urechis* embryo increases by only about 50% by the trochophore larval stage.

The investigations summarized above have surveyed the synthesis and methylation of DNA and three classes of RNA (sRNA, rRNA, and dRNA) in the mature oocyte and during embryogenesis in

Urechis caupo. The metabolism of sRNA throughout this period is of particular interest because of the postulated role of sRNA as a regulator of gene action at the level of translation. Therefore we are now investigating the developmental fate of the oocyte's sRNA, as well as comparing qualitatively the populations of sRNA molecules synthesized in the oocyte and in the trochophore larvae.

HISTONE SYNTHESIS DURING DEVELOPMENT

H. E. Kasinsky

It is of great interest to correlate the synthesis of nuclear proteins with that of nuclear DNA and RNA. Oogenesis and embryogenesis provide periods when the synthesis of these components varies greatly. Does the synthesis of nuclear proteins such as histones coordinate with cell division and DNA synthesis or does the oocyte store histones for use in nuclei made during cleavage stages?

The plan for this work includes studying the radioactive proteins synthesized by oocytes and embryos of *Xenopus laevis*. Extraction of total protein from the embryo and separation of labeled histones by cation-exchange chromatography or electrophoresis on polyacrylamide gel should enable us to compare the histone pattern of embryos at differ-

ent stages with that of adult tissues, such as liver and erythrocytes, in order to look for qualitative changes. Berlowitz and Birnstiel (*Science*, 156, 78, 1967) attempted to isolate nuclei from *Xenopus* embryos at different stages and extract histones from this organelle. However, the acid extraction procedure for isolating histones might not be equally applicable at every stage of development, nor are the "nuclei" obtained experimentally necessarily the same at every stage. An examination of the histones present in the total protein of the embryo, extracted by methods similar to those of Hallberg (*Year Book* 66, pp. 589-590; reprint pp. 17-18), should overcome such difficulties. These investigations are now in progress.

STUDIES ON MITOCHONDRIAL NUCLEIC ACIDS

A SIZE DIFFERENCE BETWEEN THE MITOCHONDRIAL DNAs OF URODELE AND ANURAN AMPHIBIA

D. R. Wolstenholme, *University of Chicago*;
and I. B. Dawid

In several laboratories, studies of mitochondrial DNAs from different vertebrate sources revealed that the size of the circular molecules was remarkably constant. Length measurements of electron micrographs of spread and shadowed preparations revealed few differences be-

tween mitochondrial DNAs from frogs, chickens, and ducks, and those from several mammalian species. Those differences that were seen might have arisen by slight modifications in the spreading technique, which is known to cause changes in the linear density of DNA.

We have studied mitochondrial DNAs from the urodele species *Siredon mexicanum* and *Necturus maculosus* and compared them with mitochondrial DNAs from the anurans *Rana pipiens* and *Xenopus laevis*. DNA was obtained from

ovarian oocytes as described earlier (*Year Book 65*, p. 518 and *Year Book 66*, p. 592; reprint, p. 20). Both urodele species possess circular mitochondrial DNA with a contour length of about 4.8 microns, while mitochondrial DNA from the anuran species was measured at about 5.8 microns in the present experiments. To ascertain that this difference was real and not due to variability between separate spreadings, the mitochondrial DNA samples were mixed in all combinations of two, then spread and measured. In mixtures of the two anuran or the two urodele DNAs all molecules fell into single length classes, but when an anuran DNA was mixed with a urodele DNA two nonoverlapping classes were always found.

In addition to the size difference, a difference was also found in the buoyant density of urodele and anuran mitochondrial DNAs. The density data indicate a content of 36% guanylic and cytidylic acid in *S. mexicanum* and *N. maculosus* DNA as compared to 43% in *R. pipiens* and *X. laevis* DNA. It should be interesting to investigate the way in which this difference in size and composition arose, especially since an answer may give a clue to the remarkable overall size constancy of the mitochondrial DNA of animals.

RNA IN FROG OOCYTE MITOCHONDRIA

I. B. Dawid, with the assistance of M. Rebbert

The presence of DNA in mitochondria and the correlation of some forms of cytoplasmic inheritance with these particles in yeast and *Neurospora* suggest that mitochondria contain genetic information. The nature of the products specified by this information and the mechanism by which such products are formed are not yet clearly understood. Mitochondria apparently possess inherent protein-synthesizing capabilities and it is believed that they also possess a special type of ribosomal particle to support such ac-

tivity. If this is true, mitochondria should contain ribosomal-type RNAs which might have different properties from the RNAs in the cytoplasmic ("usual") ribosomes. In yeast and in *Neurospora* mitochondria, the presence of two ribosomal-like RNA species has been demonstrated in the laboratories of Luck, Linnane and Noll; these RNAs are smaller than the

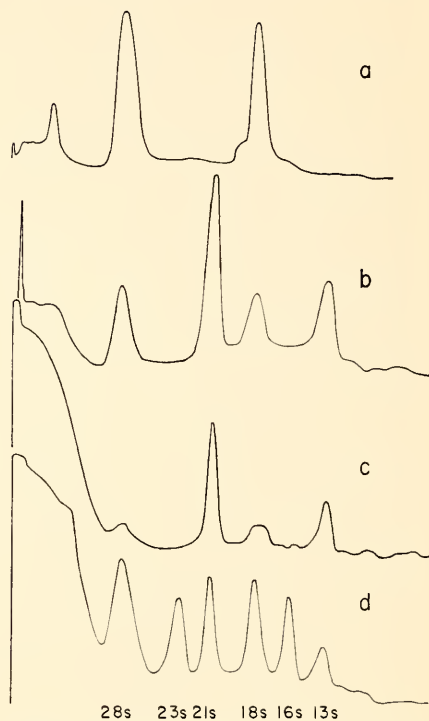


Fig. 14. Electrophoresis of RNA on polyacrylamide gels. Separation was carried out for 4 hours at about 10 V/cm and the gels were scanned in ultraviolet light. Under these conditions transfer RNA has run off the gel. The origin is to the left; ultraviolet-absorbing material at or near the origin consists of DNA and contaminating uncharged substances which diffuse into the gel. RNA was prepared from (a) *X. laevis* cytoplasmic ribosomes; (b) *X. laevis* oocyte mitochondria; (c) mitochondria treated with ribonuclease; (d) a mixture of cytoplasmic, mitochondrial and *E. coli* ribosomal RNA. At the bottom of the figure the RNA components are identified by their sedimentation coefficients; those for mitochondrial RNA were calculated from the electrophoretic mobility.

cytoplasmic ribosomal RNA components. Using the oocytes of *Xenopus laevis*, a similar situation could be demonstrated in animal mitochondria.

Electrophoresis on polyacrylamide gel, established as a method for the analysis of high-molecular-weight RNA by Loening, allows a much better resolution of RNA molecules of slightly different sizes than zone sedimentation in sucrose gradients. We have used the electrophoretic method to analyze the RNA extracted from frog oocyte mitochondria, which were prepared in the same way as in the experiments on mitochondrial DNA (see *Year Book* 65, p. 518). RNA prepared from cytoplasmic ribosomes of the same tissue was used for comparison; the two characteristic components of ribosomal RNA (28S and 18S) were found (Fig. 14a). In mitochondrial RNA (Fig. 14b) the same two components were observed, as well as two additional species of higher electrophoretic mobility, i.e., lower molecular weight. The 28S and 18S RNA components in the mitochondrial extract are presumably contaminating cytoplasmic material, since most of them could be removed by treatment of the intact

mitochondria with ribonuclease (Fig. 14c). The mitochondrial RNA itself is not degraded by this procedure, probably because the ribonuclease cannot enter the particle. Frog mitochondrial RNA is also smaller than ribosomal RNA from *Escherichia coli*; the electrophoretic method allows the separation of all six RNA species considered in a single run (Fig. 14d). A relation between size and mobility established by Loening allows us to assign a molecular weight of 9.4×10^5 to the larger, and 4.5×10^5 to the smaller mitochondrial RNA component. The two components of mitochondrial RNA have a guanylic plus cytidylic acid content of about 40%, very different from that of the cytoplasmic ribosomal RNA (63%). It may be significant that the composition of mitochondrial RNA is close to that of mitochondrial DNA.

These results suggest that animal mitochondria contain ribosomal-like RNA of distinct properties. If this suggestion can be corroborated by additional experiments it will support our belief that animal mitochondria possess an endogenous and distinct protein-synthesizing machinery.

CLONAL CULTURE OF DIFFERENTIATED CELLS FROM MAMMALS: RAT LIVER CELL CULTURE

H. G. Coon

(with the technical assistance of Isabelle Williams)

The variety in number and morphology of the chromosomes in the karyotypes of mammals makes them more suitable markers for studies of cellular hybridization than are the karyotypes of domestic birds. Furthermore, men and mice may soon become the best described material for genetic study in higher animals, apart from the insects. These were the principal reasons for shifting our attention from the culture of avian cells to the culture of differentiated cells from laboratory mammals. It has proven remarkably easy to adapt the methods of clonal culture of differentiated cells to the tissues of rats,

rabbits, hamsters, and, hopefully, soon also to man. The techniques we have used have been adapted from those originated in our laboratory for clonal culture of chick embryo cells and have been described in detail in a recently published compendium of methods edited by Wilt and Wessells. Cell suspensions were prepared by sequential trypsinization (0.2%) and collagenase (0.4 mg/ml) in the presence of 2% chicken serum (CTC). Cultures were nourished by our modification of Ham's F12 medium supplemented with 5% selected fetal calf serum which was especially tested for plating efficiency

and differentiation of chick cartilage cells and rat liver cells.

We have enjoyed the collaboration of Rechsteiner in investigating a variety of tissues from infant rats (2–5 weeks old). Salivary gland, thyroid, liver, kidney, pancreas, and spleen have yielded epithelial cell colonies as well as typical fibroblastlike colonies from dilute single cell suspensions. Skeletal muscle and cardiac muscle, as well as sternal and rib cartilage, have produced differentiated colonies which behave like their counterparts from avian tissues. We believe that these tissues will all provide excellent sources of differentiated cells in clonal culture and will prove especially valuable for studies of their hybridization. Propagating hybrid strains have already been isolated between each of these cell types and the selectable strain of mouse L cells (Cl 1 D).

Of the tissues which produced colonies that appeared to be differentiated, we have chosen to concentrate first upon liver. Many attempts have been made to culture the parenchymal cells of mammalian liver. These attempts have varied from organ cultures showing zones of outgrowth of epithelial cells (Hillis and Bang) to cell cultures (Katsuta and Takaoka). However, cultures of this kind have either undergone very little growth while maintaining liverlike morphology and functions, or they have shown cell division with concomitant evolution of the cultures into populations of cells more typical of fibroblasts in morphology and function (Sato). Our cultures differ from these in that we have used very low initial density (10^4 cells/100-mm petri plate) and have obtained primary colonies from single cell suspensions with a plating efficiency varying from 0.1 to 1%. Under these conditions two principal kinds of colonies are formed: typical epithelial pavement cells, showing phase-dense cytoplasm and tightly packed nuclei, which appear very similar to the parenchymal cells of the liver (Plate 4) and a few large colonies of spreading

fibroblastlike cells which we interpret to be derived from a nonparenchymal component of the liver. Both of these cell types have been serially subcultured, yielding plating efficiencies of 10–20%. It has been verified that individual cells from the primary colonies do form colonies upon transfer, and thus they may properly be called clones.

Attempts to characterize the liverlike properties of these cells are now being made in our laboratory by radioimmuno-electrophoresis, assay of enzyme activities thought to be specific to liver, and tests for certain complex liver functions such as bile production and glycogen metabolism. Our results have already established that clonally purified lines of rat liver produce several of the normal serum antigens. Extracts of these cells exhibit activities of two liver enzymes, serum glutamicpyruvic transaminase (SGPT) and serum glutamic oxalacetic transaminase (SGOT) comparable (per milligram protein) to extracts of whole fresh rat liver. The cell strains from the liver which exhibit fibroblastlike morphology do not share these liverlike presumed parenchymal cell functions. The activities of other specialized enzymes are now being investigated in our clonal cell strains by a number of different laboratories long experienced in this exacting kind of work.

It has been difficult to construct a growth curve for liver cells because a variable number (30–60%) of the cells die each time the cultures are transferred. We suspect that the persistent connections which we see between neighboring cells are very tight and that in the process of making single cell suspensions from trypsinized groups of cells, many of the delicate cells are torn and die. However, from observations of small clones we are able to estimate that the average doubling time is approximately two days. We estimate that our oldest liver cell lines (now eight months old) have undergone about 80 doublings. They are still predominantly diploid. It is, perhaps, not

surprising that we find many tetraploids (1 to 5%) in the populations which have been passed as mass cultures, because polyploidy is common in normal liver. Clonally passed populations show a lower frequency of tetraploidy. Binucleate cells are frequently seen in both kinds of culture.

Considerable interest attaches to the study of differentiated liver cultures. Much of the work now done on the control of inducible enzyme synthesis in higher animals is done with perfused livers or short-term organ cultures of liver fragments. If it continues to be found that our cultures of liver cells possess many of the normal functions of the liver, then clonal culture will make a large simplification in many current research projects. If human liver cells can be cultured it might be possible for the first time to culture hepatitis virus and hasten production of a vaccine.

We find liver cells especially intriguing because they are among the most complex in the diversity of their known differentiated functions. Liver cells should provide a large number of functions for assay in somatic cell hybrids. A question of interest to cell biologists is the number of unrelated specialized functions that can occur in a single cell. One might ask whether all of the primary clones from a liver synthesize serum albumin as well as some other serum proteins or a liver-specific transaminase. One should be able to test the idea that a complexly functioning but largely homogeneous organ like the liver is composed of a mosaic of

cells, each pursuing one or at most a few among the many specialized synthetic functions. We are presently examining primary colonies and their subclones for evidence of difference in the synthesis of serum antigens.

We hypothesize that the reason for the difference between our liver cultures and the partially successful methods of liver culture previously reported is that our cells have been clonally purified virtually from the beginning of their life in culture. When we have tried to initiate mass cultures from freshly prepared suspensions of rat liver, we too have obtained cultures dominated by fibroblastlike elements. We have seen that small nests of the epithelial, parenchymalike cells die selectively in mass cultures as cell densities approach packed monolayers. Those cultures soon appear to contain only fibroblasts. On the other hand, clonally purified, parenchymalike cells can be maintained in densely crowded cultures without degeneration. These observations suggest that there are unanticipated interactions among different cell types derived from a single organ which seriously prejudice the persistence of differentiated function in tissue culture. Our experience with a number of different tissues of infant and adult rats implies that differentiated function may be relatively easy to maintain in clonal cultures or in cultures made homogeneous by cloning, but that mixed mass cultures often provide minimal opportunity for continued expression of differentiation.

AN ESTABLISHED CELL LINE OF FIBROBLASTS FROM GOOSE CELLS

*H. G. Coon and Isabelle Williams
(with the technical assistance of Virginia Hicks)*

The phenomenon of senescence in cell cultures has occasioned much interest since it was described by Hayflick as a regular feature of populations of primary

diploid human cell cultures. If a cumulative growth curve is kept for a cell population which is repeatedly transferred at constant initial density and al-

lowed to grow to saturation before the next passage, then unexpectedly a typical sigmoid growth curve is generated. After a rather constant number of passage generations in vitro the cells simply cease to grow; these live but nondividing cells are termed "senescent." The limited lifetime in culture of many primary diploid cell strains must be contrasted with the sudden adaptation to life in culture which can occur with the formation of a permanent established line of cells such as the famous HeLa or L cells. Ostensibly a minority of the cells transforms in culture and these cells usually show a gross karyotypic change. Hayflick has emphasized that the number of cell generations in culture is related to the onset of senescence.

Notorious among the animals whose cells become senescent quickly and reproducibly in cell culture are those from the embryos of the gallinaceous birds. Chicken heart fibroblasts are reported to have lives in cell culture of from the low estimates of 15 to 35 cell generations to extreme values of 40 to 55 cell generations for cloned populations of differentiated cells. The techniques vary but the consistent observation of a finite lifetime in culture is noteworthy. The gallinaceous birds differ from many vertebrates in that their cells are not known to form permanent cell lines in culture. The well-known example of the immortal line of chicken heart fibroblasts perpetuated by Alexis Carrel is now generally discounted because of an error in technique which could have continuously reinoculated the cultures with fresh cells. In spite of many diligent efforts to produce established avian cell strains, senescence usually occurs within 50 cell generations.

In the course of our survey to find avian species with distinguishable nuclear and chromosomal morphology (see *Year Book 66*) we found that cultures from embryonic domestic geese (*Anser anser*) were unusual in that senescence occurred much later than in other avian species.

Consequently, we decided to discover when in a series of continuous passages senescence might occur for goose cells under the same clonal culture conditions which were known to permit only fifty doublings of chicken cells. Figure 15 shows the cumulative growth curves of the sternal cells of several geese. Two of the three cell lines became senescent after only 65 generations, but one, CGBQ, has continued to grow well past 100 cell generations in culture. This has been considered indicative of the form of an "established cell line." At the time of this writing that cell line had undergone nearly 150 cell doublings during 30 passages by trypsinization in cell culture in the course of one year. Furthermore, a record of the karyotype of the cells has been made at each passage and as far as it can be determined from the preliminary examination an overwhelming majority of the cells have remained diploid.

Geese, like other gallinaceous birds, have karyotypes which are very difficult to analyze. Two thirds of their chromosomes are exceedingly small, microchromosomes, which cannot be counted reliably or told apart. However, the large chromosomes can be compared by conventional methods and these have been found to be normal in strain CGBQ. Goose cell cultures harbor more tetraploid cells than do chicken or turkey cultures. Furthermore, it must be emphasized that Hayflick's hypothesis of limited cell culture lifetime is restricted to diploid cells and diploidy cannot, in our opinion, be vouched for in this avian material.

The existence of an apparently established line of avian cells may prove a boon to workers in a number of fields. Avian viruses such as Rous sarcoma virus may prove to be grown and assayed with greater reliability on an established cell line than it is presently possible to achieve with primary whole embryo fibroblast cultures.

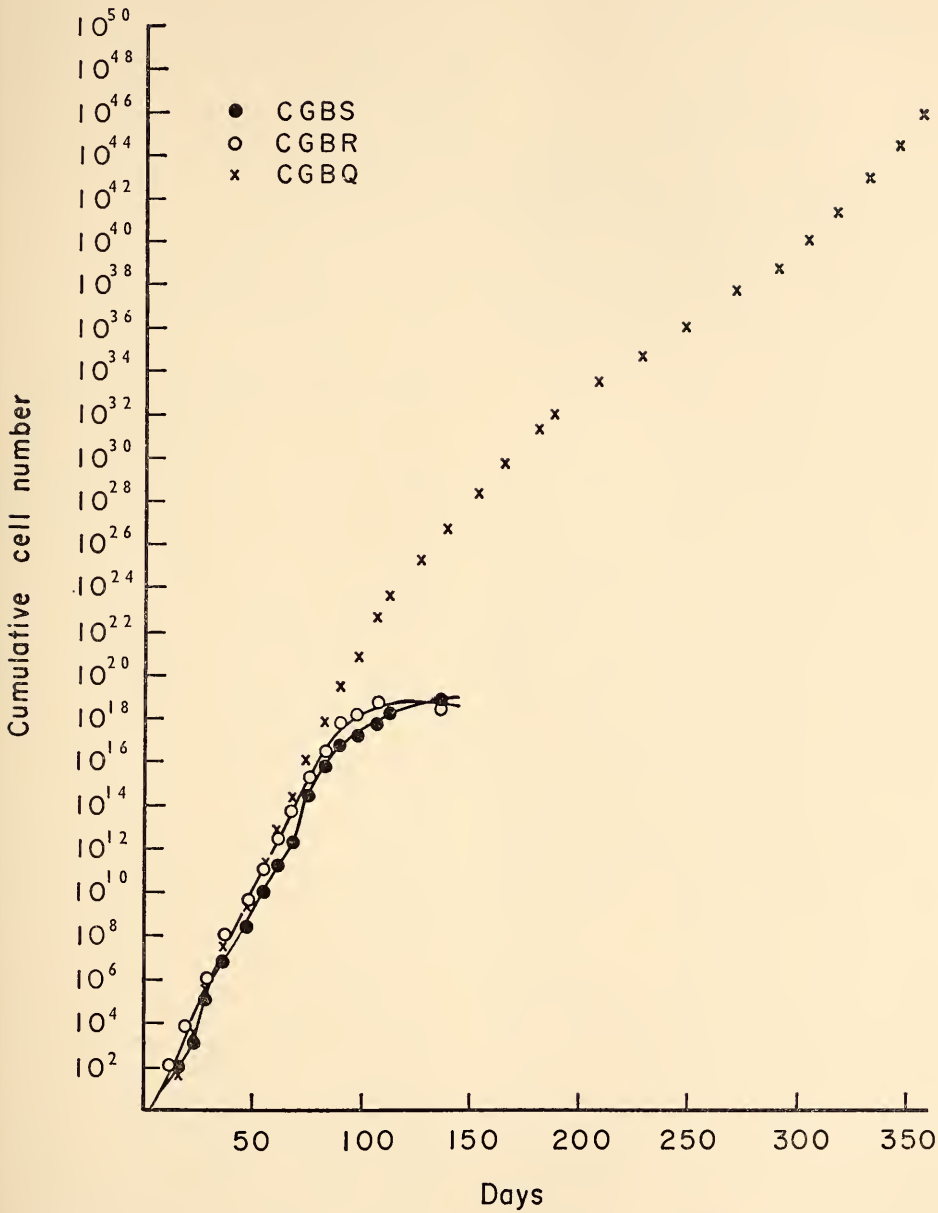


Fig. 15. Cumulative growth curves from the sternal cells of several geese, Q, R, and S. CGBR and CGBS became senescent after 65 cell generations. CGBQ has continued to grow for more than 150 cell generations.

STUDIES USING SOMATIC CELL HYBRIDS

THE PRODUCTION OF CELL HYBRIDS WITH
UV-INACTIVATED SENDAI VIRUS

H. G. Coon and M. C. Weiss
(with the technical assistance of
Isabelle Williams)

The report of Yerganian and Nell has been for several years the only instance of the successful production of somatic cell hybrids by fusion induced with inactivated Sendai virus. Our program (see *Year Book 66*) has been aimed at developing the technology of cell fusion with inactivated Sendai virus in order to produce hybrid cell strains between differentiated, normal diploid cells. It is necessary to distinguish between "heterokaryons," which consist of a single cytoplasmic mass containing two or more different nuclei, and "hybrid" cell strains, which are propagating cell lines containing the chromosomes from different parent cells within a single nucleus. Following the reasoning of Yerganian and Nell, it seemed that artificial induction of cell fusion should substantially assist the formation of propagating hybrid strains of the kind observed to occur as rare "spontaneous" events by Barski and Ephrussi. The conditions for the production of "spontaneous" somatic cell hybrids have been explored by Ephrussi and his colleagues using the selective techniques of Szybalski and Littlefield.

We have undertaken a systematic study of the influence of inactivated Sendai virus fusion upon hybridization of cells grown in medium which permits selective growth of hybrids. Hopefully, the information gathered from the study of this model system will indicate a strategy for achieving efficient hybridization between differentiated, normal diploid cells for which selective media do not exist. Our first experiments have attempted to demonstrate an effect upon the spontaneous hybridization or "mating rate" of selectable cells after their pretreatment with the inactivated virus reagent. We have studied first an example

of a fully selected cross between variants of the "L" cell (A9 and Cl 1 D), second, an example of a partially selected cross between Cl 1 D and rat liver cells, and third, an unselected cross between the clonally purified, diploid rat liver cells and freshly prepared suspensions of mouse liver cells.

*Sendai Virus-Assisted Hybridization
of the Fully Selectable Cell Lines
A9 and Cl 1 D*

Variants of the long-established mouse L cell of Earle have been used by Ephrussi and others to produce serially propagable somatic cell hybrids identifiable in the presence of marker chromosomes of both parents within the single hybrid nucleus. Both of the parental cell lines, A9 and Cl 1 D, are unable to grow in a medium containing a folic acid inhibitor, aminopterin. Because the two cell types have different enzyme deficiencies, a hybrid between the two cells will contain both of these essential enzymes and will grow in a medium containing the selective agent, aminopterin. Control experiments for "spontaneous" hybridization were done by mixing one million Cl 1 D and one million A9 cells in an 85-mm petri plate and incubating them for 24 hours (to permit attachment) before changing the medium to the selective medium containing aminopterin. After ten to fourteen days of culture in selective medium, the number of colonies per plate is counted. Under these standard conditions a "hybridization frequency" or spontaneous "mating rate" could be defined as the reciprocal of the smallest number of the least numerous parent which yielded an average of one hybrid colony per plate. If pretreatment of the parental cell suspensions with inactivated Sendai virus and the resultant fusion to yield heterokaryons were effective in producing hybrid colonies, then it should be possible to notice an increase in the mating rate.

The results of mating experiments conducted under a variety of conditions are presented in Fig. 16 (A) and (B). In experiments on spontaneous hybridization, the parental cells are mixed at the time of plating; therefore, cell fusion must occur after the cells are plated. On the other hand, in most of the experiments which involve pretreatment of the parental cells with virus, the pretreatment is done in a small volume and cell fusion occurs before plating; therefore, the number of hybrid colonies is linear with dilution of the treated cell suspensions. Finally, in the experiments shown in Fig. 16 (B) one parental cell type is added

to a constant excess of the other parent which was already attached to a plate, thereby showing that both virus-treated and untreated cells are capable of forming hybrids with the same frequency as is observed when the parental cells are mixed simultaneously. From such data as these we have calculated that the spontaneous mating rate is about $2/10^6$ and the average mating rate after virus treatment is $1/10^3$. Under standard conditions, a one-thousandfold increase in the spontaneous mating rate of A9 with Cl 1 D may be attributed to pretreatment with Sendai virus.

Hybrid colonies from virus-treated

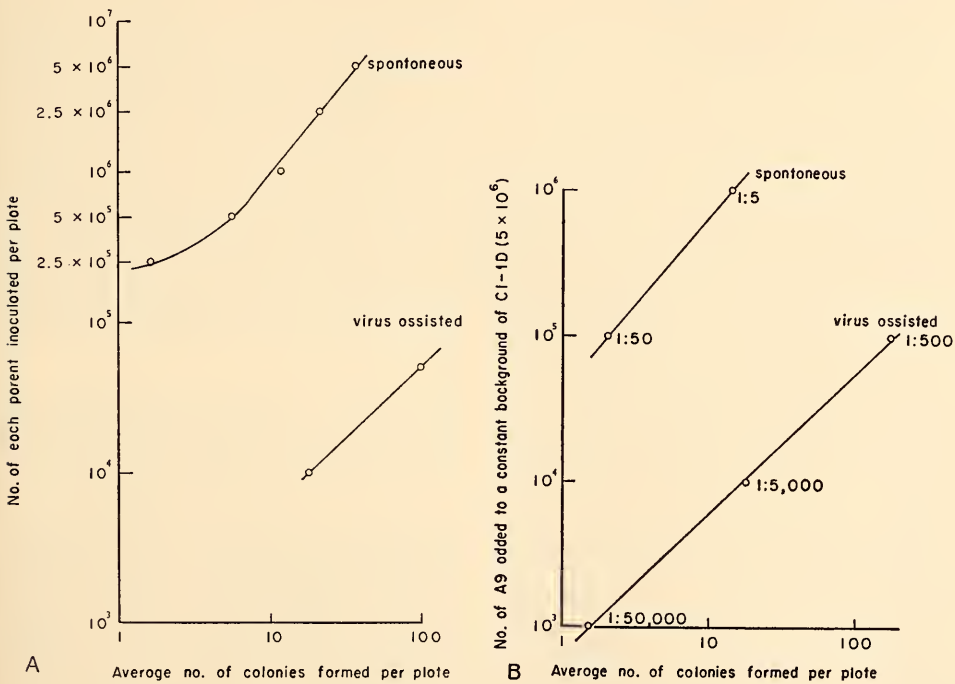


Fig. 16. The number of hybrid colonies formed between A₉ and Cl 1 D under conditions of spontaneous hybridization, detectable only at high inoculation densities, and virus-assisted hybridization. (A) Frequency of hybrid colonies when parental cells are used in equal number. The deviation from linearity in the lower part of the spontaneous hybridization curve is to be expected, since the opportunities for cell contact and fusion decrease drastically as the culture becomes subconfluent. (B) Frequency of hybrid colonies when one parent is used in limiting number in combination with a constant excess of the other parent. Since other experiments have shown that the number of hybrid colonies found is a function of the number of cells on the plate (i.e., is linear with dilution), we can conclude further that the number of hybrid colonies is also a function of the number of opportunities for fusion, clearly shown in this case as linearity with the number of cells of the limiting parent.

parental cells which occurred under conditions in which nonvirus-treated cells never produced hybrids were called "virus-assisted hybrids." At first it was thought that there might be consistent differences between the karyotypes of virus-assisted hybrids and the spontaneous hybrids. However, detailed chromosomal analysis of the karyotypes of hybrids produced under both conditions were found not to be significantly different. Virus-assisted hybridization in this model system appears to yield hybrid strains which are equivalent to those formerly known to occur only as infrequent spontaneous events.

Sendai Virus-Assisted Hybridization of a Partially Selectable Cell System: Cl 1 D and Normal Rat Liver Cells

Davidson and Ephrussi demonstrated that advantage might be taken of the ability to kill selectively one of the parents in a hybrid cross. If the ratio of the selectable parent to the unselectable parent is made sufficiently high, then among the few surviving colonies in selective medium it is often possible to distinguish hybrids from colonies of the nonselectable parent. This procedure is particularly effective when the nonselectable parent usually plates in a low efficiency, as is generally true with freshly prepared primary cell suspensions.

At a ratio of 200 Cl 1 D to one rat liver cell and a cell density of one million per 100-mm petri plate, we found the highest spontaneous mating rate to be 1/20,000. Under optimal conditions, the highest virus-assisted mating rate was found to be 1/55. Figure 17 shows that the number of hybrids formed between the cells is proportional to the number of the minority parent over a wide range when the cells are pretreated with a given concentration of virus, and that the number of hybrids formed may further be proportional to the titre of the virus used in the pretreatment.

The hybrids formed in this cross proved easy to isolate and should be of considerable interest for future analysis. About 5% of the hybrids from Sendai-assisted Cl 1 D \times rat liver hybrids (whether from freshly prepared liver suspensions or from clonally purified cultured rat liver) exhibited the epithelial morphology of the rat liver parent cell. It is possible to concentrate attention on the rare kinds of hybrids which favor the functional parent at least with respect to its morphology when there are hundreds of hybrid colonies to choose among. Plate 5 shows the morphology of Cl 1 D cells, rat liver parenchymal cells, and epithelial type and fibroblastic hybrids. It may be possible to associate the appearance of variants with fibroblastlike morphology (which occur with a frequency of about $1/10^6$ cell divisions) with the loss of one or more of the rat marker chromosomes. Functions typical of liver cells are being assayed in epithelial and fibroblastic hybrids. Surface properties of the hybrids, such as the ability to undergo histiotypic sorting in mixtures, should prove interesting to investigate in segregated hybrids.

The Use of Sendai-Assisted Hybridization to Make Possible Hybridization between Unselectable Cells: Virus Fusion as a Partial Selective Agent

Because di-heterokaryons and hybrids cannot be separated from the single nucleated parental cells it seemed likely that it would be possible to use the cell fusion procedure itself as a selective method. Our previous experience (*Year Book 66*) indicated that few if any heterokaryons enter division when normal diploid cells are fused together with UV-inactivated Sendai virus. The fusion process may be controllable to the point of making the residual number of single parental cells small relative to the number of fusion products. In this way, the few fusion products which give rise to

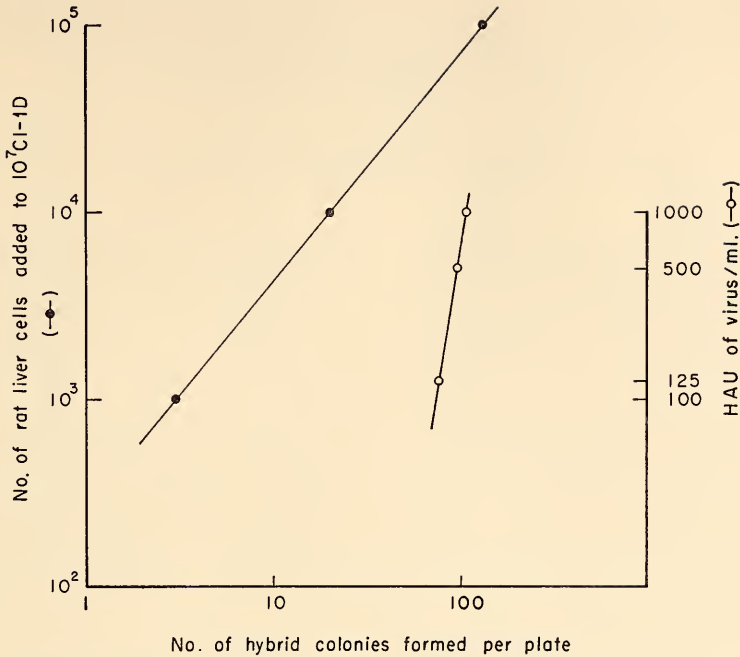


Fig. 17. The number of hybrid colonies formed in the cross of RL (rat liver) cells with Cl 1 D after pretreatment of the cells with inactivated Sendai virus. Closed circles: varying number of RL were mixed with a constant excess of Cl 1 D, and the number of hybrid colonies formed is seen to be proportional to the number of cells of the limiting parent. Open circles: mixture of 5×10^4 RL cells and 10^7 Cl 1 D were exposed to varying concentrations of virus (expressed as HAU or hemagglutinating unit). It can be seen that there is only a small difference in the number of hybrid colonies obtained between 125 and 1,000 HAU of inactivated Sendai virus.

propagating hybrid colonies (presumably binucleate heterokaryons) might be found among the colonies formed by the surviving parental cells.

One of the first unselected crosses we are attempting by this method is one which is difficult to recognize but which should prove of considerable interest. Clonally cultured rat liver cells plate with rather low efficiency (about 10%) and freshly prepared suspensions of mouse liver cells plate with an exceedingly low efficiency (less than 0.01%). It would appear that this combination should successfully mimic the partially selective system. In our first experiments we have succeeded in inducing extensive cell fusion (with more than 95% of the nuclei incorporated into heterokaryons) and we have found hybrid metaphases

produced as frequently as 10% of the total and persisting in sufficiently high frequency to be discovered as long as ten days after plating. However, it has so far proven impossible to recognize hybrid colonies. Apparently it will be difficult to distinguish between colonies of polyploid rat liver cells and the heterospecific hybrid.

In certain heterospecific crosses, as well as crosses between cells of differing morphology, it should be possible to distinguish the same intermediate morphology found in the epithelial Cl 1 D \times rat liver hybrids. It may be that a distinctive morphology will mark all hybrids between epithelial and fibroblastlike morphologies, making it possible to recognize certain intraspecific crosses such as myoblasts with liver cells.

LOSS OF SV₄₀-INDUCED T-ANTIGEN FROM SOMATIC HYBRIDS BETWEEN MOUSE CELLS AND SV₄₀-TRANSFORMED HUMAN CELLS

M. C. Weiss

(undertaken in cooperation with B. Ephrussi, University of Paris, and L. J. Scaletta, Case Western Reserve University)

Somatic cells of a number of species, including human and mouse, can be transformed by the oncogenic virus SV₄₀, and thereafter are altered in several of their properties: they lose the property of contact inhibition, become neoplastic, and possess two new (apparently non-species-specific) antigens, thought to be specified by the viral genome. However, since such transformed cells do not produce live virus, the permanent alteration of the cells and the continuous production of viral antigens have been the only sources of evidence that the viral genome is retained in the transformed cells. A more direct proof of persistence of the viral genome has recently been provided by the technique of virus reactivation, as described by Koprowski *et al.* and by Watkins and Dulbecco. This technique involves the Sendai virus-mediated fusion of transformed cells with indicator (Green monkey kidney) cells. After fusion, the indicator cells undergo a lytic response and infectious SV₄₀ is produced. One major question which has remained unanswered is the nature of the relationship of the viral genome to the transformed cell. Two major hypotheses have been that (1) the virus is somehow integrated into the genome of the transformed cell, or (2) it is present as a free particle (episomalike) in the cytoplasm of the nucleus of the transformed cell.

Our approach to this question has been to use the technique of somatic hybridization under conditions such that all of the chromosomes of one parent are lost from the hybrid cells. In earlier experiments by Weiss and Green, it was shown that hybrids made between human and mouse cells undergo rapid and

extensive "segregation" of human chromosomes with no concomitant loss of mouse chromosomes. Thus, one might predict that if hybrids are made between normal mouse cells and human cells transformed by SV₄₀, and if all human chromosomes are lost from the hybrid cells, then if the viral genome is integrated into a human chromosome, it will disappear with the human chromosomes. On the other hand, if the viral genome is present as a free particle in the transformed cell, since both parental cell types are susceptible to transformation by SV₄₀ and can express the viral antigens, then the viral genome should be retained in the hybrid cells, even if all human chromosomes are lost.

Three different hybrid cell lines have been made for these experiments, each of them between non(viral)-transformed mouse cells (all of which are negative for the viral T-antigen) and SV₄₀-transformed human cells (all of which are positive for the T-antigen). All hybrid lines have been found to be viable mononucleate cells which proliferate rapidly in tissue culture, and some of them have been maintained for more than 150 cell generations. The properties of only one of these hybrid lines will be presented in detail.

Using the half selective system of Davidson and Ephrussi, hybrid cells were made between Cl 1 D, a mouse line deficient for the enzyme thymidine kinase and therefore unable to grow in nutrient medium containing aminopterin, and SV-SD-C, a clone of human fibroblasts transformed by SV₄₀. One hybrid clone was isolated and found to contain 5-15 human chromosomes. The cells of this clone have been maintained under

TABLE 3. T-antigen Production by Various Populations of HM-SV, a Hybrid Line Derived from the "Cross" of Cl 1 D (Mouse) \times SV-SD-C (SV₄₀ Transformed Human Line)

Hybrid Line	No. of Generations Grown	Mean No. and Range of Human Chromosomes	SV ₄₀ T-antigen
HM-SV	30	5.2 (2-10)	Mixed
clone 3a	60	2.9 (2-4)	Mixed
clone 4	60	2.0 (2)	Positive
clone 6	60	2.1 (1-3)	Positive
clone 6-1	120	2.0 (2)	Positive
clone 6-3	120	1.0 (1)	Negative
clone 6-4	140	1.9 (2)	Positive
HM-SV	80	1.9 (1-4)	Mixed
clone 1	100	0 (0)	Negative
clone 2	100	0.4 (0-1)	Negative
clone 3	100	0 (0)	Negative

conditions of continuous propagation, and every 20 generations the chromosomes of the hybrid cells were examined and the presence of T-antigen (a viral antigen) assayed. After approximately 30 generations, the hybrids contained 5.2 human chromosomes (range 2-10), and at this time some cells were found to contain T-antigen, while a proportion of them (40%) had lost this viral property. The population was cloned, and some T-antigen negative populations were isolated. The T-antigen positive clones were maintained and recloned, and from them were isolated T-antigen negative clones, thus providing direct evidence that the T-antigen negative cells (which apparently had lost the viral genome) can be derived from positive ones.

The number and kinds of human chromosomes have been determined in the T-antigen positive and negative clones, and it has been found that T-antigen is absent only from those cells which

have lost most or all of the human chromosomes (Table 3). This finding suggests that loss of the SV₄₀ antigen occurs as a result of the loss of human chromosomes, thus providing evidence that the viral genome is integrated into the chromosomes of transformed cells. The fact that loss of the antigen occurs only when most or all of the chromosomes derived from the transformed cell are lost suggests that more than one chromosome contains the viral genome. Evidence in support of this hypothesis has recently come from the laboratory of Dulbecco, who has found (by DNA-RNA hybridization techniques) that transformed cells contain between 5 and 40 copies of the viral genome.

Further experiments are in progress to determine whether the T-antigen negative cells can be transformed, and whether virus can be reactivated from the T-antigen positive and negative clones.

CELL DIFFERENTIATION AND VIRAL SUSCEPTIBILITY

*R. J. Hay, M. Yoshikawa-Fukada, S. Yuyama and J. D. Ebert
(assisted by D. Somerville and B. Smith)*

THE INTERACTIONS OF ROUS SARCOMA VIRUS WITH DEVELOPING MUSCLE

Cell colonies composed of myoblasts and myotubes can be infected with Rous sarcoma virus (RSV) to ultimately yield mononucleated cells which are trans-

formed and which produce infective virus (Kaighn, Ebert, and Stott, *Year Book 64*, pp. 483-486). The myotubes in such clones normally do not synthesize DNA but a small fraction of these do incorporate tritiated thymidine after in-

fection (Kaighn, Lee, and Ebert, *Year Book 65*, pp. 524-526). A number of interesting questions, each with its own technical hurdles, has arisen from these findings. Can myotubes be infected directly by RSV or must the myoblast serve as a vehicle for entry of the viral genome into the developing myotube? The incorporation of H^3 -thymidine can occur in nuclei situated in the central regions of infected myotubes, far removed from the site of myoblast fusion; experiments using short pulses (30 minutes) of H^3 -thymidine clearly rule out the possibility that the label is incorporated during the fusion of labeled myoblasts. However, the possibility remains that infected myoblasts, having fused earlier into myotubes, secondarily infect other nuclei in the syncytium, permitting a reactivation of DNA synthesis in nuclei previously thought to be in a highly repressed state. Studies in several laboratories with RSV and other oncogenic viruses indicate that cellular DNA synthesis is a prerequisite for transformation and synthesis of infective virus. If the DNA synthesized in myotubes is, in fact, cellular DNA, the state of differentiation in mature muscle could presumably preclude further steps required for the synthesis of complete virus and for transformation. Thus far, for example, we have not observed the initiation of mitosis following the initiation of DNA synthesis. It could be argued, also, that the DNA synthesized in RSV-infected myotubes may represent, at least in part, provirus DNA. The second general question with which we are concerned, then, has to do with the nature of the DNA synthesized in infected myotubes and the mechanism by which the virus induces its formation.

Definitive answers to these questions seem to depend initially on our ability to obtain multinucleated myotubes free from their mononucleate precursor cells, the myoblasts. Numerous different approaches to this technical problem were taken. Two of these may merit further

intensive study, since the initial results are encouraging. The first approach involved simple manipulation of the growth medium in an attempt to inhibit myoblast fusion initially, then a reversion to fusion-promoting conditions in the hope that synchronous or relatively complete fusion would occur. The second approach involved attempts at selective killing of dividing cells by exposure to antimetabolic drugs or inhibitors of DNA synthesis.

The medium generally adopted for clonal cultures of chick embryonic muscle consists basically of Ham's F12, with double the recommended concentration of amino acids, supplemented with 15% of selected horse serum and 2% embryo extract (F12 215). We found that normal myotubes did not develop, however, if fetal calf serum was substituted for horse serum. Colonies of myoblasts could be recognized by gross morphology and occasionally by the presence of a few small elongated syncytia (Plate 6). Accordingly, clonal cultures of chick skeletal muscle cells were set up using the techniques described previously. Medium in test plates consisted of F12 supplemented with 2% embryo extract and 15% fetal calf serum instead of horse serum. On the fourth and eighth day representative cultures of the fetal calf serum series were changed to horse serum supplemented medium. Companion cultures were fed using fresh medium without altering serum type. Typical results (Fig. 18) indicate that no abrupt or synchronous fusion of myoblasts occurs after the change from fetal calf to horse serum. Myoblast fusion apparently is delayed in medium supplemented with fetal calf serum and the process is gradually resumed on addition of horse serum to the culture system.

Coon and Kaighn (*Year Book 66*, p. 604; reprint, p. 32) showed that myoblast fusion was inhibited at high concentrations of the high molecular weight fraction of embryo extract. Perhaps by combining these two general findings

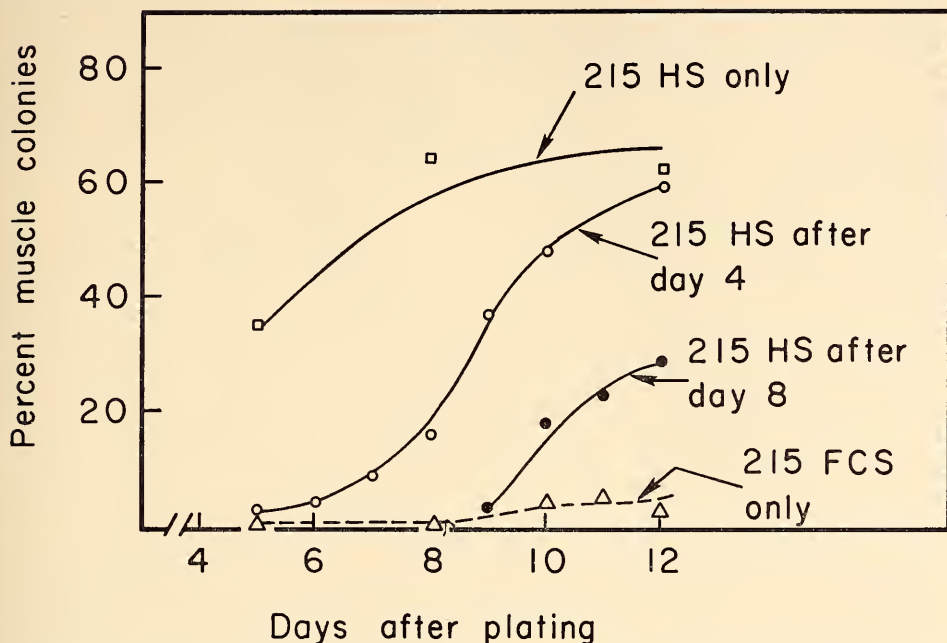


Fig. 18. Influence of serum component on development of muscle colonies. Cultures were set up in F12 medium containing 15% fetal calf serum instead of horse serum. Representative plates were changed to F12 215 (horse serum) on the 4th and 8th day. Colonies with at least one conspicuous myotube were scored as muscle colonies. Plating efficiency in F12 215 (FCS) was about 6%; in F12 215 (HS) about 19%.

with techniques for obtaining cultures of synchronously dividing cells, we might be able to promote more abrupt fusion in isolated myoblast populations.

The second approach involved cursory screening of various inhibitors of DNA synthesis and of mitosis for their ability to selectively eliminate myoblasts from muscle clones. The technique finally adopted was in some respects similar to that recently described by Bischoff and Holtzer except that vincoleucoblastine sulfate (VLB), a mitotic inhibitor, was selected for use. This inhibitor seemed to be more effective than colchicine or colcemide in arresting myoblasts in mitosis. Furthermore, "myosacs" formed after exposure to VLB elongated, developed cross striations and, very infrequently, exhibited spontaneous contractions within 48–120 hours after treatment.

On the ninth day after plating, clonal cultures of chick embryonic muscles were exposed for 2 hours at 37°C to VLB dissolved in fresh growth medium (2 $\mu\text{g}/\text{ml}$). They were then washed three times in succession with Hanks' BSS before addition of medium. This procedure removes most of the myoblasts (fibroblast colonies seem to be less severely affected) leaving rounded "myosacs" similar to those described by Bischoff and Holtzer. These return to more normal morphology after about 48 hours of incubation (Plate 7A). Studies of the effect of RSV at high multiplicities of infection on DNA synthesis in such cultures are now in progress.

RSV-RNA HYBRIDIZATION WITH AVIAN AND MAMMALIAN DNA

Although considerable evidence exists indicating that both DNA synthesis and

mitosis are essential requirements for cell transformation and synthesis of infective virus particles, the mechanisms by which the viral genome is integrated into the cell's synthetic apparatus are poorly understood. Interest in this problem prompted the initiation of experiments to determine whether DNA isolated from various cell types contains nucleotide sequences homologous to RSV-RNA.

Viral RNA with high specific activity was prepared as follows: Chick embryo fibroblast cultures were infected with RSV and incubated for 4 days. The growth medium was changed to phosphate-free medium (with 5% normal medium) and 200 $\mu\text{C}/\text{ml}$ of carrier-free P^{32}O_4 was added. The medium was collected daily for 5 days, and the RSV was precipitated with ammonium sulfate and purified by sucrose density gradient centrifugation.

Typical fractionation patterns of RSV and RSV-RNA extracted from the purified RSV peak are shown in Figs. 19 and 23(A), respectively. The specific activity of RSV-RNA in these experiments ranged from 2 to 4×10^5 CPM/ μg .

DNA was extracted from a variety of

tissues and cultured cells by the SDS-phenol method. It was purified by treatment with α -amylase, ribonuclease (RNase), and pronase, followed in some cases by passage through an MAK column.

Hybridization Technique

To test for RNA-DNA homology, heat-denatured DNA (100–200 $\mu\text{g}/\text{ml}$ of SSC/10) was mixed with labeled RNA and the salt concentration was adjusted to equal $2 \times \text{SSC}$. After incubation at 60°C for 6 hours, the RNA-DNA mixture was treated at room temperature (30 min) with 30 $\mu\text{g}/\text{ml}$ of RNase (heated at 80°C for 10 min). Cesium chloride (3.5 g) was added and the refractive index was adjusted to 1.4015 ± 0.0003 with $2 \times \text{SSC}$. The solution was then centrifuged at 33,000 rpm for 60–64 hours. Fractions were collected in 14–20 tubes and the optical density was determined. Then each fraction was diluted with 10 ml of $2 \times \text{SSC}$ and incubated at 60°C for 1 hour. Finally, the salt concentration was increased to $4 \times \text{SSC}$ and RNA-DNA hybrids were trapped on Millipore filters and their radioactivity was determined in toluene scintillator.

In some experiments DNA was pre-hybridized with unlabeled RNA and fractionated by cesium chloride centrifugation. DNA filters were then prepared as described by Brown, Weber, and Sinclair (*Year Book* 66, pp. 580–581; reprint, pp. 8–9) and the DNA was allowed to hybridize with labeled RSV-RNA. Hybrids thus formed were treated for 30 minutes at 37°C with RNase (50 $\mu\text{g}/\text{ml}$ of $2 \times \text{SSC}$ final concentration) to remove unbound RNA.

Hybridization of RSV-RNA to Chick DNA

RSV-RNA was found to hybridize with DNA isolated from uninfected chick fibroblasts as well as with DNA from cultured skeletal muscle cells which had

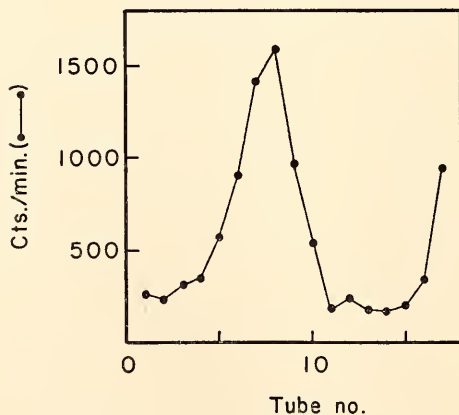


Fig. 19. Sucrose density gradient centrifugation of RSV. Ammonium sulfate-precipitated RSV was centrifuged on a sucrose gradient of 5–20% at 20,000 rpm for 60 minutes in SW 25.2 rotor.

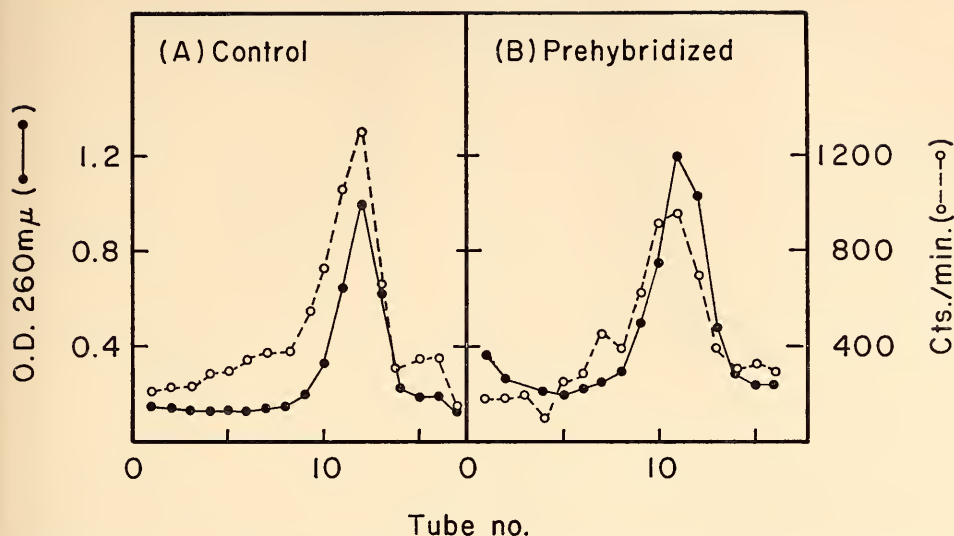


Fig. 20. Hybridization between chick embryo DNA and RSV-RNA. (A) CsCl fractionation of hybrids between chick embryo DNA and P³²-RSV-RNA. (B) Chick embryo DNA prehybridized with unlabeled RSV-RNA was fractionated by CsCl centrifugation, and each fraction was treated with alkali, neutralized, and trapped on a Millipore filter. The filter with trapped DNA was dried at 80°C for 3 hours and used for hybridization with P³²-RSV-RNA.

been infected with RSV (Figs. 20 and 21). Note that, unlike ribosomal RNA (Fig. 22), even with the prehybridized preparation (Fig. 20B), the hybrid did not fractionate as a heavier component.

The nature of the fraction of RSV-RNA which hybridizes with chick cell DNA was also studied. DNA-RNA hybrids isolated by gradient centrifugation in cesium chloride were pooled, dialyzed overnight at 4°C in 1/10 SSC (containing 10 μg polyvinyl sulfate per ml). The solution was then heated to 100°C for 2 minutes and cooled rapidly in an ice bath. The salt concentration was then adjusted to 4×SSC and the solution was filtered through a Millipore membrane. Unlabeled rRNA was then added as a carrier to the filtrate. Finally, the solution was concentrated by ethanol precipitation and the RNA was fractionated by sucrose density gradient centrifugation.

The fractionation patterns of the original RSV-RNA (A), RSV-RNA treated in essentially the same manner as the

hybrid but without centrifugation in cesium chloride (B), and RNA after hybridization with chick fibroblast DNA (C) are shown in Fig. 23 and 24. The heavy RNA component observed on fractionation of the original RSV-RNA (Fig. 23A) represents 62S viral RNA which may be broken up on heating. With the exception of the disappearance of this heavy component, there were no notable differences in fractionation pattern between the hybridized and non-hybridized viral RNA. The sedimentation coefficient was about 4S.

The material identified by each peak in Fig. 24 was then subjected to base analysis. The RNA was precipitated with ethanol and hydrolyzed in 0.3 N KOH at 37°C for 18 hours. Results of analysis of the hydrolysates are presented in Table 4. Note that the composition of the hybridized RNA differs from that of the other preparations in its high content of adenylic acid. This suggests that although the hybridized RNA has the same molecular size as the small com-

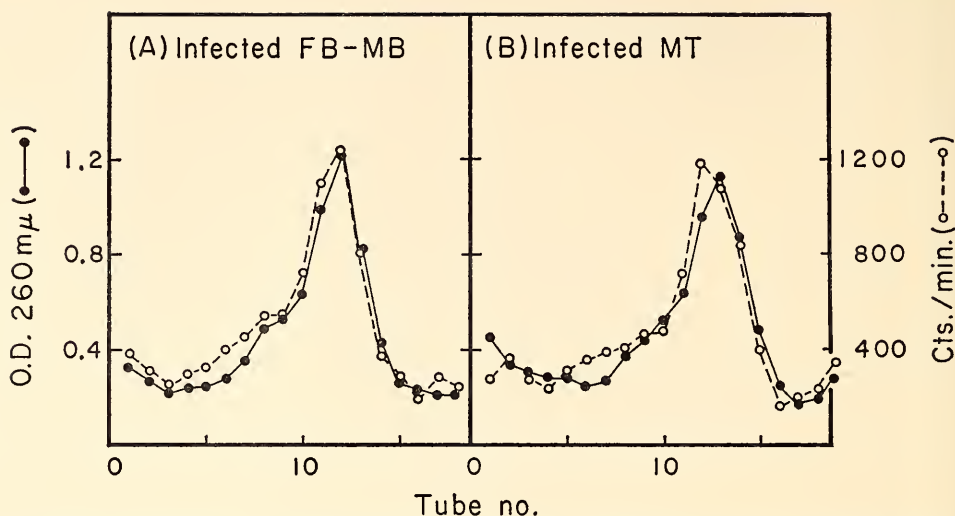


Fig. 21. Hybridization of P^{32} -RSV-RNA with infected chick embryo DNA. Hybrids between P^{32} -RSV-RNA and DNAs of fibroblast-myoblast fraction (A) and myotube fraction (B) 42 hours postinfection were obtained by centrifuging cells from mixed fibroblast and muscle cultures which had been layered over fetal calf serum ($800 \times g$ for 30 seconds). The lower fraction (B) was about threefold enriched in myotubes but still contained myoblasts and fibroblasts.

ponent of virus preparations, it represents an RNA species that is only part of the RSV-RNA molecule, presumably the portion which binds most firmly to

host DNA. This hypothesis has also been advanced by Harel and his associates. Evidence presented by Kubinski and Rose indicating that DNA from onco-

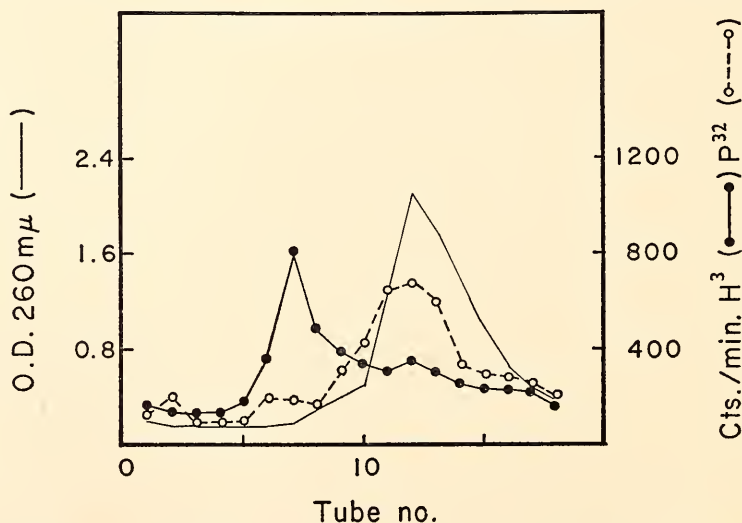


Fig. 22. Hybridization of chick embryo DNA with rRNA and RSV-RNA. Filters with trapped DNA were prepared in the same way as in Fig. 20(B) using chick embryo DNA prehybridized with unlabeled rRNA. These were incubated in a mixture of H^3 -18S rRNA and P^{32} -RSV-RNA at $65^\circ C$ for 6 hours. The labeled rRNA was isolated from chick embryo fibroblasts cultured in the presence of H^3 -uridine and had a specific activity of 1.5×10^5 cpm/ μg .

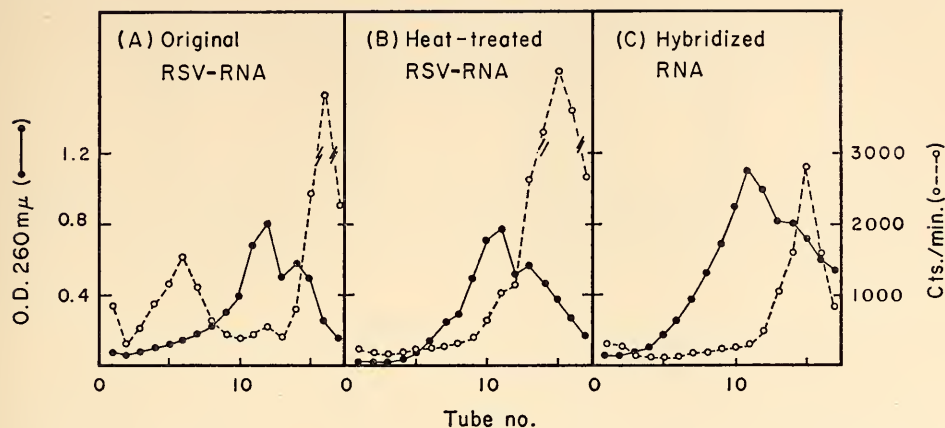


Fig. 23. Sucrose density gradient centrifugation of RSV-RNA. The original RSV-RNA was extracted from material identified by sucrose gradient peaks similar to that in Fig. 20(A). Heat treated RSV-RNA (B), and RNA recovered from the hybrid with chick embryo DNA (C) were centrifuged on a sucrose gradient of 5-20% at 36,000 rpm for 120 minutes in a SW 39 rotor.

genic adenoviruses contains more deoxy-adenosine-rich sequences than that from nononcogenic adenoviruses is also notable.

Specificity in this RSV-RNA to DNA hybridization is suggested by results of competition experiments such as that shown in Fig. 25. Note that RSV-RNA but not rRNA competed with P^{32} -labeled RSV-RNA for the receptor sites on chick fibroblast DNA.

Hybridization of RSV-RNA to DNA from Several Other Avian and Mammalian Species

The ability of RSV-RNA to hybridize with DNA isolated from several other sources was also examined. Interestingly, almost an identical pattern of hybridization was noted with all DNA types (Figs. 26 and 27) except the bacteria *M. lysodeikticus* and *E. coli* (Fig. 28). The former showed no hybridization,

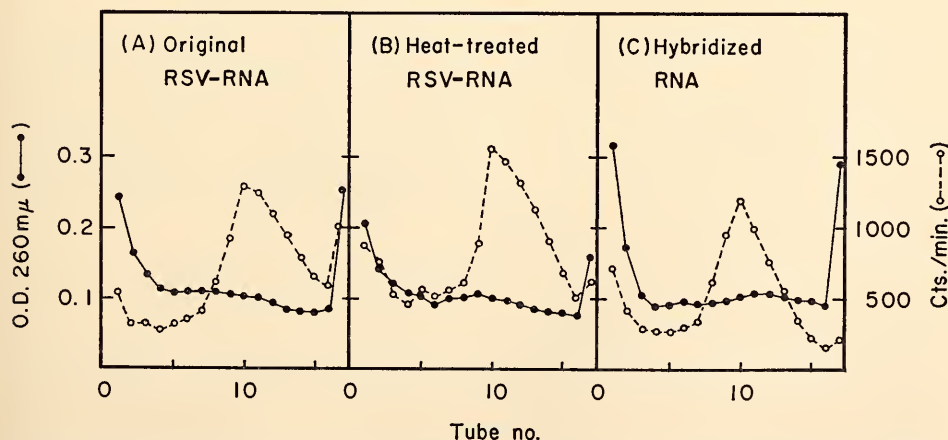


Fig. 24. Sucrose density gradient centrifugation of RSV-RNA. The same sample as in Fig. 23 was centrifuged for 18 hours.

TABLE 4. Base Composition of RSV-RNA

	62S RSV-RNA	4S RSV-RNA	Heat-treated RSV-RNA	Hybridized RNA
C	24.6	26.1	25.6	22.2
A	23.6	21.1	21.7	26.9
G	23.7	32.8	33.1	31.3
U	23.1	20.0	19.6	19.6

Note: Radioactive material identified by peaks of Fig. 23 A, B, and C were pooled, precipitated by ethanol with carrier rRNA and hydrolyzed. Each figure represents the average of six analyses on two-dimensional paper chromatography with RNA from two different preparations.

while the peak observed in the latter combination is thought to represent activity of low density, not truly associated with the *E. coli* DNA. Verification of this assumption through use of less dense cesium chloride gradient separation is in progress.

Analyses of DNA-RNA hybridization with DNA from other sources (frog, salmon, pea, yeast, etc.) and saturation experiments to try to quantitate the complementarity of RSV-RNA and chick DNA are also to be initiated.

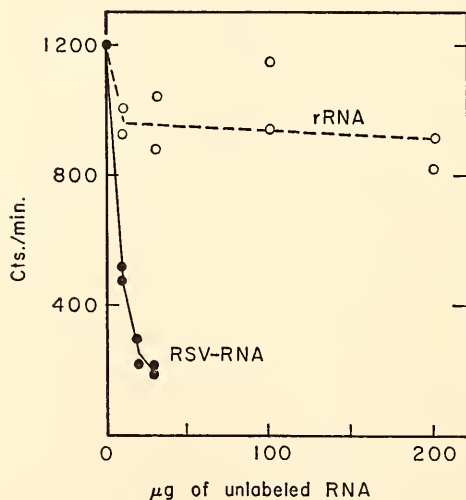


Fig. 25. Competition of RSV-RNA with rRNA. Filters containing about 100 μ g of trapped DNA isolated from infected fibroblast-myoblast preparations were incubated under hybridization conditions with P^{32} -RSV-RNA in the presence of unlabeled RSV-RNA or rRNA. Similar results were obtained when DNA from uninfected fibroblasts was used.

ADDITIONAL CELL CULTURE SYSTEMS FOR FUTURE STUDY

In addition to the aforementioned effects of RSV on chick myoblasts and fibroblasts, studies with cloned strains of chick cartilage cells indicate that they will produce infective virus and do undergo morphological change after infection (*Year Book 66*, pp. 600-602; reprint, pp. 28-30). Similar reports of effects of RSV on iris epithelial cells in monolayer culture and on liver cells in plasma clot culture have also appeared. These latter studies, however, were conducted with heterogeneous populations, and it can be argued that the changes observed could be due to the presence of connective tissue or vascular endothelial elements.

We have attempted to isolate and maintain cells from several additional chick embryonic tissues to enlarge upon the information discussed above. We hope ultimately to include studies of effects of RSV on various cell types at different stages of development and growth. This work is, however, in preliminary stages and for the most part the culture methods discussed below are still being developed.

Isolation and Maintenance of Sensory Nerve Cells

Levi-Montalcini and Angeletti have described a method for obtaining dissociated sensory and sympathetic nerve cells in culture using Eagle's medium supplemented with nerve growth factor (NGF). We were interested in this cell

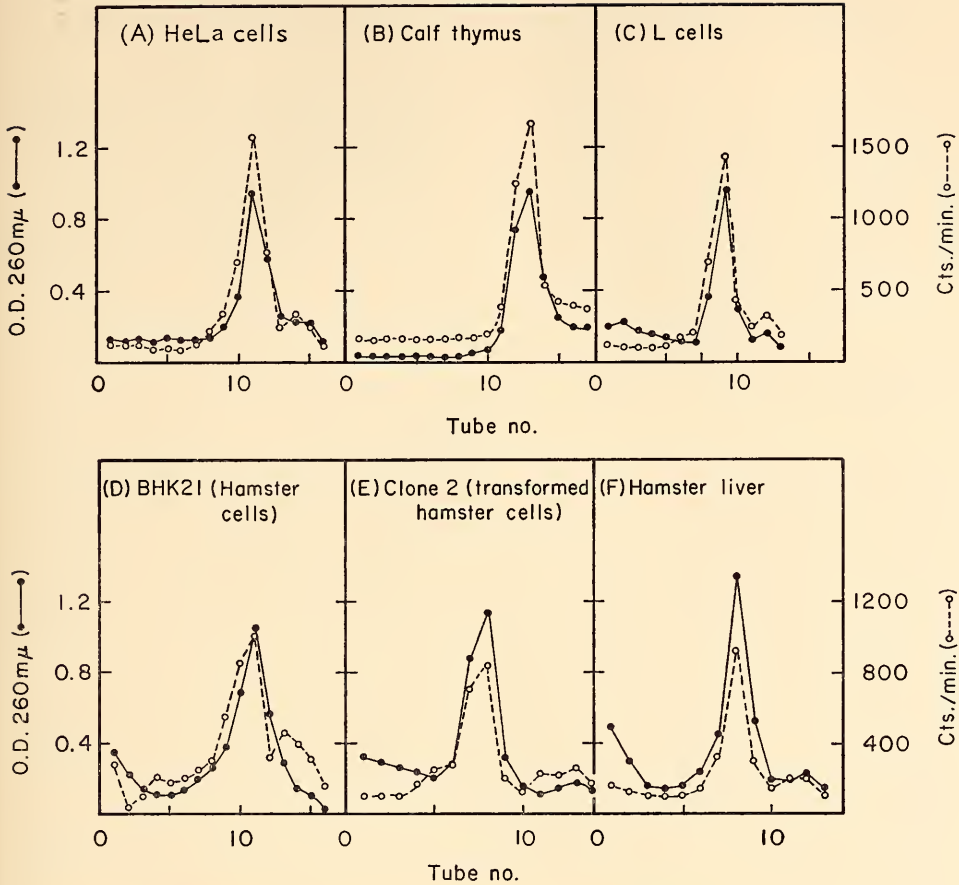


Fig. 26. Hybridization of RSV-RNA with various mammalian DNAs.

type as a postmitotic, mononucleated cell which, like muscle, might be stimulated after RSV infection to synthesize DNA. Accordingly, the standard method for obtaining muscle development in culture was adapted for use with sensory ganglia. It proved successful without addition of NGF to the culture medium.

Sensory nerve ganglia from chick embryos were removed and collected in calcium- and magnesium-free Hanks' BSS. They were dissociated with 0.05% trypsin in Ca^{++} - and Mg^{++} -free BSS by stirring rapidly at 37°C on a magnetic stirrer for 10–15 minutes. Generally, the ganglia collected from 4–6 embryos were processed in 5 ml of the trypsin

solution. The cell suspension was then filtered through bolting silk and the cells were removed by centrifugation. The cell pellet was suspended in 1 ml of F12 supplemented with 2% embryo extract and 10% calf serum (F12 210) and counted in a hemocytometer. Collagen-coated petri plates (35 mm size) containing 2.5 ml of F12 210 were then seeded with 10^4 nerve cells and incubated at 37°C .

The adhesion of sensory nerve cells to the coated culture dish is slow in comparison to fibroblastlike cells, requiring about 24 hours of incubation. This may be of use in obtaining enriched populations for long-term studies. Attempts to

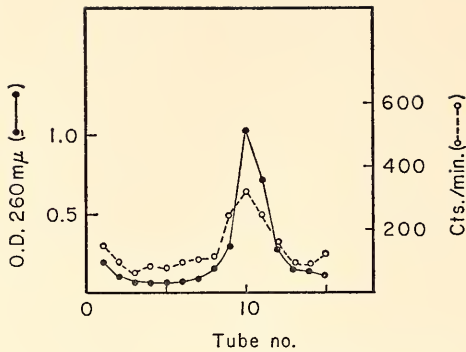


Fig. 27. Hybridization of RSV-RNA with goose DNA.

determine whether or not RSV infection leads to DNA stimulation and production of viral antigen in these cells have so far been inconclusive, primarily because of the lack of sufficiently reliable cell markers. The refractile appearance of a sensory neuron in culture is very similar to that of a transformed fibroblast, and the nerve fibers often do not withstand the repeated washings required in autoradiographic and fluorescent antibody staining techniques. Clearly we must depend on other cell specific markers to answer the questions posed above.

Aggregation Techniques for Culture of Hepatocytes

Initial attempts at obtaining clonal cultures of parenchymal cells from dissociated embryonic chick liver were unsuccessful in spite of repeated trials with various sera and several different dissociation techniques. Fibroblastlike cells could be recovered by techniques similar to those used for muscle but with plating efficiencies of only about 0.2%.

An alternative method was therefore developed, one which shows considerable promise for the hepatocyte and probably numerous other cell types as well. At this writing, liver cells isolated from embryos ranging from 10 to 19 days old have been maintained in culture without difficulty for periods of up to 2 weeks.

The heart and liver were exposed immediately after removing the embryo from the egg. Approximately 2.5 ml of Ca^{++} - and Mg^{++} -free Hanks' BSS was perfused directly into the heart using a syringe and 25-gauge needle. This procedure reduces the levels of divalent cations and erythrocytes in the liver mass. The liver was then removed, minced, and suspended in a solution containing 0.125% trypsin, 0.2% EDTA, 0.3% sodium citrate and 0.5% glucose made up in phosphate-buffered saline. The mixture

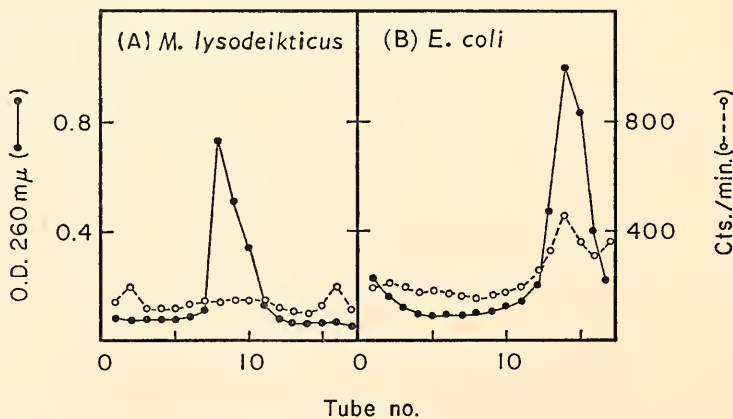


Fig. 28. Hybridization of RSV-RNA with bacterial DNA.

was agitated at room temperature for 20–30 minutes on a magnetic stirrer. The suspension was then filtered through gauze and bolting silk and the cells were removed by centrifugation. They were then washed free of the dissociation solution and finally were suspended in Eagle's minimal essential medium or F12 supplemented with 5% agamma calf serum. Approximately 3×10^7 cells could be obtained in this manner from four 13-day embryos. These cells, suspended in 5 ml of growth medium, were allowed to aggregate for 10–15 hours in a shaking water bath at 37°C. The aggregates could then be plated to 9 cm collagen-coated dishes at the equivalent of 10^5 to 10^7 cells in 5 ml of medium. Aggregate colonies adhere to the culture dishes within 5–8 hours, by 48 hours having spread out on the substratum to display typical hepatocyte morphology (Plate 7B).

The rationale behind development of this method of cell isolation was the hope that aggregate colonies free of fibroblast-like cells could be obtained. These cells are still present however, and techniques for eliminating them or discouraging their proliferation are required for any long-term studies.

Isolation and Culture of Cells from the Chorioallantoic Membrane

Long-standing interest in the chorioallantoic membrane (CAM), its morphogenetic potentialities, possible susceptibility to transformation by RSV, and also the controversy regarding initial site of infection by RSV, prompted attempts to isolate the various major cells types involved. As with the liver, fibroblastlike cells presumably of mesenchymal origin could readily be isolated in clonal culture but with low plating efficiencies of around 0.2%. These fibroblastlike cells were similar in appearance to those isolated from the liver but differed somewhat in morphology (and markedly in plating efficiency) from fibroblasts of skeletal

muscle. No colonies of epithelial cells could be obtained by this conventional method.

When the entire CAM was dissociated in the trypsin-citrate-EDTA solution (described above) and allowed to aggregate, colonies of epithelial cells, presumably from the chorionic epithelium (CE), developed. In later experiments 5 or 6 membranes from 9-day eggs were treated using a method similar to that reported by Kato and Hayashi for separating the chorionic epithelium from the mesenchyme of the CAM. The membranes were first washed in Ca^{++} - and Mg^{++} -free Hanks' BSS and placed in double strength BSS free of divalent cations but containing 0.25% EDTA. These were left at 4°C for 1½ hours. The chorionic epithelial layer could then be peeled off and the pooled layers were dissociated and allowed to aggregate as described for liver. CE clones isolated in this manner were almost completely free of fibroblastlike cells. Although these techniques require refinement, the general approach should provide conclusive evidence as to the susceptibility of these cell types to infection and transformation by RSV.

Studies Employing HeLa Cell-Erythrocyte Heterokaryons

A new system, free of some of the difficulties inherent in the muscle-RSV study for larger scale biochemical work, has also been the subject of preliminary investigation. Harris has recently shown that nuclei of adult chicken erythrocytes, which normally do not synthesize DNA, can incorporate tritiated thymidine after virus-induced fusion with HeLa cells. His findings have been confirmed and extended using erythrocytes fused to HeLa collected by the method of Robbins and presumed to be in synchrony. Although the methodology is still in developmental stages, initial results indicate that about 30% of the HeLa cells in test

populations contain at least one erythrocyte nucleus. Approximately 80% of these erythrocyte nuclei incorporate tritiated thymidine. Attempts at fractiona-

tion of the components in this system which may lead to initiation of DNA synthesis in the erythrocyte nucleus are to be initiated.

CARDIOGENESIS IN THE CHICK EMBRYO

*R. L. DeHaan, H. Stalsberg, E. E. Legum, I. Polinger,
S. Gottlieb, M. Egorin and B. Gould*

In our attempts to understand the early development of the heart, we continue to find most fruitful a multilevel approach: seeking to describe and analyze the morphogenetic events in the intact embryo; and simultaneously investigating the properties of the cells which comprise the heart when those cells are isolated in tissue culture. Our goals remain to understand the causal mechanisms underlying the emergence of form and of function in this organ. Overshadowing all else in our work during the past year is the breakthrough we have enjoyed in the electrophysiological analysis of heart cells in culture.

ELECTROPHYSIOLOGICAL IMPALEMENT OF ISOLATED CELLS

When a cell in the intact heart, or in a dense sheet of heart cells in culture is impaled with a recording microelectrode, its normal electrical activity can be seen (Fig. 29). The cell exhibits a negative electrical potential across its membrane, the maximum diastolic potential (MDP), of 60–80 mV. If it is a spontaneously active pacemaker cell, the membrane potential immediately begins to decay towards zero (shown by convention as a rising line) through characteristic points of deflection (PBA, PBO) until at some threshold level the transmembrane potential very rapidly reverses, producing, for a brief period, a small positive potential (MPP). After an action potential duration on the order of 200–500 milliseconds, the transmembrane potential is restored to the maximal diastolic level, until the next action potential cycle. It is

this rhythmic electrical discharge, characteristic of the cell membranes of pacemaker cells, which initiates the contractile activity of cardiac tissue.

With the advent of techniques for dissociating heart tissue into its component cells and growing these cells in cultures (as described in *Year Books 65* and *66*) a growing literature has developed on the electrophysiological properties of such cells. Although substantial information has been obtained by impaling sheets or aggregates of cells, successful recordings have been obtained previously only from cells cultured at relatively high densities. Yet, most of the benefits to be derived from applying these techniques to cultured cardiac cells depend upon being able to record at will either from an active cell, completely isolated from any neighbors as a singlet, or from such

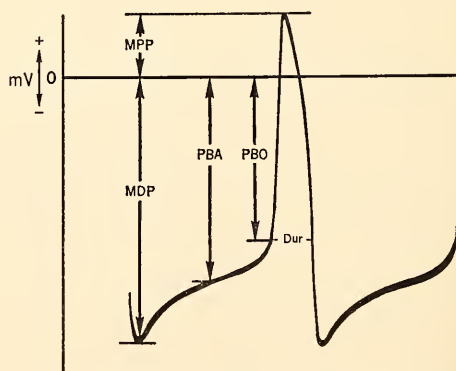


Fig. 29. Diagrammatic action potential to show parameters measured. MDP = maximal diastolic potential; MPP = maximum positive potential; Dur = duration; PBA = potential at break of afterpotential; PBO = potential at break of phase O.

a cell in electrical contact with a small group of neighbors, under circumstances where the number of cells in the group may be determined and the points of contact examined. Despite recent attempts in several laboratories, including our own (*Year Book 66*, pp. 613-615; reprint pp. 40-43), no successful recordings from actively beating singlet cells have been published, although abortive impalements have yielded low-level resting potentials from such cells. Spontaneous action potentials from singlet cells have not been reported.

Success in recording from cells in sparse sheets or those completely isolated from neighbors appears to depend upon at least three sets of variables: (1) characteristics of the microelectrode, (2) components of the culture medium, and (3) level of oxygen in the ambient atmosphere. In collaboration with Sheldon Gottlieb, we have been able, during recent months, to work out techniques which have enabled us to impale isolated single cells successfully and to record rhythmic action potentials from them over extended periods of time in culture.

Tissue culture techniques were similar to those described previously (*Year Books 65, 66*, and DeHaan, 1967a) with the exception that media with lower protein content and low-oxygen atmosphere were employed. Hearts were dissected from chick embryos incubated 7 or 12 days and dissociated into their component cells by three 8-minute cycles of trypsinization (0.05% trypsin, pH 7.3, 37°C). Damaging effects of the enzymes were minimized by collecting freed cells at the end of each 8-minute period in a trypsin-inhibitor medium. The final cell suspension was filtered through bolting silk, counted in a hemocytometer, and resuspended in growth medium. Cells were plated in small culture dishes (Falcon Plastics, 35 mm diameter), at a density of 2 or 4×10^5 cells/plate. The cultures were incubated at 37.5°C in a water-saturated atmo-

sphere of 5% CO₂, 10% oxygen, and 85% nitrogen.

Within about 4 hours after inoculation into standard medium, 25-50% of the cells adhere to the surface of the culture dish and take on their characteristic morphology as myocardial-like M-cells, or F-cells having properties typical of fibroblasts. Twenty-four hours after inoculation, nonadhering "floaters" are removed with the first change of medium, leaving behind healthy cells attached to the dish bottom at a density of 50-200 cells/mm². In most regions, the majority of cells are completely isolated one from another. However, some cells are found in groups or sparse sheets of 2-50 cells mutually in contact. Cells tend to settle at higher density in the center of the dish, and are more sparsely distributed at the periphery, especially in low-K⁺ media (DeHaan, 1967d).

In growth medium, the cells divide rapidly, increasing about tenfold in four days of cultivation. Thus, by the end of that period cell densities as high as 1000 cells/mm² are not uncommon, and isolated cells are rare. Typical cells, photographed with phase optics while recording, are shown in Plate 8. The cell impaled in Plate 8A is one of a group of seven cells in mutual contact. This cell and three others in the group (cells 1, 3, 4, and 7) are typical M-cells with a single nucleolus. Several binucleolate F-cells are also visible.

We refer here to "contacted" cells as those adhering to, and electrically interconnected with, one or more neighbors. Interconnection is generally manifested in synchronous rates of beating. Although F-cells do not usually contract, they are conductive. Therefore, all M-cells in a contacted group beat in synchrony. Neighboring cells beating at different rates indicate a lack of electrical interconnection. Cell number 8 (Plate 8A), connected to the main group by a slender strand, was not beating. In other cases, however, cells have been seen to beat in synchrony when the only con-

nection between them was a fiber of such size and appearance.

Impalability

Impalability refers to the ease with which cells may be penetrated by a micro-electrode without irreversible damage. It may be roughly quantitated by noting the ratio of successful to unsuccessful attempts to impale cells under a given set of conditions. The criteria of success are that upon recovery from impalement (usually after an initial depolarization) the cell exhibits a resting potential of at least -40 mV with or without action potentials, and the recording lasts a minimum of 10 seconds.

Attempts to impale M-cells in sheets using glass microelectrodes of the type commonly described (tip diameter 0.4 – 0.5μ ; impedance 10 – 40 megohms) were moderately successful. Cells in non-growth media and ambient atmospheres containing 40% oxygen could be impaled with 20–30% success. These recordings lasted from a few seconds to several minutes, terminating when either the electrode became dislodged from the cell, or the potential diminished to near zero as the cell exhibited visible signs of damage, becoming vacuolated and "blebby." Under these conditions, isolated cells were never successfully impaled.

In media containing 6% embryo extract, in which the cells grow rapidly, a greater degree of success was obtained from contacted cells. The electrode healed in more readily, and recordings generally lasted several minutes. Com-

parison between cells grown in atmospheres of 90%, 40%, or 10% oxygen were also striking. Cells in 90% or 40% oxygen were vacuolated in appearance and difficult to impale. Groups of cells cultured in growth medium and 10% oxygen atmospheres for 48 hours could be impaled successfully in more than 60% of the attempts. Once the electrode was sealed into a cell, recording could be continued for 15–20 minutes (frequently for 30 minutes or more) and was most often discontinued by the electrode's becoming dislodged, rather than by death of the cell.

Under these circumstances, other cells in the same dish, differing only in that they were not in contact with neighbors, could still not successfully be impaled. At best, abortive impalements, yielding low-level membrane potentials of 15–20 mV could be obtained.

With the introduction of ultramicro-electrodes with impedances of 100–150 megohms, success in impalements of contacted cells increased still further, and recording from isolated cells became feasible for the first time. The degree of success in impaling M-cells in groups and isolated cells is indicated by the results of three experiments shown in Table 5. In each case, the culture was prepared for recording, and cells were impaled one after another, systematically alternating between M-cells in groups and singlet cells. In most instances the electrode was allowed to remain in each cell no more than 3–4 minutes, by which time the impalement was declared successful or unsuccessful as defined above. All three experiments were done with cells in

TABLE 5. Impalability of Isolated and Contacted Cells

	Contacted			Singlets		
	Attempted Impalements	Successful	Unsuccessful	Attempted Impalements	Successful	Unsuccessful
Expt I	33	23	10	36	1	35
Expt II	30	23	7	30	5	25
Expt III	30	24	6	30	2	28
Total	93	70	23	96	8	88
Mean %	...	75.3	24.7	...	8.3	91.7

growth medium (729A) containing 1.2 mM K^+ , grown 48 hours in 10% oxygen. Under these conditions, cells in contact with two or more neighbors could be readily impaled about 75% of the time. This was about the same degree of success attained with dense cultures several cell-layers thick. Moreover, a large portion of the remaining unsuccessful attempts were cells in which good recordings were obtained but the resting potential did not meet the minimum criterion of -50 mV, or the electrode became dislodged a few seconds after recording began.

Under identical conditions, singlet cells in these cultures permitted 8% successful recordings. Most commonly, upon impalement a single cell exhibited a 15–

20 mV resting potential. Within a few seconds it became dotted with small black spots at its periphery (Plate 8B, cell *p*). In most cases violent blebbing and vacuolization ensued (Plate 8B, cell *b*). In a successful impalement, the singlet cell did not increase in number of intracellular vacuoles, nor did it draw pseudopodial extensions. It remained smooth-faced and healthy in appearance throughout the recording period (Plate 8C). Furthermore, after withdrawing the electrode from a successfully impaled cell, that cell could often be impaled a second time with equal success.

The action potentials shown in Fig. 30 (A) and (B) were recorded from singlet cells similar to the one shown in Plate 8 (C). They are typical in amplitude and

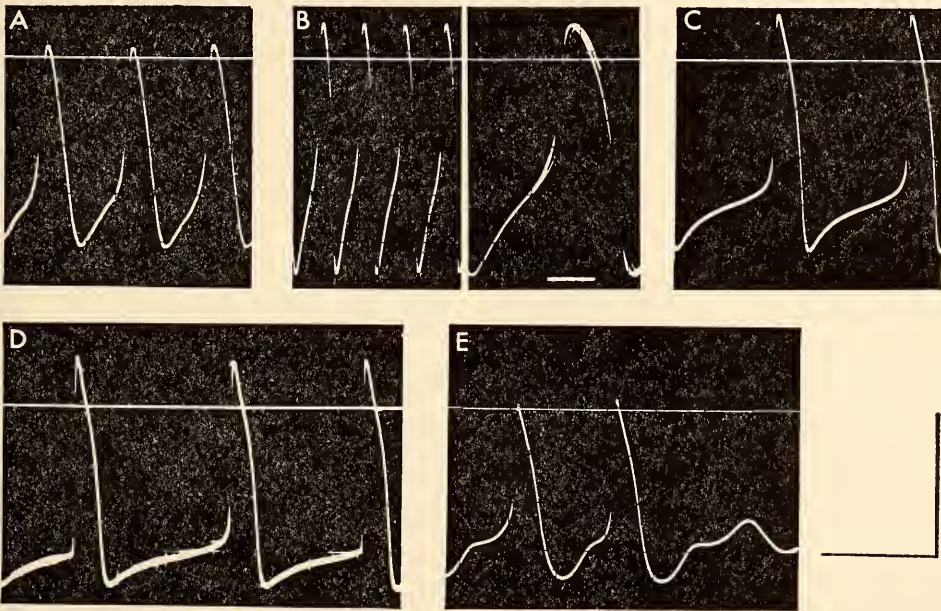


Fig. 30. Representative action potentials recorded from 7-day heart cells, 48 hours in culture medium 729A. (A) From singlet pacemaker M-cell. MDP = -64 mV; PBA = -55 mV, dur = 150 msec, rate = 170 B/M. (B) From singlet, pacemaker M-cell. MDP = -84 mV; PB = -49 mV; dur = 70 msec, rate = 450 B/M. (C) From contacted pacemaker M-cell, in sparse sheet. MDP = -64 mV; PBA = -50 mV; dur = 140 msec; rate = 103 B/M. (D) From contacted M-cell, alternating between primary and latent pacemaker MDP = -63 mV; PBA = -53 mV; dur = 130 msec. (E) From contacted M-cell in a group of three; to show the distinction between AHP and pacemaker potential. MDP = -59 mV; PBA = -47 mV; dur = 130 msec. Vertical scale = 500 msec except for the single fast sweep-speed record shown in B. The horizontal scale shown in that panel = 50 msec.

wave form. In Fig. 30 (C) are shown action potentials from a primary pacemaker in a sparse sheet of contacted cells similar to those photographed in Plate 8 (A). Except for pulsation rate (108/min) the form and amplitude of these action potentials are not substantially different from those recorded from singlets.

No one has attempted to offer an explanation for the difference in impalability between singlet and contacted cells except the more or less tacit assumption that a cell surrounded on all sides by neighbors is mechanically stronger and more stable than an isolated cell. Our experience would indicate, however, that mechanical support probably plays only a small role in the difference in ease of recording. This is shown by a comparison of Plate 8 (A) and (C). The impaled contacted cell (Plate 8A) is clearly not mechanically buttressed by any of the six neighbors with which it was electrically connected. Its only contact, in fact, is in a small region about 5 microns long where the end of the impaled cell adheres to an extension of the ruffled membrane of one of the other cells. Yet cells of this type could be impaled with 75% success (just as in very dense cultures) while recordings could be obtained only 8% of the time from singlet cells (Table 5).

An alternative explanation for the differential sensitivity to impalement is suggested by a consideration of the ultrastructure of intercellular connections. It is now well established that a variety of cell types, including cardiac muscle, exhibit "tight junctions" or "nexuses" at regions of intercellular contact where the outer leaflet of the apposed cell membranes fuse. These junctions have been associated with regions of low intercellular impedance in several cell types. They are found in intercalated discs of mammalian cardiac muscle and avian purkinje fibers, and appear to be present in electron micrographs of neonatal rat heart cells in tissue culture. Weidmann has presented compelling evidence that heart cells are connected

across highly permeable junctions in the intercalated discs by showing that K^{42} diffuses freely from cell to cell longitudinally along a strand of sheep ventricular fibers.

When an electrode 200–300 Å in diameter penetrates a cell membrane which is only 150–200 Å thick, it seems reasonable to assume that some tearing of the membrane will occur, especially a membrane weakened by trypsin. The "sealing-in" effects commonly observed within the first few minutes after cell impalement presumably represent the repair and adhesion of the membrane around the electrode. However, before this sealing is completed, substantial intracellular material could be lost to the environment. In a cell in electrical contact with several neighbors, the resultant deficit could be quickly restored after repair of the damaged membrane by flow of ions and other substances from connected cells across the intercellular low-impedance junctions. The singlet cell, in contrast, would have no such external reservoir of cytoplasmic components. If its transmembrane pump mechanisms were inadequate to transfer materials from the extracellular milieu, the cell would have to succumb. In light of these considerations, the requirements we have demonstrated for success in impaling singlet cells—ultrafine electrodes and culture conditions favoring growth and membrane synthesis—are readily understood.

Perhaps the most noteworthy result of the present study to date is the similarity in form and amplitude of action potentials recorded from singlet and contacted cells. Despite the difference in frequency of success, once an electrode was sealed in a singlet cell and the cell repolarized, it exhibited action potentials which were similar to those of pacemaker cells in contact with a few neighbors, or in dense, multilayered sheets. However, we are now in a position to begin asking questions of developmental significance. What are the changes in electrical prop-

erties of prospective myocardial cells as they differentiate pacemaker function and contractility? How do the responses of such cells to ambient ions change with development, and do ions such as potassium play regulative or causal roles in physiological differentiation? How do cells establish electrical conductivity with neighbors? Are the events which take place when cells isolated in culture begin to beat in synchrony related to those which presumably take place as the loose mesenchyme of the precardiac mesoderm condenses into the synchronously beating myocardial tube? The answers to these and many related questions must be left for the pages of future reports.

PROPERTIES OF HEART CELLS

Chick embryonic heart cells in culture are distinguishable in two apparent subpopulations by their different physiological characteristics. On morphological grounds also, we have characterized cultured heart cells as being either M-cells (myoblastlike and comprising about 65–75% of the population) or F-cells (fibroblastlike and comprising about 25–35% of the total population). Under phase optics, M-cells appear as thick, refractile cells, usually rounded and having what appears to be one nucleolus. F-cells appear as thin, well-spread, nonrefractile cells with phase dense granules surrounding a 2-nucleolate nucleus. Approximately 70–80% of the M-cells beat spontaneously in culture whereas only 1–5% of the F-cells do so. M- and F-cells also differ in their mitotic rates. Time-lapse studies have demonstrated that M-cells are generally stationary in culture and divide but rarely. On the other hand, F-cells move about very actively and have a life cycle of 11–18 hours. An additional difference between M- and F-cells, a difference probably at the cell membrane level, is reflected in their differential adhesiveness to Falcon Plastic surfaces. The F-cells attach more rapidly

and spread on the surface, while M-cells remain more rounded, and are more easily detached.

These differences, apparent in 24-hour cultures, appear to distinguish between two distinct and separate cell populations. However, any analysis of the properties of heart cells requires a test of this basic assumption. It is possible that the two sets of properties seen are manifested by the same cell type, responding to the culture conditions in one of two ways, or caught at two different times in the cell cycle by the processes of dissociation and culture. In cultures grown for many days, the sharp distinctions are lost—most cells spread well on the surface, become more or less vacuolated, and their nuclear inclusions often become granular or multiple.

For the past year Iris Polinger, a doctoral candidate at Johns Hopkins, has been concerned primarily with the problem of the disparity or identity of the two major heart-cell types. She has demonstrated clearly that these differences, while real, represent different morphological and physiological states of the same basic cell type.

The first question to be answered was whether the single or double phase-dense intranuclear inclusions are indeed nucleoli; that is, do they stain positively for RNA? Are they RNase-sensitive? Do they incorporate RNA precursors?

One of the more specific histochemical stains for RNA is azure B, which when used at 37°C, is a metachromatic stain, coloring RNA a deep purple, and DNA a blue-green. In order to determine the specificity of azure B in our system, several controls including DNase and RNase extractions were carried out. The results were unambiguous. The phase-dense spots in the nuclei apparently do contain RNA, since they stain a deep purple with azure B, and are destroyed only by RNase treatment.

To determine whether these RNA-containing structures synthesize RNA, cultured cells were incubated with 5, 10, or

12.6 $\mu\text{C}/\text{ml}$ of tritiated uridine, specific activity 9.3 or 19.5 c/mmole , for 15 or 30 minutes, washed, fixed, and coated with Kodak NTB-2 emulsion. After the appropriate exposure time, the plates were developed and stained with azure B. Nuclei which had more grains than the background number were examined to ascertain whether any of these grains were located over the azure B staining structures. Counts on 500 cells showed that 78% contained one azure B staining body in the nucleus and 22% had two such bodies. The majority of cells of both these classifications contained label. In this experiment, 90% of the one-body cells contained label over this structure, and 70% of the two-body cells contained label over both structures. About 9% of all of the cells counted did not show label over azure B staining bodies in the nucleus. Flattening the cells by air-drying before fixation in order to bring them closer to the emulsion did not seem to increase the percentage of the two-body cells which labeled in both bodies. Stimulating mitosis in cells in growth medium also did not seem to increase this percentage. Increasing the dosage of tritiated uridine or lengthening the exposure time resulted in a grain density which obscured the intranuclear contents. This still left 1-4% of the nuclei which did not label. That these unlabeled cells were not dead can be inferred from control experiments in which it was shown that all cells on sister plates were able to exclude the dye Nigrosin, indicating that they were all metabolically alive.

In sum, (1) the phase-dense bodies in M- and F-cells are RNase, but not DNase sensitive; (2) they stain with azure B; and (3) the majority of these structures incorporate tritiated uridine. On the basis of these three points, and their appearance in electron micrographs (see below), we classify them as nucleoli.

A second question asked by Polinger was whether 1-*nu* and 2-*nu* cells are present in the intact heart, and during the process of dissociation in proportions similar to those seen in cultured cells. To answer this, sections of intact seven-day heart, sections of centrifuged pellets of trypsinized cells (taken just before plating), and culture plates made from the same suspension as the pellets were stained with azure B and compared for the percentages of 1-*nu* and 2-*nu* cells. Table 6 shows that the proportion of 2-*nu* cells is approximately 58% in the intact ventricle. In sectioned pellets of trypsinized cells, the percentage of 2-*nu* cells is comparable, approximately 52%. However, when these cells were cultured, fixed at 24 hours and stained, the percentage of 2-*nu* cells was substantially decreased, to approximately 27%. About 15% of the freshly trypsinized cells took up Nigrosin, indicating that they were moribund or dead. Thus the difference in numbers of 1-*nu* and 2-*nu* cells between the intact heart and the culture plate could result from differential mortality, or from differences in the ability of the two cell types to stick to the plastic surface. However, the important point is that in the intact heart in the myocardium, epi-

TABLE 6. Number of 1-*nu* and 2-*nu* Cells in the Intact Heart, in Freshly Trypsinized Cells, and in Cells after 24 Hours in Culture

Source	Thickness of Section	% 1- <i>nu</i> \pm S.D.	% 2- <i>nu</i>	Number of Cells Counted
Intact heart: 7-day trabeculae of ventricle	7 μ	42.3 \pm 4	57.7	1900
Intact 7-day heart: epicardium	7 μ	49.5 \pm 0.8	50.5	800
Trypsinized cells in pellet prior to plating	7 μ	48.5 \pm 2.5	51.5	7000
Cultured cells	...	73.1 \pm 1	26.9	3500

cardium, and endocardium, cells containing one and two nucleoli, but otherwise indistinguishable, are present.

In the intact heart the similarities of 1-*nu* and 2-*nu* cells are also apparent in the ultrastructural level as shown in electron micrographs taken by Polinger (Plates 9 and 10). In 1-*nu* and 2-*nu* cells, a similar cytoplasmic organization, clumps of glycogen and mitochondria suggest that a single basic type is involved. Moreover, both 1-*nu* and 2-*nu* cells contain organized myofibrils with Z-bands, indicating clearly that 2-*nu* cells in the ventricle are neither endothelium nor fibroblasts. These micrographs also demonstrate that both intranuclear inclusions in 2-*nu* cells have the internal structure characteristic of nucleoli, corroborating the previous conclusion.

If the presence of one or two nucleoli and the constellation of behavioral properties associated with each, represent merely different states of the same fundamental cell type, it follows that nucleolar number should not breed true. A 2-*nu* cell should, at some point, be convertible into a 1-*nu* cell, or vice versa. DeHaan and Polinger have recently begun a collaborative study of cloning of heart cells to test this possibility. Preliminary results seem to be confirmatory. Colonies of cells, all derived from a single progenitor cell, exhibit both 1-*nu* and 2-*nu* nuclei.

MECHANISM OF ENLARGEMENT OF THE PERICARDIAL SPACE

In the chick embryo of 20–30 hours of incubation, the rostral portions of each lateral heart-forming region are converted into a pair of troughs of compact epimyocardial tissue, which gradually swing together, ventral to the forming foregut, to form the early primitive tubular heart. During the next 24 hours of incubation, the heart tube increases in length about sixfold. During the same period the rostrocaudal dimension of the pericardial cavity, in which the heart

grows, increases by a factor of about 3.5. This enlargement of the pericardial cavity is adequate to permit growth of the heart, but also keeps pace with the gradual curvature of the heart tube.

The caudal wall of the pericardial space is the anterior intestinal portal (AIP) of the foregut. Enlargement of that space occurs in conjunction with elongation of the foregut. In collaboration with DeHaan, Stalsberg has recently completed an analysis of the mechanism of foregut elongation, in an attempt to understand the interrelations of the morphogenetic events in the precardiac mesoderm and endoderm of the forming foregut.

In the chick embryo of about 24 hours of incubation, the first step in foregut formation is taken when the endoderm rostral to the tip of the lengthening notochord is thrown ventrally into a fold along a broad crescentic line. The ventral lip of this fold forms the anterior intestinal portal; the infolded pouch is the shallow rudiment of the foregut. During the ensuing 12–18 hours, the foregut lengthens from this shallow diverticulum into a fingerlike flattened tube more than a millimeter long. Despite scattered attacks on the problem, remarkably little is known about how these morphogenetic events take place. What are the topological transformations which convert the originally flat layer of endoderm into a blind tube? Where do the forces arise which bring about these tissue movements?

Stalsberg and DeHaan have approached these problems by applying visually observable markers to the endoderm of intact early embryos in culture, to trace the movements of that layer during foregut elongation. Embryos were explanted, marked with particles of iron oxide powder, and photographed at frequent intervals during a further 24 hours of development.

Measurements of the location of individually identified particles made on each photograph included the following (Fig.

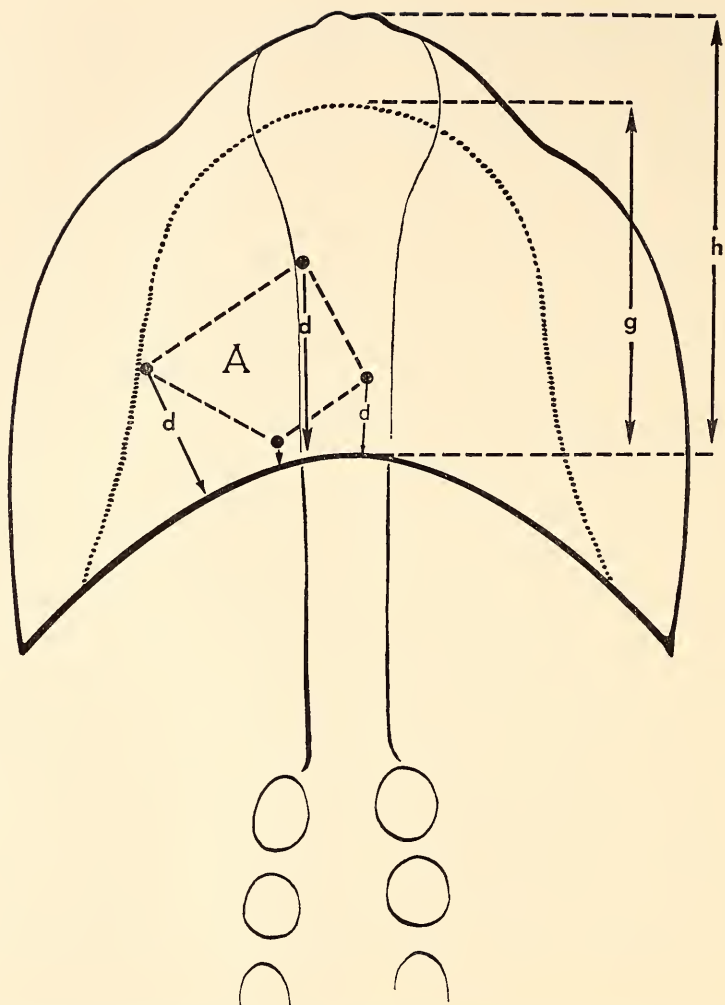


Fig. 31. Schematic drawing of the ventral surface of an embryo at stage 8. Iron oxide particles adhering to the yolk-sac endoderm are represented by solid circles. Measurements made on each embryo were: (1) distance (h) from tip of anterior neuropore to arch of AIP; length of foregut (g) was taken as 80% of h . (2) Shortest distance (d) from each particle of the edge of the AIP; (3) the area of a polygon (A) formed by connecting three or four selected particles with straight lines.

31): distance (h) from the anterior end of the embryo (neuropore) to the crest of the arch of the AIP; shortest distance (d) from each particle to the edge of the AIP; and the area of a polygon (A) enclosed by straight lines connecting three or four selected particles. At each stage, from the photographs, the polygons were traced on cellulose acetate film, cut out,

and weighed. The area measured at stage 6-7 (whenever the AIP was first seen) was given unit value for each embryo. With frequent observations, the individual particles could be readily identified from one stage to the next.

After the foregut starts to form with the appearance of the AIP, there is a steady increase in anteroposterior dis-

tance between the iron oxide particles, while lateral separation tends to decrease, bringing all particles closer to the midline. Plate 11 shows a series of photographs of a single embryo at sequential stages. For purposes of illustration, the same four iron oxide particles have been encircled at each stage.

To determine whether the apparent elongation of the yolk-sac endoderm represents merely a stretching of the tissue with compensatory narrowing, the areas of polygons comparable to the four-sided figure formed by the four encircled particles in Plate 11 were measured in all twelve embryos. When these sequential polygonal areas are plotted against foregut length (Fig. 32), the defined fields of subcephalic yolk-sac endoderm are seen to increase steadily in size. By stage 8⁺ to 9⁻ the endodermal polygons have doubled in average area; by stage 10 they

have increased threefold over their size at stage 6.

As the foregut lengthened, the particles followed a consistent pattern of behavior, increasing their longitudinal distance from each other and moving gradually toward the midline. Those particles which were positioned initially near the AIP approached the edge of the portal, while those located farther cephalad moved away from it. Measurements on 12 embryos showed, for example, that the yolk-sac endoderm, which was less than 33 microns from the AIP at the start of the early period of foregut elongation, rolled in over the portal to be incorporated as part of the foregut floor by the end of the foregut. As the foregut continued to lengthen, the amount of such inrolling decreased with time.

It was evident from the work of Stalsberg and DeHaan that anteroposterior

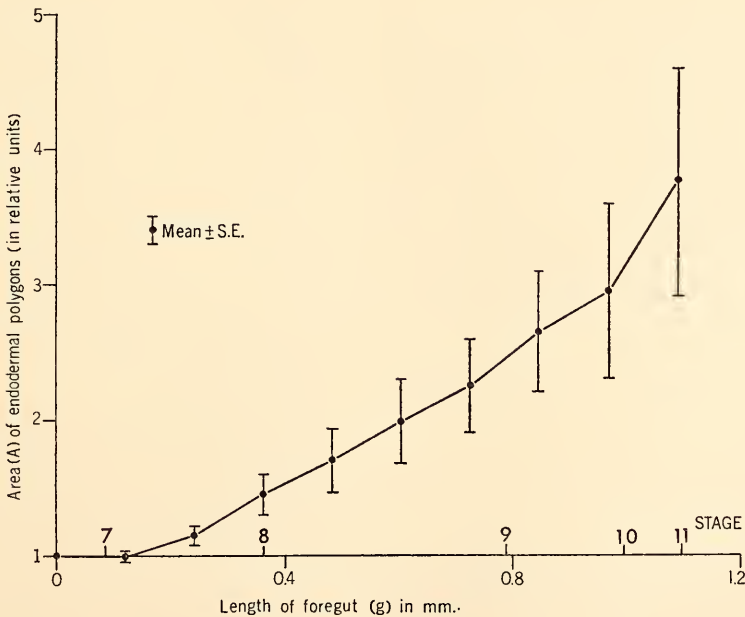


Fig. 32. Increase in area of polygonal regions of yolk-sac endoderm, defined by the positions of 3 or 4 iron oxide particles, plotted against foregut length. Each polygon was measured at intervals throughout development from about stage 6⁺ to stage 11. Each point on the curve shows a mean and standard error, calculated from individual growth curves at regular intervals. Developmental stage is given on the abscissa for comparison.

elongation of each region of endoderm in the area studied is a major factor in the morphogenetic movements forming the foregut, and moreover, that elongation occurs uniformly along the entire length of the subcephalic yolk-sac endoderm. From the elongation of radioactively labeled implants (to be reported elsewhere) it is apparent that this uniformity of elongation is not restricted to the yolk sac, but continues over the fold of the AIP along the endoderm of the foregut floor almost to its rostral tip. As diagrammed in Fig. 33, the major portion of yolk-sac endoderm anterior to the AIP at stage 7 remains extraembryonic throughout subsequent development of the foregut (Points 3, 4, Fig. 33B). However, our data indicate also that that part of the yolk-sac endoderm nearest the ridge of the AIP does roll in over the fold, accounting for a steadily decreasing fraction of the foregut elongation (Point 2, Fig. 33B).

When seen in midsagittal section (Fig. 33), these endodermal movements are reminiscent of those which occur when a rubber band, fixed at its two ends, is stretched into a U-shape by applying tension somewhere near the middle. Using this model—an elastic band under tension—Stalsberg and DeHaan have postulated a mechanism of foregut elongation which seems to fit the observed data. The model is illustrated in Fig. 34.

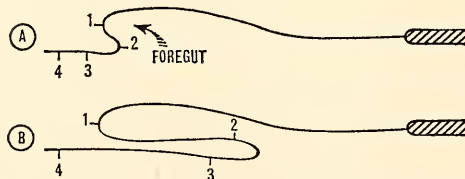


Fig. 33. Diagrammatic representation of a midsagittal section through the embryonic endoderm. Points 1-4 indicate identifiable positions on the cell sheet. (A) Stage 6⁺, shortly after the AIP was formed. Point 1, cephalic tip of the foregut; point 2, crest of the AIP, points 3 and 4, rostral yolk-sac endoderm. (B) Stage 10, foregut elongation by combined expansion and in-rolling.

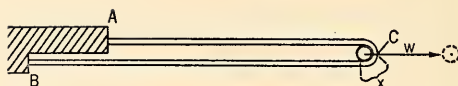


Fig. 34. Theoretical model to explain foregut elongation and in-rolling of endoderm over the AIP. A rubber band (ACB) is anchored at points A and B. Tension is exerted at point C by pulling a rod horizontally distance w . If the band is free to slip over the rod, a segment of it (x) will move around from the long limb (BC) to the short limb (AC) during stretching.

The ends of a rubber band are anchored at points A and B, which have a fixed relation to each other. At point C, a rod is inserted in such a way as to allow the rubber band to slip freely over it, permitting equalization of tensions in the two limbs. If the rod is drawn away from A and B a distance w , increasing the total length of the band (BC and AC) by factor a , then a segment x of the limb (BC) will move around to the short limb during stretching. And since the tension within the whole band is uniform, any part of it will increase by the same factor a .

Applying an analysis of the relationships seen in the simplified elastic model to the situation in the embryo, Stalsberg and DeHaan were able to show that the endoderm which forms the foregut floor at about stage 6⁺, when the foregut is 0.1 mm long, elongates to comprise 75% of the floor length when the foregut has increased to a total length of 1.0 mm, at about stage 10. The remaining 25% is derived from endoderm which was part of the yolk sac at stage 6⁺, but rolled over the AIP during the intervening period of elongation (Fig. 33).

As depicted in the model (Fig. 34), the ends of the elongating band (points A and B) are anchored, and they retain a fixed relationship to each other. In the embryo, point B would be equivalent to the junction of the yolk-sac endoderm and germ wall, at the edge of the pellucid area. It has been shown experimentally that the area pellucida is, in fact, maintained under tension by its connection with the area opaca, and that this tension is essential to normal development.

Point *A* of the model would represent the anterior tip of the foregut. The endoderm at this point is known to be firmly connected or fused with the anterior end of the head process, forming the prechordal plate. The strength of this connection was readily confirmed in experiments in which cultured embryos at stages 5+ to 7- were treated with 1% trypsin solution for a few minutes. The lateral and rostral endoderm could then be separated from its underlying attachments. In the midline, however, especially in the region of the prechordal plate, the endoderm would rupture rather than come loose from the subjacent mesodermal structures (Stalsberg, unpublished observations).

Assuming the validity of the proposed model, how might the tensions arise in the embryo which produce the folding, elongation, and in-rolling of the endoderm? A reasonable answer to this question derives from a consideration of the adhesive relations between the endoderm and mesoderm. During the time the head process forms and lengthens into the notochord, it adheres firmly to the neural plate, these two structures together giving a certain rigidity to the body axis. On its ventral side, the axial endoderm is firmly fused or anchored to the notochord along its entire length.

With regression of the primitive streak, the mesodermal streak tissue and the subjacent endoderm move backwards together. The axial endoderm rostral to the streak is thus stretched between the two terminal anchoring points (Hensen's node and the prechordal plate). This stretching was clearly demonstrated in carbon marking experiments some years ago by Bellairs.

The endoderm directly rostral to the prechordal plate would initially tend to be compressed rather than stretched. Lateral to the prechordal plate, where no such anchoring point exists for the

endoderm, the tension exerted by regression of the node could spread all the way to the edge of the area pellucida endoderm, and that layer would yield to the pulling force. In so doing, endoderm lateral to the prechordal plate would be drawn posteriorly. This movement in turn would transmit the tension to the endoderm rostral to the prechordal plate. The only way that this rostromedian endoderm could yield to the pull exerted upon it, would be by folding over the anchor point at the prechordal plate, forming the anterior intestinal portal. Thus the regressing primitive streak exerts tension on the lateral endoderm which is transmitted by a pulling force to the endodermal fold of the AIP. It is this latter tensional force which is simulated by the pull exerted at point *C* in the theoretical model. Because the prechordal plate has a certain width the transverse fold of the initial AIP will have a corresponding width, the fold tapering off into the posterolateral ridges in the direction of the pulling force.

Unlike the conditions in a sheet of rubber, the endoderm can probably yield to tension not only by deformation of the shape of cells, but also by rearrangement of the position of individual cells within the layer. Presumably, if a square piece of a cell sheet containing ten cells along each side is passively stretched in one direction, it will initially retain ten cells along each side. However, if the deformation is prolonged, the cells may rearrange themselves, for instance, into five rows of twenty cells each. Cell shape would thereby return somewhat towards normal, and the elastic tension in the sheet would be diminished. If, in a sheet of cells like the endoderm, rearrangement of cells keeps pace with the pulling movement, continued deformation of the sheet may take place without substantial increases of tension.

STUDIES ON CELL INTERACTIONS

S. Shifrin

Exploratory studies of the mechanisms by which cells move during embryogenesis and adhere to other cells in functioning tissues have been initiated thus far in two systems. The first study was carried out on the nature of forces by which 7-day embryonic heart cells adhere to the substratum. The second system was on the interaction of blastomeres in the cleaving eggs of *Urechis caupo*.

PROPERTIES OF EMBRYONIC HEART CELLS
IN TISSUE CULTURE

The properties of 7-day embryonic heart cells in tissue culture were described in *Year Book 65* (pp. 526-536). Disaggregated embryonic heart cells were plated on Falcon plastic petri dishes in growth medium 729A₁. Two distinct populations of cells could be recognized after several hours of incubation. As we have seen, they are believed to be different states of one basic cell type. One variant, designated as "M," often shows spontaneous beating activity while the other, "F" cell, is rarely found to have rhythmic activity. The difference in adhesivity of these two types of cells is suggested by their behavior as observed with time-lapse cinematography. The M-cell remains firmly attached to the substratum while the F-cell moves across the plate, constantly sending out pseudopodal extensions which often pull at the M-cell membrane. The F-cell lifts off the substratum in order to undergo a mitotic division while the M-cell has not been found to divide in the same medium.

Noncovalent Interactions in Adhesion

The interaction between cells in tissue culture and the metal ions of the substratum have been thoroughly investigated. There are few reports, however, of noncovalent interactions in tissue culture. There is considerable evidence that hy-

drophobic forces maintain the configuration of proteins such as myoglobin and that they maintain polypeptide subunits in an enzymatically active aggregate. In both examples of protein interaction, urea disrupts the hydrophobic forces. It appeared reasonable that hydrophobic bonds might also participate in cell interactions. In order for the cell to adhere to the plate or to another cell, the new bond which is formed must be more stable than its interaction with the medium. If electrostatic forces were important in cell-cell or cell-substratum interactions, the ionic content of the medium would disrupt the interaction. On the other hand, the aqueous medium which generally surrounds the individual cell must be squeezed out as the cell adheres to the substratum; i.e., a new region which repels an aqueous environment (hydrophobic bond).

Embryonic heart cells (2×10^5 cells/plate) were cultured in 729A₁ for 24 hours. The total number of cells which adhered to the plate and the number of beating cells were counted. Medium 729A₁ containing urea from 0.05 to 0.35 *M* replaced the original medium, and the plates were incubated for 7 hours. Cells which were desorbed by this treatment were removed and the plates were again examined. The results are shown on the semilogarithmic plot in Fig. 35. In the absence of urea, more than 50% of the cells which adhere to the substratum show spontaneous activity. Low concentrations of urea drastically reduce the percentage of beating cells. In addition, the distinct morphology of the two cell types is lost in the presence of urea so that it is not possible to determine whether urea selectively removes the M-cells or the F-cells. It is clear that urea irreversibly removes cells from the substratum. It is not known, however, if this results from disruption of hydrophobic forces or secondarily from the action of

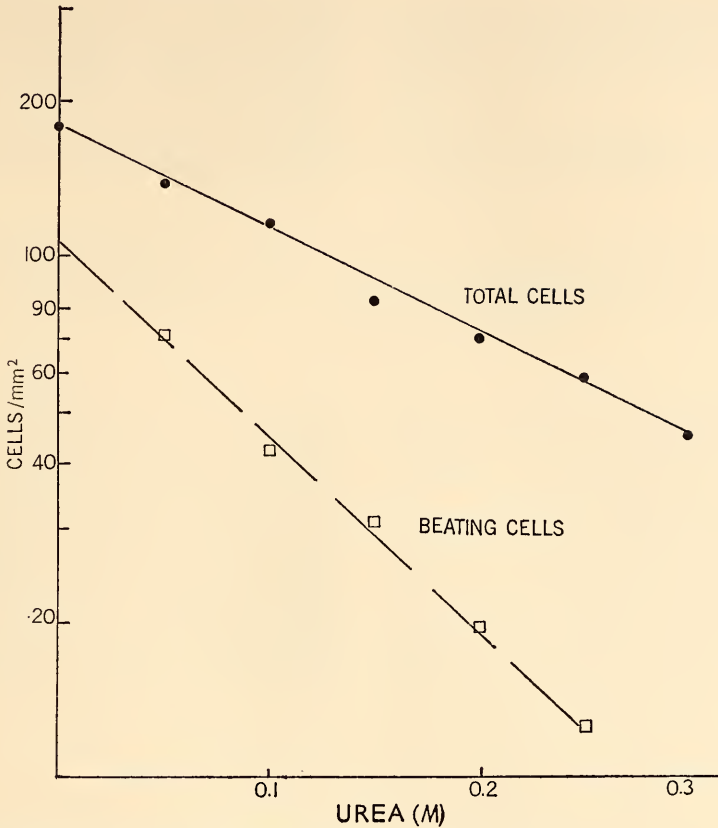


Fig. 35. Effects of urea on chick embryo heart cells. Details in text.

urea on an unrelated aspect of cell behavior. It should be mentioned that the concentration of urea employed in these studies is one tenth of that required for protein denaturation.

INTERACTION OF BLASTOMERES IN EGGS OF *Urechis caupo*

Many proteins such as the α - and β -chains of hemoglobin interact through the formation of disulfide bonds. If disulfide bonds link the blastomeres of a cleaving egg, a reducing agent such as Cleland's reagent, which is dithiothreitol (DTT), should disrupt the sulfide bond and cause the individual micromeres to fall apart. Fertilization of the eggs of *Urechis caupo* was carried out in seawater containing DTT at concentrations

ranging from $1.2 \times 10^{-4} M$ to $5.4 \times 10^{-3} M$. The appearance of the fertilization membrane, as well as the first and second cleavage stages of the embryo were normal in all but the highest concentration of DTT. However, the third cleavage, at which point the four macromeres give rise to their daughter micromeres, was normal only at the lowest concentration of DTT; i.e., 1.2 and $2.5 \times 10^{-4} M$. The macromeres did not cleave in the presence of $6.2 \times 10^{-4} M$ DTT or sometimes only one macromere would cleave. Although the concentration of the reagent appears to be somewhat high for biological systems, the permeability of the egg to this reagent is not known nor is the internal concentration known.

The effect of dithiothreitol on disrup-

tion of the already formed macromeres and micromeres could not be measured, since the fertilized egg was completely impermeable to 6×10^{-3} M DTT. Removal of the membrane with 0.53 M NaCl brought to pH 10.6 interrupted normal cleavage. Additional methods of de-

membration are being investigated. It is clear that the presence of disulfide bonds is essential for normal cleavage of *Urechis* eggs. Nevertheless, I have not ascertained whether or not an enzyme which promotes normal cleavage requires a disulfide bond for activity.

OVULATION AND GERMINAL VESICLE BREAKDOWN IN AMPHIBIAN OOCYTES: GONADOTROPHIC HORMONE SPECIFICITY

A. W. Schuetz

In amphibians two processes, the induction of ovulation and the completion of oocyte meiotic maturation as characterized by the breakdown of the germinal vesicle (GVBD), are initiated and controlled by the pituitary gland. Previous studies by this investigator have shown that progestational but not estrogenic steroid hormones are also effective stimulators of GVBD in oocytes incubated in vitro. The experimental evidence also indicates that pituitary stimulation of oocyte maturation is mediated by some intermediary intrafollicular process(es) or substances which resemble those stimulated by progestational steroids. In mammals ovarian processes and steroidogenesis are generally considered to be regulated by three gonadotrophic hormones secreted separately or in combination by the pituitary gland. These are FSH, LH, and LTH. The relative roles of these hormones in amphibian ovarian and oocyte functions are poorly understood, as is the nature of the amphibian pituitary substance(s) which stimulates ovulation and oocyte maturation. In the present study the effects of relatively purified gonadotrophic hormone on the processes of ovulation and maturation were compared. These effects were evaluated utilizing intact ovarian follicles of *Rana pipiens*. The follicles were maintained under standardized conditions in vitro. The incidence of GVBD in ovulated and unovulated oocytes was assessed. In all cases the effectiveness of the

purified hormones was compared with that of amphibian pituitary homogenates and progesterone. The biological activities of the following purified pituitary gonadotrophins, prepared by the National Institutes of Health, were compared: (1) follicle-stimulating hormone (FSH), (2) luteinizing hormone (LH), (3) luteotrophic hormone (LTH). The placental gonadotrophins (PMS and HCG) were also utilized. Fresh amphibian pituitary tissue was triturated prior to use and the equivalent of $\frac{1}{4}$ – $\frac{1}{10}$ of a pituitary was utilized for assay purposes. These data demonstrate that all doses of FSH (500 μ g), LTH (1 mg), PMS (500 I. U.), HCG (500 I. U.) tested were ineffective in stimulating either ovulation or germinal vesicle breakdown (the highest dose tested is in parenthesis). Pituitary LH, however, initiated both ovulation and GVBD when utilized at doses of 80–100 μ g. FSH, LTH, PMS, and HCG did not inhibit either (1) frog pituitary-induced ovulation and GVBD or (2) progesterone-induced GVBD. Addition of subminimal amounts of LH with 300–500 μ g of FSH did not result in a synergistic action between the FSH and LH.

On the basis of these studies mammalian pituitary appears to be the only gonadotrophin which shares with frog pituitary tissue the capacity to induce ovulation and GVBD. HCG, which is considered to be a highly potent LH-like gonadotrophin, was inactive. In view of the large quantity of LH (80–100 μ g) as

opposed to the very small amount of frog pituitary tissue required to stimulate ovulation and GVBD (the wet weight of a whole pituitary gland is less than 1 mg),

it appears that the gonadotrophic hormone(s) of the frog pituitary is a much more active molecule or of a different nature.

THE MAMMALIAN EMBRYO IN ITS RELATION TO ITS ENVIRONMENT

THE UPTAKE OF WATER BY THE RABBIT BLASTOCYST

P. H. Tuft and B. G. Böving

The formation of large, transient, liquid-filled intercellular cavities is an important and characteristic but little-understood feature of embryonic development. The rapid accumulation of fluid in the rabbit blastocyst cavity is a striking example of this phenomenon and is of special interest, because the resulting blastocyst expansion is the stimulus for equidistant spacing of blastocysts by the uterus. The expansion begins 4 days after mating, when the volume is about $6.5 \times$

10^{-5} ml. The volume then increases more and more rapidly, reaching 5.4×10^{-1} ml at 8 days after mating (Fig. 36). Since the dry weight of the blastocyst is approximately 1% of its wet weight, the bulk of the ten-thousandfold increase must be due to uptake of water either from fluid in the uterine lumen secreted by the endometrium or directly from the maternal blood after implantation has occurred. Before we can usefully speculate about the nature of the mechanisms which regulate the change in volume of the blastocyst, we need to know whether it can be accounted for simply by the passive flow of water down a chemical potential gra-

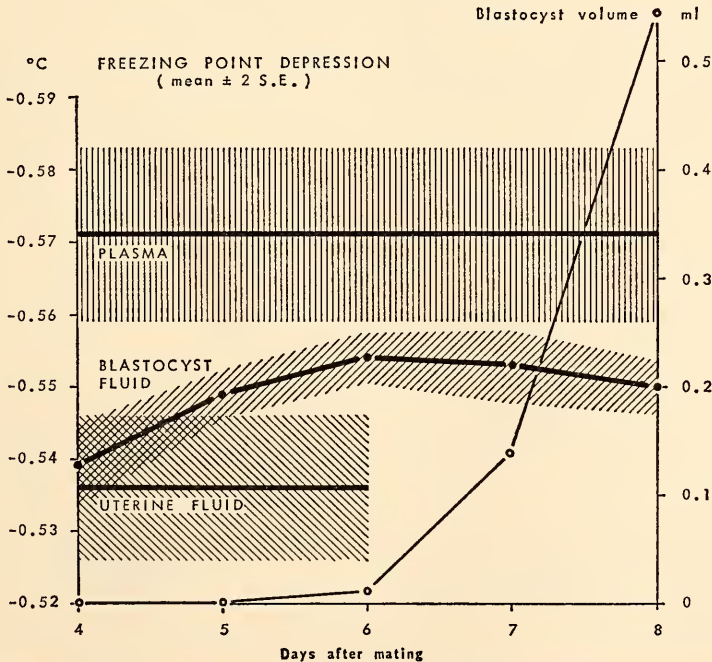


Fig. 36. Freezing point depression (ΔT_f) of fluids in various compartments and blastocyst volume on successive days.

dient or whether more complicated mechanisms are involved.

The difference between the chemical potential of pure water and water in solution ($\Delta\mu$) can be calculated with few assumptions from the depression of the freezing point (ΔT_f). Provided allowance is made for the effect of hydrostatic pressure on the potential *in situ*, the magnitude and sign of the gradients in question can be determined from the ΔT_f of samples taken from the blastocyst cavity, uterine lumen and blood and measured at atmospheric pressure. The volume of fluid in some of these compartments is very small, but Ramsay has described a method for measuring the ΔT_f of samples as small as 1×10^{-7} ml, which makes satisfactory measurements possible.

For the present investigation, a slightly modified version of the Ramsay apparatus was built by John Wiser. The principal modifications involved the rearrangement of the components and the replacement of the dry ice cooling tube by a thermoelectric cooling device. The sample holder, Beckman thermometer, cooling thimble, heating coils and stirrer were arranged in a straight line down the middle of the insulated bath. The coolant (50% each, alcohol and water) was cir-

culated along the bottom, up over the sample and thermometer bulb and back over the temperature regulating components, which ensured an even temperature distribution.

The freezing points were determined as follows. A droplet of the solution to be measured was placed in mineral oil (Nujol) in a wellled polyethylene slide. A small quantity of this sample was drawn up into a fine capillary of pure silica (I. D.=0.1 mm; O. D.=0.2 mm); see Fig. 37. The end of the capillary was sealed with sealing wax. The capillary was then put in a thin-walled glass handling tube (O. D.=1 mm) filled with oil (Fig. 37). The handling tube was then clamped in the sample holder of the apparatus and plunged into a mixture of solid CO_2 to quench the sample and transferred quickly to the bath at -1.0°C . The frozen sample was observed by transmitted light under a low power ($60\times$) microscope. The temperature of the bath was raised slowly until only two crystals of ice remained, when the heating rate was reduced to $0.001^\circ\text{C}/\text{min}$. The freezing point was taken to be that temperature at which the smallest visible crystal of ice was in equilibrium with the rest of the sample for 4 minutes. (It was

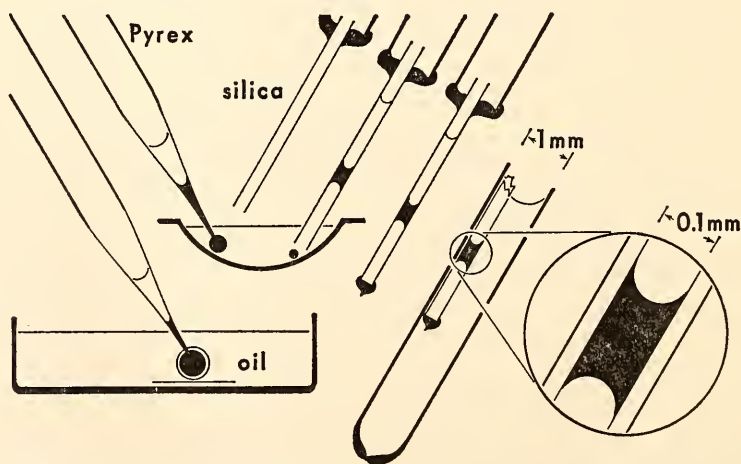


Fig. 37. Diagram showing sampling procedure.

usually necessary to raise and lower the temperature a number of times to obtain the highest precision.)

The thermometer was calibrated before each experiment by measuring the freezing point of a standard solution of NaCl (173 mmole/Kg H₂O) which had a Δ_{Tr} near that expected of the sample. The precision of the apparatus was tested by comparing the difference between the measured Δ_{Tr} of two standard solutions with the difference calculated from concentration and appropriate freezing point constant. The difference between measured and calculated values is small (Table 7); it approaches the smallest temperature difference that can be estimated on the thermometer used in these experiments.

The main problem encountered in the investigation was not the precision of the instrument but the difficulty of obtaining satisfactory samples of fluid from the blood, uterus, and blastocysts. However, after a number of preliminary experiments, a satisfactory procedure was evolved. Blood samples were taken from the unanesthetized rabbit, because it was found that the Δ_{Tr} increased after anesthesia. Blood was drawn from the ear vein into a glass syringe moistened with heparin. One half ml was placed under oil and centrifuged at 1550 *g* for 6 minutes. A droplet of plasma was transferred to clean mineral oil in the welled polyethylene slide and the freezing point sample taken as described. The rabbit was then anesthetized with intravenous sodium pentobarbital supplemented by open drop ether. After midventral incision, one of the uterine horns was drawn out, leaving the other in place to prevent cooling. Warm mineral oil was injected

into the lumen of the uterine horn at the tubal end and "milked" down with the fingers into a plastic dish through a polyethylene canula inserted in the cervix.

The warm oil containing the blastocysts and uterine fluid was then examined under a binocular dissecting microscope using transmitted light. Clear liquid droplets free of debris found in the oil were assumed to be uterine fluid and were transferred to clean oil with a fine pyrex pipet. Blastocysts were anchored to the surface of small strips of lens paper placed in the oil, and a fine oil-filled pyrex capillary, drawn to a point (0.01 mm), was introduced into the cavity, and a small quantity of the contents was removed and transferred to clean oil, and the freezing point samples were taken as before.

This procedure enabled us to obtain freezing point samples within ten minutes of the abdomen's being opened, without exposing the blastocysts to air or allowing their temperature to drop more than 2°C. This seems to be important, because preliminary experiments showed that the Δ_{Tr} of the blastocyst fluid tended to rise the longer they remained in the exposed uterus.

Between 6 and 7 days after mating, it becomes impossible to remove the blastocysts intact from the uterus, but by then the blastocyst cavity is so large that it can be sampled *in situ*. However, when we attempted to take samples through the intact wall of the uterus, the fluid tended to clot, a difficulty noted by Lutwak-Mann *et al.* We found we could avoid clotting if we stripped off most of the muscle from a small area of the antimesometrial wall before inserting the sampling capillary into the blastocyst cavity.

The results of a number of experiments using these procedures are summarized below (Table 8; Fig. 36). They show that: (1) The Δ_{Tr} of the plasma is always significantly greater than that of the uterine fluid and the fluid in the blastocyst cavity. (2) The Δ_{Tr} of the blastocyst

TABLE 7. Precision of Freezing Point Determinations

	Δ _{Tr} A-Δ _{Tr} B
Measured	- 0.297 ± 0.0026°C (n = 12)
Calculated	- 0.295°C
Solution A = 0.173 Molal NaCl	
Solution B = 0.083 Molal NaCl	

TABLE 8. Mean ΔT_r of Fluids in the Different Compartments

Compartment	Days After Mating	Animals	Samples	Mean ΔT_r °C	S.E. °C
Blastocyst	4	8	21	-0.539	± 0.0028
	5	4	20	-0.549	± 0.0016
	6	3	18	-0.554	± 0.0017
	7	3	18	-0.553	± 0.0025
	8	4	25	-0.550	± 0.0018
Uterine fluid	4-6 (combined data)	10	10	-0.536	± 0.0050
Maternal plasma	4-8 (combined data)	22	22	-0.571	± 0.0066

fluid does not differ significantly from that of the uterine fluid at 4 and 5 days after mating but is slightly greater at 6 days. (At 7 and 8 days after mating uterine fluid does not intervene between uterus and blastocyst, and none could be collected.)

In interpreting these results, it is necessary to take into account the effect of hydrostatic pressure on the potential of the water when the solutions are in the body. This is only important for the blood. If we assume an effective hydrostatic pressure difference equal to the arterial blood pressure (0.2 atm) the $\Delta\mu$ will only be raised from -3.01 cal/mol to -2.923 cal/mol, which is still appreciably less than the potential in the uterine fluid (-2.85 cal/mol). The blastocyst fluid at 4 and 5 days after mating has the same potential as the uterine fluid, but at 6 days after mating it drops to -2.93 cal/mol, so that it then has a

potential less than its surroundings. However, when implantation has occurred and the trophoblast has penetrated to the maternal blood vessels, the gradient is again reversed, because there is now no hydrostatic pressure difference and the effective potential of the water in the blood is -3.01 cal/mol. These changes are summarized in Figure 38.

If the only forces acting on the water in this system are the potential gradients between the different compartments, we would expect no uptake of water by the 4- and 5-day blastocyst, and we would expect a flow of water into the blood from the uterine lumen and the implanted blastocyst. Since the volume of the blastocyst increases more and more rapidly, the flows are all in the opposite direction, and we must conclude that either energy-coupled solute or water flows or both are involved.

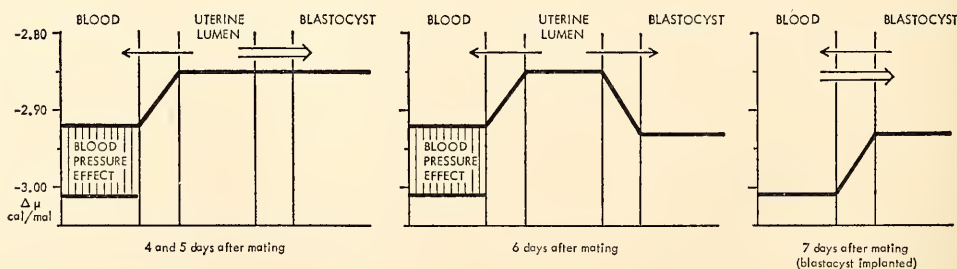


Fig. 38. The chemical potential gradients between blood, uterine fluid, and blastocyst fluid at different stages, calculated from the ΔT_r . The passive water flows are shown by single arrows, the energy coupled flows by double arrows.

ANATOMY AND PHYSIOLOGY OF THE
PLACENTA

*E. M. Ramsey, M. W. Donner,
C. B. Martin, Jr., H. R. Misenhimer
and S. I. Margulies*

Radioangiography of Placental Circulation in the Rhesus Monkey

In this ninth year of the collaboration between the Carnegie Department of Embryology and the Johns Hopkins Department of Radiology, attention has been focused upon three special facets of the general subject. Thanks to the fine facilities and skilled services available in the Radiology Research Laboratory at the Hospital and to the outstanding help of visiting associates who will be mentioned at appropriate points, it has been possible to obtain answers to several important questions in addition to pertinent data upon other matters investigated.

Standardization of technique. The success which has attended the use of radioangiography to demonstrate both the maternal and the fetal circulation of the placenta renders it likely that the method will be found applicable for many similar studies. It is important, therefore, that standards be set at the outset so that the results obtained in various laboratories may be uniform and comparable. An additional incentive prompting us to refine and standardize our technique was our desire to determine its suitability not only as a qualitative means of demonstrating pattern but also as a quantitative yardstick of placental circulation. Several parameters were regarded as fundamental and accordingly were investigated thoroughly.

Cumulative experience throughout the study has indicated the superior qualities of Conroy 60 (Meglumine iothalamate 60%) as a contrast material. This medium has lesser viscosity and is less irritating than the other substances tried (see previous *Year Books*) and is of very low toxicity. We have had no drug mortality in mothers or fetuses. Occasional

transitory muscle spasms have been noted immediately after injection but no other untoward effects have occurred when dosage was kept within reasonable limits. Highly satisfactory radiologic visualization has been obtained following injection of doses far below the level of tolerance and much smaller than those previously employed in our own studies. Injections are made into the femoral artery of mother or fetus or into the interplacental artery. We have adopted 5 ml as the standard dose in the mother and 2-3 ml in fetuses at or close to term. This dose may be repeated at least five times, with return to basal conditions between injections. The general condition of mother and fetus, reflecting the results of surgical manipulation as much as the effect of contrast medium injection, should be monitored by continuous blood pressure recording and frequent blood gas analyses.

For delivery of contrast material to the mother a plastic catheter of suitable calibre with side perforations towards its tip provides better delivery of the bolus than one with a perforation at the tip only. With such a catheter there is less likelihood of filling of the renal and mesenteric vascular beds with consequent loss of contrast material from the uterine circulation. The side hole catheters are not entirely satisfactory for direct blood pressure determination so we use a regular end hole catheter for this purpose, introducing it into a brachial artery. An end hole catheter has been found for injection of the fetal side of the placenta effected via the fetal femoral artery or an interplacental artery.

Optimum results were obtained in the mother when the end of the catheter was opposite the body of the fourth lumbar vertebra. Its position should be determined by fluoroscopy before each of the injections and necessary adjustments made to preserve constancy. This location provides maximum filling of the uterine vasculature with minimum diffusion of contrast material elsewhere. In fetal fem-

oral injections the catheter tip should be above the point of origin of the hypogastric artery so that both umbilical arteries may be filled. In injection of the interplacental artery the tip of the catheter should be pointed proximally to insure filling of as many umbilical artery branches as possible. Both fetal positions can and should be checked fluoroscopically. Injection pressure is of vital importance if a clear-cut, nondiffusing bolus is to be obtained. Experimentation with many other pressures, both up and down the scale, has shown 150 pounds per square inch to be the optimum value in maternal injections. This should be delivered by an automatically triggered pressure syringe coupled to the cine or automatic serial X-ray camera in such fashion that frame or film number one is exactly synchronous with the injection. Fetal injections are performed manually. In monkeys close to term the satisfactory radiological technical factors have been established as: Ansco roll film; 300 MA; time, 0.1 sec; KV, 60 for AP and 80 for lateral films.

The final technical decision involves which one of the films shall be taken as the criterion of the degree of intervillous space filling achieved by an injection. We have adopted as our standard the frame in a motion picture or the film of a series made 5 seconds after injection is commenced. It has been found that development of the basic number of "spurts" (entries of contrast medium to the intervillous space) is accomplished by this time in normal animals. If more appear later, they can be regarded as delayed in formation. In order that the analysis of spurts may be comprehensive, we recommend the reporting of two additional parameters: (1) the time at which the first spurt appears; (2) that at which the spurts are maximal. These together with the number of spurts at 5 seconds permit an evaluation of the circulatory conditions prevailing during the injection period. These data must, of course, be

correlated with the existing intervillous space pressure, the systemic blood pressure and, as needed, blood gas fluctuations.

The effect of anesthesia. Strong presumptive evidence that use of the anesthetic agent pentobarbital sodium did not affect the uteroplacental circulation was obtained in the studies carried out during the 1967 experimental season, as reported in *Year Book 66*. To "make assurance doubly sure" this matter was reexamined in the season just past, employing the refined techniques and criteria described above. Through the cooperation of Dr. Mary Ellen Avery of the Johns Hopkins Department of Pediatrics, we had the expert assistance of Mrs. Helen Scott of her Department in adding extensive blood chemistry determinations to our parameters of study. Again, with increased assurance, we can affirm that it is "both safe and reasonable" to use pentobarbital sodium in studies of placental circulation. From all standpoints of analysis, blood gas studies, radioangiography, or blood flow computation (see below), the results are essentially the same whether studies are carried out under pentobarbital or nitrous oxide-oxygen anesthesia.

As in 1966-1967 this phase of the study, together with that to be described in the following section, has been illuminated and implemented by the participation of Dr. John J. Bonica, Professor of Anesthesiology at the University of Washington in Seattle. Dr. Bonica has spent three extended work periods with us and, enlisting the generous cooperation of Dr. Donald W. Benson of the Johns Hopkins Department of Anesthesiology and his staff, has assisted us in carrying out highly sophisticated studies embracing anatomy, physiology, radiology, and biochemistry in a gratifyingly comprehensive investigation of our test object.

Radioangiography versus uterine blood flow determination as criterion of placental circulation. Having standardized our

technique of radioangiography so that we might attempt to quantitate the anatomical evidence obtained, we faced the question of whether spurt counts are in fact an adequate criterion of uteroplacental blood flow. The question is pertinent in view of the demonstrated effect of regional uterine activity upon intrauterine pressure (Caldeyro-Barcia) and the possibility of intrinsic vasomotion in individual spiral arteries (Martin *et al.*).

To investigate this we took advantage of the generous cooperation of yet another collaborator, Dr. C. B. Martin, Jr., of the Department of Obstetrics and Gynecology at the Medical College of Georgia. Dr. Martin, who has been a co-worker in our project for the past 5 years, brought his electromagnetic flow meter to Baltimore and we made radiography-flow meter comparisons in several animals. The anesthetized monkeys with flow probes in place in a single uterine artery, plus the usual recording and injection catheters, were subjected to drug-induced variations in systemic blood pressure and myometrial activity. Radioangiography was done during the test periods and resultant fluctuations in spurt counts were compared with changes in blood flow rate. Although the number of successful experiments is still limited, early indications are that spurts into the intervillous space and uterine blood flow are not always parallel. Further work with this exceedingly intricate and delicate technique is scheduled for next season.

Experimental Production of Hypertension

Drs. Alberto Hodari and Paul Hodgkinson of the Department of Obstetrics and Gynecology, Ford Hospital, Detroit, Michigan, placed bands upon the uterine arteries of six nonpregnant monkeys last spring, hoping to duplicate in a primate studies which they have carried out in

dogs. In the dogs this produces, in subsequent pregnancies, a hypertensive stage which resembles toxemia. Dr. Misenhimer has followed the blood pressure in these monkeys and various pertinent blood and urine constituents. Four of the monkeys became pregnant. A single year's observation is insufficient for formulation of conclusions. The study is being continued.

Incidence of Single Disc Placentas in Rhesus Monkeys

It has been commonly accepted that the placenta of the rhesus monkey (*Macaca mulatta*) is usually bidiscoid (Hill, 1932; Hartman and Straus, 1933; Wislocki and Streeter, 1938; Ramsey, 1950; Ruch, 1958). Since there is growing reason to believe, however, that single disc placentas are not rare, a survey of the findings in the Carnegie monkey colony was made by Mr. J. Sollins.

Data from 1960-1968 were reviewed. During this period of nine breeding seasons, there were 143 pregnancies. Reliable data on the placenta were collected for 90 monkeys, 64% of the total. To insure accurate interpretation, note should be taken of the methods of study of the placentas. Thirty-eight monkeys were studied by radiography: 29 by gross inspection, 23 by transillumination of the intact uterus.

The results show that 68 monkeys (75.5%) had a bidiscoid placenta; 22 (24.5%) had a placenta consisting of a single disc. There were 10 cases (14.3%) in which a monkey had a double or single placenta interchangeably over a period of years.

Thus, single placentas are by no means uncommon, as previously believed, and one may expect to encounter single placentas in one quarter of all pregnancies, even in monkeys whose placenta was bidiscoid in previous pregnancies.

THE COLLECTION OF HUMAN EMBRYOS

B. G. Böving and E. M. Ramsey

In the year covered by this report, E. M. Ramsey examined 41 specimens sent by 19 physicians from seven states. Of these specimens 22 were discarded as of no research or museum value, at the end of three months after reporting to donor, provided nothing further was heard from him. Nineteen specimens had sufficient value and were in good enough condition to justify permanent preservation.

THE DEVELOPMENT OF THE EPIPHYSIS CEREBRI AND THE SUBCOMMISSURAL COMPLEX IN STAGED HUMAN EMBRYOS

R. O'Rahilly

The pineal body first appears in the roof of the diencephalon adjacent to a shallow bay (Stadium I of Turkevitch) at stage 15 (33 postovulatory days). The primordium is covered by the encephalic basement membrane and the bay is lined by terminal bars throughout the embryonic period. Cellular migration in an external direction occurs during stages 16 and 17, during which time the posterior commissure is defined (Stadium II). By stage 18, the cellular migration forms a distinct "anterior lobe" in which follicles appear (Stadium III). A characteristic step and wedge appearance of the anterior lobe (Stadium IV) is found at stage 19. At the end of the em-

bryonic period proper (stage 23, 8 postovulatory weeks), the pineal body (Stadium V), the posterior commissure, the habenular commissure, and the subcommissural organ are all present.

DEVELOPMENT OF THE TEETH AND ORAL STRUCTURES

Two investigators have used the Collection in studies of the differentiation and morphogenesis of the teeth and oral structures.

Dr. P. E. B. Calonius of the University of Helsinki, currently a visiting scientist at the University of Maryland, has studied normal development of the teeth as part of the background of his research on the factors contributing to the retardation of dental development in human infants, and on the epithelial remnants in the jaws (where the fetal processes fuse and where the dental lamina tends to form cysts). The epithelial remnants may also be sources of odontogenic tumors. Aspects of these studies were presented at the annual meetings of the American Academy of Oral Pathology and the International Association for Dental Research.

Dr. Edmundo B. Nery of the Cleft Palate Research Center at the University of Pittsburgh has used selected younger embryos in his continuing study of the normal development of the teeth.

STAFF ACTIVITIES

Science, the hoary cliché goes, aims at truth, art at beauty. However, the criteria of truth, such as verification by experiment, are not as hard and clean as we tend to believe. The same experimental data can often be interpreted in more than one way—and that is why the history of science echoes with as many impassioned controversies as the history of literary criticism. Moreover, the verification of a discovery comes *after* the act; the creative act is for the scientist, as for the artist, a leap into the dark, where both are equally dependent on their fallible intuitions.

ARTHUR KOESTLER—*The Ghost in the Machine*, 1968

The dissemination of research findings, through presentations at informal conferences and meetings of learned societies,

publications, and teaching, serves several functions. It provides an opportunity for criticism and exchange, leading ulti-

mately to verification of discovery, and advance—the word “ultimately” being crucial, for verification may be preceded, once or even repeatedly, by failure of confirmation, by reexamination and re-direction. Teaching, especially, has another function: to convey an awareness of the forces impinging upon creativity and making it possible. Although the gap between students and teachers has widened of late, partly because many students are critical of faculty participation in research, it still seems reasonable that a sense of what it is to be involved in creative research may best be conveyed by an active participant. It is for these reasons that Staff Members and Fellows are strongly committed to teaching activities.

Formal teaching has been largely confined to the Johns Hopkins Department of Biology, but during the year lectures were offered in other departments of the University as well, among them Anatomy, Obstetrics and Gynecology, Pathobiology and Pediatrics.

Other activities directed largely toward teaching included the participation of members of the Department in a series of lectures offered for high school teachers at the National Association of Biology Teachers Regional Seminar, held at the University of North Carolina, and for the Independent School Teachers' Association, Wilmington, Delaware. Lectures and laboratory programs were also presented at Friends School, Baltimore, and the Waterville (Maine) Area Science Center.

Lectures were presented at a number of campuses, including Case Western Reserve University, Indiana University, New York University, Pennsylvania State University, State University of New York (Downstate Medical School and Stony Brook), Temple University, Tohoku University School of Medicine, Wright State University, Yale University, and the Universities of California (San Diego and Santa Barbara), Connecticut, Delaware, Kyoto, Kyushu,

Miami (Florida), Michigan, Minnesota, North Carolina, Pennsylvania, Pittsburgh, Rochester, and Wisconsin.

Special presentations included a series of E. B. Wilson Lectures at the University of Texas, a National Institutes of Health Lecture, a Thomas Alva Edison Lecture, and the Yamagiwa Memorial Lecture at the Cancer Institute, Tokyo, in addition to addresses before audiences at the Cold Spring Harbor Laboratory of Quantitative Biology, the Institute for Cancer Research, Maryland Academy of Sciences, Michael Reese Hospital, Smithsonian Institution, and Worcester Foundation.

Among the symposia and conferences in which various members of the staff participated during the past year were the following: Seventh International Congress of Biochemistry, Tokyo; Eighth International Embryological Conference, Interlaken, Switzerland; U.S.-Japan Conference on Control Mechanisms in Cells, Tokyo; Symposium on Molecular Aspects of Differentiation; Gordon Conference on Cell Structure and Metabolism; the Neurosciences Research Program Work Session on Trophic Effects of Neurons; the American Society for Cell Biology Symposium on Cytodifferentiation; Twenty-seventh Symposium of the Society for Developmental Biology; Symposium on Virus Induction by Cell Association; two Symposia dealing with the heart—one on Congenital Heart Disease, the other on Pathophysiology of Heart Disease; and two on problems of reproduction—one on Obstetrical and Fetal Physiology, the other on the Physiology and Pathology of Reproduction. Two informal Workshops in the latter field also were unusually instructive, one on Placental Biopsy, the other on Reproductive Physiology.

Members of the group took part in meetings of a number of learned societies, including, in addition to those already mentioned, the American Association of Anatomists, American Chemical Society, American College of Obstetri-

cians and Gynecologists, American Society of Biological Chemists, American Society for Cell Biology, Federation of American Societies for Experimental Biology, National Academy of Sciences, and Society for Gynecologic Investigation.

Advisory and consultative services included membership on the editorial boards of *Developmental Biology*, *International Journal of Cancer*, *Journal of Embryology and Experimental Morphology*, *Excerpta Medica* (section on Human Developmental Biology), *Current Topics in Developmental Biology*, and *Quarterly Review of Biology*.

Members of the staff continued to serve on the University Science Development Advisory Panel, National Science Foundation; and the Visiting Committees of the Departments of Biology, of Massachusetts Institute of Technology, University of Oregon, and University of Toledo. In addition, service was rendered on Advisory Committees of the Center for Oral Health Research (University of Pennsylvania) and the International Institute for the Study of Human Reproduction (Columbia University).

Members of the staff also acted in these capacities: Member of the Board of Scientific Overseers, Jackson Laboratory; Trustee, Marine Biological Laboratory; Member of the Board of Scientific Counselors, National Cancer

Institute; and Member of the Board of Directors, Oak Ridge Associated Universities.

A sampling of other posts within professional societies includes the following: in the American Association for the Advancement of Science, Committeeman-at-Large for Medical Sciences, Committee on Science in the Promotion of Human Welfare, Newcomb Cleveland Prize Committee; in the American Association of Anatomists, Representative to Division of Medical Sciences of the National Research Council, Representative to the National Society for Medical Research; in the American Institute of Biological Sciences, Chairman of the Committee on Laboratory Animal Care, and Council of Past Presidents.

Seminars. The roster of speakers at the seminars organized by the Department to serve all those working in developmental biology in the region included H. Berendes, Max-Planck-Institut, Tübingen; A. Braun, Rockefeller University; E. H. Davidson, Rockefeller University; H. Hanafusa, The Public Health Research Institute; S. Hendricks, Mineral Nutrition Laboratory, U. S. Department of Agriculture; O. Miller, Oak Ridge National Laboratory; B. Mintz, Institute for Cancer Research; C. Pelling, Max-Planck-Institut, Tübingen; H. M. Rabes, Rockefeller University.

BIBLIOGRAPHY

- Biggers, J. D., D. G. Whittingham, and R. P. Donahue, The pattern of energy metabolism in the mouse oocyte and zygote. *Proc. Natl. Acad. Sci.*, 58, 560-567, 1967.
- Böving, B. G., Laboratory animal legislation dangers. *BioScience*, 17, 771-773, 1967.
- Böving, B. G., *Review of Sir William Osler, Læge og livskunstner* by Anker Aggebo (København, Astra, 1966). *Bull. Hist. Med.*, 62, 88-89, 1968.
- Böving, B. G., Blastocyst propulsion by rabbit uterus. *Anat. Record*, 160, 520, 1968.
- Brown, D. D., Nucleic acid determination in embryos, in *Methods in Developmental Biology*, F. H. Wilt and N. K. Wessells, eds., Thomas Y. Crowell Co., New York, pp. 685-701, 1967.
- Brown, D. D., The genes for ribosomal RNA and their transcription during amphibian development, in *Current Topics in Developmental Biology*, vol. 2, A. Monroy and A. A. Moscona, eds., pp. 47-73, 1967.
- Brown, D. D., *Review of Theodor Boveri. Life and Work of a Great Biologist, 1862-1915*, by Fritz Baltzer. Translated from the German by Dorothea Rudnick. *Science*, 160, 653-654.
- Brown, D. D., and I. B. Dawid, Specific gene amplification in oocytes. *Science*, 160, 272-280, 1968.

- Brown, D. D., *see also* Sinclair, J. H.
- Brown, D. D., and C. S. Weber, Gene linkage by RNA-DNA hybridization. I. Unique DNA sequences homologous to 4S RNA, 5S RNA and ribosomal RNA. *J. Mol. Biol.*, **34**, 661-680, 1968.
- Brown, D. D., and C. S. Weber, Gene linkage by RNA-DNA hybridization. II. Arrangement of the redundant gene sequences for 28S and 18S ribosomal RNA. *J. Mol. Biol.*, **34**, 618-697, 1968.
- Cahn, M. B., *see* Cahn, R. D.
- Cahn, R. D., H. G. Coon, and M. B. Cahn, Cell culture and cloning techniques, in *Methods in Developmental Biology*, F. H. Wilt and N. K. Wessells, eds., Thomas Y. Crowell Co., New York, pp. 493-530, 1967.
- Coon, H. G., Hybrid cell strain formation by virus-induced fusion of Colcemid-arrested metaphases. *J. Cell. Biol.*, **35**, 27A, 1967.
- Coon, H. G., and G. Marzullo, Chondroitin sulfate synthesis in clonal cultures of embryonic chick cartilage. *Seventh International Biochemistry Congress, Abstracts*, Supplement I, 1082 (381)-1083 (382), 1967.
- Coon, H. G., *see also* Cahn, R. D.
- Dawid, I. B., and D. R. Wolstenholme, Ultracentrifuge and electron microscope studies on the structure of mitochondrial DNA. *J. Mol. Biol.*, **23**, 233-245, 1967.
- Dawid, I. B., and D. R. Wolstenholme, Renaturation and hybridization studies of mitochondrial DNA. *Biophys. J.*, **8**, 65-81.
- Dawid, I. B., *see also* Brown, D. D.; Wolstenholme, D. R.
- DeHaan, R. L., Avian embryo culture, in *Methods in Developmental Biology*, F. H. Wilt and N. K. Wessells, eds., Thomas Y. Crowell Co., New York, pp. 401-412, 1967(a).
- DeHaan, R. L., Introduction: Spontaneous activity of cultured heart cells, in *Factors Influencing Myocardial Contractility*, R. D. Tanz, F. Kavalier and J. Roberts, eds., Academic Press, New York, pp. 217-230, 1967(b).
- DeHaan, R. L., Regulation of spontaneous activity and growth of embryonic chick heart cells in tissue culture. *Develop. Biol.*, **16**, 216-249, 1967(c).
- DeHaan, R. L., The effects of potassium ion concentration on spacing and intercellular contact among embryonic heart cells in monolayer cultures. *J. Cell. Biol.* **35**, 32A, 1967(d).
- Donner, M. W., *see* Martin, C. B., Jr.; Ramsey, E. M.
- Ebert, J. D., *Review of Genetic Control of Differentiation*. *Quart. Rev. Biol.*, **42**, 60, 1967.
- Ebert, J. D., *Review of Essays in the History of Embryology and Biology*, by Jane M. Oppenheimer. *BioScience*, **17**, 749 (1967).
- Ebert, J. D., *Review of Control of Cellular Growth in Adult Organisms*, H. Teir and T. Rytömaa, eds. *Science*, **159**, 620, 1968.
- Ebert, J. D., Molecular and cellular interactions, in *The Neurosciences: A Study Program*, G. Quarton, T. Melnechuk and F. O. Schmitt, eds., Rockefeller University Press, New York, pp. 241-247, 1967.
- Ebert, J. D., *Review of Nobel Lectures. Physiology or Medicine, 1901-1921*. *Science*, **159**, 866-867, 1968.
- Ebert, J. D., F. E. Samson, Jr., and Y. M. Homsy, Gene expression. *Neurosciences Res. Progr. Bull.*, **5**, 223-306, 1967.
- Ebert, J. D., *see also* Lee, H. H.
- Ephrussi, B., and M. C. Weiss, Regulation of the cell cycle in mammalian cells: inferences and speculations based on observations of interspecific somatic hybrids. *Develop. Biol.*, Suppl. **1**, 136-169. (The 26th Symposium of the Society of Developmental Biology, *Control Mechanisms in Developmental Processes*, M. Locke, ed., Academic Press, Inc., 1967).
- Ephrussi, B., *see also* Weiss, M. C.
- Green, H., *see* Weiss, M. C.
- Hay, R. J., and J. Paul, Factors influencing glucose flux and the effect of insulin on cultured human cells. *J. Gen. Physiol.*, **50**, 1663-1680, 1967.
- Hay, R. J., Cell and tissue culture in aging research. *Advan. Gerontol. Res.*, **2**, 121-158, 1967.
- Hay, R. J., and B. L. Strehler, The limited growth span of cell strains isolated from the chick embryo. *Exp. Gerontol.*, **2**, 123-135, 1967.
- Hay, R. J., R. A. Menzies, H. P. Morgan, and B. L. Strehler, The division potential of cells in continuous growth as compared to cells subcultivated after maintenance in stationary phase. *Exp. Gerontol.*, **3**, 35-44, 1968.
- Homsy, Y. M., *see* Ebert, J. D.
- Kaighn, M. E., *see* Lee, H. H.
- Kimmel, C. B., Lysosomes in the spleen of the chick embryo. I. Description in the normal spleen. *J. Exp. Zool.*, **166**, 433-445, 1967.
- Kimmel, C. B., Lysosomes in the spleen of the chick embryo. II. Changes during the graft-versus-host reaction. *J. Exp. Zool.*, **166**, 447-458, 1967.
- Lee, H. H., M. E. Kaighn, and J. D. Ebert, Induction of thymidine-³H incorporation in multinucleated myotubes by Rous sarcoma virus. *Intern. J. Cancer*, **3**, 126-136, 1968.

- Lieberman, M., Effects of cell density and low K on action potentials of cultured chick heart cells. *Circulation Res.*, 21, 879-888, 1967.
- Martin, C. B., Jr., Anatomy and circulation of the placenta, in *Intrauterine Development*, A. C. Barnes, ed., Lea and Febiger, Philadelphia, pp. 35-67, 1968.
- Martin, C. B., Jr., E. M. Ramsey, and M. W. Donner, Gross anatomy of the placenta of rhesus monkeys. *Anat. Record*, 160, 389, 1968.
- Menzies, R. A., *see* Hay, R. J.
- Morgan, H. P., *see* Hay, R. J.
- O'Rahilly, R., The development of the epiphysis cerebri and the commissural complex in staged human embryos. *Anat. Record*, 160, 488-489, 1968.
- Paul, J., *see* Hay R. J.
- Ramsey, E. M., Uteroplacental circulation during labor, in *Symposium on the Physiology of Labor*, E. J. Quilligan, ed., *Clin. Obstet. Gynecol.*, 11, 78-95, 1968.
- Ramsey, E. M., M. W. Donner, and C. B. Martin, Jr., *Placental Circulation in the Rhesus Monkey*. A motion picture in color, with spoken narration. Produced with the advice and assistance of B. G. Böving, H. R. Misenhimer, S. I. Margulies, and R. D. Grill, 1968.
- Ramsey, E. M., *see also* Martin, C. B., Jr.
- Ristow, H. J., *see* Wolstenholme, D. R.
- Samson, F. E., Jr., *see* Ebert, J. D.
- Scaletta, L. J., *see* Weiss, M. C.
- Schuetz, A. W., Variable sensitivity of starfish ovarian tissue to radial nerve factor. *Exp. Cell Res.*, 43, 183-186, 1967.
- Schuetz, A. W., Action of hormones on germinal vesicle breakdown in frog (*Rana pipiens*) oocytes. *J. Exp. Zool.*, 166, 347-354, 1967.
- Sinclair, J. H., and D. D. Brown, Conservation of ribosomal DNA sequences among eukaryotes. *Federation Proc.*, 27, 335, 1967.
- Strehler, B. L., *see* Hay, R. J.
- Tiedemann, H., J. Born, and H. Tiedemann, Embryonale Induktion und Hemmung der Ribonucleinsäure-Synthese durch Actinomycin D. *Z. Naturforsch.*, 22b, 649-659, 1967.
- Todaro, G. J., *see* Weiss, M. C.
- Weiss, M. C., Discussion in *Report on the Workshop on Virus Induction by Cell Association*, S. Svoboda, D. Simkovic and H. Koprowski, eds., *Intern. J. Cancer*, 3, 317-322, 1968.
- Weiss, M. C., B. Ephrussi, and L. J. Scaletta, Loss of T-antigen from somatic hybrids between mouse cells and SV₄₀-transformed human cells. *Proc. Natl. Acad. Sci.*, 59, 1132-1135, 1968.
- Weiss, M. C., and H. Green, Human-mouse hybrid cell lines containing partial complements of human chromosomes and functioning human genes. *Proc. Natl. Acad. Sci.*, 58, 1104-1111, 1967.
- Weiss, M. C., G. J. Todaro, and H. Green, Properties of a hybrid between lines sensitive and insensitive to contact inhibition of cell division. *J. Cell. Physiol.*, 71, 105-108, 1968.
- Wolstenholme, D. R., I. B. Dawid, and H. J. Ristow, An electron microscope study of DNA molecules from *Chironomus*. *J. Cell. Biol.*, 35, 145A-146B, 1967.
- Wolstenholme, D. R., *see also* Dawid, I. B.
- Yoshikawa-Fukada, M., The intermediate state of ribosome formation in animal cells in culture. *Biochim. Biophys. Acta*, 145, 651-663, 1967.

PERSONNEL

Year Ended June 30, 1968

(including those whose services began or ended during the year)

Research Staff

Bent G. Böving, Physiology
 Donald D. Brown, Biochemistry
 Igor B. Dawid, Biochemistry
 Robert L. DeHaan, Experimental Embryology
 James D. Ebert, Director
 Elizabeth M. Ramsey, Placentology and Pathology

Assistant Investigator

Robert J. Hay

Research Associates (extramural)

Louis B. Flexner, Philadelphia
 Arthur T. Hertig, Boston
 Irwin R. Konigsberg, Charlottesville
 Samuel R. M. Reynolds, Chicago

Fellows

Hayden G. Coon, Fellow of Carnegie Institution
 Douglas M. Fambrough, Fellow of Carnegie Institution

Harold Kasinsky, Fellow of U. S. Public Health Service
 Harold R. Misenhimer, Fellow of Carnegie Institution
 Ronan O'Rahilly, Fellow of Carnegie Institution
 Ronald H. Reeder, Fellow of the Helen Hay Whitney Foundation
 John H. Sinclair, Fellow of U. S. Public Health Service
 Helge Stalsberg, Fellow of U. S. Public Health Service
 Ronald F. Swanson, Fellow of Carnegie Institution
 Peter H. Tuft, Fellow of Carnegie Institution
 Mary C. Weiss, Fellow of U. S. Public Health Service
 Masako Yoshikawa-Fukada, Fellow of Carnegie Institution
 Shuhei Yuyama, Fellow of Carnegie Institution

Students

John Chase, Graduate, Biology, Johns Hopkins University
 M. Egorin, Undergraduate, Johns Hopkins University
 Sheldon H. Gottlieb, Undergraduate, Johns Hopkins University
 B. Gould, Undergraduate, Johns Hopkins University
 R. L. Hallberg, Predoctoral Fellow, U. S. Public Health Service
 Iris S. Polinger, Graduate, Biology, Johns Hopkins University
 Merry C. Schwartz, Predoctoral Fellow, National Science Foundation

Visiting Investigators

John Bonica, Seattle
 P. E. B. Calonius, Helsinki and Baltimore
 Louis E. DeLanney, Ithaca, N. Y.
 Martin W. Donner, Baltimore
 Cary M. Dougherty, Baton Rouge, La.
 Marlene Eng, Seattle
 Daniel Goor, New York
 Peter Gruenwald, Baltimore
 R. Lawrence Kroovand, Cincinnati
 C. B. Martin, Jr., Augusta, Ga.
 Roberto Narbaitz, Baltimore and Pittsburgh

Edmundo Nery, Pittsburgh
 N. Nishida, Iwamizawa, Hokkaido
 Dorcas H. Padget, Baltimore
 Glenn C. Rosenquist, Baltimore
 A. W. Schuetz, Baltimore
 Adolph H. Sellman, New Orleans
 C. B. Severn, Ann Arbor, Mich.
 S. Shifrin, Bethesda
 D. G. Whittingham, Baltimore
 E. Witschi, New York
 M. Wharton Young, Washington, D. C.

Clerical and Technical Staff

James E. Abbott, Recorder
 Grace M. Andrews, Secretary-Receptionist
 Mary N. Barton, Librarian (part time)
 James Blackwell, Custodian
 Paul Blackwell, Custodian
 William J. Cleary, Recorder
 William H. Duncan, Senior Technician
 Wilbur F. Garde, Assistant Recorder
 Richard D. Grill, Photographer
 Elizabeth L. Hallberg, Technician
 Ernest Harper, Chief Custodian
 Virginia Hicks, Laboratory Helper
 Eddie Jordan, Technician
 Elizabeth Legum, Technician
 Edna G. Lichtenstein, Secretary
 Alice H. Mabin, Laboratory Helper
 Thomas F. Malooly, Business Manager
 Juanita Mandy, Laboratory Helper
 Arlyne Musselman, Senior Technician
 John Pazdernik, Building Engineer
 Conrad Pott, Custodian
 Margaret J. Proctor, Secretary
 Martha Rebbert, Technician
 Arthur G. Rever, Fiscal Officer
 Bessie Smith, Laboratory Helper
 Delores Somerville, Technician
 SuatLu Toh, Technician
 Isabelle P. Williams, Technician
 Leroy Williams, Custodian
 David Wilmoth, Assistant Recorder
 John L. Wiser, Machinist

Student Assistants

Lynn Billingsley, University of Maryland
 John Chase, Johns Hopkins University
 Sheldon H. Gottlieb, Johns Hopkins University
 David Rosenfeld, Johns Hopkins University
 Jeff Sollins, Drew University

PLATES

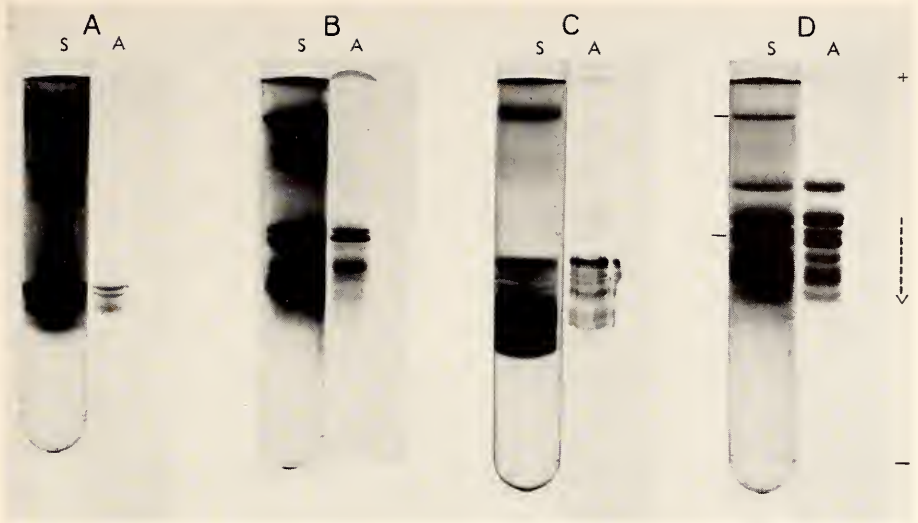


Plate 1. Disc gel electrophoresis of protein derived from fractions A-D of the CMC column shown in Fig. 8. Amido Schwartz stain pattern is on the left (S) and its radioautogram is on the right (A).

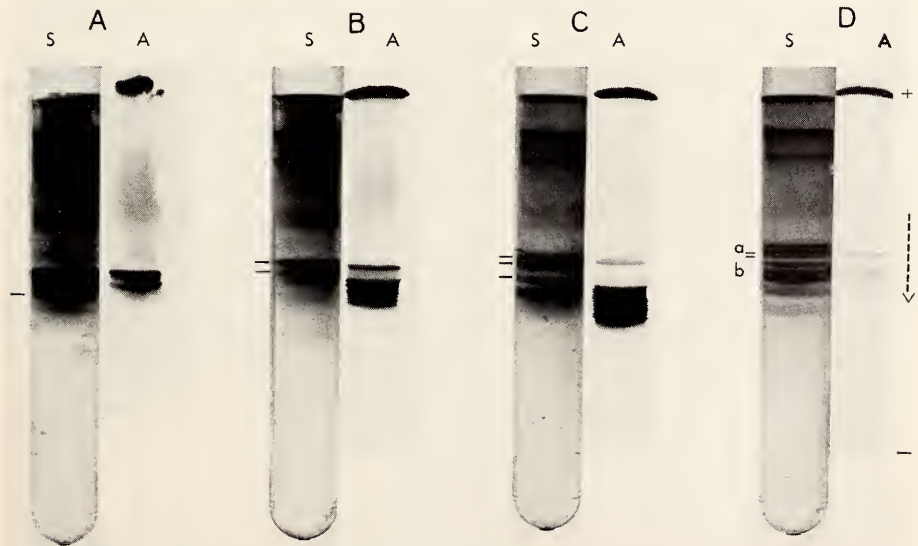


Plate 2. Disc gel electrophoresis of protein derived from fractions A-D of the CMC column shown in Fig. 9. The stained pattern (S) is compared with its autoradiogram (A).



Plate 3. Disc gel electrophoresis of protein derived from fractions A-D of CMC chromatography of radioactive mutant (0-*nu*) and control (1-*nu* and 2-*nu*) total proteins. The stained pattern (S) is compared with its autoradiogram (A).

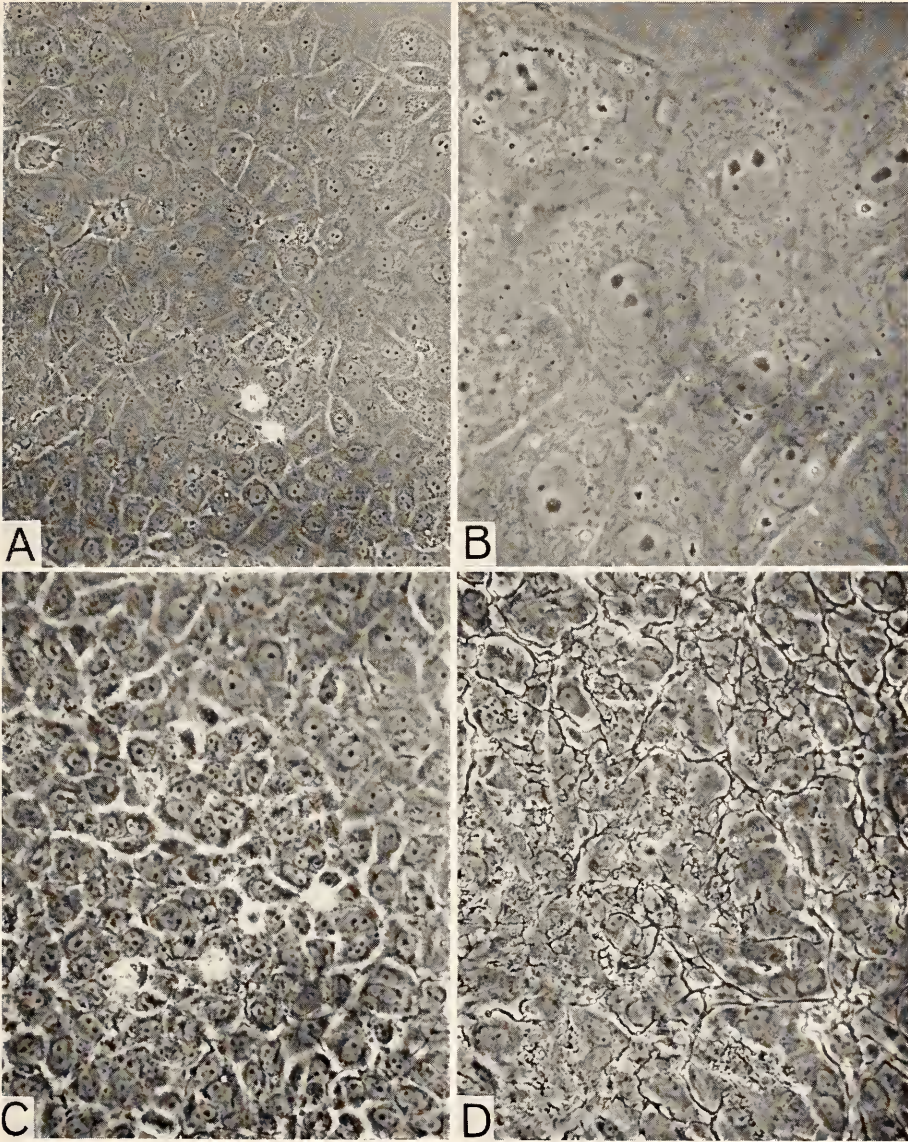


Plate 4. Phase contrast photomicrographs made of portions of live colonies of rat liver cells during the third clonal passage. (A) A portion of the edge of a young colony showing spreading epithelial morphology grading from the margin (upper righthand corner) toward the center (at the lower left). Most mitotic figures occur near the edge of the colony and are usually found in synchronous pairs as may be seen in the two metaphases visible in the upper left. (B) Margin of the colony shown in (A), oil immersion. (C) A region near the center of a young colony showing the condensed packing of cuboidal cells arranged in rosettes and cordlike patterns. (D) At the center of old colonies (5 weeks in culture) many phase-dark strands of extracellular material accumulate. This material appears by inference from its solution in purified collagenase to be analogous to the collagenous reticulin fibers which are seen in histological preparations enmeshing liver lobules. Since there are cultures of clonally purified epithelial cells, it appears that contrary to current interpretation nonfibroblast components of the liver may be responsible for this material.

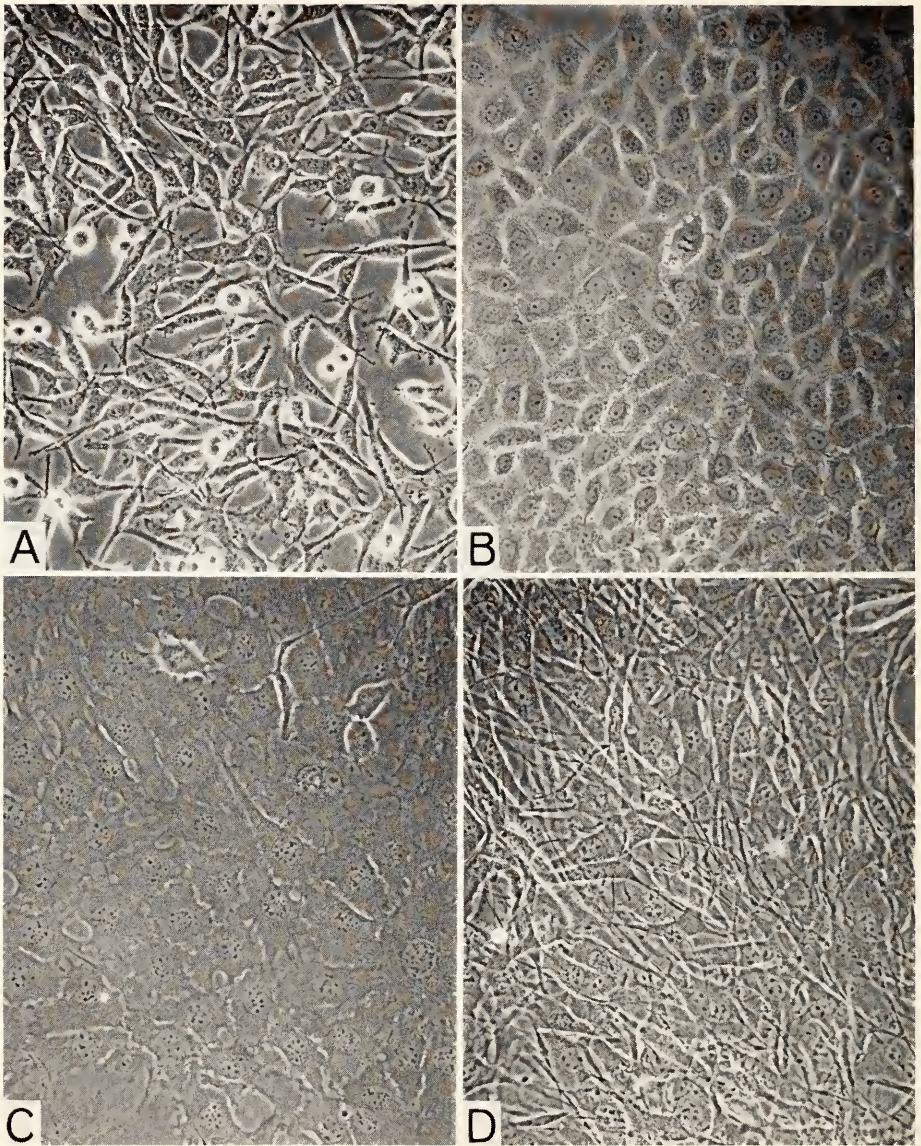


Plate 5. The parents (A, B) and two types of hybrid progeny (C, D), of virus-assisted somatic cell hybridization experiments. (A) Mouse cell line: LM (Tk⁻) Cl 1 D, fibroblastic spindle-shaped cell morphology. (B) Clonally purified culture of rat liver cells, RL-3, which show typical pavement epithelial morphology. (C) Hybrid strain RLDE-2 with morphology favoring epithelial parent. Note the predominantly epithelial morphology which is discernibly intermediate between the parental morphologies. (D) Hybrid strain RLDF-3 with morphology favoring the fibroblast parent. Note the multilayered, typically fibroblast fusiform morphology.

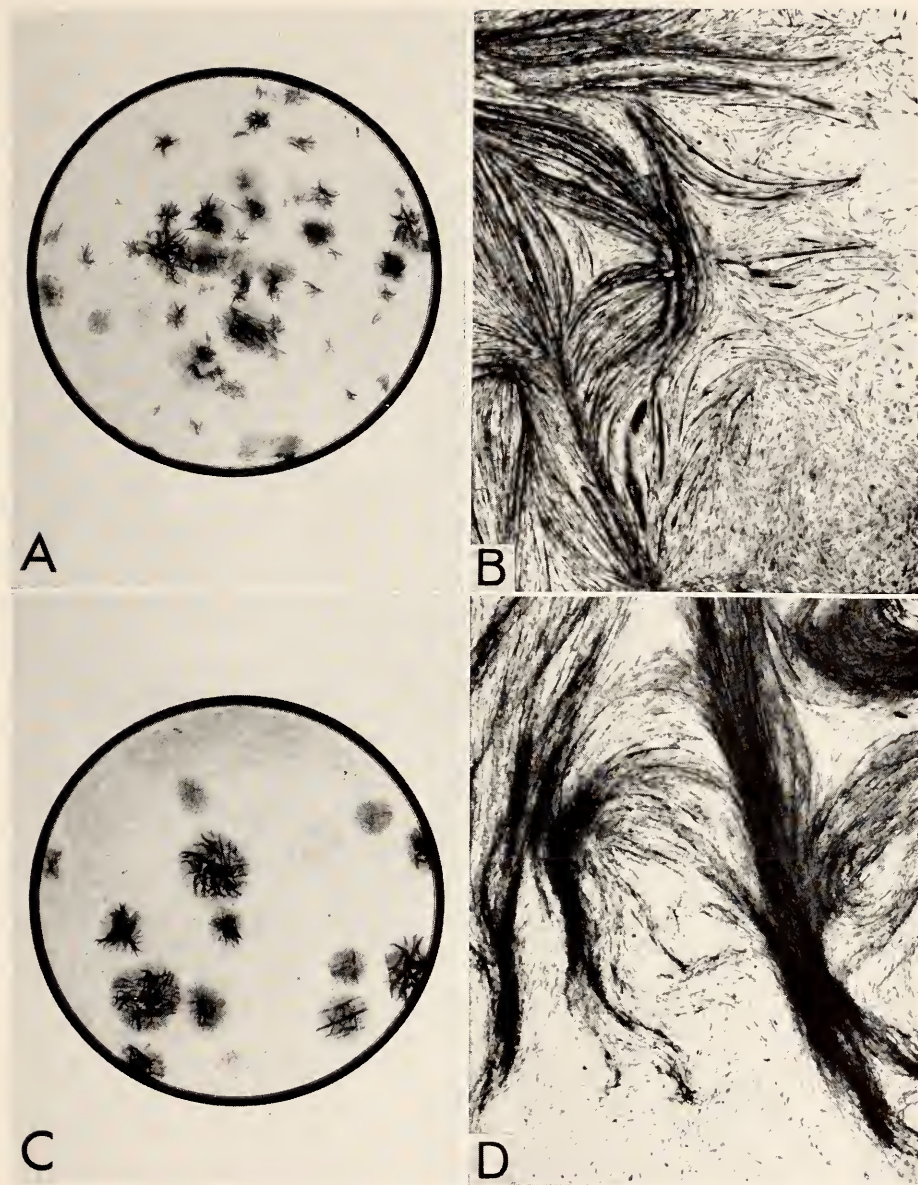


Plate 6. Clonal cultures of chick embryonic muscle grown for 12 days in F12 215. The inoculum consisted of 400 cells per plate. Note gross morphology (A) and abundance of well-developed myotubes (B) in cultures which contained horse serum. Companion cultures set up with F12 215 (fetal calf serum) generally exhibited lower plating efficiencies. Note similar gross morphology of muscle clones (C) but absence of well-developed myotubes (D).

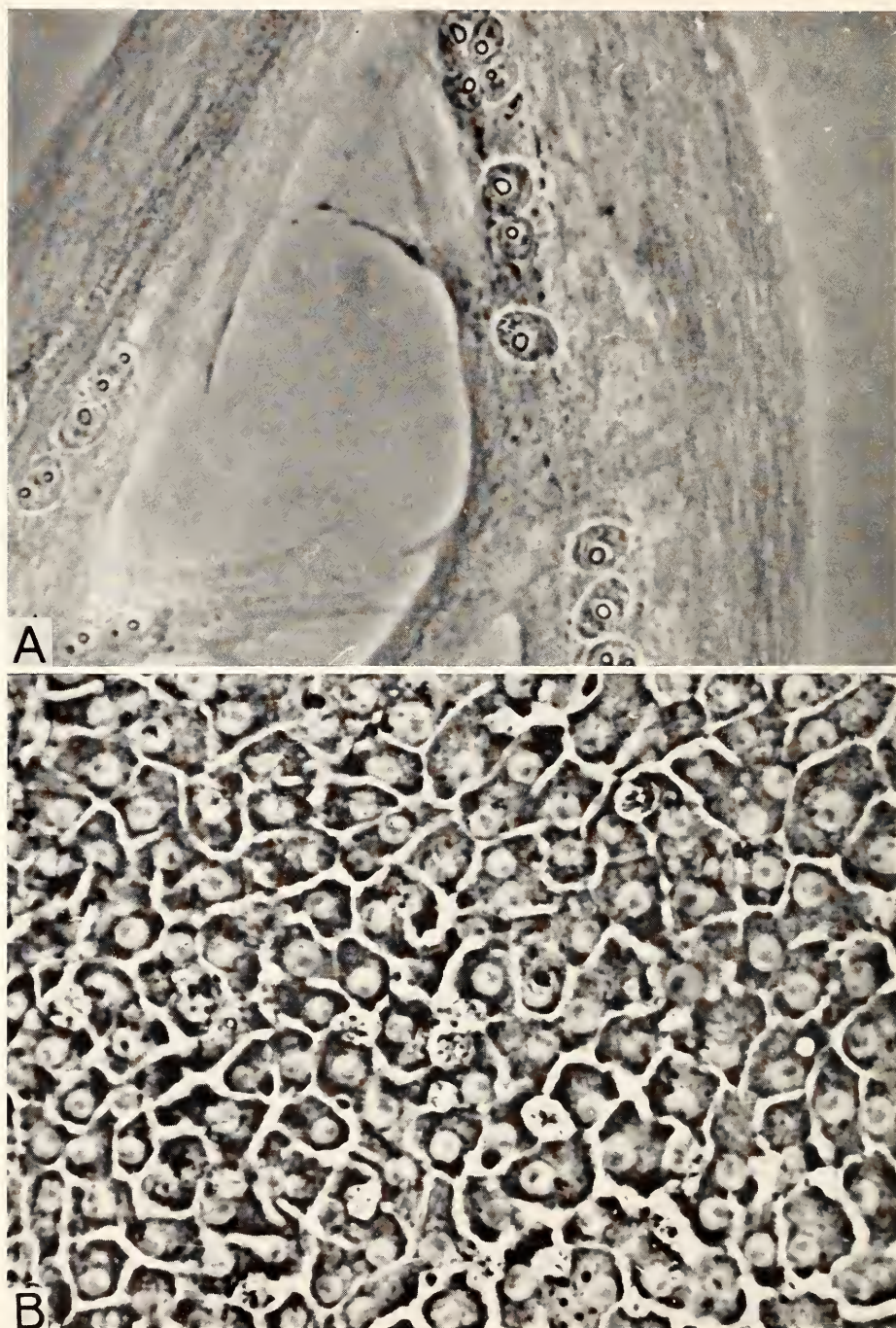


Plate 7. (A) Appearance of muscle 120 hours after treatment with VLB. Phase contrast, $\times 200$. (B) Aggregate colony of hepatocytes 96 hours after isolation. Obtained from liver of 10-day-old embryos. Phase contrast, $\times 250$.

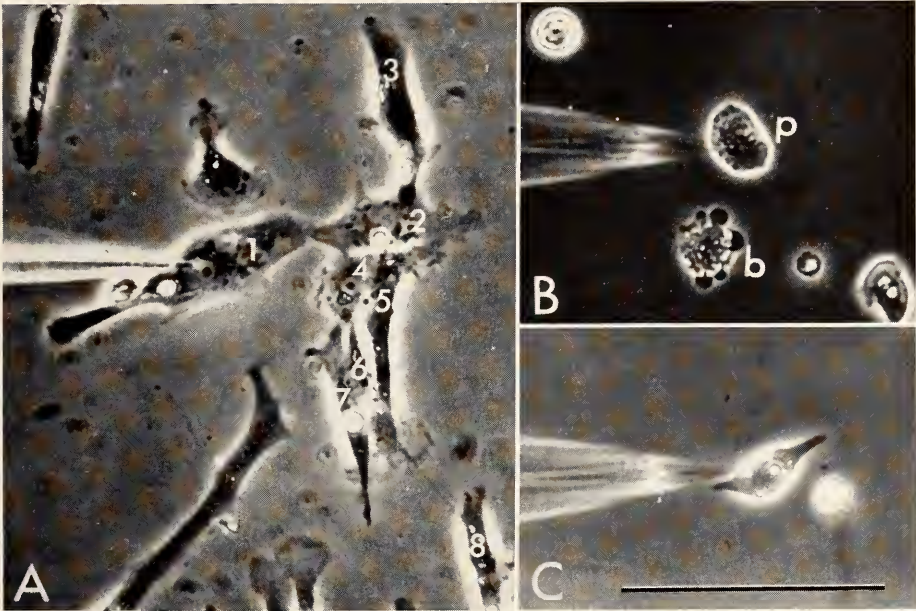


Plate 8. Seven-day heart cells 48 hours in culture photographed while recording. Phase optics; scale = 100 microns. (A) Electrode penetrating an M-cell in a group of seven contacted cells (numbered). Cell number 8, connected by a slender strand, was not beating. (B) Singlet cells, unsuccessfully impaled. Penetrated cell (*p*) is showing early signs of deleterious effects of impalement. Cell *b*, impaled four minutes previously, is exhibiting extensive blebbing and vacuolization. (C) Singlet M-cell successfully impaled.

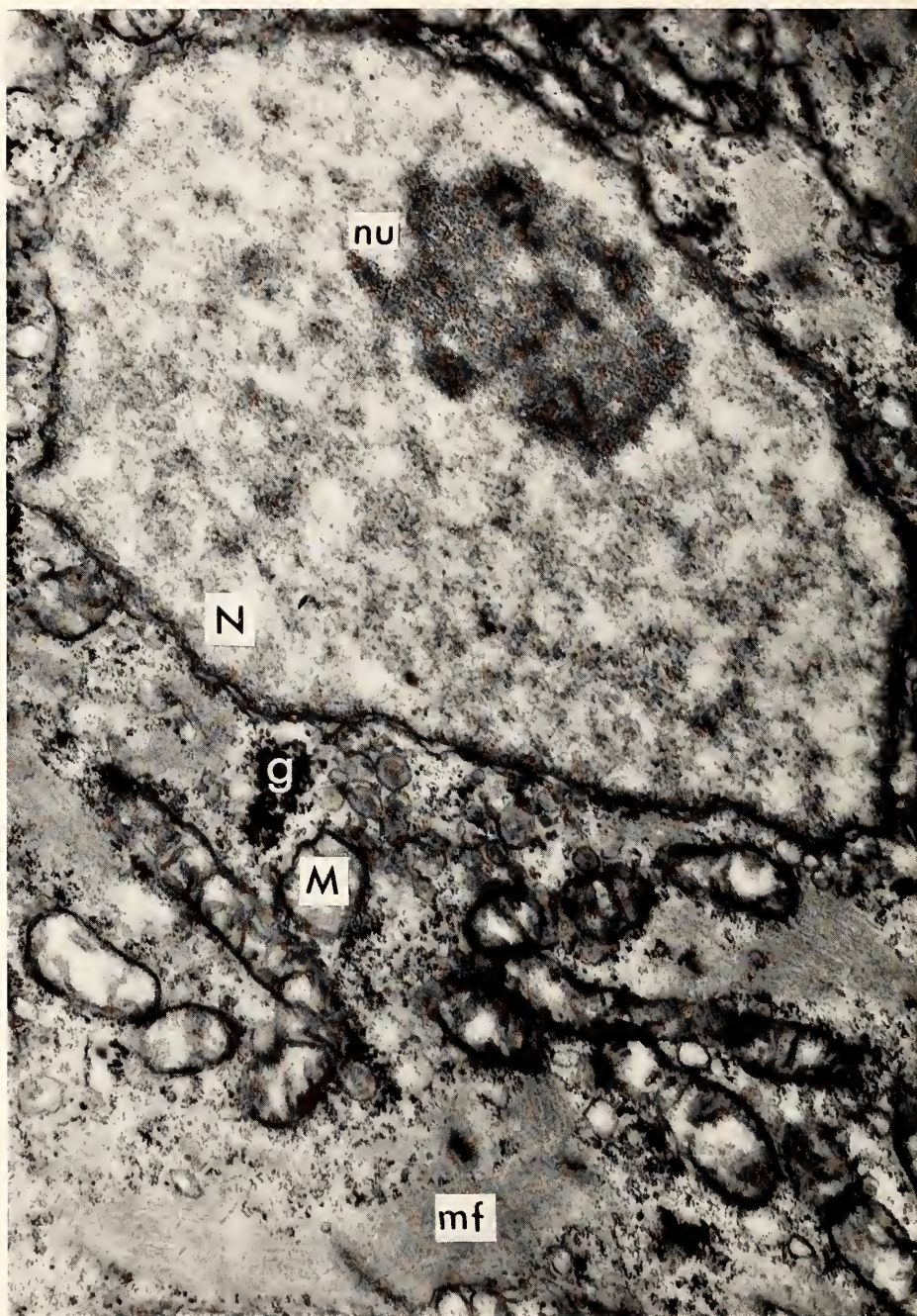


Plate 9. Electron micrograph of a one-nucleolate ventricular cell in a section of an intact 7-day heart. Palade's fixative, pH 7.4, stained with lead citrate. g = glycogen; M = mitochondrion; mf = myofibrils; N = nucleus; nu = nucleolus. ($\times 22,900$).

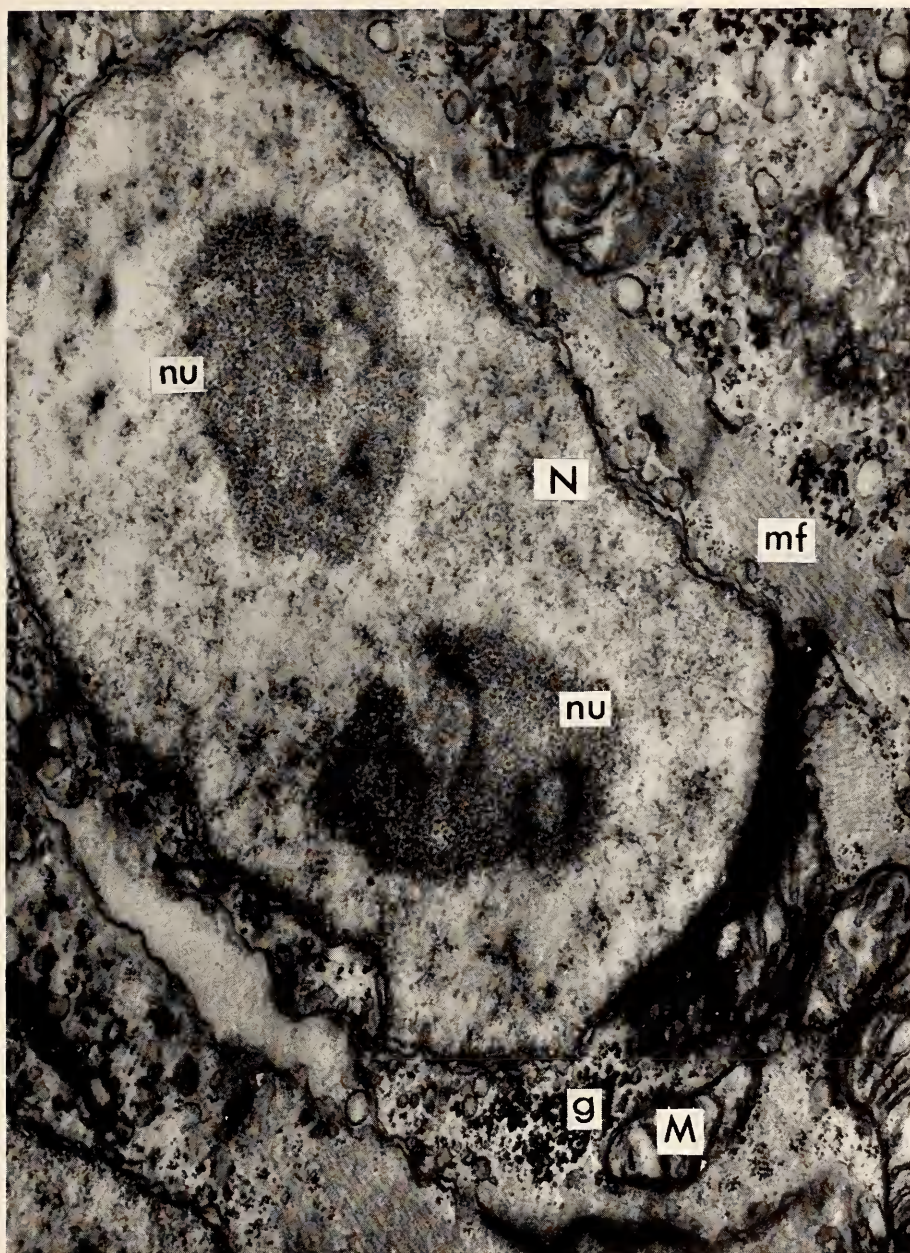


Plate 10. Electron micrograph of a two-nucleolate cell from the same heart as that shown in Plate 9. Preparation and labeling as in Plate 9 ($\times 32,200$).

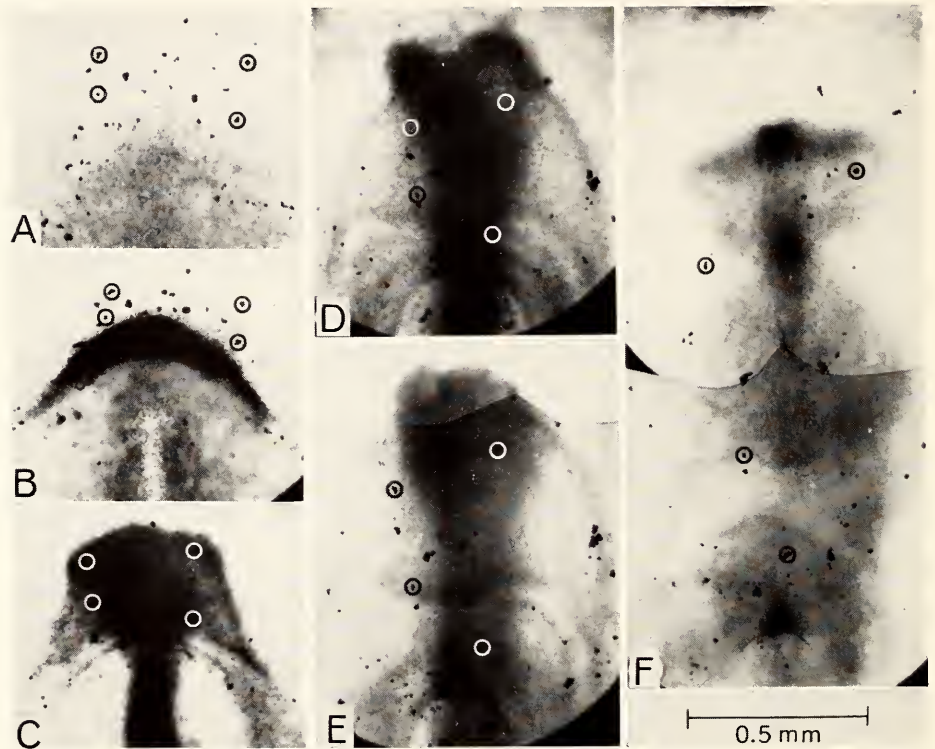


Plate 11. Sequential stages of a single embryo marked with iron oxide particles, showing the formation and elongation of the head and foregut. The same four particles on the yolk-sac endoderm are encircled at each stage. Stages and time after the particles were placed in position are: (A) stage 6, zero hours; (B) stage 7⁻, two hours and 15 minutes; (C) stage 7⁺, 4 hours and 15 minutes; (D) stage 8⁻, 7 hours and 45 minutes; (E) stage 9⁻, 10 hours and 15 minutes; (F) stage 11, 20 hours.

Department of Plant Biology

Stanford, California

C. Stacy French
Director

Contents

Introduction	473
Experimental Taxonomy Investigations	477
Growth of <i>Mimulus</i> , <i>Marchantia</i> and <i>Zea</i> under different oxygen and carbon dioxide levels	477
Comparative physiological and biochemical studies on <i>Marchantia</i> from habitats with contrasting temperatures	478
Effect of temperature and oxygen concentration on photosynthesis in <i>Marchantia polymorpha</i>	479
Differential photosynthetic performance of <i>Solanum dulcamara</i> ecotypes from shaded and exposed habitats	482
Carboxydismutase activity in shade-adapted and sun-adapted species of higher plants	487
Photosynthesis of an amphiploid <i>Mimulus</i> in comparison with its progenitors	489
Variation among ryegrasses in rates of apparent photosynthesis	491
Genetic recombination and transplant responses among F_3 progenies in <i>Mimulus</i>	493
Biochemical Investigations	496
Light-induced reactions of carotenoids in the yellow-green alga <i>Botrydiopsis</i>	496
Studies on the photosynthesis of plastome mutants of <i>Oenothera</i>	503
Effect of enzymatic digestion of chloroplast lamellae on chlorophyll absorption	505
Fractionation of the photosynthetic apparatus from broken spinach chloroplasts by sucrose density-gradient centrifugation	508
Absorption spectra of fractions obtained by sucrose gradient centrifugation from <i>Chlorella pyrenoidosa</i>	514
Absorption and fluorescence of fractions from several plants	516
Emerson enhancement at different intensities and ratios of two light beams	520
Inhibition of cyclic electron transfer in vivo by red light and oxygen	525
Factors affecting absorption and fluorescence spectra of natural chlorophyll complexes	528
Connection of the laboratory to the computation center of Stanford University	534
A curve digitizer	535
Analysis of spectra of natural chlorophyll complexes	536
Staff Activities	546
Bibliography	547
Speeches	548
Personnel	548

INTRODUCTION

The first International Congress of Photosynthesis Research was held in June 1968, in Germany. It gave an excellent opportunity to survey the present state of the subject and to see the relations between the work of this laboratory and that in progress elsewhere. This full-scale Congress developed from a smaller group previously called the Western European Conference on Photosynthesis that had met twice before.

The establishment of a Congress, to convene at three-year intervals, focuses the efforts of people from many of the traditional academic disciplines on a problem that requires investigation from widely divergent viewpoints. It also represents the evolutionary culmination of the long history of research in photosynthesis. A hundred years ago photosynthesis was primarily of interest to botanists, trained in the classification of plants. Slowly the field of plant physiology developed and the knowledge of how plants convert carbon dioxide into food with the energy of sunlight became one of its major subdivisions. As the basic questions about the process became more clearly formulated the more easily definable problems were taken up by chemists and physicists, usually with the expectation of a quick breakthrough from the application of their more sharply defined methods of experimentation and interpretation. The initial over-simplification characteristic of much of this phase in the history of our subject has, however, led to a sharper formulation of known facts and to a more precise delineation of some significant though poorly understood questions. We seem to have passed through the period of naïveté in the application of the more rigorous disciplines to biological problems. Rather than being considered a limitation on precise experimentation, the diversity of species and of physiological states of living plants is now being exploited. This

is done by selection of species particularly well adapted to specific kinds of experimentation, by specially induced and selected mutants, and by controlled preconditioning of the plant material. Excellence of chemical and physical procedures combined with weak biology, or the converse situation, is no longer a characteristic of work in our field.

At this Congress, a major fraction of the work reported was on the nature of the electron transport chain whereby two consecutive photochemical reactions, driven by different forms of chlorophyll, release oxygen from water and form reducing power. The attempt to separate those parts of chloroplasts that are responsible for each of the two separate photochemical reactions is being widely pursued. This year at the Department, Mr. J.-M. Michel and Dr. M.-R. Michel-Wolwertz, Institution Research Fellows from Belgium, have improved the still primitive art of chloroplast fractionation. Their separation methods avoid the need of adding detergents which, though widely used, may damage the material. The relative activities for two photochemical reactions of their different chloroplast fractions contrasted greatly, and they found characteristic differences in the absorption spectra of comparable fractions from several species of plants.

The absorption spectra of chlorophyll complexes in fractions prepared from chloroplasts that were nearly specific for system 1 or system 2 activity differed greatly from each other in the region from 680 to 715 nm. The fraction giving high system 1 activity had high absorption in that part of the spectrum. A striking parallelism to this situation was found in isolated but not fractionated chloroplast particles from mutant leaves. Drs. Fork, Heber, and Michel-Wolwertz found far higher absorption from 680 to 715 nm in a mutant that gave only system 1 activity than in another mutant

with only system 2 activity. The difference between these spectra presumably represents the absorbance of a specific system 1 pigment.

Eventually we may hope for improvements in the technique for measuring action spectra of specific reactions driven by the separated particles to a precision that is routine in recording absorption spectra. Then it will be possible to characterize definitely the specific forms of chlorophyll that are responsible for the activity of each system.

The function of the carotenoids is one of the persistent questions about photosynthesis that seem to have a variety of answers. All plants that do photosynthesis have these yellow pigments. Some but not all of the many carotenoids may act as light absorbers for the reaction. They are believed to work by passing on their absorbed energy to chlorophyll. Another recognized function is that of an internal light filter whereby carotenoids protect chlorophyll from bleaching by blue light. Furthermore, the reversible oxygenation of particular carotenoids is thought by some investigators to be a part of the oxygen-evolving step of photosynthesis. In last year's report Drs. Fork and Ames described rapid changes of light absorption by carotenoids in red and in brown algae. This year Dr. Fork gives the results of a detailed study of carotenoid changes in a yellow-green alga that is particularly suitable because it lacks chlorophyll *b*. Activation of either of the two photochemical systems of this alga, *Botrydiopsis*, gave identical carotenoid changes. Since the changes were in the same direction when driven by either system, the carotenoid responsible for the spectral changes cannot be located between the two photochemical reactions. There are two types of absorbance changes, one slow, the other rapid; but since they have identical spectra, the same carotenoid pigment is activated by both of the photosystems.

Another part of photosynthesis extensively discussed at the Congress was the

effect of light on CO₂ evolution by plants in an atmosphere with oxygen but devoid of CO₂. This photorespiration is another aspect of O₂ uptake by certain steps in the process of photosynthesis, long a subject of interest to our group.

The overall result of photosynthesis is evolution of oxygen from water followed by utilization of the remainder as a source of power for making reduced compounds and high-energy phosphate bonds. Nevertheless, oxygen is taken up at several different places in the photosynthetic system of plants and this utilization of some oxygen may be essential to the normal functioning of the mechanism. The uptake of oxygen may well have significance in adjusting the rates of some different steps by a feedback mechanism. The importance of this effect in understanding the details of the photosynthetic process is self evident, and investigations of the oxygen uptake have been made from many different viewpoints. Two different aspects of the subject are discussed in this year's report. Professor Heber, a Visiting Investigator from Düsseldorf, describes the interaction of oxygen with the electron transport system at a point near photosystem 1 but located on the opposite side of that system from system 2 where oxygen is produced and where there are also other sites of oxygen uptake. The action spectra of light-induced oxygen consumption measured at the Department some years ago with different procedures by Dr. Vidaver and by Dr. Fork also related one site of oxygen uptake to system 1.

Studies on the inhibiting effect of oxygen on the rate of photosynthesis and growth of whole plants have been continued this year by Dr. Björkman. New experiments on the effects of oxygen concentration on the growth of plants in controlled environments confirm and extend findings reported last year on the enhancement of growth of some plants under low concentrations of oxygen (4% to 5%) as compared with normal air (21%). The new data also indicate that

there is an interaction between O_2 and CO_2 concentrations as measured by the degree of enhancement of growth of plants caused by low oxygen concentration.

An effect possibly of appreciable significance that is, however, not yet well understood was turned up this year by Dr. Brown. She found that small increases of temperature appreciably reduce the height of the absorption bands of chlorophyll in its natural complexes. If the temperature increase is small enough, the effect is reversible. A similar response, the one that led to these experiments, had been known for cytochrome, another protein complex. This high sensitivity to the temperature, fascinating in itself as a phenomenon, may eventually contribute to a better description of the way in which chlorophyll is bound to its carrier protein. The time course of the effect, the extent of this change for the various forms of chlorophyll, and the influence of temperature changes on the shape of the spectral bands offer promising areas for future work.

In the search for improved methods of chloroplast fractionation Dr. Michel-Wolwertz investigated the effects of enzymes that digest proteins or fats. The hope was to break some of the bonds between the protein carriers of the different forms of chlorophyll and thus to facilitate the separations. Molecular sieve resins were used for testing the separability of the partially hydrolyzed chloroplast fragments. No improvement in separability resulted. However, an enzyme, protease, was found to convert one form of chlorophyll *a* to another. That such a conversion can take place by partial hydrolysis supports the idea that the longer wavelength forms of chlorophyll *a* are aggregates of smaller chlorophyll protein complexes. The action spectra for various photochemical activities of chloroplast fragments partially digested by enzymes remain to be determined. Such experiments would tell

whether the chlorophyll complex, whose absorption spectra change, also changes its activity.

One of the basic experiments leading to the realization that two separate photochemical reactions are used in photosynthesis, and that these reactions are driven by different forms of chlorophyll, was the demonstration of the enhancement effect. This effect, discovered by Robert Emerson, was that photosynthesis with two beams of light of different wavelengths is greater than the sum of photosynthesis for the two beams given separately. Dr. Eckhard Loos, a Research Fellow from Munich, had found, before coming to the laboratory, that the enhancement effect at high light intensity became smaller than the value predicted from measurements at low intensity if studied by the uptake of radioactive carbon dioxide. This year the experiments were repeated by measuring oxygen evolution instead of carbon dioxide uptake. In the recent oxygen experiments, however, the decline of activity at high intensity in different algae was attributable solely to the normal limitations of photosynthesis by non-photochemical reactions that approach a saturating rate at high light intensity.

A cable was installed this year connecting the laboratory to two of Stanford's large computer systems. One of these, ACME at the Medical School, is still an experimental enterprise. ACME operates as an on-line computer accepting data and programs and returning the computed results on an electrical typewriter in the laboratory. It is also intended to accept electrical data signals, either analogue or digital, directly from experimental equipment in the laboratory and perform on-line calculations or control operations. Thus measured data will be computed and plotted in the desired form on our own recorders during the experiments. The electrical data input systems for ACME are nearly completed for use with the measurement of light-induced absorption changes in photo-

synthetic plants and for digitizing recorded curves. Furthermore, the typewriter can be connected to Stanford's WYLBUR system for program and data input with convenient revision facilities to the large IBM 360/67 system. WYLBUR output computations and the graphs are produced at the Computation Center close to our laboratory. Much use of the WYLBUR system has been made this year for analysis of absorption spectra of the different types of chlorophyll.

The gift of a suitable program from the Shell Development Laboratory for use with the computer has made it possible to do many more and greatly improved analyses of absorption spectra. By such analysis of particularly significant new measurements we are continuing the attempt to determine the spectra of the naturally occurring forms of chlorophyll in chloroplast fractions and in certain algae. The objective is to find out how many such forms of chlorophyll exist, which of them are part of each of the two photochemical systems of photosynthesis, and to describe in detail the curves for each separate form of chlorophyll. Some progress has been made and it now appears that different forms of chlorophyll with the same wavelength peak may vary remarkably in the width of their absorption bands.

Continuing emphasis on the basic mechanisms underlying the evolution of higher plants has characterized the work of the Experimental Taxonomy group during the current year. The analysis and integration of the extensive data from the long-term cytogenetic, transplant, and physiological investigations on the Erythranthe section of *Mimulus*, begun in 1947, is progressing with the preparation for publication as Volume V of the Institution's monograph series *Experimental Studies on the Nature of Species*. This book is scheduled for completion in the coming year.

Dr. Björkman has developed a rapid

method of measuring photosynthetic rates with an oxygen electrode in green tissues of liverworts. This method makes possible the study of rapid transient effects on photosynthesis and respiration during alternating light and dark periods, and of the effects of rapid changes in temperature, CO₂ and O₂ concentrations, and light intensities. It is also an effective instrument for comparative studies on ecological races.

In *Solanum dulcamara*, a European species of nightshade, Mr. Eckard Gauhl has established the occurrence of distinct obligate shade forms of the species in contrast with other races that are capable of utilizing high light intensities efficiently in photosynthesis. This finding parallels the discovery by Björkman and Holmgren some years ago on *Solidago virgaurea*, the common European goldenrod. Mr. Gauhl has also found that races of *Solanum* that occur in marshy sites in central Germany are strongly inhibited in photosynthetic rate when subjected to mild water stress in contrast with races native to dry areas along the Dalmatian coast in southeastern Europe whose photosynthetic rate is unaffected when grown under the same conditions.

Dr. J. H. Silsbury of the Waite Agricultural Research Institute at Adelaide, South Australia, spent six months at the Stanford laboratory as a Carnegie Fellow. His major objective was to study techniques of measurement of photosynthesis and to compare the photosynthetic characteristics of an agronomically important form of *Lolium rigidum*, an annual ryegrass from the Mediterranean region, with a form of the closely related *Lolium perenne*, a perennial grass from Algeria. Dr. Silsbury was on sabbatical leave from the Waite Institute and, after visiting other laboratories in the United States and in Europe, returned to Adelaide to pursue further comparative studies under controlled conditions of various agronomic strains.

EXPERIMENTAL TAXONOMY INVESTIGATIONS

GROWTH OF *Mimulus*, *Marchantia*, AND
Zea UNDER DIFFERENT OXYGEN AND
CARBON DIOXIDE LEVELS

Olle Björkman, Eckard Gauhl, William M.
Hiesey, Frank Nicholson, and
Malcolm A. Nobs

Last year we reported that the production of dry matter in *Mimulus cardinalis* and *Phaseolus vulgaris* was markedly enhanced when the oxygen concentration of the air surrounding the green parts of the plants was reduced from the normal level of 21% to only a few percent. These comparative experiments were made at a CO₂ concentration of normal air (approx. 0.03%). This year we have studied the effect of oxygen concentration on growth at lower and higher CO₂ concentrations as well. Clone 7211-4 of *Mimulus cardinalis*, TO1-10 of the liverwort *Marchantia polymorpha*, and corn seedlings *Zea mays*, Ferry-Morse hybrid 901, were used in these studies. As in the previous work, the roots of the higher plants were aerated in nutrient solution with normal air (21% O₂, 0.03% CO₂) so that only the composition of the atmosphere surrounding the shoots was varied. With *Marchantia* the entire plants were exposed to the different O₂ and CO₂ concentrations. The temperature in all cases was 25°C.

As reported elsewhere (*Year Book 65*, pp. 446-454, *Year Book 66*, pp. 220-228, *Year Book 67*, pp. 479-482) the rate of photosynthetic CO₂ uptake in *Mimulus* and *Marchantia* is markedly enhanced when the oxygen concentration of the air is reduced from 21% to a few percent, whereas in corn oxygen has little, if any, effect. Similarly, the carbon dioxide compensation point for photosynthesis (i.e., the CO₂ concentration at which there is no net uptake or release of CO₂ in the light) has a relatively high value in *Mimulus* and *Marchantia* (0.005-0.01% CO₂) in 21% O₂, whereas at an O₂ concentration of a few percent the CO₂

compensation point approaches zero. In corn the CO₂ compensation point is close to zero also in 21% O₂.

On the basis of this information one would predict that if *Mimulus* or *Marchantia* were kept at a CO₂ concentration approaching the CO₂ compensation point for photosynthesis under normal O₂ concentration, growth would be stopped. Reducing the O₂ concentration while maintaining the CO₂ concentration at the same low level would increase photosynthesis to a positive value and should thus enable the plants to grow. Corn, on the other hand, would have a positive photosynthetic rate even at 21% O₂ and at a low CO₂ concentration, and one would expect that it would grow also under these conditions.

As shown in Table 1 and Plates 1 and 2, the results of actual growth experiments support these predictions, based on photosynthetic characteristics. Under 21% O₂ and 0.011% CO₂ growth in *Mimulus* and *Marchantia* is almost entirely inhibited, whereas at this same CO₂ concentration but at 4% O₂, the plants are able to grow at a moderate rate. The growth rate of corn at 0.011% CO₂ was unaffected by the O₂ concentration: the increase in dry matter was the same at 21% and 4% O₂ and was close to the value for *Mimulus* under 4% O₂.

When CO₂ concentration is increased beyond the CO₂ compensation point for photosynthesis, dry matter production in *Mimulus* and *Marchantia* increases both under 21% and 4% O₂. At approximately normal air CO₂ concentration (0.032%), dry matter yield is about 90% and 50% greater in 4% O₂ than in 21% O₂ for *Mimulus* and *Marchantia*, respectively. When the CO₂ concentration is increased to about twice that of normal air (0.064%), dry matter production increases both under 21% and 4% O₂, but the increase is relatively greater under 21%. This results in a lower degree of

TABLE 1. Effect of O₂ Concentration on Dry Matter Production at Different CO₂ Concentrations

% CO ₂ Concentration	Dry Weight Increase in 10 Days, mg/plant		% Increase of Growth in 4% O ₂ over 21%
	4% O ₂	21% O ₂	
<i>Mimulus cardinalis</i> , Jacksonville			
0.011	150 ¹	< 10 ¹	> 1000
0.032	1076 ²	565 ²	190
0.064	1144 ²	804 ²	142
<i>Marchantia polymorpha</i> , TO1-10			
0.011	24	7	343
0.034	83	55	151
0.064	101	78	130
<i>Zea mays</i> , Ferry-Morse hybrid 901			
0.011	196 ⁴	218 ⁴	90
0.032	1473 ³	1269 ³	116

¹ Difference between means, very highly significant: $P < 0.01$.² Difference between means, highly significant: $P < 0.05$.³ Difference between means, scarcely significant: $0.3 < P < 0.4$.⁴ Difference between means, not significant: $P > 0.5$.

enhancement by low O₂ concentration at high CO₂ concentration. Nevertheless, even at 0.064% CO₂, dry matter production in *Mimulus* and *Marchantia* is substantially higher when O₂ concentration is kept at 4% as compared with 21%.

Possibly the lower degree of enhancement of dry matter production by low O₂ at high as compared with normal CO₂ concentration reflects a decreasing effect of oxygen concentration on the rate of photosynthetic CO₂ uptake as the CO₂ level is increased. It should be pointed out, however, that these experiments were made under continuous light, a high CO₂ concentration, and at a temperature near the optimum for photosynthesis. Total photosynthesis is, therefore, very high, probably many times higher than in natural habitats. Under such conditions the capacity of growth processes other than photosynthesis may partially limit the rate of growth. If this is the case, an additional increase in the rate of photosynthesis would only be partially expressed in an increased dry matter production.

COMPARATIVE PHYSIOLOGICAL AND BIO-CHEMICAL STUDIES ON *Marchantia* FROM HABITATS WITH CONTRASTING TEMPERATURES

Olle Björkman, Eckard Gauhl, William M. Hiesey and Malcolm A. Nobs

In our comparative studies on physiological and biochemical characteristics of contrasting ecological races of the same or related species we began work this year on the liverwort *Marchantia polymorpha* L. This species has characteristics that make it an especially effective experimental subject in conjunction with current work on species of higher plants. Our principal immediate objective is to compare clones of *Marchantia* from widely contrasting latitudes in a critical comparative analysis of their photosynthetic and respiratory responses as a function of temperature. The wealth of background information already available from earlier investigations that include taxonomy, cytology, and controlled growth studies facilitates our effort.

Marchantia polymorpha provides certain experimental advantages over species of higher green plants that make possible a wider choice of experimental

techniques to probe in depth with increased precision steps that underlie such complex functions as photosynthesis and respiration in genetically and ecologically diverse races. This species occurs from arctic polar regions to the equatorial tropics. The anatomical structure of *Marchantia*, especially the absence of stomata and complex vascular tissues and its compact growth of thallus tissues, simplifies kinetic studies of photosynthesis in vivo. Genetically identical material can easily be grown in quantity through vegetative propagation of single clones, either through gemmae or small pieces of thalli. The absence of protein-precipitating substances, and apparently also of other compounds that commonly act as enzyme inhibitors in plant extracts, is of great importance in biochemical work. Finally, close genetic manipulation of experimental materials can be realized since the thalli are haploid, have a relatively low chromosome number ($n=8$), and male and female gametes are formed on different thalli.

During the summer of 1968 we plan to collect living *Marchantia* clones from the Point Barrow area in northernmost Alaska (71° N.L.) as well as from the equatorial Galapagos Islands. These clones together with those from near Point Reyes Peninsula (north of San Francisco, California, 38° N.L.) are to be used as materials in the contemplated work. This would include studies of the response of growth to a number of different temperature regimes in the laboratory, kinetic studies of photosynthesis and respiration, and studies on the extent to which photosynthetic and respiratory properties of the diverse clones can be modified by growing them under different temperature regimes. Some of the early work on the response of photosynthesis to temperature, light intensity and oxygen concentration of clone TO 1-10 from the Samuel P. Taylor State Park near the Point Reyes Peninsula in central coastal California, and on the effect on these characteristics of growing

this clone under different temperatures, is reported below.

We plan also to compare the activities and kinetic properties of some selected enzymes that are known to be of key importance in the metabolism of green plants among the clones from the different habitats and experimental growing conditions. The enzymes chosen for these studies are carboxydismutase (ribulose-1, 5-diphosphate carboxylase), phosphoribulokinase, phospho(enol)pyruvate carboxylase and citrate synthase (condensing enzyme). Methods for the preparation of extracts of these enzymes from *Marchantia* tissues and various assay procedures are currently being tested.

EFFECT OF TEMPERATURE AND OXYGEN CONCENTRATION ON PHOTOSYNTHESIS IN *Marchantia polymorpha*

Olle Björkman and Eckard Gauhl

As a first step in our comparative work on adaptation to temperature among *Marchantia polymorpha* clones from habitats with contrasting temperatures we have studied the effect of temperature on photosynthesis in clone TO1-10 originally from the Samuel P. Taylor State Park near the Point Reyes Peninsula in central coastal California. Photosynthesis measurements were made in the temperature range from 6° to 34°C on ramets previously grown at 10°, 20°, and 30°C.

As is also the case in the majority of higher plants investigated, the rate of photosynthetic CO₂ uptake in the liverwort *Marchantia polymorpha* is markedly inhibited by the oxygen in normal air (Fig. 1). There is evidence that the inhibition is caused by a reoxidation of one or several photosynthetic intermediates by molecular oxygen ("photorespiration"). The photosynthetic responses to temperature of the *Marchantia* clone were therefore also measured under an atmosphere with an oxygen content of 1% to 2%.

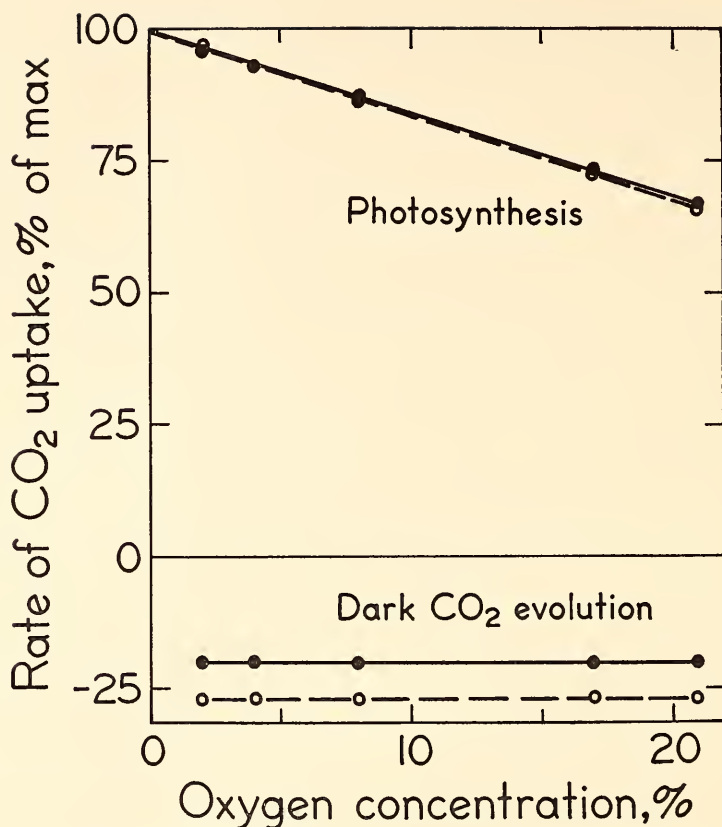


Fig. 1. Rate of apparent photosynthetic CO_2 uptake as a function of oxygen concentration in *Marchantia polymorpha* TO1-10. $[\text{CO}_2]$: 0.032%; 22°C. The clone was grown at 4% oxygen (broken line) and 21% oxygen (solid line). The temperature for growth was 20°C.

The lower part of Fig. 2 shows the temperature curve for light-saturated photosynthesis in normal air (21% O_2 , 0.032% CO_2). In this and in the following graphs the rate of CO_2 evolution in the dark has been added to the apparent rate of CO_2 uptake in the light. The rate of light-saturated photosynthesis shows a strong dependence on temperature and increases in a nearly linear fashion from 6° to 20°C. The temperature optimum occurs in the range 27° to 30°C regardless of the temperature at which the clone was previously grown.

The rate of photosynthesis on the basis of unit dry weight or thallus area is somewhat lower at all temperatures when

the clone is grown at 10° as compared with 30°C. Expressed on the basis of soluble protein the rate at all temperatures is highest when the plant is grown at 30°, and lowest when grown at 10°C.

The apparent lack of a photosynthetic acclimation to low temperature in this *Marchantia* clone is consistent with its slow growth at 10°C, but contrasts with the results found in the higher plant species *Encelia californica* and *Polygonum bistortoides* by Mooney and Shropshire, 1967. The latter species appear to possess great phenotypic plasticity in the photosynthetic characteristics since preconditioning to different temperatures for 24 hours greatly changes the temperature

dependence of light-saturated photosynthesis.

The temperature dependence of light-saturated photosynthesis at 2% O_2 for the *Marchantia* clone TO1-10 is shown in the upper part of Fig. 2. The response differs considerably from that found in *Solidago virgaurea* and *Mimulus cardinalis* (Year Book 66, p. 222). In *Marchantia* the rate of photosynthesis shows a much stronger decrease in the range from 20° down to 6°C than do the higher plants. Moreover, the enhancement by low oxygen is small, or even absent, at temperatures below 10°C in *Marchantia*. It does not reach its maximum value until the temperature exceeds 20°C, in

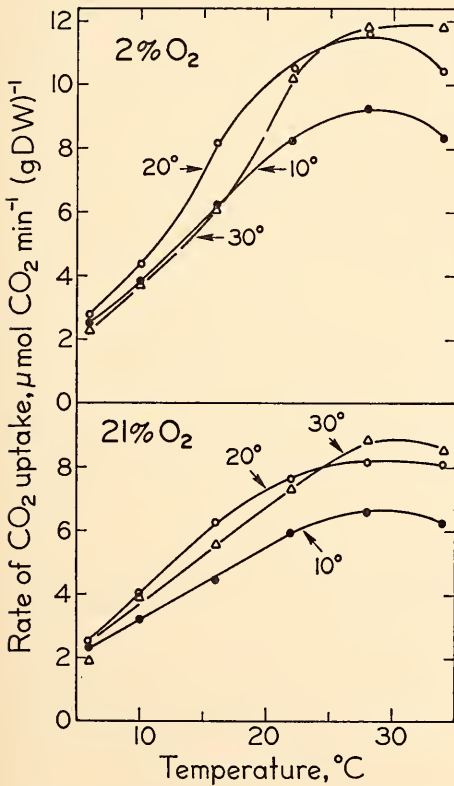


Fig. 2. Temperature dependence of light-saturated photosynthesis at low and normal oxygen in *Marchantia polymorpha* TO1-10 grown at 10°, 20°, and 30°C. $[CO_2]$: 0.032%.

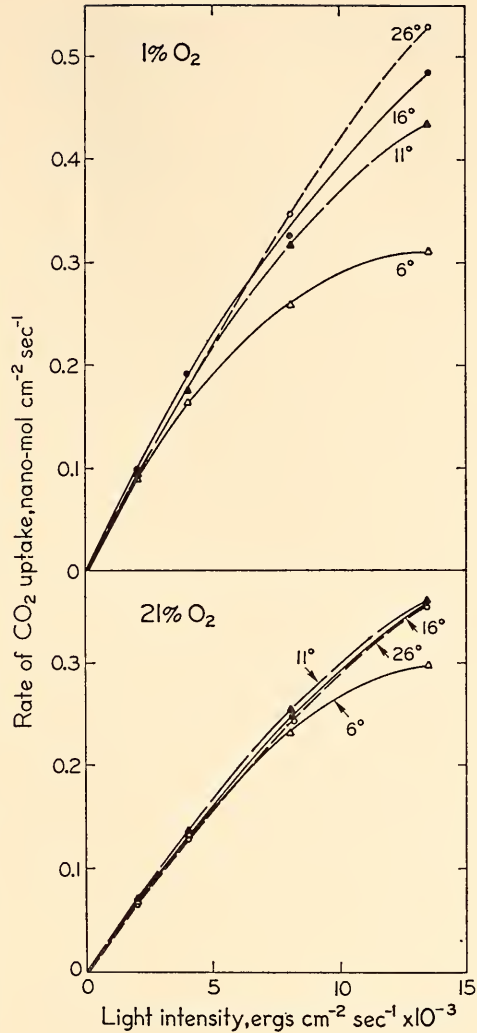


Fig. 3. Lower part of curves for photosynthesis as a function of light intensity (665 nm) at low and normal oxygen for different temperatures. *Marchantia polymorpha* TO1-10 grown at 20°C.

contrast with *Solidago* and *Mimulus* which show little change in enhancement by low O_2 with temperature change. It is noteworthy, however, that the optimum temperature for the light-saturated rate of CO_2 uptake in *Marchantia* is not markedly affected by O_2 concentration but lies in the range 28° to 31°C

both at 21% and 2% O_2 . Also, low O_2 enhances the maximum rate of CO_2 uptake to about the same degree regardless of the temperature under which the clone was previously grown even though the temperature at which enhancement occurs appears to increase with increasing temperature for growth.

Possibly, the temperature dependence of the light-saturated rate of CO_2 uptake in *Marchantia* reflects an increasing rate of reoxidation of photosynthetic products with increasing temperature. This re-oxidation would then be negligible at 6°C, and increase with temperature faster than does photosynthesis in the range 6° to 20°C. This hypothesis, however, is weakened by the finding that the enhancement by low O_2 becomes less dependent on temperature as the light intensity is decreased (Figs. 3 and 4). In the range where photosynthesis is linearly dependent on light intensity, the enhancement of CO_2 uptake that takes place when oxygen concentration is reduced from 21% to 1% seems to be independent of temperature. In the temperature range investigated (6° to 26°C), the apparent quantum yield was found to be 0.068 mole CO_2 per absorbed einstein in 21% O_2 and 0.094 in 1% O_2 . Another interesting observation is that the rise

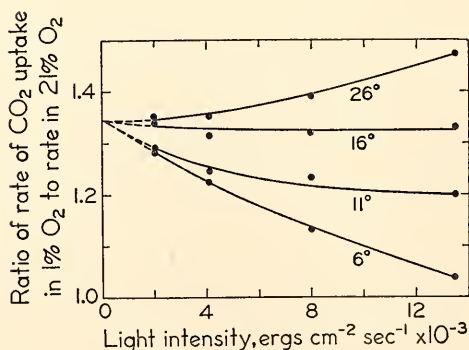


Fig. 4. Ratio of photosynthesis in 1% oxygen to that in 21% oxygen as a function of light intensity at different temperatures in *Marchantia polymorpha* TO1-10. $[CO_2]$: 0.032%. The plant was grown at 20°C.

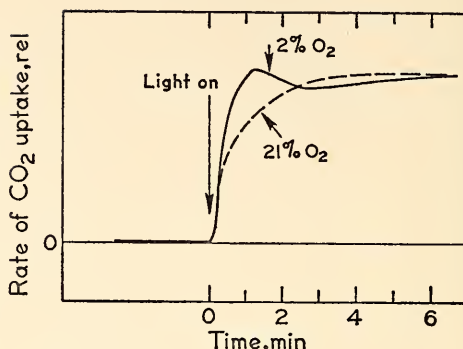


Fig. 5. Effect of oxygen on the time course of photosynthesis on exposure to saturating light at a low temperature (4°C). $[CO_2]$: 0.032%; *Marchantia polymorpha* TO1-10.

in the rate of CO_2 uptake with time upon exposure to light following darkness is considerably faster in 1% than in 21% O_2 even at low temperature where the photosynthetic rate at steady-state is the same at both oxygen concentrations (Fig. 5).

One interpretation of these results is that oxygen acts as an electron acceptor in the dark reaction chain of photosynthesis at a site before the thermal step that determines the overall rate of light-saturated photosynthesis at low temperatures. Electrons would then be drained from the chain to oxygen even at low temperatures, but this would not affect the rate of CO_2 uptake so long as the rate of flow to the step limiting the overall rate exceeds the capacity of this step.

Reference

Mooney, H. A., and F. Shropshire, *Eco. Planta*, 11, 1-13, 1967.

DIFFERENTIAL PHOTOSYNTHETIC PERFORMANCE OF *Solanum Dulcamara* ECOTYPES FROM SHADED AND EXPOSED HABITATS

Eckard Gauhl

Solanum dulcamara L. is widely distributed in many contrasting natural environments. Since it is found in open as

well as in densely shaded habitats, it is a suitable species for experimental studies on the differentiation of the photosynthetic machinery among plants native to contrasting light climates.

Several clones isolated from selected populations in exposed and shaded habitats were used in a comparative study of growth responses and photosynthetic characteristics under two different light intensities (11×10^4 and 24×10^3 ergs $\text{cm}^{-2} \text{sec}^{-1}$, 400–700 nm). Two clones representing extremes with respect to natural habitats and also in responses to preconditioning to different light intensities were later chosen for more detailed studies.

Clone Fe 2 was originally collected from an open sand dune on Fehmarn Island off the Baltic coast of Germany. The leaves of this plant are twice as thick when grown in strong light, and have three layers of palisade cells as compared with one layer when grown in weak light. Clone Mb 1 originates from a reed-grass marsh near Mönchbruch, south of Frankfurt. Its stems wind around stalks of *Phragmites communis* which form a dense, shady stand with only a few other species. Leaves of this clone are only slightly thicker when grown in strong as compared with weak light and develop only one or two layers of palisade cells.

Fig. 6 shows typical curves of photosynthetic rate as a function of light intensity for leaves of both clones grown under high and low light intensities. Leaves of clone Fe 2, when developed under strong light, are capable of markedly higher rates of CO_2 uptake at high light intensities than when developed under weak light. They also require higher light intensities to saturate photosynthesis. In contrast, the light-saturated photosynthetic rates of Mb 1 leaves are about the same regardless of whether the plant has been grown in strong or weak light. The somewhat less steep initial slope of the curve for leaves developed under strong light indicates a

reduced efficiency of utilization of light of low intensities.

To compare further the capacity of these two clones to adjust to contrasting light intensities, plants were grown under a low light intensity and subsequently exposed to a higher intensity for different lengths of time. Only mature leaves, already fully expanded at the time of transfer to the high intensity growth chamber, were used for measurements of photosynthesis and of the content of chlorophyll and soluble protein. Light-saturated photosynthesis was measured in white light of 3×10^5 ergs $\text{cm}^{-2} \text{sec}^{-1}$ (400–700 nm). At this intensity the rate in leaves of clone Mb 1 often declined with time during measurement, presumably as a result of photoinhibition.

To determine the photochemical capacity of the leaves, the rate of photosynthesis was measured in monochromatic light of low intensities in the range where photosynthesis is a linear function of light intensity. Monochromatic light was isolated by an interference filter (665 nm). The fractional absorption of light by the leaf was determined in an Ulbricht integrating sphere using the same interference filter. Quantum requirements were then calculated as einsteins absorbed per mole CO_2 taken up by the leaf. Following the photosynthesis measurements, the chlorophyll and protein contents of the same leaf were determined. Tables 2 and 3 show results from one experimental series with plants of both clones grown first under weak light and then transferred to strong light for periods ranging from one to six days.

As can be seen from Table 2, the chlorophyll content per unit leaf area of leaves of clone Mb 1 decreases considerably after transfer to strong light. On the other hand, no such decrease is found in leaves of clone Fe 2. Both clones increased in leaf thickness during the six days in strong light but to different degrees, i.e., about 25% in Mb 1 and 75% in Fe 2. This increase in thickness

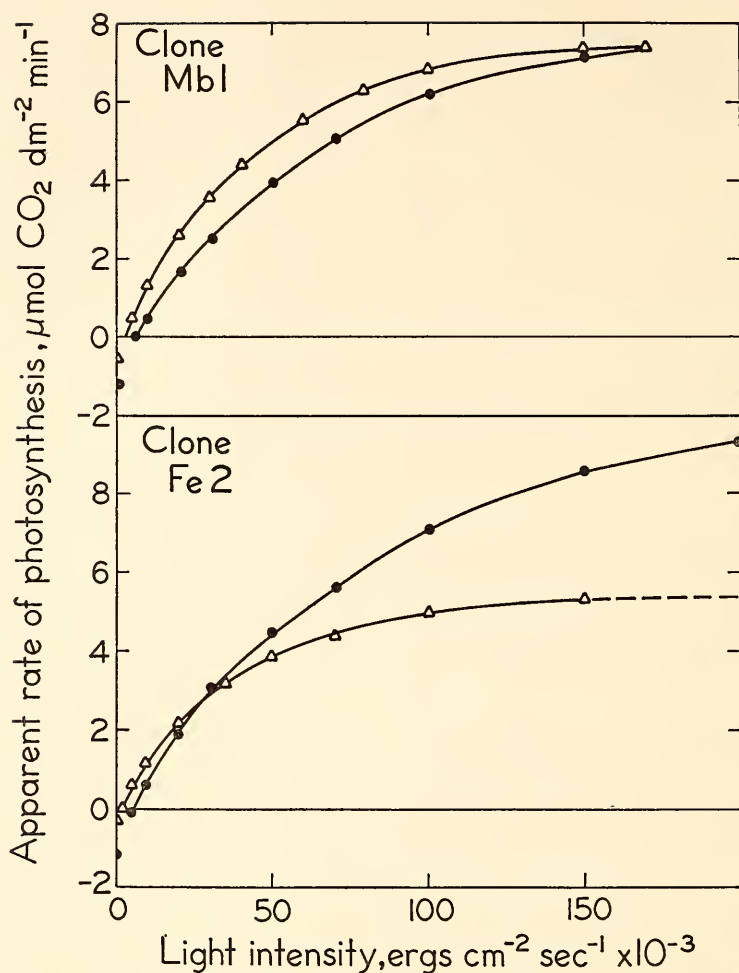


Fig. 6. Apparent rate of photosynthesis as a function of light intensity of a shade (Mb 1) and a sun (Fe 2) clone of *Solanum dulcamara* grown under a high light intensity of 11×10^4 $\text{ergs cm}^{-2} \text{ sec}^{-1}$ (solid circles) and a low intensity of 24×10^3 $\text{ergs cm}^{-2} \text{ sec}^{-1}$ (open triangles).

TABLE 2. Quantum Requirement and Chlorophyll Content of Leaves of Two Clones of *Solanum dulcamara* Grown in Weak Light and After Transfer to Strong Light for One to Six Days

		Clone Mb 1 from Shaded Habitat		Clone Fe 2 from Exposed Habitat	
		Chloro- phyll mg dm^{-2}	Quantum Requirement Einst. abs. per mole CO_2	Chloro- phyll mg dm^{-2}	Quantum Requirement Einst. abs. per mole CO_2
At start		6.1	15	5.9	15
Days in strong light	1	5.6	19	6.2	15
	2	5.1	20	5.9	16
	3	4.5	21	7.6	14
	4	4.4	21	6.6	14
	5	3.6	23	6.5	14
	6	3.4	23	7.1	17

could account for the slight increase in chlorophyll content per unit leaf area in Fe 2 leaves.

Leaves of clone Mb 1 show a continuing increase in quantum requirement for CO₂ fixation during the six-day period. This can be interpreted to be a result of inactivation of photochemical partial reactions within these leaves. Substantial damage to the photochemical apparatus already is evident the first day after transfer to the higher light intensity. This early increase in quantum requirement is accompanied by only a slight decrease in chlorophyll content which indicates that the chlorophyll destruction observed later is not a primary effect of photoinhibition. In contrast, no significant change in quantum requirement occurred in Fe 2 leaves during the same period.

Leaves of clone Fe 2 continuously increase their light-saturated photosynthesis to almost twice the original rate during six days in strong light (Table 3). Simultaneously, the concentration of soluble protein increases greatly. This suggests that the increase in light-saturated CO₂ uptake during the experimental period is caused by a synthesis of one or several photosynthetic enzymes. The light-saturated photosynthesis of clone Mb 1 leaves, by contrast, does not increase during exposure to strong light.

These leaves show no consistent increase in protein content.

These results demonstrate that within the species *Solanum dulcamara*, ecotypes have evolved that have specific physiological mechanisms to cope with the light climate prevailing in their different natural habitats.

In practically all known instances, shaded habitats of *Solanum dulcamara* are moist and some are wet all year. In contrast, some exposed habitats are very dry as, for example, the gravel mound in the Mediterranean maqui near Rovinj, Yugoslavia, where clone Yu 5 was found to grow actively during the dry summer season. In early experiments it was found that clone Sh 2, which grows in a shaded *Alnus glutinosa* swamp near Frankfurt-Schwanheim, Germany, showed no signs of photoinhibition when grown under high light intensity. Moreover, it was able to increase its light-saturated photosynthetic rate when exposed to high light intensity during growth.

In order to determine whether there is an interaction between light intensity and water stress in influencing the distribution of *Solanum dulcamara* ecotypes, comparative growth experiments were made with clones Sh 2 and Yu 5. The plants were grown outdoors in full sunlight and with identical nutrients. Some propagules of both clones were

TABLE 3. Protein Content and Light-Saturated Photosynthetic Rate of Leaves of Two Clones of *Solanum dulcamara* Grown in Weak Light and After Transfer to Strong Light for One to Six Days

		Clone Mb 1 from Shaded Habitat		Clone Fe 2 from Exposed Habitat	
		Max. CO ₂ Uptake μ mole dm ⁻² min ⁻¹ *	Sol. Protein mg dm ⁻²	Max. CO ₂ Uptake μ mole dm ⁻² min ⁻¹ *	Sol. Protein mg dm ⁻²
At start		7.0	39	7.0	32
Days in strong light	1	4.6	46	7.0	34
	2	6.6	55	10.2	43
	3	5.3	45	10.4	50
	4	6.0	49	10.7	54
	5	5.7	45	11.5	59
	6	5.3	37	13.0	69

* Light intensity for photosynthesis measurements: 3×10^5 ergs cm⁻² sec⁻¹ (400-700 nm); temperature: 24°C; [CO₂]: 0.03%.

given only one third of the normal water supply, just enough to prevent wilting.

Fig. 7 shows curves for photosynthetic rate as a function of light intensity for leaves of the two clones grown under dry and moist conditions. Although clone

Yu 5 grows more slowly under dry than under moist conditions, its photosynthetic capacity is not affected by the water stress. It should be noted, however, that the photosynthetic rate is not very high for this clone under any condition.

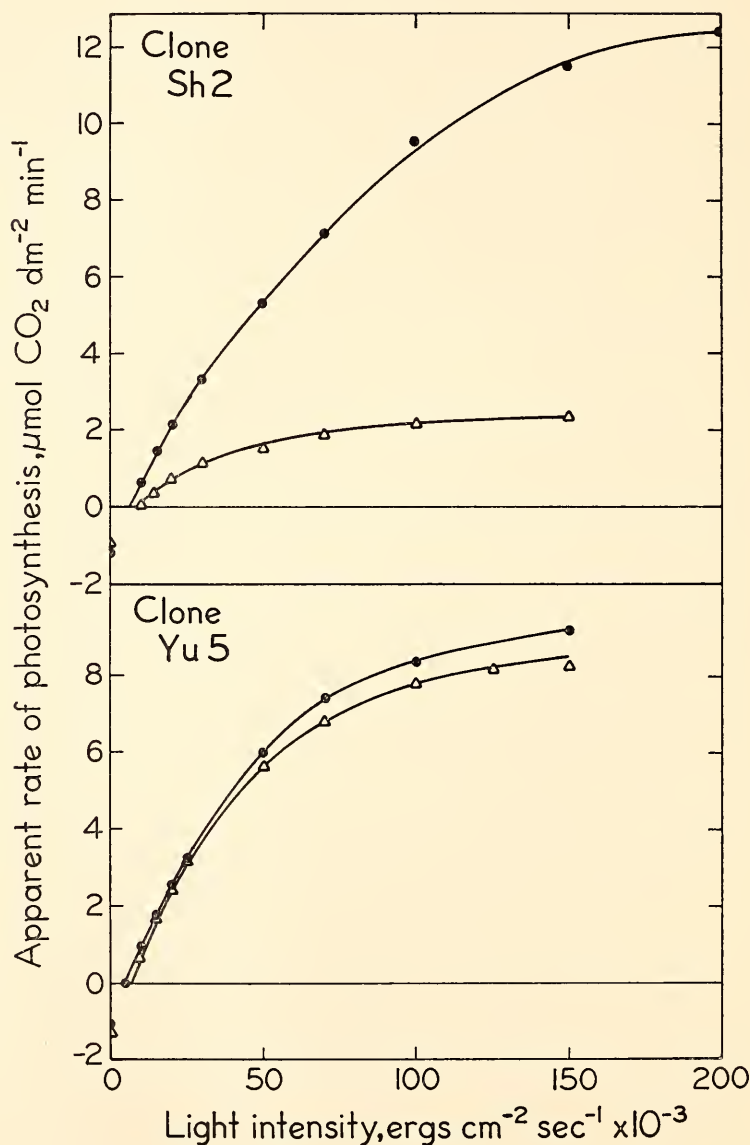


Fig. 7. Apparent rate of photosynthesis as a function of light intensity for two clones of *Solanum dulcamara* grown in strong light. Water supply normal (solid circles) and one-third of normal (open triangles).

On the other hand, the growth of clone Sh 2 is extremely retarded under the same water stress, and its light-saturated photosynthetic rate is much lower as compared with propagules given an ample water supply.

The greatly reduced initial slope of the curve for the Sh 2 leaf grown under dry conditions and high light intensity indicates that severe damage has taken place in the photochemical system. Clone Sh 2 thus appears to be photolabile only under water stress, since it is highly efficient even when grown under strong light when sufficient water is available. Clone Yu 5, on the other hand, shows only a moderate photosynthetic rate in saturating light, but it is capable of maintaining this rate even under drought.

CARBOXYDISMUTASE ACTIVITY IN SHADE-ADAPTED AND SUN-ADAPTED SPECIES OF HIGHER PLANTS

Olle Björkman

The findings that light intensity for growth markedly influences the activity of the photosynthetic enzyme carboxydismutase in the same individual plant and that *Solidago virgaurea* ecotypes from sunny and shaded habitats differ in the activity of this enzyme when

grown at a high light intensity prompted us to investigate the carboxydismutase activity among a number of sun and shade species grown in their natural habitats. A full account of this investigation has been published (Björkman, 1968).

The various species used in the investigation are listed in Table 4. The shade species are limited in natural distribution exclusively to the shaded floors of dense forests, the sun species to moist sunny locations. All are natives of California except *Plantago lanceolata*, which is a naturalized introduction from Europe. The habitats of all the plants used in the present study are situated within 40 km of the laboratory at Stanford. The shade species were collected on the floors of two redwood forests; the light intensity at plant level in these habitats on the average was only 1 to 4 percent of full sunlight.

Cell-free leaf extracts of the plants from sunny habitats that are capable of much higher rates of photosynthetic CO₂ fixation in vivo clearly have much higher activities of carboxydismutase than those of plants growing in deep shade. The enzyme activity expressed on the basis of unit leaf area is of the order of ten times higher in the sun than in the shade

TABLE 4. Carboxydismutase Activity in Leaf Extracts of Sun and Shade Species Grown in Their Natural Habitats

Species	Carboxydismutase Activity, $\mu\text{mole CO}_2 \text{ min}^{-1} *$			
	Per dm ² Leaf Area	Per g Fresh Tissue	Per mg Chlorophyll	Per mg Soluble Protein
Shade Species				
<i>Adenocaulon bicolor</i>	2.0	2.0	0.63	0.22
<i>Aralia californica</i>	2.0	2.3	0.76	0.16
<i>Disporum smithii</i>	1.0	1.1	0.40	0.20
<i>Trillium ovatum</i>	2.0	1.7	0.50	0.15
<i>Viola glabella</i>	1.0	1.2	0.38	—
Sun Species				
<i>Atriplex patula</i>	23.0	10.1	5.72	0.43
<i>Echinodorus berteroi</i>	15.0	7.6	3.26	0.24
<i>Mimulus cardinalis</i>	17.0	5.4	3.28	0.35
<i>Plantago lanceolata</i>	10.0	4.1	1.89	0.26
<i>Solidago spathulata</i>	12.0	4.9	2.81	0.23

* $[\text{HCO}_3] = 5 \times 10^{-3} M$. $[\text{RuDP}] = 3 \times 10^{-4} M$. 23°C.

species. Since the sun species have a greater ratio of volume to area (almost 50%) than the shade species, the difference between the two groups becomes somewhat smaller when the activity is expressed on the basis of leaf volume or fresh weight. Even when fresh weight is used as the basis for comparison, however, the plants show a carboxydismutase activity several times higher than the shade plants, and there is a strikingly parallel variation in the light-saturated rate of CO_2 fixation in vivo and the rate of CO_2 fixation by the enzyme in vitro among the species for which both were measured.

The chlorophyll content per unit weight of fresh leaves is higher in the shade species than in the sun species, whereas the opposite is true of the soluble protein content. Consequently, the difference in carboxydismutase activity between the two groups becomes greater when expressed on the basis of chlorophyll than it is when expressed on the basis of fresh weight, but considerably smaller when expressed on the basis of soluble protein. It is noteworthy in this connection that carboxydismutase probably accounts for a large fraction of the total soluble protein. This would, of course, tend to reduce differences in the activity of this enzyme when soluble protein is used as the basis for comparison rather than, for example, fresh weight.

The higher chlorophyll content but lower carboxydismutase activity in the shade as compared with the sun plants is of particular interest from an ecological viewpoint since it lends support to the idea that the fraction of the available chemical energy used for the synthesis of components determining the efficiency of light absorption in relation to the fraction used for the synthesis of components that determine the capacity of enzymic steps is larger among the shade plants than among the sun plants.

It seems likely that the low carboxydismutase activity in the shade plants is

at least partly responsible for their low light-saturated rates of photosynthesis. Although it can be expected on theoretical grounds that shade plants have a low activity of other enzymes in addition to carboxydismutase, no direct measurements of enzyme activity supporting this supposition have as yet been made. There is, however, evidence that shade species have greater resistance to gas diffusion than do sun plants. This also would be expected to result in a lower light-saturated photosynthetic rate in the shade plants.

Hatch and co-workers have provided evidence for the operation of a C 4-dicarboxylic acid pathway for photosynthesis in certain monocotyledons, including many tropical grasses, but not in several dicotyledons (Hatch, Slack, and Johnson, 1967; Slack and Hatch, 1967). The species in which this pathway was found to be operative had low carboxydismutase activity but high levels of phosphopyruvate carboxylase. Very recently, Johnson and Hatch (1968) reported that the pathway operates also in the dicotyledonous genera *Amaranthus* and *Atriplex*. It is very interesting that the *Atriplex* species used by Johnson and Hatch, *A. semibaccata*, showed a high level of phosphopyruvate carboxylase but a very low level of carboxydismutase, whereas the *Atriplex* species used in the present study, *A. patula* var. *hastata* had a high carboxydismutase activity, indeed the highest among the species investigated. Apparently, therefore, differentiation in photosynthetic pathway has taken place within the same genus.

References

- Björkman, O., *Physiol. Plantarum*, **21**, 1-10, 1968.
- Hatch, M. D., C. R. Slack, and H. S. Johnson, *Biochem. J.*, **102**, 417-422, 1967.
- Johnson, H. S., and M. D. Hatch, *Phytochemistry*, **7**, 375-380, 1968.
- Slack, C. R., and M. D. Hatch, *Biochem. J.*, **103**, 660-665, 1967.

PHOTOSYNTHESIS OF AN AMPHIPLOID
Mimulus IN COMPARISON WITH ITS
PROGENITORS

William M. Hiesey, Malcolm A. Nobs and
Olle Björkman

The important evolutionary role played by amphiploidy in the synthesis of new species from ancestral forms of restricted geographical and ecological distribution has been recognized for some time (Clausen, Keck, and Hiesey, 1945). Frequently amphiploids are successful in inhabiting new environments not occupied by their parent species. The physiological basis for the evolutionary success of such amphiploids has been a matter of speculation.

A unique opportunity for comparing the photosynthetic performance of an interspecific tetraploid hybrid derivative with its markedly distinct diploid parent species was afforded by the production of an amphiploid between *M. lewisii* and *M. nelsonii* described in *Year Book 65*, pp. 468-471. The F_1 hybrid between these species is normally diploid, like both parents, which have 8 pairs of chromosomes. This hybrid is highly sterile, but a tetraploid sector of one F_1 individual having 16 pairs of chromosomes yielded viable seeds giving rise to a vigorous, fertile, self-perpetuating amphiploid population.

Clones of the original parental plants and of the diploid and tetraploid sectors of the F_1 , together with an amphiploid F_2 individual, were grown as vegetative propagules under identical conditions in growth cabinets. During the growth

period prior to the photosynthetic measurements, the light intensity was maintained at approximately 100,000 ergs $\text{cm}^{-2} \text{sec}^{-1}$, the photoperiod was held at 16 hours, and day and night temperatures at 22° and 15°C, respectively. The plants were grown in perlite supplied with nutrient solution.

Light saturation curves were determined on attached leaves of intact plants with the apparatus and methods described in *Year Book 63*, pp. 430-431, and *Year Book 65*, pp. 461-468. The curve for the parental *M. lewisii*, clone 7405-4, originally from near our Timberline station at 10,500 feet elevation in the Sierra Nevada of California, is shown in Fig. 8. It is compared with that of *M. nelsonii*, clone 7422-12, originally from near El Salto, in the highlands of Central Mexico, and of the F_2 amphiploid clone 7606-8.

All three clones have essentially identical curves at low light intensities in the nearly linear range 0 to 30,000 ergs $\text{cm}^{-2} \text{sec}^{-1}$. As light-saturating intensities are approached, the curves diverge and show differences both in the light intensity required for saturation and in the maximum light-saturated rate attained. The *M. lewisii* clone saturates at a lower light intensity than the clone of *M. nelsonii* or the amphiploid. The amphiploid has a significantly higher light-saturated rate than either parent, although the F_1 progenitor on both the diploid and tetraploid levels have rates that are intermediate between the parents (Table 5). The enhanced vigor of growth

TABLE 5. Light-Saturated Rate of Photosynthesis of an Amphiploid *Mimulus* and of its Progenitors at Three Different Temperatures

	Approximate Light-Saturation Intensity, ergs $\text{cm}^{-2} \text{sec}^{-1}$	Light-Saturated Photosynthetic Rate at 22°C, mg CO_2 $\text{dm}^{-2} \text{hr}^{-1}$ *	Photosynthetic Rate, % of Maximum		
			10°C	22°C	38°C
7405-4, <i>M. lewisii</i> P_1 , $n = 8$	225,000	26.3	82.0	100.0	73.8
7422-12, <i>M. nelsonii</i> P_2 , $n = 8$	325,000	31.3	82.5	93.6	78.8
7540-2-2x, F_1 Hybrid, $n = 8$	325,000	26.4	76.5	95.0	45.0
7540-2-4x, F_1 Hybrid, $n = 16$	325,000	30.0	85.3	91.0	37.4
7606-8, Amphiploid, $n = 16$	325,000	33.4	85.0	98.5	23.4

* $[\text{CO}_2]$: 0.03%.

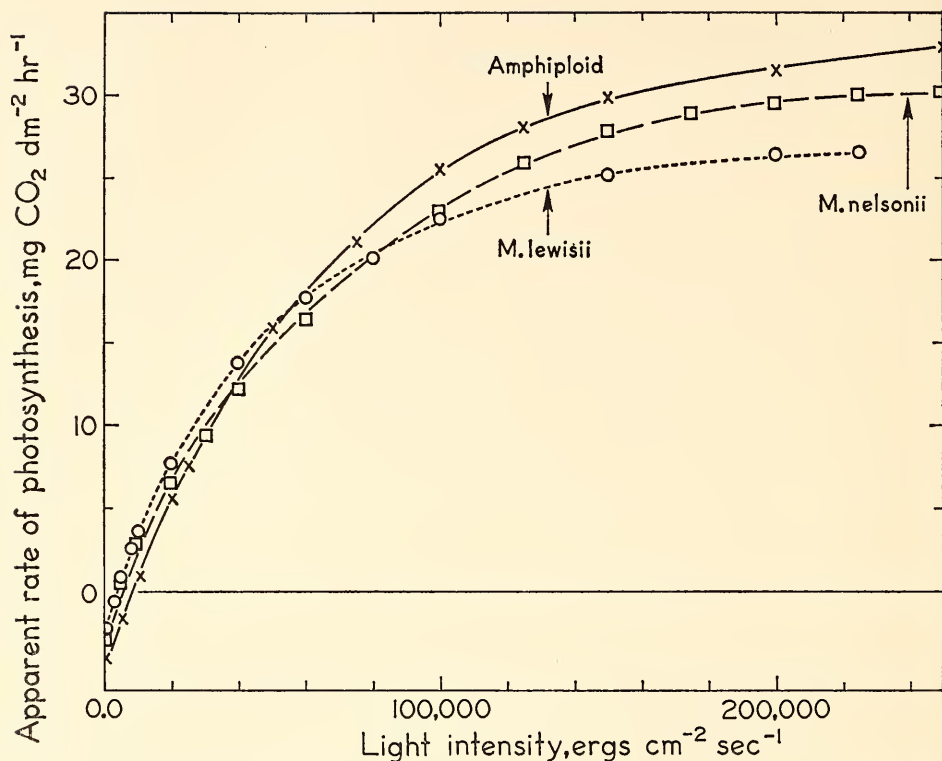


Fig. 8. Photosynthetic rates of *M. lewisii*, *M. nelsonii*, and their tetraploid amphiploid derivative as a function of light intensity (600–700 nm).

of the amphiploid, as compared with the parents when all are grown under identical conditions, may therefore be due at least in part to the higher light-saturated photosynthetic rate.

The temperature dependence of net photosynthetic rate was likewise determined at a constant light intensity of 175,000 ergs cm⁻² sec⁻¹ in the wavelength range between 600 and 700 nm. Leaf temperatures were monitored during the measurements with miniature thermocouples in direct contact with the under leaf surfaces. Fig. 9 shows curves for the same three clones depicted in Fig. 8.

The results from these measurements reveal (1) that the temperature dependence curves for the ecologically and morphologically diverse parental clones *M. lewisii* and *M. nelsonii* are remark-

ably similar and surprisingly flat over the range 10° to 38°C, showing a high degree of tolerance over this range; and (2) that the amphiploid derivative, which has a higher photosynthetic rate than either parent over the cooler temperature ranges, is much more sharply inhibited in rate at temperatures above 25°C than is either parent. Curves of a general shape similar to the amphiploid were determined at both the diploid and tetraploid levels. The relative photosynthetic rates listed in the right-hand columns of Table 5 show the drop at high temperatures of the hybrid derivatives in comparison with the parental species.

To our knowledge, these are the first data on comparative photosynthetic rates of an amphiploid with its precisely

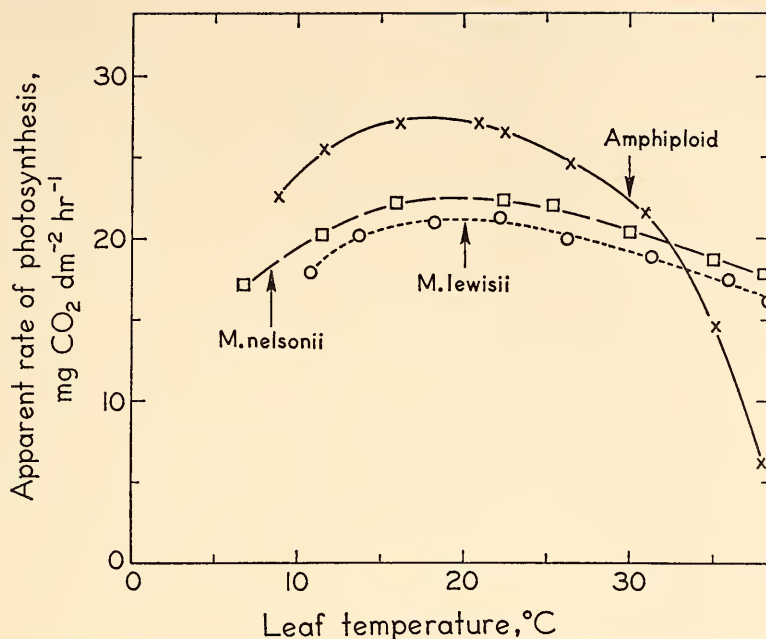


Fig. 9. Photosynthetic rate as a function of temperature of *M. lewisii*, *M. nelsonii*, and their tetraploid amphiploid derivative. (Light intensity held constant at 175×10^3 ergs cm⁻² sec⁻¹ 600-700 nm).

known parental individuals and the immediate progenitor individual plant on both the diploid and tetraploid levels. The measurements reflect the interaction of genomes of two taxonomically and ecologically distinct species on the functioning of a complex physiological character.

These data on *Mimulus* support the conclusion that the process of genome addition of two species through amphiploidy may alter basic physiological functions significantly. Such interactions at present cannot be explained in simple terms.

References

- Clausen, Jens, David D. Keck, and William M. Hiesey, *Experimental studies on the nature of species II. Plant evolution through amphiploidy and autopolyploidy, with examples from Madiinae*, Carnegie Inst. of Wash. Publ. No. 564, vii+174 pp., 1945.

VARIATION AMONG RYEGRASSES IN RATES OF APPARENT PHOTOSYNTHESIS

J. H. Silsby

The variation in rates of photosynthesis among individual plants and among plant populations is of considerable interest from the viewpoint of both ecology and plant productivity. Studies on the basic photosynthetic characteristics of ecological races of *Mimulus* and *Solidago* reported in this and previous *Year Books* show not only that such races differ in photosynthetic rates, but also that this attribute is inherited and probably has ecological significance.

Currently agricultural scientists are paying increased attention to the utilization of light energy by crop plants. Knowledge of basic differences in photosynthetic ability between species and cultivars could be of considerable value in improving crop production. Although

it is known that widely contrasting crop plants such as corn, wheat, sugar cane, and cotton differ in light-saturated rates of photosynthesis, attempts to demonstrate such differences among closely related species or varieties of cultivated plants have met only partial success.

Lolium rigidum is an annual ryegrass of predominantly Mediterranean distribution. *L. perenne* var. *Medea* is a perennial ryegrass derived from a summer-dormant form of *L. perenne* from Algeria. *L. rigidum* and *L. perenne* var. *Medea* were chosen for study because they are known to differ in both their absolute and relative growth rates. Rates of photosynthesis were determined with the techniques described in *Year Book 63*, pp. 430-431 and *Year Book 65*, pp. 461-468. In these measurements, portions of attached leaves 5.5 cm in length were used. Responses to different light intensities ($0-3 \times 10^5$ ergs $\text{cm}^{-2} \text{sec}^{-1}$) and temperatures ($10^\circ-40^\circ\text{C}$) were studied for several leaves of individual plants in order to evaluate the range of performance of that plant as a whole and in relation to different plants within the population. It was found that light-saturated rates of photosynthesis decreased when leaves began to senesce and were lower in the proximal as compared with the distal portions of the leaf. Poor mineral nutrition also resulted in reduced rates.

Plants were grown in pots with a favorable nutrient regime both outdoors and in a glasshouse under a range of light environments. The photosynthesis-light intensity curves of both species reflect the light regime under which the plants had been grown. Leaves grown under high light (about 3×10^5 ergs $\text{cm}^{-2} \text{sec}^{-1}$) had higher light-saturated rates than leaves grown under low light intensity (about 2×10^4 ergs $\text{cm}^{-2} \text{sec}^{-1}$). However, the differences in *Lolium* are small in comparison with similar effects shown by other species.

In *Lolium rigidum* there was evidence that leaves grown under low light utilize low light intensities more efficiently than

leaves grown under high light. Also it appears that high-light-grown leaves of *L. perenne* are more efficient at low light intensities than are those of *L. rigidum*.

The above results indicate that light-saturated rates of photosynthesis are quite comparable in the two species. However, it was noted that the rates varied from leaf to leaf, a greater rate generally being observed the smaller the specific leaf area (leaf area per unit leaf dry weight). The light-saturated rates of photosynthesis of a mature leaf of a number of different plants of each species grown under a range of light intensities were therefore determined, and the rate plotted against the specific leaf area (S.L.A.) of that portion enclosed in the leaf chamber. The results show that for each species, a decline in light-saturated photosynthesis is associated with an increase in S.L.A.; there is some residual variation about a regression line linking the two attributes. For a given S.L.A., *Lolium rigidum* tended to have a slightly higher photosynthetic rate than *L. perenne*.

An attempt was made to resolve these differences more clearly by measuring the light-saturated rates of the fifth leaf on the main stem of six seedling plants of each species grown under comparable conditions in the greenhouse. The average rate per unit leaf area of the six leaves of *L. perenne* was higher than that of *L. rigidum*, but the S.L.A. of the latter was lower. Plots of photosynthesis against S.L.A. again show a tendency for leaves of *L. rigidum* to have a higher rate of photosynthesis for the same S.L.A.

A situation similar to the above was found within *L. perenne* for two plants (Nos. 18 and 27) thought to differ in light-saturated rates. Plots of photosynthetic rate against S.L.A. for leaves of a number of clones grown under different light regimes show divergence between the two plants.

In conclusion, the above results show that the basic photosynthetic character-

istics of *L. rigidum* and *L. perenne* are very similar. Both tend to behave as "sun" plants in that when grown under low light intensity they retain a capacity for response to high light intensities. Maximum photosynthetic capacities are similar, but it is probable that the light-saturated rate of *L. rigidum* is slightly greater than that of *L. perenne*.

The temperature responses of the two species at a constant light energy level of 2×10^5 ergs $\text{cm}^{-2} \text{sec}^{-1}$ show apparent photosynthesis to have a wide tolerance to this factor. The optimum temperature is $18^\circ\text{--}24^\circ\text{C}$ for each species, but it is clear that the tolerance of *L. rigidum* for high temperature is much greater than that of *L. perenne*. This is in keeping with the summer-dormant behavior of the latter.

GENETIC RECOMBINATION AND TRANSPLANT RESPONSES AMONG F_3 PROGENIES OF *Mimulus*

Malcolm A. Nobs and William M. Hiesey

A logical follow-up of studies on the performance of contrasting races and species of *Mimulus* and their F_1 and F_2 hybrids at the Stanford, Mather, and Timberline transplant stations (*Year Book 66*, pp. 208–214) is a corresponding analysis of selected F_3 progenies. Data gained from this additional step strongly reinforce evidence from F_2 progenies with respect to genetic coherence. They also throw new light on natural selection among genetically heterogeneous populations.

The studies on F_3 populations of *Mimulus* have concentrated on progenies resulting from a single cross between the altitudinally and morphologically contrasting forms of *M. cardinalis* from near sea-level in coastal central California and subalpine *M. lewisii* from 3,200 meters elevation in the Sierra Nevada. The extensive recombination of the parental characters in F_2 populations of this cross, and the diverse responses of individual plants at the Stanford,

Mather, and Timberline transplant stations have been described in part in earlier reports (*Year Book 60*, pp. 381–384; and *Year Book 62*, pp. 387–392).

Segregation within F_3 progenies derived from contrasting F_2 individuals. The patterns of segregation in F_3 populations differ widely, depending on the genetic constitution of the individual F_2 parent. This is illustrated in Fig. 10 where the frequencies of individuals falling into different morphological classes, as expressed by index values, are plotted as histograms. The index value of a given individual is determined by the summed expression of 11 essentially nonmodifiable characters that distinguish the parents. The scoring of each character is made on the basis of a scale of 9 on independent observations at Stanford, Mather and Timberline during a period of three years. Plants resembling *M. lewisii* for a given character are given a rating of 1, and those resembling *M. cardinalis*, a value of 9. The sum of characters of an individual falling into the *M. lewisii* category could, therefore, have a minimum value of 11 in contrast with one of *M. cardinalis* with a possible maximum value of 99. Since progenies resulting from self-pollination of either parent vary within an appreciable range, these idealized minimal and maximal index values are rarely found.

The histograms along the top line of Fig. 10 indicate the range of variation within populations of the self-pollinated *M. lewisii* parent (left), the selfed *M. cardinalis* (right), and their F_1 progeny (center). All these data were obtained from populations grown at Stanford. On the basis of the 11 characters used in determining the index values, the F_1 population tends to resemble *M. lewisii* more than *M. cardinalis* although the F_1 hybrids may be regarded as essentially intermediate between the parents.

The histogram immediately below the topmost line in Fig. 10 shows the frequency of character distribution within

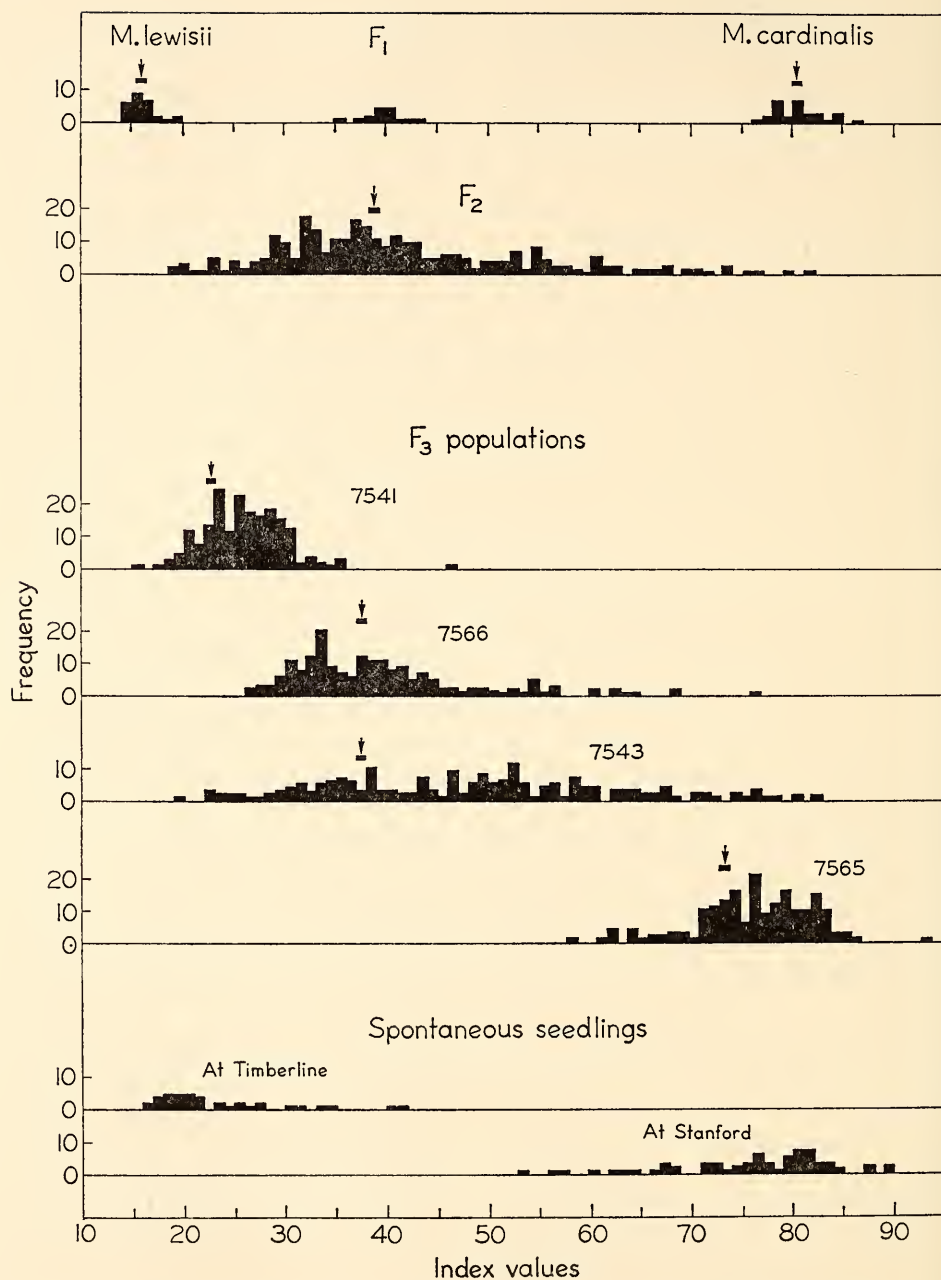


Fig. 10. Ranges of segregation of characters in parental, first, second, and third generation progenies in the cross *Mimulus lewisii* × *M. cardinalis* as observed at Stanford. The index values are based on scored values of 11 characters of individual plants. Arrows point to individuals giving rise to the progenies depicted. Spontaneous seedlings established at Timberline were brought to Stanford for maturing.

a population of 310 F_2 individuals. The broad spread reflects the wide array of character-combinations of the parental plants found in the second generation. Even within this relatively small F_2 population sample, individuals occur that fall within the ranges of the progenies of both self-pollinated parents, but do not exceed their limits.

The middle histograms of Fig. 10 show the ranges of segregation among four F_3 progenies, each consisting of 200 individuals. Each population is the product of a self-pollinated F_2 plant having characters of the index class indicated above each histogram. The populations are distinctive in having peak frequencies at different values along the index scale. The population 7541, for example, which stems from 7111-16, a plant hardly distinguishable from the *M. lewisii* parent, clusters on the left side of the index scale. There is, nevertheless, an appreciable range of segregation although much less than in the F_2 population. In contrast, the population 7565 from the *M. cardinalis*-like F_2 plant 7135-35 clusters far to the right on the index scale, and the majority fall within the morphological limits of the population derived from the selfed *M. cardinalis* parent. Populations 7566 and 7543, the progeny of plants 7111-17 and 7112-55, respectively, which fall within the morphological range of F_1 hybrids, segregate about as widely as the original F_2 population.

The F_3 progeny often show marked transgressive segregation with respect to genetic segregation of a single character distinguishing the parents. The inheritance of pistil length, described in *Year Book 63*, pp. 432-438, may be cited as an example. Even when the aggregate combination of 11 characters is pooled in terms of index value, the segregation in some F_3 populations may extend beyond the mean index value of the self-pollinated parental progenies. An example is seen in population 7565 (Fig. 10) in

which some individuals surpass the mean of selfed progeny of *M. cardinalis*.

The current season is the third during which the F_3 populations 7541, 7565, and 7566 have been tested as cloned individuals at the Stanford, Mather, and Timberline stations. It is now evident that striking differences in the response-pattern of 7541 in contrast with 7565 are being realized. Population 7541 has a markedly higher record for survival and dry weight production at Timberline than 7565, whereas at Stanford the reverse is true. Individual plants that are exceptions occur in both populations, but their frequency is low. In the F_3 population 7566 there is considerably greater diversity in response among individual plants at all three stations.

At Mather, where neither subalpine *M. lewisii* nor coastal *M. cardinalis* survive, the F_3 progeny of the *cardinalis*-like population 7565 has a higher percentage of nonsurvivors than the F_3 of the more *lewisii*-like population 7541. In population 7566 the plants vary from vigorous survivors to weak nonsurvivors; the vigorous plants invariably are morphologically similar to the F_1 hybrids. All the evidence from the F_3 populations therefore strongly supports the conclusion that morphological characters are strongly linked genetically with physiological qualities that are of importance for survival in different kinds of climates.

Spontaneous "weedlings" at the transplant stations. Additional evidence indicating that the type of coherence mentioned above is of importance in natural selection is afforded by a study of spontaneous seedlings of *Mimulus* that become established from seed of open-pollinated F_2 populations growing in the transplant gardens of Stanford, Mather and Timberline. Random samples of such "weedling" populations were taken from the gardens at each station during the spring of 1967 and grown in the nursery at Stanford to study their morphological characters. The lowermost two histograms in Fig. 10 show the frequency dis-

tribution of plants according to index values of samples taken from Stanford and Timberline. The separation of the clusters of frequencies at the two contrasting altitudinal stations is striking:

Timberline favors the establishment of plants having a preponderance of *lewisii*-like characters in contrast with Stanford where only *cardinalis*-like seedlings establish.

BIOCHEMICAL INVESTIGATIONS

LIGHT-INDUCED REACTIONS OF CAROTENOIDS IN THE YELLOW-GREEN ALGA *Botrydiopsis*

David C. Fork

A light-induced shift in the absorption spectrum of carotenoids was reported last year (*Year Book 66*, p. 160; Fork and Ames, 1967) for a number of variously colored algae and for a barley mutant lacking chlorophyll *b*. One of the requirements for clear observation of the carotenoid changes is that the plant used does not contain chlorophyll *b*, since this pigment produces prominent light-induced changes of absorbance near

475 and 515 nm which effectively mask changes produced by carotenoids. This shift toward longer wavelengths of the absorption of a carotenoid was seen particularly clearly in the yellow-green alga *Botrydiopsis alpina* (Xanthophyceae) which contains no chlorophyll *b*.

Further studies on the carotenoid shift have been made with this alga. Action spectra for *Botrydiopsis* confirm the suggestion made earlier, based on studies of the red alga *Iridaea*, that excitation of each of the photosystems produces a carotenoid shift. Detailed measurements of difference spectra indicate that the same carotenoid is apparently participat-

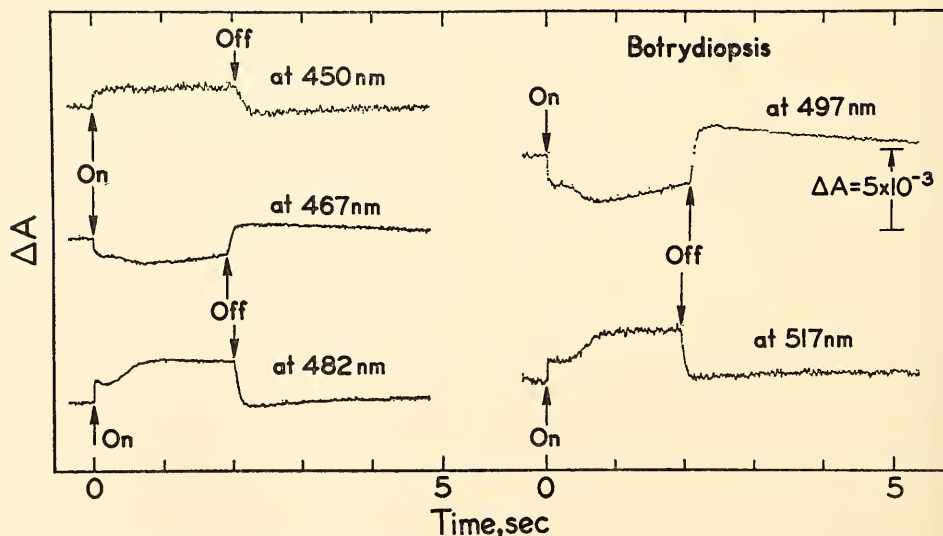


Fig. 11. Light-induced changes of absorbance in *Botrydiopsis alpina* induced by a broad band of red actinic light (2.8×10^5 ergs $\text{cm}^{-2} \text{sec}^{-1}$ between 650 and 800 nm). The magnitude of these initial deflections, the second slow changes, as well as the off deflections all depended strongly upon the schedule used. The traces shown here are those which resulted after the cells had been adapted to a schedule of 2 seconds light and 6 seconds dark. Halfband width of the measuring beam, 1.5 nm.

ing in systems 1 and 2. The kinetic behavior of the carotenoid shift as well as the effect of a number of inhibitors of photosynthesis show many similarities between this change and that produced at 515 nm mentioned earlier.

Since both chlorophyll *b* and carotenoids produce positive absorbance changes at 515 nm it is clear that care should be exercised in the interpretation of results which are based upon studies of absorbance changes at this wavelength.

Kinetics and difference spectra. Kinetics of absorbance changes at 450, 467, 482, 497 and 517 nm produced by illumination of *Botrydiopsis* with a broad band of red light are shown in Fig. 11. In each case an initial rapid change was seen which was followed by a second larger, but slower change. The rise time

of the initial change was measured at 518 nm and found to be as fast as the rise time (50 μ sec) of the flash used. A rapid deflection also resulted upon darkening.

Fig. 12 shows difference spectra obtained when cells were illuminated with high intensity red light like that used to produce the traces for Fig. 11. The spectrum for the initial change had maxima at 451, 482, and 517 nm and minima at 467 and 497 nm. The off deflections shown in Fig. 11 are in each case larger than the on deflections. The difference spectrum of Fig. 12 for the off deflection is just reversed and has its peaks located at the same wavelengths as for the on deflection. The intensity of the light used had no effect on the difference spectra. The same spectra were found when low actinic intensity was used. Integration of the difference spectra given

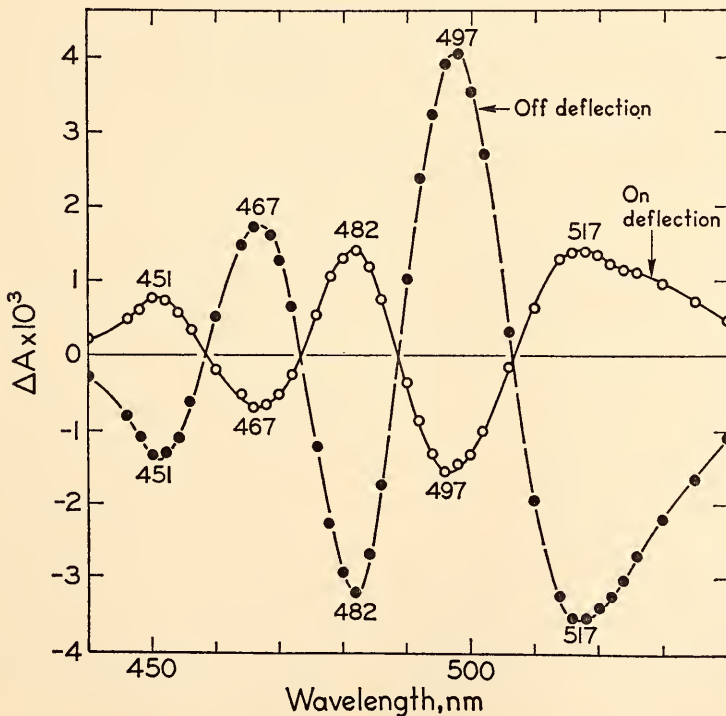


Fig. 12. Difference spectra of *Botrydiopsis* produced by red actinic light as described for Fig. 11 (8.7×10^4 ergs $\text{cm}^{-2} \text{sec}^{-1}$). The kinetics of absorbance changes at maxima and minima are given in Fig. 11.

in Fig. 12 suggests that these spectra are most likely produced by a shift toward longer wavelengths of the absorption band of a carotenoid originally having maxima at or somewhat below 440, 473 and 506 nm.

The effect of DCMU. The effect of the inhibitor DCMU [3-(3,4-dichlorophenyl)-1,1-dimethylurea] is shown in Fig. 13. Trace *a* shows the light-induced absorbance change produced at 482 nm before adding DCMU. After addition of this inhibitor, the initial positive deflection remained (trace *b*). Its height was dependent upon the length of the dark intervals between exposures and is discussed below. DCMU completely in-

hibited the slower but larger absorbance increase following the initial deflection. After the cells had been in the light for several seconds a very small positive change persisted in the presence of DCMU. The effect of DCMU on the kinetics of the absorbance changes at those wavelengths shown in Fig. 11 was the same: positive transients persisted at 450 and 517 nm, negative ones at 467 and 497 nm. The difference spectrum for cells which had been treated with DCMU is given in Fig. 14. Maxima were again found at 450, 482, and 516 nm and minima at 466 and 497 nm. The spectrum is very similar to those shown in Fig. 12.

The height of the transient absorbance change persisting in cells inhibited with DCMU is strongly dependent on the length of the dark intervals given between light exposures. Fig. 15 shows the height of the initial transient (in this case measured at 515 nm) as a function of dark intervals between light exposures. Half of the maximum change was regenerated in about 4 seconds.

The effect of DCMU on the absorbance change at 482 nm was greatly altered after the addition of the donor system DAD (2, 3, 5, 6-tetramethyl-*p*-phenylenediamine) and sodium ascorbate. This couple is known from the work of Trebst and co-workers (1965; 1966) to be an effective donor of electrons which enter the electron-transport sequence very near system 1. Trace *c* of Fig. 13 shows the effect on the absorbance change at 482 nm of adding these compounds to whole cells of *Botrydiopsis*. Addition of only ascorbate to DCMU-inhibited cells did not produce an effect. TMPD (N,N,N',N'-tetramethyl-*p*-phenylenediamine) and ascorbate gave only a very small regeneration of this change. Difference spectra (Fig. 16) for the on and off deflections regenerated by DAD and ascorbate also have their maxima and minima at the same wavelengths as those spectra given in Figs. 12 and 14.

The effect of other inhibitors on the carotenoid shift. The uncoupler of phos-

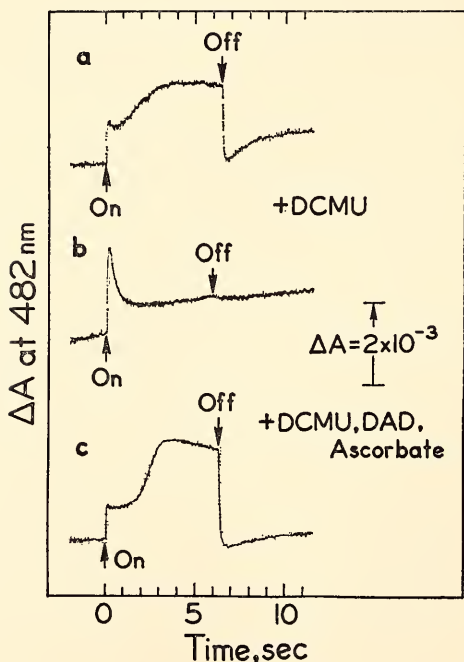


Fig. 13. Kinetics of the absorbance changes induced at 482 nm in *Botrydiopsis* by red light as described in Fig. 11 before addition of DCMU (trace *a*) and after addition of DCMU (trace *b*), and DAD and ascorbate (trace *c*). The concentrations used were: DCMU, $5 \times 10^{-5}M$; DAD, $6.6 \times 10^{-5}M$; sodium ascorbate, $2 \times 10^{-3}M$. Intensity of actinic light 1.5×10^4 ergs $cm^{-2} sec^{-1}$; halfband width of the measuring beam, 2 nm.

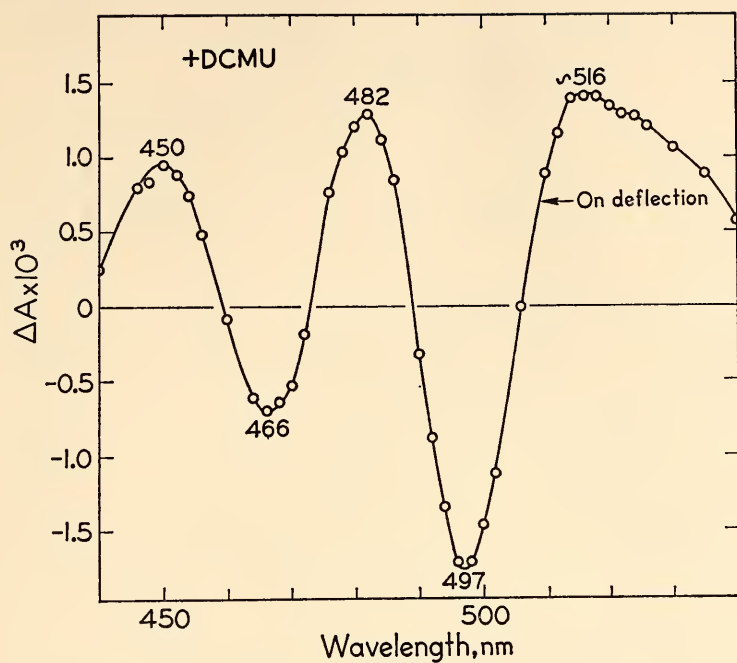


Fig. 14. Difference spectrum for the magnitude of the initial absorbance change (see trace *b*, Fig. 13) produced by *Botrydiopsis* in $10^{-8}M$ DCMU upon exposure to red light as described in Fig. 11 (7.9×10^4 ergs cm^{-2} sec^{-1}).

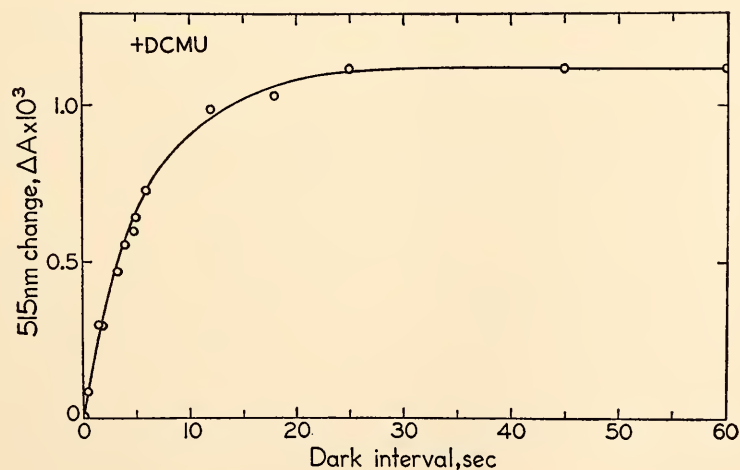


Fig. 15. Height (regeneration) of the fast, initial transient of the 515-nm absorbance change in *Botrydiopsis* (as in trace *b* of Fig. 13) as a function of varied dark intervals between 6-second exposures to actinic light of 672 nm (5.1×10^5 ergs cm^{-2} sec^{-1}). DCMU, $10^{-8}M$.

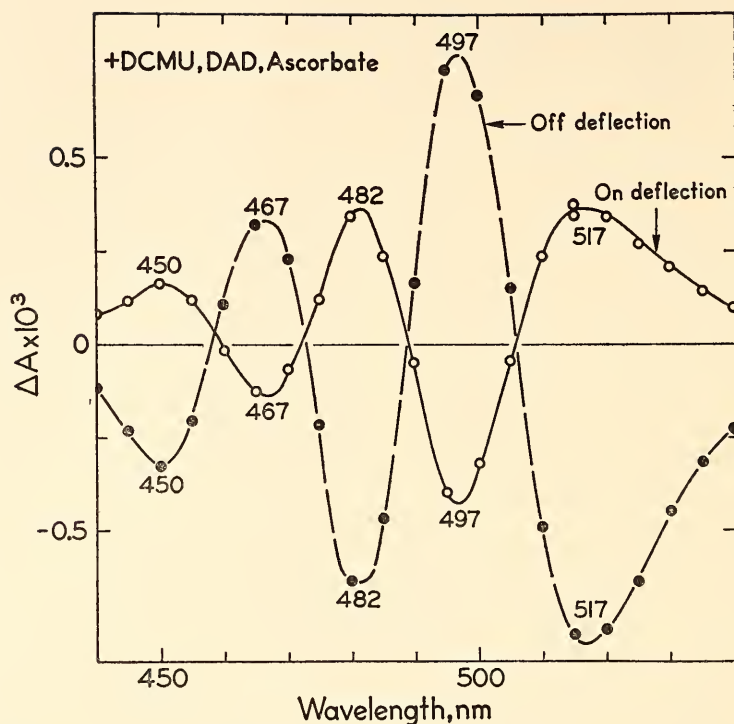


Fig. 16. Difference spectra for the magnitude of the absorbance changes of *Botrydiopsis* in DCMU, DAD, and ascorbate (as in trace *c*, Fig. 13) produced by a band of far-red actinic light (6.3×10^4 ergs $\text{cm}^{-2} \text{sec}^{-1}$ between 690 and 750 nm). DCMU, $5 \times 10^{-5} M$; DAD, $6.6 \times 10^{-5} M$, sodium ascorbate, about $2 \times 10^{-3} M$. Halfband width of the measuring beam, 2 nm.

phorylation CCCP (carbonyl cyanide, *m*-chlorophenylhydrazine) at $10^{-5} M$ had an effect after cells had been incubated for about 30 minutes which was similar to that produced by DCMU. The initial on deflection persisted and the second, slow and larger change was inhibited. Quinacrine (atebrin) at $10^{-3} M$ inhibited both the initial transient and second wave. Vitamin K_3 , which has been shown (Amesz and Fork, 1967) to poison reaction centers of system 2, inhibited the slow increase at 482 nm already at a concentration of $10^{-5} M$ but did not affect the initial transient. Hydroxylamine ($2 \times 10^{-3} M$) acted like DCMU and inhibited the second, slow increase of the absorbance change at 482 nm but did not affect the initial on transient.

Action spectra for the production of

the carotenoid shift. Action spectra, using equal numbers of incident quanta, were determined for production of the initial transient at 482 nm persisting after the addition of DCMU and for the slow increase of absorbance which occurred upon illumination of cells exposed to a continuous far-red background light. For the determination of the action spectrum of the initial transient remaining after the addition of DCMU, sufficiently low actinic intensities were used so that the rate of the initial change was linear with light intensity. The curve in Fig. 17 with a broken line shows a peak for this action spectrum near 681 nm and activity extending well beyond 700 nm. An action spectrum was also determined for the production of the 482-nm change in cells treated with DCMU, DAD and ascor-

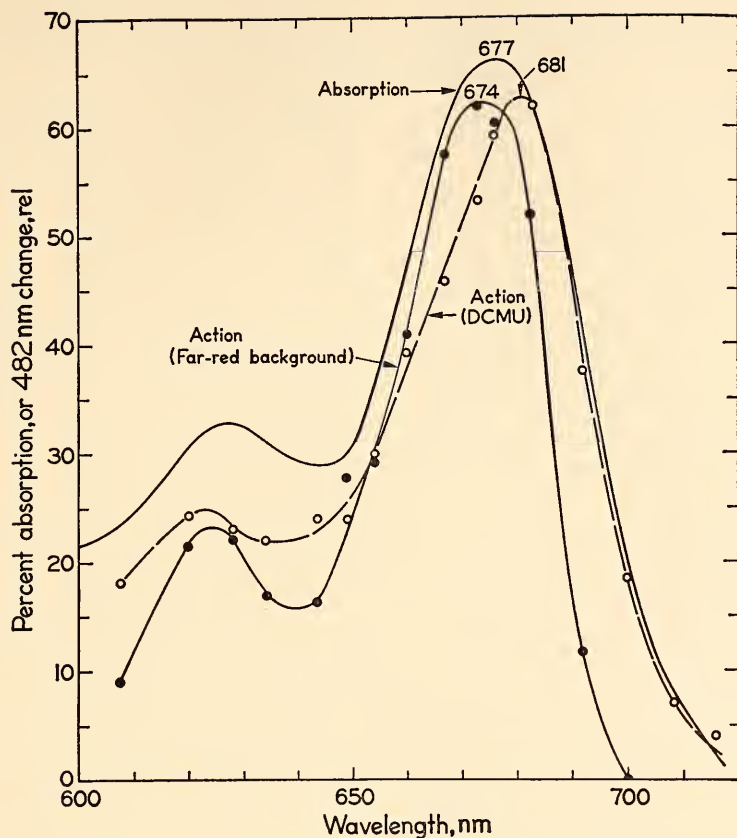


Fig. 17. Action spectra for the production of the 482-nm absorbance change in *Botrydiopsis*. Solid circles: action spectrum for the rate of the slow absorbance increase determined in the presence of far-red background light (690–750 nm; 1.1×10^4 ergs $\text{cm}^{-2} \text{sec}^{-1}$). The incident actinic intensities had halfband widths of about 9 nm and were equivalent to 1.32×10^9 einstein $\text{cm}^{-2} \text{sec}^{-1}$ at 673 nm. Open circles: action spectrum in $10^{-4}M$ DCMU (without far-red background light) for the rate of the rapid absorbance increase corresponding to trace *b* of Fig. 13. The incident actinic intensities used were equivalent to 0.77×10^9 einstein $\text{cm}^{-2} \text{sec}^{-1}$ at 683 nm. The absorption of the cell suspension was measured in an integrating sphere with the same interference filters used for the action spectra. A scattering correction of about 6% was used. The absorption spectrum and action spectra were all measured using one sample of cell suspension.

bate (see trace *c* of Fig. 13). This spectrum was like the action spectrum for the production of the initial transient in DCMU-treated cells and had a peak near 681 nm.

In cells not treated with DCMU but exposed to far-red background light, the rapid initial change upon illumination was absent. Instead, a slow increase of absorbance occurred in the light and a fast off deflection followed upon darkening.

The rates of these slow increases of absorbance at 482 nm were measured using actinic wavelengths having intensities such that they were linear with intensity. The resulting action spectrum, plotted as the solid curve in Fig. 17, has its peak near 674 nm and at 700 the activity is zero.

It is clear from the action spectra measured for *Botrydiopsis* that both photochemical systems produce a carotenoid

shift. The action spectra for the transient carotenoid change persisting in DCMU (trace b, Fig. 13) as well as that measured after the addition of DAD and ascorbate show that system 1 alone participates in this reaction, since these spectra had peaks at 681 nm and high activity extending beyond 700 nm. They are very similar to the action spectrum measured (Fork *et al.*, 1967) in the green alga *Ulva* for the oxidation of the *f*-type cytochrome, a well-known system 1 reaction. These spectra are also similar to the system 1 action spectra measured by Joliot *et al.* (1968) for the reduction of methyl viologen by chloroplasts poisoned with DCMU and supplied with DAD and ascorbate.

Measurements made last year (Year Book 66, p. 160) on the red alga *Iridaea* have also shown that each of the two photochemical systems produced a carotenoid shift. This distinction was possible because the absorption of the pigments associated with systems 1 and 2 is widely separated spectrally. Thus 684 nm, absorbed largely by chlorophyll of system 1 produced a time course for the carotenoid shift which was different from that produced by 622-nm light, absorbed predominantly by phycocyanin of system 2. Moreover, the ratios of the activity of 684- to 622-nm light in bringing about the carotenoid shift in this alga were the same as for cytochrome oxidation.

If electron flow is interrupted with DCMU in *Botrydiopsis* the excitation of system 1 produces a rapid shift of carotenoid absorption toward longer wavelengths which reverses again in the light. This same transient shift occurs in red algae excited with red light (but not treated with DCMU) because in these algae red light is unable alone to sustain complete photosynthesis efficiently.

The slower, but larger, shift of carotenoid absorption apparently accompanies sustained electron flow. The reestablishment of partial electron transport after addition of DAD and ascorbate to

DCMU-treated algae produced a lasting carotenoid shift in the light, sensitized by system 1.

System 2 also produced a sustained carotenoid shift in the light. This was seen (Fig. 17) in the action spectrum for the slowly occurring shift measured in the presence of far-red background light. This action spectrum with a peak near 674 nm and activity dropping to zero around 700 nm reflects participation by system 2. In these respects it resembles other action spectra for system 2 (Müller *et al.*, 1963) and the spectrum for system 2 measured as O₂ evolution in chloroplasts by Joliot *et al.* (1968); however, the spectrum of *Botrydiopsis* is not asymmetric, since this alga contains no chlorophyll *b*.

Vitamin K₃, among other substances, suppresses electron flow probably by acting as "artificial" traps in system 2 (Amesz and Fork, 1967). This compound, like DCMU, also selectively stopped the slow phase of the carotenoid shift. A similar effect was seen with the system 2 inhibitor, hydroxylamine. Explanation of the results obtained with the uncouplers CCCP and quinacrine on the basis of electron flow is not apparent and needs more study.

So far, there is no evidence to suggest that a different carotenoid participates in the absorption shifts taking place upon excitation of systems 1 and 2. Detailed measurements of difference spectra for the transient shift persisting in DCMU as well as those sustained by DAD and ascorbate (system 1) were similar to each other and to difference spectra obtained before poisoning. Also, difference spectra for the slow shift taking place in the presence of background light (system 2) were the same as the above-mentioned spectra.

The shifts in carotenoid absorption reported (Year Book 66, p. 160) for plants lacking chlorophyll *b* as well as those described here have many similarities in common with the 475-, 415-, 650-nm change seen in green algae and

higher plants containing chlorophyll *b*. The latter change apparently does not result from an oxidation-reduction reaction but rather seems to be caused by an alteration in the environment of chlorophyll *b* which produces a small change in its absorption spectrum. Junge and Witt (1968) have recently suggested that this change is an indicator for proton translocation across a membrane.

Both the carotenoid shift and the chlorophyll *b* changes begin with a fast, initial transient sensitized by system 1. The initial, fast carotenoid shift, like the chlorophyll *b* change, is dependent upon the preceding dark time and increases up to a certain maximum with increasing dark time. DCMU in each case only inhibits the slow, second increase of both changes. This slow change for each is sensitized by system 2.

All the similarities between the carotenoid shift, which has one of its maxima near 515 nm, and the 515-nm change, which is produced by chlorophyll *b*, make it necessary to proceed with caution in a description of what role chlorophyll *b* plays in photosynthesis. Since the carotenoid shifts were seen in a barley mutant lacking chlorophyll *b* (Year Book 66, p. 165) it is not unreasonable to assume that these shifts also occur in other higher plants as well as in green algae containing chlorophyll *b*, and that light-induced absorbance changes caused by both compounds are visible at 515 nm. Since absorbance changes attributable to carotenoids are near zero at 473 nm in *Botrydiopsis* and at 480 nm in mutant barley while the change caused by chlorophyll *b* has a negative maximum near these wavelengths, it may be possible by appropriate choice of wavelengths to observe the chlorophyll *b* change without interference from the carotenoid change.

References

Amesz, J., and D. C. Fork, *Biochim. Biophys. Acta*, **143**, 97-107, 1967.

Fork, D. C., and J. Amesz, *Photochem. Photobiol.*, **6**, 913-918, 1967.

Fork, D. C., J. Amesz, and J. M. Anderson, *Energy Conversion by the Photosynthetic Apparatus, Brookhaven Symp. in Biology*, **19**, Brookhaven National Laboratory, Upton, N.Y., pp. 81-94, 1967.

Joliot, P., A. Joliot, and B. Kok, *Biochim. Biophys. Acta*, **153**, 635-652, 1968.

Junge, W., and H. T. Witt, *Z. Naturforsch.*, **23b**, 244-254, 1968.

Müller, A., D. C. Fork, and H. T. Witt, *Z. Naturforsch.*, **18b**, 142-145, 1963.

Trebst, A., and E. Pistorius, *Z. Naturforsch.*, **20b**, 143-147, 1965.

Trebst, A., E. Pistorius, and E. Elstner, in *Currents in Photosynthesis*, J. B. Thomas, and J. C. Goedheer, eds. Ad. Donker, Rotterdam, pp. 409-419, 1966.

STUDIES ON THE PHOTOSYNTHESIS OF PLASTOME MUTANTS OF *Oenothera*

David C. Fork, Ulrich W. Heber and Marie-Rose Michel-Wohwertz

We have previously investigated (Fork and Heber, 1968) electron-transport reactions in 5 mutants of the higher plant *Oenothera hookeri* and *O. suaveolens* that are known to have deficiencies in their plastomes (the genetic material residing in the plastids). We are grateful to Prof. W. Stubbs for these mutants. Since all of these mutants also have defects in photosynthesis, we investigated their fluorescence characteristics and light-induced absorbance changes in an attempt to localize the site of the block in photosynthesis and to relate mutational changes of the plastome to specific biochemical events.

Examination of 4 of the mutants (designated I α , I δ , I γ and II γ) revealed that photosystem 2 was largely, or completely, nonfunctional. In all of these mutants the excitation of system 2 was largely, or completely, nonfunctional. In all of these mutants the excitation of system 2 did not cause reduction of oxidized cytochrome *f*. Moreover, the system-2 dependent absorbance change at 518 nm seen in normal leaves was absent. Also, these mutants had a high initial fluores-

cence in the presence or absence of DCMU [3-(3,4-dichlorophenyl)-1,1-dimethylurea] which did not change during illumination, indicating that the reaction centers of system 2 were affected by the mutations. Photosystem 1 appeared to function normally.

A fifth mutant ($\text{II}\alpha$) had an impairment in photosystem 1. Even high intensity far-red light did not lead to an accumulation of oxidized cytochrome *f* as seen in normal plants. Photosystem 2 was functioning as shown by the fast reduction of the primary system-2 oxidant (Duysens' "Q") and by the characteristics of the 518-nm absorbance change.

The studies mentioned above suggested that the reaction centers of photosystem 1 or 2 were nonfunctional or perhaps missing altogether in the mutants. We therefore measured low temperature spectra of chloroplast particles isolated from normal leaves, from a mutant deficient in photosystem 1 ($\text{II}\alpha$) and from a mutant deficient in photosystem 2 ($\text{II}\gamma$). These particles were prepared by grinding leaves in an isotonic mannitol buffer; the larger particles were removed by filtration and lowspeed centrifugation.

Chloroplast particles were collected by centrifugation at $8000\times g$ and resuspended in 0.025 *M* tris buffer, pH 7.8. Samples were cooled with liquid N_2 and absorption spectra measured with the spectrophotometer designed to minimize scattering as described in *Year Book 66*, p. 175.

Fig. 18 shows significant differences in the absorption spectra of particles derived from mutants $\text{II}\alpha$ and $\text{II}\gamma$ particularly in the region between 677 and 720 nm. The spectrum of particles obtained from normal leaves (not shown) follows closely that of mutant $\text{II}\gamma$ up to 677 nm and from there on it falls between the curves of mutant $\text{II}\gamma$ and $\text{II}\alpha$. The spectrum for chloroplast particles derived from mutant $\text{II}\alpha$, without system-1 activity, showed a steeper decline from about 677 nm toward longer wavelengths when compared with particles obtained from mutant $\text{II}\gamma$ or normal chloroplasts. At about 700 nm the absorption of these particles approached zero. By contrast, particles from mutant $\text{II}\gamma$, lacking system-2 activity, when compared to normal or mutant $\text{II}\alpha$ had absorption well beyond 677 nm and approached zero only around 720 nm.

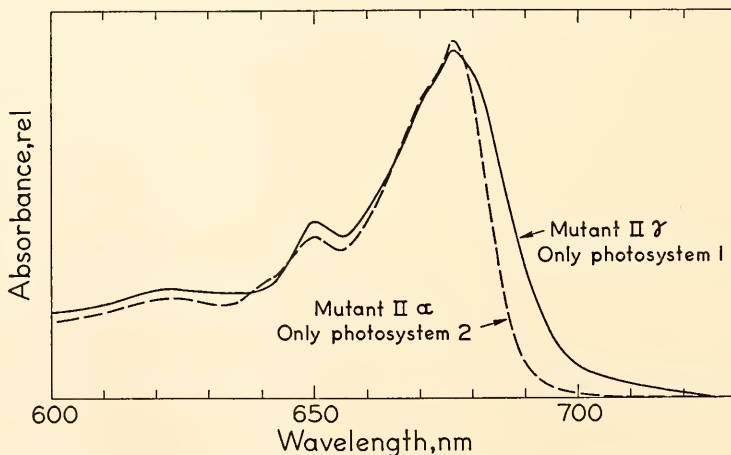


Fig. 18. Absorption spectra measured at 77° K for chloroplast particles isolated from *Oenothera* mutants $\text{II}\alpha$ (having system 2 but no system 1 activity) and $\text{II}\gamma$ (system 1 but no system 2 activity).

These findings should indeed be expected if some specialized forms of chlorophyll necessary for the conversion of light energy into biochemical energy are missing. It is known that chlorophyll *a* forms, absorbing maximally around 700 nm (Kok's P700 and Butler's C700), comprise part of the reaction centers of system 1. The low absorption of mutant II α in this region suggests that these pigments may be for the most part missing in this mutant. Conversely, the mutant (II γ) which has system-1 but no system-2 activity has pronounced absorption around 700 nm suggesting the presence of those specialized chlorophylls associated with system-1 reaction centers. The fact that the absorption of this mutant is greater than that of the normal plant beyond 677 nm may be caused by the absence of other specialized chlorophyll(s) associated with system 2 absorbing maximally at shorter wavelengths.

In addition to showing that the site of the genetic block of photosynthesis is at or close to the reaction centers of either photosystems 1 or 2, these results have a bearing on the function of the plastome. Since the genetic defect of these mutants is located in the plastome that is contained in the plastids, these experiments suggest that this genetic entity controls electron transport reactions in the lamellar structure of chloroplasts.

Reference

Fork, D. C., and U. W. Heber, *Plant Physiol.*, **5**, 606-612, 1968.

EFFECT OF ENZYMATIC DIGESTION OF CHLOROPLAST LAMELLAE ON CHLOROPHYLL ABSORPTION

Marie-Rose Michel-Wolwertz

Currently much effort is being spent in attempts to separate different forms of chlorophyll by fractionating chloroplast preparations. Hydrolytic enzymes have proved to be useful. Greenblatt *et al.*

(1960), using lipase, separated the chloroplast lamellae from one another, whereas with trypsin he disrupted the internal structure of the lamellae. By treatment of *Chromatium* chromatophores with proteolytic enzymes in the presence of Triton X-100, Vernon and Garcia (1967) isolated three distinct pigment-protein complexes.

We have investigated the effect of treatment with proteases and a lipase on the absorption spectra of fragmented chloroplasts. In one organism, *Euglena*, a selective conversion of longer to shorter wavelength forms of chlorophyll was found. The finding that modification of the carrier protein can change one of the native chlorophyll complexes into another spectroscopic type is of considerable significance to the basic problem of the nature of the structural differences between the different forms.

Euglena gracilis (Indiana Culture Col. No. 752) and *Chlorella pyrenoidosa* (Indiana Culture Col. No. 1230) were used. *Euglena*, in addition to the two absorbing forms Ca 670 and Ca 680 that are present in most plants, contains a large amount of a third form, Ca 695, when grown in dim light. *Chlorella* contains relatively more Ca 680 and Cb 650 in addition to Ca 670.

The cells were broken by forcing them three times through the needle-valve homogenizer. Chloroplast fragments were separated from soluble cellular material by centrifugation and were resuspended in buffer (0.35 M NaCl, 0.02 M tris-HCl, pH 7.4 and 0.01 M EDTA).

Enzymatic digestions were carried out at 33°C under nitrogen for 1 hour. After incubation, absorption spectra were measured for treated samples as well as for controls without enzyme.

When chloroplast fragments from *Euglena* or *Chlorella* were treated with papain or pancreatic lipase, they were immediately precipitated. Therefore we will report further only the results obtained with protease (from *Streptomyces*

griseus), with trypsin and with wheat lipase.

Enzymatic degradation of *Euglena* chloroplast fragments. Fig. 19 shows the absorption spectra, measured at room temperature, of *Euglena* chloroplast fragments treated with protease (1 μg protease/ μg chl) and of a control sample. Protease preferentially destroyed Ca 695; at the same time, an increase in absorption of "Ca 670" was observed. The spectrum of the difference measured at liquid nitrogen temperature between the control and the protease-treated sample (protease minus control) is given in Fig. 20. This spectrum clearly shows that by protease degradation, Ca 695 was transformed into "Ca 670." From a series of calculated difference spectra for these preparations the "Ca 695" was found to have a wavelength peak of 693 nm and a half width of about 24 nm (French *et al.*, 1968).

Longer incubation time (3–4 hours) or

higher enzyme concentration (20 μg protease/ μg chl) resulted in partial destruction of Ca 680 and Ca 670; the Ca 680 was the first to disappear. Similar results were obtained by trypsin degradation. No modifications of the spectrum were observed when *Euglena* chloroplast fragments were treated with wheat lipase.

Enzymatic degradation of *Chlorella* fragments. Absorption spectra, measured at -196°C , of chloroplast fragments of *Chlorella* treated for 1 hour by protease, by wheat lipase and the control sample are shown in Fig. 21. The three curves were adjusted to the same height at 678 nm. Protease preferentially destroyed the "Ca 680," lipase the "Ca 670." No change in the total chlorophyll following enzymatic degradation was detected by spectroscopic analysis of acetone extracts from enzyme-treated material.

Fractionation attempts by gel filtration. Unfortunately, attempts to separate the chlorophyll-lipoprotein complexes of

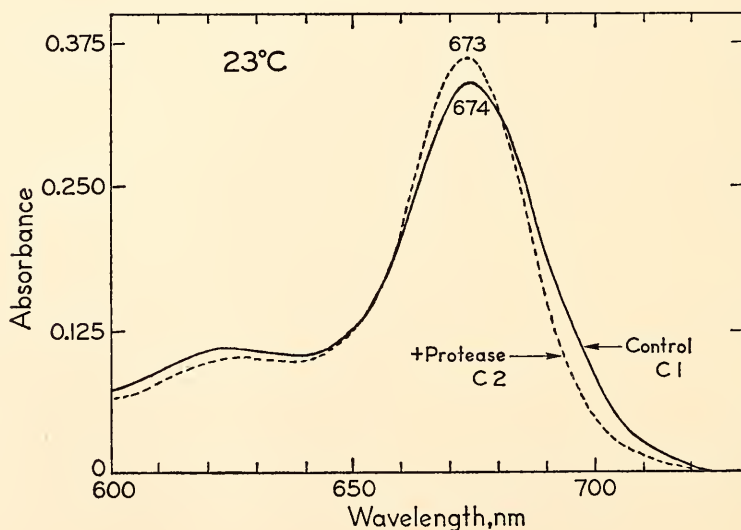


Fig. 19. Absorption spectra, at room temperature, for *Euglena* chloroplast fragments treated with 1 μg protease/ μg total chlorophyll. The enzymatic digestion and the control were incubated at 33°C for 1 hour under nitrogen.

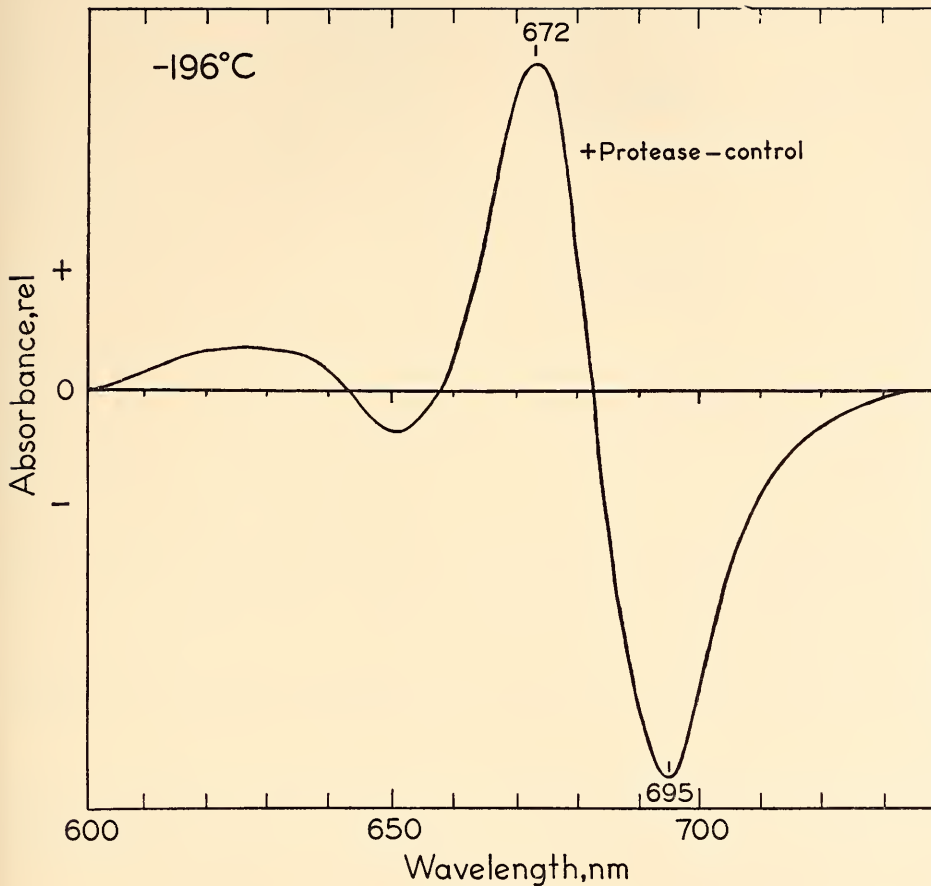


Fig. 20. The difference spectrum (protease minus control) measured at -196°C , between a sample of *Euglena* chloroplast fragments treated with protease and a control. Conditions same as for Fig. 19.

enzyme-treated chloroplast fragments by gel filtration were unsuccessful. Although the various agarose gels used offered a large range of exclusion molecular weight (from 40,000 to 150,000,000) poor resolution was obtained with all samples tested. When the sample was layered on the column it either passed through in a large band without separation, or it separated into different bands which were elutable only by use of detergents.

References

- French, C. S., M.-R. Michel-Wolwertz, J.-M. Michel, J. S. Brown, and Lillian Prager in *Symposium on Porphyrins*, T. W. Goodwin, ed., Biochem. Soc. London, 147-162 (In press) 1968.
- Greenblatt, C. L., R. A. Olson, and E. K. Engel, *J. Cell Biol.* (formerly *J. Biophys. Biochem. Cytol.*), 7, 235-238, 1960.
- Vernon, L. P., and A. F. Garcia, *Biochim. Biophys. Acta*, 143, 144-153, 1967.

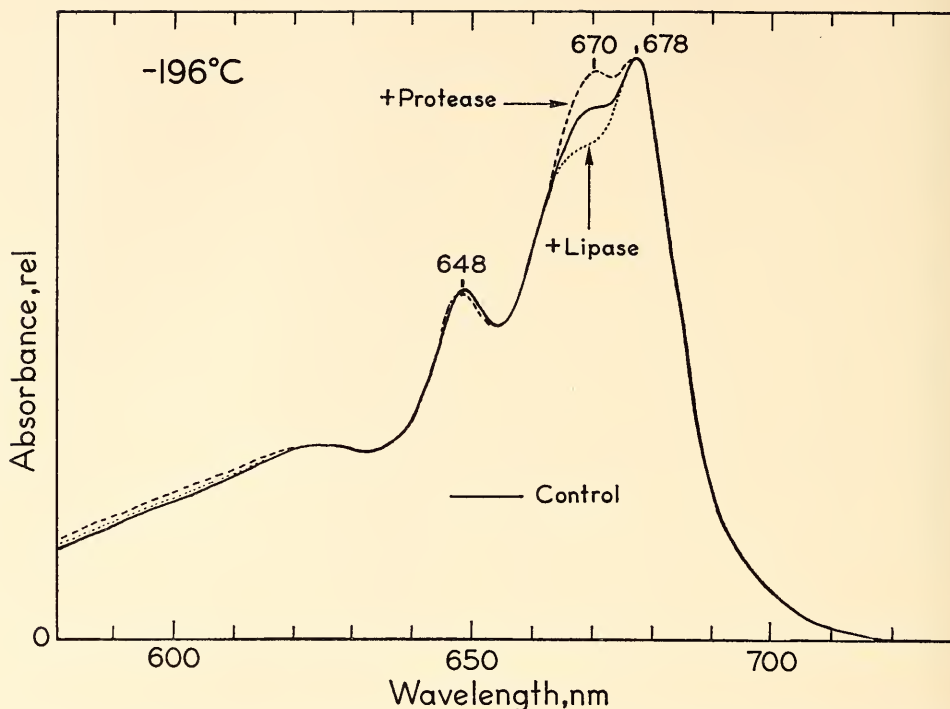


Fig. 21. Absorption spectra measured at -196°C for *Chlorella* fragments treated with wheat lipase and a control. The enzyme concentration was $5\mu\text{g}/\mu\text{g}$ total chlorophyll. The enzymatic treatments and the control were incubated at 33°C for 1 hour under nitrogen.

FRACTIONATION OF THE PHOTOSYNTHETIC
APPARATUS FROM BROKEN SPINACH
CHLOROPLASTS BY SUCROSE
DENSITY-GRADIENT
CENTRIFUGATION

Jean-Marie Michel and
Marie-Rose Michel-Wolwertz

In recent years, many attempts were made to fractionate the photosynthetic apparatus into particles containing mainly one or the other of the two photosystems. Detergents have been widely used for this purpose. The complexes usually released with detergents had often partly or completely lost their photochemical activities. The goal of the present study was to find a method of chloroplast disintegration and fractionation without use of detergents. We succeeded in separating fractions of spinach, *Chlorella* and *Euglena*. This section re-

ports the separation from broken spinach chloroplasts of three bands by centrifugation in a continuous sucrose gradient, without detergents.

The spectral properties and the photochemical activities of the three bands were studied. The results indicate that band 1 (low density) contained particles enriched in photosystem 1, whereas bands 2 and 3 (high density) contained particles enriched in photosystem 2. These particles, like the digitonin particles, are much reduced in their photochemical activities.

Fractionation method. Chloroplasts were isolated from spinach leaves purchased at the local market and suspended in 0.05 M Tricine-NaOH buffer adjusted to pH 7.8 containing 0.15 M KCl. The fresh chloroplast suspension was forced three times through a needle-valve press

operating at maximum pressure (12,500 lb/in²). The broken material, hereafter called homogenate, was fractionated on a linear sucrose density-gradient (12.5%–50%) by centrifugation at 60,000 *g* for 45 minutes. All the operations were carried out at 4°C. After centrifugation the different bands were collected separately. Their pigment contents and some of their photochemical activities were measured.

Centrifugation pattern. By centrifugation on a continuous sucrose gradient, the homogenate of broken chloroplasts separated into three green distinct bands (Fig. 22) and a few large particles sedimented on the bottom of the centrifuge tube. The three bands had about the same width. We called them band 1, band 2, and band 3, starting from the top of the gradient.

Distribution of chlorophyll *a* and *b* in the bands. The homogenate or the fractions were dialyzed and extracted with 80% acetone. Chlorophyll contents were determined spectrophotometrically according to Mackinney.

Table 6 shows the relative content of chlorophylls *a* and *b* in the homogenate and in the different bands for three different experiments. The chlorophyll content in the three bands was nearly the same. From 20 to 30% of the chlorophyll layered on the top of the gradient was found in each band and 14 to 30% of the total was lost in the sediment and between the bands. The *a/b* ratio was much higher in band 1 than in bands 2 and 3 or in the homogenate. Compared to the original homogenate, band 3 and also

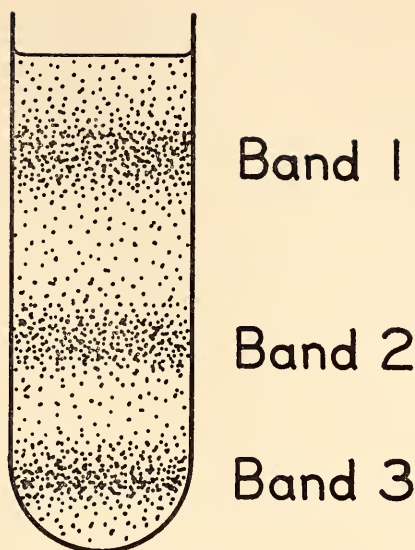


Fig. 22. The 3-band pattern of broken spinach chloroplasts centrifuged on a continuous sucrose gradient at 60,000 *g* for 45 min in a Spinco L ultracentrifuge. The sucrose gradient increased linearly from 12.5% to 50% sucrose (W/V) dissolved in the Tricine buffer of low ionic strength.

band 2 were enriched in chlorophyll *b*.

It should be pointed out, however, that if the chloroplasts were isolated and broken in a buffer of low ionic strength (0.05 *M* Tricine-NaOH at pH 7.8 containing 0.001 *M* MgCl₂, 0.005 *M* NaCl and 0.001 *M* KH₂PO₄) instead of one of high ionic strength (Tricine containing 0.15 *M* KCl) the three bands were found to have almost the same *a/b* ratio.

TABLE 6. Chlorophyll Distribution in the Bands Separated from Spinach Chloroplasts Broken in 0.05 *M* Tricine-NaOH, 0.15 *M* KCl pH 7.8

Sample	Percent of Total Chlorophyll in the Different Fractions			Chlorophyll Ratio <i>a/b</i>		
	Expt 1	Expt 2	Expt 3	Expt 1	Expt 2	Expt 3
Broken chloroplasts	100	100	100	2.97	3.00	2.78
Band 1 (low-density)	20.2	27.2	22.1	6.90	5.26	6.50
Band 2 (medium-density)	27.7	29.0	26.0	2.30	2.70	2.55
Band 3 (high-density)	21.5	29.5	22.2	2.70	2.80	2.56
Sediment + material between bands	30.4	14.1	29.5

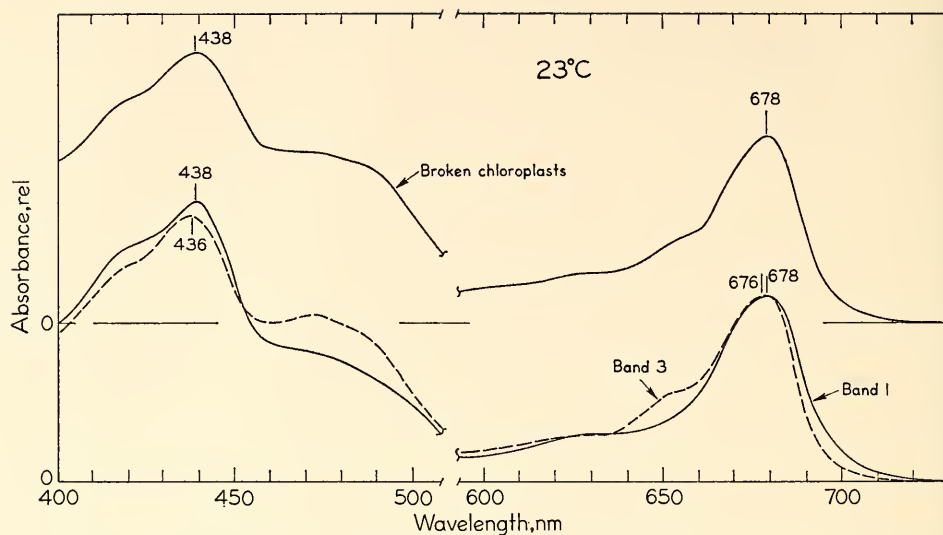


Fig. 23. Absorption spectra of the spinach chloroplast homogenate and of the bands separated from this homogenate. The bands correspond to those in Fig. 22 and were dialyzed overnight against buffer before recording the spectra; band 2 had an absorption spectrum similar to band 3.

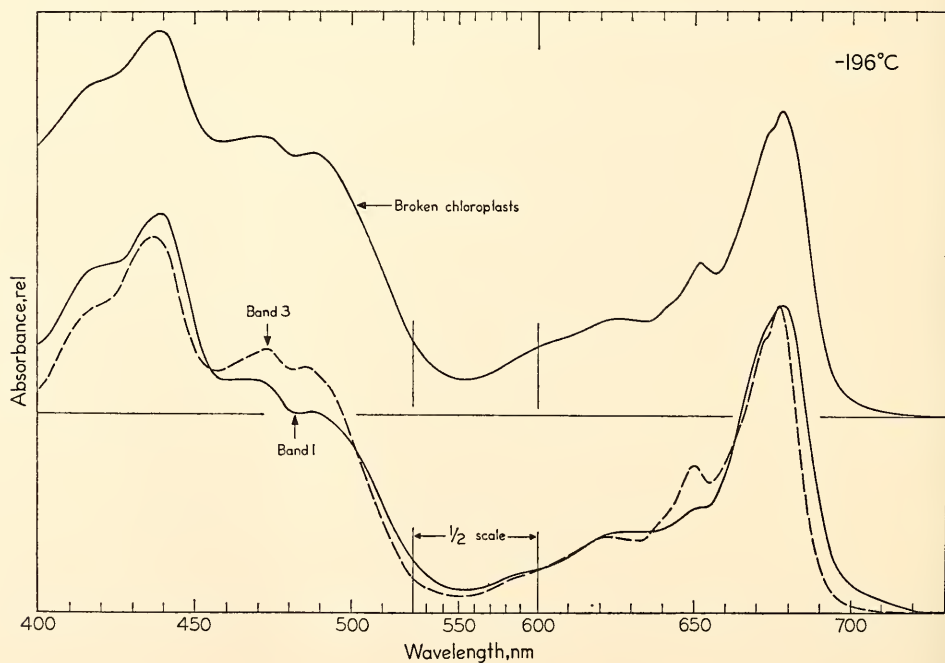


Fig. 24. Absorption spectra for the homogenate of broken spinach chloroplasts and of band 1 and band 3 after dialysis overnight against the buffer.

Absorption and fluorescence spectra. The absorption and fluorescence emission spectra were recorded at 20° and -196°C. The spectrofluorometer and the spectrophotometer used were described in *Year Book 65*, p. 483, and *Year Book 66*, p. 175. Fig. 23 shows the absorption spectra, at room temperature, of the homogenate and of bands 1 and 3. The curves were adjusted to the same height at the maximum in the red. The absorption band of chlorophyll *b*, located near 650 nm, was clearly visible in band 3, whereas it appeared only as a shoulder in band 1. Again it is important to note that almost no differences were observed in the spectra of band 1 and band 3 when chloroplast material was broken in buffer of low ionic strength. Near 700 nm, band 1 absorbed more than band 3 and even more than the homogenate. Also in

the 450–500 nm region, band 1 showed a greater absorbance than band 3.

Spectra of these samples measured at -196°C and matched to the same height at the maximum in the red are given in Fig. 24. At low temperature, the main peak of both the homogenate and the bands appeared as a double structure: a well-defined peak near 678 nm and a shoulder at about 670 nm. The relative heights of these two spectral bands were not the same in all the fractions. In band 1, the absorbance at 670 nm was almost equal to the absorbance at 678 nm, whereas in band 3, the peak located near 678 nm was higher than the shoulder situated at 672 nm. Identical results were obtained by Briantais (1967) for fractions separated by centrifugation from Triton X-100 treated chloroplasts.

Fig. 25 compares the fluorescence emis-

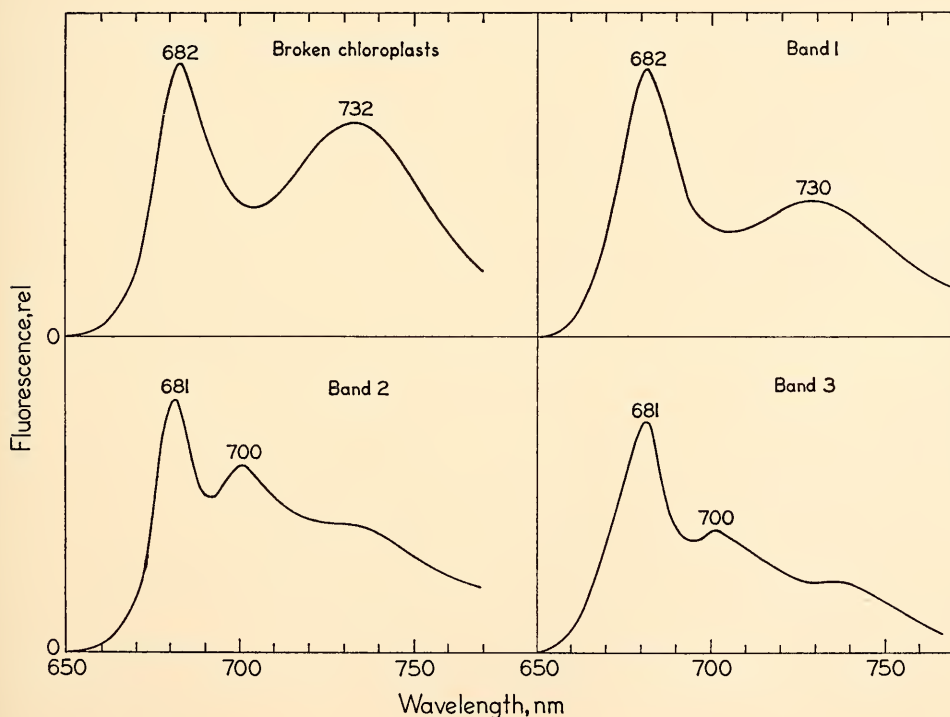


Fig. 25. Fluorescence emission spectra, at -196°C, of the homogenate of broken spinach chloroplasts and of the bands. Excitation at 435 nm.

sion spectra at -196°C of the homogenate and of the three bands that were isolated. All the samples showed an emission peak at 681 to 682 nm (F 682); a second broad emission band was present at 730 nm (F 730). However, the F 730/F 682 ratio was greater in band 1 than in bands 2, 3 or the homogenate. In bands 2 and 3 a supplementary emission peak was visible at 700 nm whereas this peak was absent from band 1 and the homogenate.

Photochemical Activities

NADP reduction. The rate of NADP reduction was calculated from the increase in absorbance at 340 nm using an extinction coefficient of $6.22 \times 10^6 \text{ cm}^2 \text{M}^{-1}$. We used diaminodiuril (DAD) and Na ascorbate as electron donors. Table 7 shows that band 1 had a rate of NADP reduction close to the rate of broken chloroplasts whereas the ability of band 2 and especially of band 3 to reduce the NADP was much lower on the same chlorophyll basis.

DCPIP reduction. Hill activity was measured using 2,6-dichlorophenol-indophenol (DCPIP) as electron acceptor

TABLE 7. NADP Photoreduction by Broken Spinach Chloroplasts and by Their Fractions*

Sample	Rate of NADP Photoreduction, $\mu\text{moles NADP (mg chlor.)}^{-1} \text{ hr.}^{-1}$
Broken chloroplasts	9.40
Band 1 (low-density)	7.40
Band 2 (medium-density)	1.11
Band 3 (high-density)	0.39

* The reaction mixture, 2.5 ml, contained the sample with a chlorophyll (*a* + *b*) content of 33 μg and (in μmoles) DCPIP, 0.05; Na Ascorbate, 2; Tricine, 33; ADP, 1.5; KH_2PO_4 , 1.3; NADP, 0.5; NaCl, 20; MgCl_2 , 2.3; and 0.6 ml of a crude preparation of ferredoxin and NADP reductase (obtained from broken spinach chloroplasts); light: 660 nm ($W = 7.5 \text{ nm}$) $1.9 \times 10^4 \text{ ergs cm}^{-2} \text{ sec}^{-1}$.

by following the decrease in absorbance at 620 nm. The rate of DCPIP reduction was calculated using an extinction coefficient of $20.6 \times 10^3 \text{ cm}^2 \text{M}^{-1}$. Fig. 26 shows the absorbance changes observed at 620 nm when broken chloroplasts and the fractions were illuminated with blue actinic light. After turning on the light, a decrease of the absorbance at 620 nm was observed with broken chloroplasts and bands 2 and 3 while almost no decrease was seen with band 1. The rate of DCPIP reduction was obtained from

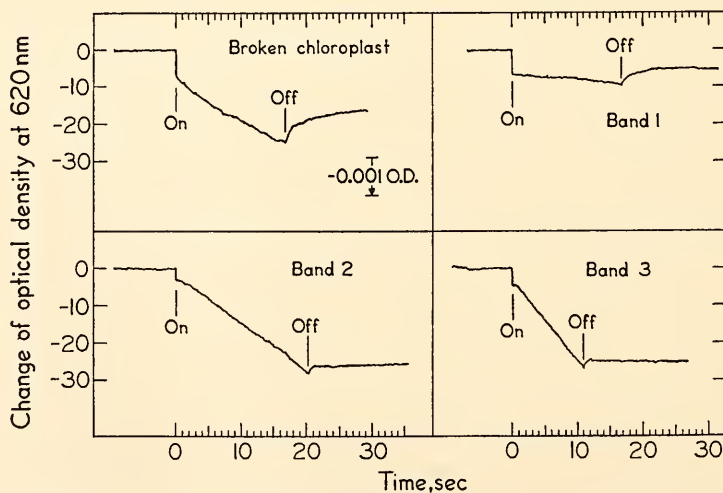


Fig. 26. Absorbance changes recorded for a reaction mixture containing 2.5 ml of a sample fraction with a chlorophyll (*a* + *b*) content of 50 μg and 0.08 μmoles of DCPIP; light: 430 nm ($W_{0.5} = 70 \text{ nm}$), $1.8 \times 10^4 \text{ ergs cm}^{-2} \text{ sec}^{-1}$.

the slope of the slow decrease of absorbance which was measured after the light had been on for several seconds. Band 1 hardly reduced any DCPIP whereas bands 2 and 3 had a rate of DCPIP reduction almost two times higher than the homogenate.

P700 content. The relative amount of P700 in the different samples was estimated by measuring the light-induced bleaching of P700 at 700 nm. The photomultiplier was located at about 30 cm below the sample in order to minimize the effect of chlorophyll fluorescence. The signal of the P700 change was corrected for these fluorescence changes. The extinction coefficient for P700 was assumed to be the same as for chlorophyll *a* in acetone at 663 nm. The results are given in Table 8. It appears that band 1 contained more P700 in proportion to the chlorophyll content than the two other fractions. These results were confirmed by the measurement of light-induced optical density changes between 400 and 450 nm in the presence of DAD-Na ascorbate as an electron donor system. These difference spectra are given in Fig. 27. The importance of the change around 430 nm, generally attributed to P700, was three times higher in band 1 than in bands 2 or 3.

Fluorescence measurements. The time course of fluorescence was measured at 684 nm with the photomultiplier at an angle of 45° with respect to the blue actinic beam. The time response was 1 msec. Chlorophyll concentrations for the different samples were adjusted to the same value by dilution; the ap-

TABLE 8. The P700 Content of Different Fractions Obtained from Spinach Chloroplasts

Sample	Moles Chl (a + b)/ Moles P700	
	Expt 1	Expt 2
Broken chloroplasts	535	560
Band 1	350	337
Band 2	950	1230
Band 3	825	840

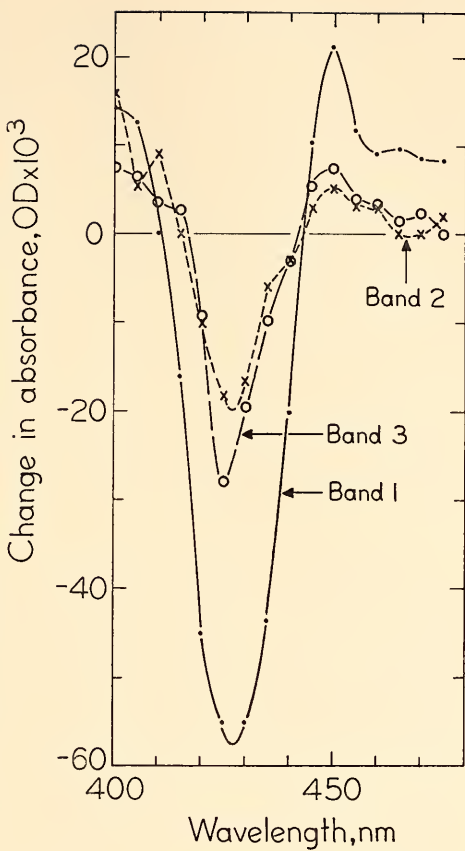


Fig. 27. Light-minus-dark difference spectra of the bands obtained from broken spinach chloroplasts. Actinic light, red 3.18×10^6 ergs $\text{cm}^{-2} \text{sec}^{-1}$.

paratus setting and the intensity of the blue actinic light were kept the same for the different measurements to permit a comparison of the relative fluorescence yield of the different samples. The fluorescence was measured after a dark period of 60 sec. Fig. 28 shows that the relative yield of fluorescence and the amount of variable fluorescence (defined in *Year Book 66*, p. 166) were both much higher in bands 2 and 3 than in the chloroplast homogenate or in band 1. The addition of DCMU to the sample slightly increased the total fluorescence but decreased the variable fluorescence.

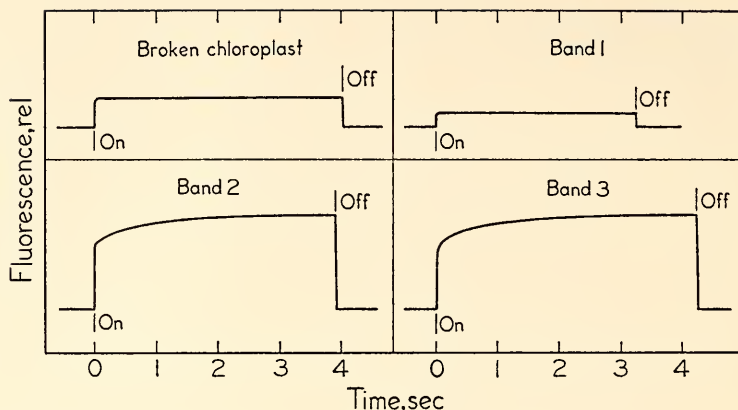


Fig. 28. Time course of fluorescence for the three bands after 60 sec in darkness. All the samples had the same chlorophyll ($a + b$) content.

Summary

Our experiments show that without the use of detergent, spinach chloroplasts can be broken into particles that separate into three distinct bands when centrifuged in a sucrose gradient. The low-density particles (band 1) are different from the high-density particles (bands 2 and 3) with respect to pigment content and photochemical activities. Band 1 particles are enriched in chlorophyll a and reduce NADP, whereas particles of bands 2 and 3 do not reduce NADP but exhibit the Hill reaction and are relatively enriched in chlorophyll b . Moreover, particles of band 2 show an enhanced yield and greater variable fluorescence than those of band 1.

Our lighter particles are similar in their spectra and photochemical activities to the small particles obtained by fractionation of detergent-treated chloroplasts, showing the properties associated with photosystem 1. Our heavier particles are similar to the large particles obtained from detergent-treated chloroplasts, showing almost exclusively the characteristics of photosystem 2.

Reference

- Briantais, J. M., *Photochem. Photobiol.*, **6**, 155-162, 1967.

ABSORPTION SPECTRA OF FRACTIONS OBTAINED BY SUCROSE GRADIENT CENTRIFUGATION FROM *Chlorella Pyrenoidosa*

Marie-Rose Michel-Wolwertz and
Jean-Marie Michel

The previous report has shown that spinach chloroplasts, fragmented by three passages through the needle-valve homogenizer, may be separated without use of detergents into three distinct bands by centrifugation in a sucrose gradient. These bands were different with respect to their photochemical activities and pigment content. Band 1 (low-density particles) was enriched in photosystem 1, and the heavier bands 2 and 3 (high-density particles), in system 2.

The aim of this study was to investigate the absorption properties of fractions obtained from another green plant by the method described for spinach. We chose *Chlorella pyrenoidosa* (Indiana Culture Col. No. 1230) and compared the absorption spectra, at low temperature, of the different bands with the absorption spectrum of the homogenate of broken *Chlorella*, and also with the absorption spectra, at room temperature, of acetone extracts of bands 1 and 3.

Results

After centrifugation in the sucrose gradient, the pigmented material was located in three distinct bands of the same width. The bands were numbered 1, 2, and 3 starting from the top of the gradient tube. The distribution of chlorophyll in the different bands was similar to that in the fractionation of spinach chloroplasts.

Absorption spectra at low temperature. The upper part of Fig. 29 gives the absorption spectrum, at -196°C , of the original homogenate of broken *Chlorella* cells. Chlorophyll *a* showed a distinct peak at 678 nm and a shoulder near 670 nm. The absorption band of chlorophyll *b* at about 648 nm was clearly visible. In the blue region, the main peak was located at 438 nm with a shoulder at 417 nm. Between 450 and 500 nm, three small maxima were distinguishable: near 477 nm (due to chlorophyll *b*) and near 486 and 495 nm (the carotenoid region). The lower part

of Fig. 29 compares the absorption spectra, at -196°C , of bands 1 and 3. The two spectra were adjusted at the time of recording to the same height at 678 nm. In the red part of the spectrum, all peaks and shoulders of bands 1 and 3 were located at the same wavelengths: 678, 670, and 648 nm; however, the relative heights of the maxima were different in the two bands. The absorbance of chlorophyll *b* at 648 nm appeared as a well-defined peak in band 3 and only as a shoulder in band 1. Band 1, on the contrary, absorbed relatively more at 670 nm and on the long-wavelength side of the 678-nm peak than did band 3. This suggests that the long wavelength absorption band of the light particles has a different shape and greater width than a band with a similar 678-nm maximum in the heavier particles.

In the Soret region, band 3 absorbed less at 437–438 nm and at 417 nm than band 1 whereas its absorption between

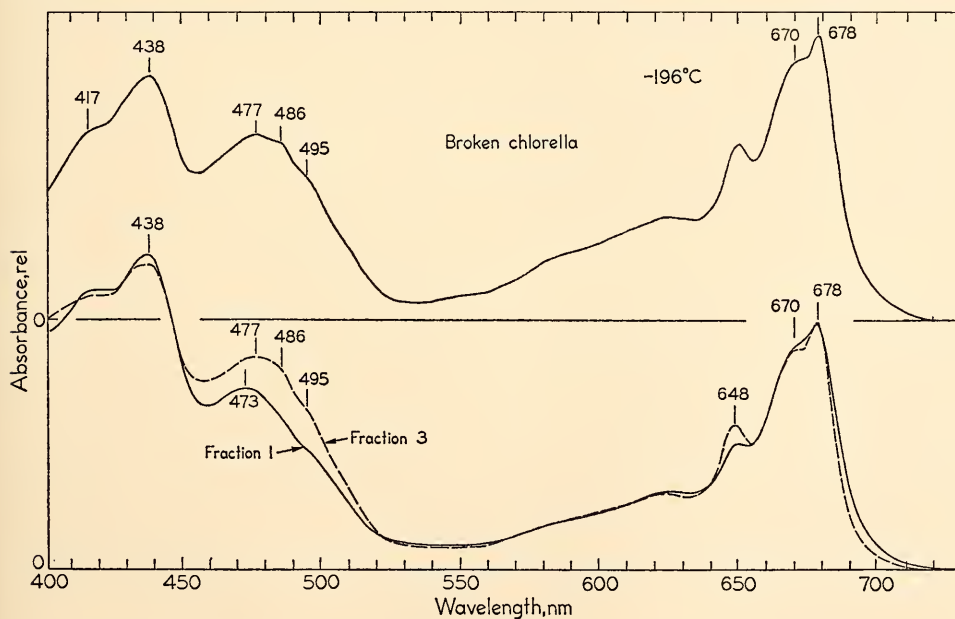


Fig. 29. Absorption spectra of the homogenate of broken *Chlorella* cells (upper) and of band 1 and band 3 separated from the homogenate by sucrose density-gradient centrifugation (lower). The spectra were adjusted to the same height at 678 nm.

460 and 500 nm was greater than that of band 1, especially near 476 where chlorophyll *b* absorbs.

Absorption spectra of acetone extracts. The differences in pigment composition in the fractions observed in the absorption spectra at low temperature were also evident from the absorption spectra of acetone extracts shown in Fig. 30. The two curves were adjusted to give an equal absorption at 664 nm. The acetone extract of band 3 as compared with that of band 1 had a greater absorbance near 645 nm where chlorophyll *b* absorbs in solution. In the blue region, band 3 also absorbed relatively more, especially between 450 and 480 nm. This difference in the 450 to 480 nm region proves that the chlorophyll *b* and the carotenoid content of band 1 and band 3 were different.

Measurements of photochemical activity showed that band 1 obtained from *Chlorella* cells was enriched in photosystem 1 whereas bands 2 and 3 had higher activity for photosystem 2. These results obtained with *Chlorella* were exactly the same as those obtained with fractions separated from broken spinach chloroplasts.

These results with *Chlorella* parallel those with spinach fractions: photosys-

tem 1 particles (band 1), separated by the fractionation method described above, have relatively greater absorbance between 680 and 700 nm whereas photosystem 2 particles (bands 2 and 3) are relatively enriched in Cb 650.

ABSORPTION AND FLUORESCENCE OF FRACTIONS FROM SEVERAL PLANTS

J. S. Brown and L. Prager

After the successful fractionation of spinach chloroplasts and *Chlorella* on a sucrose gradient, described above, a series of similar experiments was performed on other plants. We have examined some aspects of the procedure itself and have noted differences and similarities that exist between widely different plants fractionated in the same way.

Our four criteria for determining a successful fractionation or separation were that the lighter fraction (1) have a higher chlorophyll *a/b* ratio than the heavier fraction or the homogenate; (2) have a higher absorbance in the 680 to 710 nm region than the heavier fraction; (3) have a lower ratio of F680 to F725 fluorescence and (4) have a lower fluorescence yield.

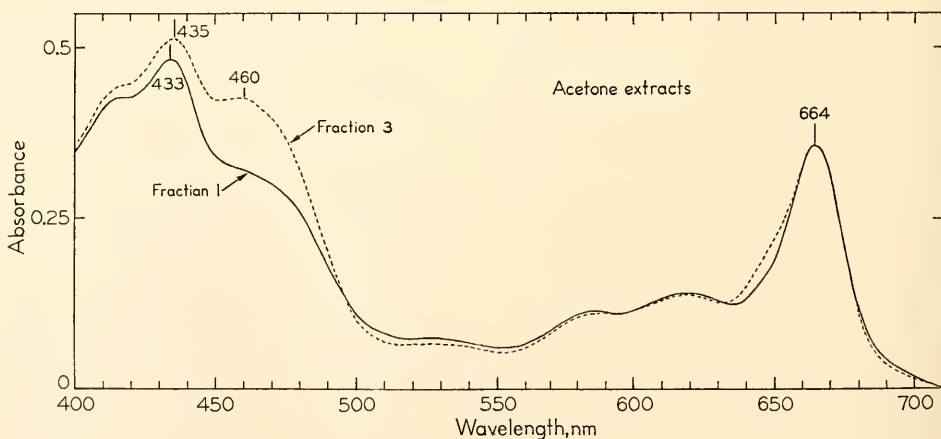


Fig. 30. Absorption spectra, at room temperature, of acetone extracts of band 1 and band 3 separated from the homogenate of broken *Chlorella* cells. The two spectra were adjusted to the same height at 665 nm.

Procedure

The algae were centrifuged from their growth medium, rinsed with distilled water, and resuspended in buffer for breaking. With the higher plants and the liverwort, about 40 g of leafy material was blended in a sorbitol buffer and filtered through cheese cloth. The chloroplasts in the filtrate were sedimented by centrifugation, washed with distilled water, resuspended in Tricine buffer and forced through the needle-valve press three times. This was essentially the same procedure followed by the Michels. A modification added by us was to centrifuge the broken mixture for 10 min at 3,000 *g* and to discard the sediment in order to have a relatively clear homogenate that could be compared spectroscopically with the fractions.

With spinach we attempted to determine what steps of the procedure were essential for a successful fractionation. Aliquots of washed chloroplasts were suspended in 0.05 *M* Tricine, pH 8 containing 0.45 *M*, 0.15 *M* or 0.05 *M* KCl and also in 0.05 *M* Tris, pH 8 containing 0.45 *M*, 0.15 *M* or no KCl before passing through the press. The sucrose solution contained 0.05 *M* Tricine, pH 8, and 0.15 *M* KCl in all six cases.

Following centrifugation in linear sucrose gradients for 30–45 min at 60,000 *g*, three green bands were observed in each case. As judged by criteria 1 and 2 above, the three fractions in each buffer-KCl combination corresponded to the system 1 (top fraction) and system 2 (both of the heavier fractions) particles in 0.15 *M* KCl-Tricine as described above by the Michels (*Year Book 67*, pp. 508–514). The KCl concentration influenced the amount of chlorophyll found in each fraction after a given period of centrifugation. Without KCl, only a little material reached the lower level after one hour whereas with 0.45 *M* KCl more than 50% of the chlorophyll was in the denser layer after 15 min. Possibly KCl causes the system 2 particles to contract

and become denser, thereby facilitating their separation from system 1 particles.

Since fractions 2 and 3 from the linear gradient were alike according to the above criteria and also in NADP reduction and Hill activity as reported by the Michels, a sucrose step gradient was sought that would retain system 1 particles near the top and system 2 particles in a single lower band. A three-step gradient of 12%, 30% and 50% sucrose was found to achieve this purpose. Of course the fact that system 2 particles of two different densities do exist should not be forgotten. Eventually differences between them in other respects than density may be found.

The relative fluorescence yield was measured for the original homogenate and dialyzed fractions from the sucrose gradient. A drop of diluted sample was placed in a 0.2-mm deep slot of an aluminum strip and covered with a glass coverslip. Fluorescence emission spectra were recorded at room temperature as described in *Year Book 65*, p. 494. At least two dilutions were measured to be sure that self-absorption was minimal. The relative yield was calculated from the peak height near 680 nm, corrected for the response of photomultiplier at the voltage used and divided by the total chlorophyll concentration. The latter was determined in acetone extracts according to Mackinney.

Results

The results with each kind of plant are described below, and the relative fluorescence yields presented in Table 9.

Marchantia polymorpha. Three fractions were observed in the linear gradient. The lighter fraction could be distinguished from the lower two fractions by the four criteria stated above. Fig 31(A) shows absorption spectra of the light and heavy fractions measured at -196°C .

Hordeum vulgare. Normal barley and a mutant lacking chlorophyll *b* (Boardman and Highkin, 1966) were fraction-

TABLE 9. The Relative Fluorescence Yield on a Chlorophyll Basis of the Homogenate and Fractions from Sucrose Gradients

Material	Original Homogenate	Fractions	
		Light	Heavy
Spinach	3.8	1.8	4.9
<i>Marchantia polymorpha</i>	1.9	0.4	2.3
Barley, wild type	1.68	0.59	2.02
Barley, mutant lacking chlorophyll <i>b</i>	0.98	0.68	3.08
<i>Stichococcus</i>	2.5	1.35	3.7
<i>Tribonema</i>	2.7	0.83	1.1
<i>Euglena</i> -Hutner's	1.23	1.75	3.15
<i>Euglena</i> -CM-citrate	3.16	2.75	4.45
<i>Euglena</i> -CM-EDTA	2.0	1.4	2.0

ated. The homogenate from normal barley separated into three fractions in the linear sucrose gradient. Spectra of these fractions showed a good separation of fraction 1 and 2 (and 3) similar to that illustrated for *Marchantia* in Fig. 31(A). On the other hand, the *b*-less mutant separated into only two fractions, a broad band at the top and narrow band just above the bottom, having identical absorption spectra at -196°C .

However, the emission spectra measured at either 20° or -190°C were very different, the long wavelength emission maximum near 720 nm being enhanced in the lighter fraction. The heavier fraction from both normal and mutant plants had a higher fluorescence yield than the lighter fraction of the original homogenate (Table 9). Boardman and Thorne, 1968, treated this same mutant barley with digitonin and found no differences in the fluorescence yields of the centrifugal fractions. Apparently chloroplast particles from the mutant are more susceptible to damage by detergents than are normal plants.

We conclude that two kinds of particles were obtained from the mutant as well as the normal plants, but that the enhancement of long wavelength absorption usually observed in the lighter (criterion 2) did not occur in the mutant particles.

Stichococcus bacillaris. Two bands differing in absorption and fluorescence, as shown in Figs. 31(B) and 32, were observed near the top and bottom of a

linear sucrose gradient. This alga, Indiana Culture Col. No. 419, has an unusually large proportion of chlorophyll *b* ($a/b=1.6$) that may be correlated with proportionally low level of Ca 670.

The fluorescence spectra in Fig. 32 illustrate the relatively greater emission at longer wavelengths from the lighter fraction 1. This higher ratio of long to shorter wavelength fluorescence in fraction 1 has been seen in all the plants that have been successfully fractionated. But when homogenates or fractions from different plants are compared, the relative proportion and peak positions of the long wavelength emission bands seen at -190°C vary considerably. The same unknown reason may account for the variation in shape of the red absorption band of chlorophyll *in vivo* as well as for the differences in the emission bands.

Tribonema sp. A successful fractionation of this alga, Indiana Culture Col. No. 639, has not been achieved according to the absorption and fluorescence criteria. Two bands were observed in the linear sucrose gradient but they had very similar absorption and emission spectra. The component that absorbed the longer wavelengths was unusually labile in the broken cell homogenate, probably because of a destructive factor in the mixture since it was stable in the fractions from the gradient.

Euglena gracilis. When *Euglena*, Indiana Culture Col. No. 752, are cultured under light-limiting conditions, their proportion of chlorophyll *b* decreases and

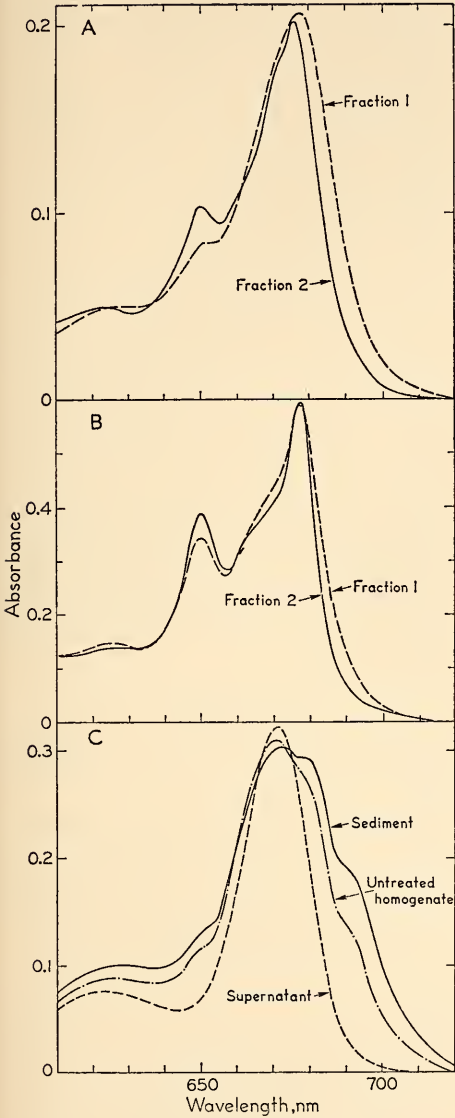


Fig. 31(A). Absorption spectra of fractions 1 and 2 from *Marchantia* recorded at -196°C . (B). Absorption spectra of fractions 1 and 2 from *Stichococcus* measured at -196°C . (C). Absorption spectra, measured at -196°C , of centrifugal fractions of a *Euglena* homogenate treated with Na deoxycholate. Original homogenate, sediment from 50,000 g for 30 min, supernatant from 100,000 g for 60 min.

that of chlorophyll *a* 695 increases with time. Therefore, we fractionated cells grown for different periods of time to see

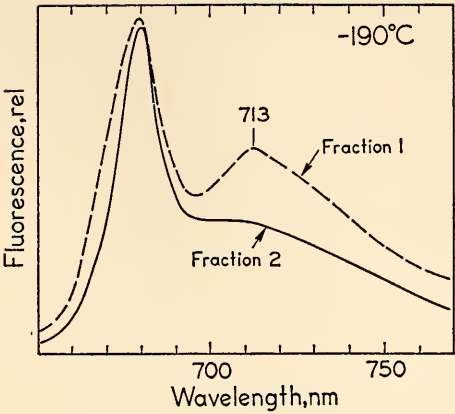


Fig. 32. Fluorescence emission spectra of fractions 1 and 2 from *Stichococcus*. Excitation at 436 nm.

whether the different relative proportions of the chlorophyll forms in the homogenates would be reflected in the absorption spectra of the fractions.

In each of four separate experiments two fractions were observed in the linear gradient, but these had nearly identical spectra and relative fluorescence yields.

For these experiments, the *Euglena* were grown in the neutral medium devised by Cramer and Myers in which EDTA had been substituted for citrate as a chelating agent in order to decrease possible bacterial and fungal contamination. Since J.-M. Michel observed that particles prepared from *Euglena* grown with EDTA had little or no photochemical activity compared to those from cells grown in the citrate medium, we fractionated *Euglena* grown in the C-M citrate medium and also in an acidic medium devised by Hutner.

Again the fractions had the same absorption spectra, but their fluorescence properties differed. Not only were the relative yields different (Table 9) but also the lighter fraction had relatively more long wavelength emission.

Euglena previously have been fractionated with the aid of deoxycholate or

digitonin (*Year Book* 64, pp. 374–379) into particles of different densities. By that procedure the heavier particles were enriched in chlorophyll *b* and Ca 695 compared to the original homogenate. The lighter fraction, showing a single absorption band at 672 nm, may have been a detergent-solubilized form of chlorophyll. Since only derivative absorption spectra were measured, the experiment with deoxycholate has been repeated, and absorption spectra of the original homogenate and centrifugal fractions recorded at -196°C (Fig. 31C).

These results with detergent-treated *Euglena* in which the heavier fraction has relatively more long wavelength-absorbing chlorophyll are different from those of either detergent or the Michels' fractions of other algae and leaves. Perhaps a unique molecular arrangement of chlorophyll *b* and Ca 695 in *Euglena* prevents the usual separation of particles having different chlorophyll forms.

Thus, in *Euglena*, attempts to obtain fractions with different proportions of chlorophyll *b* and forms of chlorophyll *a* have been unsuccessful unless a detergent is added. However, fractions with different fluorescence characteristics can be obtained on a sucrose gradient without detergent, providing the cells are grown in a medium without EDTA.

Summary

When leaves of barley and *Marchantia* were homogenized and then centrifuged in a linear sucrose gradient, three bands appeared that were similar to those observed previously in spinach. With several algae and a barley mutant lacking chlorophyll *b*, only two bands were found in the linear gradient. The heavier of these two bands corresponded to fractions 2 and 3 from spinach.

The fractions prepared from either *Tribonema* or the barley mutant had nearly identical absorption spectra. The expected relative increase in long wavelength absorption in the lighter fraction 1

did not occur in these plants lacking chlorophyll *b*. The fluorescence emission spectra and yields were also alike in *Tribonema* fractions. But the emission from the mutant barley fractions differed in the same way as it did in wild-type barley. *Euglena* fractions had the same absorption, but differences in emission similar to those in higher plants were observed provided the cells had not been cultured in a medium containing EDTA.

These results demonstrate that the fractionation procedure devised by the Michels may be successfully applied to several kinds of plants. In some plants, notably those in which chlorophyll *b* is lacking or variable in amount, the fractions can apparently have similar absorption spectra but different fluorescence spectra and yields. We presently have no explanation for this result unless the existence of additional, as yet undetected, absorbing forms of chlorophyll is postulated.

References

- Boardman, N. K., and H. R. Highkin, *Biochim. Biophys. Acta*, 126, 189–199, 1966.
- Boardman, N. K., and S. W. Thorne, *Biochim. Biophys. Acta*, 153, 448–458, 1968.

EMERSON ENHANCEMENT AT DIFFERENT INTENSITIES AND RATIOS OF TWO LIGHT BEAMS

Eckhard Loos

In a recent investigation (Loos, 1967) the Emerson enhancement effect was studied by measuring $^{14}\text{CO}_2$ uptake. Constant ratios of short-wavelength to far-red light were used while the intensity was varied. Those experiments gave lower enhancement at higher light intensities even within the linear range, a finding contrary to the results of Bannister and Vrooman (1964). Recently the variation of enhancement with light intensity has been studied by measuring oxygen evolution in *Chlorella* and in *Porphyridium* to compare with previous measurements of CO_2 uptake.

Material and methods. *Porphyridium cruentum* was grown in artificial sea water in shaken flasks aerated with 3% CO₂ in air. Cool-white fluorescent tubes provided a light intensity of 3500 Lux at the bottoms of the flasks. The extinction of the suspension at 515 nm, determined in a Beckman DU spectrophotometer with a 1-cm cuvette, was used as a measure of algal density. Cultures were started with an extinction of about 0.3 and in two to four days they had grown from 5 to 8 times the concentration of the inoculum. They were centrifuged and resuspended in enough fresh nutrient medium to give an extinction of 0.5 in a 1:10 dilution. When a suspension of this density or lower was used in the electrode compartment, the rate of O₂ evolution was proportional to the density, which shows that there was no trouble from mutual shading of the cells.

Chlorella vulgaris was grown at 6,500 Lux, whereas the other conditions, except for the medium, were the same as with *Porphyridium*. Most *Chlorella* experiments were done with four-day-old cells having an extinction of 0.6 at 515 nm in a 1:10 dilution. With this density mutual shading was probably small, for it did not occur with *Chlorella pyrenoidosa* cells showing in a 1:10 dilution at 515 nm an extinction of 0.47 or less.

Relative rates of oxygen evolution were measured with the polarized platinum electrode covered with Teflon described

by Pickett and French (1967). The electrical signal obtained from the electrode was amplified and recorded. The flow system of the electrode assembly contained nutrient medium that was equilibrated with 5% CO₂ in air. Two 150 W quartz-iodine projection lamps were used with a lens system. Light intensity was varied by adjusting the lamp voltages. To obtain the desired spectral bands the light beams were filtered through 4 cm of water, heat reflecting filters and interference filters with halfband widths of 20 nm or less. A beamsplitter divided and mixed the two beams by transmission and reflection in such a way that part of each one impinged on the algae and part on an RCA vacuum photodiode (S-1 response), the photodiode calibrated at the desired wavelengths with a calibrated thermopile in place of the algae.

Measuring procedure. Relative rates of oxygen evolution were taken from the values reached five minutes after the onset of illumination when a fairly constant rate had been established (Fig. 33). This time was chosen because it is just beyond the time of the initial rise of rate yet does not include much of the further rate increase that continued for a longer period as indicated by the dotted line in Fig. 33. Every new illumination period was separated from the preceding one by a dark interval to achieve a stable baseline rate. For a better comparison

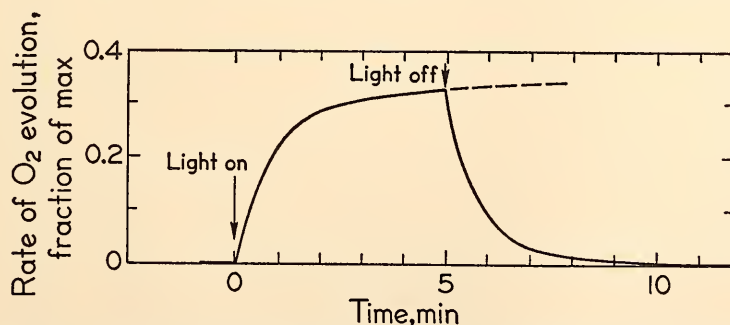


Fig. 33. Time course of oxygen exchange in *Chlorella*. Wavelength 574 nm, light intensity: 5480 ergs cm⁻² sec⁻¹. Broken line indicates time course if light had not been turned off.

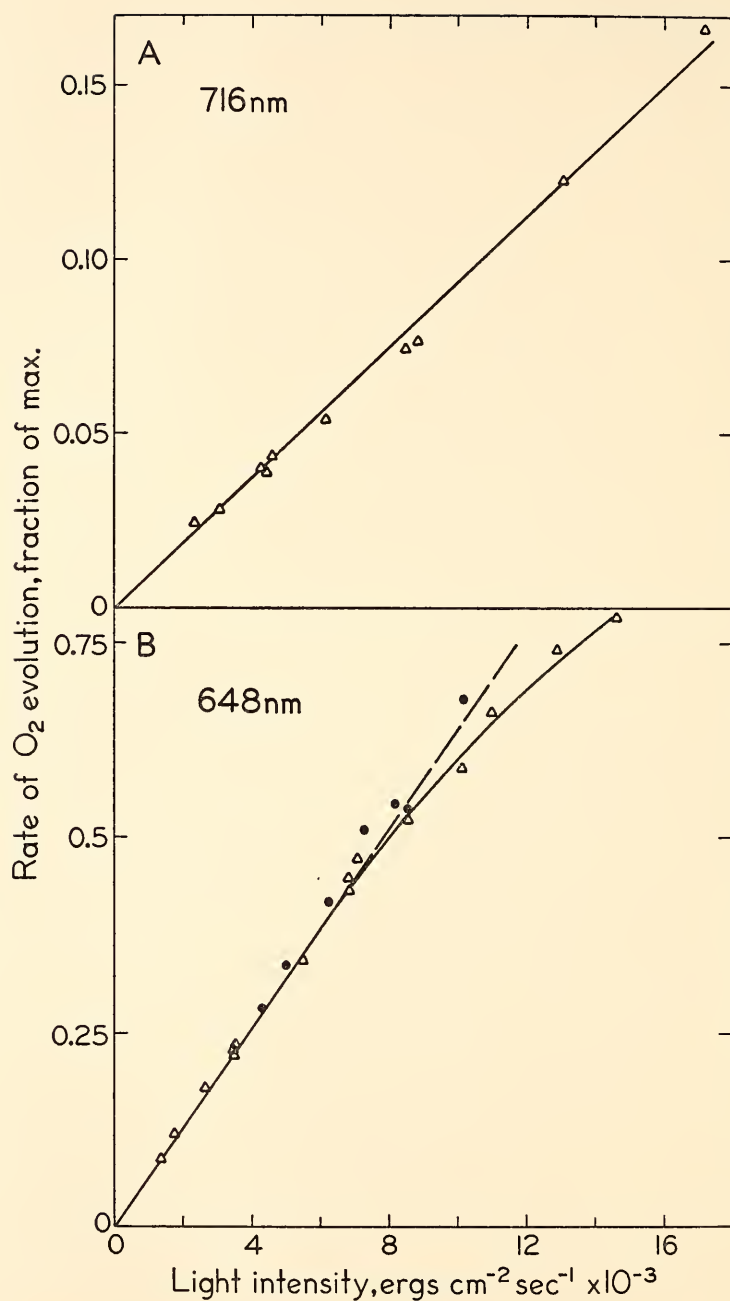


Fig. 34. Dependence of oxygen exchange on light intensity in *Chlorella* at two wavelengths. (A): 716 nm (triangles); (B): 648 nm (triangles). The solid circles indicate calculated rates of P_{1+2} for the maximum values of E found for each ratio at lower intensities.

of photosynthetic rates from different experiments, rates of O₂ evolution were expressed as fractions of the light saturated value, which was determined with short-wavelength light in every experiment.

Calculation of enhancement. Enhancement, *E*, was calculated as

$$E = \frac{P_{1+2} - P_2}{P_1}$$

where *P*₁ is the rate of O₂ evolution with the longer wavelength light primarily activating photosystem 1, *P*₂ is the rate for the shorter wavelength system 2 light and *P*₁₊₂ is the rate with both beams on together.

Results: Chlorella. With low light intensities the rate of photosynthesis was generally linear (Figs. 34 and 35). No evidence was found for the “Kok effect,” an increase in the slope of the curve at low intensity, that could have led to a lowering of enhancement values as pointed out by Myers (1963).

The result of an enhancement experiment with 648 and 716 nm for short-wavelength and far-red light, respec-

tively, are listed in Table 10. It is seen that when the ratio *P*₂/*P*₁ is kept approximately constant, the enhancement factor *E* becomes smaller as the rates *P*₂ and *P*₁ increase. Comparison with the light curve of photosynthesis (obtained in the same experiment, Fig. 34B) suggests that the lower values of *E* might be

TABLE 10. Enhancement in *Chlorella* at Various Photosynthetic Rates with Different Ratios of Rates in the Two Beams

<i>P</i> ₂ / <i>P</i> ₁	<i>E</i>	O ₂ Evolution, Fraction of Saturation Rate		
		<i>P</i> ₂ *	<i>P</i> ₁₊₂ †	<i>P</i> ₁ ‡
2.98	1.39	0.120	0.176	0.0401
3.00	1.22	0.228	0.322	0.0767
2.77	1.01	0.341	0.465	0.123
2.68	1.00	0.446	0.612	0.167
6.28	1.53	0.180	0.224	0.0286
5.70	1.42	0.224	0.279	0.0392
6.18	1.19	0.335	0.400	0.0543
5.78	1.05	0.432	0.510	0.0747
9.50	1.54	0.235	0.273	0.0247
10.9	1.32	0.474	0.530	0.0434

* 648 nm
† 648 + 716 nm
‡ 716 nm

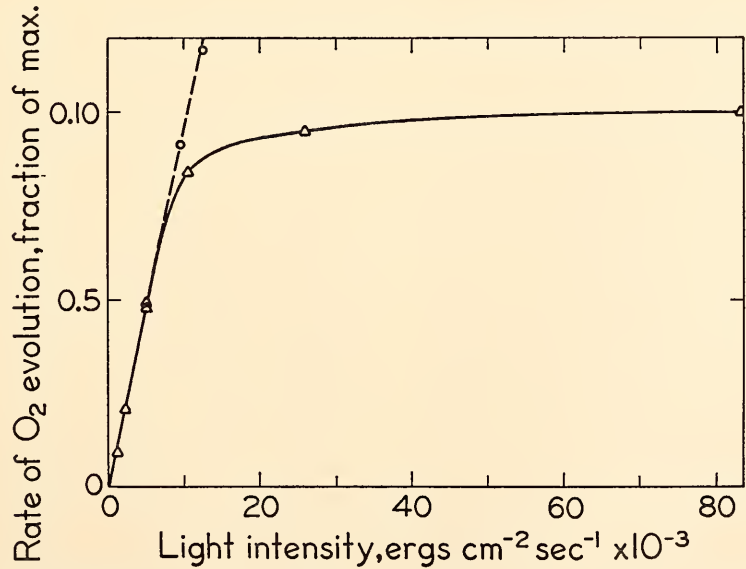


Fig. 35. Dependence of oxygen exchange on intensity in 674-nm light in *Porphyridium* (triangles). The circles have the same meaning as in Fig. 34(B).

caused by rates of P_{1+2} , which are in the bending part of the light curve. To test this the following procedure was adopted: For those cases showing low E values for a certain ratio P_2/P_1 , rates of P_{1+2} that are equivalent to the maximum enhancement factor for that ratio were calculated. If the measured rates of P_{1+2} were in the bending part of the light curve, thereby lowering the enhancement factor, the calculated P_{1+2} rate should lie on the extrapolation of the linear part of the light curve. Fig. 34(B) shows that the calculated P_{1+2} rates do coincide well with the linear part of the light curve and its extrapolation. This indicates that any decrease of E at the higher rates of P_2 and P_1 can be ascribed to the bending of the light curve of photosynthesis. Two other experiments gave results consistent with this finding.

Porphyridium. In far-red light a change in slope in the light curves indicating a "Kok effect" was occasionally observed; in four experiments on the behavior of enhancement at higher light intensities, the "Kok effect" interfered in only one case with the interpretation of the enhancement values. With green light (574 nm) no "Kok effect" was seen.

The results of the two best enhancement experiments are given in Table 11.

TABLE 11. Enhancement in *Porphyridium*

P_2/P_1	E	O ₂ Evolution, Fraction of Saturation Rate		
		P_2^*	P_{1+2}^\dagger	P_1^\ddagger
Expt 1				
0.625	1.25	0.068	0.20	0.11
0.70	1.25	0.20	0.57	0.29
1.06	1.31	0.083	0.19	0.079
1.09	1.45	0.20	0.47	0.19
1.04	0.82	0.49	0.88	0.47
1.81	1.81	0.09	0.18	0.05
1.93	1.65	0.20	0.37	0.103
2.03	1.24	0.48	0.78	0.24
Expt 2				
2.80	1.95	0.15	0.254	0.0536
2.68	1.94	0.37	0.634	0.137

* 574 nm

† Expt. 1: 574 + 684 nm; Expt. 2: 574 + 703 nm.

‡ Expt. 1: 684 nm; Expt. 2: 703 nm.

With constant ratios of P_2 to P_1 at different absolute values of P_2 and P_1 , very similar enhancement factors are obtained, except for $P_2=0.5$ where the value of E is severely diminished. In this case, however, the corresponding rates for P_{1+2} (0.88 and 0.78) lie in the bending part of the light-photosynthesis curve as shown in Fig. 35. As previously described for *Chlorella*, P_{1+2} values were calculated for *Porphyridium* on the basis of the maximum enhancement at lower intensities and plotted. Again the calculated values of P_{1+2} are found on the extrapolation of the linear part of the light curve (Fig. 35).

From these experiments with *Chlorella* and *Porphyridium* the conclusion is drawn that light saturation of photosynthesis is sufficient to explain a decline in enhancement when the rates P_2 and P_1 are increased. Bannister and Vrooman (1964) also arrived at the same conclusion in their study of enhancement of oxygen evolution under different illumination conditions with *Chlorella*.

Discussion. The discrepancy between the results presented here and the findings for $^{14}\text{CO}_2$ -assimilation does not seem easily explainable at first sight. One has, however, to consider the way in which the results for $^{14}\text{CO}_2$ -assimilation were derived. E was determined at different values of P_2/P_1 obtained by changing P_1 for two different rates of P_2 . With a large ratio, P_2/P_1 , (about 12) and large rate of P_2 , a drop of E was observed. This did not occur with a smaller ratio, P_2/P_1 . It was argued that light saturation of photosynthesis could not be the reason for this because such a drop in E should have occurred instead with the smaller ratio P_2/P_1 corresponding to the bigger P_1 rate.

This argument was based on the behavior of E with different rates of P_2 and a fairly large ratio P_2/P_1 . For a large ratio P_2/P_1 , when there is a small rate P_1 , the values of P_{1+2} and P_2 are relatively large and their difference is small; thus minor variations of P_{1+2} or P_2 may

lead to considerable changes of the value of E . (Compare also in Fig. 34B the relatively small corrections needed for P_{1+2} to obtain full reconstitution of enhancement factors). In view of this consideration, a reinvestigation of enhancement for CO_2 -assimilation at higher light intensities seems desirable.

References

- Bannister, T. T., and M. J. Vrooman, *Plant Physiol.*, **39**, 622-629, 1964.
 Loos, E., Dissertation, München, 1967.
 Myers, J., in *Photosynthetic Mechanisms of Green Plants*, NAS-NRC Publ. 1145, Washington, D. C., pp. 301-317, 1963.
 Pickett, J. M., and C. S. French, *Proc. Natl. Acad. Sci.*, **57**, 1587-1593, 1967.

INHIBITION OF CYCLIC ELECTRON TRANSPORT IN VIVO BY RED LIGHT AND BY OXYGEN

Ulrich Heber

Light-induced electron transport is known to be accompanied by ion and water transport across the membranes of the thylakoid system in isolated chloroplasts. The ensuing shrinkage of the chloroplasts changes the light-scattering properties of the preparation. We therefore used light-scattering changes to study cyclic electron flow in vivo with two different wavelengths of light at various intensities and with different oxygen concentrations. The experiments were carried out with intact leaves.

Light-scattering changes were detected in the leaf by the attenuation of a measuring beam of 530 nm with the photo-detector put in line with the measuring beam. Changes in scattering appear in this arrangement as changes in absorbance. They are distinguished from true absorbance changes by their kinetics, their magnitude, sensitivity to observation in the Ulbricht sphere and sensitivity to certain uncouplers. Fig. 36 gives the intensity dependence of changes that have been tentatively identified by these criteria as photoinduced shrinkage of chloroplasts in leaves.

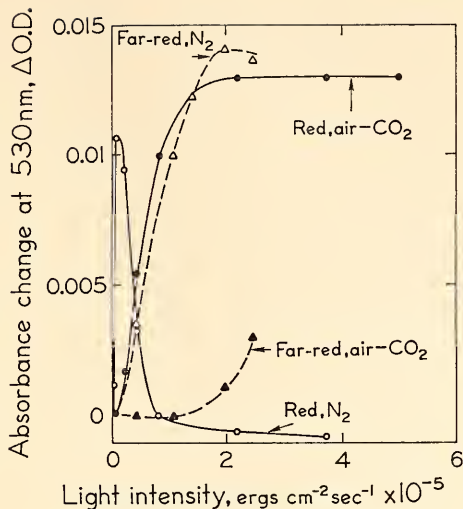


Fig. 36. The extent of photo-induced shrinkage of a *Mimulus verbenaceus* leaf in CO_2 -free air and in nitrogen as a function of the intensity of the exciting red or far-red light. Shrinkage is indicated by slow increase in the apparent absorbance of the leaf at 530 nm. Red: a broad band from about 620 to 820 nm; halfband width 125 nm, from 635 to 760 nm. Far-red: a band from about 690 to 820 nm; halfband width 60 nm, from 700 to 760 nm.

Under nitrogen, illumination with far-red light of low intensity that predominantly excites photosystem 1 causes shrinkage. Red light, exciting both photosystems 1 and 2, is also very effective at low intensities. At higher intensities of red light, however, shrinkage is progressively inhibited. In CO_2 -free air, the shrinkage in red light follows a saturation curve. With far-red light no response is observed at low intensities but shrinkage does occur at high intensities.

Interpretation of Fig. 36. As in other experiments, not described here, the action spectrum of shrinkage in nitrogen as compared with that in air was found to be shifted toward longer wavelengths. Shrinkage in far-red light under nitrogen was assumed to represent a cyclic electron flow mediated by photosystem 1. Likewise low-intensity red light in nitrogen permits cyclic electron flow to occur. At higher intensities, however, photosys-

tem 2 becomes sufficiently excited to reduce electron carriers between photosystem 1 and 2 thus rendering them ineffective as electron acceptors for cyclic electron flow. Consequently cyclic electron transport becomes inhibited and shrinkage no longer occurs.

Far-red, of an intensity sufficient to produce large shrinkage in nitrogen, is ineffective in CO_2 -free air indicating that oxygen reacts with an electron carrier connected to photosystem 1 and drains electrons from the cyclic pathway. The large increase of shrinkage seen on admission of oxygen to a leaf in nitrogen that has been inhibited by high-intensity red light marks the onset of electron flow from water to oxygen. Accordingly, the action spectrum of shrinkage in the presence of oxygen is that of a reaction involving both photosystems.

Comparison of shrinkage with cytochrome f reduction. The redox state of electron carriers involved in cyclic electron flow should also reflect the proposed inhibition of cyclic electron transport by oxygen and by strong excitation of photosystem 2 in nitrogen. Cytochrome *f*

donates electrons to the reaction centers of photosystem 1 and should in turn become reduced by carriers of the cyclic pathway during cyclic electron transfer. Its reduction should be seen in the dark immediately following a light period. If the initial rate of dark-reduction of cytochrome *f* is plotted as a function of the light intensity of a preceding illumination period the results depicted in Fig. 37 are obtained. It is obvious that the pattern of cytochrome reduction is similar to that of the photo-induced shrinkage of Fig. 36. In agreement with the interpretation of shrinkage, the dark reduction of cytochrome after exposure to far-red light is much faster in nitrogen than in CO_2 -free air, which indicates the functioning of cyclic electron flow in nitrogen and its inhibition by oxygen. The very slow dark reduction of cytochrome *f* after illumination with high-intensity red light in nitrogen demonstrates the inhibition of cyclic electron flow under these conditions.

The inhibition of cyclic electron flow by oxygen, although seen only under far-red or low-intensity red illumination in

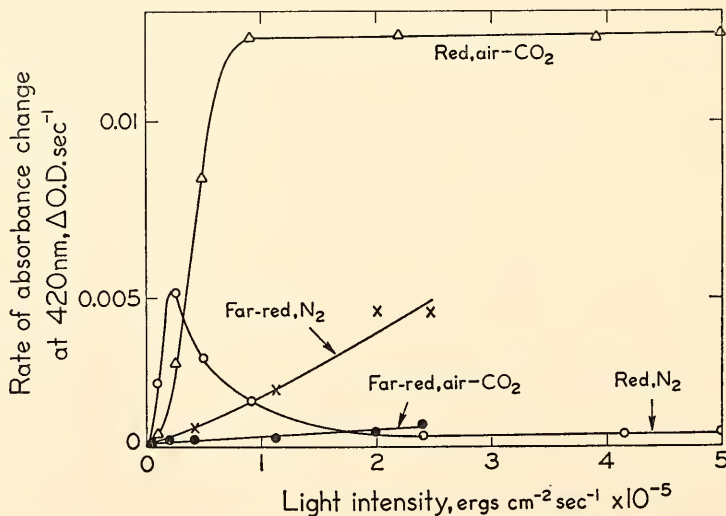


Fig. 37. The rate of dark-reduction of photo-oxidized cytochrome *f* measured at 420 nm in a leaf of *Mimulus verbenaceus* as a function of the previous illumination with red or far-red light. The rate of dark-reduction was calculated from the slope of the initial decay of the signal after darkening.

leaves, suggests that cyclic electron transport reaches significant proportions only under anaerobiosis.

The intensity dependence of shrinkage in leaves shows the interdependence of the two photosystems. The experimental results have been explained on the basis of the series formulation of photosynthesis. It appears difficult, if not impossible, to accommodate the data in a model of photosynthesis with two separate photo-reactions having independent electron transport pathways.

Dependence of shrinkage on oxygen concentration. Fig. 38 shows changes in shrinkage of a spinach leaf caused by establishing different oxygen concentrations in the previously anaerobic system.

In low-intensity red as well as in far-red light, one notices with increasing oxygen concentration a large swelling which then levels off. As outlined above, this swelling is due to a deletion of cyclic electron flow with oxygen acting as an electron trap. In strong red light, admission of oxygen again causes a large increase in scattering indicating electron flow from water to oxygen. For medium intensities of red and relatively high intensities of far-red light, two effects show up with increasing oxygen concentration: First, a large shrinkage which settles to a constant value in the range between 1% and 5% O_2 . The interpretation of this shrinkage is the same as for that of strong red light. The far-red intensities

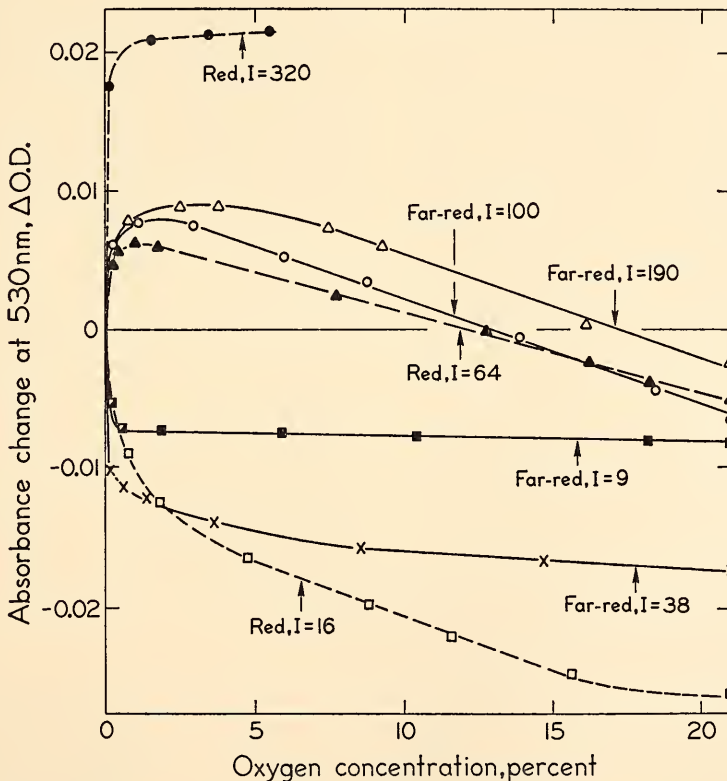


Fig. 38. Extent and direction of shrinkage or swelling induced in a spinach leaf under continuous illumination as a function of the concentration of oxygen and of light intensity. Positive changes in the optical density at 530 nm denote shrinkage; negative changes denote swelling. The reference level is the shrinkage condition produced in nitrogen.

seem now to be strong enough to provide electrons from water by excitation of pigment system 2. Second, for higher O_2 concentrations the degree of shrinkage becomes gradually smaller and when changing from nitrogen to 21% oxygen even swelling is observed. An explanation for this phenomenon is not yet at hand.

Under the simplifying assumption that the light scattering response caused by low oxygen concentrations of less than 5% is a measure of the rate of a reaction of oxygen with the electron transport chain, the affinity of the system for oxygen was determined. The half-maximal response of shrinkage or swelling was observed at an oxygen concentration of $1.4 \mu M$ or approximately 1100 ppm of oxygen in nitrogen.

Effect of CO_2 . Admission of CO_2 to a leaf kept in nitrogen and illuminated with far-red or low-intensity red light also resulted in a drastic inhibition of shrinkage. The half-maximal response to CO_2 in nitrogen was at approximately 10 ppm. Carbon dioxide is assumed, similar to oxygen, to drain electrons from the cyclic pathway and thereby to interrupt it. The high effectiveness of CO_2 in this reaction is in accord with the role of CO_2 as the main, though indirect, electron acceptor in photosynthesis.

Because O_2 and CO_2 inhibit shrinkage caused by excitation of photosystem 1 (low-intensity far-red or a monochromatic beam of 709 nm), the interaction of both O_2 and CO_2 with the electron transport chain should occur directly or via intermediates at the reducing end of photosystem 1. Preliminary experiments with isolated chloroplasts also agree with this interpretation. Isolated and washed chloroplasts, incapable of performing cyclic electron transport, still take up oxygen by a light dependent reaction even after electron flow photosystem 2 has been blocked by DCMU and a donor system is available to feed electrons to photosystem 1. The rate may be as high as $30 \mu moles$ per mg of chloro-

phyll per hour. As ferredoxin is largely missing from these preparations, interaction with oxygen seems to be at the level of the first reductant generated by photosystem 1.

Part of the work described in this report has been published in more detail (Heber and French, 1968).

Reference

Heber, U., and C. S. French, *Planta* 79, 99-112, 1968.

FACTORS AFFECTING ABSORPTION AND FLUORESCENCE SPECTRA OF NATURAL CHLOROPHYLL COMPLEXES

J. S. Brown

Although several forms of chlorophyll have been observed as peaks and shoulders in spectra for many years, their physical form is unknown. So far these chlorophyll forms have eluded our attempts to isolate them in pure form. Consequently to study the physical characteristics of chlorophyll in vivo we are restricted mainly to spectroscopic measurements.

A series of experiments in which algae or chloroplast particles have been subjected to various physical treatments has yielded some information about the natural state of chlorophyll. We have studied the effect of chlorophyll concentration within the cells, heat treatments and ultraviolet irradiation on the absorption and in some cases also the fluorescence of several organisms.

The absorption and fluorescence spectra of chloroplast fractions from a variety of plants is reported in another section.

Effect of Concentration on the Spectra of Chlorophyll in Chlorella

The shape of absorption and fluorescence emission spectra of intact algae may be distorted by a high chlorophyll concentration. Since our knowledge of the absorbing forms of chlorophyll *a* depends

upon the interpretation of complex spectra, the effect of varying the concentration of chlorophyll within the cells was investigated.

French *et al.* (*Year Book 65*, p. 492 and *Year Book 66*, p. 177) compared spectra of a series of *Claes Chlorella* mutants. Mutant No. 520 contained very little chlorophyll and nearly all of it as one form when grown in the dark. Spectra of these cells showed a single absorption maximum near 670 nm, no chlorophyll *b* and a single fluorescence emission maximum near 680 nm. (We wish to thank Mr. Norio Murata for pointing out the error in plotting Fig. 30B of *Year Book 65*, p. 495. The whole curve should have been put 10 nm toward longer wavelengths). The spectrum of Mutant 520 contrasts with that of normal green *Chlorella* that has an absorption peak at 677 nm and a shoulder at 670 nm indicating at least two forms of chlorophyll *a*. The normal fluorescence emission spectrum of *Chlorella* measured at low temperature shows two maxima, one near 680 nm and another broad band near 730 nm.

To determine whether the unusual spectra of Mutant 520 were due to a pigment mutation or to low chlorophyll concentration, a comparison was made with absorption and fluorescence spectra of *Chlorella protothecoides* (Indiana Culture Col. No. 25) in which the amount of chlorophyll formed is directly proportional to the nitrogen-carbon ratio in the growth medium (Shihira-Ishikawa and Hase, 1964). If this alga is grown on a glucose medium containing a minimal amount of nitrogen, very little chlorophyll is formed.

When grown in a medium containing 0.5% glucose and 0.05% urea, *C. protothecoides* was green, but in 1.0% glucose and 0.01% urea, the culture appeared about half as green as the usual *Chlorella* culture. An inoculum of cells from this pale green culture transferred to a medium containing 1.0% glucose and no nitrogen grew for several days, and the resulting suspension was white. However, chlorophyll was present as shown by the absorption spectrum of a dense cell suspension in Fig. 39; also shown

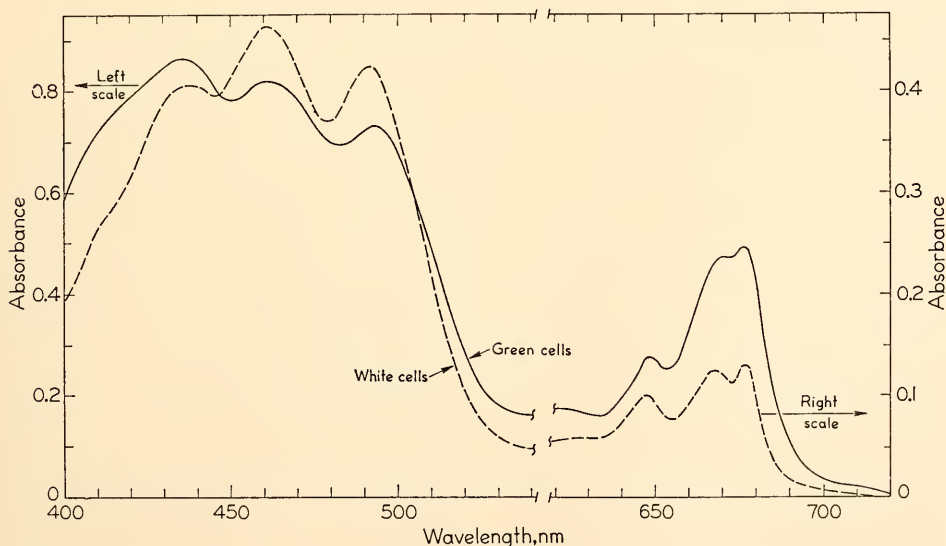


Fig. 39. Absorption spectra of *Chlorella protothecoides* measured at -196°C . Green culture grown on 0.55% glucose and 0.05% urea. White culture, measured on a much higher cell concentration, was grown on 1.0% glucose without an added nitrogen source.

is the spectrum of a thin suspension of green *Chlorella*.

Although the exact shape and relative heights of the chlorophyll *a* and *b* peaks are distorted by the high ratio of scattered to absorbed light in the cells containing very little chlorophyll, the spectra are very similar in shape and in their proportions of the chlorophyll forms. A comparison of these spectra in the blue region shows that the proportion of carotenoid to chlorophyll is greater in the cells grown in the lower nitrogen concentration.

The fluorescence emission spectra of cells from the green and the white cultures are shown in Fig. 40. The cells containing very little chlorophyll show much less long-wavelength fluorescence emission near 730 nm. The relatively enhanced long-wavelength emission seen in the green cells may be an artifact due to reabsorption of fluorescence near 680 nm by chlorophyll (Goedheer, 1964), or the normal green cells may contain a small amount of a highly fluorescent pigment that is absent in the cells grown in low nitrogen.

Absorption spectra of green *Chlorella protothecoides*, of two species of *C. pyrenoidosa* (Indiana Culture Col. Nos. 252 and 1230), and of aqueous extracts of the latter all have similar red bands.

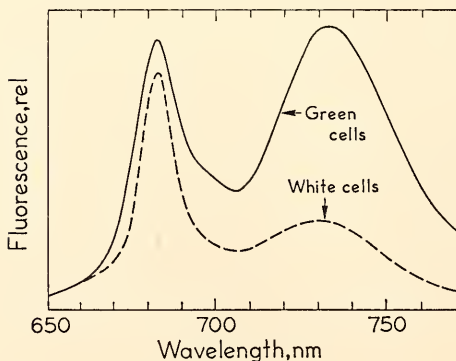


Fig. 40. Fluorescence emission spectra of *Chlorella protothecoides* measured at -190°C ; excitation at 436 nm. Growth conditions are the same as for Fig. 39.

The peak near 680 nm is always higher than the shoulder at shorter wavelengths. Algae from different genera may have different proportions of the chlorophyll *a* forms and therefore exhibit spectra of different shapes, but within specific groups, the shapes of the spectra are much alike.

We conclude that the doublet structure of the red absorption band in *Chlorella* is not caused or affected by the chlorophyll concentration within the cell although the long wavelength fluorescence emission maximum may be artificially enhanced. Assuming that chlorophylls *a* and *b* are normally attached to a lipoprotein framework, an explanation for the difference between the mutant and *C. protothecoides* may be as follows: *C. protothecoides* grown on low nitrogen may be able to synthesize only a small amount of this lipoprotein framework, but what it does make is normal, and the attached chlorophyll exhibits the usual spectrum. The mutant may be unable to form the basic structure, and therefore the small amount of chlorophyll formed is not attached in the normal way and displays only a single absorption band.

Effect of Temperature on Absorbance of Chloroplast Particles

Schejter and George (1964) observed that the 695-nm absorption band of ferri cytochrome *c* was reversibly decreased by heating the solution from 10° to 60°C , and that this effect was probably caused by a conformational change in the protein portion of the hemoprotein. These results suggested that information about the nature of chlorophyll-lipoprotein complexes might be gained from similar heating experiments. In the present study, changes in absorption with changes in temperature from 15° to 70°C were measured in chloroplast particles of different sizes. In contrast to the hemoproteins, chlorophyll-lipoprotein complexes are insoluble.

Chloroplasts or algae were broken in

the needle-valve press and centrifuged to obtain fractions of different densities. Also spinach fractions or bands from the sucrose gradient, described by the Michels, were tested. Samples were placed in a jacketed cuvette in the recording spectrophotometer and heated or cooled by flowing water. Five to ten minutes were required to change the temperature.

Two types of decreases in apparent absorption with increasing temperature were observed. One type illustrated in Fig. 41(A), could result from a decreased light scattering by the chloroplast particles when these are heated. The larger the particles, the greater was this type of change. It occurred throughout the measured spectrum and was completely reversible up to 40°C. This change may be similar to light-induced conformational changes.

The second type, illustrated by Fig. 41(B), appears to be a true decrease in absorption. This change takes place with very small green particles of *Chlorella*, and it is only partially reversible. Chlorophyll *a* 680 is more easily bleached by heat than are the shorter wavelength absorbing forms. The reversible part of the change may be attributed to a decrease in light scattering discussed above.

Since the different forms of chlorophyll bleach at different rates with heating, two spinach fractions from a sucrose gradient, top fraction 1 enriched in long wavelength chlorophyll, and lowest fraction 2 in short wavelength chlorophyll *a* and chlorophyll *b*, were heated. Each fraction, heated to 40°C, showed a reversible bleaching pattern similar to that in Fig. 41(B) for *Chlorella* particles. When each fraction was subsequently heated to 70°C and returned again to 15°C, the original peak position shifted 6–8 nm towards shorter wavelengths. Fig. 42 shows the plotted difference of absorbance of each fraction measured at 15°C before and after heating to 70°C for several minutes. The bands with

maxima at 683 nm in fraction 1 and 682 nm in fraction 2, represent the chlorophyll complex destroyed by heat.

If these fractions had contained the same chlorophyll forms in different proportions, the difference spectra would be similar in peak position and shape, and they are not. The small difference in the heights is not significant because the original peak absorbance of fraction 2 was 0.06 greater than fraction 1.

The difference spectra were dissimilar in bandwidths and peak positions. This suggests that the fractions representing photosystem 1 and 2 activities contain separate forms of chlorophyll, both of which show peak absorption near 680 nm. We arrived at a similar tentative conclusion from curve analysis of spectra of the fractions. This work is reported in another section.

Effect of Ultraviolet Irradiation on Chlorophyll Absorption and Fluorescence in Phaeodactylum

Irradiation of algae or chloroplasts with ultraviolet light preferentially destroys photosystem 2 activity (Mantai and Bishop, 1967). Since the long wavelength absorption and fluorescence bands of the diatom, *Phaeodactylum tri-cornutum*, have been attributed to photosystem 2 (Brown, 1967), it was of interest to see if ultraviolet irradiation would specifically destroy these bands.

The algae, suspended in a thin layer of culture medium in a petri dish, were exposed to a sterilamp. Absorption and fluorescence emission spectra of the cells measured before and after exposure are presented in Figs. 43 and 44.

The absorption bands near 705 and 685 nm were both diminished by the ultraviolet light. The decrease in fluorescence at 710 nm is probably correlated with the loss of the 705-nm absorption band because chlorophyll *a* 685, observed in most plants, does not fluoresce at room temperature. The total relative fluorescence, measured as the area under the

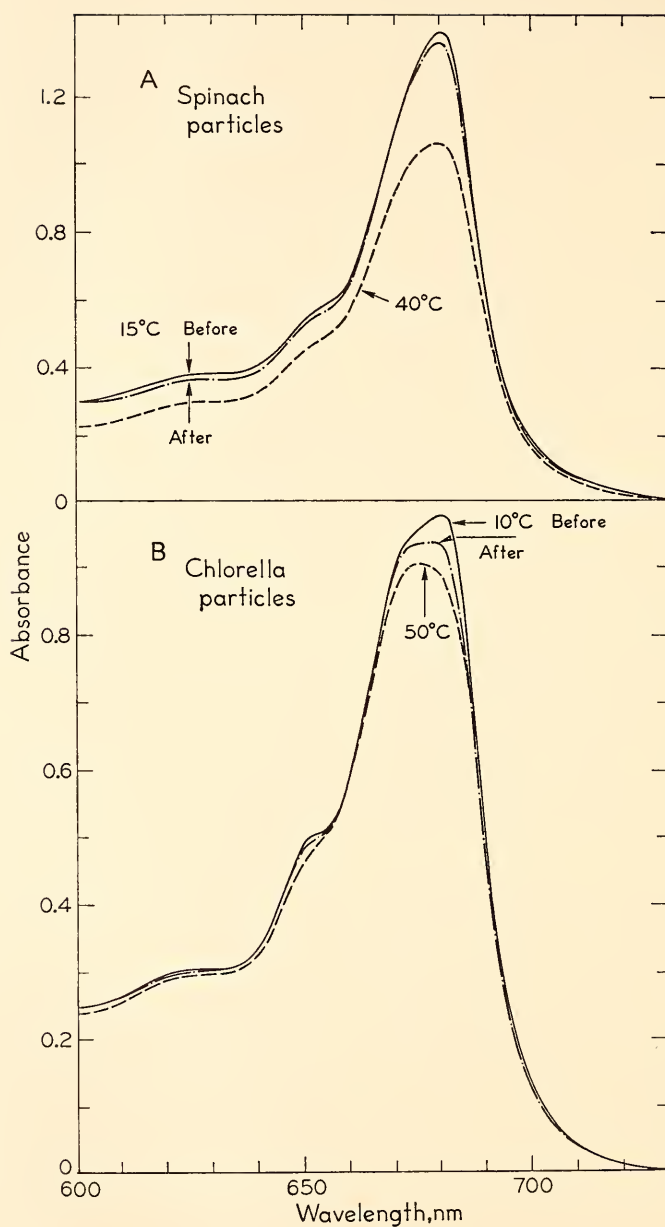


Fig. 41. (A) Absorption spectra of spinach chloroplast fragments suspended in 0.01 *M* Tris, pH 8.5 measured at 15°, 40°, and again at 15°C. (B) Absorption spectra of supernatant from broken *Chlorella*, centrifuged at 10,000 *g* for 15 min, measured at 10°, 50°, and again at 10°C.

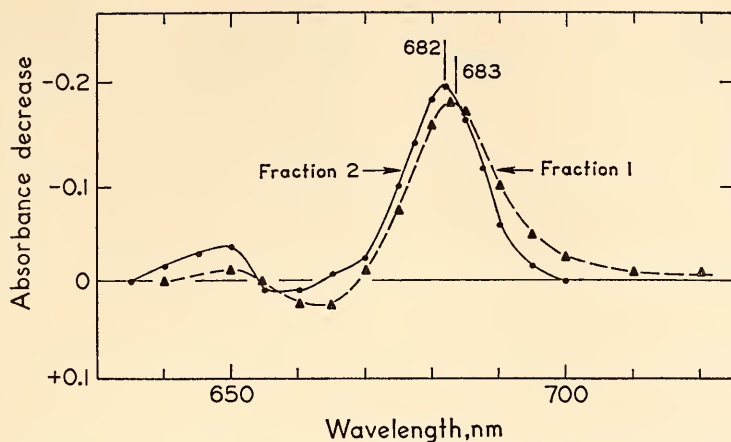


Fig. 42. Difference in absorbance between spectra measured at 15°C before and after heating to 70°C. Spinach fraction 1 from top of sucrose gradient and fraction 2 from lower part of gradient. Original absorbance approximately 0.6 at 678 nm. Fractionation carried out in 0.45 *M* KCl, 0.05 *M* Tricine at pH 8.0. The fractions were dialyzed to remove the sucrose before measuring the spectra.

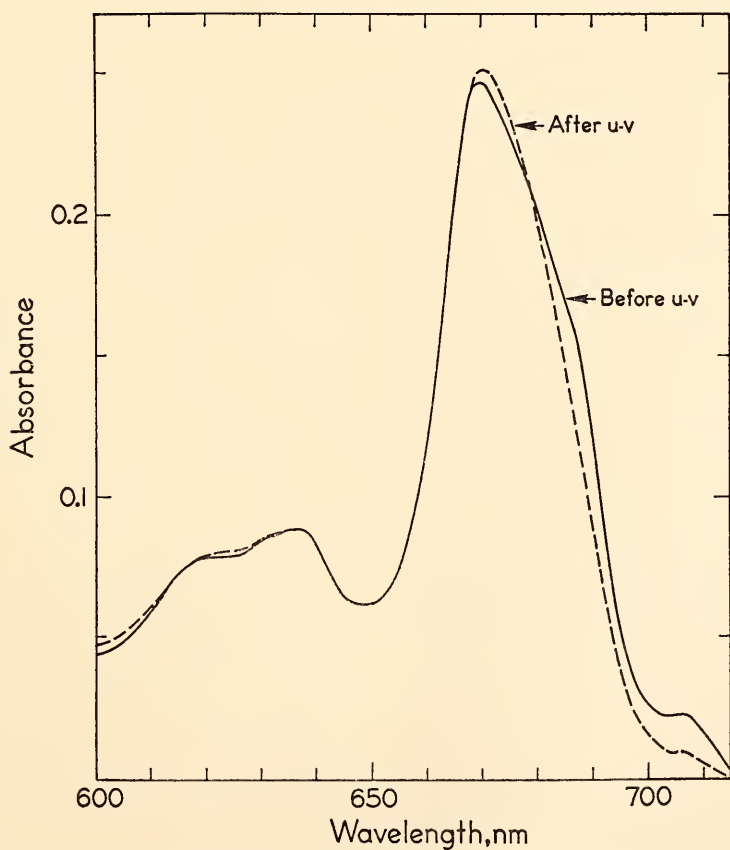


Fig. 43. Absorption spectra of *Phaeodactylum tricornutum* at -196°C before and after irradiation with ultraviolet light, 253.7 nm, for 10 min.

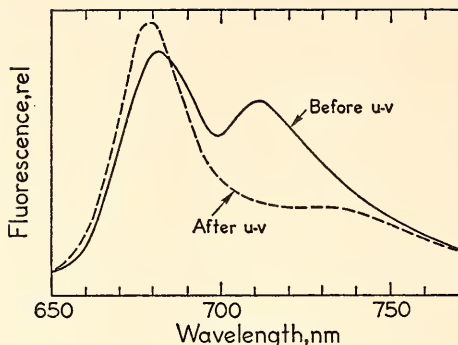


Fig. 44. Fluorescence emission spectra of *Phaeodactylum tricornutum* before and after irradiation with ultraviolet light, 253.7 nm, 10 min; measured at 20°C, excitation at 436 nm.

curves, was also decreased by the ultraviolet irradiation.

The long wavelength absorption bands are easily destroyed by several mild treatments such as heating to 40° for 10 min, freezing and thawing, or exposure to 10% ethanol for several hours (Brown, 1967). Following each of these previously studied treatments the chloroplast within the cells disintegrated, and the suspension changed color from brown to green simultaneously with the disappearance of the long wavelength fluorescence band. Following ultraviolet irradiation, no immediate change in the cell structure corresponding to the change in fluorescence could be observed, although after several hours the cell interior did break up, indicating the lethality of the irradiation. Thus the loss of long wavelength fluorescence need not be correlated with gross morphological change.

These results are consistent with the hypothesis that the absorption band near 704 nm that fluoresces at 710 nm in *Phaeodactylum* is associated with photosystem 2.

Phaeophytin Formation in Ochromonas

In *Year Book 66*, p. 196, it was reported that mild heating or freezing and thawing of *Ochromonas danica* caused a change in its chlorophyll absorption

spectrum from three maxima between 665 and 695 nm to a single band at 670 nm. Subsequent experiments have shown that this change results from the conversion of chlorophyll *a* to phaeophytin or phaeophorbide within the cell. Even in cells from a culture only just beyond the logarithmic growth phase, considerable phaeophytin was detected. Thus, the spectrum of the damaged cells may represent phaeophytin rather than an altered form of chlorophyll *a*.

This conclusion also changes the previous interpretation of the fluorescence spectra. In *Ochromonas* it appears that the main fluorescence emission band may be shifted from 680–685 to 690 nm by self-absorption.

No method has yet been found to extract pigment lipoprotein particles from *Ochromonas* without converting chlorophyll to phaeophytin.

References

- Brown, J. S., *Biochim. Biophys. Acta*, **143**, 391–398, 1967.
- Goedheer, J. C., *Biochim. Biophys. Acta*, **88**, 304–317, 1964.
- Mantai, K. E., and N. I. Bishop, *Biochim. Biophys. Acta*, **131**, 350–356, 1967.
- Schejter, A., and P. George, *Biochem. J.*, **104**, 1045–1049, 1964.
- Shihira-Ishikawa, Ikuko, and Eiji Hase, *Plant Cell Physiol.*, **5**, 227–240, 1964.

CONNECTION OF THE LABORATORY TO THE COMPUTATION CENTER OF STANFORD UNIVERSITY

David C. Fork

We have recently installed a cable connection between this laboratory and two facilities of the Computation Center at Stanford University.

One of the facilities now available for our use, called ACME for Advanced Computer for Medical Research, is an on-line computer system for data collection and control of experiments which is sponsored by the Macy Foundation and the National Institutes of Health.

The main computer of the ACME system is an IBM 360 Model 50. The ACME system also uses an IBM 1800 computer linked by a special channel to the Model 50. We have access to the computer "on line" on a time-sharing basis by means of an IBM 2741 typewriter terminal located in the laboratory. In addition to using the typewriter terminal, data can be sent to the computer as analogue signals (6 inputs) or digital signals (1 input), both via the 1800. The system will also accept direct input into the 360 for high speed experiments or data from small computers via high speed parallel data links.

Results of experiments may be obtained in the laboratory on the same typewriter terminal used to put in data or via the 1800 as analogue (4 outputs) or digital output (1 output) signals to drive various display equipment. The input and output system includes file handling and retrieval facilities.

One of the uses planned for ACME is to facilitate the analysis of large amounts of data which can be generated in a short time during studies of light-induced absorbance changes or the polarographic determination of O_2 exchange.

The other facility on the Stanford campus which can be used from our terminal contains an IBM 360 Model 67 computer. The terminal may be used for text editing, and computation jobs may be submitted through the terminal for standard batch processing.

The program for curve analysis described in another section of this report, for example, was stored on the disk file of this computer, the data for curves to be analyzed was sent to the computer via our terminal, and the results printed out on the high-speed printer and plotted on the Calcomp plotter at the Computation Center.

A CURVE DIGITIZER

C. S. French, R. W. Hart and Mark Lawrence

Direct digital recording of absorption spectra for data handling by computer

is being developed by instrument manufacturers and appears to be on its way in for future routine use. We have considered, but at least temporarily abandoned, the thought of digitizing our spectrophotometer output through the ACME computer. The reasons for not taking this step are: the limited times of day that ACME is operational, the need to keep the ACME connection free for more pressing uses, and the cost.

There are many useful spectra on hand that we wish to put through the digital curve analysis procedure. Therefore, we have made a device to convert plotted curves into tabulated numbers for the computer input. This device moves a table carrying the plotted curve by a definite distance each time a knee switch is closed. This step distance on the x-axis is selected by a double set of change gears in wavelength steps of 0.5, 1.0, 2.0, 3.0, 4.0, or 5.0 nm. Our usual wavelength scales are $\frac{2}{3}$ inch = 10 nm for absorbance or $\frac{1}{2}$ inch = 10 nm for fluorescence spectra. A cursor observed under magnification is set by a hand wheel on the curve at each wavelength step. The counter, presently in use, reads 0.00842 inch per unit giving a precision of about 0.1% f.s. for the original record of a spectrum 8 inches high. A typical spectrum covering 160 nm can be converted in about 20 minutes to a table of heights at 1-nm intervals by reading a digital counter. A shaft angle encoder is being installed to provide a direct connection to the on-line ACME computer for more rapid read-in. The manual cursor setting will be retained since it provides a convenient way to average visually the minor irregularities of the record. The range on the x-scale is 16 $\frac{5}{8}$ inches and on the y-scale 15 $\frac{1}{2}$ inches.

The unfortunate custom of publishing absorbance spectra on too short a wavelength scale makes it very difficult, even with this device, to make adequately accurate measurements of absorbance values at particular wavelengths from most of the spectra in the literature. To

make important data retrievable from published curves the wavelength scale needs to be adjusted at the time of recording or of plotting so the maximum slope on the side of a steep band is less than 80°. Few published spectra meet this criterion. As digital methods become more widely used in spectroscopy, and as the shape, as well as the peak position of the curves, becomes of interest to more workers, we may hope for editors' encouragement of the publication of data tables as well as curves in the routine reporting of absorption spectra. When digital recording of spectra combined with curve analysis becomes routine, complicated spectra can be reported in complete detail with high accuracy as a table of parameters for the component curves. Then curve fitting, even where it does not necessarily further theoretical understanding, can be used to record spectral measurements in a compact and accurately retrievable fashion.

ANALYSIS OF SPECTRA OF NATURAL CHLOROPHYLL COMPLEXES

*C. S. French, J. S. Brown, Lillian Prager, and
Mark Lawrence*

We are continuing the attempts to define the absorption spectra of the various naturally occurring chlorophyll complexes so often discussed in this *Year Book*.

What is the significance of this concern about the spectra of the separate forms of chlorophyll in plants? In the first place comes the simple description of the spectroscopy of the most obvious colored substance on earth. Secondly, precise knowledge of the spectra of the separate forms should not only show the number of existing natural chlorophyll complexes but also may lead to some understanding of the structural relations of the chlorophyll molecules to each other and to the remainder of the protein complex. Thirdly, there is the pressing need, for use in kinetic studies of photosynthesis, to know from analyses

of absorption spectra what fraction of the incident light of a particular wavelength is absorbed by each photochemical system. Now, that information can be obtained only from action spectra for the two photochemical effects.

The problem we face is illustrated in Fig. 45 where the absorption spectrum of extracted and purified chlorophyll *a* is compared with the absorption spectrum of chloroplast fragments from *Euglena* at liquid nitrogen temperature. In the *Euglena* spectrum the small shoulder at 649 nm is due to chlorophyll *b* while the other humps at longer wavelengths show the presence of four different kinds of chlorophyll *a* complexes. The purpose of the work in progress is to derive the individual absorption spectra of each of these and of other naturally occurring forms of chlorophyll.

One theory about the natural chlorophyll *a* complexes is that there is a comparatively small number of definite and universally distributed forms of chlorophyll *a* each with its own definite and constant absorption spectrum. Accordingly the variation in the shape of measured absorption spectra for different algae and for fractions prepared from chloroplasts is attributed to variations in the relative proportions of these few specific compounds. For many years this concept has been implicit in the work of this laboratory. Another theory, apparently of greater validity, is that the forms of chlorophyll are pigments with absorption maxima of slightly different wavelength positions and widths depending on the source or treatment of the material. A third concept is that there may be such a large number of chlorophyll *a* complexes that their absorption peaks may be found more or less at random from 662 to beyond 715 nm. We expect that the work in progress may clarify the relative merits of these three contrasting ideas.

The effect of anomalous dispersion on the measurements of absorption spectra of chlorophyll complexes is an ever re-

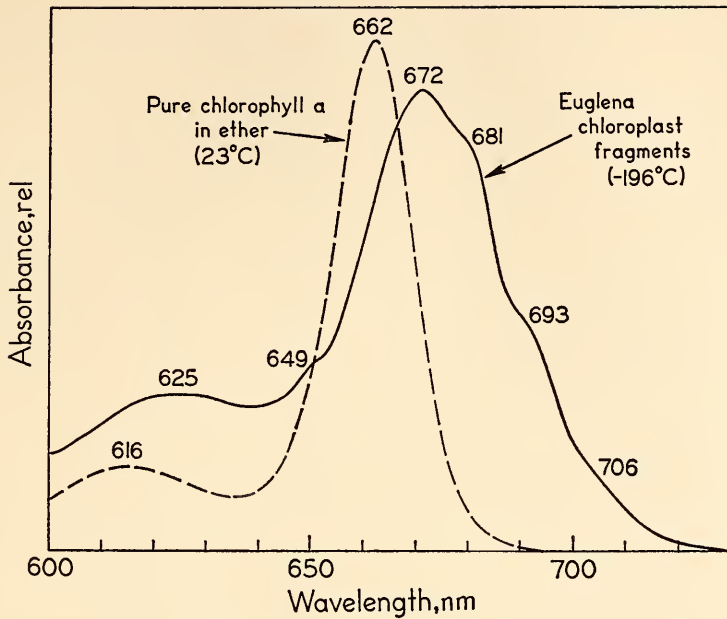


Fig. 45. The spectrum of the alga *Euglena* shows bands due to four different forms of chlorophyll *a* at 672, 681, 693 and 706 nm. Each of these forms has its own characteristic spectrum presumably somewhat similar to that for isolated chlorophyll *a* (broken line) but shifted in wavelength. The small band at 649 nm is due to chlorophyll *b*.

curing question. This large change of refractive index of a solid pigment near its absorption band makes the light scattering from pigment particles highly wavelength dependent. The light-scattering and hence the average length of the light path, both within an individual particle and in the sample as a whole, are greater on the long wavelength side of an absorption band. The direct effect of changes of scattering with wavelength is reasonably well taken care of by opal glass plates or similar means of insuring that a nearly constant fraction of the light from the sample reaches the detector. However, the increased average path length of the beam on the long wavelength side of an absorption band remains a potential source of error. This is because a large increase in path length, even in a region of actually decreasing absorbance, could give the appearance of an absorption band that in reality may be due only to increased path length.

To take an extremely sceptical point of view one may ask if the absorption band near 680 nm is a real absorption band from which the presence of a particular form of chlorophyll "Ca 680" may be identified or if this observed peak is at least partially due to increased scattering on the long wavelength side of the 670-nm absorption peak. In fact, the extreme sharpness of the "680" peak in some chloroplast fractions studied this year may eventually be attributed more to scattering by anomalous dispersion than to absorption. The studies in progress on the shapes of absorption spectra of chlorophyll complexes bear directly on the question. The application of theory, such as it is, to experimental measurements of mixed absorption and scattering phenomena (Latimer, *Year Book 56*, p. 265) is not a simple matter although such an attempt has been made elsewhere in the past year (Hagemeister, 1968) with intact *Chlorella* cells.

Some of the different chlorophyll *a* complexes are known from action spectra to be associated with two different photochemical reactions in photosynthesis. By comparison with the precision of absorption spectrophotometry, the determination of action spectra is a crude operation at best. Furthermore, the fractionated chloroplast particles whose pigment systems are of particular interest may have very low activities for the measurable photochemical reactions, which makes it more difficult to get action spectra for the fractions than for whole chloroplasts.

Action spectra must of necessity be measured at room temperature; however, it is useful to measure absorption spectra at liquid nitrogen temperature because peaks are sharpened, and overlapping components become more evident. Components resulting from the analysis of spectra at low temperature may then be used to estimate at least the number, and possibly the widths and shapes, of chlorophyll components in room temperature absorption spectra.

As emphasized in *Year Book 66*, p. 171, we are continuing to study mainly the spectra of finely disintegrated chloroplasts or of very pale mutants to avoid distortion effects that would make the data unsuitable for precise curve analysis. This year the improved chloroplast fractionation method of J.-M. Michel and M.-R. Michel-Wolwertz has made it possible to get spectral measurements of more significant material. The use of a digital computer has greatly extended our ability to analyze the shapes of the spectra. In addition to our own measurements we have obtained some original records of particularly significant spectra from colleagues in other laboratories.

Comparisons of spectra at 23° and -196°C. In order to use the sharper low-temperature spectra as a guide in the analysis of room temperature absorption curves we would like to know how the spectra of the individual forms of chlorophyll *a* change with temperature.

Fig. 46 gives the absorption spectra of a very pale *Chlorella* mutant showing only very slight narrowing of the absorption at low temperature. The middle curves of this figure, for a pale mutant *Aesculus* leaf (California buckeye), also show a small narrowing combined with a shift to shorter wavelength by low temperature. The upper curves of Fig. 46, however, illustrate the more usual effect of low temperature. Here we see a strong narrowing of Ca 677 and Cb 648 while Ca 668 appears to be only slightly sharpened. From this figure it is evident that a simple general quantitative relation between all bands at room temperature and at low temperature is not likely to exist. This effect of temperature on the shape of the absorption bands is one of the questions susceptible to investigation by curve analysis.

The RESOL program. Dr. Don D. Tunncliffe of the Shell Development Laboratory, Emeryville, California, gave us a very versatile computer program for the analysis of spectra. This was written for the IBM 7090 and 7094 computers and modified by Mrs. Gilman and Mr. Beebe of the Stanford University Computation Center, User Services Group for the 360/67 computer to which we have access. The plotting routine has been adapted to our needs and some further program modifications are still being made by one of us (Mark Lawrence).

To analyze spectra the absorbance is entered in digital form usually at 1-nm wavelength intervals. Trial component bands are estimated by inspection of the curve or from previous analyses of the same or of other curves. Their wavelength peaks, heights, halfwidths, and the proportions of Gaussian to Lorentzian shape are roughly estimated and entered. The computer will then optimize these four parameters of each band to give the best fit to the absorbance curve. Because all parameters of each component are adjusted for each iteration the convergence is rapid. A dozen or fewer

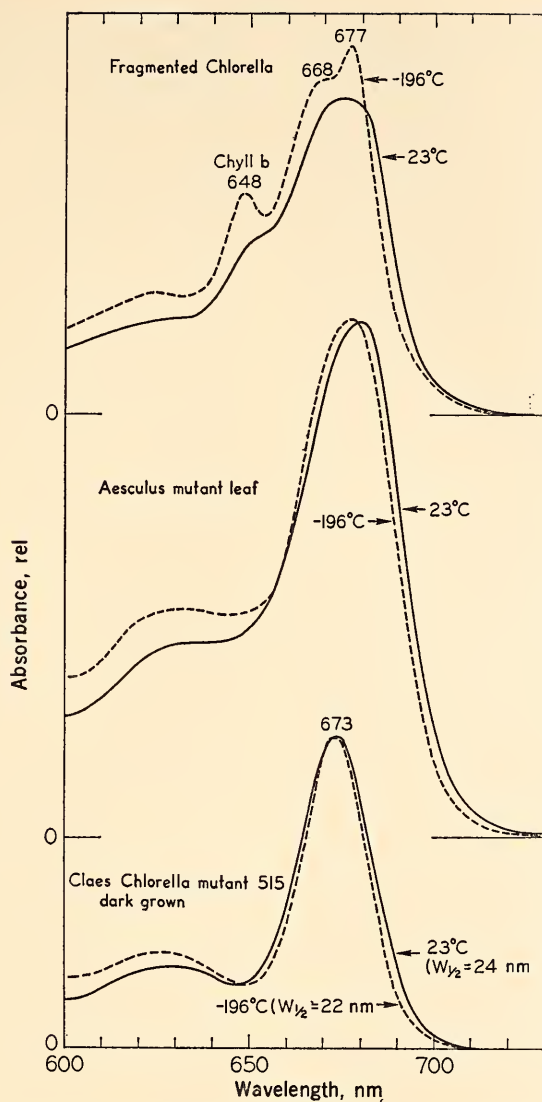


Fig. 46. The absorption spectra of three plants are shown at room temperature and at liquid nitrogen temperature. The amount of band sharpening is not the same for all plants nor for all the bands in a single plant.

iterations will usually suffice to bring the standard deviation to a value that changes less than the specified amount (usually 0.2%) per iteration.

Gaussian curves are wider near the top and narrower at the bottom than are Lorentzian curves of the same width at half height. Since the program optimizes

the proportions of the two functions for each component band, this adjustment of the band shape can improve the fit near the tails of the bands over that given by Gaussian curves alone.

By appropriate selection of the trial input bands, some "guidance" toward one or another possible combination may be

made when the number of bands entered is adequate for more than one solution. The corollary of this flexibility is that if too many bands are used, a mathematically correct solution can be achieved that may have no physical meaning in terms of pigment components. The input bands are modified by the program until the change of standard error of fit for each iteration is within the limit specified. The procedure is thus essentially a means of improving the parameters of the input bands selected by eye. By using a preliminary solution as a guide in the choice of input band parameters for a second solution, improved fits can be had and occasional absurdities may thus be avoided.

The output is given as plotted curves for the derived components, for their sum, for the original data, and for the difference between the sum and the data. The parameters of the derived components are also tabulated. This versatile program allows for choices of types of input data, for variations in the operations performed, and for various presentations of output. Assorted options of fitting procedure, weighting factors, and tolerances may be selected. Conversions of input data to frequency or wavelength scales may be made. If desired, transmission can be entered for conversion to absorbance before the curve analysis.

The provisions for handling a background correction may also be used as a means of entering known bands and using the program to evaluate the residual components. The program itself may be used to determine the number and position of bands from the peaks and inflections. Above all, results can be obtained rapidly and at reasonable cost.

The DSPEC program. It is often useful to compare spectra by subtracting one curve from another. Before doing this it is necessary to have one of the curves plotted to a scale that would make the heights attributable to one or another of the components equal in the two curves. Generally the factor needed to accomplish this objective is unknown. Therefore, a whole family of

difference curves have to be plotted with a series of factors applied to one of the curves before the subtraction. Inspection of such families of curves can often lead to an approximate estimate of the wavelength peak, the halfwidth, and shape of components that differ in their quantities in the two spectra. Furthermore, these difference spectra can show, by sharp discontinuities, if the two curves compared differ in the types of components as well as in their relative amounts.

A computer program, DSPEC, was written for this purpose with help from Mr. Beebe of the Stanford Computation Center. This program uses curve input data in the same form as does RESOL and produces a family of difference curves each with the desired adjustment factor.

The GRAPHIC program. So far, surprisingly little use has been made of log absorbance curves in analyzing the spectra of chlorophyll complexes. Absorption spectra plotted as log of absorbance against wavelength give, for a pure substance, curves of identical size and shape that differ with concentration only in their position on the height axis. A program to plot spectral data in a standardized logarithmic form has been prepared for use with the new on-line plotter at the Stanford Computation Center. Comparisons of data so plotted are used to select curves significant enough for detailed analysis by RESOL.

Comments on curve analyses. This year J.-M. Michel and M.-R. Michel-Wolwertz found that the width and shapes of components having nearly the same peak wavelength in two fractions of the same chloroplasts can be very different from each other. Thus there seems to be a distinction of width and shape as well as of peak wavelength between several natural forms of chlorophyll. This fact greatly changes the previous simple assumption that all "Ca 670" and "Ca 680" components used for curve analysis should be identical.

Each chlorophyll form must have its own complete spectrum although we can

only study the shapes of the red part of the spectrum because of carotenoids and other colored substances that interfere below about 500 nm. The major red peak has a far more distinctive shape than do the lower bands near 625 and 585 nm. We need to know not only the characteristics of the major red band but also the relation of the shorter bands to the main peak for each form of chlorophyll. At present the emphasis is on the major red peak. To match it with simple curves of known shape it is, however, necessary also to use some sort of approximation to the bands near 585 and 625 nm because the tail of the 625-nm band overlaps the main component. Attempts to resolve the 625-nm band into several components have not yet succeeded.

Some illustrations of work in progress. During the year two reports have been prepared that include curve analyses of chlorophyll in vivo (French *et al.* and French and Prager, 1968). We will give here a few examples of the potentialities and limitations of the curve fitting procedure as an aid in the understanding of complex absorption spectra.

To evaluate the comparative merits of different curve fitting procedures, the same curves were analyzed in various ways. One of these was the absorption spectrum of pure chlorophyll *a* in 80% acetone prepared from *Euglena* by M.-R. Michel-Wolwertz. Even this simple curve seems to have a "hidden" band at about 650 nm. It is unlikely that this component represents a trace amount of residual chlorophyll *b* because the starting material contained very little chlorophyll *b* even before purification and the peak of this hidden component is nearer 650 nm than 645 nm, where it would be for chlorophyll *b* in 80% acetone. Furthermore, a similar hidden component was also necessary to match the data of Smith and Benitez for pure chlorophyll *a* in ether.

The following comparisons of different curve fitting procedures were made: all

Gaussian, all Lorentzian, mixed Gaussian and Lorentzian; wavelength, wave-number; equal weights for all points, weight proportional to square of absorbance. For each case the standard error of the computed fit is given in Table 12.

Components of pure Gaussian shape gave much better fits than those of pure Lorentzian shape but mixed Gaussian and Lorentzian shapes of the same width at half height and the same wavelength center were better than pure Gaussian curves. This improvement was particularly evident on the long wavelength tail. If mixed Gaussian and Lorentzian shapes are used, the need for another small, long-wavelength band may be avoided in some cases. The fit obtained by weighting the upper part of the bands was better than with equal weighting. Matching the curve with symmetrical components on a wavenumber plot, while perhaps theoretically preferable to a wavelength plot, has so far not given appreciably better fits. The very satisfactory fit for mixed Gaussian and Lorentzian components on a wavelength plot is given in Fig. 47(A).

The standard errors refer to the error of fit between the measured heights of the spectral curves and the sum of the hypothetical components at each wavelength, as illustrated in the error curve below the analyzed spectra. The height units are the counter readings of the curve digitizer; 1 unit=0.00842 in.

TABLE 12. Standard Errors of Fit for Spectrum of Pure Chlorophyll *a* in 80% Acetone Matched in Different Ways by Four Components

Shapes of Component Curves	Wavelength Scale	Wavenumber Scale
Points Weighted Proportional to (Absorbance) ^a		
Gaussian	4.04	3.54
Lorentzian	9.98	10.44
Mixed	2.36	2.40
All Points Weighted Equally		
Mixed	2.79	2.73

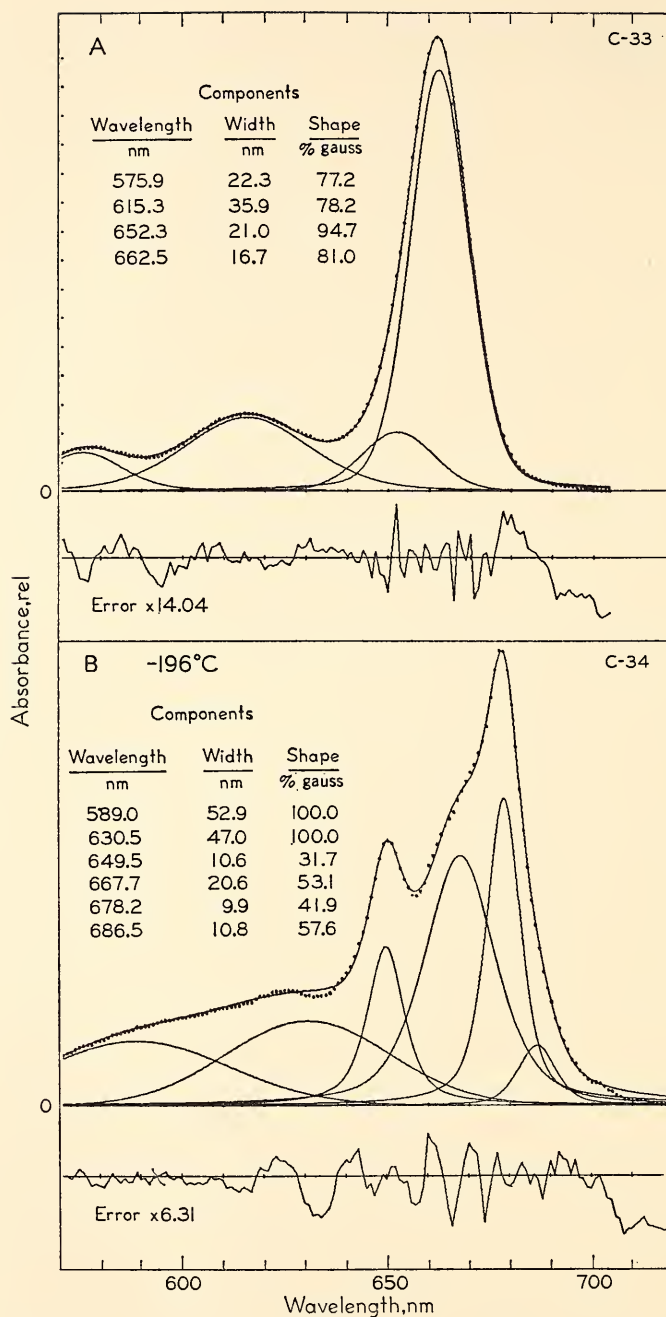


Fig. 47. (A) The absorption spectrum for pure chlorophyll *a* in 80% acetone from M.-R. Michel-Wolwertz, shown by points, was matched by the sum of four components by RESOL. The standard error of fit was 2.36. (B) The absorption spectrum at -196°C of fraction 2 from *Stichococcus* was matched by hypothetical components. The standard error of fit was 5.35.

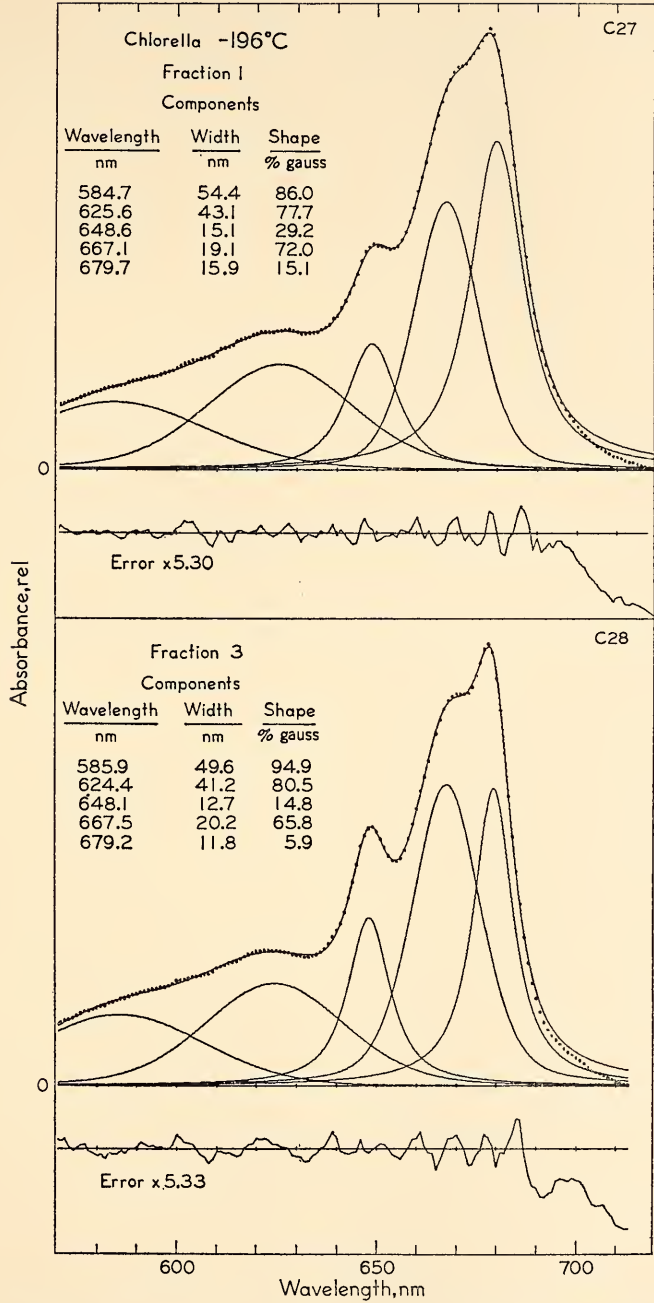


Fig. 48. Absorbance spectra of two fractions from disintegrated *Chlorella* chloroplasts separated by centrifugation in a sucrose gradient matched with hypothetical component curves. Data from M.-R. Michel-Wolwertz.

A much more complicated curve analysis is presented in Fig. 47(B) for the absorption of a fraction of chloroplast particles prepared from *Stichococcus*. This is a particularly interesting sample because of its high chlorophyll *b* content and its sharp 677.5-nm peak. This represents a second attempt but nevertheless still shows deviation from our concept of the most believable components. The 630.5-nm band is probably too broad; the chlorophyll *b* at 649.5 nm is probably nearly reasonable; the 667.7-nm band should probably be narrower and more Gaussian; and the 686.5-nm component should be lower and at a longer wavelength. Both the accuracy of fit and the plausibility of the component curves representing bands of the pigments present can certainly be improved.

In Fig. 48 are comparable analyses of two *Chlorella* chloroplast fractions of M.-R. Michel-Wolwertz. Again this is a second approximation and subject to further modification. Another component near 695 nm combined with the Lorentzian shape of the 677- and 679-nm bands would be preferable. The standard errors of fit 3.46 and 3.45 have been reduced from the previous values of 5.75 and 6.05 (French *et al.*, in press, Fig. 6). This pair of analyses is based on the idea that the main difference in the two curves is in the width of the 679-nm component rather than in the possible presence of another long wavelength pigment in fraction 1 at 687 nm.

A very rough attempt was made to characterize the difference between the two spectra for the *Oenothera* mutants in Fig. 18 of Fork, Heber, and Michel-Wolwertz (this report, p. 504). One of these mutants lacks photosystem 1 activity while the other lacks system 2 activity. The curves have their greatest difference at wavelengths longer than 680 nm. This difference may be due to an extra chlorophyll *a* component specifically active in photosystem 1. However the distinction could equally be due simply to differences in the bandwidth

and wavelength position of some chlorophyll components. On that assumption, the "Ca 680" component in the curve for the mutant with system 2 activity would have its peak at 677 nm, and a narrow bandwidth, while the "Ca 680" analogue in the curve for the system 1 pigment would have a peak near 682 nm and a larger bandwidth. A situation of that sort is believed to account for the difference in the two *Chlorella* fractions illustrated in Fig. 48.

A possible test for the plausibility of the extra component theory versus the above explanation is to examine the calculated difference spectra between the two curves, using a series of fractions applied to one curve before the subtraction. These difference curves are uninterpretable if made from spectra that differ otherwise than in the relative amounts of common components. Thus difference spectra having sharp discontinuities indicate that comparisons have been made of curves composed of dissimilar components.

The results of this application of the DSPEC program to the curves of Fig. 18 is shown in Fig. 49. The small differences between the curves are magnified about 3.5 times so most of the small irregularities have no significance in this plot. A smoothed line was drawn more or less between the two top curves, corresponding to a factor of 0.895. At 641 nm there is a dip perhaps due to a form of chlorophyll *b* in the system 2 preparation. This dip is shown inverted at the bottom of the figure. The dip was omitted in drawing the hypothetical spectrum for the extra component of photosystem 1. The hypothetical component so derived is shown in the lower part of Fig. 49. Its peak at 687 nm has a halfwidth of 13.5 nm and the side band, $H=0.26$, has a broad maximum somewhere near 650 nm. There is a wide tail possibly due to a component with a 708-nm peak. The accuracy of the records is hardly sufficient to do more than to suggest the

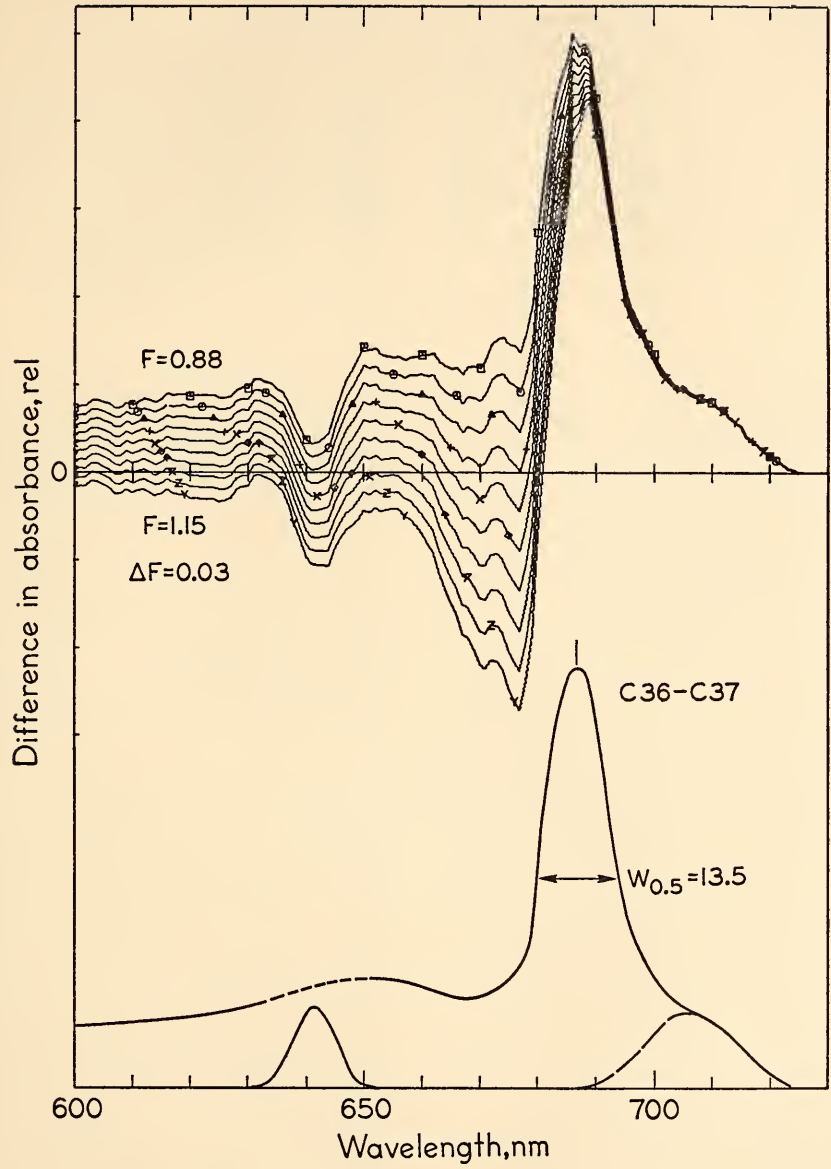


Fig. 49. Enlarged difference spectra between the curves of Fig. 18 with a series of fractions applied to the photosystem 2 curve before subtraction. If an extra component in the photosystem 1 curve that is lacking in the other is the cause of the difference between the two, the spectrum of that component will resemble the lower curve. The small component at 641 nm shown below has been omitted from the estimated difference component attributed to system 1.

possible presence of this long wavelength component.

In general the experience with curve analyses so far has been that a complete solution from a single attempt is likely only if the bands are clearly evident in the input data. For more complex curves, susceptible to being fitted by a variety of mathematically adequate solutions, some judgment in choice of input bands can be made to guide the fitting toward a solution having a reasonable physical

meaning in terms of actual pigment components.

References

- French, C. S., M.-R. Michel-Worwertz, J.-M. Michel, J. S. Brown, and Lillian Prager in *Symposium on Porphyrins*, T. W. Goodwin, ed., Biochem. Soc. London, pp. 000-000, (In press), 1968.
 French, C. S., and Lillian Prager in *Proc. Intern. Congr. Photosynthesis Research*, H. Metzner, ed., (In press), 1968.

STAFF ACTIVITIES

The Botanical Society of America awarded one of its two annual Certificates of Merit to Dr. William M. Hiesey "In recognition of distinguished achievement in and contributions to the advancement of botanical science, ecological physiology and imaginative experiments. A pioneer in elucidating the geneecological nature of species; he has done much to encourage and help students in all areas of plant science."

Dr. Olle Björkman was awarded the degree of Doctor of Philosophy "with great distinction" at the University of Uppsala in December 1967. This degree is awarded in Sweden only to outstanding scholars and confers the title of Member of the Faculty at the University of Uppsala. Dr. Björkman's paper "Comparative Studies on Photosynthetic Properties of Species and Races of Higher Plants from Ecologically Diverse Habitats" reviews some of his research that prompted the awarding of the degree.

The Experimental Taxonomy group served as host to visiting classes of biology students from Stanford University, the University of California at Berkeley, and the University of California at Santa Cruz. Classes led by Dr. Herbert Baker of Berkeley, Dr. Jean Langenheim of Santa Cruz, and Dr. John Thomas of Stanford included field trips to the Stanford, Mather, and Timberline field stations.

Members of the Institution staff have

lectured to advanced students on special topics in experimental ecology and on photosynthesis. Drs. Björkman and Fork were appointed "Associate Professor of Biology by Courtesy" at Stanford University for the year 1968-1969.

In addition to the work reported for this year, the Department facilities were used by some Stanford faculty and the following individuals:

Dr. Dan McMahon of the Department of Biophysics at the University of Chicago spent the month of September 1967 at our laboratory in an effort to isolate the enzyme ribulose diphosphate carboxylase in clones of *Mimulus cardinalis*, originally from different climates, known to differ in their capacity for CO₂ uptake at normal air concentrations. Crude extractions were made at this Department for final purification at the University of Chicago. Mrs. Mary Mantuani, a graduate student at Duke University, together with her husband, utilized the facilities at the Mather station during the summer of 1967. She obtained climatological and ecological field data as background information for experimental laboratory work being continued at Duke. Her study embraces a comparison of tolerance to water stress in ecological races of *Solidago*. Since the spring of 1967, Mr. Lafayette C. Eaton, a graduate student in the Department of Biological Sciences at Stanford, has been conducting a comparative study on the pattern of varia-

tion in morphology, seasonal responses, and survival in the *Ranunculus californicus* complex as expressed at the Stanford and Mather transplant stations.

Dr. Hiesey participated in an International Biological Planning Conference and a field trip that was held at Caracas, Venezuela, in November 1967.

Dr. Brown served as Secretary-Treasurer for the Stanford Chapter of Sigma Xi

and attended the Annual Meeting in New Hampshire in October.

This year a small lot was purchased from the fund given the Institution by Dr. Bush for staff recreation. Plans for a cabin are being considered. This heavily forested land is nearly adjacent to the Tomales Bay State Park and within a short distance of the Point Reyes National Seashore.

BIBLIOGRAPHY

- Amesz, Jan, and David C. Fork, The function of P700 and cytochrome *f* in the photo-synthetic reaction center of system 1 in red algae, *Photochem. Photobiol.*, **6**, 903-912, 1967.
- Amesz, Jan, David C. Fork, and W. Nooteboom, Function of the pigments of the reaction center of system 1, *Gatersleben Symposium, Studia Biophysica*, **5**, 175-181, 1967.
- Amesz, Jan, *see also* Fork, David C.
- Björkman, Olle, Comparative studies on photosynthetic properties of species and races of higher plants from ecologically diverse habitats. Printed privately, 1967.
- Björkman, Olle, Carboxydismutase activity in shade-adapted and sun-adapted species of higher plants, *Physiol. Plantarum*, **21**, 1-10, 1968.
- Björkman, Olle, Further studies on differentiation of photosynthetic properties in sun and shade ecotypes of *Solidago virgaurea*, *Physiol. Plantarum*, **21**, 84-99, 1968.
- Brown, Jeanette S., Fluorometric evidence for the participation of chlorophyll *a*-695 in system 2 of photosynthesis, *Biochim. Biophys. Acta*, **143**, 391-398, 1967.
- Brown, Jeanette S., Fluorescence emission spectra of a diatom, *Seventh Intern. Congr. Biochem., Tokyo, Abstracts V*, 898, 1967.
- Brown, Jeanette S., Chlorophyll absorption and fluorescence in *Ochromonas danica*, *Biochim. Biophys. Acta*, **153**, 901-902, 1968.
- Brown, Jeanette S., and M.-R. Michel-Wolwertz, Chlorophyll fluorescence near 720 m μ in *Euglena* extracts, *Biochim. Biophys. Acta*, **153**, 288-290, 1968.
- Clausen, Jens, Biosystematic consequences of ecotypic and chromosomal differentiation, *Taxon*, **16**, 271-279, 1967.
- Fork, David C., and J. Amesz, Light-induced shifts in the absorption spectrum of carotenoids in red and brown algae, *Photochem. Photobiol.*, **6**, 913-918, 1967.
- Fork, David C., and Ulrich W. Heber, Studies on electron-transport reactions of photosynthesis in plastome mutants of *Oenothera*, *Plant Physiol.*, **43**, 606-612, 1968.
- Fork, David C., and Yaroslav de Kouchkovsky, Light-induced spectroscopic changes in leaves of a higher plant and in *Chlorella*, *Biochim. Biophys. Acta*, **153**, 891-894, 1968.
- Fork, David C., *see also* Amesz, Jan.
- French, C. Stacy, Changes with age in the absorption spectrum of chlorophyll *a* in a diatom, *Arch. Mikrobiol.*, **69**, 93-103, 1967.
- French, C. S., Energy transfer between pigments of photosynthesis, *Seventh Intern. Congr. Biochem., Tokyo, Abstracts II*, 355-356, 1967.
- French, C. S., Fluorescence spectra for several forms of chlorophyll *in vivo*, *Seventh Intern. Congr. Biochem., Tokyo, Abstracts V*, 898, 1967.
- French, C. S., Chairman's remarks: Part I, Molecular and Structural Aspects, in *Comparative Biochemistry and Biophysics of Photosynthesis*, K. Shibata, A. Takamiya, A. T. Jagendorf and R. C. Fuller, eds., University of Tokyo Press, University Park Press, State College, Pa., pp. 106-110, 1968.
- French, C. S., *see also* Heber, U.
- Heber, U., and C. S. French, Effects of oxygen on the electron transport chain of photosynthesis, *Planta*, **78**, 99-112, 1968.
- Heber, U., *see also* Fork, David C.
- Kouchkovsky, Y. de, *see* Fork, David C.
- Michel-Wolwertz, M.-R., *see* Brown, Jeanette S.
- Nooteboom, W., *see* Amesz, Jan.
- Reid, August, Interactions between photosynthesis and respiration in *Chlorella*, *Biochim. Biophys. Acta*, **153**, 653-663, 1968.

SPEECHES

- Amesz, J., D. C. Fork, and W. Nooteboom, Function of the pigments of the reaction center of system 1, Symposium, Plastidenpigmente und ihre rolle im photosynthese prozess, Gatersleben, East Germany, October 2, 1967.
- Björkman, Olle, Photosynthetic differentiation and adaption in plants from ecologically diverse habitats, Seminar, Department of Biological Sciences, Stanford University, Stanford, California, May 1, 1968.
- Björkman, Olle, Differentiation of photosynthetic properties among plants native to habitats with contrasting levels of irradiance, Seminar, Department of Botanical Sciences, University of California at Los Angeles, Los Angeles, California, June 4, 1968.
- Clausen, Jens, The genetic structure of natural ecological entities, Lecture, Department of Biology, University of California at Santa Cruz, Santa Cruz, California, October 10, 1967.
- Fork, David C., Investigations on primary reactions and components involved in electron transport of photosynthesis, Seminar, Department of Biological Sciences, Stanford University, Stanford, California, November 20, 1967.
- Fork, David C., Light-induced reactions of P700, cytochrome *f*, carotenoids and chlorophyll *b* in the photosynthesis of algae and higher plants, Seminar, Department of Biology, Temple University, Philadelphia, Pennsylvania, April 22, 1968.
- French, C. S., Energy transfer between pigments of photosynthesis, Symposium on Bioenergetics, Seventh International Congress of Biochemistry, Tokyo, August 19, 1967.
- French, C. S., Photosynthesis, National Association of Biology Teachers, Annual Meeting, Anaheim, California, March 2, 1968.
- French, C. S., Closing session report on biophysics of plastid pigments, International Congress of Photosynthesis Research, Freudenstadt, Germany, June 8, 1968.
- French, C. S., and Lillian Prager, Absorption spectra for different forms of chlorophyll, International Congress of Photosynthesis Research, Freudenstadt, Germany, June 6, 1968.
- French, C. S., M.-R. Michel-Wolwertz, J.-M. Michel, J. S. Brown, and Lillian Prager, Naturally occurring chlorophyll types and their function in photosynthesis, Symposium on Porphyrins and Related Compounds, Biochemical Society, University College, London, April 19, 1968.
- Heber, Ulrich W., Photo-induced shrinkage in leaves, Seminar, Department of Biochemistry, University of California at Davis, Davis, California, April 26, 1968.
- Heber, Ulrich W., Control of cyclic electron flow in vivo by photosystem II and electron acceptors, Seminar, Laboratory of Chemical Biodynamics, Lawrence Radiation Laboratory, University of California at Berkeley, Berkeley, California, April 30, 1968.
- Heber, Ulrich W., Effects of oxygen on chloroplasts, International Congress of Photosynthesis Research, Freudenstadt, Germany, June 5, 1968.
- Michel, Jean-Marie, Fractionation of the photosynthetic apparatus in chloroplasts, Seminar, Department of Physiology, University of California at Berkeley, Berkeley, California, March 20, 1968.
- Michel, Jean-Marie, Fractionation of chloroplast lamellae by density gradient centrifugation, International Congress of Photosynthesis Research, Freudenstadt, Germany, June 7, 1968.

PERSONNEL

Biochemical Investigations

Staff: C. Stacy French, *Director*; Jeanette S. Brown, David C. Fork; James H. C. Smith, *Emeritus*

Carnegie Corporation Fellow: Ulrich W. Heber¹

Institution Research Fellows: Marie-Rose Michel-Wolwertz,² Jean-Marie Michel,² Eckhard E. Loos,³ James M. Pickett⁴

Technical Assistants: Mark C. Lawrence, Lillian K. Prager⁵

Experimental Taxonomy

Staff: Olle Björkman, William M. Hiesey, Malcolm A. Nobs; Jens C. Clausen, *Emeritus*

Institution Research Fellows: Eckard Gauh,⁶ James H. Silsby⁷

Technical Assistant: Frank Nicholson

Visiting Investigator: Daniel McMahon⁸

Gardener: Archibald H. Lawrence⁹

Summer Research Assistant: Steven G. Wood¹⁰

Part-time Garden Helpers: James M. Barnes,¹¹ Andrew J. Libertone¹²

Illustrator: Carolyn R. Clark¹³

Clerical Assistant: Marylee Eldredge

Accountant-Administrative Secretary: Clara K. Baker

General Department Secretaries: Lena R. Barton,¹⁴ Wilta M. Stewart¹⁵

Mechanical Engineer: Richard W. Hart

Custodian: Jan Kowalik

Custodian-Helper: Wayne E. Miller¹⁶

¹ From May 3, 1967, through April 30, 1968. From Botanisches Inst. der Universität Düsseldorf, Bonn.

² From January 4, 1967, through March 30, 1968. From Centre de Recherches de Gorsem-St. Trond, Belgium.

³ From January 6, 1968. From Institut für Angewandte Botanik, Technische Hochschule, Munich.

⁴ From October 1, 1965, through July 28, 1967. From Department of Zoology, University of Texas, Austin, Texas.

⁵ From July 1, 1967.

⁶ From April 11, 1967. From Botanisches Institut der Johann Wolfgang Goethe-Universität, Frankfurt.

⁷ From July 21, 1967, through May 1, 1968. From University of Adelaide, Waite Agricultural Research Institute, Glen Osmond, Australia.

⁸ From August 24, 1967, through October 2, 1967. From the Department of Biophysics, University of Chicago, Chicago, Illinois.

⁹ From July 1, 1967.

¹⁰ From June 15, 1967, through September 15, 1967, and from June 19, 1968.

¹¹ From June 8, 1967, through September 30, 1967.

¹² From October 3, 1967.

¹³ From July 5, 1967, through July 21, 1967.

¹⁴ From April 12, 1966, through October 31, 1967.

¹⁵ From November 3, 1967.

¹⁶ From August 16, 1967, through September 15, 1967.

PLATES

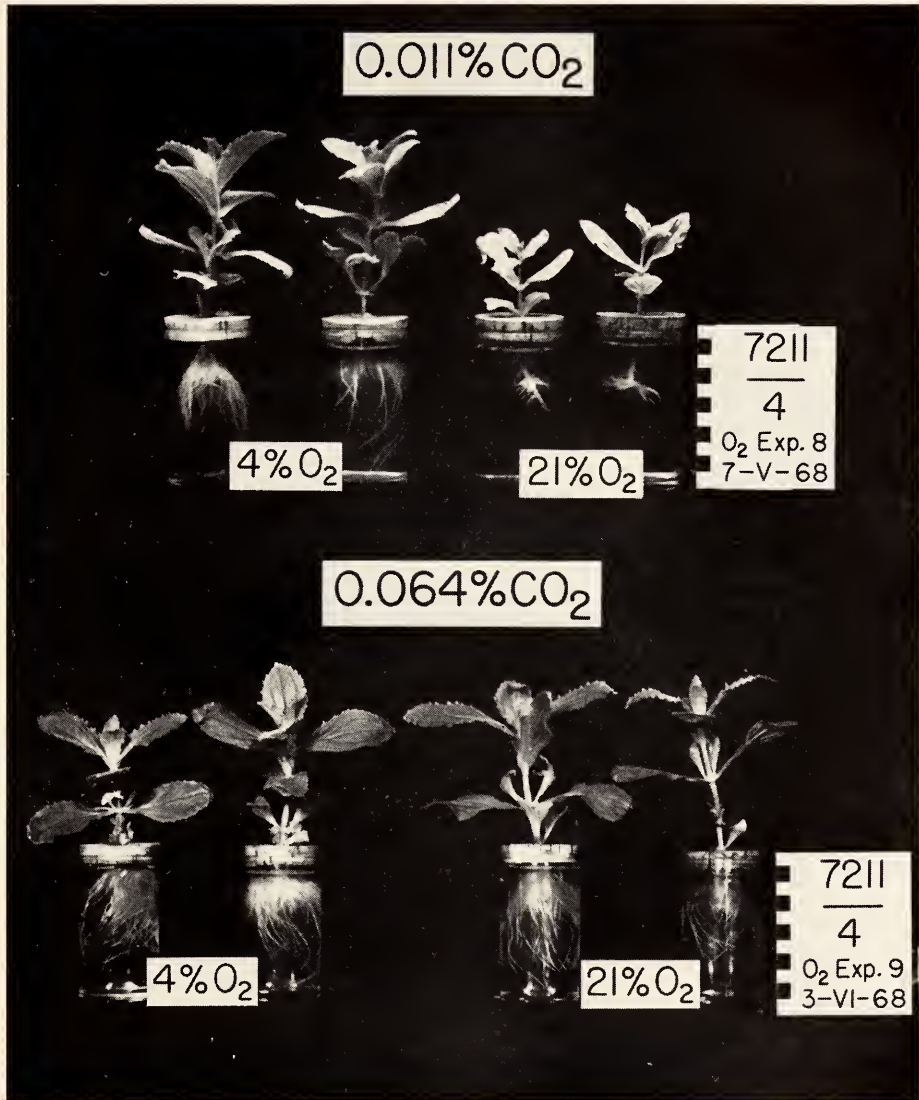


Plate 1. Growth of *Mimulus cardinalis*, Jacksonville 7211-4, under 21% and 4% oxygen and two different levels of CO_2 .

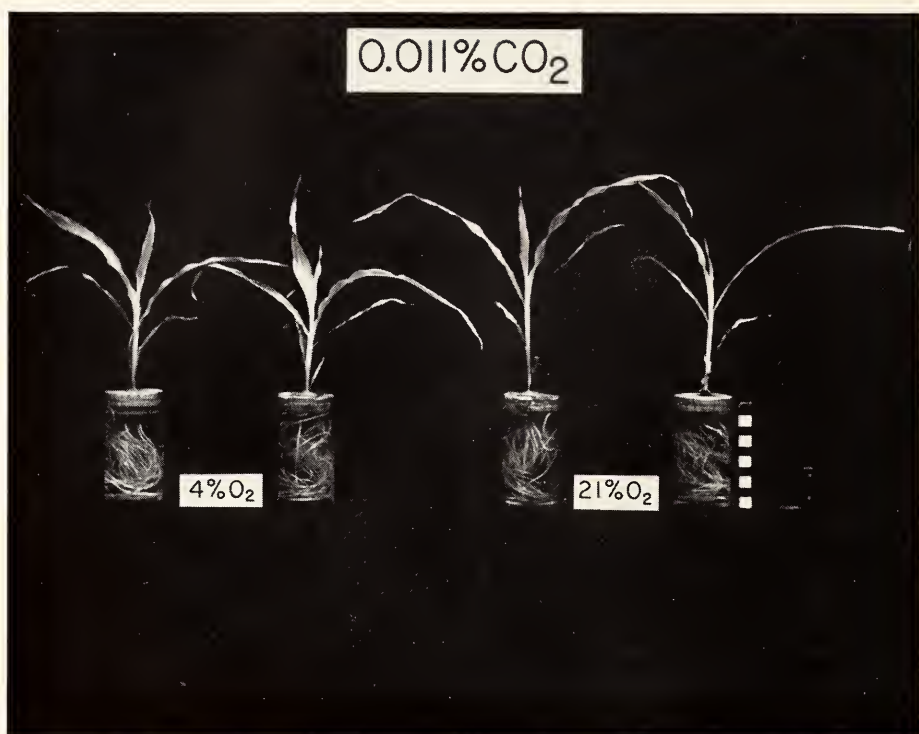


Plate 2. Growth of *Zea mays*, Ferry-Morse hybrid 901, under 21% and 4% oxygen and a low CO₂ concentration.

Genetics Research Unit

Cold Spring Harbor, New York

Alfred D. Hershey

Director

Contents

Introduction	555
Structure and Function of Phage DNA's	556
Segmental distribution of nucleotides in λ DNA	556
The molecular site of the repressor gene	557
Transducing phages	558
Phage $\phi 80$	560
Origin of λ DNA synthesis	561
Requirements for replication of T4 DNA	561
The T4- λ universe	562
Bibliography	568
Personnel	568

INTRODUCTION

Elucidation of the structure of DNA has had consequences of two sorts. As all interested people know, it set off a numerous and continuing train of successes in the analysis of the living machine. It also led to conclusions of more general significance: notably, that natural phenomena do not present immovable obstacles to human comprehension.

One of our less machinelike attributes, as humans, is our tendency to ask whether problems are soluble in principle. The answer has never been clear. In fact, human history can be epitomized in terms of modes of seeking the answer. The scientific mode, impressive as its record is in many ways, engenders its own grounds for reasoned doubt.

J. D. Watson, in his Nobel Lecture, stated part of the difficulty very clearly. "In pessimistic moods," he wrote, "we often worried that the correct structure [of DNA] might be dull—that is, that it would suggest absolutely nothing. . . ." Indeed, both the history of speculation about DNA structure, and the record of chemical pharmacodynamics as a whole, encouraged such pessimism. As it turned out, the correct structure suggested a great deal, and it is this result, not the structure itself, that illuminates.

I once publicly expressed a similar pessimism in connection with my own work on genetic recombination. Phage research, I complained, is beset with the following difficulty. One notices a phenomenon that looks interesting. After suitable thought and labor, one performs an experiment that ought to be instructive. What it actually does is to turn up a second phenomenon not related in a simple way to the first. This sequence of events makes for lively research. It does not provide explanations.

As practicing scientists we don't have to be much concerned about the search for explanations, because the discovery

and description of natural phenomena are ends in themselves. As philosophers, though, we have to consider the possibility that the sequence I have described may prove endless, giving an indefinitely complicated description of nature without making us, in human terms, appreciably wiser. To an outsider, this seems to be the state of affairs in research on the structure of matter at both ends of the scale of magnitude. For somewhat similar reasons, what goes on in atomic nuclei, outer space, and living cells might prove equally refractory to explanation. This must be roughly what Watson and Crick dreaded in their pessimistic moments.

What do we seek in a scientific explanation? Our universe is necessarily described in terms of conceptual fictions: mass, field, electromagnetic wave, energy quantum, genome, or, for that matter, gross national product. These we combine into relations that have predictive value. At this stage we have a successful theory but hardly an explanation, for Apollo's chariot serves as well as Newtonian principles in appropriate areas of prediction. According to P. W. Bridgman, we arrive at explanations by establishing, among items of experience, connections that are independent of the operations by which our fictions are defined. Apollo is manifest only in the sun, which places him in the unscientific category of hypotheses beyond dispute. By contrast, Bouguer found gravity in a Peruvian mountain, and rotational inertia must have been noticed by the inventor of the wheel.

There are not many explanations of the sort exemplified by classical mechanics, certainly not many in biology. Most biological explanations necessarily borrow their elements from mechanics and chemistry. The exceptions, such as the metabolic role of enzymes and the

evolutionary origin of species, are interesting in the present connection and share common features. Darwin's hypothesis is perfectly satisfactory as an explanation, since its elements, hereditary variation and selection, are demonstrable independently of the process they explain. It fails as a theory because, like all historical schemes, it deals with unique events, says nothing about direction, and lacks predictive value. Similar qualifications apply to metabolic principles.

In short, the DNA revolution is one of a small class of successful scientific revolutions, and should renew significantly our confidence that the structure of the universe is eventually decipherable. As Albert Einstein wrote in an earlier context, "... [scientific] endeavors are based on the belief that existence should have a completely harmonious structure. Today we have less ground than ever before for allowing ourselves to be forced away from this wonderful belief."

Note that a scientific explanation has a negative aspect: it must not introduce any new conceptual fictions. (If it does, the explanation rests in abeyance until the new fictions can be independently authorized. Hence Bouguer's search for Newton's action at a distance.) Gunther Stent, in a charming and luminous essay recently published in *Science*, has stressed this negative aspect of the DNA revolu-

tion, which uncovered no paradox unique to living things.* According to the point of view I have presented, his essay might be described as a lament for success. Of course, one may argue that discovery of primary concepts is more important than explanation, or even that explanations stale the freshness of the human outlook. But these are untestable hypotheses.

Barbara McClintock, now Distinguished Service Member of our group, continues her work on controlling mechanisms in maize. Her new status carries the privilege of aperiodic publication. Readers of this report will miss her written contribution, but may know that her influence is there just the same.

Rudolf Werner's work on replication of T4 DNA, referred to in previous *Year Books*, has been published in the *Journal of Molecular Biology*. In March he moved next door, to the Laboratory of Quantitative Biology. He no longer reports in these pages, but he too remains one of us.

Phyllis Bear left our group in December 1967 to join the faculty of the University of Wyoming.

The work described in the following pages was partly supported by a research grant, GM15876, from the National Institute of General Medical Sciences, U. S. Public Health Service.

STRUCTURE AND FUNCTION OF PHAGE DNA'S

Segmental Distribution of Nucleotides in λ DNA

Skalka, Burgi, and Hershey

For some years it has been clear that the DNA molecule in particles of phage λ contains segments of unlike composition. This is conveniently demonstrated by breaking the molecules, which are initially uniform in density, into fragments. The fragments exhibit a density that depends on average nucleotide composition and varies with place of origin in the

molecules. As shown by Nandi, Wang, and Davidson, one can accentuate the density differences by combining the DNA with mercury. We described in previous reports our principal methods of

*Stent cites Schrödinger and Bohr as prophets of "other laws of physics" presumed to reside in the hereditary substance. The curious reader should be able to find a textbook of physiological chemistry, probably out of date when I read it around 1930, whose author expressed in his preface the opinion that atoms composing living matter would turn out to possess unique attributes.

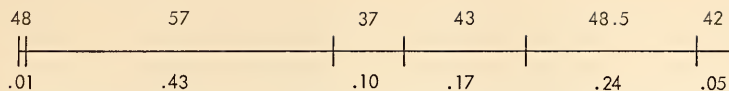


Fig. 1. Nucleotide distribution in λ DNA. The compositions of segments, expressed in mole per cent guanine plus cytosine, are given above the line; fractional molecular lengths below. The orientation places gene A on the left.

analysis (*Year Book 65*, pp. 559-562) and preliminary results (*Year Book 66*, pp. 650-651; reprint, pp. 6-7). This year we pursued the analysis about as far as the methods permit, with rather greater success than we had anticipated. We identified six intramolecular segments. Their arrangement in the molecule is illustrated in Fig. 1. A full account of the work has been published in the *Journal of Molecular Biology*. There we discuss the significance, actually obscure, of the proposed structure.

The Molecular Site of the Repressor Gene

Bear and Skalka

In bacteria lysogenic for phage λ , the functioning of most phage genes is in-

hibited by a protein, called repressor, that is the product of a gene called c_I situated in the right half of the genetic map of the phage. As far as is known, only c_I and an adjacent gene called *rex* function under these conditions, and other genes are not transcribed.

Phyllis Bear took advantage of the circumstance described above to locate the genes c_I and *rex* in our physical map of the λ DNA molecule. Though she encountered many difficulties, her experiment is simple in principle. She broke λ DNA molecules into small fragments, sorted them into fractions of unlike nucleotide composition by density analysis, and passed equal volumes of each fraction, heated to separate the DNA strands, through membrane filters. This gave her a series of filters containing

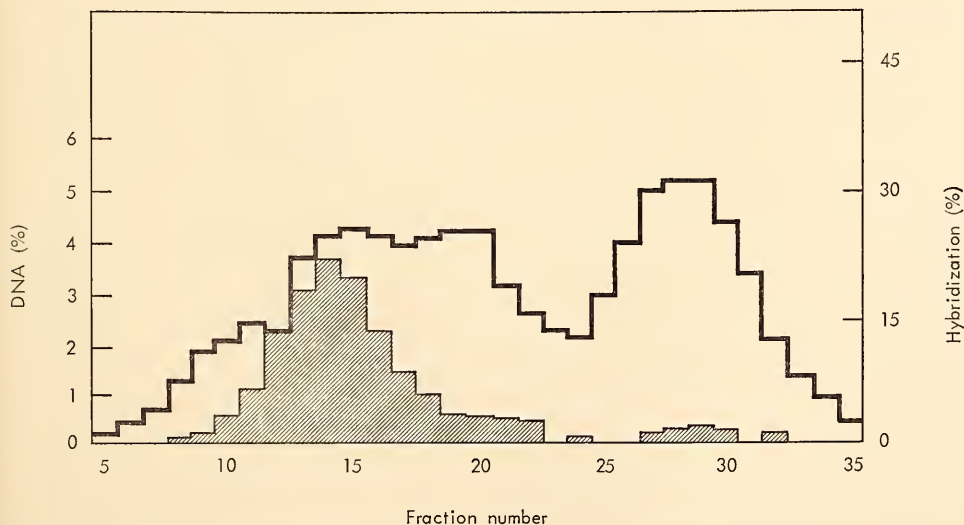


Fig. 2. Hybridization of messenger RNA with λ DNA fractions. Outer histogram: λ DNA fragments of fractional molecular length 0.05 separated according to density in 42.5% Cs_2SO_4 containing 0.22 mole HgCl_2 per mole of nucleotides. The four bands, left to right, contain DNA of 37%, 43%, 48.5%, and 57% GC. Shaded histogram: hybridization of λ messenger RNA, isolated from uninduced lysogenic bacteria, with DNA from each fraction.

various amounts of DNA but representing, in effect, equal numbers of copies of individual genes. She then isolated labeled RNA from lysogenic bacteria, fractionated it by hybridization with λ DNA to enrich for phage-specific messenger, and tested the messenger for hybridization with the DNA fractions affixed to filters. Her results, presented in Fig. 2, show that the RNA binds specifically to DNA of 43% GC content. Reference to Fig. 1 shows that this DNA originates mainly from the segment of fractional molecular length 0.17 whose center lies at fractional distance 0.38 from the right molecular end. Therefore c_1 and rex are two of perhaps five genes that could be accommodated in this segment.

Dove (*Ann. Rev. Genet.*, 1968), citing data from several sources, puts c_1 at fractional distance 0.25 from the right molecular end. His estimate is consistent with Bear's, even though neither may be very exact.

The results verify in a direct way that repression of gene function specifically suppresses the transcription of the repressed genes. Bear's experiments also demonstrate a useful means for determining the GC content of RNA.

Transducing Phages

Yamagishi and Skalka

Phage λ has contributed in many ways toward an understanding of genetic recombination. To appreciate this contribution, one must clearly distinguish three kinds of recombination seen in λ .

The first kind, observed in ordinary phage crosses involving homologous chromosomes, is the molecular equivalent of the process described in textbooks of genetics. Meselson showed that the parallels include reciprocal exchanges and, probably, four-strand exchanges. Meselson, Weigle, and others brought to light recombination by literal breakage and reunion of DNA molecules. The same authors, and, with particular clarity, Kaiser and Hogness, demonstrated the

congruence of the genetic map with molecular structure in DNA. The now commonplace fact that genetic crosses yield information about topology of DNA molecules is less than ten years old.

Ordinary genetic recombination can occur at any internucleotide bond (for example, within anticodons, as shown by Henning and Yanofsky), and is equational in the sense that the parental numbers of nucleotides per gene are conserved in recombinants (as shown by Crick, Barnett, Brenner, and Watts-Tobin in the drastic effect of exceptions). These properties place recombination in the same category as replication: processes dependent on pairing between complementary nucleotide sequences. In λ , ordinary recombination is catalyzed by the function of a phage gene, *red*, and by the function of an equivalent bacterial gene, *rec* (Signer and Weil; Echols and Gingery).

The second kind of genetic recombination seen in λ is responsible for the reversible insertion of prophage into the bacterial chromosome, a process for which Campbell invented the proper model (*Year Book 66*, pp. 651-657; reprint, pp. 7-13). Prophage insertion and excision differ from the exchanges described above in three respects: matching nucleotide sequences cannot be confidently invoked (*Year Book 66*, pp. 657-660; reprint, pp. 13-16), the exchanges occur at a unique site in each DNA, and they depend on the function of a phage gene *int* (Zissler; Gingery and Echols; Gottesman and Yarmolinsky). The function of *int* is itself site-specific, but is otherwise equivalent to that of *red*. Thus *int* function can substitute for *red* function with respect to ordinary recombination at the appropriate site, but *red* function does not measurably assist in prophage insertion. Other differences, implied by the words insertion and recombination, are topological, not mechanistic.

The third type of recombination seen in λ brings about excision of prophage

in such a manner as to give rise to structures in which both phage and bacterial genes are represented. The recoverable structures, usually chromosomes of transducing phage particles, consist of a continuous segment of prophage DNA joined to a continuous, adjacent segment of bacterial DNA (Arber, Kellenberger, and Weigle, 1957; Campbell, 1957). Kayajanian and Campbell (1966) identified this type of recombination as illegitimate crossing over, in the technical sense that it does not depend on linear homology between phage and bacterial chromosomes.

The generation of transducing phage lines by illegitimate crossing over of the sort described is a rare event largely inaccessible to direct analysis. It is not even clear as yet whether or not the process depends on *rec*, *red*, or *int* functions, because when these are not provided, transducing phage particles of an atypical kind make their appearance (Gottesman and Yarmolinsky; Gingery and Echols). This result, which may signify a fourth category of recombination catalyzed by the hypothetical enzyme that cuts the molecular ends of λ DNA, illustrates a point made in the Introduction: that in biology one process often interferes with the analysis of another.

The origin of typical transducing lines of λ can perhaps be accounted for by a process that resembles recombination of the first kind except for one known difference: the interacting DNA's are not homologous. According to this view, recombination of the third kind would depend on a nonlinear pattern of matching nucleotide sequences in the DNA's of λ and its host, *Escherichia coli*. Then the only resemblance to normal prophage excision (recombination of the second kind) would be topological.

Yamagishi and Skalka undertook to determine whether or not matching nucleotide sequences in phage and host DNA's are distributed in the same manner as the observed exchanges that generate transducing phage lines. If they

are, bacterial DNA recovered from *gal*-transducing phages must resemble the left half of λ DNA, and bacterial DNA recovered from *bio*-transducing phages must resemble the right half of λ DNA. This prediction follows from the model of Kayajanian and Campbell for the origin of transducing phage lines (*Year Book 66*, pp. 651-657; reprint, pp. 7-13).

Yamagishi and Skalka retrieved bacterial DNA from the $\lambda dg(A-J)$ of Adler and Templeton, and from the $\lambda dbio$ M55-3 of Kayajanian. Skalka's previous work with λdg illustrates the principal method (*Year Book 66*, pp. 657-659; reprint, pp. 13-15). She found that the segment of bacterial DNA lying between *gal* and the prophage has the uniform composition 51% GC, the same as that of the bacterial DNA as a whole. The segment found in $\lambda dbio$, on the contrary, proves to contain subsections ranging in GC content from 37% to 50%. Thus a certain resemblance is evident between the *gal* region of *E. coli* DNA and the left half of λ DNA (Fig. 1), and between the *bio* region of *E. coli* DNA and the right half of λ DNA.

The distribution of matching nucleotide sequences, expressed in terms of results of the appropriate DNA-DNA hybridization tests, shows the following features. (1) Bacterial DNA recovered from either transducing phage binds more efficiently to λ DNA than does unselected bacterial DNA. (2) Bacterial DNA from $\lambda dgal$ binds equally to right and left halves of λ DNA. (3) Bacterial DNA from $\lambda dbio$ binds preferentially to right halves of λ DNA. Thus the distribution of matching nucleotide sequences is such as to permit and even encourage the kinds of illegitimate crossing over that generate transducing phages.

The results suggest a resemblance between the left half of λ DNA and the *gal* region of *E. coli* DNA, and another between the right half of λ DNA and the *bio* region of *E. coli* DNA. The resemblances are weak but are perceptible both in local composition and in sequence of

nucleotides, a correlation that is obligatory if matching sequences are numerous and clustered (*Year Book 65*, pp. 562-565). Given the observed types of λ transducing phages, and the hypothesis of their origin by crossing over at match points, one sees the germ of a functional explanation for the observed distributions of nucleotides in phage and host DNA's in the constraints imposed by the pattern of their habitual interactions. Differentiated segments in two interacting DNA's should resist the manifest selective influences that otherwise favor uniformity. More important, one might expect positive selection for differences in composition between elements whose interaction could be profitably discouraged. These are not idle thoughts. They lead to the prediction that the sort of structure found in λ DNA should be characteristic of specialized transducing phages, not of phages like P1 that disseminate bacterial genes by another mechanism.

Related experiments performed by Laura Ingraham some years ago were less edifying, though not, in fact, inconsistent with the ideas just presented. Ingraham found, in collaboration with Naomi Franklin, that the DNA of bacterial strains, deleted in the vicinity of the prophage insertion site of $\phi 80$, did not show diminished ability to hybridize with the DNA of that phage. Such experiments should be repeated with appropriately defined bacterial deletion mutants.

We suggest as a general inference that all recombination processes represent variations on a single theme. Those giving rise to transducing phages are inefficient by design. Because illegitimate crossing over is a rare event, it can afford to sacrifice precision for the sake of adventure.

Phage $\phi 80$

Skalka

The phage $\phi 80$ is one of several species related in many ways to λ . Comparison of

structure of the two DNA's might be expected to clarify relatedness, on the one hand, and to provide clues to interdependence of structure and function on the other, notwithstanding the perennial difficulty that these two aspects of comparative structure tend to defeat each other.

Skalka has analyzed structure and transcription of the DNA of $\phi 80$ by methods previously applied to λ . She finds, in molecules of $\phi 80$ DNA, a GC-rich half that, by analogy with λ DNA (Fig. 1), can be called the left half. Then it turns out that the two DNA's terminate in identical cohesive sites at their left ends, as shown by the fact that left molecular halves of either DNA can join only to right molecular halves of either. Both DNA's contain long segments of high GC content (55% in $\phi 80$) in their left halves, and both terminate on the left in short segments of lower GC content. Hybridization tests show a moderate cross-reaction (20% for the unfractionated DNA's), which is strongest in the left half of each. In both DNA's the late-functioning genes reside in left molecular halves, as determined by hybridization tests with messenger RNA.

Right molecular halves of the two DNA's terminate in identical cohesive sites, contain early-functioning genes, and show similar discontinuities in nucleotide composition. They differ appreciably, however, in average composition (45% GC in λ , 51% in $\phi 80$), and show relatively weak cross-reactions in hybridization tests. The central segment of low GC content found in λ has no counterpart in $\phi 80$ detectable either by density analysis or by hybridization tests.

Messenger RNA synthesis in bacteria infected with the respective phages is entirely similar, characterized by slow transcription of right molecular halves at early times and rapid transcription of both halves, but predominantly the left, at late times.

The relatedness of the two phages is therefore clearly evident as linear homology in their DNA's. The differences are instructive, however. Our work with λ was prompted in part by our biological prejudice that structural singularities necessarily serve some useful purpose. Some of Skalka's results with λ were compatible, for instance, with the hypothesis that the switch from early to late phases of transcription depended directly on some device sensitive to local nucleotide composition (*Year Book 64*, pp. 526-527). If that were true, one should expect early and late messengers to differ markedly in composition even in a phage like $\phi 80$, where the average compositions of large DNA sections do not differ greatly. Since Skalka's results with $\phi 80$ fail to verify the prediction, she concludes that patterns of transcription are not directly dependent on nucleotide composition.

Skalka plans to extend comparative analysis along the lines indicated to a few additional phage species.

Origin of λ DNA Synthesis

Makover

If a replicating DNA molecule contains a number of growing points that started from a single origin and are moving in the same direction, a nucleotide sequence lying ahead of the first growing point should be represented only once in the replicating structure, whereas a sequence lying between the n^{th} and $n+1^{\text{th}}$ growing points should be represented $n+1$ times. Sueoka and his colleagues exploited this principle to determine the sequence of replication of genetic markers in *Bacillus subtilis*. Makover is using it to determine the sequence of replication of the segments of λ DNA of dissimilar nucleotide composition (Fig. 1).

Makover finds, first of all, that the appropriate experiments are feasible. He treats bacteria with mitomycin to destroy their capacity for synthesis of their own DNA, infects them with phage, and

feeds tritiated thymidine to the culture for just three minutes to label replicating phage DNA. He then extracts DNA from the cells, mixes it with differently labeled DNA from phage particles, breaks the DNA in the mixture to small fragments, and fractionates these according to nucleotide composition as illustrated in Fig. 2. He finds that the replicating and nonreplicating DNA's in the mixture form identical distributions except for a quantitative bias that he attributes to sequential replication of the several molecular segments. His results show that the 48.5%-GC segment is one of the first to be replicated. He hopes that further experiments will define both origin and direction of replication. What is more important, he may be able to verify the general model of replication in a single direction from a unique starting point.

Makover's results are consistent with other facts. A line of λdg from which the 57%-GC section of DNA (Fig. 1) has been deleted is able to synthesize DNA (Brooks; Echols, Skalka, and others; also analogous experiments by Dove and Franklin). A chromosomal locus (ri), situated near the right end of the genetic map, is a plausible candidate for the starting point of DNA synthesis (Dove, Hargrove, and Haugli).

R. L. Sinsheimer, in whose laboratory the mitomycin treatment was first applied in experiments with λ , furnished the requisite bacterial strain.

Requirements for Replication of T4 DNA

Mosig and Ehrling

Gisela Mosig, now at Vanderbilt University, is continuing her physical and genetic study of T4 phage particles which, by some sort of biological accident, end up with a DNA fragment of two thirds the normal molecular length (*Year Book 64*, pp. 521-524). Such particles contain a random segment of the T4 chromosome, as shown, among other ways, by the fact that two or more par-

ticles attaching to a single bacterium can usually initiate infection, whereas one particle cannot.

In the summer of 1966, Mosig returned to our laboratory to collaborate with Ruth Ehring in an effort to determine whether or not a single DNA fragment can replicate. Mosig and Ehring infected bacteria with the incomplete phage particles, added radiophosphorus to the culture, extracted DNA from it some time later, and measured the amount of radioactivity in T4 DNA by hybridization tests. Unfortunately, there is an irreducible limit to the sensitivity of such experiments, because some bacteria necessarily get infected with two or more phage particles. However, Mosig and Ehring found that little or no DNA synthesis ensued in singly infected bacteria.

In the genetic map of T4, known in great detail from the work of Epstein, Edgar, and colleagues, there are a number of genes essential for DNA synthesis. Seldom could all these genes be represented in a DNA segment of two thirds the normal length. This consideration sufficiently explains the observed result. However, as Mosig and Ehring point out in their paper, DNA fragments lack terminally repetitious nucleotide sequences, which may also be essential for DNA synthesis. Mosig is investigating this possibility.

The T4- λ Universe

Hershey

I discuss here certain aspects of DNA structure which, though not especially new, are still sufficiently novel to provoke thought. The serious reader may find it helpful to have at hand my previous discussions of related matters (*Year Book 63*, pp. 589-592; *Year Book 66*, pp. 647-657; reprint, pp. 3-13).

The main historical facts are worth recalling for their own sake. Streisinger, Edgar, and Denhardt, in the first of a series of three papers written between 1961 and 1963, and published between 1964 and 1967, predicted faithfully on the basis of genetic experiments the structure of T4 DNA verified by Thomas and Rubenstein (1964) and MacHattie, Ritchie, Thomas, and Richardson (1967). So much for the complementarity principle according to which genetics and chemistry were to provide immiscible information.

Campbell in 1962, likewise on the basis of genetic experiments, predicted a rather different structure for λ DNA. That structure was verified by Hershey, Burgi, and Ingraham (1963), Ris and Chandler (1963), and Wu and Kaiser (1968).

My universe of discourse is presented in Fig. 3, which shows information dia-

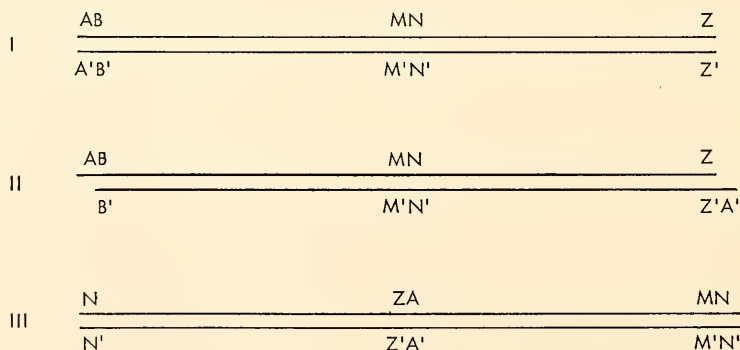


Fig. 3. Three bihelical DNA molecules represented as information diagrams. Each letter signifies a nucleotide sequence of arbitrary length; each primed letter, the corresponding complementary sequence.

grams of three bihelical DNA molecules. Each letter in the figure stands for a nucleotide sequence of arbitrary length, and each primed letter for the corresponding complementary sequence.

Structure I, though it conforms to the classic model of 1953, is not known to exist. It may be characterized as an open sequence possessing a twofold redundancy of language in a code of pairwise complementarity.

Structure II could be derived from structure I by Maxwell's demon without the performance of work. But he would have to violate the principles of information theory that dominate DNA synthesis, because structure II contains the sequence Z'A' missing in I. Structure II is slightly less than twofold redundant, and contains slightly more information per nucleotide than structure I. Note that joining the complementary ends of structure II, which does not alter information content because scientists can do it reversibly, results in a closed sequence with exactly twofold redundancy. Thus the extra information in structure II is the potentiality of closure; messages I and II contain the same number of sentences. Structure II, characterized by a non-repetitive terminal redundancy, is that of λ DNA.

Structure III could be derived from structure II by an energetic but mindless demon or, in fact, by Kornberg's DNA polymerase. The two structures have the same information content but differ in mass. The increased mass is associated with the terminal repetition, which makes structure III appreciably more than twofold redundant. Structure III also possesses the potentiality of closure, albeit in a slightly hidden form. The ends of structure III can be joined in the laboratory with the aid of nonspecific enzymes to form a closed sequence with exactly twofold redundancy.

Structure III as I have drawn it also differs from structure II in sentence order. In fact, the sentence alphabet permits 26 cyclic permutations, which are

equivalent since the cyclic structure is common to all. Structure III and its cyclic permutations represent T4 DNA, characterized by terminal repetition and circular permutation. T4 DNA molecules exist as isomeric systems representing, perhaps, 200,000 permuted structures.

Phage λ also permutes its nucleotide sequences to form prophage, but only the one cyclic permutation is known, and DNA molecules isolated from λ phage particles are all alike (*Year Book 66*, pp. 650-657; reprint, pp. 6-13).

I conclude that DNA language is not human language and that information theory of the message variety is not serviceable for both. Consider a message A through Z in which sentence Z is a paraphrase of A. Then, for purposes of human communication, we have $A-Z = A-YA = A-Y$, and Z serves only to minimize errors of transmission. In the language of DNA chemistry, A-Y and A-YA are not equivalent, and open sequences of the type A-Y may well be meaningless. Furthermore, we can write $A-YA = N-YA-N$ for DNA language, a rule implying a degree of independence in the meaning of individual sentences not common in human messages. This second difference is only one of degree, and DNA sentences must surely remain intact in the long run. Lambda sees to this by cutting between sentences. T4 sees to it by cutting terminal repetitions of generous length. In short, DNA language is a chemical language obeying special topological rules, rules that are enforced by the special kind of twofold redundancy usually found in its messages.

If the redundancy of DNA language plays a special role in reclaiming permuted messages, it also serves, of course, for the ordinary purpose of minimizing accidental losses of information. Single strands of DNA are vulnerable physically because of mechanical fragility and because they are susceptible to a variety of nucleases to which bihelical molecules are refractory. They are vulnerable as

messages because every internucleotide bond is essential to the meaning of the whole. It cannot be accidental that unpaired DNA messages of appreciable length have been found only in encapsulated form in phage particles of several species, and it seems likely, too, that production and encapsulation of single-strand DNA are more or less simultaneous events during phage particle formation. This reasoning also applies to the unpaired ends of λ DNA, which, in spite of their complementary structure, are vulnerable because they form together a joining sequence without which the whole message becomes illegible. Seen in this light, the T4 DNA molecule is no more redundant than its nonrepetitive circular equivalent, and the phrase "terminal redundancy," which derives from the theory of open messages, becomes inappropriate to DNA language theory. I therefore substitute hereafter the phrase "joining sequence."

In 1963 a number of people suggested, mainly on the basis of genetic evidence, that DNA replication starts at a unique nucleotide sequence and proceeds in one direction (Cairns; Jacob, Brenner, and Cuzin; Nagata; Sueoka and Yoshikawa). The model will probably survive as a prototype if not as a universal rule. It introduced the starting sequence as a genetic element of novel kind on which replication depends. It also contained the implication, not obvious in 1963, that joining sequences constitute a second obligatory element. (The model was actually proposed for circular structures.)

Let us notice at the outset that there are at least two difficulties in this model. One of the reasons for proposing a unique starting point in the first place was to account for the fact that not just any piece of DNA can replicate. If joining sequences are also obligatory, that particular argument evaporates. The second difficulty is more pervasive. Doermann and Boehner showed in beautiful experiments that certain heterozygotes in phage

T4 can be characterized as structures with overlapping ends that replicate as such. According to Streisinger and Stahl and their colleagues, this means that, to a limited extent, T4 replicates its terminally repetitious nucleotide sequences without joining them. Readers of the following paragraph will note that the results of Doermann and Boehner contradict all aspects of the 1963 model for DNA replication. In discussing that model, I am in effect assuming that T4 replicates its DNA in two ways: one to account for the results just mentioned, one to account for other facts. For similar reasons, I ignore evidence recently gained by Huberman and Riggs that DNA sometimes replicates in two directions from a common starting point. As it happens, the model proposed by Huberman and Riggs nicely accounts for the results of Doermann and Boehner.

If DNA replicates from a unique starting sequence, it is unlikely in general, and is clearly impossible among the permuted molecules of T4, that the starting point is situated at a molecular end. If, in addition, replication proceeds in a single direction, end-to-end joining becomes necessary for completion of the replication cycle, and DNA language is seen to have a mechanical origin. Joining of either of the two sorts seen in λ DNA can serve: ring formation or chain formation. (Incidentally, catenate and concatenate are misused verbs and adjectives. Perhaps catemer is a preferable noun.) Thus end joining, not circularity as such, is the characteristic feature of DNA messages. Both rings and chains are needed: rings to simplify replication of single molecules and to serve other genetic purposes (*Year Book 66*, pp. 651-657; reprint, pp. 7-13); chains to permit length variation in the joining sequences of T4 (Streisinger, Emrich, and Stahl, 1967). In T4, owing to the permuted sequences, chains cannot be formed by literal end-to-end joining but must be synthesized directly from a circular template or arise by recombinative processes.

In λ , the possibility that molecular chains are formed by joining is structurally plausible and cannot be excluded on kinetic grounds. In view of the vulnerable nature of open ends, few replicating DNA molecules are likely to possess them. However, in vitro λ DNA molecules with complementary ends separated by an average distance of at least 13.5 μm form rings at appreciable rates. In a bacterium, a single pair of complementary ends, whether belonging to one molecule or two, cannot be distant from each other by more than about one micrometer. Thus, other things being equal, single DNA molecules in bacterial cells should form rings at least $(13.5)^3$ times faster than they do in bulk solution. Moreover, in cells the competition between chain formation and ring formation becomes a numerical problem indifferent to DNA concentration as such. For instance, if one could introduce several λ DNA molecules into a bacterium simultaneously, formation of a unimolecular ring would be an exceptional event.

In contrast to the continuously variable joining sequences in T4, phage λ has evolved two specific kinds: the molecular ends already discussed, and the ends of the cyclically permuted prophage. For each a specific cutting mechanism must be postulated. The molecular ends are better known than the prophage ends, but a cutting mechanism has been put in evidence only for the prophage ends. The two situations reinforce the common model for λ , on the one hand, and the more general model including T4 on the other. Since I shall have few occasions to speak of the prophage ends of λ , my phrase "joining sequences" will refer to those at the molecular ends.

The nature of the T4- λ DNA message suggests that DNA replication depends on at least four categories of genetic elements: one or more starting sequences; one or more enzymes (and perhaps anti-enzymes) directly responsible for DNA synthesis, including something that rec-

ognizes starting sequences; joining sequences; and a mechanism for the regeneration of joining sequences from joined sequences. In λ , the last function is supplied by a hypothetical gene *ter* that ensures production of a hypothetical cutting enzyme able to open joined ends. In T4, the corresponding function is supplied by a hypothetical device for measuring lengths of DNA. The fourth element of either kind is not essential for DNA synthesis as such, but serves as a primitive segregation mechanism for the preservation of molecular structure (Frankel, Weissbach).

The known joining sequences provide a model for a mechanism of genetic recombination catalyzed by at least one sort of cutting enzyme. In fact, Signer and Weil have shown that the hypothetical cutting enzyme that opens λ prophage ends specifically biases recombination frequencies measured in ordinary crosses: a nice demonstration of the abstract power of genetic analysis.

In λ the specific joining sequences and the hypothetical starting sequence differ in operational respects from genes. Presumably they function without translation, and their structural role could hardly be subject to complementation. They belong to a category of DNA structures called recognition sites by Dove. The operator serves as the classic example and the joining sequences at the molecular ends in λ DNA provide the least ambiguous example. Note, however, that in the molecular ends of T4, and for purposes of genetic recombination between homologous chromosomes in general, all sequences become recognition sites.

A unique starting sequence for DNA replication is in principle identifiable by deletion analysis, which for λ has been carried out in a remarkably complete way by Kayajanian and Campbell. I state here only limited aspects of their results.

Recall that joining sequences in λ DNA lie at the center of the permuted

map of the prophage, that deletions of the right prophage end can be selected by recovery of *gal*-transducing phage lines, and that deletions of the left prophage end can be selected by recovery of *bio*-transducing phage lines (*Year Book 66*, 651-657; reprint, pp. 7-13). Deletions of either class span various lengths of DNA up to, but never including, the joining sequences. Left-end deletions, the longest of which include all the known genes essential for DNA synthesis, result in defective phage particles able to replicate DNA when helped by normal λ present in the same bacterium. Right-end deletions result in defective phage particles able to replicate DNA on their own.

From these results, Kayajanian and Campbell drew conclusions of the following sort.

1. The joining sequences are essential for encapsulation of DNA in phage particles. That they are also essential for DNA synthesis is suggested by the experiments of N. Franklin and Dove with bacteria containing partially deleted prophages.

2. A unique starting sequence for DNA synthesis cannot lie in the right half of the prophage, that is, in subterminal parts of the left half of the DNA molecule shown in Fig. 1.

3. Rather unexpectedly, the results do not put in evidence any starting sequence recognizable as a structure with non-complementable function essential for DNA synthesis. Simply interpreted, this would mean that there is no unique starting sequence, or that the starting sequence is situated in or near the joining sequence at either molecular end. It could also mean something else, and that alternative I present in the arbitrary statements that follow (also suggested, in part, by Kayajanian).

- (a) Any piece of DNA terminated by λ joining sequences can be replicated in the λ system because absence of a starting sequence in one member of a tandem complex can be made good by the starting sequence in a neighboring member.

According to this hypothesis, the starting point for λ DNA synthesis could lie anywhere in the right molecular half.

- (b) From (a) it follows that unimolecular rings cannot be strongly preferred templates for synthesis of DNA incorporated into λ phage particles.

- (c) Any piece of DNA of suitable length, bounded by λ joining sequences, can be encapsulated by the λ packaging system.

I should add that these statements are not literally true. Phages λ and $\phi 80$ possess, as far as we know, DNA's with identical joining sequences. Yet Dove (*Ann. Rev. Genet.*, 1968) finds, in contradiction to my assertion (a), that certain mutations in the DNA of one of these phages prevent its replication in the presence of the other. Dove also states that λ and $\phi 80$ possess distinct DNA-encapsulating systems, in contradiction to my assertion (c). As he points out, the latter contradiction disappears if one imagines that a species-specific cutting enzyme recognizes a few nucleotide pairs adjacent to the joining sequences proper. If that is so, assertion (a) may also be true with trivial qualifications. My point here is that a proper answer to any of these questions should include the answer to all—especially the one concerning the starting point for DNA synthesis.

Diverse evidence from the work of Dove, Weigle, Weissbach, Siminovitch, and others shows that a defect in any of several DNA encapsulation genes of λ interferes with the opening of the joining sequence in newly replicated DNA. This suggests that the encapsulation genes, lying at the left molecular end, the hypothetical gene *ter* (cutting enzyme), and the joining sequences, form a functional unit ensuring that the joining sequences will open only at the proper moment, a provision otherwise desirable in view of the vulnerable character of the open molecular ends. Synchronization could be achieved by control of transcription; localization in space could be achieved

by suitable protein-protein interactions. These considerations, together with the principle of the clustering of genes of related function, place the hypothetical gene *ter* at the left molecular end.

In λ , clustering of genes of related function is not a principle but a fact. The principle can be debated. R. Thomas pointed out a few years ago the significance of linkage between the structural gene and target site for λ repressor. According to some of my colleagues, the evolutionary significance of clustering was anticipated by R. A. Fisher in 1930. Actual clustering was first clearly demonstrated by Demerec among genes of *E. coli*.

In λ , the joining sequences at the molecular ends form the most obligatory sort of functional unit but are scarcely clustered in the genetic map. This exception to the rule of clustering is a necessary one, but is no less instructive for that. It doesn't help to say that molecular ends are joined in the prophage map, because there the prophage ends come apart. It doesn't help either to say that some historical λ possessed a circular map, because we are looking at λ now. In fact, it appears that clustering is a useful device but one seldom exploited, perhaps, in chromosomes at large. Clustering is a radical principle in relation to genetic recombination; its opposite plays a conservative role. For instance, odd numbers of crossovers (with respect to the ordinary genetic map) between λ and a phage with dissimilar joining sequences should be lethal. In view of Dove's analysis, it seems likely that the same restriction applies to crosses between λ and $\phi 80$. Otherwise, λ is the radical creature par excellence: as seen in the transducing lines; as seen in the DNA of $\phi 80$, which is λ at its conservative ends and, according to Skalka, a sort of ghost of λ in between. I suggest that Fisher's radical clustering principle is opposed by

a conservative unclustering principle, and that history is inscrutable to us precisely because, as Pareto noticed some years back, it mixes incompatible principles. That conclusion didn't daunt Pareto's thinking and doesn't mine.

Why has λ chosen to place its cluster of genes responsible for prophage insertion at the center of the DNA molecule, which automatically places the joined molecular ends at the center of the prophage map? The second consideration seems to be the crucial one. Since the molecular joint is the sole prophage structure indispensable to the formation of a transducing phage, the effect of the existing arrangement is to give λ an equal reach in both directions along the bacterial chromosome for the acquisition of transducible genes. Thus what might be mistaken for an abstract principle of symmetry actually ensures a maximum number of genes transducible in small pieces of DNA. A similar optimizing principle in message theory accounts for the fact that the DNA universe contains equimolar amounts of adenine and guanine.

I conclude this essay by turning for a moment to another phage known as P22, mainly to show that we can do so without leaving the T4- λ universe. Consider just two facts. P22 is a generalized transducing phage; it transports, in rare defective particles, pieces of bacterial DNA selected more or less at random. Its own DNA comes in terminally repetitious and circularly permuted form, like that of T4. As pointed out by Rhoades, MacHattie, and Thomas, who analyzed the DNA, the two facts are not unrelated. Both suggest that P22, like T4, encapsulates DNA by the length-measuring principle: in this case, any available DNA. Thus *E. coli*, in persuading λ to center its joining sequence in the prophage map, just made the best of a second-rate opportunity.

BIBLIOGRAPHY

- Burgi, E., *see* Skalka, A.
 Ehring, R., *see* Mosig, G.
 Hershey, A. D., *see* Skalka, A.
 McClintock, B., Genetic systems regulating gene expression during development. *Develop. Biol.*, Suppl. 1, 84-112, 1967.
 Makover, S., A preferred origin for the replication of lambda DNA. *Proc. Natl. Acad. Sci. U.S.*, 59, 1345-1348, 1968.
 Mosig, G., and R. Ehring, Failure of incomplete T4 genomes to replicate under conditions of single infection. *Virology*, 35, 171-174, 1968.
 Skalka, A., E. Burgi, and A. D. Hershey, Segmental distribution of nucleotides in the DNA of bacteriophage lambda. *J. Mol. Biol.*, 34, 1-16, 1968.
 Werner, R., Distribution of growing points in DNA of bacteriophage T4. *J. Mol. Biol.*, 33, 679-792, 1968.

PERSONNEL

Year Ended June 30, 1968

- | | |
|---|--|
| Phyllis D. Bear, Carnegie Institution Fellow | Anna Marie Skalka, Carnegie Corporation Fellow |
| Elizabeth M. Bocskay, Chief Clerk | |
| Jennie S. Buchanan, Curator of <i>Drosophila</i> Stocks | Carole E. Thomason, Technical Assistant |
| Elizabeth Burgi, Associate in Microbiology | Rudolf Werner, Associate in Research |
| Agnes C. Fisher, Secretary to Director; Editor | Hideo Yamagishi, Carnegie Institution Fellow |
| Alfred D. Hershey, Director | <i>Temporary and Part-Time</i> |
| Laura J. Ingraham, Research Assistant | Kevin Clowe, Technical Assistant |
| Shraga Makover, Carnegie Institution Fellow | John B. Earl, Technical Assistant |
| Barbara McClintock, Distinguished Service Member | Margaret Lieb, Guest Investigator |
| | Barbara A. Lutjen, Typist |

Bibliography

July 1, 1967–June 30, 1968

PUBLICATIONS OF THE INSTITUTION

Carnegie Institution of Washington Year Book 66. Octavo, xi + 76 + 119 pages, 30 plates, 271 figures, Washington, D.C., January 1968.

609. Sixth printing. Anna O. Shepard. *Ceramics for the Archaeologist*. Octavo, 414 pages, 59 figures. July 1968.

626. *Atlas of Solar Magnetic Fields, 1959–1966*. Robert Howard, V. Bumba, Sara F. Smith. 14 pages, 167 maps, boxed. Produced in cooperation with the Office of Naval Research, Washington, D. C., March 1968.

627. *Genetic Variations of Drosophila melanogaster* (Revised from *The Mutants of Drosophila melanogaster*, by C. B. Bridges and K. S. Brehme, Pub. No. 552). Don L. Lindsley and E. H. Grell. Octavo, preface + 472 pages, 8 plates, 147 figures, 4 cytogenetic maps, Washington, D. C., March 1968.

PUBLICATIONS BY THE PRESIDENT

Caryl P. Haskins

Report of the President. Reprinted from *Carnegie Institution of Washington Year Book 66*, 76 pages, 6 plates, 8 figures, January 1968. Excerpts reprinted under title "Evolution or Catastrophe," *Science*, Vol. 159, No. 3671, March 1968, p. 1055, and under title "Science Advances in 1967," in *Here and There, American Scientist*, Vol. 56, No. 2, Summer 1968, pp. 165–181.

What role for science? *Diversity and Interdependence Through Education*, Education and World Affairs, New York, November 1967, pp. 117–122.

Review of D. S. Greenberg's *The Politics of Pure Science: An Inquiry into the Relationship between Science and Government in the United States. American Scientist*, Vol. 56, No. 2, Summer 1968, pp. 140A and 142A.

PUBLICATION BY THE DIRECTOR OF PUBLICATIONS

Donald J. Patton

The United States and World Resources. Octavo, 128 pages, 7 maps, G. Etzel Percy and George W. Hoffman, eds., D. Van Nostrand Co., Inc., 1968.

Report of the Executive Committee

To the Trustees of the Carnegie Institution of Washington

Gentlemen:

In accordance with the provisions of the By-Laws, the Executive Committee submits this report to the Annual Meeting of the Board of Trustees.

During the fiscal year ending June 30, 1968, the Executive Committee held four meetings. Printed accounts of these meetings have been or will be mailed to each Trustee.

The estimate of expenditures for the fiscal year beginning July 1, 1968, has been reviewed by the Executive Committee.

The terms of office of the Chairmen of all Committees of the Board expire on May 3, 1968. The terms of the following members of Committees also expire on May 3, 1968:

Executive Committee

Robert A. Lovett
William I. Myers
Frank Stanton

Finance Committee

Crawford H. Greenewalt

Retirement Committee

Frank Stanton

May 3, 1968

HENRY S. MORGAN, *Chairman*

Report of Auditors

LYBRAND, ROSS BROS. & MONTGOMERY

REPORT OF INDEPENDENT CERTIFIED PUBLIC ACCOUNTANTS

To the Auditing Committee of
Carnegie Institution of Washington:

We have examined the statement of assets and funds balances of Carnegie Institution of Washington as of June 30, 1968, and the related summary statement of changes in funds for the year then ended and the supporting exhibits and schedules. Our examination was made in accordance with generally accepted auditing standards, and accordingly included confirmation from the custodian of investments held at June 30, 1968, and such tests of the accounting records and such other auditing procedures as we considered necessary in the circumstances. We previously examined and reported upon the financial statements of the Institution for the year ended June 30, 1967.

These statements have been prepared on the general basis of cash receipts and disbursements and, as a result, omit accrued income, liabilities and provision for depreciation. Accordingly, they do not purport to present financial position or results of operations as they would appear had generally accepted accrual basis accounting principles been applied in their preparation.

In our opinion, the accompanying financial statements and supporting exhibits and schedules (Pages 4-17) present fairly the assets and funds balances of Carnegie Institution of Washington at June 30, 1968 and 1967, and the changes in funds for the year ended June 30, 1968, on the basis indicated above consistently applied.

Lybrand, Ross Bros. & Montgomery

Washington, D. C.
August 16, 1968

STATEMENT A

ASSETS AND FUNDS

JUNE 30, 1968, and 1967

Assets

	<u>1968</u>	<u>1967</u>
Cash	\$ 273,715.58	\$ 467,505.87
Advances	44,265.83	40,339.54
Investments (cost) — Schedule 2:*		
Governmental obligations	2,907,695.31	2,907,695.31
Nongovernmental bonds	41,176,949.69	41,152,380.99
Corporate stocks	34,539,849.64	33,890,108.41
Mortgage	16,397.31	18,682.65
Land (cost)	368,760.86	362,147.71
Buildings and equipment (cost)	<u>6,497,273.68</u>	<u>6,378,397.45</u>
Total assets	<u>\$85,824,907.90</u>	<u>\$85,217,257.93</u>

Funds

Operating Fund, Exhibit I	\$ 918,043.52	\$ 898,044.58
Restricted Grants, Exhibit 2	(5,893.90)	106,318.98
Endowment and Special Funds, Exhibit 3	78,046,723.74	77,472,349.21
Land, Building, and Equipment Fund, Exhibit 4	<u>6,866,034.54</u>	<u>6,740,545.16</u>
Total funds	<u>\$85,824,907.90</u>	<u>\$85,217,257.93</u>

*Approximate market value on June 30, 1968: \$114,796,473.

STATEMENT B

SUMMARY STATEMENT OF CHANGES IN FUNDS

FOR THE YEAR ENDED JUNE 30, 1968

	Operating Fund (Exhibit 1)	Restricted Grants (Exhibit 2)	Endowment and Special Funds (Exhibit 3)	Land, Building, and Equipment (Exhibit 4)	Total
Balance July 1, 1967	\$ 898,044.58	\$106,318.98	\$77,472,349.21	\$6,740,545.16	\$85,217,257.93
Additions:					
Realized capital gain, net					
Investment income					
Interest			581,336.13		581,336.13
Dividends			2,127,786.27		2,127,786.27
Restricted grants			1,964,750.70		1,964,750.70
Gifts		464,136.06			464,136.06
Other income			38,452.09		38,452.09
Expenditures capitalized			53,413.47		53,413.47
Current year				278,450.58	278,450.58
Prior year				55,730.98	55,730.98
Appropriations					
Budget	4,490,137.00		(4,490,137.00)		
Bush Gift	16,600.00		(16,600.00)		
Transfers					
Unallocated appropriations	(314,711.11)		314,711.11		
Bush Gift	(661.76)		661.76		
	4,191,364.13	464,136.06	574,374.53	334,181.56	5,564,056.28
Deductions:					
Expenditures	4,171,365.19	576,348.94			4,747,714.13
Disposition of equipment				208,692.18	208,692.18
	4,171,365.19	576,348.94		208,692.18	4,956,406.31
Net change during year	19,998.94	(112,212.88)	574,374.53	125,489.38	607,649.97
Balance June 30, 1968	\$ 918,043.52	\$ (5,893.90)	\$78,046,723.74	\$6,866,034.54	\$85,824,907.90

EXHIBIT I

CHANGES IN OPERATING FUND
FOR THE YEAR ENDED JUNE 30, 1968

Balance July 1, 1967		\$ 898,044.58
Appropriations — Statement B:		
Budget, July 1, 1967		
to June 30, 1968 — Exhibit 3	\$4,490,137.00	
Bush Gift	16,600.00	
Transfers — Statement B:		
Bush Gift	(661.76)	
Unallocated Appropriations	<u>(314,711.11)</u>	<u>4,191,364.13</u>
Total available for expenditures		5,089,408.71
Expenditures:		
Salaries	2,113,229.72	
Laboratory	422,290.54	
Employee Benefits, Retirement Contributions	275,798.39	
Employee Benefits, Other	128,064.12	
Equipment	224,155.48	
Fellowships	205,104.01	
Building	183,807.28	
Operating	110,324.76	
Travel	104,659.28	
Publications	98,779.89	
Awards	78,663.94	
Financial advisory services	71,034.78	
Taxes	63,901.03	
Consulting fees and insurance	37,163.17	
Rent	21,347.04	
Shop	21,225.99	
Entertainment	6,418.04	
Dormitory	<u>5,397.73</u>	
Total expenditures		<u>4,171,365.19</u>
Balance June 30, 1968		<u>\$ 918,043.52</u>

EXHIBIT 2

CHANGES IN RESTRICTED GRANTS
FOR THE YEAR ENDED JUNE 30, 1968

	Balance July 1, 1967	Grants	Expenditures		Balance June 30, 1968
			Salaries	Other	
Carnegie Corporation of New York	\$113,372.37	\$ 63,486.23	\$ 49,886.14
General Services Administration	1,455.65	\$ (54.30)	1,401.35
Helen Hay Whitney Foundation	8,000.00	7,416.63	583.37
Holt, Rinehart and Winston, Inc.	1,141.00	1,141.00
Jet Propulsion Laboratory	434.16	82.98	351.18
National Aeronautics and Space Administration . .	(14,313.09)	50,721.00	\$12,346.63	56,937.86	(32,876.58)
National Science Foundation	5,568.69	340,500.00	14,261.77	344,251.94	(12,445.02)
Office of Naval Research . .	(9,691.24)	26,419.36	3,067.22	22,780.29	(9,119.39)
Public Health Service	8,351.44	35,550.00	24,186.64	23,376.98	(3,662.18)
University of Minnesota	3,000.00	1,611.42	1,388.58
Total	<u>\$106,318.98</u>	<u>\$464,136.06</u>	<u>\$53,862.26</u>	<u>\$522,486.68</u>	<u>\$ (5,893.90)*</u>

*Does not include grants to be received as follows:

National Aeronautics and Space Administration . . .	\$231,203.00
National Science Foundation	342,831.94
Office of Naval Research	33,297.00
Public Health Service	<u>11,349.00</u>
	<u>\$618,680.94</u>

EXHIBIT 3

CHANGES IN ENDOWMENT AND SPECIAL FUNDS

FOR THE YEAR ENDED JUNE 30, 1968

Endowment Fund:	Balance	Realized	Investment	Gifts and Other Income	Appropriations	Transfers	Balance
	July 1, 1967	Capital Gain, net					
Gifts							
Andrew Carnegie	\$22,000,000.00	\$22,000,000.00
Carnegie Corporation of New York	10,000,000.00	10,000,000.00
Realized capital gain, net	30,898,298.43	\$482,051.55	31,380,349.98
Unrestricted Capital Fund							
Gifts	98,528.04	\$ 6,740.95	105,268.99
Realized capital gain, net	5,202,106.46	90,275.69	5,292,382.15
Income							
Andrew Carnegie, reserve	2,500,000.00	2,500,000.00
Other	538,829.29	538,829.29
Working Capital Fund							
Income	4,781,671.12	...	\$4,030,988.22	...	\$4,455,690.00	\$368,124.58	4,725,093.92
Sales							
Assets	13,503.20	...	(13,503.20)	...
Publications	16,541.66	...	(16,541.66)	...
Refunds	17,050.72	...	(17,050.72)	...
Publication royalties	6,317.89	...	(6,317.89)	...
Special Funds:							
Astronomy	655,057.74	3,634.59	24,990.96	683,683.29
Bush Gift	34,359.02	253.54	2,195.11	...	17,760.00	661.76	19,709.43
Colburn	188,623.76	1,472.19	10,122.56	...	10,046.00	...	190,172.51
Hale Relief	6,976.95	51.98	357.45	...	390.00	...	6,996.38
Harkavy	9,398.45	64.34	442.47	...	430.00	...	9,475.26
Morgenroth	...	246.58	848.53	32,806.25
Teepie	19,200.81	143.69	988.00	...	981.00	...	19,351.50
Wood	539,299.14	3,141.98	21,603.67	...	21,440.00	...	542,604.79
Total	\$77,472,349.21	\$581,336.13	\$4,092,536.97	\$91,865.56	\$4,506,737.00	\$315,372.87	\$78,046,723.74

EXHIBIT 4

CHANGES IN LAND, BUILDING, AND EQUIPMENT FUND

FOR THE YEAR ENDED JUNE 30, 1968

	Balance July 1, 1967	Expenditures*	Deductions	Balance June 30, 1968	Classification of June 30, 1968, Balance		
					Land	Building	Equipment
Department of Plant Biology	\$ 207,192.42	\$ 6,069.60	\$ 430.95	\$ 212,831.07	\$ 75,371.81	\$ 137,459.26
Geophysical Laboratory	864,219.32	59,525.51	13,436.90	910,307.93	\$ 22,907.27	147,476.52	739,924.14
Mount Wilson Observatory	1,745,392.30	76,289.45	12,001.81	1,809,679.94	27,278.87	289,627.44	1,492,773.63
Department of Terrestrial Magnetism	1,221,606.99	114,747.38	180,777.52	1,155,576.85	74,449.98	324,385.72	756,741.15
Department of Embryology	395,830.02	56,300.68	452,130.70	452,130.70
Genetics Research Units	1,267,609.60	5,863.53	2,045.00	1,271,428.13	29,880.54	964,465.47	277,082.12
Office of Administration	1,038,694.51	15,385.41	1,054,079.92	214,244.20	718,943.49	120,892.23
Total	\$6,740,545.16	\$334,181.56	\$708,692.18	\$6,866,034.54	\$368,760.86	\$2,520,270.45	\$3,977,003.23

* Expenditures for Equipment:

Operating Fund	\$224,155.48
Restricted Grants	33,688.53
Expenditures Capitalized:	
Current Year	20,606.57
Prior Year	55,730.98
Total	\$334,181.56

SCHEDULE 1

BUDGET SUMMARY OF OPERATING FUND

FOR THE YEAR ENDED JUNE 30, 1968

Department	Unexpended Appropriations July 1, 1967	Appropriations	Transfers and Allotments	Total Expenditures	Unexpended Appropriations June 30, 1968
Research:					
Plant Biology	\$ 4,566.99	\$ 252,037.98	\$ (7,145.49)	\$ 244,275.60	\$ 5,183.88
Geophysical Laboratory	45,278.69	763,978.98	(9,571.51)	761,640.63	38,045.53
Mount Wilson Observatory	31,791.21	806,429.98	(44,485.29)	780,596.11	13,139.79
Terrestrial Magnetism	93,557.52	856,079.98	(38,634.01)	845,231.06	65,772.43
Embryology	37,411.10	609,050.98	(51,459.50)	561,650.83	33,351.75
Genetics Research Units	6,032.82	176,295.10	(31,887.74)	147,486.07	2,954.11
Research Projects, etc.	110,722.56	111,500.00	(21,257.32)	117,736.04	83,229.20
Total	329,360.89	3,575,373.00	(204,440.86)	3,458,616.34	241,676.69
Administration and General Expenses:					
Administration	14,997.19	447,464.00	1,326.45	455,301.42	8,486.22
Consulting fees, insurance, taxes	5,599.11	43,500.00	(4,528.45)	38,399.66	6,171.00
Contingent operating fund	1,750.00	200,000.00	(121,328.94)	80,421.06	80,421.06
Financial advisory services	16,000.00	70,000.00	1,774.00	71,034.78	16,739.22
General publications	14,563.17	46,400.00	15,154.32	69,617.49	6,500.00
Employee benefits, retirees	308,066.46	86,700.00	212.23	68,621.21	326,357.48
Employee benefits, special	707.76	4,000.00	13,058.38	9,774.29	7,991.85
Total	361,683.69	898,064.00	(94,332.01)	712,748.85	452,666.83
Unallocated Appropriations	207,000.00	16,700.00	223,700.00
Total	\$898,044.58	\$4,490,137.00	\$(298,772.87)	\$4,171,365.19	\$918,043.52

SCHEDULE 2

INVESTMENTS, JUNE 30, 1968

<u>Principal Amount</u>	<u>Description</u>	<u>Maturity</u>	<u>Book Value</u>	<u>Approximate Market Value</u>
Mortgage				
\$ 16,397.31	Alfred D. Hershey and Harriet D. Hershey, 5½ s	1974	\$ 16,397.31	\$ 16,397
Federal Agency Bonds				
\$1,025,000	Federal National Mortgage Association, 4½ s	1970	\$1,015,070.31	\$ 978,875
400,000	Federal National Mortgage Association, 4½ s	1970	394,500.00	389,000
500,000	Federal National Mortgage Association, 5½ s	1972	498,125.00	475,625
1,000,000	Federal National Mortgage Association, Part. Certificates, 5½ s	1973	1,000,000.00	963,750
<u>\$2,925,000</u>	Total		<u>\$2,907,695.31</u>	<u>\$2,807,250</u>
Foreign and International Bank Bonds				
\$ 700,000	Alberta Government Telephone, Commission Deb., 4½ s	1989	\$ 700,000.00	\$ 511,000
750,000	Alcan Aluminum Corporation, Prom. Note, 4½ s	1984	750,000.00	609,375
489,000	Aluminum Co. of Canada, Ltd., S. F. Deb., 4½ s	1980	494,514.76	405,870
146,000	Australia (Commonwealth of), 4½ s	1971	143,810.00	133,590
114,000	Australia (Commonwealth of), 5 s	1972	114,000.00	106,163
466,000	Australia (Commonwealth of), 5½ s	1982	468,003.48	382,120
750,000	Bell Telephone Co. of Canada, 1st Mtg. Series X, 4½ s	1988	747,300.00	564,375
250,000	British Columbia Power Commission, S. F. Deb., Series L, 4½ s	1987	245,000.00	175,000
750,000	Industrial Acceptance Corp., Ltd., Sec. Note Series Z, 5½ s	1982	750,000.00	590,625
125,000	Intl. Bank for Reconstruction & Development, 3 s	1976	125,000.00	101,875
125,000	Intl. Bank for Reconstruction & Development, 3½ s	1975	123,125.00	103,125
250,000	Intl. Bank for Reconstruction & Development, 20 Yr. Bonds, 4½ s	1977	250,000.00	217,500

INVESTMENTS — Continued

Principal Amount	Description	Maturity	Book Value	Approximate Market Value
Foreign and International Bank Bonds — Continued				
\$ 767,000	Quebec Hydro-Electric Commission, S. F. Deb., 5 s	1988	\$ 753,577.50	\$ 563,745
200,000	Shawinigan Water & Power Co., 1st Mtg. & Collat. Tr. S. F. Series M, 3 s	1971	201,080.00	178,500
1,000,000	Shell Funding Corp., Collat. Tr. Series B, 4½ s	1985	1,000,000.00	817,500
500,000	Toronto (Municipality of Metropolitan), S. F. Deb., 5 s	1979	498,637.50	412,500
<u>\$7,382,000</u>	Total		<u>\$7,364,048.24</u>	<u>\$5,872,863</u>
Public Utility Bonds				
\$ 237,000	Columbus & Southern Ohio Electric Co., 1st Mtg., 3¼ s	1970	\$ 238,563.33	\$ 219,818
125,000	Columbia Gas System, Inc., Series B, 3 s	1975	125,907.61	95,000
250,000	Columbia Gas System, Inc., Series F, 3¼ s	1981	245,937.50	182,500
300,000	Consolidated Edison Co. of N. Y., 1st & Ref. Mtg. Series N, 5 s	1987	301,486.90	252,000
4,000	Consumers Power Co., 1st Mtg., 4¼ s	1987	4,016.32	3,285
800,000	General Telephone & Electronics Corporation, Sub. Conv. Deb., 5 s	1992	800,000.00	824,000
200,000	Minnesota Power & Light Co., 1st Mtg., 3¼ s	1975	201,105.93	160,250
250,000	Niagara Mohawk Power Corp., Gen. Mtg., 3¼ s	1986	251,966.90	177,500
400,000	Niagara Mohawk Power Corp., Gen. Mtg., 4¼ s	1987	402,218.73	334,500
100,000	Ohio Power Co., 1st Mtg., 3¼ s	1968	101,500.00	98,875
200,000	Pacific Gas & Electric Co., 1st & Ref. Mtg. Series X, 3¼ s	1984	200,933.24	133,500
250,000	Pacific Gas & Electric Co., 1st & Ref. Mtg. Series BB, 5 s	1989	251,272.90	211,250
250,000	Pacific Power & Light Co., 1st Mtg., 4¼ s	1986	251,925.03	184,688
236,000	Potomac Electric Power Co., Deb., 4¼ s	1982	239,375.90	197,355
200,000	Public Service Co. of Indiana, 1st Mtg. Series F, 3¼ s	1975	201,233.45	160,750
400,000	Public Service Co. of Indiana, 1st Mtg. Series L, 4¼ s	1987	400,000.00	315,000
500,000	Public Service Electric & Gas Co., 1st & Ref. Mtg., 4¼ s	1987	503,044.93	418,125
250,000	Southern California Edison Co., 1st & Ref. Mtg. Series H, 4¼ s	1982	251,015.68	199,063

INVESTMENTS — Continued

Principal Amount	Description	Maturity	Book Value	Approximate Market Value
Public Utility Bonds — Continued				
\$ 200,000	Southern California Edison Co., 1st & Ref. Mtg. Series J, 4½ s	1982	\$ 201,220.59	\$ 166,000
500,000	Tenneco Inc., Deb., 5 s	1982	503,500.00	408,750
216,000	Tenneco Inc., 1st Mtg. Pipe Line, 5½ s	1977	216,000.00	191,700
300,000	Washington Water Power Co., 1st Mtg., 4½ s	1987	300,000.00	234,750
<u>\$6,168,000</u>	Total		<u>\$6,192,224.94</u>	<u>\$5,168,659</u>
Communication Bonds				
\$ 400,000	Illinois Bell Telephone Co., 1st Mtg. Series E, 4½ s	1988	\$ 403,194.02	\$ 305,500
200,000	Mountain States Telephone & Telegraph Co., Deb., 3½ s	1978	200,350.00	150,500
100,000	New York Telephone Co., Ref. Mtg. Series E, 3½ s	1978	100,443.77	75,625
200,000	Pacific Telephone & Telegraph Co., Deb., 3½ s	1978	201,103.60	152,750
250,000	Southern Bell Telephone & Telegraph Co., Deb., 4 s	1983	250,664.54	192,813
300,000	Southwestern Bell Telephone Co., Deb., 3½ s	1983	302,500.00	207,375
<u>\$1,450,000</u>	Total		<u>\$1,458,255.93</u>	<u>\$1,084,563</u>
Railroad Bonds				
\$ 100,000	Chesapeake & Ohio Railway Co., Gen. Mtg., 4½ s	1992	\$ 99,500.00	\$ 72,500
267,000	Fort Worth & Denver Railway Co., 1st Mtg., 4½ s Guar.	1982	268,200.59	206,925
<u>\$ 367,000</u>	Total		<u>\$ 367,700.59</u>	<u>\$ 279,425</u>
Industrial and Miscellaneous Bonds				
\$1,000,000	Aluminum Co. of America, Conv. Sub. S. F. Deb., 5½ s	1991	\$1,000,000.00	\$1,092,500
262,500	Bethlehem Steel Corporation, Sub. Deb., 4½ s	1990	183,637.50	207,703
1,000,000	Boeing Co., Notes, 6¾ s	1986	1,000,000.00	905,000
550,000	C.I.T. Financial Corp., Deb., 4½ s	1970	536,937.50	522,500
750,000	Colonial Pipeline Co., Sec. Note Series A, 4½ s	1990	750,000.00	592,500

INVESTMENTS — Continued

Principal Amount	Description	Maturity	Book Value	Approximate Market Value
Industrial and Miscellaneous Bonds — Continued				
\$1,000,000	Columbia Broadcasting System, Inc., Prom. Note, 5½ s	1991	\$1,000,000.00	\$ 870,000
400,000	Commercial Credit Co., Note, 3½ s	1976	403,313.34	310,000
700,000	Commercial Credit Co., Note, 4¾ s	1982	700,000.00	539,000
30,000	Corn Products Co., Sub. Deb., 4¾ s	1983	30,916.02	24,150
350,000	Crown Zellerbach Corp., Prom. Note, 4¾ s	1981	350,000.00	298,375
515,000	Erie Mining Company, 1st Mtg. Series B, 4½ s	1983	500,003.20	433,888
500,000	FMC Corp., S. F. Deb., 3.8 s	1981	500,000.00	380,000
500,000	First National City Bank, Capital Conv. Notes, 4 s	1990	512,215.00	548,750
204,000	Four Corners Pipe Line Co., Sec. Note, 5 s	1982	204,000.00	179,010
500,000	General Electric Credit Corp. (N.Y.), Sub. Note, 4¾ s	1987	500,000.00	365,000
500,000	General Electric Credit Corp. (N.Y.), Prom. Note, 5 s	1975	500,000.00	438,750
200,000	General Motors Acceptance Corp., Deb., 3½ s	1972	200,000.00	178,500
480,000	General Motors Acceptance Corp., Deb., 4 s	1979	435,037.50	369,600
1,000,000	General Motors Acceptance Corp., Deb., 4¾ s	1987	990,000.00	810,000
200,000	General Motors Acceptance Corp., Deb., 5 s	1977	195,000.00	173,500
200,000	General Motors Acceptance Corp., Deb., 5 s	1981	199,000.00	171,000
150,000	General Portland Cement Co., Conv. Sub. Deb., 5 s	1977	154,500.00	123,000
750,000	Household Finance Corp., Deb., 4¾ s	1993	746,250.00	581,250
1,000,000	Hyston Fibers, Inc., Notes, 5¾ s	1986	1,000,000.00	900,000
389,498.13	Instlcorp, Inc., Collat. Tr. Note, A-16	1991	376,487.53	334,968
321,097.52	Instlcorp, Inc., Collat. Tr. Note, A-19	1991	310,472.94	274,538
182,174.51	Instlcorp, Inc., Collat. Tr. Note, A-21	1991	175,798.43	156,670
231,361.68	Instlcorp, Inc., Collat. Tr. Note, A-23	1991	227,613.72	197,814
737,600.86	Instlcorp, Inc., Collat. Tr. Note, A-36	1992	707,476.92	610,364
400,000	Intl. Harvester Credit Corp., Deb., 4¾ s	1979	398,000.00	315,000

INVESTMENTS – Continued

Principal Amount	Description	Maturity	Book Value	Approximate Market Value
Industrial and Miscellaneous Bonds – Continued				
\$ 241,000	Kaiser Aluminum & Chemical Corp., 1st Mtg., 5½ s	1987	\$ 241,000.00	\$ 202,440
700,000	Kresge (S. S.) Company, Prom. Note, 4% s	1983	700,000.00	579,250
200,000	Montgomery Ward Credit Corp., Deb., 4% s	1980	199,000.00	160,000
95,000	National Dairy Products Corp., Deb., 2% s	1970	94,728.56	87,163
700,000	Owens-Illinois, Inc., Notes, 5 s	1991	700,000.00	547,750
150,000	Scovill Mfg. Co., Deb., 4% s	1982	147,686.32	128,250
525,000	Sears Roebuck Acceptance Corp., Sub. Deb., 4% s	1977	511,505.00	433,125
1,000,000	Shell Oil Company, Deb., 5 s	1991	1,000,000.00	847,500
250,000	Spiegel, Inc., Deb., 5 s	1987	250,000.00	185,000
466,000	Statewide Stations Inc., Sec. Note, 4% s	1994	466,000.00	368,140
215,000	Talcott (James) Inc., Senior Note 5½ s	1980	212,850.00	189,200
700,000	Texas Gulf Sulphur Co., Prom. Note, 4.7 s	1989	700,000.00	553,000
517,672.01	Trailer Train Co., 4% s	1976	517,672.01	487,906
340,000	Trans World Airlines, Inc., Conv. Sub. Deb., 4 s	1992	371,445.00	257,550
324,000	Tremarco Corporation, 1st Mtg. Series E, 5 s	1983	324,000.00	285,120
1,000,000	Union Carbide Corporation, S. F. Deb., 5.3 s	1997	1,000,000.00	890,000
700,000	United Air Lines, Inc., Notes, 5 s	1984	700,000.00	570,500
680,000	United Shoe Machinery Corporation, S. F. Deb., 5½ s	1992	678,300.00	618,800
542,500	U. S. Steel, S. F. Sub. Deb., 4% s	1996	443,873.50	425,863
1,000,000	Westinghouse Electric Corp., Deb., 5½ s	1992	1,000,000.00	873,750
250,000	Whirlpool Corporation, S. F. Deb., 3½ s	1980	250,000.00	188,750
500,000	Woolworth (F. W.) Company, Prom. Note, 5 s	1982	500,000.00	400,000
<u>\$26,099,404.71</u>	Total		<u>\$25,794,719.99</u>	<u>\$22,182,387</u>
<u>\$44,391,404.71</u>	Bonds, funds invested		<u>\$44,084,645.00</u>	<u>\$37,395,147</u>

INVESTMENTS — Concluded

Number of Shares	Description	Book Value	Approximate Market Value
Common Stocks			
13,100	American Can Company	\$ 731,046.93	\$ 658,275
23,110	American Electric Power Co., Inc.	162,703.74	895,513
24,700	American Smelting & Refining Company	1,360,570.39	2,223,000
42,352	American Telephone & Telegraph Company	1,161,275.59	2,133,482
16,000	Armstrong Cork Company	131,908.39	1,182,000
10,000	Avon Products, Inc.	826,947.35	1,387,500
53,600	Burlington Industries, Inc.	1,480,722.69	2,244,500
24,000	Caterpillar Tractor Co..	97,534.09	918,000
11,000	Celanese Corp..	568,604.02	603,625
24,000	Chesebrough-Pond's Inc.	746,765.43	1,089,000
16,500	Chicago Pneumatic Tool Co.	601,964.31	690,938
32,000	Clark Equipment Co.	772,393.17	912,000
39,200	Coca-Cola Company (The)	628,984.09	2,881,200
18,000	Continental Oil Company (Del.)	146,960.65	1,210,500
2,500	Corning Glass Works	59,631.83	801,250
41,172	Eastman Kodak Company	233,651.32	3,262,881
12,000	Federated Department Stores, Inc.	582,805.81	960,000
15,104	First National City Bank.	348,278.77	1,095,040
19,400	Ford Motor Company.	577,047.36	1,018,500
30,337	General Electric Company	740,512.49	2,616,566
10,800	General Foods Corp..	948,480.44	967,950
35,419	General Motors Corporation.	1,143,847.99	2,842,375
36,200	Gillette Company	1,239,112.08	1,900,500
21,712	Goodyear Tire & Rubber Company	488,401.64	1,191,446
20,006	Gulf Oil Corporation.	154,333.51	1,505,452
31,668	International Business Machines Corp..	851,095.87	1,120,555
24,470	International Nickel Co. of Canada Ltd.	1,296,074.87	2,502,058
12,900	Johnson & Johnson	750,762.93	1,193,250
45,630	Kennecott Copper Corporation	1,208,688.57	1,944,979
15,000	Merck & Co., Inc.	107,286.55	1,320,000
8,700	Minnesota Mining & Manufacturing Co.	787,138.57	928,725
30,700	Mobil Oil Corporation	1,099,916.18	1,427,550
40,000	Niagara Mohawk Power Corp.	863,803.67	825,000
34,000	Ohio Edison Co.	587,855.31	930,750
16,400	Panhandle Eastern Pipe Line Co.	431,553.54	602,700
9,000	Penn. Central Co.	614,232.68	729,000
15,000	Philip Morris Incorporated	493,240.88	821,250
4,600	Sears, Roebuck and Co.	207,078.03	325,450
32,800	Southern Co.	878,283.72	918,400
22,361	Standard Oil Co. (New Jersey)	578,043.17	1,520,548
24,190	Texaco Inc.	249,172.89	1,856,583
43,500	Texas Gulf Sulphur Co.	1,257,455.80	1,859,625
7,600	Texas Utilities Co.	104,621.78	443,650
41,500	TRW Inc.	2,097,876.40	2,391,438
28,400	U. S. Plywood-Champion Papers Inc.	697,928.16	1,608,150
35,132.67	Virginia Electric & Power Co.	636,137.24	1,097,875
20,000	Whirlpool Corporation	943,953.26	1,160,000
8,700	Xerox Corp.	1,863,165.49	2,583,900
<u>1,144,463.67</u>	Common stocks, funds invested	<u>\$34,539,849.64</u>	<u>\$ 77,384,929</u>
	Aggregate investments	<u>\$78,640,891.95</u>	<u>\$114,796,473</u>

SUMMARY OF INVESTMENT TRANSACTIONS
FOR THE YEAR ENDED JUNE 30, 1968

Cash, July 1, 1967 \$ 46,640.45

Sales and Redemptions

	Capital Gain	Capital Loss	Book Value
Mortgage			\$ 2,285.34
Bonds	\$ 8,026.14	\$ 47,697.50	1,962,230.40
Common stocks	<u>1,234,606.42</u>	<u>613,598.93</u>	<u>7,024,029.41</u>
	1,242,632.56	661,296.43	8,898,545.15
Realized capital gain, net — Statement B.	<u>.</u>	<u>581,336.13</u>	<u>581,336.13</u>
	<u>\$1,242,632.56</u>	<u>\$1,242,632.56</u>	

Total Sales and Redemptions	9,569,881.28
Income applied to amortization of bond premium	5,550.40
Morgenroth gift	<u>31,711.14</u>
	9,653,783.27
Cash transferred to current funds	<u>172,375.44</u>
Total	9,481,407.83

Acquisitions

Bonds	1,992,349.50
Common stock	<u>7,673,770.64</u>
Total Acquisitions	<u>9,666,120.14</u>
Cash, June 30, 1968	<u>\$ (184,712.31)</u>

Abstract of Minutes

of the Seventieth Meeting of the Board of Trustees

The annual meeting of the Board of Trustees was held in the Board Room of the Administration Building on Friday, May 3, 1968. Chairman James N. White called the meeting to order.

The following Trustees were present: Amory H. Bradford, Vannevar Bush, Crawford H. Greenewalt, Caryl P. Haskins, Alfred L. Loomis, Robert A. Lovett, William McC. Martin, Jr., Keith S. McHugh, Henry S. Morgan, William I. Myers, Garrison Norton, Richard S. Perkins, William R. Rubey, Frank Stanton, Juan T. Trippe, and James N. White.

The minutes of the Sixty-Ninth Meeting were approved.

The Chairman notified the Trustees of the deaths of Elihu Root, Jr., and Seeley G. Mudd. Dr. Bush and Dr. Haskins spoke of the Trustees' high esteem for Mr. Root and Dr. Mudd, and of their services and contributions to the Institution. Dr. Bush proposed the following resolution, which was unanimously adopted by the Trustees:

Be It Therefore Resolved, That we, the Trustees of the Carnegie Institution of Washington, record our keen sense of loss at the death of Elihu Root, Jr.

And Be It Further Resolved, That this resolution be entered on the minutes of the Institution, and that a copy be sent to Mrs. Root.

Dr. Haskins proposed the following resolution, which was also unanimously adopted by the Trustees:

Be It Therefore Resolved, That we, the Trustees of the Carnegie Institution, record our grief and deep sense of loss at the death of our friend and companion, Seeley Greenleaf Mudd.

And Be It Further Resolved, That this resolution be entered on the minutes of the Institution, and that a copy be sent to Mrs. Mudd.

Michael Ference, Jr., Robert M. Pennoyer, and William M. Roth were elected members of the Board of Trustees.

Mr. White was reelected Chairman of the Board for a term ending in 1971.

The following were elected for one-year terms: Henry S. Morgan as Chairman of the Executive Committee, Richard S. Perkins as Chairman of the Finance Committee, Carl J. Gilbert as Chairman of the Nominating Committee, Keith S. McHugh as Chairman of the Auditing Committee, and Frank Stanton as Chairman of the Retirement Committee.

Vacancies in standing committees, with terms ending in 1971, were filled as follows: Keith S. McHugh, William I. Myers, and Frank Stanton were elected members of the Executive Committee, Crawford H. Greenewalt was elected a member of the Finance

Committee, and Amory H. Bradford was elected a member of the Retirement Committee.

The reports of the Executive Committee, the Finance Committee, the Retirement Committee and the Auditing Committee were accepted. On the recommendation of the latter it was resolved that Lybrand, Ross Bros. and Montgomery be appointed as public accountants for the fiscal year beginning July 1, 1968.

The resignation of a Trustee, General Omar N. Bradley was reported and accepted with regret.

The annual report of the President was accepted.

Article V, Section 2, of the By-Laws was amended to read as follows:

ARTICLE V

Committees

2. All vacancies in the Standing Committees shall be filled by the Board of Trustees at the next annual meeting of the Board and may be filled at a special meeting of the Board. A vacancy in the Executive Committee, and, upon request of the remaining members of any other Standing Committee, a vacancy in such other Committee may be filled by the Executive Committee by temporary appointment to serve until the next meeting of the Board.

It was resolved that the Astronomy Fund of approximately \$600,000, and \$400,000 from the Working Capital Fund, be appropriated for use at the discretion of the President in needed site development, and the construction and location of suitable instruments for an astronomical observatory in Chile.

To provide for the operation of the Institution for the fiscal year beginning July 1, 1968, and, upon recommendation of the Executive Committee, the sum of \$4,697,212 was appropriated, the appropriation to be made specifically in the amount of \$4,644,557 from the Working Capital Fund, \$17,400 from the Astronomy Fund, \$350 from the Hale Fund, \$450 from the Harkavy Fund, \$290 from the Morgenroth Fund, \$985 from the Teeple Fund, and \$21,570 from the Wood Fund.

Articles of Incorporation

Fifty-eighth Congress of the United States of America;

At the Second Session,

Begun and held at the City of Washington on Monday, the seventh day of December, one thousand nine hundred and three.

AN ACT

To incorporate the Carnegie Institution of Washington.

Be it enacted by the Senate and House of Representatives of the United States of America in Congress assembled, That the persons following, being persons who are now trustees of the Carnegie Institution, namely, Alexander Agassiz, John S. Billings, John L. Cadwalader, Cleveland H. Dodge, William N. Frew, Lyman J. Gage, Daniel C. Gilman, John Hay, Henry L. Higginson, William Wirt Howe, Charles L. Hutchinson, Samuel P. Langley, William Lindsay, Seth Low, Wayne MacVeagh, Darius O. Mills, S. Weir Mitchell, William W. Morrow, Ethan A. Hitchcock, Elihu Root, John C. Spooner, Andrew D. White, Charles D. Walcott, Carroll D. Wright, their associates and successors, duly chosen, are hereby incorporated and declared to be a body corporate by the name of the Carnegie Institution of Washington and by that name shall be known and have perpetual succession, with the powers, limitations, and restrictions herein contained.

SEC. 2. That the objects of the corporation shall be to encourage, in the broadest and most liberal manner, investigation, research, and discovery, and the application of knowledge to the improvement of mankind; and in particular—

(a) To conduct, endow, and assist investigation in any department of science, literature, or art, and to this end to cooperate with governments, universities, colleges, technical schools, learned societies, and individuals.

(b) To appoint committees of experts to direct special lines of research.

(c) To publish and distribute documents.

(d) To conduct lectures, hold meetings, and acquire and maintain a library.

(e) To purchase such property, real or personal, and construct such building or buildings as may be necessary to carry on the work of the corporation.

(f) In general, to do and perform all things necessary to promote the objects of the institution, with full power, however, to the trustees hereinafter appointed and their successors from time to time to modify the conditions and regulations under which the work shall be carried on, so as to secure the application of the funds in the manner best adapted to the conditions of the time, provided that the objects of the corporation shall at all times be among the foregoing or kindred thereto.

SEC. 3. That the direction and management of the affairs of the corporation and the control and disposal of its property and funds shall be vested in a board of trustees, twenty-two in number, to be composed of the following individuals: Alexander Agassiz, John S. Billings, John L. Cadwalader, Cleveland H. Dodge, William N. Frew, Lyman J. Gage, Daniel C. Gilman, John Hay, Henry L. Higginson, William Wirt Howe, Charles L. Hutchinson, Samuel P. Langley, William Lindsay, Seth Low, Wayne MacVeagh, Darius O. Mills, S. Weir Mitchell, William W. Morrow, Ethan A. Hitchcock, Elihu Root, John C. Spooner, Andrew D. White, Charles D. Walcott, Carroll D. Wright, who shall constitute the first board of trustees. The board of trustees shall have power from time to time to increase its membership to not more than twenty-seven members. Vacancies occasioned by death, resignation, or otherwise shall be filled by the remaining trustees in such manner as the by-laws shall prescribe; and the persons so elected shall thereupon become trustees and also members of the said corporation. The principal place of business of the said corporation shall be the city of Washington, in the District of Columbia.

SEC. 4. That such board of trustees shall be entitled to take, hold and administer the securities, funds, and property so transferred by said Andrew Carnegie to the trustees of the Carnegie Institution and such other funds or property as may at any time be given, devised, or bequeathed to them, or to such corporation, for the purposes of the trust; and with full power from time to time to adopt a common seal, to appoint such officers, members of the board of trustees or otherwise, and such employees as may be deemed necessary in carrying on the business of the corporation, at such salaries or with such remuneration as they may deem proper; and with full power to adopt by-laws from time to time and such rules or regulations as may be necessary to secure the safe and convenient transaction of the business of the corporation; and with full power and discretion to deal with and expend the income of the corporation in such manner as in their judgment will best promote the objects herein set forth and in general to have and use all powers and authority necessary to promote such objects and carry out the purposes of the donor. The said trustees shall have further power from time

to time to hold as investments the securities hereinabove referred to so transferred by Andrew Carnegie, and any property which has been or may be transferred to them or such corporation by Andrew Carnegie or by any other person, persons, or corporation, and to invest any sums or amounts from time to time in such securities and in such form and manner as are permitted to trustees or to charitable or literary corporations for investment, according to the laws of the States of New York, Pennsylvania, or Massachusetts, or in such securities as are authorized for investment by the said deed of trust so executed by Andrew Carnegie, or by any deed of gift or last will and testament to be hereafter made or executed.

SEC. 5. That the said corporation may take and hold any additional donations, grants, devises, or bequests which may be made in further support of the purposes of the said corporation, and may include in the expenses thereof the personal expenses which the trustees may incur in attending meetings or otherwise in carrying out the business of the trust, but the services of the trustees as such shall be gratuitous.

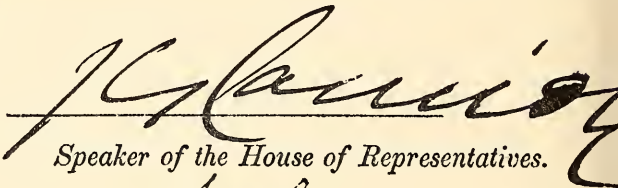
SEC. 6. That as soon as may be possible after the passage of this Act a meeting of the trustees hereinbefore named shall be called by Daniel C. Gilman, John S. Billings, Charles D. Walcott, S. Weir Mitchell, John Hay, Elihu Root, and Carroll D. Wright, or any four of them, at the city of Washington, in the District of Columbia, by notice served in person or by mail addressed to each trustee at his place of residence; and the said trustees, or a majority thereof, being assembled, shall organize and proceed to adopt by-laws, to elect officers and appoint committees, and generally to organize the said corporation; and said trustees herein named, on behalf of the corporation hereby incorporated, shall thereupon receive, take over, and enter into possession, custody, and management of all property, real or personal, of the corporation heretofore known as the Carnegie Institution, incorporated, as hereinbefore set forth under "An Act to establish a Code of Law for the District of Columbia, January fourth, nineteen hundred and two," and to all its rights, contracts, claims, and property of any kind or nature; and the several officers of such corporation, or any other person having charge of any of the securities, funds, real or personal, books or property thereof, shall, on demand, deliver the same to the said trustees appointed by this Act or to the persons appointed by them to receive the same; and the trustees of the existing corporation and the trustees herein named shall and may take such other steps as shall be necessary to carry out the purposes of this Act.

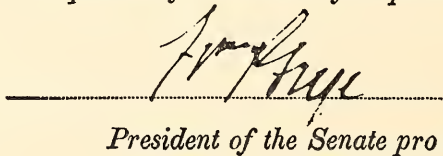
SEC. 7. That the rights of the creditors of the said existing corporation known as the Carnegie Institution shall not in any manner be impaired by the

passage of this Act, or the transfer of the property hereinbefore mentioned, nor shall any liability or obligation for the payment of any sums due or to become due, or any claim or demand, in any manner or for any cause existing against the said existing corporation, be released or impaired; but such corporation hereby incorporated is declared to succeed to the obligations and liabilities and to be held liable to pay and discharge all of the debts, liabilities, and contracts of the said corporation so existing to the same effect as if such new corporation had itself incurred the obligation or liability to pay such debt or damages, and no such action or proceeding before any court or tribunal shall be deemed to have abated or been discontinued by reason of the passage of this Act.

SEC. 8. That Congress may from time to time alter, repeal, or modify this Act of incorporation, but no contract or individual right made or acquired shall thereby be divested or impaired.

SEC. 9. That this Act shall take effect immediately.


Speaker of the House of Representatives.


President of the Senate pro tempore.

Approved.

April 28, 1904.



By-Laws of the Institution

Adopted December 13, 1904. Amended December 13, 1910, December 13, 1912, December 10, 1937, December 15, 1939, December 13, 1940, December 18, 1942, December 12, 1947, December 10, 1954, October 24, 1957, May 8, 1959, May 13, 1960, May 10, 1963, May 15, 1964, March 6, 1967, and May 3, 1968.

ARTICLE I

The Trustees

1. The Board of Trustees shall consist of twenty-four members with power to increase its membership to not more than twenty-seven members. The Trustees shall hold office continuously and not for a stated term.

2. In case any Trustee shall fail to attend three successive annual meetings of the Board he shall thereupon cease to be a Trustee.

3. No Trustee shall receive any compensation for his services as such.

4. All vacancies in the Board of Trustees shall be filled by the Trustees by ballot at an annual meeting, but no person shall be declared elected unless he receives the votes of two-thirds of the Trustees present.

5. If, at any time during an emergency period, there be no surviving Trustee capable of acting, the President, the Director of each existing Department, and the Executive Officer, or such of them as shall then be surviving and capable of acting, shall constitute a Board of Trustees *pro tem*, with full powers under the provisions of the Articles of Incorporation and these By-Laws. Should neither the President, nor any such Director, nor the Executive Officer be capable of acting, the senior surviving Staff Member of each existing Department shall be a Trustee *pro tem* with full powers of a Trustee under the Articles of Incorporation and these By-Laws. It shall be incumbent on the Trustees *pro tem* to reconstitute the Board with permanent members within a reasonable time after the emergency has passed, at which time the Trustees *pro tem* shall cease to hold office. A list of Staff Member seniority, as designated annually by the President, shall be kept in the Institution's records.

ARTICLE II

Officers of the Board

1. The officers of the Board shall be a Chairman of the Board, a Vice-Chairman, and a Secretary, who shall be elected by the Trustees, from the members of the Board, by ballot to serve for a term of three years. All vacancies shall be filled by the Board for the unexpired term; provided, however, that the Executive Committee shall have power to fill a vacancy in the office of Secretary to serve until the next meeting of the Board of Trustees.

2. The Chairman shall preside at all meetings and shall have the usual powers of a presiding officer.

3. The Vice-Chairman, in the absence or disability of the Chairman, shall perform the duties of the Chairman.

4. The Secretary shall issue notices of meetings of the Board, record its transactions, and conduct that part of the correspondence relating to the Board and to his duties.

ARTICLE III

Executive Administration

The President

1. There shall be a President who shall be elected by ballot by, and hold office during the pleasure of, the Board, who shall be the chief executive officer of the Institution. The President, subject to the control of the Board and the Executive Committee, shall have general charge of all matters of administration and supervision of all arrangements for research and other work undertaken by the Institution or with its funds. He shall prepare and submit to the Board of Trustees and to the Executive Committee plans and suggestions for the work of the Institution, shall conduct its general correspondence and the correspondence with applicants for grants and with the special advisers of the Committee, and shall present his recommendations in each case to the Executive Committee for decision. All proposals and requests for grants shall be referred to the President for consideration and report. He shall have power to remove, appoint, and, within the scope of funds made available by the Trustees, provide for compensation of subordinate employees and to fix the compensation of such employees within the limits of a maximum rate of compensation to be established from time to time by the Executive Committee. He shall be *ex officio* a member of the Executive Committee.

2. He shall be the legal custodian of the seal and of all property of the Institution whose custody is not otherwise provided for. He shall sign and execute on behalf of the corporation all contracts and instruments necessary in authorized administrative and research matters and affix the corporate seal thereto when necessary, and may delegate the performance of such acts and other administrative duties in his absence to the Executive Officer. He may execute all other contracts, deeds, and instruments on behalf of the corporation and affix the seal thereto when expressly authorized by the Board of Trustees or Executive Committee. He may, within the limits of his own authorization, delegate to the Executive Officer authority to act as custodian of and affix the corporate seal. He shall be responsible for the expenditure and disbursement of all funds of the Institution in accordance with the directions of the Board and of the Executive Committee, and shall keep accurate accounts of all receipts and disbursements. Following approval by the Executive Committee he shall transmit to the Board of Trustees before its annual meeting a written report of the operations and business of the Institution for the preceding fiscal year with his recommendations for work and appropriations for the succeeding fiscal year.

3. He shall attend all meetings of the Board of Trustees.

4. There shall be an officer designated Executive Officer who shall be appointed by and hold office at the pleasure of the President, subject to the approval of the Executive Committee. His duties shall be to assist and act for the President as the latter may duly authorize and direct.

5. The President shall retire from office at the end of the fiscal year in which he becomes sixty-five years of age.

ARTICLE IV

Meetings and Voting

1. The annual meeting of the Board of Trustees shall be held in the City of Washington, in the District of Columbia, in May of each year on a date fixed by the Executive Committee, or at such other time or such other place as may be designated by the

Executive Committee, or if not so designated prior to May 1 of such year, by the Chairman of the Board of Trustees, or if he is absent or is unable or refuses to act, by any Trustee with the written consent of the majority of the Trustees then holding office.

2. Special meetings of the Board of Trustees may be called, and the time and place of meeting designated, by the Chairman, or by the Executive Committee, or by any Trustee with the written consent of the majority of the Trustees then holding office. Upon the written request of seven members of the Board, the Chairman shall call a special meeting.

3. Notices of meetings shall be given ten days prior to the date thereof. Notice may be given to any Trustee personally, or by mail or by telegram sent to the usual address of such Trustee. Notices of adjourned meetings need not be given except when the adjournment is for ten days or more.

4. The presence of a majority of the Trustees holding office shall constitute a quorum for the transaction of business at any meeting. An act of the majority of the Trustees present at a meeting at which a quorum is present shall be the act of the Board except as otherwise provided in these By-Laws. If, at a duly called meeting, less than a quorum is present, a majority of those present may adjourn the meeting from time to time until a quorum is present. Trustees present at a duly called or held meeting at which a quorum is present may continue to do business until adjournment notwithstanding the withdrawal of enough Trustees to leave less than a quorum.

5. The transactions of any meeting, however called and noticed, shall be as valid as though carried out at a meeting duly held after regular call and notice, if a quorum is present and if, either before or after the meeting, each of the Trustees not present in person signs a written waiver of notice, or consent to the holding of such meeting, or approval of the minutes thereof. All such waivers, consents, or approvals shall be filed with the corporate records or made a part of the minutes of the meeting.

6. Any action which, under law or these By-Laws, is authorized to be taken at a meeting of the Board of Trustees may be taken without a meeting if authorized in a document or documents in writing signed by all the Trustees then holding office and filed with the Secretary.

7. During an emergency period the term "Trustees holding office" shall, for purposes of this Article, mean the surviving members of the Board who have not been rendered incapable of acting for any reason including difficulty of transportation to a place of meeting or of communication with other surviving members of the Board.

ARTICLE V

Committees

1. There shall be the following Standing Committees, *viz.* an Executive Committee, a Finance Committee, an Auditing Committee, a Nominating Committee, and a Retirement Committee.

2. All vacancies in the Standing Committees shall be filled by the Board of Trustees at the next annual meeting of the Board and may be filled at a special meeting of the Board. A vacancy in the Executive Committee and, upon request of the remaining members of any other Standing Committee, a vacancy in such other Committee may be filled by the Executive Committee by temporary appointment to serve until the next meeting of the Board.

3. The terms of all officers and of all members of Committees, as provided for herein, shall continue until their successors are elected or appointed.

Executive Committee

4. The Executive Committee shall consist of the Chairman, Vice-Chairman, and Secretary of the Board of Trustees, the President of the Institution *ex officio*, and, in addition, not less than five or more than eight Trustees to be elected by the Board by

ballot for a term of three years, who shall be eligible for re-election. Any member elected to fill a vacancy shall serve for the remainder of his predecessor's term.

5. The Executive Committee shall, when the Board is not in session and has not given specific directions, have general control of the administration of the affairs of the corporation and general supervision of all arrangements for administration, research, and other matters undertaken or promoted by the Institution. It shall also submit to the Board of Trustees a printed or typewritten report of each of its meetings, and at the annual meeting shall submit to the Board a report for publication.

6. The Executive Committee shall have power to authorize the purchase, sale, exchange, or transfer of real estate.

Finance Committee

7. The Finance Committee shall consist of not less than five and not more than six members to be elected by the Board of Trustees by ballot for a term of three years, who shall be eligible for re-election.

8. The Finance Committee shall have custody of the securities of the corporation and general charge of its investments and invested funds, including its investments and invested funds as trustee of any retirement plan for the Institution's staff members and employees, and shall care for and dispose of the same subject to the directions of the Board of Trustees. It shall have power to authorize the purchase, sale, exchange, or transfer of securities and to delegate this power. It shall consider and recommend to the Board from time to time such measures as in its opinion will promote the financial interests of the Institution and of the trust fund under any retirement plan for the Institution's staff members and employees, and shall make a report at each meeting of the Board.

Auditing Committee

9. The Auditing Committee shall consist of three members to be elected by the Board of Trustees by ballot for a term of three years.

10. Before each annual meeting of the Board of Trustees, the Auditing Committee shall cause the accounts of the Institution for the preceding fiscal year to be audited by public accountants. The accountants shall report to the Committee, and the Committee shall present said report at the ensuing annual meeting of the Board with such recommendations as the Committee may deem appropriate.

Nominating Committee

11. The Nominating Committee shall consist of the Chairman of the Board of Trustees *ex officio* and, in addition, three Trustees to be elected by the Board by ballot for a term of three years, who shall not be eligible for re-election until after the lapse of one year. Any member elected to fill a vacancy shall serve for the remainder of his predecessor's term, provided that of the Nominating Committee first elected after adoption of this By-Law one member shall serve for one year, one member shall serve for two years, and one member shall serve for three years, the Committee to determine the respective terms by lot.

12. Sixty days prior to an annual meeting of the Board the Nominating Committee shall notify the Trustees by mail of the vacancies to be filled in membership of the Board. Each Trustee may submit nominations for such vacancies. Nominations so submitted shall be considered by the Nominating Committee, and ten days prior to the annual meeting the Nominating Committee shall submit to members of the Board by mail a list of the persons so nominated, with its recommendations for filling existing vacancies on the Board and its Standing Committees. No other nominations shall be received by the Board at the annual meeting except with the unanimous consent of the Trustees present.

Retirement Committee

13. The Retirement Committee shall consist of three members to be elected by the Board of Trustees by ballot for a term of three years, who shall be eligible for re-election and the Chairman of the Finance Committee *ex officio*. Any member elected to fill a vacancy shall serve for the remainder of his predecessor's term.

14. The Retirement Committee shall, subject to the directions of the Board of Trustees, be responsible for the maintenance of a retirement plan for staff members and employees of the Institution and act for the Institution in its capacity as trustee under any such plan, except that any matter relating to investments under any such plan shall be the responsibility of the Finance Committee subject to the directions of the Board of Trustees. The Committee shall submit a report to the Board at the annual meeting of the Board.

ARTICLE VI

Financial Administration

1. No expenditure shall be authorized or made except in pursuance of a previous appropriation by the Board of Trustees, or as provided in Article V, paragraph 8, hereof.

2. The fiscal year of the Institution shall commence on the first day of July in each year.

3. The Executive Committee shall submit to the annual meeting of the Board a full statement of the finances and work of the Institution for the preceding fiscal year and a detailed estimate of the expenditures of the succeeding fiscal year.

4. The Board of Trustees, at the annual meeting in each year, shall make general appropriations for the ensuing fiscal year; but nothing contained herein shall prevent the Board of Trustees from making special appropriations at any meeting.

5. The Executive Committee shall have general charge and control of all appropriations made by the Board. Following the annual meeting, the Executive Committee may allocate these appropriations for the succeeding fiscal year. The Committee shall have full authority to reallocate available funds, as needed, and to transfer balances.

6. The securities of the Institution and evidences of property, and funds invested and to be invested, shall be deposited in such safe depository or in the custody of such trust company and under such safeguards as the Finance Committee shall designate, subject to directions of the Board of Trustees. Income of the Institution available for expenditure shall be deposited in such banks or depositories as may from time to time be designated by the Executive Committee.

7. Any trust company entrusted with the custody of securities by the Finance Committee may, by resolution of the Board of Trustees, be made Fiscal Agent of the Institution, upon an agreed compensation, for the transaction of the business coming within the authority of the Finance Committee.

8. The property of the Institution is irrevocably dedicated to charitable purposes, and in the event of dissolution its property shall be used for and distributed to those charitable purposes as are specified by the Congress of the United States in the Articles of Incorporation, Public Law No. 260, approved April 28, 1904, as the same may be amended from time to time.

ARTICLE VII

Amendment of By-Laws

1. These By-Laws may be amended at any annual or special meeting of the Board of Trustees by a two-thirds vote of the members present, provided written notice of the proposed amendment shall have been served personally upon, or mailed to the usual address of, each member of the Board twenty days prior to the meeting.

Index of Names

Numbers in *italic type* refer to the Report of the President.

- Abelson, Philip H., viii, *49, 75, 73, 78, 205, 266, 276*
 publications, 263
 studies, 203–210
- Ackerman, Edward A., x
- Adelman, Saul J., 69
- Agassiz, Alexander, vii
- Akimoto, S., 86, 87
- Albee, A., 265
- Aldrich, L. Thomas, viii, 74, 223, 281, 339, 381
 studies, 224, 224–231, 369–372
- Aller, L. H., 51, 65, 390
- Althaus, E., 265
- Anderson, Carl D., 3
- Anderson, Christopher M., 69
- Anderson, Jean H., 63
 publications, 65
- Anderson, Kurt S., 69
- Aparicio, Javier, 382
- Aparicio, Pablo, 339, 360, 382
 studies, 344–353
- Arp, Halton C., viii, *40, 42, 18, 36, 39, 48, 68*
 publications, 63, 65, 67
- Ashby, Eric, v, 2
- Assousa, George E., 381
- Atkinson, R. d'E., 51
- Avery, Mary Ellen, 460
- Baade, Walter, 63, 287
- Babcock, Horace, viii, *33, 73, 76, 3, 64, 68*
 publications, 63
 report of Director, Mount Wilson and Palomar Observatories, 3–70
- Bahcall, John, 7, 48
 publications, 63, 67
- Baker, Dennis, 69
- Baldwin, George J., vii
- Barbon, Roberto, 38, 41, 51, 52
 publications, 63, 64
- Barbour, Thomas, vii
- Barnhart, Philip E., 54
- Bartelmez, George W., 73
- Barton, R., 74
 studies, 221–222
- Bauer, Louis, 285
- Baum, William, A., 379, 387, 390
 publications, 63, 65
- Beach, Liselotte, 383
- Bear, Phyllis D., 556, 568
 studies, 557–558
- Becklin, Eric E., *43, 18, 29, 31, 33, 36, 37, 40, 44, 47, 54, 69*
 publications, 63, 66
- Belin, H. Lowell, 333
- Bell, James F., vii
- Bell, P. M., viii, *51, 53, 73, 76, 77, 78, 79, 91, 98, 101, 182, 188, 189, 191, 265, 266, 276*
 publications, 268
 studies, 97–98, 126–130, 135–137, 197–198, 198–199
- Bendich, Arnold, 382
- Benson, Donald W., 460
- Berendes, H., 464
- Bertola, F., 63, 64
- Billings, John S., vii
- Birch, F., 97, 98, 99, 100
- Bird, M., 276
- Bishop, David W., ix, 74
- Björkman, Olle, ix, *68, 69, 76, 474, 476, 546, 548*
 publications, 547
 studies, 477–478, 479–482, 487–488, 489–491
- Bliss, Robert Woods, vii
- Boesgaard, Ann Merchant, 25, 69
 publications, 63
- Bohlin, J. David, 12, 14, 15, 60, 69
- Boise, James W., x
- Bolton, Ellis T., viii, *46, 281, 300, 301, 381*
 report of the Director, Department of Terrestrial Magnetism, 281–386
- Bonica, John, 400, 460, 467
- Böving, Bent G., ix, *61, 62, 400, 466*
 publications, 464
 studies, 455–459, 462
- Bowen, Ira S., viii, *39, 46, 15, 58, 68, 390, 391*
 publications, 63
- Bowen, N. L., 81, 92, 93, 104, 113, 119, 120, 125, 153, 159, 160
- Boyd, F. R., Jr., viii, *51, 52, 73, 75, 76, 81, 87, 89, 100, 101, 131, 153, 156, 157, 158, 161, 168, 169, 276*
 publications, 268
 studies, 83–86, 130–131, 133–135, 210–215
- Braccesi, A., *41, 46, 52, 69*
 publications, 63, 65
- Bradford, Amory H., v
- Bradford, Lindsay, vii
- Bradley, Omar N., v
- Brandt, Werner, 299, 382
- Braun, E. H., 464

- Brenner, Don J., 300, 302, 381
 publications, 379
 studies, 301-310
 Brett, R., 73, 78
 studies, 198-199
 Britten, Roy J., viii, 300, 302, 381
 publications, 379
 studies, 320-325, 325-327, 327-330, 330-332,
 332-335
 Brookings, Robert S., vii
 Brookins, D. G., 131
 Brooks, Christopher, 339, 381
 Brown, Donald D., ix, 62, 63, 397, 400, 432, 466
 publications, 464, 465
 studies, 401-404, 404-408, 413
 Brown, G. M., 73, 76, 86, 96, 266, 276
 studies, 83-86
 Brown, Jeanette S., ix, 66, 475, 547, 548
 publications, 547
 studies, 516-520, 528-534, 536-546
 Brown, Louis, viii, 47, 286, 381
 publications, 379, 380
 studies, 294-299, 299-300
 Brueckel, Frank J., 69
 Bryan, W. B., 53, 74, 80, 246, 266, 276
 studies, 241-243, 243-244, 244-251
 Bumba, V., 89, 76, 9
 publications, 63, 64, 65, 67
 Burbidge, E. M., 35, 44, 46
 Burbidge, G. R., 35, 46
 Burd, Sylvia, 69
 Burgi, Elizabeth, ix, 562, 568
 publications, 568
 studies, 556-557
 Burrhus, Kenneth D., 383
 Bush, Vannevar, v, 285
 Buynitzky, Stephen J., 383

 Cabre, Ramon, S. J., 339, 382
 Cadwalader, John L., vii
 Calonius, P. E. B., 400, 462, 467
 Cameron, Robert C., 25, 63
 Campbell, William W., vii
 Canter, Dorothy, 382
 Carroll, George, 60
 Carty, John J., vii
 Casaverde, Mateo, xi, 339, 382
 studies, 369-372, 372-376
 Chamberlin, Margaret E., 383
 publications, 379
 Chambers, Robert G., 52
 Chang, Lillie O., 325
 Chao, Edward, 48, 53, 73, 77, 276
 studies, 126-130
 Chase, John, 467
 Chase, Richard A., xi
 Chayes, Felix, viii, 76, 73, 79, 80, 131, 244, 245,
 247, 266, 276
 publications, 268
 studies, 210-215, 235-236, 236, 236-239,
 239-241, 243-244
 Chinner, G. A., 265
 Chiscon, J. Alfred, 381

 Christy, J. W., 380
 Ciatti, F., 64
 Cisternas, Armando, 339, 344, 346, 382
 studies, 357-360
 Clark, S. P., Jr., 265
 Clausen, Jens C., ix, 489, 548
 publications, 547
 Clegg, Thomas B., 332
 publications, 379, 380
 Code, A. D., 390
 Cohen, J. G., 69
 publications, 64
 Cole, Whitefoord R., vii
 Conti, Peter S., 25
 publications, 64
 Coon, Hayden G., 63, 64, 399, 430, 466
 publications, 465
 studies, 419-421, 421-424, 424-428
 Cowie, Dean B., viii, 300, 304, 381
 publications, 379, 380
 studies, 301-310
 Cragg, Thomas A., 9, 69
 Craig, J. R., 73, 187, 276
 publications, 268
 studies, 177-179

 Danziger, I. John, 25, 30, 53
 publications, 64, 65
 Davidson, A. W., 54
 Davidson, E. H., 464
 Davis, B. T. C., 74, 78, 86, 87, 89, 91, 93, 98, 101,
 154, 155, 156, 157
 Davis, Dorothy N., 64, 67
 Davis, Gordon L., viii, 276
 publications, 268
 studies, 224, 224-231, 231-233
 Dawid, Igor B., ix, 62, 63, 397, 398, 400, 466
 publications, 465
 studies, 401-404, 417-418, 418-419
 DeHaan, Robert L., ix, 61, 400, 466
 publications, 465
 studies, 440-452
 DeLanney, Louis E., 467
 Delano, Frederic A., vii
 Dennison, Edwin, viii, 56, 68
 Deutsch, Armin, J., viii, 20, 22, 23, 24, 53, 57, 68
 publications, 64
 Dickel, H., 52
 Dickens, Robert J., 28, 29, 69
 publications, 64, 65
 Dickson, J. R., 248, 249
 Deza, Ernesto, 339, 382
 Doak, John B., 383
 Dodge, Cleveland H., vii
 Donnay, Gabrielle, viii, 48, 73, 74, 79, 177, 266,
 276
 publications, 268
 studies, 215-216, 218, 218-219, 219-220,
 220-221, 221-222, 222-223, 223, 223-224
 Donnay, J. D. H., 74, 276
 studies, 218-219

- Donner, Martin W., 401, 467
 publications, 465
 studies, 459-461
- Dougherty, Cary M., 467
- Drake, F. D., 40
- Dunn, Richard, 60
- Ebert, James D., ix, 37, 76, 398, 466
 publications, 465
 studies, 429-440
 report of Director, Department of Embryology, 393-467
- Ecklund, Everett T., 383
- Eggen, Olin J., 17, 18, 53, 55
 publications, 64
- Egorin, M., 467
 studies, 440-452
- Ehring, Ruth, 304, 307, 309
 publications, 568
 studies, 561-562
- El Goresy, A., 43, 53, 73, 78, 79, 133, 219, 266, 276
 studies, 182-187, 187-192, 197-198, 215-216
- Elvius, A., 390
- Emslie, R. F., 73, 78, 276
 studies, 108-112
- Eng, Marlene, 467
- England, J. L., viii, 73, 79, 80, 81, 87, 100, 101, 153, 154, 155, 156, 157, 158, 182, 188, 189, 191, 276
 publications, 268
 studies, 197-198
- Ephrussi, B., 63, 399, 424, 426, 428
 publications, 465
- Evertson, Dale, 382
- Ewald, P. P., 218
- Falkow, Stanley, 382
 publications, 379
- Fambrough, Douglas M., 400, 466
- Fanti, R., 52
 publications, 63, 64
- Fenner, Charles P., vii
- Ference, Michael, Jr., 74
- Ferguson, Homer L., vii
- Fernandez, Luis, S. J., 339, 382
- Finger, L. W., 73, 74, 76, 80, 91, 131, 266, 276
 studies, 91-92, 210-215, 216-218, 243-244
- Fisher, R. A., 567
- Flexner, Josefa B., 336, 382
- Flexner, Louis B., xi, 70, 336, 382, 466
- Flexner, Simon, vii
- Forbes, W. Cameron, vii
- Forbush, Scott E., viii, 339, 381
 publications, 379
 studies, 367-369
- Ford, W. Kent, Jr., viii, 286, 287, 381, 390
 publications, 379, 380
 studies, 286-290, 299-300
- Fork, David C., ix, 67, 473, 474, 500, 502, 546, 548
 publications, 547
 studies, 496, 503-505, 534-535
- Forrestal, James, vii
- Franklin, Naomi, 560, 566
- Fredrick, L. W., 390
- French, C. Stacy, ix, 64, 66, 69, 506, 521, 541, 548
 publications, 547
 studies, 535-536, 536-546
 report of Director, Department of Plant Biology, 470-549
- Frew, William N., vii
- Frez, Jose, 339, 382
- Gage, Lyman J., vii
- Gaines, Richard V., 48, 74, 79
 studies, 223
- Gajardo, Enrique, 339, 382
- Garrison, R. F., 22, 23, 53, 69
 publications, 64
- Gates, Howard S., 38, 69
 publications, 63, 64, 65, 68
- Gauhl, Eckard, 68, 69, 476, 548
 studies, 477-478, 478-479, 479-482, 482-487
- Gaz, Helen, ix
- Geiser, P., 276
- Gelderman, Albert H., 382
 studies, 320-325
- Giesecke, Alberto A., 339, 382
 studies, 369-372, 372-376
- Gifford, Walter S., vii
- Gilbert, Carl J., v, vi
- Gilbert, Cass, vii
- Gilbert, M. C., 52, 73, 77, 265, 266, 276
 studies, 100-101, 135-137, 167-170
- Gillett, Frederick H., vii
- Gilman, Daniel C., vii
- Goor, Daniel, 467
- Gottlieb, Sheldon H., 61, 400, 441, 467
- Gould, B., 467
 studies, 440-452
- Grasdalen, G. L., 64
- Green, H., 63
- Greene, Thomas, 56
- Greenwalt, Crawford H., v, vi
- Greenstein, Jesse L., viii, 42, 3, 7, 14, 17, 18, 20, 24, 25, 29, 31, 44, 48, 52, 68
 publications, 64, 67
- Greenwood, H. J., 265
- Grevesse, N., 39, 16
- Groth, Edward J., 23, 33, 69
- Gruenwald, Peter, 467
- Gunn, James E., 25
 publications, 64, 65
- Güven, N., 276
 publications, 268
- Haapala, Daniel, 382
- Hadidiacos, C., 219
- Hafner, S. S., 265
- Hafstad, Lawrence, 46, 285, 286
- Haggerty, S. E., 276
- Hale, George Ellery, 73, 60, 285
- Haler, Don, 31
- Hales, A. L., 372
- Hall, John S., 379, 387
- Hallberg, R. L., 398, 400, 402, 417, 467
 studies, 409-413

- Hanafusa, H., 464
Hansen, Edward, 74, 80, 251, 265, 266, 276
 studies, 254-258, 258-263, 263-265
Haraburda, Joseph M. S., x
Hare, P. E., viii, 49, 50, 73, 78, 266, 276
 studies, 205-208, 208-210
Hart, Stanley R., viii, 53, 54, 339, 381
 publications, 74, 233, 379, 380
 studies, 224, 224-231, 360-367
Hartman, Carl G., 73
Hartwick, F. David A., 27, 28, 30
Haskins, Caryl P., iv, vi, viii
Hay, John, vii
Hay, Robert J., 399, 466
 publications, 465
 studies, 429-440
Heard, J. F., 390
Heber, Ulrich W., 65, 473, 474, 548
 publications, 547
 studies, 503-505, 525-528
Heinrich, K. F. J., 213
Heintze, J. W. R., 69
Henard, Kenneth R., x
Henderson, Jack, 230
Hendricks, S., 464
Henry, Barklie McKee, vii
Herrick, Myron T., vii
Hershey, Alfred D., ix, 38, 54, 56, 57, 58, 304,
 307, 309, 568
 publications, 568
 studies, 556-557, 562-567
 report of Director, Genetics Research Unit,
 553-568
Hertig, Arthur T., 466
Herzog, Emil R., 38, 41, 69
 publications, 64
Hewish, A., 40
Hewitt, Abram S., vii
Hey, M. H., 48, 74, 219
Hicks, Virginia, 421, 467
Hiesey, William M., ix, 68, 76, 547, 548
 studies, 477-478, 478-479, 489-491, 493-496,
 546
Hietanen, A., 265
Higginson, Henry L., vii
Hilgeman, Theodore, 31, 69
Hitchcock, Ethan A., vii
Hodari, Alberto, 461
Hodgkinson, Paul, 461
Hoering, Thomas C., viii, 49, 73, 78, 192, 276
 publications, 268
 studies, 199-201, 201-203, 202-203, 203-205
Holdaway, M. J., 265
Holland, H. D., 379
Holmberg, Erik, 53
Hoover, Herbert, vii
Hornblower, Marshall, x
Howard, Robert, viii, 76, 38, 39, 9, 10, 61, 63, 68
 publications, 63, 64, 65, 67
Howe, William Wirt, vii
Hoyer, Bill H., 382
 publications, 379
Huckenholtz, H. G., 73, 76, 107, 276
 studies, 94-97, 139-153
Hutchinson, Charles L., vii
Hyland, Ardon R., 69
Iiyama, J. T., 276
Ingraham, Laura J., 304, 307, 309, 560, 562, 568
Irwin, John B.
 publications, 64
Ishizaka, Kyoichi, 74, 339, 381
 studies, 224, 224-230, 376-377
James, David E., 339, 360, 381
 publications, 379, 380
 studies, 344-353, 353-357
Jasper, H. H., 70
Jessup, Walter A., vii
Jewett, Frank B., vii
Johnson, J. J., 41
Johnson, Paul A., 383
Joy, Alfred H., 69
 publications, 64
Jugaku, Jun, 26
 publications, 64, 67
Julian, William H., 13, 49, 50, 60, 69
Kalb, J. E., 73, 76, 276
 studies, 97-98
Karpowicz, M.
 publications, 65
Kasinsky, Harold, 400, 467
 studies, 417
Katem, Basil, 27
Kato, Y., 372, 373
Katz, Margaret, 69
Kausel, Edgar, 339, 382
 studies, 357-360
Khachikian, E., 36, 53, 63
 publications, 65
Khogali, A., 65
Kinman, T. D., 390
Kleczeck, J., 65
Kleppa, O. J., 265
Kodaira, Keiichi, 19, 20, 24
Koelbloed, David, 65
Kohne, David E., viii, 58, 59, 60, 300, 302, 381
 studies, 310-320
Konigsberg, Irwin R., xi, 466
Kowal, Charles T., 38, 41, 54, 69
Kraft, Robert P., viii, 22, 29, 55, 68
 publications, 64, 65
Kristian, Jerome, 40, 44, 8, 27, 34, 40, 42, 43, 44,
 49, 69
 publications, 65, 66, 67
Krogh, Thomas E., viii, 74, 78, 267, 276
 studies, 224, 224-231
Kroovand, R. Lawrence, 467
Krüger, A., 64, 65
Krzeminski, W., 18, 29, 69
 publications, 64, 65
Kuhi, L. V., 64, 65, 390

- Kullerud, Gunnar, viii, 53, 73, 78, 267, 276
 publications, 268
 studies, 175–177, 177–179, 179–182, 182–187, 187–192
- Kushiro, I., 52, 73, 76, 77, 81, 89, 92, 105, 107, 110, 150, 276
 studies, 80–83, 98–100, 153–158, 161–167
- Lackner, Dora Russo, 39, 11, 12, 13, 69
- Lambert, David L., 39, 12, 13, 14, 16, 50, 69
 publications, 65, 67
- Langley, Samuel P., vii
- Lasker, Barry, M., 65
- Laubert, Roman, 299, 382
- Lawrence, Ernest O., vii
- Lawrence, Mark C., 66, 548
 studies, 535–536, 536–546
- Lazo, Eduardo, 339, 360, 382
 studies, 344–353
- Lazo, Melezio, 382
- Legum, Elizabeth, 467
 studies, 440–452
- Leighton, Robert B., viii, 3, 12, 63, 68
- Lieb, Margaret, 568
- Liller, William, 390
- Lindbergh, Charles A., vii
- Lindblad, P. O., 390
- Lindsay, William, vii
- Lindsley, D. H., viii, 73, 76, 78, 82, 100, 101, 170, 267, 276
 publications, 268
 studies, 86–88, 88–91, 91–92, 92–94, 108–112
- Little, Charles A., 383
- Livingston, William C., 64, 65
- Locanthi, Dorothy D., 69
- Lodge, Henry Cabot, vii
- Long, A., 276
- Loomis, Alfred L., v
- Looney, William B., 325
- Loos, Eckhard E., 475, 548
 studies, 520–525
- Losonsky, William, 382
- Lovett, Robert A., v
- Low, F. J., 53
- Low, Seth, vii
- Lowen, A. Louise, 69
- Ludwig, W. J., 379, 380
- Luyten, Willem, J., 41, 8, 45, 46, 52, 54
 publications, 63, 65, 66
- Lynds, Beverly T., 54
- Lynds, C. R., 44, 46, 390
 publications, 63, 65
- McCammon, D., 65
- McCarthy, M. F., S. J., 301, 319, 382, 390
 publications, 379
- McClintock, Barbara, ix, 75, 556, 568
 publications, 568
- McCord, Thomas B., 44, 69
- McGee, J. D., xi
 publications, 63, 65
- McGough, Sheila A., x
- McHugh, Keith S., v, vi
- MacKay, Donald, 71
- MacKenzie, W. S., 267
- McMahon, Daniel, 548
- MacVeagh, Wayne, vii
- Magnusson, E. A., 276
- Makita, Mitsugu, 65, 69
- Makover, Shraga, 568
 publications, 568
 studies, 561
- Mallia, E. A., 14, 16
 publications, 65
- Manwell, Tom, 50
 publications, 65, 67
- Marchant, J. C., 390
- Margulies, S. I.
 studies, 459–461
- Marsden, B. G., 65
 publications, 66
- Martin, C. B., Jr., 401, 461, 467
 publications, 466
 studies, 459–461
- Martin, William McC., Jr., v
- Marton, L. L., 379, 387
- Martres, M. J., 63
- Mathews, T. A., 390
- Matson, Dennis, 69
- Mayer, Oscar G., 59
- Mellon, Andrew W., vii
- Mendiguren, Jorge, 339, 382
- Merriam, John Campbell, vii
- Meyer, H. O. A., 51, 52, 75, 170, 276
 publications, 268
 studies, 130–131, 131–132, 132, 132–133
- Meyer, Robert, 46, 285, 286
- Michel, Jean-Marie, 65, 473, 540, 548
 studies, 508–514, 514–516
- Michel-Wolwertz, Marie-Rose, 65, 473, 475, 540, 541, 542, 543, 544, 548
 publications, 547
 studies, 503–505, 505–507, 508–514, 514–516
- Miller, Margaret Carnegie, vii
- Miller, O., 464
- Miller, Roswell, vii
- Miller, William C., 69
- Millikan, A. G., 390
- Mills, Darius O., vii
- Milton, Charles, 218
- Mintz, B., 464
- Misenhimer, Harold R., 400, 461, 467
 studies, 459–461
- Mitchell, S. Weir, vii
- Mitchell, Walter E., Jr., 59
- Mitterer, R. M., 49, 50, 73, 78, 276
 studies, 205–208
- Moffet, Alan T., 14, 37, 43
 publications, 65, 67
- Moh, G., 178, 179, 276
- Montague, Andrew J., vii
- Moore, Charlotte E., 73
- Morgan, Henry S., v, vi

- Morrow, William W., vii
 Morse, Stearns A., 73, 74, 78, 96, 113, 115, 267, 276
 studies, 112-120, 120-126, 224, 224-231, 231-233
 Mosig, Gisela
 publications, 568
 studies, 561-562
 Mudd, Seeley G., v, 72
 Mulholland, Thomas B., 70
 Münch, Guido, viii, 16, 23, 30, 32, 68
 publications, 65
 Munoz, J. L., 73, 76, 82, 87, 88, 92, 267
 studies, 86-88, 88-91, 91-92, 137-139, 170-175
 Murray, Bruce C., 69
 Musselman, Arlyne, 400, 467
 Myer, G. H., 73
 studies, 92-94
 Myers, William I., v, vi

 Nafe, E. S., 379
 Naldrett, A. J., 187, 276
 publications, 268
 Narbaitz, Roberto, 467
 Nery, Edmundo, 401, 462, 467
 Neugebauer, G., 42, 43, 16, 18, 29, 31, 33, 36, 37, 38, 40, 44, 47, 69
 publications, 65, 66
 Newkirk, Gordon A., 15
 publications, 65
 Newton, R. C., 98, 99, 265
 Nicholson, Frank, 548
 studies, 477-478
 Nishida, N., 467
 Nobs, Malcolm A., ix, 68, 548
 studies, 477-478, 479, 489-491, 493-496
 Norton, Garrison, v, vi
 Norton, Robert H., 64, 65, 68

 O'Brien, Peter N. S., 381
 publications, 379
 O'Connell, Robert, 69
 O'Dell, C. R., 54
 Ohmoto, H., 379
 Oke, J. B., viii, 41, 42, 44, 8, 24, 25, 26, 27, 34, 36, 37, 38, 39, 44, 47, 68
 publications, 66
 Olea, Ricardo, 339, 382
 studies, 357-360
 Olsen, Edward T., 41, 45
 Oort, Jan H., xi, 68
 O'Rahilly, Ronan, 467
 publications, 466
 studies, 462
 Orruma, Jose, 382
 Osborn, William Church, vii
 Osmer, Patrick S., 69
 Ostenso, N., 360

 Padget, Dorcas H., 467
 Parmelee, James, vii
 Parsons, William Barclay, vii
 Paton, Stewart, vii

 Patton, Donald J., x
 Peach, John V., 45, 34, 49, 69
 publications, 65, 66
 Peery, B. F., 390
 Pelling, C., 464
 Pennoyer, Robert Morgan, 74, 75
 Pepper, George W., vii
 Perkins, Richard S., v, vi
 Pershing, John J., vii
 Peterson, Arsine V., 69
 Peterson, Bruce A., 69
 Petitjean, Claude, 47, 286, 381
 publications, 379
 studies, 294-299
 Pickett, James M., 548
 Platt, R. G., 276
 Poe, Glenn R., 383
 Polinger, Iris S., 445, 467
 studies, 440-452
 Pollard, C. O., 74
 studies, 220-221
 Pollock, Harry E. D., xi
 Potter, Van R., 327
 Powell, James L., 268
 Pozo, Salvador del, 339, 382
 studies, 369-372, 372-376
 Prager, Lillian K., 66, 541, 548
 studies, 516-520, 536-546
 Prentis, Henning W., Jr., vii
 Presnall, D. C., 276
 Prewitt, C. T., 217
 Pritchett, Henry S., vii
 Proskouriakoff, Tatiana, x
 Puchelt, H. R., 73, 79, 267, 276
 studies, 192-197
 Purgathofer, Alois Th., 382

 Rabes, H. M., 464
 Racine, René, 22, 28, 29, 33, 55, 69
 publications, 66
 Rake, Adrian V., 70, 71, 300, 381
 studies, 320-325, 325-327, 335-339
 Ramsey, Elizabeth M., ix, 400, 466
 publications, 466
 studies, 459-461, 462
 Rebbert, Martha, 467
 studies, 418-419
 Reeder, Ronald H., 62, 63, 397, 400, 410, 467
 studies, 401-404
 Rees, Martin J., 50, 69
 publications, 66, 67
 Reitzel, John, 372
 Rentschler, Gordon S., vii
 Reynolds, Kathleen, 69
 Reynolds, Samuel R. M., 466
 Richardson, S. W., 73, 77, 276
 studies, 135-137
 Riley, Malcolm S., 69
 Robertson, P., 97, 98, 265
 Roberts, Richard B., viii, 46, 70, 71, 285, 286, 300, 381
 publications, 379
 studies, 335-339

- Rockefeller, David, vii
 Rodgers, John, 265, 267
 Rodman, J. P., 390
 Rodriguez, Anibal, 339, 371, 382
 Root, Elihu, vii
 Root, Elihu, Jr., vii
 Rosenfeld, David, 467
 Rosenfeld, J. L., 265, 268
 Rosenquist, Glenn C., 467
 Rosenwald, Julius, vii
 Roth, William M., v, 74, 75
 Roy, R., 364
 Rubey, William W., v
 Rubin, Vera C., viii, 286, 288, 381
 publications, 379, 380
 studies, 286-290, 299-300
 Rudnicki, K., 41
 publications, 64, 65, 66
 Rule, Bruce, viii, 59, 62
 Rust, David M., 11, 69
 publications, 66
 Ryerson, Martin A., vii
- Saa, German, S. J., 339, 381
 Sachs, Howard, 58
 Sacks, I. Selwyn, viii, 339, 360, 381
 publications, 379, 380
 studies, 339-344, 344-353, 353-357
 Salgueiro, Reynaldo, xi, 339, 382
 studies, 369-372, 372-376
 Sandage, Allan, viii, 40, 41, 44, 45, 76, 3, 8, 27,
 28, 30, 33, 34, 36, 40, 42, 43, 44, 45, 46, 47, 49,
 54, 68
 publications, 65, 66, 67
 Santa Cruz, Jaime, 339, 382
 Sargent, Annilla, 69
 Sargent, Wallace L., viii, 42, 7, 20, 24, 26, 29, 35,
 36, 37, 38, 39, 40, 42, 47, 48, 50
 publications, 63, 64, 66, 67
 Satchler, G. R., 47, 299
 Scaletta, L. J., 63, 428
 publications, 466
 Scargle, Jeffrey D., 63
 publications, 67
 Schadee, Aert
 publications, 64, 67
 Schairer, J. Frank, viii, 73, 77, 81, 92, 93, 94,
 95, 98, 105, 106, 107, 108, 111, 112, 114, 119,
 120, 142, 143, 146, 147, 148, 151, 153, 158, 160,
 162, 267
 publications, 269
 studies, 101-104, 104-105
 Schild, Rudolph E., 23, 26, 69
 publications, 66, 67
 Schmidt, Maarten, viii, 41, 7, 8, 42, 43, 45, 46,
 48, 68
 publications, 63, 65, 67
 Scholz, M. T., 69
 Schreyer, W., 265
 Schuetz, A. W., 400, 467
 publications, 466
 studies, 454-455
- Schuilling, R. D., 265
 Schwartz, Merry C., 400, 467
 studies, 413, 413-417
 Scott, William H., 74, 80, 267, 276
 studies, 251-254, 254-258, 258-263
 Seares, Frederick H., 63
 Searle, Leonard, 20, 25, 50, 68
 publications, 66, 67
 Sellman, Adolph H., 467
 Senftle, F. E., 74
 studies, 218
 Severn, C. B., 467
 Seyler, Richard G., 296, 382
 publications, 379, 380
 Sharpless, S., 390
 Shepard, Anna O., x, 74
 Shepley, Henry R., vii
 Shifrin, S., 400, 467
 studies, 452-454
 Silsbury, James H., 476, 548
 studies, 491-493
 Simon, Michal, 14, 50, 69
 publications, 65, 66, 67
 Simoni, Diglio V., 339, 382
 Simpson, E. S. W., 380
 Simpson, John A., 368, 379
 Sinclair, John H., 400, 432, 467
 publications, 466
 studies, 404-408
 Skalka, Anna Marie, 567, 568
 publications, 568
 studies, 556-557, 557-558, 558-560, 560-561
 Slater, C. H., 65, 67
 Smith, Bessie, 429, 467
 Smith, Bradford, 17
 Smith, James H. C., ix, 548
 Smith, Sara F., 9, 10, 30
 publications, 63, 64, 67
 Smith, T. Jefferson, viii, 53, 54, 339, 381
 publications, 379, 380
 studies, 360-367
 Smith, Theobald, vii
 Sollins, Jeff, 461
 Somerville, Delores, 429, 467
 Soru-Iscovi, I., 63, 67
 Sosman, Robert B., 73
 Spiegel, E. A., 67
 Spooner, John C., vii
 Stalsberg, Helge, 447, 467
 studies, 440-452
 Stanton, Frank, v, vi
 Steiger, R. H., 379, 380
 Stein, Robert F., 25, 69
 publications, 67
 Steinhart, John S., viii, 53, 54, 339, 381
 publications, 379, 380
 studies, 360-367
 Stewart, David B., 137
 publications, 269
 studies, 223-224
 Stewart, J. M., 48
 Storey, William Benson, vii

- Strong, Richard P., vii
 Stueber, Alan M., 381
 Sutherland, L. J., 249
 Suyehiro, Shigeji, xi, 339, 382
 Swanson, Ronald F., 400, 467
 Swings, J. P., 39
 Switzer, G., 222
 Swope, Henrietta H., 73, 68, 69
 publications, 67
 Taft, Charles P., v, vi
 Taft, William H., vii
 Tamayo, Lupe, 339, 382
 studies, 369-372
 Tammann, G. A.
 publications, 66, 67
 Tanenbaum, Andrew W., 11
 publications, 64, 67
 Taylor, L. A., 276
 Thackeray, A. D., 63, 67
 Thayer, William S., vii
 Thomas, Pamela W., x
 Thomas, R., 567
 Thomason, Carole E., 568
 Thompson, A. Gerald, x
 Thompson, A. R., 65, 67
 Thompson, J. B., 265
 Thorpe, A., 74
 studies, 218
 Tilley, C. E., 81, 94, 106, 112, 168, 170, 245,
 246, 247, 266, 276
 Townes, Charles H., v, 13
 Trächslin, Walter, 47, 286, 381
 publications, 379, 380
 studies, 294-299, 299-300
 Treanor, P. J., S. J., 379, 380
 Trimble, Virginia L., 32, 69
 publications, 64, 67
 Trippe, Juan T., v, vi
 Tsuju, Takashi, 18, 19, 69
 Tuft, Peter H., 61, 62, 400, 467
 studies, 455-459
 Turner, Kenneth C., viii, 43, 286, 290, 381
 publications, 380
 studies, 290-294
 Tuve, M. A., viii, 285, 286, 339, 360, 381, 387
 publications, 379, 380
 studies, 290-294, 369-372
 Utter, Merwyn, G., 9, 69
 publications, 67
 Varsavsky, Carlos, 286, 382
 studies, 290-294
 Vaughan, Arthur H., Jr., viii, 30, 58, 69
 publications, 67, 68
 Velde, Neltje W. van de, 383
 Vess, Grace D., 69
 Villiers, J. de, 276
 Visvanathan, N., 27, 36, 37, 39, 47, 59, 69
 publications, 66, 67
 Volponi, Fernando, 339, 382
 Vorontsov-Velyaminov, B. A., 42
 Wadsworth, James W., vii
 Wagner, C. E., 74, 220
 studies, 220-221
 Walburn, Marjorie H., x
 Walcott, Charles D., vii
 Walcott, Frederic C., vii
 Walcott, Henry P., vii
 Warner, B., 14, 16
 publications, 65, 67
 Weed, Lewis H., vii
 Weedman, D. W., 67
 Wehmiller, J. F., 276
 Weiss, Mary C., 63, 64, 398, 399, 467
 publications, 466
 studies, 424-428, 428-429
 Weistrop, Donna, 69
 publications, 67
 Welch, William H., vii
 Wendker, H., 52
 Werner, Rudolf, 568
 publications, 568
 Westphal, J. A., 8, 42, 43, 44, 62, 69
 publications, 65, 67
 Wheeler, R., 276
 White, Andrew D., vii
 White, Edward D., vii
 White, James N., v, vi
 White, William, 268
 Whitman, Winifred G., 285
 Whittingham, D. G., 467
 Wickersham, George W., vii
 Wilcox, John M., 39, 10, 11
 publications, 64, 67
 Wildey, Robert, 30
 publications, 66, 67
 Wilkins, R. W. T., 222
 Williams, Isabelle P., 424, 467
 studies, 421-424
 Wilson, Olin C., viii, 3, 22, 23, 32, 53, 69
 publications, 67
 Wilson, Robert E., vii
 Wiser, John L., 456, 467
 Witschi, E., 467
 Woerden, Hugo van,
 publications, 67
 Wold, R., 360
 Wolstenholme, D. R.
 publications, 466
 studies, 417-418
 Wood, Steven G., 548
 Woodward, Robert S., vii
 Wright, Carroll D., vii
 Yamagishi, Hideo, 568
 studies, 558-560
 Yoder, Hatten S., viii, 52, 73, 76, 77, 81, 94, 95,
 96, 98, 107, 108, 110, 112, 114, 115, 119, 120,
 121, 124, 142, 143, 146, 147, 148, 151, 158,
 170, 245, 246, 266, 267, 276
 publications, 269
 studies, 101-104, 104-105, 105-108, 153-158,
 161-167

Yoshikawa-Fukada, Masako, 398, 467
 publications, 466
 studies, 429-440
Young, M. Wharton, 401, 467
Young, R. A., 74
 studies, 220-221
Yuyama, Shuhei, 399, 467
 studies, 429-440

Zemann, J., 48, 74, 79, 276
 studies, 223, 223-224
Zen, E., 265
Zies, E. G., 276
Zirin, Harold, viii, 39, 7, 12, 13, 14, 26, 60, 61,
 63, 69
 publications, 65, 67, 68
Zwicky, Fritz, 42, 37, 38, 39, 40, 41, 50, 51, 68, 69
 publications, 63, 64, 65, 66, 68

